frontiers | Research Topics

Advances in brain disorders: From mechanisms to therapeutic targets

Edited by
Arianna Bellucci, Federica Bono, Sara Anna Bonini, Maria Jose Sisalli and Giulia Abate

Coordinated by
Viviana Trezza and Daniela Uberti

Published in
Frontiers in Molecular Neuroscience

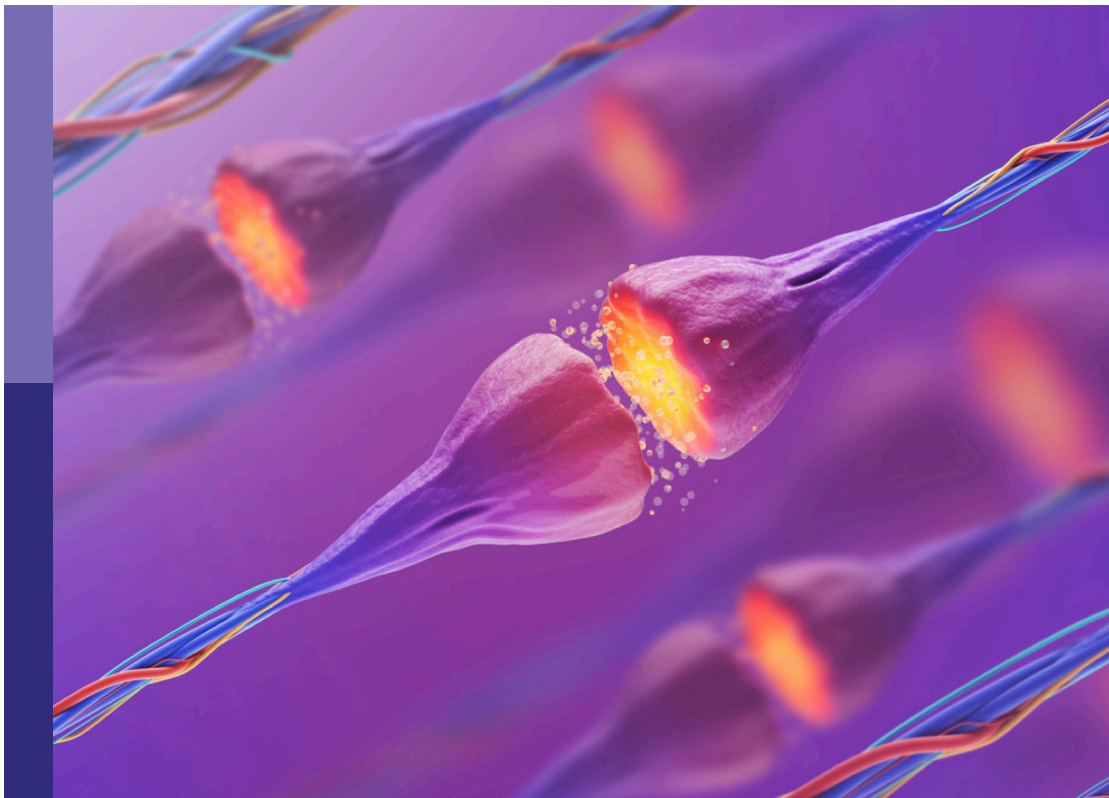

ISSN 1664-8714
ISBN 978-2-8325-4105-0
DOI 10.3389/978-2-8325-4105-0

About Frontiers

Frontiers is more than just an open access publisher of scholarly articles: it is a pioneering approach to the world of academia, radically improving the way scholarly research is managed. The grand vision of Frontiers is a world where all people have an equal opportunity to seek, share and generate knowledge. Frontiers provides immediate and permanent online open access to all its publications, but this alone is not enough to realize our grand goals.

Frontiers journal series

The Frontiers journal series is a multi-tier and interdisciplinary set of open-access, online journals, promising a paradigm shift from the current review, selection and dissemination processes in academic publishing. All Frontiers journals are driven by researchers for researchers; therefore, they constitute a service to the scholarly community. At the same time, the *Frontiers journal series* operates on a revolutionary invention, the tiered publishing system, initially addressing specific communities of scholars, and gradually climbing up to broader public understanding, thus serving the interests of the lay society, too.

Dedication to quality

Each Frontiers article is a landmark of the highest quality, thanks to genuinely collaborative interactions between authors and review editors, who include some of the world's best academicians. Research must be certified by peers before entering a stream of knowledge that may eventually reach the public - and shape society; therefore, Frontiers only applies the most rigorous and unbiased reviews. Frontiers revolutionizes research publishing by freely delivering the most outstanding research, evaluated with no bias from both the academic and social point of view. By applying the most advanced information technologies, Frontiers is catapulting scholarly publishing into a new generation.

What are Frontiers Research Topics?

Frontiers Research Topics are very popular trademarks of the *Frontiers journals series*: they are collections of at least ten articles, all centered on a particular subject. With their unique mix of varied contributions from Original Research to Review Articles, Frontiers Research Topics unify the most influential researchers, the latest key findings and historical advances in a hot research area.

Find out more on how to host your own Frontiers Research Topic or contribute to one as an author by contacting the Frontiers editorial office: frontiersin.org/about/contact

Advances in brain disorders: From mechanisms to therapeutic targets

Topic editors
Arianna Bellucci — University of Brescia, Italy
Federica Bono — University of Brescia, Italy
Sara Anna Bonini — University of Brescia, Italy
Maria Jose Sisalli — University of Naples Federico II, Italy
Giulia Abate — University of Brescia, Italy

Topic coordinators
Viviana Trezza — Roma Tre University, Italy
Daniela Uberti — University of Brescia, Italy

Citation
Bellucci, A., Bono, F., Bonini, S. A., Sisalli, M. J., Abate, G., Trezza, V., Uberti, D., eds. (2023). *Advances in brain disorders: From mechanisms to therapeutic targets*. Lausanne: Frontiers Media SA. doi: 10.3389/978-2-8325-4105-0

Table of contents

frontiers | Frontiers in Molecular Neuroscience

TYPE Editorial
PUBLISHED 28 November 2023
DOI 10.3389/fnmol.2023.1337583

OPEN ACCESS

EDITED AND REVIEWED BY
Detlev Boison,
Rutgers, The State University of New Jersey, United States

*CORRESPONDENCE
Arianna Bellucci
✉ arianna.bellucci@unibs.it

RECEIVED 13 November 2023
ACCEPTED 15 November 2023
PUBLISHED 28 November 2023

CITATION
Bono F, Abate G, Bonini SA, Sisalli MJ and Bellucci A (2023) Editorial: Advances in brain disorders: from mechanisms to therapeutic targets. *Front. Mol. Neurosci.* 16:1337583. doi: 10.3389/fnmol.2023.1337583

Editorial: Advances in brain disorders: from mechanisms to therapeutic targets

Federica Bono[1], Giulia Abate[1], Sara Anna Bonini[1], Maria Josè Sisalli[2] and Arianna Bellucci[1]*

[1]Department of Molecular and Translational Medicine, University of Brescia, Brescia, Italy, [2]Division of Pharmacology, Department of Neuroscience, School of Medicine, University of Naples "Federico II", Naples, Italy

KEYWORDS

brain disorders, brain disease mechanisms, disease biomarker discovery, therapeutic targets, therapeutic development

Editorial on the Research Topic
Advances in brain disorders: from mechanisms to therapeutic targets

Brain disorders represent one of the main challenges for global society because of their outstanding impact on human health and social welfare (Feigin et al., 2020; Arias et al., 2022). This is aggravated by the detrimental effects of COVID-19 infections on the central nervous system and more generally on human wellbeing, which predispose a large number of affected patients to the development of acute or chronic neurological disorders or mental illnesses (Heneka et al., 2020; Penninx et al., 2022).

More efficient strategies to monitor brain health are warranted in order to precociously diagnose neurological and psychiatric disorders and finely stage their progression. Still, the development of novel therapeutic approaches able to halt disease advancement without inducing severe side effects is compelling in order to factually cure patients affected by brain disorders. Such objectives can be reached only by the elucidation of the key molecular underpinnings of brain disorders and by the combination and integration of data deriving from basic and clinical research studies.

This Frontiers in Molecular Neuroscience Topic collects research articles and reviews providing novel significant advancements in our general knowledge of the biological basis of disease and opening new insights into the development of innovative biomarkers and therapeutic approaches for these disabling conditions.

Guo et al. showed that Rab20 inhibition significantly alleviates brain infarct volume, neurological deficits, and apoptosis by inhibiting mitochondrial fission and dysfunction in models of ischemia/reperfusion injury.

McClendon et al. showed that the administration of the steroid receptor co-activator MCB-10-1 in a rat model of transient cerebral ischemia reduces post-ischemic brain damage by modulating microglia and astroglia and mitigating neurologic impairment.

Shen et al. reviewed the contribution of single-cell sequencing technology to our understanding of post-stroke brain damage.

Wang et al. summarized the role of chemokines in intracerebral hemorrhage, underlining their key role as disease mediators and highlighting their relevance as therapeutic targets.

Fan G. et al. reviewed the role of glutamate in excitotoxicity and ferroptosis in the context of ischemic stroke, describing possible therapeutic approaches to modulate these events.

Shim et al. investigated the occurrence of shared pathological pathways between cerebral adrenoleukodystrophy and Alzheimer's disease through an *in silico* approach, showing that annexin A5, beta-2-microglobulin, CD44, and fibroblast growth factor 2 associate with the pathogenesis of the two neurodegenerative diseases.

Guan et al. investigated the pathogenic mechanism of abnormal cell cycle re-entry of neurons in Alzheimer's disease in *in vitro* and *in vivo* models with the β-amyloid pathology, revealing that increased expression of cyclin-dependent kinase (CDK)1/2/4 and cyclin A2/B1/D3/E1, and a parallel decrease of p18 and p21 underlie β-amyloid protein-dependent-enhanced cell cycle re-entry, which can be counteracted by aspirin administration.

Gasser et al. showed that a microglial/innate immune modulator selectively targeting microglial aberrant functions, such as synaptic overpruning, may attenuate the progression of cognitive, and motor decline in Huntington's disease.

Brembati et al. reviewed the significance of post-translational modifications in α-synuclein, a protein playing a major role in the pathophysiology of Parkinson's disease, opening insightful perspectives for the development of innovative therapeutic approaches or disease biomarkers.

In their minireview, Zhao et al. described the relevance of the vesicular glutamate transporters to Parkinson's disease pathophysiology.

Mays et al. found that plasmin inhibits the formation of pathological misfolded prion protein scrapie by mediating prion protein α-cleavage that, in turn, reduces prion conversion.

Lu et al. identified a *de novo* nonsense mutation of FOXG1 in a Chinese patient affected by neurodevelopmental disorders/intellectual disorders (NDDs/IDs) and clarified the diagnostic criteria defining the FOXG1-related clinical phenotypes.

By assessing the efficacy of dodecyl creatine ester in the Slc6a8 knockout mouse model through shotgun proteomics on brain proteins, Mabondzo et al. found that phospholipase C beta 1, kinesin family member 1A, and associated molecules are crucially involved in the pathogenesis of creatine transporter deficiency, a leading cause of intellectual disability.

Shao et al. showed that the severely impaired cognitive subtype in the early course of schizophrenia is characterized by differences in the brain's spontaneous neural activity of the prefrontal cortex and bilateral posterior cingulate cortex/precuneus.

Peng et al. described a case report of a patient diagnosed with Wiedemann–Rautenstrauch syndrome (WDRTS) complicated with the occurrence of another recessive disorder, Fanconi anemia (FA).

Zhang Z. et al. characterized plasma metabolic profiles associated with brain atrophy in individuals with alcohol dependence, reporting that glycerophospholipid metabolism may have a prominent role in the pathogenesis of alcohol-induced brain atrophy.

Nie et al. reviewed the role and the current studies of pyroptosis, ferroptosis, parthanatos, and cyclophilin D-mediated necrosis in traumatic brain injury secondary damage, discussing whether these signaling pathways may provide new insights into the treatment of craniocerebral injury.

In their review, Tian et al. discussed the regulatory mechanisms of cyclin-dependent kinase 5 (Cdk5) in a series of common neurological disorders such as neurodegenerative diseases, stroke, anxiety/depression, pathological pain, and epilepsy, emphasizing the crucial role of Cdk5 aberrant activation as a driving force for the initiation and progression of brain injury.

In their review, Fan Y. et al. summarized the most recent developments on the role of miRNAs in the regulation of reactive astrocytes in CNS diseases, elegantly discussing the clinical application of miRNA-based therapies for the modulation of reactive astrocytosis.

Finally, Zhang Y. et al. investigated the cellular and molecular mechanisms related to primary familial brain calcification by using Slc20a2 homozygous knockout mice, showing that impairment in the paracellular and transcellular pathways of the brain endothelial cells produces BBB leakage and brain T-cell invasion that, in turn, underlie the onset of brain calcification.

Author contributions

FB: Writing – original draft, Writing – review & editing. GA: Writing – original draft, Writing – review & editing. SB: Writing – original draft, Writing – review & editing. MS: Writing – original draft, Writing – review & editing. AB: Writing – original draft, Writing – review & editing.

Funding

The author(s) declare that no financial support was received for the research, authorship, and/or publication of this article.

Conflict of interest

The authors declare that the research was conducted in the absence of any commercial or financial relationships that could be construed as a potential conflict of interest.

The author(s) declared that they were an editorial board member of Frontiers, at the time of submission. This had no impact on the peer review process and the final decision.

Publisher's note

References

Arias, D., Saxena, S., and Verguet, S. (2022). Quantifying the global burden of mental disorders and their economic value. *EClinicalMedicine*. 54, 101675. doi: 10.1016/j.eclinm.2022.101675

Feigin, V. L., Vos, T., Nichols, E., Owolabi, M. O., Carroll, W. M., Dichgans, M., et al. (2020). The global burden of neurological disorders: translating evidence into policy. *Lancet Neurol.* 19, 255–265. doi: 10.1016/S1474-4422(19)30411-9

Heneka, M. T., Golenbock, D., Latz, E., Morgan, D., and Brown, R. (2020). Immediate and long-term consequences of COVID-19 infections for the development of neurological disease. *Alzheimers Res. Ther.* 12, 69. doi: 10.1186/s13195-020-00640-3

Penninx, B. W. J. H., Benros, M. E., Klein, R. S., and Vinkers, C. H. (2022). How COVID-19 shaped mental health: from infection to pandemic effects. *Nat. Med.* 28, 2027–2037. doi: 10.1038/s41591-022-02028-2

frontiers | Frontiers in Molecular Neuroscience

TYPE Original Research
PUBLISHED 02 September 2022
DOI 10.3389/fnmol.2022.990136

OPEN ACCESS

EDITED BY
Arianna Bellucci,
University of Brescia, Italy

REVIEWED BY
Giuseppe Legname,
International School for Advanced Studies (SISSA), Italy
Wenquan Zou,
Case Western Reserve University, United States

*CORRESPONDENCE
Chongsuk Ryou
cryou2@hanyang.ac.kr
Hae-Eun Kang
kanghe@korea.kr

SPECIALTY SECTION
This article was submitted to Brain Disease Mechanisms, a section of the journal Frontiers in Molecular Neuroscience

RECEIVED 09 July 2022
ACCEPTED 15 August 2022
PUBLISHED 02 September 2022

CITATION
Mays CE, Trinh THT, Telling G, Kang H-E and Ryou C (2022) Endoproteolysis of cellular prion protein by plasmin hinders propagation of prions. *Front. Mol. Neurosci.* 15:990136. doi: 10.3389/fnmol.2022.990136

Endoproteolysis of cellular prion protein by plasmin hinders propagation of prions

Charles E. Mays[1], Trang H. T. Trinh[2,3], Glenn Telling[1,4,5], Hae-Eun Kang[4,5,6]* and Chongsuk Ryou[1,2,3,4]*

[1]Department of Microbiology, Immunology, and Molecular Genetics, University of Kentucky College of Medicine, Lexington, KY, United States, [2]Department of Pharmacy, College of Pharmacy, Hanyang University, Ansan, South Korea, [3]Institute of Pharmaceutical Science and Technology, Hanyang University, Ansan, South Korea, [4]Sanders-Brown Center on Aging, University of Kentucky College of Medicine, Lexington, KY, United States, [5]Department of Microbiology, Immunology, and Pathology, Colorado State University, Fort Collins, CO, United States, [6]Reference Laboratory for Chronic Wasting Disease (CWD), Foreign Animal Disease Division, Animal and Plant Quarantine Agency, Gimcheon, South Korea

Many questions surround the underlying mechanism for the differential metabolic processing observed for the prion protein (PrP) in healthy and prion-infected mammals. Foremost, the physiological α-cleavage of PrP interrupts a region critical for both toxicity and conversion of cellular PrP (PrP^{C}) into its misfolded pathogenic isoform (PrP^{Sc}) by generating a glycosylphosphatidylinositol (GPI)-anchored C1 fragment. During prion diseases, alternative β-cleavage of PrP becomes prominent, producing a GPI-anchored C2 fragment with this particular region intact. It remains unexplored whether physical up-regulation of α-cleavage can inhibit disease progression. Furthermore, several pieces of evidence indicate that a disintegrin and metalloproteinase (ADAM) 10 and ADAM17 play a much smaller role in the α-cleavage of PrP^{C} than originally believed, thus presenting the need to identify the primary protease(s) responsible. For this purpose, we characterized the ability of plasmin to perform PrP α-cleavage. Then, we conducted functional assays using protein misfolding cyclic amplification (PMCA) and prion-infected cell lines to clarify the role of plasmin-mediated α-cleavage during prion propagation. Here, we demonstrated an inhibitory role of plasmin for PrP^{Sc} formation through PrP α-cleavage that increased C1 fragments resulting in reduced prion conversion compared with non-treated PMCA and cell cultures. The reduction of prion infectious titer in the bioassay of plasmin-treated PMCA material also supported the inhibitory role of plasmin on PrP^{Sc} replication. Our results suggest that plasmin-mediated endoproteolytic cleavage of PrP may be an important event to prevent prion propagation.

KEYWORDS

plasmin, prion, endoproteolysis, α-cleavage, PrP^{Sc} propagation

Introduction

Prion diseases are a category of ultimately fatal neurodegenerative disorders that include Creutzfeldt–Jakob disease (CJD) in humans, bovine spongiform encephalopathy (BSE) in cattle, scrapie in sheep, and chronic wasting disease (CWD) in deer. The infectious agent responsible, termed a prion, is a completely proteinaceous particle that lacks a nucleic acid component (Prusiner, 1998). Prion propagation is characterized by a major conformational alteration for the host-encoded cellular prion protein (PrP^{C}) to a misfolded isoform called scrapie prion protein (PrP^{Sc}), where transition of α-helices of PrP^{C} to β-sheets occurs (Pan et al., 1993). A hallmark of PrP^{Sc} is its relative resistance to protease digestion *in vitro*. Proteinase K (PK) treatment of PrP^{Sc} results in the partially resistant molecule, referred to as PrP27-30, consisting predominantly of amino acid residues 90-231 (Chen et al., 1995). In contrast to PrP^{Sc}, PrP^{C} is sensitive to proteolytic digestion by PK.

In addition to these biochemical differences, PrP^{C} and PrP^{Sc} are subject to diverse intracellular proteolytic processing events. The α-cleavage site that produces the C1 fragment (C1) was mapped to a variable site N-terminal to the hydrophobic domain within Lys110, His111, or Met112 [human (h) PrP^{C} sequence nomenclature], while the generation of the C2 fragment (C2) by β-cleavage was estimated to occur C-terminal to the octapeptide repeat region in the vicinity of residue 90 (Chen et al., 1995; Mangé et al., 2004; Oliveira-Martins et al., 2010). A central event in PrP conformational conversion is likely metabolic processing because the dominant C-terminal PrP endoproteolytic product switches from the normal C1 to the alternative C2 as prion disease progresses (Harris et al., 1993; Chen et al., 1995; Hachiya et al., 2007). The C2 is likely to correspond to the PrP27-30 generated by PK digestion. Therefore, disruption of the neurotoxic and amyloidogenic PrP(106-126) domain by α-cleavage may prevent the accumulation of the C2 and inhibit PrP^{Sc} propagation (Chen et al., 1995; Jimenez-Huete et al., 1998). Besides these well-described internal cleavage events, γ-cleavage of PrP^{C} results in a soluble N-terminal fragment (N3) of 20 kDa and a small GPI-anchored C3 fragment (C3) of 5 kDa, cleaved in a region between amino acid residues 170 and 200, near N-terminal of the first N-glycosylation site (Haigh and Collins, 2016). It appears to be associated with pathophysiological conditions, as increased C3 fragments are found in CJD brain samples (Kojima et al., 2014; Lewis et al., 2016).

However, the exact mechanism for PrP processing remains unclear. To date, a handful of proteases have been reported as having the ability to cleave at the α-site: ADAM8 (Liang et al., 2012), ADAM10 (Vincent et al., 2001; Cisse et al., 2005), ADAM17 (Vincent et al., 2001; Laffont-Proust et al., 2005), calpain (Hachiya et al., 2011), and plasmin (Kornblatt et al., 2003; Praus et al., 2003; Xanthopoulos et al., 2005). Unfortunately, ADAM family proteases showed higher complexity with different cleavages dependent on divalent ions (McDonald et al., 2014); ADAM8 appears to be specifically active in extraneural tissues such as muscle (Liang et al., 2012); ADAM10 plays a larger role in shedding, presumably generating N3 (Endres et al., 2009; Taylor et al., 2009; Altmeppen et al., 2011); ADAM17 contributes less frequently than ADAM10 through a pathway regulated by protein kinase C (Vincent et al., 2000; Cisse et al., 2005). The α-cleavage of PrP by calpain is dubious because of its shared ability to perform β-cleavage (Yadavalli et al., 2004).

Plasminogen is an enzymatically inactive, kringle domain-containing zymogen expressed in the liver and to a lesser extent in the brain (Basham and Seeds, 2001; Zhang et al., 2002; Kwon and Waisman, 2003; Ledesma et al., 2003; Kim et al., 2009). Plasminogen gives rise to several biologically active fragments upon proteolytic cleavage including the serine protease plasmin (Castellino and Ploplis, 2003) that is capable of processing recombinant (r) PrP and purified PrP^{C} *in vitro* at the α-cleavage site (Kornblatt et al., 2003; Praus et al., 2003). However, the details to confirm plasmin-mediated α-cleavage of PrP remain to be further investigated because the level of C1 under plasmin-deficient condition in plasminogen null mice was found to be comparable to the C1 level in wild type mice (Barnewitz et al., 2006). Separately, a line of studies suggested that PrP^{C} plays a role to stimulate activation to plasmin from plasminogen (Ellis et al., 2002; Praus et al., 2003; Epple et al., 2004a,b; Borumand and Ellis, 2022).

Numerous studies, including a report from one of us (Ryou et al., 2003), have described plasminogen as a PrP ligand and its interaction with PrP is mediated through the lysine-binding motifs of the plasminogen kringle domains (Fischer et al., 2000; Maissen et al., 2001; Ellis et al., 2002; Shaked et al., 2002; Kornblatt et al., 2003, 2004; Praus et al., 2003; Epple et al., 2004a,b; Cuccioloni et al., 2005; Hatcher et al., 2009; Bougard et al., 2016). Previously, we expanded on this discovery by demonstrating the ability of plasminogen to stimulate PrP^{Sc} formation in cultured cells chronically infected with prions as well as in a cell-free system called protein misfolding cyclic amplification (PMCA) (Mays and Ryou, 2010). Furthermore, disruption of the PrP-plasminogen interaction with L-lysine and its polymers successfully inhibited PrP^{Sc} formation in PMCA, cell culture, and mouse models of prion disease (Ryou et al., 2011). Collectively, these studies validated plasminogen as a cellular protein auxiliary factor proven to stimulate PrP^{Sc} propagation (Mays and Ryou, 2011). However, the use of plasminogen-deficient mouse models has generated incongruent data on the role of plasminogen during disease progression. Prion challenge to plasminogen null mice results in no major change of mean incubation period of disease (Salmona et al., 2005; Xanthopoulos et al., 2005), concluding that plasminogen is not functional to control prion propagation *in vivo*. Nevertheless, one must understand that the ablation of

plasminogen gene drives the deficiency of both plasminogen and plasmin and reason whether ablation of two factors (plasminogen and plasmin) with potentially opposing roles would offset each other.

We offer a "yin-yang" hypothesis for the plasmin(ogen) system, where plasminogen accelerating PrP^{Sc} replication is counteracted by enzymatically active plasmin, cleaving PrP^{C} at the α-site to generate the C1 fragment. Thus, we assessed the ability of plasmin to generate the endoproteolytic products for PrP and whether active up-regulation of α-cleavage by plasmin can inhibit PrP^{Sc} propagation. Plasmin-mediated endoproteolysis of PrP was investigated using recombinant prion protein (rPrP), PrP^{C} of prion-infected and –uninfected cultured cells, and PMCA products. To specifically address plasmin-mediated inhibition of prion propagation, we investigated PrP^{Sc} formation in biological conditions by monitoring the accumulation of PrP^{Sc} in prion-infected cell lines cultured with supplemented plasmin. Furthermore, we determined whether inhibition of prion propagation by plasmin can be recapitulated using the controlled conditions of PMCA, which avoids problems associated with plasminogen knockout animal models. Finally, we determined whether plasmin-facilitated inhibition of prion propagation affects prion infectivity using bioassay.

Materials and methods

In vitro plasmin cleavage for recombinant prion protein

His-tagged recombinant human (rh) PrP(23-231) was expressed and purified as previously described (Kim et al., 2014). Briefly, *E. coli* BL21(DE3)/RIL + cells (Invitrogen, Carlsbad, CA, United States) were transformed with the recombinant expression plasmid in which the encoding DNA fragment for hPrP(23-231) was cloned in pET100/D-TOPO (Invitrogen). The protein expression was induced at an $OD_{600} \sim 0.6$, and grown at 37°C for 2 h. rhPrP(23-231) was purified from the lysates of harvested cells via a nickel chelate affinity resin. Three μg recombinant protein was digested with 0.05, 0.1, 0.2, or 0.5 μM human plasmin (hPln, HCPM-0140, Haematologic Technologies, Inc, Essex Junction, VT, United States) for 4 h at 37°C in a volume brought to 30 μl with Dulbecco's Modified Eagle's Medium (DMEM, Invitrogen) with 10% fetal bovine serum (FBS, Invitrogen). Western blot analysis or silver staining was used to analyze 1 μg aliquot samples that were loaded and run in 12–14% Tris-glycine SDS-PAGE gels. rhPrP(23-231) (0.05 μg), not mixed with FBS and hPln, was also examined. Gels for silver staining were processed as directed by the ProteoSilver™ Silver Stain Kit (Sigma-Aldrich, St. Louis, MO, United States), while gels for western blot analysis were subsequently transferred to a PVDF membrane (Immobilon-FL, Millipore, Billerica, MA, United States) as described in detail below.

Cell culture

The Neuro2a neuroblastoma (N2a) cells (ATCC CCL-131) and scrapie-infected N2a (ScN2a) cells (Butler et al., 1988) were grown in DMEM-high glucose containing 10% inactivated FBS, 1% glutamax, and 1% streptomycin/penicillin (Invitrogen) in the presence of 5% CO_2 and humidity at 37°C.

Plasmin cleavage for cellular prion protein of cultured cells

For the study of PrP^{C} cleavage in response to plasmin, cells were passed into 6-well culture plates (Corning, Lowell, MA. United States) and maintained in serum-free DMEM with 1X N-2 supplement (Invitrogen) for 18 h in the presence of 0 or 0.1 μM hPln. Cell lysate prepared with lysis buffer (20 mM Tris, pH 8.0, 150 mM NaCl, 0.5% Non-idet-P 40 and 0.5% sodium deoxycholate) was used for digestion with or without 20 μg/ml PK for 1 h at 37°C. To investigate the fragmentation of PrP^{C} under the deglycosylated condition, PK-digested or –undigested cell lysate was further incubated with Peptide:N-Glycosidases F (PNGase F, NEB, Ipswich, MA, United States) according to manufacturer's instruction. Briefly, the samples were first incubated in denaturing buffer (0.5% SDS, 40 mM DL-dithiothreitol) for 10 min at 100°C and further incubated with ∼1000 U of PNGase F in 50 mM sodium phosphate buffer (pH 7.5) supplemented with 1% Non-idet-P 40 for 3.5 h at 37°C. The samples were analyzed by SDS-PAGE followed by Western blotting using anti-PrP antibodies.

Scrapie prion protein assay in cultured cells incubated with plasmin

For the study of PrP^{Sc} propagation in response to plasmin, cells were passed into 6-well culture plates (Corning) at an estimated 5% confluence and supplemented with the specified concentration (0 – 0.5 μM) of each treatment for 6 d. After 3 d, media was replaced with fresh media and reagents. On day 6, lysates were prepared from cell cultures with lysis buffer (20 mM Tris, pH 8.0, 150 mM NaCl, 0.5% Non-idet-P 40 and 0.5% sodium deoxycholate). *De novo* formation of PrP^{Sc} in ScN2a cells was monitored by transiently transfecting with plasmids harboring the 3F4 epitope-tagged PrP (PrP-3F4) (Scott et al., 1992). ScN2a cells maintained in Minimal Essential Media (MEM, Invitrogen) containing 10% inactivated FBS, 1% penicillin-streptomycin, and 1% glutamax were cultured in a 12-well plate (Corning) at approximately 70% confluence. Cells

were transfected with 5 μg of plasmid DNA expressing PrP-3F4 or an empty plasmid vector using transfection reagent DOTAP (Roche, Basel, Switzerland). Then, at 1 d post-transfection, they were washed twice with PBS and cultured in MEM with 2% FBS for 3 d in the presence of 0 – 0.3 μM hPln. Cell lysate was prepared as described above. Analysis of PK-digested and –undigested samples was performed by the same protocol described above.

Protein misfolding cyclic amplification

All brain materials for PMCA were obtained from 5- to 9-week-old CD-1 mice (Harlan Laboratories, Indianapolis, IN, United States) the following perfusion with phosphate-buffered saline (PBS) containing 5 mM EDTA. PrP^{C} substrate was made by homogenizing healthy brain material 10% (w/v) in PMCA buffer [PBS, pH 7.2; 150 mM NaCl; 1% Triton X-100; 4 mM EDTA; and Complete Mini (Roche) protease inhibitors]. PrP^{Sc} seeds were generated by homogenizing RML prion-infected brain material 10% (w/v) in PBS. To remove debris, the homogenate was centrifuged at 2000 × *g* for 5 min at 4°C. The supernatant was saved at −80°C for PMCA, while the pellet was discarded.

Our method for automated PMCA was conducted as previously described (Mays and Ryou, 2010). Briefly, PrP^{Sc} seeds were diluted 500- to 16000-fold in PrP^{C} substrate in a 96-well PCR plate (TempPlate III, United States Scientific, Ocala, FL, United States). Purified hPln (0–1.0 μM) or mouse plasmin (0.5 μM, mPln, MCPM-5140, Haematologic Technologies, Inc) was added in the mixture. If necessary, aprotinin (0 – 8.0 μM, A1153, Sigma-Aldrich), phenylmethylsulfonyl fluoride (PMSF, 1 mM, P7626, Sigma-Aldrich), Pefabloc SC (1 mM, Roche), or E-64 (1 mM, E3132, Sigma-Aldrich) was added as described in the text. Pre-PMCA aliquots were taken from each sample to be saved at −20°C, while the remaining mixture underwent the amplification procedure. The plates were immersed in water maintained at 37°C on the microplate horn of a microsonicator (Misonix Model 3000, Farmingdale, New York, United States) programmed for 48 h with a 40 s pulse of sonication every 30 min at a potency of 7.

Pre- and post-PMCA samples were PK-digested with 20 μg/ml PK for 1 h at 37°C and analyzed by western blotting using anti-PrP antibodies. PK-undigested, plain post-PMCA samples were further analyzed before and after PNGase F digestion, which was performed as described above.

Prion bioassay

The assay was performed as described elsewhere (Ryou et al., 2011). Age-matched groups of 5 to 6-week-old female CD-1 mice (Harlan Laboratories, Indianapolis, IN, United States)

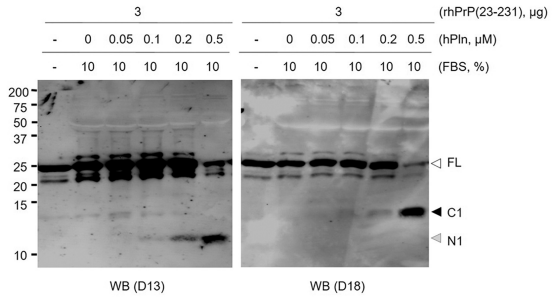

FIGURE 1
Plasmin cleaves rPrP *in vitro*. rhPrP(23-231) was treated with increasing concentrations of hPln in DMEM with 10% FBS. Western blot analysis was utilized to visualize plasmin-generated C-terminal (D18) and N-terminal (D13) fragments for rPrP. white arrow; full-length (FL) rPrP; black arrow, C1 fragment; gray arrow, N1 fragment.

were intracerebrally inoculated with PMCA material diluted 1:10 in PBS. During this procedure, isoflurane was utilized to anesthetize animals to minimize pain or discomfort. While the animal was unconscious, intracerebral inoculation was performed by injection at a depth of 2-3 mm with 30 μl of inoculum using a 26-gauge needle inserted in the middle of the left parietal lobe beside the midline. Incubation time was measured by determining the point at which multiple characteristic disease signs (including slowed movement, hunched posture, increased tone of the tail, loss of balance, and roughened coat) had progressed to the terminal stage, and the brains of the prion-infected mice were collected at this time. This protocol was approved by the Institutional Animal Care and Use Committee, University of Kentucky. Ten% (w/v) homogenate prepared from the collected brains was digested in PBS including 2% Sarkosyl with 20 μg/ml PK at 37°C for 1 h and analyzed by western blotting.

Western blotting

Immunoblotting for recombinant protein, cell lysates, PMCA samples, brain material, and their PK- or PNGase F-digested samples was performed by separation on a 12–14% Tris-glycine SDS-PAGE gel followed by western blotting as previously described (Mays and Ryou, 2010). Following gel electrophoresis and electrotransfer of proteins in the gel to PVDF membrane, blocking for 1 h with 5% skim milk was carried out. The membranes were immediately incubated with anti-β-actin antibody (ACTN05; Neomarker, Fremont, CA, United States), anti-PrP antibodies 3F4 (Signet Laboratory, Boston, MA, United States), D13, or D18 (gifted by Dr. Stanley Prusiner, University of California, San Francisco, CA, United States). ECL Plus kit (GE Healthcare, Amersham Biosciences, Piscataway, NJ, United States) was used for

chemiluminescence detection. The blots were visualized by developing on film or scanning with the Fuji Film FLA 5000 image reader (Fuji Film, Edison, NJ, United States).

Histopathologic analysis

Histology and immunohistochemistry were performed according to the methods described elsewhere (Nazor et al., 2007). Briefly, brains were dissected rapidly after sacrifice of the animal and immersion fixed in 10% buffered formalin. Tissues were embedded in paraffin and 10 μm-thick coronal microtome sections were mounted onto positively charged glass slides and stained with hematoxylin and eosin for evaluation of spongiform degeneration. Following inactivation of endogenous peroxidases by incubation in 3% H_2O_2 in methanol, peroxidase immunohistochemistry was used to evaluate the extent of reactive astrocytic gliosis using to anti-glial fibrillary acidic protein (GFAP) antibodies (Abcam, Cambridge, United Kingdom). Detection was with Vectastain ABC reagents (Vector Laboratories, Newark, CA, United States) and slides were developed with diaminobenzidine.

Statistical analysis

The Kaplan-Meier survival curve was calculated by SigmaPlot 11.0. Statistical analysis of difference in incubation time between experimental groups was performed using the log-rank test. $P < 0.05$ was considered statistically significant.

Results

Plasmin internally cleaves recombinant prion protein

Several studies reported that plasmin is able to cleave the PrP at lysine residue 110 generating an N-terminally truncated molecule that has previously been described as a major product of PrP^C metabolism (Praus et al., 2003). To address the specific proteolytic activity of plasmin, we conducted *in vitro* plasmin cleavage of rPrP in the serum conditioned buffer. rhPrP(23-231) was subjected to increasing hPln concentrations ranging from 0 to 0.5 μM. In agreement with other studies (Kornblatt et al., 2003; Praus et al., 2003; Xanthopoulos et al., 2005), antibody mapping of plasmin-digested full-length rhPrP(23-231) suggested the α-cleavage generation of an 11 kDa N-terminal fragment [N1, likely PrP amino acid residues (aa) 23-110] and a larger 13 kDa C-terminal fragment (C1, likely PrP aa 111-231). D13 antibody recognizing PrP aa 94-105 and D18 antibody recognizing PrP aa 133-157 were used to probe N1 and C1, respectively. Plasmin-mediated α-cleavage showed a dose-dependent response (**Figure 1** and **Supplementary Figure 1**).

Plasmin generates C1 fragments in cultured cells

To demonstrate the specific proteolytic activity of plasmin fragmenting PrP^C in live cells, N2a and ScN2a cells were incubated with 0.1 μM of hPln. As shown in plasmin *in vitro* cleavage assays using rPrP, C1 formation was enhanced in the presence of hPln in both cells (**Figure 2** and **Supplementary Figure 2**). N2a cells, a neuronal cell line with no prion infection, expressed variably glycosylated, GPI-anchored PrP^C of full length and C1. hPln cleaved PrP^C, generating variably glycosylated C1, which was recognized by D18 antibody (**Figure 2A**). Both PrP^C of full length and C1 were sensitive to PK digestion. Increased formation of C1 by hPln was more obvious when glycans were removed from variably glycosylated PrP^C. ScN2a cells persistently infected with prions produced PrP^C and PrP^{Sc} of full length and two endoproteolytic fragments C1 and C2. In ScN2a cells, hPln facilitated formation of endoproteolytic fragments of PrP^C, which was detected by D18 antibody similarly to the events occurred in N2a cells. However, this did not cause a significant decrease of the level of PK-resistant PrP^{Sc} (PrP27-30), which was recognized by both D13 and D18 antibodies (**Figure 2B**). When deglycosylated, increased formation of C1 by hPln was clearly demonstrated in ScN2a cells, too. When deglycosylated PrP and its fragments were hydrolyzed with PK, C2, equivalent to disease-specific PrP27-30, was recognized by both D13 and D18, and its level was unaltered by hPln. These results showed that plasmin involves in generation of C1, but not C2.

Plasmin negates scrapie prion protein formation in scrapie-infected N2a cells

To determine whether plasmin-induced C1 generation inhibits PrP^{Sc} formation under biological conditions, persistently prion-infected ScN2a cells were incubated with titrated concentrations of hPln for 6 d. PrP27-30 accumulation was significantly reduced by incubation with 0.5 μM hPln, although it appeared to be gradually increased by incubation with 0.05 – 0.2 μM hPln (**Figure 3A** and **Supplementary Figure 3A**). Incubation of ScN2a cells with hPln did not induce cell death within the concentrations employed in this experiment (data not shown). Total PrP and β-actin expression were stable, too, in all samples. To further understand how plasmin hinders PrP^{Sc} accumulation, a similar experiment was conducted with cells transiently transfected to express 3F4-tagged PrP^C [47] so that the function of plasmin on nascent PrP^{Sc} formation could be determined. Following a period of 3 d,

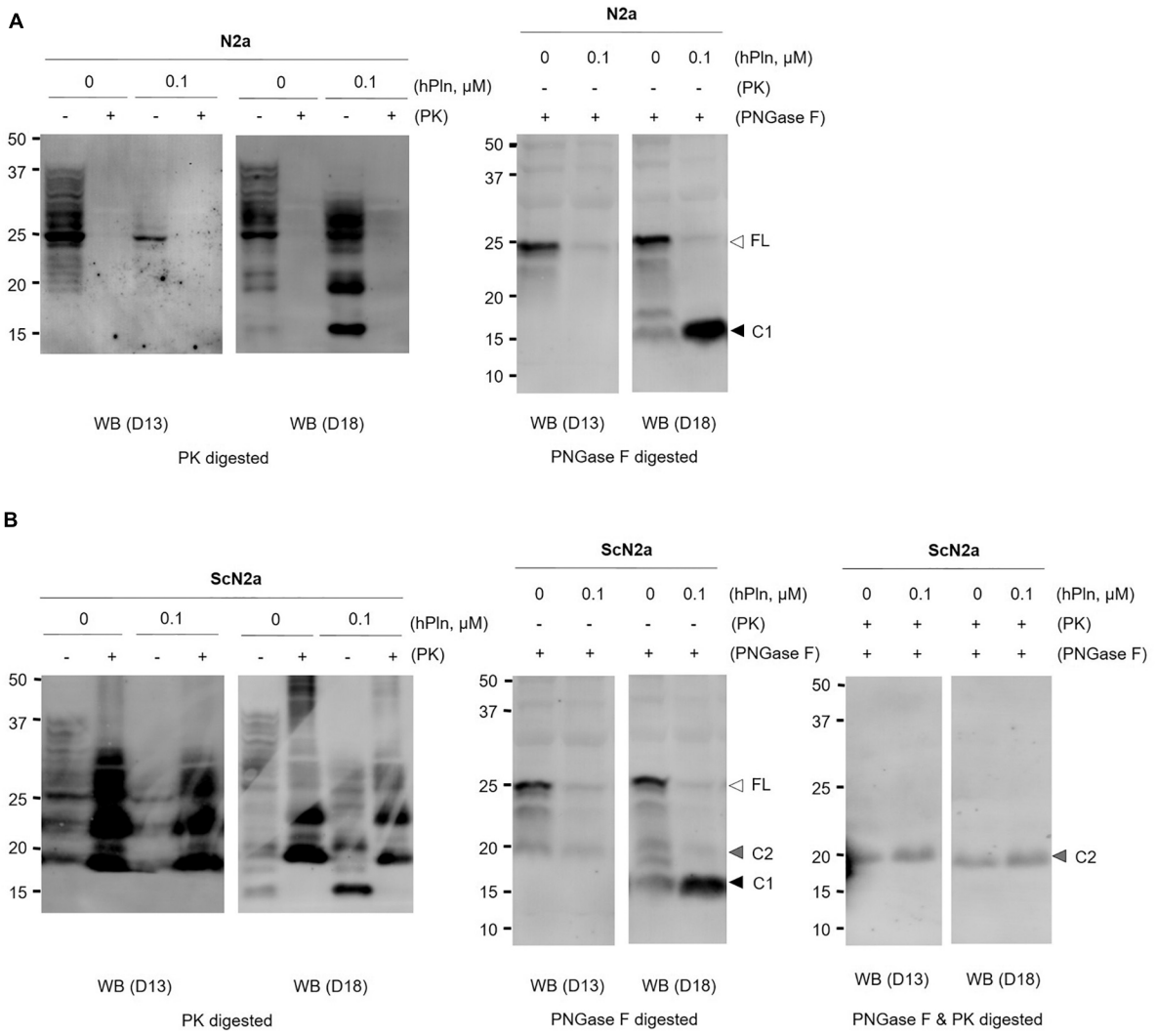

FIGURE 2
Plasmin cleaves PrP^C in cultured cells. **(A)** N2a cells were grown with supplemented hPln and analyzed the level of C1. The increased signals in the D18 blot were sensitive to PK digestion. PNGase F treatment revealed the unglycosylated C1 fragment probed with D18. **(B)** Persistently scrapie-infected ScN2a cells were grown with supplemented hPln and analyzed the level of C1. The level of C1 was increased by hPln. The level of C2 was not affected by hPln. white arrow, full-length (FL) PrP^C; black arrow, C1 fragment; gray arrow, C2 fragment.

incubation with hPln demonstrated a dose-dependent decrease in newly generated 3F4-tagged PrP^{Sc} and PrP^C (Figure 3B and Supplementary Figure 3B).

Scrapie prion protein generation in protein misfolding cyclic amplification is inhibited specifically by plasmin

An *in vitro* prion amplification technique was used to recapitulate the effects of plasmin in hPln-supplemented cell culture. PMCA was performed by diluting prion-infected brain homogenate 500-fold in that of a healthy animal. This dilution was chosen to evaluate plasmin because it consistently allowed robust PrP^{Sc} production in PMCA, while a minute amount of PrP^{Sc} could still be detected in the pre-amplification sample from the original seed. Under these conditions, the addition of 0.5 μM purified hPln and mPln successfully inhibited PrP^{Sc} generation with no obvious preference for the sources (Figure 4A and Supplementary Figure 4A). However, PrP^{Sc} propagation was not completely abolished and never reduced below levels of the original PrP^{Sc} seed, as shown by a comparison of pre- and post-PMCA samples that were supplemented with plasmin. When similar PMCA was performed with titrated concentrations of hPln ranging from 0 to 1 μM, the amount of PrP^{Sc} amplified was decreased in a dose-responsive manner (Figure 4B and Supplementary Figure 4B).

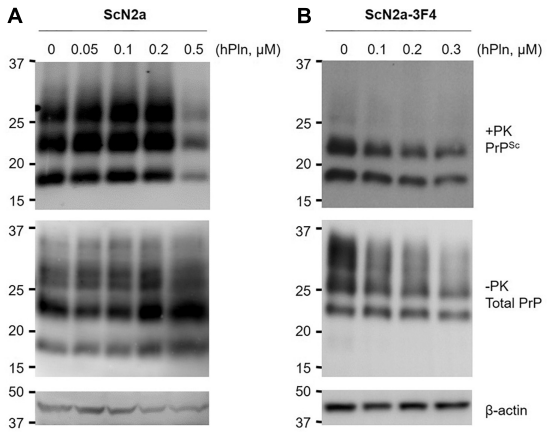

FIGURE 3
Plasmin reduces PrP^{Sc} formation in cultured cells. ScN2a cells were grown in the presence of increasing concentrations of hPln. **(A)** The levels of total endogenous PrP (−PK) and PrP^{Sc} (+ PK) accumulation in ScN2a cells cultured under the 10% FBS condition were evaluated by western blotting using anti-PrP antibody D13. **(B)** *De novo* formation of PrP^{Sc} during hPln treatment was determined in ScN2a cells transiently transfected for PrP^{C}-3F4 expression (ScN2a-3F4), which were cultured under the 2% FBS condition. PrP-3F4 (-PK) and PrP^{Sc}-3F4 (+ PK) were specifically detected in western blots probed with anti-PrP antibody 3F4. β-actin was used as a reference protein to ensure equal amounts of each cell lysate were analyzed.

The PrP^{Sc} product of hPln-supplemented PMCA performed in the presence of protease inhibitors, such as aprotinin, a specific serine protease inhibitor; PMSF, a broad-spectrum serine and cysteine protease inhibitor; Pefabloc Sc, a broad-spectrum serine protease inhibitor; and E-64, a selective cysteine protease inhibitor, was compared to determine whether the inhibitive effect was a function of plasmin. These protease inhibitors exhibit different specificity for plasmin. The inhibition constant (Ki) of aprotinin for plasmin is 4 nM (Fritz and Wunderer, 1983), which demonstrates aprotinin is most potent and specific among other inhibitors listed above. In fact, aprotinin was able to restore amplification of PrP^{Sc} in hPln-supplemented PMCA, but not others (**Figure 4C** and **Supplementary Figure 4C**). In the control PMCA performed in the presence of each protease inhibitor but without hPln supplementation, aprotinin and E-64 did not affect PrP^{Sc} generation by themselves, while Pefabloc SC failed PMCA (**Figure 4D** and **Supplementary Figure 4D**). Interestingly, PMSF appeared not to affect PMCA but to interfered with PK digestion of pre- and post-PMCA samples. Thus, plasmin-mediated inhibition of PrP^{Sc} generation in hPln-supplemented PMCA was facilitated specifically by plasmin activity, which was suppressed by aprotinin. When hPln-supplemented PMCA was performed with titrated concentrations of aprotinin ranging from 0 to 8 μM, the amount of PrP^{Sc} amplified was recovered in an aprotinin concentration-dependent fashion (**Figure 4E** and **Supplementary Figure 4E**).

Inhibition of scrapie prion protein generation in protein misfolding cyclic amplification is attributed to plasmin-mediated endoproteolysis of cellular prion protein generating C1 fragments

To eliminate detectable levels of PrP^{Sc} from the seed, PMCA supplemented with titrated concentrations of hPln was repeated under conditions in which prion-infected brain homogenate was diluted 2500-fold in brain material from a healthy animal. Addition of 0.05 and 1 μM hPln caused a concentration-dependent decrease in the level of PrP^{Sc} produced, where 0.5 and 1 μM hPln effectively prevented the appearance of newly formed PrP^{Sc} (**Figure 5A** and **Supplementary Figure 5A**). To investigate plasmin-mediated internal cleavage of PrP, the hPln-supplemented PMCA samples without PK digestion were subjected to western blot analysis probed with D13 or D18. In the D13 blot, detection of PrP gradually diminished as the hPln concentration increased, presumably due to disappearance of D13 epitope by plasmin-mediated cleavage of full length PrP^{C} and C2, which was not shown almost invisible in the blot because of its relatively low abundance. On the other hand, in the D18 blot, a band shift is observed as the hPln concentration increases, because hPln cleaved the full-length PrP^{C}, resulting in an increase of C1 (**Figure 5B** and **Supplementary Figure 5B**). The results of the PNGase F treatment further confirmed that plasmin-mediated cleavage in PMCA altered C1 and C2 generation. PNGase F deglycosylation of the hPln-supplemented PMCA samples without PK digestion showed that hPln induced the production of C1 fragments (**Figure 5C**; compare lanes 7 and 8) and simultaneously reduced C2 production (**Figure 5C** and **Supplementary Figure 5C**; compare lanes 3 and 7 to 4 and 8, respectively).

Supplemented plasmin reduces prion infectivity of protein misfolding cyclic amplification product

In addition to its effect to PrP^{Sc} generation, the role of plasmin in controlling prion infectivity was assessed. Three groups of eight wild type mice received intracranial inoculation of the hPln-supplemented PMCA product, the non-supplemented PMCA product, or the PrP^{Sc} seed used in PMCA reactions. All PMCA materials were generated by diluting prion-infected brain homogenate 16,000-fold in healthy brain material (**Supplementary Figure 6**). Infectivity of this material was

estimated by comparing the mean incubation period from each group. According to statistical analysis, injection of material obtained from PMCA conducted in the presence of hPln resulted in an incubation time of 193 ± 4 d (mean incubation time ± standard error). This incubation period was significantly longer than that of the non-supplemented PMCA product (177 ± 2 d; $P < 0.001$), but statistically equivalent to that of the PrP^{Sc} seed (198 ± 8 d; $P > 0.05$) (**Table 1**).

Western blot analysis of PK-resistant PrP^{Sc} in the mouse brains of all three groups showed that PrP^{Sc} accumulated in the end-stage animals ill with prion disease (**Supplementary Figure 7**). The neuropathology of the mouse brains of each group also supported that the prion-ill mice were due to prion disease with vacuolation and gliosis in their brains which are typical signs of prion disease (**Supplementary Figures 8**, **9**).

Discussion

Rationale

All members of the PrP superfamily (PrP, Shadoo, and Doppel) have been shown to occupy similar membrane environments and undergo congruent endoproteolytic events (Mays et al., 2014a). Transition in metabolic processing for PrP was originally described for CJD patients nearly three decades ago and has since been documented as being altered in other models of prion disease (Chen et al., 1995; Jimenez-Huete et al., 1998; Yadavalli et al., 2004; Ayers et al., 2011). In the healthy state, a proportion of mature PrP^{C} undergoes endoproteolysis at an α-cleavage site that presumably occurs N-terminal to the hydrophobic domain generating a GPI-anchored C-terminal fragment (C1) and subsequently releasing an N-terminal fragment (N1). However, during prion disease, PrP more favorably undergoes alternative β-cleavage C-terminal to the octarepeat that yields a larger C-terminal fragment (C2) and its corresponding N-terminal fragment (Chen et al., 1995; Jimenez-Huete et al., 1998). Interestingly, C2 is equivalent in size to PrP27-30, which is the protease-resistant core of PrP^{Sc}. Although the exact cleavage site has not yet been elucidated, γ-cleavage appears to be associated with pathophysiological conditions, as increased C3 is found in CJD brain samples (Lewis et al., 2016). Therefore, the initial processing of PrP^{C} at the α-cleavage site to produce the C1 has long been considered as a potential prophylactic for prion diseases by preventing the production of infectious and/or toxic forms of PrP.

Plasmin inhibits prions by specifically cleaving cellular prion protein

Successful generation of the PrP C1 in various model systems has been shown for ADAM8 (Liang et al., 2012),

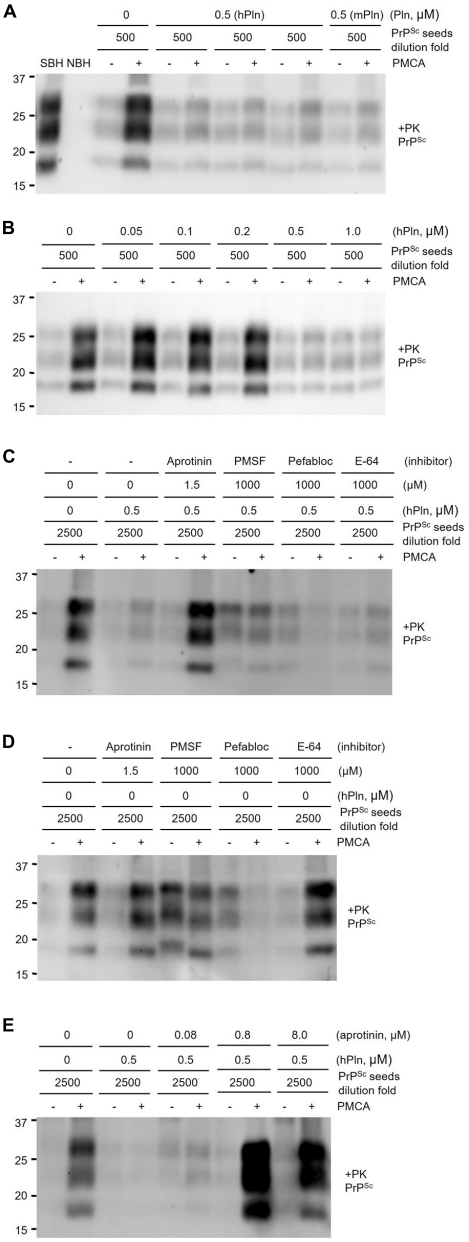

FIGURE 4
PMCA inhibited by supplementation with plasmin. Sick brain homogenate (SBH) were diluted 500 or 2500-fold in uninfected normal brain homogenate (NBH) and used as PrP^{Sc} seeds for PMCA. PK digested pre- and post-PMCA samples are denoted by (–) and (+), respectively. PMCA products were evaluated by western blot analysis of PrP^{Sc} generated. **(A)** PMCA supplemented with 0.5 μM plasmin of either human (hPln) or mouse (mPln) source was compared to identical reactions without supplementation. **(B)** PMCA conducted with increasing concentrations of hPln (ranging from 0 to 1 μM) was evaluated. **(C)** hPln-supplemented PMCA was performed in the presence or absence of protease inhibitors at an optimal working concentration for each. **(D)** PMCA with no hPln supplementation was performed in the presence or absence of protease inhibitors at an optimal working concentration for each. **(E)** hPln-supplemented PMCA was performed with increasing concentrations from 0 to 8 μM aprotinin.

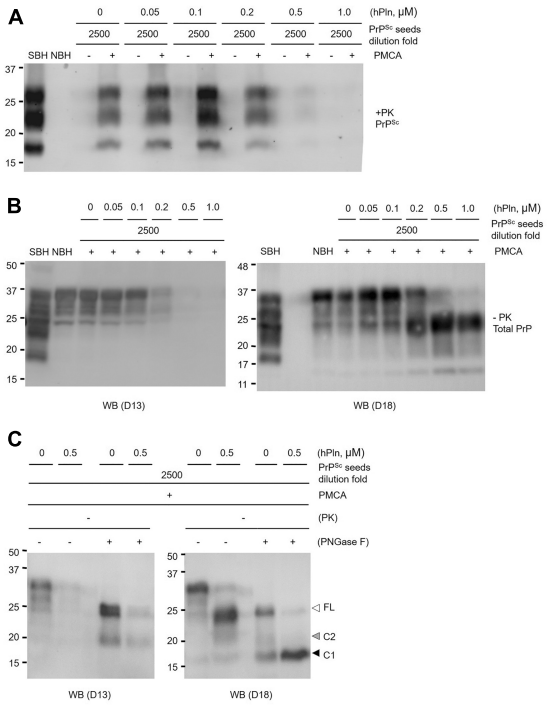

FIGURE 5
Plasmin inhibits PrP conversion in PMCA by promoting α-cleavage. Sick brain homogenate (SBH) were diluted 2500-fold in uninfected normal brain homogenate (NBH) and used as PrP^{Sc} seeds for PMCA. PMCA products were evaluated by western blot analysis. **(A)** PMCA was conducted with increasing concentrations of hPln ranging from 0 to 1 μM and the level of PrP^{Sc} was evaluated by western blot analysis with PK digestion. Pre- and post-PMCA samples are denoted by (-) and (+), respectively. **(B)** Post-PMCA (+) samples analyzed in Panel **(A)** were not subjected to PK digestion and further analyzed by western blotting with D13 or D18, recognizing full-length and fragments of PrP in different glycosylation states. **(C)** Post-PMCA (+) samples with no PK digestion from Panel **(B)** were deglycosylated by PNGase F and analyzed by western blot with D13 or D18. white arrow, full-length (FL) PrP; black arrow, C1 fragment; gray arrow, C2 fragment.

ADAM10 (Vincent et al., 2001; Cisse et al., 2005), ADAM17 (Vincent et al., 2001; Laffont-Proust et al., 2005), calpain (Hachiya et al., 2011), and plasmin (Kornblatt et al., 2003; Praus et al., 2003; Xanthopoulos et al., 2005). However, the *bona fide* protease responsible is currently a matter of debate because recent evidence questions the prominence in which the leading candidates, ADAM10 and ADAM17, play in the α-cleavage of PrP. In summary, there has been large discrepancy in the amount of C1 obtained from cultured cells over-expressing or depleted of ADAM10 or ADAM17 (Vincent et al., 2000, 2001; Taylor et al., 2009; Béland et al., 2012). Moreover, neuronal over-expression or knockdown of ADAM10 *in vivo* failed to influence α-cleavage (Endres et al., 2009; Altmeppen et al., 2011). In contrast, a convincing case was reported describing ADAM8 as the primary protease generating C1 in skeletal muscle *in vitro* and *in vivo*, but this likely cannot be recapitulated in the central nervous system due to negligible expression levels (Su et al., 2004; Liang et al., 2012). Lastly, a role for calpain contradicts the hypothesis that C1 and C2 are cleaved by separate pathways since it has demonstrated the capacity to perform α- and β-cleavage *in vitro* (Yadavalli et al., 2004).

Here, we focused on the unexplored function of plasmin in PrP endoproteolysis during PrP^{Sc} formation and prion propagation. Although primarily found in the liver, plasminogen is expressed by neuronal populations in the brain and often localizes to the lipid rafts of the plasma membrane (Ledesma et al., 2003; Kim et al., 2009). Therefore, this observation indirectly places plasmin at the site for PrP^{Sc} replication (Vey et al., 1996) because plasminogen readily converts into plasmin. To better understand the role of plasmin, we used an *in vitro* plasmin cleavage assay to recognize the nature of plasmin responsible for the C1 cleavage. We tested the specific proteolytic activity of plasmin by using rhPrP(23-231) in the presence of 10% FBS and PrP^{C} expressing-neuronal cell lines with or without chronic prion infection. In the present study, we confirmed that plasmin has the fundamental ability to internally cleave PrP at the α-cleavage site in agreement with previous reports (**Figures 1**, **2**). Inclusion of FBS in the rhPrP(23-231) cleavage reaction, which was not the case for previous reports, was carried out in this study to investigate the cleavage under a condition that is similar to the physiological environment. Because serum includes a number of regulators that control plasmin activity, the result of hPln-mediated rhPrP(23-231) cleavage in the presence of serum strongly suggests that the generation of rhPrP(23-231) fragments by hPln is not artifacts obtained under the simple *in vitro* condition. This is further expanded in the cultured cells. Plasmin increased formation of the C1, while analysis of deglycosylated PrP

TABLE 1 Bioassay of PMCA materials with or without supplementation with plasmin.

Sample	No. Mice (Prion-sick/Total)	Avg. Incubation Time ± SEM (days)	*P*-value (vs. PMCA)	*P*-value (vs. PrP^{Sc} Seeds)
PrP^{Sc} Seeds	7/8	198 ± 8	0.01	
PMCA	8/8	177 ± 2		
PMCA + hPln	8/8	193 ± 4	< 0.001	NS (> 0.05)

showed that the level of C2 was not changed by plasmin treatment in ScN2a cells.

To address that plasmin induction of C1 generation would inhibit PrP^{Sc} formation under biological conditions, ScN2a and PrP-3F4 expressing ScN2a cells were exposed to plasmin. In ScN2a cells, PrP^{Sc} accumulation was significantly, but suddenly, reduced by incubation with 0.5 μM hPln, while it was gradually increased by incubation with low concentrations of hPln (**Figure 3A**). This indicates that there is a threshold of hPln concentration to facilitate inhibition of PrP^{Sc} formation under the experimental conditions used for this study. Because ScN2a cells were cultured in the presence of 10% serum that includes the natural plasmin inhibitor such as α2-antiplasmin estimated to be 0.2 μM (Cederholm-Williams, 1981), the supplemented hPln at the low concentrations could remain inactive to cleave PrP^{C}. Interestingly, this inactive plasmin harboring Kringle domains could be virtually identical to plasminogen that enhances PrP^{Sc} formation as we reported previously (Ryou et al., 2003). Therefore, it is likely that PrP^{Sc} accumulation is stimulated until, but inhibited after, the concentration of hPln exceeds the level of natural plasmin inhibitors provided in serum. The inhibition of PrP^{Sc} accumulation found in ScN2a cells was likely due to the inhibition of *de novo* PrP^{Sc} formation as shown in ScN2a cells transiently transfected for PrP-3F4 expression (**Figure 3B**). From these results, we suggested that plasmin would inhibit the conversion of PrP^{C} to PrP^{Sc} by generating C1 lacking the neurotoxic and amyloidogenic PrP(106-126) domains without a direct effect on C2 alteration. Other studies showed that the reduction of the PrP^{C} level resulted in decreased prion replication during the transition from presymptomatic to symptomatic prion disease (Mays et al., 2014b, 2015). Interestingly, the level of total PrP in ScN2a expressing PrP-3F4 was decreased as the concertation of supplemented hPln increased, implicating the reduction of the PrP^{C} level (**Figure 3B**). Thus, plasmin-mediated cleavage of PrP^{C} could potentially contribute to the diminishing residual full-length PrP^{C} levels in the presymptomatic to symptomatic period transition.

PMCA provided a simplified system to study PrP^{Sc} formation in the presence of physiologically relevant plasmin levels (Cederholm-Williams, 1981; Whitelaw et al., 1995), while avoiding the complex pathways necessary to activate plasminogen to plasmin (Castellino and Ploplis, 2005) and intrinsic health problems associated with the plasminogen knockout mouse model (Ploplis et al., 1995; Bugge et al., 1995) that has confounded the interpretation of prion bioassays in the past. The inhibition of PrP^{Sc} generation by plasmin was confirmed using PMCA in this study (**Figures 4A,B**). The plasmin function could only be abolished with the addition of aprotinin, a serine protease inhibitor specific and potent for plasmin (**Figures 4C–E**), suggesting an apparent role of plasmin as a negative regulator in PrP^{Sc} generation. The role of plasmin to inhibit PrP^{Sc} generation was extended to its role in inhibiting prion infectivity from the bioassay using PMCA materials produced in the presence or absence of hPln (**Table 1**). In this study, the material obtained from PMCA resulted in the abbreviated incubation time over 21 d compared to the PrP^{Sc} seeds, the material without amplification, suggesting an increase of prion titer by PMCA. The plasmin supplementation in PMCA counteracted the effect of amplification and, like the PrP^{Sc} seeds, the incubation time of this material prolonged 16 d compared to the material obtained from PMCA without hPln supplementation. This delay of incubation time represents the abolition of PMCA prion titer by plasmin to the level of the PrP^{Sc} seeds because the incubation time between the PrP^{Sc} seeds and hPln-supplemented PMCA groups was not different with statistical significance. Thus, plasmin supplementation in PMCA efficiently inhibited infective prion propagation by producing an endoproteolytic fragment of PrP^{C} (**Figure 5**), which can serve as improper substrates for conversion, via α-cleavage. Because the substrate of normal brain homogenates used for PMCA was prepared in PBS with the protease inhibitor cocktail that includes the agents inhibiting plasmin, the α-cleavage of PrP^{C} by plasmin and the subsequent PrP^{Sc} formation may not be robust under the experimental conditions in this study.

The mechanistic details underlying the endoproteolysis of PrP^{C} by plasmin remain to be explored. PrP^{C} is known to interact with plasminogen and tissue-type plasminogen activator (tPA) (Fischer et al., 2000; Maissen et al., 2001; Ellis et al., 2002; Shaked et al., 2002; Kornblatt et al., 2003, 2004; Praus et al., 2003; Ryou et al., 2003; Epple et al., 2004a,b; Cuccioloni et al., 2005; Hatcher et al., 2009; Bougard et al., 2016). Because plasmin is activated from plasminogen by tPA, this event can occur in a complex with PrP^{C}, which enables plasmin readily cleaves PrP^{C} at the α-site. The substrate specificity of PrP^{C} for plasmin catalysis has not been documented. However, although not perfect, the α-site of PrP^{C} resembles the arrangement of amino acid residues (Xaa-Tyr/Phe-Lys/Arg-Xaa, where Xaa can be any amino acid) preferred by plasmin (Harris et al., 2000). Like many serine proteases, plasmin cleaves the peptide bond between Lys/Arg-Xaa, leaving a C-terminal lysine, with a preference of an aromatic amino acid reside at the N-terminal of Lys/Arg. The α-site of human and mouse PrP^{C} shows Asn-Met/Leu-Lys-His. Although aliphatic Met/Leu are not aromatic, they share the hydrophobic characteristics with Tyr/Phe and could fill the space of a specificity pocket near the catalytic triad of plasmin similar to Tyr or Phe does. Thus, PrP^{C} may not be the best substrate for plasmin, while it is sufficient enough to be cleaved by plasmin, which contributes to the prevention of PrP^{Sc} formation as demonstrated in the current study.

Implications for plasmin in neurodegenerative diseases

Defining the role of plasmin in the endoproteolysis of PrP also may have implications for other neurodegenerative diseases on multiple levels. First, the suggested involvement of multiple pathways for the metabolic processing of PrP parallels the situation in the healthy, non-amyloidogenic α-processing versus the disease-associated amyloidogenic β-processing of the β–amyloid precursor protein (βAPP) (Selkoe, 1999; Venugopal et al., 2008). Secondly, enzymatic assays demonstrated that plasmin intervenes by scission of APP at the α-cleavage site between Lys687 and Leu688 (Selkoe, 1999) as well as by degrading Aβ40 and Aβ42 via cleavage between Arg5 and His6 or at multiple other sites (Van Nostrand and Porter, 1999; Tucker et al., 2000a,b; Exley and Korchazhkina, 2001). Concomitantly, induced activation of plasminogen into plasmin has been indicated to reduce Aβ levels *in vivo* (Melchor et al., 2003; Tucker et al., 2004; Jacobsen et al., 2008; Liu et al., 2011). Thirdly, PrP^{C} contains a binding site for oligomeric Aβ located between the C1 and C2 sites, which has been shown to mediate toxicity (Lauren et al., 2009; Westaway and Jhamandas, 2012). Therefore, plasmin α-cleavage of PrP generates a GPI-anchored C1 in which oligomeric Aβ could not dock, thus preventing its toxic effect during Alzheimer's disease. It is also suggested that the proteolytic activity of plasmin is associated with Parkinson's disease. Plasmin is capable of cleaving and degrading α-synuclein in both its monomeric and aggregated forms, inhibiting the translocation of extracellular α- synuclein into the neighboring cells, and reducing the neuroinflammatory response of microglia and astrocytes. This prevents α-synuclein from aggregating and forming toxic Lewy bodies, resulting in reduced neuronal cell death (Kim et al., 2012; Park and Kim, 2013). Although the role of plasmin/plasminogen in the pathogenesis of amyotrophic lateral sclerosis remains to be elucidated, several studies have reported that plasminogen/plasmin is associated with the pathogenesis of amyotrophic lateral sclerosis (Demestre et al., 2006; Glas et al., 2007).

Summary and conclusion

In summary, we demonstrated an inhibitory role for plasmin in PrP^{Sc} formation using PMCA and observed a parallel *de novo* reduction in the accumulation of PrP^{Sc} in ScN2a cells incubated with plasmin. Although it remains to be determined whether plasmin inhibits PrP^{Sc} propagation during natural prion infectivity *in vivo*, plasmin inhibits propagation of infective prion replication during PMCA as shown in bioassays of PMCA products. While the ability to generate the PrP C1 fragment is shared by several proteases, our data presents plasmin as the first discovered to play a functional role during prion formation by cleaving PrP^{C}, but not PrP^{Sc}. Moreover, the present study complements our recent discovery that plasminogen assists in PrP^{Sc} propagation by introducing a novel regulatory role for the plasmin(ogen) system that could not be revealed in complex plasminogen knockout mouse models. Although the mechanistic details are uncertain, the "yin-yang" effect of the plasmin(ogen) system not only contributes to deciphering the intricate events involved in prion replication but presents new and attractive therapeutic targets to treat prion diseases as well as other neurodegenerative diseases.

Data availability statement

The original contributions presented in this study are included in the article/**Supplementary material**, further inquiries can be directed to the corresponding authors.

Ethics statement

The animal study was reviewed and approved by Institutional Animal Care and Use Committee, University of Kentucky.

Author contributions

CM and TT performed the experiments. CM, TT, GT, H-EK, and CR analyzed the data. CM, H-EK, and CR wrote the manuscript. All authors read and approved the final manuscript.

Funding

This work was supported by the start-up fund of University of Kentucky, KY, United States. (CR), a grant (HI16C1085) from the Korea Health Technology R&D Project through the Korea Health Industry Development Institute (KHIDI) funded by the Ministry of Health & Welfare, South Korea (CR), and a grants (2012R1A1A2043356, 2020R1F1A1074328, and 2020R1A6A1A03042854) from the Basic Science Research Program through the National Research Foundation of Korea (NRF) funded by the Ministry of Education, South Korea (CR).

Acknowledgments

We are grateful to Younghwan Kim, William B. Titlow, and Jifeng Bian for technical assistance and scientific discussion.

Conflict of interest

The authors declare that the research was conducted in the absence of any commercial or financial relationships that could be construed as a potential conflict of interest.

Publisher's note

All claims expressed in this article are solely those of the authors and do not necessarily represent those of their affiliated organizations, or those of the publisher, the editors and the reviewers. Any product that may be evaluated in this article, or claim that may be made by its manufacturer, is not guaranteed or endorsed by the publisher.

Supplementary material

The Supplementary Material for this article can be found online at: https://www.frontiersin.org/articles/10.3389/fnmol.2022.990136/full#supplementary-material

References

Altmeppen, H., Prox, J., Puig, B., Kluth, M., Bernreuther, C., Thurm, D., et al. (2011). Lack of a-disintegrin-and-metalloproteinase ADAM10 leads to intracellular accumulation and loss of shedding of the cellular prion protein in vivo. *Mol. Neurodegener.* 6:36. doi: 10.1186/1750-1326-6-36

Ayers, J. I., Schutt, C. R., Shikiya, R. A., Aguzzi, A., Kincaid, A. E., and Bartz, J. C. (2011). The strain-encoded relationship between PrPSc replication, stability and processing in neurons is predictive of the incubation period of disease. *PLoS Pathog.* 7:e1001317. doi: 10.1371/journal.ppat.1001317

Barnewitz, K., Maringer, M., Mitteregger, G., Giese, A., Bertsch, U., and Kretzschmar, H. A. (2006). Unaltered prion protein cleavage in plasminogen-deficient mice. *Neuroreport* 17, 527–530. doi: 10.1097/01.wnr.0000209003.55728.ac

Basham, M. E., and Seeds, N. W. (2001). Plasminogen expression in the neonatal and adult mouse brain. *J. Neurochem.* 77, 318–325.

Béland, M., Motard, J., Barbarin, A., and Roucou, X. (2012). PrPC homodimerization stimulates the production of PrPC cleaved fragments PrPN1 and PrPC1. *J. Neurosci.* 32, 13255–13263. doi: 10.1523/jneurosci.2236-12.2012

Borumand, M., and Ellis, V. (2022). Metal ions bound to prion protein affect its interaction with plasminogen activation system. *Prot. J.* 41, 88–96. doi: 10.1007/s10930-021-10035-4

Bougard, D., Brandel, J. P., Belondrade, M., Beringue, V., Segarra, C., Fleury, H., et al. (2016). Detection of prions in the plasma of presymptomatic and symptomatic patients with variant Creutzfeldt-Jakob disease. *Sci. Transl. Med.* 8:370ra182. doi: 10.1126/scitranslmed.aag1257

Bugge, T. H., Flick, M. J., Daugherty, C. C., and Degen, J. L. (1995). Plasminogen deficiency causes severe thrombosis but is compatible with development and reproduction. *Genes Dev.* 9, 794–807. doi: 10.1101/gad.9.7.794

Butler, D. A., Scott, M., Bockman, J. M., Borchelt, D. R., Taraboulos, A., Hsiao, K. K., et al. (1988). Scrapie-infected murine neuroblastoma cells produce protease-resistant prion proteins. *J. Virol.* 62, 1558–1564.

Castellino, F. J., and Ploplis, V. A. (2003). "Human plasminogen: Structure, activation, and function," in *Plasminogen: Structure, activation, and regulation*, ed. D. M. Waisman (Boston, MA: Springer), 3–17.

Castellino, F. J., and Ploplis, V. A. (2005). Structure and function of the plasminogen/plasmin system. *Thromb. Haemost.* 93, 647–654.

Cederholm-Williams, S. (1981). Concentration of plasminogen and antiplasmin in plasma and serum. *J. Clin. Pathol.* 34, 979–981.

Chen, S. G., Teplow, D. B., Parchi, P., Teller, J. K., Gambetti, P., and Autilio-Gambetti, L. (1995). Truncated forms of the human prion protein in normal brain and in prion diseases. *J. Biol. Chem.* 270, 19173–19180.

Cisse, M. A., Sunyach, C., Lefranc-Jullien, S., Postina, R., Vincent, B., and Checler, F. (2005). The disintegrin ADAM9 indirectly contributes to the physiological processing of cellular prion by modulating ADAM10 activity. *J. Biol. Chem.* 280, 40624–40631. doi: 10.1074/jbc.M506069200

Cuccioloni, M., Amici, M., Eleuteri, A. M., Biagetti, M., Barocci, S., and Angeletti, M. (2005). Binding of recombinant PrP^c to human plasminogen: Kinetic and thermodynamic study using a resonant mirror biosensor. *Proteins* 58, 728–734. doi: 10.1002/prot.20346

Demestre, M., Howard, R. S., Orrell, R. W., and Pullen, A. H. (2006). Serine proteases purified from sera of patients with amyotrophic lateral sclerosis (ALS) induce contrasting cytopathology in murine motoneurones to IgG. *Neuropathol. Appl. Neurobiol.* 32, 141–156. doi: 10.1111/j.1365-2990.2006.00712.x

Ellis, V., Daniels, M., Misra, R., and Brown, D. R. (2002). Plasminogen activation is stimulated by prion protein and regulated in a copper-dependent manner. *Biochemistry* 41, 6891–6896. doi: 10.1021/bi025676g

Endres, K., Mitteregger, G., Kojro, E., Kretzschmar, H., and Fahrenholz, F. (2009). Influence of ADAM10 on prion protein processing and scrapie infectiosity in vivo. *Neurobiol. Dis.* 36, 233–241. doi: 10.1016/j.nbd.2009.07.015

Epple, G., Langfeld, K., Baier, M., Holzhütter, H. G., Schleuning, W. D., Köttgen, E., et al. (2004a). Both lysine-clusters of the NH2 -terminal prion-protein fragment PrP23-110 are essential for t-PA mediated plasminogen activation. *Thromb. Haemost.* 91, 465–471. doi: 10.1160/TH03-06-0382

Epple, G., Schleuning, W. D., Kettelgerdes, G., Köttgen, E., Geßner, R., and Praus, M. (2004b). Prion protein stimulates tissue-type plasminogen activator-mediated plasmin generation via a lysine-binding site on kringle 2. *J. Thromb. Haemos.* 2, 962–968. doi: 10.1111/j.1538-7836.2004.00675.x

Exley, C. C. A., and Korchazhkina, O. V. (2001). Plasmin cleaves A[beta]42 in vitro and prevents its aggregation into [beta]-pleated sheet structures. *Neuroreport* 12, 2967–2970.

Fischer, M. B., Roeckl, C., Parizek, P., Schwarz, H. P., and Aguzzi, A. (2000). Binding of disease-associated prion protein to plasminogen. *Nature* 408, 479–483.

Fritz, H., and Wunderer, G. (1983). Biochemistry and applications of aprotinin, the kallikrein inhibitor from bovine organs. *Arzneimittelforschung* 33, 479–494.

Glas, M., Popp, B., Angele, B., Koedel, U., Chahli, C., Schmalix, W. A., et al. (2007). A role for the urokinase-type plasminogen activator system in amyotrophic lateral sclerosis. *Exp. Neurol.* 207, 350–356. doi: 10.1016/j.expneurol.2007.07.007

Hachiya, N., Komata, Y., Harguem, S., Nishijima, K., and Kaneko, K. (2011). Possible involvement of calpain-like activity in normal processing of cellular prion protein. *Neurosci. Lett.* 490, 150–155. doi: 10.1016/j.neulet.2010.12.046

Hachiya, N. S., Imagawa, M., and Kaneko, K. (2007). The possible role of protein X, a putative auxiliary factor in pathological prion replication, in regulating a physiological endoproteolytic cleavage of cellular prion protein. *Med. Hypotheses* 68, 670–673. doi: 10.1016/j.mehy.2006.07.038

Haigh, C. L., and Collins, S. J. (2016). Endoproteolytic cleavage as a molecular switch regulating and diversifying prion protein function. *Neural Regen. Res.* 11, 238–239. doi: 10.4103/1673-5374.177726

Harris, D. A., Huber, M. T., van Dijken, P., Shyng, S. L., Chait, B. T., and Wang, R. (1993). Processing of a cellular prion protein: Identification of N- and C-terminal cleavage sites. *Biochemistry* 32, 1009–1016. doi: 10.1021/bi00065a003

Harris, J. L., Backes, B. J., Leonetti, F., Mahrus, S., Ellman, J. A., and Craik, C. S. (2000). Rapid and general profiling of protease specificity by using combinatorial fluorogenic substrate libraries. *Proc. Natl. Acad. Sci. U. S. A.* 97, 7754–7759. doi: 10.1073/pnas.140132697

Hatcher, K., Zheng, J., and Chen, S. G. (2009). Cryptic peptides of the kringle domains preferentially bind to disease-associated prion protein. *J. Alz. Dis.* 16, 421–431. doi: 10.3233/JAD-2009-0980

Jacobsen, J. S., Comery, T. A., Martone, R. L., Elokdah, H., Crandall, D. L., Oganesian, A., et al. (2008). Enhanced clearance of amyloid-beta in brain by sustaining the plasmin proteolysis cascade. *Proc. Natl. Acad. Sci. U. S. A.* 105, 8754–8759. doi: 10.1073/pnas.0710823105

Jimenez-Huete, A., Lievens, P. M., Vidal, R., Piccardo, P., Ghetti, B., Tagliavini, F., et al. (1998). Endogenous proteolytic cleavage of normal and disease-associated isoforms of the human prion protein in neural and non-neural tissues. *Am. J. Pathol.* 153, 1561–1572. doi: 10.1016/S0002-9440(10)65744-6

Kim, K. S., Choi, Y. R., Park, J. Y., Lee, J. H., Kim, D. K., Lee, S. J., et al. (2012). Proteolytic cleavage of extracellular alpha-synuclein by plasmin: Implications for Parkinson disease. *J. Biol. Chem.* 287, 24862–24872. doi: 10.1074/jbc.M112.348128

Kim, S.-G., Lee, H.-M., and Ryou, C. (2014). Parameters that affect macromolecular self-assembly of prion protein. *Prot. J.* 33, 243–252. doi: 10.1007/s10930-014-9556-z

Kim, Y., Song, J., Mays, C., Titlow, W., Yoon, D., and Ryou, C. (2009). Changes in gene expression of kringle domain-containing proteins in murine brains and neuroblastoma cells infected by prions. *Mol. Cell. Biochem.* 328, 177–182. doi: 10.1007/s11010-009-0087-4

Kojima, A., Konishi, M., and Akizawa, T. (2014). Prion fragment peptides are digested with membrane type matrix metalloproteinases and acquire enzyme resistance through Cu(2)(+)-binding. *Biomolecules* 4, 510–526. doi: 10.3390/biom4020510

Kornblatt, J. A., Marchal, S., Razaei, H., and Balny, C. (2004). Characterization of a complex formed between human plasminogen and recombinant sheep prion: Pressure and thermal sensitivity of complex formation. *Cell. Mol. Biol.* 50, 387–396.

Kornblatt, J. A., Marchal, S., Rezaei, H., Kornblatt, M. J., Balny, C., Lange, R., et al. (2003). The fate of the prion protein in the prion/plasminogen complex. *Biochem. Biophys. Res. Commun.* 305, 518–522. doi: 10.1016/s0006-291x(03)00804-0

Kwon, M., and Waisman, D. M. (2003). "Mechanism of angiostatin formation from plasminogen," in *Plasminogen: Structure, activation, and regulation*, ed. D. M. Waisman (New York, NY: Kluwer Academic/Plenum Publishers), 135–156.

Laffont-Proust, I., Faucheux, B. A., Hässig, R., Sazdovitch, V., Simon, S., Grassi, J., et al. (2005). The N-terminal cleavage of cellular prion protein in the human brain. *FEBS Lett.* 579, 6333–6337. doi: 10.1016/j.febslet.2005.10.013

Lauren, J., Gimbel, D. A., Nygaard, H. B., Gilbert, J. W., and Strittmatter, S. M. (2009). Cellular prion protein mediates impairment of synaptic plasticity by amyloid-[bgr] oligomers. *Nature* 457, 1128–1132.

Ledesma, M. D., Da Silva, J. S., Schevchenko, A., Wilm, M., and Dotti, C. G. (2003). Proteomic characterisation of neuronal sphingolipid-cholesterol microdomains: Role in plasminogen activation. *Brain Res.* 987, 107–116. doi: 10.1016/s0006-8993(03)03296-7

Lewis, V., Johanssen, V. A., Crouch, P. J., Klug, G. M., Hooper, N. M., and Collins, S. J. (2016). Prion protein "gamma-cleavage": Characterizing a novel endoproteolytic processing event. *Cell. Mol. Life Sci.* 73, 667–683. doi: 10.1007/s00018-015-2022-z

Liang, J., Wang, W., Sorensen, D., Medina, S., Ilchenko, S., Kiselar, J., et al. (2012). Cellular prion protein regulates its own α-cleavage through ADAM8 in skeletal muscle. *J. Biol. Chem.* 287, 16510–16520. doi: 10.1074/jbc.M112.360891

Liu, R. M., van Groen, T., Katre, A., Cao, D., Kadisha, I., Ballinger, C., et al. (2011). Knockout of plasminogen activator inhibitor 1 gene reduces amyloid beta peptide burden in a mouse model of Alzheimer's disease. *Neurobiol. Aging* 32, 1079–1089. doi: 10.1016/j.neurobiolaging.2009.06.003

Maissen, M., Roeckl, C., Glatzel, M., Goldmann, W., and Aguzzi, A. (2001). Plasminogen binds to disease-associated prion protein of multiple species. *Lancet* 357, 2026–2028. doi: 10.1016/S0140-6736(00)05110-2

Mangé, A., Béranger, F., Peoc'h, K., Onodera, T., Frobert, Y., and Lehmann, S. (2004). Alpha- and beta- cleavages of the amino-terminus of the cellular prion protein. *Biol. Cell* 96, 125–132. doi: 10.1016/j.biolcel.2003.11.007

Mays, C. E., Coomaraswamy, J., Watts, J. C., Yang, J., Ko, K. W., Strome, B., et al. (2014a). Endoproteolytic processing of the mammalian prion glycoprotein family. *FEBS J.* 281, 862–876. doi: 10.1111/febs.12654

Mays, C. E., Kim, C., Haldiman, T., van der Merwe, J., Lau, A., Yang, J., et al. (2014b). Prion disease tempo determined by host-dependent substrate reduction. *J. Clin. Invest.* 124, 847–858. doi: 10.1172/JCI72241

Mays, C. E., and Ryou, C. (2010). Plasminogen stimulates propagation of protease-resistant prion protein in vitro. *FASEB J.* 24, 5102–5112. doi: 10.1096/fj.10-163600

Mays, C. E., and Ryou, C. (2011). Plasminogen: A cellular protein cofactor for PrPSc propagation. *Prion* 5, 22–27. doi: 10.4161/pri.5.1.14460

Mays, C. E., van der Merwe, J., Kim, C., Haldiman, T., McKenzie, D., Safar, J. G., et al. (2015). Prion Infectivity Plateaus and Conversion to Symptomatic Disease Originate from Falling Precursor Levels and Increased Levels of Oligomeric PrPSc Species. *J. Virol.* 89, 12418–12426. doi: 10.1128/JVI.02142-15

McDonald, A. J., Dibble, J. P., Evans, E. G., and Millhauser, G. L. (2014). A new paradigm for enzymatic control of alpha-cleavage and beta-cleavage of the prion protein. *J. Biol. Chem.* 289, 803–813. doi: 10.1074/jbc.M113.502351

Melchor, J. P., Pawlak, R., and Strickland, S. (2003). The tissue plasminogen activator-plasminogen proteolytic cascade accelerates amyloid-beta degradation and inhibits amyloid-beta-induced neurodegeneration. *J. Neurosci.* 23, 8867–8871. doi: 10.1523/JNEUROSCI.23-26-08867.2003

Nazor, K. E., Seward, T., and Telling, G. C. (2007). Motor behavioral and neuropathological deficits in mice deficient for normal prion protein expression. *Biochim. Biophys. Acta Mol. Basis Dis.* 1772, 645–653. doi: 10.1016/j.bbadis.2007.04.004

Oliveira-Martins, J. B., Yusa, S. I, Calella, A. M., Bridel, C., Baumann, F., Dametto, P., et al. (2010). Unexpected tolerance of α-cleavage of the prion protein to sequence variations. *PLoS One* 5:e9107. doi: 10.1371/journal.pone.0009107

Pan, K. M., Baldwin, M., Nguyen, J., Gasset, M., Serban, A., Groth, D., et al. (1993). Conversion of α-helices into β-sheets features in the formation of the scrapie prion proteins. *Proc. Natl. Acad. Sci. U. S. A.* 90, 10962–10966.

Park, S. M., and Kim, K. S. (2013). Proteolytic clearance of extracellular alpha-synuclein as a new therapeutic approach against Parkinson disease. *Prion* 7, 121–126. doi: 10.4161/pri.22850

Ploplis, V. A., Carmeliet, P., Vazirzadeh, S., Van Vlaenderen, I., Moons, L., Plow, E. F., et al. (1995). Effects of disruption of the plasminogen gene on thrombosis, growth, and health in mice. *Circulation* 92, 2585–2593. doi: 10.1161/01.cir.92.9.2585

Praus, M., Kettelgerdes, G., Baier, M., Holzhütter, H. G., Jungblut, P. R., Maissen, M., et al. (2003). Stimulation of plasminogen activation by recombinant cellular prion protein is conserved in the NH2-terminal fragment PrP23-110. *Thromb. Haemost.* 89, 812–819.

Prusiner, S. B. (1998). Prions. *Proc. Natl. Acad. Sci. U. S. A.* 95, 13363–13383.

Ryou, C., Prusiner, S. B., and Legname, G. (2003). Cooperative binding of dominant-negative prion protein to kringle domains. *J. Mol. Biol.* 329, 323–333.

Ryou, C., Titlow, W. B., Mays, C. E., Bae, Y., and Kim, S. (2011). The suppression of prion propagation using poly-L-lysine by targeting plasminogen that stimulates prion protein conversion. *Biomaterials* 32, 3141–3149. doi: 10.1016/j.biomaterials.2011.01.017

Salmona, M., Capobianco, R., Colombo, L., De Luigi, A., Rossi, G., Mangieri, M., et al. (2005). Role of plasminogen in propagation of scrapie. *J. Virol.* 79, 11225–11230.

Scott, M. R., Köhler, R., Foster, D., and Prusiner, S. B. (1992). Chimeric prion protein expression in cultured cells and transgenic mice. *Prot. Sci.* 1, 986–997.

Selkoe, D. J. (1999). Translating cell biology into therapeutic advances in Alzheimer's disease. *Nature* 399, A23–A31. doi: 10.1038/399a023

Shaked, Y., Engelstein, R., and Gabizon, R. (2002). The binding of prion proteins to serum components is affected by detergent extraction conditions. *J. Neurochem.* 82, 1–5. doi: 10.1046/j.1471-4159.2002.00995.x

Su, A. I., Wiltshire, T., Batalov, S., Lapp, H., Ching, K. A., Block, D., et al. (2004). A gene atlas of the mouse and human protein-encoding transcriptomes. *Proc. Natl. Acad. Sci. U. S. A.* 101, 6062–6067. doi: 10.1073/pnas.0400782101

Taylor, D. R., Parkin, E. T., Cocklin, S. L., Ault, J. R., Ashcroft, A. E., Turner, A. J., et al. (2009). Role of ADAMs in the ectodomain shedding and conformational conversion of the prion protein. *J. Biol. Chem.* 284, 22590–22600. doi: 10.1074/jbc.M109.032599

Tucker, H. M., Kihiko-Ehmann, M., Wright, S., Rydel, R. E., and Estus, S. (2000a). Tissue plasminogen activator requires plasminogen to modulate amyloid-beta neurotoxicity and deposition. *J. Neurochem.* 75, 2172–2177. doi: 10.1046/j.1471-4159.2000.0752172.x

Tucker, H. M., Kihiko, M., Caldwell, J. N., Wright, S., Kawarabayashi, T., Price, D., et al. (2000b). The plasmin system is induced by and degrades amyloid-beta aggregates. *J. Neurosci.* 20, 3937–3946.

Tucker, H. M., Simpson, J., Kihiko-Ehmann, M., Younkin, L. H., McGillis, J. P., Younkin, S. G., et al. (2004). Plasmin deficiency does not alter endogenous murine amyloid beta levels in mice. *Neurosci. Lett.* 368, 285–289.

Van Nostrand, W. E., and Porter, M. (1999). Plasmin cleavage of the amyloid beta-protein: Alteration of secondary structure and stimulation of tissue plasminogen activator activity. *Biochemistry* 38, 11570–11576. doi: 10.1021/bi990610f

Venugopal, C., Demos, C. M., Rao, K. S., Pappolla, M. A., and Sambamurti, K. (2008). Beta-secretase: Structure, function, and evolution. *CNS Neurol. Disord. Drug Targets* 3, 278–294.

Vey, M., Pilkuhn, S., Wille, H., Nixon, R., DeArmond, S. J., Smart, E. J., et al. (1996). Subcellular colocalization of the cellular and scrapie prion proteins in caveolae-like membranous domains. *Proc. Natl. Acad. Sci. U. S. A.* 93, 14945–14949. doi: 10.1073/pnas.93.25.14945

Vincent, B., Paitel, E., Frobert, Y., Lehmann, S., Grassi, J., and Checler, F. (2000). Phorbol ester-regulated cleavage of normal prion protein in HEK293 human cells and murine neurons. *J. Biol. Chem.* 275, 35612–35616. doi: 10.1074/jbc.M004628200

Vincent, B., Paitel, E., Saftig, P., Frobert, Y., Hartmann, D., De Strooper, B., et al. (2001). The disintegrins ADAM10 and TACE contribute to the constitutive and phorbol ester-regulated normal cleavage of the cellular prion protein. *J. Biol. Chem.* 276, 37743–37746. doi: 10.1074/jbc.M105677200

Westaway, D., and Jhamandas, J. H. (2012). The P's and Q's of cellular PrP-Aβ interactions. *Prion* 6, 359–363.

Whitelaw, A., Mowinckel, M., and Abildgaard, U. (1995). Low levels of plasminogen in cerebrospinal fluid after intraventricular haemorrhage: A limiting factor for clot lysis? *Acta Paediatr.* 84, 933–936. doi: 10.1111/j.1651-2227.1995.tb13795.x

Xanthopoulos, K., Paspaltsis, I., Apostolidou, V., Petrakis, S., Siao, C. J., Kalpatsanidis, A., et al. (2005). Tissue plasminogen activator in brain tissues infected with transmissible spongiform encephalopathies. *Neurobiol. Dis.* 20, 519–527.

Yadavalli, R., Guttmann, R. P., Seward, T., Centers, A. P., Williamson, R. A., and Telling, G. C. (2004). Calpain-dependent endoproteolytic cleavage of PrPSc modulates scrapie prion propagation. *J. Biol. Chem.* 279, 21948–21956. doi: 10.1074/jbc.M400793200

Zhang, L., Seiffert, D., Fowler, B. J., Jenkins, G. R., Thinnes, T. C., Loskutoff, D. J., et al. (2002). Plasminogen has a broad extrahepatic distribution. *Thromb. Haemost.* 87, 493–501.

frontiers | Frontiers in Molecular Neuroscience

TYPE Original Research
PUBLISHED 27 September 2022
DOI 10.3389/fnmol.2022.996698

OPEN ACCESS

EDITED BY
Daniela Uberti,
University of Brescia, Italy

REVIEWED BY
Xiao-Yan Chen,
Chinese PLA General Hospital, China
Jahan B. Ghasemi,
University of Tehran, Iran

*CORRESPONDENCE
Wonhee Jang
wany@dongguk.edu

SPECIALTY SECTION
This article was submitted to Brain Disease Mechanisms, a section of the journal Frontiers in Molecular Neuroscience

RECEIVED 18 July 2022
ACCEPTED 22 August 2022
PUBLISHED 27 September 2022

CITATION
Shim YJ, Shin MK, Jung J, Koo B and Jang W (2022) An *in-silico* approach to studying a very rare neurodegenerative disease using a disease with higher prevalence with shared pathways and genes: Cerebral adrenoleukodystrophy and Alzheimer's disease.
Front. Mol. Neurosci. 15:996698.
doi: 10.3389/fnmol.2022.996698

An *in-silico* approach to studying a very rare neurodegenerative disease using a disease with higher prevalence with shared pathways and genes: Cerebral adrenoleukodystrophy and Alzheimer's disease

Yu Jeong Shim[1], Min Kyoung Shin[1], Junghyun Jung[1], Bongseong Koo[2] and Wonhee Jang[1]*

[1]Department of Life Science, Dongguk University, Goyang-si, South Korea, [2]BPgene, Seoul, South Korea

Cerebral adrenoleukodystrophy (cALD) is a rare neurodegenerative disease characterized by inflammatory demyelination in the central nervous system. Another neurodegenerative disease with a high prevalence, Alzheimer's disease (AD), shares many common features with cALD such as cognitive impairment and the alleviation of symptoms by erucic acid. We investigated cALD and AD in parallel to study the shared pathological pathways between a rare disease and a more common disease. The approach may expand the biological understandings and reveal novel therapeutic targets. Gene set enrichment analysis (GSEA) and weighted gene correlation network analysis (WGCNA) were conducted to identify both the resemblance in gene expression patterns and genes that are pathologically relevant in the two diseases. Within differentially expressed genes (DEGs), GSEA identified 266 common genes with similar up- or down-regulation patterns in cALD and AD. Among the interconnected genes in AD data, two gene sets containing 1,486 genes preserved in cALD data were selected by WGCNA that may significantly affect the development and progression of cALD. WGCNA results filtered by functional correlation via protein–protein interaction analysis overlapping with GSEA revealed four genes (*annexin A5*, *beta-2-microglobulin*, *CD44 molecule*, and *fibroblast growth factor 2*) that showed robust associations with the pathogeneses of cALD and AD, where they were highly involved in inflammation, apoptosis, and the mitogen-activated protein kinase pathway.

This study provided an integrated strategy to provide new insights into a rare disease with scant publicly available data (cALD) using a more prevalent disorder with some pathological association (AD), which suggests novel druggable targets and drug candidates.

KEYWORDS

adrenoleukodystrophy, Alzheimer's disease, shared pathway, meta-analysis, neurodegenerative disease

Introduction

Neurodegenerative diseases (NDs) are a class of disorders that mainly affect the central nervous system (CNS) and are characterized by progressive loss of the structure and/or function of neurons (Nussbaum and Ellis, 2003). Recently, the number of patients suffering from NDs such as Alzheimer's disease (AD), Huntington's disease, Parkinson's disease, and amyotrophic lateral sclerosis has been rapidly increasing worldwide (Hou et al., 2019). Significant efforts have been dedicated to developing medications that can cure NDs; however, no current therapeutics can completely cure these diseases. Even reversing damage is improbable, only a few treatments can slow the progression or alleviate these diseases' symptoms (Crous-Bou et al., 2017). If the exact pathological pathways can be identified, it may help develop therapeutic agents that can cure NDs. The most frequent form of NDs is dementia, the most prevalent type of which is AD (Nussbaum and Ellis, 2003). In the United States about 5.8 million Americans of all ages reportedly have AD-type dementia, 200,000 of whom have AD under the age of 65 years (Alzheimer's Association, 2019). The percentage of AD patients within the population is expected to increase by 6.7–30.8% depending on the state by 2025 compared to 2020 (Alzheimer's Association, 2021).

X-linked adrenoleukodystrophy (ALD) is a rare ND characterized by fatal progressive cerebral demyelination and/or spinal cord neurodegeneration (Fourcade et al., 2008). The ALD phenotypes range from rapidly progressing childhood cerebral form to adrenomyeloneuropathy (AMN) with/without cerebral involvement in adults (Berger et al., 2014). ALD is caused by an abnormality in the *adenosine triphosphate binding cassette subfamily D member1* (*ABCD1*) gene (Xq28) that encodes an integral peroxisomal membrane protein (Fourcade et al., 2008). Childhood cerebral ALD (cALD), which develops in boys aged 5–12 years, accounts for 35% of all ALD patients (Berger et al., 2014). Symptoms of childhood cALD include autoimmune response, strong inflammatory demyelination, and rapid progression of neurological dysfunction, leading to death within a few years (Moser et al., 1992).

One feature of all ALD is the accumulation of very long-chain fatty acids (VLCFA; $\geq$ C22) caused by impaired peroxisome β oxidation (Moser et al., 1992; Berger et al., 2014). The accumulation of saturated VLCFA was also found in the cortex of AD patients (Kou et al., 2011). VLCFA aggregate throughout the body with the most severe accumulation in the white matter of the brain and adrenal glands, causing neurological problems and adrenal insufficiency (Fourcade et al., 2008; Berger et al., 2014). VLCFA was reportedly a potential risk factor contributing to neurodegeneration by inducing nerve cell damage through mitochondrial dysfunction (Schönfeld and Reiser, 2016; Nury et al., 2020). VLCFA levels can be lowered by oral administration of oleic acid (C18: 1) and erucic acid (C22: 1) at a 4:1 ratio, which is known as Lorenzo's oil. Erucic acid is an important ligand of peroxisome proliferator-activated receptor δ, the activation of which directly inhibits neuronal cell death and alleviates neuro-inflammation in AD (Moser et al., 2007; Sassa et al., 2014; Altinoz et al., 2018; Altinoz and Ozpinar, 2019). Despite the link, very few studies have focused on the commonalities between ALD and AD.

Studies on rare diseases such as ALD generally have hardships of having a small sample size due to the low prevalence among the population, leading to difficulties in drug development (Engelen et al., 2014). Meta-studies merge datasets from individual studies to increase their sample size, thereby increasing statistical power, allowing the identification of novel pathways that cannot otherwise be found in separate studies. Comparing a rare disease with a more highly prevalent disease that shares a common pathway enables the designing of a novel drug that may act on both diseases (Goh et al., 2007).

As the development of novel *in silico* tools for analyzing genetic diseases arrives, studies are also actively being conducted to understand the biological meaning of a disease based on gene expression (Subramanian et al., 2005; Langfelder and Horvath, 2008). GSEA allows single-gene expression data to be compared with a distinct type of gene set conveying the biological roles and characteristics of other diseases. In addition to GSEA, a weighted gene co-expression network analysis (WGCNA) is

a bioinformatic application for finding co-expression patterns between genes by constructing a network and is used to compare clustered genes with another set of genes. These are powerful analytical tools that can be used to investigate various diseases, even rare diseases, with which several studies have successfully elicited genetic markers (Jung et al., 2019; Bottero et al., 2021; Kim et al., 2021). After identifying these markers, drug-repositioning can be performed to develop novel drug candidates.

In this study, we designed a workflow to study cALD using AD data to discover meaningful pathogenetic pathways and novel genetic markers via combining two different bioinformatic approaches (**Figure 1**). GSEA was conducted to detect common differentially expressed genes (DEGs) to determine the similarities between the two diseases, followed by WGCNA to identify interconnected gene sets that have correlations with the pathogeneses of cALD and AD. The core genes were finally selected by overlapping genes from GSEA and WGCNA results, of which biological roles were revealed along with the pathogenic understanding of cALD. By integrating two analyses in a complementary manner, common marker genes and pathways in both diseases could be identified that can be suggested as putative targets for pathway-based drug repositioning.

Materials and methods

Data collection of cerebral adrenoleukodystrophy and Alzheimer's disease

We searched for and downloaded microarray datasets of Homo sapiens from ArrayExpress.[1] We used three datasets for cALD (E-MEXP-3288, E-GEOD-34309, E-GEOD-85804) and five datasets for AD (E-GEOD-36980, E-GEOD-5281, E-GEOD-29378, E-GEOD-48350, E-GEOD-34879) in this study that contained samples of postmortem brains and induced pluripotent stem cells (iPSCs) obtained from patients' skin fibroblasts (cALD or AD) and from healthy control subjects (Liang et al., 2007; Israel et al., 2012; Schlüter et al., 2012; Wang et al., 2012; Berchtold et al., 2013; Miller et al., 2013; Hokama et al., 2014; Jang et al., 2016). The iPSC cells obtained from AD and control samples were induced into neurons, where only the induced neurons derived from AD patients showed a significant increase in three major biochemical markers of AD, amyloid-β, active glycogen synthase kinase-3β, and phosphorylated tau/total tau (Israel et al., 2012). The microarray datasets of iPSC samples were established from the fibroblasts cultured from skin biopsies of the patients and healthy controls. For the validation, an RNA sequencing (RNA-seq) data set (PRJNA422218) in which iPSC samples derived from somatic cells from childhood cALD patients were induced into brain microvascular endothelial cells was used (Lee et al., 2018).

Data preprocessing

The downloaded raw datasets in Affymetrix platform (*.CEL files) and Illumina platform were normalized using the Robust Multi-array Average (RMA) algorithm and the neqc function in R package oligo and limma, respectively. The duplicate genes in the datasets were processed using the probe's Entrez ID in the annotation package following Jung et al. (2017). The mean values were used for the data with identical Entrez IDs (Jung et al., 2018).

Adjusting batch effects and computing *Z*-scores in merged data

The datasets were merged and adjusted the batch effect and by the R surrogate variable analysis (sva) package to maintain meaningful biological effects while eliminating non-biological effects that result from combining independent studies conducted in different environments (Johnson et al., 2006; Leek et al., 2012). A meta-analysis was conducted using the random effects model in the GeneMeta R package to obtain false discovery rates (FDRs) and *Z*-scores that represent the gene expression profiles in each disease (Choi et al., 2003). The *Z*-score was calculated to indicate how the expression of a single gene in a patient group is different from that of a control group in this study. That is, genes with positive values of the *Z*-score are expressed higher in the patient group compared with the control group, whereas genes with negative values are less expressed in the patient group compared with the control group.

Gene set enrichment analysis

A fast GSEA R package was implemented for GSEA (Subramanian et al., 2005; Sergushichev, 2016). The *Z*-scores of the AD datasets were used to make a list of ranked genes. The DEGs of cALD were used as a set of genes to be analyzed and enrichment scores were calculated based on the ranked list. GSEA is designed to test multiple hypotheses for the similarity between ranked gene lists and a set of genes and has an algorithm to calculate enrichment scores by weighting the extreme (top or bottom) of the entire ranked list (Subramanian et al., 2005). The core members of the gene set with a high enrichment score were selected as leading-edge

1 https://www.ebi.ac.uk/arrayexpress/

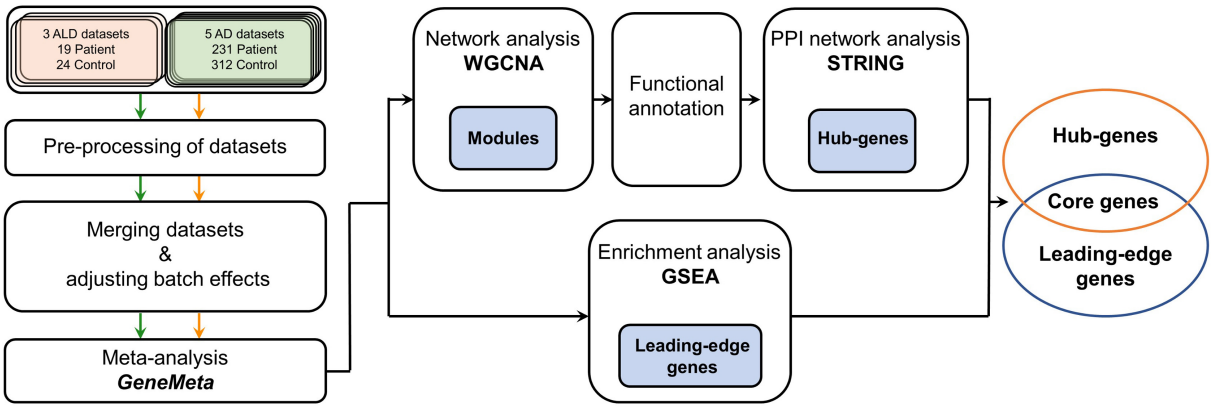

FIGURE 1
Workflow of the meta-analysis in this study. Green, orange, and black arrows indicate how cALD, AD, and the meta-analysis datasets were processed, respectively. The meta-analysis using GeneMeta was performed separately for two diseases, but the diseases were later analyzed together in the GSEA, WGCNA, and STRING processes. The blue painted boxes represent genes that were obtained from the corresponding analysis process, and those genes were used in the next analysis process. cALD, cerebral adrenoleukodystrophy; AD, Alzheimer's disease; GSEA, gene set enrichment analysis; WGCNA, weighted gene co-expression network analysis; STRING, search tool for the retrieval of interacting genes/proteins; PPI, protein–protein interaction.

genes (Subramanian et al., 2005). For the functional annotation of modules, the hallmark genes from molecular signatures database (MsigDB[2]) were used as annotated gene sets (Liberzon et al., 2015).

Weighted gene co-expression network analysis

Originally, a signed WGCNA is designed to cluster gene sets that solely consist of positively correlated genes based on Pearson correlation coefficients (Langfelder and Horvath, 2008). First, we performed a signed WGCNA using the merged datasets of AD (Jung et al., 2019; Kim et al., 2021). To describe this in detail, outliers of samples were eliminated by the hierarchical cluster method and the soft thresholding power (β) was calculated via scale-free topology analysis to a value of 10. Next, the adjacency matrix was converted into a topology overlap matrix to reflect the topology information on network formation. The modules were identified by the hierarchical cluster method and module eigengenes were calculated as summarized gene expression patterns of their respective modules. The modules were clustered with a minimum size of 30 genes. All modules were compared pair-wise, and pairs of modules showing high module eigengene correlations ($r > 0.80$) were merged. In order to find modules that showed correlations with cALD, module preservation analysis was conducted among the modules constructed from the AD dataset as the reference set and the merged cALD dataset as the test set (Langfelder et al., 2011). The evidence that a module is preserved is summarized by the Z-summary score, which was created by averaging the various preservation statistics of module robustness and reproducibility (Langfelder et al., 2011). All the above analyses were conducted in R (version 4.1.2).

Protein–protein interaction network analysis

The search tool for the retrieval of interacting genes/proteins (STRING[3].) was applied to investigate the connections between genes at the protein level (Szklarczyk et al., 2019). The STRING provides predictions of protein–protein interactions (PPIs) by taking a list of proteins as input, calculating confidence scores based on various evidence of interactions among proteins, and assigning uniform confidence scores to the same data set (Szklarczyk et al., 2019). The confidence level of the edge was adjusted to 0.7 and the nodes that were connected to fewer than two other nodes were deleted (Apostolakou et al., 2021). A PPI network constructed by STRING was visualized by cytoscape (version 3.9; Shannon et al., 2003). In the network, highly interconnected gene clusters were found by molecular complex detection (MCODE) with the cytoscape plugin (Bader and Hogue, 2003).

2 http://software.broadinstitute.org/gsea/msigdb

3 https://string-db.org/, version 11.5

Results

Data collection of cerebral adrenoleukodystrophy and Alzheimer's disease and identifying differentially expressed genes in cerebral adrenoleukodystrophy by meta-analysis

To conduct a meta-analysis that utilizes multiple datasets together, gene expression datasets were collected from EBI-arrayexpress that contained samples from healthy controls and patients (cALD or AD) who had not received any drug intervention. Only one RNA-seq dataset from cALD patients and three microarray datasets from cALD patients and control subjects were publicly available. One microarray dataset was obtained from the postmortem brains of control subjects and cALD patients. This dataset also included cerebral AMN (cAMN) patients since cAMN is a subtype that shows mild cerebral-specific symptoms of cALD. Two additional datasets were obtained from the samples of early passage cultures of iPSCs derived from the skin fibroblasts of control subjects and cALD patients. In total, 43 datasets were used for cALD (19 cALD and 24 control; Table 1). The AD microarray datasets were searched for in the same way as the cALD microarray datasets and five AD microarray datasets were selected. Four datasets were generated with postmortem brains and the other dataset produced by iPSCs-induced neurons. These neurons exhibited significantly higher levels of Aβ and phosphorylated tau, and thus mimicked a live AD patient's brain (Israel et al., 2012). In total, 534 data were obtained from control subjects and AD patients who did not receive treatment (231 AD and 313 control; Table 2).

Preprocessing was performed for each dataset and the datasets were merged based on the disease type. Batch effects, which are non-biological variants caused by two merged datasets, were removed using Combat function in the sva R package. The *Z*-scores of genes in the two merged datasets were calculated using GeneMeta R package (Johnson et al., 2006). In total, 636 cALD DEGs were screened by the cALD *Z*-scores and FDRs of the genes for GSEA ($|Z\text{-score}| > 0$ and FDR < 0.05; Figure 2A). Among cALD DEGs, 317 and 319 genes were up- and down-regulated, respectively.

Comparison of cerebral adrenoleukodystrophy and Alzheimer's disease patients' gene expression patterns

To determine whether cALD and AD have similar gene expression patterns in the brain, GSEA were conducted to examine two gene expression data sets from cALD and

TABLE 1 cALD dataset.

ArrayExpress ID	Source	Platform	Number of samples		
			*cALD	Control	Total
E-MEXP-3288	Postmortem brain	Affymetrix GeneChip Human Genome HG-U133A	11	13	24
E-GEOD-85804	*iPSCs	Illumina HumanHT-12 V4.0 expression beadchip	3	3	6
E-GEOD-34309	*iPSCs	Affymetrix Human Genome U133A 2.0 Array	5	8	13
			19	24	43

*iPSC, induced pluripotent stem cells; cALD, cerebral adrenoleukodystrophy.

TABLE 2 AD dataset.

ArrayExpress ID	Source	Platform	Number of samples		
			*AD	Control	Total
E-GEOD-36980	Postmortem brain	Affymetrix Human Gene 1.0 ST Array	32	47	79
E-GEOD-5281	Postmortem brain	Affymetrix Human Genome U133 Plus 2.0 Array	87	74	161
E-GEOD-29378	Postmortem brain	Illumina HumanHT-12 V3.0 expression beadchip	17	16	33
E-GEOD-48350	Postmortem brain	Affymetrix Human Genome U133 Plus 2.0 Array	80	173	253
E-GEOD-34879	*iPSC-induced neurons	Illumina HumanHT-12 V4.0 expression beadchip	15	2	17
			231	312	543

*iPSC, induced pluripotent stem cells; AD, Alzheimer's disease.

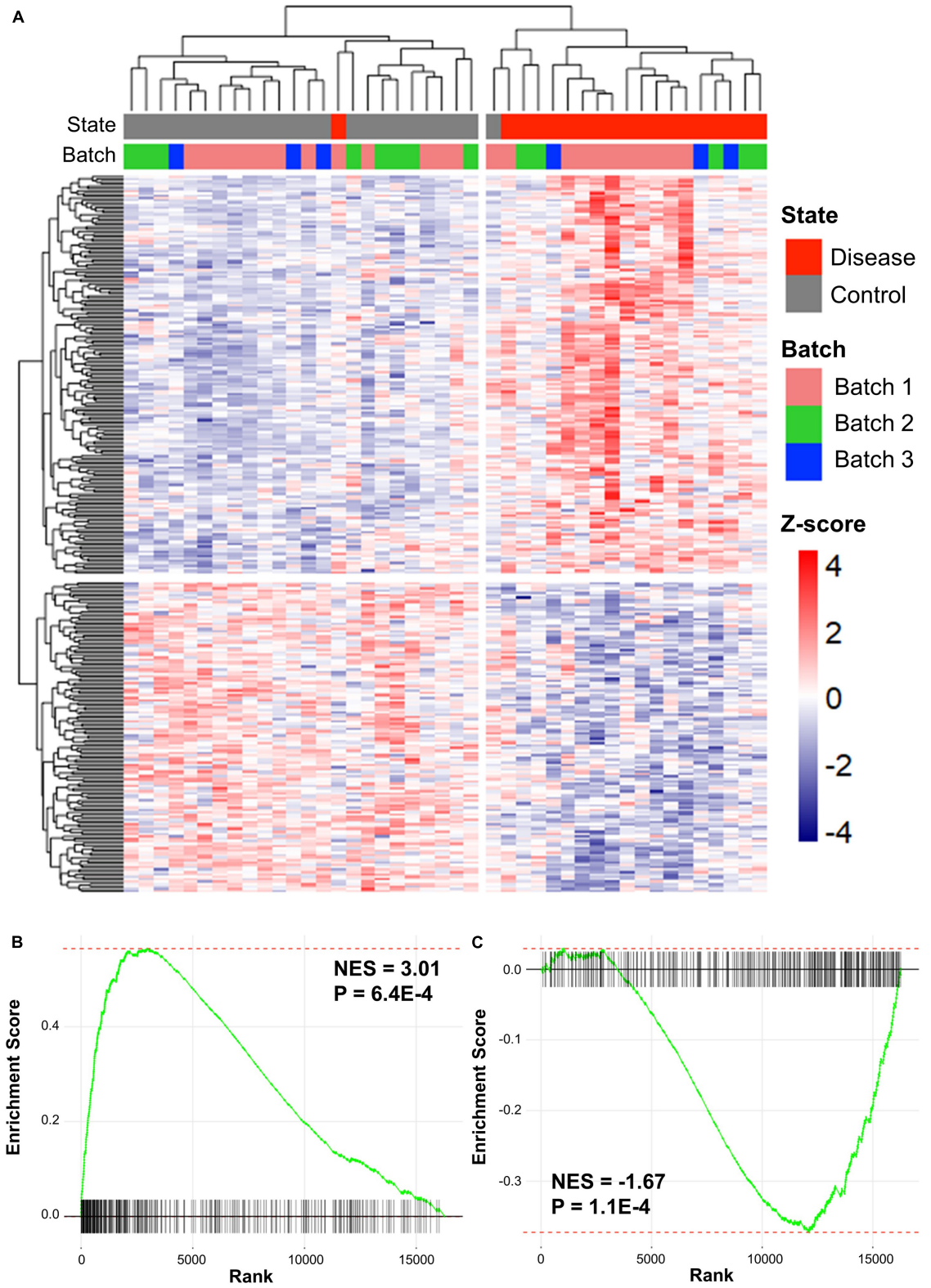

FIGURE 2
Clustered results of DEGs and GSEA plots of cALD and AD. **(A)** Heatmap showing expression patterns of DEGs in cALD (FDR < 0.05). The disease states of individuals are shown as red and gray bars, and the batch represents the three datasets of cALD as green, blue, and pink bars above the heatmap. The color inside the heatmap shows the *Z*-score of cALD. GSEA plot comparing the expression of the AD dataset to DEGs that were significantly up-regulated **(B)** and down-regulated **(C)** in cALD. The normalized enrichment score (NES) indicates the degree to which DEGs of cALD were overexpressed at the top or bottom of ranked expression in the AD dataset.

AD. GSEA is a gene rank-based analysis method extensively used in meta-analysis when evaluating two gene expression datasets. Therefore, GSEA was utilized to observe whether the expression of the cALD dataset was similar to that of the AD dataset (Subramanian et al., 2005). The *Z*-scores of the entire AD dataset (16,265 genes) were ranked from highest to lowest and then up- and down-regulated DEGs in cALD were examined to place them in the ordered gene list of AD. Using GSEA, the normalized enrichment scores (NES) of DEGs in cALD were calculated from the *Z*-scores of the same DEGs obtained from the AD gene list. The NES value increases when the DEG in cALD is ranked high in AD data and *vice versa*. The GSEA results showed that both up- and down-regulated DEGs were positively and negatively enriched with p-values < 0.05 (up-regulated DEGs: NES = 3.01 and p-value = 6.4×10^{-4} and down-regulated DEGs: NES = -1.67 and p-value = 1.1×10^{-4}; **Figures 2B,C** (Subramanian et al., 2005). The leading-edge genes are key genes that contribute to the NES, which are considered shared DEGs in two diseases (Subramanian et al., 2005). We identified 144 and 122 up- and down-leading-edge genes in cALD and AD via GSEA (**Supplementary Table 1**). The GSEA results indicate that cALD and AD have similar gene expression patterns with significant NES and leading-edge genes.

Identification of co-expressed gene modules in cerebral adrenoleukodystrophy and Alzheimer's disease by weighted gene correlation network analysis

WGCNA was conducted to comprehend the gene expression profile that is applicable in cALD from interconnected genes in AD. WGCNA provides network topology information and modules that indicate correlated gene sets by performing correlation network analysis on a high-dimensional dataset. We constructed a correlation weighted network of the AD dataset with preserved sign information of gene expression. Eight modules (black, blue, green, magenta, orange, pink, purple, and red) were detected by constructing a network of AD (**Figure 3A**). To identify applicable modules in cALD, we performed module preservation analysis using AD modules and the cALD dataset. Preservation median rank and *Z*-summary scores were obtained from preservation analysis and the scores were considered to have strong, weak-to-moderate, or little-or-no preservation when the score was > 10, 2–10, or < 2, respectively (Langfelder et al., 2011). The green and orange modules were highly preserved in the cALD dataset (green: 12 and orange: 14) and the other modules were moderately preserved in the cALD dataset (blue: 10; black: 7.2; magenta: 5.6; purple: 5.4; gold: 5.1; pink: 3.3; red: 2.0; **Figures 3B,C**). The Pearson correlation coefficients of both disease states and batches in the cALD dataset were calculated with the module eigengenes, which contains the expression profile of each module (**Figure 3D**). The p-value of the correlation coefficient indicates whether the correlation coefficient is significantly different from 0. The green and orange modules were considered significantly different in gene expression between the control and patient groups (green: r = 0.59 and $P = 3 \times 10^{-5}$; orange: r = -0.39 and $P = 0.01$) and the number of genes in the two modules were 652 and 834, respectively. The results of WGCNA indicated that the green and orange modules were important for the causal genetic relationship between cALD and AD.

Preservation module related to immune process and cell death

In order to gain insights into the biological processes of the cALD-related preserved modules, functional annotation was performed using GSEA with gene ontology biological process gene sets. We performed gene annotation with biological process of gene ontology using green and orange modules and screened biological processes at $P < 0.01$. There were 24 and 53 biological processes that met the criteria of $P < 0.01$ in gene annotation of the green and orange modules, respectively. Biological processes were ordered by NES of overlapped genes between annotated modules and the genes constituting individual biological processes. In the orange module, the top 12 enriched biological processes were myeloid leukocyte activation (NES = 2.03 and $P < 0.001$), vascular process in circulatory system (NES = 1.92 and $P = 2.0 \times 10^{-3}$), positive regulation of anion transport (NES = 1.89 and $P < 0.001$), myeloid leukocyte-mediated immunity (NES = 1.86 and $P < 0.001$), cell activation (NES = 1.86 and $P < 0.001$), nuclear transport (NES = 1.84 and $P < 0.001$), receptor-mediated endocytosis (NES = 1.84 and $P = 4.3 \times 10^{-3}$), protein localization to nucleus (NES = 1.82 and $P = 6.8 \times 10^{-3}$), negative regulation of immune system process (NES = 1.78 and $P = 6.8 \times 10^{-3}$), immune effector process (NES = 1.78 and $P = 2.3 \times 10^{-3}$), cell activation involved in immune response (NES = 1.77 and $P < 0.001$), and leukocyte-mediated immunity (NES = 1.76 and $P < 0.001$; **Figure 4A**). In the green module, the top 12 enriched biological processes were blood vessel morphogenesis (NES = 2.28 and $P < 0.001$), anatomical structure formation involved in morphogenesis (NES = 2.22 and $P < 0.001$), vasculature development (NES = 2.21 and $P < 0.001$), circulatory system development (NES = 2.14 and $P < 0.001$), tube morphogenesis (NES = 2.13 and $P < 0.001$), regulation of vasculature development (NES = 2.00 and $P < 0.001$), tube development (NES = 1.98 and $P < 0.001$), regulation of multicellular organismal development (NES = 1.97 and $P < 0.001$), regulation of cellular component movement (NES = 1.97 and $P < 0.001$),

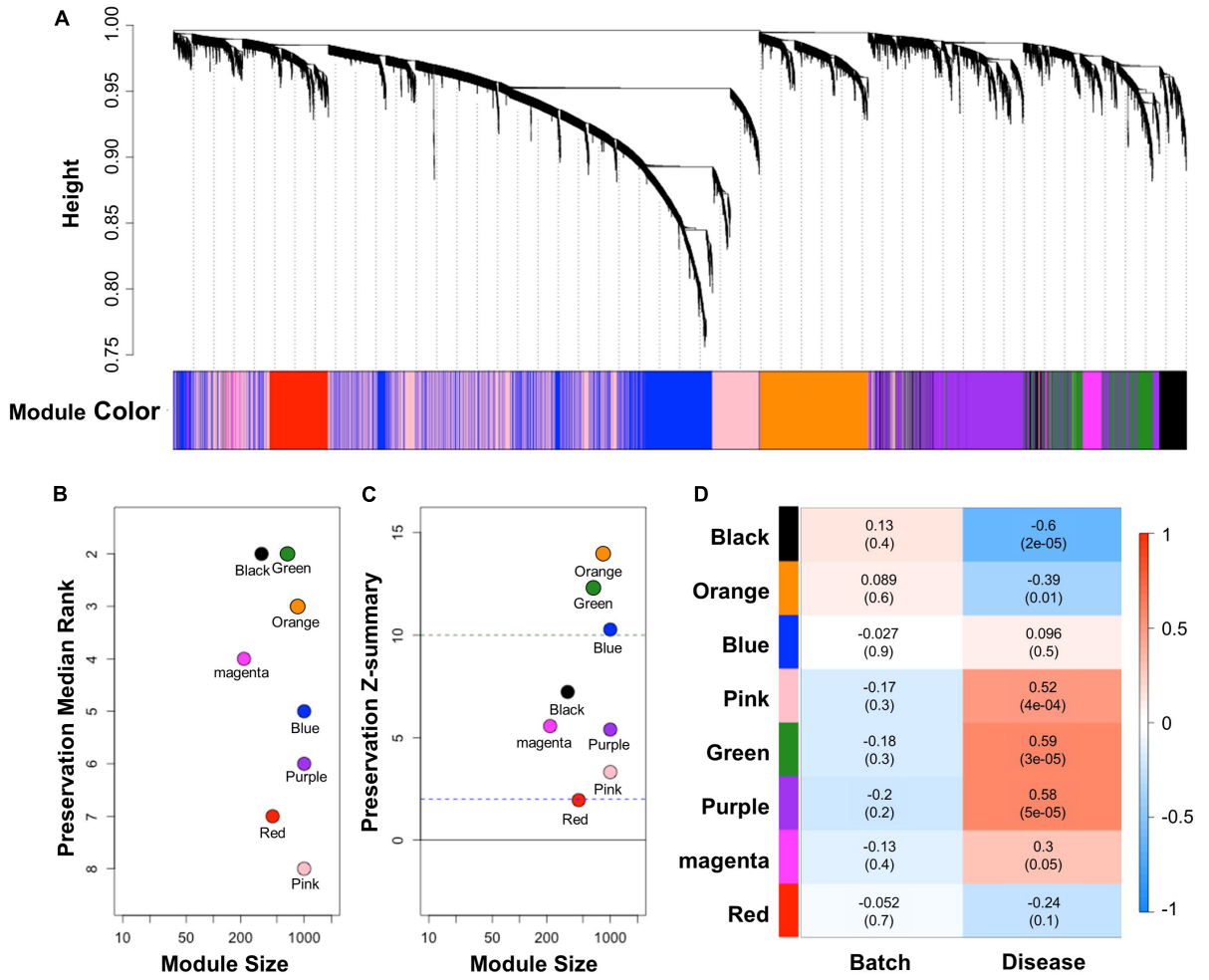

FIGURE 3
Results of WGCNA and module preservation analysis. **(A)** Dendrogram showing the modules obtained from the signed network based on the dissimilarity of the topology overlap matrix of the AD modules. A total of eight modules were clustered and are represented by color. The modules were sorted by their respective module size and aligned by preservation median rank **(B)** and preservation *Z*-summary score **(C)** against cALD data. The dashed line at 10 indicates a strong preservation threshold, whereas the dashed line at 2 indicates no preservation threshold. **(D)** Matrix showing the correlation of characteristics of the samples in the merged cALD dataset and the genes in the modules. The numbers in parentheses are their respective *p*-values.

muscle system process (NES = 1.97 and $P < 0.001$), positive regulation of multicellular organismal process (NES = 1.96 and $P < 0.001$), and apoptotic signaling pathway (NES = 1.97 and $P < 0.001$; **Figure 4B**).

As a result of functional annotation of the orange module, immune effector process, inflammatory response (NES = 1.74 and $P = 2.0 \times 10^{-3}$), and the regulation of immune system process (NES = 1.65 and $P = 2.0 \times 10^{-3}$) were immune-related pathways related to the pathogenesis of both diseases (**Figures 4C–E**). The green module was enriched with cell death-related processes including the apoptotic signaling pathway and the regulation of cell death (NES = 1.92 and $P < 0.001$). In addition, mitogen-activated protein kinase (MAPK) activity (NES = 1.91 and $P = 2.0 \times 10^{-3}$), which was involved in inflammation and cell death, was also enriched in the green module (**Figures 4F–H**). Although the role of the MAPK pathway in cALD has not been thoroughly revealed, it is known to regulate several cellular processes including development, apoptosis, and inflammation in AD (Cui et al., 2013; Thei et al., 2018).

Identification hub-genes of cerebral adrenoleukodystrophy and Alzheimer's disease by protein–protein interactionnetwork analysis

To identify hub-genes that affect the pathogenesis of cALD and AD, we conducted PPI network analysis by

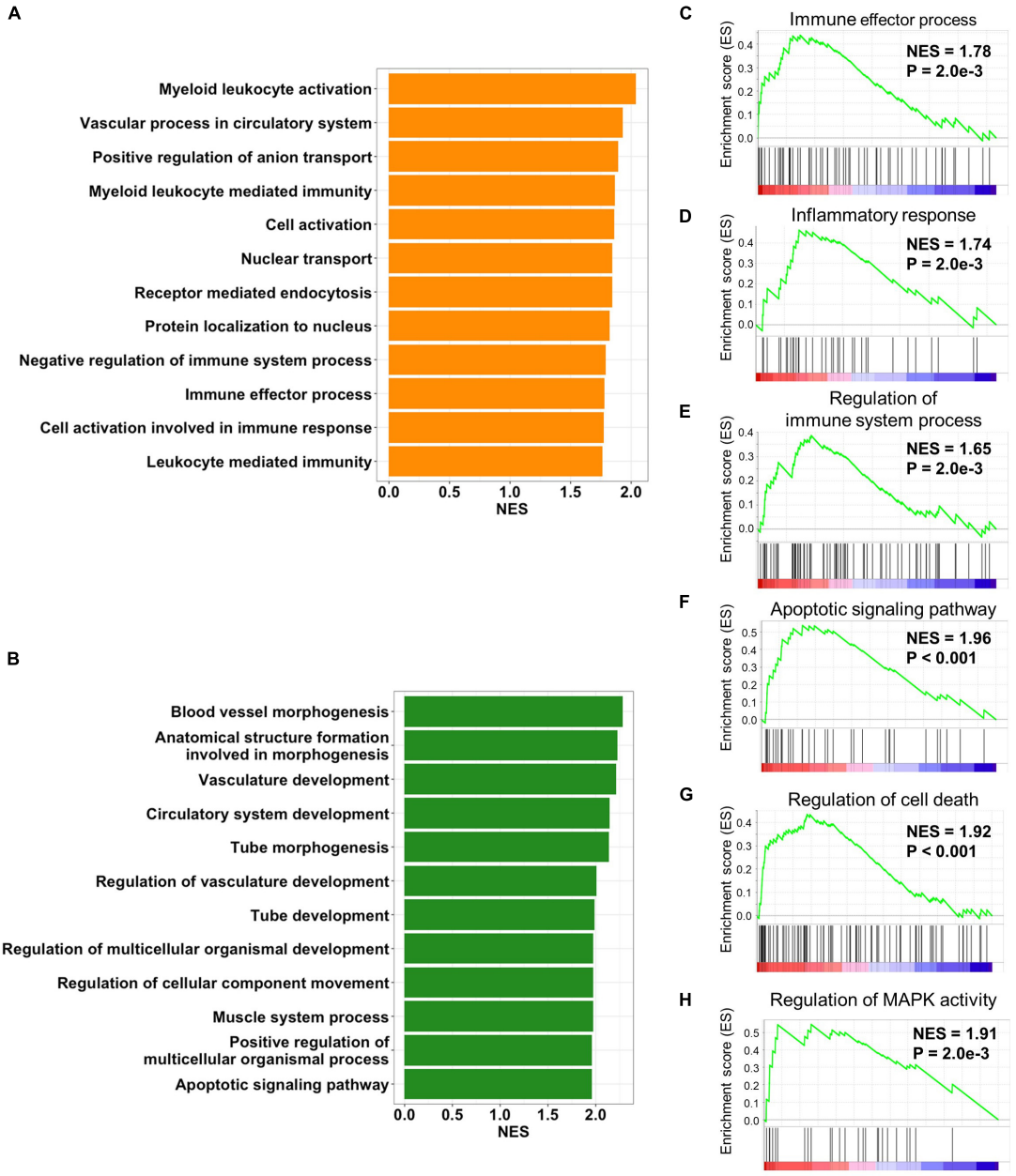

FIGURE 4
Biological processes of preserved modules. Bar plots represent *p*-values of biological process of gene ontology from **(A)** orange and **(B)** green modules. The top 12 biological processes with the most overlapped genes between the annotated gene list and module genes are displayed. The orange module was positively enriched with **(C)** the immune effector process, **(D)** inflammatory response, and **(E)** regulation of the immune system process. The green module was positively enriched with **(F)** the regulation of MAPK activity, **(G)** the regulation of cell death, and **(H)** the apoptotic signaling pathway.

STRING to discover the connection of genes at the protein level. STRING provides interaction information between gene-encoded proteins using a network that contains proteins' structural and functional information. The numbers of genes in the green and orange modules were reduced to 167 based on | *Z*-score| > 2 in cALD and AD (Bai et al., 2020). In addition, we obtained 38 genes that correspond to relevance score > 2 in cALD from the GeneCards[4] to identify how the selected genes interact with the known cALD genes, of which 19 genes overlapped (**Supplementary Table 2**; Rappaport et al., 2017). As described above, PPI network analysis was

4 www.genecards.org/

conducted using 186 genes composed of module genes and known cALD genes (**Figure 4A**). The entire PPI network was formed by 106 genes excluding unlinked genes, and the *p*-value was calculated as 2.22×10^{-16}. The *p*-value suggested that the analyzed genes have statistically higher interactions and shared more biologically significant links than a random geneset of the same size and linkage distribution (**Figure 5A**). *apolipoprotein E* (*APOE*; cALD *Z*-score = 2.97 and AD *Z*-score = 2.07) and *ATP binding cassette subfamily A member 1* (*ABCA1*) genes served as bridges between cALD-related genes and the module genes. *ABCA1* (cALD *Z*-score = 3.86 and AD *Z*-score = 5.05) was a leading-edge gene in this study.

We then utilized MCODE to detect highly interconnected genes—called hub-genes—as clusters based on the topology of the constructed PPI network (**Supplementary Table 3**). *APOE* was identified as a seed node around which the remaining eight genes, namely *annexin A5* (*ANXA5*), *beta-2-microglobulin* (*B2M*), *C-C motif chemokine ligand 2* (*CCL2*), *CD44 molecule* (*CD44*), *fibroblast growth factor 2* (*FGF2*), *syndecan 1* (*SDC1*), *syndecan 4* (*SDC4*), and *signal transducer and activator of transcription 3* (*STAT3*) were clustered. *APOE* is a well-known major genetic risk factor for late-onset AD. Even though the correlation between *APOE* and cALD pathogenesis has not been completely revealed, a recent proteomic study on the cerebrospinal fluid of active cALD patients showed that APOE is an inflammatory marker for the disease (Orchard et al., 2019). The hub-genes were highly interconnected among themselves and were also connected with other gene networks of the green and orange modules (**Figures 5B,C**). The distinction between control subjects and cALD patients in RNA-seq data were validated from the expression of hub-genes via principal component analysis (PCA; **Supplementary Figure 1**). This confirms that the hub-genes of cALD and AD were reliably discovered in this study.

To identify genes that have robust associations with the pathogenesis of diseases, four core genes—*B2M*, *CD44*, *FGF2*, and *ANXA5*—were selected from the hub-genes that overlapped with the GSEA results. Among the biological processes we discovered (**Figures 4C–H**), core genes were closely related to inflammation and apoptosis. *B2M* (cALD *Z*-score = 3.81 and AD *Z*-score = 5.35) serves as an inflammatory marker in the CNS (Liu et al., 2014; Topçiu-Shufta et al., 2016), and *CD44* (cALD *Z*-score = 4.67 and AD *Z*-score = 4.96) is positively correlated with apoptosis and inflammation by regulating cytokine expression (McKallip et al., 2002). *FGF2* (cALD *Z*-score = 3.58 and AD *Z*-score = 6.10) increased susceptibility to oxidative stress that induces neuronal cell death in astrocytes. The level of *ANXA5* (cALD *Z*-score = 2.98 and AD *Z*-score = 4.79), which is associated with familial late-onset AD from whole exome sequencing, in the cerebrospinal fluid of AD patients increased proportionally with the severity of the disease state as Aβ accumulates, playing a protective role against Aβ toxicity (Zhang et al., 2019; Bartolome et al., 2020).

Discussion

In-silico approaches can be applied as tools to expand our understanding of diseases and suggest new therapeutic targets, which may reduce the time spent on laborious and time-consuming pre-screening processes. Meta-analyses combine multiple studies to increase both the sample size and statistical power and can particularly be effective when studying rare diseases as they usually consist of studies with small samples (Bradburn et al., 2007). cALD is a rare disease characterized by complex metabolic disorders in the cerebral and adrenal cortexes, the exact pathogenesis and molecular mechanisms of which remain unclear due to the near absence of data. Currently available treatment options include, but are not limited to, medication for relieving stiffness and seizures, Lorenzo's oil (Moser et al., 1992), and stem cell transplantation (Cartier et al., 2009). In order to develop novel therapeutic options, a deeper understanding of the disease is required by overcoming the problem of data insufficiency (Berger et al., 2014). In comparison, numerous studies have been conducted because of the worldwide prevalence of AD, resulting in the discovery of various novel pathogenic mechanisms and treatments. Based on the fact that both diseases are NDs and share a common remedy (erucic acid), the purpose of this study was to utilize the large amount of data on AD to discover new pathological targets for cALD. Therefore, we analyzed the expression profiles and co-expression network of cALD and AD in parallel based on meta-analyses and revealed that the two diseases share distinct gene expressions, leading to the discovery of novel genes that may affect the pathogenesis of cALD (**Figure 1**).

To conduct our meta-analysis, we first constructed individual datasets for cALD and AD. As far as we know, other than one RNA-seq data obtained from iPSC-induced endothelial cells from cALD patients that we used for validation, only one microarray data composed of postmortem brain samples from cALD was available in the public database (**Table 1**). To increase the quantity of data and to estimate the disease state of the brain closer to its living state (Manchia et al., 2017), we used gene expression profiles of iPSCs from cALD patients. Wang et al. reported the suggestible transcriptome-level coherence between iPSCs of cALD patients and the known pathogenetic characteristics of cALD, including neuro-inflammation and peroxisome abundance (2012). One pathogenetic hypothesis of cALD includes that mutation in *ABCD1* gene impacts the endothelia of the brain microvasculature, leading to inflammatory demyelination in the brain (Lauer et al., 2017). Gene mutations promote the accumulation of VLCFA, oxidative stress, and cell death

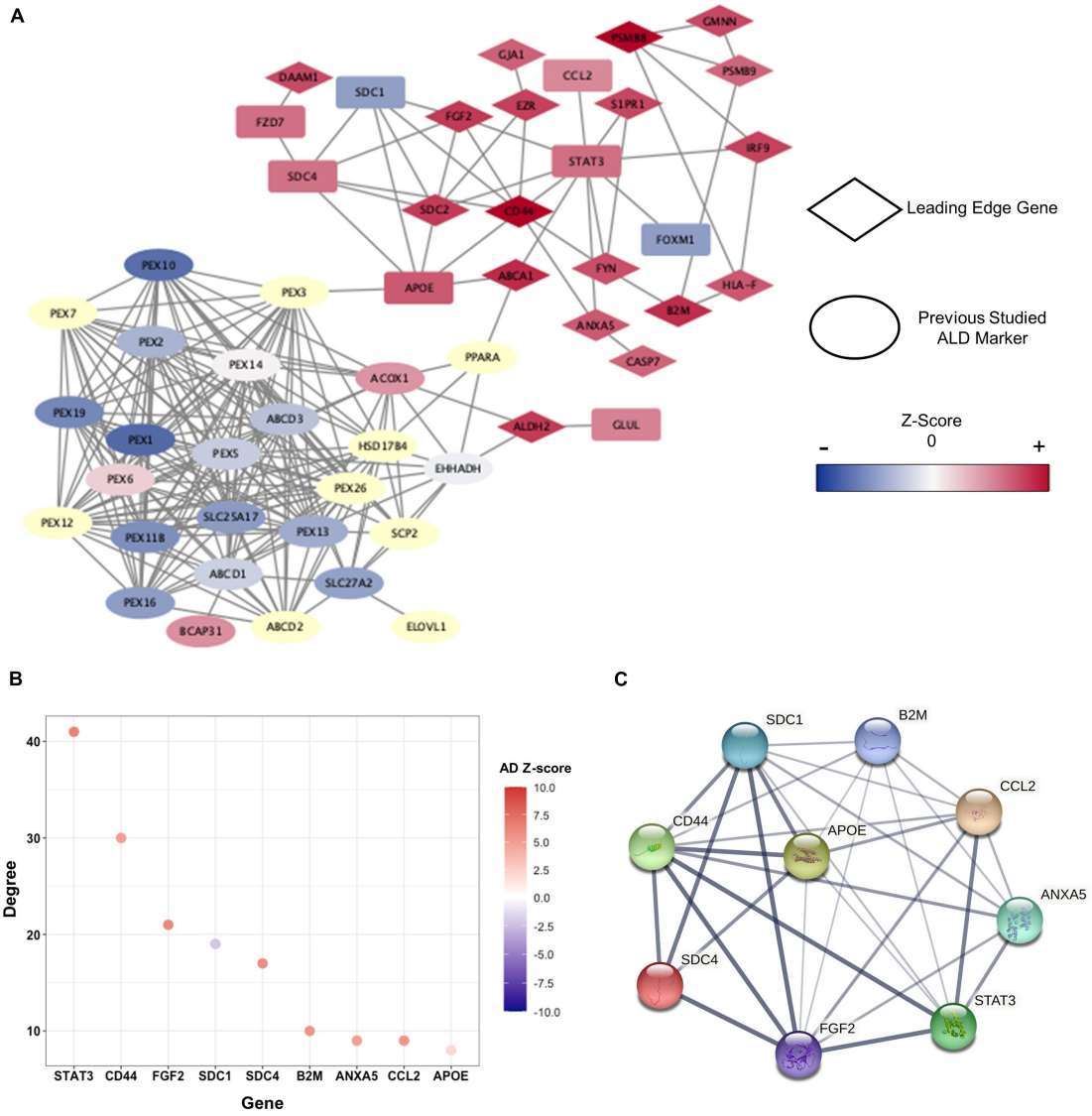

FIGURE 5
Clusters within the PPI network and characteristics of hub-genes. **(A)** PPI network presented by cALD-related genes and genes of $|Z\text{-score}| > 2$ in cALD and AD among green and orange modules. The leading-edge genes are indicated by rhombi, and previously studied cALD marker genes are indicated by ellipses. The range of *Z*-score values in the cALD dataset of the nodes is represented by a color bar at the right. The undetected genes in the microarray are shown as pale-yellow nodes and were not used in meta-analysis. **(B)** The degree of hub-genes was obtained using green and orange modules. The degree of each node represents the total number of connections to other nodes in a network, and the colors of dots represent *Z*-scores of AD. **(C)** Protein interaction among hub-genes clustered around APOE. The thickness of the connected lines represents the strength of correlation between two hub-genes.

(Wiesinger et al., 2013). Since this study was mainly focused on the neuronal pathophysiology of cALD, the RNA-seq dataset of iPSC-induced endothelial cells was excluded from the meta-analysis and only used as a validation dataset. In addition, the cALD-related genes provided by the GeneCards were used to validate the results of WGCNA conducted in this study by utilizing the results of previous studies. Among cALD-related genes, genes without *Z*-scores for cALD and AD were not detected or designed to be undetected in at least one cALD microarray dataset (**Supplementary Table 2**). Even after adding these data, the insufficiencies remained in the cALD data.

There are abundant RNA-seq and microarray data on AD brains; however, there are almost no publicly available data obtained from live brains as far as we know. Most data were generated using postmortem brains due to the special nature of the brain itself. The iPSC-induced neuron dataset from AD patients showed conforming biological characteristics with the

original neurons of AD patients (**Table 2**; Almeida et al., 2013; Chen et al., 2013). Therefore, the aforementioned dataset was included when constructing a combined gene expression matrix for AD in this study. There was much less RNA-seq AD data than that of the microarray dataset, consisting of 71 patients and 87 controls, which is less than one-third of the microarray dataset in this study (**Supplementary Table 4**). The merged data including an AD RNA-seq dataset had even fewer genes than the AD microarray dataset. In order to minimize the loss of genes that may provide potential signatures, merged data were constructed with only microarray platforms.

After data preparation, two statistically powerful approaches (GSEA and WGCNA) based on meta-analysis were performed to investigate the sharing transcriptomic aspects of cALD and AD. Gene set-level correlation analysis between cALD and AD was performed using GSEA, which suggested 144 up- and 122 down-regulated leading-edge genes that can be regarded as key driver genes in the shared genetic mechanisms (**Figure 2**). To simultaneously consider the co-expression structure of cALD and AD, WGCNA was conducted by constructing a gene network (**Figure 3A**). Among the eight modules identified in AD data, the network connectivity and correlation structures of the green and orange modules were conserved and significantly correlated with the disease state of cALD (Z-summary score > 10 and $P < 0.05$), which suggests a shared co-expression structure between cALD and AD (**Figure 3**). Among the significantly enriched biological pathways from both cALD and AD, immune response and cell death are known to occur via oxidative stress associated with the MAPK signaling pathway in AD (**Figure 4**; Kamat et al., 2014). Most biological processes of functional annotation were related to the pathogenesis of cALD and AD; the results suggested that most functional annotation results were in line with previous studies. The accumulation of VLCFA is reported to be the key contributor to oxidative stress in cALD, where excessive oxidative stress causes neuro-inflammation and eventually leads to the apoptosis of neuronal cells in cALD and AD (Behl, 1999; Berger et al., 2014). Even though the role of MAPK signaling pathway was not clearly revealed in cALD, the MAPK pathway may be suggested as an intermediating mechanism between oxidative stress and immune response and/or cell death considering the pathway-level similarity of cALD and AD.

Through systemic analysis of the PPI network, nine hub-genes were identified, led by *APOE* as the seed node of the cluster (**Figure 5**). APOE is a lipid transport protein that regulates the lipid metabolism, oxidative stress, neurite outgrowth, and the mitochondrial metabolism (Orchard et al., 2019). As the association between *APOE* and AD has been well-established for decades, the APOE's role as a potential biomarker for cALD has been recently proposed (Orchard et al., 2019). Considering the statistical significance from GSEA and WGCNA along with network topology from the PPI network analysis, *B2M*, *CD44*, *FGF2*, and *ANXA5* were identified as core genes. In accordance with the result from the functional enrichment analysis of WGCNA modules, the core genes were related to inflammation, apoptosis, and MAPK in AD. In detail, B2M plays a critical role in inflammation and apoptosis and has been demonstrated to induce cognitive impairment in AD (Topçiu-Shufta et al., 2016; Zhong et al., 2020). *CD44* encodes cell-surface glycoproteins involved in cell–cell and cell–extracellular matrix interaction, where its expression on immune cells is known to regulate inflammation and apoptosis in CNS (McKallip et al., 2002). By contributing to a variety of biological activities, FGF2 plays significant role in apoptosis and differentiation in CNS and can activate the MAPK pathway (Liu et al., 2014). While four core genes were reported as the causal genetic risk factors for AD, the expression level of *ANXA5* is known to have a negative correlation with AD risk. *ANXA5* encodes protein that has inhibitory effects on inflammation and early apoptosis, contributing to tissue homeostasis (Bartolome et al., 2020). Despite the insufficient evidence explaining the pathological roles of these four core genes in cALD, the results of this study showed the potential of the core genes as the biomarker candidates for cALD. We finally suggested the four genes as novel targets for cALD as they are closely related to the common pathological phenotypes of cALD and AD.

In conclusion, the knowledge on pathological mechanisms and genes of cALD was successfully expanded through combination of the results of GSEA and WGCNA using AD datasets based on meta-analysis. The study showed the shared pathway between cALD and AD, finally determining the novel target genes of cALD. These findings can help fill in gaps in previously unknown pathways in cALD, which were found through two main approaches: increasing sample sizes for cALD and comparing the gene expression patterns of cALD with a disease with a higher prevalence and some common features, AD. The putative gene markers can potentially be applied not only to therapeutic targets or genetic diagnosis, but also to the potential drug repositioning for cALD, which is further augmented by rapid study on AD (Ashburn and Thor, 2004). To the best of our knowledge, this is the first meta-analysis to discover genetic similarities and common pathological factors derived from the correlation between cALD and AD. Because this study was conducted using *in silico* analyses, rigorous validation through functional studies might be necessary. Despite this limitation, this research demonstrated an approach for studying pathologically relevant diseases by deriving novel biological meaning of a very rare disease, which suggests a potential extension for various approaches.

Data availability statement

The datasets presented in this study are included in the article/**Supplementary material**,

further inquiries can be directed to the corresponding author.

Author contributions

YS devised this study and conducted *in silico* analysis. YS and MKS wrote the manuscript. JJ, BK, and WJ supervised the research. WJ edited and gave final approval of the manuscript. All authors contributed to the article and approved the submitted version.

Funding

This work was supported by the National Research Foundation of Korea (NRF) grant funded by the Korea government (MSIT; No. NRF-2021R1A2C1008804).

Acknowledgments

We thank Byungjo Lee, Jaeseung Song, Hyeon Jun Yoon, Youngtae Won, and Yeonbin Jeong for their comments in editing the draft.

Conflict of interest

BK is employed by BPgene.

The remaining authors declare that the research was conducted in the absence of any commercial or financial relationships that could be construed as a potential conflict of interest.

Publisher's note

All claims expressed in this article are solely those of the authors and do not necessarily represent those of their affiliated organizations, or those of the publisher, the editors and the reviewers. Any product that may be evaluated in this article, or claim that may be made by its manufacturer, is not guaranteed or endorsed by the publisher.

Supplementary material

The Supplementary Material for this article can be found online at: https://www.frontiersin.org/articles/10.3389/fnmol.2022.996698/full#supplementary-material

References

Almeida, S., Gascon, E., Tran, H., Chou, H. J., Gendron, T. F., DeGroot, S., et al. (2013). Modeling key pathological features of frontotemporal dementia with C9ORF72 repeat expansion in iPSC-derived human neurons. *Acta Neuropathol.* 126, 385–399. doi: 10.1007/s00401-013-1149-y

Altinoz, M. A., Bilir, A., and Elmaci, I. (2018). Erucic acid, a component of Lorenzo's oil and PPAR-δ ligand modifies C6 glioma growth and toxicity of doxorubicin. Experimental data and a comprehensive literature analysis. *Chem. Biol. Interact.* 294, 107–117. doi: 10.1016/j.cbi.2018.08.024

Altinoz, M. A., and Ozpinar, A. (2019). PPAR-δ and erucic acid in multiple sclerosis and Alzheimer's disease. Likely benefits in terms of immunity and metabolism. *Int. Immunopharmacol.* 69, 245–256. doi: 10.1016/j.intimp.2019.01.057

Alzheimer's Association. (2019). 2019 Alzheimer's disease facts and figures. *Alzheimers Dement.* 15, 321–387. doi: 10.1016/J.JALZ.2019.01.010

Alzheimer's Association. (2021). 2021 Alzheimer's disease facts and figures. *Alzheimers Dement.* 17, 327–406. doi: 10.1002/ALZ.12328

Apostolakou, A. E., Sula, X. K., Nastou, K. C., Nasi, G. I., and Iconomidou, V. A. (2021). Exploring the conservation of Alzheimer-related pathways between *H. sapiens* and *C. elegans*: A network alignment approach. *Sci. Rep.* 11, 1–11. doi: 10.1038/s41598-021-83892-9

Ashburn, T. T., and Thor, K. B. (2004). Drug repositioning: Identifying and developing new uses for existing drugs. *Nat. Rev. Drug Discov.* 3, 673–683. doi: 10.1038/nrd1468

Bader, G. D., and Hogue, C. W. V. (2003). An automated method for finding molecular complexes in large protein interaction networks. *BMC Bioinform.* 4:2. doi: 10.1186/1471-2105-4-2/FIGURES/12

Bai, B., Wang, X., Li, Y., Chen, P. C., Yu, K., Dey, K. K., et al. (2020). Deep multilayer brain proteomics identifies molecular networks in Alzheimer's disease progression. *Neuron* 105, 975–991.e7. doi: 10.1016/J.NEURON.2019.12.015

Bartolome, F., Krzyzanowska, A., de la Cueva, M., Pascual, C., Antequera, D., Spuch, C., et al. (2020). Annexin A5 prevents amyloid-β-induced toxicity in choroid plexus: Implication for Alzheimer's disease. *Sci. Rep.* 10:9391. doi: 10.1038/s41598-020-66177-5

Behl, C. (1999). Alzheimer's disease and oxidative stress: implications for novel therapeutic approaches. *Prog. Neurobiol.* 57, 301–323. doi: 10.1016/S0301-0082(98)00055-0

Berchtold, N. C., Coleman, P. D., Cribbs, D. H., Rogers, J., Gillen, D. L., and Cotman, C. W. (2013). Synaptic genes are extensively downregulated across multiple brain regions in normal human aging and Alzheimer's disease. *Neurobiol. Aging* 34, 1653–1661. doi: 10.1016/j.neurobiolaging.2012.11.024

Berger, J., Forss-Petter, S., and Eichler, F. S. (2014). Pathophysiology of X-linked adrenoleukodystrophy. *Biochimie* 98, 135–142. doi: 10.1016/j.biochi.2013.11.023

Bottero, V., Alrafati, F., Santiago, J. A., and Potashkin, J. A. (2021). Transcriptomic and network meta-analysis of frontotemporal dementias. *Front. Mol. Neurosci.* 14:239. doi: 10.3389/FNMOL.2021.747798/BIBTEX

Bradburn, M. J., Deeks, J. J., Berlin, J. A., and Localio, A. R. (2007). Much ado about nothing: A comparison of the performance of meta-analytical methods with rare events. *Stat. Med.* 26, 53–77. doi: 10.1002/sim.2528

Cartier, N., Hacein-Bey-Abina, S., Bartholomae, C. C., Veres, G., Schmidt, M., Kutschera, I., et al. (2009). Hematopoietic stem cell gene therapy with a lentiviral vector in X-linked adrenoleukodystrophy. *Science* 326, 818–823. doi: 10.1126/science.1171242

Chen, J., Lin, M., Foxe, J. J., Pedrosa, E., Hrabovsky, A., Carroll, R., et al. (2013). Transcriptome comparison of human neurons generated using induced pluripotent stem cells derived from dental pulp and skin fibroblasts. *PLoS One* 8:e75682. doi: 10.1371/journal.pone.0075682

Choi, J. K., Yu, U., Kim, S., and Yoo, O. J. (2003). Combining multiple microarray studies and modeling interstudy variation. *Bioinformatics* 19(Suppl. 1), 84–90. doi: 10.1093/bioinformatics/btg1010

Crous-Bou, M., Minguillón, C., Gramunt, N., and Molinuevo, J. L. (2017). Alzheimer's disease prevention: From risk factors to early intervention. *Alzheimers Res. Ther.* 9:71. doi: 10.1186/s13195-017-0297-z

Cui, H., Freeman, C., Jacobson, G. A., and Small, D. H. (2013). Proteoglycans in the central nervous system: Role in development, neural repair, and Alzheimer's disease. *IUBMB Life* 65, 108–120. doi: 10.1002/IUB.1118

Engelen, M., Kemp, S., and Poll-The, B. T. (2014). X-linked adrenoleukodystrophy: Pathogenesis and treatment. *Curr. Neurol. Neurosci. Rep.* 14, 1–8. doi: 10.1007/s11910-014-0486-0

Fourcade, S., López-Erauskin, J., Galino, J., Duval, C., Naudi, A., Jove, M., et al. (2008). Early oxidative damage underlying neurodegeneration in X-adrenoleukodystrophy. *Hum. Mol. Genet.* 17, 1762–1773. doi: 10.1093/hmg/ddn085

Goh, K.-I., Cusick, M. E., Valle, D., Childs, B., Vidal, M., and Szló Barabá, A.-L. (2007). *The human disease network*. Available online at: www.pnas.org/cgi/content/full/ (accessed February 24, 2022).

Hokama, M., Oka, S., Leon, J., Ninomiya, T., Honda, H., Sasaki, K., et al. (2014). Altered expression of diabetes-related genes in Alzheimer's disease brains: The Hisayama study. *Cereb. Cortex* 24, 2476–2488. doi: 10.1093/cercor/bht101

Hou, Y., Dan, X., Babbar, M., Wei, Y., Hasselbalch, S. G., Croteau, D. L., et al. (2019). Ageing as a risk factor for neurodegenerative disease. *Nat. Rev. Neurol.* 15, 565–581. doi: 10.1038/s41582-019-0244-7

Israel, M. A., Yuan, S. H., Bardy, C., Reyna, S. M., Mu, Y., Herrera, C., et al. (2012). Probing sporadic and familial Alzheimer's disease using induced pluripotent stem cells. *Nature* 482, 216–220. doi: 10.1038/nature10821

Jang, J., Park, S., Jin Hur, H., Cho, H. J., Hwang, I., Pyo Kang, Y., et al. (2016). 25-hydroxycholesterol contributes to cerebral inflammation of X-linked adrenoleukodystrophy through activation of the NLRP3 inflammasome. *Nat. Commun.* 7:13129. doi: 10.1038/ncomms13129

Johnson, W. E., Li, C., and Rabinovic, A. (2006). Adjusting batch effects in microarray expression data using empirical Bayes methods. *Biostatistics* 8, 118–127. doi: 10.1093/biostatistics/kxj037

Jung, J., Hah, K., Lee, W., and Jang, W. (2017). Meta-analysis of microarray datasets for the risk assessment of coplanar polychlorinated biphenyl 77 (PCB77) on human health. *Toxicol. Environ. Health Sci.* 9, 161–168. doi: 10.1007/s13530-017-0317-1

Jung, J., Kim, G. W., Lee, B., Joo, J. W. J., and Jang, W. (2019). Integrative genomic and transcriptomic analysis of genetic markers in Dupuytren's disease. *BMC Med. Genomics* 12:98. doi: 10.1186/s12920-019-0518-3

Jung, J., Kim, G. W., Lee, W., Mok, C., Chung, S. H., and Jang, W. (2018). Meta- and cross-species analyses of insulin resistance based on gene expression datasets in human white adipose tissues. *Sci. Rep.* 8:3747. doi: 10.1038/s41598-017-18082-7

Kamat, P. K., Kalani, A., Rai, S., Swarnkar, S., Tota, S., Nath, C., et al. (2014). Mechanism of oxidative stress and synapse dysfunction in the pathogenesis of Alzheimer's disease: Understanding the therapeutics strategies. *Mol. Neurobiol.* 53, 648–661. doi: 10.1007/S12035-014-9053-6

Kim, D., Song, J., Lee, S., Jung, J., and Jang, W. (2021). An Integrative transcriptomic analysis of systemic juvenile idiopathic arthritis for identifying potential genetic markers and drug candidates. *Int. J. Mol. Sci.* 22:712. doi: 10.3390/IJMS22020712

Kou, J., Kovacs, G. G., Höftberger, R., Kulik, W., Brodde, A., Forss-Petter, S., et al. (2011). Peroxisomal alterations in Alzheimer's disease. *Acta Neuropathol.* 122, 271–283. doi: 10.1007/s00401-011-0836-9

Langfelder, P., and Horvath, S. (2008). WGCNA: An R package for weighted correlation network analysis. *BMC Bioinformatics* 9:559. doi: 10.1186/1471-2105-9-559

Langfelder, P., Luo, R., Oldham, M. C., and Horvath, S. (2011). Is my network module preserved and reproducible? *PLoS Comput. Biol.* 7:e1001057. doi: 10.1371/journal.pcbi.1001057

Lauer, A., Da, X., Hansen, M. B., Boulouis, G., Ou, Y., Cai, X., et al. (2017). ABCD1 dysfunction alters white matter microvascular perfusion. *Brain* 140, 3139–3152. doi: 10.1093/BRAIN/AWX262

Lee, C. A. A., Seo, H. S., Armien, A. G., Bates, F. S., Tolar, J., and Azarin, S. M. (2018). Modeling and rescue of defective blood-brain barrier function of induced brain microvascular endothelial cells from childhood cerebral adrenoleukodystrophy patients. *Fluids Barriers CNS* 15:9. doi: 10.1186/s12987-018-0094-5

Leek, J. T., Johnson, W. E., Parker, H. S., Jaffe, A. E., and Storey, J. D. (2012). The sva package for removing batch effects and other unwanted variation in high-throughput experiments. *Bioinformatics* 28, 882–883. doi: 10.1093/bioinformatics/bts034

Liang, W. S., Dunckley, T., Beach, T. G., Grover, A., Mastroeni, D., Walker, D. G., et al. (2007). Gene expression profiles in anatomically and functionally distinct regions of the normal aged human brain. *Physiol. Genomics* 28, 311–322. doi: 10.1152/physiolgenomics.00208.2006

Liberzon, A., Birger, C., Thorvaldsdóttir, H., Ghandi, M., Mesirov, J. P., and Tamayo, P. (2015). The molecular signatures database (MSigDB) hallmark gene set collection. *Cell Syst.* 1:417. doi: 10.1016/J.CELS.2015.12.004

Liu, X., Albano, R., and Lobner, D. (2014). FGF-2 induces neuronal death through upregulation of system xc-. *Brain Res.* 1547, 25–33. doi: 10.1016/J.BRAINRES.2013.12.018

Manchia, M., Piras, I. S., Huentelman, M. J., Pinna, F., Zai, C. C., Kennedy, J. L., et al. (2017). Pattern of gene expression in different stages of schizophrenia: Down-regulation of NPTX2 gene revealed by a meta-analysis of microarray datasets. *Eur. Neuropsychopharmacol.* 27, 1054–1063. doi: 10.1016/j.euroneuro.2017.07.002

McKallip, R. J., Do, Y., Fisher, M. T., Robertson, J. L., Nagarkatti, P. S., and Nagarkatti, M. (2002). Role of CD44 in activation-induced cell death: CD44-deficient mice exhibit enhanced T cell response to conventional and superantigens. *Int. Immunol.* 14, 1015–1026. doi: 10.1093/INTIMM/DXF068

Miller, J. A., Woltjer, R. L., Goodenbour, J. M., Horvath, S., and Geschwind, D. H. (2013). Genes and pathways underlying regional and cell type changes in Alzheimer's disease. *Genome Med.* 5:48. doi: 10.1186/gm452

Moser, H. W., Moser, A. B., Hollandsworth, K., Brereton, N. H., and Raymond, G. V. (2007). "Lorenzo's oil" therapy for X-linked adrenoleukodystrophy: Rationale and current assessment of efficacy. *J. Mol. Neurosci.* 33, 105–113.

Moser, H. W., Moser, A. B., Smith, K. D., Bergin, A., Borel, J., Shankroff, J., et al. (1992). Adrenoleukodystrophy: Phenotypic variability and implications for therapy. *J. Inherit. Metab. Dis.* 15, 645–664. doi: 10.1007/BF01799621

Nury, T., Doria, M., Lizard, G., and Vejux, A. (2020). Docosahexaenoic acid attenuates mitochondrial alterations and oxidative stress leading to cell death induced by very long-chain fatty acids in a mouse oligodendrocyte model. *Int. J. Mol. Sci.* 21:641. doi: 10.3390/ijms21020641

Nussbaum, R. L., and Ellis, C. E. (2003). Alzheimer's disease and Parkinson's disease. *N. Engl. J. Med.* 348, 1356–1364. doi: 10.1056/NEJM2003ra020003

Orchard, P. J., Markowski, T. W., Higgins, L. A., Raymond, G. V., Nascene, D. R., Miller, W. P., et al. (2019). Association between APOE4 and biomarkers in cerebral adrenoleukodystrophy. *Sci. Rep.* 9:7858. doi: 10.1038/s41598-019-44140-3

Rappaport, N., Fishilevich, S., Nudel, R., Twik, M., Belinky, F., Plaschkes, I., et al. (2017). Rational confederation of genes and diseases: NGS interpretation via GeneCards, MalaCards and VarElect. *Biomed. Eng.* 16, 1–14. doi: 10.1186/S12938-017-0359-2/FIGURES/6

Sassa, T., Wakashima, T., Ohno, Y., and Kihara, A. (2014). Lorenzo's oil inhibits ELOVL1 and lowers the level of sphingomyelin with a saturated very long-chain fatty acid. *J. Lipid Res.* 55, 524–530. doi: 10.1194/jlr.M044586

Schlüter, A., Espinosa, L., Fourcade, S., Galino, J., Lśpez, E., Ilieva, E., et al. (2012). Functional genomic analysis unravels a metabolic-inflammatory interplay in adrenoleukodystrophy. *Hum. Mol. Genet.* 21, 1062–1077. doi: 10.1093/hmg/ddr536

Schönfeld, P., and Reiser, G. (2016). Brain lipotoxicity of phytanic acid and very long-chain fatty acids. Harmful cellular/mitochondrial activities in refsum disease and X-linked adrenoleukodystrophy. *Aging Dis.* 7, 136–149. doi: 10.14336/AD.2015.0823

Sergushichev, A. A. (2016). An algorithm for fast preranked gene set enrichment analysis using cumulative statistic calculation. *bioRxiv* [Preprint].

Shannon, P., Markiel, A., Ozier, O., Baliga, N. S., Wang, J. T., Ramage, D., et al. (2003). Cytoscape: A software Environment for integrated models of biomolecular interaction networks. *Genome Res.* 13, 2498–2504. doi: 10.1101/gr.1239303

Subramanian, A., Tamayo, P., Mootha, V. K., Mukherjee, S., Ebert, B. L., Gillette, M. A., et al. (2005). Gene set enrichment analysis: A knowledge-based approach for interpreting genome-wide expression profiles. *Proc. Natl. Acad. Sci. U.S.A.* 102, 15545–15550. doi: 10.1073/pnas.0506580102

Szklarczyk, D., Gable, A. L., Lyon, D., Junge, A., Wyder, S., Huerta-Cepas, J., et al. (2019). STRING v11: Protein-protein association networks with increased coverage, supporting functional discovery in genome-wide experimental datasets. *Nucleic Acids Res.* 47, D607–D613. doi: 10.1093/nar/gky1131

Thei, L., Imm, J., Kaisis, E., Dallas, M. L., and Kerrigan, T. L. (2018). Microglia in Alzheimer's disease: A role for ion channels. *Front. Neurosci.* 12:676. doi: 10.3389/FNINS.2018.00676/BIBTEX

Topçiu-Shufta, V., Miftari, R., Haxhibeqiri, V., and Haxhibeqiri, S. (2016). Association of beta-2 microglobulin with inflammation and dislipidemia in high-flux membrane hemodialysis patients. *Med. Arch.* 70:348. doi: 10.5455/MEDARH.2016.70.348-350

Wang, X. M., Yik, W. Y., Zhang, P., Lu, W., Dranchak, P. K., Shibata, D., et al. (2012). The gene expression profiles of induced pluripotent stem cells from individuals with childhood cerebral adrenoleukodystrophy are consistent with proposed mechanisms of pathogenesis. *Stem Cell Res. Ther.* 3, 39–39.

Wiesinger, C., Kunze, M., Regelsberger, G., Forss-Petter, S., and Berger, J. (2013). Impaired very long-chain Acyl-CoA β-oxidation in human X-linked adrenoleukodystrophy fibroblasts is a direct consequence of ABCD1 transporter dysfunction. *J. Biol. Chem.* 288:19269. doi: 10.1074/JBC.M112.445445

Zhang, X., Zhu, C., Beecham, G., Vardarajan, B. N., Ma, Y., Lancour, D., et al. (2019). A rare missense variant in CASP7 is associated with familial late-onset Alzheimer disease. *Alzheimers Dement.* 15:441. doi: 10.1016/J.JALZ.2018.10.005

Zhong, Q., Zou, Y., Liu, H., Chen, T., Zheng, F., Huang, Y., et al. (2020). Toll-like receptor 4 deficiency ameliorates β2-microglobulin induced age-related cognition decline due to neuroinflammation in mice. *Mol. Brain* 13, 1–15. doi: 10.1186/S13041-020-0559-8/FIGURES/8

frontiers | Frontiers in Molecular Neuroscience

TYPE Original Research
PUBLISHED 03 October 2022
DOI 10.3389/fnmol.2022.983995

OPEN ACCESS

EDITED BY
Arianna Bellucci,
University of Brescia, Italy

REVIEWED BY
Johanna Seitz-Holland,
Brigham and Women's Hospital and Harvard Medical School, United States
Tianhong Zhang,
Shanghai Jiao Tong University, China
Li Hui,
Suzhou Guangji Hospital, China
Bing Liu,
Beijing Normal University, China

*CORRESPONDENCE
Renrong Wu
wurenrong@csu.edu.cn

†These authors have contributed equally to this work

SPECIALTY SECTION
This article was submitted to Brain Disease Mechanisms, a section of the journal Frontiers in Molecular Neuroscience

RECEIVED 01 July 2022
ACCEPTED 07 September 2022
PUBLISHED 03 October 2022

CITATION
Shao T, Wang W, Hei G, Yang Y, Long Y, Wang X, Xiao J, Huang Y, Song X, Xu X, Gao S, Huang J, Wang Y, Zhao J and Wu R (2022) Identifying and revealing different brain neural activities of cognitive subtypes in early course schizophrenia. *Front. Mol. Neurosci.* 15:983995. doi: 10.3389/fnmol.2022.983995

Identifying and revealing different brain neural activities of cognitive subtypes in early course schizophrenia

Tiannan Shao[1†], Weiyan Wang[1†], Gangrui Hei[2], Ye Yang[1], Yujun Long[1], Xiaoyi Wang[1], Jingmei Xiao[1], Yuyan Huang[1], Xueqin Song[2], Xijia Xu[3], Shuzhan Gao[3], Jing Huang[1], Ying Wang[1], Jingping Zhao[1] and Renrong Wu[1]*

[1]Department of Psychiatry, and National Clinical Research Center for Mental Disorders, The Second Xiangya Hospital of Central South University, Changsha, China, [2]Department of Psychiatry, The First Affiliated Hospital of Zhengzhou University, Zhengzhou, China, [3]Department of Psychiatry, Affiliated Nanjing Brain Hospital, Nanjing Medical University, Nanjing, China

Background: Cognitive subtypes of schizophrenia may exhibit different neurobiological characteristics. This study aimed to reveal the underlying neurobiological features between cognitive subtypes in the early course of schizophrenia (ECS). According to prior studies, we hypothesized to identify 2–4 distinct cognitive subtypes. We further hypothesized that the subtype with relatively poorer cognitive function might have lower brain spontaneous neural activity than the subtype with relatively better cognitive function.

Method: Cognitive function was assessed by the MATRICS Consensus Cognitive Battery (MCCB). Resting-state functional magnetic resonance imaging scanning was conducted for each individual. There were 155 ECS individuals and 97 healthy controls (HCs) included in the subsequent analysis. Latent profile analysis (LPA) was used to identify the cognitive subtypes in ECS individuals, and amplitude of low-frequency fluctuations (ALFFs) was used to measure brain spontaneous neural activity in ECS individuals and HCs.

Results: LPA identified two cognitive subtypes in ECS individuals, containing a severely impaired subtype (SI, $n = 63$) and a moderately impaired subtype (MI, $n = 92$). Compared to HCs, ECS individuals exhibited significantly increased ALFF in the left caudate and bilateral thalamus and decreased ALFF in the bilateral medial prefrontal cortex and bilateral posterior cingulate cortex/precuneus (PCC/PCu). In ECS cognitive subtypes, SI showed significantly higher ALFF in the left precentral gyrus (PreCG) and lower ALFF in the left PCC/PCu than MI. Furthermore, ALFFs of left PreCG were negatively correlated with several MCCB cognitive domains in ECS individuals, while ALFF of left PCC/PCu presented opposite correlations.

Conclusion: Our findings suggest that differences in the brain spontaneous neural activity of PreCG and PCC/PCu might be the potential neurobiological features of the cognitive subtypes in ECS, which may deepen our

understanding of the role of PreCG and PCC/PCu in the pathogenesis of cognitive impairment in schizophrenia.

KEYWORDS

schizophrenia, cognitive subtypes, latent profile analysis, MCCB, MRI, ALFF

Introduction

Cognitive impairment is a core component of schizophrenia, which exists not only in the acute phase but also in the ultra-high risk stage of psychosis and persists during the clinical remission of psychiatric symptoms (Keefe et al., 2006; Bora and Murray, 2014). In schizophrenia, cognitive impairment is manifested in multiple domains, including verbal and visual learning, working memory, processing speed, problem solving, attention, and executive function (Nuechterlein et al., 2004; Sheffield et al., 2018), which could contribute to poor functional outcomes (Green, 2016). Although there is a generalized cognitive deficit in schizophrenia, not all individuals exhibit the same pattern of cognitive deficits, i.e., degrees of impairment in different cognitive dimensions from different sample groups are manifested differently (Carruthers et al., 2019). These heterogeneous patterns of cognitive impairment make it difficult to understand the pathophysiology of schizophrenia.

Accumulating evidence has successfully classified individuals with psychiatric disorders with similar cognitive characteristics and compared differences between distinct cognitive features. Participants could be classified according to their current cognitive function scores based on artificial classification (Ammari et al., 2010; Ortiz-Gil et al., 2011), or could be classified by data-driven approaches (Lim et al., 2020; Smucny et al., 2020). Instead of appearing to be limited to dividing participants into relatively intact or cognitively impaired subtypes by prior defined classification criteria, the data-driven approach could provide valuable insight into multiple cognitive subtypes that exist in psychiatric disorders (Carruthers et al., 2019).

Abnormal cognitive function also has relevant neuroimaging features. Growing attention has been paid to identifying the neurobiological changes of cognitive subtypes in schizophrenia through neuroimaging (Van Rheenen et al., 2018; Lewandowski et al., 2019). Several studies using data-driven methods have illustrated the different patterns of brain structure or resting-state functional connectivity among cognitive subtypes in individuals with schizophrenia. For brain structure, near-normal cognitive groups and impaired cognitive groups of individuals with schizophrenia or schizoaffective disorders were found at varying levels of cortex thickness (Cobia et al., 2011), or different gray and white matter volumes (Wexler et al., 2009; Van Rheenen et al., 2018). For brain function connectivity networks, three cognitive subtypes classified by *k*-means clustering method from 67 individuals with schizophrenia spectrum disorders showed unique hyper- or hypo-connectivity in specific functional networks (Rodriguez et al., 2019). However, previous neuroimaging studies have used structural measurements and functional connectivity approaches to investigate the neurobiological features between cognitive subtypes in schizophrenia; to the best of our knowledge, there was no study investigating differences in brain spontaneous neural activity between cognitive subtypes of ECS yet.

The amplitude of low-frequency fluctuations (ALFFs) is often used to characterize brain spontaneous neural activity (Zang et al., 2007). Several studies have investigated the association between ALFF and cognitive function in schizophrenia (Zhou et al., 2014; Wang et al., 2019). Therefore, the purpose of this study was to determine the differences in brain spontaneous neuronal activity measured by ALFF between cognitive subtypes of individuals with ECS. We compared the cognitive subtypes derived from latent profile analysis (LPA) with healthy controls (HCs) to assess the condition of cognitive impairment (Miettunen et al., 2016). Based on two recent systematic reviews on cognitive subtypes in schizophrenia, we expected to find 2–4 distinct cognitive subtypes: a severely impaired subgroup, 1–2 moderately impaired subgroups, and a relatively intact cognitive subgroup (Carruthers et al., 2019, 2021). We further hypothesized that cognitive subtypes might exhibit different brain spontaneous neuronal activities, and the brain spontaneous neuronal activity may be lower in the subtype with poorer cognitive function than in the subtype with better cognitive function.

Methods

Participants

We recruited ECS individuals and HCs from three clinical medical centers, the Second Xiangya Hospital of Central South University (Center 1), the Affiliated Nanjing Brain Hospital of Nanjing Medical University (Center 2), and the First Affiliated Hospital of Zhengzhou University (Center 3). All recruited ECS individuals met the criteria of the Diagnostic and Statistical Manual of Mental Disorders, Fourth Edition (DSM-IV) based on a Structured Clinical Interview for DSM-IV Axis-I Disorder

(First et al., 1997), which were assessed by two well-trained psychiatrists in each center.

For ECS individuals, the further inclusion criteria were as follows: (1) aged 16–60; (2) experienced the first episode of psychiatric symptoms or illness duration within 3 years but in the acute phase currently; (3) Positive and Negative Syndrome Scale (PANSS) total score >60. The exclusion criteria were: (1) comorbidity of physical diseases, or other psychiatric disorders that met the DSM-IV criteria; (2) comorbidity of substance abuse or addiction; (3) unable to complete cognitive function tests and magnetic resonance imaging (MRI) examinations; (4) pregnant or lactating women. In addition, HCs with first-degree relatives that had any psychiatric disorders were also excluded.

Written informed consents were obtained from all participants or first-degree relatives of ECS individuals before participating in the study. This study was approved by the Ethics Committee of the Second Xiangya Hospital of Central South University, the Ethics Committee of the Affiliated Nanjing Brain Hospital of Nanjing Medical University, and the Ethics Committee of the First Affiliated Hospital of Zhengzhou University.

Our study totally enrolled 181 ECS individuals and 107 HCs. After neuroimaging preprocessing, 155 ECS individuals and 97 HCs were included in the subsequent analysis (subjects with head motion exceeding 2 mm or head rotation exceeding 2° were excluded). Among 155 ECS individuals, 119 (76.8%) individuals received risperidone, 16 (10.3%) olanzapine, 11 (7.1%) amisulpride, seven (4.5%) aripiprazole, and two (1.3%) paliperidone. The doses of antipsychotic drugs were equivalent to chlorpromazine dose by the defined daily doses (DDDs) method (Leucht et al., 2016). The remaining subjects of each center were as follows: 34 ECS individuals and 18 HCs (Center 1); 38 ECS individuals and 36 HCs (Center 2); 83 ECS individuals and 43 HCs (Center 3). Demographic and clinical data of ECS individuals and HCs from three centers are shown in Supplementary Table 1.

Cognitive assessment

We used Measurement and Treatment Research to Improve Cognition in Schizophrenia Consensus Cognitive Battery (MCCB) to evaluate cognitive function (Kern et al., 2008; Nuechterlein et al., 2008). The MCCB was widely used and translated into Chinese version (Shi et al., 2015). It includes nine tasks across seven cognitive domains: (1) speed of processing (Trail Making Test, part A; Brief Assessment of Cognition in Schizophrenia, Symbol Coding; Category Fluency Test, Animal); (2) attention and vigilance (Continuous Performance Test-Identical Pairs); (3) working memory (Wechsler Memory Scale, spatial span); (4) verbal learning (Hopkins Verbal Learning Test-Revised); (5) visual learning (Brief Visuospatial Memory Test); (6) reasoning and problem solving (Neuropsychological Assessment Battery, mazes test); (7) social cognition (Mayer–Salovey–Caruso Emotional Intelligence Test, managing emotions test). It takes 1–1.5 h for each subject to finish MCCB. Raw scores were converted to scale scores, then to Chinese-normalized *T* scores. *T* scores of seven cognitive domains and composite scores (the average *T* score of nine tasks) were calculated. In this study, all ECS individuals and HCs completed the MCCB.

Neuroimaging data acquisition

The thorough description of this section is described in the Supplementary material.

Neuroimaging data preprocessing

Image preprocessing was performed by the Data Processing & Analysis of Brain Imaging toolbox (DPABI, V4.2, http://rfmri.org/dpabi) running on MATLAB software (The MathWorks, Inc., Natick, MA, USA; Yan et al., 2016). We removed the first 10 scanning volumes in order to stabilize the magnetic resonance signal and reduce the impact of subjects not adapting to the scanning environment. Slice timing and head motion were corrected for each subject, and those whose head motion exceeded 2 mm or head rotation exceeded 2° were excluded. Afterward, images were spatially normalized to the standard Montreal Neurological Institute template by using warping parameters estimated from T1 images with a resampling standard voxel size of 3 mm × 3 mm × 3 mm. We used a 6 mm full-width at half-maximum Gaussian kernel to spatially smooth images and performed linear detrending. Then the nuisance signals were regressed out, including head motion effects (Friston 24-parameter model; Friston et al., 1996), white matter, and cerebrospinal fluid. Finally, band-pass filtering (0.01–0.08 Hz) was applied for the time series of each voxel to remove the effects of very-low-frequency drifts and high-frequency noise (Zang et al., 2007). After that, the time series of each voxel for each subject was transformed into the frequency domain under a fast Fourier transformation way in order to get the power spectrum. To standardize the ALFF values, the ALFF of each voxel would be converted into *Z* scores by subtracting the global mean and then dividing the global standard deviation.

Multi-site effect harmonization

Before statistical analysis, we used the ComBat Harmonization method (http://github.com/Jfortin1/ComBatHarmonization) for preprocessed data to eliminate the inter-site effects (Fortin et al., 2017). This widely used method could effectively remove unwanted variation introduced by the

site, and increase statistical power (Fortin et al., 2018; Radua et al., 2020). In addition, group, age, sex, and education level were protected during the removal of inter-site effects.

Latent profile analysis

Latent profile analysis is used to classify individuals into heterogeneous subtypes based on latent variable models. It could explain the associations between the observed continuous indicator variables by regressing the continuous indicator variables onto a set of one or more latent class variables (Miettunen et al., 2016). LPA is a model-based approach, and thus has fewer prerequisites for application, more reasonable clustering criteria and result testing, and less arbitrariness than traditional clustering methods (e.g., *k*-means; Brusco et al., 2017; Schreiber, 2017). The flexibility of LPA makes it adaptable to the heterogeneous study of complex psychiatric and psychological phenomena with effective classification of cognitive subtypes (Lim et al., 2020; Smucny et al., 2020; De Meo et al., 2021).

Latent profile analysis was conducted by Mplus version 7.11 to identify potential homogenous subtypes of ECS individuals based on cognitive performance in seven MCCB cognitive domains (Muthén and Muthén, 2015). The number of classes was determined from an examination of models fit statistics rather than hypothesized. These model fit indices included log-likelihood ratio (LLR; Woolf, 1957), Akaike's information criteria (AIC; Akaike, 1987), Bayesian information criteria (BIC; Schwarz, 1978), sample-size adjusted BIC (ABIC; Sclove, 1987), and entropy (Celeux and Soromenho, 1996). Lo-Mendell-Rubin (LMR) tests and bootstrapped likelihood ratio tests (BLRTs) were also conducted to evaluate the significance of model improvement between n and n – 1 number of classes (McLachlan, 1978; Lo et al., 2001). A total of five models were estimated specifying from 1 to 5 latent classes.

Statistical analysis

Once the potential subtypes were identified, group differences in demographic data, clinical data, PANSS scores, and MCCB scores were analyzed by SPSS version 22.0 (IBM, Armonk, NY, USA) by using one-way analysis of variance (ANOVA), two-sample *t*-test, or chi-squared test. Furthermore, eta-squared (η^2) was used to calculate the effect size of comparisons of each MCCB cognitive domain (Cohen, 1988). Post-hoc comparisons were carried out by Bonferroni correction if ANOVA showed significant differences between subtypes. Generally, *p*-values of <0.05 were accepted as statistically significant.

ALFF analysis was conducted in the Statistical Parametric Mapping 12 toolbox (SPM12, https://www.fil.ion.ucl.ac.uk/spm/software/spm12). Two-sample *t*-test was designed for the comparison of ALFF maps between ECS individuals and HCs, and in ECS cognitive subtypes, with age, sex, education, and mean frame-wise displacement Jenkinson as covariates. In addition, PANSS total score was also controlled for subtypes comparison to investigate whether the result was consistent after subtracting out the effect of symptom severity. Multiple comparisons were corrected using the cluster-wise family-wise error (FWE) rates correction (cluster-wise FWE $p < 0.05$) with a combined individual voxel threshold of $p < 0.001$. Significant brain regions with discrepant ALFF between ECS cognitive subtypes were regarded as regions of interest (ROI) to extract ALFF values for subsequent correlation analysis in SPSS. To further explore the specific associations between ALFF in ROIs and MCCB scores, their correlations coefficient between ALFF values in ROIs and MCCB scores in ECS and HCs were calculated, respectively. Pearson's r was used to calculate the effect size of correlations between ALFF in ROIs and MCCB cognitive scores (Cohen, 1988). The significant level of correlations was corrected by the false discovery rate (FDR) at $q < 0.05$.

Results

LPA results based on MCCB cognitive domains

According to the results of model estimation, the 2-class solution presented a better fit than the 1-class solution. Though the other solutions suggested better fits than the 2-class solution based on AIC, BIC, and ABIC, there was no significant improvement over the 2-class solution according to the *p*-value of LMR and the *p*-value of BLRT (Table 1, Supplementary Figure 1). The 2-class solution classified 40.6% of the ECS individuals into the severely impaired subtype (SI, $n = 63$) and 59.4% into the moderately impaired subtype (MI, $n = 92$), respectively.

Demographic and clinical characteristics

Demographic and clinical characteristics of two ECS cognitive subtypes and HCs are shown in Table 2. The sex composition of SI significantly differed from MI. Besides, education levels were similar in both subtypes but significantly lower than the HCs. For symptom severity, PANSS scores of SI were significantly higher than MI except for positive score. Significant pairwise differences in MCCB domains were exhibited among the three groups, while differences in the working memory domain and reasoning/problem-solving domain between MI and HCs were not significant (Table 2). In addition, the MCCB performance of HC were taken as the

TABLE 1 Model estimations of latent profile analysis based on MCCB cognitive domains.

Classes	LLR	AIC	BIC	ABIC	Entropy	*p*-value of LMR	*p*-value of BLRT
1	−4208.287	8444.573	8487.181	8442.868	–	–	–
2	−4093.591	8231.181	8298.137	8228.502	0.822	<0.001	<0.001
3	−4065.038	8190.077	8281.379	8186.422	0.808	0.498	<0.001
4	−4047.426	8170.852	8286.502	8166.223	0.798	0.132	<0.001
5	−4032.352	8156.704	8296.701	8151.101	0.781	0.759	<0.001

LLR, log-likelihood ratio; AIC, Akaike's information criteria; BIC, Bayesian information criteria; ABIC, sample-size adjusted Bayesian information criteria; LMR, Lo-Mendell-Rubin test; BLRT, bootstrap likelihood ratio test.

TABLE 2 Demographic and clinical data of ECS cognitive subtypes and HCs.

	SI ($n = 63$)	MI ($n = 92$)	HC ($n = 97$)	$F/\chi^2/t$	*p*	Effect size (η^2)	*Post hoc*[a]
Age, years	23.84 (7.06)	25.38 (8.37)	25.03 (5.42)	0.944	0.391	–	–
Sex, female/male	26/37	59/33	54/43	7.918	0.019	–	SI ≠ MI, SI = HC, MI = HC
Education, years	11.24 (2.56)	11.32 (2.97)	13.49 (3.27)	16.255	<0.001	–	SI, MI < HC
Duration, months	8.10 (10.09)	10.09 (10.23)	–	−1.197	0.233	–	–
CPZ-DDD, mg	254.92 (61.80)	278.15 (123.24)	–	−1.546	0.124	–	–
PANSS							
Positive symptoms	23.38 (5.41)	21.90 (6.27)	–	1.523	0.130	–	–
Negative symptoms	27.06 (6.14)	22.25 (5.91)	–	4.903	<0.001	–	–
General psychopathology	46.60 (6.82)	43.90 (6.31)	–	2.531	0.012	–	–
Total score	97.05 (13.19)	88.26 (12.54)	–	4.195	<0.001	–	–
MCCB							
Speed of processing	20.61 (7.74)	37.86 (7.17)	46.59 (7.38)	236.768	<0.001	0.655	SI < MI < HC
Attention/vigilance	25.51 (11.09)	40.15 (10.81)	48.55 (9.25)	95.440	<0.001	0.434	SI < MI < HC
Working memory	32.16 (9.82)	41.07 (9.41)	41.27 (12.40)	16.586	<0.001	0.118	SI < MI, HC
Verbal learning	27.57 (8.31)	41.73 (8.60)	44.25 (9.23)	75.085	<0.001	0.376	SI < MI < HC
Visual learning	28.38 (13.39)	44.33 (10.29)	48.77 (11.01)	63.938	<0.001	0.339	SI < MI < HC
Reasoning/problem solving	28.87 (7.49)	39.86 (11.64)	41.37 (10.63)	31.027	<0.001	0.199	SI < MI, HC
Social cognition	30.54 (9.60)	39.67 (10.85)	46.45 (9.98)	46.427	<0.001	0.272	SI < MI < HC
Composite score	26.10 (4.89)	40.04 (4.88)	45.60 (5.63)	274.783	<0.001	0.688	SI < MI < HC

Values are presented as mean (SD). SI and MI represent the two cognitive subtypes in ECS.
[a]Post-hoc comparisons were conducted using Bonferroni correction.
ECS, early course schizophrenia; SI, severely impaired subtype; MI, moderately impaired subtype; HC, healthy control; CPZ-DDD, chlorpromazine-defined daily dose; MCCB, MATRICS Consensus Cognitive Battery; PANSS, Positive and Negative Syndrome Scale; SD, standard deviation.

norm to standardize the cognitive score of ECS into *Z* scores (see Figure 1 and Supplementary Table 2).

ALFF differences between groups

Results of the independent two-sample *t*-test (cluster-wise FWE $p < 0.05$) and cluster information are shown in Table 3 and Figure 2. Compared with HCs, ECS exhibited higher ALFF in the left caudate and bilateral thalamus, while lower ALFF was observed in the bilateral medial prefrontal cortex (MPFC) and bilateral posterior cingulate cortex/precuneus (PCC/PCu). For the subtypes comparison, ALFF of the left precentral gyrus (PreCG) was significantly higher in SI. On the contrary, the ALFF of left PCC/PCu in SI was significantly lower than MI. To control for the effect of PANSS and medication effects (chlorpromazine dose equivalence), we conducted the additional analysis with PANSS total score and medication effects as covariates. This result was similar to the previous result without controlling for the two covariates (see Supplementary material).

Correlations between ALFF of ROIs and cognition

For ECS individuals, there were significantly positive correlations between ALFF values of left PCC/PCu with MCCB speed of processing, attention/vigilance, verbal

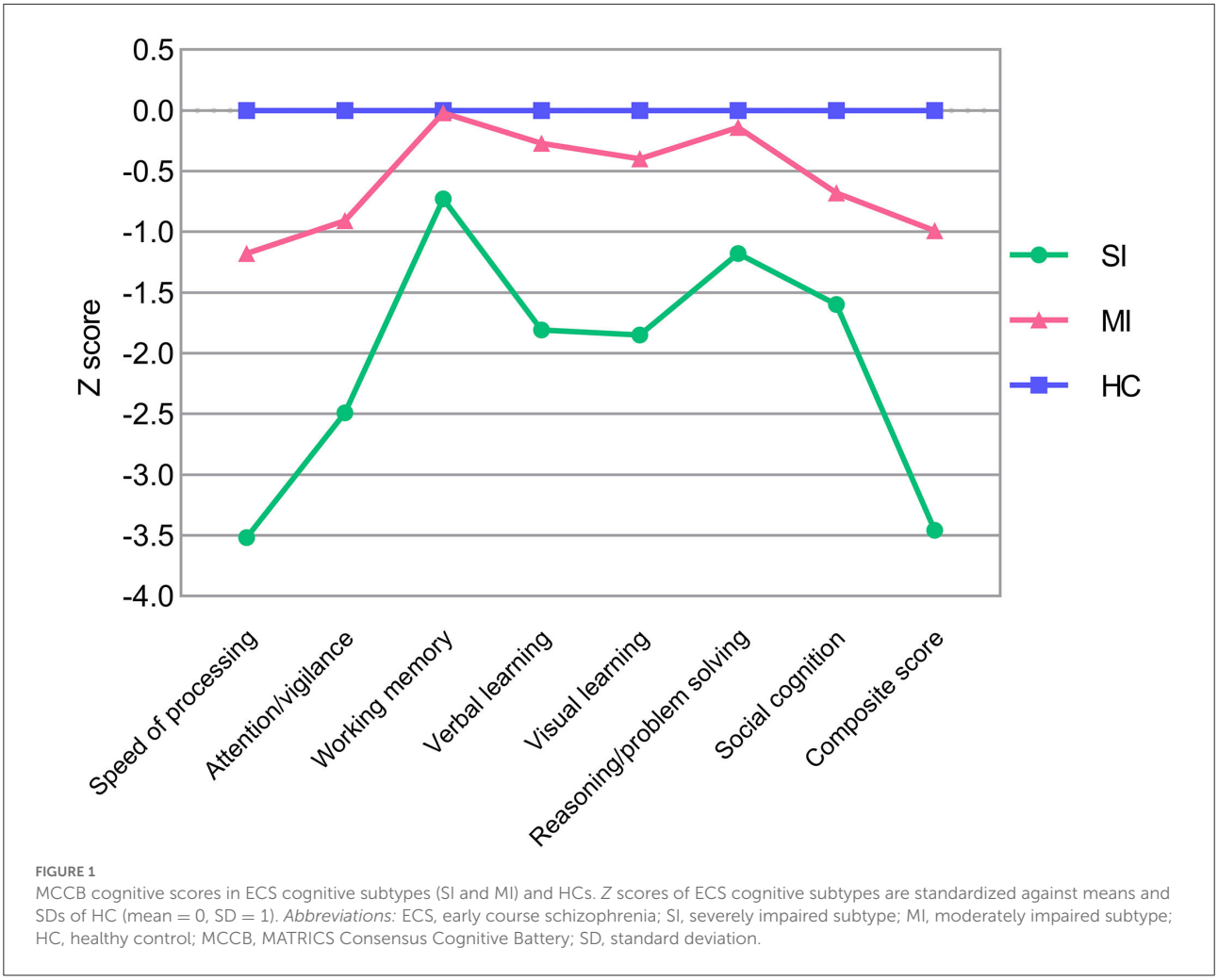

FIGURE 1
MCCB cognitive scores in ECS cognitive subtypes (SI and MI) and HCs. *Z* scores of ECS cognitive subtypes are standardized against means and SDs of HC (mean = 0, SD = 1). *Abbreviations:* ECS, early course schizophrenia; SI, severely impaired subtype; MI, moderately impaired subtype; HC, healthy control; MCCB, MATRICS Consensus Cognitive Battery; SD, standard deviation.

TABLE 3 Brain regions with ALFF differences in ECS and HCs and in ECS cognitive subtypes.

	Brain regions	Cluster size	Peak coordinate (mm)[a]			Peak *t*-value
			x	*y*	*z*	
ECS > HC	Caudate L	98	−9	9	0	5.0849
	Thalamus B	54	−9	−6	9	4.7638
ECS < HC	MPFC B	49	3	48	−24	−4.4362
	PCC/PCu B	100	3	−54	21	−4.5327
SI > MI	PreCG L	47	−56	5	19	4.9245
SI < MI	PCC/PCu L	142	−6	−57	26	−5.488

SI and MI represent the two cognitive subtypes in ECS.
[a]Peak coordinate refers to the peak voxel location of the significant cluster in the Montreal Neurological Institute space.
ALFF, amplitude of low-frequency fluctuations; ECS, early course schizophrenia; SI, severely impaired subtype; MI, moderately impaired subtype; HC, healthy control; MPFC, medial prefrontal cortex; PCC/PCu, posterior cingulate cortex/precuneus; PreCG, precentral gyrus; L, left; B, bilateral.

learning, reasoning/problem solving, and composite score (Figure 3). The effect sizes of the correlations were small to moderate. Moreover, ALFF in left PreCG was significantly negatively correlated with MCCB seven cognitive domains and composite score (Figure 3). Importantly, some correlations of ALFF in left PreCG had moderate to large effect sizes. No significant correlations were found in HCs.

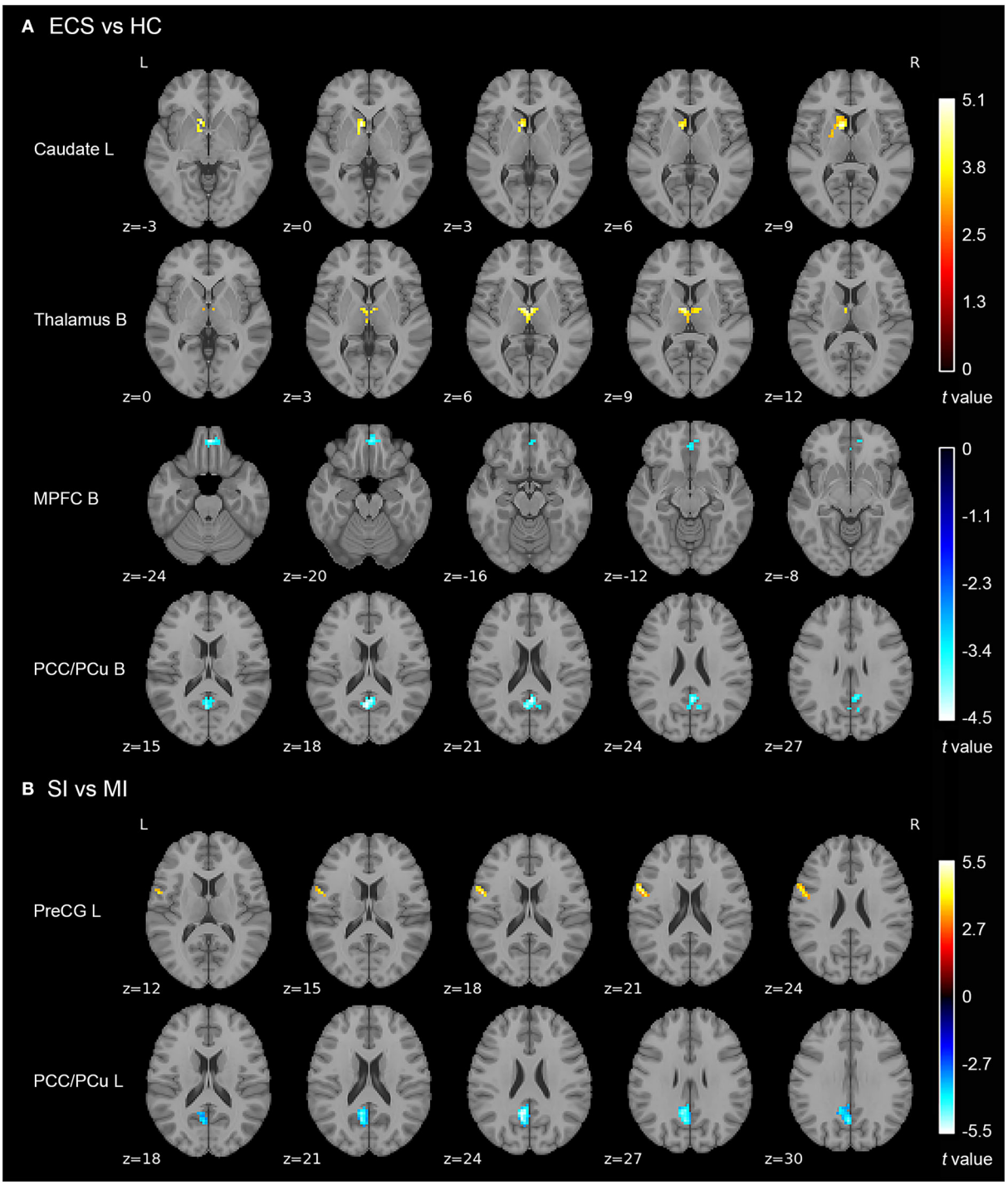

FIGURE 2
ALFF differences in ECS, HCs, and ECS cognitive subtypes (SI and MI). **(A)** Abnormal ALFF in ECS relative to HCs. **(B)** Increased ALFF in left PreCG and decreased ALFF in left PCC/PCu in SI relative to MI. Results were cluster-wise FWE corrected. *Abbreviations:* ALFF, amplitude of low-frequency fluctuations; ECS, early course schizophrenia; SI, severely impaired subtype; MI, moderately impaired subtype; HC, healthy control; MPFC, medial prefrontal cortex; PCC/PCu, posterior cingulate cortex/precuneus; PreCG, precentral gyrus; L, left; B, bilateral; FWE, family-wise error.

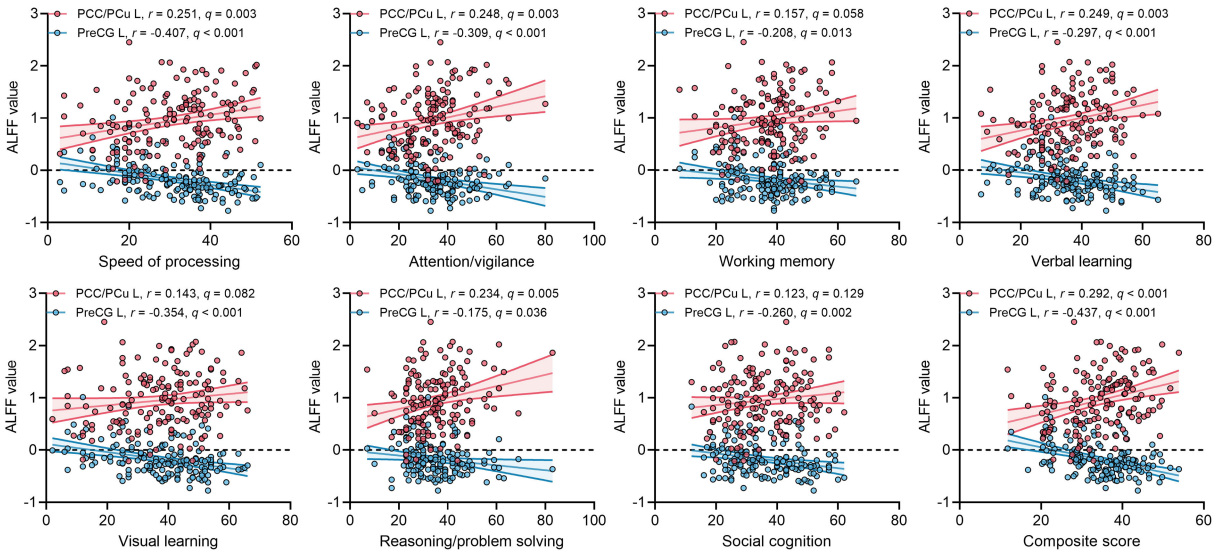

FIGURE 3
Correlations between ALFF values of two ROIs and MCCB cognitive scores in ECS. *q*, *p*-values corrected by FDR correction. *Abbreviations:* ALFF, amplitude of low-frequency fluctuations; ECS, early course schizophrenia; MCCB, MATRICS Consensus Cognitive Battery; PCC/PCu, posterior cingulate cortex/precuneus; PreCG, precentral gyrus; ROI, region of interest; FDR, false discovery rate; L, left.

Discussion

The present study revealed the relationship between cognitive impairment and neurobiology in ECS individuals grouped according to their different patterns of cognitive deficit using a data-driven approach. We reported two patterns of cognitive impairment in ECS individuals. Compared to HCs, ECS individuals showed significantly increased ALFF in the left caudate and bilateral thalamus and decreased ALFF in bilateral MPFC and bilateral PCC/PCu. Interestingly, we first found that ALFF of left PreCG and left PCC/PCu were different in the two identified impaired cognitive subtypes. In addition, ALFF of left PreCG and left PCC/PCu exhibited significant correlations with MCCB cognitive domains in ECS individuals. These findings suggest that the different spontaneous neural activities of PreCG and PCC/PCu at resting-state may be the potential neurobiological features of cognitive impairment subtypes in ECS.

Consistent with the grouping results of previous studies (Morar et al., 2011; Green et al., 2013), our LPA recognized two different patterns of cognitive impairment in ECS individuals. SI exhibited the worst performance in all MCCB cognitive scores, which manifested wide deficits in whole cognitive domains, ranging from 0.7 to 3.5 standard deviations below HCs (Figure 1 and Supplementary Table 2). MI showed an intermediate deficient speed of processing, attention/vigilance, verbal learning, visual learning, and social cognition, but maintained intact working memory and reasoning/problem solving, within ∼1.2 standard deviations of HCs (Figure 1 and Supplementary Table 2).

In line with previous studies, a common phenomenon in both subtypes is that the speed of processing was the most severely impaired cognitive domain ($\eta^2 = 0.655$, Table 2) except for the composite score. Speed of processing appears to be a core feature of cognition, it underlies other cognitive impairments such as executive functioning and working memory (Dickinson et al., 2007). Our study further supported that impaired speed of processing plays a key role in the cognitive impairment of ECS (Sheffield et al., 2018; Lim et al., 2020). Despite ECS individuals having a lower level of education, there was no difference in the educational years between the two impaired cognitive subtypes. Moreover, severely impaired individuals showed higher negative symptoms than moderately impaired individuals but with no differences in positive symptoms, which is consistent with the clinical observation that negative symptoms and cognitive impairment might share common pathophysiological substrates (Bowins, 2011; Lincoln et al., 2017).

Working memory is described as the ability to temporarily reserve and manipulate information for further cognitive processing (Baddeley, 1992). High-level cognitive processes require the support of working memory, such as reasoning, learning, and comprehension (Baddeley, 2003). The deficit in reasoning/problem-solving domain indicates executive dysfunction (Lis et al., 2005). Impaired executive function is found to predict poor functional outcomes, failure of interventions, and restricted recovery (Green et al., 2000). By using the LPA method, we identified a subtype with intact

working memory and reasoning/problem solving from 155 ECS individuals, suggesting that executive function in the subtype with mild to moderate cognitive deficits is, indeed, comparable to the healthy population. In contrast to our study hypothesis, our results found only two cognitive subtypes. A possible reason is that due to our sample size limitation, it was not possible to cluster a subtype with a small proportion of ECS individuals. Another possible reason may be that our ECS individuals had a shorter duration and more severe psychiatric symptoms compared to other studies (Carruthers et al., 2019, 2021; Lim et al., 2020).

Before analyzing brain regions with ALFF differences in the two cognitive subtypes, we first examined regions with abnormal ALFF in ECS individuals. Resting-state functional MRI analyses showed four brain regions with abnormal neural activity in ECS, including two brain regions with increased ALFF (left caudate and bilateral thalamus) and two with decreased ALFF (bilateral MPFC and bilateral PCC/PCu).

Caudate is a part of the subcortical structure, which is responsible for several neurobiological processes such as planning the behavioral execution (Grahn et al., 2008). It has been found that there was hyperactivity in caudate during working memory tasks in individuals at clinical high risk for psychosis (Thermenos et al., 2016). Individuals with schizophrenia also exhibited higher ALFF in the left caudate than HCs (Zhang et al., 2021). Thalamus is also a subcortical region, which is involved in transmitting sensory information to the cerebral cortex and regulating emotion and cognitive attention control (Sherman, 2016; Wolff and Vann, 2019). Individuals with schizophrenia exhibited reduced thalamic gray matter volume (Alemán-Gómez et al., 2020), and abnormal activation during task-related functional MRI (Byne et al., 2009). As two parts of the cortico-striatal-thalamic-cortical (CSTC) sub-circuit in the salience network (SN), abnormal functional connectivity of caudate and thalamus has been reported in previous studies (Peters et al., 2016; Huang et al., 2020). Our findings showed that increased spontaneous neural activity appeared in the CSTC sub-circuit of the SN in the early course of schizophrenia, which may suggest a compensatory mechanism to maintain normal functioning performance (Gong et al., 2020). In addition, the long-term examination should be performed to investigate whether the changes in these two brain regions still exist.

Another important finding in our study is that ECS individuals showed decreased ALFF in bilateral MPFC and bilateral PCC/PCu compared with HCs. Both MPFC and PCC/PCu are core regions of the default mode network (DMN), a crucial brain network that associates with many neurophysiological functions (Raichle, 2015). The function of MPFC and PCC/PCu was involved in introspective processes that were attenuated when attention was turned to external events (Gusnard et al., 2001). There is increasing evidence that ECS individuals exhibited decreased ALFF in MPFC and PCC/PCu compared with HCs (Ren et al., 2013; Gong et al., 2020), which is in line with our results. Taken together, our findings further support that SN and DMN play a critical role in the pathogenesis of ECS.

Although we found ALFF abnormalities in several brain regions in ECS, not all the abnormalities could reflect the neuropathological changes in cognitive impairment. We found two regions with different ALFF values between SI and MI. Compared with MI, SI presented higher ALFF values in the left precentral gyrus (PreCG) and lower ALFF values in the left PCC/PCu. After controlling the PANSS total score and medication effects, these results remained significant. Moreover, ALFF of left PCC/PCu was positively correlated with MCCB cognitive scores in ECS, while ALFF of left PreCG showed negative correlations.

Several studies focused on PCC/PCu and cognitive function have been reported. A cortical morphometric study revealed that the structural volume of PCC/PCu was associated with cognitive impairment in first-episode schizophrenia (Wang et al., 2021). Furthermore, PCC/PCu showed significant activation during the episodic memory search task (Sestieri et al., 2011). In schizophrenia individuals, the activation in PCC/PCu was not significantly enhanced during the virtual maze task, while HCs exhibited significantly enhanced activation in the same region (Siemerkus et al., 2012). PreCG, also known as the primary motor cortex, is participated in motor information processing and emotional perception (Mesulam, 1998; Watanuki et al., 2016). Abnormal regional homogeneity and voxel-mirrored homotopic connectivity of PreCG have been found in first-episode schizophrenia (Liu et al., 2018a,b). Recent evidence confirmed that the excessive activity of PreCG could result in the impairment of emotional processing in schizophrenia (Watanuki et al., 2016). Additionally, another study indicated that PreCG might be involved in some cognitive processes, such as word recognition and phonological processing (Xu et al., 2019). Based on the available evidence, our results suggest that higher spontaneous neural activity in PCC/PCu is beneficial for the preservation of cognitive function in schizophrenia individuals, whereas higher activity in PreCG plays an opposite role. In conclusion, abnormal ALFF in caudate, thalamus, MPFC, and PCC/PCu reflected the pathophysiology of ECS, with abnormal ALFF in the PCC/PCu also indicating the pathophysiology of cognitive impairment in ECS. Furthermore, the abnormal spontaneous neural activity in the PCC/PCu in schizophrenia and between cognitive subtypes provides compelling evidence for the vital effect of DMN on schizophrenia and cognitive function.

Several limitations should be considered in our study. MRI data of subjects in our study were restricted by the fact that images were collected from different acquisition centers and scanners (Jovicich et al., 2006). We used the ComBat Harmonization method to minimize the site-specific confounds and enhanced statistical power (Fortin et al., 2017). However,

the ComBAt Harmonization method cannot exclude the non-linear site and scanner effects, which is one of its drawbacks. For now, this method is still the best way to minimize linear site and scanner effects (Sun et al., 2022). Second, our sample size is relatively small, we propose to expand the sample size and make validation in the independent sample population in future. Third, our study is a cross-sectional study, and further follow-up study should be conducted to validate subtype stability and outcomes. Moreover, our study did not collect full-scale IQ from schizophrenia individuals and HCs, we will collect full-scale IQ in future studies, use the subtype classification based on MCCB to compare to the subtype classification based on full-scale IQ, and investigate the differences in full-scale IQ across cognitive subtypes.

In general, our results showed that cognitive impairment in ECS might be described as two subtypes: a severely impaired group with compromised cognition across all cognitive domains and a moderately impaired group with preserved cognition in working memory and reasoning/problem solving. Furthermore, our study identified four neurobiological features of ECS and two neurobiological features of cognitive subtypes in ECS. These brain regions associated with schizophrenia and cognitive function could be potential targets for the treatment of schizophrenia and its cognitive impairment. Meanwhile, differentiating individuals into subtypes based on cognitive function could help clinicians better understand the prognosis and recovery of social function, as well as carry out individualized interventions by combining the neuroimaging features derived from the subtypes. Our findings contribute to understanding the pathophysiology of cognitive impairment in ECS from the perspective of brain spontaneous neural activity.

Data availability statement

The raw data supporting the conclusions of this article will be made available by the authors, without undue reservation.

Ethics statement

The studies involving human participants were reviewed and approved by the Ethics Committee of the Second Xiangya Hospital of Central South University, the Ethics Committee of the Affiliated Nanjing Brain Hospital of Nanjing Medical University, the Ethics Committee of the First Affiliated Hospital of Zhengzhou University. Written informed consent to participate in this study was provided by the participants' legal guardian/next of kin.

Author contributions

RW and JZ designed this study and wrote the protocol. RW, XS, XX, GH, YY, YL, XW, JX, YH, SG, JH, and YW performed the research. TS and WW analyzed the data and wrote the manuscript. RW, XS, and XX were involved in the revision and completion of the work. All authors contributed to the final manuscript.

Funding

This work was supported by the National Natural Science Foundation of China (Grant Nos. 81622018 and 82072096).

Acknowledgments

We would like to thank all the participants that participated in this study.

Conflict of interest

The authors declare that the research was conducted in the absence of any commercial or financial relationships that could be construed as a potential conflict of interest.

Publisher's note

Supplementary material

The Supplementary Material for this article can be found online at: https://www.frontiersin.org/articles/10.3389/fnmol.2022.983995/full#supplementary-material

References

Akaike, H. (1987). Factor analysis and AIC. *Psychometrika* 52, 317–332.

Alemán-Gómez, Y., Najdenovska, E., Roine, T., Fartaria, M. J., Canales-Rodríguez, E. J., Rovó, Z., et al. (2020). Partial-volume modeling reveals reduced gray matter in specific thalamic nuclei early in the time course of psychosis and chronic schizophrenia. *Hum. Brain Mapp.* 41, 4041–4061. doi: 10.1002/hbm.25108

Ammari, N., Heinrichs, R. W., and Miles, A. A. (2010). An investigation of 3 neurocognitive subtypes in schizophrenia. *Schizophr Res* 121, 32–38. doi: 10.1016/j.schres.2010.04.014

Baddeley, A. (1992). Working memory. *Science* 255, 556–559. doi: 10.1126/science.1736359

Baddeley, A. (2003). Working memory: looking back and looking forward. *Nat. Rev. Neurosci.* 4, 829–839. doi: 10.1038/nrn1201

Bora, E., and Murray, R. M. (2014). Meta-analysis of cognitive deficits in ultra-high risk to psychosis and first-episode psychosis: do the cognitive deficits progress over, or after, the onset of psychosis? *Schizophr. Bull.* 40, 744–755. doi: 10.1093/schbul/sbt085

Bowins, B. (2011). A cognitive regulatory control model of schizophrenia. *Brain Res. Bull.* 85, 36–41. doi: 10.1016/j.brainresbull.2011.02.004

Brusco, M. J., Shireman, E., and Steinley, D. (2017). A comparison of latent class, K-means, and K-median methods for clustering dichotomous data. *Psychol. Methods* 22, 563–580. doi: 10.1037/met0000095

Byne, W., Hazlett, E. A., Buchsbaum, M. S., and Kemether, E. (2009). The thalamus and schizophrenia: current status of research. *Acta Neuropathol.* 117, 347–368. doi: 10.1007/s00401-008-0404-0

Carruthers, S. P., Van Rheenen, T. E., Gurvich, C., Sumner, P. J., and Rossell, S. L. (2019). Characterising the structure of cognitive heterogeneity in schizophrenia spectrum disorders. A systematic review and narrative synthesis. *Neurosci. Biobehav. Rev.* 107, 252–278. doi: 10.1016/j.neubiorev.2019.09.006

Carruthers, S. P., Van Rheenen, T. E., Karantonis, J. A., and Rossell, S. L. (2021). Characterising demographic, clinical and functional features of cognitive subgroups in schizophrenia spectrum disorders: a systematic review. *Neuropsychol. Rev.* 25, 1–21. doi: 10.1007/s11065-021-09525-0

Celeux, G., and Soromenho, G. (1996). An entropy criterion for assessing the number of clusters in a mixture model. *J. Classif.* 13, 195–212.

Cobia, D. J., Csernansky, J. G., and Wang, L. (2011). Cortical thickness in neuropsychologically near-normal schizophrenia. *Schizophr. Res.* 133, 68–76. doi: 10.1016/j.schres.2011.08.017

Cohen, J. (1988). *Statistical Power Analysis for the Behavioural Sciences*. Hillside, NJ: Lawrence Erlbaum Associates.

De Meo, E., Portaccio, E., Giorgio, A., Ruano, L., Goretti, B., Niccolai, C., et al. (2021). Identifying the distinct cognitive phenotypes in multiple sclerosis. *JAMA Neurol.* 78, 414–425. doi: 10.1001/jamaneurol.2020.4920

Dickinson, D., Ramsey, M. E., and Gold, J. M. (2007). Overlooking the obvious: a meta-analytic comparison of digit symbol coding tasks and other cognitive measures in schizophrenia. *Arch. Gen. Psychiatry* 64, 532–542. doi: 10.1001/archpsyc.64.5.532

First, M. B., Spitzer, R., Gibbon, M., and Williams, J. B. (1997). *Structured Clinical Interview for DSM-IV Axis I Disorders, Clinician Version (SCID-CV)*. Washington, DC: American Psychiatric Press.

Fortin, J. P., Cullen, N., Sheline, Y. I., Taylor, W. D., Aselcioglu, I., Cook, P. A., et al. (2018). Harmonization of cortical thickness measurements across scanners and sites. *Neuroimage* 167, 104–120. doi: 10.1016/j.neuroimage.2017.11.024

Fortin, J. P., Parker, D., Tunç, B., Watanabe, T., Elliott, M. A., Ruparel, K., et al. (2017). Harmonization of multi-site diffusion tensor imaging data. *Neuroimage* 161, 149–170. doi: 10.1016/j.neuroimage.2017.08.047

Friston, K. J., Williams, S., Howard, R., Frackowiak, R. S., and Turner, R. (1996). Movement-related effects in fMRI time-series. *Magn. Reson. Med.* 35, 346–355. doi: 10.1002/mrm.1910350312

Gong, J., Wang, J., Luo, X., Chen, G., Huang, H., Huang, R., et al. (2020). Abnormalities of intrinsic regional brain activity in first-episode and chronic schizophrenia: a meta-analysis of resting-state functional MRI. *J. Psychiatry Neurosci.* 45, 55–68. doi: 10.1503/jpn.180245

Grahn, J. A., Parkinson, J. A., and Owen, A. M. (2008). The cognitive functions of the caudate nucleus. *Prog. Neurobiol.* 86, 141–155. doi: 10.1016/j.pneurobio.2008.09.004

Green, M. F. (2016). Impact of cognitive and social cognitive impairment on functional outcomes in patients with schizophrenia. *J. Clin. Psychiatry* 77(Suppl 2), 8–11. doi: 10.4088/JCP.14074su1c.02

Green, M. F., Kern, R. S., Braff, D. L., and Mintz, J. (2000). Neurocognitive deficits and functional outcome in schizophrenia: are we measuring the "right stuff"? *Schizophr. Bull.* 26, 119–136. doi: 10.1093/oxfordjournals.schbul.a033430

Green, M. J., Cairns, M. J., Wu, J., Dragovic, M., Jablensky, A., Tooney, P. A., et al. (2013). Genome-wide supported variant MIR137 and severe negative symptoms predict membership of an impaired cognitive subtype of schizophrenia. *Mol. Psychiatry* 18, 774–780. doi: 10.1038/mp.2012.84

Gusnard, D. A., Raichle, M. E., and Raichle, M. E. (2001). Searching for a baseline: functional imaging and the resting human brain. *Nat. Rev. Neurosci.* 2, 685–694. doi: 10.1038/35094500

Huang, H., Botao, Z., Jiang, Y., Tang, Y., Zhang, T., Tang, X., et al. (2020). Aberrant resting-state functional connectivity of salience network in first-episode schizophrenia. *Brain Imag. Behav.* 14, 1350–1360. doi: 10.1007/s11682-019-00040-8

Jovicich, J., Czanner, S., Greve, D., Haley, E., van der Kouwe, A., Gollub, R., et al. (2006). Reliability in multi-site structural MRI studies: effects of gradient non-linearity correction on phantom and human data. *Neuroimage* 30, 436–443. doi: 10.1016/j.neuroimage.2005.09.046

Keefe, R. S., Bilder, R. M., Harvey, P. D., Davis, S. M., Palmer, B. W., Gold, J. M., et al. (2006). Baseline neurocognitive deficits in the CATIE schizophrenia trial. *Neuropsychopharmacology* 31, 2033–2046. doi: 10.1038/sj.npp.1301072

Kern, R. S., Nuechterlein, K. H., Green, M. F., Baade, L. E., Fenton, W. S., Gold, J. M., et al. (2008). The MATRICS consensus cognitive battery, part 2: co-norming and standardization. *Am. J. Psychiatry* 165, 214–220. doi: 10.1176/appi.ajp.2007.07010043

Leucht, S., Samara, M., Heres, S., and Davis, J. M. (2016). Dose equivalents for antipsychotic drugs: the DDD method. *Schizophr. Bull.* 42(Suppl 1), S90–94. doi: 10.1093/schbul/sbv167

Lewandowski, K. E., McCarthy, J. M., Öngür, D., Norris, L. A., and Liu, G. Z., Juelich, R.J., et al. (2019). Functional connectivity in distinct cognitive subtypes in psychosis. *Schizophr. Res.* 204, 120–126. doi: 10.1016/j.schres.2018.08.013

Lim, K., Smucny, J., Barch, D. M., Lam, M., Keefe, R. S. E., and Lee, J. (2020). Cognitive subtyping in schizophrenia: a latent profile analysis. *Schizophr. Bull.* 47, 712–721. doi: 10.1093/schbul/sbaa157

Lincoln, T. M., Dollfus, S., and Lyne, J. (2017). Current developments and challenges in the assessment of negative symptoms. *Schizophr. Res.* 186, 8–18. doi: 10.1016/j.schres.2016.02.035

Lis, S., Krieger, S., Wilhelm, J., and Gallhofer, B. (2005). Feedback about previous action improves executive functioning in schizophrenia: an analysis of maze solving behaviour. *Schizophr. Res.* 78, 243–250. doi: 10.1016/j.schres.2005.02.008

Liu, Y., Guo, W., Zhang, Y., Lv, L., Hu, F., Wu, R., et al. (2018a). Decreased resting-state interhemispheric functional connectivity correlated with neurocognitive deficits in drug-naive first-episode adolescent-onset schizophrenia. *Int. J. Neuropsychopharmacol.* 21, 33–41. doi: 10.1093/ijnp/pyx095

Liu, Y., Zhang, Y., Lv, L., Wu, R., Zhao, J., and Guo, W. (2018b). Abnormal neural activity as a potential biomarker for drug-naive first-episode adolescent-onset schizophrenia with coherence regional homogeneity and support vector machine analyses. *Schizophr. Res.* 192, 408–415. doi: 10.1016/j.schres.2017.04.028

Lo, Y. T., Mendell, N. R., and Rubin, D. B. (2001). Testing the number of components in a normal mixture. *Biometrika* 88, 767–778. doi: 10.1093/biomet/88.3.767

McLachlan, G. J. (1978). On bootstrapping the likelihood ratio test statistic for the number of components in a normal mixture. *Appl. Stat.* 23, 318–324.

Mesulam, M. M. (1998). From sensation to cognition. *Brain* 121(Pt 6), 1013–1052. doi: 10.1093/brain/121.6.1013

Miettunen, J., Nordström, T., Kaakinen, M., and Ahmed, A. O. (2016). Latent variable mixture modeling in psychiatric research: a review and application. *Psychol. Med.* 46, 457–467. doi: 10.1017/S0033291715002305

Morar, B., Dragović, M., Waters, F. A., Chandler, D., Kalaydjieva, L., and Jablensky, A. (2011). Neuregulin 3 (NRG3) as a susceptibility gene in a schizophrenia subtype with florid delusions and relatively spared cognition. *Mol. Psychiatry* 16, 860–866. doi: 10.1038/mp.2010.70

Muthén, L. K., and Muthén, B. O. (2015). *Mplus User's Guide, 7th Edn.* Los Angeles, CA: Muthén and Muthén.

Nuechterlein, K. H., Barch, D. M., Gold, J. M., Goldberg, T. E., Green, M. F., and Heaton, R. K. (2004). Identification of separable cognitive factors in schizophrenia. *Schizophr. Res.* 72, 29–39. doi: 10.1016/j.schres.2004.09.007

Nuechterlein, K. H., Green, M. F., Kern, R. S., Baade, L. E., Barch, D. M., Cohen, J. D., et al. (2008). The MATRICS consensus cognitive battery, part 1: test selection, reliability, and validity. *Am. J. Psychiatry* 165, 203–213. doi: 10.1176/appi.ajp.2007.07010042

Ortiz-Gil, J., Pomarol-Clotet, E., Salvador, R., Canales-Rodríguez, E. J., Sarró, S., Gomar, J. J., et al. (2011). Neural correlates of cognitive impairment in schizophrenia. *Br. J. Psychiatry* 199, 202–210. doi: 10.1192/bjp.bp.110.083600

Peters, S. K., Dunlop, K., and Downar, J. (2016). Cortico-striatal-thalamic loop circuits of the salience network: a central pathway in psychiatric disease and treatment. *Front. Syst. Neurosci.* 10, 104. doi: 10.3389/fnsys.2016.00104

Radua, J., Vieta, E., Shinohara, R., Kochunov, P., Quidé, Y., Green, M. J., et al. (2020). Increased power by harmonizing structural MRI site differences with the ComBat batch adjustment method in ENIGMA. *Neuroimage* 218, 116956. doi: 10.1016/j.neuroimage.2020.116956

Raichle, M. E. (2015). The brain's default mode network. *Annu. Rev. Neurosci.* 38, 433–447. doi: 10.1146/annurev-neuro-071013-014030

Ren, W., Lui, S., Deng, W., Li, F., Li, M., Huang, X., et al. (2013). Anatomical and functional brain abnormalities in drug-naive first-episode schizophrenia. *Am. J. Psychiatry* 170, 1308–1316. doi: 10.1176/appi.ajp.2013.12091148

Rodriguez, M., Zaytseva, Y., Cvrčková, A., Dvoraček, B., Dorazilová, A., Jonáš, J., et al. (2019). Cognitive profiles and functional connectivity in first-episode schizophrenia spectrum disorders: linking behavioral and neuronal data. *Front. Psychol.* 10, 689. doi: 10.3389/fpsyg.2019.00689

Schreiber, J. B. (2017). Latent class analysis: an example for reporting results. *Res. Soc. Adm. Pharm.* 13, 1196–1201. doi: 10.1016/j.sapharm.2016.11.011

Schwarz, G. (1978). Estimating the dimension of a model. *Ann. Stat.* 6, 461–464. doi: 10.1214/aos/1176344136

Sclove, S. L. (1987). Application of model-selection criteria to some problems in multivariate analysis. *Psychometrika* 52, 333–343.

Sestieri, C., Corbetta, M., Romani, G. L., and Shulman, G. L. (2011). Episodic memory retrieval, parietal cortex, and the default mode network: functional and topographic analyses. *J. Neurosci.* 31, 4407–4420. doi: 10.1523/JNEUROSCI.3335-10.2011

Sheffield, J. M., Karcher, N. R., and Barch, D. M. (2018). Cognitive deficits in psychotic disorders: a lifespan perspective. *Neuropsychol. Rev.* 28, 509–533. doi: 10.1007/s11065-018-9388-2

Sherman, S. M. (2016). Thalamus plays a central role in ongoing cortical functioning. *Nat. Neurosci.* 19, 533–541. doi: 10.1038/nn.4269

Shi, C., Kang, L., Yao, S., Ma, Y., Li, T., Liang, Y., et al. (2015). The MATRICS consensus cognitive battery (MCCB): co-norming and standardization in China. *Schizophr. Res.* 169, 109–115. doi: 10.1016/j.schres.2015.09.003

Siemerkus, J., Irle, E., Schmidt-Samoa, C., Dechent, P., and Weniger, G. (2012). Egocentric spatial learning in schizophrenia investigated with functional magnetic resonance imaging. *Neuroimage Clin.* 1, 153–163. doi: 10.1016/j.nicl.2012.10.004

Smucny, J., Iosif, A. M., Eaton, N. R., Lesh, T. A., Ragland, J. D., Barch, D. M., et al. (2020). Latent profiles of cognitive control, episodic memory, and visual perception across psychiatric disorders reveal a dimensional structure. *Schizophr. Bull.* 46, 154–162. doi: 10.1093/schbul/sbz025

Sun, D., Rakesh, G., Haswell, C. C., Logue, M., Baird, C. L., O'Leary, E. N., et al. (2022). A comparison of methods to harmonize cortical thickness measurements across scanners and sites. *Neuroimage* 261, 119509. doi: 10.1016/j.neuroimage.2022.119509

Thermenos, H. W., Juelich, R. J., DiChiara, S. R., Mesholam-Gately, R. I., Woodberry, K. A., Wojcik, J., et al. (2016). Hyperactivity of caudate, parahippocampal, and prefrontal regions during working memory in never-medicated persons at clinical high-risk for psychosis. *Schizophr. Res.* 173, 1–12. doi: 10.1016/j.schres.2016.02.023

Van Rheenen, T. E., Cropley, V., Zalesky, A., Bousman, C., Wells, R., Bruggemann, J., et al. (2018). Widespread volumetric reductions in schizophrenia and schizoaffective patients displaying compromised cognitive abilities. *Schizophr. Bull.* 44, 560–574. doi: 10.1093/schbul/sbx109

Wang, C., Oughourlian, T., Tishler, T. A., Anwar, F., Raymond, C., Pham, A. D., et al. (2021). Cortical morphometric correlational networks associated with cognitive deficits in first episode schizophrenia. *Schizophr. Res.* 231, 179–188. doi: 10.1016/j.schres.2021.04.001

Wang, P., Yang, J., Yin, Z., Duan, J., Zhang, R., Sun, J., et al. (2019). Amplitude of low-frequency fluctuation (ALFF) may be associated with cognitive impairment in schizophrenia: a correlation study. *BMC Psychiatry* 19, 30. doi: 10.1186/s12888-018-1992-4

Watanuki, T., Matsuo, K., Egashira, K., Nakashima, M., Harada, K., Nakano, M., et al. (2016). Precentral and inferior prefrontal hypoactivation during facial emotion recognition in patients with schizophrenia: a functional near-infrared spectroscopy study. *Schizophr. Res.* 170, 109–114. doi: 10.1016/j.schres.2015.11.012

Wexler, B. E., Zhu, H., Bell, M. D., Nicholls, S. S., Fulbright, R. K., Gore, J. C., et al. (2009). Neuropsychological near normality and brain structure abnormality in schizophrenia. *Am. J. Psychiatry* 166, 189–195. doi: 10.1176/appi.ajp.2008.08020258

Wolff, M., and Vann, S. D. (2019). The cognitive thalamus as a gateway to mental representations. *J. Neurosci.* 39, 3–14. doi: 10.1523/JNEUROSCI.0479-18.2018

Woolf, B. (1957). The log likelihood ratio test (the G-test); methods and tables for tests of heterogeneity in contingency tables. *Ann. Hum. Genet.* 21, 397–409. doi: 10.1111/j.1469-1809.1972.tb00293.x

Xu, X. M., Jiao, Y., Tang, T. Y., Lu, C. Q., Zhang, J., Salvi, R., et al. (2019). Altered spatial and temporal brain connectivity in the salience network of sensorineural hearing loss and tinnitus. *Front. Neurosci.* 13, 246. doi: 10.3389/fnins.2019.00246

Yan, C. G., Wang, X. D., Zuo, X. N., and Zang, Y. F. (2016). DPABI: data processing and analysis for (resting-state) brain imaging. *Neuroinformatics* 14, 339–351. doi: 10.1007/s12021-016-9299-4

Zang, Y. F., He, Y., Zhu, C. Z., Cao, Q. J., Sui, M. Q., Liang, M., et al. (2007). Altered baseline brain activity in children with ADHD revealed by resting-state functional MRI. *Brain Dev.* 29, 83–91. doi: 10.1016/j.braindev.2006.07.002

Zhang, Y., Liao, J., Li, Q., Zhang, X., Liu, L., Yan, J., et al. (2021). Altered resting-state brain activity in schizophrenia and obsessive-compulsive disorder compared with non-psychiatric controls: commonalities and distinctions across disorders. *Front. Psychiatry* 12, 681701. doi: 10.3389/fpsyt.2021.681701

Zhou, Y., Wang, Z., Zuo, X. N., Zhang, H., Wang, Y., Jiang, T., et al. (2014). Hyper-coupling between working memory task-evoked activations and amplitude of spontaneous fluctuations in first-episode schizophrenia. *Schizophr. Res.* 159, 80–89. doi: 10.1016/j.schres.2014.07.023

frontiers | Frontiers in Molecular Neuroscience

TYPE Original Research
PUBLISHED 03 October 2022
DOI 10.3389/fnmol.2022.1006216

OPEN ACCESS

EDITED BY
Sara Anna Bonini,
University of Brescia, Italy

REVIEWED BY
Xiangyu Zheng,
First Affiliated Hospital of Jilin University, China
Mingkai Xu,
Institute of Applied Ecology (CAS), China
Yansu Guo,
Xuanwu Hospital, Capital Medical University, China

*CORRESPONDENCE
Pu Wang
wangpu@mail.neu.edu.cn

SPECIALTY SECTION
This article was submitted to Brain Disease Mechanisms, a section of the journal Frontiers in Molecular Neuroscience

RECEIVED 29 July 2022
ACCEPTED 01 September 2022
PUBLISHED 03 October 2022

CITATION
Guan P-P, Ding W-Y and Wang P (2022) Molecular mechanism of acetylsalicylic acid in improving learning and memory impairment in APP/PS1 transgenic mice by inhibiting the abnormal cell cycle re-entry of neurons.
Front. Mol. Neurosci. 15:1006216.
doi: 10.3389/fnmol.2022.1006216

Molecular mechanism of acetylsalicylic acid in improving learning and memory impairment in APP/PS1 transgenic mice by inhibiting the abnormal cell cycle re-entry of neurons

Pei-Pei Guan, Wei-Yan Ding and Pu Wang*

College of Life and Health Sciences, Northeastern University, Shenyang, China

Alzheimer's disease (AD) is a neurodegenerative disorder accompanied by the loss and apoptosis of neurons. Neurons abnormally enter the cell cycle, which results in neuronal apoptosis during the course of AD development and progression. However, the mechanisms underlying cell cycle re-entry have been poorly studied. Using neuroblastoma (N) $2a^{SW}$ and APP/PS1 transgenic (Tg) mice as *in vitro* and *in vivo* AD models, we found that the expression of cyclin-dependent kinase (CDK)1/2/4 and cyclin A2/B1/D3/E1 was increased while the protein expression of p18 and p21 was decreased, which led to enhanced cell cycle re-entry in a β-amyloid protein (Aβ)-dependent mechanism. By preparing and treating with the temperature-sensitive chitosan-encapsulated drug delivery system (CS), the abnormal expression of CDK1/2/4, cyclin A2/B1/D3/E1 and p18/21 was partially restored by acetylsalicylic acid (ASA), which decreased the apoptosis of neurons in APP/PS1 Tg mice. Moreover, CDK4 and p21 mediated the effects of ASA on activating transcription factor (TF) EB *via* peroxisome proliferator-activated receptor (PPAR) α, thus leading to the uptake of Aβ by astrocytes in a low-density lipoprotein receptor (Ldlr)-dependent mechanism. Moreover, the mechanisms of Aβ-degrading mechanisms are activated, including the production of microtubule-associated protein light chain (LC) 3II and Lamp2 protein by ASA in a PPARα-activated TFEB-dependent manner. All these actions contribute to decreasing the production and deposition of Aβ, thus leading to improved cognitive decline in APP/PS1 Tg mice.

KEYWORDS

cell cycle re-entry, acetylsalicylic acid, apoptosis, lysosomal biogenesis, autophagy

Introduction

Alzheimer's disease (AD) is a neurodegenerative disease characterized by progressive memory loss and cognitive impairment with the deposition of β-amyloid protein (Aβ) in β-amyloid plaques (APs) and hyperphosphorylated tau in neurofibrillary tangles (NFTs) (Laferla and Oddo, 2005). Progressively, the neurons show a vacuolar degeneration and neuronal loss morphology (Laferla and Oddo, 2005). Therefore, the hypothesis of cell cycle re-entry was proposed to define the association between neurodegenerative diseases and neuronal loss (Khurana and Feany, 2007). For a long time, researchers believed that most differentiated cells will remain in the G0 phase of the cell cycle, except for cells that need active division, such as bone marrow stem cells and digestive tract mucosal cells. In the mature central nervous system (NCS), neurons are generally considered to be in the terminal state of differentiation, which means that they no longer enter the cell cycle. However, an increasing number of studies have shown that the neuronal cell cycle can abnormally restart under some pathological conditions, such as neurodegenerative disease and cerebral ischemia (Liu and Greene, 2001). For example, the expression of cyclin B and cyclin D was significantly higher in patients with mild cognitive impairment (MCI) and AD than in corresponding control subjects (Yang et al., 2003). Moreover, microchromosome maintenance complex component 2 (MDM2), which is an essential protein for DNA replication, was identified in AD patients (Bonda et al., 2009), and it can be phosphorylated by CDKs and CDC7 in S phase (Bonda et al., 2009). Immunohistochemistry (IHC) analysis showed that MDM2 was located around NFTs (Bonda et al., 2009), which provides definite evidence for aberrant cell cycle re-entry in AD neurons.

Indeed, cell cycle re-entry appears to occur earlier than the formation of APs and NFTs (Evans, 2007). Until now, there have been a series of methods to induce the cell cycle re-entry of neurons, through which its relationship with AD has been investigated. Studies have shown that mature neurons are forced to enter the cell cycle by overexpressing the antigen Simian Virus 40 T, which results in the formation of APs and NFTs. In addition, most neurons reached G2 phase according to the BrdU assay after injecting c-myc and mutated ras into primary cultured cortical neurons. More importantly, tau protein is phosphorylated and undergoes conformational changes, which is similar to the pathological changes of tau protein in AD (McShea et al., 2007). Reciprocally, Aβ treatment and tau^{P301L} expression in an AD tissue culture model act synergistically to promote aberrant cell cycle re-entry (Hoerndli et al., 2007). After cell cycle re-entry, neurons cannot continue to differentiate but induce the signaling cascades of apoptosis based on the expression of caspase 3 (Love, 2003), thus leading to neuronal loss during the course of AD development and progression.

Based on these clues, accumulating evidence suggests that factors that induce inhibition or block the progression of the cell cycle can protect neurons from death in AD, which provides a potential strategy for the treatment of AD (Snape et al., 2009). In other words, blocking cell cycle re-entry will provide insights into AD treatment. Retinoic acid (RA) can block the progression of the cell cycle to the G0/G1 phase by upregulating the expression of p62 and p56 in neurons (Lamkin et al., 2006). Similarly, simvastatin (Murakami et al., 2001), taurine (Chen et al., 2004), interleukin (IL) (Morinaga et al., 1990), and interferon (Sangfelt et al., 1999) can block the cell cycle to the G0/G1 phase, which exerts neuroprotective effects on neurons in AD.

Apart from the above interventions, epidemiological investigations have shown that long-term administration of acetylsalicylic acid (ASA) obviously decreases the risk of AD (Pomponi et al., 2008), suggesting its potential application prospect for combating the disease. Evidence has shown that ASA has the ability to block the effects of $A\beta_{1-40}$ on releasing IL-6 and tumour necrosis factor (TNF)-α, thus leading to improved learning and memory. Moreover, Tortosa et al. (2006) found that ASA can inhibit the phosphorylation of tau and the formation of NFTs. Asanuma et al. (2001) pointed out that ASA is capable of clearing nitric oxide (NO), through which it protects neurons from oxidative stress-induced impairment. Moreover, Legler et al. (2010) confirmed that ASA can reduce the synthesis of prostaglandin (PG) E_2 by inhibiting platelet activation, which alleviates inflammatory injury in neurons.

In addition to these functions, ASA may be also involved in regulating the clearance of Aβ during the course of AD development and progression. During this process, transcription factor (TF) EB overexpression potentially contribute to decrease the accumulation of Aβ *via* autophagic lysosome-degrading pathways, leading to alleviation of the progression of AD (Zhang and Zhao, 2015). Notably, peroxisome proliferator-activated receptor (PPAR)α is reported to mediate the transcriptional synthesis of TFEB in brain cells (Ghosh et al., 2015), suggesting the important roles of PPARα and TFEB pathways in mediating Aβ clearance.

Although ASA may be beneficial for AD, its effects on the cell cycle re-entry of neurons are not thoroughly known, rather than its inherent mechanisms. As a water-insoluble drug, ASA shows relatively high toxicity and side effects, which restricts its practical applications. Recently, *in vivo* temperature-sensitive chitosan gel has progressively become a good drug delivery system for decreasing the toxicity and side effects of drugs (Eve and Leroux, 2004). In detail, chitosan and glycerol phosphate are used to prepare thermosensitive hydrogels loaded with adriamycin (an effective drug for treating malignant tumors), which achieve

better therapeutic effects by decreasing toxicity and side effects. Under the condition of long-term administration, nasal mucosal administration has a natural advantage to treat AD by bypassing the blood–brain barrier (BBB) through the olfactory nerve and directly reaching brain tissue.

Based on the above clues, the current study aimed to reveal the regulatory mechanisms of cell cycle re-entry during the course of AD development and progression. Taking advantage of the ASA-CS drug delivery system, we revealed that ASA protects neurons from apoptosis by inhibiting cell cycle re-entry. In addition, we described the roles of ASA in disrupting the deposition of Aβ in APs and inducing the uptake of Aβ for degradation in the astrocytes of APP/PS1 transgenic (Tg) mice. All these actions mediate the effects of ASA on improving the cognitive decline of AD animals.

Materials and methods

Reagents

Acetylsalicylic acid, chitosan, Aβ, GW6471 and β-glycerphosphate were obtained from Sigma-Aldrich (Shanghai, China). Antibodies specific for CDK4, cyclin E1 and p21 were obtained from ImmunoWay Biotechnology Company (Suzhou, Jiangsu, China). Antibodies for low-density lipoprotein receptor (Ldlr) and PPAR α were purchased from Abcam (Shanghai, China). Antibodies for Aβ, CDK1, CDK2, cyclin A2, Cyclin B1, Cyclin D3, p18, Caspase 3, NeuN, PSD95, SYP, Bax, Bcl-2, GFAP, TFEB, LC3, Lamp2, histone, and β-actin were purchased from Cell Signaling Technology (Shanghai, China). $A\beta_{1-40}$ and $A\beta_{1-42}$ immunoassay kits were purchased from Invitrogen (Shanghai, China). The kits for RNA extraction, reverse transcription and real-time PCR were obtained from Promega Corporation (Beijing, China). The kits for IHC were purchased from MXB Biotechnologies (Fuzhou, Fujian, China). All other reagents were from Thermo Fisher Scientific (Shanghai, China) and Fuyu Chemical (Tianjin, China) unless specified otherwise.

Cell culture

D1A, neuroblastoma (N) 2a, $N2a^{WT}$ and $N2a^{SW}$ cells were cultured in 5% CO_2 at 37°C on 6 cm tissue culture dishes in dulbecco's modified eagle medium (DMEM) culture medium. In a select set of experiments, N2a cells were incubated in serum-deprived medium for an additional 24 h before treatment with the indicated concentration of ASA (5 or 10 μM) in the absence or presence of Aβo (20 nM). In a separate set of experiments, N2a cells were transfected with CDK4 shRNA or p21 cDNA before treatment with Aβo. In a separate set of experiments, D1A cells were treated with ASA (10 μM) in the absence or presence of the PPARα antagonist GW6471 (1 μM) or transfected with shRNA targeting TFEB or p21 or cDNA constructs encoding CDK4 coding sequences. After treatment, the cells were lysed for RNA or protein extraction or stained with 3-(4,5-Dimethylthiazol-2-yl)-2,5-diphenyltetrazolium bromide (MTT) assay (3 h at 37°C).

Animals

Wild-type (WT) mice were purchased from Liaoning Chengda Biotechnology Co., Ltd. (Benxi, Liaoning, China). APP/PS1 (Stock No. 004462) Tg mice were obtained from the Jackson Laboratory (Bar Harbor, ME, USA). Genotyping was per-formed after 1 month of birth. The mice were then randomly divided into different groups, which are, respectively treated with vehicle, ASA solution or ASA CS (0.2 mg/kg/d) for 3 months. The general health and body weights of the animals were monitored every day. The Morris maze test and nest construction were performed before collecting brains under anesthesia.

Preparation of the thermosensitive chitosan gels

First, 200 mg of CS (medium viscosity, degree of deacetylation is 91) was dissolved in hydrochloric acid and acetic acid (v:v, 4:1) solution under vigorous stirring. After CS was dissolved, the solution was cooled down by placing it on ice for 20 min. Then, 200 mg of β-glycerphosphate (GPS) in 0.4 ml of distilled water was slowly added to the CS solution. The mixture was heated in a 37°C water bath, after which thermosensitive chitosan gels were formed in a few minutes. To prepare ASA-CS, a certain amount of ASA was added to a 2% CS solution. After dissolving by oscillation, GPS was added to the solution to mix together on ice. Then, the mixture will be placed in a 37°C water bath until ASA-CS gels form.

Protein extraction and western blots

A total of 100 μl of lysis buffer was added to cell pellets or tissues with the inhibitors of 1 μl proteinase and 1 μl phosphatase. After smashing with 1 ml syringe, the samples were vortexed on ice every 10 min. After 1 h, the tubes were centrifuged at 15, 000 rpm for 15 min at 4°C. The supernatants were collected and stored at −80°C for use. The protein concentration was measured by BCA kits (Pierce, Shanghai, China) and calculated by standard curve. The samples were diluted according to the protein concentration, which was loaded in SDS-PAGE. After transferring to polyvinylidene

fluoride (PVDF) membrane, the protein was probed with specific antibody. After developing, the specific band was visualized by ECL (Tanon, Shanghai, China).

RNA extraction and real-time PCR

The cells and tissues were crushed by ultrasonication in 1 ml TRIzol on ice. After vortexing for 30 s, 0.2 ml of chloroform was added to the tube and then vortex vigorously for 15 s. After centrifugation at 12, 000 rpm for 10 min, the supernatant was transferred to a new tube. The RNA was then purified by RNA extraction kits (Thermo Fischer Scientific, Shanghai, China). After analyzing the concentration of RNA with NanoDrop microvolume spectrophotometer (Thermo Fischer Scientific, Shanghai, China), the RNA was diluted and used for the real-time PCR assays. In brief, real-time PCR assays were performed with the MiniOpticon Real-Time PCR detection system (Bio-Rad Laboratories, Beijing, China) with Real-Time PCR kits and the appropriate primers. The sequences of primers were listed in Table 1. The gene expression values were normalized to that of GAPDH.

Enzyme-linked immunosorbent assay

The mouse $A\beta_{1-40}$ and $A\beta_{1-42}$ kits were obtained from Thermo Fisher Scientific (Shanghai, China).

TABLE 1 The list for the sequences of primers.

Genes	F/R	Sequences
CDK1	Forward	CCAAGAAGCCGCTTTTCCAC
	Reverse	AAAGTACGGGTGCTTCAGGG
CDK2	Forward	TACCCAGTACTGCCATCCGA
	Reverse	GACACGGTGAGAATGGCAGA
CDK4	Forward	GGAGGCCTTTGAACATCCCA
	Reverse	GTTCTCTGGCTTCAGGTCCC
CyA2	Forward	GTCAACCCCGAAAAACTGGC
	Reverse	CAGCTGGCCTCTTCTGAGTC
CyB1	Forward	TCTCCAAGCCCGATGGAAAC
	Reverse	ACATGGTCTCCTGAAGCAGC
CyD3	Forward	AAACAGATGTCCTGCAGCGA
	Reverse	TGTGCGGCTTGATCTCCTTT
CyE1	Forward	GAAAAGCGAGGATAGCAGTCAG
	Reverse	CCCAATTCAAGACGGGAAGTG
p18	Forward	GATTTGGGAGAACTGCGCTG
	Reverse	TGCAGGCTGTGTGCTTCATA
p21	Forward	GTACTTCCTCTGCCCTGCTG
	Reverse	CTGACCCACAGCAGAAGAGG
GAPDH	Forward	TTCACCACCATGGAGAAGGC
	Reverse	AGTGATGGCATGGACTGTGG

The contents of $A\beta_{1-40}$ and $A\beta_{1-42}$ were measured according to the manufacturer's instructions. In brief, samples, standards or controls were added into the wells, which bind to the immobilized antibody specific for $A\beta_{1-40}$ or $A\beta_{1-42}$. By sequentially adding the secondary antibody and substrate solution, the contents of $A\beta_{1-40}$ and $A\beta_{1-42}$ were calculated according to the standard curve.

Flow cytometry

The cells were collected with 0.05% trypsin. After centrifugation at 1,000 rpm for 5 min, the cells were immobilized by 1 ml of 70% ethanol at −4°C for 2 h. Then, the cells were stained with PI in the dark before analysis using a BD Accuri C6 flow cytometer (BD, Shanghai, China).

MTT assay

The cells treated without or with the indicated concentration of chemical reagents were removed from incubator into laminar flow hood. 100 μl of MTT solution was added to 96 well plates. After incubating at 37°C for 3 h, the plates were centrifuged and replaced with MTT solvents (4 mM HCl, 0.1% NP40 in isopropanol). After 15 min, the optical density was read at 590 nm.

Intracerebroventricular injection

Aβ oligomers or vehicle was injected intracerebroventricularly (i.c.v.) into C57BL/6 mice. In selected experiments, the mice were intranasal administered with ASA solution or ASA-CS before injecting (i.c.v.) Aβo. In brief, stereotaxic apparatus was adjusted to the appropriate coordinate according to the location of bregma (mediolateral, 21.0 mm; anteroposterior, 20.22 mm, and dorsoventral, 22.8 mm). The chemical reagents were slowly injected to the ventricles of mice and the injector was slowly taken out. After injection, the mice were put on the heated pad before sobering up.

Aβ preparation

Freeze-dried Aβ monomer was dissolved in 100% HFIP to prepare 1.0 μg/μl solution. The solution was equally distributed into Eppendorf tubes and vacuum dried to store in −80°C refrigerator. The vacuum dried Aβ monomer was reconstituted with dimethyl sulfoxide (DMSO) in ultrasound water bath

for 10 min to prepare 20 μg/μl solutions. Until Aβ was thoroughly dissolved, F-12 medium without phenol red was added to adjust the final concentration to 0.2 μg/μl. The solution was incubated at 4°C for 24 h before obtaining Aβo. The quality of oligomers product was controlled by Western blot using Aβ antibody (Cell Signaling Technology, Shanghai, China).

Aβ uptake and degradation

D1A cells were incubated with Aβ for 2 h. Then, the cells were lysed to measure the uptake of Aβ by enzyme-linked immunosorbent assay (ELISA), washed with fresh medium two times and incubated in medium for an additional 46 h before determining the degradation of Aβ by ELISA.

Tissue embedding and Immunohistochemistry

Mouse brains were collected from WT or APP/PS1 Tg mice, which is treated without or with ASA. The brains were immobilized in 4% paraformaldehyde for 48 h, soaked in 70% ethanol overnight, and soaked in 80% ethanol for 1 h at room temperature. For dehydration, the tissues were soaked sequentially in 90, 95, and 100% ethanol (twice) for 0.5 h. The tissues were then placed in xylene for 2 min−2 h and a xylene: soft wax mixture for 1.5 h and hard wax for 1.5 h. After tissue embedding, serial sections (5 μm thick) were cut using a paraffin slice (Leica, RM2235, Germany), and the sections were used for morphological determination. In detail, the slides were rehydrated with xylene and gradient ethanol, which were then eliminate endogenous peroxidase antigen for 30 min and repair the antigens for 20 min. After blocking with goat serum for 0.5 h, the slides were incubated with specific antibody overnight at 4°C. After rinsing with 0.01 M PBS for three times, the slide was incubated with secondary antibody for 2 h and streptomycin anti-biotin peroxidase for 1 h. After rinsing with PBS, the slides were visualized with DAB. In selected experiments, the nuclei of the cells in the brains were stained with hematoxylin for 1 min. The slides were finally dehydrated with gradient ethanol and cleared with xylene, which were then mounted with neutral resin before observing under microscopy.

Plasmid construction and transfection

The siRNA targeted CDK4, p21, or TFEB was designed by siRNA selection tool (Thermo Fisher Scientific, Shanghai, China) and synthesized by GENEWIZ (Suzhou, Jiangsu, China). The genetic fragments were inserted into the lentiviral pLKO.1 vectors. After sequencing, the shRNA plasmids were purified and co-transfected with packaging vectors (psPAX2 and pMD2.G) into HEK293T cells. After 48 and 72 h, the lentiviral particles in the supernatant were concentrated through ultracentrifugation and resuspended in phosphate buffered saline (PBS) (−). For knocking down the expression of corresponding genes, the lentiviral particles that contained shRNA or control shRNA were adjusted to 10^6–10^7 titers prior to infecting N2a or D1A cells. For overexpression, the coding sequences of CDK4 or p21 were synthesized and inserted into the pcDNA3.1 plasmids. The vector or plasmids were transfected to N2a or D1A cells with lipofectamine 2000 according to the manufacturer's instructions (Invitrogen, Shanghai, China).

Nest construction

The mice were housed in cages with corncob bedding for 1 week before the nest construction test. 2 h before the onset of the dark phase of the light cycle, eight pieces of paper (5 cm × 5 cm) were introduced into the home cage to create conditions for nesting. The nests were recorded on the following mornings according to a 4-point system: (1) no biting/tearing, with random dispersion of the paper; (2) no biting/tearing of paper, with gathering in a corner/side of the cage; (3) moderate biting/tearing of paper, with gathering in a corner/side of the cage; and (4) extensive biting/tearing of paper, with gathering in a corner/side of the cage.

Morris maze test

The experimental training phase was carried out three times per day for 10 consecutive days. During first 2 day, put the mice into the pool and record the time required for the mice to find the visible platform. In the following 7 day of training, the time was recorded for the mice to find the underwater hidden platform from the water entry point facing the pool wall. After the mice find the platform, let the mice stand on the platform for 10 s. If the mice failed to find the platform within 60 s, gently put them on the platform for 10 s. For the last day, the platform will be removed to record the passing times of the original location of platforms.

Animal committee

All animals were handled according to the guidelines for the care and use of medical laboratory animals (Ministry of Health,

Peoples Republic of China, 1998) and the guidelines of the laboratory animal ethical standards of Northeastern University.

Statistics

All data are presented as the means ± S.E. of at least three independent experiments. The statistical significance of the differences between the means was determined using Student's *t*-test or one-way analysis of variance, where appropriate. If the means were significantly different, multiple pairwise comparisons were performed using Tukey's *post hoc* test.

Results

Aspirin attenuates amyloid plaques pathology

Given the potential roles of ASA in AD, we further determined the effects of ASA on the production and deposition of Aβ in APP/PS1 Tg mice. Although ASA solution could lower the average production of $A\beta_{1-42}$ and $A\beta_{1-40}$, ASA-CS significantly suppressed the production of $A\beta_{1-42}$ and $A\beta_{1-40}$ in the brains of APP/PS1 Tg mice (**Figures 1A,B**). To further explore the roles of ASA in the formation of APs, IHC

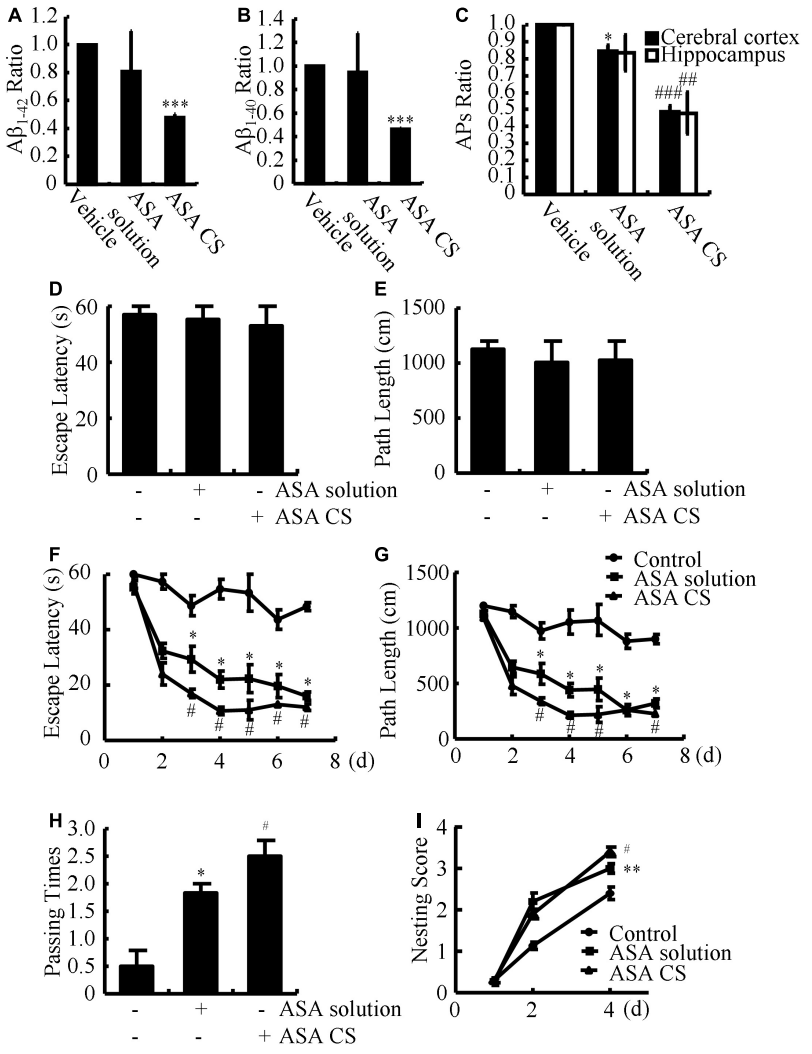

FIGURE 1
ASA-CS shows better effects on improving the cognitive decline of APP/PS1 Tg mice than that of ASA solution *via* disrupting the production and deposition of Aβ. **(A–I)** APP/PS1 Tg mice were intranasally administered with ASA solution or ASA CS (0.2 mg/kg/d) for 3 months. **(A,B)** The contents of $A\beta_{1-40}$ and $A\beta_{1-42}$ in the cerebral cortex and hippocampus were determined by ELISA. **(C)** The ratio of APs in the cerebral cortex and hippocampus of APP/PS1 Tg mice was determined using IHC. **(D,E)** Escape latency and path length of mice in the visible platform experiments. **(F,G)** Escape latency and path length of mice in the invisible platform experiments. **(H)** In the spatial exploration experiment, the number of times the animals crossed over the original platform was recorded by the software. **(I)** Nest construction of different group of mice were analyzed according to nesting scores. Data are presented as the means ± S.E. of independent experiments, $^{*}p < 0.05$; $^{**}p < 0.01$; $^{***}p < 0.001$ compared to vehicle-treated mice, $^{\#}p < 0.05$; $^{\#\#}p < 0.01$; $^{\#\#\#}p < 0.001$ compared to ASA solution-treated APP/PS1 Tg mice.

experiments were carried out. The results showed that both ASA solution and ASA-CS inhibited the deposition of Aβ in APs (Figure 1C). Notably, ASA-CS showed relatively higher efficacy in suppressing the formation of APs than ASA solution in APP/PS1 Tg mice (Figure 1C).

Acetylsalicylic acid-chitosan-encapsulated drug delivery system shows better effects on improving the cognitive decline of APP/PS1 Tg mice than acetylsalicylic acid solution

Based on the observation that ASA treatment attenuates Aβ aggregation and deposition of Aβ, we next investigated the relationship between ASA and memory deficits in APP/PS1 Tg mice. After 3 months of ASA treatment, we assessed spatial learning and memory abilities by the Morris maze test. In visible platform experiments, the distinct groups of mice did not show much difference, suggesting that neither ASA solution nor ASA-CS administration affected the motility and vision of mice (Figures 1D,E). In the following invisible platform experiments, ASA-CS showed better therapeutic effects on memory loss than ASA solution (Figures 1F,G). After removing the platform, ASA-CS increased the passing times of the original location of the platform compared to that of the ASA solution (Figure 1H). Moreover, nest construction is a natural inborn ability, and it became progressively impaired in APP/PS1 Tg mice; however, this impairment was reversed by ASA treatment, especially ASA-CS treatment (Figure 1I).

Identification of differential expression of cell cycle-regulated genes in *in vitro* and *in vivo* Alzheimer's disease models

To study differential gene expression in AD models, we initially assessed the mRNA and protein expression of cell cycle-related genes in N2a^{SW} cells compared to that of vector-transfected cells. The results demonstrated that the mRNA and protein expression of CDK1/2/4 and CyA2/B1/D3/E1 was upregulated, whereas p18 and p21 were downregulated in N2a^{SW} cells (Figure 2A and Table 2). In the hippocampus of 3-month-old APP/PS1 Tg mice, cell cycle-related genes were regulated similarly as those in N2a^{SW} cells (Figure 2B and Table 3). However, the mRNA expression of cell cycle-related genes was not always consistent with those of N2a^{SW} cells in the cerebral cortex of 3-month-old APP/PS1 Tg mice (Table 3). Given the critical roles of Aβ in AD, we further treated N2a cells and C57BL/6 mice with Aβ oligomers (Aβo). By measuring the expression of cell cycle-related genes, Aβo showed positive effects on concurrently upregulating the mRNA and protein expression of CDK1/2/4 and CyA2/B1/D3/E1 and downregulating the expression of p18 and p21 in N2a cells and the hippocampus of C57BL/6 mice (Figures 2C,D and Tables 4, 5). For their important roles in the progression of G0/G1 phase, our results suggested the re-entry of the cell cycle during the course of AD development and progression.

Preparation and *in vitro* release of acetylsalicylic acid-chitosan-encapsulated drug delivery system

To perform brain-targeted drug delivery and decrease the toxicity and side effects of ASA, ASA-CS was prepared for intranasal administration. ASA-CS is in a liquid state at room temperature while CS forms a cross-linking 3D colloidal gel under physiological conditions. Therefore, ASA-CS will form gels in the nasal cavity because of the thermosensitive properties of CS. By forming the gels, CS will control the slow release of ASA to maintain a stable blood drug concentration. Taking advantage of this approach, it can reduce the times of drug administration and prolong the biological half-life of drugs. In addition, intranasal administration will avoid the first pass effect of the liver and improve the bioavailability of the drug.

Acetylsalicylic acid-chitosan-encapsulated drug delivery system showed better effects on restoring the expression of cell cycle-regulated genes than acetylsalicylic acid solution

We next determined the effects of ASA on the progression of the cell cycle. For this purpose, N2a cells were first treated with 5 or 10 μM ASA. Treatment with ASA decreased the mRNA and protein expression of CDK1/2/4 and CyA2/B1/D3/E1, whereas the expression of p18 and p21 was increased compared to vehicle-treated controls (Figure 3A and Table 6). To validate these *in vitro* data, ASA-CS and ASA solutions were intranasally administered to APP/PS1 Tg mice. Interestingly, ASA-CS showed better effects on restoring the expression of cell cycle-regulated genes than ASA solution (Figure 3B and Table 7). These observations suggested better therapeutic effects of ASA-CS than ASA solution on restoring the expression of cell cycle-regulated genes.

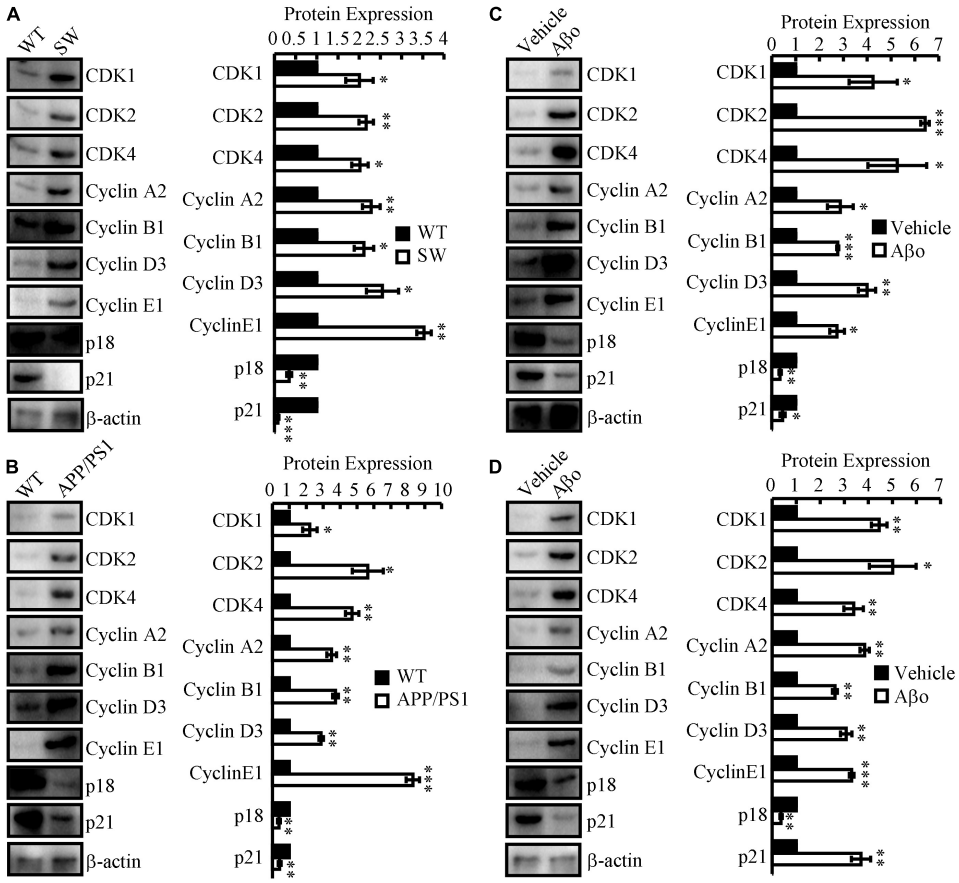

FIGURE 2
The expression of cell cycle-regulated genes in *in vitro* and *in vivo* AD models. **(A)** N2a^{SW} cells were established by transfecting N2a cells with swedish mutated APP plasmids. **(B)** The brains of 3-month-old APP/PS1 Tg mice were collected for the following experiments. **(C)** Aβo was prepared to treat N2a cells at the concentration of 20 nM. **(D)** Aβo (2 ng/5μl) was injected (i.c.v.) to the ventricles of C57BL/6 mice. **(A–D)** The total protein was extracted from the cells and brains. Western blotting was employed to detect the expression of CDK1/2/4, cyclin A2/B1/D3/E1, p18 and p21. β-actin served as an internal control. The optical density of the bands was analyzed using ImageJ software. Data are presented as the means ± S.E. of independent experiments, $^{*}p < 0.05$; $^{**}p < 0.01$, and $^{***}p < 0.001$ compared to the controls.

TABLE 2 The expression of cell cycle-associated genes in N2a^{sw} cells.

Genes cells	CDK1	CDK2	CDK4	CyA2	CyB1	CyD3	CyE1	p18	p21
N2a^{sw}	2.10	3.21	1.24	1.65	2.06	1.32	1.66	0.34	0.86

TABLE 3 The expression of cell cycle-associated genes in the brains of 3-month-old APP/PS1 mice.

Genes ER	CDK1	CDK2	CDK4	CyA2	CyB1	CyD3	CyE1	p18	p21
Hippocampus	3.38	2.09	4.68	3.63	5.48	2.40	2.23	0.27	0.43
Cortex	0.44	0.71	0.82	0.08	0.09	0.54	1.93	1.07	0.44

ER, encephalic region.

TABLE 4 The expression of cell cycle-associated genes in Aβo-treated N2a cells.

Genes N2a cells	CDK1	CDK2	CDK4	CyA2	CyB1	CyD3	CyE1	p18	p21
Aβo	1.28	3.31	1.26	1.42	3.28	12.77	2.55	0.06	0.63

TABLE 5 The expression of cell cycle-associated genes in Aβo-injected (i.c.v) mice.

Genes ER	CDK1	CDK2	CDK4	CyA2	CyB1	CyD3	CyE1	p18	p21
Hippocampus	6.66	1.37	2.01	10.41	9.85	7.54	1.05	0.01	0.02
Cortex	0.99	0.46	0.09	0.21	0.07	1.17	1.01	0.30	1.56

ER, encephalic region.

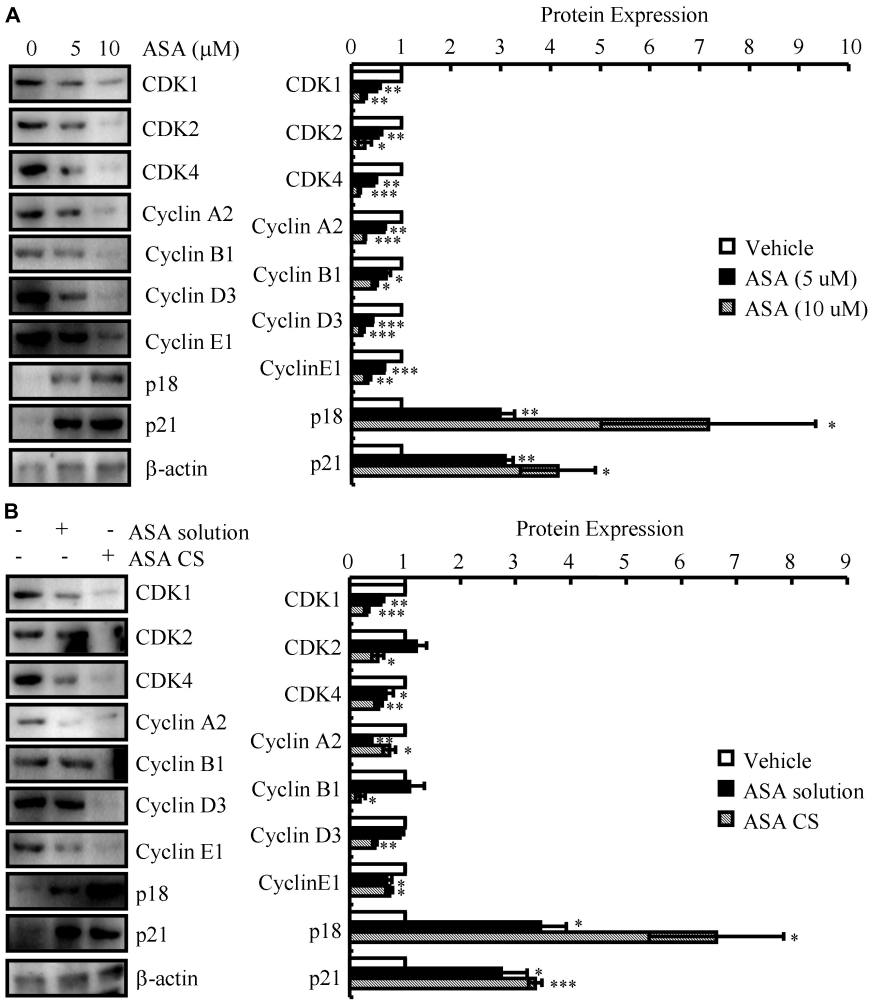

FIGURE 3
ASA-CS showed better effects on restoring the expression of cell cycle-regulated genes than that of ASA solution. **(A)** N2a cells were treated with 5 or 10 μM ASA. **(B)** ASA-CS and ASA solutions were intranasally administered to APP/PS1 Tg mice. **(A,B)** The total protein was extracted from the cells and brains. Western blotting was employed to detect the expression of CDK1/2/4, cyclin A2/B1/D3/E1, p18 and p21. β-actin served as an internal control. The optical density of the bands was analyzed using ImageJ software. Data are presented as the means ± S.E. of independent experiments, $^{*}p < 0.05$; $^{**}p < 0.01$, and $^{***}p < 0.001$ compared to the controls.

TABLE 6 The expression of cell cycle-associated genes in aspirin-treated N2a cells.

Genes Aspirin	CDK1	CDK2	CDK4	CyA2	CyB1	CyD3	CyE1	p18	p21
5 μM	0.46	0.87	0.61	0.66	0.96	1.16	0.91	1.13	0.95
10 μM	0.36	0.52	0.18	0.67	0.80	0.63	0.37	2.18	1.78

TABLE 7 The expression of cell cycle-associated genes in aspirin-administered mice.

Genes hippocampus	CDK1	CDK2	CDK4	CyA2	CyB1	CyD3	CyE1	p18	p21
Solution	0.49	0.76	0.19	0.38	0.78	0.31	0.50	2.54	1.95
Nasal gel	0.25	0.35	0.11	0.18	0.29	0.19	0.38	6.28	4.37

Cyclin-dependent kinase 4 and p21 mediate the effects of acetylsalicylic acid on protecting neurons from cell cycle re-entry, thereby inhibiting neuronal apoptosis

To further investigate the relationship with the cell cycle, flow cytometry experiments were carried out to determine the effects of ASA on the progression of the cell cycle in Aβo-treated N2a cells. The results demonstrated that Aβo obviously enhanced the proportion of N2a cells in S phase (Figure 4A). These observations indicate that Aβo triggers the cell cycle re-entry of neurons and suggest the consequences of cell cycle re-entry to neurons. For this purpose, N2a cells were used in the following experiments and treated with Aβo in the absence or presence of ASA. Based on a MTT assay, ASA showed beneficial effects on preventing neuronal death (Figure 4B). Mechanistically, Aβo induces the cleavage of caspase 3, which is attenuated by the addition of ASA to N2a cells (Figure 4C). Furthermore, N2a cells were transfected with either CDK4 shRNA or p21 cDNA before treatment with Aβo. Moreover, the MTT assay showed that knocking down the expression of CDK4 or ectopic expression of p21 ameliorated the effects of Aβo on inducing the death of neurons (Figure 4D). Of note, caspase 3 located downstream of CDK4 and p21 mediated the effects of Aβo on inducing neuronal death (Figure 4E).

To further validate these *in vitro* data, APP/PS1 Tg mice were administered ASA solution and ASA-CS for 3 months. Western blots assays showed that ASA-CS had better effects on restoring the protein levels of NeuN, PSD95, and SYP than ASA solution (Figure 4F). Moreover, ASA also showed the inhibitory effects of lowering the levels of caspase 3 in the brains of APP/PS1 Tg mice (Figure 4G). Along these lines, CDK4 and p21 mediate the effects of ASA on protecting neurons from cell cycle re-entry, leading to inhibition of neuronal death.

Aspirin induces the uptake of Aβ for degradation in astrocytes

Based on the above observations, we continued to investigate the effects of ASA on the uptake of Aβ for degradation in astrocytes since astrocytes are activated in the brains of APP/PS1 Tg mice (Figure 5A). For this purpose, D1A cells were used in the following experiments. Treatment with ASA showed that the expression of Ldlr was up-regulated in D1A cells (Figure 5B), whose expression is critical for the uptake of Aβ in astrocytes. A report showed that the activation of the nuclear receptor PPARα by its agonist fenofibrate induces the expression of Ldlr; thus, we determined the effects of ASA on the activity of PPARα in astrocytes. As expected, ASA treatment induced the expression of not only PPARα but also its downstream target, TFEB, in astrocytes (Figures 5C,D). To further determine the uptake of Aβ by astrocytes, D1A cells were transfected with TFEB shRNA or treated with the PPARα antagonist GW6471 in the presence of ASA. By incubating with Aβ, the contents of Aβ in the cell lysates were determined by ELISA after 2 h of treatment with ASA. The results demonstrated that the contents of Aβ in cell lysates were induced by ASA treatment, which was blocked by TFEB knockdown and GW6471 treatment in D1A cells (Figure 5E), suggesting that ASA induces the uptake of Aβ *via* PPARα-dependent TFEB-activating mechanisms. Moreover, questions are easily raised regarding whether cell cycle re-entry is involved in regulating the uptake of Aβ by ASA treatment. For this purpose, we overexpressed CDK4 and knocked down the expression of p21 in ASA-treated D1A cells. Western blot assays showed that ASA induced the translocation of TFEB from the cytosol to the nucleus, which was partially blocked by CDK4 overexpression and p21 knockdown in D1A cells (Figure 5F). As a consequence, the uptake of Aβ was elevated by ASA treatment, which was attenuated by ectopically expressing CDK4 or p12 knockdown in D1A cells (Figure 5G). Therefore, our data revealed that cell cycle re-entry is involved in regulating the uptake of Aβ in an ASA-stimulated PPARα-dependent TFEB-activating mechanism.

Since ASA has shown its effects on inducing the uptake of Aβ in astrocytes, we investigated whether ASA has the ability to trigger the degradation of Aβ in cells. As expected, we further found that ASA treatment augmented the production of LC3II in D1A cells (Figure 6A), suggesting that autophagy might be activated by ASA to degrade Aβ. Because lysosomes are responsible for Aβ degradation, we continued to measure the activity of lysosomes in ASA-treated D1A cells. Western blot assays showed that ASA has the ability to upregulate the expression of Lamp2, a marker for lysosomes, which was blocked by GW6471 treatment or TFEB knockdown in D1A cells (Figures 6B,C). More interestingly, we found that ASA treatment for 24 h did not elevate the contents of Aβ but reduced the contents of Aβ in the cell lysates of D1A cells (Figure 6D), suggesting the ability of ASA to degrade Aβ. Moreover, GW6471 treatment or TFEB knockdown blocked the effects of ASA on inducing the degradation of Aβ in D1A

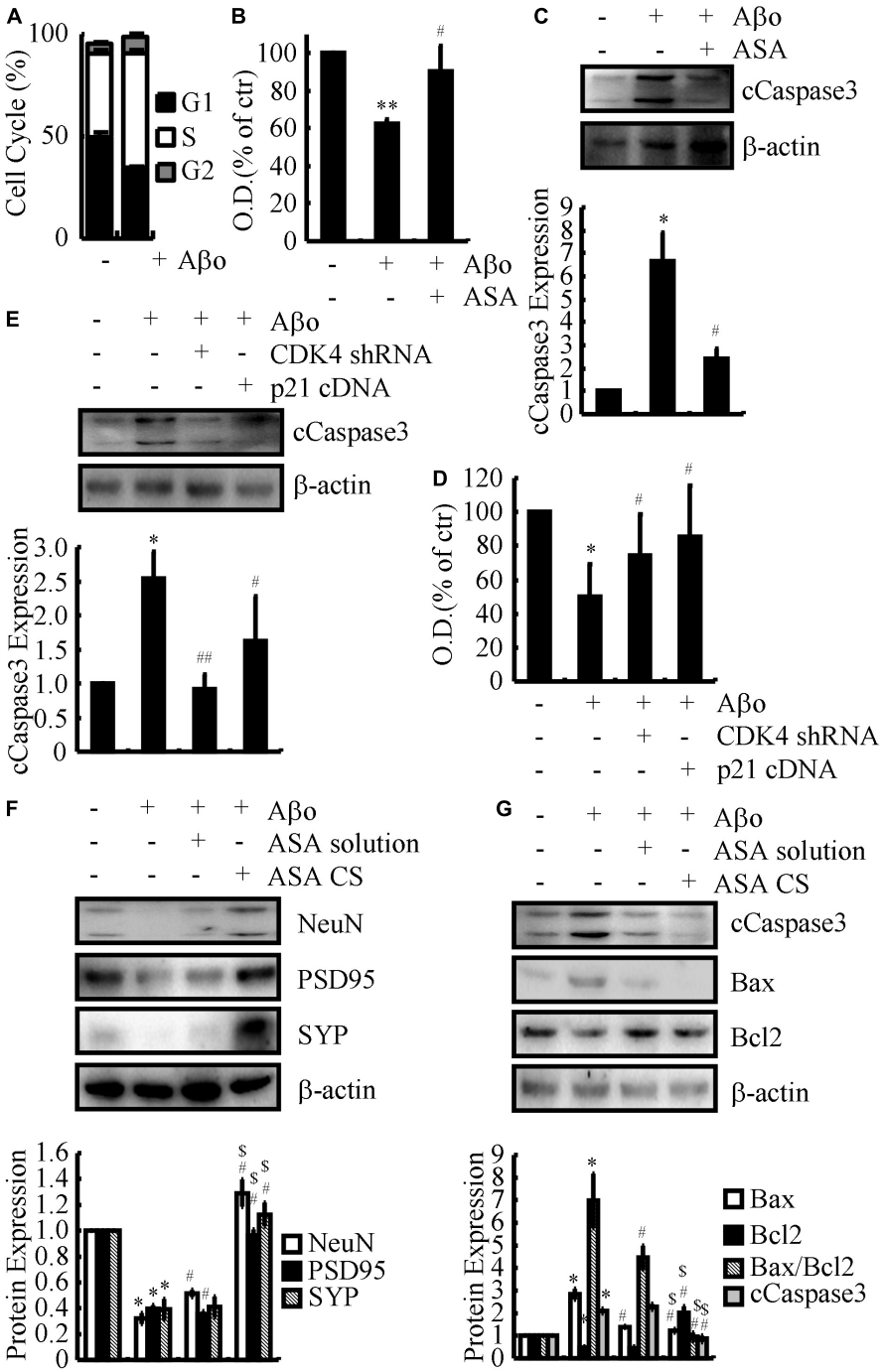

FIGURE 4
CDK4 and p21 mediate the effects of ASA on protecting neurons from cell cycle re-entry, leading to inhibit the apoptosis of neurons. **(A–C)** N2a cells were treated with Aβo (20 nM) in the absence or presence of ASA (10 μM). **(D,E)** N2a cells were treated with Aβo (20 nM) in the absence or presence of transfecting CDK4 shRNA or p21 cDNA. **(F,G)** C57BL/6 mice were injected (i.c.v.) with Aβo (2 ng/5 μl) in the absence or presence of intranasally administrating ASA solution or ASA CS. **(A)** The cell cycle was determined by flow cytometry. **(B–D)** The survival rate of N2a cells were determined by MTT assay. **(C,E–G)** The production of caspase 3 and the protein expression of NeuN, PSD95, SYP, Bax, and Bcl2 were determined by western blots. β-actin served as an internal control. The optical density of the bands was analyzed using ImageJ software. Data are presented as the means ± S.E. of independent experiments, $^{*}p < 0.05$; $^{**}p < 0.01$ compared to vehicle-treated controls, $^{\#}p < 0.05$; $^{\#\#}p < 0.01$ compared to Aβo-treated alone, $^{\$}p < 0.05$ compared to ASA solution-treated alone.

10.3389/fnmol.2022.1006216

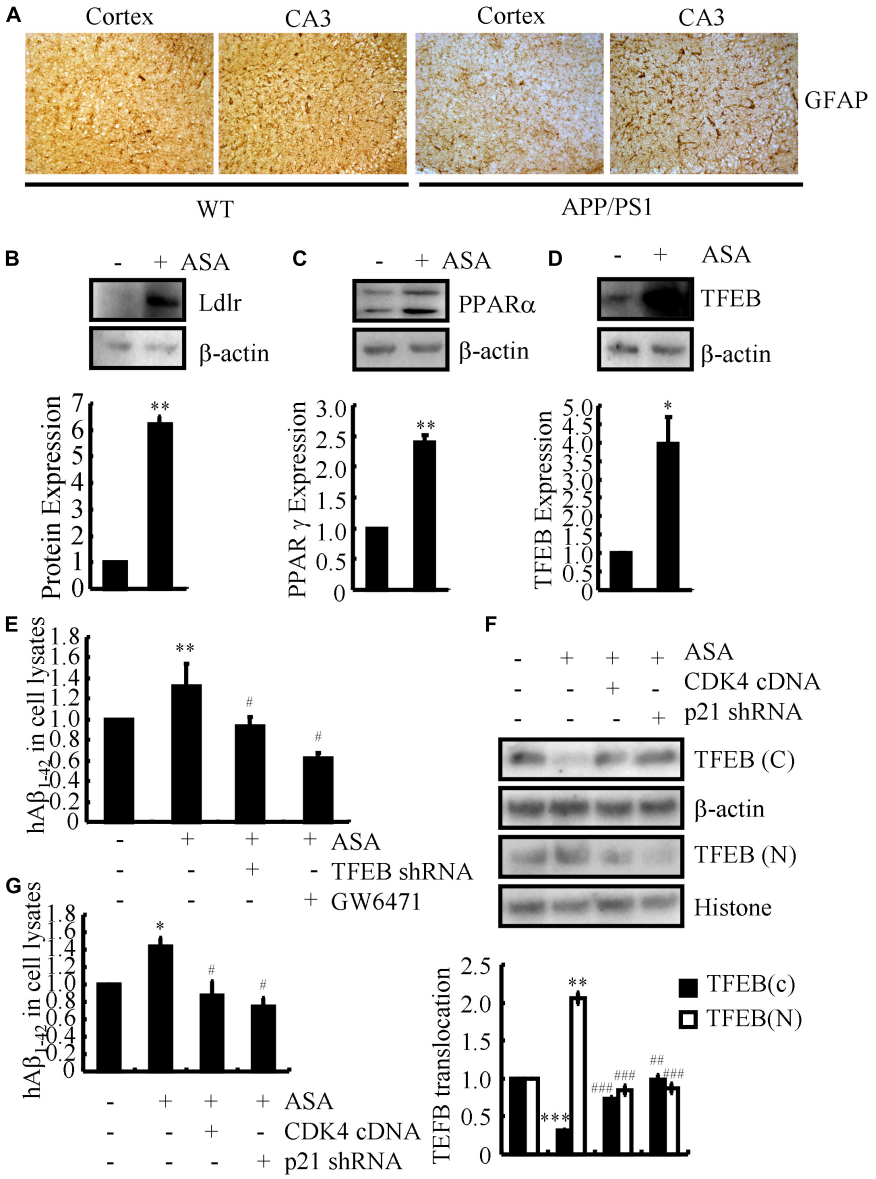

FIGURE 5
Aspirin induces the uptake of Aβ in astrocytes. **(A)** The brains of WT and APP/PS1 Tg mice were collected and sectioned after paraffin embedding. The morphology of astrocytes were determined by IHC. **(B–D)** In select experiments, D1A cells were treated with ASA (10 μM). The protein expression of Ldlr, PPARα, and TFEB were determined by western blots. β-actin served as an internal control. The optical density of the bands was analyzed using ImageJ software. **(E)** In separate experiments, D1A cells were transfected with TFEB shRNA or pre-treated with GW6471 (1 μM) before incubating in ASA (10 μM). **(F,G)** In distinct experiments, D1A cells were transfected with CDK4 cDNA and p21 shRNA before incubating with ASA (10 μM). **(E–G)** The uptake of $A\beta_{1-42}$ was determined by ELISA. **(F)** The protein levels of TFEB in cytosol and nucleus was determined by western blots. β-actin and histone served as internal controls. The optical density of the bands was analyzed using ImageJ software. Data are presented as the means ± S.E. of independent experiments, $^{*}p < 0.05$; $^{**}p < 0.01$; $^{***}p < 0.001$ compared to vehicle-treated controls, $^{\#}p < 0.05$; $^{\#\#}p < 0.01$; $^{\#\#\#}p < 0.001$; compared to ASA-treated alone.

cells (Figure 6D). More importantly, cell cycle re-entry was also involved in regulating the degradation of Aβ in D1A cells (Figure 6E). Collectively, these observations demonstrate that ASA attenuates AP pathology by inhibiting the production and deposition of Aβ and enhancing the uptake and degradation of Aβ in AD.

Discussion

In the present study, we revealed an early but poorly understood mechanism for the pathogenesis of AD: neuronal cell cycle re-entry. Insights from a previous study suggested that Aβo induces microglial cell activity, which results

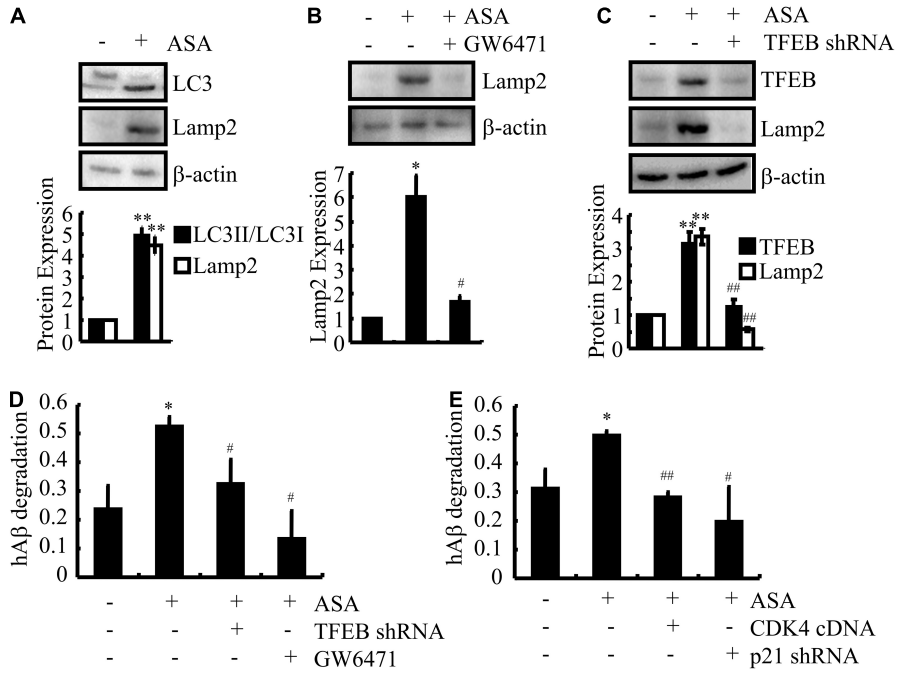

FIGURE 6
Aspirin induces the degradation of Aβ in astrocytes. **(A–D)** D1A cells were transfected with TFEB shRNA or pre-treated with GW6471 (1 μM) before incubating in ASA (10 μM). **(E)** In select experiments, D1A cells were transfected with CDK4 cDNA and p21 shRNA before incubating with ASA (10 μM). **(A–C)** The protein expression of LC3, Lamp2, and TFEB were determined by western blots. β-actin served as an internal control. The optical density of the bands was analyzed using ImageJ software. **(D,E)** The degradation of Aβ was determined by ELISA in astrocytes. Data are presented as the means ± S.E. of independent experiments, $^{*}p < 0.05$; $^{**}p < 0.01$ compared to vehicle-treated controls, $^{\#}p < 0.05$; $^{\#\#}p < 0.01$; compared to ASA-treated alone.

in neuronal cell cycle re-entry *via* the TNF-α and c-Jun kinase (JNK) signaling pathways (Bhaskar et al., 2014). In particular, induction of cell cycle re-entry is toxic to terminally differentiated neurons, which is associated with neuronal cell death (TUNEL-positive) in the AD cortex (Bhaskar et al., 2014). In light of prior works, we investigated the gene regulation and cell cycle changes specifically associated with Aβo treatment and ectopic expression of APP^{SW}, both separately and in combination and revealed changes in genes with a role in cell cycle control during the course of AD development and progression. Interestingly, ASA showed neuroprotective effects on restoring the levels of cell cycle-associated genes, which potentially contribute to the production and deposition of Aβ, leading to the cognitive decline of APP/PS1 Tg mice.

Previous studies have implied that a variety of cyclins and CDKs, such as CDK4, cyclin B1, Cdc2, and p16, are enhanced in the brains of AD patients (McShea et al., 1997; Vincent et al., 1997; Busser et al., 1998). Indeed, the expression of cell cycle proteins could be activated in neurons by a number of stimulating factors. For example, the protein level of cyclin D1 is elevated in *cis*-platinum-treated sensory neurons (Gill and Windebank, 1998). In neuronal PC12 cells, NGF deprivation stimulates the activity of Cdc2 and the expression of cyclin D1 (Gao and Zelenka, 1995), and this behavior is also observed in sympathetic neurons (Freeman et al., 1994). For AD, Aβ induces not only cell cycle re-entry but also cell death by upregulating the expression of CDK4 and the phosphorylation of Rb before entering S phase (Giovanni et al., 1999; Copani et al., 2001). In addition, $A\beta_{1-42}$ treatment modestly upregulates the protein expression of CDK4 in SH-SY5Y cells and robustly increases the protein levels of CDK4 in tau^{P301L}-expressing cells (Hoerndli et al., 2007). Apart from CDK4, $A\beta_{1-42}$ also stimulates the protein expression of CDK1, CDK5, and Cdc25B and lowers the protein levels of 14-3-3, Cdc34, Chk1, cyclin D1, and Rb in SH-SY5Y cells (Hoerndli et al., 2007), which potentially contributes to the cell cycle re-entry of neurons during the course of AD development and progression.

However, the cell cycle re-entry in these neurons showed a highly unorganized nature since the profile of cyclin-CDK activity in the phase of each cell cycle is usually lost in normal dividing cells. For instance, CDK4 and p16 are expressed concurrently in these neurons and are not observed in normal dividing cells (McShea et al., 1997). Moreover, most of these cell cycle elements are expressed in the cytosol rather than in the nucleus, where they should be (Vincent et al., 1997; Ogawa et al., 2003). Although the consequence of such cell cycle re-entry is

unclear, all of these aberrant regulatory factors likely lead to the inadequate or failed control of the cell cycle in these neurons, which may potentially contribute to their ultimate death in AD. It is likely that the death of PC12 cells was blocked by treatment with the CDK inhibitor flavopiridol or the expression of dominant-negative CDK4/6 in the presence of Aβ (Giovanni et al., 1999). As an inhibitor of CDK, p16 protects N cells from death caused by trophic factor deprivation (Kranenburg et al., 1996). In addition, trophic factor deprivation- and DNA damage-induced sympathetic and cortical neuronal death was blocked by a pharmacological inhibitor of the cell cycle (Farinelli and Greene, 1996; Park et al., 1996, 1997b, 1998b). Virus-induced expression of CDK inhibitors, including p16 and p27, and the dominant negative forms of CDK4 and CDK6 suppress neuronal loss (Park et al., 1997a, 1998a). Consistent with these prior works, we also found that CDK1, CDK4, and cyclin B1 were upregulated in Aβ-treated neuronal cells (**Figure 2C** and **Table 3**). In addition, we extended prior works and found that Aβ treatment concurrently induced the expression of CDK2 and cyclin A2/D3/E1 and reduced the expression of p18 and p21 in neuronal cells (**Figure 2C** and **Table 3**). Moreover, similar regulatory activities were further observed in N2a^{SW} cells, Aβ-injected (i.c.v.) C57BL/6 mice and APP/PS1 Tg mice (**Figures 2A,B,D** and **Tables 1**, **2**, **4**), thus leading to cell cycle re-entry and apoptosis of neurons (**Figure 4**).

Notably, aberrantly regulated proteins in the cell cycle do not appear exclusively at the late stage of neuropathology but rather the earliest neuronal changes to occur in the disease (McShea et al., 1997; Nagy et al., 1997; Busser et al., 1998; Zhu et al., 2000). Cell cycle markers occur even prior to the appearance of gross cytopathological changes (Vincent et al., 1997). The proximal time of cell cycle re-entry appears in pre-AD patients with MCI, which is a prodromal stage of AD (Yang et al., 2003). From the point of view, it might be better to intervene in AD as early as the appearance of gross cytopathological changes or even cell cycle re-entry. Based on the above clues, ASA was selected for the current study for the following reasons. First, numerous cytokines, chemokines and inflammatory components, including COX-2, NO and IL-1β, are elevated in AD brains by activating microglia and astrocytes (Akiyama et al., 2000), which occurs earlier than Aβ deposition in different AD animals (Dudal et al., 2004). Second, COX-2 overexpression induces alteration of the neuronal cell cycle in APP/PS1 Tg mice, which provides a rational basis for targeting neuronal COX-2 in therapeutic research aimed at slowing the clinical progression of AD (Xiang et al., 2002). Third, NSAIDs have shown beneficial effects on decreasing the risk of AD in retrospective studies (McGeer et al., 1996). Although clinical trials of NSAIDs are unsuccessful, this may simply reflect its premorbid but not therapeutic effects. As an inhibitor of COX-2, ASA exhibited an ∼50% decreased risk of AD (Zandi et al., 2002). On the basis of these clues, we also made the novel discovery that ASA has the ability to protect neurons from cell cycle re-entry, which results in the apoptosis of neurons (**Figure 4**).

Apart from its powerful anti-inflammatory effects, ASA disrupts the oligomerization of Aβ in an *in vitro* study (Parmer et al., 2017). In light of these prior works, our data further revealed that ASA treatment clearly inhibited the production and deposition of Aβ in the brains of APP/PS1 Tg mice (**Figures 1A–C**). However, we could still not fill the gaps between cell cycle re-entry and Aβ deposition. This problem might be resolved by the expected experiments to knock out or overexpress CDKs, cyclins or p18/p21 in APP/PS1 Tg mice. Despite lacking connections, CDK5 has shown negative regulatory effects on the production of Aβ in HEK293 $_{751}$APP$_{SW}$ cells (Ryder et al., 2003), which is caused by the activity of BACE1 (Sadleir and Vassar, 2012). Although the roles of cell cycle proteins in the production and deposition of Aβ are quite limited, accumulating evidence has shown that Aβ is able to regulate the progression of the cell cycle and the expression of associated regulatory proteins (Wang et al., 2012). Therefore, crosstalk might exist between cell cycle re-entry and the production and deposition of Aβ during the course of AD development and progression.

In addition to the above functions, ASA also shows the ability to enhance astrocyte uptake of Aβ, leading to the degradation of Aβ in lysosomes (**Figure 5**). In line with our observations, oral administration of ASA can upregulate lysosomal markers, including Lamp2, in the hippocampus of 5 × fAD mice, which decreases the loading of APs (Chandra et al., 2018). During this process, TFEB was found to be transcriptionally upregulated by a PPARα-dependent mechanism under the ASA treatment (**Figures 5C,D**). Consistent with our findings, TFEB activation enhances the function of lysosomes in degrading APP, which results in decreased production of Aβ and formation of APs (Xiao et al., 2015). On the other hand, TFEB can attenuate the pathogenesis of AD by facilitating the uptake and lysosomal degradation of Aβ in astrocytes (Xiao et al., 2014), which is consistent with our observations in ASA-treated astrocytes (**Figure 6D**). In addition, Ldlr was elevated by ASA treatment in astrocytes (**Figure 5B**). Supporting our results, Ldlr has been implicated in the direct binding and internalization of Aβ by astrocytes (Basak et al., 2012), whose deficiency reduces the responses of glial cells and increases AP burden in 5 × fAD mice (Katsouri and Georgopoulos, 2011). In addition, PPARα activation by its agonist fenofibrate is also involved in Ldlr expression (Huang et al., 2008). More interestingly, CDK4 regulated the uptake and degradation of Aβ by regulating TFEB in astrocytes (**Figures 5G**, **6E**). Of note, these observations were further supported by a previous study, suggesting that CDK4 interacts with phosphorylated TFEB, which inactivates them by promoting their shuttling to the cytoplasm (Yin et al., 2010).

Given the beneficial effects of ASA on AD, we further found that ASA has the ability to improve the cognitive decline of APP/PS1 Tg mice (**Figures 1D–I**). In line with our observations, ASA enhanced memory in an $AlCl_3$-induced mouse model of neurotoxicity (Rizwan et al., 2016). In addition, ASA has been reported to reduce the activity of NF-κB *via* acetylation of COX-2, which results in enhanced phagocytosis of microglial cells to facilitate the clearance of Aβ and cognitive improvement in Tg2576 mice (Medeiros et al., 2013). Moreover, high-dose ASA is effective in lowering the prevalence of AD and improving cognition (Nilsson et al., 2003). Therefore, ASA showed protective effects against AD by inhibiting the cell cycle re-entry of neurons.

Data availability statement

The original contributions presented in this study are included in the article/**Supplementary material**, further inquiries can be directed to the corresponding author.

Ethics statement

All animals were handled according to the guidelines for the care and use of medical laboratory animals (Ministry of Health, Peoples Republic of China, 1998) and the guidelines of the laboratory animal ethical standards of Northeastern University.

Author contributions

P-PG and W-YD conceived and performed all of the experiments, participated in the design of the study, and wrote the manuscript. PW conceived the experiments, interpreted the data, and wrote the manuscript of the study. All authors contributed to the article and approved the submitted version.

Funding

This research was funded by the National Natural Science Foundation of China, grant number: 81870840.

Conflict of interest

The authors declare that the research was conducted in the absence of any commercial or financial relationships that could be construed as a potential conflict of interest.

Publisher's note

All claims expressed in this article are solely those of the authors and do not necessarily represent those of their affiliated organizations, or those of the publisher, the editors and the reviewers. Any product that may be evaluated in this article, or claim that may be made by its manufacturer, is not guaranteed or endorsed by the publisher.

Supplementary material

The Supplementary Material for this article can be found online at: https://www.frontiersin.org/articles/10.3389/fnmol.2022.1006216/full#supplementary-material

References

Akiyama, H., Arai, T., Kondo, H., Tanno, E., Haga, C., and Ikeda, K. (2000). Cell mediators of inflammation in the Alzheimer disease brain. *Alzheimer Dis. Assoc. Disord.* 14(Suppl. 1), S47–S53. doi: 10.1097/00002093-200000001-00008

Asanuma, M., Nishibayashi-Asanuma, S., Miyazaki, I., Kohno, M., and Ogawa, N. (2001). Neuroprotective effects of non-steroidal anti-inflammatory drugs by direct scavenging of nitric oxide radicals. *J. Neurochem.* 76, 1895–1904. doi: 10.1046/j.1471-4159.2001.00205.x

Basak, J. M., Verghese, P. B., Yoon, H., Kim, J., and Holtzman, D. M. (2012). Low-density lipoprotein receptor represents an apolipoprotein E-independent pathway of Abeta uptake and degradation by astrocytes. *J. Biol. Chem.* 287, 13959–13971. doi: 10.1074/jbc.M111.288746

Bhaskar, K., Maphis, N., Xu, G., Varvel, N. H., Kokiko-Cochran, O. N., Weick, J. P., et al. (2014). Microglial derived tumor necrosis factor-alpha drives Alzheimer's disease-related neuronal cell cycle events. *Neurobiol. Dis.* 62, 273–285. doi: 10.1016/j.nbd.2013.10.007

Bonda, D. J., Evans, T. A., Santocanale, C., Llosa, J. C., Vina, J., Bajic, V. P., et al. (2009). Evidence for the progression through S-phase in the ectopic cell cycle re-entry of neurons in Alzheimer disease. *Aging* 1, 382–388. doi: 10.18632/aging.100044

Busser, J., Geldmacher, D. S., and Herrup, K. (1998). Ectopic cell cycle proteins predict the sites of neuronal cell death in Alzheimer's disease brain. *J. Neurosci.* 18, 2801–2807. doi: 10.1523/JNEUROSCI.18-08-02801.1998

Chandra, S., Jana, M., and Pahan, K. (2018). Aspirin induces lysosomal biogenesis and attenuates amyloid plaque pathology in a mouse model of Alzheimer's disease *via* PPARalpha. *J. Neurosci.* 38, 6682–6699. doi: 10.1523/JNEUROSCI.0054-18.2018

Chen, Y. X., Zhang, X. R., Xie, W. F., and Li, S. (2004). Effects of taurine on proliferation and apoptosis of hepatic stellate cells *in vitro*. *Hepatobiliary Pancreat. Dis. Int.* 3, 106–109.

Copani, A., Uberti, D., Sortino, M. A., Bruno, V., Nicoletti, F., and Memo, M. (2001). Activation of cell-cycle-associated proteins in neuronal death: A mandatory or dispensable path? *Trends Neurosci.* 24, 25–31. doi: 10.1016/S0166-2236(00)01663-5

Dudal, S., Krzywkowski, P., Paquette, J., Morissette, C., Lacombe, D., Tremblay, P., et al. (2004). Inflammation occurs early during the Abeta deposition process in TgCRND8 mice. *Neurobiol. Aging* 25, 861–871. doi: 10.1016/j.neurobiolaging.2003.08.008

Evans, T. A. (2007). BRCA1 may modulate neuronal cell cycle re-entry in Alzheimer disease. *Int. J. Med. Sci.* 4, 140–145. doi: 10.7150/ijms.4.140

Eve, R.-G., and Leroux, J. C. (2004). In situ-forming hydrogels–review of temperature-sensitive systems. *Eur. J. Pharm. Biopharm.* 58, 409–426. doi: 10.1016/j.ejpb.2004.03.019

Farinelli, S. E., and Greene, L. A. (1996). Cell cycle blockers mimosine, ciclopirox, and deferoxamine prevent the death of PC12 cells and postmitotic sympathetic neurons after removal of trophic support. *J. Neurosci.* 16, 1150–1162. doi: 10.1523/JNEUROSCI.16-03-01150.1996

Freeman, R. S., Estus, S., and Johnson, E. M. Jr. (1994). Analysis of cell cycle-related gene expression in postmitotic neurons: Selective induction of Cyclin D1 during programmed cell death. *Neuron* 12, 343–355. doi: 10.1016/0896-6273(94)90276-3

Gao, C. Y., and Zelenka, P. S. (1995). Induction of cyclin B and H1 kinase activity in apoptotic PC12 cells. *Exp. Cell Res.* 219, 612–618. doi: 10.1006/excr.1995.1271

Ghosh, A., Jana, M., Modi, K., Gonzalez, F. J., Sims, K. B., Berry-Kravis, E., et al. (2015). Activation of peroxisome proliferator-activated receptor alpha induces lysosomal biogenesis in brain cells: Implications for lysosomal storage disorders. *J. Biol. Chem.* 290, 10309–10324. doi: 10.1074/jbc.M114.610659

Gill, J. S., and Windebank, A. J. (1998). Cisplatin-induced apoptosis in rat dorsal root ganglion neurons is associated with attempted entry into the cell cycle. *J. Clin. Invest.* 101, 2842–2850. doi: 10.1172/JCI1130

Giovanni, A., Wirtz-Brugger, F., Keramaris, E., Slack, R., and Park, D. S. (1999). Involvement of cell cycle elements, cyclin-dependent kinases, pRb, and E2F x DP, in B-amyloid-induced neuronal death. *J. Biol. Chem.* 274, 19011–19016. doi: 10.1074/jbc.274.27.19011

Hoerndli, F. J., Pelech, S., Papassotiropoulos, A., and Gotz, J. (2007). Abeta treatment and P301L tau expression in an Alzheimer's disease tissue culture model act synergistically to promote aberrant cell cycle re-entry. *Eur. J. Neurosci.* 26, 60–72. doi: 10.1111/j.1460-9568.2007.05618.x

Huang, Z., Zhou, X., Nicholson, A. C., Gotto, A. M. Jr., Hajjar, D. P., and Han, J. (2008). Activation of peroxisome proliferator-activated receptor-alpha in mice induces expression of the hepatic low-density lipoprotein receptor. *Br. J. Pharmacol.* 155, 596–605. doi: 10.1038/bjp.2008.331

Katsouri, L., and Georgopoulos, S. (2011). Lack of LDL receptor enhances amyloid deposition and decreases glial response in an Alzheimer's disease mouse model. *PLoS One* 6:e21880. doi: 10.1371/journal.pone.0021880

Khurana, V., and Feany, M. B. (2007). Connecting cell-cycle activation to neurodegeneration in Drosophila. *Biochim. Biophys. Acta* 1772, 446–456. doi: 10.1016/j.bbadis.2006.10.007

Kranenburg, O., Van Der Eb, A. J., and Zantema, A. (1996). Cyclin D1 is an essential mediator of apoptotic neuronal cell death. *EMBO J.* 15, 46–54. doi: 10.1002/j.1460-2075.1996.tb00332.x

Laferla, F. M., and Oddo, S. (2005). Alzheimer's disease: Aβ, tau and synaptic dysfunction. *Trends Mol. Med.* 11, 170–176. doi: 10.1016/j.molmed.2005.02.009

Lamkin, T. J., Chin, V., and Yen, A. (2006). All-trans retinoic acid induces p62DOK1 and p56DOK2 expression which enhances induced differentiation and G0 arrest of HL-60 leukemia cells. *Am. J. Hematol.* 81, 603–615. doi: 10.1002/ajh.20667

Legler, D. F., Bruckner, M., Uetz-Von Allmen, E., and Krause, P. (2010). Prostaglandin E2 at new glance: Novel insights in functional diversity offer therapeutic chances. *Int. J. Biochem. Cell Biol.* 42, 198–201. doi: 10.1016/j.biocel.2009.09.015

Liu, D. X., and Greene, L. A. (2001). Regulation of neuronal survival and death by E2F-dependent gene repression and derepression. *Neuron* 32, 425–438. doi: 10.1016/S0896-6273(01)00495-0

Love, S. (2003). Neuronal expression of cell cycle-related proteins after brain ischaemia in man. *Neurosci. Lett.* 353, 29–32. doi: 10.1016/j.neulet.2003.09.004

McGeer, P. L., Schulzer, M., and Mcgeer, E. G. (1996). Arthritis and anti-inflammatory agents as possible protective factors for Alzheimer's disease: A review of 17 epidemiologic studies. *Neurology* 47, 425–432. doi: 10.1212/WNL.47.2.425

McShea, A., Harris, P. L., Webster, K. R., Wahl, A. F., and Smith, M. A. (1997). Abnormal expression of the cell cycle regulators P16 and CDK4 in Alzheimer's disease. *Am. J. Pathol.* 150, 1933–1939.

McShea, A., Lee, H. G., Petersen, R. B., Casadesus, G., Vincent, I., Linford, N. J., et al. (2007). Neuronal cell cycle re-entry mediates Alzheimer disease-type changes. *BBA Mol. Basis Dis.* 1772, 467–472. doi: 10.1016/j.bbadis.2006.09.010

Medeiros, R., Kitazawa, M., Passos, G. F., Baglietto-Vargas, D., Cheng, D., Cribbs, D. H., et al. (2013). Aspirin-triggered lipoxin A4 stimulates alternative activation of microglia and reduces Alzheimer disease-like pathology in mice. *Am. J. Pathol.* 182, 1780–1789. doi: 10.1016/j.ajpath.2013.01.051

Morinaga, Y., Hayashi, H., Takeuchi, A., and Onozaki, K. (1990). Antiproliferative effect of interleukin 1 (IL-1) on tumor cells: G0-G1 arrest of a human melanoma cell line by IL-1. *Biochem. Biophys. Res. Commun.* 173, 186–192. doi: 10.1016/S0006-291X(05)81039-3

Murakami, M., Goto, T., Saito, Y., Goto, S., Kochi, M., and Ushio, Y. (2001). The inhibitory effect of simvastatin on growth in malignant gliomas–with special reference to its local application with fibrin glue spray *in vivo*. *Int. J. Oncol.* 19, 525–531. doi: 10.3892/ijo.19.3.525

Nagy, Z., Esiri, M. M., and Smith, A. D. (1997). Expression of cell division markers in the hippocampus in Alzheimer's disease and other neurodegenerative conditions. *Acta Neuropathol.* 93, 294–300. doi: 10.1007/s004010050617

Nilsson, S. E., Johansson, B., Takkinen, S., Berg, S., Zarit, S., Mcclearn, G., et al. (2003). Does aspirin protect against Alzheimer's dementia? A study in a Swedish population-based sample aged > or =80 years. *Eur. J. Clin. Pharmacol.* 59, 313–319. doi: 10.1007/s00228-003-0618-y

Ogawa, O., Lee, H. G., Zhu, X., Raina, A., Harris, P. L., Castellani, R. J., et al. (2003). Increased p27, an essential component of cell cycle control, in Alzheimer's disease. *Aging Cell* 2, 105–110. doi: 10.1046/j.1474-9728.2003.00042.x

Park, D. S., Farinelli, S. E., and Greene, L. A. (1996). Inhibitors of cyclin-dependent kinases promote survival of post-mitotic neuronally differentiated PC12 cells and sympathetic neurons. *J. Biol. Chem.* 271, 8161–8169. doi: 10.1074/jbc.271.14.8161

Park, D. S., Morris, E. J., Greene, L. A., and Geller, H. M. (1997b). G1/S cell cycle blockers and inhibitors of cyclin-dependent kinases suppress camptothecin-induced neuronal apoptosis. *J. Neurosci.* 17, 1256–1270. doi: 10.1523/JNEUROSCI.17-04-01256.1997

Park, D. S., Levine, B., Ferrari, G., and Greene, L. A. (1997a). Cyclin dependent kinase inhibitors and dominant negative cyclin dependent kinase 4 and 6 promote survival of NGF-deprived sympathetic neurons. *J. Neurosci.* 17, 8975–8983. doi: 10.1523/JNEUROSCI.17-23-08975.1997

Park, D. S., Morris, E. J., Stefanis, L., Troy, C. M., Shelanski, M. L., Geller, H. M., et al. (1998b). Multiple pathways of neuronal death induced by DNA-damaging agents, NGF deprivation, and oxidative stress. *J. Neurosci.* 18, 830–840. doi: 10.1523/JNEUROSCI.18-03-00830.1998

Park, D. S., Morris, E. J., Padmanabhan, J., Shelanski, M. L., Geller, H. M., and Greene, L. A. (1998a). Cyclin-dependent kinases participate in death of neurons evoked by DNA-damaging agents. *J. Cell Biol.* 143, 457–467. doi: 10.1083/jcb.143.2.457

Parmer, M., Milan, S., and Torabi, A. (2017). Calcitonin-negative neuroendocrine tumor of the thyroid. *Int. J. Surg. Pathol.* 25, 191–194. doi: 10.1177/1066896916670989

Pomponi, M., Di Gioia, A., Bria, P., and Pomponi, M. F. (2008). Fatty aspirin: A new perspective in the prevention of dementia of Alzheimer's type? *Curr. Alzheimer Res.* 5, 422–431. doi: 10.2174/156720508785908892

Rizwan, S., Idrees, A., Ashraf, M., and Ahmed, T. (2016). Memory-enhancing effect of aspirin is mediated through opioid system modulation in an AlCl3-induced neurotoxicity mouse model. *Exp. Ther. Med.* 11, 1961–1970. doi: 10.3892/etm.2016.3147

Ryder, J., Su, Y., Liu, F., Li, B., Zhou, Y., and Ni, B. (2003). Divergent roles of GSK3 and CDK5 in APP processing. *Biochem. Biophys. Res. Commun.* 312, 922–929. doi: 10.1016/j.bbrc.2003.11.014

Sadleir, K. R., and Vassar, R. (2012). Cdk5 protein inhibition and Abeta42 increase BACE1 protein level in primary neurons by a post-transcriptional mechanism: Implications of CDK5 as a therapeutic target for Alzheimer disease. *J. Biol. Chem.* 287, 7224–7235. doi: 10.1074/jbc.M111.333914

Sangfelt, O., Erickson, S., Castro, J., Heiden, T., Gustafsson, A., Einhorn, S., et al. (1999). Molecular mechanisms underlying interferon-alpha-induced G0/G1 arrest: CKI-mediated regulation of G1 Cdk-complexes and activation of pocket proteins. *Oncogene* 18, 2798–2810. doi: 10.1038/sj.onc.1202609

Snape, M., Lee, H. G., Casadesus, G., and Smith, M. A. (2009). Cell cycle aberrations in Alzheimer's disease: A novel therapeutic opportunity. *Expert Rev. Neurother.* 9, 1579–1580. doi: 10.1586/ern.09.113

Tortosa, E., Avila, J., and Perez, M. (2006). Acetylsalicylic acid decreases tau phosphorylation at serine 422. *Neurosci. Lett.* 396, 77–80. doi: 10.1016/j.neulet.2005.11.066

Vincent, I., Jicha, G., Rosado, M., and Dickson, D. W. (1997). Aberrant expression of mitotic cdc2/cyclin B1 kinase in degenerating neurons of Alzheimer's disease brain. *J. Neurosci.* 17, 3588–3598. doi: 10.1523/JNEUROSCI.17-10-03588.1997

Wang, J., Zhang, Y. J., and Du, S. (2012). The protective effect of curcumin on Aβ induced aberrant cell cycle reentry on primary cultured rat cortical neurons. *Eur. Rev. Med. Pharmacol.* 16, 445–454.

Xiang, Z., Ho, L., Valdellon, J., Borchelt, D., Kelley, K., Spielman, L., et al. (2002). Cyclooxygenase (COX)-2 and cell cycle activity in a transgenic mouse model of Alzheimer's disease neuropathology. *Neurobiol. Aging* 23, 327–334. doi: 10.1016/S0197-4580(01)00282-2

Xiao, Q., Yan, P., Ma, X., Liu, H., Perez, R., Zhu, A., et al. (2014). Enhancing astrocytic lysosome biogenesis facilitates Abeta clearance and attenuates amyloid plaque pathogenesis. *J. Neurosci.* 34, 9607–9620. doi: 10.1523/JNEUROSCI.3788-13.2014

Xiao, Q., Yan, P., Ma, X., Liu, H., Perez, R., Zhu, A., et al. (2015). Neuronal-targeted TFEB accelerates lysosomal degradation of app, reducing abeta generation and amyloid plaque pathogenesis. *J. Neurosci.* 35, 12137–12151. doi: 10.1523/JNEUROSCI.0705-15.2015

Yang, Y., Mufson, E. J., and Herrup, K. (2003). Neuronal cell death is preceded by cell cycle events at all stages of Alzheimer's disease. *J. Neurosci.* 23, 2557–2563. doi: 10.1523/JNEUROSCI.23-07-02557.2003

Yin, Q., Jian, Y., Xu, M., Huang, X., and Yang, C. (2010). CDK4/6 regulate lysosome biogenesis through TFEB/TFE3. *J. Cell Biol.* 219:e201911036. doi: 10.1083/jcb.201911036

Zandi, P. P., Anthony, J. C., Hayden, K. M., Mehta, K., Mayer, L., and Breitner, J. C. (2002). Reduced incidence of AD with NSAID but not H2 receptor antagonists: The Cache County Study. *Neurology* 59, 880–886. doi: 10.1212/WNL.59.6.880

Zhang, Y. D., and Zhao, J. J. (2015). TFEB participates in the Abeta-induced pathogenesis of Alzheimer's disease by regulating the autophagy-lysosome pathway. *DNA Cell Biol.* 34, 661–668. doi: 10.1089/dna.2014.2738

Zhu, X., Rottkamp, C. A., Raina, A. K., Brewer, G. J., Ghanbari, H. A., Boux, H., et al. (2000). Neuronal CDK7 in hippocampus is related to aging and Alzheimer disease. *Neurobiol. Aging* 21, 807–813. doi: 10.1016/S0197-4580(00)00217-7

frontiers | Frontiers in Molecular Neuroscience

TYPE Review
PUBLISHED 18 October 2022
DOI 10.3389/fnmol.2022.1005422

OPEN ACCESS

EDITED BY
Daniela Uberti,
University of Brescia, Italy

REVIEWED BY
Tang Biao,
Hunan University of Chinese Medicine, China
Norberto Gonzalez-Juarbe,
J. Craig Venter Institute, United States

*CORRESPONDENCE
Bing Wang
wangb46@mail2.sysu.edu.cn

SPECIALTY SECTION
This article was submitted to Brain Disease Mechanisms, a section of the journal Frontiers in Molecular Neuroscience

RECEIVED 28 July 2022
ACCEPTED 27 September 2022
PUBLISHED 18 October 2022

CITATION
Nie Z, Tan L, Niu J and Wang B (2022) The role of regulatory necrosis in traumatic brain injury. *Front. Mol. Neurosci.* 15:1005422. doi: 10.3389/fnmol.2022.1005422

The role of regulatory necrosis in traumatic brain injury

Zhenyu Nie, Liming Tan, Jie Niu and Bing Wang*

Department of Neurosurgery, The Second Affiliated Hospital, University of South China, Hengyang, China

Traumatic brain injury (TBI) is a major cause of death and disability in the population worldwide, of which key injury mechanism involving the death of nerve cells. Many recent studies have shown that regulatory necrosis is involved in the pathological process of TBI which includes necroptosis, pyroptosis, ferroptosis, parthanatos, and Cyclophilin D (CypD) mediated necrosis. Therefore, targeting the signaling pathways involved in regulatory necrosis may be an effective strategy to reduce the secondary injury after TBI. Meanwhile, drugs or genes are used as interference factors in various types of regulatory necrosis, so as to explore the potential treatment methods for the secondary injury after TBI. This review summarizes the current progress on regulatory necrosis in TBI.

KEYWORDS

traumatic brain injury (TBI), regulatory necrosis, ferroptosis, necroptosis, pyroptosis, parthanatos, cell death

Introduction

Traumatic brain injury (TBI) is a common traumatic disease and a serious factor causing death and disability in adults worldwide. Each year, more than 27 million new TBI cases are diagnosed around the world, imposing a huge burden on society and families (Jiang et al., 2019; Ponsford et al., 2022). TBI is a relatively complex disease, which will lead to structural damage and functional defects through primary and secondary injury mechanisms. Secondary injury occurs after primary injury, resulting from a cascade of metabolic, cellular and molecular events, and will eventually lead to brain cell death, tissue damage and atrophy (Ng and Lee, 2019). However, the cellular pathophysiological changes occurring in brain after TBI are mainly based on four major factors, namely excitotoxicity, cytokines, reactive oxygen species (ROS), and cell death (Ladak et al., 2019). In recent years, more and more studies have shown that some cell death is regulated by a certain kind of mechanism called regulatory necrosis, including

necroptosis, pyroptosis, ferroptosis, parthanatos, and Cyclophilin D (CypD) mediated cell necrosis (Galluzzi et al., 2018). The details of regulatory necrosis in TBI and its differences in various features are provided in **Table 1**.

Regulatory necrosis has been found in many diseases in central nervous system, such as traumatic brain injury, spinal cord injury, epilepsy, Alzheimer's disease (AD), Parkinson's disease (PD), stroke, etc. (Liu et al., 2015; Sekerdag et al., 2018; Weiland et al., 2019; Hu et al., 2020; Dionísio et al., 2021). In Alzheimer's disease, pTau can cause neuronal death by inducing necroptosis (Dong et al., 2022), while introducing the gene of amyloid precursor protein (App) can enhance necroptosis (Pang et al., 2022). In PD, fibrillar alpha-synuclein promotes the activation of neurotoxic astrocytes through RIP kinase signaling pathway (Chou et al., 2021). This review focuses on the role and the current studies of regulatory necrosis in the secondary injury after TBI, which may provide new targets for the treatment of craniocerebral injury.

The necroptosis involved in traumatic brain injury

Necroptosis is induced by the combination of related ligands with Tumor Necrosis Factor (TNF) family death domain receptors, pattern recognition receptors, and virus sensors. It is a regulated cell death mode independent of caspase activity, which is mediated by mixed lineage kinase domain-like protein (MLKL) by activating receptor interacting protein kinase 1 (RIPK1)/receptor interacting protein kinase 3 (RIPK3) (Galluzzi et al., 2018). The process of necroptosis is characterized by cell swelling and the loss of plasma membrane integrity (Holler et al., 2000; Cho et al., 2009; Murphy et al., 2013; Grootjans et al., 2017; Degterev et al., 2019).

Previous studies have reported that necroptosis is involved in TBI (Liu et al., 2015; Yuan et al., 2019). Necroptosis would occur after a controlled cortical impact (CCI) in mice. RIPK3 is highly expressed in the hippocampus of CCI-TBI mice. Knockout of RIPK3 gene can inhibit oxidative stress, inflammation and apoptosis after TBI through AMPK signaling pathway (Liu Z. et al., 2018). The mice with RIPK3 gene knockout and RIPK1-deficient improved cognitive function within 3 months after TBI, demonstrating that the loss of RIPK1/RIPK3 could prevent progressive neuronal death and improve cognitive memory function (Wehn et al., 2021). But Wu et al. (2021) noted that the knockout of RIPK3 and MLKL in CCI mice model indicates RIPK3 is a disease driver independent of necroptosis mechanisms, while MLKL and the drug therapy of necroptosis may have no clinical effect on the patients with cerebral contusion. In PD animal model, the knockout of RIPK3 and MLKL can reduce the degeneration of dopaminergic neuron, improving the motion performance of mice (Oñate et al., 2020). The contribution of necroptosis to TBI needs to be further confirmed.

As the role of necroptosis in TBI has already been well recognized, many relevant studies started their research on the mechanisms that affected RIPK1/RIPK3/MLKL. Recently, Carsten Culmsee et al. found that mice with the knockout of tumor-suppressor cylindromatosis (CYLD) gene have relieved nerve damage after TBI. As a key regulator of deubiquitinase, cell proliferation and inflammation, the down-regulation of CYLD can increase the ubiquitination of RIP1, inhibit the formation of RIPK1/RIPK3 complex, and reduce necroptosis to protect neuronal cells (Ganjam et al., 2018). The 2-benzofuranyl-imidazoline (2-BFI) is an effective analgesic. In recent studies, 2-BFI treatment could significantly improve the neurological dysfunction and brain edema after TBI, of which mechanism is to reduce the level of receptor interacting proteins (RIPK1), (RIPK3), and MLKL (Ni et al., 2019). Other studies have shown that TNF Alpha induced protein 3 (TNFAIP3, also known as A20) can inhibit the synthesis of protein complexes composed of RIPK1, RIPK3, and MLKL, and thus reducing necroptosis in TBI, while Nec-1 and melatonin can reduce necroptosis and inhibit HMGB1, RAGE and proinflammatory cell factors in an A20 dependent manner (Bao et al., 2019). When MLKL maps to the site of damaged membrane bubble, it will recruit transport complex III (ESCRT-III) component (Gong et al., 2017; Guo and Kaiser, 2017), including the charged multivesicular body protein 4b (CHMP4B), which can alleviate the cell membrane damage caused by p-MLKL and the necroptosis level of microglia to a great extent. The transcription factor FOXO1 enhances the transcription of CHMP4B by binding to the promoter region in microglia. Stable knockdown of FOXO1 can reduce the expression of CHMP4B, thereby increasing the level of necroptosis after microglia damage, and further reducing the pro-inflammatory effect of microglia while improving the recovery of neural function after TBI (Zhao et al., 2020). According to current studies, the immediate-early gene (IEG) encoding the protein activity-regulated cytoskeletal (Arc) is a brain-specific postsynaptic density (PSD) protein. Arc can reduce the traumatic injury (TNI) in cortical neurons by inhibiting necroptosis. The arc silencing can activate the metabotropic glutamate receptor-1 (mGluR1) -mediated ER stress-calcium overload pathway and the RIP1-dependent necroptosis (Chen et al., 2020). As a AMPAR antagonist, perampanel has recently been reported as a neuroprotective factor in hemorrhagic and ischemic stroke models, while Wang et al. found that perampanel can also act as a protective factor in the TBI-*in vitro* model, reducing RIPK1 and RIPK3 expression and subsequently alleviating necroptosis through the activation of Akt/GSK3β signaling (Chen et al., 2021b).

In fact, studies have shown that hydrogen or hydrogen-containing saline can modulate neuronal death. Hu et al. (2022) found that hydrogen-rich saline inhibits necroptosis

TABLE 1 Main morphological features, key regulators, inducers, and inhibitors of necroptosis, pyroptosis, ferroptosis, parthanatos, and CYPD-dependent necrosis.

Regulated necrosis	Main morphological features	Key regulators	Inducers	Inhibitors
Necroptosis	Loss of cytoplasmic membrane integrity, secretion of DAMP; swelling of cell bodies and organelles, chromatin fragmentation, nucleus disintegration	RIPK1, RIPK3, RIP1, RIP3, and MLKL	TNF-α,Fas, TRAIL, IFN, TNFR, TLR, and z-VAD-fmk	Nec-1, CYLD, 2-BFI, A20, CHMP4B, Arc, Hydrogen-rich saline, Perampanel, and HT
Pyroptosis	Cell swelling, cell membrane pore formation, release of bubble-like protrusions; cell membrane rupture, release of cell contents, DNA breakage; chromatin condensation, intact nuclei	NLRP3, ASC, Caspase-1, AIM2, GSDMD, IL-1β, and IL-18	ATP, LPS, PRR, HMGB1, and HIF-1α	Ac-YVAD-CMK, Ac-FLTD-CMK, PGAM5, VX765, JC124, NEK7, 2-BFI, ACE2, Dexmedetomidine, Artesunate, Resveratrol, Rhein, CORM-3, H2, and Ghrelin
Ferroptosis	Cellular mitochondria shrink in size and become smaller, with increased membrane density and reduced cristae. Insignificant morphological changes in the nucleus	Fe, GPX4, ROS, GSH, P53, and SLC7A11	Erastin, Erastin derivatives, RSL3, Glutamate, PEBP1, and 15LO	Ferrostatin-1, Liproxstatin-1, Deferoxamine, Ferristatin II, Baicalein, Prokineticin-2, Polydatin, Ruxolitinib, Tetrandrine, Melatonin, and SIRT2
Parthanatos	Loss of cell membrane integrity, intranuclear chromatin condensation, DNA breakage, and production of large amounts of DNA fragments; irreversible $\Delta\psi m$ dissipation, ATP and NADH depletion	PARP-1, PAR, AIF, and MIF	PAR polymer, AIFsol (soluble AIF)	PARP-1 inhibitors, DPQ, GPI 6150, PJ34, INO-1001, Ghrelin, TSG, OLA, and Iduna
CYPD-dependent necrosis	Mitochondrial membrane potential damage; mitochondrial swelling, mitochondrial matrix expansion; massive intracellular vacuoles, outer membrane rupture	CypD, p53, and mPTP	CypD, VDAC (anion channel)	CsA, NIM811, Resveratrol, SIRT1, and BDNF

TRAIL, TNF-related apoptosis-inducing ligand; IFN, interferon; TNFR1, TNF-receptor 1; TLR, toll-like receptors; A20, TNF-inducible protein 3; CHMP4B, multivesicular body protein 4b; Arc, activity-regulated cytoskeletal; Perampanel, an (AMPAR) antagonist; HT, hypothermia treatment.

10.3389/fnmol.2022.1005422

and neuroinflammation based on the ROS/heme oxygenase-1 (HO-1) signaling, reducing neuronal death after TBI. As a research hotpot, Nec-1 is often used to verify the contribution of necroptosis. For example, Nec-1 can alleviate brain tissue injury, motor dysfunction and spatial learning impairment after CCI in mice, and has an anti-inflammatory effect in acute brain injury (You et al., 2008). Mu et al. (2021) found that Nec-1 can protect neuronal cells and oligodendrocytes by inhibiting the nuclear transposition of cellular AIF induced by the pro-apoptotic protein called Bcl-2/adenovirus E1B 19-kDa interacting protein 3 (BNIP3). At the same time, changes in external environment can also affect necroptosis. The hypothermia (HT) treatment can significantly reduce the upregulation of RIPK-1 and protect injured CNS from tissue damage and inflammation by targeting necroptosis through TNF signaling (Liu et al., 2016; Zhang et al., 2017) after TBI. The controlled decompression (CDC) surgery can reduce brain injury, and Chen et al. (2021a) stated that performing CDC for 2 or 3 h *in vitro* and for 20 or 30 min *in vivo* can exert neuroprotective effects. CDC can inhibit neuronal necroptosis through the TREK-1-mediated intracellular Ca^{2+} overload and the depression of RIPK3 activation. As indicated by Nec-1, necroptosis can affect acute neuronal injury, and the activation of RIPK1 and RIPK3 are both observed in the rat model of liquid impact brain injury and MCAO model with TBI (Liu et al., 2016; Ni et al., 2018). Interestingly, post-traumatic hypothermia (33°C) also reduces brain damage after stroke, resulting in decreased levels of RIPK1, RIPK3, and MLKL (You et al., 2008). Thus indicates that there may exist common target for the treatment of TBI and stroke by improving necroptosis. In conclusion, these studies have emphasized the potential therapeutic significance of necroptosis related therapy for TBI. The possible signal pathways of necroptosis involved in TBI are summarized in **Figure 1**.

The pyroptosis involved in traumatic brain injury

Pyroptosis is mediated by Gasdermin D (GSDMD), the formation of plasma membrane pores as well as the extracellular release of inflammatory cytokines. In typical caspase-1 inflammatory pathway, caspase-1 is activated by apoptosis related CARD containing spotted protein (ASC) or pyridine domain 3 (NLRP3) in Nucleotide oligomerization domain (NOD) like receptor family, and processed into inflammatory cytokines such as IL-1β, IL-18 which can finally induce the release of inflammatory factors through the activation of GSDMD, resulting in cell death (Shi et al., 2017; Hu et al., 2020; Irrera et al., 2020; Zhou et al., 2022).

Therefore, most studies have been designed to explore the potential role of pyroptosis in TBI based on the regulation of inflammasome, such as caspase-1, NLRP1, NLRP3, AIM2, etc. Up to now, many of these studies have confirmed the contribution of pyroptosis to TBI by targeting inflammasomes. In the animal model of TBI, the caspase-1 plays a critical role, of which inhibition can reduce the level of IL-1β, IL-18, and GSDMD, and finally reduce the neuroinflammation and neuronal damage after TBI (Liu W. et al., 2018). Blocking the increasing level of phospho-Tau by IL-1R1$^{-/-}$ in cortex and cerebellum suggests that inflammasome activation can drive Tau phosphorylation, while the aberrantly phosphorylated Tau may also contribute to neuronal IL-1β production and impaired proteostasis in feed forward loops, leading to neuronal death (Wu L. et al., 2022). The inflammasome plays a dominant role in the development of neuroinflammation after TBI, as NLRP3-GSDMD is dominant in the regulation of neuroinflammation and neuropathology after TBI. The level of GSDMD and N-GSDMD reach the peak 3 days after TBI, equivalent to the level of NLRP3 inflammasome. After TBI, GSDMD is mainly located in microglia cells, indicating that GSDMD may involve in the polarization of microglia cells. GSDMD-KO can alleviate the neuropathological changes (synaptic protein loss, microglia activation, astrocyte increase, dendritic damage and neuronal death) caused by TBI to a great extent (Du et al., 2022). The inhibition of GSDMD is conducive to a better prognosis, as the inhibition of inflammasome can prevent the neurological dysfunction in patients with TB1, PD, AD, subarachnoid hemorrhage, vascular dementia, etc. (Wnuk and Kajta, 2017; Ising et al., 2019; Rui et al., 2020; Poh et al., 2021). After TBI, NLRs, and AIM2 inflammatory corpuscles are activated in the cerebral microvascular endothelial cells (BMVECs) in cerebral cortex. As caspase-1 inhibitors, Ac-YVAD-CMK and Ac-FLTD-CMK can block the cleavage of GSDMD and ASC oligomerization by inhibiting caspase-1, which can reduce pyroptosis (Ge et al., 2018; Wang et al., 2021). Pgam5 is a mitochondrial protein that promotes the activation of microglial inflammasome after TBI, reduces the amount of pyroptosis-related molecules, promotes the polymerization of ASC and the activation of caspase1, and ameliorates the neuronal damage and dysfunction in TBI (Chen et al., 2021e). VX765, a known caspase-1 inhibitor, can inhibit pro-inflammatory cytokines against pyroptosis through HMGB1/TLR4/NF-κB pathway (Sun et al., 2020).

Pyridine domain 3 inflammasome is an intracellular multiprotein complex which can activate the release of inflammatory factors in TBI, causing cell pyroptosis (Irrera et al., 2017). Many researchers have found that NLRP3 inhibitors can inhibit cell death and play a neuroprotective role in TBI. JC124 is a specific NLRP3 inflammatory inhibitor, which is developed from the structural optimization of sulfonylurea drugs. It can block the aggregation of ASC, inhibit the activation of caspase-1 and protect brain from TBI (Kuwar et al., 2019). NIMA-associated kinase 7 (NEK7) is an important vector for NLRP3 inflammasome activation. Liu et al. have demonstrated that the NEK7 knockdown can inhibit the activation of NLRP3 inflammasome and caspase-1 through K^+ outflow and reduce

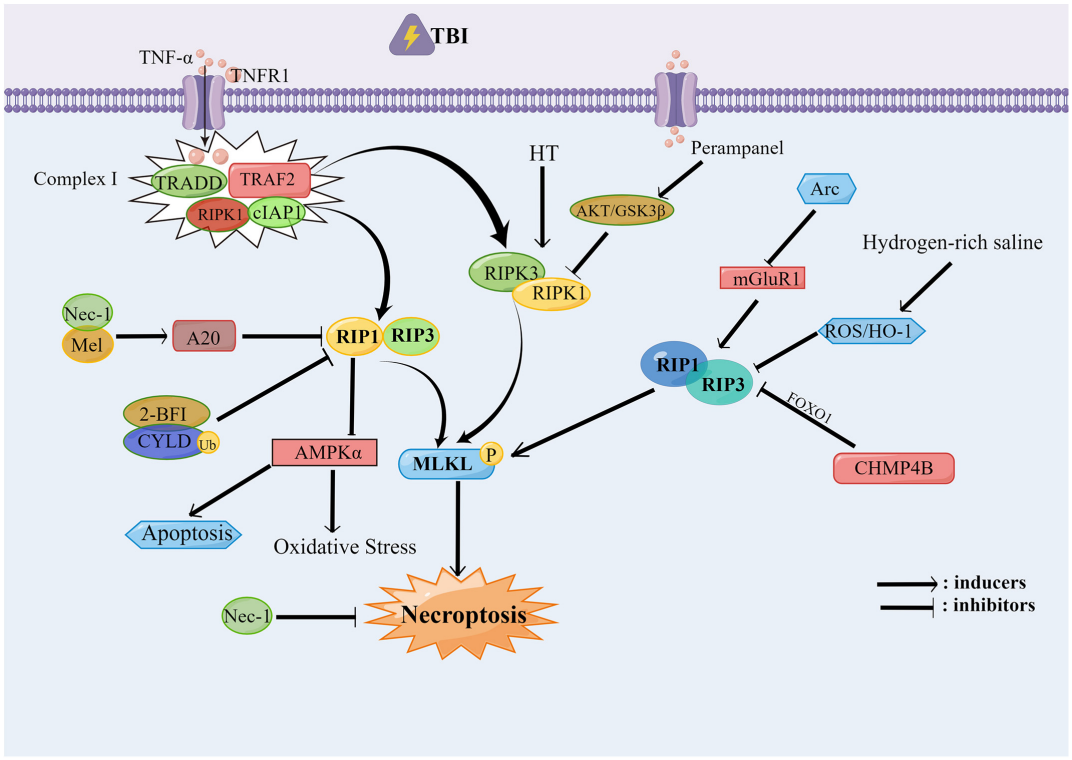

FIGURE 1
The necroptosis involved in traumatic brain injury (TBI). After TBI occurs, the RIPK1/RIPK3/MLKL pathway is activated, in which the Nec-1, Mel, 2-BFI, CYLD, and CHMP4B can alleviate the necroptosis and protect the neural function by inhibiting the RIP1 and RIP3. Hydrogen-rich saline can inhibit the RIP1 and RIP3 through the ROS/HO-1 pathway. While RIP1 can inhibit the oxidative stress and the apoptosis which occurred after TBI through the AMPK signal pathway. Perampanel can inhibit the RIPK1/RIPK3/MLKL pathway through the AKT/GSK3β pathway, thereby alleviating the necroptosis.

posttraumatic nerve injury (Chen et al., 2019). After TBI, the NLRP3 inflammasome inhibitor 2-BFI will induce inflammation and play an important role in BBB destruction and brain edema (Ni et al., 2019). Meanwhile, HIF-1α will recruit and activate microglia during the release of inflammatory factor, leading to the NLRP3 inflammasome-mediated cell pyroptosis (Yuan et al., 2021). Angiotensin converting enzyme 2 (ACE2) is an enzyme that catalyze the convert of angiotensin II to angiotensin, exerting neuroprotective effect. As proved by Meng Liang Zhou et al., ACE2 can reduce the mitogen activated protein kinase and NF in TBI- κ Phosphorylation of B, leading to the reduction of activated NLRP3 and caspase-3, thereby alleviating cell death (Li T. et al., 2022). As another effector molecule induced by the activation of NLRP3 inflammasome, high mobility group box 1 (HMGB1) is also involved in a typical damage-associated molecular pattern (DAMP), which is associated with the initiation process of NLRP3 inflammasome (Frank et al., 2015). Zhou et al. showed that NLRP3 inflammasome can impair the memory function in late TBI stages mainly through the upregulation of HMGB1 (Tan et al., 2021). Researchers have also studied some related drugs and found that dexmedetomidine, artesunate, and resveratrol can inhibit the activation of NLRP3 inflammasome, and thus presenting an anti-inflammatory function (Gugliandolo et al., 2018; Zheng et al., 2018; Zou et al., 2018).

In addition, some natural products and gas molecules can also inhibit pyroptosis to improve the prognosis of brain injury such as Rhein, which protects the neurological dysfunction after TBI by inhibiting neuronal cell pyroptosis (Bi et al., 2020). Carbon monoxide releasing molecule-3 (CORM-3) is a water-soluble exogenous carbon monoxide involved in the two-way interaction between intestinal and brain, which can inhibit cell death and improve brain injury (Zhang et al., 2021). In terms of the complications after TBI, it has been reported that molecular hydrogen (H_2) can improve the acute lung injury (ALI) after TBI in rats by reducing pyroptosis (Li T. T. et al., 2022). Meanwhile, as a neuroendocrine hormone and a new gastrointestinal hormone which can block NF-κB signaling pathway, ghrelin can improve the inflammasome induced focal necrosis and reduce the TBI induced ALI (Shao et al., 2020). Another study also showed that microglia and infiltrating $CD11b^{+}$ leukocytes, which include macrophages and neutrophils, can actively participate in the innate immune response to penetrating brain injury (PBBI) and pyroptosis,

which would lead to cell loss (Lee et al., 2019). These studies reported that pyroptosis signaling pathway might be a novel therapeutic target for TBI. The possible signal pathways of pyroptosis involved in TBI are summarized in **Figure 2**.

The ferroptosis involved in traumatic brain injury

Ferroptosis is an iron dependent regulatory form of cell death driven by lipid peroxidation. It is characterized by the accumulation of intracellular iron and lipid ROS, the reduction of glutathione (GSH) level, and the inactivation of glutathione peroxidase 4 (GPX4) (Dixon et al., 2012; Stockwell et al., 2017; Yu et al., 2017; Chen et al., 2021d). Ferroptosis has been reported to be involved in TBI (Wenzel et al., 2017; Tang et al., 2020; Geng et al., 2021; Yao et al., 2021). Meanwhile, lipid peroxidation also plays an important role in the traumatic injury of nerve tissue (Anthonymuthu et al., 2018). In the TBI animal model, iron overload, the increased expression of transferrin, the accumulation of lipid ROS and mitochondrial atrophy associated with iron metabolic pathway further verified the existence of ferroptosis. While the treatment of ferroptosis with the inhibitor Fer-1 can reduce neuronal death and improve long-term cognitive and motor function (Xie et al., 2019). TfR1 is a recognized marker of ferroptosis. Researchers reported that ferristatin II (an iron absorption and TfR1 inhibitor) can inhibit the formation of ferritin by reducing Fe^{3+} and iron positive deposits, leading to the alleviation of the neuronal damage caused by TBI (Cheng et al., 2022).

In terms of the lipid metabolism pathway, some scholars have reported that in animal models of TBI, the expression levels of 15-HpETE-PE and 15LO2, GPX4 levels and enzyme activity are decreased in cerebral cortex and hippocampus, proving the existence of PEBP1/15LO-driven ferroptosis in TBI (Wenzel et al., 2017). Lipoxygenase (LOXs) is considered to be a key factor of ferroptosis. It inhibits 12/15-LOX while also reducing infarct size and improving behavioral parameters in ischemic stroke, which confirms the feasibility of 12/15-LOX inhibitors in the treatment of stroke (Karatas et al., 2018). It is reported that the redox lipomics method with liquid chromatography tandem mass spectrometry (LC-MS/MS) identify the oxidation of phosphatidylethanolamine (PEoX) and the reduction of glutathione levels. After the identification of PEoX as a predictive biomarker in ferroptosis by gas cluster ion beam secondary ion mass spectrometry (GCIB-SIMS) imaging and cluster ion beam, mapping the distribution of PEoX in cortical/hippocampal neurons after traumatic brain injury with a spatial resolution of 1.2 mm at single cell/subcellular level can help researchers visualize lipid peroxidation (Sparvero et al., 2021). At the same time, the baicalein administration (a 12/15-lipoxase inhibitor) can significantly reduce ferroptosis in TBI (Kenny et al., 2019). Moreover, baicalin also plays a neuroprotective effect against the seizures after TBI by inhibiting ferroptosis (Li et al., 2019). In addition, it is reported that prokineticin-2, as an important secretory protein, can participate in the pathogenesis of acute and chronic nervous system diseases. It reduces ferroptosis and protect nervous function through the ubiquitination of Fbxo10, the degradation of long chain acyl-CoA synthetase 4 (ACSL4) and the inhibition of lipid peroxidation (Bao et al., 2021).

In addition, there are some molecular compounds and drugs that involved in the mechanism of GPX4 inhibition that can cause ferroptosis. These compounds and drugs include polydatin, ruxolitinib, and tetrandrine. Among them, polydatin generally plays an anti-inflammatory effect, which can improve the activity of GPX4 enzyme and reduce MDA accumulation and lipid peroxidation deposition (Huang et al., 2021). As an inhibitor of janus kinase (JAK) 1 and 2, ruxolitinib is used to treat bone marrow fibrosis, which has an inhibitory effect on ferroptosis, and can also alleviate brain edema and nerve deformation (Chen et al., 2021c). Tetrandrine is a natural bisbenzylisoquinoline alkaloid that can ameliorate TBI by activating autophagy to reduce ferroptosis (Liu et al., 2022). Meanwhile, carotenoids can inhibit ferroptosis from I/R by increasing the expression of GPX4 (Guan et al., 2019). Selenium (Se) effectively inhibits GPX4-dependent ferroptosis, thereby protecting neurons and reducing cerebral infarction (Alim et al., 2019). Regulating the inhibition of ferroptosis by GPX4 may be an effective treatment for patients with ischemic stroke and TBI.

Some non-coding RNAs also exert function in the process of ferroptosis. The miR-212-5p can regulate Ptgs2 to inhibit ferroptosis and protect injured brain (Xiao et al., 2019). Melatonin is a neuroprotective factor which can mitigate lipid peroxidation through circPtpn14/miR-351-5p/5-LOX signaling. It can also antagonize ferroptosis and relieve ER stress in TBI (Wu C. et al., 2022). Referring to the protective mechanism of melatonin, Rui et al. (2021) found that melatonin could inhibit the neuronal FTH mediated ferroptosis after TBI. Meanwhile, p53 is another factor involved in ferroptosis, of which possible target is SLC7A11 (Jiang et al., 2015). Sirtuin 2 (SIRT2) is a member of nicotinamide adenine dinucleotide (NAD+) dependent protein deacetylase family which has neuroprotective effects on TBI by inhibiting the p53 mediated ferroptosis (Gao et al., 2021). To sum up, inhibiting ferroptosis can probably improve the damage caused by TBI. The possible signal pathways of ferroptosis involved in TBI are summarized in **Figure 3**.

The parthanatos involved in traumatic brain injury

Parthanatos is a novel form of programmed cell death based on DNA damage and PARP-1 activation. In this process, the DNA repairment of poly ADP-PARP1 is over activated

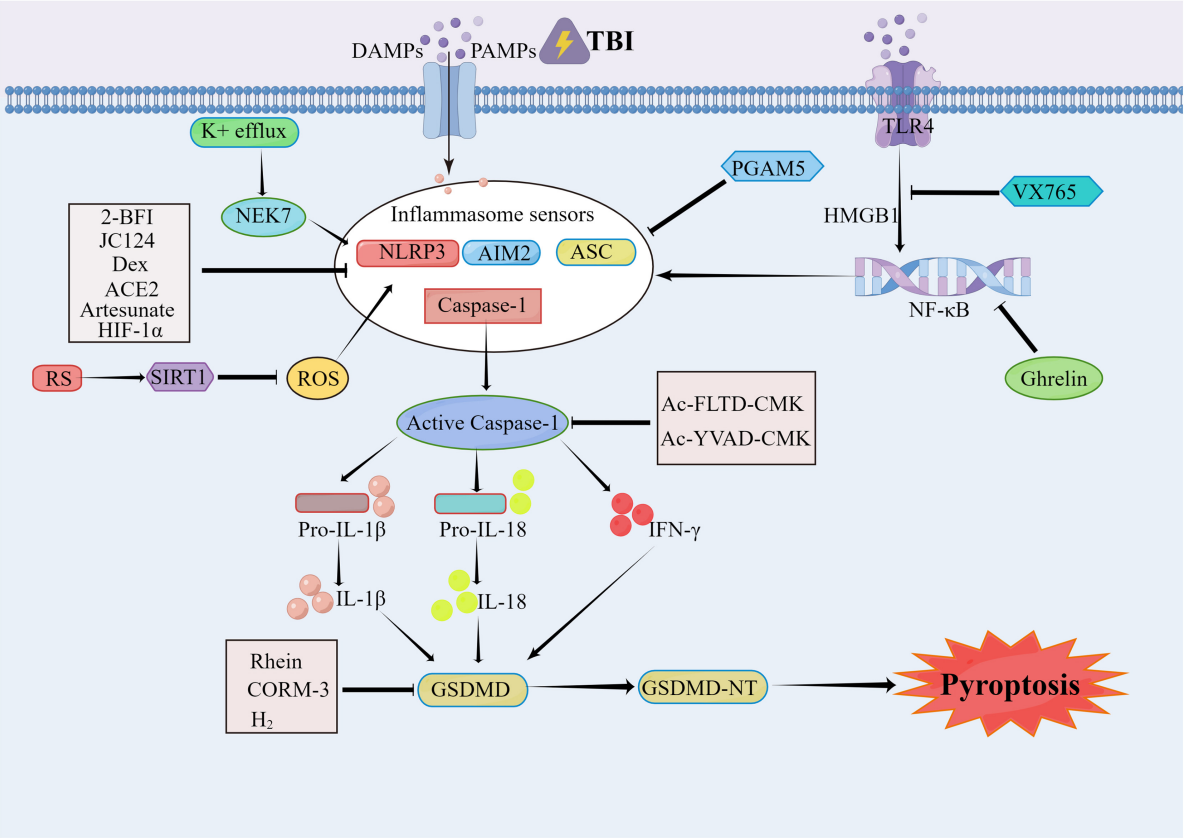

FIGURE 2
The pyroptosis involved in traumatic brain injury (TBI). After TBI occurs, the caspase-1 is mainly activated by NLRP3, AIM2, ASC, and other inflammasomes. The activated caspase-1 includes the IL-1β/18 lysed from the pro IL-1β, and the N-terminal segments of the GSDMD (GSDMD-NT) lysed from the Gasdermin D (GSDMD). The 2-BFI, JC124, Dex, ACE2, Artesunate, HIF-1α, and PGAM5 can alleviate the pyroptosis by inhibiting the inflammasomes. The VX765 can exert the neural protect function through the HMGB1/TLR4/NF-κB pathway. The Rhein, CORM-3, and H2 can inhibit the pyroptosis as well. The RS can activate the SIRT1 to inhibit the activation of NLRP3, thereby relieving the TBI. As the inhibitors of the Caspase-1, the Ac-YVAD-CMK and Ac-FLTD-CMK can inhibit the lysis of GSDMS and the oligomerization of ASC to alleviate the pyroptosis.

with the accumulation of intracellular poly ADP ribose (PAR) polymer, resulting in the depletion of NAD^+ and ATP. PAR also combines with mitochondrial apoptosis which can induce the release of factor AIF to cell membrane. Combined macrophage migration inhibitory factor (MIF) can move to nucleus and split the genomic DNA into large fragments, causing chromatin condensation and fragmentation, and further leading to cell death (Virag and Szabó, 2002; Yu et al., 2006; Wang et al., 2011; Fatokun et al., 2014).

Multiple lines of evidence can support a certain role of parthanatos in TBI (Fatokun et al., 2014; Galluzzi et al., 2018). Secondary damage caused by oxidative stress after TBI will lead to DNA strand breakage, the over activation of PARP-1, and neuronal death. In some studies, the functional prognosis of TBI was improved by inactivation of PARP. This protective effect was confirmed by the use of a new PARP inhibitor named GPI 6150 (Virag and Szabó, 2002). PJ34 and INO-1001 are the other two structural PARP inhibitors except benzamide, which can reduce cell death and the microglia activation of primary cortical neurons exposed to *n*-methyl-*n*'-nitro-*N*-nitrosoguanidine (MNNG). They can also reduce reactive oxygen species neuroinflammation, and protect the neurons in cerebral cortex and thalamus. While neither of them can improve cognitive performance in morris water maze (MWM) test, nor can they reduce the loss of nerve cells in hippocampus (Stoica et al., 2014). INO-1001 can exert a neuroprotective effect in the rat TBI model by preventing NAD^+ depletion (Besson et al., 2005; Clark et al., 2007). Meanwhile, the inhibition of NF-B-dependent gene transcription by PARP inhibition will prevent microglial activation. The inhibitor should be administered within 20 h after TBI, which will alleviate inflammation and improve histological and functional outcomes (d'Avila et al., 2012). Ghrelin also has the functions about improving sensormotor and reflex function and reducing cleaved PARP-1 levels in cortex, the PARP-1-dependent cell death, and the mortality after TBI (Qi et al., 2012). It is

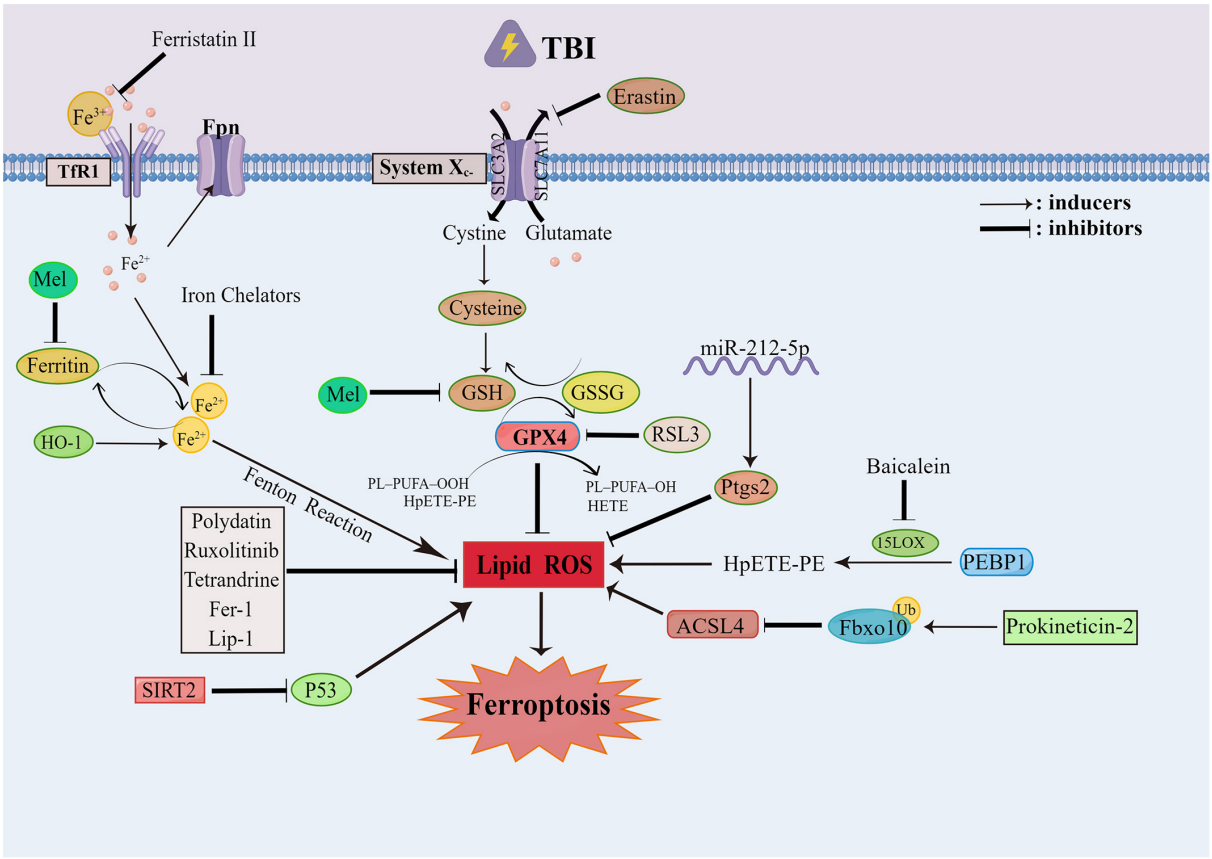

FIGURE 3
The ferroptosis involved in traumatic brain injury (TBI). The ferroptosis generally occurs after TBI, which can be targeted to improve the prognosis of TBI. The ferroptosis can be alleviated by the inhibition of the Xc-system and GPX4. The Mel can reduce the fenton reaction by inhibiting Ferritin. The Polydatin, Ruxolitinib, Tetrandrine can all alleviate the ferroptosis by mitigating the lipid peroxidation. While the SIRT2 can mitigate the lipid peroxidation through the inhibition of P53. The Prokineticin-2 can promote the ubiquitination of Fbxo10 to accelerate the degradation of Acsl4 and inhibit the lipid peroxidation. The miR-212-5p can inhibit the lipid peroxidation through Ptgs2. And the PEBP1/15LO can drive the occurrence of ferroptosis.

reported that tetrahydroxystilbene glucoside (TSG) is an active component of the traditional Chinese herbal medicine called polygonum multiflorum, which has neuroprotective effect. Its specific mechanism may be explicated as the reduction of oxidative stress and neuroinflammation and the inhibition of PARP1 to negatively regulate Ras/JNK signaling pathway (Cao et al., 2020). A large number of studies have focused on the pathway about transporting PARP inhibitors. Nanostructured lipid carriers (RBCNLCs) encapsulated by red blood cells (RBC) were used in brain neuron mitochondria together with C3 and ss31 peptides (C3/SS31-RBCNLCs). The high-concentration delivery of PARP inhibitor olapali (Ola) to brain mitochondria by C3/SS31-RBCNLCs-Ola has effectively improved mitochondrial function (Sun et al., 2022). Various lines of evidence suggested that the inhibition of PARP1 has a protective effect, as some studies found that PARP1 inhibition in ShRNA could promote axon regeneration, while the inhibition of other PARP isoforms would reduce axon regeneration with no improvement of motor function (Wang et al., 2016). The timing of pharmacological inhibition and the direction of inhibitor selection also need to be further investigated.

In addition to directly inhibiting PARP-1, aiming at PAR/MIF or NAD^+ depletion pathway is also an option to improve the prognosis of TBI. It has been reported that the intranasal delivery of NAD^+ can increase NAD^+ levels in hippocampus and reduce the TBI induced hippocampal neuronal death (Won et al., 2012). Furthermore, MIF can mediate the TBI-induced neurodegeneration, neuronal death, and neurobehavioral dysfunction via its nuclease activity, while it shows no pro-inflammatory effects (Ruan et al., 2021). Recent studies demonstrated that iduna is a newly discovered ubiquitin E3 ligase and an endogenous regulator of parthanatos, which can reduce PARP activation and nuclear translocation of AIF to prevent parthanatos, indicating that ubiquitin-proteasome pathway may also play a role in parthanatos (Xu et al., 2019). At the same time, iduna may promote docosahexaenoic acid

(DHA) through Wnt/MDM2 pathway and reduce the damage of TBI cell and mitochondrial dysfunction (Shi et al., 2022). Based on these reports, targeting PARP1-dependent parthanatos may be a potential strategy for the treatment of secondary injury after TBI.

The cyclophilin D-mediated necrosis involved in traumatic brain injury

Cyclophilin D (CypD) is a member of cyclophilin family with various biological functions which can cause mitochondrial dysfunction through promoting the opening of mitochondrial permeability transitionpore (mPTP). For example, the loss of mitochondrial membrane potential, ATP depletion, mitochondrial swelling, and final mitochondrial outer membrane rupture can all induce the CypD pathway-dependent cell necrosis (Baines et al., 2005; Schinzel et al., 2005; Yamaguchi et al., 2005; Alam et al., 2015).

Evidence suggests that in the secondary damage generated after TBI, Cyclosporin A (CsA) can inhibit the opening of mPTP by interacting with CypD, resulting in the alleviation of mitochondrial dysfunction and neuronal damage in a TBI rat model (Sullivan et al., 2005; Kim et al., 2014; Springer et al., 2018). Studies have shown that the mice lacking CypD coding gene Ppif can retain mitochondrial function for 6 h after injury with fewer loss of subacute cortical tissue and hippocampal cells within 18 days after injury. As an effective inhibitor of CypD, CSA has many benefits about its usage on disease treatment (Readnower et al., 2021). There are many CSA related studies, some of them reported the function of CSA about suppressing mPTP opening that can maintain mitochondrial membrane potential and calcium balance in isolated mitochondria, and alleviate acute mitochondrial dysfunction after TBI (Sullivan et al., 1999). However, synaptic mitochondria will suffer more damage than non-synaptic mitochondria 24 h after CCI. While the intraperitoneal injection of CSA (20 mg/kg) at 15 mins after injury can improve synaptic and non-synaptic respiration to a significant extent, especially in the synaptic groups enduring more severe damage (Kulbe et al., 2017). As a non-immunosuppressive CSA analog, NIM811 as well as CSA can significantly reduce lipid peroxidation and protein nitrating damage of mitochondria 12 h after TBI. The neuroprotection provided by nim811 is dose-dependent with the most appropriate dose of 10 mg/kg. This dose can improve cognitive function and reduce mitochondrial damage (Mbye et al., 2008; Readnower et al., 2011). In preclinical experiments, positive improvements in brain metabolism and mitochondrial function were observed in TBI models in large animals, validating the neuroprotective effects of cyclosporine (Karlsson et al., 2019). At the same time, researchers have employed some research on the intervention of CypD. For example, CypD knockout can improve the abnormalities of excitatory synapses, while inhibiting CypD can reduce the synaptic overexcitation after TBI (Sun and Jacobs, 2016). But the knockdown of CypD was unable to reduce the pathology within axon initiation node (AIS), suggesting that axonal interval is regulated under different mechanism (Hanell et al., 2015).

Other studies have focused on the regulation of Cypd/mPTP in drugs or targeted molecules to improve mitochondrial function and produce protective effects. (1) Resveratrol can reduce mPTP opening by inhibiting the ROS mediated function, and protect the TBI mitochondrial function of GSK3 (Lin et al., 2014). (2) With an neuroprotective activity in p38 MAPK pathway, SIRT1 has been reported to protect mitochondria from damage (Yang et al., 2017). (3) Treatment of recombinant human erythropoietin or carbamylated erythropoietin can reduce mPTP opening caused by TBI, thereby improving mitochondrial disorders (Millet et al., 2016). (4) In rat brain mitochondria (RBM), the oxidative phosphorylation capacity (OXPHOS) can evaluate the respiratory effect of mitochondria. Etofoxine can restore mitochondrial oxidative phosphorylation and improve cognitive recovery after TBI (Palzur et al., 2021). (5) Brain-derived neurotrophic factor (BDNF) can inhibit the opening of MPTP, promote the accumulation of pCREB in mitochondrial intima and matrix and the synthesis of mitochondrial complex V, while alleviate the metabolic defects of neurons after mechanical injury (Xu et al., 2018). To sum up, the role of CypD-mediated necrosis in TBI can provide therapeutic implications for mitochondrial dysfunction after TBI.

Discussion

Necroptosis, pyroptosis, ferroptosis, parthanatos, and CypD mediated necrosis are all important to the secondary injury after TBI. Several different types of regulatory necrosis can be triggered by nerve cells under death-inducing stimuli. However, under various complex pathophysiological mechanisms in TBI, these kinds of regulated necrosis may be interrelated and coexist with each other, or be alterable in cells with ever-changing levels. For example, (1) necroptosis may play a major role in the early stage after CCI, but other cell death pathways such as autophagy, apoptosis, pyroptosis, and ferroptosis are associated with the subsequent pathological process (Ganjam et al., 2018). (2) Silencing of RIPK1 can alleviate TBI by inhibiting inflammation and autophagy in neurons through NF-κB signaling pathway (Liu et al., 2020). (3) Nec-1 can prevent BNIP3 from integrating into mitochondria by modifying the binding site of BNIP3 on mitochondria. Therefore, Nec-1 can effectively inhibit the collapse of mitochondrial membrane potential induced by BNIP3 and reduce the opening efficiency of mPTP (Mu et al., 2021). Autophagy is significantly enhanced

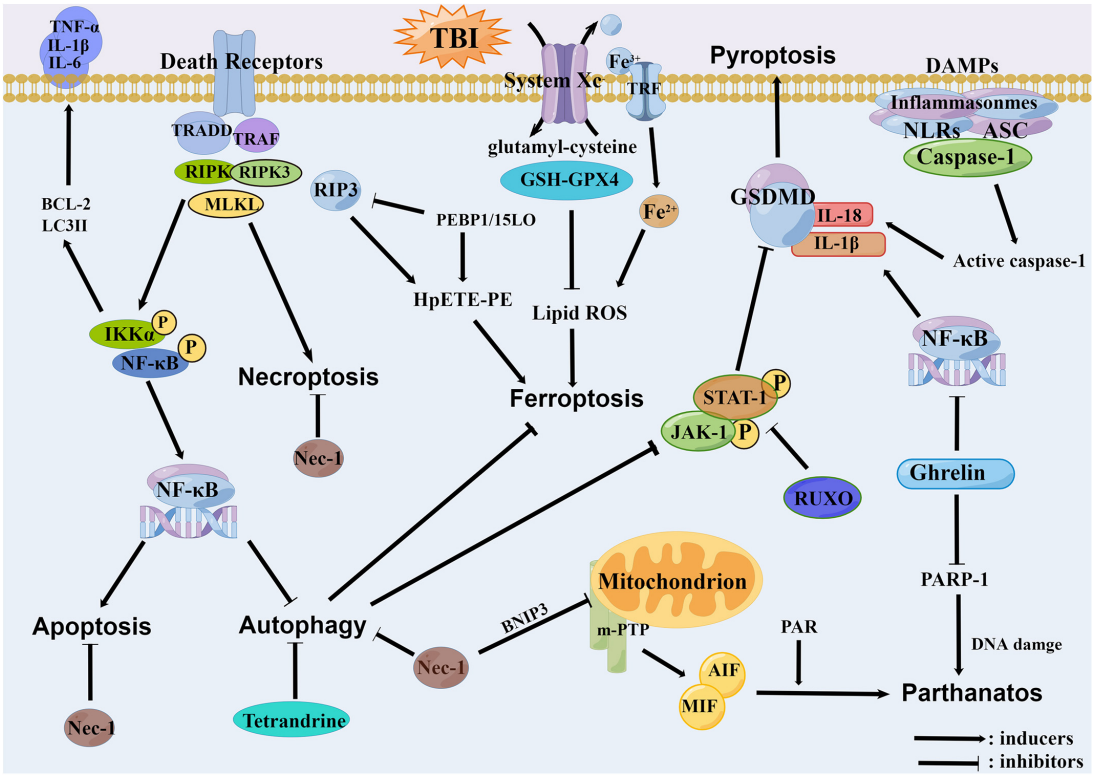

FIGURE 4
The relationships among all the regulatory necrosis involved in traumatic brain injury (TBI). The necroptosis can promote the apoptosis and inhibit the autophagy through the NF-κB pathway. The PEBP1 can interact with RIP3 or 15LOX to initiate the necroptosis and the ferroptosis. The Tetrandrine can inhibit the ferroptosis through the inhibition of autophagy. Meanwhile, the autophagy can inhibit the pyroptosis through the JAK1/STAT1 pathway. As an inhibitor of the necroptosis, the Nec-1 can concurrently inhibit the BNIP3 and decrease the open efficiency of mPTP, thereby reducing the parthanatos. The Ghrelin also has anti-inflammatory properties, which can alleviate the pyroptosis, and furthermore alleviate the parthanatos by reducing the PARP-1.

in TBI and ischemic stroke. The knockout of BNIP3 in mice can inhibit mitosis through the interaction of BNIP3 and LC3, with the manifestations of increased autophagy, decreased apoptosis and reduced cerebral infarction, indicating that the silencing of BNIP3 may be conducive to the neuroprotection after stroke (Shi et al., 2014). Meanwhile, Nec-1 can also inhibit the activation of necrotizing apoptosis as well as cell apoptosis and autophagy, while reducing the tissue damage and functional defects caused by TBI (Wang et al., 2012). (4) Autophagy activation can inhibit cell death in a mouse model of moderate traumatic brain injury through IL-13 and JAK1/STAT1 pathways (Gao et al., 2020). Inactivation of RIPK3 K51A kinase can enhance ferroptosis, causing worse outcomes after TBI. As a regulator of cell death, PEBP1 can inhibit the activity of pro-metabolic RIP3, and activate 15LOX to trigger pro-ferroptotic HpETE-PE signaling (Lamade et al., 2022). All these kinds of regulatory necrosis may occur simultaneously.

Interestingly, there are interactions between different types of cell death. Some reports showed that some inhibitors or hormones could be sensitive to another by blocking any way of cell death. For example, tetrahydropyrrole can improve TBI by regulating autophagy and reducing ferroptosis (Liu et al., 2022). It has been shown that treatment with 2-BFI could reduce both necroptosis and pyroptosis, thus exerting a role of neurofunctional protection (Ni et al., 2019). In some hormone treatments, ghrelin can reduce the level of cleaved PARP-1 in cortex, the PARP-1 dependent cell death and the mortality after TBI, while improving the sensorimotor and reflex functions. Its protective effect is related to its anti-inflammatory properties and pyroptosis (Shao et al., 2020). Upregulation of NIX reduces neuronal apoptosis and brain water content by increasing mitophagy in TBI rat model (Ma et al., 2019). Inhibition of autophagy and apoptosis and reduction of neuronal death using intranasal WNT3α therapy in TBI mice model can reduce the death of neurons (Zhang et al., 2018). In clinical stroke, Dl-3n-butylphthalide (Dl-NBP) has neuroprotective effects with anti-inflammatory, antioxidant, anti-apoptotic and mitochondrial protective functions. Dl-NBP treatment improves motor recovery after TBI by inhibiting the activation of autophagy and consequently blocking connexin loss and neuronal apoptosis (Wu et al., 2020). Therefore, regulatory necrosis may occur simultaneously with mutual transformation

and interaction to some extent. The relationships among all the regulatory necrosis involved in TBI are summarized in **Figure 4**.

Secondary injury following TBI is a critical factor which affects prognosis. The cell death is an important cause of secondary injury and there is increasing number of researchers who have found that various regulatory necrosis could contribute to the development of TBI, providing many new perspectives for us to understand and treat TBI. Therefore, the intervention of regulatory necrosis related pathway may be an effective strategy to reduce the secondary injury after TBI, and the relationships among different necrosis are worthy of further study.

Author contributions

ZN and BW: concept and design. ZN, LT, JN, and BW: writing, review, and revision of the manuscript. ZN: figures design. All authors approved the final version of the manuscript.

Funding

The present investigation was funded by the Natural Science Foundation of Hunan Province (No. 2022JJ30520) and the Postgraduate Scientific Research Innovation Project of Hunan Province (CX20221014).

Acknowledgments

We thank Figdraw (www.figdraw.com) for expert assistance in the pattern drawing.

Conflict of interest

The authors declare that the research was conducted in the absence of any commercial or financial relationships that could be construed as a potential conflict of interest.

Publisher's note

References

Alam, M. R., Baetz, D., and Ovize, M. (2015). Cyclophilin D and myocardial ischemia-reperfusion injury: A fresh perspective. *J. Mol. Cell. Cardiol.* 78, 80–89. doi: 10.1016/j.yjmcc.2014.09.026

Alim, I., Caulfield, J. T., Chen, Y., Swarup, V., Geschwind, D. H., Ivanova, E., et al. (2019). Selenium drives a transcriptional adaptive program to block ferroptosis and treat stroke. *Cell* 177, 1262–1279. doi: 10.1016/j.cell.2019.03.032

Anthonymuthu, T. S., Kenny, E. M., Lamade, A. M., Kagan, V. E., and Bayır, H. (2018). Oxidized phospholipid signaling in traumatic brain injury. *Free Radic Biol. Med.* 124, 493–503. doi: 10.1016/j.freeradbiomed.2018.06.031

Baines, C. P., Kaiser, R. A., Purcell, N. H., Blair, N. S., Osinska, H., Hambleton, M. A., et al. (2005). Loss of cyclophilin D reveals a critical role for mitochondrial permeability transition in cell death. *Nature* 434, 658–662. doi: 10.1038/nature03434

Bao, Z., Fan, L., Zhao, L., Xu, X., Liu, Y., Chao, H., et al. (2019). Silencing of A20 aggravates neuronal death and inflammation after traumatic brain injury: A potential trigger of necroptosis. *Front. Mol. Neurosci.* 12:222. doi: 10.3389/fnmol.2019.00222

Bao, Z., Liu, Y., Chen, B., Miao, Z., Tu, Y., Li, C., et al. (2021). Prokineticin-2 prevents neuronal cell deaths in a model of traumatic brain injury. *Nat. Commun.* 12:4220. doi: 10.1038/s41467-021-24469-y

Besson, V. C., Zsengeller, Z., Plotkine, M., Szabo, C., and Marchand-Verrecchia, C. (2005). Beneficial effects of PJ34 and INO-1001, two novel water-soluble poly(ADP-ribose) polymerase inhibitors, on the consequences of traumatic brain injury in rat. *Brain Res.* 1041, 149–156. doi: 10.1016/j.brainres.2005.01.096

Bi, F., Ma, H., Ji, C., Chang, C., Liu, W., and Xie, K. (2020). Rhein protects against neurological deficits after traumatic brain injury in mice via inhibiting neuronal pyroptosis. *Front. Pharmacol.* 11:564367. doi: 10.3389/fphar.2020.564367

Cao, Y., Chen, Y., Wang, F., Wang, Y., and Long, J. (2020). PARP1 might enhance the therapeutic effect of tetrahydroxystilbene glucoside in traumatic brain injury via inhibition of Ras/JNK signalling pathway. *Folia Neuropathol.* 58, 45–56. doi: 10.5114/fn.2020.94006

Chen, T., Yang, L., Zhu, J., Hang, C., and Wang, Y. (2021b). The AMPAR antagonist perampanel regulates neuronal necroptosis via Akt/GSK3β signaling after acute traumatic injury in cortical neurons. *CNS Neurol. Disord. Drug Targets* 20, 266–272. doi: 10.2174/1871527319666201001110937

Chen, T., Qian, X., Zhu, J., Yang, L. K., and Wang, Y. H. (2021a). Controlled decompression attenuates compressive injury following traumatic brain injury via TREK-1-mediated inhibition of necroptosis and neuroinflammation. *Oxid. Med. Cell. Longev.* 2021:4280951. doi: 10.1155/2021/4280951

Chen, Y., Gong, K., Guo, L., Zhang, B., Chen, S., Li, Z., et al. (2021e). Downregulation of phosphoglycerate mutase 5 improves microglial inflammasome activation after traumatic brain injury. *Cell Death Discov.* 7:290. doi: 10.1038/s41420-021-00686-8

Chen, X., Kang, R., Kroemer, G., and Tang, D. (2021d). Broadening horizons: The role of ferroptosis in cancer. *Nat. Rev. Clin. Oncol.* 18, 280–296. doi: 10.1038/s41571-020-00462-0

Chen, X., Gao, C., Yan, Y., Cheng, Z., Chen, G., Rui, T., et al. (2021c). Ruxolitinib exerts neuroprotection via repressing ferroptosis in a mouse model of traumatic brain injury. *Exp. Neurol.* 342:113762. doi: 10.1016/j.expneurol.2021.113762

Chen, T., Zhu, J., Wang, Y., and Hang, C. (2020). Arc silence aggravates traumatic neuronal injury via mGluR1-mediated ER stress and necroptosis. *Cell Death Dis.* 11:4. doi: 10.1038/s41419-019-2198-5

Chen, Y., Meng, J., Bi, F., Li, H., Chang, C., Ji, C., et al. (2019). EK7 regulates NLRP3 inflammasome activation and neuroinflammation post-traumatic brain injury. *Front. Mol. Neurosci.* 12:202. doi: 10.3389/fnmol.2019.00202

Cheng, Y., Qu, W., Li, J., Jia, B., Song, Y., Wang, L., et al. (2022). Ferristatin II, an iron uptake inhibitor, exerts neuroprotection against traumatic brain injury via suppressing ferroptosis. *ACS Chem. Neurosci.* 13, 664–675. doi: 10.1021/acschemneuro.1c00819

Cho, Y. S., Challa, S., Moquin, D., Genga, R., Ray, T. D., Guildford, M., et al. (2009). Phosphorylation-driven assembly of the RIP1-RIP3 complex regulates programmed necrosis and virus-induced inflammation. *Cell* 137, 1112–1123. doi: 10.1016/j.cell.2009.05.037

Chou, T. W., Chang, N. P., Krishnagiri, M., Patel, A. P., Lindman, M., Angel, J. P., et al. (2021). Fibrillar alpha-synuclein induces neurotoxic astrocyte activation via RIP kinase signaling and NF-kappaB. *Cell Death Dis.* 12:756. doi: 10.1038/s41419-021-04049-0

Clark, R. S., Vagni, V. A., Nathaniel, P. D., Jenkins, L. W., Dixon, C. E., and Szabo, C. (2007). Local administration of the poly(ADP-ribose) polymerase inhibitor INO-1001 prevents NAD+ depletion and improves water maze performance after traumatic brain injury in mice. *J. Neurotrauma* 24, 1399–1405. doi: 10.1089/neu.2007.0305

d'Avila, J. C., Lam, T. I., Bingham, D., Shi, J., Won, S. J., and Kauppinen, T. M. (2012). Microglial activation induced by brain trauma is suppressed by post-injury treatment with a PARP inhibitor. *J. Neuroinflammation* 9:31. doi: 10.1186/1742-2094-9-31

Degterev, A., Ofengeim, D., and Yuan, J. (2019). Targeting RIPK1 for the treatment of human diseases. *Proc. Natl. Acad. Sci. U.S.A.* 116, 9714–9722. doi: 10.1073/pnas.1901179116

Dionísio, P. A., Amaral, J. D., and Rodrigues, C. M. P. (2021). Oxidative stress and regulated cell death in Parkinson's disease. *Ageing Res. Rev.* 67:101263. doi: 10.1016/j.arr.2021.101263

Dixon, S. J., Lemberg, K. M., Lamprecht, M. R., Skouta, R., Zaitsev, E. M., Gleason, C. E., et al. (2012). Ferroptosis: An iron-dependent form of nonapoptotic cell death. *Cell* 149, 1060–1072. doi: 10.1016/j.cell.2012.03.042

Dong, Y., Yu, H., Li, X., Bian, K., Zheng, Y., Dai, M., et al. (2022). Hyperphosphorylated tau mediates neuronal death by inducing necroptosis and inflammation in Alzheimer's disease. *J. Neuroinflammation* 19:205. doi: 10.1186/s12974-022-02567-y

Du, H., Li, C. H., Gao, R. B., Cen, X. Q., and Li, P. (2022). Ablation of GSDMD attenuates neurological deficits and neuropathological alterations after traumatic brain injury. *Front. Cell Neurosci.* 16:915969. doi: 10.3389/fncel.2022.915969

Fatokun, A. A., Dawson, V. L., and Dawson, T. M. (2014). Parthanatos: Mitochondrial-linked mechanisms and therapeutic opportunities. *Br. J. Pharmacol.* 171, 2000–2016. doi: 10.1111/bph.12416

Frank, M. G., Weber, M. D., Watkins, L. R., and Maier, S. F. (2015). Stress sounds the alarmin: The role of the danger-associated molecular pattern HMGB1 in stress-induced neuroinflammatory priming. *Brain Behav. Immun.* 48, 1–7. doi: 10.1016/j.bbi.2015.03.010

Galluzzi, L., Vitale, I., Aaronson, S. A., Abrams, J. M., Adam, D., Agostinis, P., et al. (2018). Molecular mechanisms of cell death: Recommendations of the Nomenclature Committee on Cell Death 2018. *Cell Death Differ.* 25, 486–541. doi: 10.1038/s41418-017-0012-4

Ganjam, G. K., Terpolilli, N. A., Diemert, S., Eisenbach, I., Hoffmann, L., Reuther, C., et al. (2018). Cylindromatosis mediates neuronal cell death in vitro and in vivo. *Cell Death Differ.* 25, 1394–1407. doi: 10.1038/s41418-017-0046-7

Gao, C., Yan, Y. N., Chen, G., Wang, T., Luo, C., Zhang, M., et al. (2020). Autophagy activation represses pyroptosis through the IL-13 and JAK1/STAT1 pathways in a mouse model of moderate traumatic brain injury. *ACS Chem. Neurosci.* 11, 4231–4239. doi: 10.1021/acschemneuro.0c00517

Gao, J., Li, Y., and Song, R. (2021). SIRT2 inhibition exacerbates p53-mediated ferroptosis in mice following experimental traumatic brain injury. *Neuroreport* 32, 1001–1008. doi: 10.1097/WNR.0000000000001679

Ge, X., Li, W., Huang, S., Yin, Z., Xu, X., Chen, F., et al. (2018). The pathological role of NLRs and AIM2 inflammasome-mediated pyroptosis in damaged blood-brain barrier after traumatic brain injury. *Brain Res.* 1697, 10–20. doi: 10.1016/j.brainres.2018.06.008

Geng, Z., Guo, Z., Guo, R., Ye, R., Zhu, W., and Yan, B. (2021). Ferroptosis and traumatic brain injury. *Brain Res. Bull.* 172, 212–219. doi: 10.1016/j.brainresbull.2021.04.023

Gong, Y. N., Guy, C., Olauson, H., Becker, J. U., Yang, M., Fitzgerald, P., et al. (2017). ESCRT-III Acts downstream of MLKL to regulate necroptotic cell death and its consequences. *Cell* 169, 286–300. doi: 10.1016/j.cell.2017.03.020

Grootjans, S., Vanden, B. T., and Vandenabeele, P. (2017). Initiation and execution mechanisms of necroptosis: An overview. *Cell Death Differ.* 24, 1184–1195. doi: 10.1038/cdd.2017.65

Guan, X., Li, X., Yang, X., Yan, J., Shi, P., Ba, L., et al. (2019). The neuroprotective effects of carvacrol on ischemia/reperfusion-induced hippocampal neuronal impairment by ferroptosis mitigation. *Life Sci.* 235:116795. doi: 10.1016/j.lfs.2019.116795

Gugliandolo, E., D'Amico, R., Cordaro, M., Fusco, R., Siracusa, R., Crupi, R., et al. (2018). Neuroprotective effect of artesunate in experimental model of traumatic brain injury. *Front. Neurol.* 9:590. doi: 10.3389/fneur.2018.00590

Guo, H., and Kaiser, W. J. (2017). ESCRTing necroptosis. *Cell* 169, 186–187. doi: 10.1016/j.cell.2017.03.030

Hanell, A., Greer, J. E., McGinn, M. J., and Povlishock, J. T. (2015). Traumatic brain injury-induced axonal phenotypes react differently to treatment. *Acta Neuropathol.* 129, 317–332. doi: 10.1007/s00401-014-1376-x

Holler, N., Zaru, R., Micheau, O., Thome, M., Attinger, A., Valitutti, S., et al. (2000). Fas triggers an alternative, caspase-8-independent cell death pathway using the kinase RIP as effector molecule. *Nat. Immunol.* 1, 489–495. doi: 10.1038/82732

Hu, X., Chen, H., Xu, H., Wu, Y., Wu, C., Jia, C., et al. (2020). Role of pyroptosis in traumatic brain and spinal cord injuries. *Int. J. Biol. Sci.* 16, 2042–2050. doi: 10.7150/ijbs.45467

Hu, Y., Feng, X., Chen, J., Wu, Y., and Shen, L. (2022). Hydrogen-rich saline alleviates early brain injury through inhibition of necroptosis and neuroinflammation via the ROS/HO-1 signaling pathway after traumatic brain injury. *Exp. Ther. Med.* 23:126. doi: 10.3892/etm.2021.11049

Huang, L., He, S., Cai, Q., Li, F., Wang, S., Tao, K., et al. (2021). Polydatin alleviates traumatic brain injury: Role of inhibiting ferroptosis. *Biochem. Biophys. Res. Commun.* 556, 149–155. doi: 10.1016/j.bbrc.2021.03.108

Irrera, N., Pizzino, G., Calo, M., Pallio, G., Mannino, F., Fama, F., et al. (2017). Lack of the Nlrp3 inflammasome improves mice recovery following traumatic brain injury. *Front. Pharmacol.* 8:459. doi: 10.3389/fphar.2017.00459

Irrera, N., Russo, M., Pallio, G., Bitto, A., Mannino, F., Minutoli, L., et al. (2020). The Role of NLRP3 inflammasome in the pathogenesis of traumatic brain injury. *Int. J. Mol. Sci.* 21:6204. doi: 10.3390/ijms21176204

Ising, C., Venegas, C., Zhang, S., Scheiblich, H., Schmidt, S. V., Vieira-Saecker, A., et al. (2019). NLRP3 inflammasome activation drives tau pathology. *Nature* 575, 669–673. doi: 10.1038/s41586-019-1769-z

Jiang, J., Gao, G., Feng, J., Mao, Q., Chen, L., Yang, X., et al. (2019). Traumatic brain injury in China. *Lancet Neurol.* 18, 286–295. doi: 10.1016/S1474-4422(18)30469-1

Jiang, L., Hickman, J. H., Wang, S. J., and Gu, W. (2015). Dynamic roles of p53-mediated metabolic activities in ROS-induced stress responses. *Cell Cycle* 14, 2881–2885. doi: 10.1080/15384101.2015.1068479

Karatas, H., Eun, J. J., Lo, E. H., and van Leyen, K. (2018). Inhibiting 12/15-lipoxygenase to treat acute stroke in permanent and tPA induced thrombolysis models. *Brain Res.* 1678, 123–128. doi: 10.1016/j.brainres.2017.10.024

Karlsson, M., Pukenas, B., Chawla, S., Ehinger, J. K., Plyler, R., Stolow, M., et al. (2019). Neuroprotective effects of cyclosporine in a porcine pre-clinical trial of focal traumatic brain injury. *J. Neurotrauma* 36, 14–24. doi: 10.1089/neu.2018.5706

Kenny, E. M., Fidan, E., Yang, Q., Anthonymuthu, T. S., New, L. A., Meyer, E. A., et al. (2019). Ferroptosis contributes to neuronal death and functional outcome after traumatic brain injury. *Crit. Care Med.* 47, 410–418. doi: 10.1097/CCM.0000000000003555

Kim, S. Y., Shim, M. S., Kim, K. Y., Weinreb, R. N., Wheeler, L. A., and Ju, W. K. (2014). Inhibition of cyclophilin D by cyclosporin A promotes retinal ganglion cell survival by preventing mitochondrial alteration in ischemic injury. *Cell Death Dis.* 5:e1105. doi: 10.1038/cddis.2014.80

Kulbe, J. R., Hill, R. L., Singh, I. N., Wang, J. A., and Hall, E. D. (2017). Synaptic mitochondria sustain more damage than non-synaptic mitochondria after traumatic brain injury and are protected by cyclosporine A. *J. Neurotrauma* 34, 1291–1301. doi: 10.1089/neu.2016.4628

Kuwar, R., Rolfe, A., Di, L., Xu, H., He, L., Jiang, Y., et al. (2019). A novel small molecular NLRP3 inflammasome inhibitor alleviates neuroinflammatory response following traumatic brain injury. *J. Neuroinflammation* 16:81. doi: 10.1186/s12974-019-1471-y

Ladak, A. A., Enam, S. A., and Ibrahim, M. T. (2019). A review of the molecular mechanisms of traumatic brain injury. *World Neurosurg.* 131, 126–132. doi: 10.1016/j.wneu.2019.07.039

Lamade, A. M., Wu, L., Dar, H. H., Mentrup, H. L., Shrivastava, I. H., Epperly, M. W., et al. (2022). Inactivation of RIP3 kinase sensitizes to 15LOX/PEBP1-mediated ferroptotic death. *Redox Biol.* 50:102232. doi: 10.1016/j.redox.2022.102232

Lee, S. W., de Rivero Vaccari, J. P., Truettner, J. S., Dietrich, W. D., and Keane, R. W. (2019). The role of microglial inflammasome activation in pyroptotic cell death following penetrating traumatic brain injury. *J. Neuroinflammation* 16:27. doi: 10.1186/s12974-019-1423-6

Li, Q., Li, Q., Jia, J., Sun, Q., Zhou, H., Jin, W., et al. (2019). Baicalein Exerts neuroprotective effects in FeCl3-induced posttraumatic epileptic seizures via suppressing ferroptosis. *Front. Pharmacol.* 10:638. doi: 10.3389/fphar.2019.00638

Li, T. T., Sun, T., Wang, Y. Z., Wan, Q., Li, W. Z., and Yang, W. C. (2022). Molecular hydrogen alleviates lung injury after traumatic brain injury: Pyroptosis and apoptosis. *Eur. J. Pharmacol.* 914:174664. doi: 10.1016/j.ejphar.2021.174664

Li, T., Huang, H. Y., Wang, H. D., Gao, C. C., Liang, H., Deng, C. L., et al. (2022). Restoration of brain angiotensin-converting enzyme 2 alleviates neurological deficits after severe traumatic brain injury via mitigation of pyroptosis and apoptosis. *J. Neurotrauma* 39, 423–434. doi: 10.1089/neu.2021.0382

Lin, C. J., Chen, T. H., Yang, L. Y., and Shih, C. M. (2014). Resveratrol protects astrocytes against traumatic brain injury through inhibiting apoptotic and autophagic cell death. *Cell Death Dis.* 5:e1147. doi: 10.1038/cddis.2014.123

Liu, H., He, S., Wang, J., Li, C., Liao, Y., Zou, Q., et al. (2022). Tetrandrine ameliorates traumatic brain injury by regulating autophagy to reduce ferroptosis. *Neurochem. Res.* 47, 1574–1587. doi: 10.1007/s11064-022-03553-9

Liu, J., Zhu, Z., Wang, L., Du, J., Zhang, B., Feng, X., et al. (2020). Functional suppression of Ripk1 blocks the NF-κB signaling pathway and induces neuron autophagy after traumatic brain injury. *Mol. Cell. Biochem.* 472, 105–114. doi: 10.1007/s11010-020-03789-5

Liu, T., Bao, Y. H., Wang, Y., and Jiang, J. Y. (2015). The role of necroptosis in neurosurgical diseases. *Braz. J. Med. Biol. Res.* 48, 292–298. doi: 10.1590/1414-431X20144310

Liu, T., Zhao, D., Cui, H., Chen, L., Bao, Y., Wang, Y., et al. (2016). Therapeutic hypothermia attenuates tissue damage and cytokine expression after traumatic brain injury by inhibiting necroptosis in the rat. *Sci. Rep.* 6:24547. doi: 10.1038/srep24547

Liu, W., Chen, Y., Meng, J., Wu, M., Bi, F., Chang, C., et al. (2018). Ablation of caspase-1 protects against TBI-induced pyroptosis *in vitro* and *in vivo*. *J. Neuroinflammation* 15:48. doi: 10.1186/s12974-018-1083-y

Liu, Z., Chen, Q., Chen, Z., Tian, D., Li, M., Wang, J., et al. (2018). RIP3 deficiency protects against traumatic brain injury (TBI) through suppressing oxidative stress, inflammation and apoptosis: Dependent on AMPK pathway. *Biochem. Biophys. Res. Commun.* 499, 112–119. doi: 10.1016/j.bbrc.2018.02.150

Ma, J., Ni, H., Rui, Q., Liu, H., Jiang, F., Gao, R., et al. (2019). Potential roles of NIX/BNIP3L pathway in rat traumatic brain injury. *Cell Transplant.* 28, 585–595. doi: 10.1177/0963689719840353

Mbye, L. H., Singh, I. N., Sullivan, P. G., Springer, J. E., and Hall, E. D. (2008). Attenuation of acute mitochondrial dysfunction after traumatic brain injury in mice by NIM811, a non-immunosuppressive cyclosporin A analog. *Exp. Neurol.* 209, 243–253. doi: 10.1016/j.expneurol.2007.09.025

Millet, A., Bouzat, P., Trouve-Buisson, T., Batandier, C., Pernet-Gallay, K., Gaide-Chevronnay, L., et al. (2016). Erythropoietin and Its derivates modulate mitochondrial dysfunction after diffuse traumatic brain injury. *J. Neurotrauma* 33, 1625–1633. doi: 10.1089/neu.2015.4160

Mu, J., Weng, J., Yang, C., Guan, T., Deng, L., Li, M., et al. (2021). Necrostatin-1 prevents the proapoptotic protein Bcl-2/adenovirus E1B 19-kDa interacting protein 3 from integration into mitochondria. *J. Neurochem.* 156, 929–942. doi: 10.1111/jnc.14993

Murphy, J. M., Czabotar, P. E., Hildebrand, J. M., Lucet, I. S., Zhang, J., Alvarez-Diaz, S., et al. (2013). The Pseudokinase MLKL mediates necroptosis via a molecular switch mechanism. *Immunity* 39, 443–453. doi: 10.1016/j.immuni.2013.06.018

Ng, S. Y., and Lee, A. Y. W. (2019). Traumatic brain injuries: Pathophysiology and potential therapeutic targets. *Front. Cell. Neurosci.* 13:528. doi: 10.3389/fncel.2019.00528

Ni, H., Rui, Q., Lin, X., Li, D., Liu, H., and Chen, G. (2019). 2-BFI provides neuroprotection against inflammation and necroptosis in a rat model of traumatic brain injury. *Front. Neurosci.* 13:674. doi: 10.3389/fnins.2019.00674

Ni, Y., Gu, W. W., Liu, Z. H., Zhu, Y. M., Rong, J. G., Kent, T. A., et al. (2018). RIP1K Contributes to neuronal and astrocytic cell death in ischemic stroke via activating autophagic-lysosomal pathway. *Neuroscience* 371, 60–74. doi: 10.1016/j.neuroscience.2017.10.038

Oñate, M., Catenaccio, A., Salvadores, N., Saquel, C., Martinez, A., Moreno-Gonzalez, I., et al. (2020). The necroptosis machinery mediates axonal degeneration in a model of Parkinson disease. *Cell Death Differ.* 27, 1169–1185. doi: 10.1038/s41418-019-0408-4

Palzur, E., Edelman, D., Sakas, R., and Soustiel, J. F. (2021). Etifoxine restores mitochondrial oxidative phosphorylation and improves cognitive recovery following traumatic brain injury. *Int. J. Mol. Sci.* 22:12881. doi: 10.3390/ijms222312881

Pang, K., Jiang, R., Zhang, W., Yang, Z., Li, L. L., Shimozawa, M., et al. (2022). An App knock-in rat model for Alzheimer's disease exhibiting Abeta and tau pathologies, neuronal death and cognitive impairments. *Cell Res.* 32, 157–175. doi: 10.1038/s41422-021-00582-x

Poh, L., Fann, D. Y., Wong, P., Lim, H. M., Foo, S. L., Kang, S. W., et al. (2021). AIM2 inflammasome mediates hallmark neuropathological alterations and cognitive impairment in a mouse model of vascular dementia. *Mol. Psychiatry* 26, 4544–4560. doi: 10.1038/s41380-020-00971-5

Ponsford, J., Spitz, G., and Hicks, A. J. (2022). Highlights in traumatic brain injury research in 2021. *Lancet Neurol.* 21, 5–6. doi: 10.1016/S1474-4422(21)00424-5

Qi, L., Cui, X., Dong, W., Barrera, R., Nicastro, J., Coppa, G. F., et al. (2012). Ghrelin attenuates brain injury after traumatic brain injury and uncontrolled hemorrhagic shock in rats. *Mol. Med.* 18, 186–193. doi: 10.2119/molmed.2011.00390

Readnower, R. D., Hubbard, W. B., Kalimon, O. J., Geddes, J. W., and Sullivan, P. G. (2021). Genetic approach to elucidate the role of cyclophilin d in traumatic brain injury pathology. *Cells* 10:199. doi: 10.3390/cells10020199

Readnower, R. D., Pandya, J. D., McEwen, M. L., Pauly, J. R., Springer, J. E., and Sullivan, P. G. (2011). Post-injury administration of the mitochondrial permeability transition pore inhibitor, NIM811, is neuroprotective and improves cognition after traumatic brain injury in rats. *J. Neurotrauma* 28, 1845–1853. doi: 10.1089/neu.2011.1755

Ruan, Z., Lu, Q., Wang, J. E., Zhou, M., Liu, S., Zhang, H., et al. (2021). MIF promotes neurodegeneration and cell death via its nuclease activity following traumatic brain injury. *Cell. Mol. Life Sci.* 79:39. doi: 10.1007/s00018-021-04037-9

Rui, T., Wang, H., Li, Q., Cheng, Y., Gao, Y., Fang, X., et al. (2021). Deletion of ferritin H in neurons counteracts the protective effect of melatonin against traumatic brain injury-induced ferroptosis. *J. Pineal Res.* 70:e12704. doi: 10.1111/jpi.12704

Rui, W., Li, S., Xiao, H., Xiao, M., and Shi, J. (2020). Baicalein Attenuates neuroinflammation by inhibiting NLRP3/caspase-1/GSDMD Pathway in MPTP Induced mice model of Parkinson's Disease. *Int. J. Neuropsychopharmacol.* 23, 762–773. doi: 10.1093/ijnp/pyaa060

Schinzel, A. C., Takeuchi, O., Huang, Z., Fisher, J. K., Zhou, Z., Rubens, J., et al. (2005). Cyclophilin D is a component of mitochondrial permeability transition and mediates neuronal cell death after focal cerebral ischemia. *Proc. Natl. Acad. Sci. U.S.A.* 102, 12005–12010. doi: 10.1073/pnas.0505294102

Sekerdag, E., Solaroglu, I., and Gursoy-Ozdemir, Y. (2018). Cell death mechanisms in stroke and novel molecular and cellular treatment options. *Curr. Neuropharmacol.* 16, 1396–1415. doi: 10.2174/1570159X16666180302115544

Shao, X. F., Li, B., Shen, J., Wang, Q. F., Chen, S. S., Jiang, X. C., et al. (2020). Ghrelin alleviates traumatic brain injury-induced acute lung injury through pyroptosis/NF-kappaB pathway. *Int. Immunopharmacol.* 79:106175. doi: 10.1016/j.intimp.2019.106175

Shi, J., Gao, W., and Shao, F. (2017). Pyroptosis: Gasdermin-mediated programmed necrotic cell death. *Trends Biochem. Sci.* 42, 245–254. doi: 10.1016/j.tibs.2016.10.004

Shi, R. Y., Zhu, S. H., Li, V., Gibson, S. B., Xu, X. S., and Kong, J. M. (2014). BNIP3 interacting with LC3 triggers excessive mitophagy in delayed neuronal death in stroke. *CNS Neurosci. Ther.* 20, 1045–1055. doi: 10.1111/cns.12325

Shi, X., Yang, F., Ge, Z., Tang, Z., Zhang, K., Chen, B., et al. (2022). Iduna contributes to the therapeutic effect of DHA in a cell and mouse model of traumatic brain injury via Wnt/MDM2 pathway. *Folia Neuropathol.* 60:92. doi: 10.5114/fn.2021.112567

Sparvero, L. J., Tian, H., Amoscato, A. A., Sun, W. Y., Anthonymuthu, T. S., Tyurina, Y. Y., et al. (2021). Direct mapping of phospholipid ferroptotic death signals in cells and tissues by gas cluster ion beam secondary ion mass spectrometry (GCIB-SIMS). *Angew. Chem. Int. Ed. Engl.* 60, 11784–11788. doi: 10.1002/anie.202102001

Springer, J., Prajapati, P., and Sullivan, P. (2018). Targeting the mitochondrial permeability transition pore in traumatic central nervous system injury. *Neural Regen. Res.* 13, 1338–1341. doi: 10.4103/1673-5374.235218

Stockwell, B. R., Friedmann, A. J., Bayir, H., Bush, A. I., Conrad, M., Dixon, S. J., et al. (2017). Ferroptosis: A regulated cell death nexus linking metabolism, redox biology, and disease. *Cell* 171, 273–285. doi: 10.1016/j.cell.2017.09.021

Stoica, B. A., Loane, D. J., Zhao, Z., Kabadi, S. V., Hanscom, M., Byrnes, K. R., et al. (2014). PARP-1 inhibition attenuates neuronal loss, microglia activation and neurological deficits after traumatic brain injury. *J. Neurotrauma* 31, 758–772. doi: 10.1089/neu.2013.3194

Sullivan, P. G., Rabchevsky, A. G., Waldmeier, P. C., and Springer, J. E. (2005). Mitochondrial permeability transition in CNS trauma: Cause or effect

of neuronal cell death? *J. Neurosci. Res.* 79, 231–239. doi: 10.1002/jnr.20292

Sullivan, P. G., Thompson, M. B., and Scheff, S. W. (1999). Cyclosporin A attenuates acute mitochondrial dysfunction following traumatic brain injury. *Exp. Neurol.* 160, 226–234. doi: 10.1006/exnr.1999.7197

Sun, J., and Jacobs, K. M. (2016). Knockout of cyclophilin-D provides partial amelioration of intrinsic and synaptic properties altered by mild traumatic brain injury. *Front. Syst. Neurosci.* 10:63. doi: 10.3389/fnsys.2016.00063

Sun, J., Liu, J., Gao, C., Zheng, J., Zhang, J., Ding, Y., et al. (2022). Targeted delivery of PARP inhibitors to neuronal mitochondria via biomimetic engineered nanosystems in a mouse model of traumatic brain injury. *Acta Biomater.* 140, 573–585. doi: 10.1016/j.actbio.2021.12.023

Sun, Z., Nyanzu, M., Yang, S., Zhu, X., Wang, K., Ru, J., et al. (2020). VX765 Attenuates pyroptosis and HMGB1/TLR4/NF-kappaB pathways to improve functional outcomes in TBI mice. *Oxid. Med. Cell. Longev.* 2020:7879629. doi: 10.1155/2020/7879629

Tan, S. W., Zhao, Y., Li, P., Ning, Y. L., Huang, Z. Z., Yang, N., et al. (2021). HMGB1 mediates cognitive impairment caused by the NLRP3 inflammasome in the late stage of traumatic brain injury. *J. Neuroinflammation* 18:241. doi: 10.1186/s12974-021-02274-0

Tang, S., Gao, P., Chen, H., Zhou, X., Ou, Y., and He, Y. (2020). The role of iron, its metabolism and ferroptosis in traumatic brain injury. *Front. Cell. Neurosci.* 14:590789. doi: 10.3389/fncel.2020.590789

Virag, L., and Szabó, C. (2002). The therapeutic potential of poly(ADP-Ribose) polymerase inhibitors. *Pharmacol. Rev.* 54, 375–429. doi: 10.1124/pr.54.3.375

Wang, P., Pan, B., Tian, J., Yang, L., Chen, Z., Yang, L., et al. (2021). Ac-FLTD-CMK inhibits pyroptosis and exerts neuroprotective effect in a mice model of traumatic brain injury. *Neuroreport* 32:188. doi: 10.1097/WNR.0000000000001580

Wang, X., Sekine, Y., Byrne, A. B., Cafferty, W. B., Hammarlund, M., and Strittmatter, S. M. (2016). Inhibition of Poly-ADP-ribosylation fails to increase axonal regeneration or improve functional recovery after adult mammalian CNS injury. *eNeuro* 3:ENEURO.0270–16.2016. doi: 10.1523/ENEURO.0270-16.2016

Wang, Y. Q., Wang, L., Zhang, M. Y., Wang, T., Bao, H. J., Liu, W. L., et al. (2012). Necrostatin-1 suppresses autophagy and apoptosis in mice traumatic brain injury model. *Neurochem. Res.* 37, 1849–1858. doi: 10.1007/s11064-012-0791-4

Wang, Y., Kim, N. S., Haince, J. F., Kang, H. C., David, K. K., Andrabi, S. A., et al. (2011). Poly(ADP-ribose) (PAR) binding to apoptosis-inducing factor is critical for PAR polymerase-1-dependent cell death (parthanatos). *Sci. Signal.* 4:a20. doi: 10.1126/scisignal.2000902

Wehn, A. C., Khalin, I., Duering, M., Hellal, F., Culmsee, C., Vandenabeele, P., et al. (2021). RIPK1 or RIPK3 deletion prevents progressive neuronal cell death and improves memory function after traumatic brain injury. *Acta Neuropathol. Commun.* 9:138. doi: 10.1186/s40478-021-01236-0

Weiland, A., Wang, Y., Wu, W., Lan, X., Han, X., Li, Q., et al. (2019). Ferroptosis and Its role in diverse brain diseases. *Mol. Neurobiol.* 56, 4880–4893. doi: 10.1007/s12035-018-1403-3

Wenzel, S. E., Tyurina, Y. Y., Zhao, J., St, C. C., Dar, H. H., Mao, G., et al. (2017). PEBP1 wardens ferroptosis by enabling lipoxygenase generation of lipid death signals. *Cell* 171, 628–641. doi: 10.1016/j.cell.2017.09.044

Wnuk, A., and Kajta, M. (2017). Steroid and xenobiotic receptor signalling in apoptosis and autophagy of the nervous system. *Int. J. Mol. Sci.* 18:2394. doi: 10.3390/ijms18112394

Won, S. J., Choi, B. Y., Yoo, B. H., Sohn, M., Ying, W., Swanson, R. A., et al. (2012). Prevention of traumatic brain injury-induced neuron death by intranasal delivery of nicotinamide adenine dinucleotide. *J. Neurotrauma* 29, 1401–1409. doi: 10.1089/neu.2011.2228

Wu, C., Du, M., Yu, R., Cheng, Y., Wu, B., Fu, J., et al. (2022). A novel mechanism linking ferroptosis and endoplasmic reticulum stress via the circPtpn14/miR-351-5p/5-LOX signaling in melatonin-mediated treatment of traumatic brain injury. *Free Radic. Biol. Med.* 178, 271–294. doi: 10.1016/j.freeradbiomed.2021.12.007

Wu, F., Xu, K., Xu, K., Teng, C., Zhang, M., Xia, L., et al. (2020). Dl-3n-butylphthalide improves traumatic brain injury recovery via inhibiting autophagy-induced blood-brain barrier disruption and cell apoptosis. *J. Cell. Mol. Med.* 24, 1220–1232. doi: 10.1111/jcmm.14691

Wu, L., Chung, J. Y., Cao, T., Jin, G., Edmiston, W. R., Hickman, S., et al. (2021). Genetic inhibition of RIPK3 ameliorates functional outcome in controlled cortical impact independent of necroptosis. *Cell Death Dis.* 12:1064. doi: 10.1038/s41419-021-04333-z

Wu, L., Kalish, B. T., Finander, B., Cao, T., Jin, G., Yahya, T., et al. (2022). Repetitive mild closed head injury in adolescent mice is associated with impaired proteostasis, neuroinflammation, and tauopathy. *J. Neurosci.* 42, 2418–2432. doi: 10.1523/JNEUROSCI.0682-21.2021

Xiao, X., Jiang, Y., Liang, W., Wang, Y., Cao, S., Yan, H., et al. (2019). miR-212-5p attenuates ferroptotic neuronal death after traumatic brain injury by targeting Ptgs2. *Mol. Brain* 12:78. doi: 10.1186/s13041-019-0501-0

Xie, B. S., Wang, Y. Q., Lin, Y., Mao, Q., Feng, J. F., Gao, G. Y., et al. (2019). Inhibition of ferroptosis attenuates tissue damage and improves long-term outcomes after traumatic brain injury in mice. *CNS Neurosci. Ther.* 25, 465–475. doi: 10.1111/cns.13069

Xu, H., Li, X., Wu, X., Yang, Y., Dai, S., Lei, T., et al. (2019). Iduna protects HT22cells by inhibiting parthanatos: The role of the p53-MDM2 pathway. *Exp. Cell. Res.* 384:111547. doi: 10.1016/j.yexcr.2019.111547

Xu, Z., Lv, X. A., Dai, Q., Lu, M., and Jin, Z. (2018). Exogenous BDNF Increases Mitochondrial pCREB and alleviates neuronal metabolic defects following mechanical injury in a MPTP-dependent way. *Mol. Neurobiol.* 55, 3499–3512. doi: 10.1007/s12035-017-0576-5

Yamaguchi, O., Watanabe, T., Kubo, T., Yamagata, H., Shimizu, S., Tsujimoto, Y., et al. (2005). Cyclophilin D-dependent mitochondrial permeability transition regulates some necrotic but not apoptotic cell death. *Nature* 434, 652–658. doi: 10.1038/nature03317

Yang, H., Gu, Z., Li, L., Maegele, M., Zhou, B., Li, F., et al. (2017). SIRT1 plays a neuroprotective role in traumatic brain injury in rats via inhibiting the p38 MAPK pathway. *Acta Pharmacol. Sin.* 38, 168–181. doi: 10.1038/aps.2016.130

Yao, M., Liu, T., Zhang, L., Wang, M., Yang, Y., and Gao, J. (2021). Role of ferroptosis in neurological diseases. *Neurosci. Lett.* 747:135614. doi: 10.1016/j.neulet.2020.135614

You, Z., Savitz, S. I., Yang, J., Degterev, A., Yuan, J., Cuny, G. D., et al. (2008). Necrostatin-1 reduces histopathology and improves functional outcome after controlled cortical impact in mice. *J. Cereb. Blood Flow Metab.* 28, 1564–1573. doi: 10.1038/jcbfm.2008.44

Yu, H., Guo, P., Xie, X., Wang, Y., and Chen, G. (2017). Ferroptosis, a new form of cell death, and its relationships with tumourous diseases. *J. Cell. Mol. Med.* 21, 648–657. doi: 10.1111/jcmm.13008

Yu, S. W., Andrabi, S. A., Wang, H., Kim, N. S., Poirier, G. G., Dawson, T. M., et al. (2006). Apoptosis-inducing factor mediates poly(ADP-ribose) (PAR) polymer-induced cell death. *Proc. Natl. Acad. Sci. U.S.A.* 103, 18314–18319. doi: 10.1073/pnas.0606528103

Yuan, D., Guan, S., Wang, Z., Ni, H., Ding, D., Xu, W., et al. (2021). HIF-1alpha aggravated traumatic brain injury by NLRP3 inflammasome-mediated pyroptosis and activation of microglia. *J. Chem. Neuroanat.* 116:101994. doi: 10.1016/j.jchemneu.2021.101994

Yuan, J., Amin, P., and Ofengeim, D. (2019). Necroptosis and RIPK1-mediated neuroinflammation in CNS diseases. *Nat. Rev. Neurosci.* 20, 19–33. doi: 10.1038/s41583-018-0093-1

Zhang, H. B., Cheng, S. X., Tu, Y., Zhang, S., Hou, S. K., and Yang, Z. (2017). Protective effect of mild-induced hypothermia against moderate traumatic brain injury in rats involved in necroptotic and apoptotic pathways. *Brain Inj.* 31, 406–415. doi: 10.1080/02699052.2016.1225984

Zhang, J. Y., Lee, J. H., Gu, X., Wei, Z. Z., Harris, M. J., Yu, S. P., et al. (2018). Intranasally Delivered Wnt3a improves functional recovery after traumatic brain injury by modulating autophagic, apoptotic, and regenerative pathways in the mouse brain. *J. Neurotrauma* 35, 802–813. doi: 10.1089/neu.2016.4871

Zhang, L. M., Zhang, D. X., Zheng, W. C., Hu, J. S., Fu, L., Li, Y., et al. (2021). CORM-3 exerts a neuroprotective effect in a rodent model of traumatic brain injury via the bidirectional gut-brain interactions. *Exp. Neurol.* 341:113683. doi: 10.1016/j.expneurol.2021.113683

Zhao, P., Li, C., Chen, B., Sun, G., Chao, H., Tu, Y., et al. (2020). Up-regulation of CHMP4B alleviates microglial necroptosis induced by traumatic brain injury. *J. Cell. Mol. Med.* 24, 8466–8479. doi: 10.1111/jcmm.15406

Zheng, B., Zhang, S., Ying, Y., Guo, X., Li, H., Xu, L., et al. (2018). Administration of Dexmedetomidine inhibited NLRP3 inflammasome and microglial cell activities in hippocampus of traumatic brain injury rats. *Biosci Rep.* 38:BSR20180892. doi: 10.1042/BSR20180892

Zhou, C., Zheng, J., Fan, Y., and Wu, J. (2022). TI: NLRP3 inflammasome-dependent pyroptosis in CNS trauma: A potential therapeutic target. *Front. Cell. Dev. Biol.* 10:821225. doi: 10.3389/fcell.2022.821225

Zou, P., Liu, X., Li, G., and Wang, Y. (2018). Resveratrol pretreatment attenuates traumatic brain injury in rats by suppressing NLRP3 inflammasome activation via SIRT1. *Mol. Med. Rep.* 17, 3212–3217. doi: 10.3892/mmr.2017.8241

frontiers | Frontiers in Molecular Neuroscience

TYPE Original Research
PUBLISHED 25 October 2022
DOI 10.3389/fnmol.2022.986710

OPEN ACCESS

EDITED BY
Sara Anna Bonini,
University of Brescia, Italy

REVIEWED BY
Mei Li,
Children's Hospital of Soochow University, China
Yu-Feng Wang,
Harbin Medical University, China

*CORRESPONDENCE
Jia Guo
ery_guojer@lzu.edu.cn

SPECIALTY SECTION
This article was submitted to Brain Disease Mechanisms, a section of the journal Frontiers in Molecular Neuroscience

RECEIVED 05 July 2022
ACCEPTED 20 September 2022
PUBLISHED 25 October 2022

CITATION
Guo J, Zhang L, Bu Y, Li W, Hu J and Li J (2022) Ras-related protein Rab-20 inhibition alleviates cerebral ischemia/reperfusion injury by inhibiting mitochondrial fission and dysfunction.
Front. Mol. Neurosci. 15:986710.
doi: 10.3389/fnmol.2022.986710

Ras-related protein Rab-20 inhibition alleviates cerebral ischemia/reperfusion injury by inhibiting mitochondrial fission and dysfunction

Jia Guo*, Lu Zhang, Yujie Bu, Wenjuan Li, Jianping Hu and Jianxiong Li

Department of Neurology, Lanzhou University Second Hospital, Lanzhou, Gansu, China

Ras-related protein Rab-20 (Rab20) is induced in hypoxia and contributes to hypoxia-induced apoptosis. However, the role and mechanism of Rab20 in cerebral ischemia/reperfusion (I/R) injury need to be elucidated. We established a cerebral I/R injury model in the mice and an oxygen-glucose deprivation/reoxygenation (OGD/R) model in HT22 cells to determine the effects of Rab20 in cerebral I/R injury. Rab20 expression was upregulated in mice after I/R and in HT22 cells after OGD/R. Upregulated Rab20 was mainly located in neurons. Rab20 inhibition significantly alleviated brain infarct volume, neurological deficits, and neuronal apoptosis in mice after I/R. Moreover, Rab20 knockdown significantly ameliorated the OGD/R-induced inhibition of cell viability and apoptotic cell death in HT22 cells. Rab20 knockdown significantly alleviated OGD/R-induced mitochondrial fission by repressing mitochondrial dynamin-related protein 1 (Drp-1) recruitment and increasing Drp-1 (Ser637) phosphorylation and ameliorated mitochondrial dysfunction by reducing the mitochondrial reactive oxygen species (ROS) and cellular calcium accumulation and increasing the mitochondrial membrane potential. In addition, Rab20 knockdown significantly alleviated cytochrome c release from the mitochondria into the cytosol in HT22 cells after OGD/R. Rab20 contributes to cerebral I/R injury by regulating mitochondria-associated apoptosis pathways. Targeting Rab20 may be an attractive strategy for the treatment of cerebral I/R injury.

KEYWORDS

Rab20, cerebral ischemia/reperfusion, mitochondria, mitochondrial fission, apoptosis

Introduction

Stroke, a cerebrovascular accident, is a leading cause of mortality and long-term disability in adults (Campbell et al., 2019). Ischemic stroke is the major type that is caused by the sudden blockage of blood flow, leading to brain tissue injury due to reduced blood and oxygen supply (Gąsecki et al., 2021). At present, the primary therapeutic approach for ischemic stroke treatment is immediate recanalization of the occluded artery and reperfusion of the brain tissue. Intravenous thrombolysis is the only FDA-approved drug for patients with cerebral ischemia. Although its use is limited by a narrow therapeutic window (within 4.5 h of symptom onset) and hemorrhagic complication, this treatment is the most effective for patients with cerebral ischemia (Prabhakaran et al., 2015; Liu et al., 2018). However, reperfusion causes accelerated neuronal damage due to a significant increase in oxidative stress and inflammation (Lin et al., 2016). Reperfusion injury has become a critical challenge in stroke treatment. Thus, it is importance to understand the mechanisms of ischemia/reperfusion (I/R) injury in the brain to develop effective therapeutics.

After ischemic stroke, the depletion of blood and oxygen supply causes the release of glutamate into the extracellular space, thereby producing an influx of calcium into the cell, which can rapidly induce neuronal death in the ischemic core, and the damage is irreversible (Hermann et al., 2001; Zhou et al., 2018). However, I/R-induced neuronal loss in the transition or penumbra zone is not irreversible (Zhou et al., 2018). Although I/R-induced neuronal death in the penumbra zone is not usually lethal, it contributes substantially to the loss of neurologic function and cognitive deficits (Hermann et al., 2001). Thus, reducing neuronal apoptosis in the ischemic penumbra is a potential treatment method for I/R injury.

Ras-related protein Rab-20 (Rab20) belongs to the Rab subfamily of small GTPases. Rab20 was first reported to be located in apical dense tubules which contribute to apical endocytosis/recycling (Lutcke et al., 1994). Rab20 plays an important role in immune regulation by controlling endosome maturation in macrophages (Egami and Araki, 2012; Zhao et al., 2020). In retinal endothelial cells and retinal Müller cells, high glucose induced Rab20 expression, and upregulated Rab20 contributed to high glucose-induced cell apoptosis (Kim et al., 2020). In a hypoxic microenvironment, Rab20 is directly induced by hypoxia-inducible transcription factor 1 (HIF-1) and is involved in hypoxia induced apoptosis (Hackenbeck et al., 2011). Moreover, Rab20 expression was substantially upregulated in an experimental model of brain inflammation in mice (Liang et al., 2012). Hypoxia and inflammation are important causes of I/R injury. Therefore, these findings suggested that Rab20 may play an important role in I/R injury.

In this study, we determined the role and mechanisms of Rab20 in I/R injury. Rab20 expression was significantly elevated in mice after I/R and in HT22 cells after oxygen-glucose deprivation/reoxygenation (OGD/R). Rab20 knockdown significantly alleviated brain infarct volume, neurological deficits, and neuronal apoptosis by inhibiting mitochondria-associated apoptosis pathways. Rab20 may be a novel target gene for the treatment of the cerebral I/R injury.

Materials and methods

Experimental animals

A total of 120 male C57BL/6J mice, 6–8 weeks old, were purchased from the Lanzhou University Second Hospital. Mice were housed in a specific pathogen-free (SPF) animal facility with a 12 h light/12 h dark cycle and given free access to water or food. Animals for each group were randomized. All animal procedures were approved by the Ethics Committee of Lanzhou University Second Hospital (D2020-046). Animal experiments were conducted in accordance with the guidelines of the Institutional Animal Care and Use Committee of the Institute of Nutrition and Health.

Construction of middle cerebral artery occlusion and reperfusion models and treatment

Ischemia/reperfusion surgery were performed on male C57BL/6J mice using the intraluminal filament method as described previously (Liu et al., 2003, 2019). Briefly, mice were anesthetized with ketamine (12 mg/kg) and xylazine (10 mg/kg) by intramuscular injection. The neck was depilated, and the right common carotid bifurcation was exposed. To induce stroke, a silicone-coated 8-0 filament was inserted to the internal carotid artery to occlude the origin of the right middle cerebral artery for 1 h. The regional cerebral blood flow during surgery was measured with a laser Doppler flowmetry (PeriFlux System 5000; Perimed, Stockholm, Sweden). A reduction of 80% in the cerebral blood flow during surgery was considered successful. After 1 h of occlusion, the filament was removed to recover the cerebral blood flow. In the sham group, right carotid arteries of mice were surgically exposed and the suture was not inserted.

To knockdown the expression of Rab20, adeno-associated virus (AAV) vectors were constructed. AAV9-Syn-GFP-U6-shRab20 (shRab20) and AAV9-Syn-GFP-U6-negative control (shNC) were constructed by Sunbio Medical Biotechnology (Shanghai, China). The shRab20 and shNC sequences inserted in the AAV9 vector were shown in **Table 1**. After concentrating, the shRab20 and shNC AAV particles were diluted in PBS to 1×10^{11} genome copies/100 μl. AAV particles containing either shRab20 or shNC were stereotactically injected into the right lateral ventricle (bregma: −2.2 mm, dorsoventral: 3 mm, lateral: 1 mm) for 4 weeks prior to middle cerebral artery occlusion

TABLE 1 shRNA, siRNA, and primers.

Name	Sequence
shRab20	5′-CCGGGAAGATCCTGAAGTACAAGATCTCGAGATCTTGTACTTCAGGATCTTCTTTTTT-3′
shNC	5′-CCGGTTCTCCGAACGTGTCACGTCTCGAGACGTGACACGTTCGGAGAATTTTTT-3′
siRab20	5′-GAAGAUCCUGAAGUACAAGAUTT-3′
siNC	5′-UUCUCCGAACGUGUCACGUTT-3′.
Rab20 Fwd	5′-TCTCCACAGGTACCAAG-3′
Rab20 Rev	5′-CCACAGTCAACAAGTT-3′
β-Actin Fwd	5′-GTGACGTTGACATCCGTAAAGA-3′
β-Actin Rev	5′-GCCGGACTCATCGTACTCC-3′

(MCAO) operation (Zhao et al., 2013; Choi et al., 2015). A total of 3×10^9 genome copies of shRab20 or shNC AAV virus in 3 μl were injected into each animal at a rate of 200 nl/min (Jin et al., 2019).

Neurological score

Neurobehavioral score was counted at 72 h after I/R, as described previously (Jin et al., 2015). In a typical procedure, neurobehavioral evaluation was determined according to the following scoring system: 0, no deficit; 1, forelimb flexion; 2, the same as 1, plus decreased resistance to lateral push; 3, unidirectional circling; 4, longitudinal spinning or seizure activity; and 5, no movement.

Brain infarction measurement

Infarct volume was determined by 2,3,5-triphenyltetrazolium chloride (TTC) staining at 72 h after I/R. Mice were anesthetized. The brain was removed from each animal and cut into 2 mm-thick slices. The slices were incubated with 2% TTC solution (Coolaber, Beijing, China) at 37°C for 30 min. Finally, the slices were fixed in 4% paraformaldehyde overnight and the infarction volume was quantified using ImageJ software (National Institutes of Health, Bethesda, MD, USA).

Immunofluorescence

Mice were anesthetized at 72 h after I/R and perfused with PBS and 4% paraformaldehyde. The brain was removed from each animal and fixed with 4% paraformaldehyde overnight, transferred to 20 and 30% sucrose, and cut into 5 μm-thick sections on a freezing microtome. After washing and blocking, the sections were incubated overnight at 4°C with the following primary antibodies: anti-Rab20 (1:200; 11616-1-AP, Proteintech Group, Inc., Wuhan, China), anti-NeuN (1:100; 66836-1-Ig, Proteintech Group, Inc.), anti-IBA1 (1:500; 011-27991, Fujifilm Wako, Japan), and anti-GFAP (1:200; ab279290, Abcam, Cambridge, MA, USA). After washing, the sections were incubated with donkey anti-rabbit Alexa fluor 488 secondary antibody (1:500; ab150073, Abcam), donkey anti-rabbit Alexa fluor 555 secondary antibody (1:500; A31572, Thermo Fisher Scientific, MA, USA), donkey anti-mouse Alexa fluor plus 555 secondary antibody (1:500; A32773, Thermo Fisher Scientific, MA, USA), and donkey anti-goat Alexa fluor plus 555 secondary antibody (1:500; A32816, Thermo Fisher Scientific) for 2 h at room temperature in the dark. Finally, the nuclei were stained by 4′,6-diamidino-2-phenylindole (DAPI) for 15 min.

Terminal deoxynucleotidyl transferase-mediated dUTP nick end labeling staining

For terminal deoxynucleotidyl transferase-mediated dUTP nick end labeling (TUNEL) staining in brain tissues, the sections were stained with TUNEL solution (Roche Diagnostics, Indianapolis, IN, USA) for 1 h at 37°C. After washing, the neurons were stained with anti-NeuN (1:100; 66836-1-Ig, Proteintech Group, Inc.) for 1 h at 37°C. The sections were incubated with donkey anti-mouse IgG (1:100; 715-685-150, Jackson ImmunoResearch Inc., West Grove, PA, USA). The sections were photographed using a microscope with a digital camera (Olympus, Tokyo, Japan). Both TUNEL (red) and NeuN (blue) positive cells were counted as the apoptotic neurons. Five different fields were taken from the ischemic penumbra of each section using 40 × objective lens (Zhang et al., 2013; Liu et al., 2020). Eight consecutive sections per mouse and six mice per group were analyzed. The percentages of TUNEL-positive neurons relative to neurons were counted by an investigator who was blinded to the experimental groups.

HT22 cells after treatment were fixed in 4% paraformaldehyde for 30 min at room temperature. After washing three times with PBS, the cells were incubated in 0.3% Triton X-100 for 5 min. Then, the cells were incubated with TUNEL solution (Roche Diagnostics, Indianapolis, IN, USA) for 1 h at 37°C and DAPI was used to stain the cell nuclei. TUNEL-positive cells were observed under a light microscope (Olympus, Tokyo, Japan). Both TUNEL (red)

and DAPI (blue) positive cells were counted as the apoptotic cells. Average number of three images under a fluorescence microscope at 200× magnification from each treatment group was presented as the final results, and each group was repeated three times independently.

Oxygen-glucose deprivation/reoxygenation model

HT22 is an immortalized mouse hippocampal neuron cell line and was purchased from Procell Life Science & Technology Co., Ltd. (Wuhan, China). Cells were cultured in DMEM (Gibco, Carlsbad, CA, USA) containing 10% FBS (Gibco, Carlsbad, CA, USA) at 37°C. HT22 cells were cultured in glucose-free DMEM solution supplemented with 100 U/ml penicillin and 100 mg/ml streptomycin and placed into a hypoxic chamber (Thermo Fisher Scientific Inc.) with 1% O_2, 5% CO_2, and 94% N_2 for 0, 1, 2, 4 or 8 h to mimic OGD (Zhang et al., 2021). After OGD, cells were given normal DMEM with 10% FBS for 24 h.

Cell transfection

Ras-related protein Rab-20 siRNA (siRab20) and scramble negative control siRNA (siNC) were synthesized by GenePharma (Shanghai, China). The siRab20 and siNC sequences were shown in **Table 1**. HT22 cells were transfected using Lipofectamine® 2000 Reagent (Invitrogen, Carlsbad, CA, USA) according to the manufacturer's instructions.

Cell viability assay

Cell Counting Kit-8 (CCK-8) assay was used to analyze the cell viability of HT22 cells according to the manufacturer's instructions. HT22 cells were cultured on 96-well plates at a density of 1×10^4 cells/well for 24 h and treated with OGD/R. CCK-8 solution (Beyotime, Shanghai, China) at 10 μl was added to each well. Cells were then incubated for 1 h at 37°C. The optical density (OD) value of each well was measured at 450 nm using an automatic microplate reader (Bio-Tek M200, Tecan, Austria).

Real-time quantitative polymerase chain reaction

Total RNA was isolated from brain tissues and HT22 cells using TRIzol reagent (Invitrogen) according to the manufacturer's protocol. The quantity and integrity of total RNA were analyzed by nanodrop spectrophotometer and gel electrophoresis. Total RNA was reverse transcribed into cDNA by M-MLV RTase (Promega, Madison, WI, USA). The Rab20 mRNA expression was determined using SYBR Master Mixture (TAKARA, Dalian, China). The $2^{-\Delta\Delta Ct}$ analysis method with normalization to β-actin expression was used to calculate the relative expression of Rab20. Primers used in this study were shown in **Table 1**.

Western blot

Brain tissues and HT22 cells were lysed using RIPA lysis buffer (Beyotime) containing proteinase inhibitor to obtain the whole cell proteins. For the analysis of mitochondrial proteins from cells, a Cell Mitochondria Isolation Kit (Beyotime) was used to isolate mitochondria according to the manufacturer's instruction. Mitochondria were lysed with a cold mitochondrial protein extraction kit (KeyGEN Biotech, Nanjing, China) to obtain mitochondrial proteins. The concentrations of the total proteins were measured by a BCA protein assay kit (Beyotime). Protein samples were denatured and separated by 10% SDS-PAGE. After SDS-PAGE, proteins were transferred to PVDF membrane. The PVDF membranes were then blocked with PBS containing 7.5% non-fat milk and incubated overnight with the primary antibodies at 4°C as follows: anti-Rab20 (1:1,000; 11616-1-AP, Proteintech Group, Inc.), anti-β-actin (1:2,000; 20536-1-AP, Proteintech Group, Inc.), anti-Bcl-2 (1:2000; 26593-1-AP, Proteintech Group, Inc.), anti-Bax (1:2,000; 60267-1-Ig, Proteintech Group, Inc.), anti-COX-4 (1:5,000; 11242-1-AP, Proteintech Group, Inc.), anti-Drp1 (1:2,000; 12957-1-AP, Proteintech Group, Inc.), anti-p-Drp1 (ser637; 1:1,000; ab193216, Abcam), and anti-cytochrome c (Cyto c; 1:4,000; 10993-1-AP, Proteintech Group, Inc.). After washing, membranes were incubated with HRP-conjugated anti-rabbit or anti-mouse secondary antibodies for 1 h. Immunoreactivity was detected using enhanced chemiluminescence reagents (Pierce Biotech, IL, USA).

Mitochondrial fission assay

For mitochondrial fission assay, HT22 cells were cultured in confocal dishes. After treatment, cells were washed and incubated with 200 nM MitoTracker® Deep Red FM (Yeasen, Shanghai, China) for 30 min at 37°C. Images were obtained by a confocal microscope (LSM 750, Zeiss, Gottingen, Germany).

Mitochondrial membrane potential (Δψm) assay

For mitochondrial membrane potential (Δψm) assay, HT22 cells were grown on glass-bottom dishes. After treatment, cells

were washed and incubated with tetramethylrhodamine ethyl ester perchlorate (TMRE, Beyotime) for 30 min at 37°C. Images were obtained by a confocal microscope (LSM 750, Zeiss).

Mitochondrial reactive oxygen species production

For mitochondrial reactive oxygen species (ROS) assay, HT22 cells were grown on glass-bottom dishes. After treatment, cells were washed and incubated with 100 nM MitoTracker® Green FM (Yeasen) and 5 μM MitoSOX Red Mitochondrial Superoxide Indicator (Yeasen) for 10 min at 37°C, as previously described (Wu et al., 2017).

Intracellular calcium assay

For intracellular calcium assay, HT22 cells were grown on glass-bottom dishes. After treatment, cells were washed and loaded with 2.5 μM Fluo-3AM (Beyotime) in the dark for 30 min. After washing, a confocal microscope (LSM 750, Zeiss) was used to obtain images, and the fluorescent intensity was analyzed using ImageJ software (National Institutes of Health, Bethesda, MD, USA) (Liao et al., 2018).

Statistical analysis

Three or more independent experiments were performed for all experiments. Data analyses were blinded by using different investigators. All the data are presented as mean ± SD. SPSS 19.0 software (IBM Corp., Chicago, IL, USA) was used for data analysis. The comparisons between groups were analyzed using Student's *t*-test or one-way ANOVA. $P < 0.05$ was considered to be statistically significant. GraphPad Prism 5 software (GraphPad Software Inc., San Diego, CA, USA) was used for statistical graphing.

Results

Ras-related protein Rab-20 expression is significantly increased in mice after ischemia/reperfusion

Ras-related protein Rab-20 expression levels were determined at 12 h, 1 day, 3 days, 5 days, and 7 days in mice after I/R using real-time quantitative polymerase chain reaction (RT-qPCR) and Western blot. As shown in **Figures 1A,B**, **Supplementary Table 1**, and **Supplementary Data Sheet 1**, Rab20 mRNA and protein levels were significantly elevated at 12 h, peaked at 3 days, and decreased at 5 days after I/R compared with the sham group. Double-label immunofluorescence staining was performed to analyze the cellular localization of Rab20 in the penumbral area of cortex at 3 days after I/R. The Rab20 was significantly increased in neurons. Rab20 was mainly expressed in neurons (NeuN) in mice after I/R and not in astrocytes (GFAP) and microglia (IBA1) (**Figure 1C**).

Ras-related protein Rab-20 knockdown ameliorated the functional outcomes after cerebral ischemia/reperfusion

To determine the role of Rab20 during cerebral I/R injury, we administrated shRab20 AAV particles into the right lateral ventricle for 4 weeks prior to MCAO operation (**Figure 2A**). As shown in **Figure 2A**, a robust GFP signal was observed at 4 weeks after AAV infection. After I/R for 3 days, shRab20 significantly reduced the expression of Rab20 in the peri-infarct region of the cortex and hippocampus compared with the shNC group (**Figures 2B,C**). Data from the Western blot assay demonstrated that Rab20 protein levels in the peri-infarct region of the cortex and hippocampus at 3 days after I/R were significantly increased compared with the sham group, whereas Rab20 protein levels were significantly inhibited in the I/R + shRab20 group compared with those in the I/R + shNC group (**Figure 2D**). To determine the effect of Rab20 inhibition on cerebral infarction, a TTC analysis of brain sections was performed. As shown in **Figure 2E**, mice at 3 days after I/R exhibited significantly increased infarct volume, whereas the infarct volume in the I/R + shRab20 group was significantly lower than that in the I/R + shNC group. We counted the neurological deficit score to determine the effect of Rab20 on neurological function after I/R. As shown in **Figure 2F**, mice at 3 days after I/R exhibited significantly worse neurological deficit score, whereas Rab20 knockdown significantly ameliorated the I/R-induced neurobehavioral deficits.

Ras-related protein Rab-20 knockdown attenuated neuronal apoptotic death after cerebral ischemia/reperfusion

To determine the effect of Rab20 on cerebral I/R-induced neuronal apoptotic death, TUNEL assay was performed. Results from **Figure 3A** showed that TUNEL-positive neurons of peri-infarct region in cortex and hippocampus at 3 days after cerebral I/R significantly increased compared with the sham group, whereas Rab20 knockdown significantly reduced the percentage of TUNEL-positive neurons induced by cerebral I/R. The expression levels of the apoptotic molecular markers Bcl-2

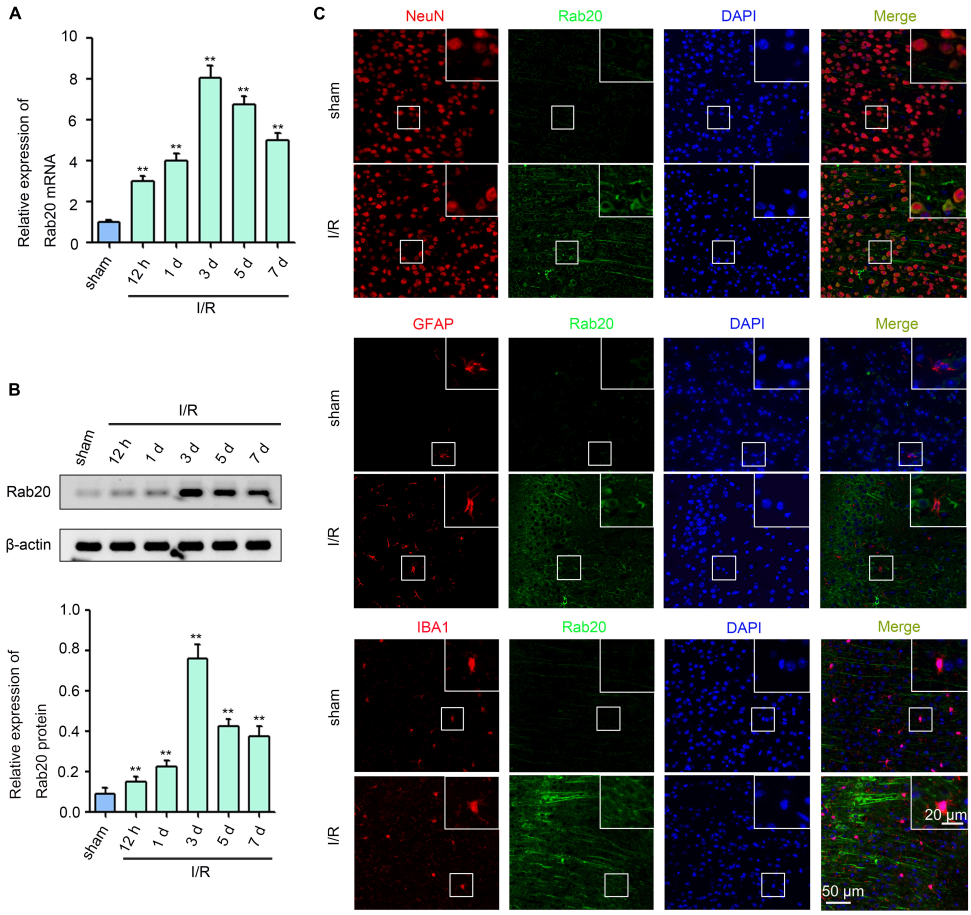

FIGURE 1
Ras-related protein Rab-20 expression was significantly increased in mice after I/R. **(A)** Rab20 mRNA levels were determined by RT-qPCR after I/R (n = 6). **(B)** Representative Western blot images and quantitative analyses of Rab20 protein in mouse brain after I/R (n = 6). **(C)** Double immunofluorescence staining for Rab20 (green) in neuron (NeuN, red), astrocytes (GFAP, red), and microglia (IBA1, red) in the penumbra after I/R. Scale bar, 20 and 50 μm. $^{**}P < 0.01$ vs. the sham group.

and Bax were determined by Western blot at 3 days after cerebral I/R. The expression of Bcl-2 protein was significantly decreased and the expression of Bax protein was significantly increased in the peri-infarct region of cortex and hippocampus at 3 days after cerebral I/R (Figure 3B). However, Rab20 knockdown significantly reversed the decrease in Bcl-2 protein levels and the increase in Bax protein levels induced by cerebral I/R (Figure 3B).

Ras-related protein Rab-20 knockdown attenuated oxygen-glucose deprivation/reoxygenation -induced neuronal injury in HT22 cells

To further confirm the effect of Rab20 on neuronal injury after cerebral I/R, we established an OGD/R model *in vitro*. As shown in Figure 4A, HT22 cells were exposed to OGD for 0, 1, 2, 4, or 8 h, followed by reperfusion for 24 h. Cell viability was decreased with increasing OGD treatment time (Figure 4A). The cell viability of HT22 cells after OGD for 4 h was 48.0%, whereas the cell viability of HT22 cells after OGD for 2 h was 33.3%. Therefore, 4 h was selected as the optimum OGD treatment time. Western blot assay was used to determine the effect of OGD/R on Rab20 mRNA and protein levels in HT22 cells. The results showed that Rab20 mRNA and protein levels were significantly increased in the OGD/R group compared with the normal group (Figures 4B,C). To determine the role of Rab20 in neuronal injury after OGD/R, Rab20 expression was inhibited by Rab20 siRNA (Figure 4D). In addition, we found that Rab20 siRNA significantly reversed the decrease in cell viability induced by OGD/R (Figure 4E). OGD/R significantly increased apoptosis in HT22 cells, whereas Rab20 knockdown significantly inhibited OGD/R-induced apoptosis (Figure 4F). Correspondingly, the

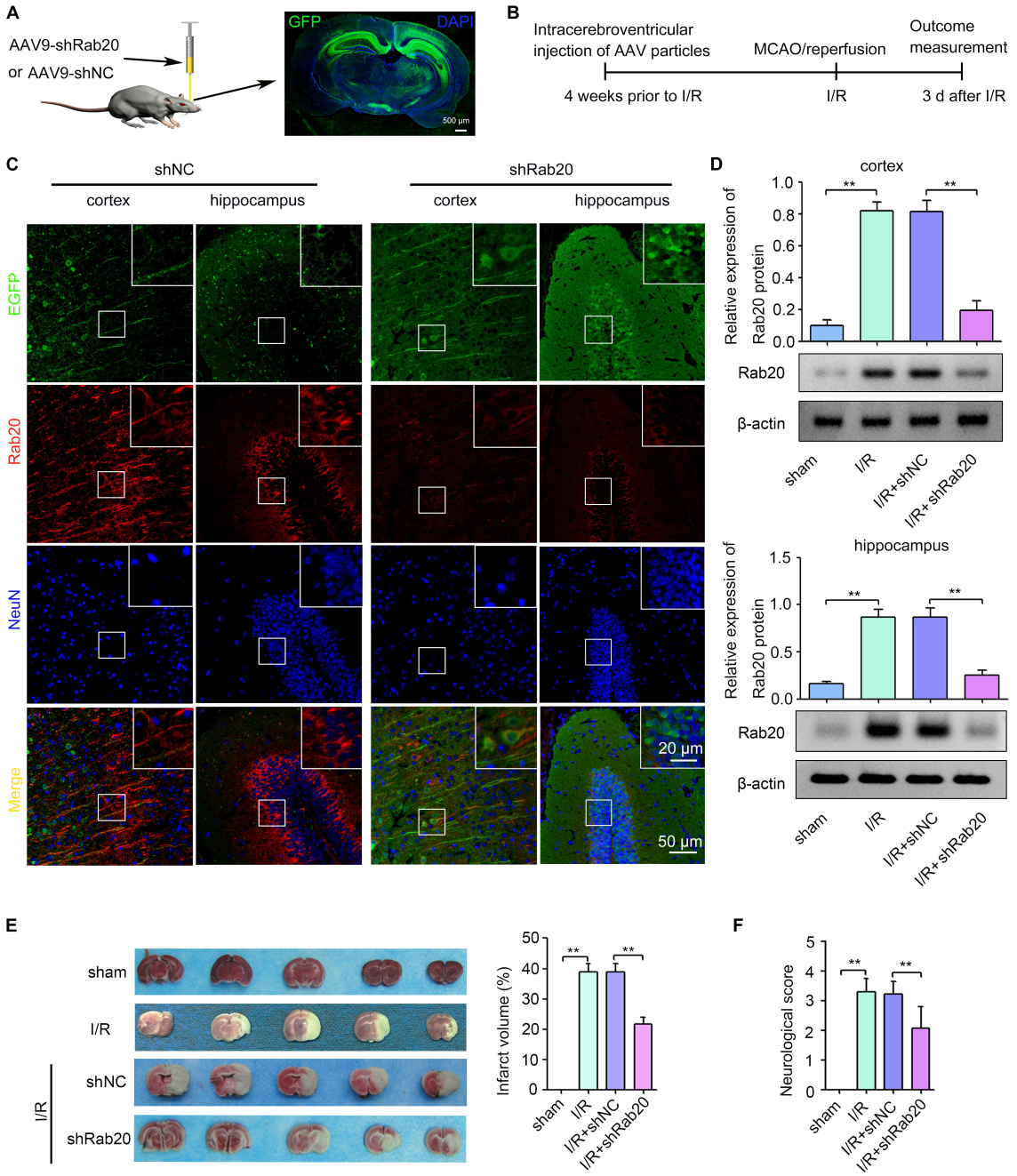

FIGURE 2
Ras-related protein Rab-20 knockdown significantly reduced the cerebral infarction and ameliorated the neurological outcome after cerebral I/R. **(A)** The shRab20 and shNC AAV particles were stereotactically injected into the right lateral ventricle for 4 weeks prior to MCAO operation. Scale bar, 500 μm. **(B)** Diagram of the experimental procedure. **(C)** The silencing efficiency of the shRab20 AAV particles in the penumbra of the cortex and hippocampus was determined by double immunofluorescence staining for Rab20 (red) in neuron (NeuN, blue) at 3 days after I/R. Scale bar, 20 and 50 μm. **(D)** Western blot assay was used to confirm the silencing efficiency of the shRab20 AAV particles in the penumbra of the cortex and hippocampus at 3 days after I/R (n = 6). **(E)** Representative photographs of coronal brain sections stained by TTC showing decreased infarct volume in shRab20-treated mice as compared to the shNC-treated mice at 3 days after I/R (n = 6). **(F)** Neurological scores were used to evaluate the neurological function at 3 days after I/R (n = 18). $^{**}P < 0.01$.

expression of Bcl-2 protein was significantly decreased, and the expression of Bax protein was significantly increased in HT22 cells after OGD/R (Figure 4G). However, Rab20 knockdown significantly reversed the decrease in Bcl-2 protein levels and the increase in Bax protein levels induced by OGD/R (Figure 4G).

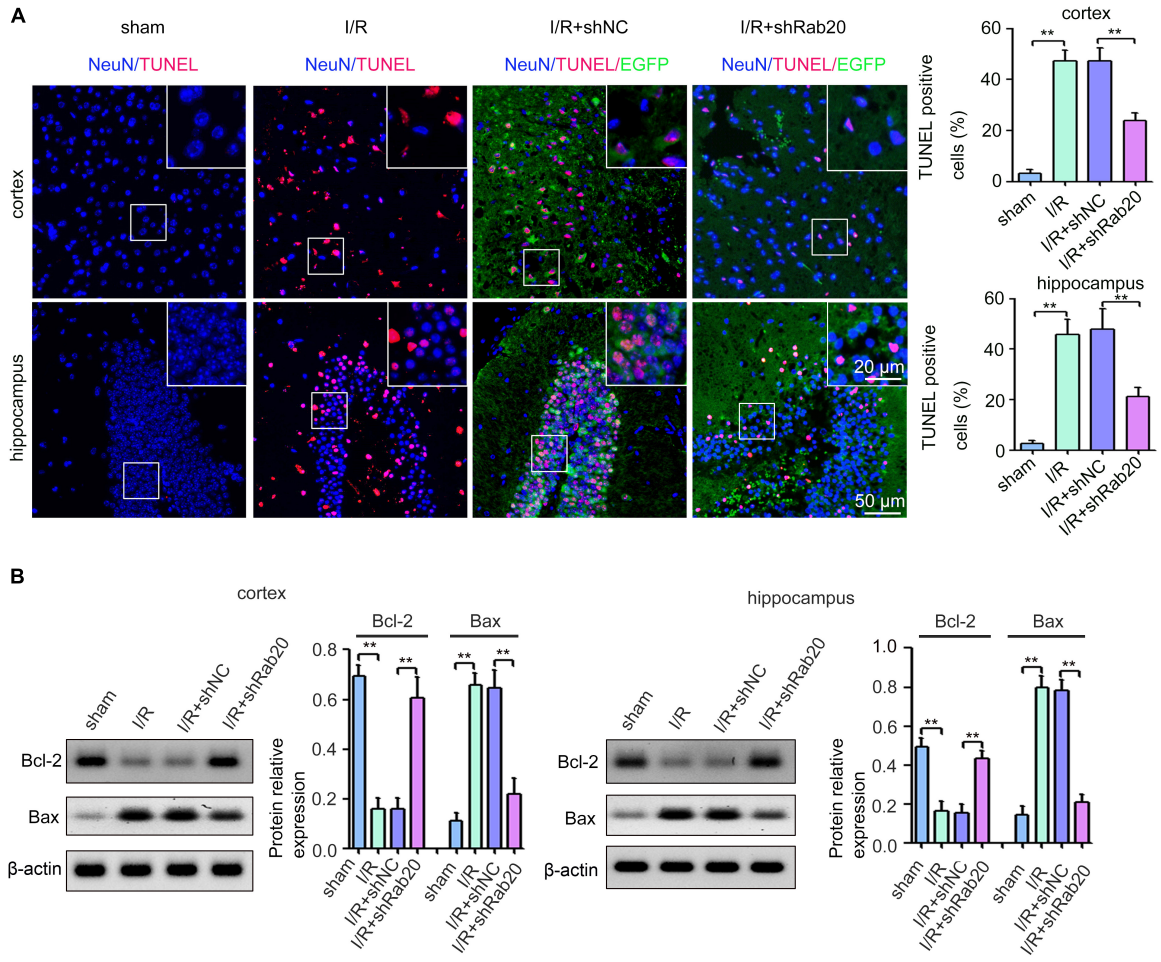

FIGURE 3
Ras-related protein Rab-20 knockdown significantly reduced I/R-induced neuronal apoptosis in mice. **(A)** Representative images and quantitative analyses of TUNEL-positive neurons in the penumbra of the cortex and hippocampus after I/R (n = 6). Scale bar, 20 and 50 μm. **(B)** Representative Western blot images and quantitative analyses of the apoptotic molecular markers Bcl-2 and Bax in the penumbra of the cortex and hippocampus after I/R (n = 6). $^{**}P < 0.01$.

Ras-related protein Rab-20 knockdown alleviated excessive mitochondrial fission in the HT22 cells after oxygen-glucose deprivation/reoxygenation

Ras-related protein Rab-20 has been shown as a predominant mitochondrial protein (Hackenbeck et al., 2011). Thus, we determined whether increased Rab20 expression induced by OGD/R was mainly located in mitochondria in HT22 cells. **Figure 5A** shows that mitochondria were visualized by the mitochondrial marker MitoTracker Green, and Rab20 protein was stained with a Rab20 antibody (red). All cells showed a colocalization with labeled mitochondria and Rab20 (**Figure 5A**). Rabs and Rab effectors have been implicated in mitochondrial fission (Farmer and Caplan, 2020). After stroke, mitochondrial fission was induced to increase mitochondrial energy production for the maintenance of neural function, whereas excessive mitochondrial fission was detrimental to neurons (Andrabi et al., 2019). Thus, we determined whether increased Rab20 expression was associated with mitochondrial fission. As shown in **Figure 5B**, mitochondria in the HT22 cells had an elongated tubular structure in the normal group, whereas OGD/R treatment caused punctuated structures in HT22 cells. The proportion of fragmented mitochondria was increased in HT22 cells after OGD/R, whereas Rab20 knockdown significantly reduced OGD/R-induced mitochondrial fission in HT22 cells (**Figure 5B**). Rab proteins are involved in dynamin-related protein 1 (Drp-1)-mediated mitochondrial fragmentation (Landry et al., 2014; Liang et al., 2020). Thus, we determined whether Rab20 alleviated OGD/R-induced mitochondrial fission by mediating Drp-1. Drp-1 phosphorylation at Ser637 decreased in HT22

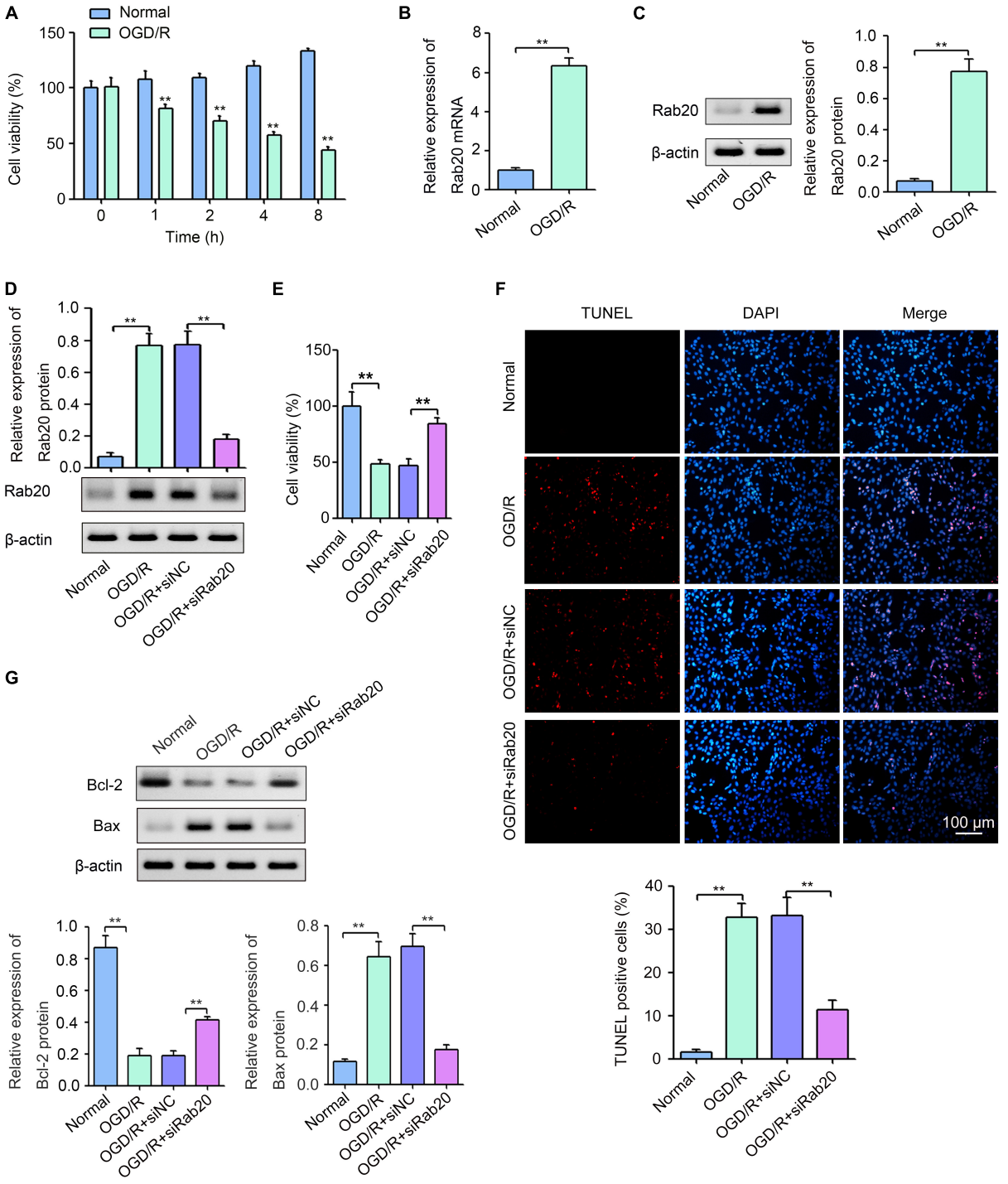

FIGURE 4
Ras-related protein Rab-20 knockdown significantly reduced OGD/R-induced neuronal injury *in vitro*. **(A)** HT22 cells were cultured in a glucose-free DMEM solution and placed into a hypoxic chamber at 1% O_2, 5% CO_2, and 94% N_2 for 0, 1, 2, 4, or 8 h to mimic OGD. After OGD, cells were then given normal DMEM with 10% FBS for 24 h. CCK-8 was used to determine the cell viability (n = 3). **(B,C)** RT-qPCR and Western blot assays were used to determine the expression levels of Rab20 mRNA and protein in HT22 cells after OGD for 4 h and reperfusion for 24 h, respectively (n = 3). **(D)** HT22 cells were transfected with siRab20 and siNC for 48 h prior to OGD/R operation, and then Western blot assay was used to determine the silencing efficiency of the siRab20 in HT22 cells after OGD for 4 h and reperfusion for 24 h (n = 3). **(E,F)** Cell viability and cell apoptosis was detected by CCK-8 and TUNEL after OGD for 4 h and reperfusion for 24 h, respectively (n = 3). **(G)** Representative Western blot images and quantitative analyses of the apoptotic molecular markers Bcl-2 and Bax in HT22 cells after OGD for 4 h and reperfusion for 24 h (n = 3). $^{**}P < 0.01$.

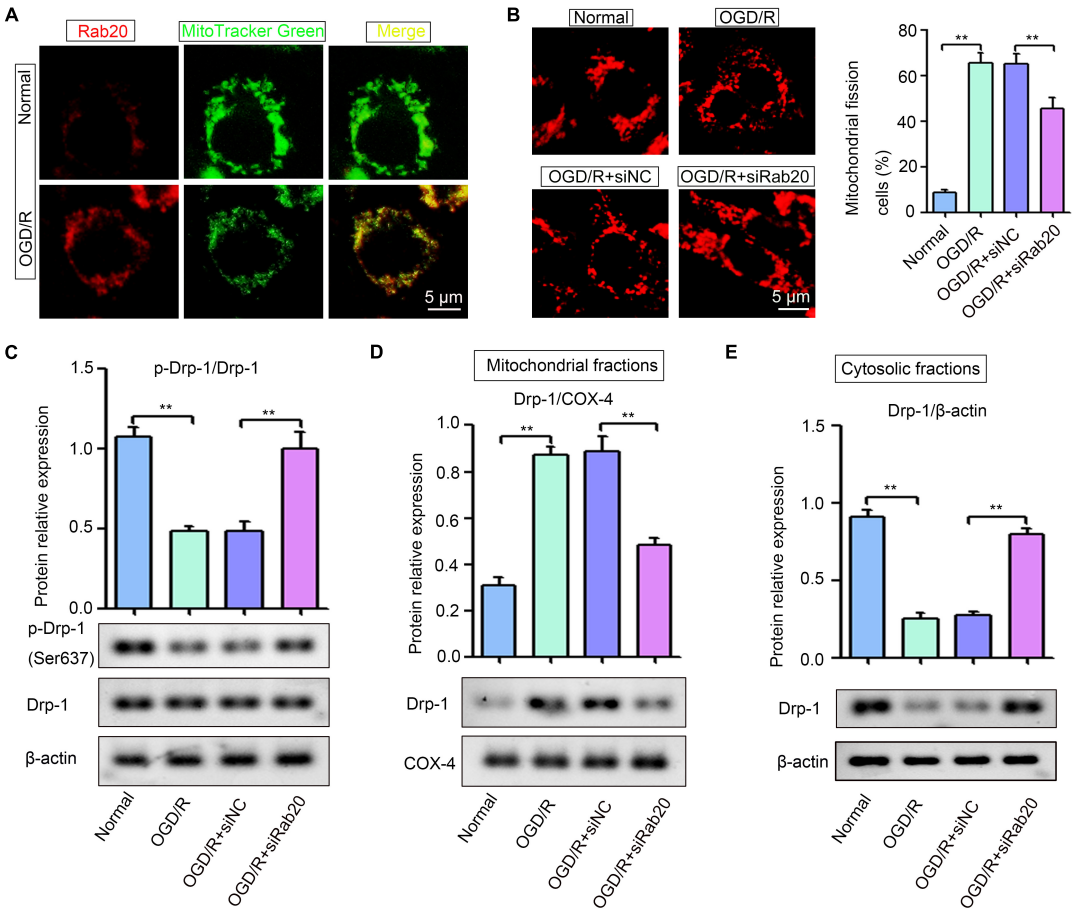

FIGURE 5
Ras-related protein Rab-20 knockdown significantly inhibited mitochondrial fission in HT22 cells after OGD/R. **(A)** HT22 cells were transfected with siRab20 and siNC for 48 h prior to OGD/R operation, and then double immunofluorescence staining for Rab20 (red) in mitochondria (MitoTracker Green, green) was performed in HT22 cells after OGD for 4 h and reperfusion for 24 h. Scale bar, 5 μm. **(B)** MitoTracker® Deep Red FM staining was used to determine the mitochondrial morphology (n = 3). Scale bar, 5 μm. **(C)** Total levels of Drp-1 and p-Drp1 (Ser637) were determined by Western blot (n = 3). **(D,E)** Drp-1 expression levels in the mitochondrial and cytosolic fractions were determined by Western blot (n = 3). $^{**}P < 0.01$.

cells after OGD/R (Figure 5C). As shown in Figures 5D,E, OGD/R induced the location of Drp-1 at mitochondria and inhibited the location of Drp-1 at cytoplasm. However, Rab20 knockdown significantly attenuated the location of Drp-1 at mitochondria and the inhibition of Drp-1 phosphorylation at Ser637 induced by OGD/R (Figures 5C–E).

Ras-related protein Rab-20 knockdown improved mitochondrial dysfunction in HT22 cells after oxygen-glucose deprivation/reoxygenation

Ras-related protein Rab-20 knockdown significantly alleviated excessive mitochondrial fission. Thus, we further determined the effect of Rab20 on mitochondrial dysfunction, as indicated by mitochondrial membrane potential (Δψm) collapse, excessive ROS production, cellular calcium accumulation and Cyto c release. To measure mitochondrial membrane potential (Δψm) collapse, TMRE staining was performed. As shown in Figure 6A, TMRE signal was significantly inhibited in HT22 cells after OGD/R, whereas Rab20 knockdown significantly reversed the inhibition of TMRE signal induced by OGD/R. To measure mitochondrial-derived ROS, HT22 cells were stained by MitoSox Red and MitoTracker Green. The mitochondrial-derived ROS was significantly increased in HT22 cells after OGD/R, whereas Rab20 knockdown significantly reversed OGD/R-induced ROS production (Figure 6B). Fluo-3AM staining showed that cellular calcium accumulation was significantly increased in HT22 cells after OGD/R, whereas this alteration was significantly reversed by Rab20 knockdown (Figure 6C). As

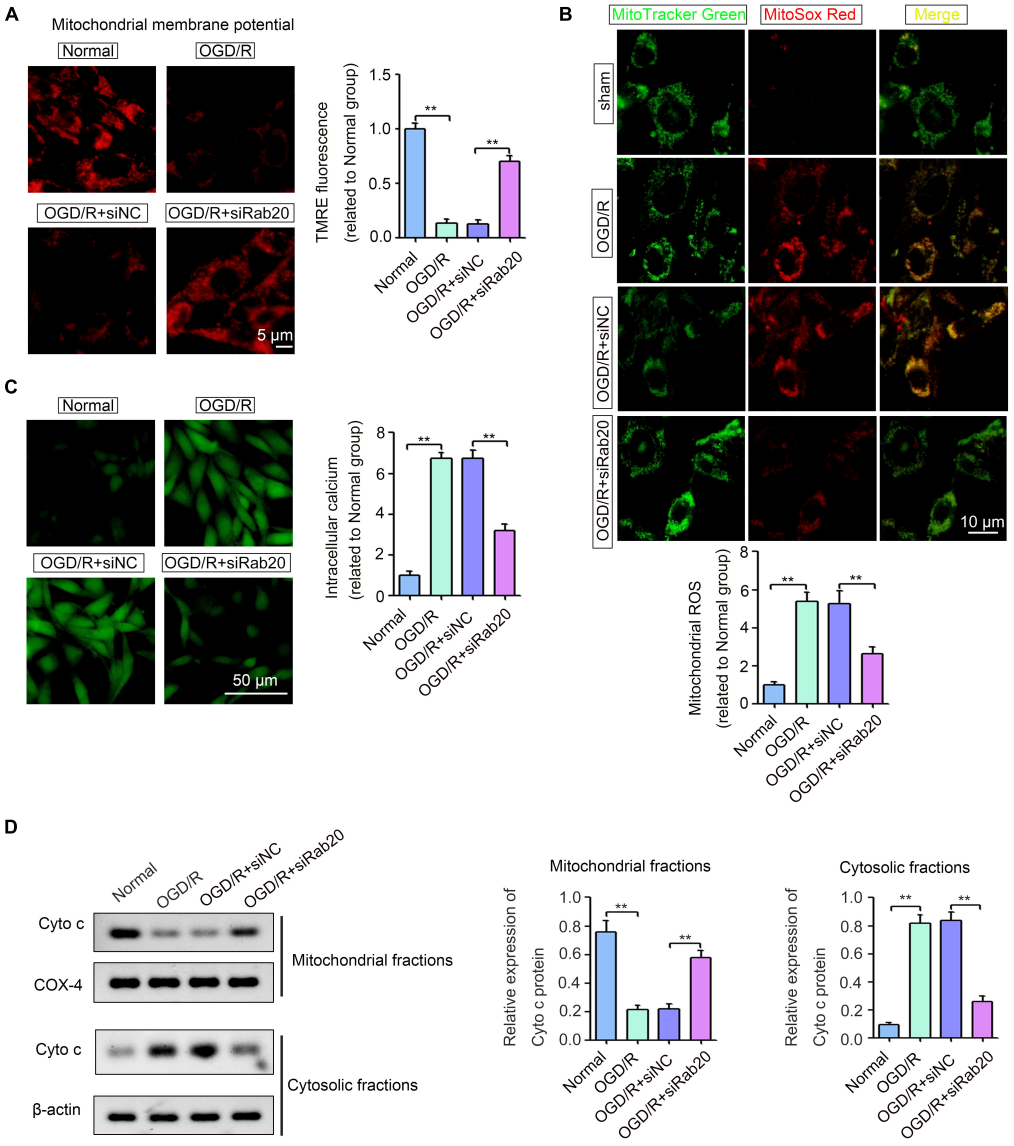

FIGURE 6
Ras-related protein Rab-20 knockdown significantly ameliorated mitochondrial dysfunction in HT22 cells after OGD/R. **(A)** HT22 cells were transfected with siRab20 and siNC for 48 h prior to OGD/R operation, and then TMRE staining was used to analyze mitochondrial membrane potential ($\Delta\psi m$) in HT22 cells after OGD for 4 h and reperfusion for 24 h. Scale bar, 5 μm. **(B)** Mitochondrial-derived ROS was stained by MitoSox Red and MitoTracker Green (n = 3). Scale bar, 10 μm. **(C)** Fluo-3AM staining was used to determine the intracellular calcium accumulation (n = 3). Scale bar, 50 μm. **(D)** Cyto c expression levels in the mitochondrial and cytosolic fractions were determined by Western blot (n = 3). $^{**}P < 0.01$.

shown in Figure 6D, OGD/R treatment significantly induced Cyto c release from the mitochondria into the cytosol, whereas this alteration was significantly reversed by Rab20 knockdown.

Discussion

Ras-related protein Rab-20 is among the Rab family of small GTPases, which are involved in membrane traffic in all eukaryotic cells (Stenmark, 2009). Interestingly, Rab20 was induced under stress. For example, Rab20 expression was increased in retinal endothelial cells and retinal Müller cells exposed to high glucose (Kim et al., 2020). In a hypoxic microenvironment, HIF-1 upregulation induced Rab20 expression (Görgens et al., 2017). In the present study, we found for the first time that Rab20 was significantly increased in the injured hemisphere after I/R (Figures 1A,B), and elevated Rab20 was mainly expressed in neurons but not in astrocytes and microglia (Figure 1C). Consistent with our findings, Rab20 was upregulated during the acute phase of inflammation in mice

(Liang et al., 2012). However, upregulated Rab20 was observed in active microglial cells during the acute phase of inflammation (Liang et al., 2012). Thus, Rab20 may show diverse cellular localization under different pathological conditions.

Ras-related protein Rab-20 was reportedly involved in stress-induced apoptosis (Hackenbeck et al., 2011; Kim et al., 2020). For instance, upregulated Rab20 induced by high glucose contributed to cell apoptosis in retinal endothelial cells and retinal Müller cells (Kim et al., 2020). Rab20 induced by HIF-1 also contributed to hypoxia-induced apoptosis (Hackenbeck et al., 2011). Whether the neuronal injury was influenced by Rab20 under cerebral I/R was unknown. Here, we found that Rab20 knockdown caused by injecting shRab20 AAV particles into the mouse brain significantly ameliorated the neurological outcome (**Figures 2E,F**) and reduced I/R-induced neuronal apoptosis, which was stained intensively by the TUNEL reaction (**Figure 3A**). To further verify the role of Rab20 in I/R-induced cell apoptosis, we assessed the effect of Rab20 on several key apoptosis-associated signal proteins including Bax and Bcl-2. As expected, Rab20 knockdown significantly reversed the decrease in Bcl-2 protein levels and the increase in Bax protein levels induced by cerebral I/R (**Figure 3B**). To further confirm the effect of Rab20 on neurological injury *in vitro*, we established an OGD/R model. Rab20 expression was significantly increased in HT22 cells after OGD/R (**Figures 4B,C**), and Rab20 inhibition by siRNA significantly ameliorated OGD/R-induced inhibition of cell viability (**Figure 4E**) and apoptosis (**Figure 4F**) in the HT22 cells. Moreover, Rab20 knockdown significantly restored the decrease in Bcl-2 protein levels and the increase in Bax protein levels induced by OGD/R (**Figure 4G**). These results further supported the proapoptotic action of Rab20 in I/R-induced neuronal injury.

A previous study has reported that Rab20 mainly colocalizes with mitochondria in HeLa and HKC-8 cells (Hackenbeck et al., 2011). We showed that upregulated Rab20 protein was mainly located in mitochondria after OGD/R (**Figure 5A**). Mitochondria are the powerhouse of the cell and organized in a highly dynamic tubular network characterized by fusion and fission (Cardoso et al., 2010). Mitochondrial dynamics is essential for maintaining the normal physiological function of cells through continuous fusion-division. However, excessive mitochondrial fission affects energy metabolism in cells, and induces apoptosis after ischemic stroke (Doyle et al., 2008). Rabs and Rab effectors are associated with mitochondrial fission (Farmer and Caplan, 2020). For instance, Rab7 can mark the mitochondria for fission by promoting contact sites between lysosomes and mitochondria (Wong et al., 2018). Rab32, a mitochondrial PKA anchoring protein, is involved in the assembly of mitochondrial fission complex (Alto et al., 2002). These studies led to the hypothesis that Rab20 may affect the I/R-induced neuronal injury by mediating mitochondrial fission. As expected, our data showed that Rab20 knockdown significantly reduced OGD/R-induced mitochondrial fission in HT22 cells (**Figure 5B**). Drp-1 plays a crucial role in regulating mitochondrial fission. Under homeostatic states, Drp-1 is allocated in the cytoplasm, whereas during ischemic stroke, Drp-1 is activated by dephosphorylation at Ser637, thereby promoting the recruitment of Drp-1 to the mitochondria *via* its receptor proteins, mitochondrial fragmentation, and exacerbated apoptotic cell death after ischemic stroke (Flippo et al., 2020; Tian et al., 2022). Rabs are involved in Drp-1-mediated mitochondrial fragmentation (Landry et al., 2014; Liang et al., 2020). For example, Rab11a regulates Drp1-mediated fission by promoting the stable association of Drp-1 with mitochondrial membranes (Landry et al., 2014). These important observations have promoted further exploration of the interaction between Rab20 and Drp-1 in mitochondrial fragmentation after ischemic stroke. Our results showed that Rab20 knockdown significantly ameliorated the inhibition of Drp-1 phosphorylation at Ser637 induced by OGD/R *in vitro* (**Figure 5C**). In addition, Rab20 inhibition significantly reversed the mitochondrial Drp1 recruitment induced by OGD/R in HT22 cells (**Figures 5D,E**). Thus, Rab20 may promote mitochondrial fragmentation by inhibiting Drp-1 phosphorylation at Ser637, thereby inducing mitochondrial Drp1 recruitment and neuronal apoptosis after ischemic stroke.

When mitochondrial fission is induced, the number of dysfunctional mitochondria in neurons increases after I/R (Yang et al., 2018). Mitochondrial dysfunction, which can lead to mitochondrial membrane potential ($\Delta\Psi m$) collapse, leads to the overproduction of ROS, calcium accumulation and Cyto c release, and promotes neural apoptosis in ischemic stroke (Andrabi et al., 2020). The interaction between calcium overload, ROS production, and the mitochondrial permeability transition pores (MPTP) leads to the increase in mitochondrial fission and apoptotic death in ischemic stroke (Andrabi et al., 2019). Our results showed that Rab20 knockdown significantly alleviated mitochondrial membrane potential ($\Delta\psi m$) collapse, the accumulation of mitochondrial-derived ROS and cellular calcium induced by OGD/R in HT22 cells (**Figures 6A–C**). In addition, Rab20 knockdown significantly reversed Cyto c release from mitochondria to cytosol, which was induced by OGD/R in HT22 cells (**Figure 6D**). Increasing evidence indicate that mitochondrial events, such as ROS production and cellular calcium accumulation, leads to Cyto c release from the mitochondria to the cytosol, thereby promoting apoptotic cascade during ischemic stroke (Andrabi et al., 2019). Thus, targeting Rab20 may be a novel approach for alleviating the mitochondrial dysfunction induced by I/R.

Conclusion

In summary, Rab20 expression was increased in neurons after I/R, and upregulated Rab20 induced mitochondrial fission and dysfunction, which in turn caused neuronal apoptosis in I/R injury.

Data availability statement

The original contributions presented in this study are included in the article/**Supplementary material**, further inquiries can be directed to the corresponding author.

Ethics statement

The animal study was reviewed and approved by the Ethics Committee of Lanzhou University Second Hospital.

Author contributions

JG and JL conceived and designed the study. JG, JL, YB, and WL performed the experiments. JG, YB, LZ, and JH analyzed the data. JG and YB wrote and revised the manuscript. All authors read and approved the final manuscript.

Funding

This study was supported by Cuiying Scientific and Technological Innovation Program of Lanzhou University Second Hospital (CY2017-QN17) and Cuiying Scientific Training Program for Undergraduates of Lanzhou University Second Hospital (CYXZ2019-24).

Acknowledgments

We thank Xiang Huang (AAV Technologist, Sunbio Medical Biotechnology) for their technical assistance.

Conflict of interest

The authors declare that the research was conducted in the absence of any commercial or financial relationships that could be construed as a potential conflict of interest.

Publisher's note

Supplementary material

The Supplementary Material for this article can be found online at: https://www.frontiersin.org/articles/10.3389/fnmol.2022.986710/full#supplementary-material

References

Alto, N. M., Soderling, J., and Scott, J. D. (2002). Rab32 is an A-kinase anchoring protein and participates in mitochondrial dynamics. *J. Cell Biol.* 158, 659–668. doi: 10.1083/jcb.200204081

Andrabi, S. S., Ali, M., Tabassum, H., Parveen, S., and Parvez, S. (2019). Pramipexole prevents ischemic cell death via mitochondrial pathways in ischemic stroke. *Dis. Model. Mech.* 12:dmm033860. doi: 10.1242/dmm.033860

Andrabi, S. S., Parvez, S., and Tabassum, H. (2020). Ischemic stroke and mitochondria: Mechanisms and targets. *Protoplasma* 257, 335–343. doi: 10.1007/s00709-019-01439-2

Campbell, B. C. V., De Silva, D. A., Macleod, M. R., Coutts, S. B., Schwamm, L. H., Davis, S. M., et al. (2019).). Ischaemic stroke. *Nat. Rev. Dis. Primers* 5:1. doi: 10.1038/s41572-019-0118-8

Cardoso, A. R., Queliconi, B. B., and Kowaltowski, A. J. (2010). Mitochondrial ion transport pathways: Role in metabolic diseases. *Biochim. Biophys. Acta Bioenerg.* 1797, 832–838. doi: 10.1016/j.bbabio.2009.12.017

Choi, D. H., Kim, J. H., Lee, K. H., Kim, H. Y., Kim, Y. S., Choi, W. S., et al. (2015). Role of neuronal NADPH oxidase 1 in the peri-infarct regions after stroke. *PLoS One* 10:e0116814. doi: 10.1371/journal.pone.0116814

Doyle, K., Simon, R., and Stenzel-poore, M. (2008). Mechanisms of Ischemic Brain Damage – Review Article. *Neuropharmacology* 55, 310–318. doi: 10.1016/j.neuropharm.2008.01.005.Neuropharmacology

Egami, Y., and Araki, N. (2012). Rab20 regulates phagosome maturation in RAW264 macrophages during Fc gamma receptor-mediated phagocytosis. *PLoS One* 7:e35663. doi: 10.1371/journal.pone.0035663

Farmer, T., and Caplan, S. (2020). *Chapter 15 Black Bride of Christ.* United Kingdom: Vanderbilt University Press. doi: 10.2307/j.ctv15vwj9v.23

Flippo, K. H., Lin, Z., Dickey, A. S., Zhou, X., Dhanesha, N. A., Walters, G. C., et al. (2020). Deletion of a neuronal Drp1 activator protects against cerebral ischemia. *J. Neurosci.* 40, 3119–3129. doi: 10.1523/JNEUROSCI.1926-19.2020

Gąsecki, D., Kwarciany, M., Kowalczyk, K., Narkiewicz, K., and Karaszewski, B. (2021). Blood Pressure Management in Acute Ischemic Stroke. *Curr. Hypertens. Rep.* 23:3. doi: 10.1007/s11906-020-01120-7

Görgens, S. W., Benninghoff, T., Eckardt, K., Springer, C., Chadt, A., Melior, A., et al. (2017). Hypoxia in Combination With Muscle Contraction Improves Insulin Action and Glucose Metabolism in Human Skeletal Muscle via the HIF-1a Pathway. *Diabetes* 66, 2800–2807. doi: 10.2337/DB16-1488

Hackenbeck, T., Huber, R., Schietke, R., Knaup, K. X., Monti, J., Wu, X., et al. (2011). The GTPase RAB20 is a HIF target with mitochondrial localization mediating apoptosis in hypoxia. *Biochim. Biophys. Acta* 1813, 1–13. doi: 10.1016/j.bbamcr.2010.10.019

Hermann, D. M., Kilic, E., Hata, R., Hossmann, K. A., and Mies, G. (2001). Relationship between metabolic dysfunctions, gene responses and delayed cell death after mild focal cerebral ischemia in mice. *Neuroscience* 104, 947–955. doi: 10.1016/S0306-4522(01)00125-7

Jin, J., Sun, H., Liu, D., Wang, H., Liu, Q., Chen, H., et al. (2019). LRG1 Promotes Apoptosis and Autophagy through the TGFβ-smad1/5 Signaling Pathway to Exacerbate Ischemia/Reperfusion Injury. *Neuroscience* 413, 123–134. doi: 10.1016/j.neuroscience.2019.06.008

Jin, Z., Liang, J., Wang, J., and Kolattukudy, P. E. (2015). MCP-induced protein 1 mediates the minocycline-induced neuroprotection against cerebral ischemia/reperfusion injury in vitro and in vivo. *J. Neuroinflammation* 12:39. doi: 10.1186/s12974-015-0264-1

Kim, D., Lewis, C. S., Sarthy, V. P., and Roy, S. (2020). High-glucose-induced rab20 upregulation disrupts gap junction intercellular communication and promotes apoptosis in retinal endothelial and müller cells: Implications for diabetic retinopathy. *J. Clin. Med.* 9:3710. doi: 10.3390/jcm9113710

Landry, M. C., Champagne, C., Boulanger, M. C., Jetté, A., Fuchs, M., Dziengelewski, C., et al. (2014). A functional interplay between the small GTPase rab11a and mitochondria-shaping proteins regulates mitochondrial positioning and polarization of the actin cytoskeleton downstream of Src family kinases. *J. Biol. Chem.* 289, 2230–2249. doi: 10.1074/jbc.M113.516351

Liang, X., Wang, S., Wang, L., Ceylan, A. F., Ren, J., and Zhang, Y. (2020). Mitophagy inhibitor liensinine suppresses doxorubicin-induced cardiotoxicity through inhibition of Drp1-mediated maladaptive mitochondrial fission. *Pharmacol. Res.* 157:104846. doi: 10.1016/j.phrs.2020.104846

Liang, Y., Lin, S., Zou, L., Zhou, H., Zhang, J., Su, B., et al. (2012). Expression profiling of Rab GTPases reveals the involvement of Rab20 and Rab32 in acute brain inflammation in mice. *Neurosci. Lett.* 527, 110–114. doi: 10.1016/j.neulet.2012.08.039

Liao, C., Xu, D., Liu, X., Fang, Y., Yi, J., Li, X., et al. (2018). Iridium (III) complex-loaded liposomes as a drug delivery system for lung cancer through mitochondrial dysfunction. *Int. J. Nanomed.* 13, 4417–4431. doi: 10.2147/IJN.S170035

Lin, L., Wang, X., and Yu, Z. (2016). Ischemia-reperfusion Injury in the Brain: Mechanisms and Potential Therapeutic Strategies. *Biochem. Pharmacol.* 5:213. doi: 10.4172/2167-0501.1000213.Ischemia-reperfusion

Liu, D., Guo, H., Griffin, J. H., Fernández, J. A., and Zlokovic, B. V. (2003). Protein S confers neuronal protection during ischemic/hypoxic injury in mice. *Circulation* 107, 1791–1796. doi: 10.1161/01.CIR.0000058460.34453.5A

Liu, H., Wu, X., Luo, J., Wang, X., Guo, H., Feng, D., et al. (2019). Pterostilbene attenuates astrocytic inflammation and neuronal oxidative injury after ischemia-reperfusion by inhibiting nf-κb phosphorylation. *Front. Immunol.* 10:2408. doi: 10.3389/fimmu.2019.02408

Liu, M., Xu, Z., Wang, L., Zhang, L., Liu, Y., Cao, J., et al. (2020). Cottonseed oil alleviates ischemic stroke injury by inhibiting the inflammatory activation of microglia and astrocyte. *J. Neuroinflammation* 17:270. doi: 10.1186/s12974-020-01946-7

Liu, S., Feng, X., Jin, R., and Li, G. (2018). Tissue plasminogen activator-based nanothrombolysis for ischemic stroke Shan. *Expert Opin. Drug Deliv.* 15, 173–184. doi: 10.1080/17425247.2018.1384464.Tissue

Lutcke, A., Parton, R. G., Murphy, C., Olkkonen, V. M., Dupree, P., Valencia, A., et al. (1994). Cloning and subcellular localization of novel rab proteins reveals polarized and cell type-specific expression. *J. Cell Sci.* 107, 3437–3448. doi: 10.1242/jcs.107.12.3437

Prabhakaran, S., Ruff, I., and Bernstein, R. A. (2015). Acute stroke intervention: A systematic review. *JAMA* 313, 1451–1462. doi: 10.1001/jama.2015.3058

Stenmark, H. (2009). Rab GTPases as coordinators of vesicle traffic. *Nat. Rev. Mol. Cell Biol.* 10, 513–525. doi: 10.1038/nrm2728

Tian, H., Chen, X., Liao, J., Yang, T., Cheng, S., Mei, Z., et al. (2022). Mitochondrial quality control in stroke: From the mechanisms to therapeutic potentials. *J. Cell. Mol. Med.* 26, 1000–1012. doi: 10.1111/jcmm.17189

Wong, Y. C., Ysselstein, D., and Krainc, D. (2018). Mitochondria-lysosome contacts regulate mitochondrial fission via RAB7 GTP hydrolysis. *Nature* 554, 382–386. doi: 10.1038/nature25486.Mitochondria-lysosome

Wu, B., Luo, H., Zhou, X., Cheng, C., Yi Lin, L., Liu, B., et al. (2017). Succinate-induced neuronal mitochondrial fission and hexokinase II malfunction in ischemic stroke: Therapeutical effects of kaempferol. *Biochim. Biophys. Acta Mol. Basis Dis.* 1863, 2307–2318. doi: 10.1016/j.bbadis.2017.06.011

Yang, J. L., Mukda, S., Chen, S., and Der. (2018). Diverse roles of mitochondria in ischemic stroke. *Redox Biol.* 16, 263–275. doi: 10.1016/j.redox.2018.03.002

Zhang, L., Cai, Q., Lin, S., Chen, B., Jia, B., Ye, R., et al. (2021). Qingda granule exerts neuroprotective effects against ischemia/reperfusion-induced cerebral injury via lncRNA GAS5/miR-137 signaling pathway. *Int. J. Med. Sci.* 18, 1687–1698. doi: 10.7150/ijms.53603

Zhang, L., Hu, X., Luo, J., Li, L., Chen, X., Huang, R., et al. (2013). Physical exercise improves functional recovery through mitigation of autophagy, attenuation of apoptosis and enhancement of neurogenesis after MCAO in rats. *BMC Neurosci.* 14:46. doi: 10.1186/1471-2202-14-46

Zhao, H., Wang, J., Gao, L., Wang, R., Liu, X., Gao, Z., et al. (2013). MiRNA-424 protects against permanent focal cerebral ischemia injury in mice involving suppressing microglia activation. *Stroke* 44, 1706–1713. doi: 10.1161/STROKEAHA.111.000504

Zhao, S., Xi, D., Cai, J., Chen, W., Xiang, J., Peng, N., et al. (2020). Rab20 is critical for bacterial lipoprotein tolerization-enhanced bactericidal activity in macrophages during bacterial infection. *Sci. China Life Sci.* 63, 401–409. doi: 10.1007/s11427-019-9527-3

Zhou, Z., Lu, J., Liu, W. W., Manaenko, A., Hou, X., Mei, Q., et al. (2018). Advances in stroke pharmacology. *Pharmacol. Ther.* 191, 23–42. doi: 10.1016/j.pharmthera.2018.05.012

frontiers | Frontiers in Molecular Neuroscience

TYPE Original Research
PUBLISHED 28 October 2022
DOI 10.3389/fnmol.2022.1026530

OPEN ACCESS

EDITED BY
Federica Bono,
University of Brescia,
Italy

REVIEWED BY
Francisco Javier del Castillo,
Ramón y Cajal University Hospital, Spain
Gonzalo Arboleda,
National University of Colombia, Colombia
Marco Baralle,
International Centre for Genetic Engineering and Biotechnology, Italy
Edoardo Monfrini,
University of Milan,
Italy
Gabriel Gutiérrez-Ospina,
National Autonomous University of Mexico, Mexico

*CORRESPONDENCE
Guanting Lu
guantlv@126.com
Xiaowu Hu
hxw0535@163.com

†These authors have contributed equally to this work

SPECIALTY SECTION
This article was submitted to Brain Disease Mechanisms, a section of the journal Frontiers in Molecular Neuroscience

RECEIVED 24 August 2022
ACCEPTED 11 October 2022
PUBLISHED 28 October 2022

CITATION
Peng Q, Zhang Y, Xian B, Wu L, Ding J, Ding W, Zhang X, Ding B, Li D, Wu J, Hu X and Lu G (2022) A synonymous variant contributes to a rare Wiedemann-Rautenstrauch syndrome complicated with mild anemia *via* affecting pre-mRNA splicing.
Front. Mol. Neurosci. 15:1026530.
doi: 10.3389/fnmol.2022.1026530

A synonymous variant contributes to a rare Wiedemann-Rautenstrauch syndrome complicated with mild anemia *via* affecting pre-mRNA splicing

Qiongling Peng[1†], Yan Zhang[2†], Binqiang Xian[1], Lianying Wu[3,4], Jianying Ding[1], Wuwu Ding[4], Xin Zhang[1], Bilan Ding[1], Ding Li[3], Jin Wu[3], Xiaowu Hu[5]* and Guanting Lu[3,4]*

[1]Department of Child Healthcare, Shenzhen Baoan Women's and Children's Hospital, Jinan University, Shenzhen, China, [2]Department of Obstetrics and Gynecology, Strategic Support Force Medical Center, Beijing, China, [3]Laboratory of Translational Medicine Research, Deyang People's Hospital, Deyang, China, [4]Deyang Key Laboratory of Tumor Molecular Research, Department of Pathology, Deyang People's Hospital, Deyang, China, [5]Clinical Laboratory, Sichuan Provincial Rehabilitation Hospital, Chengdu, China

Wiedemann-Rautenstrauch syndrome (WDRTS) is an extremely rare autosomal recessive neonatal disorder. Currently, over 50 cases with variable phenotypes of WDRTS have been reported. In our cohort of prenatal and postnatal growth retardation, a female proband was found to have general growth retardation, neurocutaneous syndrome, and anemia. Karyotype test and array-CGH detected no obvious chromosomal aberrations. Trio-based whole-exome sequencing (Trio-WES) identified bi-allelic compound mutations in the coding sequence (CDS) of *POLR3A* gene (c.3342C>T, p.Ser1114=and c.3718G>A, p.Gly1240Ser). For the mild anemia phenotype, the underlying causal genetic factors could be attributed to the compound heterozygous mutations in *FANCA* gene (c.2832dup, p.Ala945CysfsTer6 and c.1902T>G, p.Asp634Glu). Mini-gene reporter assays revealed that the synonymous variant of *POLR3A* and the missense variant of *FANCA* could affect pre-mRNA splicing of each gene. For *POLR3A*, the synonymous mutation (c.3342C>T, p.Ser1114=) generated three types of aberrant isoforms. Therefore, the female patient was finally diagnosed as WDRTS caused by *POLR3A*. For *FANCA*, the missense variant (c.1902T>G, p.Asp634Glu) disrupted the normal splicing between exon 21 and 22, and produced two types of abnormal isoforms, one carrying the 1902G and the other spliced between exon 21 and 23 to exclude exon 22. Network analysis showed that POLR3A and FANCA could be STRINGed, indicating both proteins might collaborate for some unknown functions. Current investigation would broaden the knowledge for clinicians and genetic counselors and remind them to interpret those synonymous or predicted "benign" variants more carefully.

KEYWORDS

Wiedemann-Rautenstrauch syndrome, Fanconi anemia, whole-exome sequencing, POLR3A, FANCA, pre-mRNA splicing

Introduction

Wiedemann-Rautenstrauch syndrome (WDRTS, OMIM#264090), an extremely rare progeroid disorder, was initially reported in two sisters by Rautenstrauch in 1977 (Rautenstrauch and Snigula, 1977). It was characterized by multiple distinct clinical features such as intrauterine growth retardation (IUGR), a progeroid appearance, lipodystrophy, failure to thrive, short stature, hypotonia, prominent scalp veins, teeth abnormalities and variable mental impairment (Toriello, 1990; Pivnick et al., 2000; Paolacci et al., 2017). In 1979, Wiedemann and Rautenstrauch considered this distinct neonatal progeroid syndrome to be transmitted under an autosomal recessive (AR) inheritance mode (Wiedemann, 1979).

Till now, over 50 individuals with variable phenotypes of WDRTS have been reported (Paolacci et al., 2017). Homozygous or bi-allelic heterozygous mutations of RNA polymerase III subunit A (*POLR3A*, OMIM#614258) were proved to be the causal for WDRTS (Jay et al., 2016; Paolacci et al., 2018; Wambach et al., 2018; Temel et al., 2020). A few other cases with neonatal-onset progeria and lipodystrophy were identified to be caused by mutations in fibrillin 1 (*FBN1*, OMIM#134797; Graul-Neumann et al., 2010; Garg and Xing, 2014), caveolin 1 (*CAV1*,OMIM#601047; Garg et al., 2015; Schrauwen et al., 2015), catalytic subunit of DNA polymerase delta 1 (*POLD1*, OMIM#174761; Elouej et al., 2017; Sasaki et al., 2018) and solute carrier family 25 member 24 (*SLC25A24*, OMIM#608744; Ehmke et al., 2017; Rodríguez-García et al., 2018). Since neonatal-onset progeria and lipodystrophy were also core clinical phenotypes of WDRTS, it would pose a big challenge to discriminate WDRTS from other neonatal-onset progeria and lipodystrophy disorders in the early period, and to give appropriate and timely symptomatic treatments.

Fanconi Anemia (FA, OMIM#227650) was a group of well-known clinically and genetically heterogeneous disorders (Bogliolo and Surralles, 2015), and characterized by distinct clinical features including developmental abnormalities in major organ systems, early-onset bone marrow failure, cellular sensitivity to DNA crosslinking agents, and a high predisposition to cancer (Nepal et al., 2017). The prevalence of FA was estimated at 1–5 in 1,000,000 live births (D'Andrea, 2010; Kottemann and Smogorzewska, 2013). It had been reported that FA could be caused by autosomal biallelic germline inactivation of any one of the 22 genes (*FANCA*-*FANCW*), except for the X-chromosomal *FANCB* gene (Niraj et al., 2019). Mutations in *FANCA* (OMIM#607139), *FANCC* (OMIM#613899) and *FANCG* (OMIM#602956) genes accounted for 60 ~ 65%, ~15% and ~10% of all the reported FA cases, respectively (D'Andrea and Grompe, 2003; Dimishkovska et al., 2018; Repczynska et al., 2022).

In our clinic, a 3-years-old female patient was presumptively diagnosed as general growth retardation, neurocutaneous syndrome, left hip dysplasia and anemia. Later, she was diagnosed as WDRTS according to the clinical phenotypes and bi-allelic mutations in *POLR3A* gene detected by Trio-based whole exome sequencing (trio-WES). Besides, two heterozygous mutations were also detected in *FANCA* gene, resulted in a mild form of Fanconi Anemia. It is worth noting that one benign variant was identified in each gene and confirmed to affect proper pre-mRNA splicing to generate abnormal transcripts.

To our knowledge, this was the first report for a WDRTS complicated with the occurrence of another recessive disorder, Fanconi Anemia (FA). It would broaden the molecular knowledge about WDRTS to clinicians and genetic counselors and reminded them to be more careful for analyzing genetic data and other relevant laboratory results.

Materials and methods

Sample collection

This study was conducted in accordance with the Code of Ethics of the World Medical Association (Declaration of Helsinki) for experiments involving humans. This study was approved by the Ethical Committee of the Shenzhen Bao'an Women's and Children's Hospital and Deyang People's Hospital. Written informed consents were obtained from the female's parent.

Peripheral venous blood was collected from the proband and her parent. Genomic DNA was extracted using the TIANamp Blood DNA Kit (DP348, Tiangen Biotech, Beijing, China) according to the manufacturer's instructions.

Array-comparative genomic hybridization

Oligonucleotide Array-comparative genomic hybridization (array-CGH) was performed using the Fetal DNA Chip (Version 1.2) designed by the Chinese University of Hong Kong (CUHK) (Huang et al., 2014). The chip contains a total of 60,000 probes for more than 100 diseases caused by known microduplication/microdeletions. It does not include small fragment chromosomal abnormalities, copy number polymorphism, chimerism and chromosomal rearrangement (Iafrate et al., 2004). The

experimental procedures were performed according to the standard Agilent protocol [Agilent Oligonucleotide Array-Based CGH (Array-CGH) for Genomic DNA Analysis, version 3.5]. Hybridized slides were scanned with SureScan High-Resolution Microarray Scanner (G2505B, Agilent Technologies), and the image data were extracted and converted to text files using Agilent Feature Extraction software. The data were graphed and analyzed using Agilent CGH Analytics software.

Trio-based whole exome sequencing

To investigate the genetic cause of the disease, whole-exome sequencing (WES) was performed for the trio at MyGenostics. Briefly, the fragmented genomic DNAs were ligated with the 3′ end of the Illumina adapters and amplified by polymerase chain reaction (PCR). The amplified DNA was captured with Gencap Human whole Exon Kit (52 M) at MyGenostics. The capture procedure was performed in accordance with the manufacturer's protocol. Finally, the generated libraries were sequenced on Illumina HiSeq 2,500 platform for paired-end sequencing. The sequencing depth was about 100x for each sample.

The analysis of the WES data was carried out according to our previous reports (Lu et al., 2021, 2022). Briefly, clean reads were obtained after removal of adaptors and low-quality reads (multiple Ns and shorter than 40 bp) by Cutadapt (version 1.16) from raw data in fastq format (Kechin et al., 2017). The trimmed clean reads were aligned to the human reference genome (UCSC hg19) using BWA software (version 0.7.10) (Li and Durbin, 2010). The obtained files would be converted to bam format by SAMtools (version 1.2) (Li et al., 2009) and then filtered by BamTools (version 2.4.0) (Barnett et al., 2011). GATK (Genome Analysis Toolkit, version 4.0.8.1) was used to remove duplicated reads (by GATK/MarkDuplicates.jar), to recalibrate bases (by GATK/BaseRecalibrator.jar), and to obtain new bam files (by GATK/ApplyBQSR.jar) for subsequent variant calling by HaplotypeCaller (Auwera et al., 2013). Functional annotation for the GATK-called variants was performed by ANNOVAR (version 2018-04-16; Wang et al., 2010). Variants with a minor allele frequency (MAF) > 1% in the 1,000 Genome Project, or in-house data were removed. Synonymous single nucleotide variants (SNVs) were also removed. SNVs that caused splicing, frameshift, stopgain, or stoploss were retained for subsequent analysis. A position was called as heterozygous if 25% or more of the reads identified the minor allele. The location, type, conservation of the identified variants was obtained from several public databases, such as UCSC Genome Browser, NCBI dbSNP, NCBI ClinVar, 1000Genome, ExAC, TOPMED, gnomAD and gnomAD_exomes. Nonsynonymous SNVs were submitted to PolyPhen-2 (Polymorphism Phenotyping v2; Adzhubei et al., 2013) and PROVEAN (Protein Variation Effect Analyzer; Choi and Chan, 2015) for functional prediction. The pathogenicity of identified variants were also annotated according to the guidelines of American College of Medical Genetics (ACMG) (Riggs et al., 2020). The selected variants were confirmed by Sanger sequencing with an ABI3730xl sequencer (Applied Biosystems, Waltham, Massachusetts, United States). The possibility of identified variant for aberrant splicing was analyzed by SpliceAI (version 1.3.1)[1] under default settings (Jaganathan et al., 2019).

Molecular analysis for the identified mutations

The protein sequences of POLR3A and FANCA were downloaded from NCBI GenBank, including 3 primates (*Homo sapiens*, *Pan troglodytes*, and *Macaca mulatta*), 1 cattle (*Bos taurus*), 2 rodents (*Mus musculus*, and *Rattus norvegicus*), 1 Chiroptera (*Artibeus jamaicensis*), 1 bird (*Gallus gallus*), 2 amphibians (*Bufo bufo* and *Xenopus tropicalis*), 2 fishes (*Danio rerio* and *Nothobranchius furzeri*). The protein sequences were aligned by the built-in ClustalW alignment algorithms of MEGA 11 (Gap opening penalty and Gap extension penalty for pairwise alignment and multiple alignment were set as 10.00, 0.10 and 10.00, 0.20, respectively; the Delay divergent cutoff was 30%). The effects of missense mutations on the structural changes were analyzed by the Missense3D and visualized using 3D View.[2] The gene expressions were evaluated according to the normalized signal intensity of probe 227872_at for POLR3A and 236976_at for FANCA, which were extracted from a gene atlas of human protein-encoding transcriptomes for 79 human tissues (NCBI GEO#GSE1133; Su et al., 2004). The protein interaction network with POLR3A and FANCA was generated by STRING (version 11.5) under default settings. Gene Ontology (GO) analysis was performed for the 10 members of the network under default parameters in the Gene Ontology knowledgebase.[3]

Mini-gene reporter assays

The genomic regions containing the two mutations (c.3342C > T for *POLR3A* and c.1902 T > G for *FANCA*) were synthesized and cloned into the multiple cloning site (MCS) of pEGFP-N1 plasmid for minigene splicing reporter assays to test their effects on pre-mRNA splicing. As for c.3342C > T of *POLR3A*, the 1,646 bp genomic DNA spanning exon 25 to exon 27 (10:79,742,411-79,744,056, hg19) was cloned into the MCS of pEGFP-N1. For c.1902 T > G of *FNACA*, the 4,135 bp genomic DNA from exon 21 to exon 23 (16:89,838,089-89,842,223, hg19) was cloned into the MCS of pEGFP-N1. The two mutations were introduced by site-directed mutagenesis.

1 https://github.com/Illumina/SpliceAI
2 https://www.pdbus.org/3d-view
3 http://geneontology.org/

The human embryonic kidney 293 cells (HEK293) or HeLa cells were cultured in high glucose DMEM medium (FI101-01, TransGen, Beijing, China) supplied with 5% fetal bovine sera (FBS) in 5% CO_2. The constructs were transfected into HEK293 or HeLa cells by *TransIntro* EL/PL Transfection Reagent (FT231-02, TransGen) according to the manufacturer's protocol. 24 h after transfection, cells were harvested, and lysed by adding 5 ml TransZol (ET101-01, TransGen). The wild-type (WT) and mutated (Mut) constructs were transfected into cells, respectively. Total RNAs were extracted and reversely transcribed into complementary DNAs (cDNAs) by TransScript Reverse Transcriptase (AT101-02, TransGen). The cDNAs were amplified by polymerase chain reaction (PCR) with paired primers (Supplementary Table S1), electrophoresed with agarose gel (1.5%, 120 V for 25 min), and then visualized by ChemiDoc XRS+ Gel Imaging System (Bio-Rad, Hercules, California, United States). DNAs of the bands were extracted and sequenced with an ABI3730xl sequencer (Applied Biosystems, United States).

Single cell gel electrophoresis assay

The single cell gel electrophoresis (SCGE) assay was performed as previously described with minor modifications (Li et al., 2014; Ji et al., 2018). After separated from 0.5 ml peripheral blood, lymphocytes were washed and resuspended at a density of 10^5 cells/mL in phosphate-buffered saline (PBS). 30 ml lymphocyte suspension were added in 70 µl of 0.75% low-melting-point agarose. The cell/agarose mixture was added onto the CometSlides which were precoated with 300 µl normal-melting-point agarose (0.75%) and was covered by a coverslip. After solidification, the coverslips were removed from the CometSlides. The CometSlides were submersed in cold fresh alkaline lysis solution for 1.5 h at 4°C. After lysis, the slides were electrophoresed at 30 V for 20 min in a horizontal tank which was filled with cold TBE buffer. Then, the slides were submerged in neutralization buffer for 20 min and stained with ethidium bromide (EB) in darkroom. The comets were observed using a digital fluorescence microscope (ECLIPSE 90i, Nikon, Tokyo, Japan), and images of 200 comets collected for each sample. The comets were analyzed by CASP (Comet Assay Software Project) software. The percentages of DNA in the comet head (HeadDNA%), DNA in the comet tail (TailDNA%), tail length (pix), tail moment (TM) and Olive tail moment (OTM) were calculated to evaluate the DNA damage of lymphocytes.

Statistical analysis

The statistical analysis was conducted using the SPSS software (version 13) with Student's t test for the mitomycin C-induced chromosome stress assay, and SCGE assay. p value less than 0.05 was considered as significance.

Results

Patient description

The female proband (46, XX) was born naturally to a non-consanguineous couple in 2019. She has one unaffected healthy elder sister (Figure 1A). Her gestational period was 40^{+3} weeks. Her birth weight was 2.59 kg (P3). Her head occipitofrontal circumference (OFC) and body length at birth were 33 cm (P11) and 48 cm (P14), respectively. At the age of three, her weight, height and OFC were 11.5 kg (P6), 89.0 cm (P4), and 49.6 cm (P76), respectively (Figure 1D). Her mother accepted all regular inspections as required during her pregnancy. No abnormalities were found except for intrauterine growth retardation (IUGR) at 36 weeks of gestation. Her mother had no history of smoking or exposure to harmful hazards during pregnancy. She was breast fed in the first 6 months after birth. Mild feeding difficulty and sucking weakness were observed during that period. After 6 months of age, she gradually established a normal daily diet, but had persistent poor postnatal growth.

Manifestations of progeroid phenotypes of WDRTS

The patient had presented progeroid appearance, with sparse scalp hair, poorly developed teeth, and thin subcutaneous fat (Figures 1B,C). Facial dysmorphic features were observed, such as triangular face, prominent forehead with frontal bossing, prominent scalp veins, sparse and broad eyebrows, deep set and long spaced eyes, pinched nose, small mouth with downturned corners, high-arched palate, malformed and low-set ears, and pointed chin. At birth, the patient had two natal teeth in the upper jaw and a gingival cyst of mucous gland in the lower jaw. At 6 months of age, the two natal teeth were removed by a dentist. No new teeth had grown at the same positions up to date.

She was found mild neurodevelopmental delay and hypermyotonia at 3 months of age and received rehabilitation which lasted for 5 months till she could creep and sit without support. Neuropsychological development assessment was performed using the Children Neuropsychological and Behavioral Scale-Revision 2016 (CNBS-R2016) and the parent-rated Adaptive Behavior Assessment System II (ABAS-II) infant version at 3 years old. Her full-scale developmental quotient (DQ) of CNBS-R2016 was 115. The DQ in the five subscales involving gross motor, fine motor, adaptive behavior, language, personal-social of CNBS-R2016 were 120, 112, 112,120, and 112, respectively. The overall adaptive function score of ABAS-II was 106 (95% CI: 102–110, P66). The scores of social skills, conceptual skills, and practical skills in the three composite areas of adaptive function were 108 (95% CI 101–115, P70), 102 (95% CI 94–110, P55), and 106 (95% CI 99–113, P66), respectively. According to the neuropsychological development assessments, her intellectual development level was similar to that of children of the same age.

Her brain magnetic resonance imaging (MRI) scan at 4 months old revealed no parenchymal abnormality except for

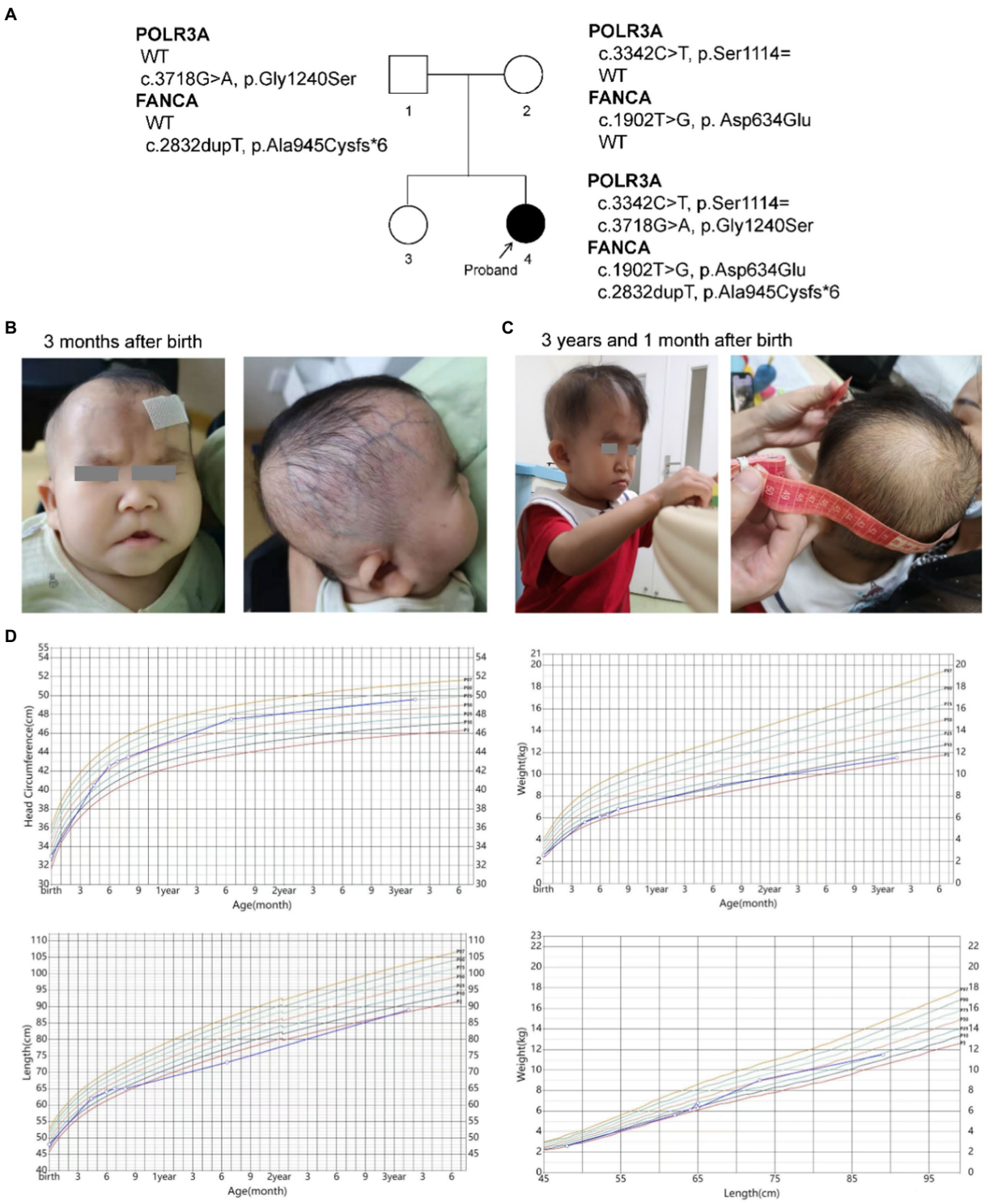

FIGURE 1
Descriptions of the proband. **(A)** Pedigree of the proband; **(B,C)** Facial and skin features of the proband; **(D)** Growth curves of the proband.

a left arachnoid cyst (20.1 mm × 11.5 mm × 10.1 mm). Electroencephalogram (EEG) at the same time showed partial spikes at left occipital-parietal and anterior temporal region during sleep. Possible hereditary metabolic diseases were screened from blood and urine samples by liquid chromatography tandem mass spectrometry (LC–MS/MS), and no abnormalities were found. No structural abnormalities of urinary, cardiac and digestive systems were found by color Doppler ultrasound when

she was 4 months old. Ultrasonic diagnosis revealed dysplasia of her left hip joint at 1 month after birth, but returned to normal at 6 months of age.

Persistent mild anemia

Routine blood tests were performed seven times from 4 months to 3 years and 3 months after birth (Figure 2; Supplementary Table S2). No abnormality was found for the leukocyte and thrombocyte. Persistent mild anemia (HGB 88 ~ 98 g/L) with reduced mean corpuscular volume (MCV) and mean corpuscular hemoglobin (MCH) were observed, while the reticulocyte count was normal (36.3×10^9/L, 0.9%). Peripheral blood smear showed normal morphology of leukocytes and platelets, and smaller volume of mature red blood cells with enlarged central light stained area. Bone marrow puncture was refused by her parent.

Mutations in POLR3A and FANCA were identified by trio-WES

Karyotype analysis of G-banding chromosomes on peripheral blood mononuclear cells (PBMCs) detected no evident chromosomal abnormalities. Array-CGH analysis revealed no clinically significant microduplications or microdeletions. Trio-based whole exome sequencing (Trio-WES) was performed, and 53 rare variants were identified in the proband (Supplementary Table S3). All of the variants were inherited either from her father (parentally) or from her mother (maternally). Since the parent displayed no symptoms, genes with *de novo*, bi-allelic heterozygous or homozygous mutations were selected for subsequent analysis. Only one gene, *FANCA,* was remained in the list. Since homozygous or compound heterozygous mutations of *FANCA* gene resulted in the recessive Fanconi anemia of complementation group A (FANCA), this gene might be the unlying molecular factor for the anemia phenotype of the proband. However, no other genes were identified to be responsible for other clinical presentations.

A Phenotype Profile Search was carried out at Human Phenotype Ontology (HPO) using eight key clinical features of the patient, such as progeroid facial appearance (HP:0005328), prominent scalp veins (HP:0001043), natal tooth (HP:0000695), intrauterine growth retardation (HP:0001511), and hypotonia (HP:0001252), sparse eyebrow (HP:0045075), sparse scalp hair (HP:0002209) and minimal (/thin) subcutaneous fat (HP:0003717). All eight input phenotypes were covered only in WDRTS, which was caused by mutations of *POLR3A* gene (Supplementary Table S4; Figure 3).

Only one rare mutation (c.3718G > A, p.Gly1240Ser) of *POLR3A* gene (NM_007055.4) was identified in the proband (Supplementary Table S3). Since WDRTS was an autosomal recessive (AR) disorder, the removed variants of *POLR3A* were revisited and one synonymous variant (c.3342C > T, p.Ser1114=) was retrieved (Table 1).

Molecular analysis of the bi-allelic mutations of *POLR3A* gene

For *POLR3A* gene, c.3718G > A (rs1003620056) in the exon 28 (28/31) was transmitted maternally (Figures 4A,B) and generated a missense mutation from Gly1240 to Ser1240 (NP_008986.2, p.Gly1240Ser) in the RNA_pol_Rpb1_5 domain of POLR3A (Figures 4C,D). The Gly1240 residual was highly conserved in different vertebrate species. This mutation was extremely rare in TOPMED ($n = 158{,}470$, MAF = 0.000016), ExAC ($n = 60{,}706$, MAF = 0.000017), gnomAD ($n = 76{,}156$, MAF = 0.000007), and gnomAD Exomes ($n = 125{,}748$, MAF = 0.000028). Besides, this mutation had been reported in two patients (4H-42 and 4H-67) with 4H leukodystrophy (Wolf et al., 2014). Functional predictions by Polyphen-2 and PROVEAN showed this variant to be "Damaging" (score = 0.995) or "Deleterious" (score = −5.480) to the proper function of POLR3A, respectively. According to the ACMG guidelines, this mutation was classified as "Uncertain Significance" (PM2 + PP5). The structural changes introduced by Gly1240Ser were analyzed by Missense3D according to the cryo-EM structure of human POLR3A protein (7d58, chain A, 2.9 Å resolution). It's revealed that Gly1240 was originally buried in a bend curvature (RAS 0.0%), which could be disrupted by the substitution with the Ser1240 residue (RSA 1.5%). The Serine could form new hydrogen bonds with Arg1104, Thr1238, and Tyr1097 (Figure 4E), which changed the surfaces of the local structure (Figure 4F). The splicing potential of this mutation on the pre-mRNA of POLR3A was evaluated by SpliceAI and obtained negative index (score = 0.00; Supplementary Table S5). The retrieved variant, c.3342C > T (rs183347762) in exon 26 (26/31) of *POLR3A* gene, was inherited paternally. It was synonymous without changing the amino acid Serine at position 1,114 (p.Ser1114=) in the RNA_pol_Rpb1_5 domain of POLR3A protein, and conserved in different species (Figures 4C,D). This variant was extremely rare in the international projects for large human cohorts, such as 1,000 Genomes ($n = 2{,}504$, MAF = 0.000200), TOPMED ($n = 158{,}470$, MAF = 0.000038), ExAC ($n = 60{,}706$, MAF = 0.000036), gnomAD ($n = 76{,}156$, MAF = 0.000043), and gnomAD_exomes ($n = 125{,}748$, MAF = 0.000036). It was assessed to be "Benign" (score = 0.0000) or "Neutral" (score = 0.0000) by Polyphen-2 and PROVEAN, respectively. According to ACMG guidelines, this mutation was annotated as "Likely Benign" (PM2 + BP4 + BP6 + BP7). Although as a synonymous mutation, c.3342C > T was only six nucleotides away from the canonical splicing acceptor site (c.3337-1G, 10:79743771) of the intron 25 (IVS25). SpliceAI displayed negative result (score = 0.00, Supplementary Table S5). The prediction by SPIDEX indicated that this mutation might affect the proper pre-mRNA splicing of *POLR3A* to generate abnormal transcripts. According to the analysis by ESEFinder (version 3.0), the mutated allele (3,342 T) might generate a novel binding site (C**T**GAGTAT) for serine and arginine rich splicing factor 1 (SRSF1), which might affect the splicing pattern or efficiency of *POLR3A*.

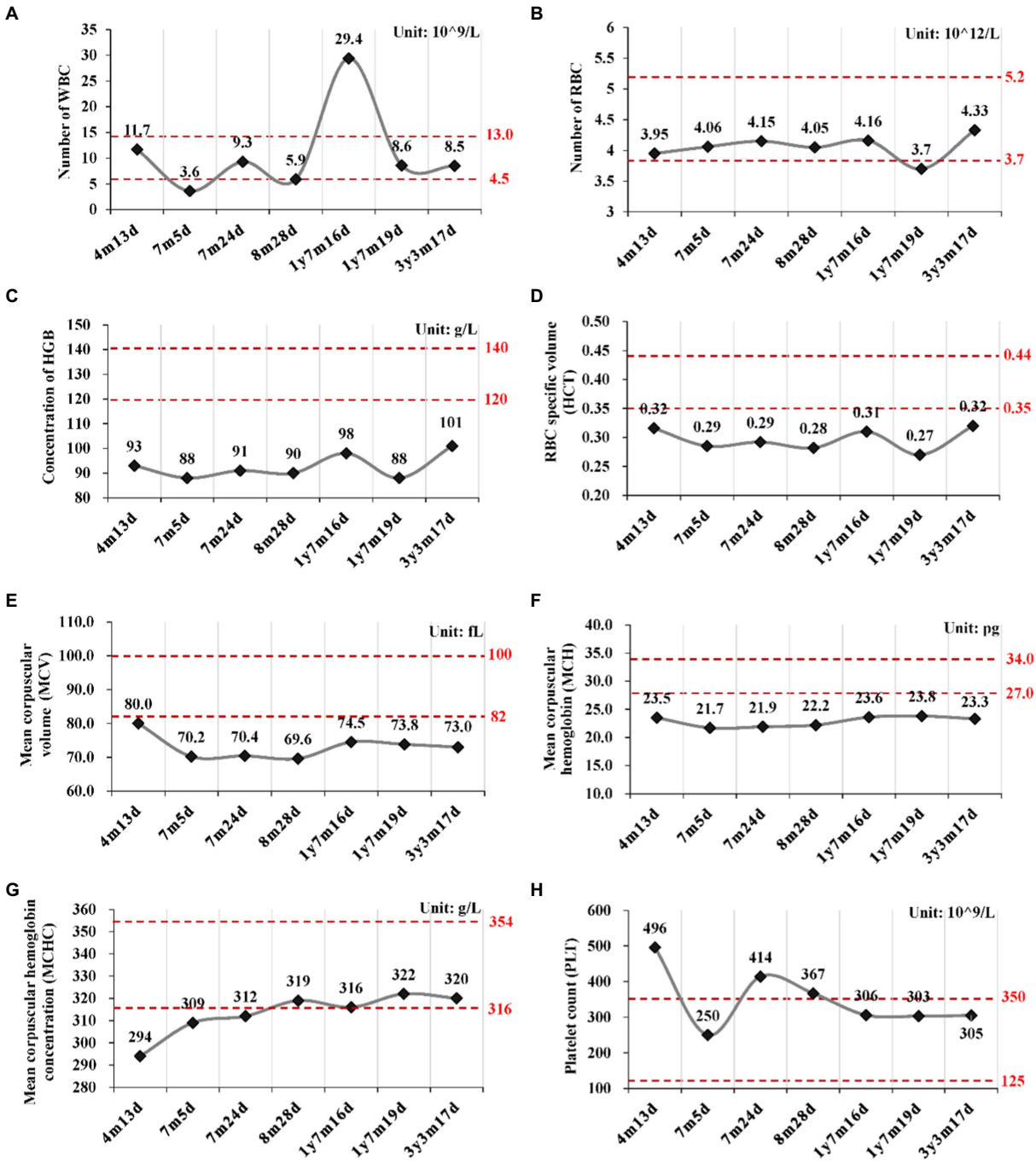

FIGURE 2
Routine blood tests at different time points. **(A)** Number of white blood cell (WBC); **(B)** Number of red blood cell; **(C)** Concentration of hemoglobin (HGB); **(D)** Hematocrit (HCT); **(E)** Mean corpuscular volume (MCV); **(F)** Mean corpuscular hemoglobin (MCH); **(G)** Mean corpuscular hemoglobin concentration (MCHC); **(H)** Platelet count (PLT). y, year; m, month; d, day.

Molecular analysis of the bi-allelic mutations of *FANCA* gene

For the anemia phenotype, two rare mutations in the CDS of *FANCA* gene (NM_000135.4) were detected by trio-WES (Table 1). A single-nucleotide insertion (c.2832dup, 16:89828377) in the exon 29 (29/43) was identified to cause a frameshift to the FANCA protein (p.Ala945CysfsTer6, NP_000126.2; Figures 5A,B). This mutation had been reported in an 8-year-old female patient (Li et al., 2018). However, this mutation had not been identified in any of the four public human genome projects, 1000Genomes, TOPMED, ExAC, gnomAD and

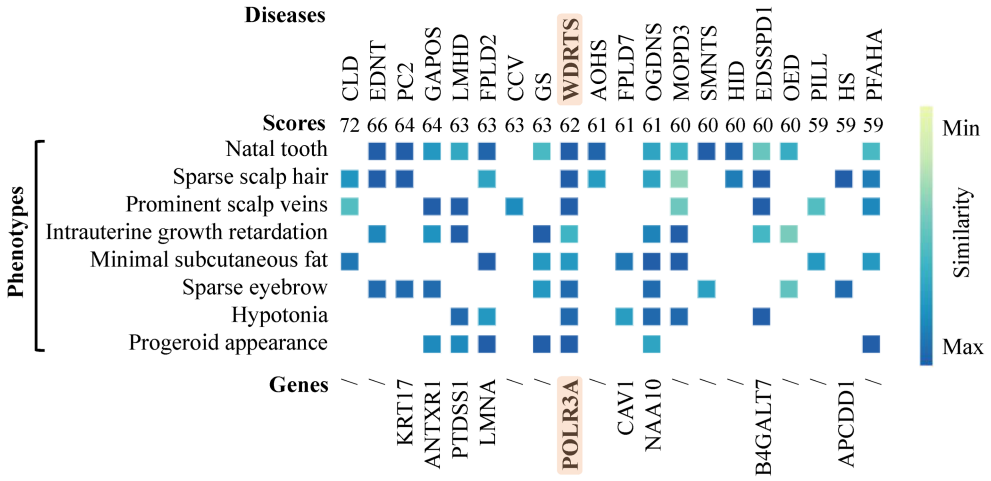

FIGURE 3
Phenotype profile search.

gnomAD_exomes databases. It was poorly conserved in different animal species (Figure 5C). The mutant transcript might be the target of nonsense-mediated mRNA decay (NMD) or encode a putative shortened protein lacking the transmembrane (TM) and C-terminal Fanconi_A domain (Figure 5D). According to ACMG guidelines, this mutation was annotated as "Pathogenic" (PVS1 + PM2 + PP5).

Another mutation in *FANCA*, c.1902 T > G (rs187300458) in exon 22 (22/43), was inherited maternally and changed the amino acid Aspartic acid (Asp., GAT) at position 634 to Glutamic acid (Glu, GAG; p.Asp634Glu; Figures 5A,B,D). This mutation was very rare in 1,000 Genome (n = 2,504, MAF = 0.000200), TOPMED (n = 158,470, MAF = 0.000008), gnomAD (n = 76,156, MAF = 0.000007), and GnomAD_exomes (n = 125,748, MAF = 0.000006). The conservation of this amino acid was very poor in different species (Figure 5C). This variant was predicted to be "Benign" (score = 0.255) or "Neutral" (score = −0.42) to the normal function of FANCA by Polyphen-2 or PROVEAN, respectively. According to ACMG guidelines, this mutation was annotated as "Likely Benign" (PM2 + BP3 + BP4). The structural changes introduced by Asp634Glu were analyzed by Missense3D according to the cryo-EM structure of human FANCA (7kzp, chain A, 3.1 Å resolution) and no structural damage was detected (Figures 5E,F). The c.1902 T > G was only two nucleotides away from the splicing acceptor site (c.1901-1G, 16:89839793, hg19) in intron 21 (IVS21) and might generate a novel putative splicing acceptor site (AT→AG). Negative impact (score = 0.03) of this missense on splicing of FANCA was identified by spliceAI (Supplementary Table S5). According to the prediction by ESEFinder (version 3.0), the mutant allele (1902G) might introduce novel binding sites for SRSF1 (CAGAGGC) and SRSF5 (ACAGAGG), and destroy a binding site for SRSF6 (TGCAGC). Although annotated to be benign, this mutation might affect the splicing pattern or efficiency of *FANCA* gene.

Variants affected pre-mRNA splicing of *POLR3A* and *FANCA*

Minigene reporter assay was carried out to verify the effects of c.3342C > T (*POLR3A*) and c.1902 T > G (*FANCA*) on pre-mRNA splicing. The genomic DNAs containing the selected mutations were cloned into the MCS of pEGFP-N1 and the mutations introduced by site-directed mutagenesis. As for c.3342C > T of *POLR3A*, the 1,646 bp genomic DNA spanning exon 25 to exon 27 (10:79,742,411-79,744,056) was cloned into the MCS (Figures 6A,B). Agarose electrophoresis revealed four different bands in the Mut samples, 435, 300, 243 bp and a short band (150 bp; Figure 6C). Sanger sequencing were carried out for the PCR products of these four bands and the band 300 bp was a non-specific product (pointed by the red arrow). The intensity of band 243 bp in Mut sample was about 70.60% of that in wild-type sample. The other two bands accounted for about 30% (Figure 6D). The band 243 bp was spliced with 3 exons (E25-E26-E27) and contained two types of isoforms, one wild type (Figure 6E) and one with 3,342 T (Figure 6F). The band 150 bp was produced by splicing between exon 25 and 27 to exclude the exon 26 (Figure 6G). In addition to the three consecutive exons, the band 435 bp retained the whole intron 25 (Figure 6H). After aligned all the Sanger-sequenced bands against *POLR3A* reference, three types of aberrant isoforms were revealed (Figure 6I).

For c.1902 T > G of *FANCA* gene, the 4,135 bp genomic DNA from exon 21 to exon 23 (16:89,838,089-89,842,223) was cloned into the MCS of pEGFP-N1 (Figures 7A,B). Agarose electrophoresis revealed a novel short band (175 bp), in addition to the long band (289 bp) in the Mut sample (Figure 7C). However, the staining of the short band was rather weak. Sanger sequencing were carried out for PCR products of the two bands. It is verified that the long band was produced by the consecutive splicing of three exons (E21-E22-E23; Figures 7D,E). The long band in the

TABLE 1 Characterizations of mutations of POLR3A and FANCA.

Genes	Location (GRCh37/hg19)	HGVS annotation	SNP IP	Zygosity P/F/M	ACMG classification	PROVEIN (score)	PolyPhen (score)	Minor allele frequencies (MAF) 1000Genome ($n = 2,504$)	TOPMED ($n = 158,470$)	ExAC ($n = 60,706$)	gnomAD ($n = 76,156$)	gnomAD_Exomes ($n = 125,748$)
POLR3A	10:79,743,765	c.3342C > T (p.Ser1114=)	rs183347762	Het/Het/WT	Likely Benign (PM2 + BP4 + BP6 + BP7)	Neutral 0.000	Benign 0.000	0.000200	0.000038	0.000036	0.000043	0.000036
POLR3A	10:79,741,953	c.3718G > A (p.Gly1240Ser)	rs1003620056	Het/WT/Het	Uncertain significance (PM2 + PP5)	Deleterious −5.480	Damaging 0.944	/	0.000016	0.000017	0.000007	0.000028
FANCA	16:89,839,791	c.1902 T > G (p.Asp634Glu)	rs187300458	Het/WT/Het	Likely Benign (PM2 + BP3 + BP4)	Neutral −0.420	Benign 0.034	0.000200	0.000008	/	0.000007	0.000006
FANCA	16:89,828,377	c.2832dup (p.Ala945CysfsTer6)	Novel	Het/Het/WT	Pathogenic (PVS1 + PM2 + PP5)	/	/	/	/	/	/	

HGVS, Human Genome Variation Society; P, patient; F, father; M, mother; Het, heterozygous; WT, wild type; ACMG, The American College of Medical Genetics and Genomics; PVS, Pathogenic, Very Strong; PM, Pathogenic, Moderate; PP, Pathogenic, Supporting; BP, Benign, Supporting; dup, duplication; Ter, termination.

Mut sample contained the 1902G allele. The short band was spliced between exon 21 and exon 23, excluding exon 22 (Figures 7F,G).

Anemia analysis

Alimentary anemia due to deficiencies of iron, vitamin B12, vitamin D and folic acid was not considered according to relevant biochemical tests (Supplementary Table S6). Regular supplementation of iron for 3 months was ineffective. Trio-WES found no mutations for thalassemia-related genes such as *HBA1* and *HBA2* for α-thalassemia and *HBB* for β-thalassemia (Supplementary Table S1). It had been reported that thalassemia could also be caused by long-fragment deletions, recombinations and mutations in locus control regions (LCRs) involving α- or β-globin genes, which could not be detected by WES. Therefore, a third-generation single molecule real-time (SMRT) sequencing for long-molecules containing thalassemia-related genes were carried out and no mutations were identified (Supplementary Table S7).

The mitomycin C (MMC)-induced chromosome stress assay was carried out for the peripheral blood samples from the patient and her mother, which was refused firmly by her father. After treated with different concentrations of MMC, 100 cells per sample were checked for chromosomal aberrations. However, no significant differences were observed between the two groups (Supplementary Figure S1).

Genomic DNA damages were measured through cell-based alkaline comet assay, which was performed by the single cell gel electrophoresis (SCGE). As shown in Figure 8, after exposure to alkaline lysis solutions, the control lymphocytes (mother) failed to show any comet-like fashion (Figures 8A–C). About 17% of the patient's lymphocytes showed the appearance of an obscure "halo" around the nucleus (Figures 8D–F), but no apoptotic cells were identified. The comet tail length of the patient sample was longer than that of the control (Supplementary Table S8). TailDNA%, TM, and OTM of the patient were much higher than those of her mother ($p < 0.001$), indicating that the level of DNA damage in the patient who carried FANCA mutations was higher than those in the control.

RNA polymerase III was essential for the homologous recombination-dependent repair of DNA double-strand breaks (DSBs) (Liu et al., 2021) and FANCA was involved in inter-strand cross-link repair (Knipscheer et al., 2009). These two genes might act synergistically in this patient. According to the gene expression data of 79 human tissues, *POLR3A* and *FANCA* were co-expressed in many different tissues (Figure 9A). Ten proteins involving POLR3A and FANCA could form a stringed network (PPI enrichment *value of* $p = 5.92E-10$). The network showed that POLR3A could interact directly with POLR3B, POLR1A, POLR2F, and POLR2L to form a multi-subunit RNA polymerase complex possessing the DNA-directed 5′-3′ RNA polymerase activity (FDR = 4.63E-08; Figure 9B). FANCA could bind directly with

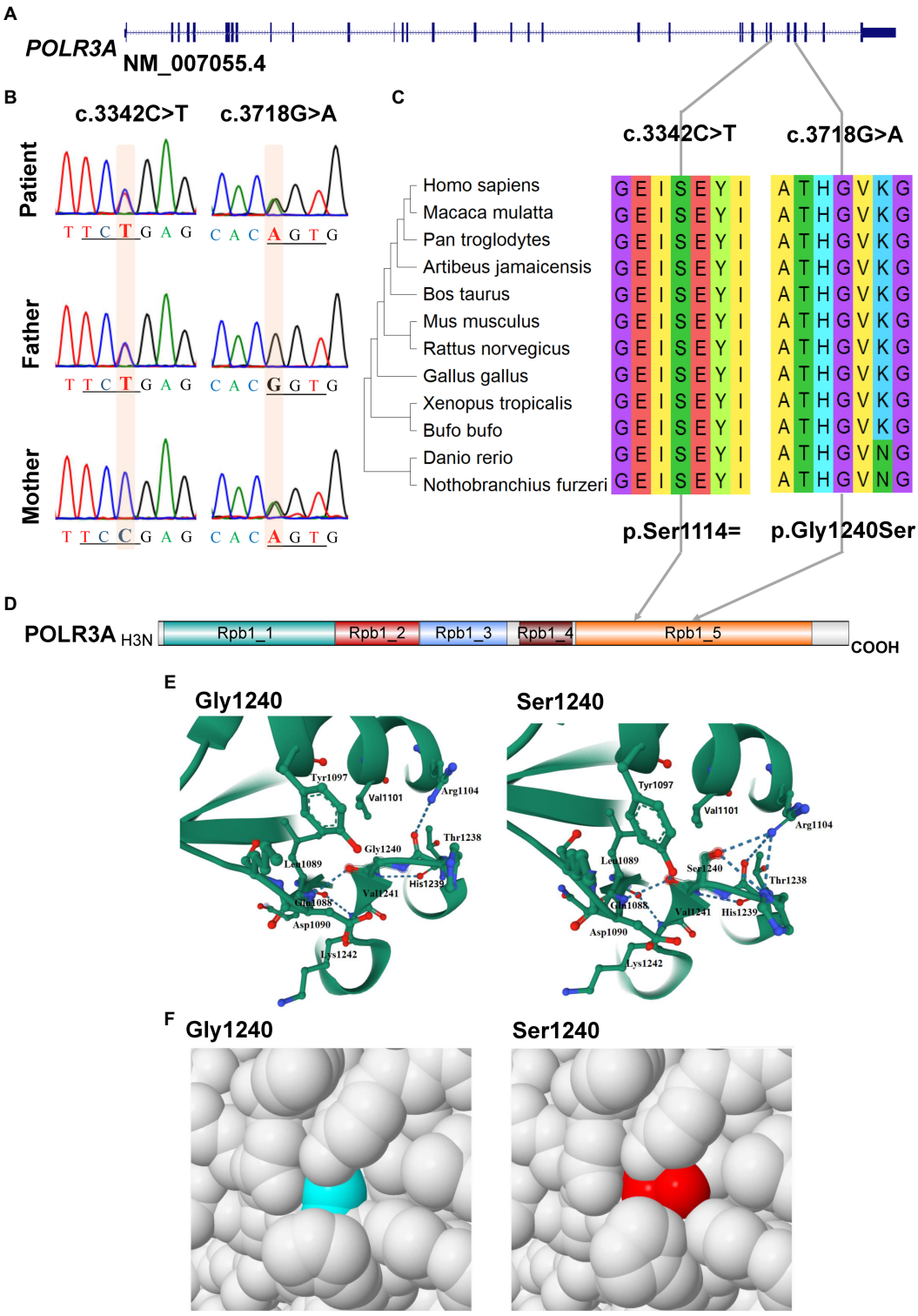

FIGURE 4
Characterization of mutations in *POLR3A* gene. **(A)** Diagram of genomic structure of *POLR3A*; **(B)** Sanger sequencing of the mutations; **(C)** Conservation analysis; **(D)** Diagram of protein structure of POLR3A; **(E)** 3-D structure of POLR3A; **(F)** Spacefill model.

BRCA1, which was an important component of the BRCA1-A complex (BRCA1, BARD1, BABAM1, and BRE; FDR = 1.92E-08). Interestingly, through the nodes of BRCA1 and POLR2F, FANCA could be stringed with POLR3A. Although all of the 10 proteins were involved in the nucleic acid metabolic process (FDR = 3.84E-06; Figure 9C), the synergistic function of FANCA on RNA

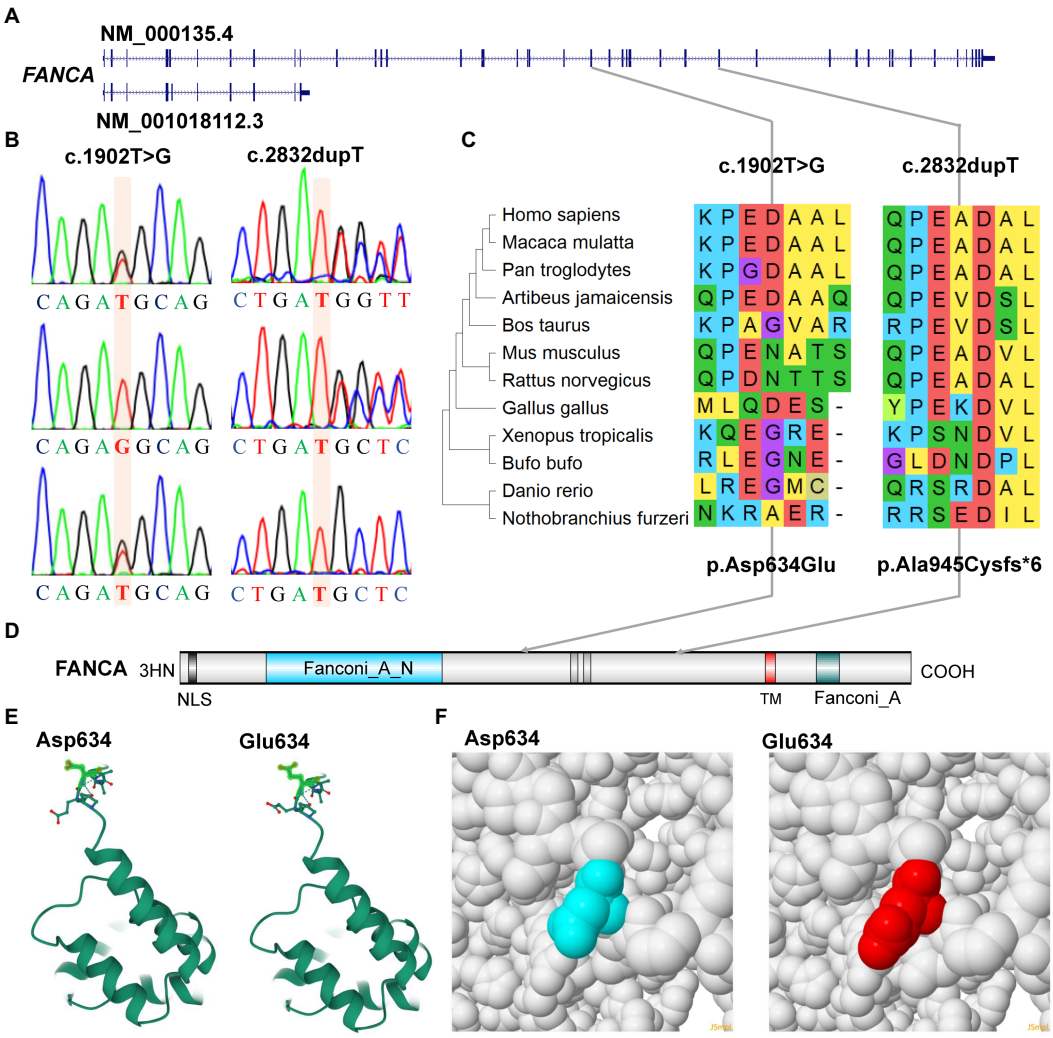

FIGURE 5
Characterization of mutations of *FANCA* gene. **(A)** Diagram of genomic structure of FANCA; **(B)** Sanger sequencing of the mutations; **(C)** Conservation of the mutations in different vertebrates; **(D)** Diagram of protein structure of FANCA; **(E)** 3-D structure of FANCA; **(F)** Space-filling model.

polymerization III or *vise verse* was remained for further exploration.

Discussion

The gene *POLR3A* is located on chromosome 10q22.3, with 31 exons to encode a protein of 1,391 amino acid having a molecular mass of 154.7 kilodaltons. POLR3A is the largest catalytic subunit of the DNA-directed RNA polymerase III complex, which transcribes genes responsible for many small non-coding RNAs (ncRNAs), such as ribosomal 5S RNA, tRNAs, U6 small nuclear RNA, RNA components of mitochondrial RNA processing endoribonuclease (RMRP), ribonuclease P RNA component H1 (RPPH1), Ro60-associated RNA Y1 (RNY1), RNA component of signal recognition particle 7SL1 (RN7SL1) and RNA component of 7SK nuclear ribonucleoprotein (RN7SK). Some of these ncRNAs, such as RN7SL1 and RN7SK, regulate the activity of DNA-dependent RNA polymerase II, hence POLR3A mutations can also affect expression levels of polymerase II-transcribed genes (Azmanov et al., 2016; Flynn et al., 2016; Egloff et al., 2018). POLR3A also acts as a sensor to detect foreign viral DNAs and triggers an innate immune response (Ablasser et al., 2009). Recently, it has been reported that RNA polymerase III is an essential factor in the homologous recombination-dependent repair of DNA double-strand breaks (DSBs; Liu et al., 2021; Liu and Kong, 2021). Inhibition of POLR3A (also called Rpc1) could lead to the loss of genes in the DSB regions (Liu et al., 2021). Since POLR3A is ubiquitously expressed, the disability of this gene might be fatal to the prenatal and postnatal development of many systems.

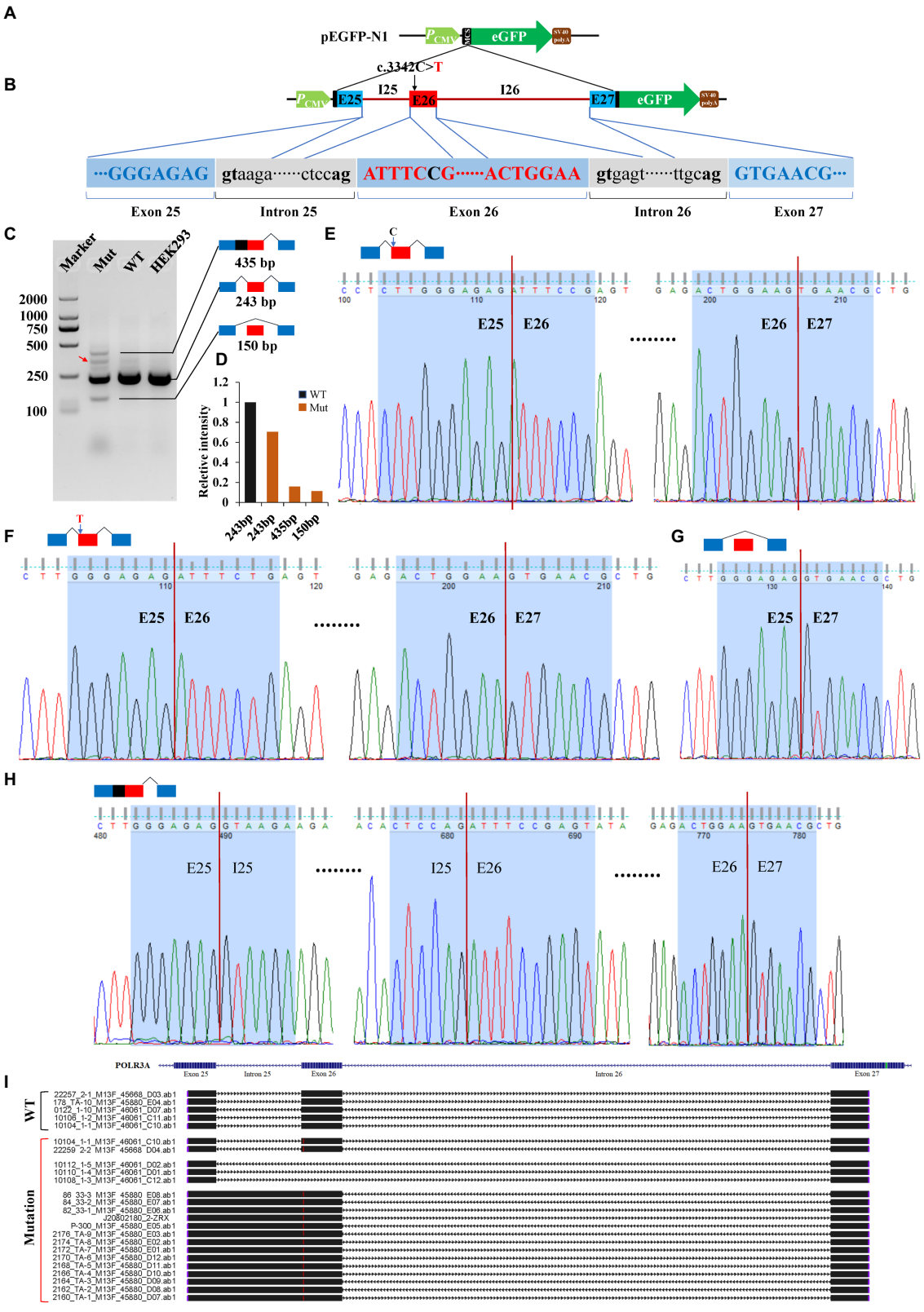

FIGURE 6
Minigene reporter assay for 3,342C>T in *POLR3A*. **(A)** Diagram of pEGFP-N1; **(B)** Positions of mutations; **(C)** Gel electrophoresis; **(D)** Intensity of bands; **(E)** Sanger sequencing for band 243 bp with 3,342C; **(F)** Sanger sequencing for band 243 bp with 3,342 T; **(G)** Sanger sequencing for band 150 bp; **(H)** Sanger sequencing for band 435 bp; **(I)** Alignment for sequenced PCR products. Red arrow indicates a non-specific band. WT, Wild type; Mut, Mutation; E, Exon; I, Intron.

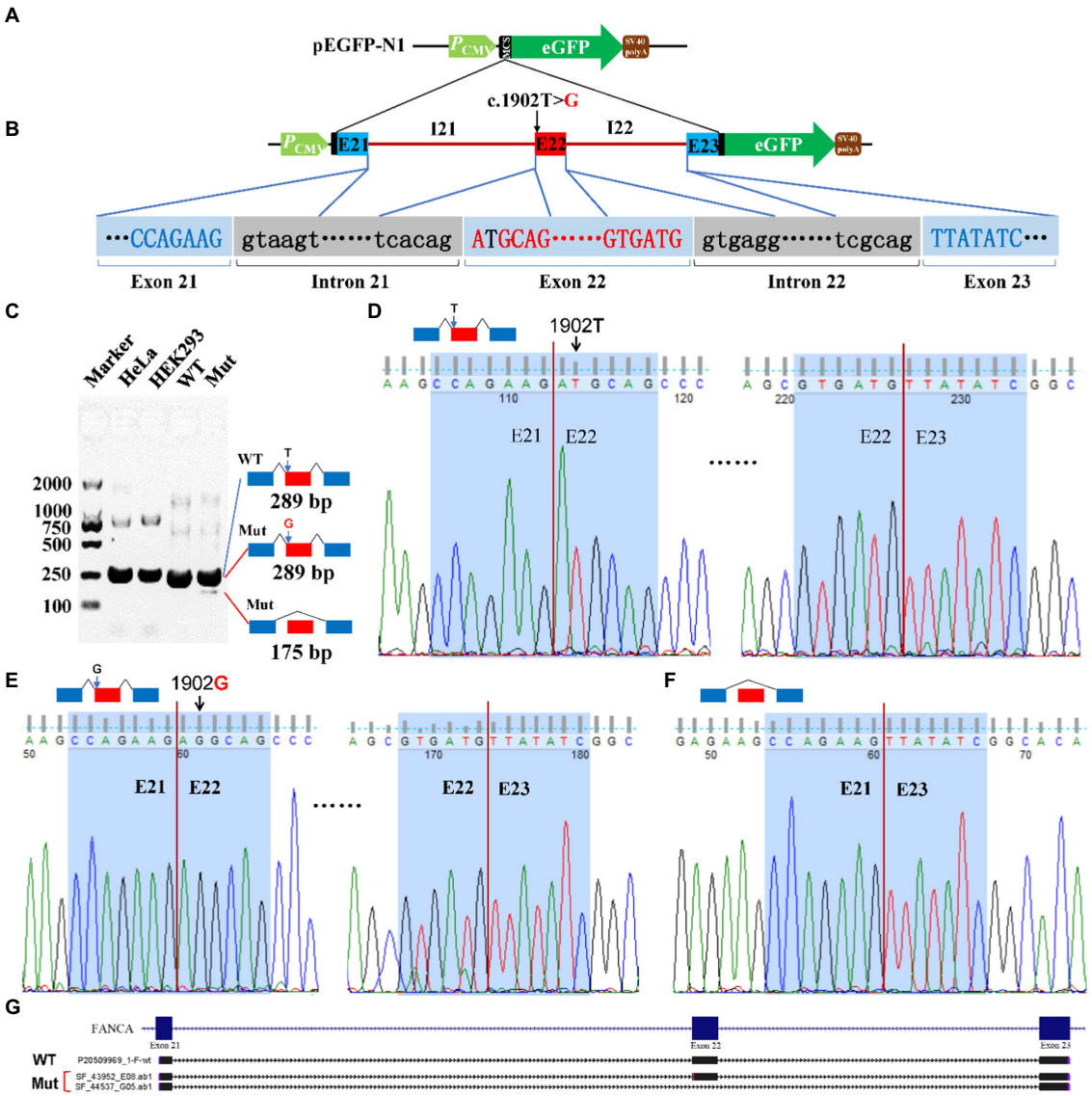

FIGURE 7
Minigene reporter assay for 1,902T>G in *FANCA*. **(A)** Diagram of pEGFP-N1; **(B)** Positions of mutations; **(C)** Gel electrophoresis; **(D)** Sanger sequencing for the band 289 bp with 1,902T; **(E)** Sanger sequencing for the band 289 bp with 1,902G; **(F)** Sanger sequencing for the band 175 bp; **(G)** Alignment for sequenced PCR products. WT, Wild type; Mut, Mutation; E, Exon; I, Intron.

It had been reported that pathologic homozygous or bi-allelic heterozygous mutations in *POLR3A* could cause the occurrence of Wiedemann-Rautenstrauch syndrome (WDRTS; Paolacci et al., 2018) or Hypomyelinating leukodystrophy 7 (HLD7, OMIM# 607694) (Bernard et al., 2011) under an autosomal recessive (AR) mode of inheritance. WDRTS was one of the rare disorders having neonatal progeroid phenotype. The others included fontaine progeroid syndrome (FPS, OMIM#612289) (Writzl et al., 2017), autosomal recessive cutis laxa type IIIA (ARCL3A, OMIM#219150), and some forms of Marfan syndrome (MFS; Graul-Neumann et al., 2010; Takenouchi et al., 2013; Garg and Xing, 2014; Jacquinet et al., 2014). These syndromes had some characteristics similar to WDRTS. Besides, the clinical phenotypes of WDRTS were highly variable involving many systems. In addition, a variant of WDRTS was reported to have some atypical WDRST features (such as no lipodystrophy, no natal teeth and no sparse scalp hair), which was caused by a homozygous mutation in *POLR3GL* (c.358C > T, p.Arg120Ter) (Beauregard-Lacroix et al., 2020). These factors together made it difficult to accurately discriminate the WDRTS from other disorders having similar phenotypes. After checking clinical presentations of the above-mentioned syndromes, patients affected with WDRTS had neonatal tooth or teeth abnormalities, those with other neonatal progeroid phenotypes did not. It seemed that neonatal tooth might be an essential marker to discriminate WDRTS from other disorders having progeroid facial features.

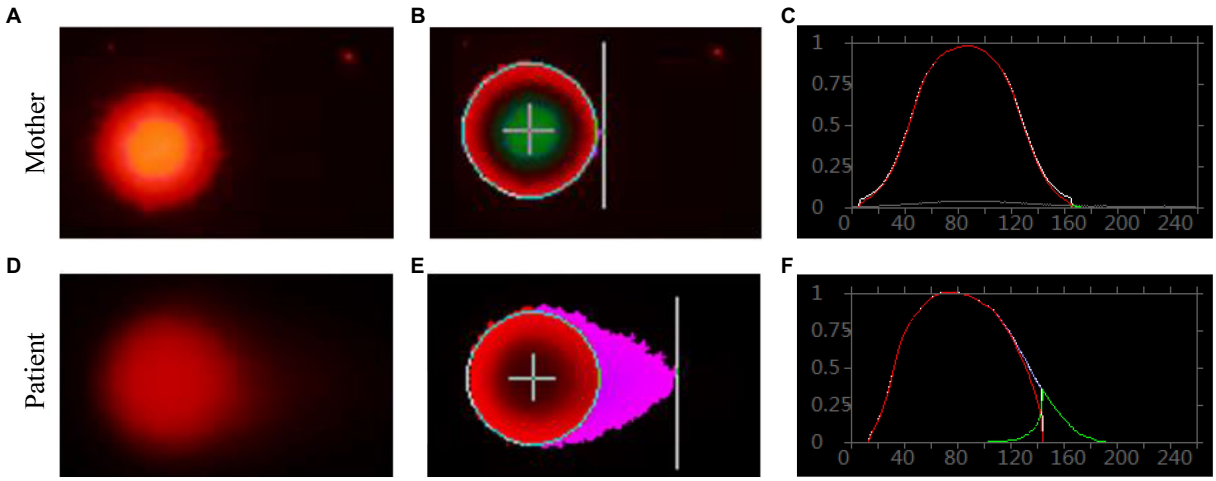

FIGURE 8
Single cell gel electrophoresis assay. Comet image of single lymphocyte from her mother **(A)**, and the patient **(D)**; CASP-analyzed comet image of single lymphocyte from her mother **(B)**, and the patient **(E)**; CASP analysis for her mother **(C)**, and the patient. **(F)** STRING network analysis involving POLR3A and FANCA.

For our patient, she carried bi-allelic mutations in the CDS of *POLR3A* (c.3342C > T, p.Ser1114 = and c.3718G > A, p.Gly1240Ser). Except for c.3718G > A (p.Gly1240Ser) which could affect the structural conformation of POLR3A protein, the synonymous variant (c.3342C > T, p.Ser1114=) could lead to three types of abnormally spliced isoforms. The isoform 243 bp was consecutively spliced with three exons and carried the mutant allele. The isoform 435 bp was generated by the retention of intron 25, plus the three consecutive exons. After analyzed by Open Reading Frame Finder (ORF Finder), there was a premature stop codon in the intron 25 and might be translated into an aberrant protein (p.Glu1112GlufsTer7) or degraded by the nonsense-mediated mRNA decay (NMD; Lykke-Andersen and Jensen, 2015; Karousis and Muhlemann, 2019). As for the short isoform 150 bp, it only contained two exons (exon 25 and 27). Since the length of exon 26 was 93 base pairs (a multiple of three), the CDS of *POLR3A* should be left intact but missing 31 amino acids (aa1113-1,143) in the RNA_pol_Rpb1_5 domain (aa841-1,315). There were 4 missense mutations in the excluded exon 26 which were recruited in the NCBI ClinVar database, c.3350 T > C (p.Ile1117Thr), c.3388G > A (p.Val1130Ile), c.3392A > G (p.Lys1131Arg) and c.3407G > A (p.Arg1136Gln). These mutations were identified in patients with WDRTS or HLD7. In addition, c.3392A > G (p.Lys1131Arg) had been reported in a Caucasian WDRTS patient by targeted parallel sequencing (Paolacci et al., 2018). This indicated that the excluded region might be important for the function of POLR3A. Since also having core clinical phenotypes of WDRTS (Paolacci et al., 2017), the female proband was finally diagnosed as WDRTS caused by bi-allelic mutations in *POLR3A*. According to the mini-gene reporter assay, there were about 70% full-length wild-type and synonymous-containing transcripts. This indicated that a pathogenic hierarchy might be related to the two mutations. The missense mutation, c.3718G > A (p.Gly1240Ser), was the major contributor to the clinical presentations of our patient, with c.3342C > T (p.Ser1114=) as the minor one.

Except for missense, nonsense, frameshifting, and mutations disrupting canonical splicing sites, there were 10 intronic mutations to affect pre-mRNA splicing of *POLR3A* (Hiraide et al., 2020), such as c.645 + 312C > T (Hiraide et al., 2020), c.1048 + 5G > T (Minnerop et al., 2017), c.1770 + 5G > C (Yan et al., 2021), c.1771-6C > G (Rydning et al., 2019; Wu et al., 2019), c.1771-7C > G (Minnerop et al., 2017), c.1909 + 22G > A (Minnerop et al., 2017; Morales-Rosado et al., 2020), c.1909 + 18G > A (Lessel et al., 2018), c.2003 + 18G > A (Bernard et al., 2011), c.3337-5 T > A (Lessel et al., 2018; Wambach et al., 2018), c.3337-11 T > C (Wambach et al., 2018). Among them, c.1909 + 22G > A was the most commonly reported mutations. However, synonymous variants affecting the pre-mRNA splicing of POLR3A were rarely reported. Till now, only one homozygous synonymous (c.3336G > A, p.Glu1112=) has been reported to generate two types of abnormal splicing isoforms, one with the retention of intron 25, and another with the exclusion of exon 25 (Lessel et al., 2022). Our patient was the second report of a synonymous variant to affect the pre-mRNA splicing of POLR3A.

In order to have a comprehensive view of the phenotypes of WDRTS and HLD7, a literature review was made. Features of craniofacial dysmorphism and soft tissues were exclusively confined to WDRTS (Figures 10A,B). However, the majority of the abnormal phenotypes in central nervous system were mainly found in patients suffering from HLD7 (Figure 10B). The reported mutations of POLR3A in WDRTS and HLD7 were compiled and arranged according to their genomic position. To our surprise, there were a few different "hot spots" between WDRTS and HLD7. Mutations in intron 13, exon 19 and exon 28 were almost exclusively related to HLD7. For WDRTS, most of the mutations

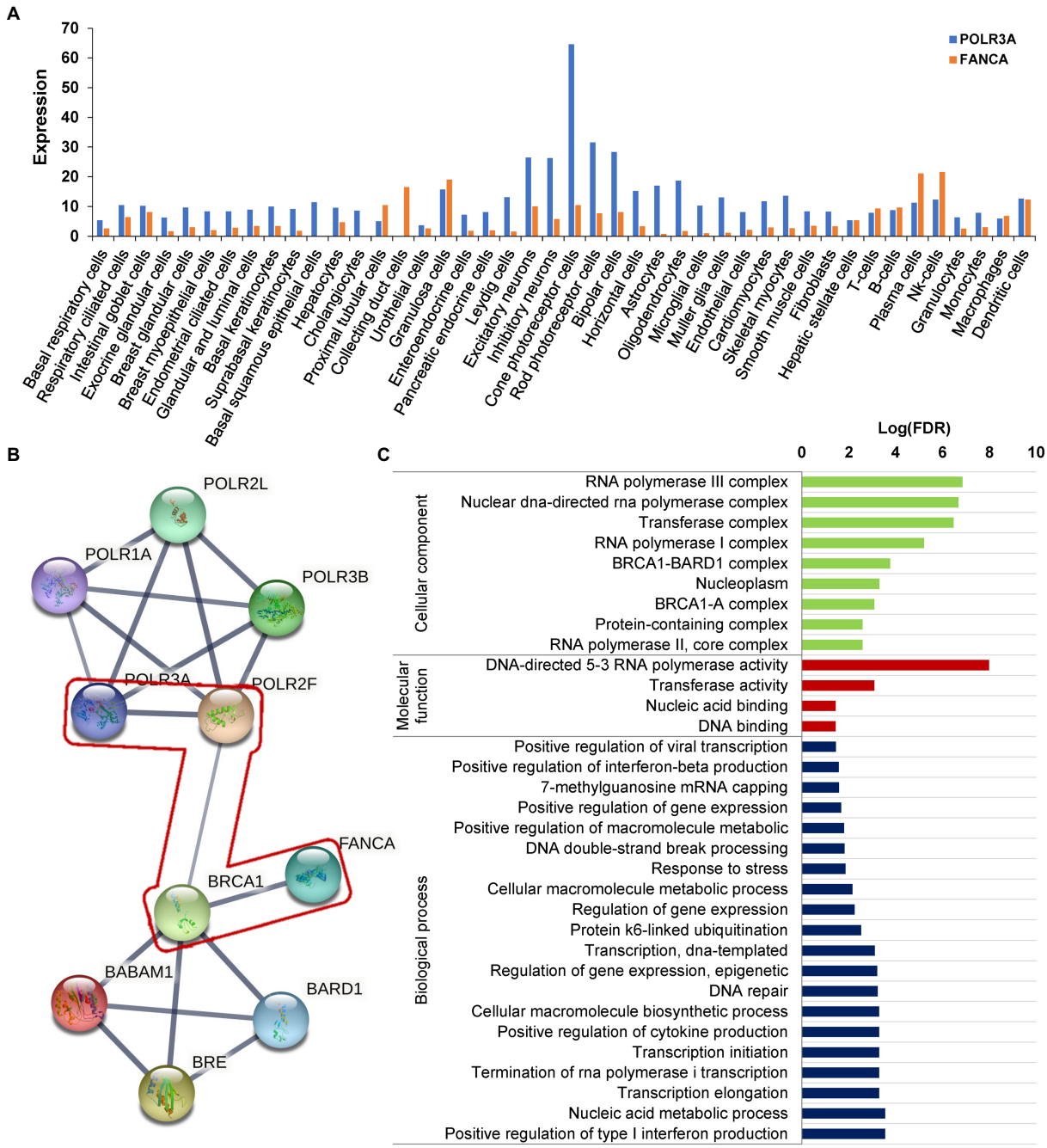

FIGURE 9
Protein network analysis of POLR3A and FANCA. **(A)** Expression in different human tissues; **(B)** STRINGed Network of POLR3A and FANCA; **(C)** GO analysis of the members of the network.

were distributed in exon 1, exon 6, intron 25 and 3'-UTR, with intron 25 as the highest (Figure 10C). For our patient, the splicing-altering mutation c.3342C > T was located at the junction between exon 25 and intron 25. It seemed that the aberrant pre-mRNA splicing at intron 25 might be correlated with the occurrence of WDRTS.

Efforts to establish animal models with Polr3a mutation had been tried in mice, but had not been successful. It had been reported that double knockout (KO) of polr3a in mice was embryonically lethal (Choquet et al., 2019). Furthermore, no neurological or developmental abnormalities were identified in mice with whole-body homozygous knock-in (KI/KI) or heterozygous KI/KO of the pathogenic c.2015G > A (p.Gly672Glu) mutation of polr3a (Choquet et al., 2017). For RNA polymerase III (POLR3) in animals, it composed of 17 subunits to form a catalytic core, the stalk domain and Pol

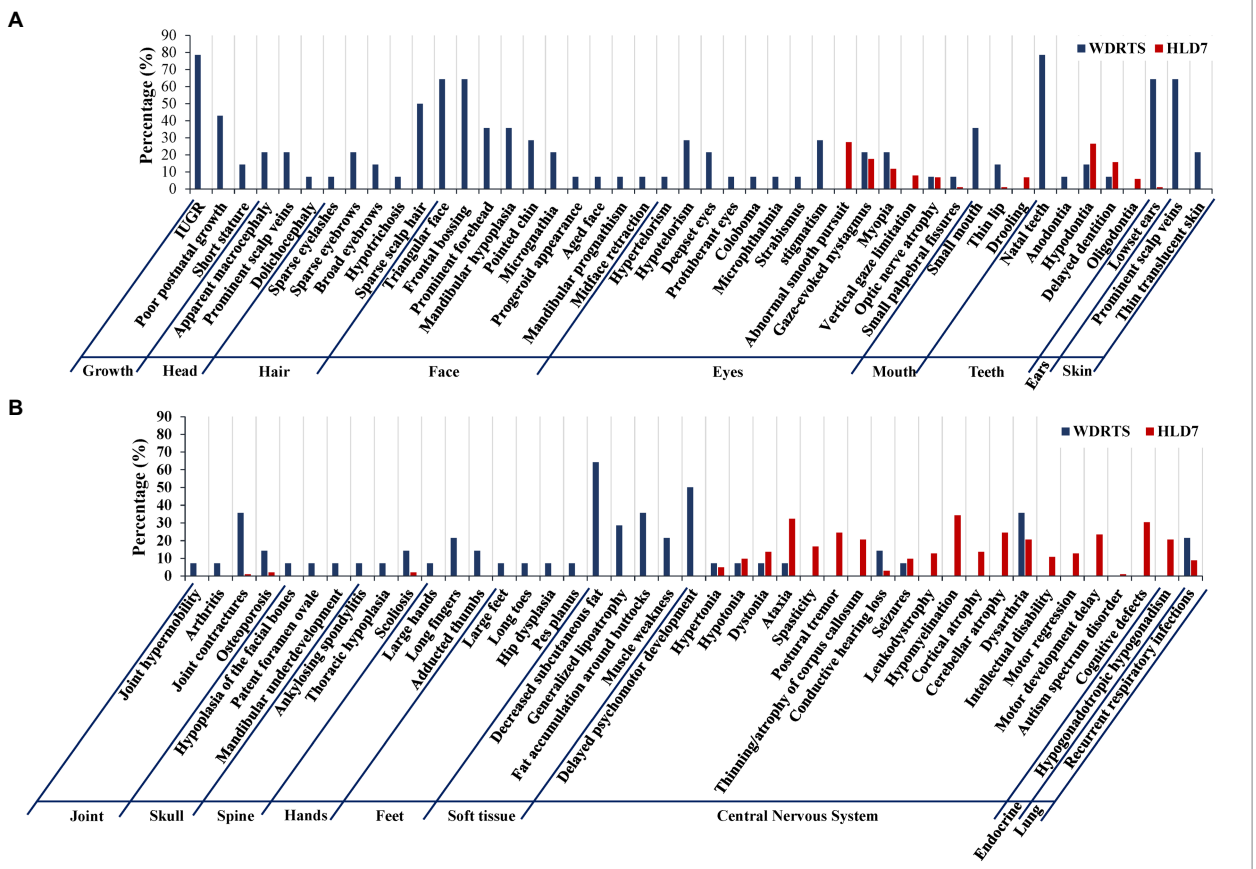

FIGURE 10
Phenotype and genotype analysis for WDRTS and HLD7. **(A,B)** Phenotypes in different organs; **(C)** Distributions of mutations in exons and introns of POLR3A. E, exon; I, intron. UTR, untranslated region.

III-specific subcomplexes (Vannini and Cramer, 2012; Girbig et al., 2021). Till now, only six of 17 subunits (35.29%) were reported to be the causal for a spectrum of rarely inherited disorders. Mutations in *POLR3A* were responsible for WDRTS or HLD7 (Bernard et al., 2011; Wambach et al., 2018), *POLR3B* for HLD8 (OMIM#614381; Saitsu et al., 2011), *POLR1C* for HLD11 (OMIM#616494) (Thiffault et al., 2015), *POLR3K* for HLD21 (OMIM#619310) (Dorboz et al., 2018), *POLR3GL* for short stature, oligodontia, dysmorphic facies, and motor delay (SOFM, OMIM#619234; Terhal et al., 2020) and *POLR3H* for primary ovarian insufficiency (POI; Franca et al., 2019). Since only 35.29% of the members of POLR3 could be related to inheritable disorders, there might be a functional redundancy among other subunits.

Inferred from the time-coursed routine blood testing, the patient had a moderate level of anemia. The anemia belonged to small cell hypochromic anemia, similar to iron deficiency anemia or thalassemia. However, the concentrations of serum ferritin, vitamin B12, folic acid and vitamin D were within a normal range, indicating that the anemia might be caused by other unknown reasons. Through trio-WES, two mutations were identified in the CDS of *FANCA*, a causal gene for Fanconi anemia of complementation group A (FANCA, OMIM#227650). No mutations were identified in genes responsible for thalassemia by trio-WES and the third-generation SMRT sequencing. For *FANCA*, the pathogenic insertion (c.2832dup) in exon 29 introduced a premature termination codon (PTC), which caused a frameshift of the FANCA protein (p.Ala945CysfsTer6) or

rendered the resultant transcripts to be rapidly degraded by NMD. Another missense mutation (c.1902 T > G, p.Asp634Glu) was predicted to be benign. After carefully analyzing the genomic sequence containing c.1902 T > G, it was only two nucleotides away from the canonical splicing acceptor site (SA1, c.1901-1_1901–2, AG) in intron 21. The mutation might introduce a potential splicing acceptor site (SA2, c.1902_1903, AG) juxtaposed with SA1. Minigene reporter assay identified two types of aberrant isoforms. One carried the 1902G and translated into a full-length FANCA protein with Glu634. The other isoform was produced by splicing between exon 21 and 23 to exclude exon 22, but at a very low level. Since the length of exon 22 was 114 base pairs (a multiple of three), the CDS of *FANCA* should be left intact but missing 38 amino acids (aa634-672). However, the function of this region was not clear. There were seven pathogenic mutations in this excluded region recruited in the ClinVar database, namely, c.1912G > T (p.Gly638Ter), c.1944del (p.Glu648AspfsTer13; Levran et al., 1997), c.1951G > T (p.Gly651Ter), c.1979 T > C (p.Leu660Pro; Ameziane et al., 2008), c.1981A > T (p.Arg661Ter), c.2001dup (p.Ser668GlnfsTer4; Moghrabi et al., 2009), and c.2005C > T (p.Gln669Ter). This indicated that the excluded region was important for the function of FANCA protein. According to the mini-gene reporter assay, there were more than 80% full-length wild-type and missense-containing transcripts. A pathogenic hierarchy might be related to the two mutations. The frameshift mutation, c.2832dup (p.Ala945CysfsTer6), was the major contributor to the clinical presentations of our patient, with the missense c.1902 T > G (p.Asp634Glu) as the minor one. This indicated that there might be a delicate balance between wild-type and mutated transcripts to prevent the occurrence of macroscopic clinical phenotypes.

In order to verify the phenotype of Fanconi's anemia (FA), mitomycin C-induced chromosome stress (MMC) assay and single cell gel electrophoresis (SCGE) assay were performed for blood samples from the patient and her mother. MMC assay detected no significant chromosome aberrations. For SCGE assay, good-shaped comets were observed in the patient's sample, indicating that the genomic DNA was seriously damaged. This implied that the patient might suffer from a mild type of FA without obvious classical phenotypes.

To our knowledge, this was the first report of a patient with a rare Wiedemann-Rautenstrauch syndrome (WDRTS) complicated with another recessive disorder, Fanconi anemia of complementation group A (FANCA). It had been reported that both POLR3A and FANCA were involved in the homologous recombination-dependent repair of DNA double-strand breaks (DSBs) (Liu et al., 2021; Liu and Kong, 2021) and inter-strand DNA cross-link repair (Howard et al., 2015; Benitez et al., 2018) to maintain the chromosome stability. A network analysis showed that POLR3A could be STRINGed with FANCA *via* two nodes of BRCA1 and POLR2F (Krum et al., 2003; Lane, 2004). It is implied that both proteins might act synergistically to contribute to the complexity of clinical phenotypes. This should be verified by further cellular and model animal experiments.

Conclusion

Generally, a WDRTS patient was identified to have rare bi-allelic compound mutations in *POLR3A*, one damaging missense and one synonymous. The synonymous mutation could affect the pre-mRNA splicing of *POLR3A* and should be pathogenic. It generated about 30% of aberrantly splicing transcripts. As for the anemia phenotype, the predicted benign missense mutation 1902 T > G could generate a small proportion of abnormally spliced isoform of FANCA. The expressed ratio between the aberrant and wild type isoforms might be correlated to the severity of the disease. Even patients carrying same splicing-altering mutations presented different phenotypes, other unidentified regulatory polymorphisms might be the modifying factors for the different penetration. Since the detrimental level of mutations vary greatly, different combinations of these mutations might be one of the underlying mechanisms for the varied clinical phenotype penetrance and prognosis. It might be very useful for clinical genetic consultors to have a comprehensive analysis for the relationship between genetic factors and clinical features.

Data availability statement

The datasets presented in this study can be found in online repositories. The names of the repository/repositories and accession number(s) can be found in the article/Supplementary material.

Ethics statement

The studies involving human participants were reviewed and approved by Ethical Committee of the Shenzhen Baoan Women's and Children's Hospital. Written informed consent to participate in this study was provided by the participants' legal guardian/next of kin.

Author contributions

GL and QP designed the study. GL and YZ analyzed gnomic data. QP, BX, JD, ZX, and BD provided phenotype information. QP and BD performed followup inquiries. LW, WD, DL, and JW performed the minigene reporter assay, SCGE assay, and MMC assay. GL wrote the manuscript. GL, XH, and QP revised the manuscript. All authors contributed to the article and approved the submitted version.

Funding

This work was supported by fundings from the Science and Technology Research and Development Foundation of Shenzhen (JCYJ20180305164359668), Natural Science Foundation of Sichuan (2022NSFSC0714), Key Research and Development

Project of Deyang science and Technology Bureau (2021SZ003 and 2020SZZ085), and Special Fund for Incubation Projects of Deyang People's Hospital (FHG202004).

Acknowledgments

The authors appreciate the assistance from the families and referring doctors who participated in this study.

Conflict of interest

The authors declare that the research was conducted in the absence of any commercial or financial relationships that could be construed as a potential conflict of interest.

Publisher's note

All claims expressed in this article are solely those of the authors and do not necessarily represent those of their affiliated organizations, or those of the publisher, the editors and the reviewers. Any product that may be evaluated in this article, or claim that may be made by its manufacturer, is not guaranteed or endorsed by the publisher.

Supplementary material

The Supplementary material for this article can be found online at: https://www.frontiersin.org/articles/10.3389/fnmol.2022.1026530/full#supplementary-material

References

Ablasser, A., Bauernfeind, F., Hartmann, G., Latz, E., Fitzgerald, K. A., and Hornung, V. (2009). RIG-I-dependent sensing of poly(dA:dT) through the induction of an RNA polymerase III-transcribed RNA intermediate. *Nat. Immunol.* 10, 1065–1072. doi: 10.1038/ni.1779

Adzhubei, I., Jordan, D. M., and Sunyaev, S. R. (2013). Predicting functional effect of human missense mutations using PolyPhen-2. *Curr. Protoc. Hum. Genet.* 7:Unit7.20. doi: 10.1002/0471142905.hg0720s76

Ameziane, N., Errami, A., Léveillé, F., Fontaine, C., de Vries, Y., van Spaendonk, R. M. L., et al. (2008). Genetic subtyping of Fanconi anemia by comprehensive mutation screening. *Hum. Mutat.* 29, 159–166. doi: 10.1002/humu.20625

Auwera, G. A., Carneiro, M. O., Hartl, C., Poplin, R., del Angel, G., Levy-Moonshine, A., et al. (2013). From FastQ data to high confidence variant calls: the genome analysis toolkit best practices pipeline. *Curr. Protoc. Bioinformatics* 43:11 10 11-11 10 33. doi: 10.1002/0471250953.bi1110s43

Azmanov, D. N., Siira, S. J., Chamova, T., Kaprelyan, A., Guergueltcheva, V., Shearwood, A. M. J., et al. (2016). Transcriptome-wide effects of a POLR3A gene mutation in patients with an unusual phenotype of striatal involvement. *Hum. Mol. Genet.* 25, 4302–4314. doi: 10.1093/hmg/ddw263

Barnett, D. W., Garrison, E. K., Quinlan, A. R., Stromberg, M. P., and Marth, G. T. (2011). BamTools: a C++ API and toolkit for analyzing and managing BAM files. *Bioinformatics* 27, 1691–1692. doi: 10.1093/bioinformatics/btr174

Beauregard-Lacroix, E., Salian, S., Kim, H., Ehresmann, S., D'Amours, G., Gauthier, J., et al. (2020). A variant of neonatal progeroid syndrome, or Wiedemann-Rautenstrauch syndrome, is associated with a nonsense variant in POLR3GL. *Eur. J. Hum. Genet.* 28, 461–468. doi: 10.1038/s41431-019-0539-6

Benitez, A., Liu, W., Palovcak, A., Wang, G., Moon, J., An, K., et al. (2018). FANCA promotes DNA double-Strand break repair by Catalyzing single-Strand annealing and Strand exchange. *Mol. Cell* 71, 621–628.e4. doi: 10.1016/j.molcel.2018.06.030

Bernard, G., Chouery, E., Putorti, M. L., Tétreault, M., Takanohashi, A., Carosso, G., et al. (2011). Mutations of POLR3A encoding a catalytic subunit of RNA polymerase pol III cause a recessive hypomyelinating leukodystrophy. *Am. J. Hum. Genet.* 89, 415–423. doi: 10.1016/j.ajhg.2011.07.014

Bogliolo, M., and Surralles, J. (2015). Fanconi anemia: a model disease for studies on human genetics and advanced therapeutics. *Curr. Opin. Genet. Dev.* 33, 32–40. doi: 10.1016/j.gde.2015.07.002

Choi, Y., and Chan, A. P. (2015). PROVEAN web server: a tool to predict the functional effect of amino acid substitutions and indels. *Bioinformatics* 31, 2745–2747. doi: 10.1093/bioinformatics/btv195

Choquet, K., Pinard, M., Yang, S., Moir, R. D., Poitras, C., Dicaire, M. J., et al. (2019). The leukodystrophy mutation Polr3b R103H causes homozygote mouse embryonic lethality and impairs RNA polymerase III biogenesis. *Mol. Brain* 12:59. doi: 10.1186/s13041-019-0479-7

Choquet, K., Yang, S., Moir, R. D., Forget, D., Larivière, R., Bouchard, A., et al. (2017). Absence of neurological abnormalities in mice homozygous for the Polr3a G672E hypomyelinating leukodystrophy mutation. *Mol. Brain* 10:13. doi: 10.1186/s13041-017-0294-y

D'Andrea, A. D. (2010). Susceptibility pathways in Fanconi's anemia and breast cancer. *N. Engl. J. Med.* 362, 1909–1919. doi: 10.1056/NEJMra0809889

D'Andrea, A. D., and Grompe, M. (2003). The Fanconi anaemia/BRCA pathway. *Nat. Rev. Cancer* 3, 23–34. doi: 10.1038/nrc970

Dimishkovska, M., Kotori, V. M., Gucev, Z., Kocheva, S., Polenakovic, M., and Plaseska-Karanfilska, D. (2018). Novel founder mutation in FANCA gene (c.3446_3449dupCCCT) among Romani patients from the Balkan region. *Balkan Med. J.* 35, 108–111. doi: 10.4274/balkanmedj.2017.0618

Dorboz, I., Dumay-Odelot, H., Boussaid, K., Bouyacoub, Y., Barreau, P., Samaan, S., et al. (2018). Mutation in POLR3K causes hypomyelinating leukodystrophy and abnormal ribosomal RNA regulation. *Neurol. Genet.* 4:e289. doi: 10.1212/NXG.0000000000000289

Egloff, S., Studniarek, C., and Kiss, T. (2018). 7SK small nuclear RNA, a multifunctional transcriptional regulatory RNA with gene-specific features. *Transcription* 9, 95–101. doi: 10.1080/21541264.2017.1344346

Ehmke, N., Graul-Neumann, L., Smorag, L., Koenig, R., Segebrecht, L., Magoulas, P., et al. (2017). De novo mutations in SLC25A24 cause a Craniosynostosis syndrome with Hypertrichosis, Progeroid appearance, and mitochondrial dysfunction. *Am. J. Hum. Genet.* 101, 833–843. doi: 10.1016/j.ajhg.2017.09.016

Elouej, S., Beleza-Meireles, A., Caswell, R., Colclough, K., Ellard, S., Desvignes, J. P., et al. (2017). Exome sequencing reveals a de novo POLD1 mutation causing phenotypic variability in mandibular hypoplasia, deafness, progeroid features, and lipodystrophy syndrome (MDPL). *Metabolism* 71, 213–225. doi: 10.1016/j.metabol.2017.03.011

Flynn, R. A., do, B. T., Rubin, A. J., Calo, E., Lee, B., Kuchelmeister, H., et al. (2016). 7SK-BAF axis controls pervasive transcription at enhancers. *Nat. Struct. Mol. Biol.* 23, 231–238. doi: 10.1038/nsmb.3176

Franca, M. M., Han, X., Funari, M. F. A., Lerario, A. M., Nishi, M. Y., Fontenele, E. G. P., et al. (2019). Exome sequencing reveals the POLR3H gene as a novel cause of primary ovarian insufficiency. *J. Clin. Endocrinol. Metab.* 104, 2827–2841. doi: 10.1210/jc.2018-02485

Garg, A., Kircher, M., Del Campo, M., Amato, R. S., and Agarwal, A. K. (2015). University of Washington Center for Mendelian G. whole exome sequencing identifies de novo heterozygous CAV1 mutations associated with a novel neonatal onset lipodystrophy syndrome. *Am. J. Med. Genet. A* 167A, 1796–1806. doi: 10.1002/ajmg.a.37115

Garg, A., and Xing, C. (2014). De novo heterozygous FBN1 mutations in the extreme C-terminal region cause progeroid fibrillinopathy. *Am. J. Med. Genet. A* 164A, 1341–1345. doi: 10.1002/ajmg.a.36449

Girbig, M., Misiaszek, A. D., Vorländer, M. K., Lafita, A., Grötsch, H., Baudin, F., et al. (2021). Cryo-EM structures of human RNA polymerase III in its unbound and transcribing states. *Nat. Struct. Mol. Biol.* 28, 210–219. doi: 10.1038/s41594-020-00555-5

Graul-Neumann, L. M., Kienitz, T., Robinson, P. N., Baasanjav, S., Karow, B., Gillessen-Kaesbach, G., et al. (2010). Marfan syndrome with neonatal progeroid syndrome-like lipodystrophy associated with a novel frameshift mutation at the 3′ terminus of the FBN1-gene. *Am. J. Med. Genet. A* 152A, 2749–2755. doi: 10.1002/ajmg.a.33690

Hiraide, T., Kubota, K., Kono, Y., Watanabe, S., Matsubayashi, T., Nakashima, M., et al. (2020). POLR3A variants in striatal involvement without diffuse hypomyelination. *Brain Dev.* 42, 363–368. doi: 10.1016/j.braindev.2019.12.012

Hiraide, T., Nakashima, M., Ikeda, T., Tanaka, D., Osaka, H., and Saitsu, H. (2020). Identification of a deep intronic POLR3A variant causing inclusion of a pseudoexon derived from an Alu element in pol III-related leukodystrophy. *J. Hum. Genet.* 65, 921–925. doi: 10.1038/s10038-020-0786-y

Howard, S. M., Yanez, D. A., and Stark, J. M. (2015). DNA damage response factors from diverse pathways, including DNA crosslink repair, mediate alternative end joining. *PLoS Genet.* 11:e1004943. doi: 10.1371/journal.pgen.1004943

Huang, J., Poon, L. C., Akolekar, R., Choy, K. W., Leung, T. Y., and Nicolaides, K. H. (2014). Is high fetal nuchal translucency associated with submicroscopic chromosomal abnormalities on array CGH? *Ultrasound Obstet. Gynecol.* 43, 620–624. doi: 10.1002/uog.13384

Iafrate, A. J., Feuk, L., Rivera, M. N., Listewnik, M. L., Donahoe, P. K., Qi, Y., et al. (2004). Detection of large-scale variation in the human genome. *Nat. Genet.* 36, 949–951. doi: 10.1038/ng1416

Jacquinet, A., Verloes, A., Callewaert, B., Coremans, C., Coucke, P., de Paepe, A., et al. (2014). Neonatal progeroid variant of Marfan syndrome with congenital lipodystrophy results from mutations at the 3′ end of FBN1 gene. *Eur. J. Med. Genet.* 57, 230–234. doi: 10.1016/j.ejmg.2014.02.012

Jaganathan, K., Kyriazopoulou Panagiotopoulou, S., McRae, J. F., Darbandi, S. F., Knowles, D., Li, Y. I., et al. (2019). Predicting splicing from primary sequence with deep learning. *Cells* 176, 535–548.e24. doi: 10.1016/j.cell.2018.12.015

Jay, A. M., Conway, R. L., Thiffault, I., Saunders, C., Farrow, E., Adams, J., et al. (2016). Neonatal progeriod syndrome associated with biallelic truncating variants in POLR3A. *Am. J. Med. Genet. A* 170, 3343–3346. doi: 10.1002/ajmg.a.37960

Ji, K., Kong, Y., Liu, Y., Wang, Y., du, L., Xu, C., et al. (2018). Evaluation on the genetic instability detecting methods for rapid diagnose of Fanconi anemia used in the undeveloped areas of China. *Int. J. Lab. Hematol.* 40, 630–636. doi: 10.1111/ijlh.12878

Karousis, E. D., and Muhlemann, O. (2019). Nonsense-mediated mRNA decay begins where translation ends. *Cold Spring Harb. Perspect. Biol.* 11:a032862. doi: 10.1101/cshperspect.a032862

Kechin, A., Boyarskikh, U., Kel, A., and Filipenko, M. (2017). cutPrimers: a new tool for accurate cutting of primers from reads of targeted next generation sequencing. *J. Comput. Biol.* 24, 1138–1143. doi: 10.1089/cmb.2017.0096

Knipscheer, P., Räschle, M., Smogorzewska, A., Enoiu, M., Ho, T. V., Schärer, O. D., et al. (2009). The Fanconi anemia pathway promotes replication-dependent DNA interstrand cross-link repair. *Science* 326, 1698–1701. doi: 10.1126/science.1182372

Kottemann, M. C., and Smogorzewska, A. (2013). Fanconi anaemia and the repair of Watson and Crick DNA crosslinks. *Nature* 493, 356–363. doi: 10.1038/nature11863

Krum, S. A., Miranda, G. A., Lin, C., and Lane, T. F. (2003). BRCA1 associates with processive RNA polymerase II. *J. Biol. Chem.* 278, 52012–52020. doi: 10.1074/jbc.M308418200

Lane, T. F. (2004). BRCA1 and transcription. *Cancer Biol. Ther.* 3, 528–533. doi: 10.4161/cbt.3.6.843

Lessel, D., Ozel, A. B., Campbell, S. E., Saadi, A., Arlt, M. F., McSweeney, K. M., et al. (2018). Analyses of LMNA-negative juvenile progeroid cases confirms biallelic POLR3A mutations in Wiedemann-Rautenstrauch-like syndrome and expands the phenotypic spectrum of PYCR1 mutations. *Hum. Genet.* 137, 921–939. doi: 10.1007/s00439-018-1957-1

Lessel, D., Rading, K., Campbell, S. E., Thiele, H., Altmüller, J., Gordon, L. B., et al. (2022). A novel homozygous synonymous variant further expands the phenotypic spectrum of POLR3A-related pathologies. *Am. J. Med. Genet. A* 188, 216–223. doi: 10.1002/ajmg.a.62525

Levran, O., Erlich, T., Magdalena, N., Gregory, J. J., Batish, S. D., Verlander, P. C., et al. (1997). Sequence variation in the Fanconi anemia gene FAA. *Proc. Natl. Acad. Sci. U. S. A.* 94, 13051–13056. doi: 10.1073/pnas.94.24.13051

Li, N., Ding, L., Li, B., Wang, J., D'Andrea, A. D., and Chen, J. (2018). Functional analysis of Fanconi anemia mutations in China. *Exp. Hematol.* 66, 32–41.e8. doi: 10.1016/j.exphem.2018.07.003

Li, H., and Durbin, R. (2010). Fast and accurate long-read alignment with burrows-wheeler transform. *Bioinformatics* 26, 589–595. doi: 10.1093/bioinformatics/btp698

Li, H., Handsaker, B., Wysoker, A., Fennell, T., Ruan, J., Homer, N., et al. (2009). The sequence alignment/map format and SAMtools. *Bioinformatics* 25, 2078–2079. doi: 10.1093/bioinformatics/btp352

Li, J., Wang, Y., Du, L. I. Q. I. N. G., Xu, C., Cao, J., Wang, Q., et al. (2014). Nested PCR for mtDNA-4977-bp deletion and comet assay for DNA damage - a combined method for radiosensitivity evaluation of tumor cells. *Oncol. Lett.* 7, 1083–1087. doi: 10.3892/ol.2014.1819

Liu, S., Hua, Y., Wang, J., Li, L., Yuan, J., Zhang, B., et al. (2021). RNA polymerase III is required for the repair of DNA double-strand breaks by homologous recombination. *Cells* 184, 1314–1329.e10. doi: 10.1016/j.cell.2021.01.048

Liu, S., and Kong, D. (2021). A direct role of RNA polymerase III and RNA in DNA homologous recombination. *Mol. Cell. Oncol.* 8:1935173. doi: 10.1080/23723556.2021.1935173

Lu, G., Ma, L., Xu, P., Xian, B., Wu, L., Ding, J., et al. (2022). A de novo ZMIZ1 pathogenic variant for neurodevelopmental disorder with dysmorphic Facies and distal skeletal anomalies. *Front. Genet.* 13:840577. doi: 10.3389/fgene.2022.977902

Lu, G., Peng, Q., Wu, L., Zhang, J., and Ma, L. (2021). Identification of de novo mutations for ARID1B haploinsufficiency associated with coffin-Siris syndrome 1 in three Chinese families via array-CGH and whole exome sequencing. *BMC Med. Genet.* 14:270. doi: 10.1186/s12920-021-01119-2

Lykke-Andersen, S., and Jensen, T. H. (2015). Nonsense-mediated mRNA decay: an intricate machinery that shapes transcriptomes. *Nat. Rev. Mol. Cell Biol.* 16, 665–677. doi: 10.1038/nrm4063

Minnerop, M., Kurzwelly, D., Wagner, H., Soehn, A. S., Reichbauer, J., Tao, F., et al. (2017). Hypomorphic mutations in POLR3A are a frequent cause of sporadic and recessive spastic ataxia. *Brain* 140, 1561–1578. doi: 10.1093/brain/awx095

Moghrabi, N. N., Johnson, M. A., Yoshitomi, M. J., Zhu, X., al-Dhalimy, M. J., Olson, S. B., et al. (2009). Validation of Fanconi anemia complementation group a assignment using molecular analysis. *Genet. Med.* 11, 183–192. doi: 10.1097/GIM.0b013e318193ba67

Morales-Rosado, J. A., Macke, E. L., Cousin, M. A., Oliver, G. R., Dhamija, R., and Klee, E. W. (2020). Interpretation challenges of novel dual-class missense and splice-impacting variant in POLR3A-related late-onset hereditary spastic ataxia. *Mol. Genet. Genomic Med.* 8:e1341. doi: 10.1002/mgg3.1341

Nepal, M., Che, R., Zhang, J., Ma, C., and Fei, P. (2017). Fanconi Anemia Signaling and cancer. *Trends Cancer* 3, 840–856. doi: 10.1016/j.trecan.2017.10.005

Niraj, J., Farkkila, A., and D'Andrea, A. D. (2019). The Fanconi Anemia pathway in cancer. *Annu Rev. Cancer Biol.* 3, 457–478. doi: 10.1146/annurev-cancerbio-030617-050422

Paolacci, S., Bertola, D., Franco, J., Mohammed, S., Tartaglia, M., Wollnik, B., et al. (2017). Wiedemann-Rautenstrauch syndrome: a phenotype analysis. *Am. J. Med. Genet. A* 173, 1763–1772. doi: 10.1002/ajmg.a.38246

Paolacci, S., Li, Y., Agolini, E., Bellacchio, E., Arboleda-Bustos, C. E., Carrero, D., et al. (2018). Specific combinations of biallelic POLR3A variants cause Wiedemann-Rautenstrauch syndrome. *J. Med. Genet.* 55, 837–846. doi: 10.1136/jmedgenet-2018-105528

Pivnick, E. K., Angle, B., Kaufman, R. A., Hall, B. D., Pitukcheewanont, P., Hersh, J. H., et al. (2000). Neonatal progeroid (Wiedemann-Rautenstrauch) syndrome: report of five new cases and review. *Am. J. Med. Genet.* 90, 131–140. doi: 10.1002/(SICI)1096-8628(20000117)90:2<131::AID-AJMG9>3.0.CO;2-E

Rautenstrauch, T., and Snigula, F. (1977). Progeria: a cell culture study and clinical report of familial incidence. *Eur. J. Pediatr.* 124, 101–111. doi: 10.1007/BF00477545

Repczynska, A., Julga, K., Skalska-Sadowska, J., Kacprzak, M. M., Bartoszewska-Kubiak, A., Lazarczyk, E., et al. (2022). Next-generation sequencing reveals novel variants and large deletion in FANCA gene in polish family with Fanconi anemia. *Orphanet J. Rare Dis.* 17:282. doi: 10.1186/s13023-022-02424-4

Riggs, E. R., Andersen, E. F., Cherry, A. M., Kantarci, S., Kearney, H., Patel, A., et al. (2020). Technical standards for the interpretation and reporting of constitutional copy-number variants: a joint consensus recommendation of the American College of Medical Genetics and Genomics (ACMG) and the clinical genome resource (ClinGen). *Genet. Med.* 22, 245–257. doi: 10.1038/s41436-019-0686-8

Rodríguez-García, M. E., Cotrina-Vinagre, F. J., Cruz-Rojo, J., Garzón-Lorenzo, L., Carnicero-Rodríguez, P., Pozo, J. S. D., et al. (2018). A rare male patient with Fontaine progeroid syndrome caused by p.R217H de novo mutation in SLC25A24. *Am. J. Med. Genet. A* 176, 2479–2486. doi: 10.1002/ajmg.a.40496

Rydning, S. L., Koht, J., Sheng, Y., Sowa, P., Hjorthaug, H. S., Wedding, I. M., et al. (2019). Biallelic POLR3A variants confirmed as a frequent cause of hereditary ataxia and spastic paraparesis. *Brain* 142:e12. doi: 10.1093/brain/awz041

Saitsu, H., Osaka, H., Sasaki, M., Takanashi, J. I., Hamada, K., Yamashita, A., et al. (2011). Mutations in POLR3A and POLR3B encoding RNA polymerase III subunits cause an autosomal-recessive hypomyelinating leukoencephalopathy. *Am. J. Hum. Genet.* 89, 644–651. doi: 10.1016/j.ajhg.2011.10.003

Sasaki, H., Yanagi, K., Ugi, S., Kobayashi, K., Ohkubo, K., Tajiri, Y., et al. (2018). Definitive diagnosis of mandibular hypoplasia, deafness, progeroid features and lipodystrophy (MDPL) syndrome caused by a recurrent de novo mutation in the POLD1 gene. *Endocr. J.* 65, 227–238. doi: 10.1507/endocrj.EJ17-0287

Schrauwen, I., Szelinger, S., Siniard, A. L., Kurdoglu, A., Corneveaux, J. J., Malenica, I., et al. (2015). A frame-shift mutation in CAV1 is associated with a severe neonatal Progeroid and Lipodystrophy syndrome. *PLoS One* 10:e0131797. doi: 10.1371/journal.pone.0131797

Su, A. I., Wiltshire, T., Batalov, S., Lapp, H., Ching, K. A., Block, D., et al. (2004). A gene atlas of the mouse and human protein-encoding transcriptomes. *Proc. Natl. Acad. Sci. U. S. A.* 101, 6062–6067. doi: 10.1073/pnas.0400782101

Takenouchi, T., Hida, M., Sakamoto, Y., Torii, C., Kosaki, R., Takahashi, T., et al. (2013). Severe congenital lipodystrophy and a progeroid appearance: mutation in the penultimate exon of FBN1 causing a recognizable phenotype. *Am. J. Med. Genet. A* 161A, 3057–3062. doi: 10.1002/ajmg.a.36157

Temel, S. G., Ergoren, M. C., Manara, E., Paolacci, S., Tuncel, G., Gul, S., et al. (2020). Unique combination and in silico modeling of biallelic POLR3A variants as a cause of Wiedemann-Rautenstrauch syndrome. *Eur. J. Hum. Genet.* 28, 1675–1680. doi: 10.1038/s41431-020-0673-1

Terhal, P. A., Vlaar, J. M., Middelkamp, S., Nievelstein, R. A. J., Nikkels, P. G. J., Ross, J., et al. (2020). Biallelic variants in POLR3GL cause endosteal hyperostosis and oligodontia. *Eur. J. Hum. Genet.* 28, 31–39. doi: 10.1038/s41431-019-0427-0

Thiffault, I., Wolf, N. I., Forget, D., Guerrero, K., Tran, L. T., Choquet, K., et al. (2015). Recessive mutations in POLR1C cause a leukodystrophy by impairing biogenesis of RNA polymerase III. *Nat. Commun.* 6:7623. doi: 10.1038/ncomms8623

Toriello, H. V. (1990). Wiedemann-Rautenstrauch syndrome. *J. Med. Genet.* 27, 256–257. doi: 10.1136/jmg.27.4.256

Vannini, A., and Cramer, P. (2012). Conservation between the RNA polymerase I, II, and III transcription initiation machineries. *Mol. Cell* 45, 439–446. doi: 10.1016/j.molcel.2012.01.023

Wambach, J. A., Wegner, D. J., Patni, N., Kircher, M., Willing, M. C., Baldridge, D., et al. (2018). Bi-allelic POLR3A loss-of-function variants cause autosomal-recessive Wiedemann-Rautenstrauch syndrome. *Am. J. Hum. Genet.* 103, 968–975. doi: 10.1016/j.ajhg.2018.10.010

Wang, K., Li, M., and Hakonarson, H. (2010). ANNOVAR: functional annotation of genetic variants from high-throughput sequencing data. *Nucleic Acids Res.* 38:e164. doi: 10.1093/nar/gkq603

Wiedemann, H. R. (1979). An unidentified neonatal progeroid syndrome: follow-up report. *Eur. J. Pediatr.* 130, 65–70. doi: 10.1007/BF00441901

Wolf, N. I., Vanderver, A., van Spaendonk, R. M. L., Schiffmann, R., Brais, B., Bugiani, M., et al. (2014). Clinical spectrum of 4H leukodystrophy caused by POLR3A and POLR3B mutations. *Neurology* 83, 1898–1905. doi: 10.1212/WNL.0000000000001002

Writzl, K., Maver, A., Kovačič, L., Martinez-Valero, P., Contreras, L., Satrustegui, J., et al. (2017). De novo mutations in SLC25A24 cause a disorder characterized by early aging, bone dysplasia, characteristic face, and early demise. *Am. J. Hum. Genet.* 101, 844–855. doi: 10.1016/j.ajhg.2017.09.017

Wu, S., Bai, Z., Dong, X., Yang, D., Chen, H., Hua, J., et al. (2019). Novel mutations of the POLR3A gene caused POLR3-related leukodystrophy in a Chinese family: a case report. *BMC Pediatr.* 19:289. doi: 10.1186/s12887-019-1656-7

Yan, H., Ji, H., Kubisiak, T., Wu, Y., Xiao, J., Gu, Q., et al. (2021). Genetic analysis of 20 patients with hypomyelinating leukodystrophy by trio-based whole-exome sequencing. *J. Hum. Genet.* 66, 761–768. doi: 10.1038/s10038-020-00896-5

frontiers | Frontiers in Molecular Neuroscience

TYPE Review
PUBLISHED 10 November 2022
DOI 10.3389/fnmol.2022.1030639

OPEN ACCESS

EDITED BY
Federica Bono,
University of Brescia, Italy

REVIEWED BY
Maria Pennuto,
University of Padua, Italy
Pei-Lin Cheng,
Academia Sinica, Taiwan

*CORRESPONDENCE
Zhen Tian
zhentianzh@163.com
Jiao Tian
jiaotianji07@163.com

†These authors share first authorship

SPECIALTY SECTION
This article was submitted to Brain Disease Mechanisms, a section of the journal Frontiers in Molecular Neuroscience

RECEIVED 29 August 2022
ACCEPTED 25 October 2022
PUBLISHED 10 November 2022

CITATION
Tian Z, Feng B, Wang X-Q and Tian J (2022) Focusing on cyclin-dependent kinases 5: A potential target for neurological disorders. *Front. Mol. Neurosci.* 15:1030639. doi: 10.3389/fnmol.2022.1030639

Focusing on cyclin-dependent kinases 5: A potential target for neurological disorders

Zhen Tian[1*†], Bin Feng[2†], Xing-Qin Wang[3] and Jiao Tian[4*]

[1]College of Pharmaceutical Sciences, Southwest University, Chongqing, China, [2]State Key Laboratory of Military Stomatology, National Clinical Research Center for Oral Diseases, Shaanxi International Joint Research Center for Oral Diseases, Department of Pharmacy, School of Stomatology, Fourth Military Medical University, Xi'an, China, [3]Department of Neurosurgery, Nanfang Hospital, Southern Medical University, Guangzhou, China, [4]Department of Infection, Children's Hospital of Chongqing Medical University, National Clinical Research Center for Child Health and Disorders, Ministry of Education Key Laboratory of Child Development and Disorders, Chongqing Key Laboratory of Child Infection and Immunity, The First Batch of Key Disciplines On Public Health in Chongqing, Chongqing, China

Cyclin-dependent kinases 5 (Cdk5) is a special member of proline-directed serine threonine kinase family. Unlike other Cdks, Cdk5 is not directly involved in cell cycle regulation but plays important roles in nervous system functions. Under physiological conditions, the activity of Cdk5 is tightly controlled by p35 or p39, which are specific activators of Cdk5 and highly expressed in post-mitotic neurons. However, they will be cleaved into the corresponding truncated forms namely p25 and p29 under pathological conditions, such as neurodegenerative diseases and neurotoxic insults. The binding to truncated co-activators results in aberrant Cdk5 activity and contributes to the initiation and progression of multiple neurological disorders through affecting the down-stream targets. Although Cdk5 kinase activity is mainly regulated through combining with co-activators, it is not the only way. Post-translational modifications of Cdk5 including phosphorylation, S-nitrosylation, sumoylation, and acetylation can also affect its kinase activity and then participate in physiological and pathological processes of nervous system. In this review, we focus on the regulatory mechanisms of Cdk5 and its roles in a series of common neurological disorders such as neurodegenerative diseases, stroke, anxiety/depression, pathological pain and epilepsy.

KEYWORDS

Cdk5, p35, neurological disorders, Parkinson's disease, Alzheimer's disease, stroke

Introduction

Cyclin-dependent kinases (Cdks) are a group of small proline-directed serine/threonine kinases mainly involved in the modulation of cell cycle, gene transcription and cell differentiation (Malumbres, 2014; Xie et al., 2022). Cyclin dependent kinase 1 (Cdk1) was the first discovered Cdk, which was initially named as cell division cycle 2 (Cdc2) because of its high homology with a yeast fission kinase

of the same name (Lee and Nurse, 1987). Until now, twenty-one genes encoding Cdks and five genes encoding Cdk-like kinases have been found in human genome (Malumbres et al., 2009). Generally, Cdks are activated through associating with specific cyclin regulatory subunits and regulated through phosphorylation of specific T-loops by Cdk-activating kinase (Malumbres et al., 2009). Among the family of Cdks, Cdk5 is a special one though it shares significant sequence homology with other members (Hellmich et al., 1992). It can neither be activated by cyclins nor involved in cell division directly. Cdk5 is ubiquitous in kinds of tissues, but its activity is extremely high in post-mitotic neurons because its activators p35 and p39 are selectively expressed in these cells (Tsai et al., 1994; Ko et al., 2001). P35 and p39 are different from cyclins as they lack the typically conserved amino acid sequences. The expression of Cdk5 and p35/p39 transcripts overlaps spatially and temporally in the developing brain, and upon directly binding, they form active complexes and induces the alterations of downstream signal pathways.

In the developing nervous system, Cdk5 seems to be expressed mainly in terminally differentiated neurons but not proliferating cells. Because the expression and kinase activity of Cdk5 was shown to increase progressively from embryonic day 15 (E15) and reaches the peak at E17 in developing mouse forebrain, which period is a critical time widow for neuronal differentiation (Tsai et al., 1993). During the embryonic brain development of rats, the expression pattern of Cdk5 is similar to that of mouse, with a gradual increase from E12 to E18 and reaches a peak at postnatal day 7 (P7), which is then maintained at this level through adulthood and aged phase (up to 18 months old) (Wu et al., 2000). In the adult central nervous system, Cdk5 is distributed throughout the brain and spinal cord, especially in the hippocampus, cerebellum, cerebral cortex, olfactory bulb, amygdala and brain stem. Generally, the level of Cdk5 is higher in the large-sized and medium-sized neurons such as hippocampal and cortical pyramidal cells, cerebellar Purkinje cells, motoneurons in spinal cord (Ino et al., 1994). The expression level of Cdk5 in various brain regions was also compared and quantified. The results showed that there was no obvious difference about Cdk5 level in the cerebral cortex, hippocampus, cerebellum and striatum of rats aged from postnatal day 14 (P14) to 18 months old (18 M) (Wu et al., 2000).

As for p35, the co-activator of Cdk5, its expression becomes detectable in E16 rat brains and gradually increases to its peak level at P7–P14, then declines in the adult and aged rat brains. The Cdk5 kinase activity is low at E12 and it also progressively reaches a peak between P7 and P14, and then declines from 1 to 3 M, a timetable correlating well with the expression pattern of p35 (Wu et al., 2000). Different from the expression pattern of Cdk5 protein, p35 expression and Cdk5 kinase activity were persistently higher in the hippocampus and cerebral cortex than cerebellum or striatum in rats from P14 to 18 M, indicating that Cdk5/p35 complex may have region-specific functions (Wu et al., 2000). P39 is the isoform of p35 with over 50% homology in genomic sequence, the functions of p39 largely overlap with those of p35. However, their spatial and temporal expression patterns are different, with p35 being highly expressed from embryonic to postnatal stage while p39 is scarcely expressed until postnatal (Tsai et al., 1994; Ko et al., 2001). In addition, the expression of p35 is mostly prominent in cerebral cortex while p39 is primarily expressed in brain stem, cerebellum and spinal cord (Ko et al., 2001). Furthermore, the binding affinity of p39 with Cdk5 is lower whereas the Cdk5-p39 complex is more stable compared with Cdk5-p35 (Yamada et al., 2007; Minegishi et al., 2010).

Cyclin-dependent kinases 5 complex plays a very important role in neuronal functions from embryogenesis to postnatal brain modulation. During embryogenesis, Cdk5 is essential for normal brain development and conditional deletion of Cdk5 is lethal (Ohshima et al., 1996; Shah and Lahiri, 2014). It is because that Cdk5 governs multiple steps of cortical neuronal migration, including the formation of multipolar processes (Kawauchi et al., 2006), gain of neuronal polarity (Ohshima et al., 2007) and the locomotion mode (Nishimura et al., 2010). Cdk5 deficiency will lead to the lack of cerebral cortical laminar structure and cerebellar foliation in mice (Ohshima et al., 1996). Mice lacking p35 show less severe corticogenesis defect and only suffer from sporadic adult lethality, which may be attributed to functional compensation by another Cdk5 activator, p39 (Chae et al., 1997). Although loss of 39 is not lethal, it attenuates overall Cdk5 activity in neurons as well as leads to aberrant axonal growth and impaired dendritic spine formation through affecting Cdk5 targets governing neuronal differentiation and network formation (Li et al., 2016). In adult brain, emerging evidences have indicated that Cdk5 complex regulated multiple neuronal functions including neuronal survival, neurite and axon outgrowth, synaptic plasticity, neurotransmission (Ye et al., 2014; Sasamoto et al., 2017; Takahashi et al., 2022). Because of its extensive and crucial roles in nervous system, the dysfunction of Cdk5 is critically involved in numerous neurological disorders such as neurodegenerative diseases, stroke, psychiatric disorders, pathological pain, epilepsy and so on. The multifaceted roles of Cdk5 make it to be an attractive target for therapeutic intervention. An updated review on the relationship between Cdk5 and nervous system dysfunction can help us better understand its potential clinical value. Therefore, we comprehensively summarized the role of Cdk5 in a series of common neurological disorders in this paper. The synthesis of these scientific evidences about Cdk5 could facilitate future research to further explore the potentiality of drugs targeting Cdk5 for clinical therapy.

Regulation of cyclin-dependent kinases 5 kinase activity

The aberrant Cdk5 activity is critically involved in the pathogenesis of neurological disorders, so the regulation of

kinase activity may be a potential strategy for disease treatment. Cdk5 kinase activity is mainly regulated by the available protein amounts of p35/p39 and their truncated fragments. p35 and p39 levels are determined by the balance between synthesis and degradation, which are cleavage by the ubiquitin-proteasome system with a half-life of about 30 and 120 min for p35 and p39, respectively (Minegishi et al., 2010). Calpain, a Ca^{2+} activated protease, is involved in multiple physiological processes and plays an important role in maintaining normal neuronal function. The activation of calpain depends on Ca^{2+} concentration, which makes it vulnerable to changes of Ca^{2+} homeostasis (Metwally et al., 2021). Following neurotoxic insults, sustained Ca^{2+} elevation leads to the over-activation of calpain, which in turn cleaved p35 and p39 into N-terminal p10 and C-terminal p25 or p29 truncated fragments (Lee et al., 2000). However, the half-life of truncated protein fragment is much longer than that of mother molecule and it can form a more stable complex with Cdk5, resulting in the prolonged activation of Cdk5 (Patrick et al., 1999; Minegishi et al., 2010). In addition, the N-terminal p10 region of p39 and p35 contains a second Gly for myristoylation and Lys clusters, the localization motifs helping to anchor the active complex at membrane. However, the truncated forms derived from cleavage of p35 or p39 lost the myristoylation signal that normally maintains Cdk5 at the membrane, leading to accumulation of the complex in nuclear and perinuclear regions (Asada et al., 2008). This aberrant subcellular localization of Cdk5/co-activator complex disturbs its substrate specificity and makes it target not only physiological substrates but also non-physiological substrates, resulting in neurotoxicity and cell death (Mushtaq et al., 2016). Thus, the hyperactivation and mislocalization of Cdk5 caused by p25 accumulation lead to the dysfunction of Cdk5, which contributes to the pathogenesis of various neurological diseases.

Although binding with the regulatory subunits is sufficient to activate Cdk5, its kinase activity can also be regulated by other pathways, such as phosphorylation, S-nitrosylation, sumoylation, and acetylation. Thr14, Tyr15, and Ser159 are the three phosphorylation sites of Cdk5 found so far. Phosphorylation at the sites of Thr14 and Ser159 produces opposite outcomes on Cdk5 activity, with the former inhibiting Cdk5 activity and the latter increasing its activity (Lee et al., 2014). The effect of phosphorylation at Tyr15 on kinase activity is still controversial. Some studies found that Cdk5 activity was enhanced by phosphorylation at Tyr15 while other study got the negative results. For example, Sasaki et al. (2002) reported that phosphorylation of Tyr15 by a non-receptor Src family tyrosine kinase Fyn increased Cdk5 enzymatic activity. However, Kobayashi et al. (2014) found that phosphorylation of Tyr15 had no effect on the activation of Cdk5. Thus, future studies are still needed to further clarify the function of Tyr15 phosphorylation as it is helpful for uncovering new regulatory pathway of Cdk5 activity.

Besides phosphorylation, the S-nitrosylation of Cdk5 is another mechanism to regulate kinase activity. It has been shown that the S-nitrosylation at cysteine residues (Cys) 83 and 157 contributed to the elevation of Cdk5 kinase activity (Qu et al., 2011, 2012). The S-nitrosylation of Cdk5 will cause transnitrosylation, a process of transferring NO group to dynamin-related protein 1 (Drp1), a protein controlling the process of mitochondrial fission (Westermann, 2010). S-nitrosylated Drp1 then stimulates excessive mitochondrial fission and damages the synapses, resulting in dendritic spine loss and synaptic failure finally (Cho et al., 2009). However, it is worth noting that the effect of S-nitrosylation at Cys83 on Cdk5 activity may be determined by the levels of exogenous NO. Cys83 S-nitrosylation by very high levels (non-physiological level) of NO could conversely inhibit Cdk5 activity though the concentrations of NO donors are never reached *in vivo* (Zhang et al., 2010). The cysteine residues of p35 can also be S-nitrosylated, it was found that S-nitrosylation of p35 at Cys92 by NO signaling led to its ubiquitination and degradation, which resulted in the reduction of Cdk5 activity (Zhang et al., 2015).

Sumoylation and acetylation are two other ways of post-translational modifications of Cdk5 activity. It has been shown that p35 is a novel sumoylation target and the sumoylation of p35 can enhance the activity of Cdk5/p35 complex (Buchner et al., 2015). However, it is still unclear whether Cdk5 can be sumoylated directly. With regard to acetylation, Cdk5 can be acetylated at the lysine residue site 33 (K33), a residue comprising the ATP binding pocket. The acetylation of Cdk5 at K33 causes an impairment of kinase activity due to the loss of ATP binding ability. The Cdk5 acetylation is negatively regulated by Sirtuin-1 (SIRT1), inhibition of SIRT1 will enhance nuclear Cdk5 acetylation whereas SIRT1 activation results in deacetylation of nuclear Cdk5 (Lee et al., 2018). Whether there are any other acetylation sites remains unclear, and the role of Cdk5 acetylation in neurological diseases is also still needed to be further investigated.

Cyclin-dependent kinases 5: A culprit in neurological disorders

Cyclin-dependent kinases 5 dysfunction triggers Parkinson's disease

Parkinson's disease (PD) is a common neurodegenerative movement disorder characterized by widespread degeneration of dopaminergic neurons located in the substantia nigra pars compacta (SNpc) and subsequent loss of dopamine reaching striatal projecting neurons (Obeso et al., 2010). The formation of intra-neuronal inclusions called Lewy bodies (LB) is a pathologic hallmark of PD and often correlates with the

degree of cognitive decline (Schneider et al., 2012). Cdk5 and p35 has been found to be localized in LB in the SNpc of postmortem patients brains with PD (Nakamura et al., 1997). There is also sustained calpain-dependent conversion of p35 to p25 and enhanced Cdk5 activity in the brain of PD patients and animal models (Smith et al., 2003; Alvira et al., 2008). Quantitative phosphoproteomic analysis of α-synuclein transgenic mice showed that elevated Cdk5/p25 pathway activity contributed to SNpc dopaminergic neuronal death in model mice (Stillwell and Myers, 1988), which was also observed in mice administrated with 1-methyl-4-phenyl-1, 2, 3, 6-tetrahydropyridine (MPTP), a toxin used to induce PD model through destroying the nigrostriatal dopaminergic pathway (Binukumar et al., 2015). TFP5, a specific inhibitory peptide of Cdk5/p25 complex, suppressed the dopaminergic neuronal loss in SNpc and striatum, improved motor function of PD mice (Binukumar et al., 2015).

The mitochondrial dysfunction and subsequent oxidative stress are important mechanisms underlying the pathogenesis of PD. Abnormal Cdk5 activity contributes to mitochondrial dysfunction in PD by aberrant modulation of several key proteins involved in mitochondrial function. Drp1 is a GTPase that controls the process of mitochondrial fission. Drp1 is translocalized from the cytosol to the mitochondrial outer membrane (MOM) and then assembled into ring-like structures wrapping around MOM. Following GTP hydrolysis, Drp1 incises the membrane and instigates mitochondrial fission (Westermann, 2010). In non-human primate PD model, Cdk5 hyperactivity was shown to increase the phosphorylation of Drp1 at Ser616, which in turn increased GTPase activity and accelerated mitochondrial fission, ultimately induced dopaminergic neuronal loss in the SNpc (Park et al., 2019). Inhibition of Cdk5 activity prevented Drp1-dependent mitochondrial fission and neuron death following MPP+ treatment (Yang et al., 2020). Dysfunction of E3 ubiquitin ligases has a close relationship with mitochondrial defects and disruption of protein degradation. Parkin is an E3 ubiquitin ligase and plays an important role in maintaining mitochondrial function. It is able to prevent cell death from toxicity elicited by diverse insults (Petrucelli et al., 2002). However, the aggregation of insoluble Parkin will inhibit its catalytic activity and lead to dopaminergic neuron death caused by accumulation of toxic Parkin substrates, such as p38 (Avraham et al., 2007), ultimately contributing to the pathogenesis of PD (Rubio de la Torre et al., 2009). Cdk5 was demonstrated to phosphorylate Parkin at Ser131 both *in vitro* and *in vivo*, decreased its solubility, induced its accumulation and subsequently reduced E3 ubiquitin-ligase activity (Avraham et al., 2007). Consistent with this, enhanced p25 level and elevated Parkin phosphorylation were also found in several brain areas of PD patients (Rubio de la Torre et al., 2009). Glycoprotein 78 (GP78), another E3 ubiquitin ligase, is involved in regulating mitochondrial function. Cdk5 was found to directly phosphorylate GP78 at Ser516, which promoted its ubiquitination and degradation, ultimately caused neuronal death in both cellular and animal PD models (Wang et al., 2018).

Mitochondrial dysfunction and aggregation of damaged mitochondria can cause remarkable oxidative stress indicating by excessive accumulation of cellular reactive oxygen species (ROS). Peroxidases are a series of antioxidant enzymes with the capacity to catalyze hydrogen peroxide into stable non-toxic molecules. Cdk5 was demonstrated to phosphorylate peroxidases 2 (Prx2) at Thr89 and this phosphorylation decreased its peroxidase activity and induced ROS over-generation and dopaminergic neuron loss in the SNc following MPTP insult (Qu et al., 2007). Increased Prx2 phosphorylation in nigral neurons was also observed in brain tissue of postmortem PD patients. Interestingly, the insults-induced cleavage of p35 could also generate p10, a pro-survival N-terminal domain of p35 with the ability of preventing Cdk5/p25-mediated Prx2 phosphorylation and ROS accumulation (Zhang L. et al., 2012). Neuroinflammation is another outcome of mitochondrial dysfunction. Cdk5-mediated inflammasomes activation was observed in the SNpc of PD mouse model and in cerebrospinal fluid of PD patients. Inhibition or deletion of Cdk5 both could inhibit the inflammasome activation and delay the progression of PD in animal models (Zhang P. et al., 2016).

Excessive autophagy is closely related with neuronal death and there is over-production of autophagy markers in PD brains (Anglade et al., 1997). Knockdown of Cdk5 inhibited autophagy-mediated α-synuclein aggregation and promoted the functional recovery in PD mice (Su et al., 2015). Endophilin B1 (EndoB1) has been reported to be implicated in autophagy induction (Takahashi et al., 2007). In MPTP-induced PD model, elevated Cdk5 activity led to EndoB1 phosphorylation at Thr145 and then promoted EndoB1 dimerization, beclin-1 recruitment and autophagy induction, resulting in neuronal loss. EndoB1 or Cdk5 knockdown both remarkably attenuated the neuronal death in PD through inhibiting aberrant autophagy (Wong et al., 2011). Besides autophagy, several other cell death pathways mediated by Cdk5 were also shown to be involved in PD. Myocyte enhancer factor 2 (MEF2), one member of transcription factors family, is an endpoint for diverse signaling pathways that control cellular survival and apoptosis (Mao et al., 1999). Abnormal Cdk5/MEF2 signaling pathway contributes to dopaminergic neuronal death. Upon MPTP insult, the hyperactivity of Cdk5/p25 inactivated MEF2 and led to dopaminergic neuronal loss in the SNpc and formation of LB. Inhibition of Cdk5/p25 complex with TFP5 decreased the levels of MEF2 inactive form, thus significantly suppressed dopaminergic neuronal death (Zhang Q. et al., 2016). Nur77 is one important downstream survival effector of MEF2. Nur77 deficient mice are more sensitive to dopaminergic neuronal loss and exhibit more serious nigrostriatal damage in response to MPTP treatment (Mount et al., 2013). Cdk5-mediated MEF2 phosphorylation led to its inactivation and

subsequently resulted in markedly Nur77 reduction in the nigrostriatal region following MPTP injection (Mount et al., 2013). These results imply that Cdk5-MEF2-Nur77 pathway is involved in the dopaminergic neuronal loss. Raf kinase inhibitor protein (RKIP) is able to block Ras/Raf/MEK/ERK signaling pathway by inhibiting Raf1-mediated MEK1 phosphorylation (Yeung et al., 1999). Downregulation of RKIP will lead to over-activation of ERK/MAPK pathway, which is resulted from losing control of Raf-1 (Granovsky and Rosner, 2008). Cdk5 was reported to phosphorylate RKIP at Thr42 and promote the degradation of RKIP. In PD animal models and post-mortal PD patients, Cdk5-mediated RKIP phosphorylation and degradation were demonstrated to occur with excessive activation of the ERK/MAPK cascade followed by cell cycle re-entry and neuron death (Wen et al., 2014).

The pathways related with Cdk5 in PD are summarized and presented as **Figure 1**.

Cyclin-dependent kinases 5 facilitates the initiation and progression of Alzheimer's disease

Alzheimer's disease (AD) is the primary reason for dementia among people over the age of 65. It has two main pathological characteristics, one is senile plaques mainly composed by amyloid-β (Aβ) peptides which is resulted from aberrant amyloid precursor protein (APP) cleavage, and the other is neurofibrillary tangles (NFTs) basically consisting of paired helical filaments (PHFs) which are derived from hyperphosphorylated tau proteins (Lau and Ahlijanian, 2003). These two proteinopathies are the basic changes underlying the progressive neuronal degeneration and cognitive dysfunction in AD patients. In a population-based study, it was found that there was a correlation between the genetic variation of Cdk5 gene and the risk of AD (Arias-Vasquez et al., 2008). Elevated p25/p35 ratio was observed in multiple brain areas including frontal cortex, inferior parietal cortex and hippocampus in human AD brains (Tseng et al., 2002). P25 transgenic mouse model showed AD-like pathological changes such as tau hyperphosphorylation, NFTs, and neuronal loss. Transgenic expression of Cdk5 inhibitory peptide before and after the insult of p25 could both suppress hippocampal tau phosphorylation and neuronal death, improve the cognitive dysfunction of model mice (Xu et al., 2019; Huang et al., 2020). Inhibition of Cdk5/p25 complex also reduced hippocampal Aβ production and tau hyperphosphorylation, improved learning and memory abilities of AD model mice (Zhao et al., 2021).

Amyloid-β peptides are produced from the sequential cleavage of APP by β-amyloid cleavage enzyme 1 (BACE1) and γ-secretase. Aβ40 and Aβ42 are two main forms of Aβ peptide, the longer Aβ42 has a much stronger tendency to oligomerize and aggregate than the shorter Aβ40, and exhibits more neurotoxic effect. Accumulation of oligomerized Aβ peptides forms amyloid plaques, which is closely related with neuronal loss and cognitive decline in AD. Cdk5/p25 activity was upregulated and significantly correlated with BACE1 elevation in brains of AD patients and transgenic mouse models (Sadleir and Vassar, 2012). Wen et al. (2008) found that Cdk5 facilitated Aβ generation through modulation of BACE1 synthesis *via* signal transducer and activator of transcription 3 (STAT3), who binded to BACE1 promoter and phosphorylated it at Ser727. In cultured primary rat hippocampal neurons, Cdk5 activation triggered peroxisome proliferators-activated receptor γ (PPARγ) phosphorylation at Ser273, then increased BACE1 activity and Aβ production (Quan et al., 2019). Presenilin 1 gene mutation is the main reason for autosomal dominant familial forms of AD (Fraser et al., 2000). As the core subunit of γ-secretase, presenilin-1 (PS1) is essential for the catalytic activity of γ-secretase. Presenilin-1 dysfunction will result in the increase of Aβ42/Aβ40 ratio, which is more toxic than the rising of Aβ42 absolute amounts (Chavez-Gutierrez et al., 2012). Cdk5/p35 is reported to regulate PS1 stability and metabolism through phosphorylating PS1 at Thr354 (Lau et al., 2002), and the aberrant Cdk5 activity will cause γ-secretase dysfunction and the alteration of Aβ42/Aβ40 ratio.

Tau is a microtubule-associated protein primarily distributed in axons. Tauopathy is characterized by abnormal tau aggregation and NFT formation in the brain, which is a hallmark of AD. Cdk5/p25 can promote tau dimerization through phosphorylating it at different sites, which subsequently aggregate into PHF-like filament, resulting in microtubule collapse and neurite retraction (Paudel, 1997). The Cdk5 and hyperphosphorylated tau are found to be co-existed in the neocortical pyramidal neurons and cerebellar neurons of AD (Pei et al., 1998). Moreover, enhanced Cdk5 immunoreactivity was observed in neurons undergoing early stage of NFTs degeneration and plaque-neurites in several regions of human AD brain (Pei et al., 1998). Cdk5 hyperactivation was also found to induce the accumulation of hyperphosphorylated tau, Aβ plaques, and neuronal loss in animal models. TFP5, an inhibitory peptide of Cdk5/p25, significantly reduced tau hyperphosphorylation, neurofilament accumulation and restored synaptic function and behavior abnormalities in transgenic AD model mice as well as the mice overexpressing p25 through attenuating Cdk5 hyperactivity (Shukla et al., 2013, 2017). Long-term and short-term Cdk5 knockdown also both inhibited insoluble tau aggregation in the hippocampus of 3xTg-AD mice and improved their spatial memory (Castro-Alvarez et al., 2014). Collapsin response mediating protein-2 (CRMP2) is capable of promoting microtubule assembly through binding tubulin heterodimers (Fukata et al., 2002). It was reported that Cdk5 phosphorylated CRMP2 at Ser522 and reduced its binding to tubulin (Uchida et al., 2005). And this hyperphosphorylated CRMP2 was demonstrated to be a component of PHF (Yoshida et al., 1998), and were observed in the brain of AD transgenic

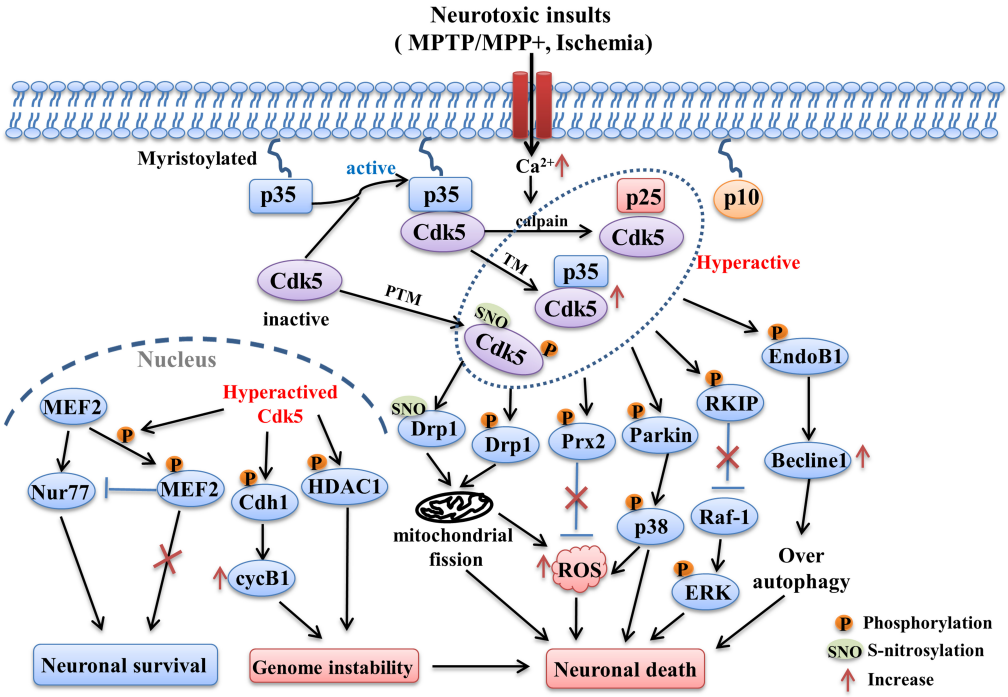

FIGURE 1
The Cdk5-related pathways involved in PD and stroke. Following neurotoxic insults, sustained Ca^{2+} elevation induces the over-activation of calpain, which in turn cleaves p35 into p25 and p10 fragments. The half-life of p25 is much longer than p35, it can form more stable complex with Cdk5 and lead to abnormally elevated Cdk5 activity. Its activity can also be regulated by post-translational modulations (PTM). The phosphorylation and S-nitrosylation of certain specific sites are able to hyperactive Cdk5 (e.g., phosphorylation at Ser159, S-nitrosylation at Cys83 and Cys157). In addition, transcriptional modulation (TM) of Cdk5 and p35 can also increase their expression and activity, which is mediated by some related transcription factors (e.g., Fos, CREB). Hyper-activation of Cdk5 then triggers the phosphorylation of multiple substrates including EndoB1, RKIP, Parkin, Prx2, Drp1, MEF2, Cdh1, and HDAC1. Changes in the phosphorylation state of these key substrates induced the occurrence of detrimental events such as mitochondrial dysfunction, oxidative stress, over-autophagy, which in turn contribute to the neuronal loss in PD and stroke.

mouse model (Cole et al., 2007). Cdk5 was also reported to activate microtubule affinity-regulating kinases 4 (MARK4) and increased tau phosphorylation and accumulation through increasing the phosphorylation of MARK4 at Ser262 (Saito et al., 2019).

Besides the above-mentioned Aβ generation and NFT formation, CNS inflammation caused by microglia activation is another main feature of AD, which correlates with the plaque accumulation and may exacerbate the pathology of AD (Kitazawa et al., 2005). Aβ oligomers caused long-lasting activation of microglia and profound neuroinflammation in the hippocampus, which was mediated by over-activation of Cdk5/p25 complex. Cdk5 inhibitor roscovitine suppressed the inflammatory processes evoked by Aβ (Wilkaniec et al., 2018). Increased phospholipase A2 (PLA2) activity is centrally involved in inflammatory responses associated with several neurological disorders including AD (Farooqui et al., 2006). Soluble lipid mediator lysophosphatidylcholine (LPC) is generated through PLA2-mediated phosphatidylcholine hydrolysis (Steinbrecher et al., 1984). It has been demonstrated that p25 overexpression lead to glia activation, neuroinflammation and neurodegeneration partially through cytosolic PLA2-mediated LPC release in neurons (Sundaram et al., 2012). In addition, hyperactivation of Cdk5 mediated by p25 accumulation also accounts for exacerbation of tau pathology caused by lipopolysaccharide, a toxin used to induce nervous system inflammation (Kitazawa et al., 2005).

Oxidative stress and dysfunctional mitochondria appear at the early stages of AD. Cdk5 is an upstream activator of mitochondrial dysfunction in AD. The mitochondrial damage results in more ROS generation and Ca^{2+} level elevation, which in turn lead to even higher Cdk5 activity, then shapes a vicious circle and contributes to neuron loss in AD (Sun et al., 2008). A variety of molecules and signaling pathways are involved in the oxidation caused by aberrant Cdk5. Sun et al. (2008) reported that over-activation of Cdk5 led to mitochondrial damage and ROS accumulation through inactivating Prx1 and Prx2. Drp1 is a direct target of Cdk5, and Cdk5-mediated phosphorylation of Drp1 at Serine 579 regulates Aβ1-42 induced mitochondrial fission and neuronal toxicity. Inhibition of Cdk5 attenuated Aβ1-42 induced mitochondrial fission by inhibiting Drp1 phosphorylation in primary cultured

neurons (Guo et al., 2018). In cultured hippocampus HT-22 cells, Cdk5 inhibition also blocked mitochondrial fragmentation and AD-like hallmarks induced by streptozotocin through suppressing Drp1 phosphorylation (Park et al., 2020). JNK and p38 MAPK signaling pathways are able to be activated by oxidative stress and they are critically involved in Aβ-induced neurotoxicity and NFT formation (Yoshida et al., 2004). Enhanced JNK activity and increased p38 expression were observed in the affected brain areas of AD patients (Pei et al., 2001). Cdk5 interacts with p38/JNK pathways and contributes to the progressive Aβ deposits and AD development. In transgenic AD mouse model, co-immunoprecipitation of p-JNK and p-p38 with Cdk5 was significantly enhanced (Otth et al., 2003). Dysregulated Cdk5 caused elevation of p38 activity by increasing ROS in response to β-amyloid neurotoxic stimuli (Chang et al., 2010). As the major substrate involved in JNK-induced neurotoxicity, c-Jun is also over-activated in the several brain regions of AD patients. Cdk5 is reported to activate c-Jun through phosphorylating it at Ser63 and Ser73 *via* ROS-mediated activation of JNK (Sun et al., 2009). Myeloid cell leukemia sequence 1 (Mcl-1) is a member of the B-cell lymphoma 2 (Bcl-2) family, which is essential for neuronal survival (Arbour et al., 2008). The disease severity of AD patients was shown to be inversely correlated with Mcl-1 levels. Mcl-1 could be phosphorylated at Thr92 by Cdk5 following neurotoxic insults and this phosphorylation in turn caused Mcl-1 degradation and mitochondrial dysfunction, which promoted the neurodegenerative process of AD (Nikhil and Shah, 2017).

The aberrant Cdk5 activity seen in the progressive neurodegeneration of AD can also be caused by other mechanisms besides the dysfunction of its co-activators. Cancino et al. (2011) reported that Aβ-induced c-Abelson tyrosine kinase (c-Abl) activation facilitated tau phosphorylation *via* phosphorylating Cdk5 at Tyr15 *in vitro*. In the brains of AD mice, there was also an elevated Tyr15 phosphorylation of Cdk5 correlating with increased c-Abl levels (Cancino et al., 2011). Cdk5 could be S-nitrosylated by endogenously generated NO (Foster et al., 2009) and S-nitrosylated Cdk5 (SNO-Cdk5) in turn transnitrosylated Drp1 and resulted in mitochondrial fission in dendritic spines, which contributed to dendritic spine loss following Aβ treatment (Qu et al., 2011). Glutathione-S-transferase pi 1 (GSTP1) is able to dislodge p25/p35 and clear ROS accumulation and negatively regulates Cdk5 activity. There was a significant correlation between reduced GSTP1 levels and hyper-activation of Cdk5 in prefrontal cortex (PFC) of human AD brain (Sun et al., 2011). Furthermore, GSTP1 is capable of suppressing the activation of JNK/c-Jun pathway whereas it will lose its control following oxidative or chemical stress (Adler et al., 1999). GSTP1 was also shown to relieve the inhibition of Prx1 mediated by Cdk5 and reactivate it directly (Ralat et al., 2006).

The summation of above molecular pathways related with Cdk5 in AD is presented in **Figure 2**.

The role of cyclin-dependent kinases 5 in Huntington's disease

Huntington's disease (HD) is a progressive neurodegenerative disease characterized by chorea, personality changes and dementia (Kaminosono et al., 2008). It is mainly caused by selective loss of striatal medium-sized spiny neurons, resulted from abnormal polyglutamine (polyQ) expansion in the protein huntingtin (htt) (MacDonald et al., 2003). The role of Cdk5 and its co-activators in HD is still controversial. Some studies have reported their neuroprotective effects, while others have shown the opposite results.

It has been demonstrated that htt co-localized with Cdk5 in cellular membrane (Luo et al., 2005). Cdk5 could phosphorylate htt at Ser1181 and Ser1201 both in primary striatal cultures and in the mouse striatum following DNA damage, which prevented neuronal death and exerted neuroprotective effects. In the brain of HD mouse model, decreased Cdk5/p35 association at the late stage resulting from sustained DNA damage led to htt dephosphorylation and polyQ-induced p53 mediated neuronal death (Anne et al., 2007). Low levels of Cdk5 and p35 have been found in the striatum of postmortem HD patients and in HdhQ111 mutant mice (Luo et al., 2005; Paoletti et al., 2008). Consistent with this, there was an accumulation of p25 and increased p25/p35 ration in rat striatum following delivery of quinolinic acid (QA) (Park et al., 2012), a neurotoxin used to make experimental model of HD.

Phosphorylation of huntingtin at Ser421 has been shown to be neuroprotective against intrastriatal QA injection (Metzler et al., 2010). In contrary to the above results, Park et al. (2017) found that single p35 allele deletion resulted in a 17% enhancement of htt phosphorylation at Ser421, indicating that genetic reduction of p35 may be neuroprotective in the context of HD. Moreover, p35 hemizygous knockout mice also showed a much smaller striatal lesion size induced by QA compared with control (Park et al., 2012). Cherubini et al. (2015) reported that the increased activity and translocation of Drp1 to the mitochondria mediated by Cdk5 contributed to striatal neurodegeneration in HD. Inhibition of Cdk5 activity could attenuate mitochondrial fragmentation in striatal cells through modulating Drp1 activity and subcellular location. Cdk5 was also shown to be involved in the hippocampal and corticostriatal-dependent learning and memory impairment relevant to HD. Genetic reduction of Cdk5 alleviated corticostriatal-dependent learning deficits by increasing GluN2B surface levels in the cortex and striatum of HD model mice. Cdk5 knockdown enhanced Rac1 activity and subsequently increased hippocampal dendritic spine density,

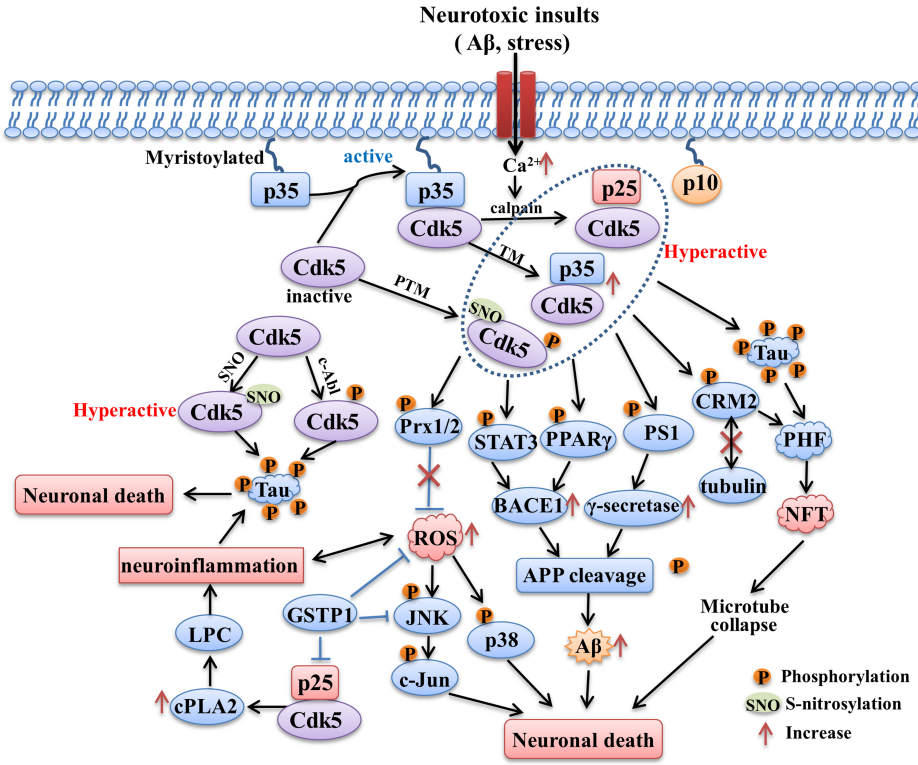

FIGURE 2
The role of Cdk5 in AD. Sustained activation of Cdk5 hyperphosphorylated tau protein and contributes to formation of PHF and NFT. CdK5 over-activation also induces intracellular Aβ accumulation through increasing APP processing mediated by BACE1 and γ-secretase. The phosphorylation of STAT3, PPARγ and PS1 contributed to the above process. Phosphorylation of Prx2 caused by aberrant Cdk5 activity inhibits its ROS scavenging ability and induces the activation of p38 MAPK and JNK pathways. Hyperactivation of Cdk5 also leads to neuroinflammation mediated by LPC accumulation through increasing cPLA2 activity. In addition, Cdk5 activity could be upregulated through being S-nitrosylated by endogenously generated NO and phosphorylated by c-Abl, both of process contribute to tau hyperphosphorylation. The tau hyperphosphorylation, NFT formation, intracellular Aβ generation, oxidative stress and neuroinflammation caused by aberrant Cdk5 activity all contribute to the neuronal death and neurodegeneration in AD.

which may be the mechanism underlying the improvement of hippocampal-dependent memory (Alvarez-Periel et al., 2018).

These findings suggest the multifaceted roles of Cdk5 in HD. Future studies are still needed to further clarify the relationship between Cdk5 dysfunction and HD pathogenesis.

Cyclin-dependent kinases 5 dysfunction contributes to stroke

Stoke is an acute neurologic event caused by dramatic reduction of cerebral blood flow to a localized part of brain (Bacigaluppi and Hermann, 2008). According to the affected brain regions, the cerebral ischemia can be divided into focal and global ischemia stroke (Traystman, 2003). A study analyzed the causes of death in Chinese residents from 1990 to 2017 and surprisingly found that stroke ranked the first, not cancer (Zhou M. et al., 2019). Many patients are disabled or died because of the untimely treatment due to the narrow time window of thrombolytic therapy. In addition, quite a few patients are not suitable for thrombolysis. Therefore, it is still necessary to further identify the pathological mechanisms underlying stroke and search for the potential pharmacological targets.

Disruption of the tight regulation of Cdk5 has been observed in stoke-affected brain tissue of patients (Mitsios et al., 2007), as well as in animal and cellular models of stroke (Meyer et al., 2014). The analysis of Cdk5 expression in human post-mortem brain showed that Cdk5- and p-Cdk5-positive neurons and microvessels increased dramatically in stroke-affected regions, accompanied by irregular arrangement and clumped in the cytoplasm (Mitsios et al., 2007). Ischemia induced either by oxygen glucose deprivation (OGD) in brain slices or middle cerebral artery occlusion (MCAO) *in vivo* both induced the cleavage of p35 into p25 (Meyer et al., 2014). Pharmacological inhibition or Cdk5 knockdown using the approach of peptide-directed lysosomal degradation prevented neuronal death, reduced infarction size and promoted the recovery of neurological functions following MCAO in mice (Meyer et al., 2014; Zhou Y. F. et al., 2019). In rat hypoxia/ischemia (HI) injury model, Cdk5 activity and p25

level were also significantly increased, and inhibiting Cdk5 with small peptide reduced cerebral infarct volume and promoted functional recovery (Tan et al., 2015).

The mitochondrial dysfunction and oxidative stress are also critically involved in the pathogenesis of stroke. Mitochondrial fusion and fission are two important ways to regulate mitochondrial function, balanced fusion/fission is essential for maintaining normal cellular physiology and fusion/fission imbalance will cause mitochondrial dysfunction and degeneration. Drp1 is a GTPase that controls the process of mitochondrial fission, and the elevated Drp1 phosphorylation will cause excessive mitochondrial fission. Hyper-activation of Cdk5 could increase the phosphorylation of Drp1 at Ser616, which in turn increased GTPase activity and accelerated mitochondrial fission, ultimately contributed to mitochondrial dysfunction and neuronal death following OGDR insults (Chen et al., 2021). Inhibition of Cdk5 hyperactivity could attenuate mitochondrial fragmentation and neuronal loss through reducing Drp1 phosphorylation at Ser616 (Chen et al., 2021). In human body, the oxidative/antioxidative balance is kept by a large group of antioxidant enzymes under physiological condition, which can catalyze hydrogen peroxide into stable non-toxic molecules (Apel and Hirt, 2004). Prx2 is such an antioxidant enzyme. Cdk5 phosphorylates Prx2 at Thr89 and this phosphorylation decreases Prx2 peroxidase activity and lowers its capacity to eliminate ROS which contributes to neuron loss subsequently (Qu et al., 2007). In both focal and global ischemia, elevated phosphorylation of Prx2 at Thr89 and ROS accumulation were found due to upregulated cytoplasmic Cdk5 activity (Rashidian et al., 2009). And p35 knockout mice displayed remarkably smaller infarct size following stroke insult due to a lower level of Prx2 phosphorylation (Rashidian et al., 2009).

The dysfunction of *N*-methyl-D-aspartate receptors (NMDARs) contributed to a variety of neurological diseases including stroke. Phosphorylation of NMDAR subunits at the cytoplasmic carboxyl termini is an important way to regulate NMDAR function. It has been shown that Cdk5 can phosphorylate NMDAR at multiple sites. The phosphorylation of GluN2A at Ser1232 by Cdk5 enhanced receptor function and promoted CA1 pyramidal neuron death following transient forebrain ischemia (Wang et al., 2003). The phosphorylation of GluN2B at Tyr1472 by Cdk5 promoted receptor internalization (Zhang et al., 2008), similarly phosphorylation of regulatory site Ser1116 also inhibited the membrane trafficking of GluN2B-containing NMDARs (Plattner et al., 2014). Cdk5 was also shown to phosphorylate GluN2B at Ser1284, which may contribute to the ischemic injury in both cultured neurons suffered from OGD-reperfusion and mice subjected to transient global ischemia (Lu et al., 2015). The anaphase-promoting complex/cyclosome (APC/C) is a E3 ubiquitin ligase that controls cell cycle progression (Peters, 2002). Cdh1 is the activator of APC/C and cyclin B1 is one substrate of APC/C–Cdh1, whose nuclear level is increased in affected neurons of stroke patients (Love, 2003). It is well known that abnormal release of glutamate caused by NMDAR overactivation is involved in stroke (Bossy-Wetzel et al., 2004). Cdk5 contributes to NMDAR-mediated neuronal excitotoxicity by phosphorylating Cdh1 at residues Ser40, Thr121, and Ser163, resulting in Cdh1 inactivation and cyclinB1 accumulation in the nucleus (Maestre et al., 2008).

Cyclin-dependent kinases 5 can modulate the process of cell apoptosis and cell cycle through regulating the function of transcription-related molecules, which may be another mechanism involved in stroke. MEF2 is a factor critical for neuronal survival. Activating MEF2 is pro-survival, whereas hyperphosphorylation of MEF2 contributes to neuronal apoptosis (Mao and Wiedmann, 1999). MEF2 can be phosphorylated at Ser408 and Ser444 directly by Cdk5 and this phosphorylation will lead to reduced MEF2 function due to the inhibition of MEF2 transactivation activity (Gong et al., 2003). Nuclear Cdk5 contributes to neuronal death following focal ischemia but not global ischemia by phosphorylating MEF2 (Tang et al., 2005). Histone deacetylase 1 (HDAC1) is critically involved in suppressing transcription of cell cycle genes and regulating the cell cycle (Lagger et al., 2002). Cdk5 was shown to inhibit HDAC1 function and induce double-strand DNA breaks and cell cycle reentry, resulting in neurodegeneration and neurologic defects following ischemia (Kim et al., 2008).

The Cdk5-modulated pathways involved in stroke are shown in **Figure 1**.

Cyclin-dependent kinases 5 dysfunction triggers anxiety/depression

Anxiety is the emotional response to threatening or potentially threatening stimuli (Sandford et al., 2000) and it is beneficial for the animals to cope with the stress. However, excessive anxious state or pathological anxiety is harmful, characterized by hypervigilance to threatening stimuli or negative events (Rosen and Schulkin, 1998). Depression is mainly manifested by anhedonia, loss of motivation and abnormal neurovegetative functions (Nestler and Carlezon, 2006). Anxiety and depression have become major public health issues and bring multiple challenges to the society. The current clinical strategies for depression and anxiety mainly act through modulating serotonergic system or GABAergic system. However, these medical approaches often have inadequate efficacy and can't meet clinical needs. Therefore, an urgent need to find new potential therapeutic targets emerges.

More and more evidences have shown that Cdk5 dysfunction plays important roles in psychiatric disorders. Analyzing postmortem brains of patients with major depression showed that Cdk5 activity was significantly increased in

Brodmann's area 25, a subregion of the PFC, which was implicated in major depression and treatment response (Papadopoulou et al., 2015). In rat depressive model induced by chronic mild stress, Cdk5 activity and p35 trafficking was enhanced in the hippocampal dentate gyrus, which was suppressed by the antidepressant venlafaxine (Zhu et al., 2012). The elevation of Cdk5 activity was also observed in several brain regions of anxious mice including basolateral amygdala, septal and lateral septum (Bignante et al., 2008). Pharmacological inhibition or genetic knockout of Cdk5 both significantly attenuated the depressive-like symptoms or aberrant anxiety-like phenotype in mice (Li G. et al., 2014).

There are multiple mechanisms involved in the regulation of anxiety/depression by Cdk5. The dysfunction of glucocorticoid receptor (GR) signaling critically contributed to the pathology of psychiatric disorders. Cdk5 was shown to phosphorylate GR at serine 232 and there was a significant correlation between elevated Cdk5 activity and enhanced GR phosphorylation in hippocampus and PFC of the depressive rats (Mitic et al., 2013). The mechanism study revealed that the aberrant GR phosphorylation may be attributed to the dysfunction of Cav1.2 subunit of the L-type calcium channel, which was closely related with stress-induced neuropsychiatric conditions. Lower levels of p25 production and GR phosphorylation was observed in the Cav1.2 heterozygous ($Cav1.2^{+/-}$) mice compared with control mice following chronic unpredictable stress, correlating with reduced depressive-like and anxiety-like behaviors (Bavley et al., 2017). Depression is the most common psychiatric comorbidity of HD. Inhibition of Cdk5 activity in the nucleus accumbens attenuated the depressive-like behaviors of HD mice through modulating dendritic spine plasticity mediated by dopamine- and cAMP-regulated phosphoprotein 32 (DARPP32)/β-adducin signaling pathway (Brito et al., 2019). Anomalous neurotransmission is an important mechanism underlying anxiety disorder. Cdk5 was shown to regulate anxiety-like behaviors through modulating neurotransmission and neuronal excitability. Conditional deletion of Cdk5 in parvalbumin (PV) interneurons results in increased GABAergic neurotransmission which in turn alleviated the anxiety-like behavior of mice (Rudenko et al., 2015). Optogenetic study showed that Cdk5 activation led to the decreased activation of excitatory neurons in the prelimbic cortex, and Cdk5 knockdown reversed the deactivation of these excitatory neurons and alleviated the anxiety-like behaviors induced by chronic inflammation (Wang et al., 2015).

Cyclin-dependent kinases 5 dysfunction elicits pathological pain

Acute nociceptive pain is the physiological sensation of injury that helps animals survive by promoting them to withdrawal from the harmful stimuli and avoid further contacting with such stimuli. However, pathological and chronic pain seems meaningless and will cause much distress. Allodynia and hyperalgesia are two kinds of behavioral phenotypes indicated by decreased threshold or amplification in the responsiveness to noxious stimulation following chronic pain (Rahn et al., 2013). Mounting evidences have shown that Cdk5 is a key molecule involved in pain modulation. In mice model of peripheral inflammatory pain, there were both an elevation of Cdk5 activity in dorsal root ganglia (DRG) and spinal dorsal horn (Wang et al., 2005; Yang et al., 2007). Roscovitine, a Cdk5 inhibitor, alleviated heat hyperalgesia induced by CFA and formalin in a dose-dependent manner (Wang et al., 2005). Conditional deletion of p35 in mice (p35-/-) resulted in decreased sensitivity to painful thermal stimulation due to reduced Cdk5 activity, whereas mice overexpressing p35 exhibited thermal hyperalgesia (Pareek et al., 2006).

Cyclin-dependent kinases 5 participates in the inflammatory pain-induced hypersensitivity through diverse pathways. Extracellular signal-regulated kinase 1 and 2 (ERK1/2) is fast activated in response to innocuous and noxious stimulation (Ji et al., 2002; Cruz et al., 2005). The levels of phosphorylated ERK1/2 (p-ERK) and phosphorylated Cdk5 at Ser159 (p-Cdk5) are increased in spinal cord dorsal horn following adjuvant-mediated inflammatory pain (Zhang X. et al., 2014). And inhibition of ERK1/2 significantly suppresses the nociceptive responses and enhancement of p-ERK and p-Cdk5 (Zhang X. et al., 2014). Tumor necrosis factor-α (TNF-α), a proinflammatory cytokines, participates in the onset and development of inflammatory pain. The release of TNF-α is elevated following peripheral inflammation, which triggers the activation of ERK1/2 and then results in the induction of early growth response 1 (Egr-1), a member of zinc-finger *trans*-activators. Subsequently, Egr-1 binds to the promoter region of p35 and increases Cdk5 activity (Utreras et al., 2009). These results indicate that ERK-mediated Cdk5 activation plays a vital role in the hypersensitivity of peripheral inflammatory pain.

Transient receptor potential vanilloid 1 (TRPV1) is mainly expressed in the nociceptive sensory neurons and potentiate pain sensitization in different pain models (Caterina et al., 1997; Davis et al., 2000). The phosphorylation of TRPV1 plays an important role in responding to a pain stimulus by regulating intracellular calcium levels (Pareek et al., 2007). Cdk5 regulates TRPV1 membrane trafficking through phosphorylating TRPV1 at the site of Thr407. Conditional Cdk5 knockout in small diameter sensory neurons (C-fibers) abolishes TRPV1 phosphorylation and leads to hypoalgesia (Pareek et al., 2006, 2007). Transforming growth factor-β1 (TGF-β1) signaling pathway is involved in modulating Cdk5-mediated TRPV1 phosphorylation under the condition of inflammation pain. TGF-β1 treatment increased Cdk5-mediated phosphorylation of TRPV1 at Thr407 *in vitro*. The conditional TGF-β1 knockout reduced Cdk5 activity and Cdk5-dependent TRPV1 phosphorylation with attenuation of thermal hyperalgesia in

mice following inflammatory pain (Utreras et al., 2012). TNF-α was shown to increase p35 expression, causing Cdk5-mediated TRPV1 phosphorylation and ROS production in nociceptive neurons and increased pain sensation (Sandoval et al., 2018). These results indicate that TRPV1 and TGF-β signaling participate in the modulation of pain sensation by Cdk5. BDNF-tyrosine kinase, type 2 (TrkB) signaling pathway has been shown to be critically involved in pain modulation. TrkB activation contributes to initiation and maintenance of both heat and mechanical hypersensitivity produced by tissue injury (Wang et al., 2009). Cdk5 is demonstrated to phosphorylate and activate TrkB at Ser478 residue (Lai et al., 2012). Inhibiting Cdk5 attenuates CFA-induced hypersensitivity through suppressing TrkB expression and blocking BDNF/TrkB signaling pathway, implying that the interaction between Cdk5 and BDNF/TrkB also plays a role in pain hypersensitivity induced by inflammation (Zhang H. H. et al., 2014).

Besides its involvement in inflammatory pain, Cdk5 has been also shown to modulate several other kinds of pain such as neuropathic pain (Li K. et al., 2014; Yang et al., 2014), bone cancer pain (Zhang R. et al., 2012), visceral pain (Chang et al., 2011), post-operative pain (Liu et al., 2014), orofacial pain (Prochazkova et al., 2013; Hu et al., 2022). For example, in the mouse neuropathic pain model induced by spinal nerve ligation, the expression of Cdk5 and its activators in DRG was elevated, which contributed to the mechanical allodynia (Gomez et al., 2020). Cdk5 inhibition attenuated mechanical allodynia and thermal hyperalgesia through suppressing mGluRs and (or) NMDAR phosphorylation in both bone cancer pain (Zhang R. et al., 2012) and post-operative pain (Liu et al., 2014) models. Depletion or overexpression of p35 caused mice to be less or more sensitive to orofacial mechanical stimulation, respectively (Prochazkova et al., 2013). Inhibition of Cdk5 activity could also alleviate facial pain by suppressing calcium-mediated trigeminal peripheral sensory neurons activation (Hu et al., 2022). The crucial roles of Cdk5 in pain modulation make it a promising non-opioid target for pain treatment.

Cyclin-dependent kinases 5 dysfunction contributes to epilepsy

Epilepsy affects over 70 million people worldwide, which is mainly manifested by recurrent seizures and brings a variety of physiological and psychosocial consequences (Thijs et al., 2019). The levels of Cdk5, p-Cdk5 and its kinase activity were significantly increased in the anterior temporal lobe samples from the patients with mesial temporal lobe

TABLE 1 List of major Cdk5 substrates reviewed in neurological disorders.

Substrates	Phosphorylation sites	Outcome	References
Drp1	Ser616 and Ser579	Promoting mitochondrial fission	Cherubini et al., 2015; Guo et al., 2018; Park et al., 2019; Chen et al., 2021
Parkin	Ser131	Reducing its E3 ubiquitin-ligase activity	Avraham et al., 2007
Glycoprotein 78	Ser516	Ubiquitination and degradation	Wang et al., 2018
Peroxidases 2	Thr89	Reducing its peroxidase activity and inducing ROS accumulation	Qu et al., 2007; Sun et al., 2008; Rashidian et al., 2009
EndoB1	Thr145	Autophagy induction	Wong et al., 2011
MEF2	Ser408 and Ser444	Inhibition of MEF2 transactivation activity and neuronal death	Gong et al., 2003; Zhang Q. et al., 2016
RKIP	Thr42	Cell cycle re-entry and neuron death	Wen et al., 2014
PPARγ	Ser273	Promoting BACE1 activity and Aβ production	Quan et al., 2019
Presenilin-1	Thr354	Dysfunction of γ-secretase and the alteration of Aβ42/Aβ40 ratio.	Lau et al., 2002
Tau	Multiple sites	Microtubule collapse and neurite retraction	Paudel, 1997
CRMP2	Ser522	Reducing microtubule assembly	Uchida et al., 2005
MARK4	Ser262	Tau phosphorylation and accumulation	Saito et al., 2019
Peroxidases 1	Thr90	Mitochondrial damage and ROS accumulation	Sun et al., 2008
c-Jun	Ser63 and Ser73	Activation of JNK pathway	Sun et al., 2009
Mcl-1	Thr92	Mcl-1 degradation and mitochondrial dysfunction	Nikhil and Shah, 2017
Huntingtin	Ser1181, Ser1201, and Ser421	Reducing neuronal death	Anne et al., 2007; Metzler et al., 2010
GluN2A	Ser1232	Enhancing receptor function	Wang et al., 2003
GluN2B	Tyr1472 and Ser1116	Promoting receptor internalization	Zhang et al., 2008; Plattner et al., 2014
Cdh1	Ser40, Thr121, and Ser163	CyclinB1 accumulation and neurotoxicity	Maestre et al., 2008
Glucocorticoid receptor	serine 232	Depressive phenotype	Mitic et al., 2013
TRPV1	threonine 407	Hyperalgesia	Pareek et al., 2007
TrkB	Ser478	Allodynia and hyperalgesia	Lai et al., 2012; Zhang X. et al., 2014

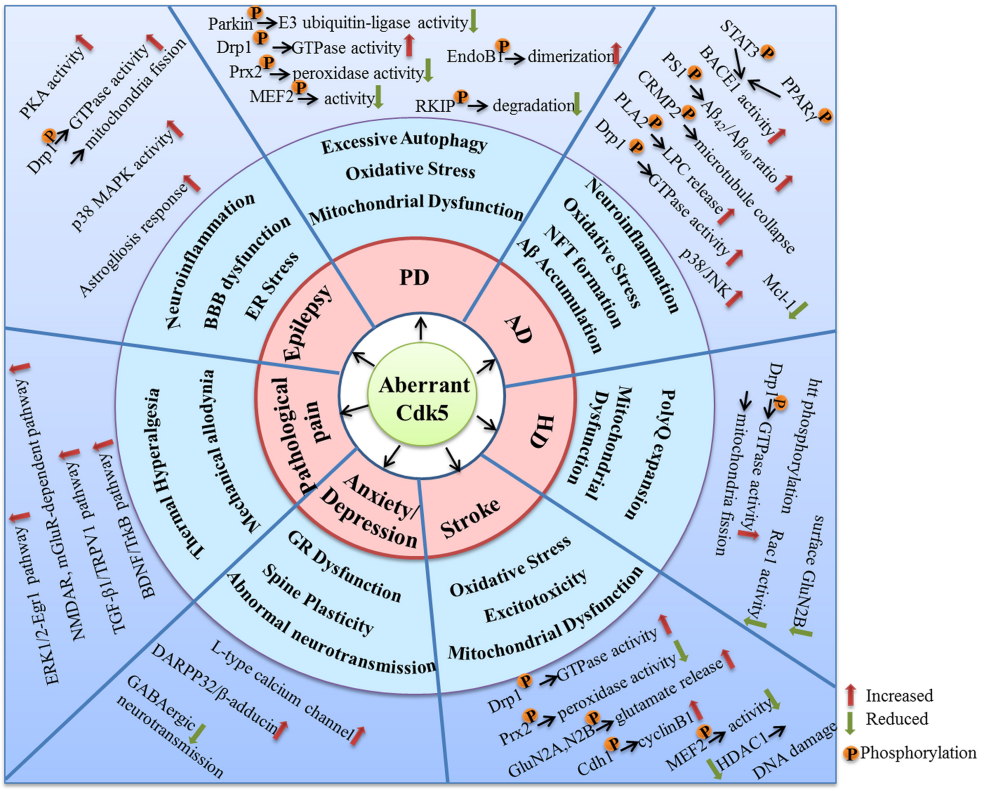

FIGURE 3
The molecular targets and mechanisms involved in the neurological disorders caused by aberrant Cdk5 activity.

epilepsy accompanied by hippocampal sclerosis (Banerjee et al., 2021). Hippocampal sclerosis (HS), characterized by segmental neuronal loss and gliosis, is the most common cause of refractory epilepsy in adults. The ratio of p25 to p35 and activity of Cdk5/p25 complex increased remarkably in the diseased hippocampi compared with the adjacent normal temporal lobe, indicating a pathological role of Cdk5/p25 in HS (Sen et al., 2006).

Sustained endoplasmic reticulum (ER) stress triggers the regional specific astroglial responses, which contributed to the status epilepticus (SE). Cdk5 phosphorylation was shown to be upregulated in the astrocytes within the hippocampus CA1 region and dentate gyrus following ER stress. Inhibition of Cdk5 with roscovitine markedly suppressed hippocampal astroglial response induced by ER stress (Lee and Kim, 2021), which may be mediated by reducing PKA activity and Drp1 phosphorylations (Hyun et al., 2017). Roscovitine was also shown to suppress SE-induced neuroinflammation mediated by glial responses *via* p38 MAPK inhibition in rat frontoparietal cortex (Kim et al., 2019). Blood–brain barrier (BBB) dysfunction is critically involved in epilepsy. Specific deletion of Cdk5 in the endothelial cells of BBB resulted in spontaneous seizures in mice, which may be attributed to the decreased astrocytic glutamate reuptake and elevated glutamatergic synaptic function (Liu et al., 2020).

Cyclin-dependent kinases 5 substrates

As one up-stream kinase in the nervous system, Cdk5 triggers the down-stream signaling pathways through interacting with its substrates. Numerous Cdk5 substrates have been detected and their abnormal alterations following aberrant Cdk5 activity are closely related with initiation and progression of neurological disorders. In this review, some important substrates of Cdk5 are listed in **Table 1**. The readers can be referred to prior reviews with a more comprehensive list of Cdk5 substrates (Dhavan and Tsai, 2001; Su and Tsai, 2011; Pao and Tsai, 2021).

Conclusion

As a kinase distributed extensively in the nervous system, Cdk5 plays crucial roles in various kinds of neuronal function. Aberrant activation of Cdk5 appears to be a

driving force for the initiation and progression of multiple neurological disorders. Numerous molecular targets and pharmacological mechanisms are involved in the Cdk5-mediated neurodysfunction (Figure 3). The extensive actions of Cdk5 discussed in this review suggest that it is a promising therapeutic target for neurological diseases. In fact, many small-molecule inhibitors and peptides have been synthetized and their beneficial effects in nervous system have been examined. Although quite a few inhibitors exhibit good neuroprotective properties in various preclinical studies, no selective Cdk5 kinase inhibitors have ever entered clinical trials for therapeutic intervention. A successful Cdk5 inhibitor for neurological diseases should be able to pass the BBB and have a high Cdk5 selectivity. Non-selective Cdk inhibitors are generally unfavorable and ineffective due to the potential off-target toxic and side effects. For example, roscovitine, one of the best known Cdk inhibitors, have been shown promising protective effects in nervous system through inhibiting Cdk5. However, roscovitine can also inhibit Cdk1, Cdk2, Cdk7, and Cdk9, the low selectivity for Cdk5 reduces its potential as a drug candidate targeting neurological disorders.

As the aberrant Cdk5 activity is generally caused by p25 accumulation, so small molecule protein-protein interaction (PPI) inhibitors targeted to disturb the interactions between Cdk5 and p25 may represent a promising strategy. It can not only eliminate Cdk5/p25 complex-induced hyper-activation but also retain the physiological function of Cdk5/p35. In addition, there is no concern about the selectivity, as the inhibitors are developed to target the specific PPI site of Cdk5 and p25 without affecting other Cdks kinase activity. However, it can be predicted that the development of any kind of drugs, including the small molecule PPI inhibitors, will not always be smooth. But it may shed light upon the treatment of Cdk5-related neurological diseases. Future extensive studies are still needed to define more precisely the role of Cdk5 hyperactivation in brain function impairments, and it will facilitate the discovery of more effective therapeutic strategies targeting Cdk5 aberrant activity implicated in neurological disorders.

Author contributions

ZT and JT designed the review. JT and X-QW searched the literature. ZT and BF made the figures and table. ZT, X-QW, BF, and JT wrote and edited the original draft. All authors have read and agreed to the published version of the manuscript.

Funding

Work in our laboratories was supported by National Natural Science Foundation of China (No. 81801329), Chongqing Natural Science Foundation (No. cstc2021jcyj-msxmX0610), Science and Technology Research Project of Chongqing Education Commission (No. KJQN202100213), Fundamental Research Funds for the Central Universities (No. SWU-KQ22018) to ZT, and Guangdong Basic and Applied Basic Research Foundation (No. 2020A1515110564) to X-QW.

Conflict of interest

The authors declare that the research was conducted in the absence of any commercial or financial relationships that could be construed as a potential conflict of interest.

Publisher's note

All claims expressed in this article are solely those of the authors and do not necessarily represent those of their affiliated organizations, or those of the publisher, the editors and the reviewers. Any product that may be evaluated in this article, or claim that may be made by its manufacturer, is not guaranteed or endorsed by the publisher.

References

Adler, V., Yin, Z., Fuchs, S. Y., Benezra, M., Rosario, L., Tew, K. D., et al. (1999). Regulation of JNK signaling by GSTp. *EMBO J.* 18, 1321–1334. doi: 10.1093/emboj/18.5.1321

Alvarez-Periel, E., Puigdellivol, M., Brito, V., Plattner, F., Bibb, J. A., Alberch, J., et al. (2018). Cdk5 contributes to Huntington's disease learning and memory deficits *via* modulation of brain region-specific substrates. *Mol. Neurobiol.* 55, 6250–6268. doi: 10.1007/s12035-017-0828-4

Alvira, D., Ferrer, I., Gutierrez-Cuesta, J., Garcia-Castro, B., Pallas, M., and Camins, A. (2008). Activation of the calpain/cdk5/p25 pathway in the girus cinguli in Parkinson's disease. *Parkinsonism Relat. Disord.* 14, 309–313. doi: 10.1016/j.parkreldis.2007.09.005

Anglade, P., Vyas, S., Javoy-Agid, F., Herrero, M. T., Michel, P. P., Marquez, J., et al. (1997). Apoptosis and autophagy in nigral neurons of patients with Parkinson's disease. *Histol. Histopathol.* 12, 25–31.

Anne, S. L., Saudou, F., and Humbert, S. (2007). Phosphorylation of huntingtin by cyclin-dependent kinase 5 is induced by DNA damage and regulates wild-type and mutant huntingtin toxicity in neurons. *J. Neurosci.* 27, 7318–7328. doi: 10.1523/JNEUROSCI.1831-07.2007

Apel, K., and Hirt, H. (2004). Reactive oxygen species: Metabolism, oxidative stress, and signal transduction. *Annu. Rev. Plant Biol.* 55, 373–399. doi: 10.1146/annurev.arplant.55.031903.141701

Arbour, N., Vanderluit, J. L., Le Grand, J. N., Jahani-Asl, A., Ruzhynsky, V. A., Cheung, E. C., et al. (2008). Mcl-1 is a key regulator of apoptosis during CNS development and after DNA damage. *J. Neurosci.* 28, 6068–6078. doi: 10.1523/JNEUROSCI.4940-07.2008

Arias-Vasquez, A., Aulchenko, Y. S., Isaacs, A., van Oosterhout, A., Sleegers, K., Hofman, A., et al. (2008). Cyclin-dependent kinase 5 is associated with risk for Alzheimer's disease in a Dutch population-based study. *J. Neurol.* 255, 655–662. doi: 10.1007/s00415-008-0770-5

Asada, A., Yamamoto, N., Gohda, M., Saito, T., Hayashi, N., and Hisanaga, S. (2008). Myristoylation of p39 and p35 is a determinant of cytoplasmic or nuclear localization of active cyclin-dependent kinase 5 complexes. *J. Neurochem.* 106, 1325–1336. doi: 10.1111/j.1471-4159.2008.05500.x

Avraham, E., Rott, R., Liani, E., Szargel, R., and Engelender, S. (2007). Phosphorylation of Parkin by the cyclin-dependent kinase 5 at the linker region modulates its ubiquitin-ligase activity and aggregation. *J. Biol. Chem.* 282, 12842–12850. doi: 10.1074/jbc.M608243200

Bacigaluppi, M., and Hermann, D. M. (2008). New targets of neuroprotection in ischemic stroke. *ScientificWorldJournal* 8, 698–712. doi: 10.1100/tsw.2008.94

Banerjee, J., Srivastava, A., Sharma, D., Dey, S., Tripathi, M., Sharma, M. C., et al. (2021). Differential regulation of excitatory synaptic transmission in the hippocampus and anterior temporal lobe by cyclin dependent kinase 5 (Cdk5) in mesial temporal lobe epilepsy with hippocampal sclerosis (MTLE-HS). *Neurosci. Lett.* 761:136096. doi: 10.1016/j.neulet.2021.136096

Bavley, C. C., Fischer, D. K., Rizzo, B. K., and Rajadhyaksha, A. M. (2017). Cav1.2 channels mediate persistent chronic stress-induced behavioral deficits that are associated with prefrontal cortex activation of the p25/Cdk5-glucocorticoid receptor pathway. *Neurobiol. Stress* 7, 27–37. doi: 10.1016/j.ynstr.2017.02.004

Bignante, E. A., Rodriguez Manzanares, P. A., Mlewski, E. C., Bertotto, M. E., Bussolino, D. F., Paglini, G., et al. (2008). Involvement of septal Cdk5 in the emergence of excessive anxiety induced by stress. *Eur. Neuropsychopharmacol.* 18, 578–588. doi: 10.1016/j.euroneuro.2008.02.007

Binukumar, B. K., Shukla, V., Amin, N. D., Grant, P., Bhaskar, M., Skuntz, S., et al. (2015). Peptide TFP5/TP5 derived from Cdk5 activator P35 provides neuroprotection in the MPTP model of Parkinson's disease. *Mol. Biol. Cell* 26, 4478–4491. doi: 10.1091/mbc.E15-06-0415

Bossy-Wetzel, E., Schwarzenbacher, R., and Lipton, S. A. (2004). Molecular pathways to neurodegeneration. *Nat. Med.* 10 Suppl, S2–S9. doi: 10.1038/nm1067

Brito, V., Giralt, A., Masana, M., Royes, A., Espina, M., Sieiro, E., et al. (2019). Cyclin-dependent kinase 5 dysfunction contributes to depressive-like behaviors in Huntington's disease by altering the DARPP-32 phosphorylation status in the nucleus accumbens. *Biol. Psychiatry* 86, 196–207. doi: 10.1016/j.biopsych.2019.03.001

Buchner, A., Krumova, P., Ganesan, S., Bahr, M., Eckermann, K., and Weishaupt, J. H. (2015). Sumoylation of p35 modulates p35/cyclin-dependent kinase (Cdk) 5 complex activity. *Neuromolecular Med.* 17, 12–23. doi: 10.1007/s12017-014-8336-4

Cancino, G. I., Perez de Arce, K., Castro, P. U., Toledo, E. M., von Bernhardi, R., and Alvarez, A. R. (2011). c-Abl tyrosine kinase modulates tau pathology and Cdk5 phosphorylation in AD transgenic mice. *Neurobiol. Aging* 32, 1249–1261. doi: 10.1016/j.neurobiolaging.2009.07.007

Castro-Alvarez, J. F., Uribe-Arias, S. A., Kosik, K. S., and Cardona-Gomez, G. P. (2014). Long- and short-term CDK5 knockdown prevents spatial memory dysfunction and tau pathology of triple transgenic Alzheimer's mice. *Front. Aging Neurosci.* 6:243. doi: 10.3389/fnagi.2014.00243

Caterina, M. J., Schumacher, M. A., Tominaga, M., Rosen, T. A., Levine, J. D., and Julius, D. (1997). The capsaicin receptor: A heat-activated ion channel in the pain pathway. *Nature* 389, 816–824. doi: 10.1038/39807

Chae, T., Kwon, Y. T., Bronson, R., Dikkes, P., Li, E., and Tsai, L. H. (1997). Mice lacking p35, a neuronal specific activator of Cdk5, display cortical lamination defects, seizures, and adult lethality. *Neuron* 18, 29–42. doi: 10.1016/s0896-6273(01)80044-1

Chang, C. H., Peng, H. Y., Wu, H. C., Lai, C. Y., Hsieh, M. C., and Lin, T. B. (2011). Cyclophosphamide induces NR2B phosphorylation-dependent facilitation on spinal reflex potentiation. *Am. J. Physiol. Renal Physiol.* 300, F692–F699. doi: 10.1152/ajprenal.00531.2010

Chang, K. H., de Pablo, Y., Lee, H. P., Lee, H. G., Smith, M. A., and Shah, K. (2010). Cdk5 is a major regulator of p38 cascade: Relevance to neurotoxicity in Alzheimer's disease. *J. Neurochem.* 113, 1221–1229. doi: 10.1111/j.1471-4159.2010.06687.x

Chavez-Gutierrez, L., Bammens, L., Benilova, I., Vandersteen, A., Benurwar, M., Borgers, M., et al. (2012). The mechanism of gamma-Secretase dysfunction in familial Alzheimer disease. *EMBO J.* 31, 2261–2274. doi: 10.1038/emboj.2012.79

Chen, C., Peng, X., Tang, J., Hu, Z., Tan, J., and Zeng, L. (2021). CDK5 inhibition protects against OGDR induced mitochondrial fragmentation and apoptosis through regulation of Drp1S616 phosphorylation. *Life Sci.* 269:119062. doi: 10.1016/j.lfs.2021.119062

Cherubini, M., Puigdellivol, M., Alberch, J., and Gines, S. (2015). Cdk5-mediated mitochondrial fission: A key player in dopaminergic toxicity in Huntington's disease. *Biochim. Biophys. Acta* 1852(10 Pt A), 2145–2160. doi: 10.1016/j.bbadis.2015.06.025

Cho, D. H., Nakamura, T., Fang, J., Cieplak, P., Godzik, A., Gu, Z., et al. (2009). S-nitrosylation of Drp1 mediates beta-amyloid-related mitochondrial fission and neuronal injury. *Science* 324, 102–105. doi: 10.1126/science.1171091

Cole, A. R., Noble, W., van Aalten, L., Plattner, F., Meimaridou, R., Hogan, D., et al. (2007). Collapsin response mediator protein-2 hyperphosphorylation is an early event in Alzheimer's disease progression. *J. Neurochem.* 103, 1132–1144. doi: 10.1111/j.1471-4159.2007.04829.x

Cruz, C. D., Neto, F. L., Castro-Lopes, J., McMahon, S. B., and Cruz, F. (2005). Inhibition of ERK phosphorylation decreases nociceptive behaviour in monoarthritic rats. *Pain* 116, 411–419. doi: 10.1016/j.pain.2005.05.031

Davis, J. B., Gray, J., Gunthorpe, M. J., Hatcher, J. P., Davey, P. T., Overend, P., et al. (2000). Vanilloid receptor-1 is essential for inflammatory thermal hyperalgesia. *Nature* 405, 183–187. doi: 10.1038/35012076

Dhavan, R., and Tsai, L. H. (2001). A decade of CDK5. *Nat. Rev. Mol. Cell Biol.* 2, 749–759. doi: 10.1038/35096019

Farooqui, A. A., Ong, W. Y., and Horrocks, L. A. (2006). Inhibitors of brain phospholipase A2 activity: Their neuropharmacological effects and therapeutic importance for the treatment of neurologic disorders. *Pharmacol. Rev.* 58, 591–620. doi: 10.1124/pr.58.3.7

Foster, M. W., Forrester, M. T., and Stamler, J. S. (2009). A protein microarray-based analysis of S-nitrosylation. *Proc. Natl. Acad. Sci. U.S.A.* 106, 18948–18953. doi: 10.1073/pnas.0900729106

Fraser, P. E., Yang, D. S., Yu, G., Levesque, L., Nishimura, M., Arawaka, S., et al. (2000). Presenilin structure, function and role in Alzheimer disease. *Biochim. Biophys. Acta* 1502, 1–15. doi: 10.1016/S0925-4439(00)00028-4

Fukata, Y., Itoh, T. J., Kimura, T., Menager, C., Nishimura, T., Shiromizu, T., et al. (2002). CRMP-2 binds to tubulin heterodimers to promote microtubule assembly. *Nat. Cell Biol.* 4, 583–591. doi: 10.1038/ncb825

Gomez, K., Calderon-Rivera, A., Sandoval, A., Gonzalez-Ramirez, R., Vargas-Parada, A., Ojeda-Alonso, J., et al. (2020). Cdk5-dependent phosphorylation of CaV3.2 T-type channels: Possible role in nerve ligation-induced neuropathic allodynia and the compound action potential in primary afferent C fibers. *J. Neurosci.* 40, 283–296. doi: 10.1523/JNEUROSCI.0181-19.2019

Gong, X., Tang, X., Wiedmann, M., Wang, X., Peng, J., Zheng, D., et al. (2003). Cdk5-mediated inhibition of the protective effects of transcription factor MEF2 in neurotoxicity-induced apoptosis. *Neuron* 38, 33–46. doi: 10.1016/s0896-6273(03)00191-0

Granovsky, A. E., and Rosner, M. R. (2008). Raf kinase inhibitory protein: A signal transduction modulator and metastasis suppressor. *Cell Res.* 18, 452–457. doi: 10.1038/cr.2008.43

Guo, M. Y., Shang, L., Hu, Y. Y., Jiang, L. P., Wan, Y. Y., Zhou, Q. Q., et al. (2018). The role of Cdk5-mediated Drp1 phosphorylation in Abeta1-42 induced mitochondrial fission and neuronal apoptosis. *J. Cell Biochem.* 119, 4815–4825. doi: 10.1002/jcb.26680

Hellmich, M. R., Pant, H. C., Wada, E., and Battey, J. F. (1992). Neuronal cdc2-like kinase: A cdc2-related protein kinase with predominantly neuronal expression. *Proc. Natl. Acad. Sci. U.S.A.* 89, 10867–10871. doi: 10.1073/pnas.89.22.10867

Hu, M., Doyle, A. D., Yamada, K. M., and Kulkarni, A. B. (2022). Visualization of trigeminal ganglion sensory neuronal signaling regulated by Cdk5. *Cell Rep.* 38:110458. doi: 10.1016/j.celrep.2022.110458

Huang, Y., Huang, W., Huang, Y., Song, P., Zhang, M., Zhang, H. T., et al. (2020). Cdk5 inhibitory peptide prevents loss of neurons and alleviates behavioral changes in p25 transgenic mice. *J. Alzheimers Dis.* 74, 1231–1242. doi: 10.3233/JAD-191098

Hyun, H. W., Min, S. J., and Kim, J. E. (2017). CDK5 inhibitors prevent astroglial apoptosis and reactive astrogliosis by regulating PKA and DRP1 phosphorylations in the rat *Hippocampus*. *Neurosci. Res.* 119, 24–37. doi: 10.1016/j.neures.2017.01.006

Ino, H., Ishizuka, T., Chiba, T., and Tatibana, M. (1994). Expression of CDK5 (PSSALRE kinase), a neural cdc2-related protein kinase, in the mature and developing mouse central and peripheral nervous systems. *Brain Res.* 661, 196–206. doi: 10.1016/0006-8993(94)91197-5

Ji, R. R., Befort, K., Brenner, G. J., and Woolf, C. J. (2002). ERK MAP kinase activation in superficial spinal cord neurons induces prodynorphin and NK-1 upregulation and contributes to persistent inflammatory pain hypersensitivity. *J. Neurosci.* 22, 478–485. doi: 10.1523/JNEUROSCI.22-02-00478.2002

Kaminosono, S., Saito, T., Oyama, F., Ohshima, T., Asada, A., Nagai, Y., et al. (2008). Suppression of mutant Huntingtin aggregate formation by Cdk5/p35 through the effect on microtubule stability. *J. Neurosci.* 28, 8747–8755. doi: 10.1523/JNEUROSCI.0973-08.2008

Kawauchi, T., Chihama, K., Nabeshima, Y., and Hoshino, M. (2006). Cdk5 phosphorylates and stabilizes p27kip1 contributing to actin organization and cortical neuronal migration. *Nat. Cell Biol.* 8, 17–26. doi: 10.1038/ncb1338

Kim, D., Frank, C. L., Dobbin, M. M., Tsunemoto, R. K., Tu, W., Peng, P. L., et al. (2008). Deregulation of HDAC1 by p25/Cdk5 in neurotoxicity. *Neuron* 60, 803–817. doi: 10.1016/j.neuron.2008.10.015

Kim, J. E., Park, H., Choi, S. H., Kong, M. J., and Kang, T. C. (2019). Roscovitine Attenuates microglia activation and monocyte infiltration *via* p38 MAPK inhibition in the rat frontoparietal cortex following status epilepticus. *Cells* 8:746. doi: 10.3390/cells8070746

Kitazawa, M., Oddo, S., Yamasaki, T. R., Green, K. N., and LaFerla, F. M. (2005). Lipopolysaccharide-induced inflammation exacerbates tau pathology by a cyclin-dependent kinase 5-mediated pathway in a transgenic model of Alzheimer's disease. *J. Neurosci.* 25, 8843–8853. doi: 10.1523/JNEUROSCI.2868-05.2005

Ko, J., Humbert, S., Bronson, R. T., Takahashi, S., Kulkarni, A. B., Li, E., et al. (2001). p35 and p39 are essential for cyclin-dependent kinase 5 function during neurodevelopment. *J. Neurosci.* 21, 6758–6771. doi: 10.1523/JNEUROSCI.21-17-06758.2001

Kobayashi, H., Saito, T., Sato, K., Furusawa, K., Hosokawa, T., Tsutsumi, K., et al. (2014). Phosphorylation of cyclin-dependent kinase 5 (Cdk5) at Tyr-15 is inhibited by Cdk5 activators and does not contribute to the activation of Cdk5. *J. Biol. Chem.* 289, 19627–19636. doi: 10.1074/jbc.M113.501148

Lagger, G., O'Carroll, D., Rembold, M., Khier, H., Tischler, J., Weitzer, G., et al. (2002). Essential function of histone deacetylase 1 in proliferation control and CDK inhibitor repression. *EMBO J.* 21, 2672–2681. doi: 10.1093/emboj/21.11.2672

Lai, K. O., Wong, A. S., Cheung, M. C., Xu, P., Liang, Z., Lok, K. C., et al. (2012). TrkB phosphorylation by Cdk5 is required for activity-dependent structural plasticity and spatial memory. *Nat. Neurosci.* 15, 1506–1515. doi: 10.1038/nn.3237

Lau, K. F., Howlett, D. R., Kesavapany, S., Standen, C. L., Dingwall, C., McLoughlin, D. M., et al. (2002). Cyclin-dependent kinase-5/p35 phosphorylates Presenilin 1 to regulate carboxy-terminal fragment stability. *Mol. Cell Neurosci.* 20, 13–20. doi: 10.1006/mcne.2002.1108

Lau, L. F., and Ahlijanian, M. K. (2003). Role of cdk5 in the pathogenesis of Alzheimer's disease. *Neurosignals* 12, 209–214. doi: 10.1159/000074622

Lee, D. S., and Kim, J. E. (2021). Regional specific activations of ERK1/2 and CDK5 differently regulate astroglial responses to ER stress in the rat hippocampus following status epilepticus. *Brain Res.* 1753:147262. doi: 10.1016/j.brainres.2020.147262

Lee, J., Ko, Y. U., Chung, Y., Yun, N., Kim, M., Kim, K., et al. (2018). The acetylation of cyclin-dependent kinase 5 at lysine 33 regulates kinase activity and neurite length in hippocampal neurons. *Sci. Rep.* 8:13676. doi: 10.1038/s41598-018-31785-9

Lee, J., Yun, N., Kim, C., Song, M. Y., Park, K. S., and Oh, Y. J. (2014). Acetylation of cyclin-dependent kinase 5 is mediated by GCN5. *Biochem. Biophys. Res. Commun.* 447, 121–127. doi: 10.1016/j.bbrc.2014.03.118

Lee, M. G., and Nurse, P. (1987). Complementation used to clone a human homologue of the fission yeast cell cycle control gene cdc2. *Nature* 327, 31–35. doi: 0.1038/327031a0

Lee, M. S., Kwon, Y. T., Li, M., Peng, J., Friedlander, R. M., and Tsai, L. H. (2000). Neurotoxicity induces cleavage of p35 to p25 by calpain. *Nature* 405, 360–364. doi: 10.1038/35012636

Li, G., Liu, T., Kong, X., Wang, L., and Jin, X. (2014). Hippocampal glycogen synthase kinase 3beta is critical for the antidepressant effect of cyclin-dependent kinase 5 inhibitor in rats. *J. Mol. Neurosci.* 54, 92–99. doi: 10.1007/s12031-014-0254-2

Li, K., Zhao, G. Q., Li, L. Y., Wu, G. Z., and Cui, S. S. (2014). Epigenetic upregulation of Cdk5 in the dorsal horn contributes to neuropathic pain in rats. *Neuroreport* 25, 1116–1121. doi: 10.1097/WNR.0000000000000237

Li, W., Allen, M. E., Rui, Y., Ku, L., Liu, G., Bankston, A. N., et al. (2016). p39 is responsible for increasing Cdk5 activity during postnatal neuron differentiation and governs neuronal network formation and epileptic responses. *J. Neurosci.* 36, 11283–11294. doi: 10.1523/JNEUROSCI.1155-16.2016

Liu, X. X., Yang, L., Shao, L. X., He, Y., Wu, G., Bao, Y. H., et al. (2020). Endothelial Cdk5 deficit leads to the development of spontaneous epilepsy through CXCL1/CXCR2-mediated reactive astrogliosis. *J. Exp. Med.* 217:e20180992. doi: 10.1084/jem.20180992

Liu, X., Liu, Y., Zhang, J., Zhang, W., Sun, Y. E., Gu, X., et al. (2014). Intrathecal administration of roscovitine prevents remifentanil-induced postoperative hyperalgesia and decreases the phosphorylation of N-methyl-D-aspartate receptor and metabotropic glutamate receptor 5 in spinal cord. *Brain Res. Bull.* 106, 9–16. doi: 10.1016/j.brainresbull.2014.04.008

Love, S. (2003). Neuronal expression of cell cycle-related proteins after brain ischaemia in man. *Neurosci. Lett.* 353, 29–32. doi: 10.1016/j.neulet.2003.09.004

Lu, W., Ai, H., Peng, L., Wang, J. J., Zhang, B., Liu, X., et al. (2015). A novel phosphorylation site of N-methyl-D-aspartate receptor GluN2B at S1284 is regulated by Cdk5 in neuronal ischemia. *Exp. Neurol.* 271, 251–258. doi: 10.1016/j.expneurol.2015.06.016

Luo, S., Vacher, C., Davies, J. E., and Rubinsztein, D. C. (2005). Cdk5 phosphorylation of huntingtin reduces its cleavage by caspases: Implications for mutant huntingtin toxicity. *J. Cell Biol.* 169, 647–656. doi: 10.1083/jcb.200412071

MacDonald, M. E., Gines, S., Gusella, J. F., and Wheeler, V. C. (2003). Huntington's disease. *Neuromolecular Med.* 4, 7–20.

Maestre, C., Delgado-Esteban, M., Gomez-Sanchez, J. C., Bolanos, J. P., and Almeida, A. (2008). Cdk5 phosphorylates Cdh1 and modulates cyclin B1 stability in excitotoxicity. *EMBO J.* 27, 2736–2745. doi: 10.1038/emboj.2008.195

Malumbres, M. (2014). Cyclin-dependent kinases. *Genome Biol.* 15:122.

Malumbres, M., Harlow, E., Hunt, T., Hunter, T., Lahti, J. M., Manning, G., et al. (2009). Cyclin-dependent kinases: A family portrait. *Nat. Cell Biol.* 11, 1275–1276.

Mao, Z., and Wiedmann, M. (1999). Calcineurin enhances MEF2 DNA binding activity in calcium-dependent survival of cerebellar granule neurons. *J. Biol. Chem.* 274, 31102–31107. doi: 10.1074/jbc.274.43.31102

Mao, Z., Bonni, A., Xia, F., Nadal-Vicens, M., and Greenberg, M. E. (1999). Neuronal activity-dependent cell survival mediated by transcription factor MEF2. *Science* 286, 785–790.

Metwally, E., Zhao, G., and Zhang, Y. Q. (2021). The calcium-dependent protease calpain in neuronal remodeling and neurodegeneration. *Trends Neurosci.* 44, 741–752.

Metzler, M., Gan, L., Mazarei, G., Graham, R. K., Liu, L., Bissada, N., et al. (2010). Phosphorylation of huntingtin at Ser421 in YAC128 neurons is associated with protection of YAC128 neurons from NMDA-mediated excitotoxicity and is modulated by PP1 and PP2A. *J. Neurosci.* 30, 14318–14329. doi: 10.1523/JNEUROSCI.1589-10.2010

Meyer, D. A., Torres-Altoro, M. I., Tan, Z., Tozzi, A., Di Filippo, M., DiNapoli, V., et al. (2014). Ischemic stroke injury is mediated by aberrant Cdk5. *J. Neurosci.* 34, 8259–8267. doi: 10.1523/JNEUROSCI.4368-13.2014

Minegishi, S., Asada, A., Miyauchi, S., Fuchigami, T., Saito, T., and Hisanaga, S. (2010). Membrane association facilitates degradation and cleavage of the cyclin-dependent kinase 5 activators p35 and p39. *Biochemistry* 49, 5482–5493. doi: 10.1021/bi100631f

Mitic, M., Simic, I., Djordjevic, J., Radojcic, M. B., and Adzic, M. (2013). Gender-specific effects of fluoxetine on hippocampal glucocorticoid receptor phosphorylation and behavior in chronically stressed rats. *Neuropharmacology* 70, 100–111. doi: 10.1016/j.neuropharm.2012.12.012

Mitsios, N., Pennucci, R., Krupinski, J., Sanfeliu, C., Gaffney, J., Kumar, P., et al. (2007). Expression of cyclin-dependent kinase 5 mRNA and protein in the human brain following acute ischemic stroke. *Brain Pathol.* 17, 11–23. doi: 10.1111/j.1750-3639.2006.00031.x

Mount, M. P., Zhang, Y., Amini, M., Callaghan, S., Kulczycki, J., Mao, Z., et al. (2013). Perturbation of transcription factor Nur77 expression mediated by myocyte enhancer factor 2D (MEF2D) regulates dopaminergic neuron loss in response to 1-methyl-4-phenyl-1,2,3,6-tetrahydropyridine (MPTP). *J. Biol. Chem.* 288, 14362–14371. doi: 10.1074/jbc.M112.439216

Mushtaq, G., Greig, N. H., Anwar, F., Al-Abbasi, F. A., Zamzami, M. A., Al-Talhi, H. A., et al. (2016). Neuroprotective mechanisms mediated by CDK5 inhibition. *Curr. Pharm. Des.* 22, 527–534.

Nakamura, S., Kawamoto, Y., Nakano, S., Akiguchi, I., and Kimura, J. (1997). p35nck5a and cyclin-dependent kinase 5 colocalize in Lewy bodies of brains with Parkinson's disease. *Acta Neuropathol.* 94, 153–157. doi: 10.1007/s004010050687

Nestler, E. J., and Carlezon, W. A. Jr. (2006). The mesolimbic dopamine reward circuit in depression. *Biol. Psychiatry* 59, 1151–1159.

Nikhil, K., and Shah, K. (2017). The Cdk5-Mcl-1 axis promotes mitochondrial dysfunction and neurodegeneration in a model of Alzheimer's disease. *J. Cell Sci.* 130, 3023–3039. doi: 10.1242/jcs.205666

Nishimura, Y. V., Sekine, K., Chihama, K., Nakajima, K., Hoshino, M., Nabeshima, Y., et al. (2010). Dissecting the factors involved in the locomotion mode of neuronal migration in the developing cerebral cortex. *J. Biol. Chem.* 285, 5878–5887. doi: 10.1074/jbc.M109.033761

Obeso, J. A., Rodriguez-Oroz, M. C., Goetz, C. G., Marin, C., Kordower, J. H., Rodriguez, M., et al. (2010). Missing pieces in the Parkinson's disease puzzle. *Nat. Med.* 16, 653–661.

Ohshima, T., Hirasawa, M., Tabata, H., Mutoh, T., Adachi, T., Suzuki, H., et al. (2007). Cdk5 is required for multipolar-to-bipolar transition during radial neuronal migration and proper dendrite development of pyramidal neurons in the cerebral cortex. *Development* 134, 2273–2282. doi: 10.1242/dev.02854

Ohshima, T., Ward, J. M., Huh, C. G., Longenecker, G., Veeranna, Pant, H. C., et al. (1996). Targeted disruption of the cyclin-dependent kinase 5 gene results in abnormal corticogenesis, neuronal pathology and perinatal death. *Proc. Natl. Acad. Sci. U.S.A.* 93, 11173–11178. doi: 10.1073/pnas.93.20.11173

Otth, C., Mendoza-Naranjo, A., Mujica, L., Zambrano, A., Concha, I. I., and Maccioni, R. B. (2003). Modulation of the JNK and p38 pathways by cdk5 protein kinase in a transgenic mouse model of Alzheimer's disease. *Neuroreport* 14, 2403–2409. doi: 10.1097/00001756-200312190-00023

Pao, P. C., and Tsai, L. H. (2021). Three decades of Cdk5. *J. Biomed. Sci.* 28:79. doi: 10.1186/s12929-021-00774-y

Paoletti, P., Vila, I., Rife, M., Lizcano, J. M., Alberch, J., and Gines, S. (2008). Dopaminergic and glutamatergic signaling crosstalk in Huntington's disease neurodegeneration: The role of p25/cyclin-dependent kinase 5. *J. Neurosci.* 28, 10090–10101. doi: 10.1523/JNEUROSCI.3237-08.2008

Papadopoulou, A., Siamatras, T., Delgado-Morales, R., Amin, N. D., Shukla, V., Zheng, Y. L., et al. (2015). Acute and chronic stress differentially regulate cyclin-dependent kinase 5 in mouse brain: Implications to glucocorticoid actions and major depression. *Transl. Psychiatry* 5:e578. doi: 10.1038/tp.2015.72

Pareek, T. K., Keller, J., Kesavapany, S., Agarwal, N., Kuner, R., Pant, H. C., et al. (2007). Cyclin-dependent kinase 5 modulates nociceptive signaling through direct phosphorylation of transient receptor potential vanilloid 1. *Proc. Natl. Acad. Sci. U.S.A.* 104, 660–665. doi: 10.1073/pnas.0609916104

Pareek, T. K., Keller, J., Kesavapany, S., Pant, H. C., Iadarola, M. J., Brady, R. O., et al. (2006). Cyclin-dependent kinase 5 activity regulates pain signaling. *Proc. Natl. Acad. Sci. U.S.A.* 103, 791–796.

Park, J., Seo, J., Won, J., Yeo, H. G., Ahn, Y. J., Kim, K., et al. (2019). Abnormal mitochondria in a non-human primate model of MPTP-induced Parkinson's disease: Drp1 and CDK5/p25 signaling. *Exp. Neurobiol.* 28, 414–424. doi: 10.5607/en.2019.28.3.414

Park, J., Won, J., Seo, J., Yeo, H. G., Kim, K., Kim, Y. G., et al. (2020). Streptozotocin induces Alzheimer's disease-like pathology in hippocampal neuronal cells *via* CDK5/Drp1-mediated mitochondrial fragmentation. *Front. Cell Neurosci.* 14:235. doi: 10.3389/fncel.2020.00235

Park, K. H. J., Franciosi, S., Parrant, K., Lu, G., and Leavitt, B. R. (2017). p35 hemizygosity activates Akt but does not improve motor function in the YAC128 mouse model of Huntington's disease. *Neuroscience* 352, 79–87. doi: 10.1016/j.neuroscience.2017.03.051

Park, K. H., Lu, G., Fan, J., Raymond, L. A., and Leavitt, B. R. (2012). Decreasing levels of the cdk5 activators, p25 and p35, reduces excitotoxicity in striatal neurons. *J. Huntingtons Dis.* 1, 89–96.

Patrick, G. N., Zukerberg, L., Nikolic, M., de la Monte, S., Dikkes, P., and Tsai, L. H. (1999). Conversion of p35 to p25 deregulates Cdk5 activity and promotes neurodegeneration. *Nature* 402, 615–622.

Paudel, H. K. (1997). Phosphorylation by neuronal cdc2-like protein kinase promotes dimerization of Tau protein in vitro. *J. Biol. Chem.* 272, 28328–28334. doi: 10.1074/jbc.272.45.28328

Pei, J. J., Braak, E., Braak, H., Grundke-Iqbal, I., Iqbal, K., Winblad, B., et al. (2001). Localization of active forms of C-jun kinase (JNK) and p38 kinase in Alzheimer's disease brains at different stages of neurofibrillary degeneration. *J. Alzheimers Dis.* 3, 41–48. doi: 10.3233/jad-2001-3107

Pei, J. J., Grundke-Iqbal, I., Iqbal, K., Bogdanovic, N., Winblad, B., and Cowburn, R. F. (1998). Accumulation of cyclin-dependent kinase 5 (cdk5) in neurons with early stages of Alzheimer's disease neurofibrillary degeneration. *Brain Res.* 797, 267–277.

Peters, J. M. (2002). The anaphase-promoting complex: Proteolysis in mitosis and beyond. *Mol. Cell* 9, 931–943.

Petrucelli, L., O'Farrell, C., Lockhart, P. J., Baptista, M., Kehoe, K., Vink, L., et al. (2002). Parkin protects against the toxicity associated with mutant alpha-synuclein: Proteasome dysfunction selectively affects catecholaminergic neurons. *Neuron* 36, 1007–1019. doi: 10.1016/s0896-6273(02)01125-x

Plattner, F., Hernandez, A., Kistler, T. M., Pozo, K., Zhong, P., Yuen, E. Y., et al. (2014). Memory enhancement by targeting Cdk5 regulation of NR2B. *Neuron* 81, 1070–1083. doi: 10.1016/j.neuron.2014.01.022

Prochazkova, M., Terse, A., Amin, N. D., Hall, B., Utreras, E., Pant, H. C., et al. (2013). Activation of cyclin-dependent kinase 5 mediates orofacial mechanical hyperalgesia. *Mol. Pain* 9:66. doi: 10.1186/1744-8069-9-66

Qu, D., Rashidian, J., Mount, M. P., Aleyasin, H., Parsanejad, M., Lira, A., et al. (2007). Role of Cdk5-mediated phosphorylation of Prx2 in MPTP toxicity and Parkinson's disease. *Neuron* 55, 37–52. doi: 10.1016/j.neuron.2007.05.033

Qu, J., Nakamura, T., Cao, G., Holland, E. A., McKercher, S. R., and Lipton, S. A. S. – (2011). Nitrosylation activates Cdk5 and contributes to synaptic spine loss induced by beta-amyloid peptide. *Proc. Natl. Acad. Sci. U.S.A.* 108, 14330–14335. doi: 10.1073/pnas.1105172108

Qu, J., Nakamura, T., Holland, E. A., McKercher, S. R., and Lipton, S. A. (2012). S-nitrosylation of Cdk5: Potential implications in amyloid-beta-related neurotoxicity in Alzheimer disease. *Prion* 6, 364–370. doi: 10.4161/pri.21250

Quan, Q., Qian, Y., Li, X., and Li, M. (2019). CDK5 Participates in amyloid-beta production by regulating PPARgamma phosphorylation in primary rat hippocampal neurons. *J. Alzheimers Dis.* 71, 443–460. doi: 10.3233/JAD-190026

Rahn, E. J., Guzman-Karlsson, M. C., and David Sweatt, J. (2013). Cellular, molecular, and epigenetic mechanisms in non-associative conditioning: Implications for pain and memory. *Neurobiol. Learn. Mem.* 105, 133–150. doi: 10.1016/j.nlm.2013.06.008

Ralat, L. A., Manevich, Y., Fisher, A. B., and Colman, R. F. (2006). Direct evidence for the formation of a complex between 1-cysteine peroxiredoxin and glutathione S-transferase pi with activity changes in both enzymes. *Biochemistry* 45, 360–372. doi: 10.1021/bi0520737

Rashidian, J., Rousseaux, M. W., Venderova, K., Qu, D., Callaghan, S. M., Phillips, M., et al. (2009). Essential role of cytoplasmic cdk5 and Prx2 in multiple ischemic injury models, in vivo. *J. Neurosci.* 29, 12497–12505. doi: 10.1523/JNEUROSCI.3892-09.2009

Rosen, J. B., and Schulkin, J. (1998). From normal fear to pathological anxiety. *Psychol. Rev.* 105, 325–350.

Rubio de la Torre, E., Luzon-Toro, B., Forte-Lago, I., Minguez-Castellanos, A., Ferrer, I., and Hilfiker, S. (2009). Combined kinase inhibition modulates parkin inactivation. *Hum. Mol. Genet.* 18, 809–823. doi: 10.1093/hmg/ddn407

Rudenko, A., Seo, J., Hu, J., Su, S. C., de Anda, F. C., Durak, O., et al. (2015). Loss of cyclin-dependent kinase 5 from parvalbumin interneurons leads to hyperinhibition, decreased anxiety, and memory impairment. *J. Neurosci.* 35, 2372–2383. doi: 10.1523/JNEUROSCI.0969-14.2015

Sadleir, K. R., and Vassar, R. (2012). Cdk5 protein inhibition and Abeta42 increase BACE1 protein level in primary neurons by a post-transcriptional mechanism: Implications of CDK5 as a therapeutic target for Alzheimer disease. *J. Biol. Chem.* 287, 7224–7235. doi: 10.1074/jbc.M111.333914

Saito, T., Oba, T., Shimizu, S., Asada, A., Iijima, K. M., and Ando, K. (2019). Cdk5 increases MARK4 activity and augments pathological tau accumulation and toxicity through tau phosphorylation at Ser262. *Hum. Mol. Genet.* 28, 3062–3071. doi: 10.1093/hmg/ddz120

Sandford, J. J., Argyropoulos, S. V., and Nutt, D. J. (2000). The psychobiology of anxiolytic drugs. Part 1: Basic neurobiology. *Pharmacol. Ther.* 88, 197–212. doi: 10.1016/s0163-7258(00)00082-6

Sandoval, R., Lazcano, P., Ferrari, F., Pinto-Pardo, N., Gonzalez-Billault, C., and Utreras, E. (2018). TNF-alpha increases production of reactive oxygen species through Cdk5 activation in nociceptive neurons. *Front. Physiol.* 9:65. doi: 10.3389/fphys.2018.00065

Sasaki, Y., Cheng, C., Uchida, Y., Nakajima, O., Ohshima, T., Yagi, T., et al. (2002). Fyn and Cdk5 mediate semaphorin-3A signaling, which is involved in regulation of dendrite orientation in cerebral cortex. *Neuron* 35, 907–920. doi: 10.1016/s0896-6273(02)00857-7

Sasamoto, K., Nagai, J., Nakabayashi, T., He, X., and Ohshima, T. (2017). Cdk5 is required for the positioning and survival of GABAergic neurons in developing mouse striatum. *Dev. Neurobiol.* 77, 483–492. doi: 10.1002/dneu.22424

Schneider, J. A., Arvanitakis, Z., Yu, L., Boyle, P. A., Leurgans, S. E., and Bennett, D. A. (2012). Cognitive impairment, decline and fluctuations in older community-dwelling subjects with Lewy bodies. *Brain* 135(Pt 10), 3005–3014. doi: 10.1093/brain/aws234

Sen, A., Thom, M., Martinian, L., Jacobs, T., Nikolic, M., and Sisodiya, S. M. (2006). Deregulation of cdk5 in Hippocampal sclerosis. *J. Neuropathol. Exp. Neurol.* 65, 55–66.

Shah, K., and Lahiri, D. K. (2014). Cdk5 activity in the brain–multiple paths of regulation. *J. Cell Sci.* 127(Pt 11), 2391–2400. doi: 10.1242/jcs.147553

Shukla, V., Seo, J., Binukumar, B. K., Amin, N. D., Reddy, P., Grant, P., et al. (2017). TFP5, a peptide inhibitor of aberrant and hyperactive Cdk5/p25, attenuates pathological phenotypes and restores synaptic function in CK-p25Tg mice. *J. Alzheimers Dis.* 56, 335–349. doi: 10.3233/JAD-160916

Shukla, V., Zheng, Y. L., Mishra, S. K., Amin, N. D., Steiner, J., Grant, P., et al. (2013). A truncated peptide from p35, a Cdk5 activator, prevents Alzheimer's disease phenotypes in model mice. *FASEB J.* 27, 174–186. doi: 10.1096/fj.12-217497

Smith, P. D., Crocker, S. J., Jackson-Lewis, V., Jordan-Sciutto, K. L., Hayley, S., Mount, M. P., et al. (2003). Cyclin-dependent kinase 5 is a mediator of dopaminergic neuron loss in a mouse model of Parkinson's disease. *Proc. Natl. Acad. Sci. U.S.A.* 100, 13650–13655. doi: 10.1073/pnas.2232515100

Steinbrecher, U. P., Parthasarathy, S., Leake, D. S., Witztum, J. L., and Steinberg, D. (1984). Modification of low density lipoprotein by endothelial cells involves lipid peroxidation and degradation of low density lipoprotein phospholipids. *Proc. Natl. Acad. Sci. U.S.A.* 81, 3883–3887.

Stillwell, T. J., and Myers, R. P. (1988). Adenomatous polyp in defunctionalized colonic segment used as a urinary bladder. *Urology* 32, 538–540. doi: 10.1016/s0090-4295(98)90038-3

Su, L. Y., Li, H., Lv, L., Feng, Y. M., Li, G. D., Luo, R., et al. (2015). Melatonin attenuates MPTP-induced neurotoxicity *via* preventing CDK5-mediated autophagy and SNCA/alpha-synuclein aggregation. *Autophagy* 11, 1745–1759. doi: 10.1080/15548627.2015.1082020

Su, S. C., and Tsai, L. H. (2011). Cyclin-dependent kinases in brain development and disease. *Annu. Rev. Cell Dev. Biol.* 27, 465–491.

Sun, K. H., Chang, K. H., Clawson, S., Ghosh, S., Mirzaei, H., Regnier, F., et al. (2011). Glutathione-S-transferase P1 is a critical regulator of Cdk5 kinase activity. *J. Neurochem.* 118, 902–914. doi: 10.1111/j.1471-4159.2011.07343.x

Sun, K. H., de Pablo, Y., Vincent, F., and Shah, K. (2008). Deregulated Cdk5 promotes oxidative stress and mitochondrial dysfunction. *J. Neurochem.* 107, 265–278. doi: 10.1111/j.1471-4159.2008.05616.x

Sun, K. H., Lee, H. G., Smith, M. A., and Shah, K. (2009). Direct and indirect roles of cyclin-dependent kinase 5 as an upstream regulator in the c-Jun NH2-terminal kinase cascade: Relevance to neurotoxic insults in Alzheimer's disease. *Mol. Biol. Cell* 20, 4611–4619. doi: 10.1091/mbc.e09-05-0433

Sundaram, J. R., Chan, E. S., Poore, C. P., Pareek, T. K., Cheong, W. F., Shui, G., et al. (2012). Cdk5/p25-induced cytosolic PLA2-mediated lysophosphatidylcholine production regulates neuroinflammation and triggers neurodegeneration. *J. Neurosci.* 32, 1020–1034. doi: 10.1523/JNEUROSCI.5177-11.2012

Takahashi, M., Nakabayashi, T., Mita, N., Jin, X., Aikawa, Y., Sasamoto, K., et al. (2022). Involvement of Cdk5 activating subunit p35 in synaptic plasticity in excitatory and inhibitory neurons. *Mol. Brain* 15:37. doi: 10.1186/s13041-022-00922-x

Takahashi, Y., Coppola, D., Matsushita, N., Cualing, H. D., Sun, M., Sato, Y., et al. (2007). Bif-1 interacts with Beclin 1 through UVRAG and regulates autophagy and tumorigenesis. *Nat. Cell Biol.* 9, 1142–1151.

Tan, X., Chen, Y., Li, J., Li, X., Miao, Z., Xin, N., et al. (2015). The inhibition of Cdk5 activity after hypoxia/ischemia injury reduces infarct size and promotes functional recovery in neonatal rats. *Neuroscience* 290, 552–560. doi: 10.1016/j.neuroscience.2015.01.054

Tang, X., Wang, X., Gong, X., Tong, M., Park, D., Xia, Z., et al. (2005). Cyclin-dependent kinase 5 mediates neurotoxin-induced degradation of the transcription factor myocyte enhancer factor 2. *J. Neurosci.* 25, 4823–4834.

Thijs, R. D., Surges, R., O'Brien, T. J., and Sander, J. W. (2019). Epilepsy in adults. *Lancet* 393, 689–701.

Traystman, R. J. (2003). Animal models of focal and global cerebral ischemia. *ILAR J.* 44, 85–95.

Tsai, L. H., Delalle, I., Caviness, V. S. Jr., Chae, T., and Harlow, E. (1994). p35 is a neural-specific regulatory subunit of cyclin-dependent kinase 5. *Nature* 371, 419–423.

Tsai, L. H., Takahashi, T., Caviness, V. S. Jr., and Harlow, E. (1993). Activity and expression pattern of cyclin-dependent kinase 5 in the embryonic mouse nervous system. *Development* 119, 1029–1040.

Tseng, H. C., Zhou, Y., Shen, Y., and Tsai, L. H. (2002). A survey of Cdk5 activator p35 and p25 levels in Alzheimer's disease brains. *FEBS Lett.* 523, 58–62.

Uchida, Y., Ohshima, T., Sasaki, Y., Suzuki, H., Yanai, S., Yamashita, N., et al. (2005). Semaphorin3A signalling is mediated *via* sequential Cdk5 and GSK3beta phosphorylation of CRMP2: Implication of common phosphorylating mechanism underlying axon guidance and Alzheimer's disease. *Genes Cells* 10, 165–179. doi: 10.1111/j.1365-2443.2005.00827.x

Utreras, E., Futatsugi, A., Rudrabhatla, P., Keller, J., Iadarola, M. J., Pant, H. C., et al. (2009). Tumor necrosis factor-alpha regulates cyclin-dependent kinase 5 activity during pain signaling through transcriptional activation of p35. *J. Biol. Chem.* 284, 2275–2284. doi: 10.1074/jbc.M805052200

Utreras, E., Keller, J., Terse, A., Prochazkova, M., Iadarola, M. J., and Kulkarni, A. B. (2012). Transforming growth factor-beta1 regulates Cdk5 activity in primary sensory neurons. *J. Biol. Chem.* 287, 16917–16929.

Wang, C. H., Chou, W. Y., Hung, K. S., Jawan, B., Lu, C. N., Liu, J. K., et al. (2005). Intrathecal administration of roscovitine inhibits Cdk5 activity and attenuates formalin-induced nociceptive response in rats. *Acta Pharmacol. Sin.* 26, 46–50. doi: 10.1111/j.1745-7254.2005.00007.x

Wang, G. Q., Cen, C., Li, C., Cao, S., Wang, N., Zhou, Z., et al. (2015). Deactivation of excitatory neurons in the prelimbic cortex *via* Cdk5 promotes pain sensation and anxiety. *Nat. Commun.* 6:7660.

Wang, J., Liu, S., Fu, Y., Wang, J. H., and Lu, Y. (2003). Cdk5 activation induces hippocampal CA1 cell death by directly phosphorylating NMDA receptors. *Nat. Neurosci.* 6, 1039–1047. doi: 10.1038/nn1119

Wang, Q., Jiao, F., Zhang, P., Yan, J., Zhang, Z., He, F., et al. (2018). CDK5-mediated phosphorylation-dependent ubiquitination and degradation of E3 ubiquitin ligases GP78 accelerates neuronal death in Parkinson's disease. *Mol. Neurobiol.* 55, 3709–3717. doi: 10.1007/s12035-017-0579-2

Wang, X., Ratnam, J., Zou, B., England, P. M., and Basbaum, A. I. (2009). TrkB signaling is required for both the induction and maintenance of tissue and nerve injury-induced persistent pain. *J. Neurosci.* 29, 5508–5515. doi: 10.1523/JNEUROSCI.4288-08.2009

Wen, Y., Yu, W. H., Maloney, B., Bailey, J., Ma, J., Marie, I., et al. (2008). Transcriptional regulation of beta-secretase by p25/cdk5 leads to enhanced amyloidogenic processing. *Neuron* 57, 680–690. doi: 10.1016/j.neuron.2008.02.024

Wen, Z., Shu, Y., Gao, C., Wang, X., Qi, G., Zhang, P., et al. (2014). CDK5-mediated phosphorylation and autophagy of RKIP regulate neuronal death in Parkinson's disease. *Neurobiol. Aging* 35, 2870–2880. doi: 10.1016/j.neurobiolaging.2014.05.034

Westermann, B. (2010). Mitochondrial fusion and fission in cell life and death. *Nat. Rev. Mol. Cell Biol.* 11, 872–884.

Wilkaniec, A., Gassowska-Dobrowolska, M., Strawski, M., Adamczyk, A., and Czapski, G. A. (2018). Inhibition of cyclin-dependent kinase 5 affects early neuroinflammatory signalling in murine model of amyloid beta toxicity. *J. Neuroinflammation* 15:1. doi: 10.1186/s12974-017-1027-y

Wong, A. S., Lee, R. H., Cheung, A. Y., Yeung, P. K., Chung, S. K., Cheung, Z. H., et al. (2011). Cdk5-mediated phosphorylation of endophilin B1 is required for induced autophagy in models of Parkinson's disease. *Nat. Cell Biol.* 13, 568–579. doi: 10.1038/ncb2217

Wu, D. C., Yu, Y. P., Lee, N. T., Yu, A. C., Wang, J. H., and Han, Y. F. (2000). The expression of Cdk5, p35, p39, and Cdk5 kinase activity in developing, adult, and aged rat brains. *Neurochem. Res.* 25, 923–929. doi: 10.1023/a:1007544106645

Xie, Z., Hou, S., Yang, X., Duan, Y., Han, J., Wang, Q., et al. (2022). Lessons learned from past cyclin-dependent kinase drug discovery efforts. *J. Med. Chem.* 65, 6356–6389. doi: 10.1021/acs.jmedchem.1c02190

Xu, M., Huang, Y., Song, P., Huang, Y., Huang, W., Zhang, H. T., et al. (2019). AAV9-mediated Cdk5 inhibitory peptide reduces hyperphosphorylated tau and inflammation and ameliorates behavioral changes caused by overexpression of p25 in the brain. *J. Alzheimers Dis.* 70, 573–585. doi: 10.3233/JAD-190099

Yamada, M., Saito, T., Sato, Y., Kawai, Y., Sekigawa, A., Hamazumi, Y., et al. (2007). Cdk5–p39 is a labile complex with the similar substrate specificity to Cdk5–p35. *J. Neurochem.* 102, 1477–1487. doi: 10.1111/j.1471-4159.2007.04505.x

Yang, L., Gu, X., Zhang, W., Zhang, J., and Ma, Z. (2014). Cdk5 inhibitor roscovitine alleviates neuropathic pain in the dorsal root ganglia by downregulating N-methyl-D-aspartate receptor subunit 2A. *Neurol. Sci.* 35, 1365–1371. doi: 10.1007/s10072-014-1713-9

Yang, S. H., Huang, C. Y., Hsieh, C. Y., and Chuang, J. I. (2020). CDK4 and CDK5 inhibition have comparable mild hypothermia effects in preventing Drp1-Dependent mitochondrial fission and neuron death induced by MPP. *Mol. Neurobiol.* 57, 4090–4105. doi: 10.1007/s12035-020-02014-0

Yang, Y. R., He, Y., Zhang, Y., Li, Y., Li, Y., Han, Y., et al. (2007). Activation of cyclin-dependent kinase 5 (Cdk5) in primary sensory and dorsal horn neurons by peripheral inflammation contributes to heat hyperalgesia. *Pain* 127, 109–120. doi: 10.1016/j.pain.2006.08.008

Ye, T., Ip, J. P., Fu, A. K., and Ip, N. Y. (2014). Cdk5-mediated phosphorylation of RapGEF2 controls neuronal migration in the developing cerebral cortex. *Nat. Commun.* 5:4826. doi: 10.1038/ncomms5826

Yeung, K., Seitz, T., Li, S., Janosch, P., McFerran, B., Kaiser, C., et al. (1999). Suppression of Raf-1 kinase activity and MAP kinase signalling by RKIP. *Nature* 401, 173–177.

Yoshida, H., Hastie, C. J., McLauchlan, H., Cohen, P., and Goedert, M. (2004). Phosphorylation of microtubule-associated protein tau by isoforms of c-Jun N-terminal kinase (JNK). *J. Neurochem.* 90, 352–358. doi: 10.1111/j.1471-4159.2004.02479.x

Yoshida, H., Watanabe, A., and Ihara, Y. (1998). Collapsin response mediator protein-2 is associated with neurofibrillary tangles in Alzheimer's disease. *J. Biol. Chem.* 273, 9761–9768.

Zhang, H. H., Zhang, X. Q., Xue, Q. S., Yan, L., Huang, J. L., Zhang, S., et al. (2014). The BDNF/TrkB signaling pathway is involved in heat hyperalgesia mediated by Cdk5 in rats. *PLoS One* 9:e85536. doi: 10.1371/journal.pone.0085536

Zhang, L., Liu, W., Szumlinski, K. K., and Lew, J. (2012). p10, the N-terminal domain of p35, protects against CDK5/p25-induced neurotoxicity. *Proc. Natl. Acad. Sci. U.S.A.* 109, 20041–20046. doi: 10.1073/pnas.1212914109

Zhang, P., Fu, W. Y., Fu, A. K., and Ip, N. Y. (2015). S-nitrosylation-dependent proteasomal degradation restrains Cdk5 activity to regulate hippocampal synaptic strength. *Nat. Commun.* 6:8665. doi: 10.1038/ncomms9665

Zhang, P., Shao, X. Y., Qi, G. J., Chen, Q., Bu, L. L., Chen, L. J., et al. (2016). Cdk5-dependent activation of neuronal inflammasomes in Parkinson's disease. *Mov. Disord.* 31, 366–376. doi: 10.1002/mds.26488

Zhang, P., Yu, P. C., Tsang, A. H., Chen, Y., Fu, A. K., Fu, W. Y., et al. (2010). S-nitrosylation of cyclin-dependent kinase 5 (cdk5) regulates its kinase activity and dendrite growth during neuronal development. *J. Neurosci.* 30, 14366–14370. doi: 10.1523/JNEUROSCI.3899-10.2010

Zhang, Q., Xie, H., Ji, Z., He, R., Xu, M., He, Y., et al. (2016). Cdk5/p25 specific inhibitory peptide TFP5 rescues the loss of dopaminergic neurons in a sub-acute MPTP induced PD mouse model. *Neurosci. Lett.* 632, 1–7. doi: 10.1016/j.neulet.2016.08.023

Zhang, R., Liu, Y., Zhang, J., Zheng, Y., Gu, X., and Ma, Z. (2012). Intrathecal administration of roscovitine attenuates cancer pain and inhibits the expression of NMDA receptor 2B subunit mRNA. *Pharmacol. Biochem. Behav.* 102, 139–145. doi: 10.1016/j.pbb.2012.03.025

Zhang, S., Edelmann, L., Liu, J., Crandall, J. E., and Morabito, M. A. (2008). Cdk5 regulates the phosphorylation of tyrosine 1472 NR2B and the surface expression of NMDA receptors. *J. Neurosci.* 28, 415–424. doi: 10.1523/JNEUROSCI.1900-07.2008

Zhang, X., Zhang, H., Shao, H., Xue, Q., and Yu, B. (2014). ERK MAP kinase activation in spinal cord regulates phosphorylation of Cdk5 at serine 159 and contributes to peripheral inflammation induced pain/hypersensitivity. *PLoS One* 9:e87788. doi: 10.1371/journal.pone.0087788

Zhao, Y., Wang, C., He, W., and Cai, Z. (2021). Ameliorating Alzheimer's-like pathology by Minocycline *via* inhibiting Cdk5/p25 signaling. *Curr. Neuropharmacol.* 20, 1783–1792. doi: 10.2174/1570159X19666211202124925

Zhou, M., Wang, H., Zeng, X., Yin, P., Zhu, J., Chen, W., et al. (2019). Mortality, morbidity, and risk factors in China and its provinces, 1990-2017: A systematic analysis for the Global Burden of Disease Study 2017. *Lancet* 394, 1145–1158.

Zhou, Y. F., Wang, J., Deng, M. F., Chi, B., Wei, N., Chen, J. G., et al. (2019). The Peptide-directed lysosomal degradation of CDK5 exerts therapeutic effects against stroke. *Aging Dis.* 10, 1140–1145. doi: 10.14336/AD.2018.1225

Zhu, W. L., Shi, H. S., Wang, S. J., Xu, C. M., Jiang, W. G., Wang, X., et al. (2012). Increased Cdk5/p35 activity in the dentate gyrus mediates depressive-like behaviour in rats. *Int. J. Neuropsychopharmacol.* 15, 795–809. doi: 10.1017/S1461145711000915

frontiers | Frontiers in Molecular Neuroscience

TYPE Original Research
PUBLISHED 01 December 2022
DOI 10.3389/fnmol.2022.1055295

OPEN ACCESS

EDITED BY
Arianna Bellucci,
University of Brescia, Italy

REVIEWED BY
Shinsuke Nakagawa,
Fukuoka University, Japan
Naomi Sayre,
The University of Texas Health Science Center at San Antonio, United States

*CORRESPONDENCE
Bert W. O'Malley
berto@bcm.edu

†These authors have contributed equally to this work and share first authorship

‡These authors share last authorship

SPECIALTY SECTION
This article was submitted to Brain Disease Mechanisms, a section of the journal Frontiers in Molecular Neuroscience

RECEIVED 27 September 2022
ACCEPTED 10 November 2022
PUBLISHED 01 December 2022

CITATION
McClendon LK, Garcia RL, Lazaro T, Robledo A, Vasandani V, Luna ZAE, Rao AS, Srivatsan A, Lonard DM, Dacso CC, Kan P and O'Malley BW (2022) A steroid receptor coactivator small molecule "stimulator" attenuates post-stroke ischemic brain injury. Front. Mol. Neurosci. 15:1055295. doi: 10.3389/fnmol.2022.1055295

A steroid receptor coactivator small molecule "stimulator" attenuates post-stroke ischemic brain injury

Lisa K. McClendon[1,2†], Roberto L. Garcia[3†], Tyler Lazaro[4], Ariadna Robledo[3], Viren Vasandani[3], Zean Aaron Evan Luna[3], Abhijit S. Rao[3], Aditya Srivatsan[4], David M. Lonard[1,2], Clifford C. Dacso[1,2], Peter Kan[3‡] and Bert W. O'Malley[1,2*‡]

[1]Department of Molecular and Cellular Biology, Baylor College of Medicine, Houston, TX, United States, [2]CoRegen, Inc., Baylor College of Medicine, Houston, TX, United States, [3]Department of Neurosurgery, University of Texas Medical Branch, Galveston, TX, United States, [4]Department of Neurosurgery, Baylor College of Medicine, Houston, TX, United States

Introduction: Pathologic remodeling of the brain following ischemic stroke results in neuronal loss, increased inflammation, oxidative stress, astrogliosis, and a progressive decrease in brain function. We recently demonstrated that stimulation of steroid receptor coactivator 3 with the small-molecule stimulator MCB-613 improves cardiac function in a mouse model of myocardial ischemia. Since steroid receptor coactivators are ubiquitously expressed in the brain, we reasoned that an MCB-613 derivative (MCB-10-1), could protect the brain following ischemic injury. To test this, we administered MCB-10-1 to rats following middle cerebral artery occlusion and reperfusion.

Methods: Neurologic impairment and tissue damage responses were evaluated on day 1 and day 4 following injury in rats treated with control or 10-1.

Results: We show that 10-1 attenuates injury post-stroke. 10-1 decreases infarct size and mitigates neurologic impairment. When given within 30 min post middle cerebral artery occlusion and reperfusion, 10-1 induces lasting protection from tissue damage in the ischemic penumbra concomitant with: (1) promotion of reparative microglia; (2) an increase in astrocyte NRF2 and GLT-1 expression; (3) early microglia activation; and (4) attenuation of astrogliosis.

Discussion: Steroid receptor coactivator stimulation with MCB-10-1 is a potential therapeutic strategy for reducing inflammation and oxidative damage that cause neurologic impairment following an acute ischemic stroke.

KEYWORDS

steroid receptor coactivator stimulation, transcriptional regulation, astrocytes, neuroprotection, cerebral ischemia, inflammation, oxidative stress

Introduction

Stroke is a pervasive disease worldwide, and a leading cause of morbidity and the fifth leading cause of death in the United States, with acute ischemic stroke (AIS) being the most common etiology (Goyal et al., 2016). Currently, the only FDA-approved medication for AIS is tissue plasminogen activator (tPA), which promotes clot degradation and reperfusion. In select patients with a large vessel occlusion, the addition of mechanical thrombectomy (MT) with thrombolysis with tPA has become the standard of care for revascularization (Albers et al., 2018; Nogueira et al., 2018). Nonetheless, AIS patients are still at an unacceptably high risk of death and disability (Albers et al., 2018; Nogueira et al., 2018) thus other therapies are sorely needed. While reperfusion focuses on restoring blood flow after AIS, neuroprotection refers to strategies that can reduce cerebral injury secondary to ischemia, but this currently remains an unmet clinical need.

While many other neuroprotective candidates have been explored in animal experiments and some in human trials (Saver et al., 2015; Hill et al., 2020), none have successfully improved AIS outcomes. Although they have largely been negative trials, these studies have provided valuable insights into how future trials might be designed to achieve better responses—specifically, therapies that appreciate the complexities of the ischemic cascade by affecting multiple injury response pathways. We recently discovered a small molecule stimulator of steroid receptor coactivators (SRC), called MCB-613 (Wang et al., 2015), that reduces ischemic injury after myocardial infarction by direct cardiomyocyte protection, mitigation of immune cell infiltration, and attenuation of pathologic fibroblast remodeling (Mullany et al., 2020). While the results of the study are very promising for cardioprotection, we considered this to also be a prime candidate for neuroprotection after AIS, as the heart and brain share many of the primary drivers of tissue damage after acute ischemic injury, including oxidative stress and inflammation.

SRCs are a family of nuclear proteins (SRC-1, -2, and -3) that are ubiquitously expressed and required for the transcription of ∼80% of all genes (Lanz et al., 2010). As a result, SRC activation has been implicated in a broad array of cellular functions, including cell proliferation, regeneration, immune modulation, antioxidant defense, and angiogenesis (Lonard and O'Malley, 2007; Lanz et al., 2010). Our team has demonstrated that SRCs are extensive organizers of growth and repair since their discovery 27 years ago (Onate et al., 1995). For optimal tissue healing after injury, injury responses necessitate a strong transcriptome response coupled with cellular reprogramming including coordinating gene expression programs. After tissue injury, SRCs work to maintain cellular homeostasis by coordinating various gene expression programs including antioxidant-defense, cell survival, and angiogenesis (Lonard and O'Malley, 2007; Chen X. et al., 2010; Lanz et al., 2010; Chen et al., 2015). Thus, unlike single target therapies, the ability of SRCs to serve as coordinators of many wound healing gene expression programs predisposes SRCs to be ideal therapeutic targets for repair after ischemic injury. Moreover, the SRCs are expressed in all areas of the brain (Sun and Xu, 2020).

Considering SRC activation has been shown to beneficially regulate the drivers of cardiac ischemic injury in our previous experiments (Mullany et al., 2020), we tested the application of a more metabolically stable and potent MCB-613 derivative, 10-1, in a rat model for middle cerebral artery occlusion followed by reperfusion (MCAO R). We assessed the neurologic impairment and infarct size, and neuronal injury. We also assessed expression of key inflammatory, neuronal excitotoxicity, and oxidative injury markers.

Materials and methods

Animal procedures were approved under our Institutional Animal Care and Use Committee and conducted under National Institutes of Health guidelines for the Care and Use of Laboratory Animals. All experimental methods were standardized and performed by specified investigators to minimize potential confounders. All investigators were blinded throughout the experiment. Using computer-based randomization, rodents were assigned to the treatment groups prior to the initial procedure. Forty male Sprague Dawley rats (Charles River Laboratories), aged 7–9 weeks and weighing 225–250 grams, were divided into two experiments: 24-h (n = 20) and 4-day survival (n = 20). Due to their bigger size, only male mice were employed in this study in order to rule out the influence of gender and treatment response on stroke recovery. The subjects received equal volume intraperitoneal (IP) injections of either 10-1 (20 mg/kg) or saline control 30 min after reperfusion or sham surgery then injected daily if they survived for more than 24 h.

For the 24-h survival experiment, 10 rodents were randomly assigned to 10-1 and 10 rats were assigned to the control groups. In the 4-day experiment, 10 rodents were randomly assigned to the 10-1 and 10 to the control groups.

Surgical preparation

Atropine sulfate (0.5 mg/kg IP), buprenorphine SR (1 mg/kg SQ), and meloxicam SR (2 mg/kg SQ) were injected 1 h before anesthesia. General anesthesia was induced using 5% isoflurane in 100% oxygen, by placing the rats in an induction chamber for approximately 3–5 min. The animals were then intubated with a 16-gauge angiocatheter and mechanically ventilated using a Harvard Apparatus VentElite ventilator. A surgical plane of anesthesia was maintained throughout the procedure with 2% isoflurane at 100% medical air. Rectal

temperature, respirations, and pulse oximetry were monitored *via* an automated monitoring system (HPMS Model# 75-1501, Harvard Apparatus, Holliston, MA, USA). Body temperature was continuously monitored and maintained between 36.5 and 37°C throughout the procedure.

The scalp was shaved and cleaned using an iodine-based solution. The surgical field was draped with sterile linens. With the animal placed in a prone position, a 2–2.5 cm midline sagittal incision was performed and the scalp with periosteum was reflected to expose the left parietal bone. A laser doppler flowmetry (LDF) probe and holder were affixed to the left parietal bone using cyanoacrylate adhesive. The animal was then placed in a supine position for the remainder of the procedure.

Middle cerebral artery occlusion

Following the methodology described in Longa et al. (1989), under microscopy, blunt dissection was performed through the carotid triangle to expose the left common carotid artery (CCA) and bifurcation of the external carotid artery (ECA) and internal carotid artery (ICA). The superior thyroid artery (STA) of the ECA was then isolated and coagulated, followed by the occipital artery. The ICA was carefully isolated from the adjacent vagus nerve. Next, two 3–0 silk sutures were placed around the ECA with one ligated distal to the STA. Cerebral blood flow (CBF) was monitored and recorded for baseline readings with the LDF system (moorVMS-LDF2, Moor Instruments) for 5 min. Two micro-vascular clips were placed on the CCA and ICA to prevent any bleeding, and the ECA was partially severed with microscissors. A 4–0 monofilament nylon suture with an occlusive diameter of 0.41 mm was inserted through the proximal ECA into the ICA, and the remaining ECA was severed. The micro-vascular clip on the ICA was removed and the filament was advanced until the LDF showed a 70% decrease from baseline CBF. The silk suture around the ECA stump was tightened around the intraluminal nylon suture to prevent bleeding. Occlusion time was set for 90 min then the filament was removed to allow for reperfusion.

Exclusion criteria and stroke-related deaths

Criteria for exclusion consisted of excessive bleeding occurring during surgery, operation time exceeded 120 min, anesthesia recovery time exceeded 30 min, animals died prior to the scheduled euthanasia date or if subarachnoid hemorrhage was found during postmortem examination. Stroke-related deaths were defined as post-operative deaths due to neurologic devastation not associated with the above exclusion criteria. One animal was excluded in the 24 h cohort and six animals (four 10-1 and two control) were excluded in the 4 day cohort due to stroke-related death. No data were collected from these animals and there was no statistical difference due to stroke-related death.

Neurologic assessment

A modified Bederson test was used to assess for neurologic impairments beginning on post-operative day 1. The scoring was as follows: (1) Forearm Flexion was graded 0–1; (2) resistance to Lateral Push was graded 0–2; and (3) circling Behavior was graded 0–3. The sum of these assessments determined the final score of 0 (normal) to 6 (severe) each day (17).

Infarct volume measurements

Brains were sliced coronally into 2 mm slices and incubated at 37°C for 20 min in 2,3,5-triphenyltetrazolium chloride (TTC; Liu et al., 2009). Brains were then fixed in formalin and then paraffin was embedded. Brain slices were photographed and infarct volume was measured using Image J (NIH.gov). Infarct area was calculated by tracing unstained regions in each section (both sides) and multiplied by slice thickness to calculate infarct volume. For measurements of cortical and subcortical infarction sizes, hematoxylin and eosin (H&E) slides were made from paraffin embedded brain sections. Cortical and subcortical structures were consistently identified using the Rat Brain Atlas as a reference (Swanson, 2018).

Immunofluorescence staining

Five micron sections were cut and placed onto slides. Immunofluorescence was performed by first removing the paraffin and then rehydrating the sections. After that, antigen retrieval was performed (Antigen unmasking solution, Tris-based, Vector Labs cat#H-3301). Sections were permeablized with 0.4% Tritonx-100-PBS, blocked with 10% normal goat serum (NGS) in PBS with 0.4% Triton X-100, and then incubated with primary antibody in blocking solution NeuN (1:200, Thermo Fisher, 26975-1-AP) ARG1 (1:200, Santa Cruz, SC-18354), GFAP (1:200, Invitrogen, MA5-12023), IBA1 (1:200, Invitrogen, MA5-41621) GLT-1 (1:200, AB1783, Sigma-Aldrich, NRF2 (1:200, Invitrogen, PA5-27882) followed by secondary (1:400 sary), and then DAPI (1:400 Thermo Fisher Scientific Cat#62248). Fluorescence was counted from three images per high-powered field (HPF) at 20× and quantified using ImageJ software. TUNEL stain was performed according to the manufacturer's instructions (Sigma, ApopTag Fluoresce in *in situ* Apoptosis Detection Kit, S7100) and was detected with Cleaved Caspase-3 (Asp175) Antibody (Alexa Fluor® 488 Conjugate,

Cell Signaling cat #9669). $n = 10$ control and $n = 10$ drug treated brains at each time point.

Quantification of microglial activation by cell shape

Microglia were visualized by immunohistochemical staining for Iba-1. ImageJ software analysis of three images of the penumbra region from three control and three drug-treated rats was used to determine cell body size.

Statistics

Results are reported as the mean ± SEM. The statistical significance of the difference between means was assessed using IBM SPSS Software using the unpaired 2-tailed Student's *t*-test (for the comparison of two groups). Pless than 0.05 was considered significant. With 10 animals per group, we had 80% power to detect a 1.3 standard deviation difference between the two groups.

Results

10-1 reduces infarct size and neurologic impairment

To determine if 10-1 could ameliorate acute ischemic brain injury, both treatments were administered following reperfusion (**Figure 1A**). Infarct volume was assessed from TTC stained brain sections at 24 h and 4 days (**Figures 1B,C**). Overall, 10-1 showed significantly decreased infarct volumes compared to control at 24 h and 4 days (**Figure 1C**). Neurologic assessment indicated that when compared with the control group, 10-1 treated rats had significantly lower Bederson scores (**Figure 1D**) at 24 h and 4 days post-injury, indicating early and sustained protection against post-ischemia neurologic impairment.

10-1 treatment attenuates progression of cerebral tissue damage

Following MCAO R, neuronal degeneration was determined by the presence of darkly stained pyknotic nuclei, cell body shrinkage, perineuronal vacuolization, and granular necrotic debris at days 1 and 4 (arrows in **Figure 2A**). Infarcted cerebral tissue is present in the cortex and subcortex (**Figure 2B**). Quantification of infarcted tissue in the cortex and subcortical structures revealed that 10-1 significantly decreased total infarct size and cortical infarct size at 24 h but not subcortical infarction (**Figure 2C**). On the other hand, 10-1 decreased cortex and subcortical infarct areas significantly at 4 days post-injury (**Figure 2C**). Thus, the damage is more severe in the subcortical tissue supplied by the proximal branches of the MCA (*e.g.*, lenticulostriates), with fewer collaterals should the blood supply be interrupted. In contrast, cortical tissue seems to be less vulnerable to immediate cell death (*i.e.*, necrosis) due to collateral circulation, and often represents at-risk tissue at early time points (*e.g.*, the penumbra). Based on this data, 10-1 appears to lead to an attenuated progression of cerebral ischemic injury 24 h and 4 days post-injury (**Figure 2B**).

NeuN staining, a neuronal cell body-specific marker, and terminal deoxynucleotidyl transferase dUTP nick end labeling (TUNEL) assay, a measure of apoptotic activity, were then performed in the infarct penumbra (**Figure 2D**). The ischemic penumbra represents vulnerable but salvageable cerebral tissue (Ramos-Cabrer et al., 2011). Cells that are positive for NeuN and TUNEL represent apoptotic neurons. Overall, the portion of apoptotic neurons was significantly decreased in the penumbra of 10-1 treated animals at 24 h and 4 days post-injury (**Figure 2D**).

10-1 promotes anti-inflammatory microglia in the ischemic penumbra and Tregs in the ischemic core

Next, expression of the glial cell markers, ionized calcium-binding adaptor protein-1 (IBA1), CD86, and arginase-1 (ARG1) were evaluated. Resident microglia are characterized by small cell bodies, long-branched processes, and relatively low intensity of IBA1 staining (**Figure 3** and **Supplementary Figure 1A**, Morizawa et al., 2017). In our subjects, IBA1 positive microglia in the penumbra of control animals 24 h post-injury were highly branched with elongated processes (**Figure 3** and **Supplementary Figure 1A**). In contrast, microglial cells in the penumbra of 10-1-treated rats showed larger body sizes and had fewer branching processes, resembling active microglia (Davis et al., 2017). At day 4, differences in the activated-amoeboid phenotype in treated and control groups were less pronounced (**Figure 3** and **Supplementary Figure 1A**).

Moreover, quantitative analysis shows a prominent increase in IBA1 expression in the penumbra of 10-1 rodents 24 h post-injury (**Figures 3A,B**). In addition, IBA1 expression was not increased in drug-treated animals as compared to controls on day 4, indicating an earlier peak in IBA1 expression in penumbral microglia (**Figure 3B**). Immunostaining was performed for CD86 to examine the effect of 10-1 on M1 microglia. We did not observe any changes in CD86 expression (data not shown).

We next investigated the expression of an alternative microglial activation marker, ARG1 (Munder et al., 1999;

10.3389/fnmol.2022.1055295

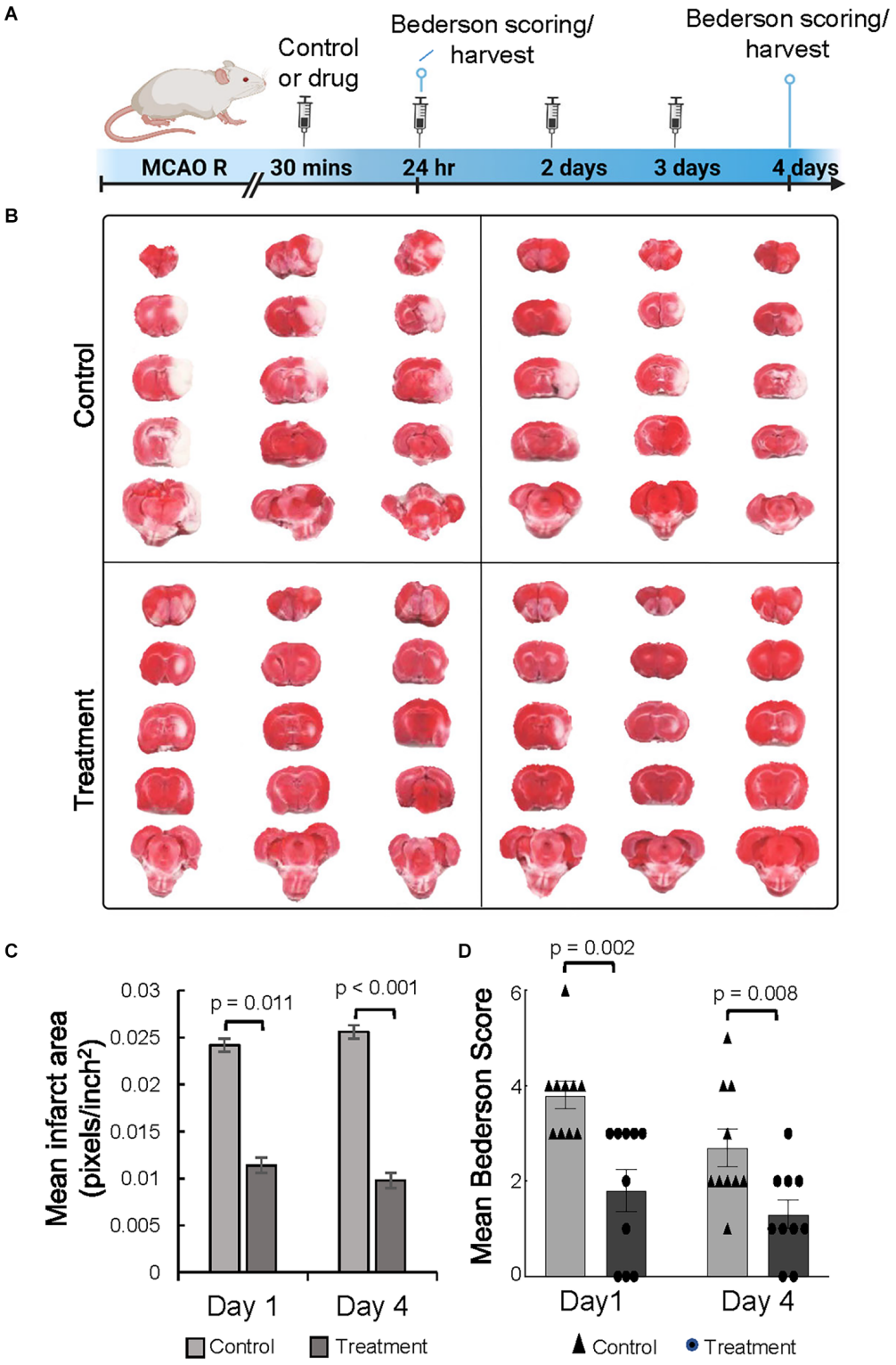

FIGURE 1
The SRC activator 10-1 attenuates cerebral ischemic injury and performance activity post-MCAO R. **(A)** Schematic representation of experimental procedures. Rats were injected with 10-1 (20 mg/kg) or control 30 min after a 90-min occlusion of the middle cerebral artery and every 24 h up to harvest at day 1 (n = 20) and day 4 (n = 20) after surgery. **(B)** Brains were harvested and stained with TTC to delineate and calculate infarct size. **(C)** Mean area of infarct was calculated at day 1 and day 4 post-MCAO R. **(D)** Neurological testing was done 24 h and 4 days after stroke onset using a modified Bederson score. n = 10 control and n = 10, 10-1.

10.3389/fnmol.2022.1055295

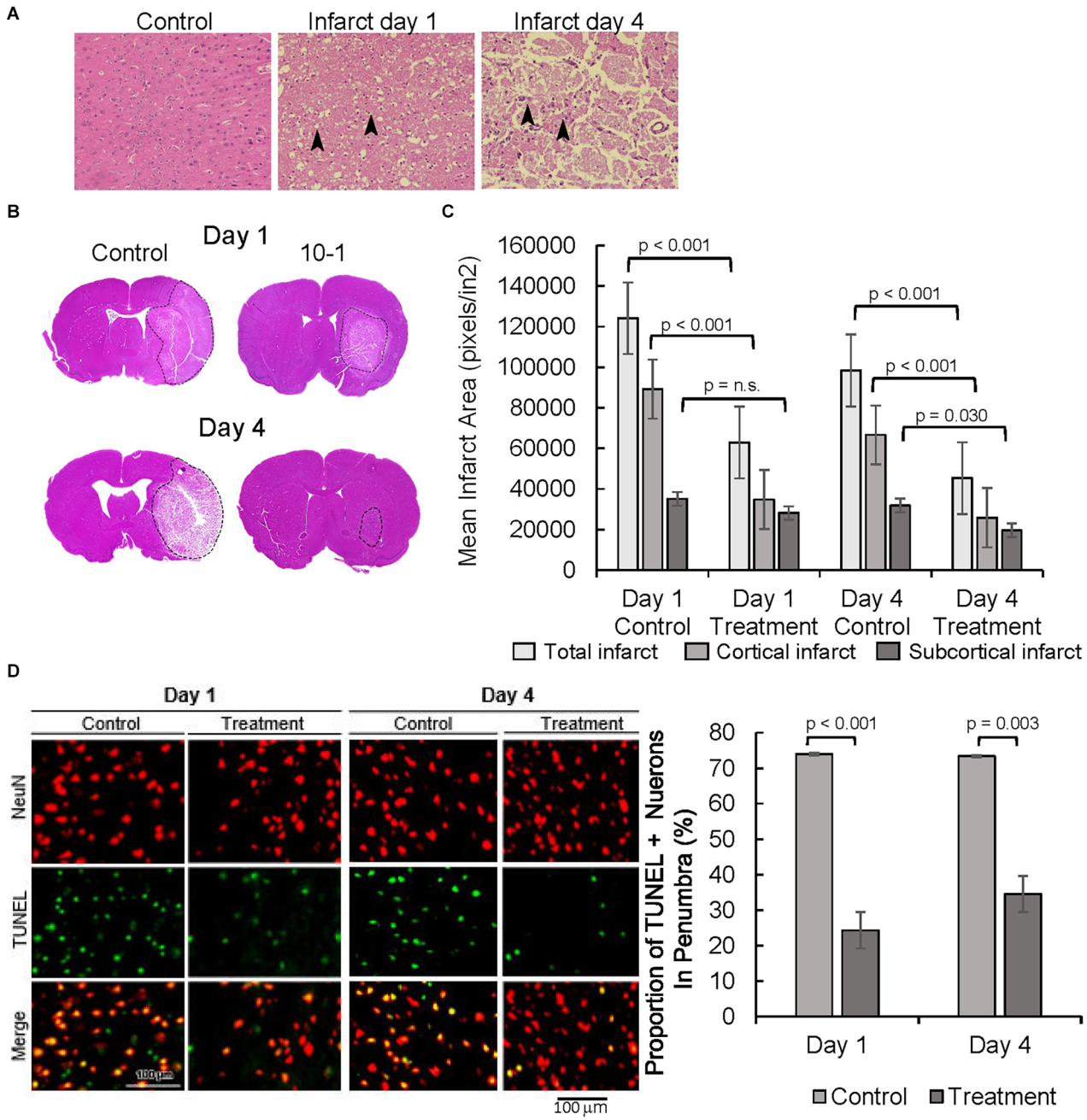

FIGURE 2
10-1 treatment attenuates progression of tissue damage post-MCAO R. **(A)** H&E tissue sections from the contralateral side (control, 1 day post-MCAO) and infarct areas at day 1 and day 4. Arrows indicate areas containing darkly stained pyknotic nuclei, cell body shrinkage, perineuronal vacuolization, and granular necrotic debris. **(B)** Representative H and E sections day 1 and day 4 post-MCAO. **(C)** Cortical and sub-cortical infarct size were measured in H&E stained brain tissue sections 1 day and 4 days post-MCAO R. **(D)** Representative images of TUNEL and NeuN immunostaining showing neuronal apoptosis one and 4 days post-MCAO R. Quantification of TUNEL positive NeuN positive cells. Day 1 and day 4 *n* = 10 control, 10 drug-treated, three images per section.

Cherry et al., 2014), specific to M2 microglia that is considered to be related to a more pro-reparative phenotype (Figures 3A,C) Co-localization of ARG1 and IBA1 was notably absent 24 h post-injury (Figure 3A). In contrast, expression of the ARG1 microglia marker was increased in IBA1 positive cells in 10-1 treated animals compared to control 4 days post-injury (Figures 3A,C). These results suggest that activated M2 microglia may contribute to improved recovery by day 4

10.3389/fnmol.2022.1055295

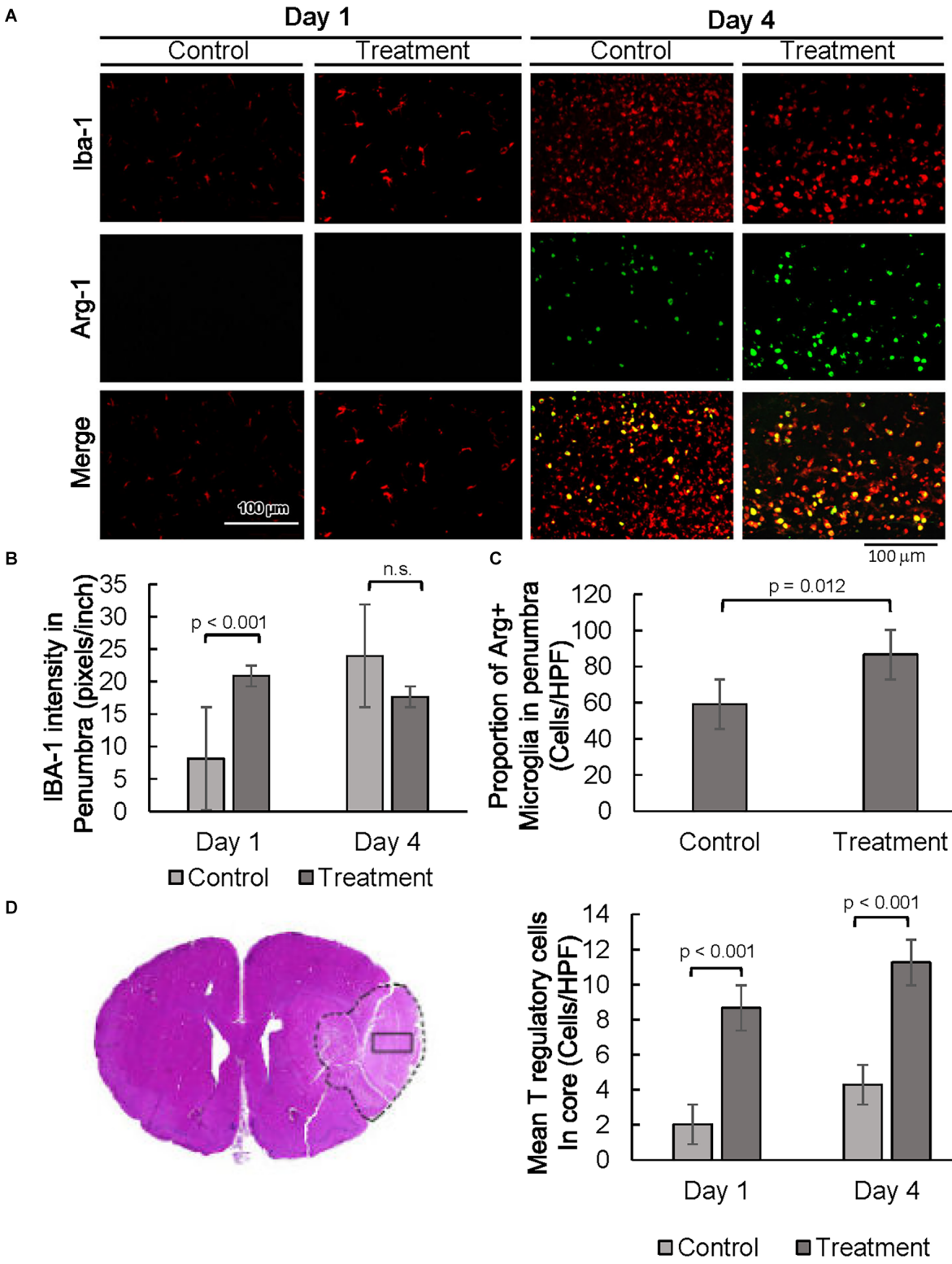

FIGURE 3
SRC activation promotes a pro-reparative immune response. **(A)** Representative images of IBA1 and ARG1 immunostaining showing per cent of pro-reparative M2 microglia 1 day and 4 days post-MCAO R. **(B)** Quantification of mean IBA1 intensity 1 and 4 days post-MCAO R. Day 1 and day 4 *n* = 10 control, 10 drug-treated, three images per section. **(C)** Quantification of IBA1 positive and ARG1 positive cells at day 4. **(D)** Quantification of average numbers of Tregs in the core infarct. Day 1 and day 4 *n* = 10 control, 10 drug-treated, three images per section.

after ischemic injury. Overall, SRC coactivator activation with 10-1 channels early post-stroke microglia activation into the more reparative M2 state during the later part of the post-injury response.

Lastly, we had recently shown enrichment of SRC-3 expression in regulatory T cells (Tregs; Nikolai et al., 2021). Given the protective effects of Tregs in post-stroke outcomes in other studies (Zhang et al., 2021), we performed immunostaining for Foxp3, a specific nuclear marker for Tregs (**Figure 3D** and **Supplementary Figure 1B**). Foxp3 staining was exclusive to the core, indicating Tregs are absent in the penumbral region 24 h and 4 days after injury. Foxp3 expression was elevated in the infarct core in 10-1 group as compared with controls at 24 h and 4 days following injury (**Figure 3D**).

10-1 treatment attenuated astrogliosis and promoted oxidative stress protection in astrocytes

Expression of astrocyte-specific glial fibrillary acidic protein (GFAP) was evaluated as a marker of astrogliosis in the stroke penumbra (**Figure 4A**). Quantitative GFAP analysis showed that GFAP expression at 4 days post-injury was significantly decreased in the stroke penumbra of 10-1 group as compared to controls, suggesting an attenuation in astrogliosis (**Supplementary Figure 2A**, Yang and Wang, 2015). On the other hand, analysis of the number of GFAP positive cells showed that the number of astrocytes in the penumbra of 10-1 animals was slightly increased from controls and was not significantly different from the contralateral normal side of the brain at 24 h (**Figures 4A,B**), suggesting a relative preservation of astrocytes. As expected, by day 4, GFAP positive cells were significantly increased in the stroke penumbra of control animals, beyond the mean number in the 10-1 group or contralateral normal side (**Figure 4B**). Quantitative analysis of GFAP positive cells showed that the number of astrocytes was significantly decreased in the penumbra of 10-1 treated animals compared to controls (**Figure 4B**).

The oxidative stress marker NFE2 Like BZIP Transcription Factor 2 (NFE2L2/NRF2) was examined next, as a measure of antioxidant protection in the stroke penumbra (**Figure 4A**). Overall, NRF2 expression was increased in the stroke penumbra of 10-1 subjects 4 days post-injury, but not significantly at 24 h (**Supplementary Figure 2B**). However, co-staining of GFAP and NRF2, a measure of astrocyte-specific expression of NRF2, showed increased co-expression at 24 h and 4 days post-injury (**Figure 4C**).

Lastly, we investigated the expression of astrocytic solute carrier family 1 member 2 (SLC1A2, also known as glutamate transporter glutamate transporter-1, GLT-1) as a marker of excitotoxic astrocytic cell death (Fontana, 2015). GLT-1 expression is well described in astrocytes in response to ischemic injury, peaks at 24–48 h, and dissipates rapidly after 4 days (Peterson and Binder, 2019). Quantification of GLT-1 staining intensity at 24 h post-injury suggests an increase in GLT-1 expression in penumbral astrocytes compared to the core infarct (**Figures 4D,E** and **Supplementary Figure 2B**).

Discussion

Neuroprotection is an important unmet need in the management of AIS. In this study, we have shown that SRC activation with 10-1 provides protection against cerebral injury following ischemia and reperfusion. In our model, infarct volumes were decreased by over 50% after treatment as compared with control animals and neurologic function remained relatively preserved. We showed that this effect most likely represents protection from ischemia rather than tissue regeneration. Furthermore, our analysis of neuronal apoptosis in the ischemic penumbra of 10-1 treated subjects was likewise decreased by over 50%. As SRCs are highly expressed in the brain and coordinate the activation of multiple gene expression programs necessary for cerebral repair (Sun and Xu, 2020), we hypothesized that this apparent neuroprotection could be explained by changes in the phenotypes of immune and glial cells.

Our findings indicate that 10-1 activates microglia to take on a more pro-reparative, M2 phenotype, that can help attenuate neurodegeneration in response to ischemic injury. Studies have shown that the presence of infiltrating macrophages from the peripheral circulation is low on the first day after stroke (Schilling et al., 2003). Thus, our data is highly suggestive that the increase in IBA1 expression we have noted is most likely a result of resident microglia activation. M2 microglia secrete anti-inflammatory cytokines that promote neuronal growth and are considered to be overwhelmingly neuroprotective (Deng et al., 2020). Nuclear receptors have well-described actions in modulating inflammatory processes (Glass and Ogawa, 2006). SRC-3 expression prevents NF-κB activation and protects against lymphoma formation in mice, indicating that SRC-3 can function to suppress the innate immune response (Wu et al., 2002; Coste et al., 2006). While our previous studies show that SRC activation suppresses inflammatory signaling (Coste et al., 2006; Yu et al., 2007; Chen Q. et al., 2010; Mullany et al., 2021), these results suggest 10-1 also provides neuroprotection by promoting early microglial activation in the acute tissue response (up to 48 h after stroke). We previously reported SRC activation suppressed macrophage inflammatory signaling and promoted M2 reparative macrophages in ischemic hearts (Mullany et al., 2020). In the current study, we found that early microglial activation is followed by the polarization of M2 microglia

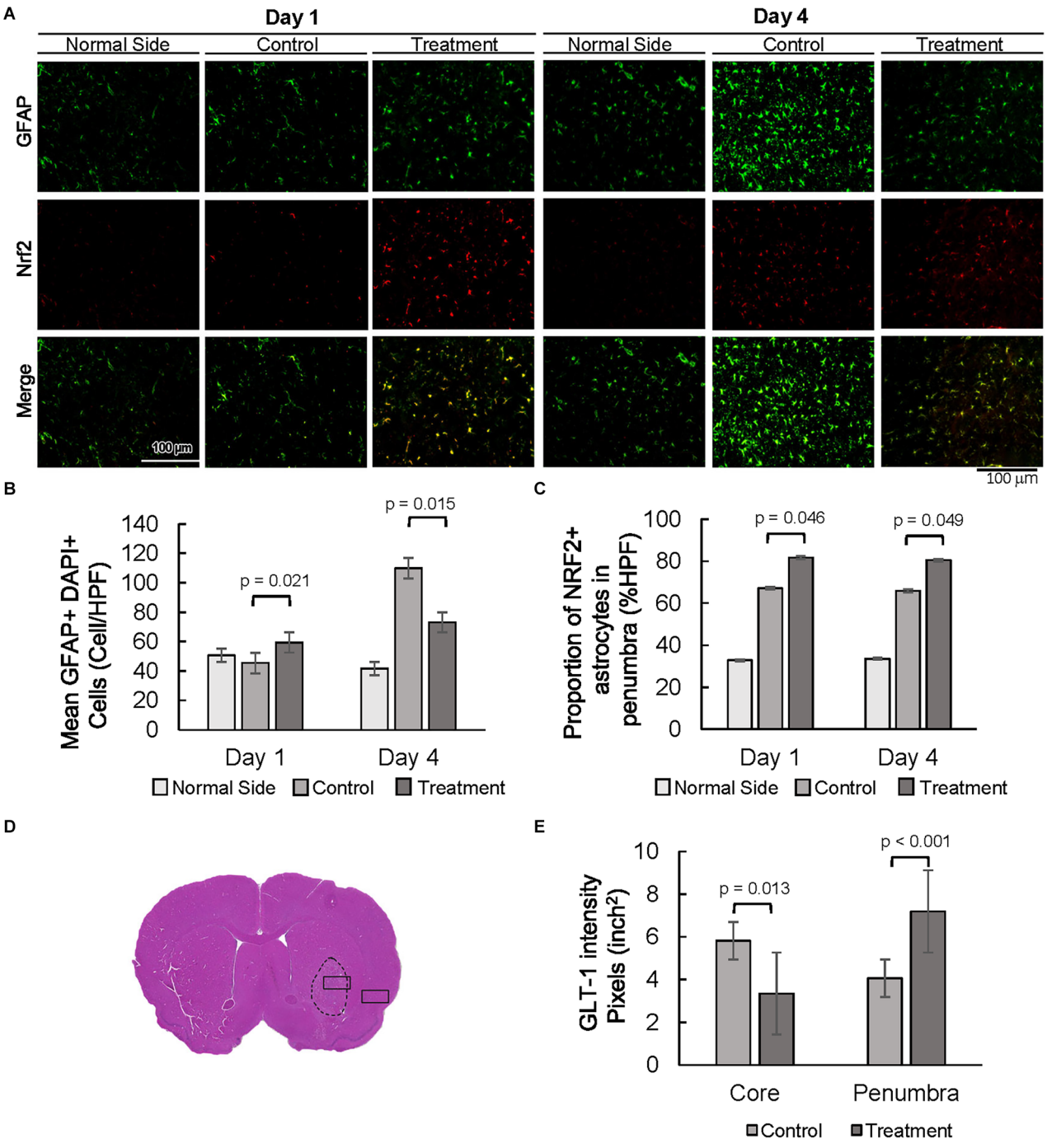

FIGURE 4
Decreased astrogliosis is associated with an increased proportion of NRF2 and GLT-1 positive astrocytes. **(A)** Representative images of GFAP and NRF2 in the contralateral side (normal side) and penumbra 1 day and 4 days post-MCAO R. **(B)** Number of astrocytes in the penumbra. **(C)** The proportion of GFAP positive, NRF2 positive astrocytes in the penumbra. **(D)** Representative H&E section with area of sampling in core (box inside dashed area) and penumbra (box outside dashed area). **(E)** Quantification of the intensity of GLT-1 staining in the core and penumbra as shown in **Supplementary Figure 2**. Day 1 and day 4 *n* = 10 control, 10 drug-treated, three HPF per section.

in the subacute phase (3–6 days after stroke), which may ultimately be contributing to the robust neuroprotection that we see. Although these findings are consistent with previously documented SRC actions, further research is needed to identify the receptors and signaling pathways involved in 10-1's regulation of microglial functions.

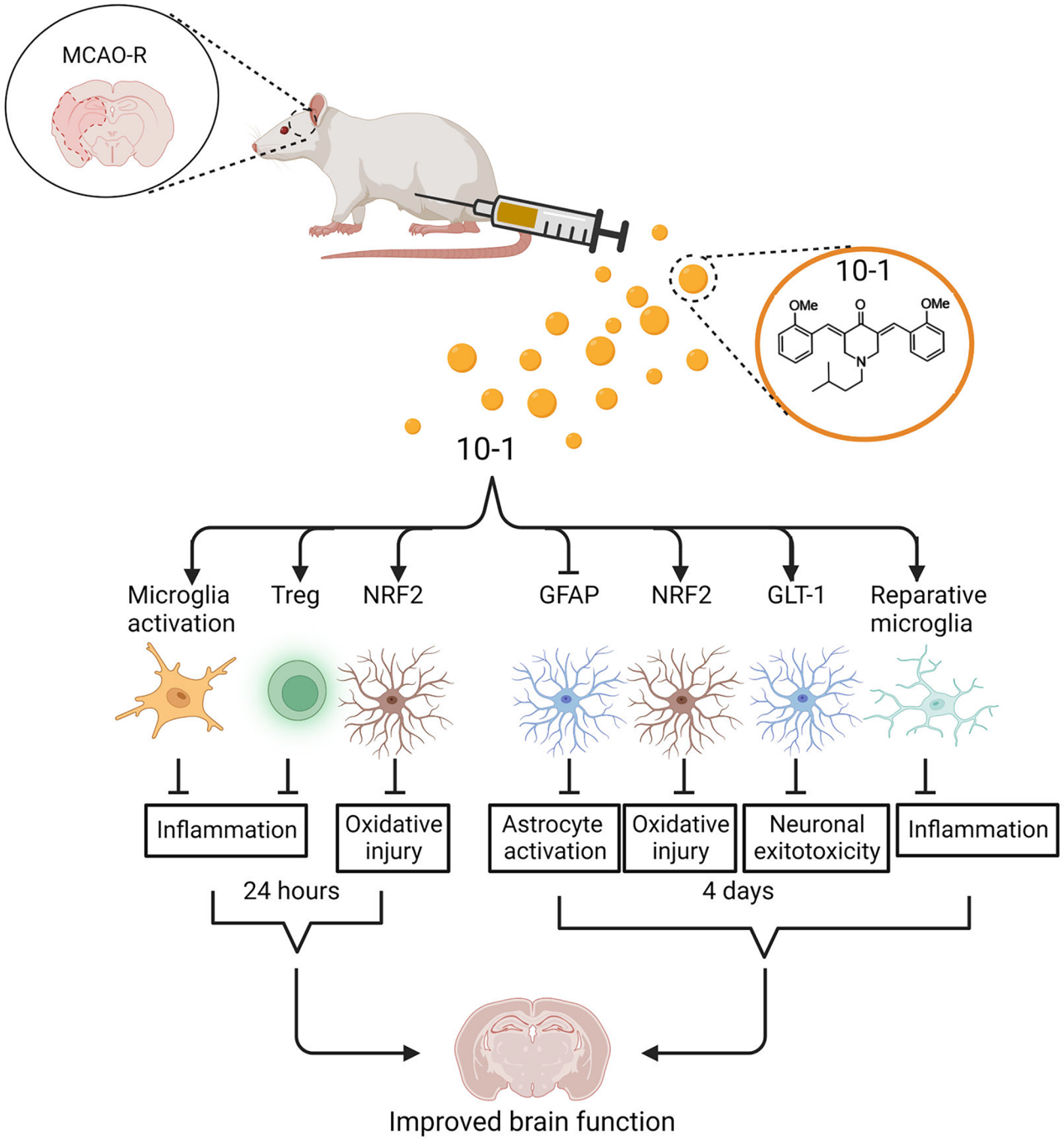

FIGURE 5
Schematic of regulation of ischemic stroke injury following 10-1 treatment. 10-1 treatment attenuated neuronal injury following robust transient activation of microglia, increased Treg numbers, and increased representation of NRF2 positive astrocytes 24 h after ischemic injury. Four days after ischemia injury, the 10-1 therapy also enhanced NRF2 positive astrocytes, polarized M2 reparative microglia, and reduced astrogliosis. Created with BioRender.com.

Ongoing inflammation in the brain following stroke is a major contributor to tissue damage (Chamorro et al., 2012). Animal studies show that Tregs can suppress inflammation and promote recovery in both the acute and chronic phases (Zhang et al., 2021). In this study, we show an increased number of Tregs at 24 h and 4 days in the post-stroke infarct core. Other animal studies have shown that Tregs migrate to the ischemic infarct core 7–14 days after stroke onset

(Ito et al., 2019). Treg functions have been implicated in many neuroprotective processes, such as the suppression of astrogliosis by producing amphiregulin and the promotion of reparative microglia by secretion of osteopontin (Shi et al., 2021). Recently, we discovered that SRC-3 expression is enriched in Tregs, and that inhibition of SRC-3 blocks their immunosuppressive functions (Nikolai et al., 2021). These findings reveal another mechanism by which SRC activation in AIS may prevent ongoing inflammation, supporting improved tissue recovery.

While microglia and other immune cells comprise a relatively small population of cells in the brain, glia are even more numerous than neurons. Astrocytes are a large part of the glial population, especially in the cortical regions of the brain, and perform multiple homeostatic functions necessary for proper cerebral function and maintenance (Pajarillo et al., 2019). Astrocytes function to modulate synaptic function, promote angiogenesis, and provide antioxidant protection (Becerra-Calixto and Cardona-Gomez, 2017). However, similar to microglia, astrocytes are not fate-arrested and can alter their morphology and function in response to environmental cues (Liddelow and Barres, 2017). Astrocyte glutamate transport by GLT-1, responsible for over 90% of synaptic clearance of excess glutamate, is critical for neuronal survival following cerebral ischemia (Pajarillo et al., 2019). Thus, an increase in astrocyte GLT-1 expression in the stroke penumbra of 10-1 treated animals suggests that GLT-1 is a key player in attenuating neuronal cell death and infarct progression.

In addition, oxidative stress-induced cerebral damage is an important mechanism of injury potentiation in ischemic stroke. NRF2 serves as the transcriptional master regulator of basal and stress-induced cytoprotective responses in the brain and in many other organs (Liu et al., 2019). Furthermore, NRF2 is highly expressed in astrocytes (Shih et al., 2003), where previous neuroprotection studies have implicated NRF2-regulated genes as the likely target of neuron–astrocyte interactions after injury (Habas et al., 2013). Increased NRF2 expression in astrocytes from 10-1 treated animals supports the notion that astrocytes are major contributors to oxidative stress management in response to stroke. In addition, higher expression of NRF2 in stroke penumbral astrocytes at 4 days post-MCAO R, suggests a higher propensity for 10-1 conditioned astrocytes to adapt and survive when exposed to oxidative stress. Previous research has previously shown that SRC-3 is required for transcriptional activation of the anti-oxidative enzyme catalase (CAT; Chen Q. et al., 2010) and is recruited to the promoters of CAT (Chen Q. et al., 2010) and NRF2 (Kim et al., 2013). This suggests SRC-3 activation contributes directly to the regulation of astrocyte antioxidant signaling pathways. These findings suggest that 10-1 may contribute to early and sustained neuroprotection by promoting the NRF2 and GLT-1 astrocyte responses, which may work to attenuate neuronal excitotoxicity and oxidative injury. Taken together, these findings indicate that 10-1 treatment promoted early microglial activation along with reparative microglia and increased Tregs. 10-1 also improved astrocyte oxidative stress responses and attenuated astrogliosis.

While we believe that the results of this study are robust and represent a breakthrough in neuroprotection research, we do appreciate several limitations. Firstly, the phenotypic changes seen in neurons, microglia, and astrocytes do not provide complete insight into gene expression. Further detailed studies are required to provide insights into the transcriptional regulation of anti-inflammatory microglial cells and the pro-survival oxidative responses of astrocytes. Ultimately, understanding the differential gene expression programs will help us to clarify what cell types are most implicated in the neuroprotective effects of 10-1, which will help us identify the drug's optimal use in AIS. Additionally, although the concern for sex differences with 10-1 therapy in the current study is eliminated, the fact that we only employed male rats for our tests is a weakness in our findings. For example, in another rodent study of the central nervous system, there was an increased expression of SRC-1 in female mice after spinal cord injury, which lead to better neurologic recovery than in male mice (Xiao et al., 2017), emphasizing the importance of future studies using female rodents.

We demonstrate that SRC-coactivator activation with MCB-10-1 provides extensive neuroprotection in a mouse MCAO R model through a coordinated, multicellular process, which is consistent with previously documented SRC activities in tissue formation and homeostasis. We have shown that not only are infarct sizes and neurologic function improved in the 10-1 treatment group but that the secondary injury response of inflammatory cells and astrocytes also is attenuated. 10-1 improved recovery after MCAO R in the acute phase, and was associated with increased M2 microglial activation, increased astrocyte NRF2 and GLT-1 expression, and increased Treg cell numbers recruited into the stroke penumbra (**Figure 5**). In addition to attenuating damage from injury, SRC stimulation with 10-1 could provide a potential therapeutic approach to extend the therapeutic window for revascularization strategies. In summary, SRC activation may be able to fill the unmet clinical need for an effective neuroprotectant in stroke patients.

Data availability statement

The raw data supporting the conclusions of this article will be made available by the authors, without undue reservation.

Ethics statement

The animal study was reviewed and approved by Institutional Animal Care and Use Committee, University of Texas Medical Branch at Galveston.

Author contributions

BO'M, LM, CD, DL, RG, and PK: conceptualization. LM: writing—original draft. LM, DL, BO'M, CD, PK, RG, AR, VV, ASR, ZL, AS, and TL: investigation, methodology, and formal analysis. BO'M, PK, and DL: resources. LM, DL, BO'M, CD, PK, RG, and TL: writing—review and editing. RG and TL: data curation and visualization. All authors contributed to the article and approved the submitted version.

Funding

This work was supported by NSF: NeTS 1801865, Philip J. Carroll, Jr. Professorship, Brockman Foundation, Rene and Kay Joyce Family Foundation, Sonya T. and William A. Carpenter, Jr. to CD.

Conflict of interest

SRC stimulator compounds are being developed for stroke and other ischemic injury-related diseases by CoRegen, Inc. affiliated with LM, DL, CD, and BO'M.

The remaining authors declare that the research was conducted in the absence of any commercial or financial relationships that could be construed as a potential conflict of interest.

Publisher's note

All claims expressed in this article are solely those of the authors and do not necessarily represent those of their affiliated organizations, or those of the publisher, the editors and the reviewers. Any product that may be evaluated in this article, or claim that may be made by its manufacturer, is not guaranteed or endorsed by the publisher.

Supplementary material

The Supplementary Material for this article can be found online at: https://www.frontiersin.org/articles/10.3389/fnmol.2022.1055295/full#supplementary-material.

References

Albers, G. W., Marks, M. P., Kemp, S., Christensen, S., Tsai, J. P., Ortega-Gutierrez, S., et al. (2018). Thrombectomy for stroke at 6 to 16 hours with selection by perfusion imaging. *N. Engl. J. Med.* 378, 708–718. doi: 10.1056/NEJMoa1713973

Becerra-Calixto, A., and Cardona-Gomez, G. P. (2017). The role of astrocytes in neuroprotection after brain stroke: potential in cell therapy. *Front. Mol. Neurosci.* 10:88. doi: 10.3389/fnmol.2017.00088

Chamorro, A., Meisel, A., Planas, A. M., Urra, X., van de Beek, D., and Veltkamp, R. (2012). The immunology of acute stroke. *Nat. Rev. Neurol.* 8, 401–410. doi: 10.1038/nrneurol.2012.98

Chen, Q., Chen, T., Xu, Y., Zhu, J., Jiang, Y., Zhao, Y., et al. (2010). Steroid receptor coactivator 3 is required for clearing bacteria and repressing inflammatory response in *Escherichia coli*-induced septic peritonitis. *J. Immunol.* 185, 5444–5452. doi: 10.4049/jimmunol.0903802

Chen, X., Liu, Z., and Xu, J. (2010). The cooperative function of nuclear receptor coactivator 1 (NCOA1) and NCOA3 in placental development and embryo survival. *Mol. Endocrinol.* 24, 1917–1934. doi: 10.1210/me.2010-0201

Chen, X., Qin, L., Liu, Z., Liao, L., Martin, J. F., and Xu, J. (2015). Knockout of SRC-1 and SRC-3 in mice decreases cardiomyocyte proliferation and causes a noncompaction cardiomyopathy phenotype. *Int. J. Biol. Sci.* 11, 1056–1072. doi: 10.7150/ijbs.12408

Cherry, J. D., Olschowka, J. A., and O'Banion, M. K. (2014). Neuroinflammation and M2 microglia: the good, the bad and the inflamed. *J. Neuroinflammation* 11:98. doi: 10.1186/1742-2094-11-98

Coste, A., Antal, M. C., Chan, S., Kastner, P., Mark, M., and O'Malley, B. W. (2006). Absence of the steroid receptor coactivator-3 induces B-cell lymphoma. *EMBO J.* 25, 2453–2464. doi: 10.1038/sj.emboj.7601106

Davis, B. M., Salinas-Navarro, M., Cordeiro, M. F., Moons, L., and De Groef, L. (2017). Characterizing microglia activation: a spatial statistics approach to maximize information extraction. *Sci. Rep.* 7:1576. doi: 10.1038/s41598-017-01747-8

Deng, W., Mandeville, E., Terasaki, Y., Li, W., Holder, J., Chuang, A. T., et al. (2020). Transcriptomic characterization of microglia activation in a rat model of ischemic stroke. *J. Cereb. Blood Flow Metab.* 40, S34–S48. doi: 10.1177/0271678X20932870

Fontana, A. C. (2015). Current approaches to enhance glutamate transporter function and expression. *J. Neurochem.* 134, 982–1007. doi: 10.1111/jnc.13200

Glass, C. K., and Ogawa, S. (2006). Combinatorial roles of nuclear receptors in inflammation and immunity. *Nat. Rev. Immunol.* 6, 44–55. doi: 10.1038/nri1748

Goyal, M., Menon, B. K., van Zwam, W. H., Dippel, D. W., Mitchell, P. J., Demchuk, A. M., et al. (2016). Endovascular thrombectomy after large-vessel ischaemic stroke: a meta-analysis of individual patient data from five randomised trials. *Lancet* 387, 1723–1731. doi: 10.1016/S0140-6736(16)00163-X

Habas, A., Hahn, J., Wang, X., and Margeta, M. (2013). Neuronal activity regulates astrocytic Nrf2 signaling. *Proc. Natl. Acad. Sci. U S A* 110, 18291–18296. doi: 10.1073/pnas.1208764110

Hill, M. D., Goyal, M., Menon, B. K., Nogueira, R. G., McTaggart, R. A., Demchuk, A. M., et al. (2020). Efficacy and safety of nerinetide for the treatment of acute ischaemic stroke (ESCAPE-NA1): a multicentre, double-blind, randomised controlled trial. *Lancet* 395, 878–887. doi: 10.1016/S0140-6736(20)30258-0

Ito, M., Komai, K., Mise-Omata, S., Iizuka-Koga, M., Noguchi, Y., Kondo, T., et al. (2019). Brain regulatory T cells suppress astrogliosis and potentiate neurological recovery. *Nature* 565, 246–250. doi: 10.1038/s41586-018-0824-5

Kim, J. H., Yu, S., Chen, J. D., and Kong, A. N. (2013). The nuclear cofactor RAC3/AIB1/SRC-3 enhances Nrf2 signaling by interacting with transactivation domains. *Oncogene* 32, 514–527. doi: 10.1038/onc.2012.59

Lanz, R. B., Bulynko, Y., Malovannaya, A., Labhart, P., Wang, L., Li, W., et al. (2010). Global characterization of transcriptional impact of the SRC-3 coregulator. *Mol. Endocrinol.* 24, 859–872. doi: 10.1210/me.2009-0499

Liddelow, S. A., and Barres, B. A. (2017). Reactive astrocytes: production, function and therapeutic potential. *Immunity* 46, 957–967. doi: 10.1016/j.immuni.2017.06.006

Liu, L., Locascio, L. M., and Dore, S. (2019). Critical role of Nrf2 in experimental ischemic stroke. *Front. Pharmacol.* 10:153. doi: 10.3389/fphar.2019.00153

Liu, F., Schafer, D. P., and McCullough, L. D. (2009). TTC, fluoro-Jade B and NeuN staining confirm evolving phases of infarction induced by middle cerebral

artery occlusion. *J. Neurosci. Methods* 179, 1–8. doi: 10.1016/j.jneumeth.2008.12.028

Lonard, D. M., and O'Malley, B. W. (2007). Nuclear receptor coregulators: judges, juries and executioners of cellular regulation. *Mol. Cell* 27, 691–700. doi: 10.1016/j.molcel.2007.08.012

Longa, E. Z., Weinstein, P. R., Carlson, S., and Cummins, R. (1989). Reversible middle cerebral artery occlusion without craniectomy in rats. *Stroke* 20, 84–91. doi: 10.1161/01.str.20.1.84

Morizawa, Y. M., Hirayama, Y., Ohno, N., Shibata, S., Shigetomi, E., Sui, Y., et al. (2017). Reactive astrocytes function as phagocytes after brain ischemia via ABCA1-mediated pathway. *Nat. Commun.* 8:28. doi: 10.1038/s41467-017-00037-1

Mullany, L. K., Lonard, D. M., and O'Malley, B. W. (2021). Wound healing-related functions of the p160 steroid receptor co-activator family. *Endocrinology* 162:bqaa232. doi: 10.1210/endocr/bqaa232

Mullany, L. K., Rohira, A. D., Leach, J. P., Kim, J. H., Monroe, T. O., Ortiz, A. R., et al. (2020). A steroid receptor coactivator stimulator (MCB-613) attenuates adverse remodeling after myocardial infarction. *Proc. Natl. Acad. Sci. U S A* 117, 31353–31364. doi: 10.1073/pnas.2011614117

Munder, M., Eichmann, K., Moran, J. M., Centeno, F., Soler, G., and Modolell, M. (1999). Th1/Th2-regulated expression of arginase isoforms in murine macrophages and dendritic cells. *J. Immunol.* 163, 3771–3777.

Nikolai, B. C., Jain, P., Cardenas, D. L., York, B., Feng, Q., McKenna, N. J., et al. (2021). Steroid receptor coactivator 3 (SRC-3/AIB1) is enriched and functional in mouse and human Tregs. *Sci. Rep.* 11:3441. doi: 10.1038/s41598-021-82945-3

Nogueira, R. G., Jadhav, A. P., Haussen, D. C., Bonafe, A., Budzik, R. F., Bhuva, P., et al. (2018). Thrombectomy 6 to 24 hours after stroke with a mismatch between deficit and infarct. *N. Engl. J. Med.* 378, 11–21. doi: 10.1056/NEJMoa1706442

Onate, S. A., Tsai, S. Y., Tsai, M. J., and O'Malley, B. W. (1995). Sequence and characterization of a coactivator for the steroid hormone receptor superfamily. *Science* 270, 1354–1357. doi: 10.1126/science.270.5240.1354

Pajarillo, E., Rizor, A., Lee, J., Aschner, M., and Lee, E. (2019). The role of astrocytic glutamate transporters GLT-1 and GLAST in neurological disorders: potential targets for neurotherapeutics. *Neuropharmacology* 161:107559. doi: 10.1016/j.neuropharm.2019.03.002

Peterson, A. R., and Binder, D. K. (2019). Post-translational regulation of GLT-1 in neurological diseases and its potential as an effective therapeutic target. *Front. Mol. Neurosci.* 12:164. doi: 10.3389/fnmol.2019.00164

Ramos-Cabrer, P., Campos, F., Sobrino, T., and Castillo, J. (2011). Targeting the ischemic penumbra. *Stroke* 42, S7–S11. doi: 10.1161/STROKEAHA.110.596684

Saver, J. L., Starkman, S., Eckstein, M., Stratton, S. J., Pratt, F. D., Hamilton, S., et al. (2015). Prehospital use of magnesium sulfate as neuroprotection in acute stroke. *N. Engl. J. Med.* 372, 528–536. doi: 10.1056/NEJMoa1408827

Schilling, M., Besselmann, M., Leonhard, C., Mueller, M., Ringelstein, E. B., and Kiefer, R. (2003). Microglial activation precedes and predominates over macrophage infiltration in transient focal cerebral ischemia: a study in green fluorescent protein transgenic bone marrow chimeric mice. *Exp. Neurol.* 183, 25–33. doi: 10.1016/s0014-4886(03)00082-7

Shi, L., Sun, Z., Su, W., Xu, F., Xie, D., Zhang, Q., et al. (2021). Treg cell-derived osteopontin promotes microglia-mediated white matter repair after ischemic stroke. *Immunity* 54, 1527–1542.e8. doi: 10.1016/j.immuni.2021.04.022

Shih, A. Y., Johnson, D. A., Wong, G., Kraft, A. D., Jiang, L., Erb, H., et al. (2003). Coordinate regulation of glutathione biosynthesis and release by Nrf2-expressing glia potently protects neurons from oxidative stress. *J. Neurosci.* 23, 3394–3406. doi: 10.1523/JNEUROSCI.23-08-03394.2003

Sun, Z., and Xu, Y. (2020). Nuclear receptor coactivators (NCOAs) and corepressors (NCORs) in the brain. *Endocrinology* 161:bqaa083. doi: 10.1210/endocr/bqaa083

Swanson, L. W. (2018). Brain maps 4.0-Structure of the rat brain: an open access atlas with global nervous system nomenclature ontology and flatmaps. *J. Comp. Neurol.* 526, 935–943. doi: 10.1002/cne.24381

Wang, L., Yu, Y., Chow, D. C., Yan, F., Hsu, C. C., Stossi, F., et al. (2015). Characterization of a steroid receptor coactivator small molecule stimulator that overstimulates cancer cells and leads to cell stress and death. *Cancer Cell* 28, 240–252. doi: 10.1016/j.ccell.2015.07.005

Wu, R. C., Qin, J., Hashimoto, Y., Wong, J., Xu, J., Tsai, S. Y., et al. (2002). Regulation of SRC-3 (pCIP/ACTR/AIB-1/RAC-3/TRAM-1) coactivator activity by I kappa B kinase. *Mol. Cell. Biol.* 22, 3549–3561. doi: 10.1128/MCB.22.10.3549-3561.2002

Xiao, J., Zhang, J., Zhao, Y., Huang, W., Guo, Z., Su, B., et al. (2017). Sex differences of steroid receptor coactivator-1 expression after spinal cord injury in mice. *Neurol. Res.* 39, 1022–1027. doi: 10.1080/01616412.2017.1367077

Yang, Z., and Wang, K. K. (2015). Glial fibrillary acidic protein: from intermediate filament assembly and gliosis to neurobiomarker. *Trends Neurosci.* 38, 364–374. doi: 10.1016/j.tins.2015.04.003

Yu, C., York, B., Wang, S., Feng, Q., Xu, J., and O'Malley, B. W. (2007). An essential function of the SRC-3 coactivator in suppression of cytokine mRNA translation and inflammatory response. *Mol. Cell* 25, 765–778. doi: 10.1016/j.molcel.2007.01.025

Zhang, Y., Liesz, A., and Li, P. (2021). Coming to the rescue: regulatory T cells for promoting recovery after ischemic stroke. *Stroke* 52, e837–e841. doi: 10.1161/STROKEAHA.121.036072

frontiers | Frontiers in Molecular Neuroscience

TYPE Original Research
PUBLISHED 07 December 2022
DOI 10.3389/fnmol.2022.1039990

OPEN ACCESS

EDITED BY
Federica Bono,
University of Brescia, Italy

REVIEWED BY
Maurizio Elia,
IRCCS Oasi Maria SS, Italy
Daniela Tropea,
Trinity College Dublin, Ireland
Xiao Chang,
Children's Hospital of Philadelphia, United States
Sheng Sun,
Massachusetts General Hospital and Harvard Medical School, United States
Wengeng Zhang,
Sichuan University, China

*CORRESPONDENCE
Qiongling Peng
pql1016@126.com
Jin Wu
Jin.wu@roswellpark.org

†PRESENT ADDRESS
Jin Wu,
Department of Molecular and Cellular Biology, Roswell Park Comprehensive Cancer Center, Buffalo, NY, United States

‡These authors have contributed equally to this work

SPECIALTY SECTION
This article was submitted to Brain Disease Mechanisms, a section of the journal Frontiers in Molecular Neuroscience

RECEIVED 08 September 2022
ACCEPTED 11 November 2022
PUBLISHED 07 December 2022

CITATION
Lu G, Zhang Y, Xia H, He X, Xu P, Wu L, Li D, Ma L, Wu J and Peng Q (2022) Identification of a *de novo* mutation of the *FOXG1* gene and comprehensive analysis for molecular factors in Chinese FOXG1-related encephalopathies.
Front. Mol. Neurosci. 15:1039990.
doi: 10.3389/fnmol.2022.1039990

Identification of a *de novo* mutation of the *FOXG1* gene and comprehensive analysis for molecular factors in Chinese FOXG1-related encephalopathies

Guanting Lu[1,2‡], Yan Zhang[3‡], Huiyun Xia[4], Xiaoyan He[1,2], Pei Xu[1,2], Lianying Wu[1,2], Ding Li[2], Liya Ma[4], Jin Wu[1,2*†] and Qiongling Peng[4*]

[1]Laboratory of Translational Medicine Research, Department of Pathology, Deyang People's Hospital, Deyang, China, [2]Key Laboratory of Tumor Molecular Research of Deyang, Deyang, China, [3]Department of Obstetrics and Gynecology, Strategic Support Force Medical Center, Beijing, China, [4]Department of Child Healthcare, Shenzhen Baoan Women's and Children's Hospital, Jinan University, Shenzhen, China

Background: FOXG1-related encephalopathy, also known as FOXG1 syndrome or FOXG1-related disorder, affects most aspects of development and causes microcephaly and brain malformations. This syndrome was previously considered to be the congenital variant of Rett syndrome. The abnormal function or expression of FOXG1, caused by intragenic mutations, microdeletions or microduplications, was considered to be crucial pathological factor for this disorder. Currently, most of the FOXG1-related encephalopathies have been identified in Europeans and North Americans, and relatively few Chinese cases were reported.

Methods: Array-Comparative Genomic Hybridization (Array-CGH) and whole-exome sequencing (WES) were carried out for the proband and her parent to detect pathogenic variants.

Results: A *de novo* nonsense mutation (c.385G>T, p.Glu129Ter) of FOXG1 was identified in a female child in a cohort of 73 Chinese children with neurodevelopmental disorders/intellectual disorders (NDDs/IDs). In order to have a comprehensive view of FOXG1-related encephalopathy in China, relevant published reports were browsed and twelve cases with mutations in FOXG1 or copy number variants (CNVs) involving FOXG1 gene were involved in the analysis eventually. Feeding difficulties, seizures, delayed speech, corpus callosum hypoplasia and underdevelopment of frontal and temporal lobes occurred in almost all cases. Out of the 12 cases, eight patients (66.67%) had single-nucleotide mutations of FOXG1 gene and four patients (33.33%) had CNVs involving FOXG1 (3 microdeletions and 1 microduplication). The expression of FOXG1 could also be potentially disturbed by deletions of several brain-active regulatory elements located in intergenic FOXG1-PRKD1 region. Further analysis indicated that PRKD1 might be a cooperating factor to regulate the expression of FOXG1, MECP2 and CDKL5 to contribute the RTT/RTT-like disorders.

Discussion: This re-analysis would broaden the existed knowledge about the molecular etiology and be helpful for diagnosis, treatment, and gene therapy of FOXG1-related disorders in the future.

KEYWORDS

Rett syndrome, FOXG1-related encephalopathy, FOXG1, PRKD1, haploinsufficiency, intergenic regulatory elements

Introduction

Rett syndrome (RTT; OMIM#312750) is a severe syndromic disorder that affects almost exclusively females with a prevalence of 1/10,000 under an X-linked dominant (XLD) mode of inheritance (Grillo et al., 2012). The characterized clinical phenotypes include arrested growth at an early stage (usually between 6 months and 18 months after birth), loss of speech, withdrawal of acquired skills, hand stereotypies, microcephaly, seizures, and intellectual disability (Moog et al., 2003).

It has been reported that mutations of the Xq28-localized *MECP2* gene are responsible for about 90% of RTT cases. Except for *MECP2*, *CDKL5* (Zhu and Xiong, 2019) and *FOXG1* (Byun et al., 2015) are two other well-known RTT causal genes. Recently, *STXBP1* (Cogliati et al., 2019), *KIF1A* (Wang et al., 2019), *GRIN1* (Wang et al., 2019), *NTNG1* (Borg et al., 2005; Archer et al., 2006; Nectoux et al., 2007; Aldosary et al., 2020), *NTNG2* (Heimer et al., 2020), *MEF2C* (Wang et al., 2018; Anitha et al., 2022), *SATB2* (Lee et al., 2016), and *WDR45* (Hoffjan et al., 2016; Kulikovskaja et al., 2018) have also been implicated as genetic factors of RTT or RTT-like syndromes. According to the molecular assays for two large cohorts recruited 486 Chinese patients with RTT, *MECP2* accounted for 83.74% (407/486) and *CDKL5* for 0.82% of the cases. No mutations of *FOXG1* were detected (Li et al., 2007; Zhang et al., 2012). In 2017, four *de novo* *FOXG1* mutations were first reported in a cohort of 451 Chinese patients with RTT or RTT-like disorders (Zhang et al., 2017). Except for intragenic mutations, CNVs containing the *FOXG1* gene were also reported in Chinese patients with neurodevelopmental disorders (Wang et al., 2017; Li et al., 2021).

Previously, patients carrying pathogenic *FOXG1* mutations were initially diagnosed as a congenital variant of the RTT syndrome (OMIM#613454), for having global development delay and disease onset from early infancy (before 6 months of age) and seizure onset after 3 months of birth (Ariani et al., 2008; Jacob et al., 2009). However, with the accumulation of clinical phenotypes associated with FOXG1 mutations, the patients generally lacked social eye contact, faced more severe sleep difficulty, and experienced difficulty in the postnatal development of language and ambulation (Papandreou et al., 2016; Mitter et al., 2018; Vegas et al., 2018). More importantly, the patients also lacked obvious regression of required psychomotor abilities as observed in RTT (Caporali et al., 2018). Therefore, the spectrum associated with FOXG1 mutations has been considered to be a separate clinical entity and termed "FOXG1-related encephalopathy," (Wong et al., 2019b) "FOXG1-related disorder," (McMahon et al., 2015) or "FOXG1-related syndrome" (Wong et al., 2019a).

Recently, a *de novo* non-sense mutation (c.385G>T, p.Glu129Ter) of the *FOXG1* gene was identified in a Chinese female patient with neurodevelopmental disorders/intellectual disorders (NDD/IDs). Currently, most of the patients of FOXG1-related encephalopathy are of European and North American origins, and only 12 Chinese cases have been identified so far. In the current project, a comprehensive reanalysis of the genotypes of *FOXG1* was carried out for the Chinese FOXG1-related encephalopathies. Four main types of underlying molecular

Abbreviations: CNV, copy number variant; RTT, Rett syndrome; ACMG, American College of Medical Genetics and Genomics; MAF, minor allele frequency; ExAC, Exome Aggregation Consortium; gnomAD, Genome Aggregation Database; GO-ESP, NHLBI Grand Opportunity Exome Sequencing Project; TOPMED, NHLBI Trans-Omics for Precision Medicine; CNKI, Chinese National Knowledge Infrastructure; GEO, gene expression omnibus; OFC, occipitofrontal head circumference; ACTH, adrenocorticotropic hormone; EEG, electroencephalogram; fVEP, flash visually evoked potential; ABR, auditory brainstem response; MRI, magnetic resonance imaging; CNS, central nervous system; CGH, comparative genomic hybridization; WES, whole exome sequencing; WGS, whole genome sequencing; CMA, chromosomal molecular analysis; CDS, coding sequence; DD, developmental delay; ID, intellectual disability; FHD, fork-head domain; JBD, JARID1B binding domain; GBD, Groucho-binding domain; CHD, congenital heart disease; CHDED, congenital heart defects and ectodermal dysplasia; ENCODE, Encyclopedia of DNA Elements Consortium; SECR, strongly-evolutionarily conserved region; ORegAnno, Open Regulatory Annotation; Hi-C, High-through Chromosome Conformation Capture; TAD, topologically associating domain; LD, linkage disequilibrium; NMD, nonsense-mediated mRNA decay; GTEx, Genotype-Tissue Expression project; eQTL, expression quantitative trait locus; GO, Gene Ontology.

etiologies for this disorder were categorized, such as intragenic mutations, CNVs containing *FOXG1*, CNVs containing the intergenic region *FOXG1-PRKD1*, and the contributing gene *PRKD1*.

Materials and methods

Sample collection

This study was conducted in accordance with the Code of Ethics of the World Medical Association (Declaration of Helsinki) for experiments involving humans. This study was approved by the Ethical Committee of the Shenzhen Bao'an Women's and Children's Hospital (LLSC-2022-02-05-16-KS). Written informed consent was obtained from the parent. Peripheral venous blood was collected from the infant and her parent.

Array-comparative genomic hybridization

Genomic DNA was extracted using the TIANamp Blood DNA Kit (DP348, TianGen Biotech, Beijing, China) according to the manufacturer's instructions. Genomic aberrations were detected by array-CGH using the Fetal DNA Chip (version 1.2) designed by The Chinese University of Hong Kong (CUHK) (Leung et al., 2011; Huang et al., 2014). Procedures of array-CGH were conducted according to the public Agilent protocol (Agilent Oligonucleotide Array-Based CGH for Genomic DNA Analysis, version 3.5). Briefly, hybridized slides were scanned with SureScan High-Resolution Microarray Scanner (G2505B, Agilent Technologies, Santa Clara, CA, USA), and the image data were extracted and converted to text files using the Agilent Feature Extraction software (version 10.5.1.1). The data were graphed and analyzed using the Agilent CGH Analytics software. Only duplications or deletions that were covered by at least three consecutive probes on the Fetal DNA Chip were considered.

Trio-whole exome sequencing

Whole exome sequencing for the trio (Trio-WES) was conducted by the Illumina HiSeq 2500 platform (Illumina, San Diego, CA, United States) according to our previous reports (Lu et al., 2021; Peng et al., 2022). Briefly, 1 mg of sheared DNA was ligated with adaptors and then amplified by PCR. The amplified fragments were hybridized and captured with xGen Exome Research Panel v2.0 (Integrated DNA Technologies, Coralville, IA, USA) according to the manufacturer's protocol. The captured products were amplified, purified, and quantified using an Agilent Bioanalyzer 2100 (Agilent Technologies, Santa Clara, CA, USA). Finally, the established libraries were sequenced on the Illumina HiSeq 2500 platform and the NextSeq CN500 platform (Berry Genomics, Beijing, China) for paired-end sequencing.

The sequencing reads were aligned against the human reference genome (hg19/GRCh37) using the BWA software (version 0.7.10) (Li and Durbin, 2010). The Verita Trekker® Variants Detection System (version 2.0, Berry Genomics, Beijing, China) was used for variant calling. The annotation and interpretation of the variants were conducted using Enliven Variants Annotation Interpretation System (Berry Genomics, Beijing, China) (Yang et al., 2019). A position was called heterozygous if 25% or more of the reads identify the minor allele. The retained variants for subsequent interpretation should have a minor allele frequency (MAF) <1% in 1000 Genomes Project, Exome Aggregation Consortium (ExAC) (Lek et al., 2016), NHLBI GO Exome Sequencing Project (ESP) (Fu et al., 2013), Genome Aggregation Database (gnomAD), NHLBI Trans-Omics for Precision Medicine (TOPMed) (Taliun et al., 2021). We also removed non-functional variants such as synonymous mutation and non-coding region mutation. According to the criteria for interpretation of genetic variants proposed by American College of Medical Genetics and Genomics (ACMG) guidelines, the annotated variants could be categorized into five classes, namely, "pathogenic," "likely pathogenic," "uncertain significance," "likely benign," and "benign" (Richards et al., 2015). The candidate variants were confirmed by Sanger sequencing.

Compilation of Chinese patients with FOXG1-related disorder

Using "FOXG1", "Forkhead box G1", "14q12", "Rett syndrome", "RTT", "Rett", "Intellectual disability", "Developmental delay", "Chinese", and "China" as keywords to search the English-written articles in NCBI PubMed (https://pubmed.ncbi.nlm.nih.gov/), and Chinese-written articles in WANFANG DATA (https://c.wanfangdata.com.cn/periodical), Chinese National Knowledge Infrastructure (CNKI) (https://www.cnki.net/), and VIP (http://www.cqvip.com/) periodical databases. Twenty-one relative articles were obtained from public periodical databases. After removing duplicates and reviews, eight articles (four English and four Chinese) were selected for subsequent analysis. After careful evaluation, one family was reported two times due to seeking medical consultations at different hospitals. Totally, six articles were qualified. The workflow chart was depicted in Supplementary Figure S1. Twelve cases with *FOXG1* mutations or CNVs involving the *FOXG1* gene were compiled for subsequent analysis.

Molecular analysis of FOXG1-related Rett syndrome

To have a comprehensive analysis for mutations of the *FOXG1* gene, single nucleotide mutations, microduplications, and microdeletions were extracted from NCBI ClinVar, DECIPHER (Firth et al., 2009), ClinGen (the Clinical Genome Resource) (Rehm et al., 2015), copy number variants from 29,083 cases (nstd100) and 15,767 cases (nstd54) of Developmental Delay and Intellectual Disability (DD/ID) (Cooper et al., 2011; Coe et al., 2014), and Database of Genomic Variants (DGV) (MacDonald et al., 2014). The CNVs were mapped against the human genome (hg19) by the UCSC genome browser. The protein sequences of FOXG1 were downloaded from the NCBI gene track (https://www.ncbi.nlm.nih.gov/gene) and aligned with the integrated CLUSTALW tool of MEGA (version 11.0.8) under default settings. The protein structures of FOXG1 with Ser197Ile (S197I) and Asn232Tyr (N232Y) mutations were predicted with AlphaFold2. As for protein-coding genes, pHI (the probability of being a haploinsufficient gene) and pAD (the probability of being autosomal dominant) were analyzed by DECIPHER and DOMINO (https://wwwfbm.unil.ch/domino/index.php), respectively. The genomic conservation evolution analysis was carried out by the ECR browser (https://ecrbrowser.dcode.org/). The Hi-C (high-through chromosome conformation capture) data for seven human cell lines (namely, GM12878, K562, KBM7, HMEC, HUVEC, IMR90, and NHEK) were downloaded from gene expression omnibus (GEO) (https://www.ncbi.nlm.nih.gov/geo/query/acc.cgi?acc=GSE63525).

Results

Clinical features of our patient with a *FOXG1* mutation

This patient was a 1 year and 11 months old female infant who was referred to our department because of early-onset delay of psychomotor development. The proband was delivered uneventfully at full-term to a 34-year-old mother by cesarean section due to breech position in 2019. Her birth weight was 3.09 kg. Her mother accepted all of the regular inspections as required and no abnormalities were found during her pregnancy. She was the second child of a non-consanguineous couple. Her 5-year-old brother had a normal developmental trajectory (Figure 1A). The patient was found obvious developmental delay after birth and was diagnosed with developmental delay till she was 7 months old. She had typical clinical phenotypes involving impaired social interaction, lack of speech development, delayed motor development, stereotypic movements of hands, hypotonia, bruxism while awake, sleep rhythm disorder, and seizure (Figure 1B).

For physical development, her height was 77 cm (<P3) and her weight was 10 kg (P18), which was suggested to be short stature. Her occipitofrontal head circumference (OFC) was 42 cm (<P3), referred to be microcephalus. For psychomotor development, she could not gain full head control and smooth roll over. She could neither sit nor stand without assistance. She could not develop hand grasping with a specific purpose. Excessive unconscious hand movements were observed, such as shaking and flapping. Eye contact was very few. A lack of speech development was observed. Hypotonia was observed after birth. Feeding difficulties were seen after adding semisolid food. Sleeping disturbance has been observed soon after birth and lasted till now. She also had bruxism while awake.

When she was 1 year and 6 months old, the seizure was first observed with a sudden loss of consciousness, eye gaze, and limb spasms that spontaneously resolved after 1–3 min. An episode of seizure occurred almost daily. She was diagnosed with generalized tonic-clonic seizures and began to receive antiseizure therapy 2 months later with oral antiepileptic drugs, such as topiramate, Depakin, Topamax, and i.v. drip of adrenocorticotropic hormone (ACTH). The seizures were relieved but not completely controlled. At present, the seizures still occurred two or three times a month.

Her first regular electroencephalogram (EEG) at 7 months old was normal. Her 24-h video of EEG at 1 year and 8 months showed generalized temporal spike and spike-slow waves during the wakefulness and sleep stages. Her first brain magnetic resonance imaging (MRI) scan at 7 months old showed widened bilateral temporal extracerebral space (the widest spaces were 14 mm on the right and 19 mm on the left, respectively), small bilateral temporal lobes, and delayed myelination development (equivalent to 3–4 months). At the age of 1 year and 2 months, she took her second MRI scan. Except widened bilateral temporal extracerebral space, small bilateral temporal lobes, and delayed myelination development (equivalent to 6–7 months) as before, corpus callosum hypoplasia was also observed (Figure 1C).

She accepted examinations of neural electrophysiological examinations involving flash visually evoked potential (fVEP) and auditory brainstem response (ABR) when she was 9 months old. The fVEP showed bilateral prolonged baseline P100 and N145 latencies. Auditory brainstem response (ABR) showed bilateral prolonged latencies of waves I, III, and V. No abnormality of the urinary system was found by color Doppler ultrasound at 10 months old. DR X-ray film for hip joint anteroposterior and abducent projections at 1 year and 11 months old found no abnormalities.

Molecular analysis with whole exome sequencing identified a *de novo* non-sense mutation of FOXG1 (c.385G>T, rs1555321264, and 14:29236870) in the patient (Figure 1D) and further confirmed by Sanger sequencing (Figure 1E).

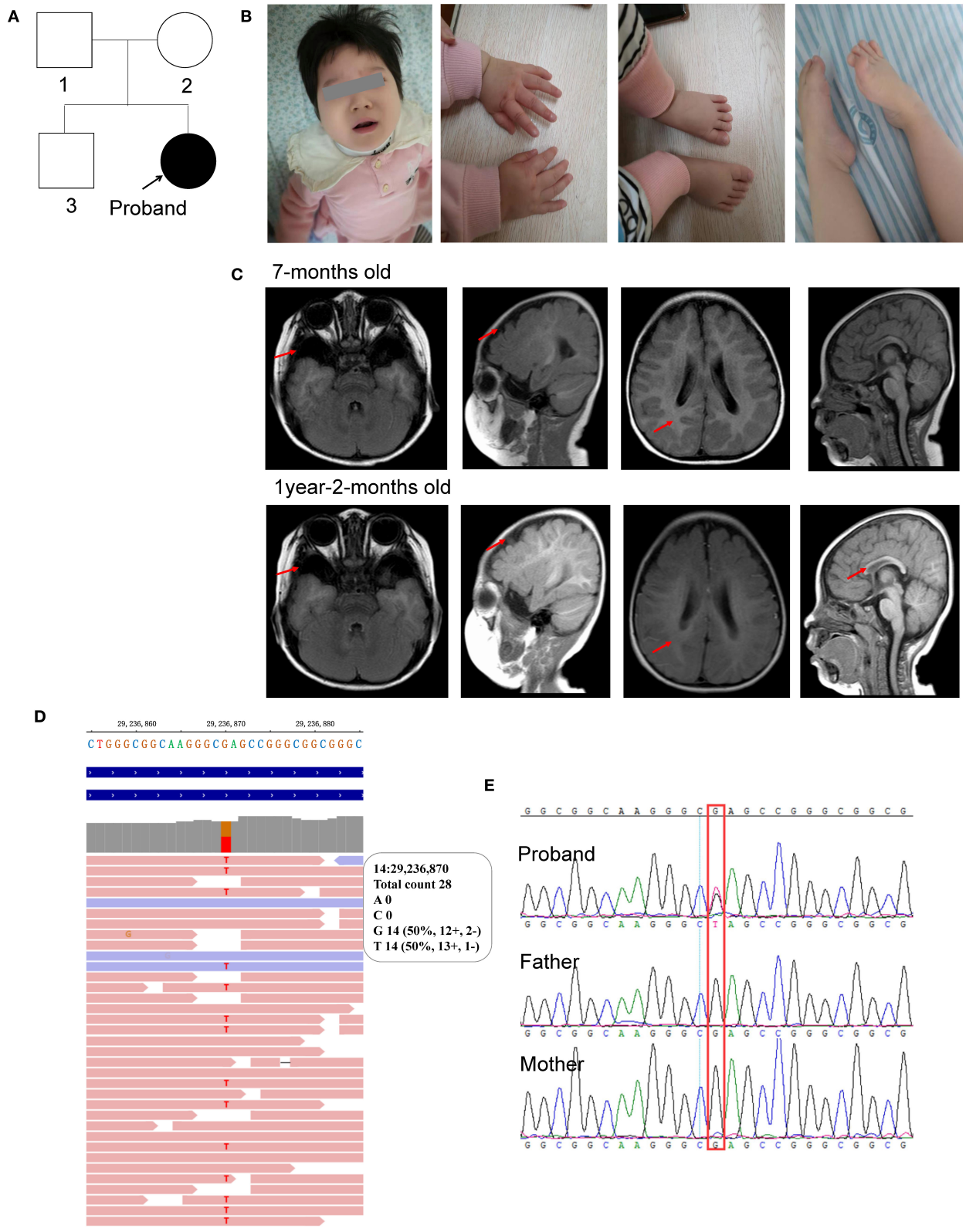

FIGURE 1
Characterization of the clinical features of the proband. **(A)** Pedigree of the proband; **(B)** photos of the facial, hands, and foot; **(C)** brain MRI scan taken at 7-months old and 1-year-2-months old; **(D)** WES identified c.385G>T in the proband; **(E)** sanger sequencing. The red arrow represents the abnormal region.

The c.385G>T mutation generated a premature stop codon at position 129 (GAG) for glutamic acid (Glu, E) to (TAG, X) (p.Glu129Ter). This mutation was not been detected in any of the four public human genome projects, such as 1000 Genomes ($n = 2,504$), GO-ESP ($n = 6,503$), ExAC ($n = 60,706$), gnomAD Genomes ($n = 15,708$), gnomAD Exomes ($n = 125,748$), and TOPMED ($n = 25,199,470$) databases. According to the ACMG guideline, this mutation was classified to be pathogenic (PVS1+PM2+PP5).

Combined with characteristic clinical phenotypes, brain MRI, and molecular analysis, the child was diagnosed as a congenial variant of Rett syndrome, (OMIM#613454), which was also named FOXG1-related encephalopathy.

Comprehensive analysis of 12 Chinese with FOXG1 mutations

Previous articles have reported 11 individual Chinese cases with 11 *de novo* FOXG1 mutations. To have a comprehensive reanalysis of these mutations, the medical records and clinical phenotypes of all the patients (11 + 1) were carefully inquired and compiled (Table 1). Pedigrees of all 12 patients were depicted in Figure 2. The ranking of the pedigrees was based on the mutation's location on the FOXG1 protein.

After compiling the described clinical features of the 12 patients (Table 1), we noticed that 11 of them were female (91.67%) and only 1 male (8.33%). Since the clinical descriptions for patients 10 and 11 were scarce, they were removed for the subsequent clinical spectrum analysis. The head size development of eight patients (8/10) was lagging behind the standard of the same age and displayed a microcephaly phenotype. The regression was reported in three patients with the progressive disappearance of acquired language skills. Bruxism was also identified in four patients. As for abnormalities of the musculoskeletal system, hypotonia and stereotypic movements with limited functional hand use were reported in almost all the patients. In the early stages, no patients could walk or sit normally; however, with increasing age, six patients could sit without aid after 10 months. Patient 11 could walk without aid at 3 years old. As for the eyes, almost all the patients had poor eye contact and could not follow moving objects.

As for the features concerning the central nervous system (CNS), delayed speech, feeding difficulties, seizures, abnormal EEGs, and stereotypic movements were reported in most of the patients. As for seizures, the onset time was at or after 4 months, and in patient 1, it was at 18 months. Two types of seizures were reported in these patients, such as partial or generalized tonic-clonic. According to the reported MRI/CT results, corpus callosum hypoplasia and underdevelopment of the frontal and temporal lobes were seen in most of the patients. Delayed myelination or hypomyelination was reported in only two patients.

Single-nucleotide mutations identified by next-generation sequencing

The *FOXG1* gene was mapped to an evolutionarily conserved region (Figure 3A), including only one exon (Figure 3B). To date, there are eight heterozygous single-nucleotide mutations of *FOXG1* detected in Chinese patients with intellectual disability (ID). The details of these mutations were described in Table 1. For our patient (patient 1), the *de novo* nonsense mutation, c.385G>T (Figure 3C) generated a premature stop codon at position 129 (GAG) for glutamic acid (Glu, E) to (TAG, X) (p.Glu129Ter). As far as we know, this mutation has been detected in an individual with unknown diseases by GeneDx in 2017 and recruited in ClinVar. Besides, no pathogenic mutations were detected in other genes for RTT/RTT-like disorders. As for mutations in patients 2, 4, 5, and 6, all four mutations were insertions with one nucleotide, which caused frame-shifting of the original coding sequence (CDS) of *FOXG1* (Figures 3C–E). c.460dup (rs398124204 in patient 2) was reported more than 10 times in European patients (Bahi-Buisson et al., 2010; Van der Aa et al., 2010; Kortüm et al., 2011; Bean et al., 2013; Seltzer et al., 2014; Richards et al., 2015; Cellini et al., 2016; Nykamp et al., 2017; Mitter et al., 2018; Vegas et al., 2018) and only once in Chinese patients (Zhang et al., 2017). c.506dup (rs1450095073 in patient 3) and the other two frame-shift mutations (c.858dup in patent 5 and c.974dup in patient 6) had been submitted to the NCBI ClinVar database by GeneDx and reported in two Chinese patients with Rett syndrome (Zhang et al., 2017; Niu et al., 2020). Although the inserted locations of the mutations were varied, the CDSs containing these four frame-shifting mutations terminated at the same premature stop codon to produce a truncated protein with 455 amino acids (Figure 3F). According to the criteria of ACMG classification, these mutations were annotated as "pathogenic" (PVS1+PS2+PM2).

As for the two missense mutations (c.590G>T, p.Ser197Ile in patient 4 and c.694A>T, p.Asn232Tyr in patient 5), they were located in the DNA-binding forkhead domain (FHD). Both amino acids (such as Ser197 and Asn232) were strongly conserved (Figure 3D) during evolution and not detected in the known public genomic databases, such as 1000 Genome ($n = 2,504$), NHLBI GO-ESP ($n = 6,503$), ExAC ($n = 60,706$), gnomAD ($n = 15,708$), and TOPMED ($n = 60,000$). According to the criteria of ACMG classification, they were annotated as "likely pathogenic" (Table 1). For c.590G>T (p.Ser197Ile), it has been submitted to the ClinVar database by the Genetic Services Laboratory of the University of Chicago (Accession: SCV002069287.1) and identified in a 47-month-old patient (Mitter et al., 2018). Analyzed by Missense3D, the 197Ile substitution disrupts all side-chain/main-chain H-bonds formed by the buried Ser residue (RSA 2.3%) (CO197-Ser OG/CO194-Ile O, CO197-Ser OG/CO201-Arg O; CO200-Lys NZ/CO197Ser O, CO200Lys N/CO197Ser OG, CO201-Arg N/CO197Ser OG).

TABLE 1 Characterizations of the 12 Chinese patients with FOXG1 mutations.

General information												
Cases	**Our project**	**Zhang et al. (2017)**	**Yang et al. (2019)**	**Bai et al. (2021)**	**Zhang et al. (2017)**	**Zhang et al. (2017)**	**Bai et al. (2021)**	**Zhang et al. (2017)**	**Bai et al. (2021)**	**Li et al. (2021)**	**Tang et al. (2021)**	**Wang et al. (2017)**
Patient No.	Patient 1	Patient 2	Patient 3	Patient 4	Patient 5	Patient 6	Patient 7	Patient 8	Patient 9	Patient 10	Patient 11	Patient 12
Sex	Female	Female	Female	Female	Female	Female	Female	Female	Female	Male	Female	Female
Age	1 y 11 m	1 y	2 y 5 m	1 y 6 m	4 y 6 m	1 y 8 m	2 y	2 y	2 y 6 m	8 d	3 y	9 y
Molecular analysis												
Locations (hg19)	14:29236870	14:29236945	14:29236986	14:29236986	14:29237179	14:29237343	14:29237408	14:29237457	14:29128665-30217058	14:25084632-34690056	14:26622393-31444468	14:28904992-30805462
Genetic mutations	c.385G>T (p.Glu129Ter)	c.460dup (p.Glu154 GlyfsTer301)	c.506dup (p.Lys170 GlnfsTer285)	590G>T (p.Ser197Ile)	c.694A>T (p.Asn232Tyr)	c.858dup (p.Lys287 GlnfsTer168)	c.923G>A (p.Trp308Ter)	c.974dup (p.Leu325 PhefsTer130)	/	/	/	/
CMAs	/	/	/	/	/	/	/	/	arr[hg19]14q12 (29128665-30217058)x1	arr[hg19]14 q12q13.1 (25084632-34690056)x1	arr[hg19]14q12 (26622393-31444468)x1	arr[hg19]14q12 (28904992-30805462)x3
Consequence	Stopgain	Frameshift	Frameshift	Missense	Missense	Frameshift	Stopgain	Frameshift	Microdeletion	Microdeletion	Microdeletion	Microduplication
Karyotypes	46, XX	46, XX	46, XX	46, XX	46, XX	46, XX	46, XX	46, XX	46, XX del(14)(q12)	46, XY del(14)(q12q13.1)	46, XX del(14)(q12)	46, XX dup(14)(q12)
ACMG classification	Pathogenic PVS1+ PS2+PM2	Pathogenic PVS1+ PS2+PM2	Pathogenic PVS1+ PS2+PM2	Likely pathogenic M1+ PM2+PP2+ PP3+PP5	Likely pathogenic PS2+ PM2+PP3	Pathogenic PVS1+ PS2+PM2	Pathogenic PVS1+ PM2+PP5	Pathogenic PVS1+ PS2+PM2	/	/	/	/
dbSNP ID	rs1555321264	rs398124204	rs1452295073	/	rs786205486	/	/	/	/	/	/	/
Inheritance	*De novo*	*De novo*	*De novo*	*De novo*	*De novo*	*De novo*	*De novo*	*De novo*	*De novo*	*De novo*	*De novo*	*De novo*
Head circumstance (cm)	42	43	40.5	39	49	42	38.5	45.5	/	/	/	46
Microcephaly	Y	Y	Y	Y	N	Y	Y	Y	/	/	/	Y

(Continued)

10.3389/fnmol.2022.1039990

TABLE 1 (Continued)

General information Cases	Our project	Zhang et al. (2017)	Yang et al. (2019)	Bai et al. (2021)	Zhang et al. (2017)	Zhang et al. (2017)	Bai et al. (2021)	Zhang et al. (2017)	Bai et al. (2021)	Li et al. (2021)	Tang et al. (2021)	Wang et al. (2017)
Regression	N	N	Y	N	N	Y	N	N	Y	/	/	/
Bruxism	Y	Y, 12 m	/	/	Y, 12 m	Y, 19 m	/	N	/	/	/	/
Hypotonia	Y	Y	Y	Y	Y	Y	Y	Y	Y	Y, 8 d	/	Y
Stereotypic movements	Y	Y, 3 m	Y	Y	Y, 10 m	Y, 12 m	Y	Y, 8 m	Y	/	/	Y
Limited functional hand use	Y	Y	/	Y	Y	Y	Y	Y	Y	/	/	Y
Rising head (m)	Y,10 m	Y, 8 m	Y, 11 m	Y	Y, 5 m	Y, 7 m	Y	Y, 2 m	Y,9 m	/	/	Y, 36 m
Sitting	N	N	N	Y	Y, 12 m	N	Y	Y, 10 m	Y,11 m	/	/	Y, 48 m
Walking	N	N	N	N	N, standing with aid at 24 m	N	N	N	N	/	/	Y,72 m
Poor eye contact	Y	Y	Y	Y	Y	/	Y	Y	Y	/	Y	Y
Delayed speech	Y	Y	Y	Y	Y	Y	Y	Y	Y	/	Y	Y
Feeding difficulties	Y	Y	Y	/	Y	/	/	Y	/	Y, 8 d	/	Y
EEG abnormalities	Y	Y	Y	N	Y	Y	N	Y	N	/	Y	Y
Seizure onset time (m)	Y, 18 m	Y, 10 m	Y, 16 m	N	Y, 6 m	Y, 10.5 m	N	Y, 10.5 m	Y, 13–15 m	/	Y, ?	Y, 4 m
Seizure types	Generalized tonic-clonic	Partial	Generalized tonic-clonic	N	Partial	Partial	N	Partial	/	/	?	?
Seizure with cyanosis	N	Y	/	N	Y	Y	N	Y	Y	/	/	/
Sleep disturbances	Y	Y	Y	/	Y	N	/	Y	/	/	/	/

(Continued)

10.3389/fnmol.2022.1039990

TABLE 1 (Continued)

General information														
Cases	Our project	Zhang et al. (2017)	Yang et al. (2019)	Bai et al. (2021)	Zhang et al. (2017)	Zhang et al. (2017)	Bai et al. (2021)	Zhang et al. (2017)	Bai et al. (2021)	Li et al. (2021)	Tang et al. (2021)	Wang et al. (2017)
Corpus callosum hypoplasia	Y	Y	Y	N	Y	Y	N	Y	N	Y	/	Y
Delayed myelination or hypomyelination	Y	N	N	N	N	Y	N	N	N	/	/	/
Underdevelopment of frontal and temporal lobes		Y	Y	Y	Y	Y	Y	Y, mild	Y	/	/	Y

This mutation also results in a switch from the buried Ser (RSA 2.3%) to exposed Ile (26.6%) (Figures 3G,H). The buried H-bond breakage and buried/exposed switch might disrupt the local structure of the PHD domain. For c.694A>T (p.Asn232Tyr), it has been submitted to the ClinVar database by the DGU-KFSHRC (Developmental Genetics Unit, King Faisal Specialist Hospital & Research Centre) and reported in a Chinese patient with RTT (Zhang et al., 2017). The side chain of Asn (N) is a small-sized amino carbonyl but a bulky p-hydroxyphenyl for Tyr (Y). Analyzed by Missense3D, this mutation led to a switch from a buried Asn (RSA 7.0%) to an exposed Tyr (63.4%), which disrupted all side-chain/side-chain H-bonds (AO187-Asn ND2/AO232-Asn OD1; AO232-Asn ND2/AO231-His NE2; AO236-Asn ND2/AO232-Asn OD1) and two side-chain/main-chain H-bonds (AO232-Asn ND2/AO228-Ser O and AO236-Asn ND2/AO232-Asn OD1). The Tyr232 only forms one side-chain/main-chain H-bond with Asn236 (AO236-Asn ND2/AO232-Tyr O) (Figures 3I,J).

To comprehensively explore the mutation patterns of *FOXG1*, variants annotated as "pathogenic" and "likely pathogenic" from NCBI ClinVar and DECIPHER were aligned against the CDS of *FOXG1* (Supplementary Figure S2). Totally, 171 mutations in the CDS of *FOXG1* were recruited in both databases. Among 38.60% (66/171) were missense mutations, 37.43% (64/171) were frame-shift mutations, and 23.98% (41/171) were non-sense mutations. For the missense mutations, about 93.94% (62/66) were located in the forkhead domain (FHD) which was responsible for DNA binding, 4.55% (3/66) in the JARID1B binding domain (JBD) responsible for the interaction between FOXG1 and JARID1B (also called as KDM5B). Only one likely-pathogenic missense (c.1439A>G, p.Gln480Arg) was localized in the C-terminal disordered region. As for the pathogenic insertion/deletions (ins/del), they were distributed throughout the whole region of FOXG1.

Copy number variations containing the *FOXG1* gene

Through oligonucleotide array-CGH, four different CNVs were identified, three microdeletions in patients 9, 10, and 11, and one microduplication in patient 12 (Table 1). As for the three microdeletions, the one in Li et al. (2021) was about 9.61 Mb in length (14:25,084,632–34,690,056) and contained 19 protein-encoding genes, including *FOXG1* (Li et al., 2021). Another 4.82 Mb microdeletion (14:26,622,393–31,444,468) in Tang et al. (2021) was completely covered by Li et al. (2021) and contained seven protein-coding genes (such as *NOVA1, FOXG1, PRKD1, G2E3, SCFD1, COCH,* and *STRN3*) (Table 2). The last microdeletion in Bai et al. (2021) was the shortest (14:29,128,665–30,217,058, 1.09Mb) and covered only two genes, such as *FOXG1* and *PRKD1* (Figures 4A,B) (Bai et al.,

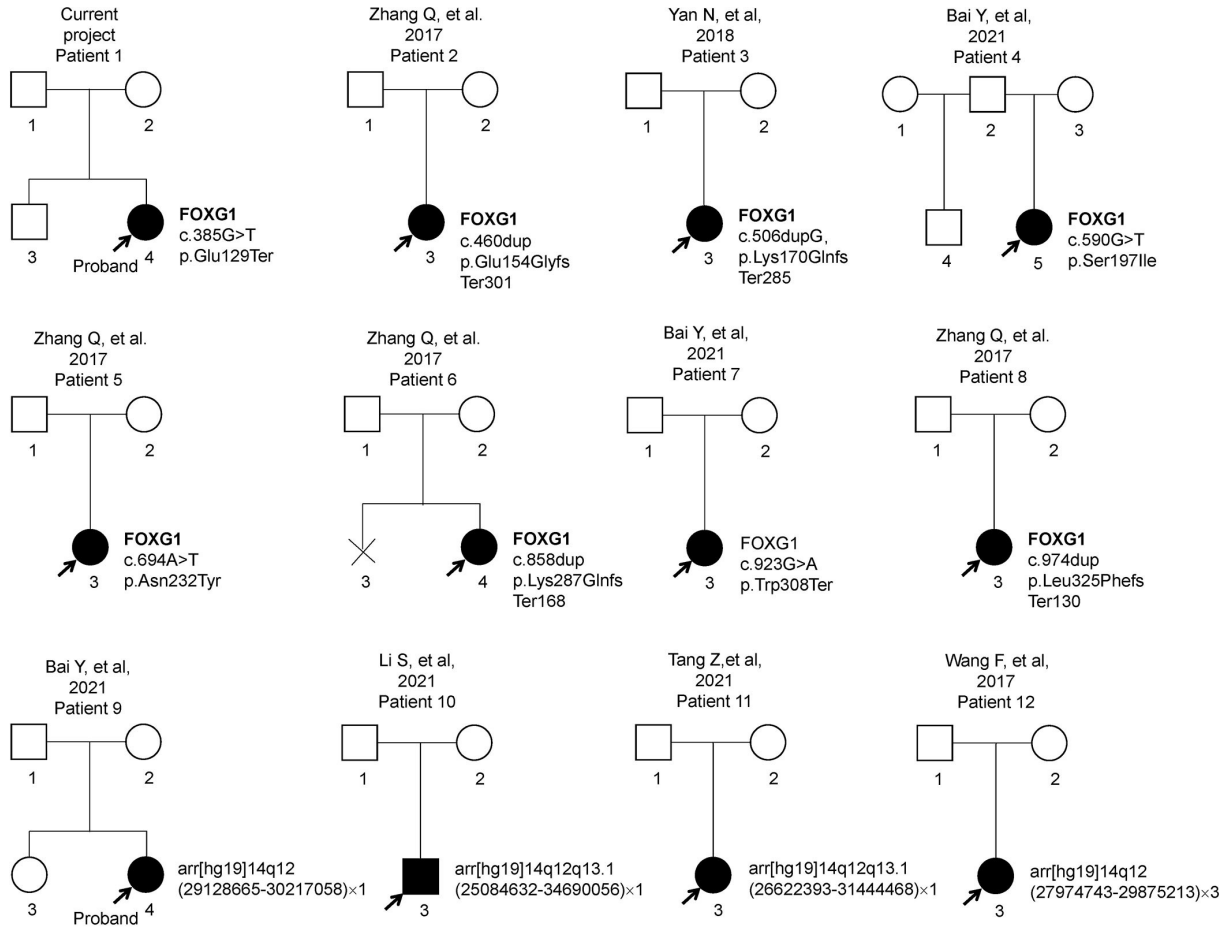

FIGURE 2
Pedigrees of 12 patients with FOXG1-related encephalopathy.

2021). A 1.90 Mb microduplication at 14q12 (14:27,974,743–29,875,213) was discovered in patient 12 and contained only the *FOXG1* gene (Supplementary Figure S3) (Wang et al., 2017). There were no obvious chromosomal aberrations detected in their parents.

About 76 individual deletions in the genomic region [Li et al. (2021), chr14: 25,084,632–34,690,056] were recruited in different public databases, such as 10 in ClinGen (Clinical Genome Resource), 21 in ClinVar, 16 in DECIPHER, and 29 in the Copy Number Variation Morbidity Map of Developmental Delay (Figures 4C–F) databases. Out of these microdeletions, 31 of them (40.79%) spanned the CDS of the *FOXG1* gene, 5 in ClinGen, 14 in ClinVar, 4 in DECIPHER, and 8 in the Developmental Delay databases. The Database of Genomic Variants (DGV) involving healthy individuals were also checked and only one short microdeletion (nsv1042959) was obtained (Figure 4G). Six short deletions just contained the *FOXG1* gene in which the three shortest deletions, 1057648 (chr14: 29,236,486–29,237,955, 1.47 Kb, ClinVar), 820618 (chr14: 29,236,466–29,237,975, 1.51 Kb, ClinVar), and 290100 (chr14: 29,236,278–29,237,804, 1.52 Kb, DECIPHER), just covered the protein-coding sequence of *FOXG1*.

Mutation analysis of *PRKD1* gene

PRKD1 was also contained in the two microdeletions of patients 8 and 9. Therefore, it is necessary to assess the contribution of *PRKD1* to the clinical phenotype of FOXG1-related disorder. After compiling the pathogenic mutations in the CDS of *PRKD1* from published articles, the ClinVar and DECIPHER databases, 13 patients were found to have single nucleotide mutations annotated as pathogenic or likely pathogenic (Figure 5A and Supplementary Table S1). Based on the mode of inheritance of these patients, five were heterozygous (4 *de novo* and 1 unknown), seven were homozygous (from two consanguineous families), and one was unknown. It is worth noting that patients with homozygous mutations, all of them suffered only from non-syndromic congenital heart diseases

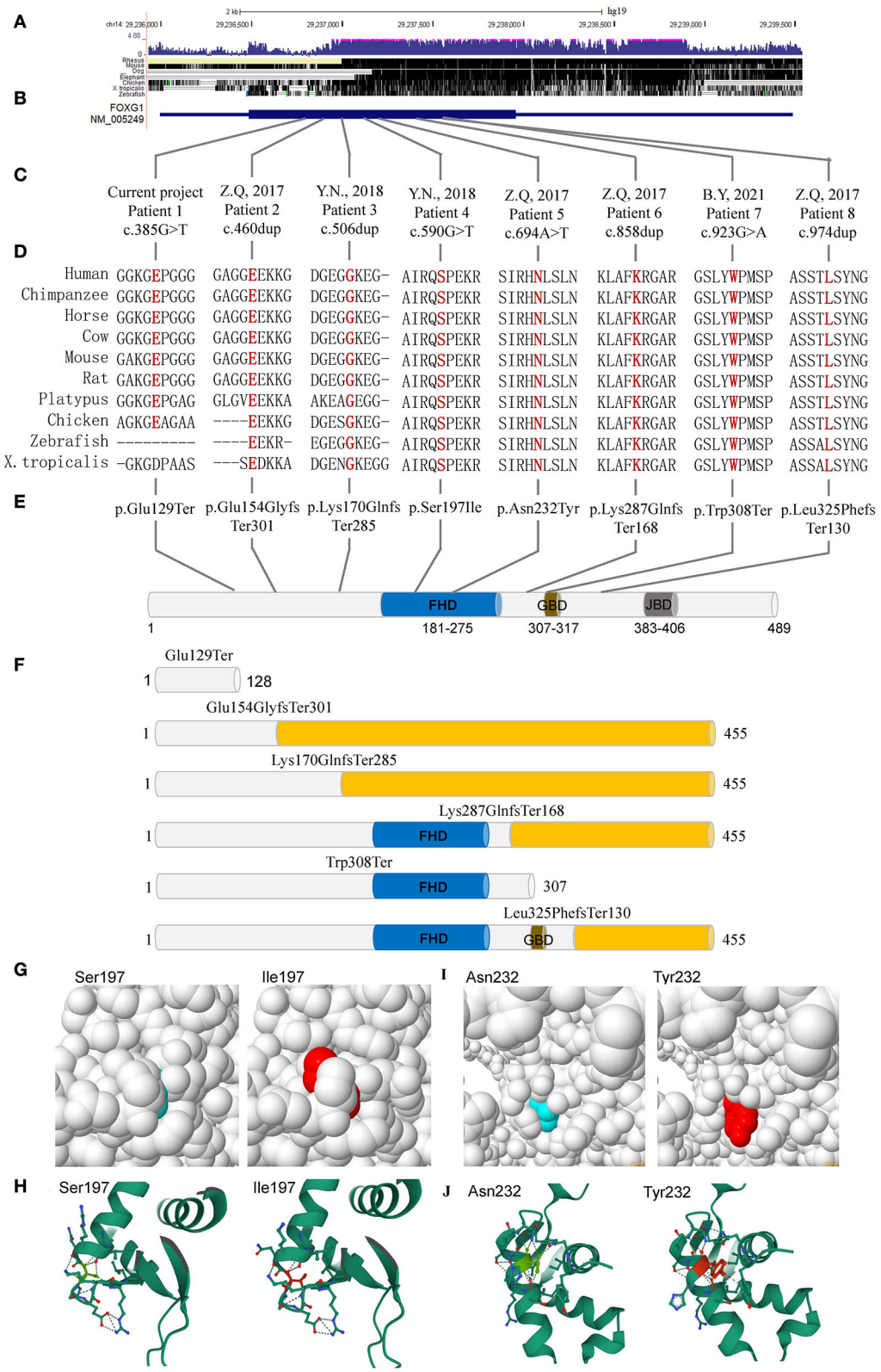

FIGURE 3
Single-nucleotide mutations of FOXG1 identified in Chinese patients. **(A)** Conservation of the genomic region; **(B)** Gene structure of FOXG1; **(C)** Nucleotide changes of the mutations; **(D)** Conservation analysis of the mutations; **(E)** Amino acid changing of the mutations; **(F)** Proteins containing truncating mutations. **(G)** Structure of FHD domain with Ser197; **(H)** Structure of FHD domain with Ile197; **(I)** Structure of FHD domain with N232; **(J)** Structure of FHD domain with Y232. FHD, DNA binding fork-head domain; GBD, Groucho-binding domain; JBD, JARID1B binding domain. The yellow cylinder represents the aberrant amino acids caused by frameshifting mutations.

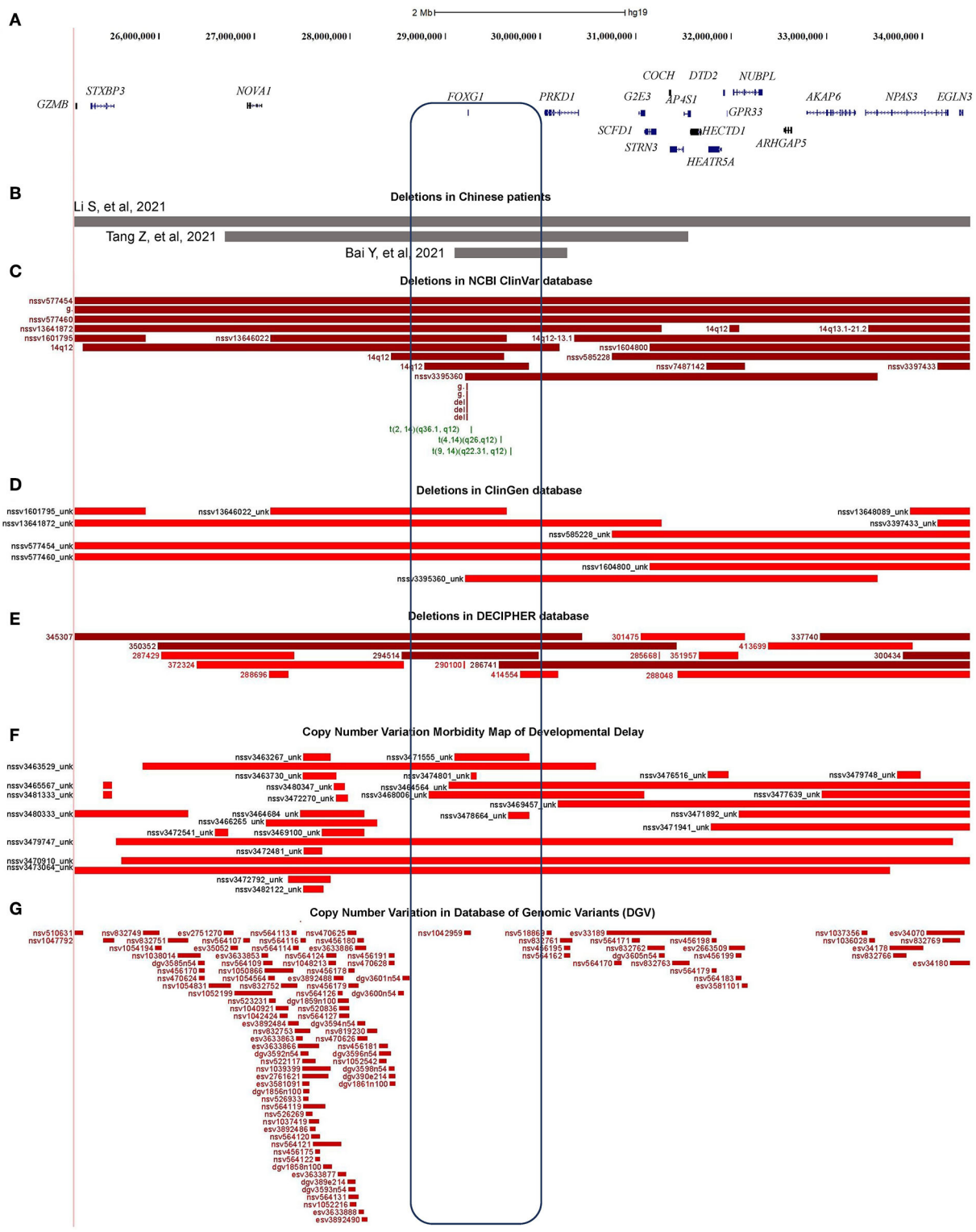

FIGURE 4
Characterization of the microdeletions containing FOXG1. **(A)** Genomic regions and protein coding genes of microdeletion in patients 9, 10, and 11; **(B)** Covered regions of the two Chinese microdeletions; **(C)** Microdeletions in ClinGen database; **(D)** Microdeletions in NCBI's ClinVar database; **(E)** Microdeletions in DECIPHER database; **(F)** Microdeletions in Developmental Delay; **(G)** Microdeletions in Database of Genomic Variants (DGVs).

FIGURE 5
Distribution of mutations in PRKD1. **(A)** Distribution of SNMs of PRKD1; **(B)** Copy number variations of PRKD1; **(C)** Ratios of clinical phenotypes in patients with CNVs containing PRKD1.

(CHDs) and no other systemic phenotypes were manifested (Shaheen et al., 2015; Massadeh et al., 2021). The heterozygous mutations could lead to not only CHDs but also abnormalities of the CNS, such as intellectual disability, global developmental delay, hearing impairment, delayed language development, or microcephaly (Swaminathan et al., 2012; Sifrim et al., 2016).

There were also five microduplications and nine microdeletions completely or partially covering only *PRKD1* recruited in the ClinVar and DECIPHER databases (Figure 5B, Supplementary Table S2). Since there were no clinical phenotypes for 4 microduplications (14q12, nssv13647033, and nssv13643620 in ClinVar and 380299 in DECIPHER), 10 CNVs (9 microdeletions and 1 microduplication) were remained for subsequent analysis. Except for abnormalities of the cardiovascular system (Tetralogy of Fallot, Ventricular septal defect, and hypertension) in 6.45% (4/62) of all the reported

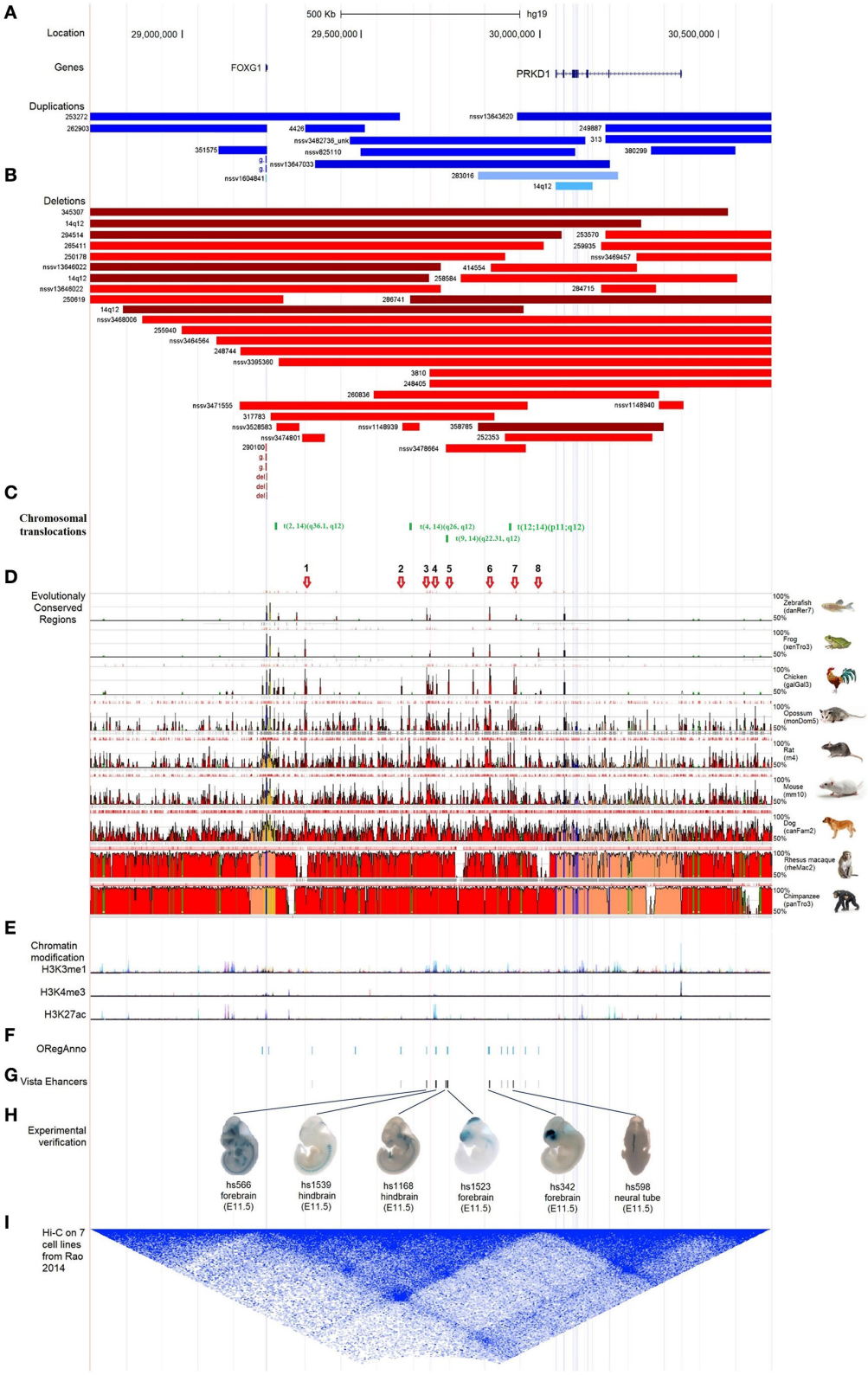

FIGURE 6
Characterization of the regulatory elements in the intergenic region between FOXG1 and PRKD1. **(A)** Partially-covered microduplications; **(B)** Partially-covered microdeletions; **(C)** Chromosomal translocations; **(D)** Evolutional conservation analysis by ECR browser; **(E)** Chromatin modification of 7 human cells from ENCODE; **(F)** Regulatory elements in ORegAnno database; **(G)** Enhancers in VISTA enhancer browser; **(H)** 6 neuronal active enhancers in mouse embryos; **(I)** In situ Hi-C for seven human cell lines.

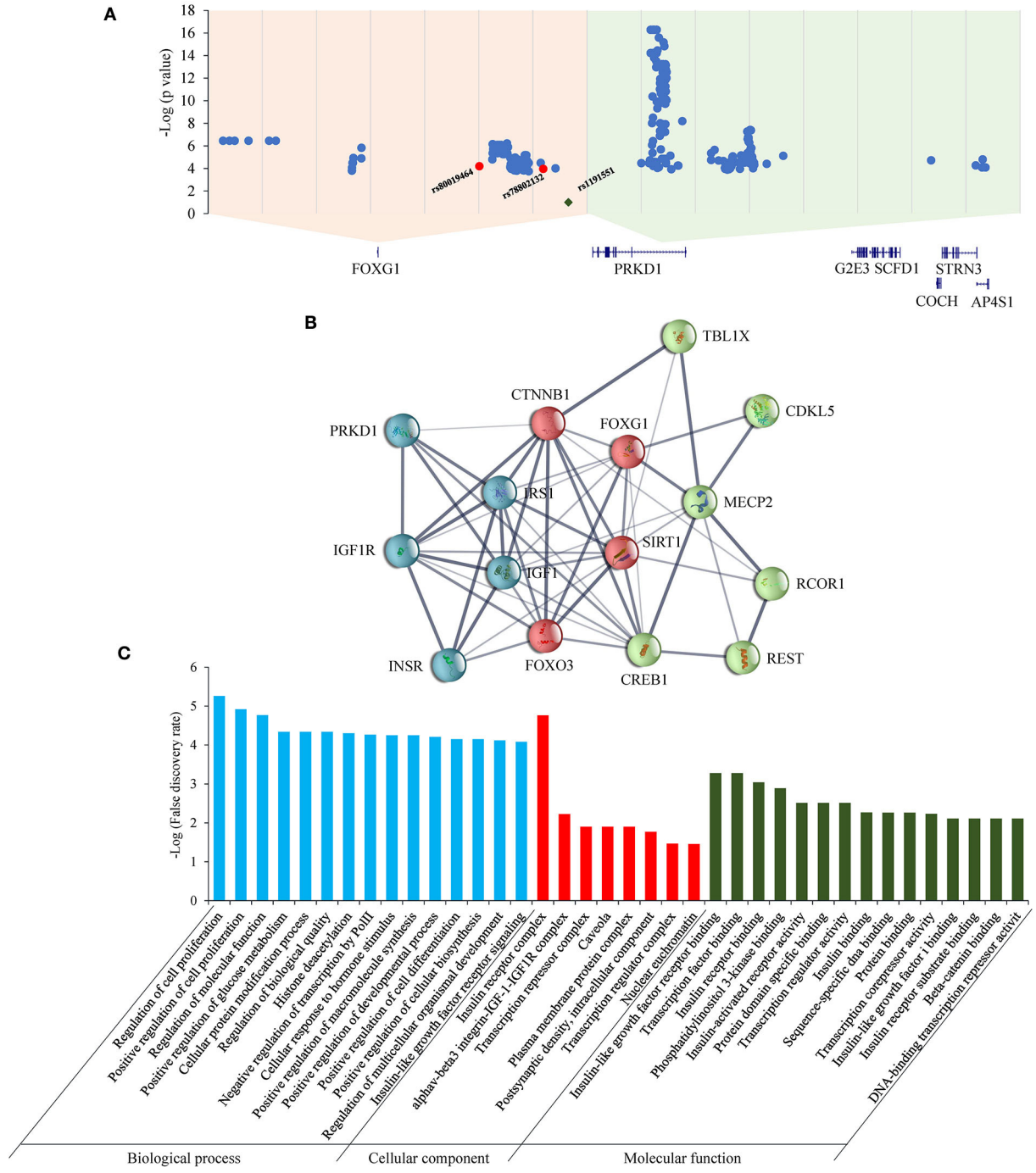

FIGURE 7
eQTLs and STRINGed network analysis for FOXG1 and PRKD1. **(A)** eQTLs for FOXG1 and PRKD1; **(B)** STRINGed protein interaction network. **(C)** GO analysis for the interacting components.

clinical phenotypes, there also exhibited RTT-like phenotypes, such as facial dysmorphisms (17.74%, 11/62), intellectual disability (11.29%, 7/62), microcephaly (8.06%,5/62), hypotonia (6.45%, 4/62), seizure (4.84%, 3/62), hypoplasia of the corpus callosum (3.23%, 2/62), delayed language development (3.23%, 2/62), behavioral abnormality (3.23%, 2/62), feeding difficulties (3.23%, 2/62), global developmental delay (1.61%, 1/62), agenesis of corpus callosum (1.61%, 1/62), delayed myelination (1.61%, 1/62), simplified gyral pattern (1.61%, 1/62), and others (11.29%, 7/62) (Figure 5C). As for others, it included

TABLE 2 Haploinsufficiency predictions for the 7 shared genes in microdeletions of three patients.

Name	pHI	Inheritance model (pA(D)	Phenotype/ OMIM	Development disorder genotype – phenotype (DDG2P)	Gene curation coalition (GenC(C)	ClinGen
NOVA1	2.330	0.977: VLD	/	/	/	/
FOXG1	**3.110**	**0.998: VLD**	613454/Rett syndrome, congenital variant	Monoallelic; Loss of function; Congenital Variant of Rett Syndrome;	Definitive: 3 Strong: 1	Definitive: AD Haploinsufficiency: 3 Triplosensitivity: 0
PRKD1	**2.790**	**0.698: LD**	617364/Congenital heart defects and ectodermal dysplasia (CHDE(**D**)	Monoallelic; All missense/in frame; Syndromic Congenital Heart Defects	Limited: 1	/
G2E3	13.460	0.213: LR	/	/	/	/
SCFD1	9.330	0.822: VLD	/	/	/	/
COCH	15.090	0.355: LR	601369/Deafness, autosomal dominant 9 (DFNA9) 618094/Deafness, autosomal recessive 110 (DFNB110)	/	Definitive: 1	Definitive: AD
STRN3	7.730	0.725: LD	/	/	/	/

VLD, Very likely dominant; LD, Likely dominant; VLR, Very likely recessive; LR, Likely recessive; pAD, probability of being autosomal dominant.
The bold means the two genes, FOXG1 and PRKD1, contained in the shortest microdeletion.

bruxism, hypothyroidism, intrauterine growth retardation, microdontia, nystagmus, obesity, and short stature. It is very likely that serine/threonine-protein kinase D1 (PRKD1) acts as an independent contributor or collaborator with *FOXG1*, for the clinical phenotypes of a congenital variant form of Rett syndrome.

Intergenic regulatory elements in the region between *FOXG1* and *PRKD1*

According to the reports regarding the large-scale identification of functional elements in the human genome revealed by the Encyclopedia of DNA Elements (ENCODE) Consortium, intergenic non-coding regions often contain multiple regulatory elements, such as enhancers, silencers, or insulators (Maurano et al., 2012). There were many pathogenic CNVs covered the intergenic genomic region between *FOXG1* and *PRKD1* (*FOXG1-PRKD1*) (Figures 6A,B). It is implied that the *FOXG1-PRKD1* might be involved in the pathogenesis of FOXG1-related encephalopathy. Interestingly, four *de novo* inter-chromosomal translocations involving the intergenic region *FOXG1-PRKD1* were identified in patients with Rett syndrome, congenital variant (OMIM:613454) (Goubau et al., 2013; Mehrjouy et al., 2018), which was also named as FOXG1-related encephalopathy. These translocations were $t_{(2,14)}$ (q36.1, q12), $t_{(4,14)}$ (q26, q12), $t_{(9,14)}$ (q22.31, q12), and $t_{(12,14)}$ (p11, q12) (Figure 6C). The CDS of FOXG1 in these patients was intact and could produce proteins with normal functions, implying that the missing genomic regions might be able to regulate the expression levels of *FOXG1*.

To evaluate the contribution of intergenic CNVs to the phenotypes of *FOXG1*-related encephalopathy, longer CNVs spanning the whole region of *FOXG1* plus *PRKD1* were removed and only those partially covering *FOXG1* or *PRKD1* were left for subsequent analysis. Genomic sequences from zebrafish, *Xenopus tropicalis*, chicken, opossum, rat, mouse, dog, Rhesus macaque, and chimpanzee were compared against the human genome (chr14:28,827,675–30,608,124, hg19), *FOXG1* was strongly conserved during evolution in all the selected animals. As for *PRKD1*, it appeared in mammals and might be a mammalian-specific gene (Figure 6D). Besides, eight strongly evolutionarily conserved regions (SECRs) were identified in the intergenic *FOXG1-PRKD1* region (Figure 6D). According to the chromatin modification patterns from ENCODE project, the *FOXG1-PRKD1* region might contain several regulatory

elements, such as enhancers or silencers (Figure 6E). Fourteen annotated regulatory elements were contained in this genomic region, which was collected in the Open Regulatory Annotation (version 3.0, ORegAnno) database (Lesurf et al., 2016) (Figure 6F). Most of them overlapped with the SECRs. For the annotated regulatory elements, 12 of them (70.59%, 12/14) were tested for enhancer activity in transgenic mouse embryos (E11.5) with LacZ staining in the VISTA enhancer browser (Visel et al., 2007). Six of the SECRs acted as active enhancers, three in the mouse forebrain (hs566, hs1523, and hs342), two in the hindbrain (hs1539 and hs1168), and one in the neural tube (hs598) (Figures 6G,H). After analyzing the *in situ* Hi-C (High-through Chromosome Conformation Capture) data for seven human cell lines (GM12878, K562, KBM7, HMEC, HUVEC, IMR90, and NHEK), this region has three topologically associating domains (TADs). *FOXG1* and the intergenic region (*FOXG1-PRKD1*) were completely constrained in the second TAD (Figure 6I), which was completely encompassed by linkage disequilibrium (LD) blocks that were divided by recombination hotspots.

Discussion

The *FOXG1* (OMIM#164874) is a single exon gene, located in 14q12, which encodes a forkhead transcription repressor. *FOXG1* is expressed highly in the telencephalon, nasal retina, otic vesicles, and olfactory placodes, and serves as a hallmark of the telencephalon in vertebrates (Toresson et al., 1998). It plays a determining role in the development of the telencephalon, cerebral cortex, and genesis of corpus callosum (Manuel et al., 2010). The expression level of *FOXG1* at specific developmental timing is critical for the development of neuronal GABAergic inhibitory circuits. In mouse models, no matter increased or decreased expression of *FOXG1* in both excitatory and inhibitory neurons could be detrimental to the inhibitory circuit formation and result in ASD-like social impairments (Miyoshi et al., 2021). It also plays an important role in the patterning of the early rostral brain and pacing of the telencephalic neurogenesis, specifically stimulating the dendrite elongation (Chiola et al., 2019). Although controlling the neurological development of the telencephalon in the embryonic period, the expression of *FOXG1* continues after birth and through adulthood to prevent the apoptosis and promote the survival of postmitotic neurons (Dastidar et al., 2011), to maintain the neural plasticity (Yu et al., 2019), and to promote the formation of the hippocampal dentate gyrus, especially during early postnatal stage (Tian et al., 2012), which is vital to high-grade function.

In recent years, with the application of molecular genetic testing approaches including chromosomal microarray analysis (CMA), exome array, gene-targeted testing (multigene panel), whole exome sequencing (WES), and whole genome sequencing (WGS), it is found that unlike many other monogenic diseases with clear and single mutation sites and mutation modes, the genomic region of the *FOXG1* gene is very unstable, resulting in diversified mutation types. The reported cases carried dozens of mutation types, such as non-sense, missense, frameshift, initiator loss, terminator loss, large fragment duplication, and large fragment deletion. These mutations were distributed in different functional regions of *FOXG1* (Wong et al., 2019b). Since the *FOXG1* gene contains only one exon, the resultant non-sense and frameshifting transcripts could be translated into aberrant proteins, instead of being degraded by the non-sense-mediated mRNA decay (NMD) (Kurosaki et al., 2019). The diversity of mutation sites and mutation types could affect the brain developmental events regulated by FOXG1 to varying degrees, which eventually led to the diversity of clinical manifestations of FOXG1-related encephalopathies.

Currently, there were four Chinese patients identified to have heterozygous large fragment abnormalities in their genomes, three microdeletions, and one microduplication. In order to find out if there existed other 14q12 copy number variants (CNVs), large-scale CNV screening analyses for Chinese patients with developmental delay/intellectual disability (DD/ID) were reviewed. Totally, in 2,870 DD/ID complied cases, 707 pathologic/likely pathologic CNVs were identified, accounting for 24.86% of the patients. However, no more 14q12 CNVs involving FOXG1 were identified. It is indicated that the occurrence of FOXG1-related disorder was extremely rare in China. The minimally overlapped region of the three microdeletions contains two protein-coding genes (*FOXG1* and *PRKD1*). *FOXG1* and *PRKD1* were reported to cause the occurrence of a congenital variant of Rett syndrome (OMIM#613454) and congenital heart defects and ectodermal dysplasia (CHDED) (OMIM#617364), respectively. In the ClinGen database, *FOXG1* was curated as a haploinsufficient gene with dosage pathogenicity. Although no annotations about *PRKD1* in the ClinGen database, it has many similar features to *FOXG1*, such as being haploinsufficient, dominantly inherited, and contained in the same microdeletions or microduplications with *FOXG1*, it is very difficult to exclude *PRKD1* from the underlying genetic factors for FOXG1-related disorder.

After compiling CNVs recruited in several databases, such as ClinGen, ClinVar, and DECIPHER, six shortest CNVs just covered the CDS of *FOXG1*, four microdeletions (nssv3442672 in ClinGen, 1073841 and 830776 in ClinVar, and 290100 in DECIPHER) and two microduplications (1020268 and 471463 in ClinVar). It has been reported that *FOXG1* was vital for the telencephalon development, the survival of postmitotic neurons, neural plasticity, and the formation of the hippocampal dentate gyrus, therefore, *FOXG1* should be the crucial molecular factor for disorders with 14q12 abnormalities.

The *PRKD1* gene was known as the molecular etiology for CHDED (Sifrim et al., 2016). In the case of patients with heterozygous mutations in the CDS of the *PRKD1*

gene, they suffered from not only CHDs but also intellectual disability, global developmental delay, hearing impairment, delayed language development, or microcephaly (Swaminathan et al., 2012; Sifrim et al., 2016). These clinical features were very similar to those of FOXG1-related disorders. To further understand the possibility of *PRKD1* to FOXG1-related disorder, clinical features were compiled from patients with deletions or duplications containing only the *PRKD1* gene. As for the one microduplication and nine microdeletions covering only the *PRKD1* gene with detailed clinical phenotypes in the ClinVar and DECIPHER databases (Figure 5B, Supplementary Table S2), in addition to abnormalities of the cardiovascular system, clinical features similar to FOXG1-related encephalopathy were also identified. The encoded protein PRKD1 is a serine/threonine protein kinase involved in many cellular processes, such as Golgi body membrane integrity and transport, cell migration and differentiation, and cell survival. It is important for neuronal polarity, synapse formation, and synaptic plasticity (Bisbal et al., 2008; Yin et al., 2008; Cen et al., 2018). PRKD1 also plays an important anti-apoptotic survival role for dopaminergic neurons during the early stage of oxidative stress (Asaithambi et al., 2011). It had been reported that *PRDK1* was associated with intelligence (Hill et al., 2019), cognitive performance (Lee et al., 2018), depressive symptoms (Baselmans et al., 2019), and susceptibility to schizophrenia (a kind of psychiatric disorder) (Pantelis et al., 2014; Wu et al., 2020). Overall, *PRKD1* might be a contributing factor for the varying clinical phenotypes of FOXG1-related encephalopathies.

As for the *FOXG1-PRKD1* intergenic region, most of the CNVs overlapped partially or completely with the intergenic region (Figure 6), it is inferred that the *FOXG1–PRKD1* region might play some unknown functions for the disease. Six of the SECRs in the intergenic region were experimentally verified as active enhancers in the embryonic mouse brain (Visel et al., 2007). Based on the *in situ* Hi-C data for human cells (Rao et al., 2014), *FOXG1* and the *FOXG1-PRKD1* region were completely contained in a large topologically associating domain (TAD). In this TAD, a schizophrenia-related SNP, rs1191551 was localized in close vicinity to the last putative enhancer (element_555), which was 760 kb away from the gene body of *FOXG*1. Reporter assay and genomic editing by CRISPR/Cas9 showed that the short region containing rs1191551 regulated the expression of *FOXG1* but not the nearby *PRKD1* (Won et al., 2016). According to the significant single tissue expression quantitative trait loci (eQTLs) for *FOXG1* and *PRKD1* curated in the Genotype-Tissue Expression (GTEx) project, there were 137 eQTLs that were exclusively located in the FOXG1-specific TAD. As for the 214 eQTLs of *PRKD1*, only two (rs80019464 and rs78802132, 0.93%) were located in the FOXG1-specific TAD (Figure 7A). These imply that the intergenic regulatory elements primarily regulate the expression of *FOXG1*, instead of *PRKD1*, by a cis-acting model. However, it is not clear about the plethora of transcription factors and regulatory manners of the intergenic enhancers to control the expression of FOXG1.

The STRINGed network for the 14 proteins involving well-known RTT or RTT-like genes, such as MECP2, CDKL5, and FOXG1, plus PRKD1 was constructed using Cytoscape (version 3.9.0) (Figure 7B). FOXG1 could interact with MECP2 and CDKL5. IGF1-IGF1R complex and INSR-IRS1 complex could regulate directly the expression of FOXG1 and indirectly the expression of MECP2 and CKDL5. As for PRKD1, it had been reported that PRKD1 could interact with IGF1R (Hermanto et al., 2002). Gene Ontology (GO) analysis revealed that genes in the GO term "regulation of cell proliferation" in the biological process were the most significantly enriched ($p = 5.54E-06$) (Figure 7C). Genes in the "insulin receptor complex" in cellular component and "IGF1R binding" were the second and third most enriched. It implied that insulin or insulin-like factor pathways might play an important role in the pathogenesis of RTT or RTT-like syndrome. It has been reported that IGF1 could ameliorate RTT-relevant phenotypes in animal models and improve some clinical manifestations in clinical trials (Pini et al., 2012; Keogh et al., 2020). Since possessing the ability to bind and regulate the expression of IGF1R, it is very likely that *PRKD1* is a novel contributor to the clinical phenotypes of FOXG1-related disorder. Experiments under cellular and animal levels should be carried out to provide solid evidence showing the involvement of PRKD1 in the pathogenesis of FOXG1-related encephalopathy.

Conclusion

Based on our comprehensive reanalysis of FOXG1 mutations, the molecular etiologies for FOXG1-related encephalopathies were quite complex. It could result from mutations in the CDS of FOXG1 itself, microdeletion/microduplication of the whole FOXG1, microdeletion/microduplication of the regulatory elements in the intergenic *FOXG1-PRKD1* region, and modified by PRKD1. The management of FOXG1-related encephalopathy is a great challenge for medical practitioners.

Data availability statement

The datasets presented in this study can be found in online repositories. The names of the repository/repositories and accession number(s) can be found in the article/Supplementary material.

Ethics statement

The studies involving human participants were reviewed and approved by Shenzhen Baoan Women's and Children's

Hospital. Written informed consent to participate in this study was provided by the participants' legal guardian/next of kin. The animal study was reviewed and approved by Shenzhen Baoan Women's and Children's Hospital. Written informed consent was obtained from the individual(s), and minor(s)' legal guardian/next of kin, for the publication of any potentially identifiable images or data included in this article.

Author contributions

GL and JW conceived the project, wrote, and revised the manuscript. QP and YZ performed genetic counseling, analyzed the clinical data, and revised the manuscript. HX and XH performed the bibliographic search and analyzed the data. PX, LW, and DL collected data and recruited mutations. All authors critically revised the article for important intellectual content.

Funding

This work was supported by the Science and Technology Research and Development Foundation of Shenzhen City (JCYJ20180305164359668 and JCYJ201908809183601667), Key Research and Development Project of Deyang City's Science and Technology Bureau (2021SZ003), Special Fund for Incubation Projects of Deyang People's Hospital (FHG202004), Natural Science Foundation of Sichuan Province (2022NSFSC0714), and Special Program of Department of Science and Technology of Sichuan Province (2018JY0389 and 2019YFS0443).

Acknowledgments

We sincerely appreciate the cooperation of the participants of our cohort of NDD/ID.

Conflict of interest

The authors declare that the research was conducted in the absence of any commercial or financial relationships that could be construed as a potential conflict of interest.

Publisher's note

All claims expressed in this article are solely those of the authors and do not necessarily represent those of their affiliated organizations, or those of the publisher, the editors and the reviewers. Any product that may be evaluated in this article, or claim that may be made by its manufacturer, is not guaranteed or endorsed by the publisher.

Supplementary material

The Supplementary Material for this article can be found online at: https://www.frontiersin.org/articles/10.3389/fnmol.2022.1039990/full#supplementary-material

References

Aldosary, M., Al-Bakheet, A., Al-Dhalaan, H., Almass, R., Alsagob, M., Al-Younes, B., et al. (2020). Rett syndrome, a neurodevelopmental disorder, whole-transcriptome, and mitochondrial genome multiomics analyses identify novel variations and disease pathways. *OMICS Mar.* 24, 160–171. doi: 10.1089/omi.2019.0192

Anitha, A., Poovathinal, S. A., Viswambharan, V., Thanseem, I., Iype, M., Anoop, U., et al. (2022). MECP2 mutations in the Rett syndrome patients from South India. *Neurol. India.* 70, 249–253. doi: 10.4103/0028-3886.338714

Archer, H. L., Evans, J. C., Millar, D. S., Thompson, P. W., Kerr, A. M., Leonard, H., et al. (2006). NTNG1 mutations are a rare cause of Rett syndrome. *Am. J. Med. Genet. A.* 140, 691–694. doi: 10.1002/ajmg.a.31133

Ariani, F., Hayek, G., Rondinella, D., Artuso, R., Mencarelli, M. A., Spanhol-Rosseto, A., et al. (2008). FOXG1 is responsible for the congenital variant of Rett syndrome. *Am. J. Hum. Genet.* 83, 89–93. doi: 10.1016/j.ajhg.2008.05.015

Asaithambi, A., Kanthasamy, A., Saminathan, H., Anantharam, V., and Kanthasamy, A. G. (2011). Protein kinase D1 (PKD1) activation mediates a compensatory protective response during early stages of oxidative stress-induced neuronal degeneration. *Mol. Neurodegener.* 6, 1–19. doi: 10.1186/1750-1326-6-43

Bahi-Buisson, N., Nectoux, J., Girard, B., Van Esch, H., De Ravel, T., Boddaert, N., et al. (2010). Revisiting the phenotype associated with FOXG1 mutations: two novel cases of congenital Rett variant. *Neurogenetics.* 11, 241–249. doi: 10.1007/s10048-009-0220-2

Bai, Y., Yi, A., Xin, J., Xu, J., and Huang, M. (2021). Genotype-phenotype implications from three representative clinical FOXG1 variants associated with FOXG1 syndrome. *Seizure.* 89, 45–47. doi: 10.1016/j.seizure.2021.04.023

Baselmans, B. M., Jansen, R., Ip, H. F., van Dongen, J., Abdellaoui, A., van de Weijer, M. P., et al. (2019). Multivariate genome-wide analyses of the well-being spectrum. *Nat. Genet.* 51, 445–451. doi: 10.1038/s41588-018-0320-8

Bean, L. J., Tinker, S. W., da Silva, C., and Hegde, M. R. (2013). Free the data: one laboratory's approach to knowledge-based genomic variant classification and preparation for EMR integration of genomic data. *Hum. Mutat.* 34, 1183–1188. doi: 10.1002/humu.22364

Bisbal, M., Conde, C., Donoso, M., Bollati, F., Sesma, J., Quiroga, S., et al. (2008). Protein kinase d regulates trafficking of dendritic membrane proteins in developing neurons. *J. Neurosci.* 28, 9297–9308. doi: 10.1523/JNEUROSCI.1879-08.2008

Borg, I., Freude, K., Kübart, S., Hoffmann, K., Menzel, C., Laccone, F., et al. (2005). Disruption of Netrin G1 by a balanced chromosome translocation in a girl with Rett syndrome. *Eur. J. Hum. Genet.* 13, 921–927. doi: 10.1038/sj.ejhg.5201429

Byun, C. K., Lee, J. S., Lim, B. C., Kim, K. J., Hwang, Y. S., Chae, J. H., et al. (2015). FOXG1 mutation is a low-incidence genetic cause in atypical Rett syndrome. *Child Neurol. Open.* 2, 2329048X.14568151. doi: 10.1177/2329048X14568151

Caporali, C., Signorini, S., De Giorgis, V., Pichiecchio, A., Zuffardi, O., Orcesi, S., et al. (2018). Early-onset movement disorder as diagnostic marker in genetic syndromes: Three cases of FOXG1-related syndrome. *Eur. J. Paediatr. Neurol.* 22, 336–339. doi: 10.1016/j.ejpn.2018.01.007

Cellini, E., Vignoli, A., Pisano, T., Falchi, M., Molinaro, A., Accorsi, P., et al. (2016). The hyperkinetic movement disorder of FOXG 1-related epileptic–dyskinetic encephalopathy. *Dev. Med. Child Neurol.* 58, 93–97. doi: 10.1111/dmcn.12894

Cen, C., Luo, L. D., Li, W. Q., Li, G., Tian, N. X., Zheng, G., et al. (2018). PKD1 promotes functional synapse formation coordinated with N-cadherin in hippocampus. *J. Neurosci.* 38, 183–199. doi: 10.1523/JNEUROSCI.1640-17.2017

Chiola, S., Do, M. D., Centrone, L., and Mallamaci, A. (2019). Foxg1 overexpression in neocortical pyramids stimulates dendrite elongation via Hes1 and pCreb1 upregulation. *Cerebral Cortex.* 29, 1006–1019. doi: 10.1093/cercor/bhy007

Coe, B. P., Witherspoon, K., Rosenfeld, J. A., Van Bon, B. W., Vulto-van Silfhout, A. T., Bosco, P., et al. (2014). Refining analyses of copy number variation identifies specific genes associated with developmental delay. *Nat. Genet.* 46, 1063–1071. doi: 10.1038/ng.3092

Cogliati, F., Giorgini, V., Masciadri, M., Bonati, M. T., Marchi, M., Cracco, I., et al. (2019). Pathogenic variants in STXBP1 and in genes for GABAa receptor subunities cause atypical rett/rett-like phenotypes. *Int. J. Mol. Sci.* 20, 3621. doi: 10.3390/ijms20153621

Cooper, G. M., Coe, B. P., Girirajan, S., Rosenfeld, J. A., Vu, T. H., Baker, C., et al. (2011). A copy number variation morbidity map of developmental delay. *Nat. Genet.* 43, 838–846. doi: 10.1038/ng.909

Dastidar, S. G., Landrieu, P. M. Z., and D'Mello, S. R. (2011). FoxG1 promotes the survival of postmitotic neurons. *J. Neuroscience.* 31, 402–413. doi: 10.1523/JNEUROSCI.2897-10.2011

Firth, H. V., Richards, S. M., Bevan, A. P., Clayton, S., Corpas, M., Rajan, D., et al. (2009). DECIPHER: database of chromosomal imbalance and phenotype in humans using ensembl resources. *Am. J. Hum. Genet. Apr.* 84, 524–533. doi: 10.1016/j.ajhg.2009.03.010

Fu, W., O'connor, T. D., Jun, G., Kang, H. M., Abecasis, G., Leal, S. M., et al. (2013). Analysis of 6,515 exomes reveals the recent origin of most human protein-coding variants. *Nature.* 493, 216–220. doi: 10.1038/nature11690

Goubau, C., Devriendt, K., Van der Aa, N., Crepel, A., and Wieczorek, D., Kleefstra Tet al. (2013). Platelet defects in congenital variant of Rett syndrome patients with FOXG1 mutations or reduced expression due to a position effect at 14q12. *Eur. J. Hum. Genet.* 21, 1349–1355. doi: 10.1038/ejhg.2013.86

Grillo, E., Villard, L., Clarke, A., Ben Zeev, B., Pineda, M., Bahi-Buisson, N., et al. (2012). Rett networked database: an integrated clinical and genetic network of Rett syndrome databases. *Hum. Mutat.* 33, 1031–1036. doi: 10.1002/humu.22072

Heimer, G., van Woerden, G. M., Barel, O., Marek-Yagel, D., Kol, N., Munting, J. B., et al. (2020). Netrin-G2 dysfunction causes a Rett-like phenotype with areflexia. *Hum. Mutat.* 41, 476–486. doi: 10.1002/humu.23945

Hermanto, U., Zong, C. S., Li, W., and Wang, L. H. (2002). RACK1, an insulin-like growth factor I (IGF-I) receptor-interacting protein, modulates IGF-I-dependent integrin signaling and promotes cell spreading and contact with extracellular matrix. *Mol. Cell Biol.* 22, 2345–2365. doi: 10.1128/MCB.22.7.2345-2365.2002

Hill, W. D., Marioni, R. E., Maghzian, O., Ritchie, S. J., Hagenaars, S. P., McIntosh, A. M., et al. (2019). A combined analysis of genetically correlated traits identifies 187 loci and a role for neurogenesis and myelination in intelligence. *Mol Psychiatry.* 24, 169–181. doi: 10.1038/s41380-017-0001-5

Hoffjan, S., Ibisler, A., Tschentscher, A., Dekomien, G., Bidinost, C., Rosa, A. L., et al. (2016). WDR45 mutations in Rett (-like) syndrome and developmental delay: Case report and an appraisal of the literature. *Mol. Cell Probes.* 30, 44–49. doi: 10.1016/j.mcp.2016.01.003

Huang, J., Poon, L., Akolekar, R., Choy, K. W., Leung, T. Y., Nicolaides, K., et al. (2014). Is high fetal nuchal translucency associated with submicroscopic chromosomal abnormalities on array CGH? *Ultrasound Obstetr. Gynecol.* 43, 620–624. doi: 10.1002/uog.13384

Jacob, F. D., Ramaswamy, V., Andersen, J., and Bolduc, F. V. (2009). Atypical Rett syndrome with selective FOXG1 deletion detected by comparative genomic hybridization: case report and review of literature. *Eur. J. Hum. Genet.* 17, 1577–1581. doi: 10.1038/ejhg.2009.95

Keogh, C., Pini, G., Gemo, I., Kaufmann, W. E., and Tropea, D. (2020). Functional network mapping reveals state-dependent response to IGF1 treatment in rett syndrome. *Brain Sci.* 10, 515. doi: 10.3390/brainsci10080515

Kortüm, F., Das, S., Flindt, M., Morris-Rosendahl, D. J., Stefanova, I., Goldstein, A., et al. (2011). The core FOXG1 syndrome phenotype consists of postnatal microcephaly, severe mental retardation, absent language, dyskinesia, and corpus callosum hypogenesis. *J. Med. Genet.* 48, 396–406. doi: 10.1136/jmg.2010.087528

Kulikovskaja, L., Sarajlija, A., Savic-Pavicevic, D., Dobricic, V., Klein, C., Westenberger, A., et al. (2018). WDR45 mutations may cause a MECP2 mutation-negative Rett syndrome phenotype. *Neurol. Genet.* 4, e227. doi: 10.1212/NXG.0000000000000227

Kurosaki, T., Popp, M. W., and Maquat, L. E. (2019). Quality and quantity control of gene expression by nonsense-mediated mRNA decay. *Nat. Rev. Mol. Cell Biol.* 20, 406–420. doi: 10.1038/s41580-019-0126-2

Lee, J. J., Wedow, R., Okbay, A., Kong, E., Maghzian, O., Zacher, M., et al. (2018). Gene discovery and polygenic prediction from a genome-wide association study of educational attainment in 1.1 million individuals. *Nat. Genet.* 50, 1112–1121. doi: 10.1038/s41588-018-0147-3

Lee, J. S., Yoo, Y., Lim, B. C., Kim, K. J., Choi, M., Chae, J. H., et al. (2016). SATB2-associated syndrome presenting with Rett-like phenotypes. *Clin. Genet.* 89, 728–732. doi: 10.1111/cge.12698

Lek, M., Karczewski, K. J., Minikel, E. V., Samocha, K. E., Banks, E., Fennell, T., et al. (2016). Analysis of protein-coding genetic variation in 60,706 humans. *Nature.* 536, 285–291. doi: 10.1038/nature19057

Lesurf, R., Cotto, K. C., Wang, G., Griffith, M., Kasaian, K., Jones, S. J., et al. (2016). ORegAnno 3.0: a community-driven resource for curated regulatory annotation. *Nucleic Acids Res.* 44, D126–D132. doi: 10.1093/nar/gkv1203

Leung, T. Y., Vogel, I., Lau, T. K., Chong, W., Hyett, J. A., Petersen, O. B., et al. (2011). Identification of submicroscopic chromosomal aberrations in fetuses with increased nuchal translucency and apparently normal karyotype. *Ultrasound in obstetrics and gynecology.* 38, 314–319. doi: 10.1002/uog.8988

Li, H., and Durbin, R. (2010). Fast and accurate long-read alignment with Burrows-Wheeler transform. *Bioinformatics Mar* 1. 26, 589–595. doi: 10.1093/bioinformatics/btp698

Li, M. R., Pan, H., Bao, X. H., Zhang, Y. Z., and Wu, X. R. (2007). MECP2 and CDKL5 gene mutation analysis in Chinese patients with Rett syndrome. *J. Human Genet.* 52, 38–47. doi: 10.1007/s10038-006-0079-0

Li, S., Sun, G., Zhao, G., and Kong, X. (2021). Analysis of a case with heterozygous 14q12 deletion and FOXG1 gene-related disease. *Chin. J. Med. Genet.* 38, 366–368. doi: 10.3760/cma.j.cn511374-20200307-00142

Lu, G., Peng, Q., Wu, L., Zhang, J., and Ma, L. (2021). Identification of de novo mutations for ARID1B haploinsufficiency associated with Coffin-Siris syndrome 1 in three Chinese families via array-CGH and whole exome sequencing. *BMC Med. Genom.* 14, 270. doi: 10.1186/s12920-021-01119-2

MacDonald, J. R., Ziman, R., Yuen, R. K., Feuk, L., and Scherer, S. W. (2014). The Database of Genomic Variants: a curated collection of structural variation in the human genome. *Nucleic Acids Res.* 42, D986–D992. doi: 10.1093/nar/gkt958

Manuel, M., Martynoga, B., Yu, T., West, J. D., Mason, J. O., Price, D. J., et al. (2010). The transcription factor Foxg1 regulates the competence of telencephalic cells to adopt subpallial fates in mice. *Development.* 137, 487–497. doi: 10.1242/dev.039800

Massadeh, S., Albeladi, M., Albesher, N., Alhabshan, F., Kampe, K. D., Chaikhouni, F., et al. (2021). Novel autosomal recessive splice-altering variant in PRKD1 is associated with congenital heart disease. *Genes.* 12, 612. doi: 10.3390/genes12050612

Maurano, M. T., Humbert, R., Rynes, E., Thurman, R. E., Haugen, E., Wang, H., et al. (2012). Systematic localization of common disease-associated variation in regulatory DNA. *Science.* 337, 1190–1195. doi: 10.1126/science.1222794

McMahon, K. Q., Papandreou, A., Ma, M., Barry, B. J., Mirzaa, G. M., Dobyns, W. B., et al. (2015). Familial recurrences of FOXG1-related disorder: Evidence for mosaicism. *Am. J. Med. Genet. A.* 167A, 3096–3102. doi: 10.1002/ajmg.a.37353

Mehrjouy, M. M., Fonseca, A. C., Ehmke, N., Paskulin, G., Novelli, A., Benedicenti, F., et al. (2018). Regulatory variants of FOXG1 in the context of its topological domain organisation. *Eur. J. Hum. Genet.* 26, 186–196. doi: 10.1038/s41431-017-0011-4

Mitter, D., Pringsheim, M., Kaulisch, M., Plümacher, K. S., Schröder, S., Warthemann, R., et al. (2018). FOXG1 syndrome: genotype-phenotype association in 83 patients with FOXG1 variants. *Genet. Med.* 20, 98–108. doi: 10.1038/gim.2017.75

Miyoshi, G., Ueta, Y., Natsubori, A., Hiraga, K., Osaki, H., Yagasaki, Y., et al. (2021). FoxG1 regulates the formation of cortical GABAergic circuit during an early postnatal critical period resulting in autism spectrum disorder-like phenotypes. *Nat. Commun.* 12, 1–17. doi: 10.1038/s41467-021-23987-z

Moog, U., Smeets, E. E., van Roozendaal, K. E., Schoenmakers, S., Herbergs, J., Schoonbrood-Lenssen, A. M., et al. (2003). Neurodevelopmental disorders in males related to the gene causing Rett syndrome in females (MECP2). *Eur. J. Paediatr. Neurol.* 7, 5–12. doi: 10.1016/S1090-3798(02)00134-4

Nectoux, J., Girard, B., Bahi-Buisson, N., Prieur, F., Afenjar, A., Rosas-Vargas, H., et al. (2007). Netrin G1 mutations are an uncommon cause of atypical Rett syndrome with or without epilepsy. *Pediatr. Neurol.* 37, 270–274. doi: 10.1016/j.pediatrneurol.2007.06.002

Niu, Y., Cao, L., Zhao, P., and Cai, C. (2020). A. case of congenital Rett variant in a Chinese patient caused by a FOXG1 mutation. *Ann. Saudi Med.* 40, 347–353. doi: 10.5144/0256-4947.2020.347

Nykamp, K., Anderson, M., Powers, M., Garcia, J., Herrera, B., Ho, Y. Y., et al. (2017). Sherloc: a comprehensive refinement of the ACMG–AMP variant classification criteria. *Genet. Med.* 19, 1105–1117. doi: 10.1038/gim.2017.37

Pantelis, C., Papadimitriou, G. N., Papiol, S., Parkhomenko, E., Pato, M. T., Paunio, T., et al. (2014). Biological insights from 108 schizophrenia-associated genetic loci. *Nature.* 511, 421. doi: 10.1038/nature13595

Papandreou, A., Schneider, R. B., Augustine, E. F., Ng, J., Mankad, K., Meyer, E., et al. (2016). Delineation of the movement disorders associated with FOXG1 mutations. *Neurology.* 86, 1794–1800. doi: 10.1212/WNL.0000000000002585

Peng, Q., Lu, G., Ma, L., Xu, P., Xian, B., Wu, L., et al. (2022). A de Novo ZMIZ1 pathogenic variant for neurodevelopmental disorder with dysmorphic facies and distal skeletal anomalies. *Front. Genet.* 13, 840577. doi: 10.3389/fgene.2022.840577

Pini, G., Scusa, M. F., Congiu, L., Benincasa, A., Morescalchi, P., Bottiglioni, I., et al. (2012). IGF1 as a Potential Treatment for Rett Syndrome: Safety Assessment in Six Rett Patients. *Autism. Res. Treat.* 2012, 679801. doi: 10.1155/2012/679801

Rao, S. S., Huntley, M. H., Durand, N. C., Stamenova, E. K., Bochkov, I. D., Robinson, J. T., et al. (2014). A 3D map of the human genome at kilobase resolution reveals principles of chromatin looping. *Cell.* 159, 1665–1680. doi: 10.1016/j.cell.2014.11.021

Rehm, H. L., Berg, J. S., Brooks, L. D., Bustamante, C. D., Evans, J. P., Landrum, M. J., et al. (2015). ClinGen–the clinical genome resource. *N. Engl. J. Med.* 372, 2235–2242. doi: 10.1056/NEJMsr1406261

Richards, S., Aziz, N., Bale, S., Bick, D., Das, S., Gastier-Foster, J., et al. (2015). Standards and guidelines for the interpretation of sequence variants: a joint consensus recommendation of the American College of Medical Genetics and Genomics and the Association for Molecular Pathology. *Genet. Med.* 17, 405–423. doi: 10.1038/gim.2015.30

Seltzer, L. E., Ma, M., Ahmed, S., Bertrand, M., Dobyns, W. B., Wheless, J., et al. (2014). Epilepsy and outcome in FOXG1-related disorders. *Epilepsia.* 55, 1292–1300. doi: 10.1111/epi.12648

Shaheen, R., Al Hashem, A., Alghamdi, M. H., Seidahmad, M. Z., Wakil, S. M., Dagriri, K., et al. (2015). Positional mapping of PRKD1, NRP1 and PRDM1 as novel candidate disease genes in truncus arteriosus. *J. Med. Genet.* 52, 322–329. doi: 10.1136/jmedgenet-2015-102992

Sifrim, A., Hitz, M. P., Wilsdon, A., Breckpot, J., Al Turki, S. H., Thienpont, B., et al. (2016). Distinct genetic architectures for syndromic and nonsyndromic congenital heart defects identified by exome sequencing. *Nat. Genet.* 48, 1060–1065. doi: 10.1038/ng.3627

Swaminathan, G. J., Bragin, E., Chatzimichali, E. A., Corpas, M., Bevan, A. P., Wright, C. F., et al. (2012). DECIPHER: web-based, community resource for clinical interpretation of rare variants in developmental disorders. *Hum. Mol. Genet.* 21, R37–44. doi: 10.1093/hmg/dds362

Taliun, D., Harris, D. N., Kessler, M. D., Carlson, J., Szpiech, Z. A., Torres, R., et al. (2021). Sequencing of 53,831 diverse genomes from the NHLBI TOPMed Program. *Nature.* 590, 290–299. doi: 10.1038/s41586-021-03205-y

Tang, Z., Tong, G., Hong, L., Zhou, T., and Xu Y. (2021). Application value of chromosome microarray analysis in the genetic etiology of children with unexplained intellectual disability/developmental delay. *J. Anhui Health Vocat. Technic. Coll.* 20, 121–124. doi: 10.1159/000509645

Tian, C., Gong, Y., Yang, Y., Shen, W., Wang, K., Liu, J., et al. (2012). Foxg1 has an essential role in postnatal development of the dentate gyrus. *J. Neurosci.* 32, 2931–2949. doi: 10.1523/JNEUROSCI.5240-11.2012

Toresson, H., Martinez-Barbera, J. P., Bardsley, A., Caubit, X., and Krauss, S. (1998). Conservation of BF-1 expression in amphioxus and zebrafish suggests evolutionary ancestry of anterior cell types that contribute to the vertebrate telencephalon. *Dev. Genes. Evol.* 208, 431–439. doi: 10.1007/s004270050200

Van der Aa, N., Van den Bergh, M., Ponomarenko, N., Verstraete, L., Ceulemans, B., Storm, K., et al. (2010). Analysis of FOXG1 is highly recommended in male and female patients with Rett syndrome. *Mol. Syndromol.* 1, 290–293. doi: 10.1159/000330755

Vegas, N., Cavallin, M., Maillard, C., Boddaert, N., Toulouse, J., Schaefer, E., et al. (2018). Delineating FOXG1 syndrome: From congenital microcephaly to hyperkinetic encephalopathy. *Neurol. Genet.* 4, e281. doi: 10.1212/NXG.0000000000000281

Visel, A., Minovitsky, S., Dubchak, I., and Pennacchio, L. A. (2007). VISTA Enhancer Browser—a database of tissue-specific human enhancers. *Nucleic Acids Res.* 35, D88–D92. doi: 10.1093/nar/gkl822

Wang, F., Luo, R., Zhou, B., Yu, T., and Chen, X. (2017). Report of a case with 14q12 triplication and literature review for FOXG1 related diseases. *Chin. J. Med. Genet.* 34, 671–675.

Wang, J., Zhang, Q., Chen, Y., Yu, S., Wu, X., Bao, X., et al. (2018). Novel MEF2C point mutations in Chinese patients with Rett (-like) syndrome or non-syndromic intellectual disability: insights into genotype-phenotype correlation. *BMC Med. Genet.* 19,191. doi: 10.1186/s12881-018-0699-1

Wang, J., Zhang, Q., Chen, Y., Yu, S., Wu, X., Bao, X., et al. (2019). Rett and Rett-like syndrome: Expanding the genetic spectrum to KIF1A and GRIN1 gene. *Molec. Genet. Genom. Med.* 7, e968. doi: 10.1002/mgg3.968

Won, H., de La Torre-Ubieta, L., Stein, J. L., Parikshak, N. N., Huang, J., Opland, C. K., et al. (2016). Chromosome conformation elucidates regulatory relationships in developing human brain. *Nature.* 538, 523–527. doi: 10.1038/nature19847

Wong, L. C., Singh, S., Wang, H. P., Hsu, C. J., Hu, S, C., Lee, W. T., et al. (2019b). FOXG1-related syndrome: from clinical to molecular genetics and pathogenic mechanisms. *Int. J. Mol. Sci.* 20, 4176. doi: 10.3390/ijms20174176

Wong, L. C., Wu, Y. T., Hsu, C. J., Weng, W. C., Tsai, W. C., Lee, W. T., et al. (2019a). Cognition and Evolution of Movement Disorders of FOXG1-Related Syndrome. *Front Neurol.* 10, 641. doi: 10.3389/fneur.2019.00641

Wu, Y., Cao, H., Baranova, A., Huang, H., Li, S., Cai, L., et al. (2020). Multi-trait analysis for genome-wide association study of five psychiatric disorders. *Transl. Psychiatry.* 10, 1–11. doi: 10.1038/s41398-020-00902-6

Yang, K., Shen, M., Yan, Y., Tan, Y. A., Zhang, J., Wu, J., et al. (2019). Genetic analysis in fetal skeletal dysplasias by trio whole-exome sequencing. *Biomed. Res. Int.* 2019, 2492590. doi: 10.1155/2019/2492590

Yin, D.-., M., Huang, Y-, H., Zhu, Y.-., B., and Wang, Y. (2008). Both the establishment and maintenance of neuronal polarity require the activity of protein kinase D in the Golgi apparatus. *J. Neurosci.* 28, 8832–8843. doi: 10.1523/JNEUROSCI.1291-08.2008

Yu, B., Liu, J., Su, M., Wang, C., Chen, H., Zhao, C., et al. (2019). Disruption of Foxg1 impairs neural plasticity leading to social and cognitive behavioral defects. *Mol. Brain.* 12, 1–12. doi: 10.1186/s13041-019-0484-x

Zhang, Q., Wang, J., Li, J., Bao, X., Zhao, Y., Zhang, X., et al. (2017). Novel FOXG1 mutations in Chinese patients with Rett syndrome or Rett-like mental retardation. *BMC Med. Genet.* 18, 96. doi: 10.1186/s12881-017-0455-y

Zhang, X., Bao, X., Zhang, J., Zhao, Y., Cao, G., Pan, H., et al. (2012). Molecular characteristics of Chinese patients with Rett syndrome. *Eur J Med Genet.* 55, 677–681. doi: 10.1016/j.ejmg.2012.08.009

Zhu, Y. C., and Xiong, Z. Q. (2019). Molecular and synaptic bases of CDKL5 disorder. *Dev. Neurobiol.* 79, 8–19. doi: 10.1002/dneu.22639

frontiers | Frontiers in Molecular Neuroscience

TYPE Original Research
PUBLISHED 13 December 2022
DOI 10.3389/fnmol.2022.999938

OPEN ACCESS

EDITED BY
Giulia Abate,
University of Brescia,
Italy

REVIEWED BY
Vidhya Kumaresan,
Boston University,
United States
Hui Li,
Beijing Center for Disease Prevention and Control (Beijing CDC), China

*CORRESPONDENCE
Xuhui Zhou
330115@hnucm.edu.cn

†These authors have contributed equally to this work

SPECIALTY SECTION
This article was submitted to Brain Disease Mechanisms, a section of the journal Frontiers in Molecular Neuroscience

RECEIVED 21 July 2022
ACCEPTED 16 November 2022
PUBLISHED 13 December 2022

CITATION
Zhang Z, Zhang S, Huang J, Cao X, Hou C, Luo Z, Wang X, Liu X, Li Q, Zhang X, Guo Y, Xiao H, Xie T and Zhou X (2022) Association between abnormal plasma metabolism and brain atrophy in alcohol-dependent patients.
Front. Mol. Neurosci. 15:999938.
doi: 10.3389/fnmol.2022.999938

Association between abnormal plasma metabolism and brain atrophy in alcohol-dependent patients

Zheyu Zhang[1,2†], Sifang Zhang[1,2†], Jianhua Huang[3], Xiaoyun Cao[1,4], Chao Hou[1,4], Zhihong Luo[1,4], Xiaoyan Wang[1,4], Xuejun Liu[1,4], Qiang Li[1,4], Xi Zhang[1,4], Yujun Guo[1,4], Huiqiong Xiao[1,4], Ting Xie[1,4] and Xuhui Zhou[1,4]*

[1]Department of Addiction Medicine, Hunan Institute of Mental Health, Brain Hospital of Hunan Province (The Second People's Hospital of Hunan Province), Changsha, China, [2]Department of Integrated Traditional Chinese & Western Medicine, The Second Xiangya Hospital, Central South University, Changsha, China, [3]Hunan Academy of Chinese Medicine, Hunan University of Chinese Medicine, Changsha, China, [4]The School of Clinical Medicine, Hunan University of Chinese Medicine, Changsha, China

Objective: In this study, we aimed to characterize the plasma metabolic profiles of brain atrophy and alcohol dependence (s) and to identify the underlying pathogenesis of brain atrophy related to alcohol dependence.

Methods: We acquired the plasma samples of alcohol-dependent patients and performed non-targeted metabolomic profiling analysis to identify alterations of key metabolites in the plasma of BA-ADPs. Machine learning algorithms and bioinformatic analysis were also used to identify predictive biomarkers and investigate their possible roles in brain atrophy related to alcohol dependence.

Results: A total of 26 plasma metabolites were significantly altered in the BA-ADPs group when compared with a group featuring alcohol-dependent patients without brain atrophy (NBA-ADPs). Nine of these differential metabolites were further identified as potential biomarkers for BA-ADPs. Receiver operating characteristic curves demonstrated that these potential biomarkers exhibited good sensitivity and specificity for distinguishing BA-ADPs from NBA-ADPs. Moreover, metabolic pathway analysis suggested that glycerophospholipid metabolism may be highly involved in the pathogenesis of alcohol-induced brain atrophy.

Conclusion: This plasma metabolomic study provides a valuable resource for enhancing our understanding of alcohol-induced brain atrophy and offers potential targets for therapeutic intervention.

KEYWORDS

alcohol, brain atrophy, cognitive dysfunction, glycerophospholipid metabolism, metabolomic

Introduction

Excessive and chronic alcohol consumption, caused by addictive behaviors in alcoholic patients, is closely related to the reduced viability of neuronal cells (neurons and glial cells) and axonal degradation, thus resulting in brain atrophy (Sutherland et al., 2014; Angebrandt et al., 2022). It has been reported that the degree of brain atrophy correlates with the rate and amount of alcohol consumed over a lifetime (de la Monte and Kril, 2014). Moreover, the latest research has detected negative relationships between alcohol consumption and gray and white matter volumes across the brain (Daviet et al., 2022). Abnormal patterns of macroscopic and microstructural changes in the brain, especially brain atrophy, are closely related to the cognitive dysfunction of alcoholics in the clinical setting (Zahr et al., 2011). Cognitive impairment, including deficits in memory, executive abilities, visuospatial processing, speed of processing and, to a lesser extent, attention and general intelligence, may dramatically influence a patient's social function and quality-of-life (Godin et al., 2019). In view of the high prevalence of alcohol-related brain atrophy (ARBA) and its associated cognitive dysfunction, a comprehensive analysis of the mechanisms underlying ARBA and the identification of potential biomarkers for this disease are urgently needed.

Metabolomics, a systematic method for the qualitative and quantitative analysis of all low-molecular-weight metabolites, is suitable for identifying metabolic indicators and can provide a basis for individualized diagnosis and treatment (Ribbenstedt et al., 2018). Moreover, the discovery of new markers can provide new ideas for the diagnosis and treatment of difficult diseases and can provide a useful guide for clinical diagnosis and treatment (Vuckovic, 2018). Metabolomic research based on untargeted/targeted mass spectrometry (MS) and proton nuclear magnetic resonance (1H-NMR) spectroscopy approaches may represent a valuable research tool to identify the underlying pathogenesis of alcohol-related disorders. Mittal and Dabur previously studied the influence of an aqueous extract of *Tinospora cordifolia* on the urinary metabolic signature of chronic alcohol using liquid chromatography–tandem mass spectrometry (LC–MS/MS; Mittal and Dabur, 2015). In another study, Zhu et al. identified discriminatory metabolic profiles between healthy and alcohol dependent individuals by using metabolomics technology (Zhu et al., 2021). To our knowledge, no previous study has identified alterations in the metabolic and protein profiles of plasma samples taken from alcohol-dependent patients with brain atrophy.

Machine learning, as a field of artificial intelligence (AI), provides intelligent data processing while facilitating reasoning and the initial settings to determine functional relationships (Deo, 2015). Due to the diversification of algorithms, machine learning is gradually emerging in the field of multi-omics, including artificial neural networks (ANNs), and random forest (RF) algorithms (Liebal et al., 2020). The main applications of machine learning in disease-related multi-omics data analysis include (1) the stratification of patients to discover various subtypes of human diseases and to discover different treatment/prognostic outcomes, and (2) the investigation of various diseases by identifying biomarkers of omics features under various state (Nicora et al., 2020). Traditional methods for processing metabolomics data tend to only focus on bridging sample differences within groups. However, in applied pharmaceutical research (such as candidate target discovery and drug sensitivity), we also need to consider data perturbation and sensitivity to sample size (Schrimpe-Rutledge et al., 2016). Based on their specific characteristics, a combination of traditional single evaluation and machine learning algorithms could provide an efficient means of evaluating the performance of metabolomics data processing from multiple perspectives (Mirza et al., 2019; Picard et al., 2021). Specifically, this strategy can achieve effective data processing from five relatively independent directions: reducing within-group sample differences, differential metabolic analysis, the stability of marker identification, classification accuracy, and the consistency of biological gold standards.

In this study, we used a LC–MS/MS-based metabonomics approach to provide a robust technical platform to investigate the profiles of plasma metabolites in ARBA patients and identify characteristic metabolites that can be used to discriminate ARBA from non-ARBA. MetaboAnalyst version 5.0 was then used to identify metabolites and metabolic pathways showing significant enrichment in ARBA. Then, machine learning algorithms were used to identify the most important distinctive metabolites that might be associated with patients with ARBA. The findings of the present study may help to identify the molecular mechanisms that underlie ARBA.

Materials and methods

Study design and participants

This study was approved by the Ethics Committee of the Hunan Brain Hospital (Reference: 2016121). Signed and informed consent was obtained from each patient.

A total of 126 patients with alcohol addiction were enrolled from Hunan Brain Hospital between March 2019 and January 2020. Brain MRI were performed in all patients to evaluate the extent of brain atrophy.

The inclusion and exclusion criteria were described in our previous publication (Liu et al., 2020). Briefly, the inclusion criteria were as follows: (1) age 18–60 years, Han Chinese; (2) no contraindications for MRI. The exclusion criteria were as follows: (1) patients had any general medical conditions or neurological disorders, including infectious, hepatic, or endocrine disease; (2) patients with a history of severe head injury with skull fracture or loss of consciousness of more than 10 min; (3) patients had any current or previous psychiatric disorder; (4) patients had a family history of psychiatric disorder. The diagnosis of alcohol dependence was made according to the Structured Clinical Interview (SCID) based on the Diagnostic and Statistical Manual

of Mental Disorders DSM-IV criteria (Battle, 2013). Alcohol-dependent patients were divided into two subgroups based on whether they have brain atrophy (the experimental group) or not (the control group).

Evaluation of brain atrophy

Brain MRI were performed in all patients after blood samples collection. The extent of brain atrophy was evaluated by at least two independent neuroradiologists using the global cortical atrophy scale (Pasquier et al., 1996). Both cortical regions (frontal, temporal, parietal and occipital) and subcortical regions (peri-insular, basal, and vault) were assessed. The severity of atrophy (low, moderate, or severe) was detected by the widening of sulci and narrow of gyri, as well as the reduction in amplitude of the respective regions. Figure 1 shows examples of different severity of brain atrophy.

Sample collection and preparation

Blood samples were taken from all inpatients after hospital admission but prior to starting treatment. Blood samples were taken from the experimental and control patients between 6:00 and 6:30 am and placed into plasma collecting tubes. Samples were then centrifuged at 3,000 rpm for 10 min at 4°C and the plasma was aliquoted into 1.5 ml microcentrifuge tubes and immediately stored at −80°C.

For LC–MS, we removed 100 µl of each plasma sample and added 0.4 ml of pre-cooled 0.2% methanol-acetonitrile mixture (1:1, v/v); this was followed by vortex-mixing and ultrasonic extraction on iced water. Next, the solution was centrifuged at 13,000 × *g* for 15 min at 4°C; 400 µl of the supernatant was taken and dried with nitrogen. Finally, 100 µl of acetonitrile water (1:1, v/v) was added and the re-dissolved solution was injected into a sample bottle for detection. Quality control samples (a mixture of equal quantities of all sample extractions) were injected after every 10 analytical samples to monitor the stability of the LC–MS system.

LC–MS data acquisition and processing

Data acquisition was performed by UPLC-Q-TOF-MS/MS with the following parameter settings: an ethylene bridged hybrid C18 column (2.1 mm × 100 mm id, 1.7 µm; Waters), mobile phase A (water with 0.1% formic acid), and mobile phase B (acetonitrile with 0.1% formic acid). The gradient of the mobile phase was consistent with our previous metabolomic studies (Zhang et al., 2020). The MS signal was acquired in positive-ion and negative-ion modes.

Raw files for the acquired LC–MS/MS data were imported into the metabolomics-processing software Progenesis QI

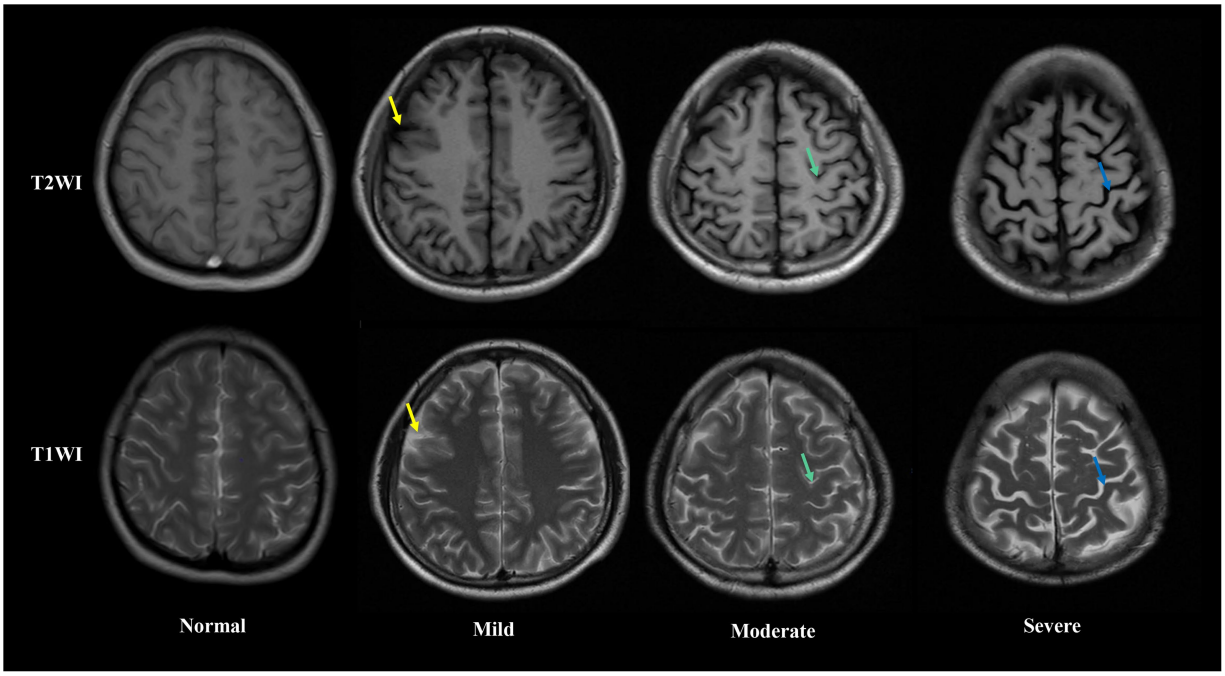

FIGURE 1
Axial T1 weight (up) and T2 weight (down) magnetic resonance images showing different extent of brain atrophy in Alcohol-dependent patients. From left to right, columns represent absent, low, moderate and sever brain atrophy. In low brain atrophy, sulcal opening peripherally (yellow arrows) is observed. In moderate brain atrophy, widening along the length of the sulcus (green arrows) are observed. In severe brain atrophy, gyral thining (red arrows) is observed.

(Waters) to obtain matched and aligned peak data. Subsequently, peak data containing retention time (RT), molecular formula, along with accurate relative molecular mass and peak area information, were imported into Microsoft Excel so that we could normalize the peak area for further analysis.

Analyses of metabolomics data and pathways

Following normalization of the peak area, data were subjected to principal component analysis (PCA), partial least squares discriminant analysis (PLS-DA), and orthogonal partial least squares discriminant analysis (OPLS-DA). The variables showing the most significant differences were identified by selecting those with a VIP > 1 from an S-plot and $p < 0.05$ from an independent samples t-test. Based on the Human Metabolome Database (HMDB) and secondary fragment ions, we were then able to identify differential variables. Then, we performed metabolic pathway analysis for differentially expressed metabolites with MetaboAnalyst version 5.0 to gain insight into the pathogenesis of ARBA, as described previously (Zhang et al., 2020).

Machine learning methods for biomarker screening

Three machine learning methods (Extreme Gradient Boosting (XGBoost), random forest (RF), and AdaBoost Classifier) were used to identify potential biomarkers from differential metabolites or proteins. The five most important metabolites were identified by XGBoost, RF and AdaBoost, and then combined for subsequent analysis. Machine learning was then performed using the Extreme Smart Analysis Platform.[1]

The sensitivity and specificity of the combined biomarkers were further analyzed using logistic regression analysis and receiver operating characteristic (ROC) curves. In ROC analysis, the area enclosed by the curve and the x-axis ($x = 1$ line) was defined as the area under the curve (AUC). Logistic regression analysis was performed using OmicStudio.[2]

Results

Baseline characteristics of the study population

A total of 226 participants were recruited for the present study: 62 were assigned to the NBA-ADP group, 64 were assigned to the BA-ADP group, and 100 were assigned to the Healthy Control (HC) group. Clinical and demographic characteristics were summarized in Table 1. The sex, age, and duration of alcohol dependence between NBA-ADP and BA-ADP group were equivalent. There was no statistical difference in Repeatable Battery for the Assessment of Neuropsychological Status (RBANS) scores between two groups. However, the RBANS scores (including attention, delay memory, immediate memory, language, visuospatial) in BA-ADP group were all slightly higher than these in NBA-ADP group.

TABLE 1 Demographic and baseline patient characteristics.

Characteristics	NBA-ADPs	BA-ADPs
	$n = 62$	$n = 64$
Gender		
Male (n)	62	64
Female (n)	0	0
Age (years)	40.71 ± 9.01	38.63 ± 9.21
Duration of alcohol dependence (years)	11.94 ± 6.80	13.11 ± 8.63
Duration of alcohol dependence (g) *	147.02 ± 67.81	153.41 ± 71.06
RBANS total score	77.87 ± 12.33	77.58 ± 8.08
Attention	84.79 ± 13.99	83.48 ± 9.86
Delay memory	78.47 ± 19.52	77.04 ± 16.57
Immediate memory	73.19 ± 11.90	73.03 ± 15.30
Language	78.56 ± 11.83	76.90 ± 13.56
Visuospatial	76.14 ± 14.65	75.63 ± 13.47

Abbreviations: NBA-ADPs, Alcohol-dependent patients (ADP) without brain atrophy; BA-ADPs, Alcohol-dependent patients (ADP) with brain atrophy; HC, Heathy controls. RBANS, Repeatable Battery for the Assessment of Neuropsychological Status. Data are shown as mean ± SD. *$p < 0.05$.

Global metabolomic profiling

A total of 13,601 peaks were obtained, including 6,189 positive-mode features and 8,432 negative-mode features. A total of 178 positive-mode and 253 negative-mode metabolites were annotated and mapped to public databases. Corresponding to the two modes, 52 and 84 metabolites were, respectively, annotated and mapped to the Kyoto Encyclopedia of Genes and Genomes (KEGG) database. These metabolites belonged to 15 different KEGG compound classifications. Figure 2A shows that these metabolites were mainly classified as phospholipids. According to the KEGG database, these metabolites belonged to 25 different KEGG pathways (Figure 2B). Of these, the lipid metabolism pathway was the pathway that contained the most metabolites.

According to the HMDB version 4.0 database, 431 selected metabolites belonged to 9 predominant super-classes (Figure 3A) and 21 subclasses (Figure 3B). The former included lipids and lipid-like molecules (63.03%), organic acids and derivatives (11.61%), organoheterocyclic compounds (7.21%), and organic oxygen compounds (6.98%). The latter includes glycerophosphocholines (10.00%), amino acids, peptides, and analo (9.07%), fatty acids and conjugat (8.14%), bile acids, alcohols and deves (6.98%), and glycerophosphoethanolamines (5%).

1 https://www.xsmartanalysis.com/

2 https://www.omicstudio.cn/tool/58

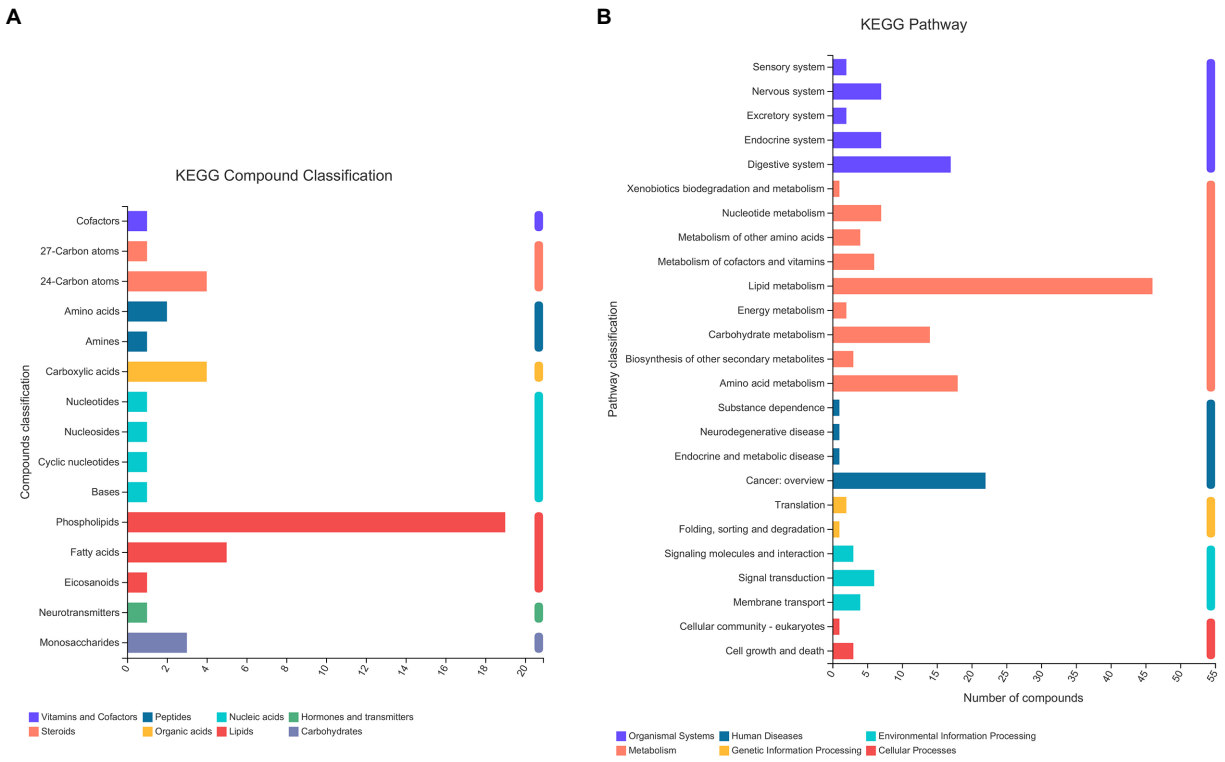

FIGURE 2
The KEGG classification of metabolites identified in all plasma samples. The classification criteria were: **(A)** KEGG Compound Classification; **(B)** KEGG Pathway.

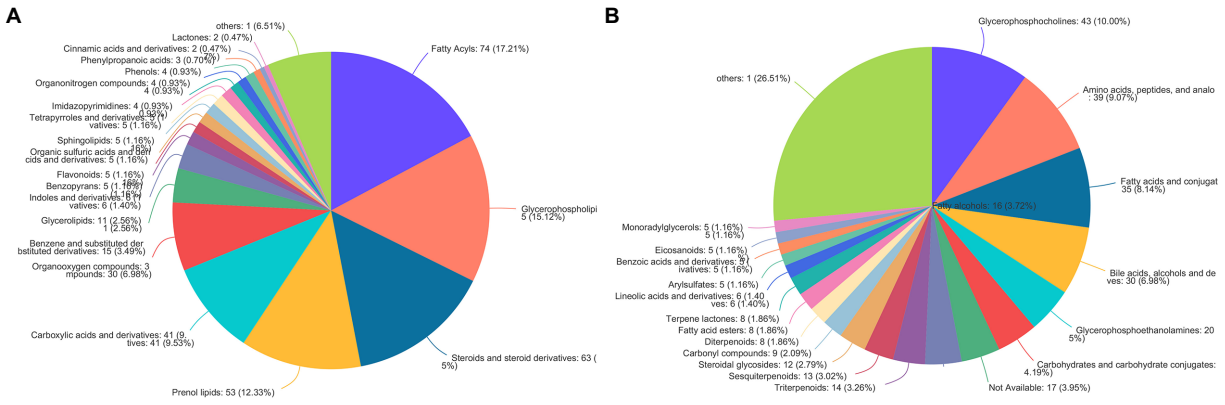

FIGURE 3
The HMDB classification of metabolites identified in all plasma samples. Pie chart illustrating the abundance ratio of different classes of plasma metabolites detected with untargeted metabolic profiling. The classification level was: **(A)** Superclass; **(B)** Subclass.

Identification of dysregulated metabolites

A total of 172 significant differential metabolites (FDR < 0.05) among the three groups were detected by analysis of variance (ANOVA). To further identify group differences in the metabolic profiles between groups, we performed OPLS-DA score plots; these identified notable separations between both the BA-ADP and HC group and between the NBA-ADP and HC group (Figure 4).

Differentially expressed metabolites were identified using multivariate and univariate statistical significance criteria (VIP > 1

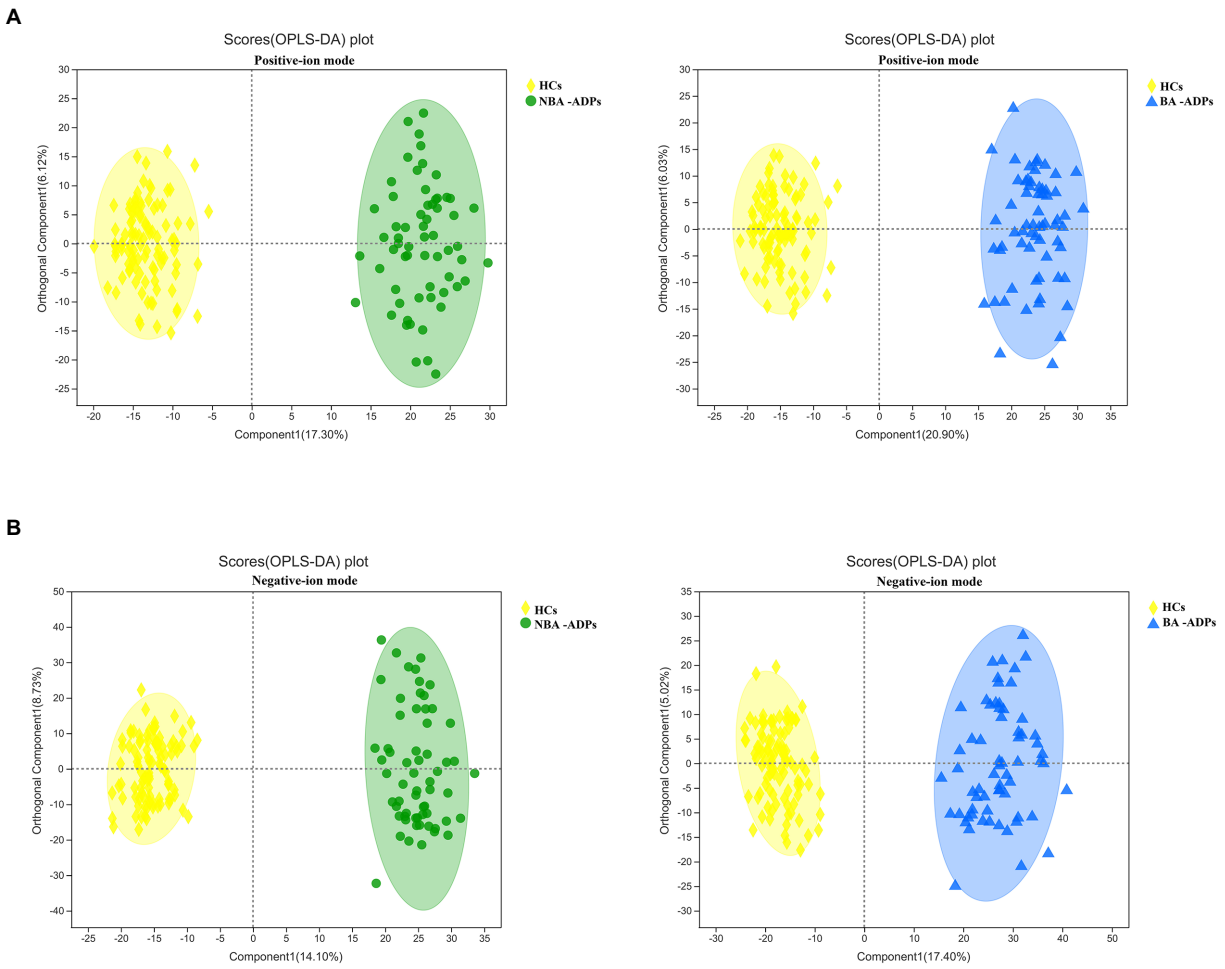

FIGURE 4
OPLS-DA score plots of alcohol-dependent patients (ADP) versus healthy controls. **(A)** OPLS-DA score plots of NBA-ADP vs. HC; **(B)** OPLS-DA score plots of BA-ADP vs. HC.

and FDR < 0.05). In total, 139 metabolites were identified to be significantly different between the NBA-ADP and HC group and 26 metabolites between the BA-ADP and NBA-ADP group (Figure 5; Table 2).

Functional analysis of differentially expressed plasma metabolites from alcohol-dependent patients

To gain a further understanding of the metabolic disturbances between the NBA-ADP and HC group and between the BA-ADP and NBA-ADP group, we performed KEGG pathway enrichment analysis; we also used MetaboAnalyst version 5.0 to perform a functional analysis of plasma metabolites.

As shown in Figure 6A, primary bile acid biosynthesis (map00120), taurine and hypotaurine metabolism (map00430) were the most important metabolic pathways that showed alterations in the alcohol-dependent patients (both the NBA-ADP group and the BA-ADP group) when compared with the HC group. In contrast, pentose and glucuronate interconversions (map00040) and glycerophospholipid metabolism (map00564) were detected in the BA-ADP group when compared with the NBA-ADP group (Figure 6B).

Screening of potential metabolic biomarkers for alcohol-dependent patients with brain atrophy

The five most important metabolites selected by AdBooST were Sulfolithocholylglycine PC (16:0/18:2(9Z,12Z)), Allolithocholic acid, MG(0:0/22:1(13Z)/0:0), and Cyclopassifloic acid E (Figure 7A). The five most important metabolites selected by Random forest were PC (16:0/18:2(9Z,12Z)), N-[(3a,5b,7a)-3-hydroxy-24-oxo-7-(sulfooxy)cholan-24-yl]-Glycine, Cyclopassifloic acid E, 2,4-Dihydroxyacetophenone 5-sulfate, and Allolithocholic

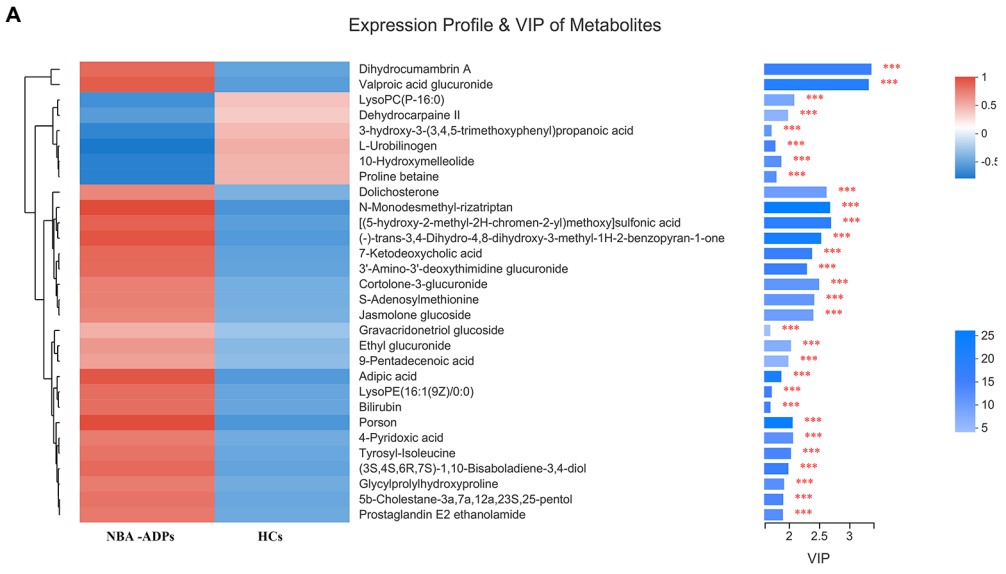

FIGURE 5
Differential plasma metabolic profiles of alcohol-dependent patients vs. healthy controls. The hierarchical clustering and heat map in the left panel shows the top 30 metabolites that were significantly differentially abundant between NBA-ADP and HC **(A)**, and 26 metabolites that were significantly differentially abundant between BA-ADP and NBA-ADP **(B)**. The histogram in the right panel represents variable importance in projection (VIP) scores derived from the OPLS-DA model for each metabolite. *** indicates P<0.001.

acid (Figure 7B). The five most important metabolites selected by Naive Bayes were Deoxycholic acid 3-glucuronide, Sulfolithocholylglycine, Cholic Acid, N-[(3a,5b,7a)-3-hydroxy-24-oxo-7-(sulfooxy)cholan-24-yl]-Glycine, and 2,4-Dihydroxyacetophenone 5-sulfate (Figure 7C). Nine metabolites (Cholic Acid, PC (16:0/18:2(9Z,12Z)), allolithocholic acid, sulfolithocholylglycine, N-[(3a,5b,7a)-3-hydroxy-24-oxo-7-(sulfooxy)cholan-24-yl]-Glycine, cyclopassifloic acid E, MG(0:0/22:1(13Z)/0:0), deoxycholic acid 3-glucuronide, 2,4-Dihydroxyacetophenone 5-sulfate) were identified as potential metabolic biomarkers for alcohol-dependent patients with brain atrophy. As shown in Figure 7D, the AUC of the ROC curve reached was 0.7719 for distinguishing between BA-ADP and NBA-ADP patients.

Discussion

It is well-known that alcohol can causes serious health problems, long-term abuse, and irreversible alterations in the structure and function of the brain (Rehm et al., 2017; Kranzler and Soyka, 2018). However, to the best of our knowledge, this is the first study that sought to identify potential plasma biomarkers of alcohol-dependent patients

TABLE 2 Differentially expressed endogenous metabolites detected by UHPLC-QTOF/MS.

Metabolite	Library ID	M/Z	Formula	RT	log2FC	-log10(p_value)
Positive-ion mode						
Taurodeoxycholic Acid	HMDB0000896	464.282	C26H45NO6S	5.113	0.074	1.394
LysoPC(P-18:0)	HMDB0013122	508.375	C26H54NO6P	8.648	0.017	2.404
Cholic Acid	HMDB0000619	373.273	C24H40O5	5.377	0.06	1.555
Hebevinoside IV	HMDB0036060	587.427	C36H60O7	9.547	−0.016	1.329
PC(16:0/18:2(9Z,12Z))	HMDB0007973	758.568	C42H80NO8P	10.753	0.007	2.103
Allolithocholic acid	HMDB0000381	394.33	C24H40O3	9.127	0.035	1.599
Muricatacin	HMDB0038685	591.459	C17H32O3	9.57	−0.016	1.626
LysoPC(20:0/0:0)	HMDB0010390	574.383	C28H58NO7P	9.48	−0.021	1.432
Erythrodiol 3-decanoate	HMDB0034510	635.482	C40H68O3	9.326	−0.03	1.672
Negative-ion mode						
Sulfolithocholylglycine	HMDB0002639	512.269	C26H43NO7S	6.36	0.072	1.821
N-[(3a,5b,7a)-3-hydroxy-24-oxo-7-(sulfooxy)cholan-24-yl]-Glycine	HMDB0002496	528.264	C26H43NO8S	4.687	0.066	2.229
N-[(3a,5b,7b)-7-hydroxy-24-oxo-3-(sulfooxy)cholan-24-yl]-Glycine	HMDB0002409	528.264	C26H43NO8S	5.624	0.044	1.456
Taurochenodeoxycholate-7-sulfate	HMDB0002498	288.62	C26H45NO9S2	4.118	0.078	1.636
Chenodeoxycholic acid sulfate	HMDB0002522	471.242	C24H40O7S	6.13	0.104	2.529
Hexadecanedioic acid	HMDB0000672	285.207	C16H30O4	7.344	0.041	1.884
Riesling acetal	HMDB0037562	271.155	C13H22O3	4.938	0.098	2.829
Suberic acid	HMDB0000893	173.081	C8H14O4	2.983	0.029	1.426
D-Glucuronic acid	HMDB0000127	193.035	C6H10O7	0.614	0.034	2.152
Cyclopassifloic acid E	HMDB0036298	597.365	C31H52O8	6.291	0.124	1.981
10Z-Nonadecenoic acid	HMDB0013622	341.27	C19H36O2	7.023	−0.123	1.312
MG(0:0/22:1(13Z)/0:0)	HMDB0011552	457.353	C25H48O4	9.031	−0.041	1.669
LysoPE(0:0/20:2(11Z,14Z))	HMDB0011483	550.314	C25H48NO7P	7.504	−0.054	1.487
Deoxycholic acid 3-glucuronide	HMDB0002596	567.318	C30H48O10	5.601	0.057	1.904
Vanillin	HMDB0012308	151.039	C8H8O3	2.576	0.064	1.811
2,4-Dihydroxyacetophenone 5-sulfate	HMDB0041646	230.996	C8H8O6S	2.576	0.157	2.999
(Z)-6-Tetradecene-1,3-diyne-5,8-diol	HMDB0038996	255.114	C14H20O2	1.707	0.052	1.586

Abbreviations: FC: fold change, as determined by average relative quantitation obtained from group BA-ADPs/NBA-ADPs; RT (min): retention time.

who have brain atrophy by applying non-targeted metabolomics and machine learning.

In this study, a total of 26 metabolites were found to show significant changes between the BA-ADP and NBA-ADP group. Each of the identified metabolites were searched against synonyms in HMDB. These metabolites covered a range of chemical classes; lipids and lipid-like molecules were ranked highest and featured 22 of the metabolites. The obtained metabolites were classified based on the KEGG compound annotation database.[3] Phospholipids and phospholipid metabolism were ranked first in the secondary classification category of KEGG compounds. As the main substance of the brain, lipids not only act as the building blocks of all membrane structures but also act as the repository for chemical energy and play a significant role in cellular signaling pathways (Holthuis and Menon, 2014; Van Deijk et al., 2017). Characteristic alterations in lipid—including structure, composition, or distribution—are thought account for alterations in neuronal function, synaptic signaling, and neurotransmitter transmission. A previous lipidomics study investigating the links between chronic alcohol infusion and whole brain lipid profile, demonstrated that specific lipid categories, mainly PS, PC and PE, appeared to be related to neuro-pathology (Wang et al., 2019). To further identify the potential metabolic biomarkers of BA-ADP, machine learning was used and nine metabolites ((Cholic Acid, PC (16:0/18:2(9Z,12Z)), Allolithocholic acid, Sulfolithocholylglycine, N-[(3a,5b,7a)-3-hydroxy-24-oxo-7-(sulfooxy) cholan-24-yl]-Glycine, Cyclopassifloic acid E, MG(0:0/22:1(13Z)/0:0), Deoxycholic acid 3-glucuronide, 2,4-Dihydroxyacetophenone 5-sulfate) were identified. The AUC of these metabolite biomarkers was 0.7719, thus indicating an acceptable correlation using metabolite biomarkers and an outstanding correlation using protein biomarkers.

Of the nine differential metabolites identified in this study, there were several different species of bile acids, including cholic acid, allolithocholic acid, and deoxycholic acid 3-glucuronide. Bile

3 https://www.kegg.jp/kegg/compound/

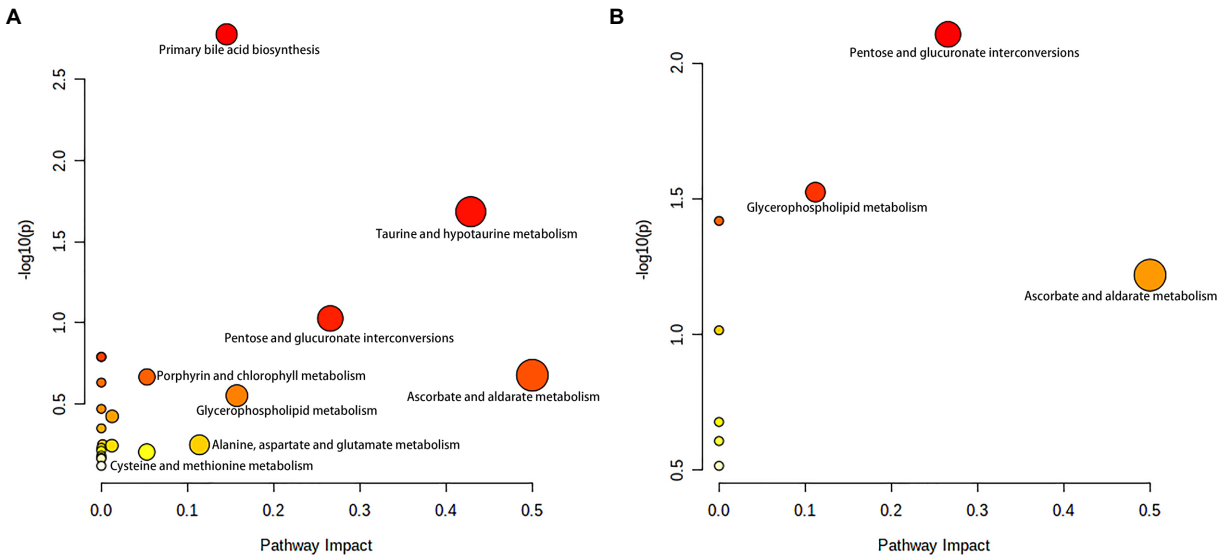

FIGURE 6
Metabolite pathway changes identified using MetaboAnalyst 5.0. Pathway analysis of the differential plasma metabolites between NBA-ADP vs. HC **(A)**, and BA-ADP vs. NBA-ADP **(B)**. The y axis shows the *p*-values and the x axis, representing pathway impact values; node color is based on its *p*-value and node size reflects the pathway impact values.

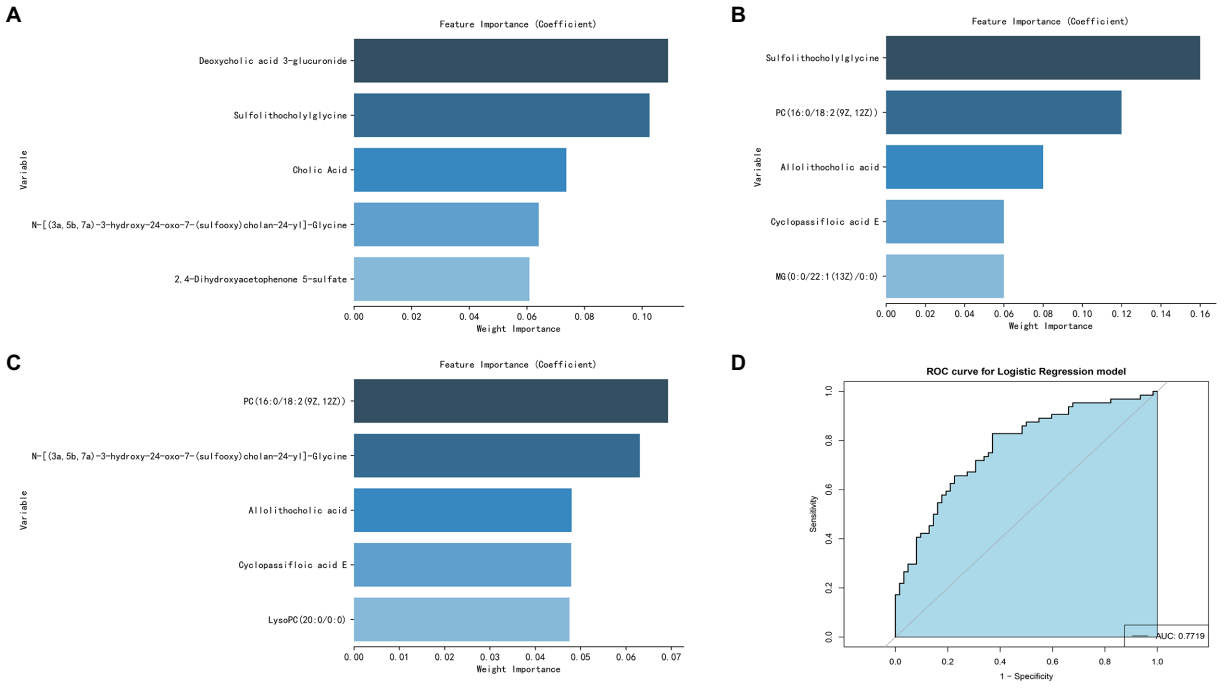

FIGURE 7
Screening of potential plasma metabolite biomarkers of alcohol-dependent patients with brain atrophy. The nine most important metabolites selected by Naive Bayes **(A)**, AdaBoost **(B)**, and Random Forest **(C)**. The AUC value of the ROC curve of potential plasma metabolite biomarkers for distinguishing BA-ADP patients from NBA-ADP **(D)**.

acids readily cross the blood–brain barrier and their receptors are expressed in central tissues, suggesting that they may have important functional roles (Romanazzi et al., 2021). The bile acid signaling pathway plays an extremely important role in diseases and is a target for drug intervention. Drugs related to bile acids include chenodeoxycholic acid and its derivatives, ursodeoxycholic

acid and its derivatives, bile acid sequestrants (such as cholestyramine), and apical sodium-dependent bile acid transporter (ASBT) inhibitors. In the nervous system, ASBT-mediated bile acid reabsorption significantly increases the level of bile acid in the serum and brain tissue, reduces the acidity of the intestinal cavity, increases the pH of the intestine, and promotes the conversion of intestinal ammonium into ammonia, thus resulting in abnormally increased levels of neurotoxic ammonia and cytotoxic bile acid in the blood and brain. Previous studies have confirmed that changes in bile acid occur in patients who progress from cognitive impairment to Alzheimer's disease, and the relationship between this change and cognitive decline is well documented. In addition, our study identified two metabolites related to bile acids. The expression of these two-acyl glycine and bile acid-glycine conjugates varied significantly between the BA-ADP and NBA-ADP group. Therefore, we assumed that bile acids may strongly associated with alcohol-related brain atrophy. And additional targeted absolute quantitative analyze of the bile acid spectrum in future studies may be helpful.

Interestingly, another class of potential metabolic biomarkers here we identified are lipid metabolites. It is widely documented that the homeostasis of lipid metabolism plays a significant role in the central nervous system. Many lipidomic-based studies have reported the relationship between the dysregulation of specific lipids and pathological conditions, including diabetes, Alzheimer's disease, hypertension, and cancer. It has been reported that long-term alcohol exposure significantly modifies the serum lipid profile, especially the metabolic pathways involving glycerophospholipid, sphingolipid and glycerolipids. Alcohol exposure can dramatically influence the lipidome of both the prefrontal cortex and striatum, thus leading to alcohol-related neurotoxicity and neuroplasticity. In the present study, by applying metabolomics analysis, we found that some glycerophospholipid (GP) metabolites, such as PC(P-16:0/18:2(9Z,12Z)), were significantly altered in alcohol-dependent patients with brain atrophy. GPs are the main components of the membrane structure. Different cell types, organelles, and inner/outer membranes in mammalian mitochondria, are known to have distinct glycerophospholipid compositions; these differences relate to the specific biological functions of these structures (Klaming et al., 2019). As GPs provide neural membranes with stability, fluidity and permeability, they are necessary for the normal biological function of integral membrane proteins, receptors, and ion-channels. Our present results suggest that chronic alcohol exposure may lead to brain atrophy and affect brain functionality by altering the composition of GPs. Alterations of the GP composition in neural membranes could therefore be related to neurological disorders. In addition, we found that some glycerolipids, such as MG(0:0/22:1(13Z)/0:0), were significantly altered in alcohol-dependent patients with brain atrophy. Further research now needs to investigate the key metabolic enzymes that mediate alcohol-induced dysfunction of lipidome profiling in the brain.

Based on the identified metabolites, we further identified two significantly altered metabolic pathways (primary bile acid biosynthesis, and taurine and hypotaurine metabolism) that were most closely related to alcohol dependence irrespective of whether brain atrophy was involved or not. As endogenous signaling molecules, bile acids are synthesized in the liver and secreted into the gastrointestinal tract for postprandial nutrient absorption and to control the overgrowth of microbial growth. In addition, gut microbes metabolize bile acids and in doing so, determine the composition of the circulating bile acids, thus regulating host metabolism (Chiang and Ferrell, 2019). Patients with acute alcohol intake exhibit increased serum levels of bile acids and cholestatic liver injury; alcohol intake also increases bile acid pool size and reduces bile acid flow and fecal excretion (Donepudi et al., 2018). Wang et al. found that the abundance of firmicutes and clostridium was notably increased in alcohol-addicted mice, and the levels of secondary bile acids produced by firmicutes had increased (Wang et al., 2018). In conclusion, compared with healthy individuals, there are certain changes in the expression levels of bile acid metabolites (including tauroursodeoxycholic acid, cholic acid and allocholic acid) in alcohol-addicted patients. The analysis showed that regulation of bile acid biosynthesis is likely to contribute to the occurrence and development of alcohol-related diseases.

As for taurine and hypotaurine metabolism, taurine has already been shown to protect mice with alcoholic liver injury by reducing hepatic oxidative stress and interrupting the alcohol-induced renal inflammatory cycle (Tang et al., 2019). It is well known that taurine can also prevent and repair liver damage and balance liver lipid metabolism indicators in a mouse model of alcoholic liver disease. The mechanism involved in this protection may be related to the regulation of related enzymes and transcriptional regulators involved in lipid metabolism (Latchoumycandane et al., 2014). In another study, Xia et al. suggested that the metabolic pathways of ascorbic acid, taurine, and hypotaurine, may play an active role in the protection against Antrodin A secreted by *Antrodia camphorata* and thus protect against alcoholic liver injury (Yi et al., 2021). Our present study also found that the BA-ADP group showed an elevation in taurine, compared with the NBA-ADP group. Thus, those imply that the metabolic pathways of taurine and hypotaurine may be also associated with alcohol-related brain atrophy.

To further identify the potential pathways that may be associated with alcohol-related brain atrophy, the KEGG pathway analysis using difference metabolites between BA-ADP and NBA-ADP was performed. We found that glycerophospholipid metabolism, along with pentose and glucuronate interconversions, were significantly associated with alcohol-related brain atrophy. This finding is in line with previous studies that demonstrated the impact of glycerophospholipid metabolism on neurodegenerative changes (Frisardi et al., 2011). Previous studies have shown that the degradation products of glycerophospholipids have pro-inflammatory effects and that their production is often accompanied by the activation of astrocytes and microglia and the release of inflammatory cytokines; these changes lead to oxidative

stress and neuroinflammation (Bonelli et al., 2020). Changes in glycerophospholipid metabolism have also been shown to lead to changes in cell membrane permeability and ion homeostasis, thus leading to oxidative stress and neurodegenerative changes (Fuller and Futerman, 2018). Increased small vascular disease load was linked to changes in glycerophospholipid metabolism, as seen by increased white matter hyperintensity volume, decreased mean diffusivity normalized peak height, increased brain atrophy, and decreased cognition (Harshfield et al., 2022). Previous report has found that pentose and glucuronate interconversions is associated with the cognitive impairment in Alzheimer disease (He et al., 2020). In the present study, we report, for the first time, that pentose and glucuronate interconversions are also associated with alcohol-related brain atrophy. However, the precise role of these two regulatory metabolic pathways in the pathophysiological mechanism of alcohol dependence-related brain atrophy requires further investigation.

Limitations

This study has several limitations that need to be considered. First, the metabolomic analysis performed in the present study did not provide absolute quantification. If this model is to be applied clinically, more rigorous quantification and extensive validation of metabolites would be needed. Targeted metabolomics could be used to validate these specific plasma metabolomic biomarkers. Second, the sample size of this study was rather small, particularly in proteomic analysis; thus, additional patients are required for future analysis. Third, only XGBoost, RF, and AdaBoost Classifier were used to screen for potential biomarkers. Other machine learning methods, such as Support Vector Machine and Boruta could be used in future analyses. Fourth, due to the complex genetic and microenvironmental backgrounds of our patients, other biofluids, such as urine, serum, and cerebrospinal fluid, could also be used to identify additional novel biomarkers. This will provide a more to comprehensive understanding of the pathogenesis of brain atrophy in alcohol-dependent patients. Last, we failed to reveal any differences in cognitive tests between control patients and those identified as having brain atrophy in this study, more detailed cognitive tests may be help in future research.

Conclusion

This was the first attempt to conduct a metabolomic analysis of plasma samples from healthy control groups and alcohol-dependent patients. Our data showed that patients with alcohol-dependent brain atrophy had distinct metabolic profiles compared with healthy controls and alcohol-dependent patients who do not have brain atrophy. Furthermore, bioinformatic analysis suggested that alterations in the metabolome may be involved in disease pathogenesis. Although further research is needed, our results offer useful diagnostic and therapeutic clues for the management of alcohol-dependent patients with brain atrophy.

Data availability statement

The original contributions presented in the study are included in the article/Results, and further inquiries can be directed to the corresponding author.

Ethics statement

The studies involving human participants were reviewed and approved by The Ethics Committee of the Hunan Brain Hospital (Reference: 2016121). The patients/participants provided their written informed consent to participate in this study.

Author contributions

SZ and XHZ designed the study. XC, CH, ZL, XW, XL, QL, XZ, YG, HX, and TX managed the data collection. SZ, JH, ZZ, and XHZ undertook the statistical analysis. ZZ wrote the first draft of the manuscript. All authors contributed to the article and approved the submitted version.

Funding

This work was financially supported by the National Key Research and Development Program of China (No. 2018YFC1314401), Hunan Provincial Natural Science Foundation of China (Nos. 2018JJ3284, 2020JJ4803, 2022JJ2540, 2022JJ2615, 2021JJ70013, 2021JJ70089, and 2022JJ40728), The Scientific Research Project of the Hunan Health Commission (Nos. A202303096949, 20200620, and 202103092373), Special Project on Science and Technology Development and First-class Discipline Construction of Clinical Medicine Discipline of Hunan University of Chinese Medicine in the 13th Five-Year Plan Period (2091007), and Key Clinical Specialty Construction Project of the Hunan Health Commission (Improvement of Diagnosis and Treatment Ability of Severe Psychiatric Diseases in Hunan Province).

Conflict of interest

The authors declare that the research was conducted in the absence of any commercial or financial relationships that could be construed as a potential conflict of interest.

Publisher's note

References

Angebrandt, A., Abulseoud, O. A., Kisner, M., Diazgranados, N., Momenan, R., Yang, Y., et al. (2022). Dose-dependent relationship between social drinking and brain aging. *Neurobiol. Aging* 111, 71–81. doi: 10.1016/j.neurobiolaging.2021.11.008

Battle, D. E. (2013). Diagnostic and statistical manual of mental disorders (DSM). *Codas* 25, 191–192. doi: 10.1590/s2317-17822013000200017

Bonelli, R., Woods, S. M., Ansell, B. R. E., Heeren, T. F. C., Egan, C. A., Khan, K. N., et al. (2020). Systemic lipid dysregulation is a risk factor for macular neurodegenerative disease. *Sci. Rep.* 10:12165. doi: 10.1038/s41598-020-69164-y

Chiang, J. Y. L., and Ferrell, J. M. (2019). Bile acids as metabolic regulators and nutrient sensors. *Annu. Rev. Nutr.* 39, 175–200. doi: 10.1146/annurev-nutr-082018-124344

Daviet, R., Aydogan, G., Jagannathan, K., Spilka, N., Koellinger, P. D., Kranzler, H. R., et al. (2022). Associations between alcohol consumption and gray and white matter volumes in the UK Biobank. *Nat. Commun.* 13:1175. doi: 10.1038/s41467-022-28735-5

de la Monte, S. M., and Kril, J. J. (2014). Human alcohol-related neuropathology. *Acta Neuropathol.* 127, 71–90. doi: 10.1007/s00401-013-1233-3

Deo, R. C. (2015). Machine learning in medicine. *Circulation* 132, 1920–1930. doi: 10.1161/CIRCULATIONAHA.115.001593

Donepudi, A. C., Ferrell, J. M., Boehme, S., Choi, H. S., and Chiang, J. Y. L. (2018). Deficiency of cholesterol 7α-hydroxylase in bile acid synthesis exacerbates alcohol-induced liver injury in mice. *Hepatol. Commun.* 2, 99–112. doi: 10.1002/hep4.1129

Frisardi, V., Panza, F., Seripa, D., Farooqui, T., and Farooqui, A. A. (2011). Glycerophospholipids and glycerophospholipid-derived lipid mediators: a complex meshwork in Alzheimer's disease pathology. *Prog. Lipid Res.* 50, 313–330. doi: 10.1016/j.plipres.2011.06.001

Fuller, M., and Futerman, A. H. (2018). The brain lipidome in neurodegenerative lysosomal storage disorders. *Biochem. Biophys. Res. Commun.* 504, 623–628. doi: 10.1016/j.bbrc.2018.03.042

Godin, J., Armstrong, J. J., Wallace, L., Rockwood, K., and Andrew, M. K. (2019). The impact of frailty and cognitive impairment on quality of life: employment and social context matter. *Int. Psychogeriatr.* 31, 789–797. doi: 10.1017/S1041610218001710

Harshfield, E. L., Sands, C. J., Tuladhar, A. M., de Leeuw, F. E., Lewis, M. R., and Markus, H. S. (2022). Metabolomic profiling in small vessel disease identifies multiple associations with disease severity. *Brain* 145, 2461–2471. doi: 10.1093/brain/awac041

He, R., Liu, J., Huang, C., Liu, J., Cui, H., and Zhao, B. (2020). A urinary metabolomics analysis based on UPLC-MS and effects of Moxibustion in APP/PS1 mice. *Curr. Alzheimer Res.* 17, 753–765. doi: 10.2174/1567205017666201109091759

Holthuis, J., and Menon, A. K. (2014). Lipid landscapes and pipelines in membrane homeostasis. *Nature* 510, 48–57. doi: 10.1038/nature13474

Klaming, R., Spadoni, A. D., Veltman, D. J., and Simmons, A. N. (2019). Expansion of hippocampal and amygdala shape in posttraumatic stress and early life stress. *NeuroImage Clin.* 24:101982. doi: 10.1016/j.nicl.2019.101982

Kranzler, H. R., and Soyka, M. (2018). Diagnosis and pharmacotherapy of alcohol use disorder: a review. *JAMA* 320, 815–824. doi: 10.1001/jama.2018.11406

Latchoumycandane, C., Nagy, L. E., and McIntyre, T. M. (2014). Chronic ethanol ingestion induces oxidative kidney injury through taurine-inhibitable inflammation. *Free Radic. Biol. Med.* 69, 403–416. doi: 10.1016/j.freeradbiomed.2014.01.001

Liebal, U. W., Phan, A. N. T., Sudhakar, M., Raman, K., and Blank, L. M. (2020). Machine learning applications for mass spectrometry-based metabolomics. *Meta* 10:243. doi: 10.3390/metabo10060243

Liu, C., Tian, X., Ling, Y., Xu, J., and Zhou, X. (2020). Alterations of metabolites in the frontal cortex and amygdala are associated with cognitive impairment in alcohol dependent patients with aggressive behavior. *Front. Psychol.* 11:694. doi: 10.3389/fpsyt.2020.00694

Mirza, B., Wang, W., Wang, J., Choi, H., Chung, N. C., and Ping, P. (2019). Machine learning and integrative analysis of biomedical big data. *Genes (Basel)* 10:87. doi: 10.3390/genes10020087

Mittal, A., and Dabur, R. (2015). Detection of new human metabolic urinary markers in chronic alcoholism and their reversal by aqueous extract of Tinospora cordifolia stem. *Alcohol Alcohol.* 50, 271–281. doi: 10.1093/alcalc/agv012

Nicora, G., Vitali, F., Dagliati, A., Geifman, N., and Bellazzi, R. (2020). Integrated multi-omics analyses in oncology: a review of machine learning methods and tools. *Front. Oncol.* 10:1030. doi: 10.3389/fonc.2020.01030

Pasquier, F., Leys, D., Weerts, J. G., Mounier-Vehier, F., Barkhof, F., and Scheltens, P. (1996). Inter- and intraobserver reproducibility of cerebral atrophy assessment on MRI scans with hemispheric infarcts. *Eur. Neurol.* 36, 268–272.

Picard, M., Scott-Boyer, M. P., Bodein, A., Périn, O., and Droit, A. (2021). Integration strategies of multi-omics data for machine learning analysis. *Comput. Struct. Biotechnol. J.* 19, 3735–3746. doi: 10.1016/j.csbj.2021.06.030

Rehm, J., Gmel, G. E. Sr., Gmel, G., Hasan, O. S. M., Imtiaz, S., Popova, S., et al. (2017). The relationship between different dimensions of alcohol use and the burden of disease-an update. *Addiction* 112, 968–1001. doi: 10.1111/add.13757

Ribbenstedt, A., Ziarrusta, H., and Benskin, J. P. (2018). Development, characterization and comparisons of targeted and non-targeted metabolomics methods. *PLoS One* 13:e0207082. doi: 10.1371/journal.pone.0207082

Romanazzi, T., Zanella, D., Cheng, M. H., Smith, B., Carter, A. M., Galli, A., et al. (2021). Bile acids gate dopamine transporter mediated currents. *Front. Chem.* 9:753990. doi: 10.3389/fchem.2021.753990

Schrimpe-Rutledge, A. C., Codreanu, S. G., Sherrod, S. D., and McLean, J. A. (2016). Untargeted metabolomics strategies-challenges and emerging directions. *J. Am. Soc. Mass Spectrom.* 27, 1897–1905. doi: 10.1007/s13361-016-1469-y

Sutherland, G. T., Sheedy, D., and Kril, J. J. (2014). Neuropathology of alcoholism. *Handb. Clin. Neurol.* 125, 603–615. doi: 10.1016/B978-0-444-62619-6.00035-5

Tang, R., Yang, Q., Lin, S., Feng, Y., Yang, J., Lv, Q., et al. (2019). Preventive or curative Administration of Taurine Regulates Lipid Metabolism in the liver of rats with alcoholic liver disease. *Adv. Exp. Med. Biol.* 1155, 119–131. doi: 10.1007/978-981-13-8023-5_11

Van Deijk, A. L. F., Camargo, N., Timmerman, J., Heistek, T., Brouwers, J. F., Mogavero, F., et al. (2017). Astrocyte lipid metabolism is critical for synapse development and function in vivo. *Glia* 65, 670–682. doi: 10.1002/glia.23120

Vuckovic, D. (2018). Improving metabolome coverage and data quality: advancing metabolomics and lipidomics for biomarker discovery. *Chem. Commun. (Camb.)* 54, 6728–6749. doi: 10.1039/C8CC02592D

Wang, L., Li, M., Bu, Q., Li, H., Xu, W., Liu, C., et al. (2019). Chronic alcohol causes alteration of lipidome profiling in brain. *Toxicol. Lett.* 313, 19–29. doi: 10.1016/j.toxlet.2019.05.010

Wang, G., Liu, Q., Guo, L., Zeng, H., Ding, C., Zhang, W., et al. (2018). Gut microbiota and relevant metabolites analysis in alcohol dependent mice. *Front. Microbiol.* 9:1874. doi: 10.3389/fmicb.2018.01874

Yi, Z., Liu, X., Liang, L., Wang, G., Xiong, Z., Zhang, H., et al. (2021). Antrodin a from Antrodia camphorata modulates the gut microbiome and liver metabolome in mice exposed to acute alcohol intake. *Food Funct.* 12, 2925–2937. doi: 10.1039/D0FO03345F

Zahr, N. M., Kaufman, K. L., and Harper, C. G. (2011). Clinical and pathological features of alcohol-related brain damage. *Nat. Rev. Neurol.* 7, 284–294. doi: 10.1038/nrneurol.2011.42

Zhang, Z., Yi, P., Yang, J., Huang, J., Xu, P., Hu, M., et al. (2020). Integrated network pharmacology analysis and serum metabolomics to reveal the cognitive improvement effect of Bushen Tiansui formula on Alzheimer's disease. *J. Ethnopharmacol.* 249:112371. doi: 10.1016/j.jep.2019.112371

Zhu, X., Huang, J., Huang, S., Wen, Y., Lan, X., Wang, X., et al. (2021). Combining metabolomics and interpretable machine learning to reveal plasma metabolic profiling and biological correlates of alcohol-dependent inpatients: what about tryptophan metabolism regulation? *Front. Mol. Biosci.* 8:760669. doi: 10.3389/fmolb.2021.760669

frontiers | Frontiers in Molecular Neuroscience

TYPE Review
PUBLISHED 10 January 2023
DOI 10.3389/fnmol.2022.1091498

OPEN ACCESS

EDITED BY
Arianna Bellucci,
University of Brescia,
Italy

REVIEWED BY
Rong Jin,
Penn State Milton S. Hershey Medical Center, United States
Minshu Li,
Tianjin Medical University General Hospital, China

CORRESPONDENCE
Jingjing Lu
✉ lujingjing666@gmail.com
Xingquan Zhao
✉ zxq@vip.163.com

SPECIALTY SECTION
This article was submitted to Brain Disease Mechanisms, a section of the journal Frontiers in Molecular Neuroscience

RECEIVED 07 November 2022
ACCEPTED 12 December 2022
PUBLISHED 10 January 2023

CITATION
Wang J, Bian L, Du Y, Wang D, Jiang R, Lu J and Zhao X (2023) The roles of chemokines following intracerebral hemorrhage in animal models and humans. *Front. Mol. Neurosci.* 15:1091498. doi: 10.3389/fnmol.2022.1091498

The roles of chemokines following intracerebral hemorrhage in animal models and humans

Jinjin Wang[1,2], Liheng Bian[1,2], Yang Du[1,2], Dandan Wang[1,2], Ruixuan Jiang[1,2], Jingjing Lu[1,2]* and Xingquan Zhao[1,2,3,4]*

[1]Department of Neurology, Beijing Tiantan Hospital, Capital Medical University, Beijing, China, [2]China National Clinical Research Center for Neurological Diseases, Beijing, China, [3]Research Unit of Artificial Intelligence in Cerebrovascular Disease, Chinese Academy of Medical Sciences, Beijing, China, [4]Beijing Institute of Brain Disorders, Collaborative Innovation Center for Brain Disorders, Capital Medical University, Beijing, China

Intracerebral hemorrhage (ICH) is one common yet devastating stroke subtype, imposing considerable burdens on families and society. Current guidelines are limited to symptomatic treatments after ICH, and the death rate remains significant in the acute stage. Thus, it is crucial to promote research to develop new targets on brain injury after ICH. In response to hematoma formation, amounts of chemokines are released in the brain, triggering the infiltration of resident immune cells in the brain and the chemotaxis of peripheral immune cells *via* the broken blood–brain barrier. During the past decades, mounting studies have focused on the roles of chemokines and their receptors in ICH injury. This review summarizes the latest advances in the study of chemokine functions in the ICH. First, we provide an overview of ICH epidemiology and underlying injury mechanisms in the pathogenesis of ICH. Second, we introduce the biology of chemokines and their receptors in brief. Third, we outline the roles of chemokines in ICH according to subgroups, including CCL2, CCL3, CCL5, CCL12, CCL17, CXCL8, CXCL12, and CX3CL1. Finally, we summarize current drug usage targeting chemokines in ICH and other cardio-cerebrovascular diseases. This review discusses the expressions of these chemokines and receptors under normal or hemorrhagic conditions and cell-specific sources. Above all, we highlight the related data of these chemokines in the progression and outcomes of the ICH disease in preclinical and clinical studies and point to therapeutic opportunities targeting chemokines productions and interactions in treating ICH, such as accelerating hematoma absorption and alleviating brain edema.

KEYWORDS

chemokines, receptors, roles, intracerebral hemorrhage, preclinical study, clinical study

1. Introduction

1.1. Epidemiology of intracerebral hemorrhage

Intracerebral hemorrhage (ICH), or hemorrhagic stroke, is one common yet disproportionately deadly stroke subtype, with a significant death rate and morbidity among survivors (Collaborators, 2021; O'Carroll et al., 2021). Spontaneous ICH is defined as bleeding into the brain parenchyma due to the rupture of cerebral blood vessels resulting from hypertension or cerebral amyloid angiopathy (CAA). Given the data from the Global Burden of Disease Study 2019, ~3.41 million patients were first diagnosed with hemorrhagic strokes worldwide each year, whereas the absolute number of deaths was 2.89 million caused by acute compression and related complications after ICH (Collaborators, 2021). Nowadays, there is a total of 20.66 million patients with current ICH worldwide, placing substantial burdens on families and society for post-stroke care and rehabilitation.

During the past decades, the rapid advance has been achieved in new therapeutic strategies, thereby contributing to prognosis improvements, such as acute blood pressure management and minimally invasive surgery for ICH (Xue and Yong, 2020; Greenberg et al., 2022). However, the death rate remains notably high at the ultra-early stage of ICH. Thus, it is crucial to clarify the etiology, pathogenesis, and underlying injury mechanisms for establishing reliable prognostic biomarkers in predicting prognosis, prompting specific therapies in managing ICH, and reducing the devastating effects of ICH eventually.

1.2. Injury mechanisms of intracerebral hemorrhage

Intracerebral hemorrhage is a complex pathophysiology marked by primary and secondary injury. Initial bleeding leads to hematoma formation, mass effects, and further high intracranial pressure, contributing to compressed brain tissue, broken blood flow, and even cerebral hernia. Secondary injury results from a cascade of events initiated by the hematoma and corresponding body responses, such as hemostasis, inflammation, and erythrocyte lysis (Keep et al., 2012).

1.2.1. Inflammatory and immune cells

Mounting evidence has demonstrated that ICH is a systemic disease affecting more than the brain (Saand et al., 2019). Once ICH occurs, systemic inflammation and immune responses are rapidly activated and exert an essential role in stroke-related injury and recovery, characterized by resident immune cells in the central nervous system (CNS) and infiltrated cells in the peripheric immune system. Microglia is recognized as the first immune cell activated by brain injury within a few minutes of ICH onset and acts as the primary source of inflammatory factors at the early stage (Wang, 2010). The role of microglia following ICH is complex (Liu et al., 2021). Contrarily, microglia also play a neuroprotective effect on anti-inflammatory and neural repair actions by releasing anti-inflammatory cytokines, extracellular matrix proteins, and other substances (Zlokovic, 2008). Astrocyte intertwines with blood vessels and synapses, affecting neuronal function and blood flow after ICH (Scimemi, 2018). A wide variety of molecules are secreted by astrocytes, including proinflammatory cytokines (IL-6 and IL-1β), anti-inflammatory cytokines (IL-10), and chemokines (CCL2, CXCL1, CXCL10, and CXCL12), through which controlling microglia differentiation and macrophage activation (Mantovani et al., 2004; McKimmie and Graham, 2010; Allaman et al., 2011; Nash et al., 2011; Lan et al., 2017).

Human data have consistently suggested that bleeding triggers a rapid increase of peripheral leukocyte counts that mainly infiltrates the brain parenchyma through the damaged blood–brain barrier (BBB), dependent on cytokines and chemokines. Previous studies reported that neutrophil was the first infiltrating immune cell detected in the perihematomal region at 5–8 h and remained at a high level at 12 days of ICH onset (Mackenzie and Clayton, 1999; Shtaya et al., 2019). However, Li and his colleagues recently identified the swift arrival of natural killer (NK) cells to the perihematomal regions within 12 h of ICH onset, even earlier than other mobilized neutrophils and T cells (Li et al., 2020). Lymphocytes were mainly observed in the perihematomal brain with lower concentrations on days 1–3, with moderate accumulation later (Mackenzie and Clayton, 1999; Shtaya et al., 2019). For monocyte/macrophage, it was found to migrate into the injury site within 12 h and peaked at days 3–5 post-ICH (Hammond et al., 2012; Bonsack et al., 2016). Increased leukocyte counts and related indexes are associated with disease severity, in-hospital death, and poor outcomes in hemorrhagic strokes (Du et al., 2022; Wang et al., 2022).

1.2.2. Inflammatory and immune factors

In the inner responses of post-stroke, inflammatory and immune mediators play a major role in the acute injury and ensuing recovery, mainly including cytokines and chemokines. Cytokines are small proteins secreted by various cell types, especially activated lymphocytes and macrophages. It regulates the balance between cellular and humoral immunity (Zhu et al., 2019). Like cytokines, chemokines also belong to a family of small proteins constitutively produced by leukocytes and tissue cells or induced after events. However, chemokines are much smaller than cytokines and exert their effects *via* heptahelical G-protein coupled receptors (GPCRs), typical for leukocyte attractants (Baggiolini, 2001). Chemokines contain roughly 70–130 amino acids (Baggiolini et al., 1997). The function of chemokines in ischemic stroke has been well documented, but their role in hemorrhagic stroke has not been completely understood. Specially, we examined potential cellular and molecular mediators from animal and human data in ICH progression and prognosis. This review summarizes the emerging evidence describing the chemokines and their receptors following ICH in preclinical and clinical studies.

2. Biology of chemokines and their receptors

Chemokines were first identified in the late 1980s. In the early 1990s, IL-8 (CXCL8) was reported to be involved in recruiting neutrophils in acute inflammation models (Matsushima, 2000; Zlotnik and Yoshie, 2012). According to the positions of critical cysteine residues, chemokines are subdivided into C, CC, CXC, and CX3C subgroups. CXC, CC, and CX3C chemokines have four conserved cysteines, while C chemokines have only two cysteines. CXC and CX3C chemokines are distinguished by the presence of one (CXC) or three (CX3C) amino acids between the first and second cysteines, but the first two cysteines of CC chemokines are adjacent (Bajetto et al., 2001). Chemokines activate several different signal transduction pathways *via* binding with their specific or shared GPCRs. Most receptors are also grouped into four subfamilies according to their major chemokine ligands, including the CXCR subfamily, CCR subfamily, XCR subfamily, and CX3CR subfamily, except for several atypical receptors (Zlotnik and Yoshie, 2012).

The chemokine family is classified as inflammatory, homeostatic, and dual-functional factors according to their chemotaxis to leukocytes or/and subsets of lymphocytes or dendritic cells (Zlotnik and Yoshie, 2012). Chemokines participate in the inflammation, immune responses, and immune system establishment. In addition, they regulate angiogenesis in inflammation, neoplasia, reproductive systems, hematopoietic systems, and organ development (Matsushima, 2000).

All microglial cells, astrocytes, and neurons can secrete chemokines. Under physiological conditions, homeostatic chemokines can originate from the vasculature of blood-brain barrier (BBB) to participate in the development of CNS, regulating the entry of leukocytes for immunosurveillance, such as CXCL12, CCL19, CCL20, and CCL21 (Chen K. et al., 2018). Unlike homeostatic chemokines, inflammatory chemokines are expressed by numerous cell types at almost any tissue location and remain low in the CNS. However, their expressions increase significantly on circulating leukocytes and other cell types activated by acute brain injury (Yao and Tsirka, 2012b; Le Thuc et al., 2015), allowing for recruiting and positioning immune cells in the damaged tissues (Yao and Tsirka, 2012b; Le Thuc et al., 2015; Kothur et al., 2016; Chen C. et al., 2018; Trettel et al., 2020). In the procedure of ICH, specific chemokines and their receptors play an essential part in secondary injury and neurological recovery (Table 1). Next, we will discuss their roles following ICH according to their subfamilies and summarize the data in preclinical and clinical studies (Tables 2, 3).

3. Chemokines and their receptors in intracerebral hemorrhage

3.1. CC chemokine family

The members of the CC chemokine family usually relate to the infiltration of monocytes, basophils, eosinophils, and T lymphocytes but have little effect on neutrophils (Bajetto et al., 2001). The most studied CC chemokines associated with ICH were CCL2, CCL3, CCL4, CCL5, CCL17, and CCL20.

3.1.1. CCL2

CCL2, also known as monocyte chemoattractant protein-1 (MCP-1), is the first human CC chemokine on chromosome 17 (chr.17, q11.2). Human CCL2 consists of 76 amino acids, and the molecular weight is 13 kDa (Van Coillie et al., 1999). Many types of cells can produce CCL2, such as monocytes/macrophages, endothelial cells, fibroblasts, epithelial cells, smooth muscle cells, and mesangial cells. In the CNS, CCL2 is predominantly secreted by astrocytes, resident microglial cells, neurons, and endothelial cells. The monocyte/macrophage has been found as the primary source (Deshmane et al., 2009). CCL2 exerts effects by bonding its cognate receptor CCR2, although it can bind to CCR4 expressed on Th2 lymphocytes (Zhang et al., 2006). Unlike CCL2, CCR2 is relatively restricted to certain types of cells according to the forms of CCR2, including CCR2A and CCR2B. In the peripheral system, CCR2A is the major isoform expressed by mononuclear cells and vascular smooth muscle cells, whereas CCR2B is predominantly expressed by monocytes and activated NK cells (Deshmane et al., 2009; Chu et al., 2014). In the CNS, CCR2 expresses on the surfaces of microglia, astrocyte, neurons, and brain microvascular endothelial cells (Semple et al., 2010).

CCL2/CCR2 axis mainly induces the egression and chemotaxis of monocyte/macrophage (Bajetto et al., 2001), shaping macrophage polarization to participate in the inflammation process (Sierra-Filardi et al., 2014). In addition, the network is vital in regulating neutrophils, T lymphocytes, and NK cells (van Helden et al., 2012; Vasanthakumar et al., 2020; Shibuya et al., 2022). The production of CCL2 is constitutive in specific cells, but its expression is upregulated by proinflammatory cytokines such as IL-1β and tumor necrosis factor (TNF)-α, growth factors, reactive oxygen species (ROS), and oxidized low-density lipoproteins (oxLDLs; Barlic and Murphy, 2007; Hinojosa et al., 2011; Gruber et al., 2015; Bianconi et al., 2018; Akhter et al., 2021). The upregulated CCL2 recruits immune cells into inflamed tissues by binding to CCR2. Recent studies have also reported the role of CCL2/CCR2 in promoting angiogenesis and regeneration (Pan et al., 2020). In cerebral ischemic stroke, this axis is involved in neuroinflammation and contributes to brain injury in the acute stage (Cisbani et al., 2018), but also promotes the migration of neuroblasts and neurological recovery (Pedragosa et al., 2020; Geng et al., 2022).

CCL2 has been studied widely in ICH. The functional network map indicates that CCL2 is a key molecule in the pathogenesis of the innate immune response and regulation of the immune effector process after ICH (Xu et al., 2021). CCL2 is produced by astrocytes, microvascular endothelial cells, microglia, and neurons, whereas CCR2 is detected on the surface of astrocytes and brain microvascular endothelial cells (BMECs; Guo et al., 2020). In the autologous blood models of the mouse, CCL2 was detected elevated at day 1, continuously higher up to 3 days, and

TABLE 1 Summary of chemokines and their receptor.

Subfamily	Main functions	Receptor	Cell expression	Chemokine ligand(s)	Reference
C C chemokine	Regulate the infiltration of monocytes, basophils, eosinophils, and T lymphocytes but have little effect on neutrophils.	CCR1	Monocytes, macrophages, neutrophils, T cells, basophils, microglia, neurons, astrocytes	CCL3, CCL5, CCL7, CCL8, CCL13, CCL14, CCL15, CCL16, CCL23	White et al. (2013)
		CCR2	Monocytes/macrophages, endothelial cells, leukocytes, smooth muscle cells, basophils, DC, natural killer cells, activated T lymphocytes, microglia, astrocyte, neurons, brain microvascular endothelial cells	CCL2, CCL7, CCL8, CCL12, CCL13, CCL16	Chu et al. (2014) and França et al. (2017)
		CCR3	Eosinophil, basophils, mast cells, vascular endothelial cells, astrocytes, microglia, oligodendrocytes	CCL5, CCL11, CCL13, CCL24	Pease and Horuk (2014) and Huber et al. (2018)
		CCR4	T cells, astrocytes, microglia, neurons	CCL17, CCL22	Scheu et al. (2017)
		CCR5	Resting memory/effector T-lymphocytes, monocytes, macrophages, immature dendritic cells, astrocytes, microglia, neurons	CCL3, CCL5, CCL8	Blanpain et al. (2002)
		CCR6	Treg cells, Th17 cells	CCL20	Meitei et al. (2021)
		CCR7	B cells, mature DC, T cells, neurons	CCL19, CCL21	Liu et al. (2007) and Förster et al. (2008)
		CCR8	Th2 cells, Treg cells, Tconv cells, NK cells, thymocytes, endothelial cells, neurons	CCL1, CCL8, CCL18	Liu et al. (2007) and Moser (2022)
		CCR9	DC, neutrophils, lymphocytes, monocytes, macrophages, and vascular endothelial cells, neurons	CCL25	Liu et al. (2007) and Wu et al. (2021)
		CCR10	T cells, Langerhans cells, melanocytes, endothelial cells, microvascular endothelial cells, fibroblasts, neurons	CCL27, CCL28	Liu et al. (2007) and Xiong et al. (2012)
XC chemokine	Regulate DC-mediated cytotoxic immune response and the thymic establishment of self-tolerance and the generation of regulatory T cells	XCR1	DC subpopulation, $CD8^+$ cells, NK cells, B cells, $CD3^+$ T cells, $CD4^+$ T cells, neutrophils	XCL1, XCL2	Lei and Takahama (2012)

(Continued)

TABLE 1 (Continued)

Subfamily	Main functions	Receptor	Cell expression	Chemokine ligand(s)	Reference
CXC chemokine	Attract neutrophils, lymphocytes, and monocytes	CXCR1	Neutrophils, CD8 T cells, monocytes, NK cells, mast cells, fibroblasts, endothelial cells, SMCs, astrocytes, microglia, neurons, oligodendrocytes	CXCL1, CXCL2, CXCL3, CXCL4, CXCL6, CXCL8	Mamik and Ghorpade (2016) and Dhayni et al. (2022)
		CXCR2	Neutrophils, CD8 T cells, monocytes, NK cells, mast cells, fibroblasts, endothelial cells, SMCs, astrocytes, microglia, neurons, oligodendrocytes	CXCL1, CXCL2, CXCL3, CXCL4, CXCL5, CXCL6, CXCL7, CXCL8	Semple et al. (2010), Mamik and Ghorpade (2016) and Dhayni et al. (2022)
		CXCR4	Lymphocytes, endothelial, epithelial and hematopoietic stem cells, stromal fibroblasts, neurons, microglia, astrocytes, oligodendrocytes	CXCL12	Jiang et al. (2013) and Pozzobon et al. (2016)
		CXCR5	Mature B cells, subpopulations of $CD4^+$ T cells, DCs	CXCL13	Pan et al. (2022)
CX3C chemokine	Induce the chemotaxis of monocytes and cytotoxic T cells.	CX3CR1	Monocytes, NK cells, T cells, smooth muscle cells microglia, neurons, astrocytes	CX3CL1	Subbarayan et al. (2022)

Th, T helper; Treg cells, regulatory T cells; DC, dendritic cells; CD, cluster of differentiation; NK, natural kill; SMC, smooth muscle cells.

decreased at 7 days after ICH. Another study showed an elevation of CCL2 at 12 h after experimental ICH induced by collagenase (Hammond et al., 2014; Huang et al., 2022). CCL2/CCR2 system mediates inflammation after ICH. $CCR2^{-/-}$ mice exhibited decreased recruited monocytes and fewer motor deficits in the early ICH (Hammond et al., 2014). CCL2/CCR2 knockout could also inhibit the proliferation and cytotoxicity of microglial cells, reduce infiltration of monocytes in the brain, ameliorate neurological deficits, and improve brain edema (Hammond et al., 2014; Yang et al., 2016). Receptor-interacting protein kinase 3 (RIPK3), a key kinase in the necroptosis pathway, may interact with CCL2 to modulate inflammatory responses and RIPK3-dependent necroptosis (Huang et al., 2022). S1PR3 modulator CAY10444 also could alleviate early inflammation and exert neuroprotective effects *via* the S1P-CCL2-p-p38 MAPK pathway (Xu et al., 2021). The expression of CCL2 has also been found to contribute to BBB disruption *via* the p38 MAPK signaling pathway following ICH (Guo et al., 2020). Consequently, the administration of CCR2 inhibitor propagermanium (PG) effectively maintained the BBB integrity, reduced brain edema, and improved neurobehavioral functions. Moreover, the CCL2-CCR2 signaling pathway affects the progression and resolution of the hematoma. At early times, CCL2/CCR2 deficiency might decrease hematoma size but delay long-term recovery (Yao and Tsirka, 2012a). This may be associated with inflammation being a double-edged sword, with beneficial or detrimental effects depending on the timing and environment.

In human studies, a small-sample study showed that cerebrospinal fluid (CSF) CCL2 peaked early on days 1–2 and then decreased in patients with spontaneous intracerebral ventricular hemorrhage (IVH; Ziai et al., 2021). The serum concentration of CCL2 was found to increase on days 1–3 after onset and then dropped slightly on days 7–14 but elevated after 14 days (Li et al., 2012). CCL2 has been thought to be an indicator of early ICH severity. The analysis of human PHE tissue showed an elevated level of CCL2. A positive relationship was observed between elevated CCL2 expression and PHE volume (Guo et al., 2020; Ziai et al., 2021). However, this association was not found in a cohort of 25 patients, which might be explained by a smaller sample (Li et al., 2012). Several studies also reported that CCL2 level was associated with ICH prognosis. In a cohort of 85 patients, higher serum CCL2 levels within 24 h were independently associated with functional outcomes at 7 days after ICH (Hammond et al., 2014). Another prospective study including 115 patients with ICH suggested that elevated serum CCL2 level at 6 h was associated with a 90-day worse modified

TABLE 2 Summary of animal studies investigating the role of chemokines in intracerebral hemorrhage.

Chemokine	Receptor	Species	ICH Model	Methods of inhibition/ activation	Time	Effect of chemokines/ receptors	References
CCL2	CCR2	C57BL/6 mice	Collagenase	Genetic deletion	1 day, 3 days, 7 days, 14 days	CCL2/CCR2 deficiency might decrease hematoma size at early time points but delay the recovery.	Yao and Tsirka (2012a)
CCL2	CCR2	SD rat	Collagenase	Pharmacological intervention (CCR2 inhibitor propagermanium, oral gavage, three times a day, 25 mg/ kg/day for 1 day or 3 days)	1 day, 3 days	Propagermanium maintain BBB integrity, reduce brain edema, and improve neurobehavioral functions.	Guo et al. (2020)
CCL2	CCR2	SD rat	Collagenase	Pharmacological intervention (S1PR3 antagonist CAY10444, I.P., 0.5 mg/kg/day for 1 day or 3 days)	1 day, 3 days	S1PR3 inhibition exerts a neuroprotective effect *via* the S1P-CCL2-p-p38 MAPK pathway.	Xu et al. (2021)
CCL2	CCR2	C57BL/6 mice	Collagenase	Genetic deletion; Pharmacological intervention (CCR2 antibody MC-21, I.P., 20 μg before ICH and again 24 h later)	1 day, 3 days, 7 days	CCR2 deletion and MC-21 decreased inflammatory monocyte recruitment and are protected from early motor deficits	Hammond et al. (2014)
CCL2	/	mouse	Autologous blood	Gene silencing by shRNA	48 h	MCP-1 shRNA inhibited inflammation response and improved neurological injury	Yang et al. (2016)
CCL5	CCR5	CD1 mice	Autologous blood	Pharmacological intervention (CCR5 antagonist Maraviroc, intranasally, 50 μg/kg or 150 μg/kg or 450 μg/kg per day for 3 days)	3 h, 6 h, 12 h, 24 h, 72 h	MVC improved neurobehavioral deficits and decreased neuronal pyroptosis in ipsilateral brain tissues, partially through the CCR5/PKA/CREB/ NLRP1 signaling pathway	Yan et al. (2021)
CCL5	CCR1	CD1 mice	Autologous blood	Pharmacological intervention (CCR1 inhibitor Met-RANTES, intranasally, 0.15 μg/ kg or 0.5 μg/kg or 1.5 μg/kg at 1 h post-ICH)	3 h, 6 h, 12 h, 24 h, 72 h	CCR1 inhibition with Met-RANTES attenuated neuroinflammation, thereby reducing brain edema and improving neurobehavioral functions	Yan et al. (2020)

(Continued)

TABLE 2 (Continued)

Chemokine	Receptor	Species	ICH Model	Methods of inhibition/ activation	Time	Effect of chemokines/ receptors	References
CCL5	CCR1	CD1 mice	Autologous blood	Pharmacological intervention (CCR1 antagonist Met-RANTES, intranasally, 0.15 μg/kg or 0.5 μg/kg or 1.5 μg/kg at 1 h post-ICH)	1 h, 24 h, 72 h, 7 days, 14 days, 21 days, 25 days	Met-R treatment attenuated blood–brain barrier permeability and ameliorated neurobehavioral deficits through inhibiting CCR1/SRC/Rac1 signaling pathway in mice.	Yan et al. (2022)
CCL12	/	C57BL/6 mice	Autologous blood	Genetic deletion. Pharmacological intervention (CCL12 antibody, I.P.)	1 day, 3 days, 5 days, 7 days	CCL12 deletion attenuated ICH damage in the brain	Huang et al. (2020)
CCL17	CCR4	CD1 mice	Autologous blood	Pharmacological intervention (CCR4 activator rCCL17, intranasally, 10 μg/kg, 30 μg/kg, 90 μg/kg, at 1 h following ICH)	6 h, 12 h, 24 h, 72 h, 5 days, 7 days, 14 days, 21 days, 22–27 days	CCR4 activation with rCCL17 promoted hematoma resolution by increasing CD163 expression and CCR4/ERK/Nrf2 pathway, thereby reducing brain edema and improving neurological function	Deng et al. (2020)
CCL17	CCR4	CD1 mice	Autologous blood	Pharmacological intervention (CCR4 activator, rCCL17, 10 μg/kg, 30 μg/kg, 90 μg/kg, intranasally at 1 h following ICH)	6 h, 12 h, 24 h, 72 h, 5 days, 7 days, 14 days, 21 days, 22–27 days	rCCL17-dependent CCR4 activation ameliorated neurological deficits, reduced brain edema, and ameliorated neuroinflammation and neuronal apoptosis, at least in part, through the PI3K/AKT/Foxo1 signaling pathway after ICH	Deng et al. (2021)
CXCL2	CXCR1/2	C57BL/6J mice	Collagenase	Pharmacological intervention (CXCR1/2 antagonist, reparixin)	0, 3 h, 6 h, 12 h, 24 h	CXCR1/2 antagonist reparixin ameliorated neurological deficits	Matsushita et al. (2014)
/	CXCR4	SD rats, C57BL/6 mice	Collagenase	Pharmacological intervention (CXCR4 agonist CX807, I.P., 3 mg/kg/day for 3 days)	30 min, 60 min, 90 min, 3 days, 4 days	CX807 is neuroprotective and anti-inflammatory against ICH	Yu et al. (2020)

(Continued)

TABLE 2 (Continued)

Chemokine	Receptor	Species	ICH Model	Methods of inhibition/ activation	Time	Effect of chemokines/ receptors	References
CXCL12	CXCR4	SD rats	Collagenase	Pharmacological intervention (CXCL12, I.V., 10 μL every other day; CXCR4 agonist, AMD3100, S.C., 120 μg/kg, twice daily)	24 h, 14 days	CXCL12 stimulates EPCs to induce angiogenesis though the CXCR4 pathway after ICH	Li et al. (2015)
CX3CL1	CX3CR1	C57BL/6 mice	Collagenase	Pharmacological intervention (CX3CL1 and a CX3CR1 inhibitor AZD8797, lateral ventricular injection)	6 h, 12 h, 24 h, 3 days, 7 days	CX3CL1 significantly decreased the hematoma size and Hb content and improved neurological deficits	You et al. (2022)
CX3CL1	CX3CR1	C57BL/6 mice	Collagenase	Genetic overexpression	6 h, 12 h, 1 day, 2 days, 3 days, 5 days, 7 days	The overexpression of CX3CR1 increased the migration ability of adipose derived stem cells, reduced cell death and improved sensory and motor functions	Li G. et al. (2019)

BBB, blood–brain barrier; I.P., intraperitoneal injection; I.V., intravenous injection; S.C., subcutaneous injection; EPCs, endothelial progenitor cells.

Rankin Scale (mRS) score (Landreneau et al., 2018). Nevertheless, no correlation was found between CSF CCL2 level and in-hospital mortality.

It is widely acknowledged that CCL2 acts as a critical molecule in the pathogenesis of ICH, especially in the early stage. Serum CCL2 level is an effective biomarker for identifying ICH severity and predicting prognosis. Thus, CCL2/CCR2 axis is a promising target to alleviate brain injury. However, the time window for inhibiting this axis needs to be further clarified to prevent delaying the protective inflammatory responses. In addition, the prognostic value of the CCL2 level should be verified in a large-sample cohort study.

3.1.2. CCL3

CCL3 is also called macrophage inflammatory protein-1α (MIP-1α), belonging to the MIP-1 CC chemokine subfamily that contains four proteins called CCL3 (MIP-1α), CCL4 (MIP-1β), CCL9/10 (MIP-1δ), and CCL15 (MIP-1γ; Maurer and von Stebut, 2004). The human CCL3 gene is identified on chromosome 17 (LD78α, LD78β, and LD78γ). It can be secreted by various mature hematopoietic cells, such as monocytes, macrophage cell lines, mast cells, Langerhans cells, fibroblasts, and lymphocytes (Cook, 1996). MIP-1α proteins could bind with CCR1, CCR3, and CCR5 to exert their chemotactic and proinflammatory effects. Moreover, it can promote homeostasis (Maurer and von Stebut, 2004). CCL3 contributes to the migration of monocytes, B lymphocytes, activated $CD8^+$ T cells, NK cells, and eosinophils (Cook, 1996). It also stimulates the expression of cell adhesion molecule 1 (ICAM-1) and the production of TNF-α, IL-1, and IL-6. IL-1β, lipopolysaccharide (LPS), and HIV-1 infection induce an increased expression of CCL3 (Menten et al., 2002). In the CNS, CCL3 is released from microglia, astrocytes, hippocampal neurons, and cerebral endothelial cells (Rezaie et al., 2002; Xu et al., 2009; Chui and Dorovini-Zis, 2010; Cudaback et al., 2015). It is implicated in numerous diseases, including ischemic stroke, seizure, and traumatic injury (Arisi et al., 2015; Huang et al., 2018; Ciechanowska et al., 2020).

The roles of CCL3 in hemorrhagic stroke have not been studied as extensively as CCL2. The studies of CCL3 in ICH are relatively limited. In the mice brain after ICH, mRNA expression of CCL3 exhibited a peak increase earlier at 6 h, a decrease at 12 h, and a stable status at 24 h (Matsushita et al., 2014). Subarachnoid hemorrhage (SAH) also caused an elevated level of CCL3 (Cobelens et al., 2010). In addition, RNA sequencing analysis revealed the recruitment of macrophages *via* CCL3 in the progression of intracranial aneurysms (Aoki et al., 2019). In the preterm infants with post-hemorrhagic hydrocephalus (PHH), there was an increased level of CSF CCL3, but the team did not observe a correlation

TABLE 3 Summary of human studies investigating the role of chemokines in intracerebral hemorrhage.

Chemokine/ receptor	Study	Population	Sample source	Time	Effects of chemokines/receptors	References
CCL2, CXCL10	prospective cohort	115 ICH patients	Serum	6 h, 24 h, 72 h	Patients with elevated CCL2 had worse mRS score at day 90. Elevation in CXCL10 was independently associated with worse 90-d mRS score	Landreneau et al. (2018)
CCL2	prospective, multi-center	28 ICH/IVH patients	CSF, serum	1–10 days	Significant correlation was found between CCL2 level and IVH volume at 3–8 days and ICH at day 1–2. Significant correlations were found with PHE volume for IL-6, IL-10 and CCL2 at day 1–2	Ziai et al. (2021)
CCL2	prospective cohort	85 ICH patients	Serum	24 h	Serum CCL2 levels are independently associated with functional outcomes	Hammond et al. (2014)
CCL5	prospective cohort	15 ICH patients, 10 controls	Serum	1–3 days, 7 days, 14 days, 30 days	No significant association was found	Li et al. (2012)
CCL23	prospective	94 ICH patients, 47 controls	Serum	Within 24 h	Serum CCL23 levels was highly related to ICH severity and inflammatory response; CCL23 ≥ 62.95 pg./mL served as an independent predictor of 6-month unfavorable outcome and death	Lin et al. (2022)
CXCL8	/	4 deceased ICH patients, 24 ICH patients, 20 controls	Brain samples, serum	Within 24 h	CXCL8 elevated in blood samples of ICH patients	Rosell et al. (2011)
CXCL12	cohort	105 ICH patients, 105 healthy controls	Serum	Within 24 h	CXCL12 concentrations had positive correlation with NIHSS scores and hematoma volume. Serum CXCL12 was independently associated with the mortality, overall survival, and unfavorable outcome	Shen et al. (2017)
CX3CL1/CX3CR1	prospective cohort	30 ICH patients	Serum	Within 7 days	Serum CX3CL1 concentration was relative to smaller hematoma volume and better outcome	You et al. (2022)
CX3CL1/CX3CR1	/	15 TBI/ICH patients, 5 patients with unruptured intracranial aneurysms	Brain tissue	/	Higher CX3CR1 expression in neurons was associated with better clinical conditions of patients at admission	Gaetani et al. (2013)

ICH, intracerebral hemorrhage; mRS, modified Rankin Scale; IVH, intraventricular hemorrhage; CSF, cerebrospinal fluid; TBI, traumatic brain injury.

with CSF inflammatory cell counts (Habiyaremye et al., 2017). No clinical studies were searched about CCL3 in patients with hemorrhagic strokes. Therefore, the underlying mechanism of CCL3 in ICH currently needs to be clarified, requiring more directly related research.

3.1.3. CCL5

CCL5, or RANTES (regulated on activation, normal T-cell expressed and secreted), was first discovered in normal T cells, acting as a critical proinflammatory chemokine (Schall et al., 1988). The production of CCL5 was also generated

predominantly in $CD8^+$ T cells, epithelial cells, fibroblasts, platelets, and macrophages. It has been indicated to contribute to the migration and recruitment of T cells, monocytes, dendritic cells, eosinophils, NK cells, mast cells, and basophils (Appay and Rowland-Jones, 2001). In the CNS, CCL5 was found expressed in oligodendrocytes, astrocytes, microglia, and some dopaminergic neurons (Lanfranco et al., 2017). CCL5 and its source cells participate in numerous biological processes, such as controlling pathogens, enhancing inflammation, and repairing wounds in many diseases (Levy, 2009; Marques et al., 2013).

CCL5 can attach to CCR1, CCR3, CCR4, and CCR5. There is a greater affinity for CCL5 binding to CCR1 and CCR5, but less affinity for CCR3 and CCR4 (Appay and Rowland-Jones, 2001; Blanpain et al., 2001). The CCR1 is widely expressed in multiple leukocyte types. It initiates and exacerbates inflammation and thus is considered a potential therapeutic target for autoimmune and inflammatory diseases. CCR1 signaling pathway contributes to tissue damage and inflammation *via* activating T cells, regulating Th1/Th2 cytokine polarization, and stimulating macrophage function and proteases (Cheng and Jack, 2008). CCR5 is also expressed on plenty of leukocytes, for instance, resting memory/effector T-lymphocytes, monocytes, macrophages, and immature dendritic cells (Blanpain et al., 2002). More importantly, it also serves as the main coreceptor for the entry of R5 strains of the human immunodeficiency virus (HIV-1, HIV-2). Maraviroc, an effective CCR5 antagonist at inhibiting HIV-1 entry into cells, has been approved by the United States Food and Drug Administration for the therapy of R5-tropic HIV-1 infection (Woollard and Kanmogne, 2015). Recently, accumulating evidence implicates the roles of the CCR5 axis in other infectious illnesses, autoimmune diseases, cerebrovascular events, and neurocognitive disorders (Martin-Blondel et al., 2016).

In the stroke subtype of ICH, CCL5 related signaling pathway participates in the secondary injury and provides a promising therapeutic approach for definitively managing conditions. Yan and his colleagues systematically explored the roles of CCL5 and its receptors in experimental ICH. In the hemorrhagic models induced by autologous blood, there was a notable elevation of CCL5 level starting at early 3 h, peaking at 24 h, and then decreasing at 72 h (Yan et al., 2022). The time courses of CCR1 and CCR5 expressions were parallel to that of CCL5 (Yan et al., 2021, 2022). In the hemorrhagic brain, CCR1 was localized in microglia, neurons, and astrocytes in the perihematomal area. The administration of CCR1 inhibitor with Met-RANTES significantly improved neurological deficits and decreased brain swelling after ICH *via* inhibiting inflammatory responses. The neuroprotective effects were achieved through the CCR1/TPR1/ERK1/2 signaling pathway (Yan et al., 2020). Besides, the latest research reported that Met-RANTES could preserve BBB integrity by inhibiting the CCR1/SRC/Rac1 pathway, which also partly explained the neuroprotective roles of Met-RANTES (Yan et al., 2022). The inhibition of CCR5 by Maraviroc also alleviated post-ICH neurological deficits, partially ameliorating neuronal proptosis through the CCR5/PKA/CREB/NLRP1 signaling (Yan et al., 2021). Given the effects of CCL5 and its receptors on neuroinflammation after ICH, the axis may serve as a potential target for secondary injury.

There are limited clinical data about CCL5 and its receptors levels in patients with ICH. Li collected serum samples to obtain the level of CCL5 at days 1–3, day 7, day 14, and day 30 of ICH, finding no correlation between CCL5 level and ICH severity or functional outcomes (Li et al., 2012). The results may be limited to fewer patients and later time points. In patients with subarachnoid hemorrhage, serum CCL5 level on day 7 was independently associated with clinical outcomes at discharge (Chaudhry et al., 2020). Moreover, a higher level of serum CCL5 is also related to an increased risk of DCI (Ahn et al., 2019).

In summary, further research is needed to identify the association between CCL5 level and ICH prognosis. In recent years, CCR5 has been developed as a promising therapeutic target for post-stroke recovery, including cognitive function (Joy et al., 2019; Feng et al., 2022). Therapeutic approaches targeting CCL5 and its receptors might be beneficial in ICH, especially for neurorehabilitation. However, there is no human research to discuss this correlation in ICH. CCR5 antagonist Maraviroc has been identified with promising potential for neurological recovery in ischemic stroke, and the translational process may be easier for its validated safety and wide application in AIDS patients. Therefore, the administration of Maraviroc may provide a promising therapeutic approach to managing patients with ICH.

3.1.4. CCL12

CCL12, also named monocyte chemoattractant protein (MCP)-5, is a potent chemoattractant for peripheral monocytes. CCL12 is weakly active on eosinophils, whereas it is inactive on neutrophils (Jia et al., 1996; Sarafi et al., 1997). Its expression was detected in mice's lymph nodes, macrophages, and lungs (Sarafi et al., 1997). CCR2 is the sole receptor of CCL12. In CNS diseases, CCL12 is associated with acute brain injury, including complement pathways and hypoxia-inducible inflammation (Mojsilovic-Petrovic et al., 2007; Popiolek-Barczyk et al., 2020). A recent study reported the effect of CCL12 on aged mice with ICH (Huang et al., 2020). Brain and plasma CCL12 levels increased significantly after ICH, aggravating secondary injury *via* recruiting macrophage and T cells. The genetic knockout of CCL12 could alleviate brain damage, including neurological deficits, survival rates, brain edema, and inflammatory responses. The results also provide a potential approach for ICH management, especially in the elderly with ICH.

3.1.5. CCL17

CCL17 is originally named thymus-and activation-regulated chemokine (TARC) for its constitutive expression in the thymus (Yoshie and Matsushima, 2015; Catherine and Roufosse, 2021). The gene for TARC/CCL17 was mapped to chromosome 16q13 (Nomiyama et al., 1998). Murine studies have shown that steady-state TARC/CCL17 synthesis occurs in various tissues, including

the thymus, lymph nodes (LNs), gut, and bronchi, but not in the spleen (Alferink et al., 2003). The cellular sources of this chemokine were Langerhans cells (LCs) and mature myeloid dendritic cells (DCs; Alferink et al., 2003). It is the first CC chemokine chemotactic for lymphoid cells but not for monocytes. CCL17 is an inflammatory chemokine with a high organ-restricted and DC-restricted expression profile (Yoshie and Matsushima, 2015). In humans, monocyte-derived DCs were shown to synthesize CCL17 in response to IL-3 and TNF-α *in vitro* cultures (Imai et al., 1999). CCL17 selectively binds to CCR4, which was found to be expressed on a fraction of Treg cells, cutaneous lymphocyte antigen (CLA), skin-homing T cells, and Th2-polarized cells (Yoshie and Matsushima, 2015). The critical role of the CCL17/CCR4 axis in immune suppression by Treg cells has also been well documented in animal models and human samples. CCL17 is expressed by DCs in the autoimmune encephalomyelitis models and promotes the pathogenesis of the disease (Ruland et al., 2017). In the hippocampus, CCL17 was identified as a homeostatic neuromodulator affecting the presence and morphology of microglia and synaptic transmission (Fülle et al., 2018).

Regarding the role of CCL17 in ICH, its expression increased after ICH from 6 h, reached a peak on day 5, and then decreased on day 7, while CCR4 significantly increased from 12 h to 5 days (Deng et al., 2021). The recombinant CCL17 (rCCL17) administration might promote hematoma resolution by increasing the expression of CD163 on microglia/macrophages, further reducing perihematomal edema and improving neurobehavior outcomes. The haptoglobin-CD163 scavenging system plays a critical role in the endogenous elimination of blood metabolites from the ICH-affected brain (Garton et al., 2017). In addition to the effects of CCL17 on hematoma resolution, the axis also could alleviate neuroinflammation and neuronal apoptosis *via* the CCR4/PI3K/AKT/Foxo1 signaling pathway at 72 h post-ICH (Deng et al., 2021). In experimental SAH rats, CCL17 presents neuroprotective effects by activating CCR4/mTORC2 axis in microglia (Zhang A. et al., 2022). There is no other clinical study about CCL17 in patients with ICH. Given the neuroprotective roles of CCL17, its activation has become a promising therapeutic approach for early therapy of ICH and contributing to hematoma absorption. Future study needs to focus more on the crossing influence of CCL17 and Treg cells.

3.2. CXC chemokine family

Based on the presence or the absence of a tripeptide motif glutamic acid–leucine–arginine (ELR) in the N-terminal domain, CXC chemokines are stratified into ELR$^+$ or ELR$^-$ molecules. The CXC-ELR$^+$ chemokines are chemoattractants mainly for neutrophils, compared to CXC-ELR-chemokines primarily attracting lymphocytes and monocytes (Bajetto et al., 2001). The presence of ELR has also been proposed to induce angiogenesis and to be chemotactic for endothelial cells (Bizzarri et al., 2006), including CXCL1, CXCL2, CXCL3, CXCL5, CXCL6, CXCL7, and CXCL8 (Murphy et al., 2000). In contrast, the non-ELR-CXC chemokines guide the recruitment of activated T cells and possess anti-angiogenic properties, such as CXCL4, CXCL10, and CXCL9 (Erdem et al., 2007; Repnik et al., 2015). Additionally, CXCL12 was observed to induce neovascularization *in vivo* (Dimova et al., 2019).

The family also plays an essential role in the pathogenic events after ICH. CXCL1 and CXCL2 were significantly elevated in the ipsilateral hemisphere at 6 h after induction of ICH (Matsumoto et al., 2020). CXCL2 exerts key effects in ICH models with axonal tract injury (Katsuki and Hijioka, 2017). Here, we mainly introduce CXCL8 and CXCL12.

3.2.1. CXCL8

CXCL8, also known as interleukin 8 (IL-8), is the first identified chemokine (Yoshimura, 2015). IL-8 is released by multiple cell types, such as monocytes, lymphocytes, granulocytes, fibroblasts, endothelial cells, and epithelial cells (Zlotnik et al., 1999). IL-1 and TNF-α can activate IL-8 gene expression through the IL-1R and TNFR signaling pathways (Hoffmann et al., 2002). CXCL8 is initially thought to act as a neutrophil mobilizer and engaged in acute inflammation, but it is also discovered to have chemotaxis to endothelial cells contributing to angiogenesis (Matsushima et al., 2022). CXCL8 interacts with CXCR1 and CXCR2 receptors expressed on T cells, monocytes, NK cells, basophils, and other non-hematopoietic cells in regulating angiogenesis, pain, and cardiovascular diseases (Strieter et al., 1995; Liu et al., 2016; Matsushima et al., 2022). In the CNS, the sources of CXCL8 include active microglia, astrocyte, endothelial cells, and infiltrated neutrophils, which is upregulated in pathological conditions (Lu et al., 2005; Vallès et al., 2006). CXCR2 has been reported to express on activated microglia or astrocytes surface. The CXCL8 and its receptors seem to be involved in various brain pathologies, such as ischemic brain injury, multiple sclerosis, and traumatic brain injury (TBI; Semple et al., 2010).

In the pathology of ICH, the CXCL8 gene was expressed upregulated in the perihematomal areas obtained from deceased patients (Rosell et al., 2011). CSF level of CXCL8 is correlated with relative PHE volume in patients with ICH, which supports CXCL8 as a biomarker for ICH severity (Ziai et al., 2021). Heme oxygenase-1 (HO-1) inhibitor was also reported to regulate the expression of CXCL8 (Fan and Mu, 2017). CXCL8 may be a novel candidate susceptibility gene for ICH. Notably, it may serve as a predictive marker for ICH severity, especially for serum concentrations.

3.2.2. CXCL12

CXCL12 (also named stromal cell-derived factor-1, SDF-1), interacting with CXCR4 and CXCR7, is one number of homeostatic chemokines. Thus, it is produced by bone marrow stromal cells and epithelial cells in many other organs, which is indispensable for lymphopoiesis and embryogenesis (Nagasawa et al., 1996; Janssens et al., 2018b). CXCL12 is also a crucial

molecule in the procedure of inflammation, mediating the activation and migration of monocyte, macrophage, Treg cell, and microglia (Li Y. et al., 2019; Wang et al., 2019; Mai et al., 2021; Zhang L. et al., 2022). CXCL12 mainly recruits progenitor cells and white blood cells through CXCR4, while CXCR7 mainly inhibits the CXCL12/CXCR4 axis (Janssens et al., 2018a). Its secretion increases in these organs during tissue damage such as heart infarction, cerebral ischemia, toxic liver damage, excessive bleeding, and total body irradiation. Furthermore, CXCR4 also functions as a co-receptor for virus entry into T cells (Huang et al., 2021). It is now recognized that CXCL12/CXCR4 signaling regulates the development of nervous tissue in different ways, particularly due to its effects on cell migration and axon guidance (Mithal et al., 2012).

The related research about the effects of CXCL12/CXCR4 on ICH is rare and controversial. A cohort study was conducted on 105 ICH patients, indicating that baseline serum CXCL12 concentrations were enhanced after ICH. Higher concentrations of CXCL12 were related to ICH severity and poor outcomes (Shen et al., 2017). Yu suggested the neuroprotective and anti-inflammatory action of CXCR4 antagonist CX807 (Yu et al., 2020). The results may be explained by inhibiting inflammatory and apoptotic markers, such as TLR4, TNF-α, IL-6, and CD8. In addition, CXCL12 has been reported to stimulate endothelial progenitor cells (EPCs) to induce angiogenesis through the CXCR4 pathway after ICH (Li et al., 2015). However, human data suggested that patients harboring the Tp53 Arg72 Pro single-nucleotide polymorphism (SNP) had better functional outcomes but higher SDF-1α levels (Rodríguez et al., 2017). In TBI models, pharmacological blockers of CXCR4 improved recovery (Friedman-Levi et al., 2021). These studies provide a new therapeutic potential for preventing and reducing ICH-related injury, but it needs to clarify the underlying mechanisms of a CXCR4 antagonist in ICH.

3.3. CX3C chemokine family

CX3CL1 (Fractalkine, FKN) is the only member of the CX3C chemokine family as a transmembrane protein or soluble chemokine. It is constitutively expressed in neurons, microglia, astrocytes, and vascular endothelial cells (Harrison et al., 1998; Yoshida et al., 2001). CX3CR1 is the exclusive receptor of CX3CL1 existing on the surface of neuron and microglial cells (Harrison et al., 2001; Hatori et al., 2002). The CX3CL1/CX3CR1 axis in physiological conditions appears critical for normal brain functions (Zhan et al., 2014). After brain injury, CX3CL1 binding to CX3CR1 regulates the activation of microglial cells and mediates interactions between neurons and microglia (Chapman et al., 2000). Nevertheless, current data are still somewhat controversial. Many studies have suggested the neuroprotective effects of CXC3R1 in ischemic stroke and other diseases (Meucci et al., 2000; Wang et al., 2018).

In recent decades, substantial data from ICH have consistently demonstrated that CX3CL1/CX3CR1 signaling can achieve some neuroprotective effects in the pathology of ICH, including contributing to the absorption of hematoma size and reducing cellular death. Gaetani first highlighted the expression of CX3CL1 and CX3CR1 in the human brain after ICH and TBI, finding that significant upregulation of CXC3L1/CXC3R1 might be involved in limiting brain damage (Gaetani et al., 2013). You further speculated on the specific mechanism of CX3CL1 promoting hematoma clearance (You et al., 2022). The expressions of both CX3CL1 and CX3CR1 increased early at 6 h of ICH onset, peaked at 3 days, and then decreased gradually in the following days. By administrating CX3CL1, it could increase the chemotactic ability of microglia toward the hematoma, accelerate hematoma absorption, and thus improve neurological function recovery. Moreover, PPAR-γ was found to mediate the increase in the CD163/HO-1 axis expression and erythrophagocytosis induced by CX3CL1 in microglia. However, Min (Min et al., 2016) have suggested that the $CX3CR1^{+}$ cells after ICH are mainly due to macrophage infiltration rather than microglia proliferation, which increased from 1 day until 7 days of ICH. Numerous macrophages were polarized to the M2 phenotype at delayed time points (3 and 7 days), playing a protective role by presumably facilitating recovery from ICH injury. The study is partially inconsistent with previous studies and may be explained by the discrepancy between the animal model and different stages of ICH. Furthermore, stem cell therapy has emerged as a promising therapeutic strategy for ICH, but it has low retention and engraftment after delivery (Gao et al., 2018).

Interestingly, a study reported that the overexpression of CX3CR1 in adipose-derived stem cells promotes cell migration and functional recovery after experimental ICH, which might contribute to the development of stem cell therapy (Li G. et al., 2019). Clinically, a prospective cohort including 30 ICH patients recently showed the relevance of serum CX3CL1 concentration and better prognosis (You et al., 2022). Given the effects of CX3CL1 on hematoma absorption, it might be a promising target for ICH treatment in the ultra-early stage. Because of inadequate data, more research is required to explore its neuroprotective effects further.

4. Chemokines and their receptors as drug targets

Based on the up-regulated expression of chemokines and their receptors after ICH, some studies primarily target chemokine receptors with pharmacological drugs in ICH models, enabling the system as a preferential approach. We summarized the usage and effects of these drugs in preventing ICH-induced injury, including Propagermanium, Maraviroc, and Reparixin (Table 4). Nevertheless, clinical ICH trials about drugs targeting chemokine or receptors currently lag. We also list more studies of corresponding drugs in clinical usage or under clinical trials in other cardiovascular and cerebrovascular diseases (Table 5). For example, the CCR5 inhibitor Maraviroc is the first targeting drug

TABLE 4 Summary of studies evaluating the effects of drugs targeting chemokines and their receptors in ICH.

Drug	Mechanism	Disease model	Drug administration details	Main effects	Signaling pathway	Reference
Propagermanium	CCR2 inhibitor	collagenase	Oral gavage: 3 times a day (25 mg/kg/day) for 1 day or 3 days	Reduce brain edema, improve neurobehavioral functions	CCL2-CCR2-p38 MAPK	Guo et al. (2020)
Maraviroc	CCR5 inhibitor	autologous blood	Intranasal delivery: once per day (50 μg/kg or 150 μg/kg or 450 μg/kg) for 3 days	Improve neurobehavioral deficits, decrease neuronal pyroptosis	CCR5/PKA/CREB	Yan et al. (2021)
Reparixin	CXCR1/2 antagonist	collagenase	Intravenous and intraperitoneal administrations: three times a day (15 mg/kg) for 3 days	Ameliorate neurological dysfunction	/	Matsushita et al. (2014)

tested in patients with IS (Francisci et al., 2019). Relevant results are not well-documented, but it opens a window for neurorehabilitation after IS (Feng et al., 2022). In addition, it was reported that Maraviroc could attenuate atherosclerotic progression in HIV patients, as well as anti-CCR2 monoclonal antibody MLN1202 for its anti-inflammation (Gilbert et al., 2011; Francisci et al., 2019). JVS-100 was developed to treat ischemic cardiovascular diseases as a nonviral, naked DNA plasmid encoding human CXCL12. The endomyocardial injection of JVS-100 was safe and improved heart failure symptoms *via* the critical role of the CXCL12/CXCR4 axis in tissue repair (Penn et al., 2013).

Chemokines and their receptors have been consistently identified as critical molecules of the pharmacological target. Its characteristic of regulating immune cell migration and recruitment contributes to the progression of ICH, which prompts the research from bench to bedside. On the one hand, chemokines can be developed as effective biomarkers for predicting ICH severity and prognosis, as mentioned above, such as CCL2, CXCL12, and CX3CL1. On the other hand, modulation of chemokine expression can be further explored to alleviate secondary injury despite the low clinical translation rate. For example, Maraviroc also has a promising potential in facilitating the translation of basic science to the clinical setting in ICH for its confirmed safety and neuroprotective effects on ICH. The role of Maraviroc in post-stroke recovery may also be the main impetus for rehabilitation after ICH. One major drawback in limiting its translational potential is the redundancy in the function through both spatial and temporal differential expression. Thus, chemokine receptor antagonists may be a more efficient approach with specificity for multiple targets. Moreover, several mechanisms are involved in ICH pathophysiology more than neuroinflammation. Thus, therapies of chemokines should be combined with other targets to test the effects on ICH.

5. Conclusion

The mechanisms underlying ICH-induced brain injury are currently unclear. Because chemokines are expressed temporally and spatially in the pathogenesis of acute ICH and post-ICH recovery. It will be vital to determine when and how chemokines influence immune responses. These mediators have various functions, including pro-inflammatory, anti-inflammatory, homeostatic, angiogenic, and neuromodulatory effects, which are intertwined and relatively complex. Many cell types produce chemokines in damaged brain tissues after ICH, including resident cells and infiltrating immune cells. Clarifying which cell types are the primary sources of chemokines in human or animal ICH is challenging. In addition, the interactions between chemokines and their receptors are highly relevant to the clinical procedure. Correspondingly, different chemokine receptors are also expressed on many cell subtypes in the brain and from peripheral immune systems. However, it is exactly because of these multiple functions serving a promising therapy with multi-targets on several chemokines or different mechanisms.

In summary, the local concentrations of chemokines in CSF or serum may provide promising predictors for ICH severity to aid decision-making in managing conditions. Their interactions with receptors determine the progression and outcome of relevant brain damage, contributing to developing new targets for hematoma absorbance, alleviating brain edema, and neurological recovery. Recently, rapid technology advances will shed light on the specific sources and activating time windows of different chemokines in ICH. Furthermore, more signaling pathways and transcription factors will be illustrated. It is conceivable that the work targeting specific chemokines and/or their receptors can effectively eliminate injury and improve prognosis in treating ICH. Nevertheless, exploring more new insights and discoveries on chemokines and their interactions with receptors is warranted. Moreover, more studies are necessary before those new findings can be translated into clinical targets.

TABLE 5 Summary of drugs in clinical usage or under clinical trials targeting on chemokines and chemokine receptors in cerebrovascular diseases.

Target	Drug	Conditions	Aim of study	Study outcomes and status	Phase	Clinical trial number
CCL2	Bindarit	Coronary restenosis	Assess the efficacy and safety of different dosages in preventing restenosis	Completed. No significant differences in in-segment, and MACE rates; significant reduction in the in-stent late loss	Phase 2	NCT01269242 Colombo et al. (2016)
CCR2	MLN1202	Atherosclerosis	Evaluate the potential of MLN1202 to reduce circulating levels of C-reactive protein in patients with risk factors for atherosclerotic cardiovascular disease	Completed. MLN1202 treatment resulted in significant reductions in high-sensitivity C-reactive protein levels	Phase 2	NCT00715169 Gilbert et al. (2011)
CCR5	Maraviroc	Stroke	Maraviroc to augment rehabilitation outcomes after stroke (MAROS)	Terminated. Only 2 participants were enrolled; No data displayed; Participants exited study prior to 6-month assessment	Phase 2/3	NCT03172026
CCR5	Maraviroc	Stroke	RCT to analyze the effect of Maraviroc and exercise to improve extremity recovery after a stroke	Not yet recruiting	Phase 2	NCT04789616
CCR5	Maraviroc	Post-stroke cognitive impairment	Investigate the safety and efficacy of Maraviroc in post-stroke impairment	Recruiting. No results.	Phase 2	NCT04966429 Assayag et al. (2022)
CCR5	Maraviroc	Atherosclerosis in HIV Patients	Efficacy of Maraviroc in modulating atherosclerosis in HIV patients	Completed. Maraviroc intensification modulates atherosclerotic progression in HIV-suppressed patients at high cardiovascular risk	Phase 4	NCT03402815 Francisci et al. (2019)
CXCL12	JVS-100	Severe peripheral arterial disease	Investigate the efficacy of JVS-100 on composite endpoints of wound progression, healing, and limb loss in patients with severe peripheral arterial disease	Unknown. JVS-100 failed to improve wound healing or hemodynamic measures at 3 months	Phase 2	NCT02544204 Shishehbor et al. (2019)
CXCL12	JVS-100	Ischemic heart failure	Assess the safety and efficacy of using JVS-100 to treat heart failure	Completed. JVS-100 improved heart failure symptoms in patients with ischemic cardiomyopathy	Phase 1	NCT01643590 Penn et al. (2013)
CXCL12	ACRX-100	Ischemic heart failure	Evaluate the safety of a single escalating dose of ACRX-100 in adults with ischemic heart failure	Completed. No results posted	Phase 1	NCT01082094

(Continued)

TABLE 5 (Continued)

Target	Drug	Conditions	Aim of study	Study outcomes and status	Phase	Clinical trial number
CXCR2	AZD5069	Atherosclerotic coronary disease	Determine whether CXCR2 inhibition will improve coronary endothelial function in patients following PCI for atherosclerotic coronary disease	Ongoing. No results posted	Phase 2	EudraCT 2016-000775-24
CXCR4	POL6326	Large reperfused ST-elevation myocardial infarction	Investigate the effects of POL6326 as a stem cell mobilizing agent on cardiac function and infarct size	Completed. No results posted	Phase 2	NCT01905475

MACE, major adverse cardiovascular events; RCT, randomized controlled trial; HIV, human immunodeficiency virus; PCI, percutaneous transluminal coronary intervention.

Author contributions

JW: conceptualization, data curation, investigation, methodology, project administration, visualization, and writing the original draft. LB: conceptualization, data curation, investigation, methodology, project administration, and visualization. YD, DW, and RJ: conceptualization and methodology. JL: supervision and writing—review and editing. XZ: funding acquisition, resources, supervision, and writing—review and editing. All authors contributed to the article and approved the submitted version.

Funding

The research was supported by the National Key Research and Development Program of the People's Republic of China (grant nos. 2018YFC1312200/2018YFC131224 and 2018YFC1705003), CAMS Innovation Fund for Medical Sciences (2019-I2M-5-029), Beijing Hospitals Authority Innovation Studio of Young Staff Funding Support (202112), and Beijing Municipal Committee of Science and Technology (Z201100005620010).

Conflict of interest

The authors declare that the research was conducted in the absence of any commercial or financial relationships that could be construed as a potential conflict of interest.

Publisher's note

References

Ahn, S. H., Savarraj, J. P. J., Parsha, K., Hergenroeder, G. W., Chang, T. R., Kim, D. H., et al. (2019). Inflammation in delayed ischemia and functional outcomes after subarachnoid hemorrhage. *J. Neuroinflammation* 16:213. doi: 10.1186/s12974-019-1578-1

Akhter, N., Wilson, A., Thomas, R., Al-Rashed, F., Kochumon, S., Al-Roub, A., et al. (2021). ROS/TNF-α crosstalk triggers the expression of IL-8 and MCP-1 in human monocytic THP-1 cells via the NF-κB and ERK1/2 mediated Signaling. *Int. J. Mol. Sci.* 22:10519. doi: 10.3390/ijms221910519

Alferink, J., Lieberam, I., Reindl, W., Behrens, A., Weiss, S., Hüser, N., et al. (2003). Compartmentalized production of CCL17 in vivo: strong inducibility in peripheral dendritic cells contrasts selective absence from the spleen. *J. Exp. Med.* 197, 585–599. doi: 10.1084/jem.20021859

Allaman, I., Bélanger, M., and Magistretti, P. J. (2011). Astrocyte-neuron metabolic relationships: for better and for worse. *Trends Neurosci.* 34, 76–87. doi: 10.1016/j.tins.2010.12.001

Aoki, T., Koseki, H., Miyata, H., Itoh, M., Kawaji, H., Takizawa, K., et al. (2019). RNA sequencing analysis revealed the induction of CCL3 expression in human intracranial aneurysms. *Sci. Rep.* 9:10387. doi: 10.1038/s41598-019-46886-2

Appay, V., and Rowland-Jones, S. L. (2001). RANTES: a versatile and controversial chemokine. *Trends Immunol.* 22, 83–87. doi: 10.1016/S1471-4906(00)01812-3

Arisi, G. M., Foresti, M. L., Katki, K., and Shapiro, L. A. (2015). Increased CCL2, CCL3, CCL5, and IL-1β cytokine concentration in piriform cortex, hippocampus, and neocortex after pilocarpine-induced seizures. *J. Neuroinflammation* 12:129. doi: 10.1186/s12974-015-0347-z

Assayag, E. B., Molad, J., Seyman, E., Rotschild, O., Zeltzer, E., Sadeh-Gonik, U., et al. (2022). Preventing post-stroke dementia. The MARCH trial. protocol and statistical analysis plan of a randomized clinical trial testing the safety and efficacy of maraviroc in post-stroke cognitive impairment. *Eur. Stroke J.* 7, 314–322. doi: 10.1177/23969873221098857

Baggiolini, M. (2001). Chemokines in pathology and medicine. *J. Intern. Med.* 250, 91–104. doi: 10.1046/j.1365-2796.2001.00867.x

Baggiolini, M., Dewald, B., and Moser, B. (1997). Human chemokines: an update. *Annu. Rev. Immunol.* 15, 675–705. doi: 10.1146/annurev.immunol.15.1.675

Bajetto, A., Bonavia, R., Barbero, S., Florio, T., and Schettini, G. (2001). Chemokines and their receptors in the central nervous system. *Front. Neuroendocrinol.* 22, 147–184. doi: 10.1006/frne.2001.0214

Barlic, J., and Murphy, P. M. (2007). An oxidized lipid-peroxisome proliferator-activated receptor gamma-chemokine pathway in the regulation of macrophage-vascular smooth muscle cell adhesion. *Trends Cardiovasc. Med.* 17, 269–274. doi: 10.1016/j.tcm.2007.09.004

Bianconi, V., Sahebkar, A., Atkin, S. L., and Pirro, M. (2018). The regulation and importance of monocyte chemoattractant protein-1. *Curr. Opin. Hematol.* 25, 44–51. doi: 10.1097/MOH.0000000000000389

Bizzarri, C., Beccari, A. R., Bertini, R., Cavicchia, M. R., Giorgini, S., and Allegretti, M. (2006). ELR+ CXC chemokines and their receptors (CXC chemokine receptor 1 and CXC chemokine receptor 2) as new therapeutic targets. *Pharmacol. Ther.* 112, 139–149. doi: 10.1016/j.pharmthera.2006.04.002

Blanpain, C., Buser, R., Power, C. A., Edgerton, M., Buchanan, C., Mack, M., et al. (2001). A chimeric MIP-1alpha/RANTES protein demonstrates the use of different regions of the RANTES protein to bind and activate its receptors. *J. Leukoc. Biol.* 69, 977–985. doi: 10.1189/jlb.69.6.977

Blanpain, C., Libert, F., Vassart, G., and Parmentier, M. (2002). CCR5 and HIV infection. *Recept. Channels* 8, 19–31.

Bonsack, F. T., Alleyne, C. H., and Sukumari-Ramesh, S. (2016). Augmented expression of TSPO after intracerebral hemorrhage: a role in inflammation? *J. Neuroinflammation* 13:151. doi: 10.1186/s12974-016-0619-2

Catherine, J., and Roufosse, F. (2021). What does elevated TARC/CCL17 expression tell us about eosinophilic disorders? *Semin. Immunopathol.* 43, 439–458. doi: 10.1007/s00281-021-00857-w

Chapman, G. A., Moores, K., Harrison, D., Campbell, C. A., Stewart, B. R., and Strijbos, P. J. (2000). Fractalkine cleavage from neuronal membranes represents an acute event in the inflammatory response to excitotoxic brain damage. *J. Neurosci.* 20:Rc87. doi: 10.1523/JNEUROSCI.20-15-j0004.2000

Chaudhry, S. R., Kinfe, T. M., Lamprecht, A., Niemelä, M., Dobreva, G., Hänggi, D., et al. (2020). Elevated level of cerebrospinal fluid and systemic chemokine CCL5 is a predictive biomarker of clinical outcome after aneurysmal subarachnoid hemorrhage (aSAH). *Cytokine* 133:155142. doi: 10.1016/j.cyto.2020.155142

Chen, K., Bao, Z., Tang, P., Gong, W., Yoshimura, T., and Wang, J. M. (2018). Chemokines in homeostasis and diseases. *Cell. Mol. Immunol.* 15, 324–334. doi: 10.1038/cmi.2017.134

Chen, C., Chu, S. F., Liu, D. D., Zhang, Z., Kong, L. L., Zhou, X., et al. (2018). Chemokines play complex roles in cerebral ischemia. *Neurochem. Int.* 112, 146–158. doi: 10.1016/j.neuint.2017.06.008

Cheng, J. F., and Jack, R. (2008). CCR1 antagonists. *Mol. Divers.* 12, 17–23. doi: 10.1007/s11030-008-9076-x

Chu, H. X., Arumugam, T. V., Gelderblom, M., Magnus, T., Drummond, G. R., and Sobey, C. G. (2014). Role of CCR2 in inflammatory conditions of the central nervous system. *J. Cereb. Blood Flow Metab.* 34, 1425–1429. doi: 10.1038/jcbfm.2014.120

Chui, R., and Dorovini-Zis, K. (2010). Regulation of CCL2 and CCL3 expression in human brain endothelial cells by cytokines and lipopolysaccharide. *J. Neuroinflammation* 7:1. doi: 10.1186/1742-2094-7-1

Ciechanowska, A., Popiolek-Barczyk, K., Pawlik, K., Ciapała, K., Oggioni, M., Mercurio, D., et al. (2020). Changes in macrophage inflammatory protein-1 (MIP-1) family members expression induced by traumatic brain injury in mice. *Immunobiology* 225:151911. doi: 10.1016/j.imbio.2020.151911

Cisbani, G., Le Behot, A., Plante, M. M., Préfontaine, P., Lecordier, M., and Rivest, S. (2018). Role of the chemokine receptors CCR2 and CX3CR1 in an experimental model of thrombotic stroke. *Brain Behav. Immun.* 70, 280–292. doi: 10.1016/j.bbi.2018.03.008

Cobelens, P. M., Tiebosch, I. A., Dijkhuizen, R. M., Van Der Meide, P. H., Zwartbol, R., Heijnen, C. J., et al. (2010). Interferon-β attenuates lung inflammation following experimental subarachnoid hemorrhage. *Crit. Care* 14:R157. doi: 10.1186/cc9232

Collaborators, G. S. (2021). Global, regional, and national burden of stroke and its risk factors, 1990-2019: a systematic analysis for the global burden of disease study 2019. *Lancet Neurol.* 20, 795–820. doi: 10.1016/S1474-4422(21)00252-0

Colombo, A., Basavarajaiah, S., Limbruno, U., Picchi, A., Lettieri, C., Valgimigli, M., et al. (2016). A double-blind randomised study to evaluate the efficacy and safety of bindarit in preventing coronary stent restenosis. *EuroIntervention* 12, e1385–e1394. doi: 10.4244/EIJY15M12_03

Cook, D. N. (1996). The role of MIP-1 alpha in inflammation and hematopoiesis. *J. Leukoc. Biol.* 59, 61–66. doi: 10.1002/jlb.59.1.61

Cudaback, E., Yang, Y., Montine, T. J., and Keene, C. D. (2015). APOE genotype-dependent modulation of astrocyte chemokine CCL3 production. *Glia* 63, 51–65. doi: 10.1002/glia.22732

Deng, S., Jin, P., Sherchan, P., Liu, S., Cui, Y., Huang, L., et al. (2021). Recombinant CCL17-dependent CCR4 activation alleviates neuroinflammation and neuronal apoptosis through the PI3K/AKT/Foxo1 signaling pathway after ICH in mice. *J. Neuroinflammation* 18:62. doi: 10.1186/s12974-021-02112-3

Deng, S., Sherchan, P., Jin, P., Huang, L., Travis, Z., Zhang, J. H., et al. (2020). Recombinant CCL17 enhances hematoma resolution and activation of CCR4/ERK/Nrf2/CD163 Signaling pathway after intracerebral Hemorrhage in mice. *Neurotherapeutics* 17, 1940–1953. doi: 10.1007/s13311-020-00908-4

Deshmane, S. L., Kremlev, S., Amini, S., and Sawaya, B. E. (2009). Monocyte chemoattractant protein-1 (MCP-1): an overview. *J. Interferon Cytokine Res.* 29, 313–326. doi: 10.1089/jir.2008.0027

Dhayni, K., Zibara, K., Issa, H., Kamel, S., and Bennis, Y. (2022). Targeting CXCR1 and CXCR2 receptors in cardiovascular diseases. *Pharmacol. Ther.* 237:108257. doi: 10.1016/j.pharmthera.2022.108257

Dimova, I., Karthik, S., Makanya, A., Hlushchuk, R., Semela, D., Volarevic, V., et al. (2019). SDF-1/CXCR4 signalling is involved in blood vessel growth and remodelling by intussusception. *J. Cell. Mol. Med.* 23, 3916–3926. doi: 10.1111/jcmm.14269

Du, Y., Wang, A., Zhang, J., Zhang, X., Li, N., Liu, X., et al. (2022). Association between the neutrophil-to-lymphocyte ratio and adverse clinical prognosis in patients with spontaneous intracerebral Hemorrhage. *Neuropsychiatr. Dis. Treat.* 18, 985–993. doi: 10.2147/NDT.S358078

Erdem, H., Pay, S., Musabak, U., Simsek, I., Dinc, A., Pekel, A., et al. (2007). Synovial angiostatic non-ELR CXC chemokines in inflammatory arthritides: does CXCL4 designate chronicity of synovitis? *Rheumatol. Int.* 27, 969–973. doi: 10.1007/s00296-007-0317-6

Fan, X., and Mu, L. (2017). The role of heme oxygenase-1 (HO-1) in the regulation of inflammatory reaction, neuronal cell proliferation and apoptosis in rats after intracerebral hemorrhage (ICH). *Neuropsychiatr. Dis. Treat.* 13, 77–85. doi: 10.2147/NDT.S120496

Feng, Y. Q., Xu, Z. Z., Wang, Y. T., Xiong, Y., Xie, W., He, Y. Y., et al. (2022). Targeting C-C chemokine receptor 5: key to opening the neurorehabilitation window after ischemic stroke. *Front. Cell. Neurosci.* 16:876342. doi: 10.3389/fncel.2022.876342

Förster, R., Davalos-Misslitz, A. C., and Rot, A. (2008). CCR7 and its ligands: balancing immunity and tolerance. *Nat. Rev. Immunol.* 8, 362–371. doi: 10.1038/nri2297

França, C. N., Izar, M. C. O., Hortêncio, M. N. S., Do Amaral, J. B., Ferreira, C. E. S., Tuleta, I. D., et al. (2017). Monocyte subtypes and the CCR2 chemokine receptor in cardiovascular disease. *Clin. Sci.* 131, 1215–1224. doi: 10.1042/CS20170009

Francisci, D., Pirro, M., Schiaroli, E., Mannarino, M. R., Cipriani, S., Bianconi, V., et al. (2019). Maraviroc intensification modulates atherosclerotic progression in HIV-suppressed patients at high cardiovascular risk. A randomized, crossover pilot study. *Open Forum. Infect. Dis.* 6:ofz112. doi: 10.1093/ofid/ofz112

Friedman-Levi, Y., Liraz-Zaltsman, S., Shemesh, C., Rosenblatt, K., Kesner, E. L., Gincberg, G., et al. (2021). Pharmacological blockers of CCR5 and CXCR4 improve recovery after traumatic brain injury. *Exp. Neurol.* 338:113604. doi: 10.1016/j.expneurol.2021.113604

Fülle, L., Offermann, N., Hansen, J. N., Breithausen, B., Erazo, A. B., Schanz, O., et al. (2018). CCL17 exerts a neuroimmune modulatory function and is expressed in hippocampal neurons. *Glia* 66, 2246–2261. doi: 10.1002/glia.23507

Gaetani, P., Pisano, P., Solinas, G., Colombo, P., Destro, A., Levi, D., et al. (2013). Immunohistohemical expression of the chemokine fractalkine and its receptor in the human brain cortex after severe traumatic brain injury and brain hemorrhage. *J. Neurosurg. Sci.* 57, 55–62. PMID: 23584220

Gao, L., Xu, W., Li, T., Chen, J., Shao, A., Yan, F., et al. (2018). Stem cell therapy: A promising therapeutic method for intracerebral Hemorrhage. *Cell Transplant.* 27, 1809–1824. doi: 10.1177/0963689718773363

Garton, T., Keep, R. F., Hua, Y., and Xi, G. (2017). CD163, a Hemoglobin/haptoglobin scavenger receptor, after intracerebral Hemorrhage: functions in microglia/macrophages versus neurons. *Transl. Stroke Res.* 8, 612–616. doi: 10.1007/s12975-017-0535-5

Geng, H., Chen, L., Tang, J., Chen, Y., and Wang, L. (2022). The role of CCL2/CCR2 Axis in cerebral ischemia-reperfusion injury and treatment: from animal experiments to clinical trials. *Int. J. Mol. Sci.* 23:3485. doi: 10.3390/ijms23073485

Gilbert, J., Lekstrom-Himes, J., Donaldson, D., Lee, Y., Hu, M., Xu, J., et al. (2011). Effect of CC chemokine receptor 2 CCR2 blockade on serum C-reactive protein in individuals at atherosclerotic risk and with a single nucleotide polymorphism of the monocyte chemoattractant protein-1 promoter region. *Am. J. Cardiol.* 107, 906–911. doi: 10.1016/j.amjcard.2010.11.005

Greenberg, S. M., Ziai, W. C., Cordonnier, C., Dowlatshahi, D., Francis, B., Goldstein, J. N., et al. (2022). 2022 guideline for the management of patients with spontaneous intracerebral hemorrhage: a guideline from the American Heart Association/American Stroke Association. *Stroke* 53, e282–e361. doi: 10.1161/STR.0000000000000407

Gruber, H. E., Hoelscher, G. L., Ingram, J. A., Bethea, S., Cox, M., and Hanley, E. N. (2015). Proinflammatory cytokines modulate the chemokine CCL2 (MCP-1) in human annulus cells in vitro: CCL2 expression and production. *Exp. Mol. Pathol.* 98, 102–105. doi: 10.1016/j.yexmp.2014.12.002

Guo, F., Xu, D., Lin, Y., Wang, G., Wang, F., Gao, Q., et al. (2020). Chemokine CCL2 contributes to BBB disruption via the p38 MAPK signaling pathway following acute intracerebral hemorrhage. *FASEB J.* 34, 1872–1884. doi: 10.1096/fj.201902203RR

Habiyaremye, G., Morales, D. M., Morgan, C. D., Mcallister, J. P., Crevecoeur, T. S., Han, R. H., et al. (2017). Chemokine and cytokine levels in the lumbar cerebrospinal fluid of preterm infants with post-hemorrhagic hydrocephalus. *Fluids Barriers CNS* 14:35. doi: 10.1186/s12987-017-0083-0

Hammond, M. D., Ai, Y., and Sansing, L. H. (2012). Gr1+ macrophages and dendritic cells dominate the inflammatory infiltrate 12 hours after experimental intracerebral Hemorrhage. *Transl. Stroke Res.* 3, s125–s131. doi: 10.1007/s12975-012-0174-9

Hammond, M. D., Taylor, R. A., Mullen, M. T., Ai, Y., Aguila, H. L., Mack, M., et al. (2014). CCR2+ Ly6C(hi) inflammatory monocyte recruitment exacerbates acute disability following intracerebral hemorrhage. *J. Neurosci.* 34, 3901–3909. doi: 10.1523/JNEUROSCI.4070-13.2014

Harrison, J. K., Fong, A. M., Swain, P. A., Chen, S., Yu, Y. R., Salafranca, M. N., et al. (2001). Mutational analysis of the fractalkine chemokine domain. Basic amino acid residues differentially contribute to CX3CR1 binding, signaling, and cell adhesion. *J. Biol. Chem.* 276, 21632–21641. doi: 10.1074/jbc.M010261200

Harrison, J. K., Jiang, Y., Chen, S., Xia, Y., Maciejewski, D., Mcnamara, R. K., et al. (1998). Role for neuronally derived fractalkine in mediating interactions between neurons and CX3CR1-expressing microglia. *Proc. Natl. Acad. Sci. U. S. A.* 95, 10896–10901. doi: 10.1073/pnas.95.18.10896

Hatori, K., Nagai, A., Heisel, R., Ryu, J. K., and Kim, S. U. (2002). Fractalkine and fractalkine receptors in human neurons and glial cells. *J. Neurosci. Res.* 69, 418–426. doi: 10.1002/jnr.10304

Hinojosa, A. E., Garcia-Bueno, B., Leza, J. C., and Madrigal, J. L. (2011). CCL2/MCP-1 modulation of microglial activation and proliferation. *J. Neuroinflammation* 8:77. doi: 10.1186/1742-2094-8-77

Hoffmann, E., Dittrich-Breiholz, O., Holtmann, H., and Kracht, M. (2002). Multiple control of interleukin-8 gene expression. *J. Leukoc. Biol.* 72, 847–855. doi: 10.1189/jlb.72.5.847

Huang, S., Hu, W., Rao, D., Wu, X., Bai, Q., Wang, J., et al. (2022). RIPK3-dependent necroptosis activates MCP-1-mediated inflammation in mice after intracerebral Hemorrhage. *J. Stroke Cerebrovasc. Dis.* 31:106213. doi: 10.1016/j.jstrokecerebrovasdis.2021.106213

Huang, L., Ma, Q., Li, Y., Li, B., and Zhang, L. (2018). Inhibition of microRNA-210 suppresses pro-inflammatory response and reduces acute brain injury of ischemic stroke in mice. *Exp. Neurol.* 300, 41–50. doi: 10.1016/j.expneurol.2017.10.024

Huang, L. S. M., Snyder, E. Y., and Schooley, R. T. (2021). Strategies and Progress in CXCR4-targeted anti-human immunodeficiency virus (HIV) therapeutic development. *Clin. Infect. Dis.* 73, 919–924. doi: 10.1093/cid/ciab160

Huang, J., Yang, G., Xiong, X., Wang, M., Yuan, J., Zhang, Q., et al. (2020). Age-related CCL12 aggravates intracerebral Hemorrhage-induced brain injury via recruitment of macrophages and T lymphocytes. *Aging Dis.* 11, 1103–1115. doi: 10.14336/AD.2019.1229

Huber, A. K., Giles, D. A., Segal, B. M., and Irani, D. N. (2018). An emerging role for eotaxins in neurodegenerative disease. *Clin. Immunol.* 189, 29–33. doi: 10.1016/j.clim.2016.09.010

Imai, T., Nagira, M., Takagi, S., Kakizaki, M., Nishimura, M., Wang, J., et al. (1999). Selective recruitment of CCR4-bearing Th2 cells toward antigen-presenting cells by the CC chemokines thymus and activation-regulated chemokine and macrophage-derived chemokine. *Int. Immunol.* 11, 81–88. doi: 10.1093/intimm/11.1.81

Janssens, R., Struyf, S., and Proost, P. (2018a). Pathological roles of the homeostatic chemokine CXCL12. *Cytokine Growth Factor Rev.* 44, 51–68. doi: 10.1016/j.cytogfr.2018.10.004

Janssens, R., Struyf, S., and Proost, P. (2018b). The unique structural and functional features of CXCL12. *Cell. Mol. Immunol.* 15, 299–311. doi: 10.1038/cmi.2017.107

Jia, G. Q., Gonzalo, J. A., Lloyd, C., Kremer, L., Lu, L., Martinez, A. C., et al. (1996). Distinct expression and function of the novel mouse chemokine monocyte chemotactic protein-5 in lung allergic inflammation. *J. Exp. Med.* 184, 1939–1951. doi: 10.1084/jem.184.5.1939

Jiang, Z., Zhou, W., Guan, S., Wang, J., and Liang, Y. (2013). Contribution of SDF-1α/CXCR4 signaling to brain development and glioma progression. *Neurosignals* 21, 240–258. doi: 10.1159/000339091

Joy, M. T., Ben Assayag, E., Shabashov-Stone, D., Liraz-Zaltsman, S., Mazzitelli, J., Arenas, M., et al. (2019). CCR5 is a therapeutic target for recovery after stroke and traumatic brain injury. *Cells* 176:e1113, 1143–1157. doi: 10.1016/j.cell.2019.01.044

Katsuki, H., and Hijioka, M. (2017). Intracerebral Hemorrhage as an axonal tract injury disorder with inflammatory reactions. *Biol. Pharm. Bull.* 40, 564–568. doi: 10.1248/bpb.b16-01013

Keep, R. F., Hua, Y., and Xi, G. (2012). Intracerebral haemorrhage: mechanisms of injury and therapeutic targets. *Lancet Neurol.* 11, 720–731. doi: 10.1016/S1474-4422(12)70104-7

Kothur, K., Wienholt, L., Brilot, F., and Dale, R. C. (2016). CSF cytokines/chemokines as biomarkers in neuroinflammatory CNS disorders: A systematic review. *Cytokine* 77, 227–237. doi: 10.1016/j.cyto.2015.10.001

Lan, X., Han, X., Li, Q., Yang, Q. W., and Wang, J. (2017). Modulators of microglial activation and polarization after intracerebral haemorrhage. *Nat. Rev. Neurol.* 13, 420–433. doi: 10.1038/nrneurol.2017.69

Landreneau, M. J., Mullen, M. T., Messé, S. R., Cucchiara, B., Sheth, K. N., Mccullough, L. D., et al. (2018). CCL2 and CXCL10 are associated with poor outcome after intracerebral hemorrhage. *Ann. Clin. Transl. Neurol.* 5, 962–970. doi: 10.1002/acn3.595

Lanfranco, M. F., Mocchetti, I., Burns, M. P., and Villapol, S. (2017). Glial-and neuronal-specific expression of CCL5 mRNA in the rat brain. *Front. Neuroanat.* 11:137. doi: 10.3389/fnana.2017.00137

Le Thuc, O., Blondeau, N., Nahon, J. L., and Rovère, C. (2015). The complex contribution of chemokines to neuroinflammation: switching from beneficial to detrimental effects. *Ann. N. Y. Acad. Sci.* 1351, 127–140. doi: 10.1111/nyas.12855

Lei, Y., and Takahama, Y. (2012). XCL1 and XCR1 in the immune system. *Microbes Infect.* 14, 262–267. doi: 10.1016/j.micinf.2011.10.003

Levy, J. A. (2009). The unexpected pleiotropic activities of RANTES. *J. Immunol.* 182, 3945–3946. doi: 10.4049/jimmunol.0990015

Li, B., Bai, W., Sun, P., Zhou, B., Hu, B., and Ying, J. (2015). The effect of CXCL12 on endothelial progenitor cells: potential target for angiogenesis in intracerebral hemorrhage. *J. Interf. Cytokine Res.* 35, 23–31. doi: 10.1089/jir.2014.0004

Li, Z., Li, M., Shi, S. X., Yao, N., Cheng, X., Guo, A., et al. (2020). Brain transforms natural killer cells that exacerbate brain edema after intracerebral hemorrhage. *J. Exp. Med.* 217:e20200213. doi: 10.1084/jem.20200213

Li, Z., Luo, S., Fan, Y., and Sun, H. (2012). Dynamic changes in serum monocyte chemoattractant protein-1, and regulated upon activation, normal T cell expressed and secreted levels in patients with minor intracerebral hemorrhage. *Neurosciences (Riyadh)* 17, 314–320.

Li, Y., Niu, M., Zhao, A., Kang, W., Chen, Z., Luo, N., et al. (2019). CXCL12 is involved in α-synuclein-triggered neuroinflammation of Parkinson's disease. *J. Neuroinflammation* 16:263. doi: 10.1186/s12974-019-1646-6

Li, G., Yu, H., Liu, N., Zhang, P., Tang, Y., Hu, Y., et al. (2019). Overexpression of CX3CR1 in adipose-derived stem cells promotes cell migration and functional recovery after experimental intracerebral Hemorrhage. *Front. Neurosci.* 13:462. doi: 10.3389/fnins.2019.00462

Lin, H., Shen, J., Zhu, Y., Zhou, L., Zhang, S., Liu, Z., et al. (2022). Serum CCL23 emerges as a biomarker for poor prognosis in patients with intracerebral hemorrhage. *Clin. Chim. Acta* 537, 188–193. doi: 10.1016/j.cca.2022.10.012

Liu, J. X., Cao, X., Tang, Y. C., Liu, Y., and Tang, F. R. (2007). CCR7, CCR8, CCR9 and CCR10 in the mouse hippocampal CA1 area and the dentate gyrus during and after pilocarpine-induced status epilepticus. *J. Neurochem.* 100, 1072–1088. doi: 10.1111/j.1471-4159.2006.04272.x

Liu, Q., Li, A., Tian, Y., Wu, J. D., Liu, Y., Li, T., et al. (2016). The CXCL8-CXCR1/2 pathways in cancer. *Cytokine Growth Factor Rev.* 31, 61–71. doi: 10.1016/j.cytogfr.2016.08.002

Liu, J., Liu, L., Wang, X., Jiang, R., Bai, Q., and Wang, G. (2021). Microglia: A double-edged sword in intracerebral Hemorrhage from basic mechanisms to clinical research. *Front. Immunol.* 12:675660. doi: 10.3389/fimmu.2021.773896

Lu, W., Maheshwari, A., Misiuta, I., Fox, S. E., Chen, N., Zigova, T., et al. (2005). Neutrophil-specific chemokines are produced by astrocytic cells but not by neuronal cells. *Brain Res. Dev. Brain Res.* 155, 127–134. doi: 10.1016/j.devbrainres.2005.01.004

Mackenzie, J. M., and Clayton, J. A. (1999). Early cellular events in the penumbra of human spontaneous intracerebral hemorrhage. *J. Stroke Cerebrovasc. Dis.* 8, 1–8. doi: 10.1016/S1052-3057(99)80032-9

Mai, C. L., Tan, Z., Xu, Y. N., Zhang, J. J., Huang, Z. H., Wang, D., et al. (2021). CXCL12-mediated monocyte transmigration into brain perivascular space leads to neuroinflammation and memory deficit in neuropathic pain. *Theranostics* 11, 1059–1078. doi: 10.7150/thno.44364

Mamik, M. K., and Ghorpade, A. (2016). CXCL8 as a potential therapeutic target for HIV-associated neurocognitive disorders. *Curr. Drug Targets* 17, 111–121. doi: 10.2174/1389450116666150626124544

Mantovani, A., Sica, A., Sozzani, S., Allavena, P., Vecchi, A., and Locati, M. (2004). The chemokine system in diverse forms of macrophage activation and polarization. *Trends Immunol.* 25, 677–686. doi: 10.1016/j.it.2004.09.015

Marques, R. E., Guabiraba, R., Russo, R. C., and Teixeira, M. M. (2013). Targeting CCL5 in inflammation. *Expert Opin. Ther. Targets* 17, 1439–1460. doi: 10.1517/14728222.2013.837886

Martin-Blondel, G., Brassat, D., Bauer, J., Lassmann, H., and Liblau, R. S. (2016). CCR5 blockade for neuroinflammatory diseases--beyond control of HIV. *Nat. Rev. Neurol.* 12, 95–105. doi: 10.1038/nrneurol.2015.248

Matsumoto, K., Kinoshita, K., Yoshimizu, A., Kurauchi, Y., Hisatsune, A., Seki, T., et al. (2020). Laquinimod and 3,3′-diindolylemethane alleviate neuropathological events and neurological deficits in a mouse model of intracerebral hemorrhage. *J. Neuroimmunol.* 342:577195. doi: 10.1016/j.jneuroim.2020.577195

Matsushima, K. (2000). Chemokines. Introduction. *Springer Semin. Immunopathol.* 22, 321–328. doi: 10.1007/s002810000049

Matsushima, K., Yang, D., and Oppenheim, J. J. (2022). Interleukin-8: An evolving chemokine. *Cytokine* 153:155828. doi: 10.1016/j.cyto.2022.155828

Matsushita, H., Hijioka, M., Ishibashi, H., Anan, J., Kurauchi, Y., Hisatsune, A., et al. (2014). Suppression of CXCL2 upregulation underlies the therapeutic effect of the retinoid Am80 on intracerebral hemorrhage in mice. *J. Neurosci. Res.* 92, 1024–1034. doi: 10.1002/jnr.23379

Maurer, M., and Von Stebut, E. (2004). Macrophage inflammatory protein-1. *Int. J. Biochem. Cell Biol.* 36, 1882–1886. doi: 10.1016/j.biocel.2003.10.019

Mckimmie, C. S., and Graham, G. J. (2010). Astrocytes modulate the chemokine network in a pathogen-specific manner. *Biochem. Biophys. Res. Commun.* 394, 1006–1011. doi: 10.1016/j.bbrc.2010.03.111

Meitei, H. T., Jadhav, N., and Lal, G. (2021). CCR6-CCL20 axis as a therapeutic target for autoimmune diseases. *Autoimmun. Rev.* 20:102846. doi: 10.1016/j.autrev.2021.102846

Menten, P., Wuyts, A., and Van Damme, J. (2002). Macrophage inflammatory protein-1. *Cytokine Growth Factor Rev.* 13, 455–481. doi: 10.1016/S1359-6101(02)00045-X

Meucci, O., Fatatis, A., Simen, A. A., and Miller, R. J. (2000). Expression of CX3CR1 chemokine receptors on neurons and their role in neuronal survival. *Proc. Natl. Acad. Sci. U. S. A.* 97, 8075–8080. doi: 10.1073/pnas.090017497

Min, H., Jang, Y. H., Cho, I.-H., Yu, S.-W., and Lee, S. J. (2016). Alternatively activated brain-infiltrating macrophages facilitate recovery from collagenase-induced intracerebral hemorrhage. *Mol. Brain* 9:42. doi: 10.1186/s13041-016-0225-3

Mithal, D. S., Banisadr, G., and Miller, R. J. (2012). CXCL12 signaling in the development of the nervous system. *J. Neuroimmune Pharmacol.* 7, 820–834. doi: 10.1007/s11481-011-9336-x

Mojsilovic-Petrovic, J., Callaghan, D., Cui, H., Dean, C., Stanimirovic, D. B., and Zhang, W. (2007). Hypoxia-inducible factor-1 (HIF-1) is involved in the regulation of hypoxia-stimulated expression of monocyte chemoattractant protein-1 (MCP-1/CCL2) and MCP-5 (Ccl12) in astrocytes. *J. Neuroinflammation* 4:12. doi: 10.1186/1742-2094-4-12

Moser, B. (2022). Chemokine receptor-targeted therapies: special case for CCR8. *Cancers (Basel)* 14:511. doi: 10.3390/cancers14030511

Murphy, P. M., Baggiolini, M., Charo, I. F., Hébert, C. A., Horuk, R., Matsushima, K., et al. (2000). International union of pharmacology. XXII. Nomenclature for chemokine receptors. *Pharmacol. Rev.* 52, 145–176. PMID: 10699158

Nagasawa, T., Hirota, S., Tachibana, K., Takakura, N., Nishikawa, S., Kitamura, Y., et al. (1996). Defects of B-cell lymphopoiesis and bone-marrow myelopoiesis in mice lacking the CXC chemokine PBSF/SDF-1. *Nature* 382, 635–638. doi: 10.1038/382635a0

Nash, B., Thomson, C. E., Linington, C., Arthur, A. T., Mcclure, J. D., Mcbride, M. W., et al. (2011). Functional duality of astrocytes in myelination. *J. Neurosci.* 31, 13028–13038. doi: 10.1523/JNEUROSCI.1449-11.2011

Nomiyama, H., Imai, T., Kusuda, J., Miura, R., Callen, D. F., and Yoshie, O. (1998). Human chemokines fractalkine (SCYD1), MDC (SCYA22) and TARC (SCYA17) are clustered on chromosome 16q13. *Cytogenet. Cell Genet.* 81, 10–11. doi: 10.1159/000015000

O'carroll, C. B., Brown, B. L., and Freeman, W. D. (2021). Intracerebral Hemorrhage: a common yet disproportionately deadly stroke subtype. *Mayo Clin. Proc.* 96, 1639–1654. doi: 10.1016/j.mayocp.2020.10.034

Pan, D., Acevedo-Cintrón, J. A., Sayanagi, J., Snyder-Warwick, A. K., Mackinnon, S. E., and Wood, M. D. (2020). The CCL2/CCR2 axis is critical to recruiting macrophages into acellular nerve allograft bridging a nerve gap to promote angiogenesis and regeneration. *Exp. Neurol.* 331:113363. doi: 10.1016/j.expneurol.2020.113363

Pan, Z., Zhu, T., Liu, Y., and Zhang, N. (2022). Role of the CXCL13/CXCR5 Axis in autoimmune diseases. *Front. Immunol.* 13:850998. doi: 10.3389/fimmu.2022.1061939

Pease, J. E., and Horuk, R. (2014). Recent progress in the development of antagonists to the chemokine receptors CCR3 and CCR4. *Expert. Opin. Drug Discov.* 9, 467–483. doi: 10.1517/17460441.2014.897324

Pedragosa, J., Miró-Mur, F., Otxoa-De-Amezaga, A., Justicia, C., Ruíz-Jaén, F., Ponsaerts, P., et al. (2020). CCR2 deficiency in monocytes impairs angiogenesis and functional recovery after ischemic stroke in mice. *J. Cereb. Blood Flow Metab.* 40, S98–s116. doi: 10.1177/0271678X20909055

Penn, M. S., Mendelsohn, F. O., Schaer, G. L., Sherman, W., Farr, M., Pastore, J., et al. (2013). An open-label dose escalation study to evaluate the safety of administration of nonviral stromal cell-derived factor-1 plasmid to treat symptomatic ischemic heart failure. *Circ. Res.* 112, 816–825. doi: 10.1161/CIRCRESAHA.111.300440

Popiolek-Barczyk, K., Ciechanowska, A., Ciapała, K., Pawlik, K., Oggioni, M., Mercurio, D., et al. (2020). The CCL2/CCL7/CCL12/CCR2 pathway is substantially and persistently upregulated in mice after traumatic brain injury, and CCL2 modulates the complement system in microglia. *Mol. Cell. Probes* 54:101671. doi: 10.1016/j.mcp.2020.101671

Pozzobon, T., Goldoni, G., Viola, A., and Molon, B. (2016). CXCR4 signaling in health and disease. *Immunol. Lett.* 177, 6–15. doi: 10.1016/j.imlet.2016.06.006

Repnik, U., Starr, A. E., Overall, C. M., and Turk, B. (2015). Cysteine cathepsins activate ELR chemokines and inactivate non-ELR chemokines. *J. Biol. Chem.* 290, 13800–13811. doi: 10.1074/jbc.M115.638395

Rezaie, P., Trillo-Pazos, G., Everall, I. P., and Male, D. K. (2002). Expression of beta-chemokines and chemokine receptors in human fetal astrocyte and microglial co-cultures: potential role of chemokines in the developing CNS. *Glia* 37, 64–75. doi: 10.1002/glia.1128

Rodríguez, C., Sobrino, T., Agulla, J., Bobo-Jiménez, V., Ramos-Araque, M. E., Duarte, J. J., et al. (2017). Neovascularization and functional recovery after intracerebral hemorrhage is conditioned by the Tp53 Arg72Pro single-nucleotide polymorphism. *Cell Death Differ.* 24, 144–154. doi: 10.1038/cdd.2016.109

Rosell, A., Vilalta, A., García-Berrocoso, T., Fernández-Cadenas, I., Domingues-Montanari, S., Cuadrado, E., et al. (2011). Brain perihematoma genomic profile following spontaneous human intracerebral hemorrhage. *PLoS One* 6:e16750. doi: 10.1371/journal.pone.0016750

Ruland, C., Renken, H., Kuzmanov, I., Fattahi Mehr, A., Schwarte, K., Cerina, M., et al. (2017). Chemokine CCL17 is expressed by dendritic cells in the CNS during experimental autoimmune encephalomyelitis and promotes pathogenesis of disease. *Brain Behav. Immun.* 66, 382–393. doi: 10.1016/j.bbi.2017.06.010

Saand, A. R., Yu, F., Chen, J., and Chou, S. H. (2019). Systemic inflammation in hemorrhagic strokes – A novel neurological sign and therapeutic target? *J. Cereb. Blood Flow Metab.* 39, 959–988. doi: 10.1177/0271678X19841443

Sarafi, M. N., Garcia-Zepeda, E. A., Maclean, J. A., Charo, I. F., and Luster, A. D. (1997). Murine monocyte chemoattractant protein (MCP)-5: a novel CC chemokine that is a structural and functional homologue of human MCP-1. *J. Exp. Med.* 185, 99–109. doi: 10.1084/jem.185.1.99

Schall, T. J., Jongstra, J., Dyer, B. J., Jorgensen, J., Clayberger, C., Davis, M. M., et al. (1988). A human T cell-specific molecule is a member of a new gene family. *J. Immunol.* 141, 1018–1025. PMID: 2456327

Scheu, S., Ali, S., Ruland, C., Arolt, V., and Alferink, J. (2017). The C-C chemokines CCL17 and CCL22 and their receptor CCR4 in CNS autoimmunity. *Int. J. Mol. Sci.* 18:2306. doi: 10.3390/ijms18112306

Scimemi, A. (2018). Astrocytes and the warning signs of intracerebral Hemorrhagic stroke. *Neural Plast.* 2018:7301623. doi: 10.1155/2018/7301623

Semple, B. D., Kossmann, T., and Morganti-Kossmann, M. C. (2010). Role of chemokines in CNS health and pathology: a focus on the CCL2/CCR2 and CXCL8/CXCR2 networks. *J. Cereb. Blood Flow Metab.* 30, 459–473. doi: 10.1038/jcbfm.2009.240

Shen, J., Chen, B., Zheng, G. R., Qiu, S. Z., Yin, H. M., Mao, W., et al. (2017). Detection of high serum concentration of CXC chemokine ligand-12 in acute intracerebral hemorrhage. *Clin. Chim. Acta* 471, 55–61. doi: 10.1016/j.cca.2017.05.022

Shibuya, R., Ishida, Y., Hanakawa, S., Kataoka, T. R., Takeuchi, Y., Murata, T., et al. (2022). CCL2–CCR2 Signaling in the skin drives surfactant-induced irritant contact dermatitis through IL-1β–mediated neutrophil accumulation. *J. Invest. Dermatol.* 142, 571–582.e579. doi: 10.1016/j.jid.2021.07.182

Shishehbor, M. H., Rundback, J., Bunte, M., Hammad, T. A., Miller, L., Patel, P. D., et al. (2019). SDF-1 plasmid treatment for patients with peripheral artery disease (STOP-PAD): randomized, double-blind, placebo-controlled clinical trial. *Vasc. Med.* 24, 200–207. doi: 10.1177/1358863X18817610

Shtaya, A., Bridges, L. R., Esiri, M. M., Lam-Wong, J., Nicoll, J. A. R., Boche, D., et al. (2019). Rapid neuroinflammatory changes in human acute intracerebral hemorrhage. *Ann. Clin. Transl. Neurol.* 6, 1465–1479. doi: 10.1002/acn3.50842

Sierra-Filardi, E., Nieto, C., Domínguez-Soto, A., Barroso, R., Sánchez-Mateos, P., Puig-Kroger, A., et al. (2014). CCL2 shapes macrophage polarization by GM-CSF and M-CSF: identification of CCL2/CCR2-dependent gene expression profile. *J. Immunol.* 192, 3858–3867. doi: 10.4049/jimmunol.1302821

Strieter, R. M., Polverini, P. J., Arenberg, D. A., Walz, A., Opdenakker, G., Van Damme, J., et al. (1995). Role of C-X-C chemokines as regulators of angiogenesis in lung cancer. *J. Leukoc. Biol.* 57, 752–762. doi: 10.1002/jlb.57.5.752

Subbarayan, M. S., Joly-Amado, A., Bickford, P. C., and Nash, K. R. (2022). CX3CL1/CX3CR1 signaling targets for the treatment of neurodegenerative diseases. *Pharmacol. Ther.* 231:107989. doi: 10.1016/j.pharmthera.2021.107989

Trettel, F., Di Castro, M. A., and Limatola, C. (2020). Chemokines: key molecules that orchestrate communication among neurons, microglia and astrocytes to preserve brain function. *Neuroscience* 439, 230–240. doi: 10.1016/j.neuroscience.2019.07.035

Vallès, A., Grijpink-Ongering, L., De Bree, F. M., Tuinstra, T., and Ronken, E. (2006). Differential regulation of the CXCR2 chemokine network in rat brain trauma: implications for neuroimmune interactions and neuronal survival. *Neurobiol. Dis.* 22, 312–322. doi: 10.1016/j.nbd.2005.11.015

Van Coillie, E., Van Damme, J., and Opdenakker, G. (1999). The MCP/eotaxin subfamily of CC chemokines. *Cytokine Growth Factor Rev.* 10, 61–86. doi: 10.1016/S1359-6101(99)00005-2

Van Helden, M. J., Zaiss, D. M., and Sijts, A. J. (2012). CCR2 defines a distinct population of NK cells and mediates their migration during influenza virus infection in mice. *PLoS One* 7:e52027. doi: 10.1371/journal.pone.0052027

Vasanthakumar, A., Chisanga, D., Blume, J., Gloury, R., Britt, K., Henstridge, D. C., et al. (2020). Sex-specific adipose tissue imprinting of regulatory T cells. *Nature* 579, 581–585. doi: 10.1038/s41586-020-2040-3

Wang, J. (2010). Preclinical and clinical research on inflammation after intracerebral hemorrhage. *Prog. Neurobiol.* 92, 463–477. doi: 10.1016/j.pneurobio.2010.08.001

Wang, Y., Dembowsky, K., Chevalier, E., Stüve, P., Korf-Klingebiel, M., Lochner, M., et al. (2019). C-X-C motif chemokine receptor 4 blockade promotes tissue repair after myocardial infarction by enhancing regulatory T cell mobilization and immune-regulatory function. *Circulation* 139, 1798–1812. doi: 10.1161/CIRCULATIONAHA.118.036053

Wang, J., Gan, Y., Han, P., Yin, J., Liu, Q., Ghanian, S., et al. (2018). Ischemia-induced neuronal cell death is mediated by chemokine receptor CX3CR1. *Sci. Rep.* 8:556. doi: 10.1038/s41598-017-18774-0

Wang, D., Wang, J., Li, Z., Gu, H., Yang, K., Zhao, X., et al. (2022). C-reaction protein and the severity of intracerebral Hemorrhage: A study from Chinese stroke Center Alliance. *Neurol. Res.* 44, 285–290. doi: 10.1080/01616412.2021.1980842

White, G. E., Iqbal, A. J., and Greaves, D. R. (2013). CC chemokine receptors and chronic inflammation--therapeutic opportunities and pharmacological challenges. *Pharmacol. Rev.* 65, 47–89. doi: 10.1124/pr.111.005074

Woollard, S. M., and Kanmogne, G. D. (2015). Maraviroc: a review of its use in HIV infection and beyond. *Drug Des. Devel. Ther.* 9, 5447–5468. doi: 10.2147/DDDT.S90580

Wu, X., Sun, M., Yang, Z., Lu, C., Wang, Q., Wang, H., et al. (2021). The roles of CCR9/CCL25 in inflammation and inflammation-associated diseases. *Front. Cell Dev. Biol.* 9:686548. doi: 10.3389/fcell.2021.810635

Xiong, N., Fu, Y., Hu, S., Xia, M., and Yang, J. (2012). CCR10 and its ligands in regulation of epithelial immunity and diseases. *Protein Cell* 3, 571–580. doi: 10.1007/s13238-012-2927-3

Xu, D., Gao, Q., Wang, F., Peng, Q., Wang, G., Wei, Q., et al. (2021). Sphingosine-1-phosphate receptor 3 is implicated in BBB injury via the CCL2-CCR2 axis following acute intracerebral hemorrhage. *CNS Neurosci. Ther.* 27, 674–686. doi: 10.1111/cns.13626

Xu, J. H., Long, L., Tang, Y. C., Zhang, J. T., Hut, H. T., and Tang, F. R. (2009). CCR3, CCR2A and macrophage inflammatory protein (MIP)-1a, monocyte chemotactic protein-1 (MCP-1) in the mouse hippocampus during and after pilocarpine-induced status epilepticus (PISE). *Neuropathol. Appl. Neurobiol.* 35, 496–514. doi: 10.1111/j.1365-2990.2009.01022.x

Xue, M., and Yong, V. W. (2020). Neuroinflammation in intracerebral haemorrhage: immunotherapies with potential for translation. *Lancet Neurol.* 19, 1023–1032. doi: 10.1016/S1474-4422(20)30364-1

Yan, J., Xu, W., Lenahan, C., Huang, L., Ocak, U., Wen, J., et al. (2022). Met-RANTES preserves the blood-brain barrier through inhibiting CCR1/SRC/Rac1 pathway after intracerebral hemorrhage in mice. *Fluids Barriers CNS* 19:7. doi: 10.1186/s12987-022-00305-3

Yan, J., Xu, W., Lenahan, C., Huang, L., Wen, J., Li, G., et al. (2021). CCR5 activation promotes NLRP1-dependent neuronal Pyroptosis via CCR5/PKA/CREB pathway after intracerebral Hemorrhage. *Stroke* 52, 4021–4032. doi: 10.1161/STROKEAHA.120.033285

Yan, J., Zuo, G., Sherchan, P., Huang, L., Ocak, U., Xu, W., et al. (2020). CCR1 activation promotes neuroinflammation through CCR1/TPR1/ERK1/2 Signaling pathway after intracerebral Hemorrhage in mice. *Neurotherapeutics* 17, 1170–1183. doi: 10.1007/s13311-019-00821-5

Yang, Z., Wang, J., Yu, Y., and Li, Z. (2016). Gene silencing of MCP-1 prevents microglial activation and inflammatory injury after intracerebral hemorrhage. *Int. Immunopharmacol.* 33, 18–23. doi: 10.1016/j.intimp.2016.01.016

Yao, Y., and Tsirka, S. E. (2012a). The CCL2-CCR2 system affects the progression and clearance of intracerebral hemorrhage. *Glia* 60, 908–918. doi: 10.1002/glia.22323

Yao, Y., and Tsirka, S. E. (2012b). Chemokines and their receptors in intracerebral hemorrhage. *Transl. Stroke Res.* 3, 70–79. doi: 10.1007/s12975-012-0155-z

Yoshida, H., Imaizumi, T., Fujimoto, K., Matsuo, N., Kimura, K., Cui, X., et al. (2001). Synergistic stimulation, by tumor necrosis factor-alpha and interferon-gamma, of fractalkine expression in human astrocytes. *Neurosci. Lett.* 303, 132–136. doi: 10.1016/S0304-3940(01)01699-8

Yoshie, O., and Matsushima, K. (2015). CCR4 and its ligands: from bench to bedside. *Int. Immunol.* 27, 11–20. doi: 10.1093/intimm/dxu079

Yoshimura, T. (2015). Discovery of IL-8/CXCL8 (the story from Frederick). *Front. Immunol.* 6:278. doi: 10.3389/fimmu.2015.00278

You, M., Long, C., Wan, Y., Guo, H., Shen, J., Li, M., et al. (2022). Neuron derived fractalkine promotes microglia to absorb hematoma via CD163/HO-1 after intracerebral hemorrhage. *Cell. Mol. Life Sci.* 79:224. doi: 10.1007/s00018-022-04212-6

Yu, S.-J., Wu, K.-J., Wang, Y.-S., Song, J.-S., Wu, C.-H., Jan, J.-J., et al. (2020). Protective effect of CXCR4 antagonist CX807 in a rat model of Hemorrhagic stroke. *Int. J. Mol. Sci.* 21:7085. doi: 10.3390/ijms21197085

Zhan, Y., Paolicelli, R. C., Sforazzini, F., Weinhard, L., Bolasco, G., Pagani, F., et al. (2014). Deficient neuron-microglia signaling results in impaired functional brain connectivity and social behavior. *Nat. Neurosci.* 17, 400–406. doi: 10.1038/nn.3641

Zhang, A., Liu, Y., Xu, H., Zhang, Z., Wang, X., Yuan, L., et al. (2022). CCL17 exerts neuroprotection through activation of CCR4/mTORC2 axis in microglia after subarachnoid haemorrhage in rats. *Stroke Vasc Neurol.* svn-2022-001659. doi: 10.1136/svn-2022-001659

Zhang, L., Mamillapalli, R., Habata, S., Mcadow, M., and Taylor, H. S. (2022). Myometrial-derived CXCL12 promotes lipopolysaccharide induced preterm labour by regulating macrophage migration, polarization and function in mice. *J. Cell. Mol. Med.* 26, 2566–2578. doi: 10.1111/jcmm.17252

Zhang, T., Somasundaram, R., Berencsi, K., Caputo, L., Gimotty, P., Rani, P., et al. (2006). Migration of cytotoxic T lymphocytes toward melanoma cells in three-dimensional organotypic culture is dependent on CCL2 and CCR4. *Eur. J. Immunol.* 36, 457–467. doi: 10.1002/eji.200526208

Zhu, H., Wang, Z., Yu, J., Yang, X., He, F., Liu, Z., et al. (2019). Role and mechanisms of cytokines in the secondary brain injury after intracerebral hemorrhage. *Prog. Neurobiol.* 178:101610. doi: 10.1016/j.pneurobio.2019.03.003

Ziai, W. C., Parry-Jones, A. R., Thompson, C. B., Sansing, L. H., Mullen, M. T., Murthy, S. B., et al. (2021). Early inflammatory cytokine expression in cerebrospinal fluid of patients with spontaneous intraventricular Hemorrhage. *Biomol. Ther.* 11:1123. doi: 10.3390/biom11081123

Zlokovic, B. V. (2008). The blood-brain barrier in health and chronic neurodegenerative disorders. *Neuron* 57, 178–201. doi: 10.1016/j.neuron.2008.01.003

Zlotnik, A., Morales, J., and Hedrick, J. A. (1999). Recent advances in chemokines and chemokine receptors. *Crit. Rev. Immunol.* 19, 1–47. PMID: 9987599

Zlotnik, A., and Yoshie, O. (2012). The chemokine superfamily revisited. *Immunity* 36, 705–716. doi: 10.1016/j.immuni.2012.05.008

frontiers | Frontiers in Molecular Neuroscience

TYPE Review
PUBLISHED 12 January 2023
DOI 10.3389/fnmol.2022.1061343

OPEN ACCESS

EDITED BY
Federica Bono,
University of Brescia,
Italy

REVIEWED BY
Gerald Seifert,
University Hospital Bonn,
Germany
Naomi Sayre,
The University of Texas Health Science Center at San Antonio, United States

*CORRESPONDENCE
Junfei Shao
✉ wxbrain@163.com
Weiyi Huang
✉ weiy_huang@126.com

†These authors have contributed equally to this work and share last authorship

SPECIALTY SECTION
This article was submitted to Brain Disease Mechanisms, a section of the journal Frontiers in Molecular Neuroscience

RECEIVED 04 October 2022
ACCEPTED 22 December 2022
PUBLISHED 12 January 2023

CITATION
Fan Y, Huang H, Shao J and Huang W (2023) MicroRNA-mediated regulation of reactive astrocytes in central nervous system diseases. *Front. Mol. Neurosci.* 15:1061343. doi: 10.3389/fnmol.2022.1061343

MicroRNA-mediated regulation of reactive astrocytes in central nervous system diseases

Yuansheng Fan, Hui Huang, Junfei Shao*† and Weiyi Huang*†

Department of Neurosurgery, The Affiliated Wuxi People's Hospital of Nanjing Medical University, Wuxi, Jiangsu, China

Astrocytes (AST) are abundant glial cells in the human brain, accounting for approximately 20–50% percent of mammalian central nervous system (CNS) cells. They display essential functions necessary to sustain the physiological processes of the CNS, including maintaining neuronal structure, forming the blood–brain barrier, coordinating neuronal metabolism, maintaining the extracellular environment, regulating cerebral blood flow, stabilizing intercellular communication, participating in neurotransmitter synthesis, and defending against oxidative stress et al. During the pathological development of brain tumors, stroke, spinal cord injury (SCI), neurodegenerative diseases, and other neurological disorders, astrocytes undergo a series of highly heterogeneous changes, which are called reactive astrocytes, and mediate the corresponding pathophysiological process. However, the pathophysiological mechanisms of reactive astrocytes and their therapeutic relevance remain unclear. The microRNAs (miRNAs) are essential for cell differentiation, proliferation, and survival, which play a crucial role in the pathophysiological development of CNS diseases. In this review, we summarize the regulatory mechanism of miRNAs on reactive astrocytes in CNS diseases, which might provide a theoretical basis for the diagnosis and treatment of CNS diseases.

KEYWORDS

central nervous system, microRNAs, ischemic stroke, spinal cord injury, neurodegenerative disease, reactive astrocytes

1. Introduction

Astrocytes are one of the most significant cellular components and represent the largest number of cells in the CNS, accounting for 20–50% of all CNS cells, which play an important role in maintaining endocytosis of extracellular fluid, ions, and transmitters (Verkhratsky and Nedergaard, 2018), feeding neurons (Magistretti and Allaman, 2018), regulating local blood flow (Mac Vicar and Newman, 2015), helping regulate interstitial fluid drainage (Plog and Nedergaard, 2018) as well as synaptic development and plasticity (Allen and Eroglu, 2017). There are two types of astrocytes, fibrous and protoplasmic astrocytes, based on the content of glial filaments and the shape of cytoplasmic protrusions. Fibrous astrocytes are primarily distributed in the cerebral cortex, with elongated protrusions and fewer branches. Protoplasmic astrocytes are mainly in gray matter, with

thick and short protrusions and many branches. However, this traditional classification ignores the heterogeneity of astrocytes, which exhibit transcriptomic and functional heterogeneity in different brain regions and cortical layers (Yeh et al., 2009; Zeisel et al., 2015; Lanjakornsiripan et al., 2018).

Reactive astrocytes, induced by brain injuries and disease, undergo a series of molecular, morphological, and functional alterations such as inflammatory factor release (Hasel et al., 2021), glial scar formation (Sofroniew and Vinters, 2010), downregulation of glutamate transporter-1 (GLT-1) expression (Tanaka et al., 1997), and upregulation of water channel protein aquaporin 4 (AQP4; Kitchen et al., 2020). These reactive astrocytes are crucial in regulating the neuron, microglia, and CNS microenvironment after SCI, stroke, neurodegeneration, and others (Liddelow and Barres, 2017). Studies have found that miRNAs play a profound role in mediating the activities and functions of reactive astrocytes in recent years. miRNAs are a class of endogenous small non-coding RNA molecules (20–25 nucleotides). Mature miRNAs under the action of RISC complex, namely RNA-induced silencing complex, work with the 3'UTR specific base of target gene mRNA sequence to cause the degradation of target gene mRNA or to inhibit the translation of target gene mRNA, thereby regulating the post-transcriptional expression of genes. In addition, miRNAs may interact with the target gene mRNA 5′-UTR coding sequences and the target promoter region. Researchers initially considered miRNAs critical players in CNS development (Worringer et al., 2014). Nonetheless, as research progress, studies have identified miRNAs as essential in CNS diseases. miRNAs in these diseases are often altered by genomic events such as gene mutations, deletion amplification, or transcriptional changes, or by mutations or downregulation of enzymes that regulate miRNA biogenesis, resulting in biogenetic defects (Bartel, 2004; Lin and Gregory, 2015; Rupaimoole et al., 2016). Studies have been on miRNAs as potential targets to regulate glioma cells' proliferation, migration, and invasion. Meanwhile, mounting data suggests that miRNAs could exert a range of protective effects by regulating the activities and functions of reactive astrocytes in CNS diseases such as stroke, SCI, and neurodegeneration (Hong et al., 2014; Duan et al., 2021; Li L. et al., 2021).

This article reviews the research on miRNAs in regulating the activities and functions of reactive astrocytes and summarizes the relevant mechanisms of miRNAs regulating reactive astrocytes in CNS diseases to provide a theoretical basis for diagnosing and treating CNS diseases.

2. MicroRNAs regulate the activities and functions of reactive astrocytes

2.1. Apoptosis and autophagy

Apoptosis is the orderly process of cell death through intracellular genetic mechanisms that eventually lead to the degradation and digestion of all cellular components by other living cells. Autophagy, a catabolic process, could degrade and recycle dysfunctional organelles and proteins (Fricker et al., 2018). During brain ischemia, astrocytes undergo autophagy, which represents the cell's attempt to cope with stress and protects the cell from apoptosis (Mo et al., 2020). Thus, autophagy might protect astrocytes from apoptosis injured by ischemia. In a study, circ_0025984 expression is significantly reduced in astrocytes during cerebral ischemia, and its overexpression strongly inhibits ischemia-induced astrocyte apoptosis to suppress brain injury. And it has been shown that the protective effect of circ_0025984 is associated with the inhibition of apoptosis by directly targeting the miR-134-3p/TET1/ORP150 pathway (Zhou et al., 2021). Similarly, miR-30d, which targets BECLIN1, is essential in the interplay between astrocyte autophagy and apoptosis following oxygen–glucose deprivation reperfusion (OGD/R). miR-30d could be seen as a novel target to attenuate cellular damage under hypoxic–ischemic conditions (Zhao et al., 2017).

2.2. Pathophysiological functions

Astrocytes have long been identified essential mediators in maintaining the CNS microenvironment's homeostasis under physiological conditions and performing critical physiological functions. However, studies over the past few decades have revealed that astrocytes undergo significant cellular, molecular, and functional alterations to transform into reactive astrocytes following pathological injury in the CNS. These changes are used to regulate the blood–brain barrier, excitability regulation, oxidative stress, neuroinflammation, and glial scar in response to the homeostatic dysregulation (Figure 1).

2.2.1. Blood–brain barrier

Vascular endothelial cells, astrocytes, and peripheral cells are participated in the maturation and maintenance of the blood–brain barrier, which is critical for the homeostasis and function of the CNS (Weiss et al., 2009; Daneman and Engelhardt, 2017; Liebner et al., 2018). The blood–brain barrier, which covers approximately 99% of the cerebrovascular surface, regulates blood–brain barrier integrity and cerebral blood flow (Iadecola and Nedergaard, 2007; Masamoto et al., 2015), and forms a secondary barrier that further prevents peripheral immune cells from non-neural tissue from entering the CNS (Sofroniew and Vinters, 2010). Gap junction proteins, such as connexin, AQP4, and Kir4.1 channels, which are specific dynamic sites regulating ion and water flow, and are essential for blood–brain barrier function, are abundant in the astrocyte end-food (Alvarez et al., 2013; Boulay et al., 2016). The perivascular astrocytes polarize in SCI (Nesic et al., 2006), ischemic stroke (Manley et al., 2000), and tumors (Verkman et al., 2008) to upregulate the expression of AQP4 on cell membranes, resulting in end-foot edema and vascular regression. This causes gap junctions to open and the blood–brain barrier to be damaged, which induces a series of secondary brain injuries (Xiang et al., 2016; Haley and Lawrence, 2017). Apolipoprotein E (ApoE) is a multifaceted secreted

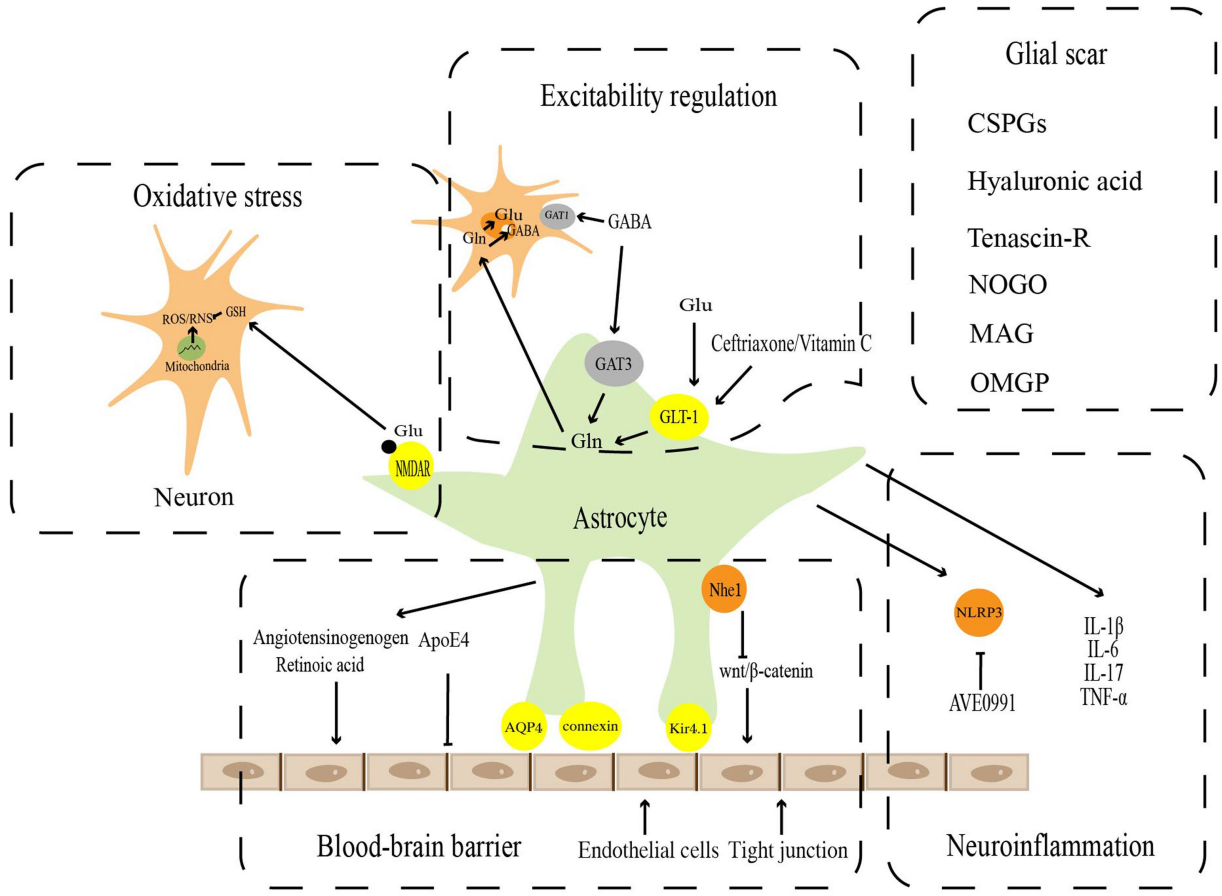

FIGURE 1
Pathophysiological functions of reactive astrocytes. Astrocytes play a key role in the maintenance of CNS homeostasis, including blood–brain barrier, excitatory regulation, oxidative stress, neuroinflammation, and Glia scar.

molecule synthesized in the CNS by astrocytes and microglia (Lanfranco et al., 2021). ApoE has been shown to impact the integrity of the blood–brain barrier (Montagne et al., 2020). Specific expression of ApoE4 alleles but not APOE2 or APOE3 derived from astrocytes results in disrupting blood–brain barrier integrity, increasing matrix metallopeptidase 9 (MMP9), impairing tight junctions, and reducing vascular coverage (Jackson et al., 2022). Wnt growth factor secreted by astrocytes maintains the integrity of the blood–brain barrier by promoting Wnt/β-linked protein activity in endothelial cells (Guérit et al., 2021). It has recently been shown that astrocytes could repair the blood–brain barrier with Nhe1 protein deficiency *via* the Wnt/β-catenin signaling pathway (Song et al., 2021). In addition, the angiotensinogen released by astrocytes could be converted into angiotensin to regulate the expression of occludin, one of the major tight junction proteins, *in vivo* (Wosik et al., 2007). Meanwhile, retinoic acid secreted by astrocytes and radial glial cells could also increase the levels of tight junction components such as ZO-1 (Mizee et al., 2013).

Ischemic stroke is caused by reduced or blocked blood flow to the CNS due to a distant embolus, *in situ* thrombus, or atherosclerotic plaque formation blocking an artery in the brain. miRNAs and astrocytes are key players in the progression of ischemic stroke. Their regulatory roles in ischemia-induced oxidative stress (Li L. et al., 2021), and apoptosis-related gene expression (Zhao et al., 2017) have been demonstrated. Growing evidence suggests that AQP4 plays a vital role in ischemic brain injury (Zhang et al., 2015). AQP4 exacerbates cerebral ischemia by increasing brain edema (Zeng et al., 2010; Thrane et al., 2011; Fukuda and Badaut, 2012). The study has found that miR-130b promotes neuroprotection by binding to the 3'UTR region of AQP4 mRNA and downregulating AQP4 levels in astrocytes at the post-transcriptional stage miR-130b may be a novel target for treating ischemic stroke (Zheng et al., 2017). Another miRNA that also targets AQP4 is miR-145. miR-145 is essential in protecting astrocytes from ischemic injury by downregulating AQP4 expression.

2.2.2. Excitability regulation

Astrocytes are involved in buffering some neurotransmitters released by neurons, such as glutamate and gamma-aminobutyric acid (GABA), to eliminate their continued effects on neurons and

provide precursors for amino acid neurotransmitters (Sofroniew and Vinters, 2010). Glutamate is the main excitatory transmitter in the brain and spinal cord. The excessive accumulation of glutamate in the synaptic gap leads to excitatory damage. There are five mammalian excitatory amino acid transporters, EAAT1, EAAT2, EAAT3, EAAT4, and EAAT5 (Arriza et al., 1994, 1997; Fairman et al., 1995). The first 2 isoforms, EAAT1 and EAAT2, are known as GLAST (Storck et al., 1992)and GLT-1 (Pines et al., 1992), respectively, which play critical roles in regulating glutamate homeostasis. Under physiological conditions, astrocytes take up glutamate from the synaptic gap *via* glutamate transporters and convert it into glutamine to prevent excitatory damage from the overaccumulation of glutamate in the synaptic gap. Glutamine could also be a substrate for glutamate resynthesis by neurons (Hamilton and Attwell, 2010). Following brain injury, the glutamate system, which relies on astrocytes, changes in several ways, including epigenetic regulation of the GLT-1 and GLAST promoters, abnormal histone methylation leading to gene dysfunction (Chisholm et al., 2015), and S-nitrosylation of GLT-1 leading to reduced activity (Yamada et al., 2006). As brain damage progresses, ATP levels in astrocytes drop, inducing glutamate transporter reversal and further exacerbating glutamate excitotoxicity (Zeevalk et al., 1998). *In vitro* and *in vivo* (Weller et al., 2008) experiments have demonstrated that upregulation of GLT-1 in astrocytes by ceftriaxone (Ouyang et al., 2007) or adenoviral vectors (Harvey et al., 2011) could reduce the area of cerebral infarction, attenuate neurological impairment, and offer neuroprotective effects against ischemic stroke. Ceftriaxone exerts the similar influence in epilepsy disease, which could upregulate GLT-1 expression by reducing glutamate in the hippocampus, mitigating the onset of seizures and the impairment of learning and memory in the chronic phase (Ramandi et al., 2021). Vitamin C acts as a neuroprotective agent by promoting astrocyte GLT-1 expression, reducing glutamate aggregation, and attenuating excitatory damage in Parkinson's disease (PD)(Zeng et al., 2022).

GABA is the primary inhibitory neurotransmitter in the brain, which is mainly transported from the synaptic gap by specific γ-aminobutyric acid transporters (GATs) expressed by neurons and surrounding astrocytes. Presynaptic neurons mainly express GAT subtype 1 (GAT1), and astrocytes mainly express GAT subtype 3 (GAT3; Zhou and Danbolt, 2013). Previous studies have found that presynaptic nerve endings express high concentrations of GAT1 (Conti et al., 2004). GABA is primarily transported from the synaptic gap by GAT1 on presynaptic neurons and stored in presynaptic neurons for later release (Schousboe et al., 2013). These imply that neurons play an imperative role in maintaining synaptic GABA homeostasis. However, recent studies have demonstrated that in contrast to neuronal GAT1, selectively inhibition of astrocyte GAT3 reduces GABA uptake of astrocyte, significantly decreases GABA metabolism, and inhibits astrocyte glutamine production (Andersen et al., 2020). The results imply that astrocytes are involved in GABA metabolism and serve a crucial metabolic function in maintaining GABA homeostasis. In flinders sensitive line (FSL) rat models, reactive astrocytes promote GABA synthesis and release, which results in increased tonic GABA inhibition. The increased synthesis and release of GABA could be blocked by monoamine oxidase B (MAO-B), which reduces tonic inhibition and has antidepressant effects (Srivastava et al., 2020). Few studies have reported that miRNAs could regulate GABA metabolism to exert neuroprotective effects in neurological disorders, which could be a novel horizon for the future.

In cerebral ischemia-induced excitotoxicity and neuronal damage, the upregulation of astrocyte GLT-1 is a potential therapeutic target. MiR-107 and GLT-1 expression were discovered to be correlated in a rat model of focal cerebral ischemia/reperfusion (I/R) damage. miR-107 inhibits GLT-1 expression, which also causes extracellular glutamate to build up (Yang et al., 2014). Additional research has demonstrated that magnesium lithospermate B (MLB) could protect the rat brain from excitatory neurotoxicity by regulating miR-107/GLT-1 and reducing extracellular glutamate aggregation after I/R (Yang et al., 2015). Similar report of miR-124 downregulation in a cerebral ischemia model has been made. GLT-1 expression of astrocytes is dramatically elevated with OGD/R when miR-124 expression improves (Huang et al., 2019).

PD is an age-related movement disorder characterized pathologically by progressive dopaminergic cell death (Olanow and Tatton, 1999). Different mechanisms of dopaminergic neuron death in PD include genetic factors (Miklya et al., 2014), environmental factors (Aguirre-Gamboa et al., 2016; Ter Horst et al., 2016), neuroinflammation (Hirsch and Hunot, 2009), and glutamate excitotoxicity (Ambrosi et al., 2014; Gardoni and Di Luca, 2015). Because the etiology of sporadic PD is unknown, there is a lack of effective therapeutic measures. Among the several etiological theories of PD, glutamate excitotoxicity theory has recently taken center stage (Chang et al., 2020). Glutamate transporters play a significant role in removing excess glutamate from the synaptic gap. GLT-1 is the critical factor in the development of PD, as it is responsible for the uptake of nearly 90% of synaptic glutamate (Storck et al., 1992; Zhang et al., 2017). Therefore, regulating GLT-1 expression in astrocytes during PD by microRNAs to delay the progression or exacerbation of PD is a potential research direction. It has been established that miR-543-3p directly regulated GLT-1 mRNA (SLC1A2 gene), and the inhibition of miR-543-3p upregulated GLT-1 protein expression and function, alleviating dyskinesia in PD models (Wu et al., 2019). The miR-30 family, which includes the mature miRNA sequences miR-30a, miR-30b, miR-30c-1, miR-30c-2, miR-30d, and miR-30, is made up of six distinct miRNAs (Chang et al., 2008). A study has reported that miR-30a-5p, which was upregulated in MPTP-treated mice (a mouse model of PD), decreased GLT-1 expression and function through the ubiquitin-proteasome degradation pathway, thereby participating in the pathological process of PD. This study provides strong evidence for miR-30a-5p as a potential therapeutic target for PD (Meng et al., 2021).

Amyotrophic lateral sclerosis (ALS) is a highly progressive disease characterized by losing motor neurons in the brain and spinal cord. The occurrence of ALS is driven spontaneously by motor neuron damage, and astrocytes strongly influence the rate of disease progression (Al-Chalabi and Hardiman, 2013). miR-218 is abundantly enriched in motor neurons and released extracellularly into the cerebrospinal fluid in ALS rats. Motor neuron-carried miR-218 could be taken up by astrocytes and downregulate EAAT2 in astrocytes. In ALS mice, the inhibition of miR-218 with antisense oligonucleotides attenuates the loss of EAAT2 and other miR-218-mediated changes, providing meaningful evidence for microRNA-mediated communication between neurons and astrocytes *in vivo* (Hoye et al., 2018). These findings imply that microRNAs from dead neurons could directly alter the glial phenotype and lead to astrocyte dysfunction, exacerbating additional neuronal damage.

2.2.3. Oxidative stress

During neurotransmission, reactive oxygen and nitrogen are inevitably created. Nerve cells generate endogenous reactive oxygen species (ROS) *via* the mitochondrial electron transport chain and the NADPH oxidation pathway, which are subsequently catalyzed by nitric oxide synthase (NOS) to produce reactive nitrogen species (RNS) (Cobley et al., 2018). Ascorbic acid and glutathione (GSH) are the two main components of the antioxidant system in brain tissues (Makar et al., 1994). Glutamate binds to N-methyl-D-aspartate (NMDA) receptors (NMDAR) on astrocytes to promote ectopic nuclear factor erythroid 2-related factor 2 (NRF2) to the nucleus, inducing antioxidant gene expression and GSH synthesis. This promotes intraneuronal GSH transport. The increasing GSH exerts a neuroprotective impact by improving the antioxidant capacity of neurons (Jimenez-Blasco et al., 2015; Skowrońska et al., 2019). In reactive astrocytes, the expression of NMDAR is usually upregulated. Two astrocyte NMDAR subunits, GluN2A and GluN2B, showed elevated expression in the transient ischemia hippocampus from day 3 and reached a peak at day 28 (Krebs et al., 2003). This upregulation of NMDAR might represent a neuroprotective response in reactive astrocytes (Jimenez-Blasco et al., 2015). The NMDAR subunit GluN3A has been found to increase in astrocytes in the middle cerebral artery occlusion (MCAO) mouse model (Dzamba et al., 2015), which could inhibit NMDARs activity and suppress the overall antioxidant capacity of astrocytes. However, there are few studies on regulating NMDAR on astrocytes by microRNAs to achieve neuroprotective effects. This may be a worthy direction for future research. Another antioxidant, ascorbic acid, which similarly shields neurons from oxidative stress, is also stored in astrocytes. As GSH synthesis declines in neurons, astrocytes manufacture and release ascorbic acid, which is then carried into neurons (Allaman et al., 2011). Recent research has shown that DJ-1, an essential antioxidant factor mainly produced by reactive astrocytes, exerts neuroprotective functions during ischemic injury by upregulating NRF2 and GSH expressions (Peng et al., 2019).

Mitochondria are central to ischemic cell death, which could regulate oxidative stress, ATP production, and intracellular calcium handling (Verdejo et al., 2012). Mitochondrial dysfunction promotes I/R injury (Stary et al., 2016). The assembly of the cytochrome C oxidase complex, which regulates ATP synthesis and mitochondrial biogenesis, relies on cytochrome C oxidase IV (COX IV) (Li et al., 2006). By targeting COX4I1, a COX IV isoform that is enriched in the brain, upregulating miR-338 in cerebral ischemia hinders COX IV protein synthesis and mitochondrial complex IV activity resulting in mitochondrial dysfunction and decreasing the ability of astrocytes to handle oxidative stress, and ultimately exacerbating ischemic brain injury (Li L. et al., 2021).

2.2.4. Neuroinflammation

While astrocytes typically sustain neuronal function and survival through multiple mechanisms, these homeostatic functions are frequently impaired in neurological disorders. Inflammatory factors released by reactive astrocytes could hasten neuronal damage (Van Damme et al., 2007; Cassina et al., 2008; Ferraiuolo et al., 2011; Madji Hounoum et al., 2017).

Alzheimer's disease (AD) is the most common cause of dementia worldwide (Wolters and Ikram, 2018), accounting for 50–70% of all cases (Querfurth and LaFerla, 2010). Amyloid β (Aβ) deposition into Aβ plaques and the formation of neurogenic fiber tangles (NFTs) composed of hyperphosphorylated tau proteins are the main neuropathological features of AD (Polanco et al., 2018). Astrocytes play a major role in regulating neuroinflammation in AD (Kwon and Koh, 2020). Activation of the NLRP3 inflammasome in astrocytes is involved in the pathogenesis of AD by triggering an inflammatory response in the brain (Heneka et al., 2013). Chronic neuroinflammation might lead to the destruction of neurons and synapses, which subsequently contribute to the deterioration of cognitive function, even if a moderate inflammatory response is necessary for the brain to clear Aβ. Previous observations showed that anti-inflammatory therapy effectively halted disease progression in animal models of AD (Brod, 2022). The inhibition of NLRP3 inflammatory vesicles might be a novel intervention for treating AD. The Ang-(1–7) analog AVE0991 could block astrocyte NLRP3 inflammasome-mediated neuroinflammation through the SNHG14/miR-223-3p/NLRP3 pathway to exert neuroprotective effects in APP/PS1 mice. These findings reveal that miR-223-3p plays a key role in regulating astrocyte-mediated inflammation in AD. More significantly, the study identifies Ang-(1–7)-targeted SNHG14/miR-223-3p as an inhibitor of neuroinflammation in AD and reveals the therapeutic potential of its non-peptide analog AVE0991 (Duan et al., 2021).

In SCI, the primary injury results in the death of local neurons and glial cells within minutes to hours. A neuroinflammatory reaction-induced secondary damage follows immediately after that (Fleming et al., 2006). The occurrence and progression of SCI are significantly influenced by the inflammatory response. Following SCI, inflammatory cells (i.e., T cells, macrophages, and

microglia) are recruited to the site of injury and clear cellular debris during the acute SCI phase (Ahuja et al., 2017). During the SCI, reactive astrocytes emit inflammatory factors, such as interleukin (IL)-17, IL-6, and tumor necrosis factor alpha (TNF-α), which might be in concert with various inflammatory mediators and other cytokines to aggravate the spinal cord damage further. A study has found that the expression of IL-1β, IL-6, and TNF-α in the serum of rats with SCI transfected with miR-136-5p was significantly higher than that of the control group, while the protein expression of A20 was significantly reduced and the expression of p-NF-κB was elevated. These results suggest that miR-136-5p could aggravate SCI injury by promoting the release of inflammatory factors from reactive astrocytes *via* the NF-κB/A20 signaling pathway. Silencing miR-136-5p could effectively diminish inflammatory factors and chemokines and protect the spinal cord through the NF-κB /A20 signaling pathway *in vivo* and *in vitro* (He et al., 2017). According to studies, miR-140 targets Brain-derived neurotrophic factor (BDNF) to regulate astrocyte proliferation through the PI3K/AKT pathway. miR-140 could inhibit the expression of BDNF, IL-6, and Transforming growth factor-alpha (TGF-α) in a lipopolysaccharide (LPS)-induced injury model. Therefore, miR-140/BDNF is expected to be a target for inhibiting the reactive proliferation of astrocytes and the release of inflammatory factors after SCI (Tu et al., 2017).

2.2.5. Glial scar

Glial scar is widespread in the pathophysiological development of CNS diseases and consists mainly of proliferating and migrating reactive astrocytes, microglia, and oligodendrocyte precursor cells (Adams and Gallo, 2018). The formation of glial scar is accompanied by changes in the expression of several related molecules: (1) glycosaminoglycan (GAG) proteoglycans, one of the main components of chondroitin sulfate proteoglycans (CSPGs), are the most abundant components of glial scar and the main inhibitors of axonal regeneration (He et al., 2020); (2) other extracellular matrix components: high molecular weight hyaluronic acid and Tenascin-R regulate the formation of glial scar and inhibit axonal growth (Khaing et al., 2011); (3) myelin-associated glycoproteins, including Nogo, myelin-associated glycoprotein (MAG), and oligodendrocyte-myelin glycoprotein (OMgp; Ohtake and Li, 2015). CSPGs are composed of core protein and GAG chain attachment sites, including lectin, phosphoglycan, and NG2 (Dyck and Karimi-Abdolrezaee, 2015). As they do during development, CSPGs effectively inhibit regenerating axons (McKeon et al., 1991). Further studies have demonstrated that the GAG residues of CSPGs interact with various neuronal developmental inhibitory receptors such as Nogo receptors 1 and 3, protein tyrosine phosphatase, and leukocyte common antigen-associated phosphatase receptor, thereby inhibiting axon regeneration (Shen et al., 2009; Dickendesher et al., 2012). Chondroitinase ABC greatly lessens the inhibitory effect of CSPGs on axon growth by eliminating the GAG chain of CSPGs or by degrading the core proteins of CSPGs with matrix metalloproteinases (MMPs) after cerebral ischemia in rats (Bradbury and Carter, 2011; Cua et al., 2013; Mukherjee et al., 2020). In addition to its effect on axons, glial scar inhibits endogenous myelin reformation. Endothelin-1 (ET-1), a negative regulator of differentiation and functional myelin formation in NG2 glial cells, raises Jagged1 expression in reactive astrocytes, activates Notch signaling in neighboring NG2 glial cells, and hinders their differentiation (Hammond et al., 2014, 2015). After focal demyelination of the corpus callosum, it has been discovered that blocking ET-1 signaling by pharmacological or genetic pathways promotes the differentiation of NG2 glial cells into oligodendrocytes and supports endogenous myelin formation (Adams and Gallo, 2018). Bone morphogenetic protein (BMP) in the glial scar has shown similar effects (Wang et al., 2011). It has recently been shown that glial scar could benefit in the CNS's recovery, while previous studies have indicated that glial scar development has adverse effects, such as limiting axonal regeneration (Hernández et al., 2021). By isolating the damaged area from the normal brain, glial scars lessen the likelihood that the inflammatory response will spread across the entire brain. Reactive astrocytes are neuroprotective by limiting the inflammatory response in damaged CNS areas (Sofroniew, 2009). These protective effects include isolation of blood-derived macrophages and repair of the blood–brain barrier. Reactive astrocytes also suppress inflammation by secreting BDNF in the initial stages of glial scar formation (Silver and Miller, 2004; Rolls et al., 2009). It has been reported that the presence of glial scar could be detected a few days after ischemic injury, and mice deficient for glial fibrillary acidic protein and vimentin (GFAP−/− Vim−/−) exhibit less organized and dense glial scar after brain injury, with an infarct area increased, suggesting that glial scar is important in protecting tissue integrity and avoiding further exacerbation of inflammation (Li et al., 2008).

In ischemic stroke, glial scar is a considerable obstacle to neuronal regeneration. Therefore, it is advantageous in stroke to employ strategies that promote their degradation and discourage their formation. miR-124 has been reported to regulate glial scar formation in ischemic stroke. M2 microglial extracellular vesicles could restrict glial scar formation and promote post-stroke recovery by upregulating miR-124 (Li Z. et al., 2021). Consequently, miR-124 might be an essential target for enhancing neuroprotection and recovery in ischemic stroke. Future research for neuroprotection will likely focus on discovering medicines that upregulate miR-124 in ischemic stroke.

Following SCI, glial scar formation is a significant self-defense mechanism (Fitch and Silver, 2008; Sofroniew, 2009; Sofroniew and Vinters, 2010). During the acute phase of SCI, astrocytes adjacent to the injury site are characterized by morphological hypertrophy, increased proliferation, and enhanced expression of the GFAP, Vim, and nestin. All these pathological processes eventually lead to the formation of the glial scar, which has beneficial effects in the acute phase of SCI, especially in repairing the blood-spinal cord barrier and limiting the spread of injury (Okada et al., 2006; Herrmann et al., 2008; Wanner et al., 2013). Certain inhibitory factors secreted by the glial scar in the chronic

phase, such as CSPGs, inhibit axonal regeneration. Therefore, coping with glial scar formation at different times of SCI to promote neuroprotection (acute phase) and axonal regeneration (subacute phase and chronic phase) is a potential research direction. It has been discovered that when the Dicer1 gene, which encodes an enzyme required for mature miRNA generation, was conditionally deleted, the injury-induced proliferation of astrocytes was blocked. Synthetic miR-17-5p mimics could rescue the proliferation defect in Dicer1-null astrocytes, while antisense inhibitors of miR-17-5p block LPS-induced astrocyte proliferation (Adams and Gallo, 2018). miR-145 is regarded as a tumor suppressor RNA in several cancer types, such as hepatocellular carcinoma (Noh et al., 2013), ovarian cancer (Kim et al., 2015), and glioma (Iorio et al., 2005). It has been found that healthy rat spinal cord neurons and astrocytes are enriched with miR-145, downregulated in astrocytes 1 week and 1 month after SCI. miR-145 overexpression in astrocytes could reduce astrocyte density at the edge of the damaged spinal cord lesion, inhibit proliferation and migration of reactive astrocytes, and hinder glial scar formation. These findings indicate that miR-145 could prevent spinal cord tissue injury by promoting astrocyte proliferation and glial scar formation (Wang et al., 2015). Similarly, miR-145-5p is a negative regulator of astrocyte proliferation, and its downregulation promotes SMAD3 activity, thereby promoting astrocyte proliferation and glial scar formation (Ye et al., 2022). LncRNAH19 as ceRNA could attenuate the inhibitory effect of miR-1-3p on C-C motif chemokine ligand 2 (CCL2) expression in SCI. The suppression of miR-1-3p could effectively reverse the effects of H19 silencing on normal astrocyte proliferation and activation, suggesting that the H19/miR-1-3p axis regulates astrocyte proliferation and glial scar formation *via* CCL2 (Li P. et al., 2020).

2.3. Transcriptomic analysis of reactive astrocytes

Researchers have concluded that differences exist between astrocytes in physiological states due to differences in developmental patterns and extracellular signals (Tsai et al., 2012). The advent of microarray and genome-wide gene expression investigations in recent years has made it clear to researchers that there is heterogeneity among astrocytes, with distinct molecular states in various CNS regions (Itoh et al., 2018) and at different developmental periods (Boisvert et al., 2018). Similarly, following dysregulation of microenvironmental homeostasis, these reactive astrocytes are highly heterogeneous that have both deleterious and beneficial effects (Zhang and Barres, 2010; Zamanian et al., 2012; Liddelow et al., 2017). These heterogeneous responses raise the question of whether there are different subtypes of reactive astrocytes that elicit different responses. Transcriptome analysis of resting and reactive astrocytes isolated from healthy and damaged brains by LPS injection or MCAO identified two distinct types of reactive astrocytes: A1 and A2. Because the different transcriptomic changes of reactive astrocytes bring different pathophysiological changes, more and more studies are now aimed at the transcriptome regulation of reactive astrocytes.

A1 astrocytes, with longer dendrites *in vivo* and *in vitro*, lose the ability to promote neuronal survival, growth, synapse formation, and phagocytosis (Liddelow et al., 2017). In addition, A1 astrocytes secrete a saturated lipid (Guttenplan et al., 2021) that rapidly and selectively kills retinal ganglion cells, cortical neurons, spinal motor neurons, and human dopaminergic neurons, but not preganglionic and gamma motor neurons (Sekar et al., 2016). Oligodendrocytes form and maintain white matter myelin sheaths around axons in the CNS (Morrison et al., 2013). A1 astrocytes conditioned medium could rapidly kill mature differentiated oligodendrocytes and impede the differentiation and maturation of oligodendrocyte precursor cells but do not directly kill oligodendrocyte precursor cells (Liddelow et al., 2017). After LPS injection in neonatal rats, C3aR expression was increased in NG2 oligodendrocyte progenitor cells in the periventricular white matter, and C3a/C3aR signaling might inhibit oligodendrocyte precursor cell differentiation and maturation *via* the Wnt/β-catenin signaling pathway. Thus, it is hypothesized that A1 astrocytes might be responsible for hindering the differentiation of oligodendrocyte precursor cells by releasing C3a, which would lower the amount of axonal myelin in mature periventricular white matter injury (Huang et al., 2020). The complement proteins C1r, C1s, C3, and C4 are upregulated as a result of the recruitment of the IL-1 receptor's TLR domain by A1 astrocytes *via* the myeloid differentiation factor 88, which also activates NF-κB and MAPK. C3 is now widely acknowledged as a decisive marker of A1 astrocytes. The expression of C3 increases in A1 astrocytes, cleaved into C3a and C3b to trigger downstream events by binding to its receptors C3aR and CR3, respectively (Stephan et al., 2012). Since both C3aR and CR3 are also expressed on microglia, the C3b/CR3 and C3a/C3aR signaling pathways are critical pathways through which A1 astrocytes exert their effects on microglia (Hong et al., 2016; Lian et al., 2016).

In PD models, an increase in A1 astrocytes is frequently accompanied by a decline in dopaminergic neurons (Luna-Herrera et al., 2020). In AD models, the absence of C3 leads to a decline in the expressions of numerous pro-inflammatory factors, including TNF-α, TNF-γ, IL-6, and IL-12, as well as the aging-related loss of synapses and neurons (Shi et al., 2017). Activating microglia CR3 enhances microglia phagocytosis, resulting in reducing synapses in a mouse AD model (Hong et al., 2016). In addition to the C3/CR3 pathway, C3 secreted by A1 astrocytes interacts with microglia C3aR to regulate microglia phagocytosis, β-amyloid, and neuroinflammation in AD models, thereby worsening cognitive function by impairing dendritic cell morphology and synaptic function (Lian et al., 2016; Litvinchuk et al., 2018; Liu et al., 2020).

In chronic cerebral ischemia, the upregulation of C3 expression leads to aberrant microglia activation and promotes microglia redistribution and myelin phagocytosis through activating microglia C3aR, thereby exacerbating brain white

matter damage and cognitive dysfunction (Zhang et al., 2020). A1 astrocyte-derived C3 prevents microglia from phagocytosing myelin debris by activating microglia C3aR, which in turn slows myelin redistribution in cerebral hemorrhage (Zheng et al., 2021). The conditioned cultures of A1 astrocytes induced by OGD/R could promote cell apoptosis and reduce the expression of synaptic proteins of cultured cortical neurons, including the scaffolding protein postsynaptic density-95, calmodulin-dependent kinase II, and synaptophysin (Hong et al., 2020). Studies have demonstrated that the neuroprotective effects of intra-arterial selective cooling infusion in hypertensive MCAO rats could be related with phenotype shifting of astrocytes (Wang et al., 2022). Therefore, studies on the neuroprotective effects of miRNAs-regulated A1/A2 astrocytes conversion in ischemic stroke deserve our attention.

The discovery of A1 neurotoxic astrocytes in SCI has provided a new research direction for treating SCI. Neuron-derived exosome-delivered miR-124-3p could reduce neuroinflammation by inhibiting the activation of M1 microglia and A1 astrocytes and promote the recovery of neurological function after SCI (Jiang et al., 2020). The study showed that the expression of miR-21a-5p and the level of A1 marker were up-regulated in spinal cord tissue 3 days after SCI, while the expression of ciliary neurotrophic factor receptor alpha (CNTFRα) was down-regulated. After ciliary neurotrophic factor (CNTF) intervention, A1 marker levels were decreased, while A2 levels were increased. With the downregulation of miR-21a-5p expression, the expression of the A1 marker was significantly reduced, while CNTFRα siRNA intervention had the opposite effects. Therefore, miR-21a-5p might promote A1 astrocyte induction through the downstream target gene CNTFRα and facilitate the inflammatory process of SCI (Zhang et al., 2021). Targeting astrocyte miR-21a-5p is a potential approach to promote SCI rehabilitation in the future.

A2 astrocytes morphologically exhibit hypertrophy with fewer dendrites (Zou et al., 2019). A2 astrocytes release several neurotrophic factors, including arginase-1, NRF2 and platelet-responsive proteins, which promote neuronal survival and synaptic repair (Zamanian et al., 2012; Liddelow and Barres, 2017). Transcriptional profiling of ischemia-induced A2-reactive astrocytes shows upregulation of anti-inflammatory genes such as corticotrophin like cytokine factor 1, S100 calcium-binding protein A10, pentapeptide 3, sphingosine kinase 1, IL-6, leukemia inhibitory factor and transglutaminase 1, as well as the upregulation of neurotrophic factors. On the other hand, A2 astrocytes could activate regulatory factors, including transcription 3, Ras homologous family member A, hypoxia-inducible factor 1α subunit and erythropoietin, which are involved in neural anti-inflammation and neural repair (Liddelow and Barres, 2017; Renault-Mihara et al., 2017; Zhang et al., 2018). Furthermore, numerous investigations have demonstrated an interaction between A2 astrocytes and microglia. The release of TGF-β from A2 astrocytes attenuates microglia activation (Norden et al., 2014). Pentraxin3 (PTX3) is a specific marker of A2 astrocytes. Under inflammatory conditions, both microglia and astrocytes secrete PTX3, which affects the phagocytic activity of microglia (Jeon et al., 2010). In addition to the release of BDNF and vascular endothelial growth factor (VEGF) to promote the differentiation of oligodendrocytes, A2 astrocytes guard against white matter injury by promoting the conversion of oligodendrocyte precursor cells into mature oligodendrocytes through mitochondrial migration. Paradoxically, A2 astrocytes produce prostaglandin E2 through a cyclooxygenase 2-dependent manner, limiting oligodendrocyte precursor cell maturation and myelin formation in a neonatal IL-1β-induced white matter injury model (Shiow et al., 2017). These results suggest that A2 astrocytes may not always benefit oligodendrocyte precursor cell differentiation and development. While in some cases, they may also have deleterious effects.

3. Clinical applications of microRNA-targeted regulation of reactive astrocytes

3.1. Diagnostic and prognostic indicators

Excitotoxic effects caused by glutamate are the leading contributor of neuronal injury in several neurological diseases. Glutamate transporters on astrocytes are the primary pathway for glutamate uptake. Typically, downregulation of glutamate transporter expression following brain injury leads to a decline in glutamate, aggravating brain injury. In ischemic stroke, miR-107 and miR-124 could worsen or ameliorate brain injury by regulating GLT-1 to promote or inhibit glutamate uptake in astrocytes. miR-107 and miR-124 could be used as new biomarkers to detect the excitotoxicity of glutamate accumulation in ischemic stroke (Yang et al., 2014; Huang et al., 2019). When miR-30a-5p and miR-543-3p bind to SLC1A2 in PD, GLT-1 expression is downregulated, exacerbating the injury. The novel biomarkers miR-30a-5p and miR-543-3p may be utilized to track excitotoxicity in PD (Wu et al., 2019; Meng et al., 2021). In ALS, miR-218 directly silences GLT-1, making astrocytes less able to absorb glutamate. miR-218 is a potential indicator for monitoring glutamate accumulation in ALS (Hoye et al., 2018).

The astrocyte protein AQP4 is pivotal in ischemic brain damage (Zhang et al., 2015). By causing more brain edema, AQP4 exacerbates cerebral ischemia in the rat model of ischemic stroke. The downregulation of AQP4 expression could result from the upregulation of miR-145 and miR-130b, which would lessen brain edema and benefit neurological recovery (Zheng et al., 2017; Wang et al., 2020). According to the above research, miR-145 and miR-130b could be used as vital indicators to determine the severity of cerebral edema during the progression of cerebral ischemia.

After brain injury, the development of the glial scar has a dual impact. In the early stage, Glial scar isolates the spread of inflammation to prevent further injury aggravation. In contrast, the glial scar in the latter stages limits neurological recovery by hindering neural repair and synaptic regeneration. The downregulation of miR-124 expression promotes reactive

astrocyte proliferation and glial scar formation in ischemic stroke (Li Z. et al., 2021). miR-124, miR-145-5p, miR-1-3p, and miR-17-5p could regulate glial scar formation in SCI (Hong et al., 2014; Li P. et al., 2020; Li Z. et al., 2021; Ye et al., 2022). miR-124, miR-145-5p, miR-1-3p, and miR-17-5p could be used as indicators of the extent of glial scar formation.

A1 astrocytes of reactive astrocytes after microenvironmental dysregulation in the CNS release inflammatory factors that aggravate brain injury, while A2 astrocytes release neurotrophic factors that play a protective role. The upregulation of miR-136-5p and miR-140 contribute to the release of inflammatory factors in reactive astrocytes in SCI (He et al., 2017; Tu et al., 2017). miR-124-3p and miR-21a-5p promote the transformation of astrocytes to A1 astrocytes (Jiang et al., 2020; Zhang et al., 2021). As a result, the level of inflammatory activity in SCI might be assessed using miR-136-5p, miR-140, miR-124-3p, and miR-21a-5p.

miR-338 is involved in regulating mitochondrial oxygen consumption, ATP production, and ROS production in axons in the CNS (Aschrafi et al., 2012). After 20 min of whole brain ischemia and 30 min of reperfusion in rats, miR-338 levels are upregulated more than 2-fold in the hippocampus of rats (Di et al., 2014), which is considerably raised in the cerebrospinal fluid (CSF) of patients with subacute ischemic stroke (Peng et al., 2015). As a highly sensitive biomarker of mitochondrial toxicity, miR-338 has been employed (Baumgart et al., 2016). MiR-338 can promote the production of COX IV and the mitochondrial ATP synthase ATP5G1 subunit, which significantly affects neuronal ROS levels and axonal development (Aschrafi et al., 2012; Figure 2; Table 1).

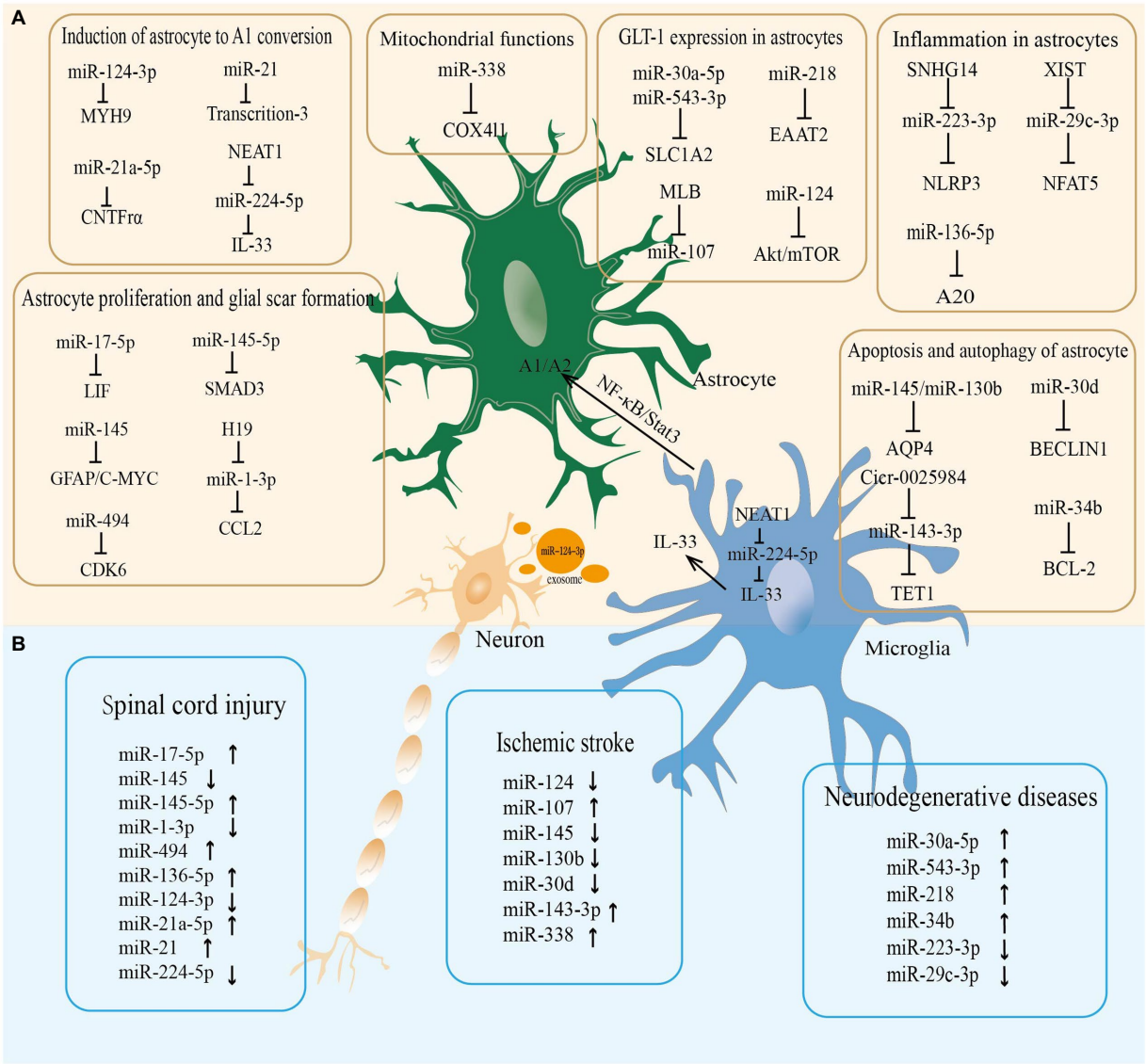

FIGURE 2
The miRNA-mRNA regulatory network in astrocytes regulated neurological diseases. **(A)** The microRNAs regulate the pathophysiological functions of astrocytes in the central nervous system. **(B)** The microRNAs altered in neurological diseases.

TABLE 1 Characteristics of miRNA involved in astrocytes in Neurological disorders.

microRNA	Disorders	Up/Downregulation	Target genes	Upstream	Influence on astrocytes
miR-17-5p	SCI	Up	LIF		Promotion of astrocyte proliferation and glial scar formation
miR-145	SCI	Down	GFAP/C-MYC		Promotion of astrocyte proliferation and glial scar formation
miR-145-5p	SCI	Up	SMAD3		Promotion of astrocyte proliferation and glial scar formation
miR-1-3p	SCI	Down	CCL2	H19	Promotion of astrocyte proliferation and glial scar formation
miR-124	Ischemic stroke	Down	STAT3		Promotion of astrocyte proliferation and glial scar formation
miR-494	SCI	Up	CDK6		Inhibition of astrocyte proliferation and synaptic remodeling
miR-107	Ischemic stroke	Up		MLB	Inhibition of GLT-1 expression in astrocytes
miR-124	Ischemic stroke	Down	AKT/mTOR		Inhibition of GLT-1 expression in astrocytes
miR-30a-5p	PD	Up	SLC1A2		Promotion of GLT-1 degradation in astrocytes
miR-543-3p	PD	Up	SLC1A2		Inhibition of GLT-1 expression in astrocytes
miR-218	ALS	Up	EAAT2		Astrocyte dysfunction
miR-145	Ischemic stroke	Down	AQP4		Promotion of apoptosis of astrocytes
miR-130b	Ischemic stroke	Down	AQP4		Promotion of apoptosis of astrocytes
miR-30d	Ischemic stroke	Down	BECLIN1		Promotion of autophagy in astrocytes and inhibition of apoptosis in astrocytes
miR-143-3p	Ischemic stroke	Up	TET1	Circ_0025984	Promotion of apoptosis and autophagy in astrocytes
miR-34b	Epilepsy	Up	BCL-2		Promotion of apoptosis in astrocyte
miR-338	Ischemic stroke	Up	COX4l1		Inhibition of Mitochondrial function
miR-136-5p	SCI	Up	A20		Promotion of astrocyte activation and inflammatory factor release
miR-223-3p	AD	Down	NLRP3	SNHG14	Promotion of neuroinflammation development
miR-29c-3p	Epilepsy	Down	NFAT5	XIST	Promotion of astrocyte activation and inflammatory factor release
miR-124-3p	SCI	Down	MYH9		Induction of astrocyte to A1 conversion
miR-21a-5p	SCI	Up	CNTFrα		Induction of astrocyte to A1 conversion
miR-21	SCI	Up	Transcription-3		Induction of A1 to A2 conversion
miR-224-5p	SCI	Down	IL-33	NEAT1	Inhibition of Induction of astrocyte to A1 conversion

SCI, spinal cord injury; PD, Parkinson's disease; ALS, amyotrophic lateral sclerosis; LIF, leukemia inhibitory factor; GFAP, glial fibrillary acidic protein; C-MYC, MYC proto-oncogene, bHLH transcription factor; SMAD3, SMAD family member 3; CCL2, C-C motif chemokine ligand 2; H19, H19 imprinted maternally expressed transcript; STAT3, signal transducer and activator of transcription 3; CDK6, cyclin dependent kinase 6; MLB, magnesium lithospermate B; AKT, AKT serine/threonine kinase 1; mTOR, mechanistic target of rapamycin kinase; SLC1A2, solute carrier family 1 member 2; EAAT2, excitatory amino acid transporter 2; AQP4, aquaporin 4; TET1, tet methylcytosine dioxygenase 1; BCL2, BCL2 apoptosis regulator; COX4l1, cytochrome c oxidase subunit 4I1 pseudogene 1; NLRP3, NLR family pyrin domain containing 3; SNHG14,small nucleolar RNA host gene 14; NFAT5, nuclear factor of activated T cells 5; XIST, X inactive specific transcript; MYH9, myosin heavy chain 9; CNTFrα, ciliary neurotrophic factor receptor α; IL-33, interleukin 33; NEAT1, nuclear paraspeckle assembly transcript 1.

3.2. Therapeutic targets

How to translate the regulatory effects of miRNAs on astrocytes in neurological disorders into clinically meaningful effects is a question that deserves our consideration. miRNA-based therapies could be divided into two different approaches: (1) the use of miRNA antagonists (antisense oligonucleotides, counterparts, and miRNA sponges) or drugs targeting miRNAs to inhibit the adverse effects of miRNAs in neurological diseases, and (2) the use of miRNA mimics, exosome-carried miRNAs or knockdown of miRNA sponges to upregulate the expression of miRNAs.

The upregulation of miR-143-3p could promote astrocyte apoptosis and autophagy *via* TET1/ORP150, exacerbating brain injury in cerebral ischemia. miR-143-3p inhibitor and circ_0025984 (a miR-143-3p sponge) have been found to drastically limit astrocyte apoptosis and autophagy, mitigating brain injury and neuronal loss in ischemic stroke (Zhou et al., 2021). Certain studies have reported that a few drugs target miRNAs to affect the activity and function of astrocytes to benefit the recovery of neurological functions in neurological diseases. For instance, MLB plays a neuronal protective role and promotes functional recovery after stroke by inhibiting the upregulation of miR-107 on astrocyte GLT-1 (Yang et al., 2015). Ang-(1–7) is a member of the renin-angiotensin system (RAS) and is produced by Angiotensin II (Ang II). Ang-(1–7) promotes functional recovery after stroke by binding to the MAS1 receptor, which is influential in the pathogenesis of several neurological disorders such as AD (Xu et al., 2011). Ang-(1–7) exerts a neuroprotective effect by inhibiting neuroinflammation mediated by astrocyte NLRP3 inflammasome through the SNHG14/miR-223-3p/NLRP3 pathway in AD (Duan et al., 2021).

The downregulation of miR-130b in astrocytes leads to the upregulation of water channel protein AQP4 and exacerbates brain injury in cerebral ischemia. miR-130b mimics could exert neuroprotective effects by decreasing the expression of AQP4 on astrocyte membranes and alleviating ischemia-induced damage (Zheng et al., 2017). Bone marrow mesenchymal stem cells (BMSCs)-carried miR-146a suppresses the release of inflammatory factors from reactive astrocytes and improves cognitive impairment in AD models (Nakano et al., 2020). In a study of depression, miR-207 is downregulated in brain tissue, weakens the inhibitory effect on TRIL, and facilitates the release of inflammatory factors in reactive astrocytes. NK cell-derived exosomes could upregulate miR-207 expression, inhibit the release of inflammatory factors in reactive astrocytes, and alleviate chronic mild stress symptoms in mice (Li D. et al., 2020). In a mouse model of tMCAO, circHECTD1, an endogenous miR-142 sponge, could inhibit miR-142 activity to downregulate TIPARP (TCDD-inducible poly [ADP-ribose] polymerase) expression, impede astrocyte autophagy, and ultimately increase infarct size. The upregulation of miR-142 by knocking down circHECTD1 drives astrocyte autophagy and shrinks infarct size (Han et al., 2018). CircHIPK2, an endogenous miR-124-2HG sponge, upregulates sigma non-opioid intracellular receptor 1 (SIGMAR1/OPRS1) expression, promotes astrocyte autophagy and neuroinflammatory responses, and finally aggravates brain tissue damage. Inhibiting circHIPK2 expression could upregulate miR-142 expression to suppress astrocyte autophagy and endoplasmic reticulum stress, preventing brain tissue damage from neuroinflammatory (Huang et al., 2017). The upregulation of miR-145 by knocking down LncRNA MALAT1 could inhibit AQP4 expression to improve brain I/R injury (Wang et al., 2020). LncRNA MEG exacerbates neuropathic pain and astrocyte activation through miR-130a-5p/CXCL12/CXCR4 axis. The pro-inflammatory effect of miR-130a-5p on reactive astrocytes is attenuated by silencing MEG3 to relieve neuropathic pain (Dong et al., 2021).

4. Discussion and conclusion

The CNS microenvironment's homeostasis is crucially maintained by astrocytes. Reactive astrocytes perform imperative pathophysiological functions in CNS diseases such as stroke, SCI, and neurodegenerative disease. miRNAs are non-coding RNAs involved in neuronal cell behavior and nervous system development. miRNAs play a positive or negative role in astrocyte-mediated neurological diseases. The regulatory mechanisms of miRNAs are related to the transcriptomic alterations, morphology, and function of reactive astrocytes. The current study has found that regulating the miRNAs-astroglial axis could inhibit the pathophysiologic progression of CNS diseases.

The current research findings indicate that miRNA-mediated regulation of reactive astrocytes in CNS diseases is a potential research direction to promote neurological recovery. However, significant obstacles must yet be overcome. (1) One is the specificity of miRNA-based therapeutics. Each miRNA has dozens of potential targets. MiRNAs have a distinct advantage in controlling intricate biological processes due to their capacity to control numerous mRNAs. It could be difficult to target miRNAs to exert protective effects on specific targets in CNS disorders. Target site blockers (TSBs) are crucial for preventing miRNAs from regulating specific mRNAs and identifying specific miRNA-mRNA interaction networks. However, the design principles of TSBs are not yet fully understood and remain a challenge. (2) The second is that astrocytes are highly heterogeneous glial cells whose transcriptomic changes, morphology, and functions are highly heterogeneous not only in different brain regions but also at different time stages after CNS injury. Whether miRNAs have different effects on other functions of the same astrocytes or on the functions of astrocytes at different time stages requires further exploration. (3) Third, How to efficiently transport miRNAs to the CNS through the blood–brain barrier to exert neuroprotective effects. miRNA mimics and inhibitors enable miRNAs to exist in circulation for longer, but most miRNAs accumulate in the liver and kidney and cannot be efficiently transported to the CNS. Therefore, it is essential to explore the ways for the targeted transport of miRNAs to the CNS. Viral and non-viral delivery systems specific to brain endothelial cells have been found to deliver nucleotide-based drugs to the brain (Marcos-Contreras et al., 2020). But it remains to be verified whether this mode of drug delivery is toxic and whether immune rejection occurs. Exosome, an important miRNA carrier discovered in recent years, is characterized by high stability, easy passage through the blood–brain barrier, and little graft response. The miRNAs-exosome targeting astrocytes is a promising treatment for neurological diseases.

In conclusion, studies based on the miRNAs-astrocyte axis are currently inadequate in CNS diseases. Focusing on the role and function of miRNAs in regulating reactive astrocytes, we summarize the regulatory mechanism of miRNAs on reactive astrocytes, which might provide a theoretical basis for the diagnosis and treatment of CNS diseases.

Author contributions

All authors listed have made a substantial, direct, and intellectual contribution to the work and approved it for publication.

Funding

This research was supported by grants from the National Natural Science Foundation of China (81701216 and 82172955), Wuxi Taihu Lake Talent Plan, Supports for Leading Talents in Medical and Health Profession (2020THRC-DJ-SNW), Natural Science Foundation of Jiangsu Province (BK20160197 and BK20180169), and Reserve Talents of Double Hundred Talent Plan (HB2020021).

Conflict of interest

The authors declare that the research was conducted in the absence of any commercial or financial relationships that could be construed as a potential conflict of interest.

Publisher's note

References

Adams, K. L., and Gallo, V. (2018). The diversity and disparity of the glial scar. *Nat. Neurosci.* 21, 9–15. doi: 10.1038/s41593-017-0033-9

Aguirre-Gamboa, R., Joosten, I., Urbano, P., van der Molen, R. G., van Rijssen, E., van Cranenbroek, B., et al. (2016). Differential effects of environmental and genetic factors on T and B cell immune traits. *Cell Rep.* 17, 2474–2487. doi: 10.1016/j.celrep.2016.10.053

Ahuja, C. S., Nori, S., Tetreault, L., Wilson, J., Kwon, B., Harrop, J., et al. (2017). Traumatic spinal cord injury-repair and regeneration. *Neurosurgery* 80, S9–S22. doi: 10.1093/neuros/nyw080

Al-Chalabi, A., and Hardiman, O. (2013). The epidemiology of ALS: a conspiracy of genes, environment and time. *Nat. Rev. Neurol.* 9, 617–628. doi: 10.1038/nrneurol.2013.203

Allaman, I., Bélanger, M., and Magistretti, P. J. (2011). Astrocyte-neuron metabolic relationships: for better and for worse. *Trends Neurosci.* 34, 76–87. doi: 10.1016/j.tins.2010.12.001

Allen, N. J., and Eroglu, C. (2017). Cell biology of astrocyte-synapse interactions. *Neuron* 96, 697–708. doi: 10.1016/j.neuron.2017.09.056

Alvarez, J. I., Katayama, T., and Prat, A. (2013). Glial influence on the blood brain barrier. *Glia* 61, 1939–1958. doi: 10.1002/glia.22575

Ambrosi, G., Cerri, S., and Blandini, F. (2014). A further update on the role of excitotoxicity in the pathogenesis of Parkinson's disease. *J. Neural Transm. (Vienna)* 121, 849–859. doi: 10.1007/s00702-013-1149-z

Andersen, J. V., Jakobsen, E., Westi, E. W., Lie, M., Voss, C. M., Aldana, B. I., et al. (2020). Extensive astrocyte metabolism of γ-aminobutyric acid (GABA) sustains glutamine synthesis in the mammalian cerebral cortex. *Glia* 68, 2601–2612. doi: 10.1002/glia.23872

Arriza, J. L., Eliasof, S., Kavanaugh, M. P., and Amara, S. G. (1997). Excitatory amino acid transporter 5, a retinal glutamate transporter coupled to a chloride conductance. *Proc. Natl. Acad. Sci. U. S. A.* 94, 4155–4160. doi: 10.1073/pnas.94.8.4155

Arriza, J. L., Fairman, W. A., Wadiche, J. I., Murdoch, G. H., Kavanaugh, M. P., and Amara, S. G. (1994). Functional comparisons of three glutamate transporter subtypes cloned from human motor cortex. *J. Neurosci.* 14, 5559–5569. doi: 10.1523/JNEUROSCI.14-09-05559.1994

Aschrafi, A., Kar, A. N., Natera-Naranjo, O., Mac Gibeny, M. A., Gioio, A. E., and Kaplan, B. B. (2012). Micro RNA-338 regulates the axonal expression of multiple nuclear-encoded mitochondrial mRNAs encoding subunits of the oxidative phosphorylation machinery. *Cell. Mol. Life Sci.* 69, 4017–4027. doi: 10.1007/s00018-012-1064-8

Bartel, D. P. (2004). MicroRNAs: genomics, biogenesis, mechanism, and function. *Cells* 116, 281–297. doi: 10.1016/s0092-8674(04)00045-5

Baumgart, B. R., Gray, K. L., Woicke, J., Bunch, R. T., Sanderson, T. P., and Van Vleet, T. R. (2016). MicroRNA as biomarkers of mitochondrial toxicity. *Toxicol. Appl. Pharmacol.* 312, 26–33. doi: 10.1016/j.taap.2015.10.007

Boisvert, M. M., Erikson, G. A., Shokhirev, M. N., and Allen, N. J. (2018). The aging astrocyte Transcriptome from multiple regions of the mouse brain. *Cell Rep.* 22, 269–285. doi: 10.1016/j.celrep.2017.12.039

Boulay, A. C., Cisternino, S., and Cohen-Salmon, M. (2016). Immunoregulation at the gliovascular unit in the healthy brain: a focus on Connexin 43. *Brain Behav. Immun.* 56, 1–9. doi: 10.1016/j.bbi.2015.11.017

Bradbury, E. J., and Carter, L. M. (2011). Manipulating the glial scar: chondroitinase ABC as a therapy for spinal cord injury. *Brain Res. Bull.* 84, 306–316. doi: 10.1016/j.brainresbull.2010.06.015

Brod, S. A. (2022). Anti-inflammatory agents: an approach to prevent cognitive decline in Alzheimer's disease. *J. Alzheimers Dis.* 85, 457–472. doi: 10.3233/JAD-215125

Cassina, P., Cassina, A., Pehar, M., Castellanos, R., Gandelman, M., de León, A., et al. (2008). Mitochondrial dysfunction in SOD1G93A-bearing astrocytes promotes motor neuron degeneration: prevention by mitochondrial-targeted antioxidants. *J. Neurosci.* 28, 4115–4122. doi: 10.1523/JNEUROSCI.5308-07.2008

Chang, C. H., Lin, C. H., and Lane, H. Y. (2020). D-glutamate and gut microbiota in Alzheimer's disease. *Int. J. Mol. Sci.* 21:2676. doi: 10.3390/ijms21082676

Chang, T. C., Yu, D., Lee, Y. S., Wentzel, E. A., Arking, D. E., West, K. M., et al. (2008). Widespread microRNA repression by Myc contributes to tumorigenesis. *Nat. Genet.* 40, 43–50. doi: 10.1038/ng.2007.30

Chisholm, N. C., Henderson, M. L., Selvamani, A., Park, M. J., Dindot, S., Miranda, R. C., et al. (2015). Histone methylation patterns in astrocytes are influenced by age following ischemia. *Epigenetics* 10, 142–152. doi: 10.1080/15592294.2014.1001219

Cobley, J. N., Fiorello, M. L., and Bailey, D. M. (2018). 13 reasons why the brain is susceptible to oxidative stress. *Redox Biol.* 15, 490–503. doi: 10.1016/j.redox.2018.01.008

Conti, F., Minelli, A., and Melone, M. (2004). GABA transporters in the mammalian cerebral cortex: localization, development and pathological implications. *Brain Res. Brain Res. Rev.* 45, 196–212. doi: 10.1016/j.brainresrev.2004.03.003

Cua, R. C., Lau, L. W., Keough, M. B., Midha, R., Apte, S. S., and Yong, V. W. (2013). Overcoming neurite-inhibitory chondroitin sulfate proteoglycans in the astrocyte matrix. *Glia* 61, 972–984. doi: 10.1002/glia.22489

Daneman, R., and Engelhardt, B. (2017). Brain barriers in health and disease. *Neurobiol. Dis.* 107, 1–3. doi: 10.1016/j.nbd.2017.05.008

Di, Y., Lei, Y., Yu, F., Changfeng, F., Song, W., and Xuming, M. (2014). MicroRNAs expression and function in cerebral ischemia reperfusion injury. *J. Mol. Neurosci.* 53, 242–250. doi: 10.1007/s12031-014-0293-8

Dickendesher, T. L., Baldwin, K. T., Mironova, Y. A., Koriyama, Y., Raiker, S. J., Askew, K. L., et al. (2012). NgR1 and NgR3 are receptors for chondroitin sulfate proteoglycans. *Nat. Neurosci.* 15, 703–712. doi: 10.1038/nn.3070

Dong, J., Xia, R., Zhang, Z., and Xu, C. (2021). lncRNA MEG3 aggravated neuropathic pain and astrocyte overaction through mediating miR-130a-5p/CXCL12/CXCR4 axis. *Aging (Albany NY)* 13, 23004–23019. doi: 10.18632/aging.203592

Duan, R., Wang, S. Y., Wei, B., Deng, Y., Fu, X. X., Gong, P. Y., et al. (2021). Angiotensin-(1-7) analogue AVE0991 modulates astrocyte-mediated Neuroinflammation via lncRNA SNHG14/miR-223-3p/NLRP3 pathway and offers

Neuroprotection in a transgenic mouse model of Alzheimer's disease. *J. Inflamm. Res.* 14, 7007–7019. doi: 10.2147/JIR.S343575

Dyck, S. M., and Karimi-Abdolrezaee, S. (2015). Chondroitin sulfate proteoglycans: key modulators in the developing and pathologic central nervous system. *Exp. Neurol.* 269, 169–187. doi: 10.1016/j.expneurol.2015.04.006

Dzamba, D., Honsa, P., Valny, M., Kriska, J., Valihrach, L., Novosadova, V., et al. (2015). Quantitative analysis of glutamate receptors in glial cells from the cortex of GFAP/EGFP mice following ischemic injury: focus on NMDA receptors. *Cell. Mol. Neurobiol.* 35, 1187–1202. doi: 10.1007/s10571-015-0212-8

Fairman, W. A., Vandenberg, R. J., Arriza, J. L., Kavanaugh, M. P., and Amara, S. G. (1995). An excitatory amino-acid transporter with properties of a ligand-gated chloride channel. *Nature* 375, 599–603. doi: 10.1038/375599a0

Ferraiuolo, L., Higginbottom, A., Heath, P. R., Barber, S., Greenald, D., Kirby, J., et al. (2011). Dysregulation of astrocyte-motoneuron cross-talk in mutant superoxide dismutase 1-related amyotrophic lateral sclerosis. *Brain* 134, 2627–2641. doi: 10.1093/brain/awr193

Fitch, M. T., and Silver, J. (2008). CNS injury, glial scars, and inflammation: inhibitory extracellular matrices and regeneration failure. *Exp. Neurol.* 209, 294–301. doi: 10.1016/j.expneurol.2007.05.014

Fleming, J. C., Norenberg, M. D., Ramsay, D. A., Dekaban, G. A., Marcillo, A. E., Saenz, A. D., et al. (2006). The cellular inflammatory response in human spinal cords after injury. *Brain* 129, 3249–3269. doi: 10.1093/brain/awl296

Fricker, M., Tolkovsky, A. M., Borutaite, V., Coleman, M., and Brown, G. C. (2018). Neuronal cell death. *Physiol. Rev.* 98, 813–880. doi: 10.1152/physrev.00011.2017

Fukuda, A. M., and Badaut, J. (2012). Aquaporin 4: a player in cerebral edema and neuroinflammation. *J. Neuroinflammation* 9:279. doi: 10.1186/1742-2094-9-279

Gardoni, F., and Di Luca, M. (2015). Targeting glutamatergic synapses in Parkinson's disease. *Curr. Opin. Pharmacol.* 20, 24–28. doi: 10.1016/j.coph.2014.10.011

Guérit, S., Fidan, E., Macas, J., Czupalla, C. J., Figueiredo, R., Vijikumar, A., et al. (2021). Astrocyte-derived Wnt growth factors are required for endothelial blood-brain barrier maintenance. *Prog. Neurobiol.* 199:101937. doi: 10.1016/j.pneurobio.2020.101937

Guttenplan, K. A., Weigel, M. K., Prakash, P., Wijewardhane, P. R., Hasel, P., Rufen-Blanchette, U., et al. (2021). Neurotoxic reactive astrocytes induce cell death via saturated lipids. *Nature* 599, 102–107. doi: 10.1038/s41586-021-03960-y

Haley, M. J., and Lawrence, C. B. (2017). The blood-brain barrier after stroke: structural studies and the role of transcytotic vesicles. *J. Cereb. Blood Flow Metab.* 37, 456–470. doi: 10.1177/0271678X16629976

Hamilton, N. B., and Attwell, D. (2010). Do astrocytes really exocytose neurotransmitters. *Nat. Rev. Neurosci.* 11, 227–238. doi: 10.1038/nrn2803

Hammond, T. R., Gadea, A., Dupree, J., Kerninon, C., Nait-Oumesmar, B., Aguirre, A., et al. (2014). Astrocyte-derived endothelin-1 inhibits remyelination through notch activation. *Neuron* 81, 588–602. doi: 10.1016/j.neuron.2013.11.015

Hammond, T. R., McEllin, B., Morton, P. D., Raymond, M., Dupree, J., and Gallo, V. (2015). Endothelin-B receptor activation in astrocytes regulates the rate of Oligodendrocyte regeneration during Remyelination. *Cell Rep.* 13, 2090–2097. doi: 10.1016/j.celrep.2015.11.002

Han, B., Zhang, Y., Zhang, Y., Bai, Y., Chen, X., Huang, R., et al. (2018). Novel insight into circular RNA HECTD1 in astrocyte activation via autophagy by targeting MIR142-TIPARP: implications for cerebral ischemic stroke. *Autophagy* 14, 1164–1184. doi: 10.1080/15548627.2018.1458173

Harvey, B. K., Airavaara, M., Hinzman, J., Wires, E. M., Chiocco, M. J., Howard, D. B., et al. (2011). Targeted over-expression of glutamate transporter 1 (GLT-1) reduces ischemic brain injury in a rat model of stroke. *PLoS One* 6:e22135. doi: 10.1371/journal.pone.0022135

Hasel, P., Rose, I., Sadick, J. S., Kim, R. D., and Liddelow, S. A. (2021). Neuroinflammatory astrocyte subtypes in the mouse brain. *Nat. Neurosci.* 24, 1475–1487. doi: 10.1038/s41593-021-00905-6

He, Y., Liu, X., and Chen, Z. (2020). Glial scar-a promising target for improving outcomes after CNS injury. *J. Mol. Neurosci.* 70, 340–352. doi: 10.1007/s12031-019-01417-6

He, J., Zhao, J., Peng, X., Shi, X., Zong, S., and Zeng, G. (2017). Molecular mechanism of MiR-136-5p targeting NF-κB/A20 in the IL-17-mediated inflammatory response after spinal cord injury. *Cell. Physiol. Biochem.* 44, 1224–1241. doi: 10.1159/000485452

Heneka, M. T., Kummer, M. P., Stutz, A., Delekate, A., Schwartz, S., Vieira-Saecker, A., et al. (2013). NLRP3 is activated in Alzheimer's disease and contributes to pathology in APP/PS1 mice. *Nature* 493, 674–678. doi: 10.1038/nature11729

Hernández, I. H., Villa-González, M., Martín, G., Soto, M., and Pérez-Álvarez, M. J. (2021). Glial cells as therapeutic approaches in brain ischemia-reperfusion injury. *Cells* 10:1639. doi: 10.3390/cells10071639

Herrmann, J. E., Imura, T., Song, B., Qi, J., Ao, Y., Nguyen, T. K., et al. (2008). STAT3 is a critical regulator of astrogliosis and scar formation after spinal cord injury. *J. Neurosci.* 28, 7231–7243. doi: 10.1523/JNEUROSCI.1709-08.2008

Hirsch, E. C., and Hunot, S. (2009). Neuroinflammation in Parkinson's disease: a target for neuroprotection. *Lancet Neurol.* 8, 382–397. doi: 10.1016/S1474-4422(09)70062-6

Hong, S., Beja-Glasser, V. F., Nfonoyim, B. M., Frouin, A., Li, S., Ramakrishnan, S., et al. (2016). Complement and microglia mediate early synapse loss in Alzheimer mouse models. *Science* 352, 712–716. doi: 10.1126/science.aad8373

Hong, P., Jiang, M., and Li, H. (2014). Functional requirement of dicer 1 and miR-17-5p in reactive astrocyte proliferation after spinal cord injury in the mouse. *Glia* 62, 2044–2060. doi: 10.1002/glia.22725

Hong, Y., Liu, Q., Peng, M., Bai, M., Li, J., Sun, R., et al. (2020). High-frequency repetitive transcranial magnetic stimulation improves functional recovery by inhibiting neurotoxic polarization of astrocytes in ischemic rats. *J. Neuroinflammation* 17:150. doi: 10.1186/s12974-020-01747-y

Hoye, M. L., Regan, M. R., Jensen, L. A., Lake, A. M., Reddy, L. V., Vidensky, S., et al. (2018). Motor neuron-derived microRNAs cause astrocyte dysfunction in amyotrophic lateral sclerosis. *Brain* 141, 2561–2575. doi: 10.1093/brain/awy182

Huang, W. Y., Jiang, C., Ye, H. B., Jiao, J. T., Cheng, C., Huang, J., et al. (2019). miR-124 upregulates astrocytic glutamate transporter-1 via the Akt and mTOR signaling pathway post ischemic stroke. *Brain Res. Bull.* 149, 231–239. doi: 10.1016/j.brainresbull.2019.04.013

Huang, R., Zhang, Y., Han, B., Bai, Y., Zhou, R., Gan, G., et al. (2017). Circular RNA HIPK2 regulates astrocyte activation via cooperation of autophagy and ER stress by targeting MIR124-2HG. *Autophagy* 13, 1722–1741. doi: 10.1080/15548627.2017.1356975

Huang, P., Zhou, Q., Lin, Q., Lin, L., Wang, H., Chen, X., et al. (2020). Complement C3a induces axonal hypomyelination in the periventricular white matter through activation of WNT/β-catenin signal pathway in septic neonatal rats experimentally induced by lipopolysaccharide. *Brain Pathol.* 30, 495–514. doi: 10.1111/bpa.12798

Iadecola, C., and Nedergaard, M. (2007). Glial regulation of the cerebral microvasculature. *Nat. Neurosci.* 10, 1369–1376. doi: 10.1038/nn2003

Iorio, M. V., Ferracin, M., Liu, C. G., Veronese, A., Spizzo, R., Sabbioni, S., et al. (2005). MicroRNA gene expression deregulation in human breast cancer. *Cancer Res.* 65, 7065–7070. doi: 10.1158/0008-5472.CAN-05-1783

Itoh, N., Itoh, Y., Tassoni, A., Ren, E., Kaito, M., Ohno, A., et al. (2018). Cell-specific and region-specific transcriptomics in the multiple sclerosis model: focus on astrocytes. *Proc. Natl. Acad. Sci. U. S. A.* 115, E302–E309. doi: 10.1073/pnas.1716032115

Jackson, R. J., Meltzer, J. C., Nguyen, H., Commins, C., Bennett, R. E., Hudry, E., et al. (2022). APOE4 derived from astrocytes leads to blood-brain barrier impairment. *Brain* 145, 3582–3593. doi: 10.1093/brain/awab478

Jeon, H., Lee, S., Lee, W. H., and Suk, K. (2010). Analysis of glial secretome: the long pentraxin PTX3 modulates phagocytic activity of microglia. *J. Neuroimmunol.* 229, 63–72. doi: 10.1016/j.jneuroim.2010.07.001

Jiang, D., Gong, F., Ge, X., Lv, C., Huang, C., Feng, S., et al. (2020). Neuron-derived exosomes-transmitted miR-124-3p protect traumatically injured spinal cord by suppressing the activation of neurotoxic microglia and astrocytes. *J Nanobiotechnol.* 18:105. doi: 10.1186/s12951-020-00665-8

Jimenez-Blasco, D., Santofimia-Castaño, P., Gonzalez, A., Almeida, A., and Bolaños, J. P. (2015). Astrocyte NMDA receptors' activity sustains neuronal survival through a Cdk5-Nrf2 pathway. *Cell Death Differ.* 22, 1877–1889. doi: 10.1038/cdd.2015.49

Khaing, Z. Z., Milman, B. D., Vanscoy, J. E., Seidlits, S. K., Grill, R. J., and Schmidt, C. E. (2011). High molecular weight hyaluronic acid limits astrocyte activation and scar formation after spinal cord injury. *J. Neural Eng.* 8:046033. doi: 10.1088/1741-2560/8/4/046033

Kim, T. H., Song, J. Y., Park, H., Jeong, J. Y., Kwon, A. Y., Heo, J. H., et al. (2015). miR-145, targeting high-mobility group A2, is a powerful predictor of patient outcome in ovarian carcinoma. *Cancer Lett.* 356, 937–945. doi: 10.1016/j.canlet.2014.11.011

Kitchen, P., Salman, M. M., Halsey, A. M., Clarke-Bland, C., MacDonald, J. A., Ishida, H., et al. (2020). Targeting Aquaporin-4 subcellular localization to treat central nervous system edema. *Cells* 181, 784–799.e19. doi: 10.1016/j.cell.2020.03.037

Krebs, C., Fernandes, H. B., Sheldon, C., Raymond, L. A., and Baimbridge, K. G. (2003). Functional NMDA receptor subtype 2B is expressed in astrocytes after ischemia in vivo and anoxia in vitro. *J. Neurosci.* 23, 3364–3372. doi: 10.1523/JNEUROSCI.23-08-03364.2003

Kwon, H. S., and Koh, S. H. (2020). Neuroinflammation in neurodegenerative disorders: the roles of microglia and astrocytes. *Transl Neurodegener* 9:42. doi: 10.1186/s40035-020-00221-2

Lanfranco, M. F., Sepulveda, J., Kopetsky, G., and Rebeck, G. W. (2021). Expression and secretion of apoE isoforms in astrocytes and microglia during inflammation. *Glia* 69, 1478–1493. doi: 10.1002/glia.23974

Lanjakornsiripan, D., Pior, B. J., Kawaguchi, D., Furutachi, S., Tahara, T., Katsuyama, Y., et al. (2018). Layer-specific morphological and molecular differences in neocortical astrocytes and their dependence on neuronal layers. *Nat. Commun.* 9:1623. doi: 10.1038/s41467-018-03940-3

Li, P., Li, Y., Dai, Y., Wang, B., Li, L., Jiang, B., et al. (2020). The LncRNA H19/miR-1-3p/CCL2 axis modulates lipopolysaccharide (LPS) stimulation-induced normal human astrocyte proliferation and activation. *Cytokine* 131:155106. doi: 10.1016/j.cyto.2020.155106

Li, L., Lundkvist, A., Andersson, D., Wilhelmsson, U., Nagai, N., Pardo, A. C., et al. (2008). Protective role of reactive astrocytes in brain ischemia. *J. Cereb. Blood Flow Metab.* 28, 468–481. doi: 10.1038/sj.jcbfm.9600546

Li, Y., Park, J. S., Deng, J. H., and Bai, Y. (2006). Cytochrome c oxidase subunit IV is essential for assembly and respiratory function of the enzyme complex. *J. Bioenerg. Biomembr.* 38, 283–291. doi: 10.1007/s10863-006-9052-z

Li, Z., Song, Y., He, T., Wen, R., Li, Y., Chen, T., et al. (2021). M2 microglial small extracellular vesicles reduce glial scar formation via the miR-124/STAT3 pathway after ischemic stroke in mice. *Theranostics* 11, 1232–1248. doi: 10.7150/thno.48761

Li, L., Voloboueva, L., Griffiths, B. B., Xu, L., Giffard, R. G., and Stary, C. M. (2021). MicroRNA-338 inhibition protects against focal cerebral ischemia and preserves mitochondrial function in vitro in astrocytes and neurons via COX4I1. *Mitochondrion* 59, 105–112. doi: 10.1016/j.mito.2021.04.013

Li, D., Wang, Y., Jin, X., Hu, D., Xia, C., Xu, H., et al. (2020). NK cell-derived exosomes carry miR-207 and alleviate depression-like symptoms in mice. *J. Neuroinflammation* 17:126. doi: 10.1186/s12974-020-01787-4

Lian, H., Litvinchuk, A., Chiang, A. C., Aithmitti, N., Jankowsky, J. L., and Zheng, H. (2016). Astrocyte-microglia cross talk through complement activation modulates amyloid pathology in mouse models of Alzheimer's disease. *J. Neurosci.* 36, 577–589. doi: 10.1523/JNEUROSCI.2117-15.2016

Liddelow, S. A., and Barres, B. A. (2017). Reactive astrocytes: production, function, and therapeutic potential. *Immunity* 46, 957–967. doi: 10.1016/j.immuni.2017.06.006

Liddelow, S. A., Guttenplan, K. A., Clarke, L. E., Bennett, F. C., Bohlen, C. J., Schirmer, L., et al. (2017). Neurotoxic reactive astrocytes are induced by activated microglia. *Nature* 541, 481–487. doi: 10.1038/nature21029

Liebner, S., Dijkhuizen, R. M., Reiss, Y., Plate, K. H., Agalliu, D., and Constantin, G. (2018). Functional morphology of the blood-brain barrier in health and disease. *Acta Neuropathol.* 135, 311–336. doi: 10.1007/s00401-018-1815-1

Lin, S., and Gregory, R. I. (2015). MicroRNA biogenesis pathways in cancer. *Nat. Rev. Cancer* 15, 321–333. doi: 10.1038/nrc3932

Litvinchuk, A., Wan, Y. W., Swartzlander, D. B., Chen, F., Cole, A., Propson, N. E., et al. (2018). Complement C3aR inactivation attenuates tau pathology and reverses an immune network deregulated in Tauopathy models and Alzheimer's disease. *Neuron* 100, 1337–1353.e5. doi: 10.1016/j.neuron.2018.10.031

Liu, L. R., Liu, J. C., Bao, J. S., Bai, Q. Q., and Wang, G. Q. (2020). Interaction of microglia and astrocytes in the neurovascular unit. *Front. Immunol.* 11:1024. doi: 10.3389/fimmu.2020.01024

Luna-Herrera, C., Martínez-Dávila, I. A., Soto-Rojas, L. O., Flores-Martinez, Y. M., Fernandez-Parrilla, M. A., Ayala-Davila, J., et al. (2020). Intranigral administration of β-Sitosterol-β-D-Glucoside elicits neurotoxic A1 astrocyte reactivity and chronic Neuroinflammation in the rat Substantia Nigra. *J Immunol Res* 2020:5907591. doi: 10.1155/2020/5907591

Mac Vicar, B. A., and Newman, E. A. (2015). Astrocyte regulation of blood flow in the brain. *Cold Spring Harb. Perspect. Biol.* 7:a020388. doi: 10.1101/cshperspect.a020388

Madji Hounoum, B., Mavel, S., Coque, E., Patin, F., Vourc'h, P., Marouillat, S., et al. (2017). Wildtype motoneurons, ALS-linked SOD1 mutation and glutamate profoundly modify astrocyte metabolism and lactate shuttling. *Glia* 65, 592–605. doi: 10.1002/glia.23114

Magistretti, P. J., and Allaman, I. (2018). Lactate in the brain: from metabolic end-product to signalling molecule. *Nat. Rev. Neurosci.* 19, 235–249. doi: 10.1038/nrn.2018.19

Makar, T. K., Nedergaard, M., Preuss, A., Gelbard, A. S., Perumal, A. S., and Cooper, A. J. (1994). Vitamin E, ascorbate, glutathione, glutathione disulfide, and enzymes of glutathione metabolism in cultures of chick astrocytes and neurons: evidence that astrocytes play an important role in antioxidative processes in the brain. *J. Neurochem.* 62, 45–53. doi: 10.1046/j.1471-4159.1994.62010045.x

Manley, G. T., Fujimura, M., Ma, T., Noshita, N., Filiz, F., Bollen, A. W., et al. (2000). Aquaporin-4 deletion in mice reduces brain edema after acute water intoxication and ischemic stroke. *Nat. Med.* 6, 159–163. doi: 10.1038/72256

Marcos-Contreras, O. A., Greineder, C. F., Kiseleva, R. Y., Parhiz, H., Walsh, L. R., Zuluaga-Ramirez, V., et al. (2020). Selective targeting of nanomedicine to inflamed cerebral vasculature to enhance the blood-brain barrier. *Proc. Natl. Acad. Sci. U. S. A.* 117, 3405–3414. doi: 10.1073/pnas.1912012117

Masamoto, K., Unekawa, M., Watanabe, T., Toriumi, H., Takuwa, H., Kawaguchi, H., et al. (2015). Unveiling astrocytic control of cerebral blood flow with optogenetics. *Sci. Rep.* 5:11455. doi: 10.1038/srep11455

McKeon, R. J., Schreiber, R. C., Rudge, J. S., and Silver, J. (1991). Reduction of neurite outgrowth in a model of glial scarring following CNS injury is correlated with the expression of inhibitory molecules on reactive astrocytes. *J. Neurosci.* 11, 3398–3411. doi: 10.1523/JNEUROSCI.11-11-03398.1991

Meng, X., Zhong, J., Zeng, C., Yung, K., Zhang, X., Wu, X., et al. (2021). MiR-30a-5p regulates GLT-1 function via a PKCα-mediated ubiquitin degradation pathway in a mouse model of Parkinson's disease. *ACS Chem. Neurosci.* 12, 1578–1592. doi: 10.1021/acschemneuro.1c00076

Miklya, I., Göltl, P., Hafenscher, F., and Pencz, N. (2014). The role of parkin in Parkinson's disease. *Neuropsychopharmacol. Hung.* 16, 67–76.

Mizee, M. R., Wooldrik, D., Lakeman, K. A., van het Hof, B., Drexhage, J. A., Geerts, D., et al. (2013). Retinoic acid induces blood-brain barrier development. *J. Neurosci.* 33, 1660–1671. doi: 10.1523/JNEUROSCI.1338-12.2013

Mo, Y., Sun, Y. Y., and Liu, K. Y. (2020). Autophagy and inflammation in ischemic stroke. *Neural Regen. Res.* 15, 1388–1396. doi: 10.4103/1673-5374.274331

Montagne, A., Nation, D. A., Sagare, A. P., Barisano, G., Sweeney, M. D., Chakhoyan, A., et al. (2020). APOE4 leads to blood-brain barrier dysfunction predicting cognitive decline. *Nature* 581, 71–76. doi: 10.1038/s41586-020-2247-3

Morrison, B. M., Lee, Y., and Rothstein, J. D. (2013). Oligodendroglia: metabolic supporters of axons. *Trends Cell Biol.* 23, 644–651. doi: 10.1016/j.tcb.2013.07.007

Mukherjee, N., Nandi, S., Garg, S., Ghosh, S., Ghosh, S., Samat, R., et al. (2020). Targeting chondroitin sulfate proteoglycans: an emerging therapeutic strategy to treat CNS injury. *ACS Chem. Neurosci.* 11, 231–232. doi: 10.1021/acschemneuro.0c00004

Nakano, M., Kubota, K., Kobayashi, E., Chikenji, T. S., Saito, Y., Konari, N., et al. (2020). Bone marrow-derived mesenchymal stem cells improve cognitive impairment in an Alzheimer's disease model by increasing the expression of microRNA-146a in hippocampus. *Sci. Rep.* 10:10772. doi: 10.1038/s41598-020-67460-1

Nesic, O., Lee, J., Ye, Z., Unabia, G. C., Rafati, D., Hulsebosch, C. E., et al. (2006). Acute and chronic changes in aquaporin 4 expression after spinal cord injury. *Neuroscience* 143, 779–792. doi: 10.1016/j.neuroscience.2006.08.079

Noh, J. H., Chang, Y. G., Kim, M. G., Jung, K. H., Kim, J. K., Bae, H. J., et al. (2013). MiR-145 functions as a tumor suppressor by directly targeting histone deacetylase 2 in liver cancer. *Cancer Lett.* 335, 455–462. doi: 10.1016/j.canlet.2013.03.003

Norden, D. M., Fenn, A. M., Dugan, A., and Godbout, J. P. (2014). TGFβ produced by IL-10 redirected astrocytes attenuates microglial activation. *Glia* 62, 881–895. doi: 10.1002/glia.22647

Ohtake, Y., and Li, S. (2015). Molecular mechanisms of scar-sourced axon growth inhibitors. *Brain Res.* 1619, 22–35. doi: 10.1016/j.brainres.2014.08.064

Okada, S., Nakamura, M., Katoh, H., Miyao, T., Shimazaki, T., Ishii, K., et al. (2006). Conditional ablation of stat 3 or Socs 3 discloses a dual role for reactive astrocytes after spinal cord injury. *Nat. Med.* 12, 829–834. doi: 10.1038/nm1425

Olanow, C. W., and Tatton, W. G. (1999). Etiology and pathogenesis of Parkinson's disease. *Annu. Rev. Neurosci.* 22, 123–144. doi: 10.1146/annurev.neuro.22.1.123

Ouyang, Y. B., Voloboueva, L. A., Xu, L. J., and Giffard, R. G. (2007). Selective dysfunction of hippocampal CA1 astrocytes contributes to delayed neuronal damage after transient forebrain ischemia. *J. Neurosci.* 27, 4253–4260. doi: 10.1523/JNEUROSCI.0211-07.2007

Peng, G., Yuan, Y., Wu, S., He, F., Hu, Y., and Luo, B. (2015). MicroRNA let-7e is a potential circulating biomarker of acute stage ischemic stroke. *Transl. Stroke Res.* 6, 437–445. doi: 10.1007/s12975-015-0422-x

Peng, L., Zhao, Y., Li, Y., Zhou, Y., Li, L., Lei, S., et al. (2019). Effect of DJ-1 on the neuroprotection of astrocytes subjected to cerebral ischemia/reperfusion injury. *J. Mol. Med. (Berl)* 97, 189–199. doi: 10.1007/s00109-018-1719-5

Pines, G., Danbolt, N. C., Bjørås, M., Zhang, Y., Bendahan, A., Eide, L., et al. (1992). Cloning and expression of a rat brain L-glutamate transporter. *Nature* 360, 464–467. doi: 10.1038/360464a0

Plog, B. A., and Nedergaard, M. (2018). The Glymphatic system in central nervous system health and disease: past, present, and future. *Annu. Rev. Pathol.* 13, 379–394. doi: 10.1146/annurev-pathol-051217-111018

Polanco, J. C., Li, C., Bodea, L. G., Martinez-Marmol, R., Meunier, F. A., and Götz, J. (2018). Amyloid-β and tau complexity - towards improved biomarkers and targeted therapies. *Nat. Rev. Neurol.* 14, 22–39. doi: 10.1038/nrneurol.2017.162

Querfurth, H. W., and LaFerla, F. M. (2010). Alzheimer's disease. *N. Engl. J. Med.* 362, 329–344. doi: 10.1056/NEJMra0909142

Ramandi, D., Elahdadi Salmani, M., Moghimi, A., Lashkarbolouki, T., and Fereidoni, M. (2021). Pharmacological upregulation of GLT-1 alleviates the cognitive impairments in the animal model of temporal lobe epilepsy. *PLoS One* 16:e0246068. doi: 10.1371/journal.pone.0246068

Renault-Mihara, F., Mukaino, M., Shinozaki, M., Kumamaru, H., Kawase, S., Baudoux, M., et al. (2017). Regulation of rho a by STAT3 coordinates glial scar formation. *J. Cell Biol.* 216, 2533–2550. doi: 10.1083/jcb.201610102

Rolls, A., Shechter, R., and Schwartz, M. (2009). The bright side of the glial scar in CNS repair. *Nat. Rev. Neurosci.* 10, 235–241. doi: 10.1038/nrn2591

Rupaimoole, R., Calin, G. A., Lopez-Berestein, G., and Sood, A. K. (2016). miRNA deregulation in cancer cells and the tumor microenvironment. *Cancer Discov.* 6, 235–246. doi: 10.1158/2159-8290.CD-15-0893

Schousboe, A., Bak, L. K., and Waagepetersen, H. S. (2013). Astrocytic control of biosynthesis and turnover of the neurotransmitters glutamate and GABA. *Front Endocrinol (Lausanne)* 4:102. doi: 10.3389/fendo.2013.00102

Sekar, A., Bialas, A. R., de Rivera, H., Davis, A., Hammond, T. R., Kamitaki, N., et al. (2016). Schizophrenia risk from complex variation of complement component 4. *Nature* 530, 177–183. doi: 10.1038/nature16549

Shen, Y., Tenney, A. P., Busch, S. A., Horn, K. P., Cuascut, F. X., Liu, K., et al. (2009). PTPsigma is a receptor for chondroitin sulfate proteoglycan, an inhibitor of neural regeneration. *Science* 326, 592–596. doi: 10.1126/science.1178310

Shi, Q., Chowdhury, S., Ma, R., Le, K. X., Hong, S., Caldarone, B. J., et al. (2017). Complement C3 deficiency protects against neurodegeneration in aged plaque-rich APP/PS1 mice. *Sci. Transl. Med.* 9:eaaf6295. doi: 10.1126/scitranslmed.aaf6295

Shiow, L. R., Favrais, G., Schirmer, L., Schang, A. L., Cipriani, S., Andres, C., et al. (2017). Reactive astrocyte COX2-PGE2 production inhibits oligodendrocyte maturation in neonatal white matter injury. *Glia* 65, 2024–2037. doi: 10.1002/glia.23212

Silver, J., and Miller, J. H. (2004). Regeneration beyond the glial scar. *Nat. Rev. Neurosci.* 5, 146–156. doi: 10.1038/nrn1326

Skowrońska, K., Obara-Michlewska, M., Zielińska, M., and Albrecht, J. (2019). NMDA receptors in astrocytes: in search for roles in neurotransmission and Astrocytic homeostasis. *Int. J. Mol. Sci.* 20:309. doi: 10.3390/ijms20020309

Sofroniew, M. V. (2009). Molecular dissection of reactive astrogliosis and glial scar formation. *Trends Neurosci.* 32, 638–647. doi: 10.1016/j.tins.2009.08.002

Sofroniew, M. V., and Vinters, H. V. (2010). Astrocytes: biology and pathology. *Acta Neuropathol.* 119, 7–35. doi: 10.1007/s00401-009-0619-8

Song, S., Huang, H., Guan, X., Fiesler, V., Bhuiyan, M., Liu, R., et al. (2021). Activation of endothelial Wnt/β-catenin signaling by protective astrocytes repairs BBB damage in ischemic stroke. *Prog. Neurobiol.* 199:101963. doi: 10.1016/j.pneurobio.2020.101963

Srivastava, I., Vazquez-Juarez, E., Henning, L., Gómez-Galán, M., and Lindskog, M. (2020). Blocking Astrocytic GABA restores synaptic plasticity in prefrontal cortex of rat model of depression. *Cells* 9:1705. doi: 10.3390/cells9071705

Stary, C. M., Sun, X., Ouyang, Y., Li, L., and Giffard, R. G. (2016). miR-29a differentially regulates cell survival in astrocytes from cornu ammonis 1 and dentate gyrus by targeting VDAC1. *Mitochondrion* 30, 248–254. doi: 10.1016/j.mito.2016.08.013

Stephan, A. H., Barres, B. A., and Stevens, B. (2012). The complement system: an unexpected role in synaptic pruning during development and disease. *Annu. Rev. Neurosci.* 35, 369–389. doi: 10.1146/annurev-neuro-061010-113810

Storck, T., Schulte, S., Hofmann, K., and Stoffel, W. (1992). Structure, expression, and functional analysis of a Na(+)-dependent glutamate/aspartate transporter from rat brain. *Proc. Natl. Acad. Sci. U. S. A.* 89, 10955–10959. doi: 10.1073/pnas.89.22.10955

Tanaka, K., Watase, K., Manabe, T., Yamada, K., Watanabe, M., Takahashi, K., et al. (1997). Epilepsy and exacerbation of brain injury in mice lacking the glutamate transporter GLT-1. *Science* 276, 1699–1702. doi: 10.1126/science.276.5319.1699

Ter Horst, R., Jaeger, M., Smeekens, S. P., Oosting, M., Swertz, M. A., Li, Y., et al. (2016). Host and environmental factors influencing individual human cytokine responses. *Cells* 167, 1111–1124.e13. doi: 10.1016/j.cell.2016.10.018

Thrane, A. S., Rappold, P. M., Fujita, T., Torres, A., Bekar, L. K., Takano, T., et al. (2011). Critical role of aquaporin-4 (AQP4) in astrocytic Ca2+ signaling events elicited by cerebral edema. *Proc. Natl. Acad. Sci. U. S. A.* 108, 846–851. doi: 10.1073/pnas.1015217108

Tsai, H. H., Li, H., Fuentealba, L. C., Molofsky, A. V., Taveira-Marques, R., Zhuang, H., et al. (2012). Regional astrocyte allocation regulates CNS synaptogenesis and repair. *Science* 337, 358–362. doi: 10.1126/science.1222381

Tu, Z., Li, Y., Dai, Y., Li, L., Lv, G., Chen, I., et al. (2017). MiR-140/BDNF axis regulates normal human astrocyte proliferation and LPS-induced IL-6 and TNF-α secretion. *Biomed. Pharmacother.* 91, 899–905. doi: 10.1016/j.biopha.2017.05.016

Van Damme, P., Bogaert, E., Dewil, M., Hersmus, N., Kiraly, D., Scheveneels, W., et al. (2007). Astrocytes regulate Glu R2 expression in motor neurons and their vulnerability to excitotoxicity. *Proc. Natl. Acad. Sci. U. S. A.* 104, 14825–14830. doi: 10.1073/pnas.0705046104

Verdejo, H. E., del Campo, A., Troncoso, R., Gutierrez, T., Toro, B., Quiroga, C., et al. (2012). Mitochondria, myocardial remodeling, and cardiovascular disease. *Curr. Hypertens. Rep.* 14, 532–539. doi: 10.1007/s11906-012-0305-4

Verkhratsky, A., and Nedergaard, M. (2018). Physiology of Astroglia. *Physiol. Rev.* 98, 239–389. doi: 10.1152/physrev.00042.2016

Verkman, A. S., Hara-Chikuma, M., and Papadopoulos, M. C. (2008). Aquaporins--new players in cancer biology. *J. Mol. Med. (Berl)* 86, 523–529. doi: 10.1007/s00109-008-0303-9

Wang, Y., Cheng, X., He, Q., Zheng, Y., Kim, D. H., Whittemore, S. R., et al. (2011). Astrocytes from the contused spinal cord inhibit oligodendrocyte differentiation of adult oligodendrocyte precursor cells by increasing the expression of bone morphogenetic proteins. *J. Neurosci.* 31, 6053–6058. doi: 10.1523/JNEUROSCI.5524-09.2011

Wang, L., Wu, L., Duan, Y., Xu, S., Yang, Y., Yin, J., et al. (2022). Phenotype shifting in astrocytes account for benefits of intra-arterial selective cooling infusion in hypertensive rats of ischemic stroke. *Neurotherapeutics* 19, 386–398. doi: 10.1007/s13311-022-01186-y

Wang, C. Y., Yang, S. H., and Tzeng, S. F. (2015). MicroRNA-145 as one negative regulator of astrogliosis. *Glia* 63, 194–205. doi: 10.1002/glia.22743

Wang, H., Zheng, X., Jin, J., Zheng, L., Guan, T., Huo, Y., et al. (2020). LncRNA MALAT1 silencing protects against cerebral ischemia-reperfusion injury through miR-145 to regulate AQP4. *J. Biomed. Sci.* 27:40. doi: 10.1186/s12929-020-00635-0

Wanner, I. B., Anderson, M. A., Song, B., Levine, J., Fernandez, A., Gray-Thompson, Z., et al. (2013). Glial scar borders are formed by newly proliferated, elongated astrocytes that interact to corral inflammatory and fibrotic cells via STAT3-dependent mechanisms after spinal cord injury. *J. Neurosci.* 33, 12870–12886. doi: 10.1523/JNEUROSCI.2121-13.2013

Weiss, N., Miller, F., Cazaubon, S., and Couraud, P. O. (2009). The blood-brain barrier in brain homeostasis and neurological diseases. *Biochim. Biophys. Acta* 1788, 842–857. doi: 10.1016/j.bbamem.2008.10.022

Weller, M. L., Stone, I. M., Goss, A., Rau, T., Rova, C., and Poulsen, D. J. (2008). Selective overexpression of excitatory amino acid transporter 2 (EAAT2) in astrocytes enhances neuroprotection from moderate but not severe hypoxia-ischemia. *Neuroscience* 155, 1204–1211. doi: 10.1016/j.neuroscience.2008.05.059

Wolters, F. J., and Ikram, M. A. (2018). Epidemiology of dementia: the burden on society, the challenges for research. *Methods Mol. Biol.* 1750, 3–14. doi: 10.1007/978-1-4939-7704-8_1

Worringer, K. A., Rand, T. A., Hayashi, Y., Sami, S., Takahashi, K., Tanabe, K., et al. (2014). The let-7/LIN-41 pathway regulates reprogramming to human induced pluripotent stem cells by controlling expression of prodifferentiation genes. *Cell Stem Cell* 14, 40–52. doi: 10.1016/j.stem.2013.11.001

Wosik, K., Cayrol, R., Dodelet-Devillers, A., Berthelet, F., Bernard, M., Moumdjian, R., et al. (2007). Angiotensin II controls occludin function and is required for blood brain barrier maintenance: relevance to multiple sclerosis. *J. Neurosci.* 27, 9032–9042. doi: 10.1523/JNEUROSCI.2088-07.2007

Wu, X., Meng, X., Tan, F., Jiao, Z., Zhang, X., Tong, H., et al. (2019). Regulatory mechanism of miR-543-3p on GLT-1 in a mouse model of Parkinson's disease. *ACS Chem. Neurosci.* 10, 1791–1800. doi: 10.1021/acschemneuro.8b00683

Xiang, J., Tang, Y., Li, C., Su, E. J., Lawrence, D. A., and Keep, R. F. (2016). Mechanisms underlying astrocyte Endfeet swelling in stroke. *Acta Neurochir. Suppl.* 121, 19–22. doi: 10.1007/978-3-319-18497-5_4

Xu, P., Sriramula, S., and Lazartigues, E. (2011). ACE2/ANG-(1-7)/mas pathway in the brain: the axis of good. *Am. J. Physiol. Regul. Integr. Comp. Physiol.* 300, R804–R817. doi: 10.1152/ajpregu.00222.2010

Yamada, T., Kawahara, K., Kosugi, T., and Tanaka, M. (2006). Nitric oxide produced during sublethal ischemia is crucial for the preconditioning-induced down-regulation of glutamate transporter GLT-1 in neuron/astrocyte co-cultures. *Neurochem. Res.* 31, 49–56. doi: 10.1007/s11064-005-9077-4

Yang, Z. B., Luo, X. J., Ren, K. D., Peng, J. J., Tan, B., Liu, B., et al. (2015). Beneficial effect of magnesium lithospermate B on cerebral ischemia-reperfusion injury in rats involves the regulation of miR-107/glutamate transporter 1 pathway. *Eur. J. Pharmacol.* 766, 91–98. doi: 10.1016/j.ejphar.2015.09.042

Yang, Z. B., Zhang, Z., Li, T. B., Lou, Z., Li, S. Y., Yang, H., et al. (2014). Up-regulation of brain-enriched miR-107 promotes excitatory neurotoxicity through down-regulation of glutamate transporter-1 expression following ischaemic stroke. *Clin. Sci. (Lond)* 127, 679–689. doi: 10.1042/CS20140084

Ye, Y., Hao, J., Hong, Z., Wu, T., Ge, X., Qian, B., et al. (2022). Downregulation of MicroRNA-145-5p in activated microglial Exosomes promotes astrocyte proliferation by removal of Smad 3 inhibition. *Neurochem. Res.* 47, 382–393. doi: 10.1007/s11064-021-03446-3

Yeh, T. H., Lee, D. Y., Gianino, S. M., and Gutmann, D. H. (2009). Microarray analyses reveal regional astrocyte heterogeneity with implications for neurofibromatosis type 1 (NF1)-regulated glial proliferation. *Glia* 57, 1239–1249. doi: 10.1002/glia.20845

Zamanian, J. L., Xu, L., Foo, L. C., Nouri, N., Zhou, L., Giffard, R. G., et al. (2012). Genomic analysis of reactive astrogliosis. *J. Neurosci.* 32, 6391–6410. doi: 10.1523/JNEUROSCI.6221-11.2012

Zeevalk, G. D., Davis, N., Hyndman, A. G., and Nicklas, W. J. (1998). Origins of the extracellular glutamate released during total metabolic blockade in the immature retina. *J. Neurochem.* 71, 2373–2381. doi: 10.1046/j.1471-4159.1998.71062373.x

Zeisel, A., Muñoz-Manchado, A. B., Codeluppi, S., Lönnerberg, P., La Manno, G., Juréus, A., et al. (2015). Brain structure. Cell types in the mouse cortex and hippocampus revealed by single-cell RNA-seq. *Science* 347, 1138–1142. doi: 10.1126/science.aaa1934

Zeng, X., Dong, X., Xiao, Q., and Yao, J. (2022). Vitamin C inhibits Ubiquitination of glutamate transporter 1 (GLT-1) in astrocytes by Downregulating HECTD1. *ACS Chem. Neurosci.* 13, 676–687. doi: 10.1021/acschemneuro.1c00845

Zeng, H. K., Wang, Q. S., Deng, Y. Y., Fang, M., Chen, C. B., Fu, Y. H., et al. (2010). Hypertonic saline ameliorates cerebral edema through downregulation of aquaporin-4 expression in the astrocytes. *Neuroscience* 166, 878–885. doi: 10.1016/j.neuroscience.2009.12.076

Zhang, Y., and Barres, B. A. (2010). Astrocyte heterogeneity: an underappreciated topic in neurobiology. *Curr. Opin. Neurobiol.* 20, 588–594. doi: 10.1016/j.conb.2010.06.005

Zhang, C., Chen, J., and Lu, H. (2015). Expression of aquaporin-4 and pathological characteristics of brain injury in a rat model of traumatic brain injury. *Mol. Med. Rep.* 12, 7351–7357. doi: 10.3892/mmr.2015.4372

Zhang, Y., He, X., Wu, X., Lei, M., Wei, Z., Zhang, X., et al. (2017). Rapamycin upregulates glutamate transporter and IL-6 expression in astrocytes in a mouse model of Parkinson's disease. *Cell Death Dis.* 8:e2611. doi: 10.1038/cddis.2016.491

Zhang, Y., Meng, T., Chen, J., Zhang, Y., Kang, J., Li, X., et al. (2021). miR-21a-5p promotes inflammation following traumatic spinal cord injury through Upregulation of neurotoxic reactive astrocyte (A1) polarization by inhibiting the CNTF/STAT3/Nkrf pathway. *Int. J. Biol. Sci.* 17, 2795–2810. doi: 10.7150/ijbs.60509

Zhang, L. Y., Pan, J., Mamtilahun, M., Zhu, Y., Wang, L., Venkatesh, A., et al. (2020). Microglia exacerbate white matter injury via complement C3/C3aR pathway after hypoperfusion. *Theranostics* 10, 74–90. doi: 10.7150/thno.35841

Zhang, Y., Xu, D., Qi, H., Yuan, Y., Liu, H., Yao, S., et al. (2018). Enriched environment promotes post-stroke neurogenesis through NF-κB-mediated secretion of IL-17A from astrocytes. *Brain Res.* 1687, 20–31. doi: 10.1016/j.brainres.2018.02.030

Zhao, F., Qu, Y., Wang, H., Huang, L., Zhu, J., Li, S., et al. (2017). The effect of miR-30d on apoptosis and autophagy in cultured astrocytes under oxygen-glucose deprivation. *Brain Res.* 1671, 67–76. doi: 10.1016/j.brainres.2017.06.011

Zheng, J., Lu, J., Mei, S., Wu, H., Sun, Z., Fang, Y., et al. (2021). Ceria nanoparticles ameliorate white matter injury after intracerebral hemorrhage: microglia-astrocyte involvement in remyelination. *J. Neuroinflammation* 18:43. doi: 10.1186/s12974-021-02101-6

Zheng, Y., Wang, L., Chen, M., Pei, A., Xie, L., and Zhu, S. (2017). Upregulation of miR-130b protects against cerebral ischemic injury by targeting water channel protein aquaporin 4 (AQP4). *Am. J. Transl. Res.* 10, 5209–5224. doi: 10.7150/thno.43640

Zhou, Y., and Danbolt, N. C. (2013). GABA and glutamate transporters in brain. *Front Endocrinol (Lausanne)* 4:165. doi: 10.3389/fendo.2013.00165

Zhou, D., Huang, Z., Zhu, X., Hong, T., and Zhao, Y. (2021). Circular RNA 0025984 ameliorates ischemic stroke injury and protects astrocytes through miR-143-3p/TET1/ORP150 pathway. *Mol. Neurobiol.* 58, 5937–5953. doi: 10.1007/s12035-021-02486-8

Zou, L. H., Shi, Y. J., He, H., Jiang, S. M., Huo, F. F., Wang, X. M., et al. (2019). Effects of FGF2/FGFR1 pathway on expression of A1 astrocytes after infrasound exposure. *Front. Neurosci.* 13:429. doi: 10.3389/fnins.2019.00429

frontiers | Frontiers in Molecular Neuroscience

TYPE Original Research
PUBLISHED 20 January 2023
DOI 10.3389/fnmol.2023.1073723

OPEN ACCESS

EDITED BY
Giulia Abate,
University of Brescia,
Italy

REVIEWED BY
Huang Weiyi,
Wuxi People's Hospital, China
Jian-Huan Chen,
Jiangnan University,
China

*CORRESPONDENCE
Lei Shi
✉ shilei_0328@hrbmu.edu.cn

†These authors have contributed equally to this work

SPECIALTY SECTION
This article was submitted to Brain Disease Mechanisms, a section of the journal Frontiers in Molecular Neuroscience

RECEIVED 18 October 2022
ACCEPTED 03 January 2023
PUBLISHED 20 January 2023

CITATION
Zhang Y, Ren Y, Zhang Y, Li Y, Xu C, Peng Z, Jia Y, Qiao S, Zhang Z and Shi L (2023) T-cell infiltration in the central nervous system and their association with brain calcification in *Slc20a2*-deficient mice.
Front. Mol. Neurosci. 16:1073723.
doi: 10.3389/fnmol.2023.1073723

T-cell infiltration in the central nervous system and their association with brain calcification in *Slc20a2*-deficient mice

Yi Zhang[1,2†], Yaqiong Ren[1†], Yueni Zhang[1,2], Ying Li[1,3], Chao Xu[1,4], Ziyue Peng[1,4], Ying Jia[2,3], Shupei Qiao[1,3], Zitong Zhang[1,2] and Lei Shi[1,2*]

[1]Human Molecular Genetics Group, NHC Key Laboratory of Molecular Probes and Targeted Diagnosis and Therapy, The Fourth Affiliated Hospital of Harbin Medical University, Harbin, China, [2]Department of Medical Genetics, College of Basic Medical Sciences, Harbin Medical University, Harbin, China, [3]Department of Child and Adolescent Health, School of Public Health, Harbin Medical University, Harbin, China, [4]Department of Pediatrics, The Second Affiliated Hospital of Harbin Medical University, Harbin, China

Primary familial brain calcification (PFBC) is a rare neurodegenerative and neuropsychiatric disorder characterized by bilateral symmetric intracranial calcification along the microvessels or inside neuronal cells in the basal ganglia, thalamus, and cerebellum. *Slc20a2* homozygous (HO) knockout mice are the most commonly used model to simulate the brain calcification phenotype observed in human patients. However, the cellular and molecular mechanisms related to brain calcification, particularly at the early stage much prior to the emergence of brain calcification, remain largely unknown. In this study, we quantified the central nervous system (CNS)-infiltrating T-cells of different age groups of *Slc20a2*-HO and matched wild type mice and found $CD45^+CD3^+$ T-cells to be significantly increased in the brain parenchyma, even in the pre-calcification stage of 1-month-old -HO mice. The accumulation of the $CD3^+$ T-cells appeared to be associated with the severity of brain calcification. Further immunophenotyping revealed that the two main subtypes that had increased in the brain were $CD3^+$ $CD4^-$ $CD8^-$ and $CD3^+$ $CD4^+$ T-cells. The expression of endothelial cell (EC) adhesion molecules increased, while that of tight and adherents junction proteins decreased, providing the molecular precondition for T-cell recruitment to ECs and paracellular migration into the brain. The fusion of lymphocytes and EC membranes and transcellular migration of CD3-related gold particles were captured, suggesting enhancement of transcytosis in the brain ECs. Exogenous fluorescent tracers and endogenous IgG and albumin leakage also revealed an impairment of transcellular pathway in the ECs. FTY720 significantly alleviated brain calcification, probably by reducing T-cell infiltration, modulating neuroinflammation and ossification process, and enhancing the autophagy and phagocytosis of CNS-resident immune cells. This study clearly demonstrated CNS-infiltrating T-cells to be associated with the progression of brain calcification. Impairment of blood–brain barrier (BBB) permeability, which was closely related to T-cell invasion into the CNS, could be explained by the BBB alterations of an increase in the paracellular and transcellular pathways of brain ECs. FTY720 was found to be a potential drug to protect patients from PFBC-related lesions in the future.

KEYWORDS

brain calcification, *Slc20a2*, T-cell, blood–brain barrier, permeability, transcytosis, FTY720

Introduction

Primary familial brain calcification (PFBC; OMIM#213600), also known as Fahr's disease, is a rare neurodegenerative disorder characterized by bilateral and symmetric calcification along the microvessels or inside neuronal cells in the basal ganglia, thalamus, and cerebellum. This disease is accompanied by multiple neurological manifestations such as movement disorders, cognitive impairment, and psychiatric signs, which commence after the age of 40 years (Tadic et al., 2015; Grangeon et al., 2019; Xu et al., 2022). Primary familial brain calcification is caused by the loss-of-function (LOF) variants, either in a dominant or recessive inheritance pattern, in one of seven genes in humans: solute carrier family 20 member 2 (*SLC20A2*; Wang et al., 2012), platelet derived growth factor receptor beta (*PDGFRB*; Nicolas et al., 2013), platelet derived growth factor subunit B (*PDGFB*; Keller et al., 2013), xenotropic and polytropic retrovirus receptor 1 (*XPR1*; Legati et al., 2015), myogenesis regulating glycosidase (putative) (*MYORG*; Yao et al., 2018), junctional adhesion molecule 2 (*JAM2*; Cen et al., 2020; Schottlaender et al., 2020) and cytidine/uridine monophosphate kinase 2 (*CMPK2*; Zhao et al., 2022).

Slc20a2 encodes a multi-transmembrane type III sodium-dependent phosphate (Pi) cotransporter 2 (Pit-2), which is essential for regulating Pi homeostasis in the cerebrospinal fluid (CSF) and brain parenchyma. Its functional deficiency impedes inward Pi transport into brain endothelial cells (ECs) or smooth muscle cells (SMCs), leading to paracellular Pi accumulation (Wallingford et al., 2017). CSF-Pi levels are significantly elevated in patients with *SLC20A2*-related PFBC (Paucar et al., 2017; Hozumi et al., 2018) and in *Slc20a2* homozygous (HO) knockout mice (Jensen et al., 2016; Wallingford et al., 2017). Excess extracellular Pi is known to cause tissue toxicity (Razzaque, 2011; Hong et al., 2015) and is associated with neuroinflammation (Brown, 2020), so as the accumulation of intracellular Pi (Legati et al., 2015; Zhao et al., 2022). The central nervous system (CNS)-resident immune cells, particularly microglia, macrophages, and astrocytes, are important sources of neuroinflammatory cytokines. Among these, $CD45^+$ microglia (Keller et al., 2013), $PDPN^+$, $LCN2^+$, or $C3^+$ neurotoxic reactive astrocytes (Zarb et al., 2019), along with novel calcification-associated microglia (Zarb et al., 2021), are known to significantly increase and cluster around the perivascular spaces of calcified microvessels in PFBC mice.

The blood–brain barrier (BBB) serves as a highly selective, restrictive, and dynamic monolayer barrier for peripheral immune cells and foreign immunogens while also overseeing the CNS immune surveillance and brain homeostasis and maintaining the normal physiological roles of the CNS (Zlokovic, 2008; Abbott et al., 2010). Microvascular ECs, the core components of the BBB, express cell adhesion molecules (CAMs) to restrict peripheral immune cell crawling and adherence and possess specific cell junction proteins to prevent harmful immunogen extravasation and maintain beneficial exchange through paracellular and transcellular pathways under physiological conditions (Wilson et al., 2010; Engelhardt and Ransohoff, 2012; Pulgar, 2018). Maintaining a low rate of endocytosis and transcytosis in the BBB also contributes to normal CNS function. Transcellular pathway could be mediated by clathrin or caveolin-1 (Cav-1) expressed on ECs (Andreone et al., 2017; Ayloo and Gu, 2019). The proto-oncogene tyrosine-protein kinases, Src and Cav-1, participate in the transcytosis process, where Src regulates the formation of endocytic vesicles by phosphorylating Cav-1, the primary structural component of caveolae (Parton et al., 1994; Kim et al., 2009).

Peripheral immune cell infiltration in the CNS has been reported as coinciding with neurological disorders, such as Alzheimer's disease, multiple sclerosis, and stroke (Ellwardt et al., 2016; Liebner et al., 2018), among which $CD4^+$ and $CD8^+$ T-cells account for the main subpopulations. FTY720 (Fingolimod) is a sphingosine-1-phosphate receptor modulator, which inhibits egress of lymphocytes from lymph nodes, potentially reducing trafficking of T-cells into the CNS (Mandala et al., 2002; Cohen and Chun, 2011), and was utilized to inhibit the circulation of peripheral T-cells to treat CNS autoimmune diseases such as multiple sclerosis (Chun et al., 2019). In $Pdgfb^{ret/ret}$ PFBC mice, $CD45^{hi}$ leukocyte infiltration modified the course of neuroinflammation, and the infiltration and neuroinflammation could be alleviated by FTY720 (Torok et al., 2021). However, in *Slc20a2*-PFBC mice, the cellular and molecular mechanisms related to brain calcification, particularly in a high-Pi microenvironment or areas of microcalcification, remain largely unknown.

Materials and methods

Mouse model

$Slc20a2^{tm1a(EUCOMM)Wtsi}$ mice were purchased from the European Mouse Mutant Archive (Munich, Germany; Skarnes et al., 2011). The mice were maintained under specific pathogen-free conditions and allowed free access to water and chow under a light–dark cycle of 12 h. Heterozygous *Slc20a2* mice were cross-mated to generate wild-type (WT) and HO mice. Littermates were used in subsequent experiments. All research procedures related to mouse models were scrutinized and approved by the Ethics Committee of the Fourth Affiliated Hospital of Harbin Medical University.

Immunofluorescence

Brain tissues embedded in optimal cutting temperature media were cut into 5 μm sections and stored at −80°C. Brain sections were fixed with 4% paraformaldehyde (PFA) for 10 min on ice and blocked with blocking buffer [5% normal goat/donkey serum, 1% bovine serum albumin (BSA), 0.3% Triton X-100, and 0.3% glycine in 0.01 M phosphate-buffered saline (PBS)] for at least 1 h at 25°C. The sections were incubated with primary antibodies overnight at 4°C, followed by incubation with secondary antibodies conjugated to Alexa Fluor 488 or 594. Images were obtained using a confocal microscope (C2 confocal system, Nikon, Japan). All the antibodies and immunofluorescence parameters are listed in Supplementary Table S1.

Leukocyte isolation and flow cytometry

The mice were anesthetized and transcardially perfused with ice-cold Hank's balanced salt solution (Ca/Mg-free). The brain was immediately isolated and homogenized mechanically through a 100 μm cell strainer, followed by digestion with Liberase (Roche, 5401020001) for 1 h at 37°C. The cell suspension was passed through a 70 μm cell strainer and rinsed with Hank's balanced salt solution (Ca/Mg-free) containing 10% fetal bovine serum with or without DNase I (Roche, 10104159001). After density gradient centrifugation using 25% Percoll to remove myelin and cell debris, the cell pellet was resuspended in

Hank's balanced salt solution (Ca/Mg-free) containing 10% fetal bovine serum. A single-cell suspension was prepared for flow cytometry with a BD Accuri C6 Plus instrument. All antibodies and additional information for flow cytometric analysis are listed in Supplementary Table S1.

Micro-computed tomography

Micro-computed tomography (IRIS PET/CT imaging system, Inviscan, France) was applied to show the distribution of calcifications in the brains of the mice. Mice were deeply anesthetized with isoflurane for approximately 5 min before the experiment. They were then placed on the imaging stage under anesthesia with isoflurane gas during the entire imaging process. A total of 1,945 coronal plane images were obtained from each mouse. Approximately 70 images showed calcification in the hypothalamus and midbrain of the brains of 12-month-old *Slc20a2*-HO mice.

Brain microvessel isolation

Mice were anesthetized with an intraperitoneal injection of 20% Ulatan (70 µl/10 g body weight). The entire brain was isolated from the skull and washed in cold isotonic sucrose buffer (0.32 mol/l sucrose, 3 mmol/l HEPES in distilled water, pH = 7.40). Each brain sample was homogenized in 5 ml sucrose buffer using a Dounce homogenizer, followed by centrifugation at 4500 × *g* for 10 min at 4°C. After removing the supernatant, the precipitate was resuspended in sucrose buffer and centrifuged again. The final pellet was resuspended in 2 ml sucrose buffer and passed through a 40 µm nylon mesh. Brain microvessels were retained on the mesh and eluted with ice-cold 0.01 M PBS (pH = 7.40) for collection. Tissue was obtained by centrifugation, and RIPA (YEASEN, 20115ES60), cell lysis buffer (CST, 9803), or TRIzol™ Reagent (Invitrogen, 15596018) were added to extract protein or RNA.

Quantitative real-time polymerase chain reaction (qRT-PCR)

Total RNA was extracted from brain microvessels using TRIzol™ Reagent (Invitrogen, 15596018) and then reverse-transcribed into first-strand complementary DNA using the SuperScript™ IV RT-PCR System (Invitrogen, 12594025). qRT-PCR was performed utilizing LightCycler® 480 SYBR Green I Master Mix (Roche, 04887352001) on a Roche 480 instrument. All assays were performed in triplicate, and the levels of each gene were normalized to those of the housekeeping gene *Hprt*. All primer sequences and additional information for qRT-PCR are listed in Supplementary Table S2.

Western blotting

Total protein was extracted from brain microvessels and quantified using a BCA Protein Assay Kit (Solarbio, PC0020). After adjusting to the consistent concentration, proteins were separated by sodium dodecyl sulfate–polyacrylamide gel electrophoresis (Bio-Rad, 161-0183), followed by the transfer of proteins from the gels to polyvinylidene difluoride membranes. 5% non-fat milk was used to avoid non-specific protein binding for 1 h at 25°C, followed by overnight incubation with primary antibodies diluted in 5% non-fat milk or 5% BSA at 4°C. After incubation with secondary antibodies, an enhanced chemiluminescence substrate was added to the membranes to highlight the target bands. All the antibodies used and additional information for western blotting are listed in Supplementary Table S1.

Blood–brain barrier (BBB) permeability/leakage detection

Mice received an intraperitoneal injection of 2% Evans Blue (Sigma-Aldrich, E2129) in normal saline (4 ml/kg body weight) 2 h before sacrifice or a tail vein injection of 100 µl of 3 or 70 kDa tetramethylrhodamine-dextran (2 and 10 mg/ml, Invitrogen, D7162 and D1818, respectively) 1 h before sacrifice. Subsequently, the mice were transcardially perfused with 30 ml of PBS, followed by 60 ml of ice-cold 4% PFA. Brain tissue was post-fixed in 4% PFA for 4 h, dehydrated in 30% sucrose overnight at 4°C, and embedded in an optimal cutting temperature medium on dry ice. Brain sections were cut into 10- or 30-µm-thick sections for Evans Blue or tetramethylrhodamine-dextran staining and visualized using a Nikon C2 confocal microscope at 555- or 580-nm emission, respectively.

Immunoelectron microscopy

Mice were transcardially perfused with a mixture of 0.2% glutaraldehyde and 4% PFA in 0.1 M phosphate buffer under deep anesthesia. The brain's basal ganglia, thalamus, and hypothalamus regions were quickly removed and cut into 1-mm^3 pieces, placed into 0.2% glutaraldehyde in 0.1 M phosphate buffer, and fixed for 2 h at 25°C. After dehydration, embedding, and sectioning, the sections were incubated with 1% BSA blocking buffer for 30 min at 25°C and then incubated with rabbit anti-CD3 antibody (1:50; Abcam, ab5690) in 1% BSA overnight at 4°C. After washing, the sections were incubated with 10 nm gold-labeled goat anti-rabbit IgG (1:50; Sigma-Aldrich, G7402) and stained with 1% aqueous uranyl acetate for 20 min, followed by lead citrate for 30 s. The sections were photographed under a HITACHI HT7800 electron microscope.

FTY720 administration

Slc20a2-HO mice, aged 1.5 months, were given 0.5 mg/kg FTY720 (Selleck, S5002) diluted in dimethyl sulfoxide or dimethyl sulfoxide alone *via* intraperitoneal administration three times a week, once every 2 days. After 12 weeks, the mice were transcardially perfused with 30 ml of PBS, and half of the brain was extracted for RNA using TRIzol™ Reagent (Invitrogen, 15596018), while the other half was fixed in ice-cold 4% PFA for 16 h. After dehydration in 30% sucrose at 4°C overnight, the brains were collected for further experiments.

von Kossa staining

von Kossa staining was applied to detect phosphate ions (PO_4^{3-}). Following the staining protocol (Abcam, ab150687), the sections were dewaxed, rehydrated, and incubated with 5% silver nitrate for 45 min

under ultraviolet rays. After rinsing several times with fresh distilled water, the sections were incubated with 5% sodium thiosulfate solution for 10 min to wash the unreacted silver ions, followed by a nuclear fast red solution.

RNA sequencing bioinformatic analysis

Brain RNA samples from mice administered the placebo/DMSO ($n = 4$), and FTY720 ($n = 6$) were collected for RNA sequencing. RNA libraries for RNA-seq were prepared using NEBNext® Ultra™ RNA Library Prep Kit for Illumina® following manufacturer's protocol. Illumina Casava 1.8 software was applied for basecalling. Raw data of fastq format were firstly processed through in-house Perl scripts. Reference genome GRCm38/mm10 and gene model annotation files were downloaded and then built and paired-end clean reads were aligned to the reference genome using Hisat2 v2.0.5. Differentially expressed genes (DEGs) were defined as the criterion $p < 0.05$ and protein-coding function. A volcano plot was constructed to map all DEGs using the Ggplot2 package (version 3.0.3). Gene Ontology (GO) and Kyoto Encyclopedia of Genes and Genomes (KEGG) enrichment analyses were applied to identify the DEG function, with the cut-off criteria of $p < 0.01$ and 0.05. Results were presented using the clusterProfiler package (version 3.0.3).

Statistical analysis

All data are presented as individual mean ± SD or SEM. $CD45^+CD3^+$ cells in the brains of 1-, 3.5-, and 8-month-old mice were counted in ten equally spaced sections covering whole brain with at least three biological replicates. The composition and percentage of T-cells in the brain parenchyma of five groups of 12-month-old mice were analyzed. For the quantitative analysis of Evans Blue leakage, under the identical conditions of sample processing and capture parameters, the average fluorescence intensity was calculated on three whole brain slices of each mouse using ImageJ (version 1.53c). For the evaluation of BBB integrity related with astrocytes and pericytes, AQP4/PDGF-Rβ and CD31 double positive areas were determined using the ImageJ area measurement tool as the percentage of AQP4-or PDGF-Rβ-positive fluorescent areas covering CD31-positive areas with five equally spaced sections in the 1- and 3.5-month-old mice. For statistical analysis, three visual fields were randomly selected in the cortex, basal ganglia, and midbrain regions of each brain slice. Simultaneously, the fluorescence intensity of AQP4- and PDGF-Rβ-positive areas was statistically analyzed. Shapiro–Wilk test and Levene's test were used to examine the normality of the data and equality of variance, respectively. All data were compared using unpaired t-test except for the data of the expression of proteins from brain microvessels using paired t-test. Statistical significance was set at $p < 0.05$. *, **, ***, ****, and n.s. represent $p < 0.05$, $p < 0.01$, $p < 0.001$, $p < 0.0001$, and "not statistically significant," respectively.

Results

T-cell infiltration positively correlated with brain calcification and aging

To determine the presence of T-cell infiltration in the brain parenchyma of *Slc20a2*-HO mice at the pre-calcification stage, CD45 and CD3 markers were used to label T-cells by immunofluorescence. $CD45^+CD3^+$ T-cells emerged in the brain parenchyma of -HO and -WT mice at the age of 1 month (Figure 1A). To explore the relationship between CNS-infiltrating T-cells and calcification severity, T-cells were quantified in 3.5- and 8-month-old mice (Figures 1B,C), representing the pathological stages of slight and moderate calcification (Wallingford et al., 2017; Jensen et al., 2018; Ren et al., 2021). There was a significant increase in the number of $CD45^+CD3^+$ T-cells in -HO mice among the three age groups, with approximately a 2-, 3-, and 4-fold increase, compared to that in -WT mice, respectively (Figure 1C). More T-cells appeared in the brains of mice with severe brain calcification and older age, suggesting that T-cells infiltrated persistently with increasing calcification and age (Figure 1C; Supplementary Figure S1A). Notably, most infiltrating T-cells clustered around the calcified regions (Figure 1B; Supplementary Figure S1A).

Central nervous system (CNS)-infiltrating T-cells mainly consisted of $CD4^+$ and $CD4^-CD8^-$ T-cell subsets

Consistent with other neuroinflammatory diseases, both $CD4^+$ and $CD8^+$ cells, two classic subsets of $CD3^+$ T-cells, were present in the brain parenchyma of 1-month-old *Slc20a2*-HO mice (Figure 1D), and these were hardly observed in -WT mice of the same age. To further precisely determine the subpopulation and proportion of infiltrated T-cells associated with brain calcification, flow cytometric analysis was performed on the brains of 12-month-old mouse pairs, as well as 14- and 21-month-old -HO mice. Firstly, micro-computed tomography had demonstrated the presence of calcified plaques in the hypothalamus, basal ganglia, and midbrain of 12-month-old -HO mice (Supplementary Figure S1B), which was consistent with previous reports (Wallingford et al., 2017; Jensen et al., 2018; Ren et al., 2021). Flow cytometric analysis confirmed an increase in $CD45^{hi}$ and $CD3^+$ cells in the brains of 12-month-old -HO, compared with -WT mice (proportion of all single cells = $CD45^{hi}$: WT: 0.980%, HO: 2.020%, $p < 0.0001$; $CD3^+$ cells = WT: 0.672%, HO: 1.532%, $p < 0.0001$). In the $CD3^+$ T-cell subpopulation, $CD4^+$ and CD4–CD8 double-negative T (DNT) cells significantly increased in the brains of -HO mice (proportion of all single cells = $CD4^+$ cells: WT: 0.218%, HO: 0.434%, $p = 0.0086$; DNT cells = WT: 0.314%, HO: 0.770%, $p = 0.0003$). However, $CD8^+$ and CD4–CD8 double-positive T (DPT) subsets were not significantly different between the -HO and -WT groups (proportion of all single cells = $CD8^+$ cells: WT: 0.070%, HO: 0.240%, $p = 0.0541$; DPT cells = WT: 0.056%, HO: 0.094%, $p = 0.2438$; Figure 1E). Furthermore, $CD3^+CD4^+$ and DNT subpopulations were increased in the older mouse groups (14- and 21-month-old), and $CD45^{hi}$ cells were also noted to increase with age (Figure 1E; Supplementary Figure S1C).

T-cells most likely travel to the brain parenchyma *via* the paracellular pathway

To explore whether T-cells have the possibility of entry into the CNS through the paracellular pathway, we evaluated the expression of EC permeability-associated proteins including selectins, CAMs and cell junctions. In isolated brain microvessels of 3.5-month-old *Slc20a2*-HO mice, the expression levels of selectin (*E-selectin* and *P-selectin*) and CAMs (*Icam-1*, *Icam-2*, and *Vcam-1*) were significantly higher than those

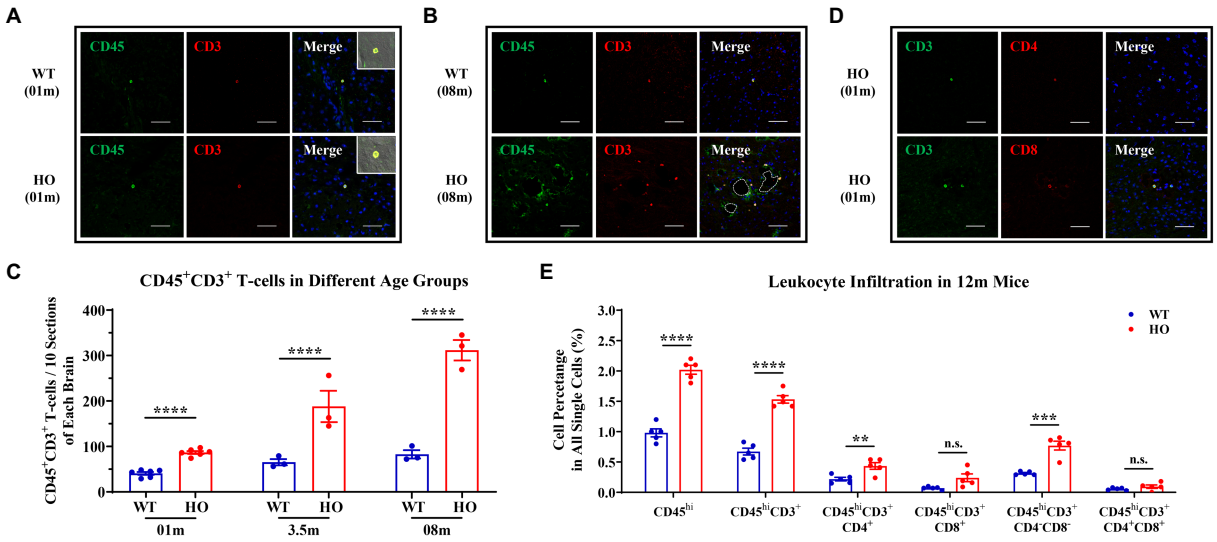

FIGURE 1
Increased CNS Infiltration of T-Cells and Their Subpopulations in *Slc20a2*-HO Mice. **(A)** CD45$^+$ CD3$^+$ T-cells in the brain parenchyma of 1-month-old *Slc20a2*-WT and -HO mice. **(B)** Accumulation of T-cells around the calcification in 8-month-old -HO mice. Dashed lines indicate the outline of the calcified spots. **(C)** Absolute number of T-cells in the brain of -WT and -HO mice at 1-, 3.5-, and 8-month-old (Data are shown as mean±SEM; 1month, n=6 pairs; 3.5months, n=3 pairs; 8months, n=3 pairs; 10 equally spaced sections covering entire brain with three biological replicates). **(D)** CD4$^+$ and CD8$^+$ T-cells in brain parenchyma of 1-month-old -HO mice. **(E)** Leukocyte immunophenotyping in 12-month-old -WT and -HO mice. Scale bar, 40μm. ****p<0.0001; ***p<0.001; **p<0.01; n.s., not statistically significant.

in -WT mice (Figure 2A), which is a prerequisite for T-cell infiltration. The endothelium of the brain vessels forms an integral and tightly sealed monolayer, which mainly depends on a series of tight junctions (TJs: occludin, claudin-5, and ZO-1) and adherents junction (AJ: VE-cadherin) expressed on the lateral and contact surfaces of each ECs. Further, they maintain the integrity of the paracellular pathways (Bazzoni and Dejana, 2004; Wallez and Huber, 2008; Tietz and Engelhardt, 2015). In our study, the expression of cell junctions decreased in the brain microvessels of 3.5-month-old -HO mice (Figure 2B); however, the distribution patterns of them, such as localization, morphology, and polarization, remained unchanged in 1-month-old -HO mice (Figure 2C). Exogenous tracers (Evans Blue, 3 kDa, and 70 kDa TMR-dextran) were utilized to directly evaluate BBB permeability in the pre-calcification stage of -HO mice. Under the consistent parameters of fluorescence intensity and exposure time, a slight but significantly increased permeability was observed in the cortex, basal ganglia, and midbrain of the 1.5-month-old pre-calcification -HO mice, compared to -WT (Figure 2D; Supplementary Figure S2). These findings indicate that the increased paracellular permeability made the entry of T-cells into the brain parenchyma more feasible, which was also the cause of neuroinflammation.

Transcytosis of brain endothelium increased in *Slc20a2*-HO mice

The expression of clathrin and phosphorylated and total Src was not altered, but that of phosphorylated and total Cav-1 was decreased in 3.5-month-old *Slc20a2*-HO mice. Mfsd2a, a key suppressor of caveolae formation and Cav-1 expression, showed slightly increased, coinciding with the decrease of Cav-1 (Figure 3A). The distribution of total Cav-1 remained unchanged in 1-month-old -HO mice (Figure 3B). Transmission electron microscopy (TEM) and immunoelectron microscopy were implemented to investigate whether T-cells traveled directly across BBB-ECs. The fusion of lymphocytes and EC membranes was observed by TEM in the brains of 6-month-old -HO mice; furthermore, immunoelectron microscopy with CD3 antibodies to label T-cells demonstrated that colloidal gold particles were present within brain ECs (Figure 3C), suggesting that CD3$^+$ T-cells or endogenous plasma proteins entered the brain parenchyma *via* the transmembrane pathway. Endogenous IgG and albumin (small molecules) could be physically transported across the intact BBB; they were substantially increased in the perivascular spaces of the neurovascular unit (NVU) of 1-month-old pre-calcification -HO mice; macromolecules, such as blood-borne fragments of fibronectin, were undetectable in the brain parenchyma of mice of the same age (Figure 3D).

Astrocyte and pericyte density and coverage of microvessels remained unchanged

Both astrocytes and pericytes play an essential role in the maintenance of BBB integrity (Zlokovic, 2008). Thus, the distribution pattern and coverage of astrocytes and pericytes in blood vessels were explored using AQP4, PDGF-Rβ, and CD31 antibodies to label astrocytes, pericytes, and vessels, respectively. There were no significant differences in the localization, morphology, polarization, and coverage of astrocytes or pericytes in *Slc20a2*-HO mice compared with -WT mice at the age of either 1 or 3.5 months (Supplementary Figure S3).

FTY720 Alleviated brain calcification probably By multiple mechanisms in *Slc20a2*-HO mice

To explore the relationship between T-cell infiltration and calcification, FTY720 was utilized to inhibit the circulation of peripheral

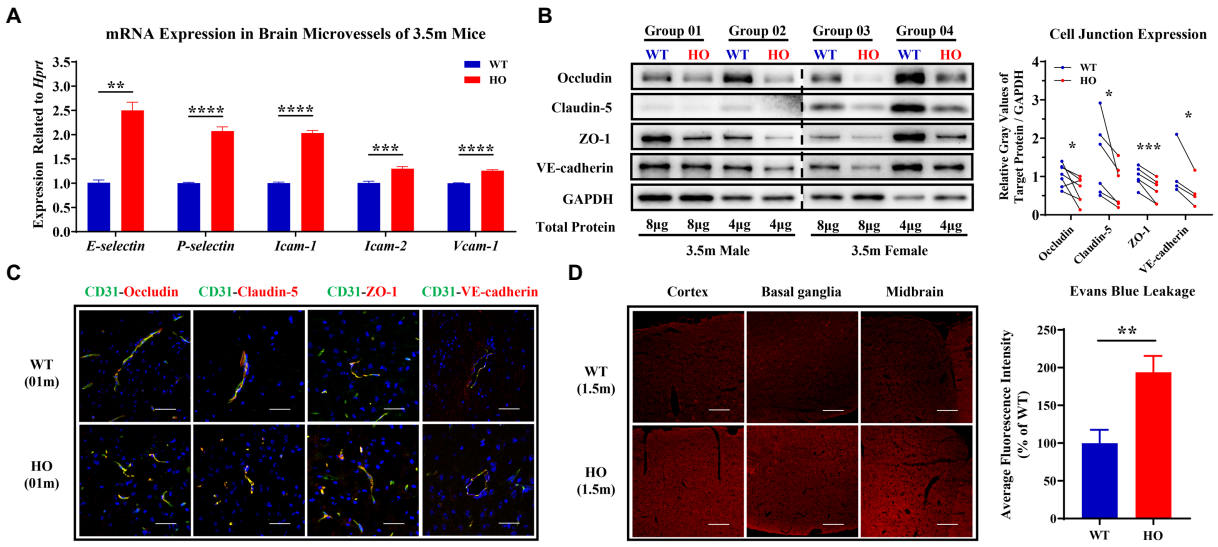

FIGURE 2
Expression and distribution pattern of core adhesion molecules and junction proteins and the blood–brain barrier (BBB) permeability of paracellular pathway. **(A)** The relatively increased expression of selectin and cell adhesion molecules (CAMs) in brain microvessels of 3.5-month-old *Slc20a2*-HO compared to that of -WT mice (n=3 pairs). **(B)** Decreased protein expression of TJs (occludin, claudin-5, and ZO-1) and AJ (VE-cadherin) in brain microvessels of 3.5-month-old -HO compared to that of -WT mice. **(C)** No difference in localization, morphology, and polarization of TJs and AJ proteins in 1-month-old -WT and -HO mice. Brain microvessels visualized by CD31. **(D)** Evans blue have slightly increased entry into the brain parenchyma of -HO compared to -WT mice at the age of 1.5months. Scale bars, 40μm **(C)**, 80μm **(D)**. ****p<0.0001; ***p<0.001; **p<0.01; *p<0.05.

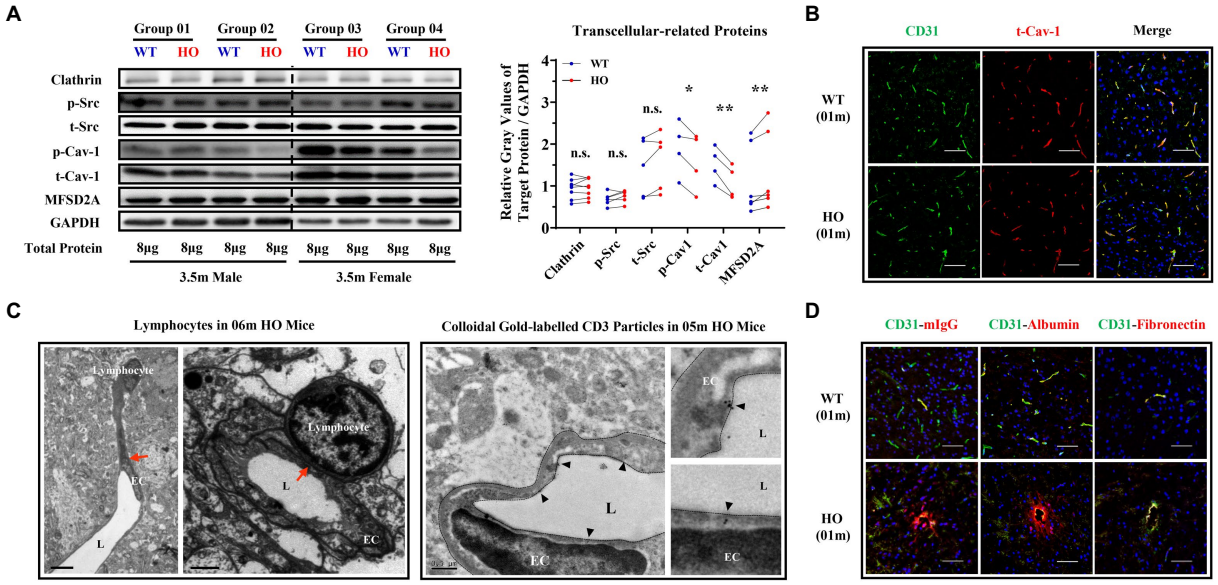

FIGURE 3
Transcellular Pathway Alterations in The brain endothelium of *Slc20a2*-HO mice. **(A)** Expression of endocytosis- and transcytosis-related proteins in brain microvessels of 3.5-month-old *Slc20a2*-WT and -HO mice. **p<0.01; *p<0.05; n.s., not statistically significant. **(B)** Distribution pattern (localization, morphology, and polarization) of total caveolin-1 in 1-month-old mice. **(C)** The fusion of endothelial and lymphocyte cell membranes (red arrows) in 6-month-old -HO mice **(C**, Left**)**. $CD3^+$ colloidal gold particles in the endothelial cell membrane of the midbrain in 5-month-old -HO mice. Black triangles indicate gold particles **(C**, Right**)**. EC, endothelial cell; L, vascular lumen. Scale bars, 6 and 1.5μm **(C**, left**)**; 0.5μm **(C**, right**)**. **(D)** Endogenous IgG and albumin, rather than fibronectin, leaked into the brains of 1-month-old -HO mice. Scale bar, 40μm **(B,D)**.

T-cells to reduce their CNS infiltration. The procedure for FTY720 administration is shown in Figure 4A. Three months after intraperitoneal administration, brain calcification was significantly reduced in FTY720-treated mice compared with that in the placebo group (FTY720: placebo = 6:4; p = 0.0181; Figure 4B). RNA sequencing helped determine the key molecular and biological mechanisms involved in FTY720's effects on the brain samples in the two groups. A total of 482 DEGs were identified using a filtering criterion of $p < 0.05$, among which 259 and 223 genes were upregulated and downregulated, respectively (Figure 4C; Supplementary Table S3, and GSE218335). GO and KEGG enrichment

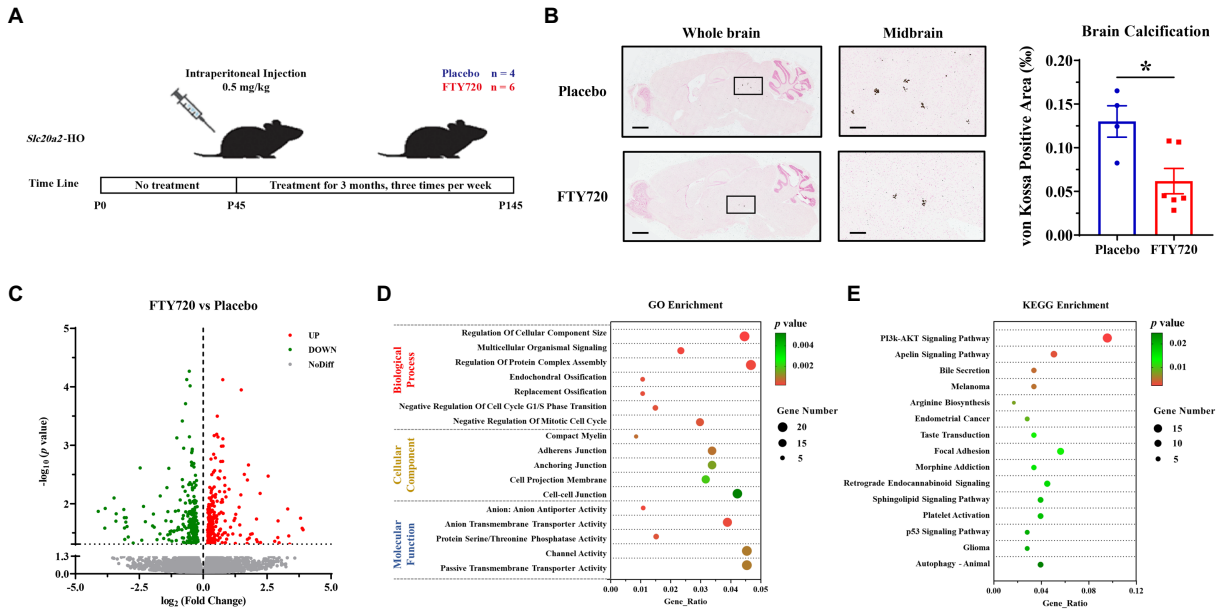

FIGURE 4
FTY720 alleviated brain calcification and mRNA profile analysis. **(A)** A schematic diagram of the FTY720 administration process. **(B)** Representative images of brain calcification between placebo- and FTY720-treated mice. Area of decreased brain calcification in FTY720-treated mice compared to the placebo group. Scale bars, 1,000μm, 150μm. *p<0.05. **(C)** A volcano plot for the DEGs revealed by RNA-seq, in which 259 and 223 genes were upregulated and downregulated, respectively, with p<0.05 as the cut-off criteria. **(D,E)** GO and KEGG enrichment analyses of the DEGs, with p<0.01 and 0.05 as the cut-off criteria, respectively.

analyses were performed to ascertain the functional changes in FTY720 treatment, and all terms were divided into the biological process (BP), cellular component (CC), and molecular function (MF) ontologies, as well as KEGG pathways. The DEGs highly enriched in GO_BP were mainly related to the "Ossification" (5 genes) and "Negative Regulation of Cell Cycle" (14 genes) terms; in the GO_CC subset, DEGs were enriched in the "Myelin" (4 genes) and various "Cell Junctions" (24 genes) terms; further, from the GO_MF perspective, the items related to transporter and channel activity (33 genes) constituted most of the enriched terms (Figure 4D; Supplementary Table S3). The "PI3K-AKT Signaling Pathway" was the top one enriched pathway in the KEGG analysis, with eight downregulated and nine upregulated genes. It is worth noting that seven genes in the autophagy pathway were also enriched in KEGG analysis (Figure 4E; Supplementary Table S3).

Discussion

Slc20a2-deficient mice exhibit the clinical symptoms of premature aging that progressively become more severe with age (Beck-Cormier et al., 2019; Ren et al., 2021). Human aging results in physiological brain calcification (Yamada et al., 2013) and a precipitous decline in the adult neural stem or progenitor cells with concomitant cognitive impairment (van Praag et al., 2005; Villeda et al., 2011), similar to the phenotypes of *Slc20a2*-HO mice (Ren et al., 2021). In aging brains, CNS-resident immune cells, such as microglia, increase, and peripheral blood-derived T-cells get recruited (Gemechu and Bentivoglio, 2012). CNS-infiltrating T-cells have been reported to play important roles in neurological diseases and are associated with neuroinflammation. $CD4^+$ T-cells can be classified into several functional subgroups based on their surface markers. The T helper (Th)1 and Th17 subgroups secrete high levels of interferon-gamma (IFN-γ) and interleukin-17-related cytokines, which contribute to chronic inflammation. In contrast, Th2 and T regulatory cells are more inclined to modulate the inflammatory responses of brain-resident immune cells (Gonzalez and Pacheco, 2014; Sonar and Lal, 2017; Solleiro-Villavicencio and Rivas-Arancibia, 2018). CNS-infiltrating DNTs were markedly increased in patients and mice with ischemic stroke and positively associated with brain injury (Meng et al., 2019; Kim et al., 2021). In *Pdgfb*$^{ret/ret}$ PFBC mice, the expression of CAMs was upregulated in the cerebral vessels, which was accompanied by more lymphocytes entering the brain parenchyma. Infiltration of peripheral leukocytes into the CNS induces susceptibility to autoimmune inflammation (Torok et al., 2021). Zarb demonstrated that in *Pdgfb*$^{ret/ret}$ mice, a novel microglial subset, calcification-associated microglia, accumulated around vascular calcified regions or in the perivascular space and effectively inhibited brain calcification (Zarb et al., 2021). Brain calcification induces the formation of neurotoxic astrocytes, although the exact functions of these cells remain unknown (Zarb et al., 2019).

The aging brain has a marked susceptibility to circulatory proteins (Conboy et al., 2005; Yang et al., 2020). Endogenous plasma proteins can pass through the BBB *via* a ligand-specific receptor-mediated pathway during adolescence, which changes into non-specific caveolin-mediated transcytosis in the aging brain (Yang et al., 2020). Similarly, increased endocytosis or transcytosis is regarded as an early event of BBB injury in migraine, brain injury, and ischemic stroke (Knowland et al., 2014; Sadeghian et al., 2018). In the brain parenchyma of *Slc20a2*-HO mice, endogenous IgG and albumin gets transported across an impaired BBB and is presented in the perivascular spaces of the NVU (Jensen et al., 2018), suggesting the enhancement of endocytosis or transcytosis. Cav-1 expression is necessary for the formation and transcytosis of caveolae as a structural protein; otherwise, it acts as a potent inhibitor of endothelial

nitric oxide synthase activity to negatively regulate paracellular permeability (Schubert et al., 2002). In an ischemic stroke mouse model, Cav-1 deficiency correlated with the increase in the degradation of TJs and the hydrolytic activity of matrix metalloproteinases, thereby enhancing BBB permeability (Choi et al., 2016).

Slc20a2 mainly expresses in the core components of the NVU, such as SMCs, ECs, pericytes, and the end-processes of astrocytes (Inden et al., 2016; Wallingford et al., 2017; Jensen et al., 2018; Vanlandewijck et al., 2018). Intracellular microcalcifications or tiny calcified granules were detected in the pericytes and astrocytes of *SLC20A2*-related patients (Miklossy et al., 2005) and mice (Jensen et al., 2018); however, neuronal and EC cell death only appeared in severely calcified areas (Kobayashi et al., 1987; Miklossy et al., 2005; Wszolek et al., 2006; Kimura et al., 2016). These findings suggest that, in the *Slc20a2*-HO mice, pericytes and astrocytes have functional defects due to intracellular calcification at an early stage, which then activates endocytosis or transcytosis of BBB-ECs (Alvarez et al., 2013; Keller et al., 2013; Villasenor et al., 2016; Jensen et al., 2018), accompanied by increased BBB permeability from the paracellular pathway.

Slc20a2 deficiency disturbed brain Pi homeostasis, forming a high-Pi microenvironment (Wallingford et al., 2017) and enhancing the sensitivity of arteriolar SMCs to induce calcification. Pi toxicity is also associated with cellular stress and neuroinflammation (Brown, 2020). *Pdgfb*$^{ret/ret}$ and *Slc20a2*-HO mice exhibited persistent retinitis (Lindblom et al., 2003; Park et al., 2017) and ocular degeneration (Ren et al., 2021), suggesting high-Pi-induced neuroinflammation. XPR1 is the only known Pi exporter in humans, its LOF mutations cause brain calcification, suggesting the essential roles of intracellular Pi homeostasis for maintaining brain health (Legati et al., 2015). *CMPK2* biallelic LOF mutations were linked to neuron mitochondrial defects and the elevated intracellular Pi levels; *Cmpk2*-KO, as well as KI mice bearing patient-derived variants developed brain calcification (Zhao et al., 2022). LOF mutations in cell junctions impair brain ECs, disrupt their integrity, enhance BBB permeability (Saitou et al., 2000; Nitta et al., 2003; Argaw et al., 2009), and cause brain calcification only in humans (Mochida et al., 2010; O'Driscoll et al., 2010; Cen et al., 2020; Schottlaender et al., 2020). *Jam2*-HO mice developed widespread prominent vacuolation instead of brain calcification in the midbrain, cerebral, and cerebellar cortexes (Schottlaender et al., 2020), suggesting that LOF mutations in cell junctions alone are insufficient to cause brain calcification in mice.

Furthermore, there were no apparent impairments in pericyte coverage and BBB integrity in humans (Paucar et al., 2017) and mice (Wallingford et al., 2017; Jensen et al., 2018; Nahar et al., 2020) with *SLC20A2*-related PFBC, which is partially consistent with our results. PDGF-B and its receptor PDGF-Rβ, two more culprits for PFBC (Keller et al., 2013; Nicolas et al., 2013), are mainly and separately expressed in brain ECs and pericytes, and they play an essential role in regulating the functions of BBB-ECs. Only *Pdgfb*$^{ret/ret}$ mice, in which the tissue distribution of PDGF-B is altered, probably due to the loss of a proteoglycan-binding motif, develop brain calcification (Keller et al., 2013; Vanlandewijck et al., 2015; Nikolakopoulou et al., 2017; Nahar et al., 2020). Inexplicably, the EC permeability was higher in the noncalcification-prone than in the calcification-prone brain areas; this region-specific heterogeneity in permeability was not associated with cell junction proteins or pericyte loss (Moura et al., 2017; Villasenor et al., 2017). *MYORG* encodes an endoplasmic reticulum-localized α-glucosidase that is specifically expressed in astrocytes, and its functional defects also cause brain calcification (Vanlandewijck et al., 2018; Yao et al., 2018; Meek et al., 2022). This evidence suggested that pericytes and astrocytes, or the differences in protein glycosylation in their supporting BBB-ECs, might affect the pathogenesis of brain calcification by regulating endocytosis or transcytosis functions (Keller et al., 2013; Villasenor et al., 2017).

FTY720 significantly alleviated autoinflammatory lesions in a *Pdgfb*$^{ret/ret}$ experimental autoimmune encephalomyelitis model and improved the survival rate of the mice (Terry et al., 2016; Torok et al., 2021). In our experiment, FTY720 partially inhibited brain calcification in *Slc20a2*-HO mice, suggesting that CNS-infiltrating T-cells could promote the pathogenesis of brain calcification. Inhibition of the PI3K-AKT pathway can activate autophagy, relieving vascular calcification phenotype *in vitro* and *in vivo*. In CD73-deficient fibroblasts, the increased activation of AKT blocked autophagy and resulted in arterial calcification (Moorhead 3rd et al., 2020). Dexamethasone accelerated the extracellular matrix calcification through activation of AKT signaling and the inhibition of autophagy in osteoarthritis mouse model (Chen et al., 2021). In the db/db mice, 9-PAHSA (a novel endogenous fatty acid) treatment down-regulated Akt–mTOR and activates autophagy in diabetic myocardium, ameliorating carotid vascular calcification (Wang et al., 2021). FTY720 was also reported to play a critical regulatory role in the bone remodeling, particularly in the regulation of osteoclasts, which were closely related to vascular calcification (Ishii et al., 2009; Xiao et al., 2018).

We demonstrated that T-cells infiltrated the CNS of *Slc20a2*-HO mice and that this infiltration rate increased with age. T-cells are likely to enter the brain parenchyma through paracellular leakage. The high restriction of BBB-ECs is a significant barrier to medications intended to cross the BBB. Targeted delivery strategies that induce endocytosis or transcytosis-mediated transport have been extensively studied. Therefore, understanding the immune mechanisms of *Slc20a2*-PFBC can increase our knowledge of disease pathogenesis and guide targeted treatment.

Data availability statement

The datasets presented in this study can be found in online repositories. The names of the repository/repositories and accession number(s) can be found at: https://www.ncbi.nlm.nih.gov/geo/, GSE218335

Ethics statement

The animal study was reviewed and approved by the Ethics Committee of The Fourth Affiliated Hospital of Harbin Medical University.

Author contributions

LS conceived and designed this study. YZ, YR, and YuZ collaboratively conducted all experiments and statistical analyses. YL, CX, ZP, and ZZ provided professional medical guidance, meanwhile, YJ and SQ provided valuable suggestion for interpreting pathophysiological and molecular results. YZ, YR, and LS prepared the original manuscript. YR, YZ, YuZ, and LS checked and revised the grammar, syntax, and

logical errors. All authors contributed to the article and approved the submitted version.

Funding

This study was funded by the National Key R&D Program of China (2020YFA0804000) and the Tou-Yan Innovation Team Program of Heilongjiang Province (2019-15).

Conflict of interest

The authors declare that the research was conducted in the absence of any commercial or financial relationships that could be construed as potential conflicts of interest.

Publisher's note

Supplementary material

The Supplementary material for this article can be found online at: https://www.frontiersin.org/articles/10.3389/fnmol.2023.1073723/full#supplementary-material

References

Abbott, N. J., Patabendige, A. A., Dolman, D. E., Yusof, S. R., and Begley, D. J. (2010). Structure and function of the blood-brain barrier. *Neurobiol. Dis.* 37, 13–25. doi: 10.1016/j.nbd.2009.07.030

Alvarez, J. I., Katayama, T., and Prat, A. (2013). Glial influence on the blood brain barrier. *Glia* 61, 1939–1958. doi: 10.1002/glia.22575

Andreone, B. J., Chow, B. W., Tata, A., Lacoste, B., Ben-Zvi, A., Bullock, K., et al. (2017). Blood-brain barrier permeability is regulated by lipid transport-dependent suppression of Caveolae-mediated transcytosis. *Neuron* 94, 581–594.e5. doi: 10.1016/j.neuron.2017.03.043

Argaw, A. T., Gurfein, B. T., Zhang, Y., Zameer, A., and John, G. R. (2009). VEGF-mediated disruption of endothelial CLN-5 promotes blood-brain barrier breakdown. *Proc. Natl. Acad. Sci. U. S. A.* 106, 1977–1982. doi: 10.1073/pnas.0808698106

Ayloo, S., and Gu, C. (2019). Transcytosis at the blood-brain barrier. *Curr. Opin. Neurobiol.* 57, 32–38. doi: 10.1016/j.conb.2018.12.014

Bazzoni, G., and Dejana, E. (2004). Endothelial cell-to-cell junctions: molecular organization and role in vascular homeostasis. *Physiol. Rev.* 84, 869–901. doi: 10.1152/physrev.00035.2003

Beck-Cormier, S., Lelliott, C. J., Logan, J. G., Lafont, D. T., Merametdjian, L., Leitch, V. D., et al. (2019). Slc20a2, encoding the phosphate transporter PiT2, is an important genetic determinant of bone quality and strength. *J. Bone Miner. Res.* 34, 1101–1114. doi: 10.1002/jbmr.3691

Brown, R. B. (2020). Stress, inflammation, depression, and dementia associated with phosphate toxicity. *Mol. Biol. Rep.* 47, 9921–9929. doi: 10.1007/s11033-020-06005-1

Cen, Z., Chen, Y., Chen, S., Wang, H., Yang, D., Zhang, H., et al. (2020). Biallelic loss-of-function mutations in JAM2 cause primary familial brain calcification. *Brain* 143, 491–502. doi: 10.1093/brain/awz392

Chen, L., Ni, Z., Huang, J., Zhang, R., Zhang, J., Zhang, B., et al. (2021). Long term usage of dexamethasone accelerating accelerates the initiation of osteoarthritis via enhancing chondrocyte apoptosis and the extracellular matrix calcification and apoptosis of chondrocytes. *Int. J. Biol. Sci.* 17, 4140–4153. doi: 10.7150/ijbs.64152

Choi, K. H., Kim, H. S., Park, M. S., Kim, J. T., Kim, J. H., Cho, K. A., et al. (2016). Regulation of Caveolin-1 expression determines early brain edema after experimental focal cerebral ischemia. *Stroke* 47, 1336–1343. doi: 10.1161/STROKEAHA.116.013205

Chun, J., Kihara, Y., Jonnalagadda, D., and Blaho, V. A. (2019). Fingolimod: lessons learned and new opportunities for treating multiple sclerosis and other disorders. *Annu. Rev. Pharmacol. Toxicol.* 59, 149–170. doi: 10.1146/annurev-pharmtox-010818-021358

Cohen, J. A., and Chun, J. (2011). Mechanisms of fingolimod's efficacy and adverse effects in multiple sclerosis. *Ann. Neurol.* 69, 759–777. doi: 10.1002/ana.22426

Conboy, I. M., Conboy, M. J., Wagers, A. J., Girma, E. R., Weissman, I. L., and Rando, T. A. (2005). Rejuvenation of aged progenitor cells by exposure to a young systemic environment. *Nature* 433, 760–764. doi: 10.1038/nature03260

Ellwardt, E., Walsh, J. T., Kipnis, J., and Zipp, F. (2016). Understanding the role of T cells in CNS homeostasis. *Trends Immunol.* 37, 154–165. doi: 10.1016/j.it.2015.12.008

Engelhardt, B., and Ransohoff, R. M. (2012). Capture, crawl, cross: the T cell code to breach the blood-brain barriers. *Trends Immunol.* 33, 579–589. doi: 10.1016/j.it.2012.07.004

Gemechu, J. M., and Bentivoglio, M. (2012). T cell recruitment in the brain during Normal aging. *Front. Cell. Neurosci.* 6:38. doi: 10.3389/fncel.2012.00038

Gonzalez, H., and Pacheco, R. (2014). T-cell-mediated regulation of neuroinflammation involved in neurodegenerative diseases. *J. Neuroinflammation* 11:201. doi: 10.1186/s12974-014-0201-8

Grangeon, L., Wallon, D., Charbonnier, C., Quenez, O., Richard, A. C., Rousseau, S., et al. (2019). Biallelic MYORG mutation carriers exhibit primary brain calcification with a distinct phenotype. *Brain* 142, 1573–1586. doi: 10.1093/brain/awz095

Hong, S. H., Park, S. J., Lee, S., Kim, S., and Cho, M. H. (2015). Biological effects of inorganic phosphate: potential signal of toxicity. *J. Toxicol. Sci.* 40, 55–69. doi: 10.2131/jts.40.55

Hozumi, I., Kurita, H., Ozawa, K., Furuta, N., Inden, M., Sekine, S. I., et al. (2018). Inorganic phosphorus (pi) in CSF is a biomarker for SLC20A2-associated idiopathic basal ganglia calcification (IBGC1). *J. Neurol. Sci.* 388, 150–154. doi: 10.1016/j.jns.2018.03.014

Inden, M., Iriyama, M., Zennami, M., Sekine, S. I., Hara, A., Yamada, M., et al. (2016). The type III transporters (PiT-1 and PiT-2) are the major sodium-dependent phosphate transporters in the mice and human brains. *Brain Res.* 1637, 128–136. doi: 10.1016/j.brainres.2016.02.032

Ishii, M., Egen, J. G., Klauschen, F., Meier-Schellersheim, M., Saeki, Y., Vacher, J., et al. (2009). Sphingosine-1-phosphate mobilizes osteoclast precursors and regulates bone homeostasis. *Nature* 458, 524–528. doi: 10.1038/nature07713

Jensen, N., Autzen, J. K., and Pedersen, L. (2016). Slc20a2 is critical for maintaining a physiologic inorganic phosphate level in cerebrospinal fluid. *Neurogenetics* 17, 125–130. doi: 10.1007/s10048-015-0469-6

Jensen, N., Schroder, H. D., Hejbol, E. K., Thomsen, J. S., Bruel, A., Larsen, F. T., et al. (2018). Mice knocked out for the primary brain calcification-associated gene Slc20a2 show unimpaired prenatal survival but retarded growth and nodules in the brain that grow and calcify over time. *Am. J. Pathol.* 188, 1865–1881. doi: 10.1016/j.ajpath.2018.04.010

Keller, A., Westenberger, A., Sobrido, M. J., Garcia-Murias, M., Domingo, A., Sears, R. L., et al. (2013). Mutations in the gene encoding PDGF-B cause brain calcifications in humans and mice. *Nat. Genet.* 45, 1077–1082. doi: 10.1038/ng.2723

Kim, M., Kim, S. D., Kim, K. I., Jeon, E. H., Kim, M. G., Lim, Y. R., et al. (2021). Dynamics of T lymphocyte between the periphery and the brain from the acute to the chronic phase following ischemic stroke in mice. *Exp. Neurobiol.* 30, 155–169. doi: 10.5607/en20062

Kim, M. P., Park, S. I., Kopetz, S., and Gallick, G. E. (2009). Src family kinases as mediators of endothelial permeability: effects on inflammation and metastasis. *Cell Tissue Res.* 335, 249–259. doi: 10.1007/s00441-008-0682-9

Kimura, T., Miura, T., Aoki, K., Saito, S., Hondo, H., Konno, T., et al. (2016). Familial idiopathic basal ganglia calcification: histopathologic features of an autopsied patient with an SLC20A2 mutation. *Neuropathology* 36, 365–371. doi: 10.1111/neup.12280

Knowland, D., Arac, A., Sekiguchi, K. J., Hsu, M., Lutz, S. E., Perrino, J., et al. (2014). Stepwise recruitment of transcellular and paracellular pathways underlies blood-brain barrier breakdown in stroke. *Neuron* 82, 603–617. doi: 10.1016/j.neuron.2014.03.003

Kobayashi, S., Yamadori, I., Miki, H., and Ohmori, M. (1987). Idiopathic nonarteriosclerotic cerebral calcification (Fahr's disease): an electron microscopic study. *Acta Neuropathol.* 73, 62–66. doi: 10.1007/BF00695503

Legati, A., Giovannini, D., Nicolas, G., Lopez-Sanchez, U., Quintans, B., Oliveira, J. R., et al. (2015). Mutations in XPR1 cause primary familial brain calcification associated with altered phosphate export. *Nat. Genet.* 47, 579–581. doi: 10.1038/ng.3289

Liebner, S., Dijkhuizen, R. M., Reiss, Y., Plate, K. H., Agalliu, D., and Constantin, G. (2018). Functional morphology of the blood-brain barrier in health and disease. *Acta Neuropathol.* 135, 311–336. doi: 10.1007/s00401-018-1815-1

Lindblom, P., Gerhardt, H., Liebner, S., Abramsson, A., Enge, M., Hellstrom, M., et al. (2003). Endothelial PDGF-B retention is required for proper investment of pericytes in the microvessel wall. *Genes Dev.* 17, 1835–1840. doi: 10.1101/gad.266803

Mandala, S., Hajdu, R., Bergstrom, J., Quackenbush, E., Xie, J., Milligan, J., et al. (2002). Alteration of lymphocyte trafficking by sphingosine-1-phosphate receptor agonists. *Science* 296, 346–349. doi: 10.1126/science.1070238

Meek, R. W., Brockerman, J., Fordwour, O. B., Zandberg, W. F., Davies, G. J., and Vocadlo, D. J. (2022). The primary familial brain calcification-associated protein MYORG is an alpha-galactosidase with restricted substrate specificity. *PLoS Biol.* 20:e3001764. doi: 10.1371/journal.pbio.3001764

Meng, H., Zhao, H., Cao, X., Hao, J., Zhang, H., Liu, Y., et al. (2019). Double-negative T cells remarkably promote neuroinflammation after ischemic stroke. *Proc. Natl. Acad. Sci. U. S. A.* 116, 5558–5563. doi: 10.1073/pnas.1814394116

Miklossy, J., Mackenzie, I. R., Dorovini-Zis, K., Calne, D. B., Wszolek, Z. K., Klegeris, A., et al. (2005). Severe vascular disturbance in a case of familial brain calcinosis. *Acta Neuropathol.* 109, 643–653. doi: 10.1007/s00401-005-1007-7

Mochida, G. H., Ganesh, V. S., Felie, J. M., Gleason, D., Hill, R. S., Clapham, K. R., et al. (2010). A homozygous mutation in the tight-junction protein JAM3 causes hemorrhagic destruction of the brain, subependymal calcification, and congenital cataracts. *Am. J. Hum. Genet.* 87, 882–889. doi: 10.1016/j.ajhg.2010.10.026

Moorhead, W. J. 3rd, Chu, C. C., Cuevas, R. A., Callahan, J. T., Wong, R., Regan, C., et al. (2020). Dysregulation of FOXO1 (Forkhead box O1 protein) drives calcification in arterial calcification due to deficiency of CD73 and is present in peripheral artery disease. *Arterioscler. Thromb. Vasc. Biol.* 40, 1680–1694. doi: 10.1161/ATVBAHA.119.313765

Moura, D. A. P., Lemos, R. R., and Oliveira, J. R. M. (2017). New data from Pdfgb (ret/ret) mutant mice might Lead to a paradoxical association between brain calcification, Pericytes recruitment and BBB integrity. *J. Mol. Neurosci.* 63, 419–421. doi: 10.1007/s12031-017-0992-z

Nahar, K., Lebouvier, T., Andaloussi Mae, M., Konzer, A., Bergquist, J., Zarb, Y., et al. (2020). Astrocyte-microglial association and matrix composition are common events in the natural history of primary familial brain calcification. *Brain Pathol.* 30, 446–464. doi: 10.1111/bpa.12787

Nicolas, G., Pottier, C., Maltete, D., Coutant, S., Rovelet-Lecrux, A., Legallic, S., et al. (2013). Mutation of the PDGFRB gene as a cause of idiopathic basal ganglia calcification. *Neurology* 80, 181–187. doi: 10.1212/WNL.0b013e31827ccf34

Nikolakopoulou, A. M., Zhao, Z., Montagne, A., and Zlokovic, B. V. (2017). Regional early and progressive loss of brain pericytes but not vascular smooth muscle cells in adult mice with disrupted platelet-derived growth factor receptor-beta signaling. *PLoS One* 12:e0176225. doi: 10.1371/journal.pone.0176225

Nitta, T., Hata, M., Gotoh, S., Seo, Y., Sasaki, H., Hashimoto, N., et al. (2003). Size-selective loosening of the blood-brain barrier in claudin-5-deficient mice. *J. Cell Biol.* 161, 653–660. doi: 10.1083/jcb.200302070

O'Driscoll, M. C., Daly, S. B., Urquhart, J. E., Black, G. C., Pilz, D. T., Brockmann, K., et al. (2010). Recessive mutations in the gene encoding the tight junction protein occludin cause band-like calcification with simplified gyration and polymicrogyria. *Am. J. Hum. Genet.* 87, 354–364. doi: 10.1016/j.ajhg.2010.07.012

Park, D. Y., Lee, J., Kim, J., Kim, K., Hong, S., Han, S., et al. (2017). Plastic roles of pericytes in the blood-retinal barrier. *Nat. Commun.* 8:15296. doi: 10.1038/ncomms15296

Parton, R. G., Joggerst, B., and Simons, K. (1994). Regulated internalization of caveolae. *J. Cell Biol.* 127, 1199–1215. doi: 10.1083/jcb.127.5.1199

Paucar, M., Almqvist, H., Jelic, V., Hagman, G., Jorneskog, G., Holmin, S., et al. (2017). A SLC20A2 gene mutation carrier displaying ataxia and increased levels of cerebrospinal fluid phosphate. *J. Neurol. Sci.* 375, 245–247. doi: 10.1016/j.jns.2017.02.007

Pulgar, V. M. (2018). Transcytosis to cross the blood brain barrier. New advancements and challenges. *Front. Neurosci.* 12:1019. doi: 10.3389/fnins.2018.01019

Razzaque, M. S. (2011). Phosphate toxicity: new insights into an old problem. *Clin. Sci. (Lond.)* 120, 91–97. doi: 10.1042/CS20100377

Ren, Y., Shen, Y., Si, N., Fan, S., Zhang, Y., Xu, W., et al. (2021). Slc20a2-deficient mice exhibit multisystem abnormalities and impaired spatial learning memory and sensorimotor gating but Normal motor coordination abilities. *Front. Genet.* 12:639935. doi: 10.3389/fgene.2021.639935

Sadeghian, H., Lacoste, B., Qin, T., Toussay, X., Rosa, R., Oka, F., et al. (2018). Spreading depolarizations trigger caveolin-1-dependent endothelial transcytosis. *Ann. Neurol.* 84, 409–423. doi: 10.1002/ana.25298

Saitou, M., Furuse, M., Sasaki, H., Schulzke, J. D., Fromm, M., Takano, H., et al. (2000). Complex phenotype of mice lacking occludin, a component of tight junction strands. *Mol. Biol. Cell* 11, 4131–4142. doi: 10.1091/mbc.11.12.4131

Schottlaender, L. V., Abeti, R., Jaunmuktane, Z., Macmillan, C., Chelban, V., O'Callaghan, B., et al. (2020). Bi-allelic JAM2 variants Lead to early-onset recessive primary familial brain calcification. *Am. J. Hum. Genet.* 106, 412–421. doi: 10.1016/j.ajhg.2020.02.007

Schubert, W., Frank, P. G., Woodman, S. E., Hyogo, H., Cohen, D. E., Chow, C. W., et al. (2002). Microvascular hyperpermeability in caveolin-1 (−/−) knock-out mice. Treatment with a specific nitric-oxide synthase inhibitor, L-NAME, restores normal microvascular permeability in Cav-1 null mice. *J. Biol. Chem.* 277, 40091–40098. doi: 10.1074/jbc.M205948200

Skarnes, W. C., Rosen, B., West, A. P., Koutsourakis, M., Bushell, W., Iyer, V., et al. (2011). A conditional knockout resource for the genome-wide study of mouse gene function. *Nature* 474, 337–342. doi: 10.1038/nature10163

Solleiro-Villavicencio, H., and Rivas-Arancibia, S. (2018). Effect of chronic oxidative stress on Neuroinflammatory response mediated by CD4(+)T cells in neurodegenerative diseases. *Front. Cell. Neurosci.* 12:114. doi: 10.3389/fncel.2018.00114

Sonar, S. A., and Lal, G. (2017). Differentiation and transmigration of CD4 T cells in Neuroinflammation and autoimmunity. *Front. Immunol.* 8:1695. doi: 10.3389/fimmu.2017.01695

Tadic, V., Westenberger, A., Domingo, A., Alvarez-Fischer, D., Klein, C., and Kasten, M. (2015). Primary familial brain calcification with known gene mutations: a systematic review and challenges of phenotypic characterization. *JAMA Neurol.* 72, 460–467. doi: 10.1001/jamaneurol.2014.3889

Terry, R. L., Ifergan, I., and Miller, S. D. (2016). Experimental autoimmune encephalomyelitis in mice. *Methods Mol. Biol.* 1304, 145–160. doi: 10.1007/7651_2014_88

Tietz, S., and Engelhardt, B. (2015). Brain barriers: crosstalk between complex tight junctions and adherens junctions. *J. Cell Biol.* 209, 493–506. doi: 10.1083/jcb.201412147

Torok, O., Schreiner, B., Schaffenrath, J., Tsai, H. C., Maheshwari, U., Stifter, S. A., et al. (2021). Pericytes regulate vascular immune homeostasis in the CNS. *Proc. Natl. Acad. Sci. U. S. A.* 118. doi: 10.1073/pnas.2016587118

van Praag, H., Shubert, T., Zhao, C., and Gage, F. H. (2005). Exercise enhances learning and hippocampal neurogenesis in aged mice. *J. Neurosci.* 25, 8680–8685. doi: 10.1523/JNEUROSCI.1731-05.2005

Vanlandewijck, M., He, L., Mae, M. A., Andrae, J., Ando, K., Del Gaudio, F., et al. (2018). A molecular atlas of cell types and zonation in the brain vasculature. *Nature* 554, 475–480. doi: 10.1038/nature25739

Vanlandewijck, M., Lebouvier, T., Andaloussi Mae, M., Nahar, K., Hornemann, S., Kenkel, D., et al. (2015). Functional characterization of germline mutations in PDGFB and PDGFRB in primary familial brain calcification. *PLoS One* 10:e0143407. doi: 10.1371/journal.pone.0143407

Villasenor, R., Kuennecke, B., Ozmen, L., Ammann, M., Kugler, C., Gruninger, F., et al. (2017). Region-specific permeability of the blood-brain barrier upon pericyte loss. *J. Cereb. Blood Flow Metab.* 37, 3683–3694. doi: 10.1177/0271678X17697340

Villasenor, R., Ozmen, L., Messaddeq, N., Gruninger, F., Loetscher, H., Keller, A., et al. (2016). Trafficking of endogenous immunoglobulins by endothelial cells at the blood-brain barrier. *Sci. Rep.* 6:25658. doi: 10.1038/srep25658

Villeda, S. A., Luo, J., Mosher, K. I., Zou, B., Britschgi, M., Bieri, G., et al. (2011). The ageing systemic milieu negatively regulates neurogenesis and cognitive function. *Nature* 477, 90–94. doi: 10.1038/nature10357

Wallez, Y., and Huber, P. (2008). Endothelial adherens and tight junctions in vascular homeostasis, inflammation and angiogenesis. *Biochim. Biophys. Acta* 1778, 794–809. doi: 10.1016/j.bbamem.2007.09.003

Wallingford, M. C., Chia, J. J., Leaf, E. M., Borgeia, S., Chavkin, N. W., Sawangmake, C., et al. (2017). SLC20A2 deficiency in mice leads to elevated phosphate levels in cerbrospinal fluid and glymphatic pathway-associated arteriolar calcification, and recapitulates human idiopathic basal ganglia calcification. *Brain Pathol.* 27, 64–76. doi: 10.1111/bpa.12362

Wang, C., Li, Y., Shi, L., Ren, J., Patti, M., Wang, T., et al. (2012). Mutations in SLC20A2 link familial idiopathic basal ganglia calcification with phosphate homeostasis. *Nat. Genet.* 44, 254–256. doi: 10.1038/ng.1077

Wang, Y. M., Mi, S. L., Jin, H., Guo, Q. L., Yu, Z. Y., Wang, J. T., et al. (2021). 9-PAHSA improves cardiovascular complications by promoting autophagic flux and reducing myocardial hypertrophy in Db/Db mice. *Front. Pharmacol.* 12:754387. doi: 10.3389/fphar.2021.754387

Wilson, E. H., Weninger, W., and Hunter, C. A. (2010). Trafficking of immune cells in the central nervous system. *J. Clin. Invest.* 120, 1368–1379. doi: 10.1172/JCI41911

Wszolek, Z. K., Baba, Y., Mackenzie, I. R., Uitti, R. J., Strongosky, A. J., Broderick, D. F., et al. (2006). Autosomal dominant dystonia-plus with cerebral calcifications. *Neurology* 67, 620–625. doi: 10.1212/01.wnl.0000230141.40784.09

Xiao, L., Zhou, Y., Zhu, L., Yang, S., Huang, R., Shi, W., et al. (2018). SPHK1-S1PR1-RANKL Axis regulates the interactions between macrophages and BMSCs in inflammatory bone loss. *J. Bone Miner. Res.* 33, 1090–1104. doi: 10.1002/jbmr.3396

Xu, X., Sun, H., Luo, J., Cheng, X., Lv, W., Luo, W., et al. (2022). The pathology of primary familial brain calcification: implications for treatment. *Neurosci. Bull.* doi: 10.1007/s12264-022-00980-0

Yamada, M., Asano, T., Okamoto, K., Hayashi, Y., Kanematsu, M., Hoshi, H., et al. (2013). High frequency of calcification in basal ganglia on brain computed tomography images in Japanese older adults. *Geriatr. Gerontol. Int.* 13, 706–710. doi: 10.1111/ggi.12004

Yang, A. C., Stevens, M. Y., Chen, M. B., Lee, D. P., Stahli, D., Gate, D., et al. (2020). Physiological blood-brain transport is impaired with age by a shift in transcytosis. *Nature* 583, 425–430. doi: 10.1038/s41586-020-2453-z

Yao, X. P., Cheng, X., Wang, C., Zhao, M., Guo, X. X., Su, H. Z., et al. (2018). Biallelic mutations in MYORG cause autosomal recessive primary familial brain calcification. *Neuron* 98, 1116–1123 e5. doi: 10.1016/j.neuron.2018.05.037

Zarb, Y., Sridhar, S., Nassiri, S., Utz, S. G., Schaffenrath, J., Maheshwari, U., et al. (2021). Microglia control small vessel calcification via TREM2. *Sci. Adv.* 7. doi: 10.1126/sciadv.abc4898

Zarb, Y., Weber-Stadlbauer, U., Kirschenbaum, D., Kindler, D. R., Richetto, J., Keller, D., et al. (2019). Ossified blood vessels in primary familial brain calcification elicit a neurotoxic astrocyte response. *Brain* 142, 885–902. doi: 10.1093/brain/awz032

Zhao, M., Su, H. Z., Zeng, Y. H., Sun, Y., Guo, X. X., Li, Y. L., et al. (2022). Loss of function of CMPK2 causes mitochondria deficiency and brain calcification. *Cell Discov.* 8:128. doi: 10.1038/s41421-022-00475-2

Zlokovic, B. V. (2008). The blood-brain barrier in health and chronic neurodegenerative disorders. *Neuron* 57, 178–201. doi: 10.1016/j.neuron.2008.01.003

frontiers | Frontiers in Molecular Neuroscience

TYPE Review
PUBLISHED 23 March 2023
DOI 10.3389/fnmol.2023.1113081

OPEN ACCESS

EDITED BY
Sara Anna Bonini,
University of Brescia,
Italy

REVIEWED BY
Franca Codazzi,
San Raffaele Hospital (IRCCS),
Italy
Eun Hee Ahn,
Hallym University,
Republic of Korea

*CORRESPONDENCE
Yuhong Huang
✉ hyh101@126.com

SPECIALTY SECTION
This article was submitted to
Brain Disease Mechanisms,
a section of the journal
Frontiers in Molecular Neuroscience

RECEIVED 01 December 2022
ACCEPTED 06 March 2023
PUBLISHED 23 March 2023

CITATION
Fan G, Liu M, Liu J and Huang Y (2023) The initiator of neuroexcitotoxicity and ferroptosis in ischemic stroke: Glutamate accumulation. *Front. Mol. Neurosci.* 16:1113081. doi: 10.3389/fnmol.2023.1113081

The initiator of neuroexcitotoxicity and ferroptosis in ischemic stroke: Glutamate accumulation

Genhao Fan[1], Menglin Liu[1], Jia Liu[2] and Yuhong Huang[2]*

[1]Graduate School, Tianjin University of Chinese Medicine, Tianjin, China, [2]Department of Clinical Pharmacology, The Second Affiliated Hospital of Tianjin University of Chinese Medicine, Tianjin, China

Glutamate plays an important role in excitotoxicity and ferroptosis. Excitotoxicity occurs through over-stimulation of glutamate receptors, specifically NMDAR, while in the non-receptor-mediated pathway, high glutamate concentrations reduce cystine uptake by inhibiting the System Xc-, leading to intracellular glutathione depletion and resulting in ROS accumulation, which contributes to increased lipid peroxidation, mitochondrial damage, and ultimately ferroptosis. Oxidative stress appears to crosstalk between excitotoxicity and ferroptosis, and it is essential to maintain glutamate homeostasis and inhibit oxidative stress responses *in vivo*. As researchers work to develop natural compounds to further investigate the complex mechanisms and regulatory functions of ferroptosis and excitotoxicity, new avenues will be available for the effective treatment of ischaemic stroke. Therefore, this paper provides a review of the molecular mechanisms and treatment of glutamate-mediated excitotoxicity and ferroptosis.

KEYWORDS

neuroexcitotoxicity, ferroptosis, glutamate, cystine-glutamate antiporter, ischemic stroke

1. Introduction

Ischemic stroke is the primary cause of death and disability in Chinese adults, characterized by high morbidity, disability, mortality, and recurrence rate (Sturm et al., 2002; Gao J. et al., 2022). According to statistics, the age-standardized prevalence of stroke in China in 2013 was 1114.8 per 100,000, with an incidence rate of 246.8 per 100,000 and a mortality rate of 114.8 per 100,000 (Wang W. et al., 2017), The Continuous Stroke Surveillance Program in 31 Chinese provinces reported an annual increase of 8.3% in the incidence of first stroke in adults, from 189 cases per 100,000 people in 2002 to 379 cases per 100,000 people in 2013， with the incidence of ischaemic stroke and hemorrhagic stroke at 335 per 100,000 population and 44 per 100,000 population, respectively, in 2013 (He et al., 2022). In the United States, more than 795,000 people suffer a stroke each year, accounting for about one in 10 deaths in the United States, and is the leading cause of long-term disability in the country (Engler-Chiurazzi et al., 2017; Ho et al., 2019; Barthels and Das, 2020). By 2050, more than 150 million people worldwide will be 65 and over (Feigin et al., 2014; Thomazi et al., 2018; He and Zhou, 2020)， the number of people suffering from stroke is expected to increase steadily in the coming decades as the population ages (Boudreau et al., 2013; Ji et al., 2022; Kevdzija et al., 2022; Tsao et al., 2022; Zhou et al., 2022).

The central premise of ischaemic stroke treatment is to limit infarction by rapid and effective recanalization of occluded vessels, leading to reperfusion of the ischaemic semidark zone, and there have been significant advances in the treatment of patients with ischaemic stroke over the last decade or so of research (Bivard et al., 2017; Malysz-Cymborska et al., 2021). Currently,

drugs commonly used to treat ischaemic stroke include drugs to improve cerebral circulation, neuroprotective agents, and herbs to activate blood circulation and resolve blood stasis. The only thrombolytic medication that has received FDA approval is tissue fibrinogen activator (tPA), but its clinical application is restricted to a certain time window (Fukuta et al., 2017; Hu et al., 2022; Yoon et al., 2022). A recent meta-analysis of individual participant data on alteplase showed that, regardless of age or stroke severity, giving alteplase within 4–5 h of stroke onset significantly improved the overall odds of a good stroke prognosis, despite an increased risk of fatal intracranial hemorrhage within a few days of treatment, and the earlier the treatment, the greater the proportion of benefit. However, recanalisation success rates were lower with intravenous administration of alteplase, thus reducing overall efficacy (Emberson et al., 2014; Leiva-Salinas et al., 2016). Although numerous studies have shown that inflammation, oxidative stress, excitotoxicity, calcium overload, apoptosis, and disruption of the blood–brain barrier are causative mechanisms of ischaemic stroke, preclinical protective agents targeting one of these mechanisms have not been used in the clinic (Dirnagl et al., 1999; He et al., 2013). Therefore, there is an urgent need to better understand the physio-pathological mechanisms that regulate these complex molecular effects in order to facilitate the research and development of new drugs and improve patient prognosis (Zou et al., 2022). This article critically discusses the role of glutamate receptor-mediated excitotoxicity and cystine/glutamate antiporter-mediated ferroptosis in ischemic stroke, as shown in Figure 1.

2. Glutamate receptor-mediated excitotoxicity

2.1. The role of glutamate in synaptic transmission

Glutamate is the main excitatory neurotransmitter in the central nervous system (CNS) and is closely linked to synaptic activity, plasticity, cell death and survival, learning and memory, and pain perception (Byrnes et al., 2009; Arteaga Cabeza et al., 2021). Excitotoxicity, a toxic effect of excessive or prolonged glutamate activation of the receptor, was first studied by Dr. Olney (Wang S. et al., 2017; McCaughey-Chapman and Connor, 2022). Excitotoxicity, excessive and pathological stimulation of neurons, associated with neuronal death in many neurological diseases, including ischaemia, traumatic brain injury, and neurodegenerative diseases (Connolly et al., 2016; Krasil'nikova et al., 2019). All intercellular signaling is dependent on chemical signals, and glutamate is one of the most important intercellular chemical signals in the nervous system (Özel et al., 2014; Teng et al., 2016).

Glutamate is approximately 5–15 mmol/kg in brain tissue, 5–10 mM in neurons, and 30–50 μM in plasma, with glutamate concentrations fluctuating in response to body metabolism, diet, etc. (Bramham et al., 1990; Ottersen et al., 1990, 1992; Osen et al., 1995; Danbolt, 2001). Glutamate concentrations in neurons are highest at axon terminals, which means that axon terminals somehow restrict glutamate movement or local synthesis and utilization of glutamate, and glutaminase is responsible for glutamate synthesis in most neurons (Márquez et al., 2009; Barbano et al., 2020; Pietrancosta et al., 2020). Glutamate in neurons is concentrated in synaptic vesicles *via* the vesicular glutamate transporter (VGLUT) and released into the extracellular space when the neuron is depolarized (Takamori et al., 2000; Takamori, 2006). Glutamate concentrations are highest in teleneuron and up to 100 mM in synaptic vesicles (Riveros et al., 1986; Burger et al., 1989; Shupliakov et al., 1992). When an action potential reaches the presynaptic terminal, Ca^{2+} influx *via* voltage-gated calcium channels (VGCC) triggers the fusion of vesicles loaded with neurotransmitter with the cell membrane, thereby releasing neurotransmitter in the synaptic cleft (Nishimune et al., 2016; Liang et al., 2021; Tukker and Westerink, 2021; Fedorovich and Waseem, 2022). Glutamate is secreted into the synaptic gap where it can diffuse around the neuron and interact with surrounding targets (Clewett et al., 2017), closest to the axon terminal is the postsynaptic membrane, which contains a large number of membrane-associated proteins, these "postsynaptic densities (PSD)" can be seen under the electron microscope (Kennedy, 1997; Xu Y. et al., 2021), PSDs contains a large number of glutamate receptors, which bind to glutamate and then trigger the postsynaptic cell to complete the synaptic transmission of glutamate signals from the presynaptic to the postsynaptic cell (Guo and Cordeiro, 2008; Terauchi and Umemori, 2012; Katayama et al., 2017). The transport pattern of glutamate is shown in Figure 2.

2.2. Type of glutamate receptor and mechanism of action

Excitotoxicity was one of the first mechanisms of ischemic cell death to be identified and one of the most intensively studied, with the term "excitotoxicity" describing the process by which excess glutamate overactivates NMDA receptors (NMDARs) and induces neuronal toxicity (Choi et al., 1988; Garthwaite et al., 1992). There are two types of glutamate receptors: ionotropic glutamate receptors (iGluRs), which are ligand-gated ion channels, and metabotropic glutamate receptors (mGluRs), which are G protein-coupled receptors (Pin and Duvoisin, 1995; Ferraguti and Shigemoto, 2006). The ionotropic receptors include kainate (KA) receptors, alpha-amino-3-hydroxy-5-methyl-4-isoxazole propionic acid (AMPA) receptors, and N-methyl-D-aspartate (NMDA) receptors (Takahashi, 2019; Burada et al., 2020). iGluRs are ligand-gated ion channels that allow cations such as calcium and potassium to cross the plasma membrane after glutamate binding to the receptor (Wei et al., 2011; Rocha-Ferreira and Hristova, 2016).

NMDA receptors require a basic NR1 subunit and one or more regulatory NR2 subunits (NR2A-D), and also NR3 subunits (NR3A-B), in some specific cases (Ye et al., 2013; Rebas et al., 2020). In the resting state, NMDAR channels are normally blocked by Mg^{2+}, but when large amounts of glutamate accumulate, activated AMPAR causes partial depolarization of the postsynaptic membrane, sufficient to clear the Mg^{2+} on the NMDAR. Among the currently known ionotropic and metabotropic glutamate receptors, NMDAR play an important role in allowing excess Ca^{2+} inward flow, leading to ischemic cell death (Mao et al., 2022). Calcium overload activates a large number of downstream pro-death signals such as calpain activation, reactive oxygen species (ROS) production, and mitochondrial damage (Fujimura et al., 1998; Kristián and Siesjö, 1998; Eliasson et al., 1999; Lau and Tymianski, 2010), resulting in cell necrosis or apoptosis (Köhr, 2006; Shi et al., 2017; Yoo et al., 2017;

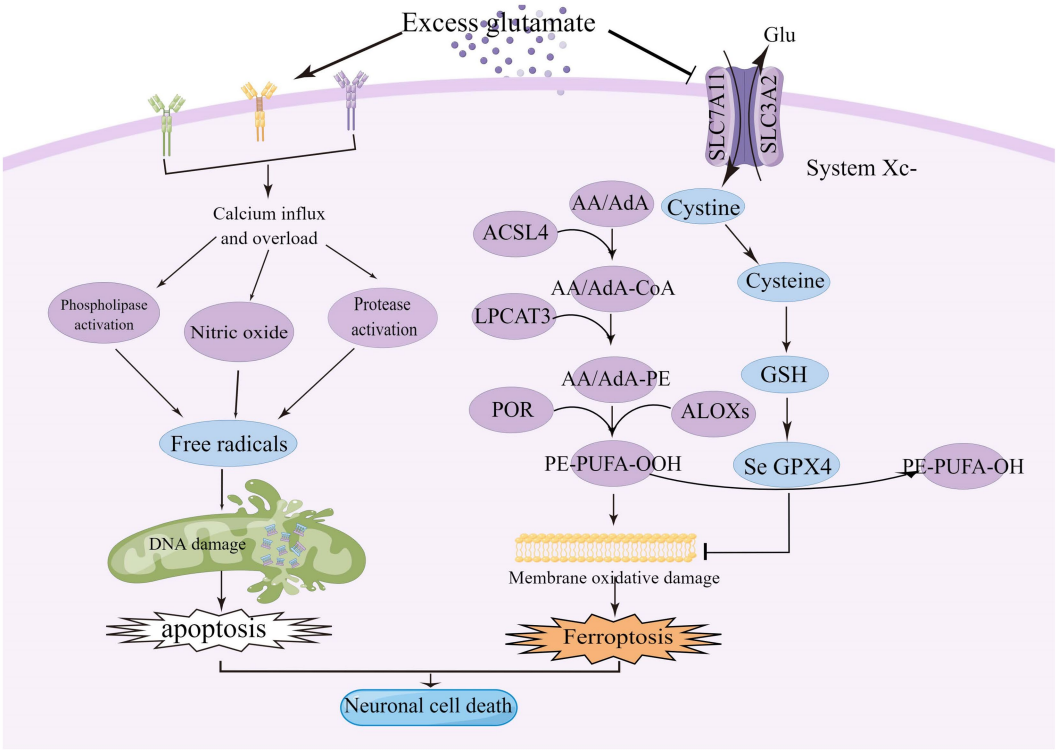

FIGURE 1
Excitotoxicity is caused by over-stimulation of glutamate receptors, particularly NMDAR, leading to high calcium influx, mitochondrial dysfunction, and DNA breakage. High levels of glutamate reduce the uptake of cystine *via* the Xc-system, leading to intracellular glutathione depletion resulting in the accumulation of reactive oxygen species (ROS), which increases lipid peroxidation, mitochondrial damage and ultimately ferroptosis. ACSL4, acyl-coenzyme A synthase long chain family member 4; System Xc-, cystine/glutamate reverse transporter; LPCAT3, lysophosphatidylcholine acyltransferase 3; AA, arachidonic acid; AdA, adrenoyl acid; ALOXs, lipoxygenases; CoA, coenzyme A; POR, cytochrome p450 oxidoreductase; GPX4, glutathione peroxidase 4; and GSH, glutathione.

Maher et al., 2018). GluN2A and GluN2B play opposite roles in ischaemic stroke, with activation of GluN2B leading to excitotoxicity and neuronal apoptosis, while activation of GluN2A protects neurons (Liu et al., 2007; Chen et al., 2008). Under stress conditions, NMDAR2A activates the PI3K/Akt kinase pathway, promoting the expression of cAMP response element binding protein (CREB) related genes and inhibiting the expression of pro-death genes, and Akt promotes cell survival by phosphorylating many downstream targets (Wu and Tymianski, 2018). Akt also inactivates the pro-apoptotic Bcl-2 family member BAD (Bcl2/Bcl-XL-antagonist causing cell death) by phosphorylation, thus stopping its interaction with and blockade of the pro-survival Bcl-2 family members Bcl-2 and Bcl-XL (Papadia and Hardingham, 2007). The JNK/p38 activator ASK1 is also inhibited by phosphorylation by Akt, and the activity of p53 is inhibited by Akt, resulting in reduced Bax expression (Kim et al., 2001; Yamaguchi et al., 2001). CREB target genes include the anti-apoptotic BTG2, the apoptotic p53 inhibitor BCL6, and the neurotrophic factor BDNF (Hardingham et al., 2002; Hardingham, 2009). During synaptic contact, these receptors are present in high density in a specific region of the postsynaptic membrane, which is closely associated with the presynaptic active zone of glutamate release (Sheng and Hoogenraad, 2007). PSD-95 was found to bind to NMDAR2B and intracellular neuronal nitric oxide synthase (nNOS) as part of a scaffold synaptic protein, and in the presence of intracellular calcium, PSD-95 plays a crucial role in the mechanism by which NMDAR activity triggers the production of nitric oxide production by nNOS and excitotoxicity (Cui et al., 2007; Forder and Tymianski, 2009; Abergel, 2020). NO combines with superoxide radicals to produce large amounts of nitrite, which leads to protein oxidation, lipid peroxidation, and DNA damage (Lipton et al., 1993), as shown in the Figure 3.

AMPAR is constructed from four subunits (GluR1-4; Hwang and Lupica, 2020; Zhang et al., 2022). Under resting conditions, the NMDAR channel pores are blocked by Mg^{2+} ions and once sufficient membrane depolarization has been established, the Mg^{2+} block is removed, allowing the influx of cations (Lin et al., 2008; Olive, 2009). AMPAR activation increases Na^{+} influx into neurons, depolarizes membranes, and activates voltage-dependent Ca^{2+} channels and NMDARs (Andriessen et al., 2010), the substitution of a positively-charged arginine residue for a neutrally-charged glutamine residue at the apex of the membrane reentrant pore loop (M2) changes the conductance properties of channels containing an edited GluR2 subunit (Köhr et al., 1998; Hood and Emeson, 2012). Most GluR2 subunits expressed in the mature rat cochlea are edited form and therefore, when incorporated into AMPA receptors, render the GluR complex calcium impermeable (Carriedo et al., 1996; Graham et al., 2011; Basappa et al., 2012). Molecular cloning has identified five isoforms, named GluK1, GluK2, GluK3, GluK4, and GluK5 according to the new IUPHAR nomenclature, which form functional receptors in various combinations (Dingledine et al., 1999).

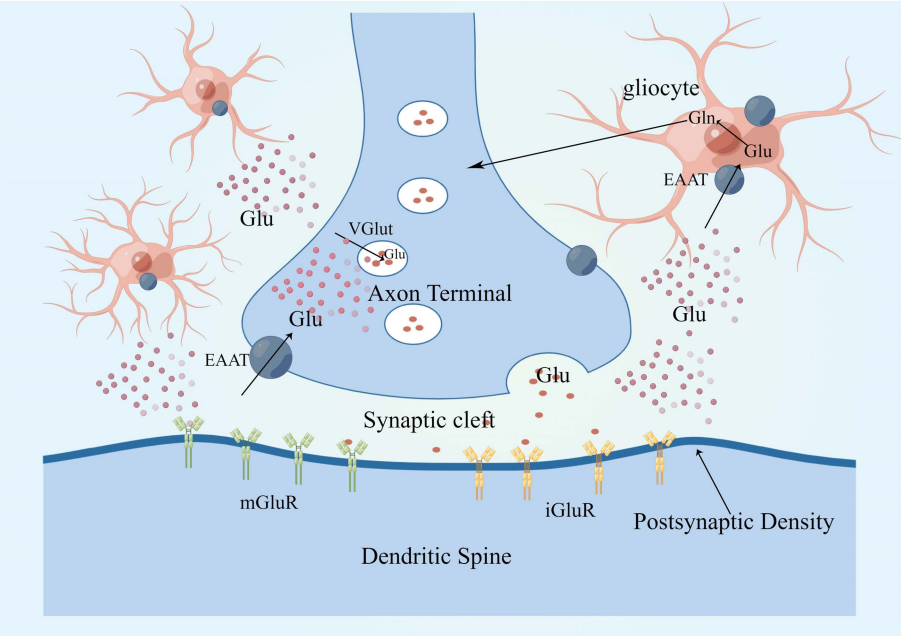

FIGURE 2
Glutamate in neurons is concentrated in synaptic vesicles *via* VGLUT and is released into the extracellular space in response to neuronal depolarization. There are two main classes of glutamate receptors, that is, mGluRs and iGluRs, glutamate clearance from the extracellular space takes place mostly through the high-affinity EAATs, EAAT 1 and 2 are mainly expressed in astrocytes. Glutamate enters glial cells *via* EAAT1 and EAAT2, where it is metabolized to glutamine, which is released into the extracellular space and converted to glutamate after uptake by neurons, completing a cycle. EAAT, excitatory amino acid transporter; mGluR, metabotropic glutamate receptor; iGluRs, ionotropic glutamate receptors; VGLUT, vesicular glutamate transporters; and PSD, postsynaptic density.

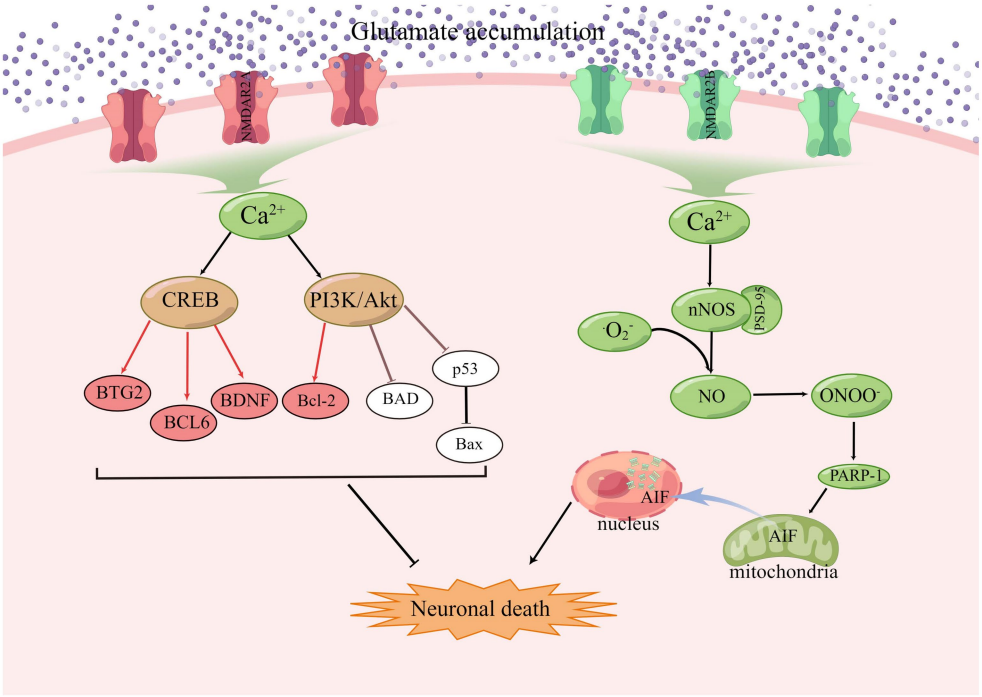

FIGURE 3
In ischaemic stroke, GluN2A and GluN2B play opposing roles, with GluN2B activation leading to excitotoxicity and apoptosis and GluN2A activation promoting cell survival.

3. Excess glutamate accumulation can inhibit the cystine/glutamate reverse transporter and lead to ferroptosis

Since 2005, the Nomenclature Committee on Cell Death (NCCD) has updated the classification system and in 2018 introduced an updated version based on molecular mechanisms, in which cell death is divided into two parts, accidental cell death (ACD), and regulated cell death (RCD; Galluzzi et al., 2018; Čepelak et al., 2020). There are several types of RCD, including apoptotic and non-apoptotic (Shen et al., 2022). Ferroptosis cells often show a necrotic appearance, such as cell swelling, plasma membrane rupture, and mitochondrial damage, unlike apoptotic cells, which are characterized by membrane blistering and contraction (Hou et al., 2021). Ferroptosis is a newly identified form of cell death caused by iron-dependent lipid peroxidation. Which leads to cell membrane damage and the accumulation of reactive lipid hydroperoxides to lethal levels (Munro et al., 2022). Our original knowledge of the molecular mechanisms of ferroptosis stemmed from studies using small molecule compounds to selectively inhibit cancer cells with oncogenic RAS mutations (Chen et al., 2021; Andreani et al., 2022). Ca^{2+} plays a fundamental role in glutamate-mediated excitotoxicity or oxidation-mediated cell death, a form of programmed cell death similar to or possibly identical to ferroptosis (Tan et al., 2001; Maher et al., 2018). Inhibiting System Xc- and inactivating GSH peroxidase-4 (GPX4) causes cellular glutathione (GSH) depletion and impaired ROS scavenging, resulting in disruption of cellular redox homeostasis, accumulation of ROS in the lipid peroxidation or Fenton reaction, and ultimately cell death (Shi et al., 2021).

3.1. Characteristics of ferroptosis

Ferroptosis cells undergo morphological changes at both the cellular and ultrastructural levels: the plasma membrane loses its integrity, the cytoplasm becomes enlarged, the mitochondria become smaller than normal cells, the mitochondrial cristae shrink or disappear, the outer mitochondrial membrane ruptures and the membrane density increases (Dolma et al., 2003; Yagoda et al., 2007; Dixon et al., 2012; Friedmann Angeli et al., 2014; Vanden Berghe et al., 2014). Mitochondria are an important source of ROS. Recent studies have found that impaired mitochondrial function leading to ROS production, DNA stress, and metabolic reprogramming is responsible for lipid peroxidation and ferroptosis (Gao et al., 2019; Lee et al., 2020; Li et al., 2021). Ferroptosis is mainly associated with iron accumulation and lipid peroxidation. Excess iron combines with hydrogen peroxide in a Fenton reaction to produce large amounts of hydroxyl radicals, increasing oxidative damage. Iron also increases the activity of lipoxygenase (ALOX) or prolyl hydroxylase (PHD), further aggravating lipid peroxidation (Chen X. et al., 2020; Lin et al., 2021; Tang D. et al., 2021). Lipid peroxidation occurs as a free radical-driven reaction that primarily affects the metabolism of polyunsaturated fatty acids (PUFAs) in cell membranes (Gao Q. et al., 2022; Nie et al., 2022). Lipopolymer peroxidation products include the initial lipid hydroperoxide (LOOH) and the subsequent reactive aldehyde (MDA,4-HNE), which increase during ferroptosis (Nie et al., 2022). The PTGS2 gene encodes prostaglandin endoperoxide synthase (PTGS), a key enzyme in prostaglandin biosynthesis (Yang et al., 2014). Acyl-Coenzyme A synthase long chain family member 4 (ACSL4) is thought to be a specific biomarker and driver of ferroptosis as it is a key enzyme involved in fatty acid metabolism. Upregulation of ACSL4 leads to an increase in polyunsaturated fatty acid content in phospholipids, which are particularly susceptible to oxidative reactions and ultimately ferroptosis (Yuan et al., 2016; Doll et al., 2017). Activation of transcriptional pathways of genes responsible for antioxidant defense (GSH, CoQ10, and NRF2) and membrane repair (ESCRT-III) limits membrane damage during ferroptosis (Dixon et al., 2012; Sun et al., 2016; Bersuker et al., 2019; Doll et al., 2019; Dai et al., 2020). The dynamic balance between damage and resistance to damage determines the survival or death of cells.

3.2. Critical role of amino acid metabolism and lipid metabolism in ferroptosis

3.2.1. Amino acid metabolism

Cystine/glutamate reverse transporter (System Xc-) is an amino acid reverse transporter protein that mediates the inward flow of cystine and the outward flow of glutamate (Kagami et al., 2018; Wang et al., 2020; Marcoli et al., 2022). The cystine taken into the cell is reduced to cysteine, part of which participates in intracellular GSH synthesis and the other part flows out of the cell to be converted to cystine and re-involved in the System Xc- (Liu N. et al., 2020; Tang Z. et al., 2021). Glutathione is an antioxidant and an important indicator of oxidative stress in cells (Guo et al., 2012). When there is too much extracellular glutamate, it inhibits the function of the System Xc-, resulting in less cystine entering the cell, which is an excitatory neurotransmitter with neurotoxic and excitatory effects (Liao et al., 2018; Ratan, 2020). System Xc- mediates the uptake of cystine and the release of glutamate, thereby promoting the synthesis of GSH, which acts as a co-molecule with GPX-4 to assist in the scavenging of lipid peroxides to protect cells (Zhao et al., 2021). System Xc- is a heterodimeric protein consisting of one light chain and one heavy chain with a disulfide bond between the two chains (Chen et al., 2022; Wang Y. et al., 2022). The light chain subunit SLC7A11 is the primary transporter and is highly sensitive to cystine and glutamate, while the heavy chain subunit SLC3A2 acts essentially as a chaperone protein and plays an important role in the transport of SLC7A11 to the plasma membrane (Koppula et al., 2018). SLC7A11 is a 12-channel transmembrane protein with both its N and C termini in intracellular locations, whereas SLC3A2 is a single-transmembrane protein with its N terminus in intracellular locations and its c terminus in extracellular locations (Sato et al., 1999; Xu C. et al., 2021; Chen et al., 2022). In addition, Knockdown of SLC3A2 has been shown to result in a significant lowering of SLC7A11 protein levels, suggesting that SLC3A2 is critical in sustaining SLC7A11 protein stability (Nakamura et al., 1999; Shin et al., 2017; Koppula et al., 2018). Intracellular cysteine is an essential precursor of glutathione. Glutathione is a tripeptide synthesized by cysteine, glutamate and glycine (Koppula et al., 2018; Gan, 2019; Zhao et al., 2022). The biosynthesis of GSH involves two crucial steps, first by formation of gamma-glutamylcysteinyl linkage by formation of gamma-glutamyl cysteine, followed by the addition of glycine *via* glutathione synthase (GSS) to produce the tripeptide glutathione (Raza et al., 2022). Endogenous enzymes protect cells from damage caused by excess ROS, including superoxide dismutase which converts superoxide (O_2^-) to hydrogen

peroxide (H_2O_2), glutathione peroxidase (GPX) which converts free H_2O_2 to water, glutathione reductase which converts glutathione disulfide to the sulfhydryl form and catalytic breakdown of H_2O_2 to water and oxygen by peroxidase (Mahmoud et al., 2014). Oxidation of glutathione by the action of GPX and reduction of glutathione by glutathione reductase (GR) at the expense of NADPH (Koppula et al., 2018). Thus, System Xc- is critically important for the uptake of cystine to produce cysteine for the maintenance of intracellular GSH levels.

Two transcription factors were identified that regulate SLC7A11, nuclear factor red lineage 2-related factor 2 (NRF2) and activating transcription factor 4 (ATF4). NRF2 is a master transcription factor that accounts for antioxidant responses (Becker et al., 2016; Kuo et al., 2022). Under normal physiological conditions, Nrf2 is ubiquitinated by the Keap1-Cullin3 ubiquitin ligase complex and is conventionally fragmented by the 26 s proteasome. In contrast, under oxidative stress conditions, ubiquitin ligase activity is blocked by modifying the cysteine residues in Keap1, thereby stabilizing and activating (Noguchi et al., 2018), stable NRF2 then translocates into the nucleus, binds to antioxidant response elements in the gene promoter region and regulates the transcription of a range of target genes involved in antioxidant defense and cellular redox maintenance (Ooi et al., 2018; Koppula et al., 2021a), Similarly, overexpression of NRF2 upregulated the expression levels of antioxidant genes such as SLC7A11 and promoted the synthesis of GSH (Shih et al., 2003). Consequently, SLC7A11 is one of the most important transcriptional targets that can mediate the anti-oxidant response.

Transcription factor ATF4 regulates the expression of genes involved in amino acid metabolism, redox homeostasis and endoplasmic reticulum stress response (Pakos-Zebrucka et al., 2016; Sazonova et al., 2021). Translation of ATF4 mRNA is silenced by two short UORFs located in the 5′ untranslated region (UTR). The kinase that is catalyzed by eIF2α phosphorylation is activated by various cellular stresses, such as amino acid deprivation, endoplasmic reticulum stress, and viral infection (Koppula et al., 2018; Scalise et al., 2020). Inhibition of eIF2alpha phosphorylation levels led to inhibition of ATF4 mRNA translation and decreased ATF4 protein levels, while increased eIF2alpha phosphorylation levels led to enhanced ATF4 mRNA translation and increased ATF4 protein (Pathak et al., 2019). One upstream kinase of eIF2α is general control non-repressor-2 (GCN2), which is activated by free tRNAs in the presence of amino acid deprivation (Scalise et al., 2020). Thus, during amino acid deletion, GCN2 phosphorylates eIF2α, leading to the inhibition of protein synthesis in general, while increasing the translation of the specific transcription factor ATF4 (Ferraz-Bannitz et al., 2021). ATF4 associates with amino acid response elements (AARE) and promotes the transcription of genes related to amino acid metabolism and stress response, in particular SLC7A11, thereby enabling cells to cope with amino acid-limited conditions (Koppula et al., 2021b). Indeed, SLC7A11 expression can be strongly induced by deprivation of a variety of amino acids, and SLC7A11 expression induced by amino acid deprivation is mainly mediated by ATF4 (Koppula et al., 2021b). In summary, these data support that amino acid deletion induces SLC7A11 expression through the GCN2-eIF2α-ATF4 signaling axis.

Several studies have shown that the above transcription factors regulate downstream biological effects, including ferroptosis, antioxidant, and nutrient-dependent, through the regulation of SLC7A11 expression. SLC7A11 inhibits ferroptosis by increasing intracellular cystine and promoting glutathione synthesis (Dixon et al., 2012). By increasing SLC7A11 expression, ATF4 and NRF2 at least partially inhibit ferroptosis, whereas p53 stimulates ferroptosis by repressing SLC7A11 expression (Jiang et al., 2015; Fan et al., 2017; Roh et al., 2017). A study showed that p53 inhibits cystine uptake and leads to ferroptosis by suppressing SLC7A11, a component of the cystine/glutamate countertransport protein. In addition, mutant p533KR is defective in p53-dependent cell cycle arrest, apoptosis and senescence, but retains the ability to inhibit SLC7A11 expression, thereby regulating cystine metabolism and ferroptosis (Jiang et al., 2015).

3.2.2. Lipid metabolism

Fatty acid metabolism is divided into anabolic and catabolic pathways, both of which are regulated by a variety of enzymes (Wakil and Abu-Elheiga, 2009). Fatty acid β-oxidation (FAO) in mitochondria normally consumes most of the fatty acids, leading to a reduction in lipid peroxidation. Cytoplasmic lipid droplets form the energy hub of almost all eukaryotic cells and when energy is available, they store energy in the form of esterified fatty acids and release them to local or distant tissues for oxidation (Goodman, 2019).

Lipids play an important role in cellular functions, including membrane formation, energy production, intra- and intercellular signaling, and the regulation of cell death. Oxidation of phospholipids contributes to ferroptosis in cells (Yang et al., 2016). Lipid peroxides are produced in cells by three main pathways: first, lipid ROS from iron *via* a non-enzymatic Fenton reaction, second, lipid peroxides from oxidation and esterification of PUFAs, and third, lipid peroxides from iron-catalyzed lipid autoxidation. AA is a PUFAs that can be converted to adrenal acid (AdA) by prolonged enzymes. The accumulation of oxygenated AA-PE and AdA-PE evokes intracellular ferroptosis. Free PUFAs can be ultimately converted to phosphatidylethanolamine (PE)-PUFAs-OOH by three important enzymes, ACSL4, lysophosphatidylcholine acyltransferase 3 (LPCAT3), and lipoxygenases (LOXs; Jiang et al., 2020). The formation of lipid peroxides involves the formation of AA-PE from phosphatidylethanolamine (PE), an essential component of cell membranes, and arachidonic acid (AA), a PUFA, catalyzed by ACSL4 and LPCAT3, which is then peroxidized by iron-dependent LOX to form AA- OH -PE, the major actuator of ferroptosis (Protchenko et al., 2021; Liu et al., 2022), this is shown in Figure 4. ACSL family made up of proteins on the endoplasmic reticulum and outer membrane, ACSLs are responsible for the formation of fatty acid acyl coenzyme a esters from free long-chain fatty acids. The ACSL family contains five enzymes, ACSL4 is one of a family of five isomers, but only ACSL4 has a specific effect on ferroptosis (Yan and Zhang, 2019; Capelletti et al., 2020).

4. Crosstalk between excitotoxicity and ferroptosis

Excitotoxicity is mainly due to excessive glutamate release during ischemia leading to excessive activation of NMDAR, which leads to intracellular calcium overload, ROS-induced oxidative stress, mitochondrial dysfunction, and impaired membrane permeability (Yoo et al., 2017), Ca^{2+} overload *via* glutamate receptor-induced cPLA2 activation produces neurotoxic metabolites such as

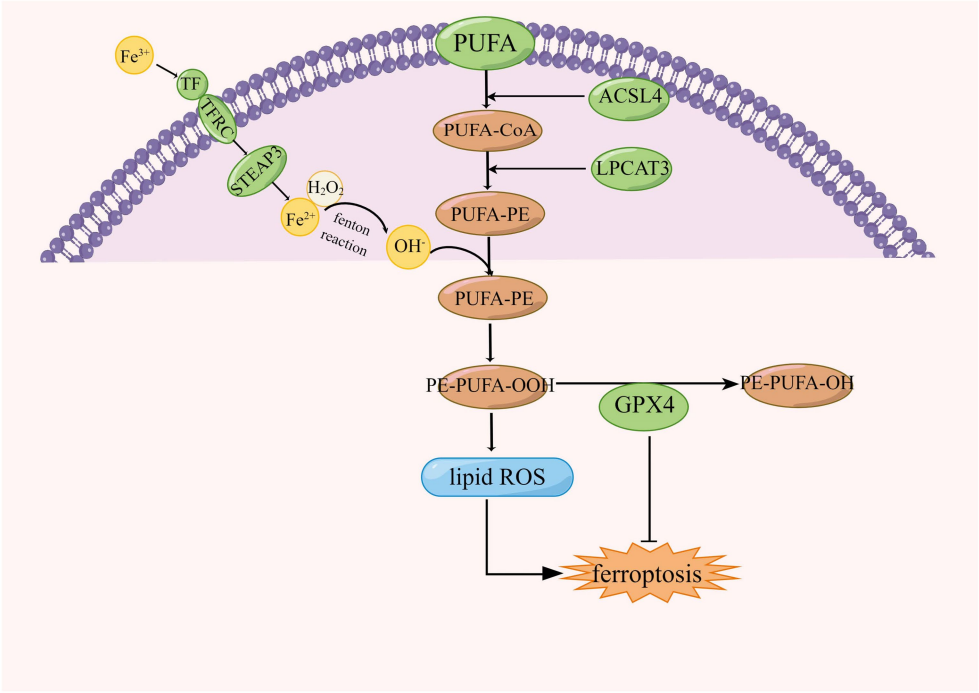

FIGURE 4
Regulation of lipid peroxidation in ferroptosis, ACSL4, acyl-coenzyme A synthase long chain family member 4; LPCAT3, lysophosphatidylcholine acyltransferase 3; CoA, coenzyme A; GPX4, glutathione peroxidase 4; and PUFA, polyunsaturated fatty acid.

prostaglandins, leukotrienes, ROS, and platelet-activating factor *via* AA and lysophospholipid metabolism. It is known to be particularly sensitive to ferroptosis as AA and ADA are the main substrates of lipid peroxidation (Liu Y. et al., 2020; She et al., 2020; Hong et al., 2022), this is shown in Figure 5. The ROS generation cascade also includes the reaction of superoxide with nitric oxide to form peroxynitrite, hydrogen peroxide catalyzed by peroxidase to form hypochlorous acid, and the Fenton reaction catalyzed by iron to form hydroxyl radicals (Lin et al., 2016; Griendling et al., 2021). Mitochondrial ROS are essential not only for apoptosis but also for ferroptosis, although the common mechanisms determining the relationship between the two different types of cell death remain obscure (Gao et al., 2019; Lee et al., 2020; Li et al., 2021; Tang Z et al., 2021). However, there appears to be crosstalk between oxidative stress and ferroptosis during the development of ischaemic stroke. Excess glutamate accumulates extracellularly during stroke, causing excessive NMDAR activation and neuroexcitotoxicity, as well as inducing NMDAR-mediated iron uptake (Cheah et al., 2006), as BBB dysfunction during stroke allows iron-containing substances to enter the brain and accumulate in areas of ischaemic brain tissue prior to neurodegeneration (Helal, 2008; DeGregorio-Rocasolano et al., 2019). Thus, crosstalk between iron and glutamate in neurons is a target for intervention that cannot be ignored.

AMPK, a family member of serine/threonine kinases, is an invaluable endogenous defense factor against cerebral ischemia. During cerebral ischemia or hypoxia, the deprivation of energy and the consequent increase in the AMP/ATP ratio facilitates AMPK phosphorylation and initiates autophagy to bolster energy production (Jiang et al., 2014; Fang et al., 2018; Qin et al., 2022). AMPK activator A-769662 mimics the effects of silymarin and inhibits ROS production and neuronal cell death after OGD/R. In conclusion, these results suggest that silymarin-mediated neuroprotection may in part require activation of AMPK signaling (Xie et al., 2014). Under oxidative stress, Nrf2 is released from Keap1 and translocated to the nucleus, where it binds to the antioxidant response element (ARE) and upregulates the expression of NQO1 and HO-1 (Meng et al., 2014). The Nrf2/ARE signaling pathway counteracts ischemia–reperfusion injury by enhancing endogenous antioxidant defense factors and suppressing ROS production during reperfusion, which indicates that enhanced antioxidant properties can protect neurons (Young Park et al., 2019), and more importantly, NRF2 plays a key role in mediating iron/hemoglobin metabolism. NRF2 regulates the light and heavy chains of the iron storage protein ferritin (FTL/FTH1), and the iron transporter (SLC40A1) responsible for iron efflux from cells (Harada et al., 2011; Agyeman et al., 2012; Kerins and Ooi, 2018). NRF2 controls many of the enzymes that participate in glutathione synthesis and metabolism, including the catalytic and regulatory subunits of glutamate-cysteine ligase (GCLC/GCLM), glutathione synthase (GSS) and the subunit of the cystine/glutamate transporter xCT (SLC7A11), all of which are required for glutathione synthesis (Kwak et al., 2002; Sasaki et al., 2002). Among the multiple AMPK-related signaling pathways, the Nrf2 signaling pathway plays an important role in the regulation of genes and proteins with cytoprotective functions (Jiang et al., 2021). AMPK/NRF2 not only protects cells from oxidative stress damage, but also effectively regulates the expression of related genes to inhibit ferroptosis.

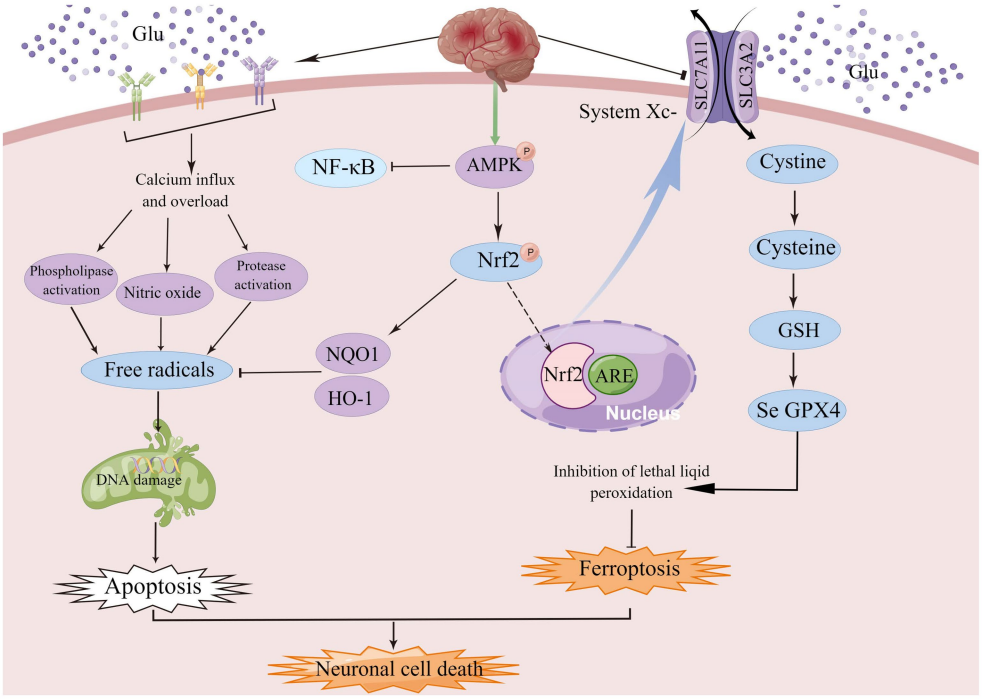

FIGURE 5
AMPK, a member of the serine/threonine kinase family, is an important endogenous defense factor against ischemia, and the Nrf2/ARE signaling pathway counteracts ischemia–reperfusion injury by inducing endogenous antioxidant defense factors and attenuating ROS production during reperfusion injury.

5. Treatment of ischemic stroke

5.1. Maintaining glutamate homeostasis

Glutamate is an important transmitter that plays a vital role in a variety of biological processes. Excess glutamate leads to over-stimulation of postsynaptic glutamatergic receptors, particularly NMDARs and AMPARs, allowing calcium to enter the cell, causing neuronal depolarisation and further neuronal death (Glotfelty et al., 2019), Inhibition of glutamate release, enhancement of glutamate clearance and blockade of glutamate receptors may be major directions for future stroke research. Methionine sulfoximine was found to be effective in inhibiting glutamate synthesis in mice (Ghoddoussi et al., 2010)，Dextromethorphan can inhibit glutamate release by inhibiting presynaptic voltage-dependent calcium channels (VDCC; Lin et al., 2009). In terms of glutamate clearance, ceftriaxone effectively increases GLT expression in glial cells and enhances glutamate clearance (Lai et al., 2011). NMDAR inhibitors are widely studied drugs, and magnesium sulfate has shown a prominent role in protecting neurons from excitotoxicity by inhibiting NMDAR, reducing the transmission of the excitatory neurotransmitter glutamate, and reducing the inward flow of calcium ions (Ovbiagele et al., 2003). Memantine is a non-competitive NMDAR inhibitor. Memantine selectively blocks the over-activation of NMDAR in excitotoxicity and memantine increases the upregulation of brain-derived neurotrophic factor (BDNF) and glial cell-derived neurotrophic factor (Martínez-Coria et al., 2021). A meta-analysis showed no improvement in key outcome indicators and mortality in acute ischaemic stroke treated with magnesium sulfate (Avgerinos et al., 2019), it seems to be due to the fact that it is more difficult to treat effectively within the time window. Peritoneal dialysis has been demonstrated to decrease peripheral blood glutamate levels in rats with cerebral ischemia (Godino Mdel et al., 2013). Therefore, inhibition of glutamate synthesis, enhancement of glutamate clearance and inhibition of glutamate receptors play an important role in the protection of ischemic stroke.

5.2. Inhibition of calcium increase and oxidative stress

Calcium ions are a commonly present second messenger that regulates a variety of activities such as excitability, cytoplasmic division, motility, transcription and apoptosis in eukaryotic cells (Bootman, 2012; Carafoli and Krebs, 2016; Pchitskaya et al., 2018). The initial calcium influx following excitotoxic glutamate stimulation is known to trigger a secondary intracellular calcium overload, and this secondary response strongly correlates with neuronal death (Randall and Thayer, 1992; Tymianski et al., 1993). The plasma membrane sodium-calcium exchanger (NCX) is an essential modulator of intracellular calcium levels, using the force of sodium influx to expel calcium ions. The action of the NCX partially restores calcium ions to physiological levels following glutamate stimulation (White and Reynolds, 1995). Another major player in intracellular calcium homeostasis is the mitochondria, which can restore intracellular calcium concentrations by absorbing large amounts of calcium themselves (Valdinocci et al., 2019; Sanz-Morello et al., 2021), and by facilitating ATP-dependent calcium extrusion (Budd and

Nicholls, 1996; White and Reynolds, 1996). Mitochondrial uptake of calcium in response to excitotoxic glutamate stimulation leads to ROS production (Castilho et al., 1999), excessive opening of the mitochondrial membrane permeability transition pore leads to a decrease in mitochondrial membrane potential (Castilho et al., 1999), induction of neuronal death (Stout et al., 1998; Ward et al., 2000). Therefore, inhibition of calcium increase and oxidative stress may be a therapeutic target in ischaemic stroke. Studies have demonstrated that the influx of calcium ions into cells during excitotoxicity is an essential pathway causing cell death, so interruption of the inward flow of extracellular calcium ions and decreasing the degree of calcium overload could theoretically protect neuronal cells to a large extent. Calcium antagonists have been proven in animal experiments to dramatically reduce the size of brain infarcts in rats and to have a protective neuronal effect (Zapater et al., 1997; Choi et al., 2011). Results of a meta-analysis show no effect of calcium antagonists on primary patient outcomes or death, and researchers show no evidence to support the use of calcium antagonists in patients with ischaemic stroke as beneficial (Zhang et al., 2019). 4,1-benzothiazoles are non-calcium antagonist drugs that reduce calcium levels in neurons by modulating mitochondria (Viejo et al., 2021). Calcium antagonists continue to be the subject of stroke research, although they have not achieved the desired results in clinical trials, probably because of intolerable side effects, low efficacy and short treatment windows. Uric acid is the final oxidation product of purine catabolism in the body and accounts for about two-thirds of the total antioxidant capacity of plasma (Becker, 1993). Uric acid has been shown to prevent glutamate-induced cell death *in vitro* and to inhibit ROS and RNS to reduce infarct size and improve prognosis in rodents after transient or permanent cerebral ischemia (Squadrito et al., 2000; Romanos et al., 2007; Onetti et al., 2015; Chamorro et al., 2016). Edaravone is an antioxidant drug that has been shown to scavenge the accumulation of free radicals and lipid peroxidation products in both clinical trials and basic experiments (Kasuya et al., 2014; Fidalgo et al., 2022).

5.3. Inhibition of ferroptosis

As ferroptosis is characterized by excessive lipid peroxidation, iron chelators, lipophilic antioxidants, and lipid peroxidation inhibitors can inhibit ferroptosis (Wang K. et al., 2022). Four types of ferroptosis inhibitors have been identified: GPX4 specifically catalyzes the loss of lipid peroxide oxidation activity in a GSH-dependent manner, FSP1 converts ubiquitin ketone on cell membranes to reduced ubiquitin, which can inhibit peroxidation and prevent iron droopy, GCH1/BH4 pathway is an endogenous antioxidant pathway, GCH1 protects cells from ferroptosis mainly through the antioxidant effect of BH4, and DHODH protects cells from ferroptosis in mitochondria by regulating the production of dihydrobisquinone in the inner mitochondrial membrane (Wang D. et al., 2022), this is shown in Figure 6. Some compounds inhibit ferroptosis directly or indirectly by targeting lipid peroxidation and iron metabolism (Chen G. et al., 2020). Both iron chelators (2,2′-pyridine, deferoxamine, deferoxamine mesylate) and inhibitors of lipid peroxides (Ferrostatin-1, Liproxstatin-1, Vitamin E) suppressed ferroptosis (Čepelak et al., 2020; Li et al., 2020). In additional, GSH, GPX4, heat shock protein β-1 and Nrf2 negatively modulate ferroptosis by restraining ROS production and repressing cellular uptake of iron (Sun et al., 2015; Qin et al., 2021). DFO, the most widely used iron chelator approved by the FDA, inhibits lipid peroxide chelation by inhibiting the Fenton reaction, and one study found that DFO effectively protects neurons by increasing the expression of hypoxia-inducible factor 1 (HIF-1; Baranova et al., 2007; Zhang et al., 2021). The widely

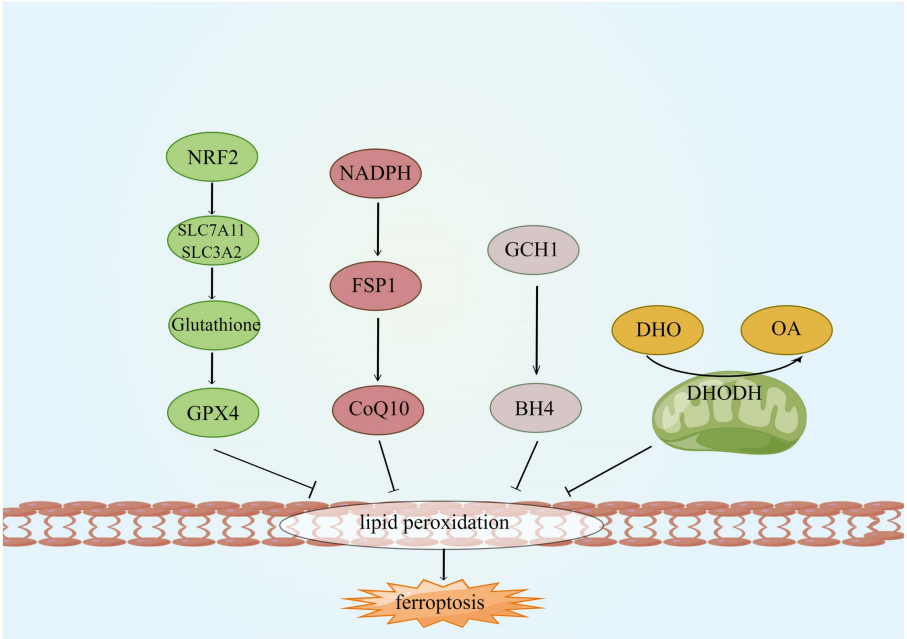

FIGURE 6
Four ferroptosis defense pathways. GCH1, GTP cyclohydrolyse-1; FSP1, ferroptosis suppressor protein 1; CoQ10, coenzyme Q; DHODH, dihydroorotate dehydrogenase; DHO, dihydroorotate; OA, orotate; GSH, glutathione; and BH4, tetrahydrobiopterin.

used RTAs are ferrostatin-1 and liproxstatin-1, which can inhibit lipid peroxidation linked to ferroptosis (Han et al., 2020). ACSL4 is a crucial enzyme for AA and ADA esterification and is most probably an essential target for the inhibition of ferroptosis. Thiazolidinediones (TZNs) have been shown to potentially inhibit the activity of ACSL4 specifically and to prevent ferroptosis (Doll et al., 2017; Zhang et al., 2021).

6. Conclusion and perspectives

Excessive accumulation of glutamate not only leads to excitotoxicity, but also to ferroptosis, Therefore, maintaining glutamate homeostasis is essential to inhibit excitotoxicity and ferroptosis. We can see a large number of articles using glutamate modeling to study the mechanism of excitotoxicity, most of which only look at the increase in calcium ions and mitochondrial dysfunction caused by excitotoxicity. In fact, the researchers used glutamate to create excitotoxic cell models that also caused ferroptosis, and excitotoxicity may be only part of the equation. Therefore it is also important to focus on neuronal ferroptosis when using glutamate for modeling in future studies. Neuronal excitotoxicity or ferroptosis can be effectively inhibited by compounds in most basic studies, particularly glutamate receptor inhibitors, but the role in clinical trials has been greatly reduced, probably mainly due to the failure to treat effectively within the time window in clinical trials. A number of influencing factors are essential, including informed patient consent, family cooperation and a well-established hospital system of care may all be influential in clinical trials. We remain confident in developing natural compounds that regulate both ferroptosis and excitotoxicity in future basic practice and further investigating their complex mechanisms and regulatory effects.

Author contributions

GF and YH conceived and designed this review. ML and JL contributed to the collection of literature and related information. GF and ML wrote the manuscript and examined the charts and the grammar of the manuscript. JL and YH provide guidance throughout the manuscript preparation process. All authors contributed to the article and approved the submitted version.

Funding

This project is supported by the Young Qihuang scholars program of National Administration of Traditional Chinese Medicine.

Acknowledgments

The authors thank to the editors and reviewers for their hard work and important comments. Picture was exported by FigDraw (www.figdraw.com).

Conflict of interest

The authors declare that the research was conducted in the absence of any commercial or financial relationships that could be construed as a potential conflict of interest.

Publisher's note

References

Abergel, E. (2020). The future of stroke interventions. *Rambam Maimonid. Med. J.* 11:e0018. doi: 10.5041/rmmj.10404

Agyeman, A. S., Chaerkady, R., Shaw, P. G., Davidson, N. E., Visvanathan, K., Pandey, A., et al. (2012). Transcriptomic and proteomic profiling of KEAP1 disrupted and sulforaphane-treated human breast epithelial cells reveals common expression profiles. *Breast Cancer Res. Treat.* 132, 175–187. doi: 10.1007/s10549-011-1536-9

Andreani, C., Bartolacci, C., and Scaglioni, P. P. (2022). Ferroptosis: a specific vulnerability of RAS-driven cancers? *Front. Oncol.* 12:923915. doi: 10.3389/fonc.2022.923915

Andriessen, T. M., Jacobs, B., and Vos, P. E. (2010). Clinical characteristics and pathophysiological mechanisms of focal and diffuse traumatic brain injury. *J. Cell. Mol. Med.* 14, 2381–2392. doi: 10.1111/j.1582-4934.2010.01164.x

Arteaga Cabeza, O., Zhang, Z., Smith Khoury, E., Sheldon, R. A., Sharma, A., Zhang, F., et al. (2021). Neuroprotective effects of a dendrimer-based glutamate carboxypeptidase inhibitor on superoxide dismutase transgenic mice after neonatal hypoxic-ischemic brain injury. *Neurobiol. Dis.* 148:105201. doi: 10.1016/j.nbd.2020.105201

Avgerinos, K. I., Chatzisotiriou, A., Haidich, A. B., Tsapas, A., and Lioutas, V. A. (2019). Intravenous magnesium sulfate in acute stroke. *Stroke* 50, 931–938. doi: 10.1161/strokeaha.118.021916

Baranova, O., Miranda, L. F., Pichiule, P., Dragatsis, I., Johnson, R. S., and Chavez, J. C. (2007). Neuron-specific inactivation of the hypoxia inducible factor 1 alpha increases brain injury in a mouse model of transient focal cerebral ischemia. *J. Neurosci.* 27, 6320–6332. doi: 10.1523/jneurosci.0449-07.2007

Barbano, M. F., Wang, H. L., Zhang, S., Miranda-Barrientos, J., Estrin, D. J., Figueroa-González, A., et al. (2020). VTA Glutamatergic neurons mediate innate defensive behaviors. *Neuron* 107, 368–382.e368. doi: 10.1016/j.neuron.2020.04.024

Barthels, D., and Das, H. (2020). Current advances in ischemic stroke research and therapies. *Biochim. Biophys. Acta Mol. Basis Dis.* 1866:165260. doi: 10.1016/j.bbadis.2018.09.012

Basappa, J., Graham, C. E., Turcan, S., and Vetter, D. E. (2012). The cochlea as an independent neuroendocrine organ: expression and possible roles of a local hypothalamic-pituitary-adrenal axis-equivalent signaling system. *Hear. Res.* 288, 3–18. doi: 10.1016/j.heares.2012.03.007

Becker, B. F. (1993). Towards the physiological function of uric acid. *Free Radic. Biol. Med.* 14, 615–631. doi: 10.1016/0891-5849(93)90143-i

Becker, A., Klapczynski, A., Kuch, N., Arpino, F., Simon-Keller, K., De La Torre, C., et al. (2016). Gene expression profiling reveals aryl hydrocarbon receptor as a possible target for photobiomodulation when using blue light. *Sci. Rep.* 6:33847. doi: 10.1038/srep33847

Bersuker, K., Hendricks, J. M., Li, Z., Magtanong, L., Ford, B., Tang, P. H., et al. (2019). The CoQ oxidoreductase FSP1 acts parallel to GPX4 to inhibit ferroptosis. *Nature* 575, 688–692. doi: 10.1038/s41586-019-1705-2

Bivard, A., Kleinig, T., Miteff, F., Butcher, K., Lin, L., Levi, C., et al. (2017). Ischemic core thresholds change with time to reperfusion: a case control study. *Ann. Neurol.* 82, 995–1003. doi: 10.1002/ana.25109

Bootman, M. D. (2012). Calcium signaling. *Cold Spring Harb. Perspect. Biol.* 4:a011171. doi: 10.1101/cshperspect.a011171

Boudreau, D. M., Guzauskas, G., Villa, K. F., Fagan, S. C., and Veenstra, D. L. (2013). A model of cost-effectiveness of tissue plasminogen activator in patient subgroups 3 to 4.5 hours after onset of acute ischemic stroke. *Ann. Emerg. Med.* 61, 46–55. doi: 10.1016/j.annemergmed.2012.04.020

Bramham, C. R., Torp, R., Zhang, N., Storm-Mathisen, J., and Ottersen, O. P. (1990). Distribution of glutamate-like immunoreactivity in excitatory hippocampal pathways: a semiquantitative electron microscopic study in rats. *Neuroscience* 39, 405–417. doi: 10.1016/0306-4522(90)90277-b

Budd, S. L., and Nicholls, D. G. (1996). Mitochondria, calcium regulation, and acute glutamate excitotoxicity in cultured cerebellar granule cells. *J. Neurochem.* 67, 2282–2291. doi: 10.1046/j.1471-4159.1996.67062282.x

Burada, A. P., Vinnakota, R., and Kumar, J. (2020). Cryo-EM structures of the ionotropic glutamate receptor GluD1 reveal a non-swapped architecture. *Nat. Struct. Mol. Biol.* 27, 84–91. doi: 10.1038/s41594-019-0359-y

Burger, P. M., Mehl, E., Cameron, P. L., Maycox, P. R., Baumert, M., Lottspeich, F., et al. (1989). Synaptic vesicles immunoisolated from rat cerebral cortex contain high levels of glutamate. *Neuron* 3, 715–720. doi: 10.1016/0896-6273(89)90240-7

Byrnes, K. R., Loane, D. J., and Faden, A. I. (2009). Metabotropic glutamate receptors as targets for multipotential treatment of neurological disorders. *Neurotherapeutics* 6, 94–107. doi: 10.1016/j.nurt.2008.10.038

Capelletti, M. M., Manceau, H., Puy, H., and Peoc'h, K. (2020). Ferroptosis in liver diseases: An overview. *Int. J. Mol. Sci.* 21:4908. doi: 10.3390/ijms21144908

Carafoli, E., and Krebs, J. (2016). Why calcium? How calcium became the best communicator. *J. Biol. Chem.* 291, 20849–20857. doi: 10.1074/jbc.R116.735894

Carriedo, S. G., Yin, H. Z., and Weiss, J. H. (1996). Motor neurons are selectively vulnerable to AMPA/kainate receptor-mediated injury in vitro. *J. Neurosci.* 16, 4069–4079. doi: 10.1523/jneurosci.16-13-04069.1996

Castilho, R. F., Ward, M. W., and Nicholls, D. G. (1999). Oxidative stress, mitochondrial function, and acute glutamate excitotoxicity in cultured cerebellar granule cells. *J. Neurochem.* 72, 1394–1401. doi: 10.1046/j.1471-4159.1999.721394.x

Čepelak, I., Dodig, S., and Dodig, D. (2020). Ferroptosis: regulated cell death. *Arh. High. Rada Toksikol.* 71, 99–109. doi: 10.2478/aiht-2020-71-3366

Chamorro, Á., Dirnagl, U., Urra, X., and Planas, A. M. (2016). Neuroprotection in acute stroke: targeting excitotoxicity, oxidative and nitrosative stress, and inflammation. *Lancet Neurol.* 15, 869–881. doi: 10.1016/S1474-4422(16)00114-9

Cheah, J. H., Kim, S. F., Hester, L. D., Clancy, K. W., Patterson, S. E. 3rd, Papadopoulos, V., et al. (2006). NMDA receptor-nitric oxide transmission mediates neuronal iron homeostasis via the GTPase Dexras1. *Neuron* 51, 431–440. doi: 10.1016/j.neuron.2006.07.011

Chen, G., Guo, G., Zhou, X., and Chen, H. (2020). Potential mechanism of ferroptosis in pancreatic cancer. *Oncol. Lett.* 19, 579–587. doi: 10.3892/ol.2019.11159

Chen, X., Kang, R., Kroemer, G., and Tang, D. (2021). Ferroptosis in infection, inflammation, and immunity. *J. Exp. Med.* 218:e20210518. doi: 10.1084/jem.20210518

Chen, M., Lu, T. J., Chen, X. J., Zhou, Y., Chen, Q., Feng, X. Y., et al. (2008). Differential roles of NMDA receptor subtypes in ischemic neuronal cell death and ischemic tolerance. *Stroke* 39, 3042–3048. doi: 10.1161/strokeaha.108.521898

Chen, X., Yu, C., Kang, R., and Tang, D. (2020). Iron metabolism in Ferroptosis. *Front. Cell Dev. Biol.* 8:590226. doi: 10.3389/fcell.2020.590226

Chen, Y. X., Zuliyaer, T., Liu, B., Guo, S., Yang, D. G., Gao, F., et al. (2022). Sodium selenite promotes neurological function recovery after spinal cord injury by inhibiting ferroptosis. *Neural Regen. Res.* 17, 2702–2709. doi: 10.4103/1673-5374.339491

Choi, D. W., Koh, J. Y., and Peters, S. (1988). Pharmacology of glutamate neurotoxicity in cortical cell culture: attenuation by NMDA antagonists. *J. Neurosci.* 8, 185–196. doi: 10.1523/jneurosci.08-01-00185.1988

Choi, S. K., Lee, G. J., Choi, S., Kim, Y. J., Park, H. K., and Park, B. J. (2011). Neuroprotective effects by nimodipine treatment in the experimental global ischemic rat model: real time estimation of glutamate. *J. Kor. Neurosurg. Soc.* 49, 1–7. doi: 10.3340/jkns.2011.49.1.1

Clewett, D., Sakaki, M., Huang, R., Nielsen, S. E., and Mather, M. (2017). Arousal amplifies biased competition between high and low priority memories more in women than in men: the role of elevated noradrenergic activity. *Psychoneuroendocrinology* 80, 80–91. doi: 10.1016/j.psyneuen.2017.02.022

Connolly, N. M., D'Orsi, B., Monsefi, N., Huber, H. J., and Prehn, J. H. (2016). Computational analysis of AMPK-mediated Neuroprotection suggests acute Excitotoxic bioenergetics and glucose dynamics are regulated by a minimal set of critical reactions. *PLoS One* 11:e0148326. doi: 10.1371/journal.pone.0148326

Cui, H., Hayashi, A., Sun, H. S., Belmares, M. P., Cobey, C., Phan, T., et al. (2007). PDZ protein interactions underlying NMDA receptor-mediated excitotoxicity and neuroprotection by PSD-95 inhibitors. *J. Neurosci.* 27, 9901–9915. doi: 10.1523/jneurosci.1464-07.2007

Dai, E., Meng, L., Kang, R., Wang, X., and Tang, D. (2020). ESCRT-III-dependent membrane repair blocks ferroptosis. *Biochem. Biophys. Res. Commun.* 522, 415–421. doi: 10.1016/j.bbrc.2019.11.110

Danbolt, N. C. (2001). Glutamate uptake. *Prog. Neurobiol.* 65, 1–105. doi: 10.1016/s0301-0082(00)00067-8

DeGregorio-Rocasolano, N., Martí-Sistac, O., and Gasull, T. (2019). Deciphering the iron side of stroke: neurodegeneration at the crossroads between iron Dyshomeostasis, Excitotoxicity, and Ferroptosis. *Front. Neurosci.* 13:85. doi: 10.3389/fnins.2019.00085

Dingledine, R., Borges, K., Bowie, D., and Traynelis, S. F. (1999). The glutamate receptor ion channels. *Pharmacol. Rev.* 51, 7–61.

Dirnagl, U., Iadecola, C., and Moskowitz, M. A. (1999). Pathobiology of ischaemic stroke: an integrated view. *Trends Neurosci.* 22, 391–397. doi: 10.1016/s0166-2236(99)01401-0

Dixon, S. J., Lemberg, K. M., Lamprecht, M. R., Skouta, R., Zaitsev, E. M., Gleason, C. E., et al. (2012). Ferroptosis: an iron-dependent form of nonapoptotic cell death. *Cells* 149, 1060–1072. doi: 10.1016/j.cell.2012.03.042

Doll, S., Freitas, F. P., Shah, R., Aldrovandi, M., da Silva, M. C., Ingold, I., et al. (2019). FSP1 is a glutathione-independent ferroptosis suppressor. *Nature* 575, 693–698. doi: 10.1038/s41586-019-1707-0

Doll, S., Proneth, B., Tyurina, Y. Y., Panzilius, E., Kobayashi, S., Ingold, I., et al. (2017). ACSL4 dictates ferroptosis sensitivity by shaping cellular lipid composition. *Nat. Chem. Biol.* 13, 91–98. doi: 10.1038/nchembio.2239

Dolma, S., Lessnick, S. L., Hahn, W. C., and Stockwell, B. R. (2003). Identification of genotype-selective antitumor agents using synthetic lethal chemical screening in engineered human tumor cells. *Cancer Cell* 3, 285–296. doi: 10.1016/s1535-6108(03)00050-3

Eliasson, M. J., Huang, Z., Ferrante, R. J., Sasamata, M., Molliver, M. E., Snyder, S. H., et al. (1999). Neuronal nitric oxide synthase activation and peroxynitrite formation in ischemic stroke linked to neural damage. *J. Neurosci.* 19, 5910–5918. doi: 10.1523/jneurosci.19-14-05910.1999

Emberson, J., Lees, K. R., Lyden, P., Blackwell, L., Albers, G., Bluhmki, E., et al. (2014). Effect of treatment delay, age, and stroke severity on the effects of intravenous thrombolysis with alteplase for acute ischaemic stroke: a meta-analysis of individual patient data from randomised trials. *Lancet* 384, 1929–1935. doi: 10.1016/S0140-6736(14)60584-5

Engler-Chiurazzi, E. B., Brown, C. M., Povroznik, J. M., and Simpkins, J. W. (2017). Estrogens as neuroprotectants: estrogenic actions in the context of cognitive aging and brain injury. *Prog. Neurobiol.* 157, 188–211. doi: 10.1016/j.pneurobio.2015.12.008

Fan, Z., Wirth, A. K., Chen, D., Wruck, C. J., Rauh, M., Buchfelder, M., et al. (2017). Nrf2-Keap1 pathway promotes cell proliferation and diminishes ferroptosis. *Oncogene* 6:e371. doi: 10.1038/oncsis.2017.65

Fang, W., Zhai, X., Han, D., Xiong, X., Wang, T., Zeng, X., et al. (2018). CCR2-dependent monocytes/macrophages exacerbate acute brain injury but promote functional recovery after ischemic stroke in mice. *Theranostics* 8, 3530–3543. doi: 10.7150/thno.24475

Fedorovich, S. V., and Waseem, T. V. (2022). The role of GRP81 lactate receptor in synaptic transmission regulation: does it enhance endocytosis? *Neural Regen. Res.* 17, 2657–2658. doi: 10.4103/1673-5374.335819

Feigin, V. L., Forouzanfar, M. H., Krishnamurthi, R., Mensah, G. A., Connor, M., Bennett, D. A., et al. (2014). Global and regional burden of stroke during 1990-2010: findings from the global burden of disease study 2010. *Lancet* 383, 245–254. doi: 10.1016/s0140-6736(13)61953-4

Ferraguti, F., and Shigemoto, R. (2006). Metabotropic glutamate receptors. *Cell Tissue Res.* 326, 483–504. doi: 10.1007/s00441-006-0266-5

Ferraz-Bannitz, R., Welendorf, C. R., Coelho, P. O., Salgado, W. Jr., Nonino, C. B., Beraldo, R. A., et al. (2021). Bariatric surgery can acutely modulate ER-stress and inflammation on subcutaneous adipose tissue in non-diabetic patients with obesity. *Diabetol. Metab. Syndr.* 13:19. doi: 10.1186/s13098-021-00623-w

Fidalgo, M., Ricardo Pires, J., Viseu, I., Magalhães, P., Gregório, H., Afreixo, V., et al. (2022). Edaravone for acute ischemic stroke—systematic review with meta-analysis. *Clin. Neurol. Neurosurg.* 219:107299. doi: 10.1016/j.clineuro.2022.107299

Forder, J. P., and Tymianski, M. (2009). Postsynaptic mechanisms of excitotoxicity: involvement of postsynaptic density proteins, radicals, and oxidant molecules. *Neuroscience* 158, 293–300. doi: 10.1016/j.neuroscience.2008.10.021

Friedmann Angeli, J. P., Schneider, M., Proneth, B., Tyurina, Y. Y., Tyurin, V. A., Hammond, V. J., et al. (2014). Inactivation of the ferroptosis regulator Gpx4 triggers acute renal failure in mice. *Nat. Cell Biol.* 16, 1180–1191. doi: 10.1038/ncb3064

Fujimura, M., Morita-Fujimura, Y., Murakami, K., Kawase, M., and Chan, P. H. (1998). Cytosolic redistribution of cytochrome c after transient focal cerebral ischemia in rats. *J. Cereb. Blood Flow Metab.* 18, 1239–1247. doi: 10.1097/00004647-199811000-00010

Fukuta, T., Asai, T., Yanagida, Y., Namba, M., Koide, H., Shimizu, K., et al. (2017). Combination therapy with liposomal neuroprotectants and tissue plasminogen activator for treatment of ischemic stroke. *FASEB J.* 31, 1879–1890. doi: 10.1096/fj.201601209R

Galluzzi, L., Vitale, I., Aaronson, S. A., Abrams, J. M., Adam, D., Agostinis, P., et al. (2018). Molecular mechanisms of cell death: recommendations of the nomenclature committee on cell death 2018. *Cell Death Differ.* 25, 486–541. doi: 10.1038/s41418-017-0012-4

Gan, B. (2019). DUBbing Ferroptosis in cancer cells. *Cancer Res.* 79, 1749–1750. doi: 10.1158/0008-5472.Can-19-0487

Gao, J., Liu, J., Yao, M., Zhang, W., Yang, B., and Wang, G. (2022). Panax notoginseng Saponins stimulates neurogenesis and neurological restoration after microsphere-induced cerebral embolism in rats partially via mTOR signaling. *Front. Pharmacol.* 13:889404. doi: 10.3389/fphar.2022.889404

Gao, M., Yi, J., Zhu, J., Minikes, A. M., Monian, P., Thompson, C. B., et al. (2019). Role of mitochondria in Ferroptosis. *Mol. Cell* 73, 354–363.e353. doi: 10.1016/j.molcel.2018.10.042

Gao, Q., Yin, X. D., Zhang, F., Zhu, Y. Z., and Li, Z. L. (2022). The regulatory effects of traditional Chinese medicine on Ferroptosis. *Oxidative Med. Cell. Longev.* 2022:4578381. doi: 10.1155/2022/4578381

Garthwaite, G., Williams, G. D., and Garthwaite, J. (1992). Glutamate toxicity: An experimental and theoretical analysis. *Eur. J. Neurosci.* 4, 353–360. doi: 10.1111/j.1460-9568.1992.tb00882.x

Ghoddoussi, F., Galloway, M. P., Jambekar, A., Bame, M., Needleman, R., and Brusilow, W. S. (2010). Methionine sulfoximine, an inhibitor of glutamine synthetase, lowers brain glutamine and glutamate in a mouse model of ALS. *J. Neurol. Sci.* 290, 41–47. doi: 10.1016/j.jns.2009.11.013

Glotfelty, E. J., Delgado, T., Tovar, Y. R. L. B., Luo, Y., Hoffer, B., Olson, L., et al. (2019). Incretin Mimetics as rational candidates for the treatment of traumatic brain injury. *ACS Pharmacol. Transl. Sci.* 2, 66–91. doi: 10.1021/acsptsci.9b00003

Godino Mdel, C., Romera, V. G., Sánchez-Tomero, J. A., Pacheco, J., Canals, S., Lerma, J., et al. (2013). Amelioration of ischemic brain damage by peritoneal dialysis. *J. Clin. Invest.* 123, 4359–4363. doi: 10.1172/jci67284

Goodman, J. M. (2019). LDAF1 holds the key to Seipin function. *Dev. Cell* 51, 544–545. doi: 10.1016/j.devcel.2019.11.009

Graham, C. E., Basappa, J., Turcan, S., and Vetter, D. E. (2011). The cochlear CRF signaling systems and their mechanisms of action in modulating cochlear sensitivity and protection against trauma. *Mol. Neurobiol.* 44, 383–406. doi: 10.1007/s12035-011-8203-3

Griendling, K. K., Camargo, L. L., Rios, F. J., Alves-Lopes, R., Montezano, A. C., and Touyz, R. M. (2021). Oxidative stress and hypertension. *Circ. Res.* 128, 993–1020. doi: 10.1161/circresaha.121.318063

Guo, L., and Cordeiro, M. F. (2008). Assessment of neuroprotection in the retina with DARC. *Prog. Brain Res.* 173, 437–450. doi: 10.1016/s0079-6123(08)01130-8

Guo, Y., Yang, X., Hakuna, L., Barve, A., Escobedo, J. O., Lowry, M., et al. (2012). A fast response highly selective probe for the detection of glutathione in human blood plasma. *Sensors* 12, 5940–5950. doi: 10.3390/s120505940

Han, C., Liu, Y., Dai, R., Ismail, N., Su, W., and Li, B. (2020). Ferroptosis and its potential role in human diseases. *Front. Pharmacol.* 11:239. doi: 10.3389/fphar.2020.00239

Harada, N., Kanayama, M., Maruyama, A., Yoshida, A., Tazumi, K., Hosoya, T., et al. (2011). Nrf2 regulates ferroportin 1-mediated iron efflux and counteracts lipopolysaccharide-induced ferroportin 1 mRNA suppression in macrophages. *Arch. Biochem. Biophys.* 508, 101–109. doi: 10.1016/j.abb.2011.02.001

Hardingham, G. E. (2009). Coupling of the NMDA receptor to neuroprotective and neurodestructive events. *Biochem. Soc. Trans.* 37, 1147–1160. doi: 10.1042/bst0371147

Hardingham, G. E., Fukunaga, Y., and Bading, H. (2002). Extrasynaptic NMDARs oppose synaptic NMDARs by triggering CREB shut-off and cell death pathways. *Nat. Neurosci.* 5, 405–414. doi: 10.1038/nn835

He, F., Blackberry, I., Yao, L., Xie, H., and Mnatzaganian, G. (2022). Geographical disparities in pooled stroke incidence and case fatality in mainland China, Hong Kong, and Macao: protocol for a systematic review and meta-analysis. *JMIR Res. Protoc.* 11:e32566. doi: 10.2196/32566

He, M., Zhang, B., Wei, X., Wang, Z., Fan, B., Du, P., et al. (2013). HDAC4/5-HMGB1 signalling mediated by NADPH oxidase activity contributes to cerebral ischaemia/reperfusion injury. *J. Cell. Mol. Med.* 17, 531–542. doi: 10.1111/jcmm.12040

He, Y., and Zhou, D. (2020). Can molecular targeting the TNFα-ERK-ETS1-IL27Rα pathway keep us young and healthy by protecting HSCs from aging? *Blood Sci.* 2, 148–149. doi: 10.1097/bs9.0000000000000060

Helal, G. K. (2008). Systemic administration of Zn2+ during the reperfusion phase of transient cerebral ischaemia protects rat hippocampus against iron-catalysed postischaemic injury. *Clin. Exp. Pharmacol. Physiol.* 35, 775–781. doi: 10.1111/j.1440-1681.2007.04858.x

Ho, K. C., Speier, W., Zhang, H., Scalzo, F., El-Saden, S., and Arnold, C. W. (2019). A machine learning approach for classifying ischemic stroke onset time from imaging. *IEEE Trans. Med. Imaging* 38, 1666–1676. doi: 10.1109/tmi.2019.2901445

Hong, M., Rong, J., Tao, X., and Xu, Y. (2022). The emerging role of Ferroptosis in cardiovascular diseases. *Front. Pharmacol.* 13:822083. doi: 10.3389/fphar.2022.822083

Hood, J. L., and Emeson, R. B. (2012). Editing of neurotransmitter receptor and ion channel RNAs in the nervous system. *Curr. Top. Microbiol. Immunol.* 353, 61–90. doi: 10.1007/82_2011_157

Hou, K., Shen, J., Yan, J., Zhai, C., Zhang, J., Pan, J. A., et al. (2021). Loss of TRIM21 alleviates cardiotoxicity by suppressing ferroptosis induced by the chemotherapeutic agent doxorubicin. *EBioMedicine* 69:103456. doi: 10.1016/j.ebiom.2021.103456

Hu, X., Wang, Y., Du, W., Liang, L. J., Wang, W., and Jin, X. (2022). Role of glial cell-derived oxidative stress in blood-brain barrier damage after acute ischemic stroke. *Oxidative Med. Cell. Longev.* 2022:7762078. doi: 10.1155/2022/7762078

Hwang, E. K., and Lupica, C. R. (2020). Altered Corticolimbic control of the nucleus Accumbens by long-term Δ (9)-tetrahydrocannabinol exposure. *Biol. Psychiatry* 87, 619–631. doi: 10.1016/j.biopsych.2019.07.024

Ji, X., Tian, L., Yao, S., Han, F., Niu, S., and Qu, C. (2022). A systematic review of body fluids biomarkers associated with early neurological deterioration following acute ischemic stroke. *Front. Aging Neurosci.* 14:918473. doi: 10.3389/fnagi.2022.918473

Jiang, L., Kon, N., Li, T., Wang, S. J., Su, T., Hibshoosh, H., et al. (2015). Ferroptosis as a p53-mediated activity during tumour suppression. *Nature* 520, 57–62. doi: 10.1038/nature14344

Jiang, M., Qiao, M., Zhao, C., Deng, J., Li, X., and Zhou, C. (2020). Targeting ferroptosis for cancer therapy: exploring novel strategies from its mechanisms and role in cancers. *Transl. Lung Cancer Res.* 9, 1569–1584. doi: 10.21037/tlcr-20-341

Jiang, W., Song, J., Zhang, S., Ye, Y., Wang, J., and Zhang, Y. (2021). CTRP13 protects H9c2 cells against hypoxia/Reoxygenation (H/R)-induced injury via regulating the AMPK/Nrf2/ARE signaling pathway. *Cell Transplant.* 30:9636897211033275. doi: 10.1177/09636897211033275

Jiang, T., Yu, J. T., Zhu, X. C., Wang, H. F., Tan, M. S., Cao, L., et al. (2014). Acute metformin preconditioning confers neuroprotection against focal cerebral ischaemia by pre-activation of AMPK-dependent autophagy. *Br. J. Pharmacol.* 171, 3146–3157. doi: 10.1111/bph.12655

Kagami, T., Yamade, M., Suzuki, T., Uotani, T., Tani, S., Hamaya, Y., et al. (2018). High expression level of CD44v8-10 in cancer stem-like cells is associated with poor prognosis in esophageal squamous cell carcinoma patients treated with chemoradiotherapy. *Oncotarget* 9, 34876–34888. doi: 10.18632/oncotarget.26172

Kasuya, A., Sakabe, J., and Tokura, Y. (2014). Potential application of in vivo imaging of impaired lymphatic duct to evaluate the severity of pressure ulcer in mouse model. *Sci. Rep.* 4:4173. doi: 10.1038/srep04173

Katayama, N., Yamamori, S., Fukaya, M., Kobayashi, S., Watanabe, M., Takahashi, M., et al. (2017). SNAP-25 phosphorylation at Ser187 regulates synaptic facilitation and short-term plasticity in an age-dependent manner. *Sci. Rep.* 7:7996. doi: 10.1038/s41598-017-08237-x

Kennedy, M. B. (1997). The postsynaptic density at glutamatergic synapses. *Trends Neurosci.* 20, 264–268. doi: 10.1016/s0166-2236(96)01033-8

Kerins, M. J., and Ooi, A. (2018). The roles of NRF2 in modulating cellular iron homeostasis. *Antioxid. Redox Signal.* 29, 1756–1773. doi: 10.1089/ars.2017.7176

Kevdzija, M., Bozovic-Stamenovic, R., and Marquardt, G. (2022). Stroke Patients' free-time activities and spatial preferences during inpatient recovery in rehabilitation centers. *HERD* 15, 96–113. doi: 10.1177/19375867221113054

Kim, A. H., Khursigara, G., Sun, X., Franke, T. F., and Chao, M. V. (2001). Akt phosphorylates and negatively regulates apoptosis signal-regulating kinase 1. *Mol. Cell. Biol.* 21, 893–901. doi: 10.1128/mcb.21.3.893-901.2001

Köhr, G. (2006). NMDA receptor function: subunit composition versus spatial distribution. *Cell Tissue Res.* 326, 439–446. doi: 10.1007/s00441-006-0273-6

Köhr, G., Melcher, T., and Seeburg, P. H. (1998). Candidate editases for GluR channels in single neurons of rat hippocampus and cerebellum. *Neuropharmacology* 37, 1411–1417. doi: 10.1016/s0028-3908(98)00149-x

Koppula, P., Olszewski, K., Zhang, Y., Kondiparthi, L., Liu, X., Lei, G., et al. (2021a). KEAP1 deficiency drives glucose dependency and sensitizes lung cancer cells and tumors to GLUT inhibition. *iScience* 24:102649. doi: 10.1016/j.isci.2021.102649

Koppula, P., Zhang, Y., Zhuang, L., and Gan, B. (2018). Amino acid transporter SLC7A11/xCT at the crossroads of regulating redox homeostasis and nutrient dependency of cancer. *Cancer Commun.* 38:12. doi: 10.1186/s40880-018-0288-x

Koppula, P., Zhuang, L., and Gan, B. (2021b). Cystine transporter SLC7A11/xCT in cancer: ferroptosis, nutrient dependency, and cancer therapy. *Protein Cell* 12, 599–620. doi: 10.1007/s13238-020-00789-5

Krasil'nikova, I., Surin, A., Sorokina, E., Fisenko, A., Boyarkin, D., Balyasin, M., et al. (2019). Insulin protects cortical neurons against glutamate Excitotoxicity. *Front. Neurosci.* 13:1027. doi: 10.3389/fnins.2019.01027

Kristián, T., and Siesjö, B. K. (1998). Calcium in ischemic cell death. *Stroke* 29, 705–718. doi: 10.1161/01.str.29.3.705

Kuo, T. T., Lin, L. C., Chang, H. Y., Chiang, P. J., Wu, H. Y., Chen, T. Y., et al. (2022). Quantitative proteome analysis reveals Melissa officinalis extract targets mitochondrial respiration in colon cancer cells. *Molecules* 27:4533. doi: 10.3390/molecules27144533

Kwak, M. K., Itoh, K., Yamamoto, M., and Kensler, T. W. (2002). Enhanced expression of the transcription factor Nrf2 by cancer chemopreventive agents: role of antioxidant response element-like sequences in the nrf2 promoter. *Mol. Cell. Biol.* 22, 2883–2892. doi: 10.1128/mcb.22.9.2883-2892.2002

Lai, P. C., Huang, Y. T., Wu, C. C., Lai, C. J., Wang, P. J., and Chiu, T. H. (2011). Ceftriaxone attenuates hypoxic-ischemic brain injury in neonatal rats. *J. Biomed. Sci.* 18:69. doi: 10.1186/1423-0127-18-69

Lau, A., and Tymianski, M. (2010). Glutamate receptors, neurotoxicity and neurodegeneration. *Pflugers Arch.* 460, 525–542. doi: 10.1007/s00424-010-0809-1

Lee, H., Zandkarimi, F., Zhang, Y., Meena, J. K., Kim, J., Zhuang, L., et al. (2020). Energy-stress-mediated AMPK activation inhibits ferroptosis. *Nat. Cell Biol.* 22, 225–234. doi: 10.1038/s41556-020-0461-8

Leiva-Salinas, C., Patrie, J. T., Xin, W., Michel, P., Jovin, T., and Wintermark, M. (2016). Prediction of early arterial recanalization and tissue fate in the selection of patients with the greatest potential to benefit from intravenous tissue-type plasminogen activator. *Stroke* 47, 397–403. doi: 10.1161/STROKEAHA.115.011066

Li, J., Cao, F., Yin, H. L., Huang, Z. J., Lin, Z. T., Mao, N., et al. (2020). Ferroptosis: past, present and future. *Cell Death Dis.* 11:88. doi: 10.1038/s41419-020-2298-2

Li, C., Zhang, Y., Liu, J., Kang, R., Klionsky, D. J., and Tang, D. (2021). Mitochondrial DNA stress triggers autophagy-dependent ferroptotic death. *Autophagy* 17, 948–960. doi: 10.1080/15548627.2020.1739447

Liang, C. Q., Zhang, G., Zhang, L., Chen, S. Y., Wang, J. N., Zhang, T. T., et al. (2021). Calmodulin Bidirectionally regulates evoked and spontaneous neurotransmitter release at retinal ribbon synapses. *eNeuro* 8:ENEURO.0257-20.2020. doi: 10.1523/eneuro.0257-20.2020

Liao, W. T., Liu, J., Zhou, S. M., Xu, G., Gao, Y. Q., and Liu, W. Y. (2018). UHPLC-QTOFMS-based Metabolomic analysis of the hippocampus in hypoxia preconditioned mouse. *Front. Physiol.* 9:1950. doi: 10.3389/fphys.2018.01950

Lin, C. H., Chen, P. S., and Gean, P. W. (2008). Glutamate preconditioning prevents neuronal death induced by combined oxygen-glucose deprivation in cultured cortical neurons. *Eur. J. Pharmacol.* 589, 85–93. doi: 10.1016/j.ejphar.2008.05.047

Lin, T. Y., Lu, C. W., and Wang, S. J. (2009). Inhibitory effect of glutamate release from rat cerebrocortical synaptosomes by dextromethorphan and its metabolite 3-hydroxymorphinan. *Neurochem. Int.* 54, 526–534. doi: 10.1016/j.neuint.2009.02.012

Lin, X., Wang, R., Zou, W., Sun, X., Liu, X., Zhao, L., et al. (2016). The influenza virus H5N1 infection can induce ROS production for viral replication and host cell death in A549 cells modulated by human cu/Zn superoxide dismutase (SOD1) overexpression. *Viruses* 8:13. doi: 10.3390/v8010013

Lin, L., Zhang, M. X., Zhang, L., Zhang, D., Li, C., and Li, Y. L. (2021). Autophagy, Pyroptosis, and Ferroptosis: new regulatory mechanisms for atherosclerosis. *Front. Cell Dev. Biol.* 9:809955. doi: 10.3389/fcell.2021.809955

Lipton, S. A., Choi, Y. B., Pan, Z. H., Lei, S. Z., Chen, H. S., Sucher, N. J., et al. (1993). A redox-based mechanism for the neuroprotective and neurodestructive effects of nitric oxide and related nitroso-compounds. *Nature* 364, 626–632. doi: 10.1038/364626a0

Liu, Y., Cao, X., He, C., Guo, X., Cai, H., Aierken, A., et al. (2022). Effects of Ferroptosis on male reproduction. *Int. J. Mol. Sci.* 23:7139. doi: 10.3390/ijms23137139

Liu, N., Lin, X., and Huang, C. (2020). Activation of the reverse transsulfuration pathway through NRF2/CBS confers erastin-induced ferroptosis resistance. *Br. J. Cancer* 122, 279–292. doi: 10.1038/s41416-019-0660-x

Liu, Y., Wong, T. P., Aarts, M., Rooyakkers, A., Liu, L., Lai, T. W., et al. (2007). NMDA receptor subunits have differential roles in mediating excitotoxic neuronal death both in vitro and in vivo. *J. Neurosci.* 27, 2846–2857. doi: 10.1523/jneurosci.0116-07.2007

Liu, Y., Zeng, L., Yang, Y., Chen, C., Wang, D., and Wang, H. (2020). Acyl-CoA thioesterase 1 prevents cardiomyocytes from doxorubicin-induced ferroptosis via shaping the lipid composition. *Cell Death Dis.* 11:756. doi: 10.1038/s41419-020-02948-2

Maher, P., van Leyen, K., Dey, P. N., Honrath, B., Dolga, A., and Methner, A. (2018). The role of ca(2+) in cell death caused by oxidative glutamate toxicity and ferroptosis. *Cell Calcium* 70, 47–55. doi: 10.1016/j.ceca.2017.05.007

Mahmoud, A. M., Yang, W., and Bosland, M. C. (2014). Soy isoflavones and prostate cancer: a review of molecular mechanisms. *J. Steroid Biochem. Mol. Biol.* 140, 116–132. doi: 10.1016/j.jsbmb.2013.12.010

Malysz-Cymborska, I., Golubczyk, D., Kalkowski, L., Kwiatkowska, J., Zawadzki, M., Głodek, J., et al. (2021). Intra-arterial transplantation of stem cells in large animals as a minimally-invasive strategy for the treatment of disseminated neurodegeneration. *Sci. Rep.* 11:6581. doi: 10.1038/s41598-021-85820-3

Mao, R., Zong, N., Hu, Y., Chen, Y., and Xu, Y. (2022). Neuronal death mechanisms and therapeutic strategy in ischemic stroke. *Neurosci. Bull.* 38, 1229–1247. doi: 10.1007/s12264-022-00859-0

Marcoli, M., Cervetto, C., Amato, S., Fiorucci, C., Maura, G., Mariottini, P., et al. (2022). Transgenic mouse overexpressing Spermine oxidase in Cerebrocortical neurons: astrocyte dysfunction and susceptibility to epileptic seizures. *Biomol. Ther.* 12:204. doi: 10.3390/biom12020204

Márquez, J., Tosina, M., de la Rosa, V., Segura, J. A., Alonso, F. J., Matés, J. M., et al. (2009). New insights into brain glutaminases: beyond their role on glutamatergic transmission. *Neurochem. Int.* 55, 64–70. doi: 10.1016/j.neuint.2009.02.022

Martínez-Coria, H., Arrieta-Cruz, I., Cruz, M.-E., and López-Valdés, H. E. (2021). Physiopathology of ischemic stroke and its modulation using memantine: evidence from preclinical stroke. *Neural Regen. Res.* 16, 433–439. doi: 10.4103/1673-5374.293129

McCaughey-Chapman, A., and Connor, B. (2022). Rat cortico-striatal sagittal organotypic slice cultures as ex vivo excitotoxic striatal lesion models. *Heliyon* 8:e10819. doi: 10.1016/j.heliyon.2022.e10819

Meng, X., Wang, M., Wang, X., Sun, G., Ye, J., Xu, H., et al. (2014). Suppression of NADPH oxidase- and mitochondrion-derived superoxide by Notoginsenoside R1 protects against cerebral ischemia-reperfusion injury through estrogen receptor-dependent activation of Akt/Nrf2 pathways. *Free Radic. Res.* 48, 823–838. doi: 10.3109/10715762.2014.911853

Munro, M. J., Wickremesekera, S. K., Tan, S. T., and Peng, L. (2022). Proteomic analysis of low- and high-grade human colon adenocarcinoma tissues and tissue-derived primary cell lines reveals unique biological functions of tumours and new protein biomarker candidates. *Clin. Proteomics* 19:27. doi: 10.1186/s12014-022-09364-y

Nakamura, E., Sato, M., Yang, H., Miyagawa, F., Harasaki, M., Tomita, K., et al. (1999). 4F2 (CD98) heavy chain is associated covalently with an amino acid transporter and controls intracellular trafficking and membrane topology of 4F2 heterodimer. *J. Biol. Chem.* 274, 3009–3016. doi: 10.1074/jbc.274.5.3009

Nie, Q., Hu, Y., Yu, X., Li, X., and Fang, X. (2022). Induction and application of ferroptosis in cancer therapy. *Cancer Cell Int.* 22:12. doi: 10.1186/s12935-021-02366-0

Nishimune, H., Badawi, Y., Mori, S., and Shigemoto, K. (2016). Dual-color STED microscopy reveals a sandwich structure of bassoon and piccolo in active zones of adult and aged mice. *Sci. Rep.* 6:27935. doi: 10.1038/srep27935

Noguchi, T., Suzuki, M., Mutoh, N., Hirata, Y., Tsuchida, M., Miyagawa, S., et al. (2018). Nuclear-accumulated SQSTM1/p62-based ALIS act as microdomains sensing cellular stresses and triggering oxidative stress-induced parthanatos. *Cell Death Dis.* 9:1193. doi: 10.1038/s41419-018-1245-y

Olive, M. F. (2009). Metabotropic glutamate receptor ligands as potential therapeutics for addiction. *Curr. Drug Abuse Rev.* 2, 83–98. doi: 10.2174/1874737109020100083

Onetti, Y., Dantas, A. P., Pérez, B., Cugota, R., Chamorro, A., Planas, A. M., et al. (2015). Middle cerebral artery remodeling following transient brain ischemia is linked to early postischemic hyperemia: a target of uric acid treatment. *Am. J. Physiol. Heart Circ. Physiol.* 308, H862–H874. doi: 10.1152/ajpheart.00001.2015

Ooi, S. L., Green, R., and Pak, S. C. (2018). N-Acetylcysteine for the treatment of psychiatric disorders: a review of current evidence. *Biomed. Res. Int.* 2018:2469486. doi: 10.1155/2018/2469486

Osen, K. K., Storm-Mathisen, J., Ottersen, O. P., and Dihle, B. (1995). Glutamate is concentrated in and released from parallel fiber terminals in the dorsal cochlear nucleus: a quantitative immunocytochemical analysis in Guinea pig. *J. Comp. Neurol.* 357, 482–500. doi: 10.1002/cne.903570311

Ottersen, O. P., Storm-Mathisen, J., Bramham, C., Torp, R., Laake, J., and Gundersen, V. (1990). A quantitative electron microscopic immunocytochemical study of the distribution and synaptic handling of glutamate in rat hippocampus. *Prog. Brain Res.* 83, 99–114. doi: 10.1016/s0079-6123(08)61244-3

Ottersen, O. P., Zhang, N., and Walberg, F. (1992). Metabolic compartmentation of glutamate and glutamine: morphological evidence obtained by quantitative immunocytochemistry in rat cerebellum. *Neuroscience* 46, 519–534. doi: 10.1016/0306-4522(92)90141-n

Ovbiagele, B., Kidwell, C. S., Starkman, S., and Saver, J. L. (2003). Neuroprotective agents for the treatment of acute ischemic stroke. *Curr. Neurol. Neurosci. Rep.* 3, 9–20. doi: 10.1007/s11910-003-0031-z

Özel, R. E., Ispas, C., Ganesana, M., Leiter, J. C., and Andreescu, S. (2014). Glutamate oxidase biosensor based on mixed ceria and titania nanoparticles for the detection of glutamate in hypoxic environments. *Biosens. Bioelectron.* 52, 397–402. doi: 10.1016/j.bios.2013.08.054

Pakos-Zebrucka, K., Koryga, I., Mnich, K., Ljujic, M., Samali, A., and Gorman, A. M. (2016). The integrated stress response. *EMBO Rep.* 17, 1374–1395. doi: 10.15252/embr.201642195

Papadia, S., and Hardingham, G. E. (2007). The dichotomy of NMDA receptor signaling. *Neuroscientist* 13, 572–579. doi: 10.1177/1073858407013006040l

Pathak, S. S., Liu, D., Li, T., de Zavalia, N., Zhu, L., Li, J., et al. (2019). The eIF2α kinase GCN2 modulates period and rhythmicity of the circadian clock by translational control of Atf4. *Neuron* 104, 724–735. doi: 10.1016/j.neuron.2019.08.007

Pchitskaya, E., Popugaeva, E., and Bezprozvanny, I. (2018). Calcium signaling and molecular mechanisms underlying neurodegenerative diseases. *Cell Calcium* 70, 87–94. doi: 10.1016/j.ceca.2017.06.008

Pietrancosta, N., Djibo, M., Daumas, S., El Mestikawy, S., and Erickson, J. D. (2020). Molecular, structural, functional, and pharmacological sites for vesicular glutamate transporter regulation. *Mol. Neurobiol.* 57, 3118–3142. doi: 10.1007/s12035-020-01912-7

Pin, J. P., and Duvoisin, R. (1995). The metabotropic glutamate receptors: structure and functions. *Neuropharmacology* 34, 1–26. doi: 10.1016/0028-3908(94)00129-g

Protchenko, O., Baratz, E., Jadhav, S., Li, F., Shakoury-Elizeh, M., Gavrilova, O., et al. (2021). Iron chaperone poly rC binding protein 1 protects mouse liver from lipid peroxidation and Steatosis. *Hepatology* 73, 1176–1193. doi: 10.1002/hep.31328

Qin, Y., Qiao, Y., Wang, D., Tang, C., and Yan, G. (2021). Ferritinophagy and ferroptosis in cardiovascular disease: mechanisms and potential applications. *Biomed. Pharmacother.* 141:111872. doi: 10.1016/j.biopha.2021.111872

Qin, C., Yang, S., Chu, Y.-H., Zhang, H., Pang, X.-W., Chen, L., et al. (2022). Signaling pathways involved in ischemic stroke: molecular mechanisms and therapeutic interventions. *Signal Transduct. Target. Ther.* 7:215. doi: 10.1038/s41392-022-01064-1

Randall, R. D., and Thayer, S. A. (1992). Glutamate-induced calcium transient triggers delayed calcium overload and neurotoxicity in rat hippocampal neurons. *J. Neurosci.* 12, 1882–1895. doi: 10.1523/jneurosci.12-05-01882.1992

Ratan, R. R. (2020). The chemical biology of Ferroptosis in the central nervous system. *Cell Chem. Biol.* 27, 479–498. doi: 10.1016/j.chembiol.2020.03.007

Raza, A., Xie, W., Kim, K. H., Dronamraju, V. R., Williams, J., Vince, R., et al. (2022). Dipeptide of ψ-GSH inhibits oxidative stress and Neuroinflammation in an Alzheimer's disease mouse model. *Antioxidants* 11:1075. doi: 10.3390/antiox11061075

Rebas, E., Rzajew, J., Radzik, T., and Zylinska, L. (2020). Neuroprotective polyphenols: a modulatory action on neurotransmitter pathways. *Curr. Neuropharmacol.* 18, 431–445. doi: 10.2174/1570159x18666200106155127

Riveros, N., Fiedler, J., Lagos, N., Muñoz, C., and Orrego, F. (1986). Glutamate in rat brain cortex synaptic vesicles: influence of the vesicle isolation procedure. *Brain Res.* 386, 405–408. doi: 10.1016/0006-8993(86)90181-2

Rocha-Ferreira, E., and Hristova, M. (2016). Plasticity in the neonatal brain following hypoxic-Ischaemic injury. *Neural Plast.* 2016:4901014. doi: 10.1155/2016/4901014

Roh, J. L., Kim, E. H., Jang, H., and Shin, D. (2017). Nrf2 inhibition reverses the resistance of cisplatin-resistant head and neck cancer cells to artesunate-induced ferroptosis. *Redox Biol.* 11, 254–262. doi: 10.1016/j.redox.2016.12.010

Romanos, E., Planas, A. M., Amaro, S., and Chamorro, A. (2007). Uric acid reduces brain damage and improves the benefits of rt-PA in a rat model of thromboembolic stroke. *J. Cereb. Blood Flow Metab.* 27, 14–20. doi: 10.1038/sj.jcbfm.9600312

Sanz-Morello, B., Ahmadi, H., Vohra, R., Saruhanian, S., Freude, K. K., Hamann, S., et al. (2021). Oxidative stress in optic neuropathies. *Antioxidants* 10:1538. doi: 10.3390/antiox10101538

Sasaki, H., Sato, H., Kuriyama-Matsumura, K., Sato, K., Maebara, K., Wang, H., et al. (2002). Electrophile response element-mediated induction of the cystine/glutamate exchange transporter gene expression. *J. Biol. Chem.* 277, 44765–44771. doi: 10.1074/jbc.M208704200

Sato, H., Tamba, M., Ishii, T., and Bannai, S. (1999). Cloning and expression of a plasma membrane cystine/glutamate exchange transporter composed of two distinct proteins. *J. Biol. Chem.* 274, 11455–11458. doi: 10.1074/jbc.274.17.11455

Sazonova, M. A., Sinyov, V. V., Ryzhkova, A. I., Sazonova, M. D., Kirichenko, T. V., Khotina, V. A., et al. (2021). Some molecular and cellular stress mechanisms associated with neurodegenerative diseases and atherosclerosis. *Int. J. Mol. Sci.* 22:699. doi: 10.3390/ijms22020699

Scalise, M., Console, L., Rovella, F., Galluccio, M., Pochini, L., and Indiveri, C. (2020). Membrane transporters for amino acids as players of cancer metabolic rewiring. *Cells* 9:2028. doi: 10.3390/cells9092028

She, X., Lan, B., Tian, H., and Tang, B. (2020). Cross talk between Ferroptosis and cerebral ischemia. *Front. Neurosci.* 14:776. doi: 10.3389/fnins.2020.00776

Shen, S., Ji, C., and Wei, K. (2022). Cellular senescence and regulated cell death of tubular epithelial cells in diabetic kidney disease. *Front. Endocrinol.* 13:924299. doi: 10.3389/fendo.2022.924299

Sheng, M., and Hoogenraad, C. C. (2007). The postsynaptic architecture of excitatory synapses: a more quantitative view. *Annu. Rev. Biochem.* 76, 823–847. doi: 10.1146/annurev.biochem.76.060805.160029

Shi, J., Tang, M., Zhou, S., Xu, D., Zhao, J., Wu, C., et al. (2021). Programmed cell death pathways in the pathogenesis of idiopathic inflammatory myopathies. *Front. Immunol.* 12:783616. doi: 10.3389/fimmu.2021.783616

Shi, Z., Zhu, L., Li, T., Tang, X., Xiang, Y., Han, X., et al. (2017). Neuroprotective mechanisms of Lycium barbarum polysaccharides against ischemic insults by regulating NR2B and NR2A containing NMDA receptor signaling pathways. *Front. Cell. Neurosci.* 11:288. doi: 10.3389/fncel.2017.00288

Shih, A. Y., Johnson, D. A., Wong, G., Kraft, A. D., Jiang, L., Erb, H., et al. (2003). Coordinate regulation of glutathione biosynthesis and release by Nrf2-expressing glia potently protects neurons from oxidative stress. *J. Neurosci.* 23, 3394–3406. doi: 10.1523/jneurosci.23-08-03394.2003

Shin, C. S., Mishra, P., Watrous, J. D., Carelli, V., D'Aurelio, M., Jain, M., et al. (2017). The glutamate/cystine xCT antiporter antagonizes glutamine metabolism and reduces nutrient flexibility. *Nat. Commun.* 8:15074. doi: 10.1038/ncomms15074

Shupliakov, O., Brodin, L., Cullheim, S., Ottersen, O. P., and Storm-Mathisen, J. (1992). Immunogold quantification of glutamate in two types of excitatory synapse with different firing patterns. *J. Neurosci.* 12, 3789–3803. doi: 10.1523/jneurosci.12-10-03789.1992

Squadrito, G. L., Cueto, R., Splenser, A. E., Valavanidis, A., Zhang, H., Uppu, R. M., et al. (2000). Reaction of uric acid with peroxynitrite and implications for the mechanism of neuroprotection by uric acid. *Arch. Biochem. Biophys.* 376, 333–337. doi: 10.1006/abbi.2000.1721

Stout, A. K., Raphael, H. M., Kanterewicz, B. I., Klann, E., and Reynolds, I. J. (1998). Glutamate-induced neuron death requires mitochondrial calcium uptake. *Nat. Neurosci.* 1, 366–373. doi: 10.1038/1577

Sturm, J. W., Dewey, H. M., Donnan, G. A., Macdonell, R. A. L., McNeil, J. J., and Thrift, A. G. (2002). Handicap after stroke: how does it relate to disability, perception of recovery, and stroke subtype?: the north north East Melbourne stroke incidence study (NEMESIS). *Stroke* 33, 762–768. doi: 10.1161/hs0302.103815

Sun, X., Ou, Z., Chen, R., Niu, X., Chen, D., Kang, R., et al. (2016). Activation of the p62-Keap1-NRF2 pathway protects against ferroptosis in hepatocellular carcinoma cells. *Hepatology* 63, 173–184. doi: 10.1002/hep.28251

Sun, X., Ou, Z., Xie, M., Kang, R., Fan, Y., Niu, X., et al. (2015). HSPB1 as a novel regulator of ferroptotic cancer cell death. *Oncogene* 34, 5617–5625. doi: 10.1038/onc.2015.32

Takahashi, T. (2019). Novel synaptic plasticity enhancer drug to augment functional recovery with rehabilitation. *Curr. Opin. Neurol.* 32, 822–827. doi: 10.1097/wco.0000000000000748

Takamori, S. (2006). VGLUTs: 'exciting' times for glutamatergic research? *Neurosci. Res.* 55, 343–351. doi: 10.1016/j.neures.2006.04.016

Takamori, S., Rhee, J. S., Rosenmund, C., and Jahn, R. (2000). Identification of a vesicular glutamate transporter that defines a glutamatergic phenotype in neurons. *Nature* 407, 189–194. doi: 10.1038/35025070

Tan, S., Schubert, D., and Maher, P. (2001). Oxytosis: a novel form of programmed cell death. *Curr. Top. Med. Chem.* 1, 497–506. doi: 10.2174/1568026013394741

Tang, D., Chen, X., Kang, R., and Kroemer, G. (2021). Ferroptosis: molecular mechanisms and health implications. *Cell Res.* 31, 107–125. doi: 10.1038/s41422-020-00441-1

Tang, Z., Huang, Z., Huang, Y., Chen, Y., Huang, M., Liu, H., et al. (2021). Ferroptosis: the silver lining of cancer therapy. *Front. Cell Dev. Biol.* 9:765859. doi: 10.3389/fcell.2021.765859

Teng, L., Lei, H. M., Sun, F., An, S. M., Tang, Y. B., Meng, S., et al. (2016). Autocrine glutamatergic transmission for the regulation of embryonal carcinoma stem cells. *Oncotarget* 7, 49552–49564. doi: 10.18632/oncotarget.9973

Terauchi, A., and Umemori, H. (2012). Specific sets of intrinsic and extrinsic factors drive excitatory and inhibitory circuit formation. *Neuroscientist* 18, 271–286. doi: 10.1177/1073858411404228

Thomazi, R., Silveira, L. V. A., Boas, P., and Jacinto, A. F. (2018). Frequency of dementia among elderly admitted to a geriatrics inpatients sector of a Brazilian public hospital. *Dement. Neuropsychol.* 12, 35–39. doi: 10.1590/1980-57642018dn12-010005

Tsao, C. W., Aday, A. W., Almarzooq, Z. I., Alonso, A., Beaton, A. Z., Bittencourt, M. S., et al. (2022). Heart disease and stroke Statistics-2022 update: a report from the American Heart Association. *Circulation* 145, e153–e639. doi: 10.1161/CIR.0000000000001052

Tukker, A. M., and Westerink, R. H. S. (2021). Novel test strategies for in vitro seizure liability assessment. *Expert Opin. Drug Metab. Toxicol.* 17, 923–936. doi: 10.1080/17425255.2021.1876026

Tymianski, M., Charlton, M. P., Carlen, P. L., and Tator, C. H. (1993). Secondary Ca2+ overload indicates early neuronal injury which precedes staining with viability indicators. *Brain Res.* 607, 319–323. doi: 10.1016/0006-8993(93)91523-u

Valdinocci, D., Simões, R. F., Kovarova, J., Cunha-Oliveira, T., Neuzil, J., and Pountney, D. L. (2019). Intracellular and intercellular mitochondrial dynamics in Parkinson's disease. *Front. Neurosci.* 13:930. doi: 10.3389/fnins.2019.00930

Vanden Berghe, T., Linkermann, A., Jouan-Lanhouet, S., Walczak, H., and Vandenabeele, P. (2014). Regulated necrosis: the expanding network of non-apoptotic cell death pathways. *Nat. Rev. Mol. Cell Biol.* 15, 135–147. doi: 10.1038/nrm3737

Viejo, L., Rubio-Alarcón, M., Arribas, R. L., Moreno-Castro, M., Pérez-Marín, R., Braun-Cornejo, M., et al. (2021). Synthesis and biological assessment of 4,1-Benzothiazepines with Neuroprotective activity on the ca(2+) overload for the treatment of neurodegenerative diseases and stroke. *Molecules* 26:4473. doi: 10.3390/molecules26154473

Wakil, S. J., and Abu-Elheiga, L. A. (2009). Fatty acid metabolism: target for metabolic syndrome. *J. Lipid Res.* 50, S138–S143. doi: 10.1194/jlr.R800079-JLR200

Wang, W., Jiang, B., Sun, H., Ru, X., Sun, D., Wang, L., et al. (2017). Prevalence, incidence, and mortality of stroke in China: results from a Nationwide population-based survey of 480 687 adults. *Circulation* 135, 759–771. doi: 10.1161/CIRCULATIONAHA.116.025250

Wang, S., Liao, L., Wang, M., Zhou, H., Huang, Y., Wang, Z., et al. (2017). Pin1 promotes regulated necrosis induced by glutamate in rat retinal neurons via CAST/Calpain2 pathway. *Front. Cell. Neurosci.* 11:425. doi: 10.3389/fncel.2017.00425

Wang, L., Liu, Y., Du, T., Yang, H., Lei, L., Guo, M., et al. (2020). ATF3 promotes erastin-induced ferroptosis by suppressing system xc(). *Cell Death Differ.* 27, 662–675. doi: 10.1038/s41418-019-0380-z

Wang, K., Mei, S., Cai, M., Zhai, D., Zhang, D., Yu, J., et al. (2022). Ferroptosis-related long noncoding RNAs as prognostic biomarkers for ovarian cancer. *Front. Oncol.* 12:888699. doi: 10.3389/fonc.2022.888699

Wang, D., Tang, L., Zhang, Y., Ge, G., Jiang, X., Mo, Y., et al. (2022). Regulatory pathways and drugs associated with ferroptosis in tumors. *Cell Death Dis.* 13:544. doi: 10.1038/s41419-022-04927-1

Wang, Y., Tang, B., Zhu, J., Yu, J., Hui, J., Xia, S., et al. (2022). Emerging mechanisms and targeted therapy of Ferroptosis in neurological diseases and neuro-oncology. *Int. J. Biol. Sci.* 18, 4260–4274. doi: 10.7150/ijbs.72251

Ward, M. W., Rego, A. C., Frenguelli, B. G., and Nicholls, D. G. (2000). Mitochondrial membrane potential and glutamate excitotoxicity in cultured cerebellar granule cells. *J. Neurosci.* 20, 7208–7219. doi: 10.1523/jneurosci.20-19-07208.2000

Wei, X., Walia, V., Lin, J. C., Teer, J. K., Prickett, T. D., Gartner, J., et al. (2011). Exome sequencing identifies GRIN2A as frequently mutated in melanoma. *Nat. Genet.* 43, 442–446. doi: 10.1038/ng.810

White, R. J., and Reynolds, I. J. (1995). Mitochondria and Na+/Ca2+ exchange buffer glutamate-induced calcium loads in cultured cortical neurons. *J. Neurosci.* 15, 1318–1328. doi: 10.1523/jneurosci.15-02-01318.1995

White, R. J., and Reynolds, I. J. (1996). Mitochondrial depolarization in glutamate-stimulated neurons: an early signal specific to excitotoxin exposure. *J. Neurosci.* 16, 5688–5697. doi: 10.1523/jneurosci.16-18-05688.1996

Wu, Q. J., and Tymianski, M. (2018). Targeting NMDA receptors in stroke: new hope in neuroprotection. *Mol. Brain* 11:15. doi: 10.1186/s13041-018-0357-8

Xie, Z., Ding, S. Q., and Shen, Y. F. (2014). Silibinin activates AMP-activated protein kinase to protect neuronal cells from oxygen and glucose deprivation-re-oxygenation. *Biochem. Biophys. Res. Commun.* 454, 313–319. doi: 10.1016/j.bbrc.2014.10.080

Xu, C., Liu, Z., and Xiao, J. (2021). Ferroptosis: a double-edged sword in gastrointestinal disease. *Int. J. Mol. Sci.* 22:12403. doi: 10.3390/ijms222212403

Xu, Y., Song, X., Wang, D., Wang, Y., Li, P., and Li, J. (2021). Proteomic insights into synaptic signaling in the brain: the past, present and future. *Mol. Brain* 14:37. doi: 10.1186/s13041-021-00750-5

Yagoda, N., von Rechenberg, M., Zaganjor, E., Bauer, A. J., Yang, W. S., Fridman, D. J., et al. (2007). RAS-RAF-MEK-dependent oxidative cell death involving voltage-dependent anion channels. *Nature* 447, 864–868. doi: 10.1038/nature05859

Yamaguchi, A., Tamatani, M., Matsuzaki, H., Namikawa, K., Kiyama, H., Vitek, M. P., et al. (2001). Akt activation protects hippocampal neurons from apoptosis by inhibiting transcriptional activity of p53. *J. Biol. Chem.* 276, 5256–5264. doi: 10.1074/jbc.M008552200

Yan, N., and Zhang, J. J. (2019). The emerging roles of Ferroptosis in vascular cognitive impairment. *Front. Neurosci.* 13:811. doi: 10.3389/fnins.2019.00811

Yang, W. S., Kim, K. J., Gaschler, M. M., Patel, M., Shchepinov, M. S., and Stockwell, B. R. (2016). Peroxidation of polyunsaturated fatty acids by lipoxygenases drives ferroptosis. *Proc. Natl. Acad. Sci. U. S. A.* 113, E4966–E4975. doi: 10.1073/pnas.1603244113

Yang, W. S., SriRamaratnam, R., Welsch, M. E., Shimada, K., Skouta, R., Viswanathan, V. S., et al. (2014). Regulation of ferroptotic cancer cell death by GPX4. *Cells* 156, 317–331. doi: 10.1016/j.cell.2013.12.010

Ye, Q., Zhang, X., Huang, B., Zhu, Y., and Chen, X. (2013). Astaxanthin suppresses MPP(+)-induced oxidative damage in PC12 cells through a Sp1/NR1 signaling pathway. *Mar. Drugs* 11, 1019–1034. doi: 10.3390/md11041019

Yoo, S. J., Cho, B., Lee, D., Son, G., Lee, Y. B., Soo Han, H., et al. (2017). The erythropoietin-derived peptide MK-X and erythropoietin have neuroprotective effects against ischemic brain damage. *Cell Death Dis.* 8:e3003. doi: 10.1038/cddis.2017.381

Yoon, E. J., Choi, Y., Kim, T. M., Choi, E. K., Kim, Y. B., and Park, D. (2022). The Neuroprotective effects of Exosomes derived from TSG101-overexpressing human neural stem cells in a stroke model. *Int. J. Mol. Sci.* 23:9532. doi: 10.3390/ijms23179532

Young Park, S., Jin Kim, Y., Park, G., and Kim, H.-H. (2019). Neuroprotective effect of Dictyopteris divaricata extract-capped gold nanoparticles against oxygen and glucose deprivation/reoxygenation. *Colloids Surf. B: Biointerfaces* 179, 421–428. doi: 10.1016/j.colsurfb.2019.03.066

Yuan, H., Li, X., Zhang, X., Kang, R., and Tang, D. (2016). Identification of ACSL4 as a biomarker and contributor of ferroptosis. *Biochem. Biophys. Res. Commun.* 478, 1338–1343. doi: 10.1016/j.bbrc.2016.08.124

Zapater, P., Moreno, J., and Horga, J. F. (1997). Neuroprotection by the novel calcium antagonist PCA50938, nimodipine and flunarizine, in gerbil global brain ischemia. *Brain Res.* 772, 57–62. doi: 10.1016/s0006-8993(97)00838-x

Zhang, J., Liu, J., Li, D., Zhang, C., and Liu, M. (2019). Calcium antagonists for acute ischemic stroke. *Cochrane Database Syst. Rev.* 2:Cd001928. doi: 10.1002/14651858.CD001928.pub3

Zhang, Y., Lu, X., Tai, B., Li, W., and Li, T. (2021). Ferroptosis and its multifaceted roles in cerebral stroke. *Front. Cell. Neurosci.* 15:615372. doi: 10.3389/fncel.2021.615372

Zhang, J., Wang, X., Bernardi, R. E., Ju, J., Wei, S., and Gong, Z. (2022). Activation of AMPA receptors in the lateral Habenula produces anxiolytic effects in a rat model of Parkinson's disease. *Front. Pharmacol.* 13:821975. doi: 10.3389/fphar.2022.821975

Zhao, Y. Y., Yang, Y. Q., Sheng, H. H., Tang, Q., Han, L., Wang, S. M., et al. (2022). GPX4 plays a crucial role in Fuzheng Kang'ai decoction-induced non-small cell lung cancer cell Ferroptosis. *Front. Pharmacol.* 13:851680. doi: 10.3389/fphar.2022.851680

Zhao, W. K., Zhou, Y., Xu, T. T., and Wu, Q. (2021). Ferroptosis: opportunities and challenges in myocardial ischemia-reperfusion injury. *Oxidative Med. Cell. Longev.* 2021:9929687. doi: 10.1155/2021/9929687

Zhou, S. Y., Guo, Z. N., Zhang, D. H., Qu, Y., and Jin, H. (2022). The role of Pericytes in ischemic stroke: Fom cellular functions to therapeutic targets. *Front. Mol. Neurosci.* 15:866700. doi: 10.3389/fnmol.2022.866700

Zou, J., Li, Y., Liao, N., Liu, J., Zhang, Q., Luo, M., et al. (2022). Identification of key genes associated with polycystic ovary syndrome (PCOS) and ovarian cancer using an integrated bioinformatics analysis. *J. Ovarian Res.* 15:30. doi: 10.1186/s13048-022-00962-w

frontiers | Frontiers in Molecular Neuroscience

TYPE Original Research
PUBLISHED 24 March 2023
DOI 10.3389/fnmol.2023.1118707

OPEN ACCESS

EDITED BY
Arianna Bellucci,
University of Brescia,
Italy

REVIEWED BY
David J. Picketts,
Ottawa Hospital Research Institute (OHRI),
Canada
Aniket Bhattacharya,
Rutgers, The State University of New Jersey,
United States

*CORRESPONDENCE
Aloïse Mabondzo
✉ aloise.mabondzo@cea.fr

†These authors have contributed equally to this work

‡These authors have contributed equally to this work and share senior authorship

SPECIALTY SECTION
This article was submitted to
Brain Disease Mechanisms,
a section of the journal
Frontiers in Molecular Neuroscience

RECEIVED 07 December 2022
ACCEPTED 20 February 2023
PUBLISHED 24 March 2023

CITATION
Mabondzo A, Harati R, Broca-Brisson L, Guyot A-C, Costa N, Cacciante F, Putignano E, Baroncelli L, Skelton MR, Saab C, Martini E, Benech H, Joudinaud T, Gaillard J-C, Armengaud J and Hamoudi R (2023) Dodecyl creatine ester improves cognitive function and identifies key protein drivers including KIF1A and PLCB1 in a mouse model of creatine transporter deficiency.
Front. Mol. Neurosci. 16:1118707.
doi: 10.3389/fnmol.2023.1118707

Dodecyl creatine ester improves cognitive function and identifies key protein drivers including KIF1A and PLCB1 in a mouse model of creatine transporter deficiency

Aloïse Mabondzo[1]*, Rania Harati[2,3]†, Léa Broca-Brisson[1]†, Anne-Cécile Guyot[1], Narciso Costa[1], Francesco Cacciante[4], Elena Putignano[4], Laura Baroncelli[4,5], Matthew R. Skelton[6], Cathy Saab[7], Emmanuelle Martini[7], Henri Benech[8], Thomas Joudinaud[8], Jean-Charles Gaillard[9], Jean Armengaud[9]‡ and Rifat Hamoudi[3,10,11]‡

[1]Université Paris Saclay, CEA, INRAE, Département Médicaments et Technologies pour la Santé (MTS), Gif sur Yvette, France, [2]Department of Pharmacy Practice and Pharmacotherapeutics, College of Pharmacy, University of Sharja, Sharjah, United Arab Emirates, [3]Sharjah Institute for Medical Research, University of Sharjah, Sharjah, United Arab Emirates, [4]Institute of Neuroscience, National Research Council (CNR), Pisa, Italy, [5]Department of Developmental Neuroscience, IRCCS Stella Maris Foundation, Pisa, Italy, [6]Department of Pediatrics, University of Cincinnati College of Medicine and Division of Neurology, Cincinnati Children's Research Foundation, Cincinnati, OH, United States, [7]Université de Paris and Université Paris Saclay, CEA, Stabilité Génétique Cellules Souches et Radiations, Fontenay aux Roses, France, [8]Ceres Brain Therapeutics, Paris, France, [9]Université Paris Saclay, CEA, Département Médicaments et Technologies pour la Santé (MTS), INRAE, Bagnol sur Cèze, France, [10]Clinical Sciences Department, College of Medicine, University of Sharjah, Sharjah, United Arab Emirates, [11]Division of Surgery and Interventional Science, University College London, London, United Kingdom

Creatine transporter deficiency (CTD), a leading cause of intellectual disability is a result of the mutation in the gene encoding the creatine transporter SLC6A8, which prevents creatine uptake into the brain, causing mental retardation, expressive speech and language delay, autistic-like behavior and epilepsy. Preclinical *in vitro* and *in vivo* data indicate that dodecyl creatine ester (DCE) which increases the creatine brain content, might be a therapeutic option for CTD patients. To gain a better understanding of the pathophysiology and DCE treatment efficacy in CTD, this study focuses on the identification of biomarkers related to cognitive improvement in a Slc6a8 knockout mouse model (Slc6a8−/y) engineered to mimic the clinical features of CTD patients which have low brain creatine content. Shotgun proteomics analysis of 4,035 proteins in four different brain regions; the cerebellum, cortex, hippocampus (associated with cognitive functions) and brain stem, and muscle as a control, was performed in 24 mice. Comparison of the protein abundance in the four brain regions between DCE-treated intranasally Slc6a8−/y mice and wild type and DCE-treated Slc6a8−/y and vehicle group identified 14 biomarkers, shedding light on the mechanism of action of DCE. Integrative bioinformatics and statistical modeling identified key proteins in CTD, including KIF1A and PLCB1. The abundance of these proteins in the four brain regions was significantly correlated with both the object recognition and the Y-maze tests. Our findings suggest a major role for PLCB1, KIF1A, and associated molecules in the pathogenesis of CTD.

KEYWORDS

dodecyl creatine ester, creatine transporter deficiency, target identification, cognitive function, CTD-pathophysiology

Introduction

Neurodevelopmental disorders represent a significant health problem due to the heterogeneity of the underlying causes and a lack of appropriate treatment options. Creatine transporter deficiency (CTD) is a rare genetic disorder and a subset of intellectual disability (ID). However its symptoms including autism-like symptoms with ID, expressive speech and language delay, movement disorders, and epilepsy (Salomons et al., 2001; Stockler et al., 2007; Des Roches et al., 2015) overlaps with those of common neurodevelopmental disorders. CTD is an X-linked (XL) disorder caused by mutations in *SLC6A8*, the gene encoding creatine transporter (CrT)(Braissant et al., 2011), that prevent the transport of creatine (Cr), which is essential for brain function, into the brain (van de Kamp et al., 2014) and is estimated to be the cause of 1%–2% of all cases of XL ID (Cheillan et al., 2012; Des Roches et al., 2015) and about 1% of cases with ID of unknown aethiology (Clark et al., 2006). As expected, the symptoms are most severe in males, with female carriers presenting with a milder phenotype. Some of the main difficulties in elucidating the pathogenesis of and treating ID are that there are wide variety of causes of ID, with no single cause being associated with a significant majority of ID cases.

Several combinations of nutritional supplements or Cr precursors l-arginine and l-glycine, have been studied as therapeutic approaches for CTD, but they have shown very limited success (Valayannopoulos et al., 2013; Jaggumantri et al., 2015; Bruun et al., 2018). However, our previous findings suggest that following the inhalation of dodecyl creatine ester (DCE) in Slc6a8$^{-/y}$ (CrT KO) mice, an animal model recapitulating the clinical features of human CTD, an increase of Cr brain content and synaptic markers could be achieved in the synapsis terminals and thus improving the cognitive function of Slc6a8−/y mice. These findings highlight that DCE might be a therapeutic option for CTD patients (Trotier-Faurion et al., 2013, 2015; Ullio-Gamboa et al., 2019).

To gain a better understanding of the pathophysiology of CTD and DCE treatment efficacy, we focused in this study on the identification of biomarkers related to cognitive improvement in a Slc6a8−/y mice which have low Cr content in the brain and hippocampus (Baroncelli et al., 2016). This mouse model exhibits a precocious cognitive and autistic-like defects, mimicking the early key features of human congenital creatine deficiency syndromes. Moreover, mutant mice displayed a progressive impairment of short and long-term declarative memory denoting an early brain aging. To that end, the study employed a combination of cognitive tests and molecular methods to decipher some of the molecular mechanisms involved in CTD pathophysiology. The cognitive tests included the use of object recognition test (ORT), Y-maze and Morris water maze (MWM) tests to show the decline of cognitive function in *Slc6a8*$^{-/y}$ mice and whether the treatment with DCE improves the cognitive function. The molecular methods involved the application of shotgun proteomics to four different brain regions; the cerebellum, cortex, hippocampus (associated with cognitive functions) and brain stem, and muscle as a control.

Results

Restoration of cognitive functions in DCE-treated creatine knockout mice

DCE was intranasally administered as previously reported (Ullio-Gamboa et al., 2019) to CrT KO mice for 30 days, while wild-type (WT) and vehicle-treated mice were used as controls ($N = 8$ per group). A volume of 6 µL of DCE or vehicle was placed in the nostril. DCE (4 mg/g) or vehicle was given twice bilaterally (12 µL total volume). Consistent with previous findings, CrT KO mice showed object recognition deficits when compared with WT mice. Mice were assigned to treatment groups by sorting animals based on discrimination index (DI) and alternating assignments between vehicle and treatment to avoid performance confounds.

Figure 1A shows DI data. Vehicle-treated CrT KO mice showed reductions in DI compared with both WT mice ($p = 0.023$) and DCE-treated CrT KO mice ($p < 0.05$). DCE-treated CrT KO mice spent more time exploring the novel object than vehicle-treated CrT KO mice (one-way ANOVA, $p < 0.01$; Tukey's *post hoc* test, $p < 0.05$; Figure 1B), but there was no difference between DCE-treated CrT KO mice and WT mice ($p = 0.406$). Strikingly, the median exploration time for the DCE-treated CrT KO mice was 96% of the median exploration time for the WT mice.

We used the Y-maze test measuring the spontaneous alternation rate, the single parameter with the highest accuracy in discriminating WT and CrT KO mice (Mazziotti et al., 2020). A reduction of the spontaneous alternation rate in vehicle-treated CrT KO mice (48%) was observed compared to WT mice (62%; one-way ANOVA, $p < 0.001$; Tukey's *post hoc* test, $p < 0.001$; Figure 1C). The median spontaneous alternation rate was higher in DCE-treated CrT KO mice than in vehicle-treated CrT KO mice but did not differ between DCE-treated CrT KO mice and WT mice (86%; $p = 0.058$; Figure 1C).

Memory was assessed using the MWM test. The results show that DCE did not have a beneficial effect on the performance of CrT KO mice in the MWM test (Figure 1D), suggesting that DCE treatment ameliorates some cognitive deficits seen in these mice.

Proteomic analysis identified unique proteins abundant in specific brain regions

In order to identify proteins across the different brain regions involved in the pathogenesis of CTD, proteomics based differential abundance analysis was performed in the different brain regions of 24 mice. Immediately after behavioral testing, the animals from all three groups were sacrificed. Label-free shotgun proteomics analysis of

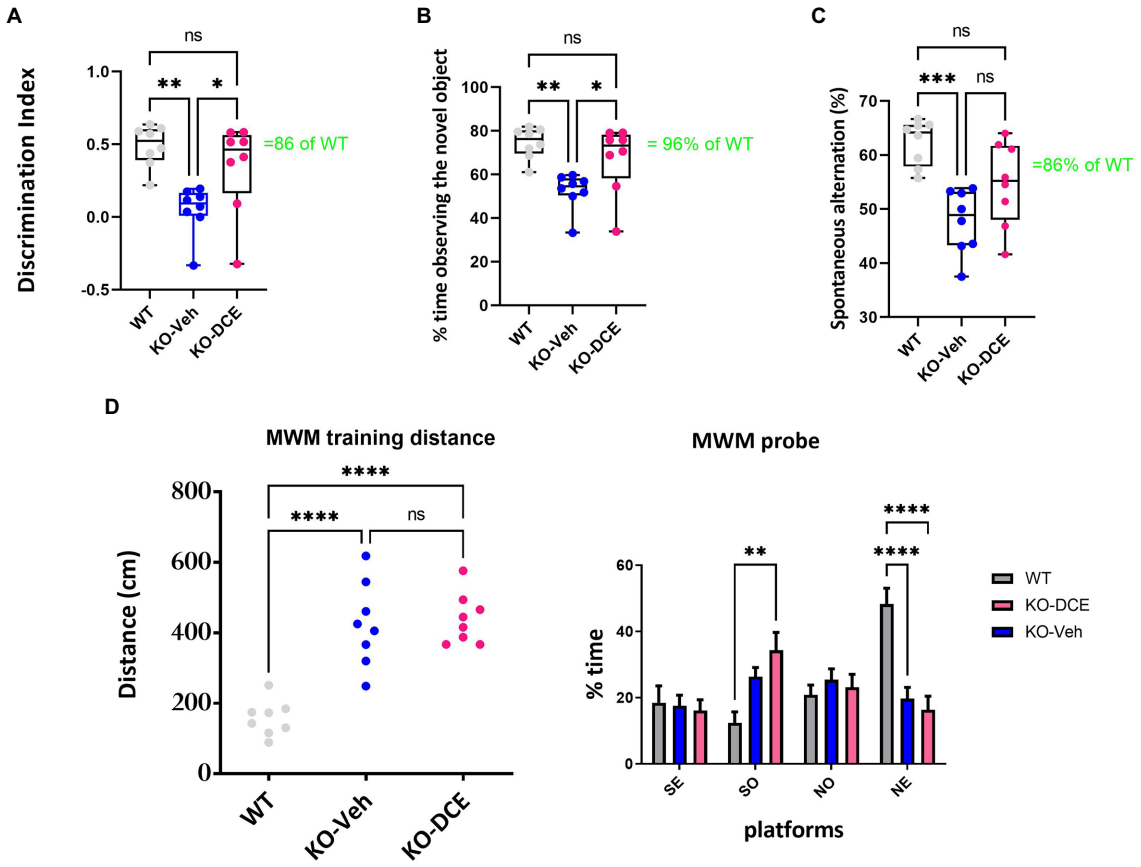

FIGURE 1
Analysis of cognition among the different experimental groups. **(A,B)** Object recognition in the ORT was impaired in CrT KO mice. **(A)**, Analysis of the object discrimination index and **(B)**, percentage of time spent exploring the novel object revealed that WT and DCE-treated CrT KO mice but not vehicle-treated CrT KO mice showed a preference for the novel object. **(C)** Early deficiency of working and spatial memory in CrT KO mice measured by the Y-maze test. CrT KO mice showed a change in the spontaneous alternation percentage in the Y-maze test, which was significantly improved by DCE treatment. **(D)** CrT deletion progressively deteriorates spatial learning and memory in KO mice. Left, learning plot for the three group of animals (WT, CrT KO mice and DCE-treated KO mice). A significant difference was detected between WT and CrT KO mice as well as between WT and DCE-treatd CrT KO mice (p<0.0001). Right histograms showing the mean swimming path covered to locate the submerged platform on the last day of training. Four starting positions arbitrarily designated North (N), South (S), East (E), and West (W) were selected, thus dividing into 4 quadarants were the mice were allowed to search for the escape platform. A significant difference was detected between WT and DCE-treated CrT KO mice in the SO position (p<0.001). In the NE position, a significant difference was detected between WT and DCE-treated KO-DCE mice as well as between WT and CrT KO mice (p<0.0001). The data are the mean±s.e.m. Statistical analysis was performed by one-way or two way ANOVA followed by Tukey's post-hoc test or 2 way ANVOA followed by. *p<0.05; **p<0.001;***p<0.0001; ns=not significant.

cortical, hippocampal, cerebellar, and brainstem tissues and muscle tissue as a control was carried out for each mouse in WT, vehicle-treated CrT KO mice and DCE-treated CrT KO mice.

High-resolution tandem mass spectrometry (MS) analysis of the 120 biological samples generated a large dataset comprising of 7,006,153 MS/MS spectra showing the abundance of 4,035 proteins for the five tissues from each mouse. Following unsupervised filtering and normalization (Hachim et al., 2020) (Supplementary Table 1), the proteins whose abundance was significantly altered by mutant CrT and DCE treatment were identified using reproducibility-optimized statistical testing in each of the five tissue types. The workflow of the bioinformatics analysis is described in Supplementary Figure 1.

The muscle was considered a control for protein analysis due to the fact that Cr levels are decreased in muscle as well. Even if the mice do have a muscle phenotype, we have shown that the learning deficits are independent of any somatic problems the mice may have hence in this study we wanted to compare various regions of the brain to tissue that is not related to the brain, which in this case is the muscle. In addition, we did a global coefficient of variation (CV) calculation of all the proteins abundance between DCE, Veh, and WT for each of the 4 brain regions as well as muscle. The results show that the least variation is in the muscle tissue with CV less than 4,000. However, all the 4 brain regions had CV of more than 5,000 [cortex (5692.59), hippocampus (5166.71), brain stem (5519.19)] with cerebellum being the highest at 5948. This shows that there are some alteration in muscle but not as much as we see in the 4 different brain regions.

A total of 376, 322, 163, and 321 proteins were found to be differentially abundant in the cortex, cerebellum, brainstem and hippocampus, respectively, between WT mice and vehicle-treated CrT KO mice. The abundances of 320, 416, 279, and 323 proteins in the cortex, cerebellum, brainstem and hippocampus, respectively, were marked altered in DCE-treated CrT KO mice compared with vehicle-treated CrT KO mice (Supplementary Figures 2A–D, 3B,D,F,H), while 413, 223, 176 and 175 proteins were differentially abundant in

DCE-treated CrT KO mice compared with WT mice (Supplementary Figures 3A,C,E,G). Overlapping proteins were observed in the comparisons of DCE-treated vs. vehicle-treated mice CrT KO, DCE-treated CrT KO vs. WT mice, and vehicle-treated CrT KO vs. WT mice. Most of the overlapping proteins in the comparison between DCE-treated vs. vehicle-treated mice CrT KO and vehicle-treated CrT KO vs. WT mice were found in the cortex (98 proteins) (Figure 2A), cerebellum (153 proteins) (Figure 2B), and hippocampus (126 proteins) (Figure 2C); conversely, fewer overlapping proteins were found in the brainstem (53 proteins) (Figure 2D; Supplementary Table 2). The proteins whose abundances were altered in vehicle-treated mice and DCE-treated mice compared with WT mice were also selected in cortex (11 proteins) (Figure 2A), cerebellum (7 proteins) (Figure 2B), hippocampus (10 proteins) (Figure 2C) and brain stem (1 protein) (Figure 2D; Supplementary Table 2).

The overlapping proteins whose abundances were significantly altered in all CrT KO mice compared to that in WT mice and in DCE-treated mice CrT KO mice compared to that in vehicle-treated CrT KO mice were then selected for pathway analysis using gene set enrichment analysis carried out using ENRICHR. The proteins found to be involved in different diseases and pathways were selected for subsequent analysis [Cortex (41 proteins), Hippocampus (53 proteins), Cerebellum (52 proteins), and brain stem (25 proteins)]. These findings suggest that lack of Cr into the brain of CrT KO mice leads to a significant alteration of protein abundance involved in the pathogenesis of CTD.

Identification of a panel of 14 proteins in the brain involved in cognitive activity using a multivariate statistical model

A multivariate statistical model comparing WT mice with vehicle-treated CrT KO mice (Figure 2E) and DCE-treated CrT KO mice with vehicle-treated CrT KO mice was used to identify key proteins (Figure 2F). Among the proteins whose abundances were affected by either CrT deficiency or DCE treatment, that were discussed in the previous section, bioinformatics analysis and statistical modelling identified 14 proteins that were the most abundant in the four different brain regions in both vehicle-treated and DCE-treated CrT KO mice. Those most abundant proteins were significantly altered by the mutation compared to WT(vehicle-treated vs. WT) and by the treatment compared to vehicle (DCE-treated vs. vehicle treated) and their abundance after treatment was restored to levels comparable to those in WT mice (Figure 3A; Supplementary Tables 3, 4).

The results showed that PLCB1 abundance in the cortex ($p = 0.0003$) (Supplementary Table 3a); MeCP2 ($p = 0.022$), ANK1 ($p = 0.0001$), and ANXA5 ($p = 0.00004$) abundance in the cerebellum (Supplementary Table 3c); and IGSF8 ($p = 0.00036$) abundance in the hippocampus (Supplementary Table 3b) were significantly downregulated in vehicle-treated CrT KO mice compared with WT mice, DCE treatment significantly rescued the abundance of these proteins in these brain regions in CrT KO mice (Figure 3A; Supplementary Table 4). In contrast, NCAM1 ($p = 1.38E-07$), PI4KA

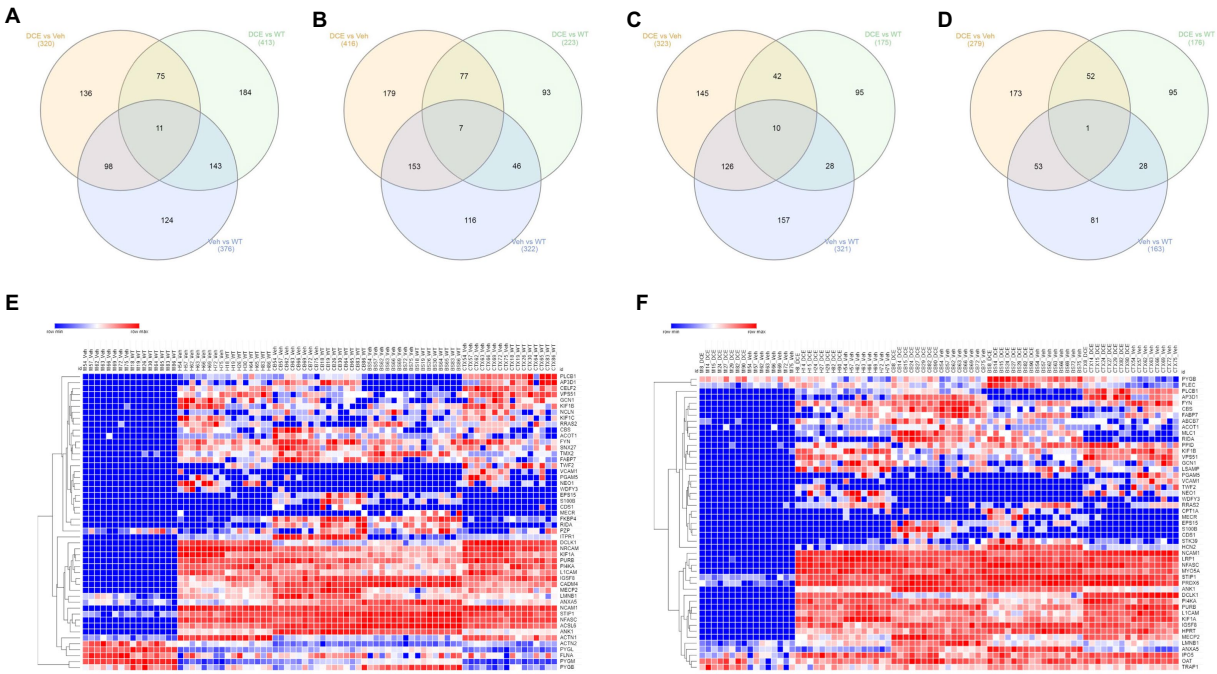

FIGURE 2
Comparison of proteomic signatures in different brain regions among the different experimental groups. **(A–D)** Venn diagram showing overlapping proteins among the three experimental groups. The proteins that showed a significant change in abundance in CrT KO mice compared with the WT and in DCE-treated mice compared with vehicle-treated mice were selected for pathway analysis. The proteins that showed a change in abundance in the vehicle-treated mice and the DCE-treated mice compared with the WT mice were also selected for pathway analysis. The abundances of these proteins in the cortex, cerebellum, brainstem, hippocampus and muscle were analyzed using a multivariate statistical model based on one-way ANOVA followed by Bonferroni's *post hoc* test. **(E)** Heatmap showing the proteins that showed a significant change in abundance in vehicle-treated CrT KO mice compared WT mice. **(F)** Heatmap showing the proteins that showed a significant change in abundance in DCE-treated CrT KO mice compared with vehicle-treated CrT KO mice.

10.3389/fnmol.2023.1118707

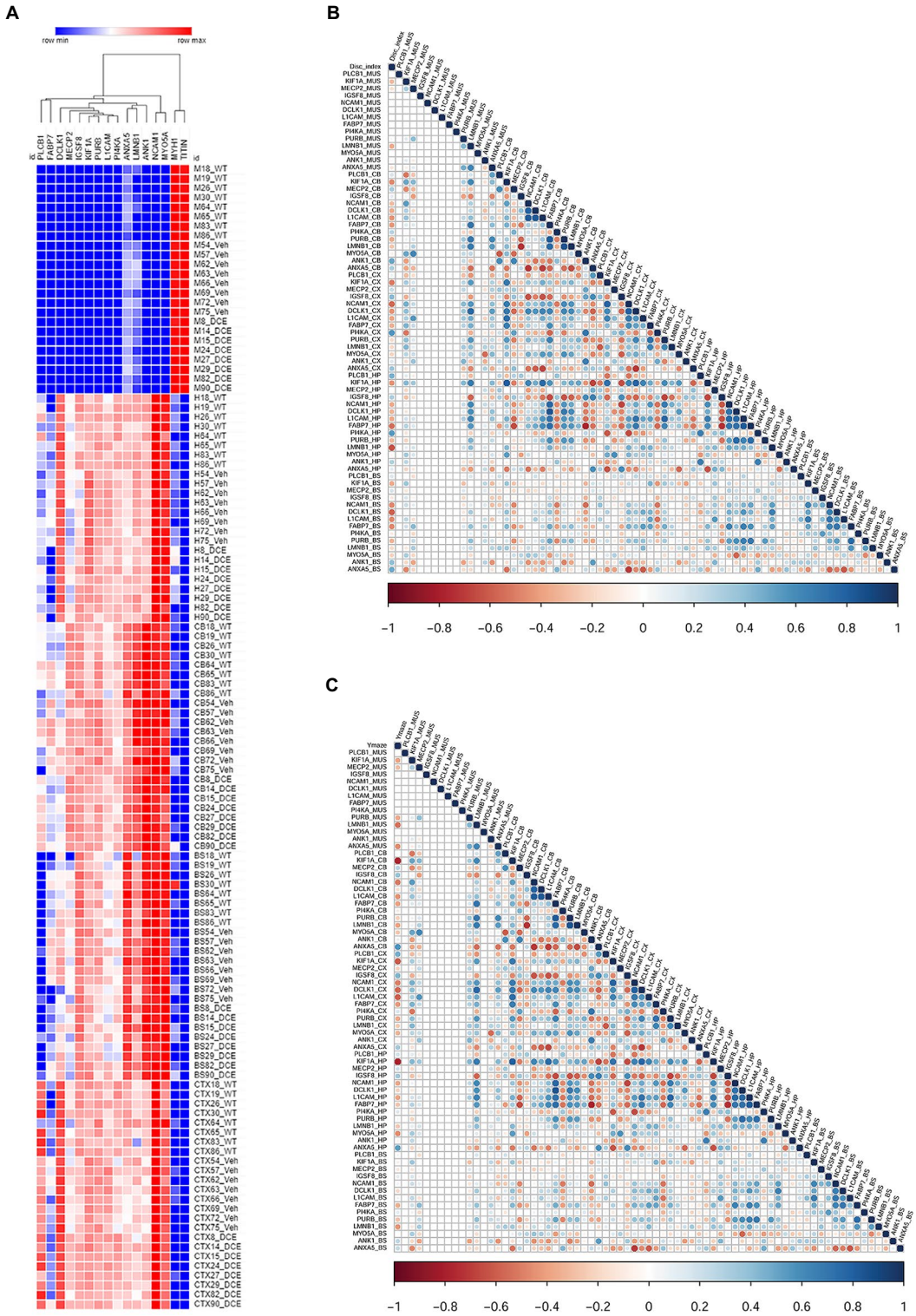

FIGURE 3
Correlation of the levels of 14 proteins with performance in different cognitive tests using a stepwise regression statistical model. **(A)** Heatmap showing the abundance levels of the 14 proteins that showed significant changes in abundance in both vehicle-treated CrT KO mice and DCE-treated CrT KO mice. **(B)** Map showing the correlation between the level of each of the 14 proteins with performance in the ORT to evaluate cognition. **(C)** Maps showing the correlation between the level of each of the 14 proteins and performance in the Y-maze test. The correlation maps were derived using a stepwise regression model to assess the correlation between the abundance each of the 14 differentially expressed proteins and performance in each of the cognitive tests. Group comparisons were carried out using a statistical model based on one-way ANOVA followed by Bonferroni's *post hoc* test for multiple comparisons.

($p = 0.026$), DCLK1 ($p = 3^{-15}$) and PURB ($p = 0.045$) abundance in the cortex (Supplementary Table 3a); KIF1A ($p = 2^{-24}$), NCAM1 ($p = 0.038$) and L1CAM ($p = 0.001$) abundance in the hippocampus (Supplementary Table 3b); and LMNB1 ($p = 1E^{-05}$), FABP7 ($p = 8.30E^{-05}$), and PURB ($p = 0.03$) abundance in the cerebellum (Supplemental Table 3c) were significantly upregulated in CrT-treated vehicle KO mice compared with WT mice but were not different between WT and DCE-treated CrT KO mice (Figure 3A; Supplementary Table 4).

Correlation of the proteins with cognitive behavioral tests using stepwise regression statistical model shows KIF1A is abundant across the brain regions

A stepwise regression model was used to assess the effect of each of the proteins of interest on cognitive outcomes to identify those that may influence cognitive function. The levels of several proteins were significantly correlated with the discrimination index (DI); the correlation between KIF1A, Fabp7 and L1CAM levels and DI was found in the hippocampus, cortex, cerebellum and brain stem ($n = 11$, Supplementary Table 5a).

We also observed that the level of LMNB1, which is involved in cerebellar ataxia and adult autosomal dominant leukodystrophy ($r^2 = -0.634$, $p < 0.0001$), and the level of Pi4KA ($r^2 = -0.634$, $p = 0.066$) in the hippocampus were correlated with the DI. Several proteins were also significantly correlated with the performance in the Y-maze test ($n = 11$, Figure 3C, Supplementary Table 5b). The level of KIF1A, a kinesin that transports synaptic vesicle precursors, was most strongly correlated with the spontaneous alternation rate in the Y-maze test (hippocampus: $r^2 = -0.795$, $p < 0.0001$; cortex: $r^2 = -0.608$, $p = 0.001$; cerebellum: $r^2 = 0.774$, $p < 0.0001$). Fabp7 and L1CAM correlated with the spontaneous alternation rate in the Y-maze test in the 3 brain regions (Supplementary Table 5b). In addition, PLCB1 is significantly more abundant in the cortex compared to other brain regions and its abundance in the cortex and hippocampus is correlated with DI and Y-maze ($p = 0.01$).

Amongst the 14 key proteins with individual animal performance in different cognitive tests, KIF1A was shown to be the protein with the most uniformly abundance across the 4 brain regions and correlated with the DI in the novel object recognition test and spontaneous alternation in the Y-maze test.

KIF1A and PLCB1 interplay is associated with DCE treatment efficacy in CrT KO mice

KIF1A participates in vesicular transport, and vesicles containing the neurotrophin BDNF have been found to be under the control of KIF1A (Kondo et al., 2012). BDNF is produced in the neocortex throughout brain development and accelerates the overall redistribution of cortical neurons (Iki et al., 2005). DCE-mediated rescue of KIF1A levels in the cortex (Figure 4A), hippocampus (Figure 4B), and cerebellum (Figure 4C) of CrT KO mice resulted in higher levels of pro-BDNF/BDNF ($p = 0.0043$; Figure 4D) a long-term potentiation (LTP) biomarkers, which are linked to cognitive function improvement. These results indicate that KIF1A is a potential key player in CTD pathogenesis.

In order to highlight the central role of KIF1A abundance across the different brain regions of CrT KO mice, proteins co-immunoprecipitated together with KIF1A were identified by MS. Shotgun proteomics revealed that KIF1A and PLCB1 could be co-immunoprecipitated with anti-KIF1A antibody from cortical and hippocampal extracts (Supplementary Table 6). In addition, PLCB1 abundance was correlated with the DI in the object recognition test (Supplementary Table 5a) and spontaneous alternation rate in the Y-maze test (Supplementary Table 5b) (hippocampus: $r^2 = 0.460$, $p = 0.012$; cortex: $r^2 = 0.469$, $p = 0.01$, respectively). Therefore, further downstream functional analysis focused on KIF1A and PLCB1 proteins.

Additional analysis confirmed the abundance of PLCB1 by Western blotting (Figures 4F–H). The results showed that PLCB1 level decreased in the cortex (Figure 4F) and hippocampus (Figure 4G) in vehicle-treated CrT KO mice, while DCE-treated CrT KO mice showed a significant increase in PLCB1 levels in the cortex ($p = 0.0004$) compared to the hippocampus and cerebellum (Figure 4H).

DCE-mediated upregulation of PLCB1 levels in the cortex might might involved the NF-κβ pathway *via* dysregulation of a PKCα inhibitor, IκBα, thereby altering the abundance of NF-κβ-inducible genes. Thus, IκBα abundance was evaluated to determine whether the DCE-induced increase in PLCB1 levels affects targets downstream of this pathway. Western blotting indicated that IκBα (Figure 4I) ($p < 0.05$) but not IκBβ (Figure 4J) was significantly downregulated in the cortex in vehicle-treated CrT KO mice, while DCE treatment rescued IκBα protein levels in CrT KO mice ($p = 0.008$), suggesting that PLCB1 is involved in NF-κβ regulation in these mice.

Discussion

The present study focuses on the CTD pathogenesis and the underlying mechanisms of DCE drug efficacy in CrT KO mouse model engineered to mimic the clinical features of CTD patients. Shotgun proteomics analysis, integrative bioinformatics and statistical modeling identified 14 key proteins that are dysregulated in the cerebellum, cortex, hippocampus and brain stem of *Slc6a8*$^{-/y}$ mice compared to WT mice and modulated by DCE. Notably, 13 of these proteins are related to ID disorders in human, including autism spectrum disorders (MECP2, Hammer et al., 2002; Shibayama et al., 2004; Wen et al., 2017), KIF1A (Weller and Gartner, 2001; Esmaeeli Nieh et al., 2015; Lee et al., 2015; Ohba et al., 2015; Padiath, 2016; Dai et al., 2017; Tomaselli et al., 2017), PLCB1 (Rusciano et al., 2021), NCAM1 (Arai et al., 2004; Atz et al., 2007; Gray et al., 2010; Varea et al., 2012), ANXA5 (Esmaeeli Nieh et al., 2015; Lee et al., 2015; Tomaselli et al., 2017), bipolar disorder (FABP7, Killoy et al., 2020), NCAM1, PLCB1 (Lo Vasco et al., 2013; Yang et al., 2016), axonal neuropathy (DCLK1), ID (KIF1A, Ohba et al., 2015), L1CAM (Weller and Gartner, 2001), regulation of neurite outgrowth (IGSF8, Ray and Treloar, 2012), leukodystrophy (LMNB1), cerebellar ataxia (LMNB1, Padiath, 2016; Dai et al., 2017), abnormal behavior (PI4KA, Pagnamenta et al., 2015), epileptic encephalopathies (PLCB1, MYO5A), or neurodegenerative diseases (ANK1, De Jager et al., 2014). Our findings suggest a profound alteration of the molecular landscape of the brain area of CrT KO mice, and DCE treatment

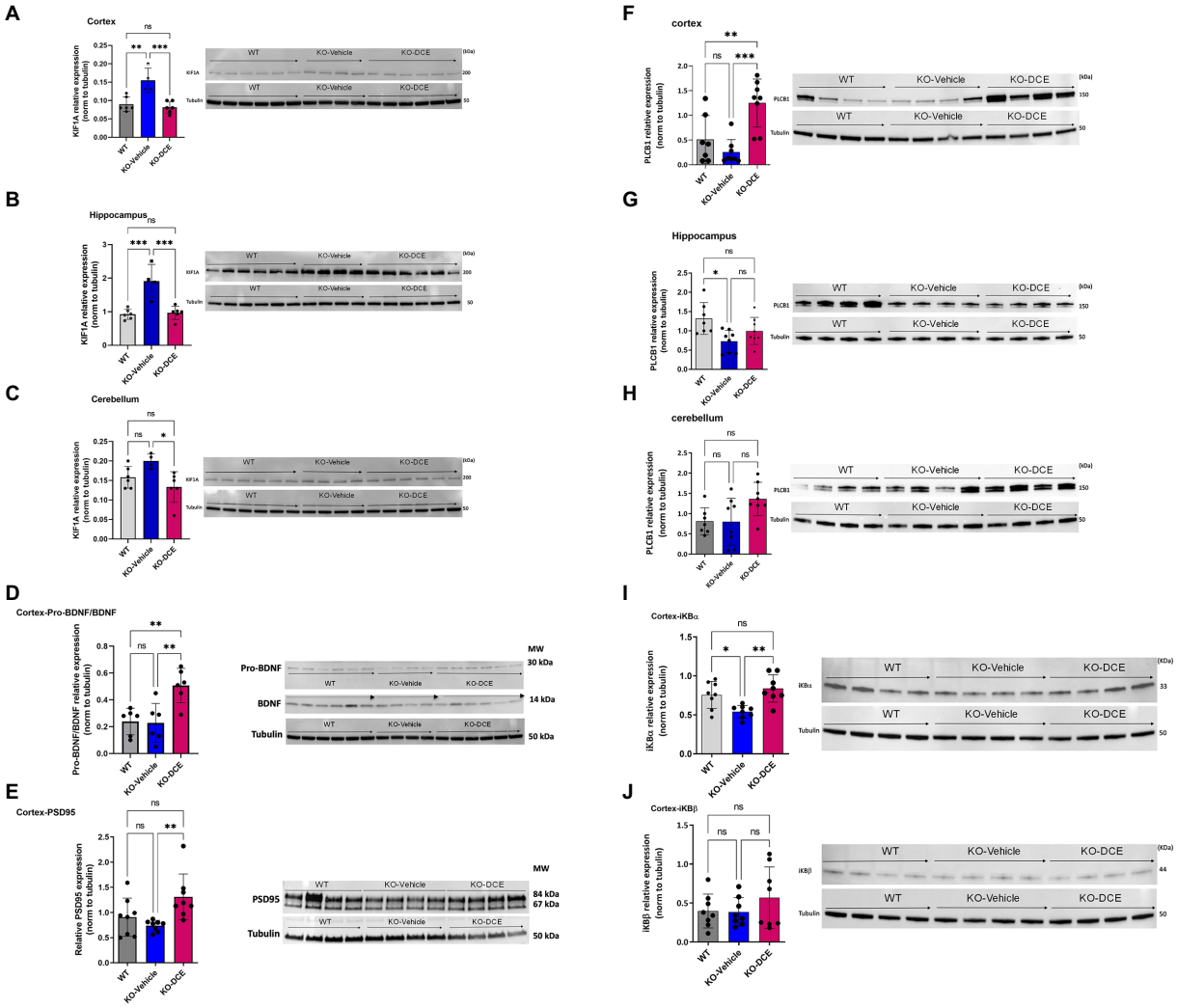

FIGURE 4
KIF1A and PLCB1 interplay is associated with DCE treatment efficacy in CrT Ko mice. **(A–C)** Western blot results showing that the KIF1A level was significantly increased in the cortex **(A)**, hippocampus **(B)** and cerebellum **(C)** in vehicle-treated CrT KO mice compared to WT mice, while DCE treatment rescued this overabundance in the three brain regions in CrT KO mice. **(D, E)** Western blot results showing that the pro-BDNF/BDNF ratio **(D)** was significantly altered in DCE-treated CrT KO mice compared to that of both WT mice and vehicle-treated CrT KO mice. In addition, the PSD95 level **(E)** was significantly altered in the cortices of vehicle-treated CrT KO mice compared to that of DCE-treated CrT KO mice. **(F–H)**, Western blotting showed that PLCB1 protein (150kDa) abundance was increased in the cortex **(F)**, hippocampus **(G)** and cerebellum **(H)** in CrT KO mice at 0days after DCE treatment. **(I,J)** Western blot results for Ibα **(I)** and IκBβ **(J)** showing that DCE promotes IκBα transcription factor abundance but not IκBβ transcription factor abundance. The data are the mean±s.e.m. (n=8/group). Statistical analysis was performed by one-way ANOVA followed by Tukey's post-hoc test. Tubulin was used as a loading control. *$p \leq 0.05$; **$p \leq 0.001$; ***$p \leq 0.0001$; ns=not significant.

changed a subset of those proteins. The hippocampus is crucial for spatial memory formation, while the Y-maze deficits are more rooted in the prefrontal cortex or the neocortex at the anterior end of the brain-than the hippocampus. The prefrontal cortex is an interconnected set of neocortical areas that have pattern of connectivity with all sensory neocortical and motor systems and a wide range of subcortical structures (Barnes and Pandya, 1992). The cerebellum is strongly interconnected with the cerebral hemispheres in both feedforward (cerebral hemispheres to cerebellum) and feedback directions (Schmahmann and Pandya, 1997). Since functional imaging and neuronal activation studies have shown that the sub-brain regions such as cortex, the cerebellum and the hippocampus are involved in the storage and retrieval of spatial memory and in the formation of spatial memory (Maviel et al., 2004), we were interested by the identification of subset of proteins correlated with the cognitive trajectory of CrT KO mice. Correlation analysis was performed using a stepwise regression model between the 14 selected proteins affected both by the mutation and DCE treatment.

Out of these 14 proteins, KIF1A abundance in the four brain regions (cortex, hippocampus, cerebellum and brain stem) was significantly correlated with DI in the object recognition test, while the abundance of this protein in the hippocampus, cortex and cerebellum correlated with the spontaneous alternation the Y-maze tests. Co-immunoprecipitation analysis using Western blotting confirmed that KIF1A interacts with PLCB1 in the various brain regions, suggesting a key role of KIF1A in CTD. The main observations of this study are summarized in Figure 5. These results confirm what has been reported in the literature regarding the association of KIF1A

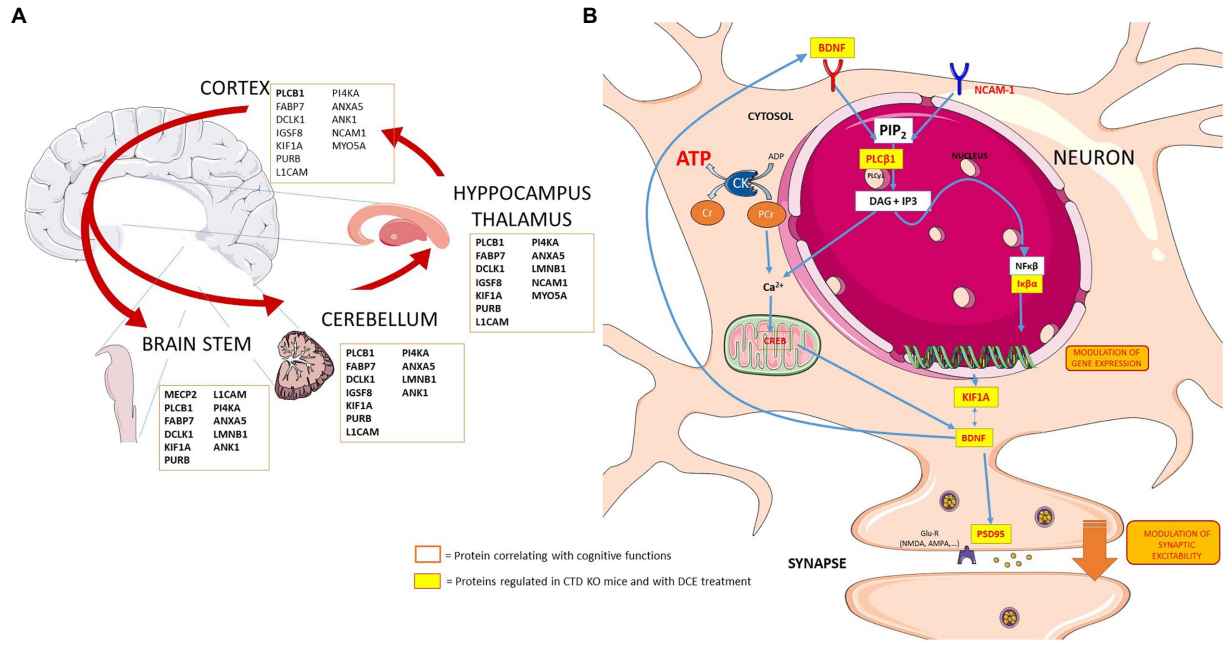

FIGURE 5
Schematic presentation showing the key players in the different brain regions and potential links between several proteins that are regulated in neurons in the context of CTD and by DCE treatment. **(A)** Proteins regulated by DCE in CrT KO mice. **(B)** DCE mediated the abundance of PLCB1. DCE-mediated upregulation of PLCB1 levels in the brain might lead to the production of inositol-1,4,5-triphosphate (IP3), and IP3 modulates the NF-κβ pathway *via* dysregulation of a PKCα inhibitor, IκBα, thereby altering the expression of NF-κβ-inducible genes which regulates the NF-κβ pathway by rescuing IκBα protein levels in CrT KO mice. NF-κβ is bound by IκBα and then translocates to the nucleus to activate target genes including KIF1A and BDNF.

and PLCB1 to cognitive function in different brain disorders (Manning et al., 2012; Lee et al., 2015).

Novel object recognition test is a valid cognitive task focusing on mostly hippocampal function. CTD increased the abundance of KIF1A. These changes suggest that anteretrograde axonal transport may be impaired in hippocampal neurons which may lead to changes in synaptic proteins, thus contributing to changes in hippocampal neurotransmission and to cognitive and memory impairments. In a rat model of α-synucleinopathy, elevated levels of KIF1A were observed in substantia nigra (Chung et al., 2009), suggesting the possibilily of the imbalance in protein degradation and synthesis and/or axonal transport deficit. KIF1A mutations have been found in patients with a severe neurodevelopmental disorder with Rett syndrome patients (Wang et al., 2019). KIF1A has been found to participate in vesicular transport. Vesicles containing the neurotrophin BDNF have been found to be under the control of KIF1A (Kondo et al., 2012). BDNF is produced in the neocortex throughout brain development and accelerates the overall redistribution of cortical neurons. DCE-mediated rescue of KIF1A levels in CrT KO mice resulted in higher levels of pro-BDNF/BDNF, which are linked to cognitive function improvement, suggesting that normal expression of KIF1A but not overexpression might be indispensable for BDNF-mediated cognitive function. The direct effect of DCE on the regulation of pro-BDNF/BDNF expression could not be excluded. KIF1A overabundance in the developing brains of CrT KO mice likely leads to synaptic dysfunction, thus contributing to cognitive and memory impairments (Iki et al., 2005; Lu et al., 2014). This is in agreement with previous data showing the reduced cortical spine density and reductions in protein levels of several synaptic markers in the brains of Slc6a8−/y mice (Chen et al., 2021). In addition, we found that in the cortex, the abundances of the presynaptic protein IgSF8 which has been reported to be a critical regulator of brain microcircuits and neuronal function (Apostolo et al., 2020), was altered in vehicle-treated CrT KO mice compared with the abundances in WT mice. Y-maze exploits the inherent motivation of an organism to explore an unknown environment. This assay is very sensitive for assessing working memory and cognitive flexibility in mice providing a simple and widely applicable behavioural assay with exceptional translational relevance. Many parts of the brain--including the hippocampus and prefrontal cortex--are involved in this task (Maviel et al., 2004). We noticed the abundance of KIF1A across the hippocampus and cortex in CrT KO mice correlating with the cognitive performance in Y-maze test. These findings indicate that KIF1A is one of a potential key player in CTD pathogenesis.

Data from co-ip experiments indicated in Supplementary File S11 suggest that it is likely a transient complex has been formed between KIF1A and PLCB1. PLCB1 plays a major role in vesicular trafficking within the cell, thus playing a direct role in axonal transport of neurotransmitters (Hannan et al., 2001). PLCB1 dysregulated signaling is linked to several brain disorders, including epilepsy, schizophrenia, bipolar disorder, Huntington's disease, depression and Alzheimer's disease (Alberini, 2009; Cholewa-Waclaw et al., 2016). We demonstrated that DCE modulates the relative abundance of PLCB1 in different brain regions. Our data showed that PLCB1 regulates the NF-κβ pathway by rescuing IκBα protein levels in CrT KO mice. Of note, NF-κβ signaling in the brain has been implicated in regulating neuronal survival and function (Meffert et al., 2003; Kaltschmidt et al., 2006). NF-κβ is bound by IκBα and then

translocates to the nucleus to activate target genes. IκBα-deficient mice display deregulated and sustained NF-κβ activation (Lian et al., 2012), indicating a critical role for IκBα in NF-κβ regulation. CrT KO mice showed a decrease in IκBα abundance in the cortex and hippocampus, which was rescued by DCE treatment. It seems likely, DCE-mediated upregulation of PLCB1 levels in the cortex might lead to the production of inositol-1,4,5-triphosphate (IP3) (Rusciano et al., 2021), and IP3 modulates the NF-κβ pathway *via* dysregulation of a PKCα inhibitor, IκBα, thereby altering the abundance of NF-κβ-inducible genes. The decrease in IκBα abundance might regulates neuroinflammation as well as spatial memory formation and synaptic plasticity, probably through BDNF signaling. Our findings are in agreement with previous observations showing that stimulation of the neuroinflammatory response through NF-κβ activation may be therapeutically beneficial (Lian et al., 2012). The regulation of neuroinflammation is also supported by the identification of NCAM1 in CrT KO mice whose abundance was altered and restored by DCE treatment; NCAM1 could participates in the structural deficits in CrT Ko mice including changes in neuronal migration and synaptogenesis.

In conclusion, the results of the study indicated that the crosstalk between KIF1A and PLCB1 mediates cognitive function in the CTD. In addition, the results identified a panel of additional 12 proteins which suggests that Slc6a8−/y mice could have structural deficits including changes in neuronal migration or synaptogenesis. To our knowledge, this is the first study that describes some of the molecular mechanisms of CTD-related cognitive dysfunction and the therapeutic effect of DCE. Furthermore, the results of the study provide further evidence regarding the efficacy of DCE in treating the cognitive symptoms of CTD and restoring the abundance of key molecular players to normal levels in several brain regions. Little is known about the underlying mechanisms of the Cr-mediated behavioral deficits. Correlating proteomic changes to behavioral deficits provide mechanistic insights into Cr-mediated changes. Future studies can be designed to investigate this relationship. This study provides a shift in research paradigms and an advancement in intervention for CTD. While CTD carrier females are reported to have a milder phenotype, it will be of interest in the future to assess the potential alteration of the molecular landscape of the brain area of for females that have a milder phenotype.

Materials and methods

Ethical considerations

All *in vivo* experiments were conducted in compliance with the European Communities Council Directive of 22 September 2010 and were approved by the Italian Ministry of Health (authorization number 259/2016-PR).

Generation of CrT KO mice

Male $CrT^{-/y}$ and $CrT^{+/y}$ mice were generated on the C57BL/6J background as previously described (Baroncelli et al., 2014). The mice were housed at 22°C on a 12–12 h light–dark cycle and provided food and water *ad libitum*.

The presence of the *Slc6a8* mutation was confirmed by PCR as previously described (Baroncelli et al., 2016). Briefly, genomic DNA was isolated from tail tissue collected from P25 mice using the DNeasy® Blood & Tissue kit from Qiagen according to the manufacturer's protocol. The following primers were used for PCR amplification: F: AGGTTTCCTCAGGTTATAGAGA; R: CCCTAGGT GTATCTAACATCT; R1: TCGTGGTATCGTTATGCGCC. The amplicon sizes were as follows: $CrT^{+/y}$ allele = 462 bp; mutant allele = 371 bp.

DCE treatment

DCE was prepared as previously described (Trotier-Faurion et al., 2013). Ten milligrams of DCE was added to 0.375 g of Maisine®CC (Gattefossé) at room temperature, and then 125 mg of DHA (Sigma–Aldrich) was added. The mixture was vortexed for 5 min and shaken at 1,000 × g in a thermomixer at 30°C for 48 h. Then, the sample was centrifuged at 20,000 × g for 10 min at room temperature, and the resulting supernatant was filtered through a 0.22 µm filter, placed in another tube and stored at +4°C prior to use.

DCE was intranasally administered to CrT KO mice for 30 days as previously reported (Ullio-Gamboa et al., 2019), while wild-type (WT) and vehicle-treated mice were used as controls ($N = 8$/group). 6 µL of DCE or vehicle (Maisine®CC with DHA) was placed in the nostril. The DCE (4 mg/g) or vehicle was given twice bilaterally (12 µL total volume).

Behavioral testing

Behavioral testing started 14 days after the start of the treatment as was done previously (Baroncelli et al., 2016). Treatment continued during behavioral testing, which lasted 2 weeks, for a total of 30 days of treatment. Each mouse was subjected to all of the behavioral assessments in following order: the 24-h ORT (3 days), Y-maze test (1 day), and hidden platform MWM test (7 days).

ORT

The ORT apparatus consisted of a square arena (60 × 60 × 30 cm) made of polyvinyl chloride with black walls and a white floor as previously described (Baroncelli et al., 2016). The day before testing, the mice were individually habituated to the empty arena for 10 min. The ORT, which is based on the tendency of rodents to spend more time exploring a novel object than a familiar object, was used to measure short-and long-term memory and consisted of the sample phase and testing phase. During the sample phase, two identical objects were placed in diagonally opposite corners of the arena (approximately 6 cm from the walls), and the mice were allowed to explore the arena for 10 min. The testing phase was performed 24 h after the sample phase. An identical copy of one of the objects from the sample phase and a novel object were placed in the same locations, and the mice were returned to the arena and allowed to explore the objects for 5 min. The DI was calculated as follows: DI = (T new − T old)/(T new + T old), where T new is the time spent exploring the novel object and T old is the time spent exploring the familiar object (Baroncelli et al., 2016).

Y-maze spontaneous alternation test

The spontaneous alternation rate was measured using a Y-shaped maze with three symmetrical gray solid plastic arms at a 120-degree angle (26 cm long, 10 cm wide, and 15 cm high) as previously described (Begenisic et al., 2014; Baroncelli et al., 2016). The mice were placed in the center of the maze one at a time, and their movements were recorded for 8 min. The number of arm entries (all four limbs within an arm) and the number of triads (successive entries into all three arms) were recorded to calculate the spontaneous alternation percentage (defined as the number of triads divided by the number of possible alternations (total arm entries minus 2) multiplied by 100).

MWM test

The mice were subjected to 4 training trials per day for a total of 7 days. The apparatus consisted of a circular water tank (diameter, 120 cm; height, 40 cm) filled with water (23°C) to a depth of 25 cm. The water was made opaque by the addition of nontoxic white paint. Four starting positions arbitrarily designated the north (N), south (S), east (E), and west (W) positions were selected, thus dividing the tank into 4 quadrants. A square escape platform (11 × 11 cm) was submerged 0.5 cm below the water surface in the middle of one of the 4 quadrants. The mice were allowed to search for the escape platform for up to 60 s, and their swimming paths were automatically recorded by the Noldus Ethovision system. The last trial on the last training day was a probe trial, during which the escape platform was removed from the tank and the swimming paths of the mice were recorded for 60 s while they searched for the missing platform.

Proteolysis and MS

Before MS analysis, total protein (15 µg) was extracted from tissues from the five tissues, i.e., muscle, cortical, cerebellar, hippocampal and brainstem tissues, then mixed with lithium dodecyl sulfate lysis buffer (Invitrogen), and incubated at 99°C for 5 min. Samples were then separated by electrophoresis for a short amount of time (5 min) at 200 V on a NuPAGE 4–12% Bis-Tris gel in 1X MES/SDS (Invitrogen) running buffer. The gels were stained with SimplyBlue SafeStain (Thermo) for 5 min followed by an overnight wash in water with gentle agitation. The band containing the whole proteome from each sample was excised from the polyacrylamide gel and treated as previously described (Hartmann and Armengaud, 2014). The proteins were in-gel proteolyzed with trypsin gold (Promega) in the presence of 0.01% Protease Max surfactant (Promega) at 50°C for 60 min. A total of 1 µL of the resulting peptide fraction (50 µL), corresponding to approximately 300 ng of peptide, was analyzed by liquid chromatography–tandem mass spectrometry (LC–MS/MS) using an Ultimate 3,000 nano-LC system coupled to a Q-Exactive HF mass spectrometer (Thermo Scientific) as described previously (Hartmann and Armengaud, 2014). The peptides were loaded on a reverse-phase PepMap 100 C18 µ-precolumn (5 µm, 100 Å, 300 µm i.d. × 5 mm, Thermo Fisher) and then resolved on a nanoscale PepMap 100 C18 nanoLC column (3 µm, 100 Å, 75 µm i.d. × 50 cm, Thermo Fisher) at a flow rate of 0.2 µL.min^{-1} using a 90-min gradient (4% B from 0 to 3 min, 4–25% B from 3 to 78 min and 25–40% B from 78 to 93 min), with 0.1% HCOOH/100% H_2O as mobile phase A and 0.1% HCOOH/80% CH3CN/20% H_2O as mobile phase B. The mass spectrometer was operated in Top20 mode, with a scan range of 350 to 1800 *m/z*, and selection and fragmentation were performed using a 10 s dynamic exclusion time for the 20 most abundant precursor ions. Only ion precursors with a 2+ or 3+ charge were selected for HCD fragmentation, which was performed at a normalized collision energy of 27 eV.

MS/MS spectra interpretation and differential proteomics

MS/MS spectra were assigned using Mascot Daemon software version 2.6.1 (Matrix Science) and the *Mus musculus* SwissProt database comprising 17,096 protein sequences. Peptide tolerance, MS/MS fragment tolerance, and the maximum number of missed cleavages were set to 5 ppm, 0.02 Da and 2, respectively. Carbamidomethylation of cysteine was considered a fixed modification, and oxidation of methionine was considered a variable modification. Peptides with p value ≤0.05 for homology threshold mode and proteins with at least two distinct peptides were selected (false discovery rate < 1%).

Bioinformatics analysis of proteomics data

The general workflow of the bioinformatics analysis is shown in Supplementary Figure 1. An in-house script was written using the R programming language to identify differentially expressed proteins between the three groups (WT, vehicle-treated CrT KO mice and DCE-treated CrT KO mice) in each of the five tissues, i.e., muscle, cortical, cerebellar, hippocampal and brainstem tissues. The following comparisons were analyzed: vehicle-treated CrT KO mice vs. WT mice; DCE-treated CrT KO mice vs. vehicle-treated CrT KO mice; and DCE-treated CrT KO mice vs. WT. Initially, the proteomics data were normalized using variance stabilizing normalization (VSN, Motakis et al., 2006). Proteins with at least 10 assigned MS/MS spectra across all samples were retained. An unsupervised variation filter was then applied to the proteomics data (Hamoudi et al., 2010), and samples of 8 proteins with MS/MS spectra were included. Differential abundance analysis of proteins among the different regions was carried out using a modified R package for reproducibility-optimized statistical testing (ROTS, Suomi et al., 2017). The data were sorted according to the adjusted p value based on a false discovery rate < 0.05. Reproducibility plots and principal component analysis (PCA) were used to assess the quality of the separation of the data between the various groups that were being compared. The identified differentially expressed proteins were visualized using volcano plots and heatmaps. The heatmaps were generated using unsupervised hierarchical clustering carried out on the basis of Ward linkage and Euclidean distance to assess the degree of proteomic profile separation across the four brain regions among the three groups.

Pathway analysis

Pathway analysis was performed to narrow down the differentially abundant proteins and identify their potential functions. To achieve

this, the proteins whose abundances were significantly altered in CrT KO vehicle-treated mice compared with WT mice and in DCE-treated mice compared with vehicle-treated mice were selected for subsequent pathway analysis. The proteins whose abundances were altered in vehicle-treated mice and DCE-treated mice compared with WT mice were also selected. Pathway analysis using gene set enrichment was carried out using Enrichr (Chen et al., 2013; Kuleshov et al., 2016) focusing on the following sets: BioCarta_2016, Elsevier_Pathway_Collection, GO_Biological_Process_2018, GO_Molecular_Function_2018, KEGG_2019_Human, KEGG_2019_Mouse, MSigDB_Hallmark_2020, WikiPathways_2019_Mouse, WikiPathways_2019_Human, ClinVar_2019, DisGeNET, Jensen_DISEASES, and OMIM_Disease. Relevant pathways were selected based on a cutoff of $p < 0.05$. The set of proteins found to be significantly involved in the different pathways and diseases were selected for further analysis.

Statistical analysis of the differentially expressed proteomics data

In order to identify the patterns of differentially expressed proteins across the different regions, the data identified by ENRICHR analysis was used to construct a multivariate statistical model using one-way ANOVA followed by Bonferroni's *post hoc* test for comparisonsacross the cortex, cerebellum, brainstem, hippocampus and muscle. The muscle was used as control for tissue other than the brain.

The stepwise regression statistical modelling was used to further reduce the marker set and identify the proteins whose abundances were significantly altered by the mutation and restored by the DCE treatment. To identify the proteins involved in cognition, a stepwise regression model was constructed to assess the correlation between the levels of the differentially expressed proteins and performance in the ORT (DI) and the Y-maze test. The results were further validated using Pearson correlation analysis of the differentially abundant proteins among the different groups.

Western blotting

Since PLCB1 and KIF1A abundance as well as their partners are associated to several brain disorders, Western blotting was used to determine their abundance as well as two inhibitors of NF-κB, IκBα and IκBβ, in dissected brain tissues. Briefly, brain tissues were homogenized in freshly prepared lysis buffer containing 20 mM Trizma-Base, 150 mM NaCl (pH 7.4) (Sigma–Aldrich, Saint-Quentin Fallavier, France), 1% Triton X-100, 4% complete protease inhibitor cocktail and 20% mix of anti-phosphatase inhibitors using a Precellys Evolution tissue homogenizer. The samples were then centrifuged at 2500 × g for 15 min followed by 10,000 x g for 20 min to obtain lysates for electrophoresis. The proteins (10 to 20 µg) and protein standards were mixed with Laemmli buffer and loaded on 4–15% Criterion TGX Stain-Free protein gels in 1 × TGS running buffer (all from Bio-Rad, Marnes-la-Coquette, France) and transferred to a 0.2 µm PVDF membrane with the Trans-Blot Turbo RTA Midi Transfer Kit (Bio-Rad, Marnes-la-Coquette, France). The membranes were blocked for 30 min in 5% low-fat milk in TBS-0.1% Tween 20 at room temperature. The blots were probed with specific primary antibodies overnight at 4°C followed by horseradish peroxidase (HRP) secondary antibodies diluted 1:5000 or 1:50000 in 5% low-fat milk in TBS-0.1% Tween 20 at room temperature. For protein detection, the membranes were treated with ECL Prime Western Blotting reagent (Amersham, UK) or Clarity Western ECL Substrate and exposed with a ChemiDoc Touch Imaging System (Bio-Rad, Marnes-la-Coquette, France). The band density was quantified with Image Lab software (Bio-Rad, Marnes-la-Coquette, France). The following antibodies were used at the indicated dilutions: anti-PLCB1 (1:1000, Abcam, ab182359), anti-IκBα (1:500, Cell Signaling Technology, 4812S), anti-IκBβ (1:500, Cell Signaling Technology, 15519S), anti-PSD95 (1:2000, Merck, MABN68), anti-tubulin (1:2000, Sigma–Aldrich, T6199), and anti-KIF1A (1:1000, Abcam, ab180153).

Co-IP

Protein extract samples (200 µg) from cortex and hippocampus were adjusted to a final volume of 600 µL with binding buffer (20 mM Tris–HCl (pH 7.5), 150 mM NaCl, 10% glycerol, 1 mM EDTA, 0.1% BSA, and 1X protease inhibitor) before the addition of 17.6 µL anti-KIF1A antibody and 100 U of Benzonase nuclease (Novagen 70,746–3). The mixture was incubated overnight at 4°C on a rotating wheel. Forty-three microliters of Dynabeads protein G (Invitrogen, 10003D) were washed 3 times with PBS + 0.05% Tween and once with binding buffer. The beads were then added to the immunoprecipitate and incubated for 1 h at room temperature with rotation. After incubation, the immunoprecipitate was washed twice with Benzonase buffer (20 mM Tris–HCl (pH 8.0), 20 mM NaCl, 10% glycerol, 2 mM MgCl2, 0.1% BSA, and 1X protease inhibitor (Roche)) and incubated in Benzonase buffer supplemented with 100 U of Benzonase nuclease for 30 min at 37°C before being washed three times with washing buffer (20 mM Tris–HCl (pH 7.5), 150 mM NaCl, 10% glycerol, 1 mM EDTA, 0.05% Tween, and 1X protease inhibitor). The immunoprecipitated proteins were eluted directly in 25 µL 1.5× Laemmli buffer supplemented with 200 mM DTT and 1 mM beta-mercaptoethanol at 95°C for 10 min before magnetic separation of the beads and MS. MS was carried out under similar conditions as those for the brain protein extracts except that the nano-UPLC gradient was reduced to 60 min.

Data availability statement

The MS and proteomics dataset is available through the ProteomeXchange Consortium via the PRIDE partner repository (https://www.ebi.ac.uk/pride/) under dataset identifiers PXD024968 and 10.6019/PXD024968.

Ethics statement

The animal study was reviewed and approved by All *in vivo* experiments were conducted in compliance with the European Communities Council Directive of 22 September 2010 and were approved by the Italian Ministry of Health (authorization number 259/2016-PR).

Author contributions

AM was responsible for project administration, conceptualization, funding acquisition and writing of the manuscript. FC and LB administered drugs to the mice, conducted behavioral studies, and collected brain samples. EP administered drugs to the mice and performed genotyping and the behavioral studies. AC-G, LBB, and NC conducted biochemistry experiments. EM and CS conducted the Co-IP experiments. J-CG and JA designed and conducted the proteomic experiments. RaH and RiH conducted mathematical and statistical modeling of the proteomics data as well as bioinformatics analysis. MS, RaH, LB, JA, RiH, HB, and TJ participated in the writing and review of the manuscript. All authors contributed to the article and approved the submitted version.

Funding

This work was supported by Jerome Fondation Lejeune grant and by X-traordinaire, which is a patient group dedicated to rare intellectual disabilities. AM is funded by Foundation Lejeune grant; RiH is funded by the University of Sharjah - Skotech collaborative Artificial Intelligence for Life (AIfoL) award (grant no: AIfoL-2201).

Conflict of interest

The authors declare that the research was conducted in the absence of any commercial or financial relationships that could be construed as a potential conflict of interest.

Publisher's note

All claims expressed in this article are solely those of the authors and do not necessarily represent those of their affiliated organizations, or those of the publisher, the editors and the reviewers. Any product that may be evaluated in this article, or claim that may be made by its manufacturer, is not guaranteed or endorsed by the publisher.

Supplementary material

The Supplementary material for this article can be found online at: https://www.frontiersin.org/articles/10.3389/fnmol.2023.1118707/full#supplementary-material

References

Alberini, C. M. (2009). Transcription factors in long-term memory and synaptic plasticity. *Physiol. Rev.* 89, 121–145. doi: 10.1152/physrev.00017.2008

Apostolo, N., Smukowski, S. N., Vanderlinden, J., Condomitti, G., Rybakin, V., Ten Bos, J., et al. (2020). Synapse type-specific proteomic dissection identifies IgSF8 as a hippocampal CA3 microcircuit organizer. *Nat. Commun.* 11:5171. doi: 10.1038/s41467-020-18956-x

Arai, M., Itokawa, M., Yamada, K., Toyota, T., Arai, M., Haga, S., et al. (2004). Association of neural cell adhesion molecule 1 gene polymorphisms with bipolar affective disorder in Japanese individuals. *Biol. Psychiatry* 55, 804–810. doi: 10.1016/j.biopsych.2004.01.009

Atz, M. E., Rollins, B., and Vawter, M. P. (2007). NCAM1 association study of bipolar disorder and schizophrenia: polymorphisms and alternatively spliced isoforms lead to similarities and differences. *Psychiatr. Genet.* 17, 55–67. doi: 10.1097/YPG.0b013e328012d850

Barnes, C. L., and Pandya, D. N. (1992). Efferent cortical connections of multimodal cortex of the superior temporal sulcus in the rhesus monkey. *J. Comp. Neurol.* 318, 222–244. doi: 10.1002/cne.903180207

Baroncelli, L., Alessandri, M. G., Tola, J., Putignano, E., Migliore, M., Amendola, E., et al. (2014). A novel mouse model of creatine transporter deficiency. *F1000Res* 3:228. doi: 10.12688/f1000research.5369.1

Baroncelli, L., Molinaro, A., Cacciante, F., Alessandri, M. G., Napoli, D., Putignano, E., et al. (2016). A mouse model for creatine transporter deficiency reveals early onset cognitive impairment and neuropathology associated with brain aging. *Hum. Mol. Genet.* 25, 4186–4200. doi: 10.1093/hmg/ddw252

Begenisic, T., Baroncelli, L., Sansevero, G., Milanese, M., Bonifacino, T., Bonanno, G., et al. (2014). Fluoxetine in adulthood normalizes GABA release and rescues hippocampal synaptic plasticity and spatial memory in a mouse model of down syndrome. *Neurobiol. Dis.* 63, 12–19. doi: 10.1016/j.nbd.2013.11.010

Braissant, O., Henry, H., Beard, E., and Uldry, J. (2011). Creatine deficiency syndromes and the importance of creatine synthesis in the brain. *Amino Acids* 40, 1315–1324. doi: 10.1007/s00726-011-0852-z

Bruun, T. U. J., Sidky, S., Bandeira, A. O., Debray, F. G., Ficicioglu, C., Goldstein, J., et al. (2018). Treatment outcome of creatine transporter deficiency: international retrospective cohort study. *Metab. Brain Dis.* 33, 875–884. doi: 10.1007/s11011-018-0197-3

Cheillan, D., Joncquel-Chevalier Curt, M., Briand, G., Salomons, G. S., Mention-Mulliez, K., Dobbelaere, D., et al. (2012). Screening for primary creatine deficiencies in French patients with unexplained neurological symptoms. *Orphanet J. Rare Dis.* 7:96. doi: 10.1186/1750-1172-7-96

Chen, E. Y., Tan, C. M., Kou, Y., Duan, Q., Wang, Z., Meirelles, G. V., et al. (2013). Enrichr: interactive and collaborative HTML5 gene list enrichment analysis tool. *BMC Bioinformatics* 14:128. doi: 10.1186/1471-2105-14-128

Chen, H.-R., Zhang-Brotzge, X., Morozov, Y. M., Li, Y., Wang, S., Zhang, H. H., et al. (2021). Creatine transporter deficiency impairs stress adaptation and brain energetics homeostasis. *JCI Insight* 6:e140173. doi: 10.1172/jci.insight.140173

Cholewa-Waclaw, J., Bird, A., von Schimmelmann, M., Schaefer, A., Yu, H., Song, H., et al. (2016). The role of epigenetic mechanisms in the regulation of gene expression in the nervous system. *J. Neurosci.* 36, 11427–11434. doi: 10.1523/JNEUROSCI.2492-16.2016

Chung, C. Y., Koprich, J. B., Siddiqi, H., and Isacson, O. (2009). Dynamic changes in presynaptic and axonal transport proteins combined with striatal neuroinflammation precede dopaminergic neuronal loss in a rat model of AAV alpha-synucleinopathy. *J. Neurosci.* 29, 3365–3373. doi: 10.1523/JNEUROSCI.5427-08.2009

Clark, A. J., Rosenberg, E. H., Almeida, L. S., Wood, T. C., Jakobs, C., Stevenson, R. E., et al. (2006). X-linked creatine transporter (SLC6A8) mutations in about 1% of males with mental retardation of unknown etiology. *Hum. Genet.* 119, 604–610. doi: 10.1007/s00439-006-0162-9

Dai, Y., Ma, Y., Li, S., Banerjee, S., Liang, S., Liu, Q., et al. (2017). An LMNB1 duplication caused adult-onset autosomal dominant Leukodystrophy in Chinese family: clinical manifestations, neuroradiology and genetic diagnosis. *Front. Mol. Neurosci.* 10:215. doi: 10.3389/fnmol.2017.00215

De Jager, P. L., Srivastava, G., Lunnon, K., Burgess, J., Schalkwyk, L. C., Yu, L., et al. (2014). Alzheimer's disease: early alterations in brain DNA methylation at ANK1, BIN1, RHBDF2 and other loci. *Nat. Neurosci.* 17, 1156–1163. doi: 10.1038/nn.3786

Des Roches, C. L., Patel, J., Wang, P., Minassian, B., Salomons, G. S., Marshall, C. R., et al. (2015). Estimated carrier frequency of creatine transporter deficiency in females in the general population using functional characterization of novel missense variants in the SLC6A8 gene. *Gene* 565, 187–191. doi: 10.1016/j.gene.2015.04.011

Esmaeeli Nieh, S., Madou, M. R., Sirajuddin, M., Fregeau, B., McKnight, D., Lexa, K., et al. (2015). De novo mutations in KIF1A cause progressive encephalopathy and brain atrophy. *Ann. Clin. Transl. Neurol.* 2, 623–635. doi: 10.1002/acn3.198

Gray, L. J., Dean, B., Kronsbein, H. C., Robinson, P. J., and Scarr, E. (2010). Region and diagnosis-specific changes in synaptic proteins in schizophrenia and bipolar I disorder. *Psychiatry Res.* 178, 374–380. doi: 10.1016/j.psychres.2008.07.012

Hachim, M. Y., Hachim, I. Y., Talaat, I. M., Yakout, N. M., and Hamoudi, R. (2020). M1 polarization markers are Upregulated in basal-like breast cancer molecular subtype and associated with favorable patient outcome. *Front. Immunol.* 11:560074. doi: 10.3389/fimmu.2020.560074

Hammer, S., Dorrani, N., Dragich, J., Kudo, S., and Schanen, C. (2002). The phenotypic consequences of MECP2 mutations extend beyond Rett syndrome. *Ment. Retard. Dev. Disabil. Res. Rev.* 8, 94–98. doi: 10.1002/mrdd.10023

Hamoudi, R. A., Appert, A., Ye, H., Ruskone-Fourmestraux, A., Streubel, B., Chott, A., et al. (2010). Differential expression of NF-kappa B target genes in MALT lymphoma

with and without chromosome translocation: insights into molecular mechanism. *Leukemia* 24, 1487–1497. doi: 10.1038/leu.2010.118

Hannan, A. J., Blakemore, C., Katsnelson, A., Vitalis, T., Huber, K. M., Bear, M., et al. (2001). PLC-beta 1, activated via mGluRs, mediates activity-dependent differentiation in cerebral cortex. *Nat. Neurosci.* 4, 282–288. doi: 10.1038/85132

Hartmann, E. M., and Armengaud, J. (2014). N-terminomics and proteogenomics, getting off to a good start. *Proteomics* 14, 2637–2646. doi: 10.1002/pmic.201400157

Iki, J., Inoue, A., Bito, H., and Okabe, S. (2005). Bi-directional regulation of postsynaptic cortactin distribution by BDNF and NMDA receptor activity. *Eur. J. Neurosci.* 22, 2985–2994. doi: 10.1111/j.1460-9568.2005.04510.x

Jaggumantri, S., Dunbar, M., Edgar, V., Mignone, C., Newlove, T., Elango, R., et al. (2015). Treatment of Creatine transporter (SLC6A8) deficiency with Oral S-Adenosyl methionine as adjunct to L-arginine, glycine, and Creatine supplements. *Pediatr. Neurol.* 53:e362, 360–363.e2. doi: 10.1016/j.pediatrneurol.2015.05.006

Kaltschmidt, B., Ndiaye, D., Korte, M., Pothion, S., Arbibe, L., Prullage, M., et al. (2006). NF-kappa B regulates spatial memory formation and synaptic plasticity through protein kinase a/CREB signaling. *Mol. Cell. Biol.* 26, 2936–2946. doi: 10.1128/MCB.26.8.2936-2946.2006

Killoy, K. M., Harlan, B. A., Pehar, M., and Vargas, M. R. (2020). FABP7 upregulation induces a neurotoxic phenotype in astrocytes. *Glia* 68, 2693–2704. doi: 10.1002/glia.23879

Kondo, M., Takei, Y., and Hirokawa, N. (2012). Motor protein KIF1A is essential for hippocampal synaptogenesis and learning enhancement in an enriched environment. *Neuron* 73, 743–757. doi: 10.1016/j.neuron.2011.12.020

Kuleshov, M. V., Jones, M. R., Rouillard, A. D., Fernandez, N. F., Duan, Q., Wang, Z., et al. (2016). Enrichr: a comprehensive gene set enrichment analysis web server 2016 update. *Nucleic Acids Res.* 44, W90–W97. doi: 10.1093/nar/gkw377

Lee, J. R., Srour, M., Kim, D., Hamdan, F. F., Lim, S. H., Brunel-Guitton, C., et al. (2015). De novo mutations in the motor domain of KIF1A cause cognitive impairment, spastic paraparesis, axonal neuropathy, and cerebellar atrophy. *Hum. Mutat.* 36, 69–78. doi: 10.1002/humu.22709

Lian, H., Shim, D. J., Gaddam, S. S., Rodriguez-Rivera, J., Bitner, B. R., Pautler, R. G., et al. (2012). Ikappa Balpha deficiency in brain leads to elevated basal neuroinflammation and attenuated response following traumatic brain injury: implications for functional recovery. *Mol. Neurodegener.* 7:47. doi: 10.1186/1750-1326-7-47

Lo Vasco, V. R., Longo, L., and Polonia, P. (2013). Phosphoinositide-specific phospholipase C β1 gene deletion in bipolar disorder affected patient. *J. Cell Commun. Signal* 7, 25–29. doi: 10.1007/s12079-012-0182-2

Lu, B., Nagappan, G., and Lu, Y. (2014). BDNF and synaptic plasticity, cognitive function, and dysfunction. *Handb. Exp. Pharmacol.* 220, 223–250. doi: 10.1007/978-3-642-45106-5_9

Manning, E. E., Ransome, M. I., Burrows, E. L., and Hannan, A. J. (2012). Increased adult hippocampal neurogenesis and abnormal migration of adult-born granule neurons is associated with hippocampal-specific cognitive deficits in phospholipase C-beta 1 knockout mice. *Hippocampus* 22, 309–319. doi: 10.1002/hipo.20900

Maviel, T., Durkin, T. P., Menzaghi, F., and Bontempi, B. (2004). Sites of neocortical reorganization critical for remote spatial memory. *Science* 305, 96–99. doi: 10.1126/science.1098180

Mazziotti, R., Cacciante, F., Sagona, G., Lupori, L., Gennaro, M., Putignano, E., et al. (2020). Novel translational phenotypes and biomarkers for creatine transporter deficiency. *Brain Commun* 2:fcaa089. doi: 10.1093/braincomms/fcaa089

Meffert, M. K., Chang, J. M., Wiltgen, B. J., Fanselow, M. S., and Baltimore, D. (2003). NF-kappa B functions in synaptic signaling and behavior. *Nat. Neurosci.* 6, 1072–1078. doi: 10.1038/nn1110

Motakis, E. S., Nason, G. P., Fryzlewicz, P., and Rutter, G. A. (2006). Variance stabilization and normalization for one-color microarray data using a data-driven multiscale approach. *Bioinformatics* 22, 2547–2553. doi: 10.1093/bioinformatics/btl412

Ohba, C., Haginoya, K., Osaka, H., Kubota, K., Ishiyama, A., Hiraide, T., et al. (2015). De novo KIF1A mutations cause intellectual deficit, cerebellar atrophy, lower limb spasticity and visual disturbance. *J. Hum. Genet.* 60, 739–742. doi: 10.1038/jhg.2015.108

Padiath, Q. S. (2016). Lamin B1 mediated demyelination: linking Lamins, lipids and Leukodystrophies. *Nucleus* 7, 547–553. doi: 10.1080/19491034.2016.1260799

Pagnamenta, A. T., Howard, M. F., Wisniewski, E., Popitsch, N., Knight, S. J., Keays, D. A., et al. (2015). Germline recessive mutations in PI4KA are associated with perisylvian polymicrogyria, cerebellar hypoplasia and arthrogryposis. *Hum. Mol. Genet.* 24, 3732–3741. doi: 10.1093/hmg/ddv117

Ray, A., and Treloar, H. B. (2012). IgSF8: a developmentally and functionally regulated cell adhesion molecule in olfactory sensory neuron axons and synapses. *Mol. Cell. Neurosci.* 50, 238–249. doi: 10.1016/j.mcn.2012.05.007

Rusciano, I., Marvi, M. V., Owusu Obeng, E., Mongiorgi, S., Ramazzotti, G., Follo, M. Y., et al. (2021). Location-dependent role of phospholipase C signaling in the brain: physiology and pathology. *Adv. Biol. Regul.* 79:100771. doi: 10.1016/j.jbior.2020.100771

Salomons, G. S., van Dooren, S. J., Verhoeven, N. M., Cecil, K. M., Ball, W. S., Degrauw, T. J., et al. (2001). X-linked creatine-transporter gene (SLC6A8) defect: a new creatine-deficiency syndrome. *Am. J. Hum. Genet.* 68, 1497–1500. doi: 10.1086/320595

Schmahmann, J. D., and Pandya, D. N. (1997). The cerebrocerebellar system. *Int. Rev. Neurobiol.* 41, 31–60. doi: 10.1016/S0074-7742(08)60346-3

Shibayama, A., Cook, E. H. Jr., Feng, J., Glanzmann, C., Yan, J., Craddock, N., et al. (2004). MECP2 structural and 3'-UTR variants in schizophrenia, autism and other psychiatric diseases: a possible association with autism. *Am. J. Med. Genet. B Neuropsychiatr. Genet.* 128B, 50–53. doi: 10.1002/ajmg.b.30016

Stockler, S., Schutz, P. W., and Salomons, G. S. (2007). Cerebral creatine deficiency syndromes: clinical aspects, treatment and pathophysiology. *Subcell. Biochem.* 46, 149–166. doi: 10.1007/978-1-4020-6486-9_8

Suomi, T., Seyednasrollah, F., Jaakkola, M. K., Faux, T., and Elo, L. L. (2017). ROTS: an R package for reproducibility-optimized statistical testing. *PLoS Comput. Biol.* 13:e1005562. doi: 10.1371/journal.pcbi.1005562

Tomaselli, P. J., Rossor, A. M., Horga, A., Laura, M., Blake, J. C., Houlden, H., et al. (2017). A de novo dominant mutation in KIF1A associated with axonal neuropathy, spasticity and autism spectrum disorder. *J. Peripher. Nerv. Syst.* 22, 460–463. doi: 10.1111/jns.12235

Trotier-Faurion, A., Dezard, S., Taran, F., Valayannopoulos, V., de Lonlay, P., and Mabondzo, A. (2013). Synthesis and biological evaluation of new Creatine fatty esters revealed dodecyl Creatine Ester as a promising drug candidate for the treatment of the Creatine transporter deficiency. *J. Med. Chem.* 56, 5173–5181. doi: 10.1021/jm400545n

Trotier-Faurion, A., Passirani, C., Bejaud, J., Dezard, S., Valayannopoulos, V., Taran, F., et al. (2015). Dodecyl creatine ester and lipid nanocapsule: a double strategy for the treatment of creatine transporter deficiency. *Nanomedicine* 10, 185–191. doi: 10.2217/nnm.13.205

Ullio-Gamboa, G., Udobi, K. C., Dezard, S., Perna, M. K., Miles, K. N., Costa, N., et al. (2019). Dodecyl creatine ester-loaded nanoemulsion as a promising therapy for creatine transporter deficiency. *Nanomedicine* 14, 1579–1593. doi: 10.2217/nnm-2019-0059

Valayannopoulos, V., Bakouh, N., Mazzuca, M., Nonnenmacher, L., Hubert, L., Makaci, F. L., et al. (2013). Functional and electrophysiological characterization of four non-truncating mutations responsible for creatine transporter (SLC6A8) deficiency syndrome. *J. Inherit. Metab. Dis.* 36, 103–112. doi: 10.1007/s10545-012-9495-9

van de Kamp, J. M., Mancini, G. M., and Salomons, G. S. (2014). X-linked creatine transporter deficiency: clinical aspects and pathophysiology. *J. Inherit. Metab. Dis.* 37, 715–733. doi: 10.1007/s10545-014-9713-8

Varea, E., Guirado, R., Gilabert-Juan, J., Marti, U., Castillo-Gomez, E., Blasco-Ibanez, J. M., et al. (2012). Expression of PSA-NCAM and synaptic proteins in the amygdala of psychiatric disorder patients. *J. Psychiatr. Res.* 46, 189–197. doi: 10.1016/j.jpsychires.2011.10.011

Wang, J., Zhang, Q., Chen, Y., Yu, S., Wu, X., and Bao, X. (2019). Rett and Rett-like syndrome: expanding the genetic spectrum to KIF1A and GRIN1 gene. *Mol. Genet. Genomic Med.* 7:e968. doi: 10.1002/mgg3.968

Weller, S., and Gartner, J. (2001). Genetic and clinical aspects of X-linked hydrocephalus (L1 disease): mutations in the L1CAM gene. *Hum. Mutat.* 18, 1–12. doi: 10.1002/humu.1144

Wen, Z., Cheng, T. L., Li, G. Z., Sun, S. B., Yu, S. Y., Zhang, Y., et al. (2017). Identification of autism-related MECP2 mutations by whole-exome sequencing and functional validation. *Mol. Autism.* 8:43. doi: 10.1186/s13229-017-0157-5

Yang, Y. R., Kang, D. S., Lee, C., Seok, H., Follo, M. Y., Cocco, L., et al. (2016). Primary phospholipase C and brain disorders. *Adv. Biol. Regul.* 61, 80–85. doi: 10.1016/j.jbior.2015.11.003

frontiers | Frontiers in Molecular Neuroscience

TYPE Review
PUBLISHED 03 April 2023
DOI 10.3389/fnmol.2023.1076016

OPEN ACCESS

EDITED BY
Arianna Bellucci,
University of Brescia,
Italy

REVIEWED BY
Abhijit Maji,
University of Texas Southwestern Medical Center,
United States
Kiran Veer Sandhu,
University College Cork,
Ireland

*CORRESPONDENCE
Zhaoming Ge
✉ 13893285120@163.com
Yongnan Li
✉ lyngyq2006@foxmail.com

†These authors have contributed equally to this work

SPECIALTY SECTION
This article was submitted to Brain Disease Mechanisms, a section of the Journal Frontiers in Molecular Neuroscience

RECEIVED 21 October 2022
ACCEPTED 13 March 2023
PUBLISHED 03 April 2023

CITATION
Shen X, Li M, Shao K, Li Y and Ge Z (2023) Post-ischemic inflammatory response in the brain: Targeting immune cell in ischemic stroke therapy.
Front. Mol. Neurosci. 16:1076016.
doi: 10.3389/fnmol.2023.1076016

Post-ischemic inflammatory response in the brain: Targeting immune cell in ischemic stroke therapy

Xueyang Shen[1†], Mingming Li[1,2,3†], Kangmei Shao[1], Yongnan Li[4*†] and Zhaoming Ge[1,2,3*†]

[1]Department of Neurology, Lanzhou University Second Hospital, Lanzhou University, Lanzhou, China, [2]Gansu Provincial Neurology Clinical Medical Research Center, The Second Hospital of Lanzhou University, Lanzhou, China, [3]Expert Workstation of Academician Wang Longde, The Second Hospital of Lanzhou University, Lanzhou, China, [4]Department of Cardiac Surgery, Lanzhou University Second Hospital, Lanzhou University, Lanzhou, China

An ischemic stroke occurs when the blood supply is obstructed to the vascular basin, causing the death of nerve cells and forming the ischemic core. Subsequently, the brain enters the stage of reconstruction and repair. The whole process includes cellular brain damage, inflammatory reaction, blood–brain barrier destruction, and nerve repair. During this process, the proportion and function of neurons, immune cells, glial cells, endothelial cells, and other cells change. Identifying potential differences in gene expression between cell types or heterogeneity between cells of the same type helps to understand the cellular changes that occur in the brain and the context of disease. The recent emergence of single-cell sequencing technology has promoted the exploration of single-cell diversity and the elucidation of the molecular mechanism of ischemic stroke, thus providing new ideas and directions for the diagnosis and clinical treatment of ischemic stroke.

KEYWORDS

neuron, immune cell, glial, single-cell sequencing, ischemic stroke

1. Introduction

Stroke threatens human life and is one of the world's most common causes of disability and death (Feigin et al., 2022). According to the Global Burden of Diseases 2019, the burden of stroke has increased significantly from 1990 to 2019 (70.0% increase in stroke events and 43.0% increase in stroke-related deaths) (Owolabi et al., 2022). Ischemic stroke accounts for 87% of all strokes globally (Virani et al., 2020). Acute ischemic stroke (AIS) is caused by a blockade of the local cerebral blood supply caused by various reasons, leading to hypoxia, ischemic changes in brain tissue, and a corresponding loss of nerve function. Since there is no effective treatment for neurological impairment caused by AIS except thrombolysis, early and accurate detection of ischemic injury is essential for initiating appropriate acute intervention and preventing recurrence strategies.

The current diagnosis of AIS is still based on clinical and neuroimaging evaluation (Bustamante et al., 2017). Therefore, it is essential to elucidate the pathophysiology of its pathogenesis further. The heterogeneity of cells in the central nervous system (CNS) has made it challenging to define the role of whole-brain cell subgroups in AIS pathogenesis and

progression, which involves complex interactions between neurons, glial cells, and other cell types (Brioschi et al., 2021; Shen et al., 2021). Therefore, identifying changes in neuronal functions, transcription factors, and molecular pathways related to the above cellular processes might help to develop new therapeutic strategies. Therefore, it is necessary to understand each cell and its subgroup caused by AIS comprehensively. The traditional research method was to study the multicellular population and obtain the average value of a particular parameter. This method leads to a loss of heterogeneity information and many other "important details." The population study can only obtain dominant cellular information for some complex tissues, such as highly heterogeneous solid tumor tissues. Some cells are ignored in the study because of their small size. Additionally, various microorganisms in nature are not only limited in number but also can not be expanded and cultured by traditional methods. Conventional techniques are of limited use for the analysis of these microorganisms, and therefore, single-cell RNA sequencing came into existence.

Single-cell sequencing mainly includes single-cell genome sequencing, single-cell epigenome sequencing, and single-cell transcriptome sequencing (scRNA-seq). There are currently many single-cell sequencing methods, such as Smart-seq, Drop-seq, and 10× genomics. Most have the same workflow: single cell isolation and collection, cell lysis, reverse transcription of RNA, cDNA amplification, library preparation, sequencing, and data analysis. The outstanding advantages of single-cell sequencing technology are that it can detect cell specificity and intercellular differences, explore the cooperative operation mode between cells, and study tissue heterogeneity from the perspective of a cell atlas. A combination of multi-omics analysis, cell and molecular imaging, and other technologies allows the generation of more accurate cell maps, deepens the understanding of disease development laws, helps find new targets for disease treatment and explores the cell development process. This article reviews the application of single-cell sequencing technology in AIS and its molecular basis in the pathological process of AIS.

2. Brain cellular damage

After an ischemic stroke, there are two zones of injury: the infarct core area and the ischemic penumbra (Heiss, 2000). Several brain cells in the ischemic penumbra, either dormant or semi-dormant, maintain the integrity of their morphology because of collateral arteries in the supply area after ischemia. Although these cells can continue to live in the brain for several hours, they cannot perform their original normal functions (Tang et al., 2022). Therefore, it is important to explicit the mechanism of ischemic cell death for the progression from penumbra towards irreversible injury. Guo et al. (2021) used scRNA-seq to comprehensively map the cell types of the ischemic penumbra in the middle cerebral artery occlusion (MCAO) mouse model and determined 24 cell clusters. All cells were divided into 13 major cell sets, and their marker genes have been confirmed in other articles. These cells include neurons (*MAP2*; Chen M.L. et al., 2021 and *TBR1*; Yook et al., 2019), astrocytes (*GFAP*; Wang et al., 2020 and *ALDOC*; Zeisel et al., 2015), microglia (*HEXB8*; Sousa et al., 2018), oligodendrocytes (*PLP1*; Marques et al., 2016), oligodendrocyte precursor cells (*PDGFRA*; Alessandrini et al., 2020), endothelial cells (*ITM2A*; Cegarra et al., 2022), pericytes (Desmin and *PDGFR-β*; Smyth et al., 2018), macrophages (*CD163*; Skytthe et al., 2020), B cells (*MS4A1* and *CD79A*; Lerman et al., 2022), T cells (*CD3*, *CD4*, *CD5*, *CD8*; Martinez-Lage et al., 2019), monocytes (*CD14* and *CD16*; Calderon et al., 2017), ependymal cells (*TTR*; Gokce et al., 2016), and fibroblasts (*COL1A1*; Bonney et al., 2022). Among them, most cells were microglia, astrocytes, and oligodendrocytes. The team of Lin and others obtained 3,186 mouse cerebrovascular cell samples from the GSE98816 dataset by examining the cerebrovascular-related databases (Kundishora et al., 2021). ScRNA-seq cell cluster analysis showed ten cell clusters and four cell subgroups, including endothelial cells, fibroblasts, oligodendrocytes, and microglia. After analyzing the differential expression of related genes in cell subgroups, it was the first time to find that calcium signaling pathway-related genes [*AC079305.10*, *BCL10*, BCL2 Related Protein A1 (*BCL2A1*), *BRE-AS1*, Dynein Light Chain LC8-Type 2 (*DYNLL2*), Epiregulin (*EREG*), and Prostaglandin-Endoperoxide Synthase 2 (*PTGS2*)] and transcription factors [Jun, Interferon Regulatory Factor 9 (IRF9), ETS Variant Transcription Factor 5 (ETV5), and Peroxisome Proliferator Activated Receptor Alpha (PPARa)] play a key role in AIS. Many cellular functions are regulated by calcium signals that are generated by different signaling pathways, and participate in the occurrence and development of many diseases (Madreiter-Sokolowski et al., 2020) such as Parkinson's disease, Alzheimer's disease, etc. *Jun* was identified to be associated with hypoxia in endothelial cells (Kundishora et al., 2021), *PPARA* is a transcription factor that regulates genes involved in fatty acid metabolism and activates hepatic autophagy, it is also an important factor regulating autophagy in the clearance of Aβ in Alzheimer's disease (Luo et al., 2020). AIS leads to a significant increase in monocyte-derived cells (the proportion of cells changed from 2 to 16%), neutrophils, and pericytes, while endothelial cells and fibroblasts decreased slightly. The expression of specific ischemic injury-related genes, such as Glycerol-3-Phosphate Dehydrogenase 1 (*GPD1*) in oligodendrocytes, C-C Motif Chemokine Ligand 11 (*CCL11*) in pericytes, CD72 Molecule (*CD72*) and Leukocyte Immunoglobulin Like Receptor B4 (*LILRB4*) in microglia, were all upregulated (Zheng et al., 2021). Rusu et al. identify *GPD1* as a specific marker for dormant and chemoresistant brain tumor stem cells (BTSCs) and show that targeting *GPD1* disrupts BTSC maintenance and extends survival (Rusu et al., 2019). *CCL11* is important in the regulation of colitis and associated carcinogenesis (Polosukhina et al., 2021). These genes are expressed in ischemic stroke and other diseases. Biomarkers are signal indicators that are abnormal due to environmental pollutants at different biological levels (molecules, cells, individuals, etc.) before organisms are seriously damaged. It can provide early warning of serious toxic injury. The onset of ischemic stroke is acute, and the pathophysiological process is complex. Currently, the commonly used clinical biomarkers do not have the high specificity of the AIS, In the future, we can use single-cell sequencing technology to seek more specific biomarkers in ischemic stroke. Neurons in the cerebral cortex are mainly excitatory neurons and interneurons (Bandler et al., 2017). Excitatory neurons originate from the precursor cells of the developing cerebral cortex, while interneurons originate from the ganglion eminence (Shi Y. et al., 2021). By RNA sequencing, Zhong et al. (2018) analyzed more than 2,300 single cells in the developing human prefrontal cortex from 8 to 26 weeks of gestation, further dividing the excitatory neurons into seven subtypes. Among them, the 13 weeks of gestation is the critical period for the migration of the newly formed neurons. In the

prefrontal cortex, the growth related gene expression of neurons increases at 16 weeks of gestation, and the functional gene expression, such as genes related to calcium input, increases at 19 weeks. At 19–26 weeks of gestation, genes related to axonogenesis were expressed in the prefrontal cortex, followed by genes related to synapse formation at 23–26 weeks, indicating that the initial formation of neural connections occurs between 19 and 26 weeks of gestation.

Interneurons were further divided into eight subtypes, and cell populations expressing interneuron markers, such as Transcription Termination Factor 1 (TTF1), LIM Homeobox 6 (Lhx6), and Distal-Less Homeobox 1 (DLX1), persisted throughout development. Calbindin 2 (Calb2) + and Somatostatin (SST) + interneurons appeared earlier, followed by Calbindin 1 (Calb1)+, Cholecystokinin (CCK)+, and Vasoactive Intestinal Peptide (VIP) + interneurons. Overall, the developmental peak of excitatory neurons appeared at 16 weeks of gestation, and that of interneurons appeared at 26 weeks. There are potential subtype-specific marker genes in each neuronal cluster (Zhong et al., 2018). Chen et al. (2017) used scRNA-seq to demonstrate the diversity of hypothalamic cells. They identified 15 glutamatergic neuron subtypes (Glu1-Glu15), 18 γ-aminobutyric acid (GABA)-ergic neuron subtypes (GABA1-GABA18), and one histaminergic neuron cluster (Hasta) expressing high levels of Histidine Decarboxylase (HDC). Kiss1 and Pomc represent Glu11 and Glu13 cell clusters, respectively, while Vip and Agouti Related Neuropeptide (Agrp) represent GABA9 and GABA15 cell clusters, consistent with their roles in controlling neuronal differentiation and identity. Recent studies have shown that RNA binding proteins CUGBP Elav-Like Family Member 1/2 (CELF1/2), Muscleblind Like Splicing Regulator 2 (Mbnl2), and KH RNA Binding Domain Containing, Signal Transduction Associated 3 (Khdrbs3) are preferentially expressed and more active in glutamatergic neurons (Feng et al., 2021). In contrast, ELAV Like RNA Binding Protein 2 (ELAVL2) and QK are preferentially expressed and more active in GABAergic neurons, indicating the hierarchical regulation of alternative splicing between different neuronal cell types and providing a basis to specify the identity and function of neurons. Single-cell sequencing studies revealed the heterogeneity among different neuronal and non-neuronal cells in various brain regions (Zeisel et al., 2015). Neuronal changes in some neurological diseases have not been described in detail. Moreover, the changes and migration of neuronal cells in the ischemic penumbra have not been reported, and therefore, further research is needed for a better understanding (Table 1).

3. Participate in inflammatory reaction

Under normal circumstances, the human CNS is separated from the peripheral immune system through a complete blood–brain barrier. The nerve cells die of ischemia within a few minutes after an ischemic stroke, releasing "danger signals" and activating the innate immune response in the brain. Promote the production of neurotoxic substances, such as inflammatory cytokines, chemokines, reactive oxygen species and nitric oxide (Shi et al., 2019), and the destruction of the blood–brain barrier is mediated, resulting in a series of inflammatory cascades. At the same time, the expression of adhesion molecules in the cerebral vascular endothelial cells increases, and immune-inflammatory cells such as polymorphonuclear neutrophils, lymphocytes, and monocyte macrophages enter the brain tissue through vascular endothelial cells. By recognizing the antigens exposed by the CNS in the brain, the immune-inflammatory cells activate the adaptive immune response, further mediating the secondary injury of neurons and aggravating the neurological defect. At the same time, to reduce the damage mentioned earlier, the body initiates peripheral immunosuppressive response after the stroke through negative feedback, thereby increasing the incidence of post-stroke infection (Iadecola et al., 2020). Different immune cells play different roles after the occurrence of AIS. Understanding the type, migration, and transformation of cells would help explore the pathogenesis of AIS further and find new intervention targets.

3.1. Microglia

Microglia play a key role in brain development, immune defense, and maintenance of CNS homeostasis (Lehnardt, 2010). Common immunological markers of microglia include CD45, CD68, HLA-DR, and IBA-1, which are slowly updated at an average rate of 28% per year. Only 2% of microglia are believed to proliferate at a specific time (Askew et al., 2017; Réu et al., 2017). Previous studies exhibited a wide range of microglial DEGs between large tissues and single cells (>50%), indicating that microglia are a core player in ischemic stroke inflammation. Meanwhile, microglia have 157 unique DEGs in all cell types, ranking first, followed by monocyte-derived cells, oligodendrocytes, endothelial cells, and CNS-related macrophages (Zheng et al., 2021). Guo et al. also confirmed that microglia accounted for the most significant number of cells after MCAO induction. Using scRNA-seq, they also showed that microglia exhibit polarization and differentiation in two different progression trajectories 24 h after MCAO (Guo et al., 2021). The most enriched signatures in subclusters 3, 4, 9, and 10 were the hypoxia pathway, as well as TNF-α, IL-6, and IL-2 genes and pathways related to inflammation. Compared with the previous M1/M2 dichotomy of microglia polarization, it would be of great significance to further study the multi-polarization of microglia by using single-cell technology. On the other hand, Li et al. found six subpopulations of microglia in aged rats after ischemia–reperfusion (Li et al., 2022). MG5 and MG6 were the main subpopulations after stroke. In MG5 cells, the expression of Top2a, Stmn1, Mki67, and Cdk1 was significantly upregulated, indicating that MG5 cells were in a highly proliferative state. Compared with MG1, expression of the steady-state genes of microglia (such as P2ry12, Tmem119, Cx3cr1, and Hexb) were downregulated in MG5. While MG6 represented a unique microglial state that appears only after stroke, was close to neutrophils on the uniform manifold approximation and projection (UMAP) map, and expressed high levels of Cxcr2, S100a8, Il1b, and Mmp9, showing a unique "neutrophil-like" phenotype and participating in the inflammatory response. Zheng et al. detected CCL7 and CCL12 in microglia, providing evidence for the molecular and cellular basis of inflammatory response after MCAO induction. They showed that the release of damage-associated molecular patterns (DAMPs) in damaged tissues initiated the secretion of these chemokines and cytokines by glial cells (Li P. et al., 2018; Zheng et al., 2021). CCL22 and many other inflammatory factors further exacerbated brain injury by enhancing cytotoxicity. Chemotactic factors direct the migration of immune cells, multipotent stem cells, and progenitor cells under physiologic and pathologic conditions. CCL7 is also highly expressed in the

TABLE 1 Application of single cell sequencing technology in the study of ischemic stroke.

Study name and years of publication	Methodology	Sample source	Number of cells sequence	Molecules/pathways identified
Chen et al. (2017)	Seurat	Mice	14,000	Defines 11 non-neuronal and 34 neuronal cell clusters with distinct transcriptional signatures on hypothalamus
Zhong et al. (2018)	Seurat and forest	Human embryonic PFCs	2,309	Found the intrinsic development-dependent signals that regulate neuron generation and circuit formation
Wang et al. (2020)	HiSeq 3000	Mice	unknown	Astrocyte-derived E2 is also critical for the activation of LIF/JAK/STAT3 signaling in astrocytes, which is a key regulatory pathway responsible for astrocyte activation
Guo et al. (2021)	10× Genomics	Mice	18,273	Identified 13 cell types and subtypes in the ischemic stroke penumbra
Lin et al. (2021)	Seurat (v. 4.0.4) and singleR (v. 1.0)	Mice	19,922	Calcium signaling pathway-related genes (AC079305.10, BCL10, BCL2A1, BRE-AS1, DYNLL2, EREG, and PTGS2) and TFs (JUN, IRF9, ETV5, and PPARA) were identified to play a key role in IS
Zheng et al. (2021)	10× Genomics	Mice	58,528	Identified 17 cell clusters
Feng et al. (2021)	Quantas pipeline	Mice	22,578	Distinct splicing programs between glutamatergic and GABAergic neurons and between subclasses within each neuronal class
Xie et al. (2021)	10× Genomics	Human glioblastoma and peritumoraltissue	97,584	ECs in GBM are associated with partially intact BBB phenotype characterized by downregulation of transporter genes and upregulation of transcytosis gene
Shi L. et al. (2021)	Seurat 2.3.4 and DESeq2	Mice	10,925	Treg cell-derived osteopontin acted through integrin receptors on microglia to enhance microglial reparative activity, consequently promoting oligodendrogenesis and white matter repair
Shi X. et al. (2021)	10× Genomics	Mice	12,000	Deleting MEGF10 and MERTK phagocytic receptors, inhibiting phagocytosis of microglia/macrophages or astrocytes in ischemic stroke improved neurobehavioral outcomes and attenuated brain damage
Cho et al. (2022)	NovaSeq 6000	Human peripheral blood	26,302	Demonstrating the increased number of NK cells and new monocyte subclusters of mild ischemic stroke
Ma et al. (2022)	10× Genomics	Mice	104,382	The astrocytes tend to play an independent role in neuroprotection or adaption in the local ischemic-reperfusion regions at 12 h
Li et al. (2022)	10× Genomics	Mice	18,755	The first scRNA-seq data set for immune cells in the stroke aged brain

tumor microenvironment of various cancers, including colorectal cancer, breast cancer, oral cancer, renal cancer, and gastric cancer (Lee and Cho, 2020). CCL12 and CCL20 also contributes to the progression of many cancers, such as liver cancer, breast cancer (Chen et al., 2020; Li B.H. et al., 2020), etc. Similarly, some studies showed that in the MCAO group, the intercellular interactions dominated by microglia and macrophages increased significantly after AIS, especially the interactions between microglia and other immune cells, astrocytes, pericytes, and oligodendrocytes (Zheng et al., 2021). These findings imply that 24 h before the onset of AIS might be a good window for intervention to help cells survive.

3.2. Macrophages

Compared with microglia, the polarization of peripheral macrophages seems complete, indicating that microglia and blood immune cells in the brain have different activation periods after AIS (Zubova et al., 2022). It has been recently found that the infiltration and polarization of macrophages can be detected in the early stage of AIS, thus promoting the progress of inflammation (Bernstein and Rom, 2020). Zheng et al. identified six macrophage subpopulations in the MCAO group, all expressing core characteristic genes *LYV1*, *CD163*, *MRC1*, and *CBR2* (Zheng et al., 2021). According to the

changes in the cell proportion of the six subpopulations after ischemia injury, it was found that the fourth and fifth subpopulations of macrophages were mainly from the MCAO group. The MHCII-related antigen-presenting molecules of the fourth subpopulation (such as H2-Aa, H2-Ab1, and Cd74) were higher. The fifth subpopulation was characterized by increased expression of genes related to oxidative phosphorylation and respiratory electron transport chain, such as Cox7b, Cox8a, and Uqcr11. Therefore, obstructing the initial recruitment of peripheral immune cells might be an effective measure to alleviate stroke inflammation.

3.3. Neutrophils

Neutrophils are short-lived but influential immune cells that can provide an early and robust inflammatory response after tissue injury, including AIS (Aronowski and Roy-O'reilly, 2019). Neutrophils are also one of the most abundant cell populations in the injured brain, and their number rapidly peaks at the lesion site 1 to 3 days after the occurrence of AIS (Grønberg et al., 2013). At the same time, Neutrophils could also worsen AIS through multiple mechanisms, including physical blockade within microvessels to reduce cerebral blood flow further and direct entry into the brain parenchyma, followed by the release of particles containing antimicrobial enzymes and chemical components, such as MMP9 that may further damage brain tissue. scRNA-seq provides a unique insight into the cellular heterogeneity of inflammatory response after AIS, revealing immune cell subpopulations with different functions in the pathophysiology of ischemic stroke and seeking a better target for inflammatory intervention in the subsequent stroke.

3.4. Monocytes

Cho et al. used individual peripheral blood mononuclear cells (PBMCs) prepared using ddSEQ (Illumina BioRad) and sequenced on the Illumina NovaSeq 6000 platform (Shi X. et al., 2021). They found that the overall gene expression of NK cells in AIS patients showed a strong increase in cell activity and a significant decrease in the number of CD14+ monocytes subdivided into dendritic cells and CD14+ monocytes associated with NK cells. Patients with mild to moderate AIS show a slight increase in the proportion of NK cells in the blood on day 7 (Yan et al., 2009), but patients with moderate to severe stroke do not exhibit any changes in the proportion of NK cells (Peterfalvi et al., 2009; Jiang et al., 2017). Reduced NK cell numbers are associated with reduced cytokine levels in the blood. Cytokine deficiency in the blood of patients with ischemic stroke leads to immunosuppression and post-stroke infection (Wang et al., 2019). This is a severe complication leading to poor outcomes of AIS, and previous reports have also shown that NK cells are involved in this process (Chen et al., 2019; Wang et al., 2019). Gene set variation analysis (GSVA) showed that oligodendrocytes contained nine subpopulations rich in IL-6, complement system, TNF-α Pathway, and KRAS signaling, indicating that serum-and glucocorticoid-inducible kinases 3 (SGK3) from oligodendrocytes may play an essential role in regulating oligodendrocyte viability and inflammatory response in the acute phase of ischemic stroke (Inoue et al., 2016).

3.5. Others

Zheng et al. detected an upregulation of CCL7 and CCL12 in microglia, CCL4 and CDKN1a in astrocytes, and CCL4 in ependymal cells, providing evidence for the molecular and cellular basis of inflammatory response after MCAO. They showed that the release of DAMPs in damaged tissues initiates the secretion of these chemokines and cytokines by glial cells (Li P. et al., 2018; Zheng et al., 2021). CCL7, CCL12 and CCL4 are proinflammatory chemokines belonging to the CC family, and their expression is not specific in ischemic stroke. Increase in mRNA and protein levels of CCL4 in the animal model of temporal lobe epilepsy (Guzik-Kornacka et al., 2011). Subsequently, many infiltrating monocytes and lymphocytes were characterized by increased expression of CCRL2, CXCL3, CCL7, and CCL22, and many other inflammatory factors further exacerbated brain injury by enhancing cell excitotoxicity. Furthermore, AIS reduces the correlation between fibroblasts and other cells (Zheng et al., 2021). Similarly, 24 h after ischemia–reperfusion, astrocytes can act as a signal amplifier to release inflammatory signals such as cytokines and attract assistance from distal sites (Figure 1; Ma et al., 2022).

We have checked the Figure 1 carefully and corrected the "I11b" into "Il1b" in the MG6 part.

4. Destroy the blood–brain barrier

The blood–brain barrier (BBB) is a highly selective semi-permeable border of brain microvascular endothelial cells regulated by tight junctions. Pericytes, basement membranes, and glial cells induce and maintain the essential functions of the blood–brain barrier. The complex they form governs the movement of molecules, ions, and cells between the blood and CNS through interaction so that the blood–brain barrier can strictly regulate CNS homeostasis (Daneman and Prat, 2015; Profaci et al., 2020). This complex also plays an essential role in maintaining the physiological function of neurons and protecting the CNS from toxins, pathogens, inflammation, and damage. After the occurrence of AIS, activated immune cells successively reach the ischemic area through the breakdown of the blood–brain barrier. They could play a double-edged sword role by destroying or protecting the integrity of the blood–brain barrier (Li Y. et al., 2018).

4.1. Endothelial cells

Endothelial cells (ECs) are critical cellular components of BBB. Brain ECs establish a continuous complex of tight and adhesive junctions along the EC-EC contact, providing a size-selective barrier that can further express different inflow and outflow transporters. Brain ECs also have a deficient level of vesicle transport, further limiting the passage of blood-derived water-soluble molecules of various sizes in the blood (Daneman and Prat, 2015). Zheng et al. Identified six endothelial cell subpopulations in the MCAO group using scRNA-seq. Ischemia-induced inflammation and oxidative stress increased the death of endothelial cells, thus decreasing the cell proportion of the MCAO group. In contrast, the cells of BBB-related clusters increase, including a series of BBB functional disorder module-related gene expressions, such as ADAMTS4, UPP1, TIMP1, and PDLIM1 (Munji et al., 2019).

Moreover, BBB enriched endothelial cell subpopulation 3 highly expresses the *KRAS* gene and participates in the regulation of the RAS/

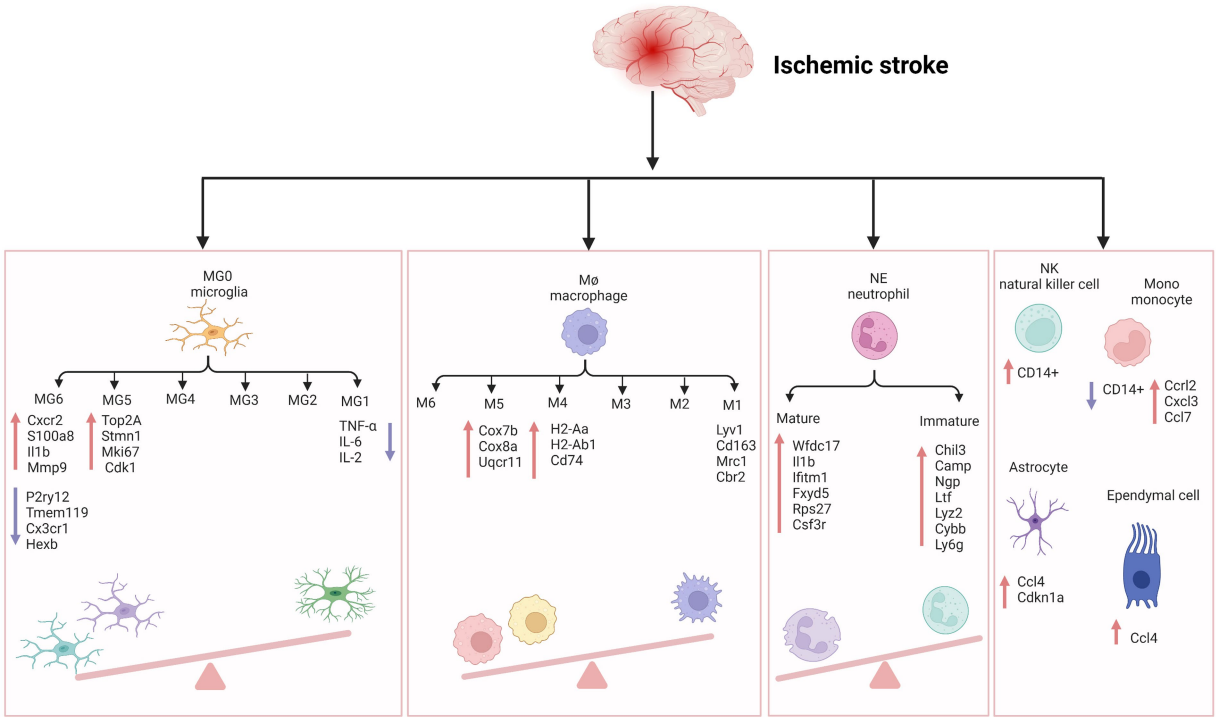

FIGURE 1
The inflammatory reaction of ischemic stroke. MG, microglia; Cxcr2, cxc chemokine receptor 2; Il1b, interleukin-1 beta; Mmp-9, matrix metallopeptidase 9; P2ry12, recombinant purinergic receptor P2Y, G protein poupled 12; Tmem119, transmembrane protein 119; Cx3cr1, c-x3-c motif chemokine receptor 1; Hexb, hexosaminidase subunit beta; Top2A, DNA topoisomerase II alpha; Stmn1, stathmin1; Mki67, marker of proliferation ki-67; TNF-α, tumor necrosis factor-α; IL-6, interleukin- 6; IL-2, interleukin-2; Cdk1, cyclin-dependent kinases 1; Cox7b, cytochrome c oxidase subunit 7b; Cox8a, cytochrome c oxidase subunit 8a; Uqcr11, ubiquinol-cytochrome c reductase, complex III subunit XI; H2-Aa, histocompatibility 2, class II antigen A, alpha; H2-Ab1, histocompatibility 2, class II antigen A, beta 1; Mrc1, mannose receptor C-Type 1; Cbr2, carbonyl reductase 2; NE, neutrophil; Wfdc17, WAP four-disulfide core domain 17; Ifitm1, interferon induced transmembrane protein 1; Fxyd5, FXYD Domain Containing Ion Transport Regulator 5; Rps27, Ribosomal Protein S27; Csf3r, colony stimulating factor 3 receptor; Chil3, Chitinase-3-like protein 3; Ltf, lactotransferrin; Lyz2, lysozyme 2; Cybb, cytochrome b-245 beta chain; Ly6g, lymphocyte antigen 6 complex locus G6D; NK, natural kill cell; Mono, monocyte; Ccrl2, c-c motif chemokine receptor like 2; Cxcl3, c-x-c motif chemokine ligand 3; Ccl7, c-c motif chemokine ligand 7; Ccl4, c-c motif chemokine ligand 4; Cdkn1a, cyclin dependent kinase inhibitor 1a. Figure was created with Biorender.com.

MAPK pathway, which is closely related to the apoptosis of cerebral microvascular endothelial cells in AIS (Yong et al., 2019). ScRNA-seq of human glioblastoma showed that ECs in the surrounding tissues have a quiescent phenotype characterized by high expression of BBB-enriched genes, including SLC2A1 and KLF2 (Xie et al., 2021). KLF2 is a crucial transcription factor that coordinates a gene network that promotes EC response to blood flow (Dekker et al., 2006) and is one of the top ten enriched genes in the brain EC cluster. GLUT1 encoded by *SLC2A1* is highly expressed in BBB ECs and promotes glucose transport across the BBB (Yong et al., 2019). Depleting GLUT1 in adult brain ECs leads to inflammation and activation of extracellular matrix-related genes (Veys et al., 2020). These results contradict the common belief that glioblastoma EC has a partially intact BBB phenotype characterized by the downregulation of transporter genes. At the same time, the expression of linker molecules remains normal or increased, and the vascular marker of BBB destruction—plasmalemma vesicle-associated protein (PLVAP) is in a high expression state.

4.2. Glial cells

The glial cells in the CNS mainly include astrocytes, microglia, and oligodendrocytes. Different glial cells are interconnected to neurons and surrounding blood vessels, forming a complex information exchange network (Huang et al., 2019). Glial cells support nerve transmission, maintain extracellular ion balance, insulate axons, and accelerate electrical signal transmission (Allen and Lyons, 2018). Guo et al. showed that in the MCAO group, Cyr61 in astrocytes and Sgk3 in oligodendrocytes were overexpressed (Guo et al., 2021). These genes might be potential therapeutic targets in this stage of AIS. Overexpression of the *CYR61* gene may contribute to the survival of astrocytes after AIS. Although there is a lack of research on AIS, previous studies have shown that the *CYR61* gene is closely related to stress and tumor cell proliferation (Sun et al., 2020). A study examining the relationship between astrocytes and BBB in heat stroke rats showed that astrocytes, but not neuronal DEGs, were rich in clusters of leukocyte chemotaxis and cytokine signals as cytokines/chemokines, toll-like receptors, and NF-κB signaling pathway (Niu et al., 2017). These chemokine-related genes were not found in neurons but combined into a regulatory sub-network in the protein–protein interaction network of astrocyte DEGs. In primary cultured astrocytes, scRNA-seq and qPCR showed upregulation of C6, CCL3, and CCR1 after heat stress but downregulation in heat stroke rats (Niu et al., 2017), while the transcriptional levels of CCL3 and CCR1 were downregulated in heat stroke rats (Audet et al., 2016). Glial cells are one of the essential components of BBB. Further exploring the regulatory

mechanism of BBB injury might be one of the targets of AIS intervention in the future.

4.3. Others

Other immune cells also play an essential role in BBB injury. Neutrophils cause the breakdown of the blood–brain barrier by releasing MMP9 and other substances, further aggravating neuroinflammation (Amantea et al., 2009). MMP9 has the ability to degrade the extracellular matrix components and has important role in the pathophysiological functions (Mondal et al., 2020). Some studies have shown that blood neutrophils in AIS patients increase and are closely related to the severity of AIS, infarct volume, and worse neurological function (Kim et al., 2012). In addition, peripheral macrophages are generally recruited to the lesion through the damaged BBB within 24 h (Jian et al., 2019). Previous studies have shown that MMP9 is highly expressed in microglia, leading to hydrolysis and vascular damage, thereby causing changes in BBB (Rosenkranz et al., 2020). Another study showed that MMPs could induce the physical destruction of BBB by digesting BBB matrix proteins (Ji et al., 2017). Guo et al. showed that MMP9 and MMP8 were overexpressed in macrophages of the MCAO group (Guo et al., 2021), indicating that in addition to microglia in the ischemic penumbra, the breakdown of BBB may also be caused by macrophages recruited from the periphery. Compared with microglia and macrophages, subpopulations of astrocytes and oligodendrocytes showed less polarization in the early stage of AIS in scRNA-seq analysis. Inflammatory mediators such as cytokines and chemokines are released through the extracellular BBB when astrocyte gap junctions are damaged during AIS (Ma et al., 2018). The mechanism of cerebral edema after cerebral ischemia is complex, caused by the interaction between many factors, and can lead to high mortality. Therefore, effective treatment measures are necessary to improve the functional prognosis of patients with cerebral ischemia (Figure 2).

5. Promote nerve repair

In the recovery stage of ischemic stroke, microglia, astrocytes, and NG2 glia proliferate highly, forming reactive gliosis and glial

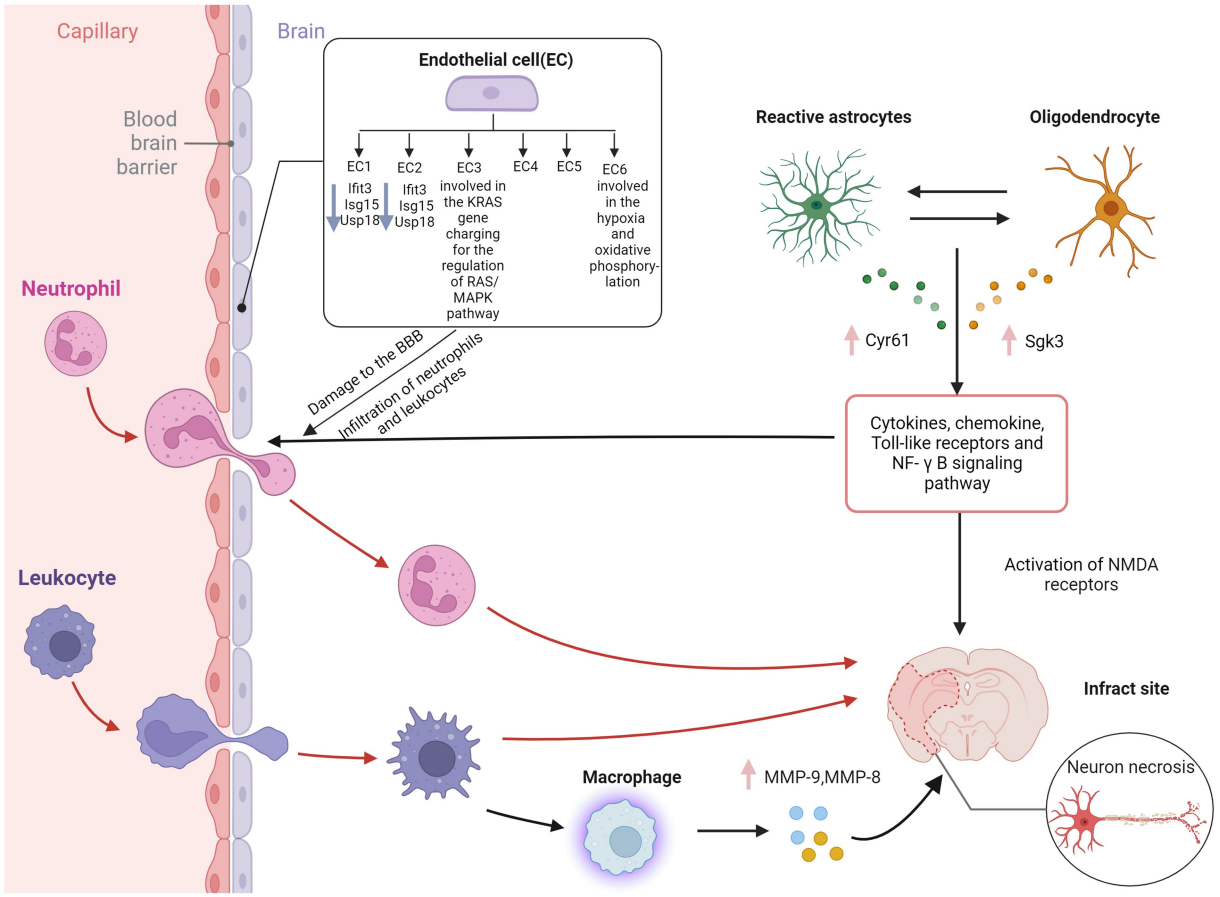

FIGURE 2
Blood–brain barrier disruption in ischemic stroke. EC, endothelial cell; IFIT3, interferon induced protein with tetratricopeptide repeats 3; Isg15, interferon-stimulated gene 15; USP18, ubiquitin-specific protease 18; Cyr61, cysteine-rich protein 61; Sgk3, serum and glucocorticoid induced kinase; MMP-9, matrix metallopeptidase 9; MMP-8, matrix metallopeptidase 8; NF-κB, nuclear factor kappa-B; NMDA receptor, N-methyl-D-aspartic acid receptor; BBB, blood–brain barrier. Figure was created with Biorender.com.

scars in the lesion area (Wanner et al., 2013). Glial scars have traditionally been thought to hinder axon regeneration and myelin sheath regeneration (Fawcett and Asher, 1999). However, there is increasing evidence that the formation of glial scars also contributes to CNS axons regeneration (Rolls et al., 2009; Anderson et al., 2016).

5.1. Microglia

Studies show that microglia and astrocytes are activated in mice with ischemic brain injury to form glial scars (Shi X. et al., 2021). The phagocytic capacity of these glial cells was enhanced in the scar area, and more synapses were phagocytized. The phagocytic ability of microglia was more substantial than that of astrocytes. High-resolution transmission electron microscopy further confirmed that synapses existed in the cell bodies of microglia and astrocytes. The GSVA results of the sixth and eighth subpopulations of microglia by Guo et al. showed that these subpopulations are MG2 type, mainly rich in the KRAS signaling pathway (Heiss, 2000), and are closely related to the survival of cancer cells (Saad et al., 2019), and may also be related to repair, neurogenesis, axon remodeling and angiogenesis (Hu et al., 2015).

5.2. Astrocytes

ScRNA-seq analysis revealed ten different astrocyte subpopulations with different cellular functional characteristics, and synaptic pruning-related processes significantly upregulated the astrocyte transcriptomic characteristics of subpopulation three. During the post-AIS repair and remodeling phase, reactive microglial proliferation and astrogliosis actively phagocytize synapses through MEGF10 and MERTK-related pathways and inhibit microglial proliferation or astrogliosis-mediated synaptic phagocytosis by improving the prognosis of AIS mice (Shi X. et al., 2021). MEGF10-knockout mice show defective long-term synaptic plasticity and impaired formation of hippocampal memories (Lee et al., 2021). Previous studies have shown that hypoxia and focal cerebral ischemia increase the number of neural stem/progenitor cells (NS/PCS) in the hippocampal and subependymal area of MCAO mice after 1 month with an increase in neuroblasts. The canonical Wnt signaling pathway is involved in this process (Knotek et al., 2020). Kraska et al. evaluated the effect of the classical Wnt signaling pathway on the differentiation potential of NS/PCS under physiological conditions and after ischemia (Kriska et al., 2021). They showed that focal cerebral ischemia increased the expression of target genes and cell type-specific proteins in the Wnt signaling pathway, affected the electrophysiological characteristics of differentiated NS/PCS, and promoted neurogenesis. ScRNA-seq provided an essential clue for analyzing the role of the Wnt signaling pathway in patients with ischemic stroke. A recent study found that astrocytes play an independent neuroprotective role 12 h after ischemia–reperfusion, mainly manifested by the activation of oxidative phosphorylation, gap junction and tight junction, ferroptosis, and other pathways (Ma et al., 2022).

5.3. Treg cells

Using scRNA-seq and flow cytometry, Shi et al. showed that the number of Treg cells in the brain significantly increased from 1 to 5 weeks after MCAO mouse modeling (Shi L. et al., 2021). Treg cells-derived osteopontin acts through integrin receptors on microglia to enhance the repair activity of microglia, thus promoting oligodendrocytes regeneration and white matter repair in the chronic phase of AIS. A recent study further confirmed that Treg cells contribute to the recovery of the CNS in the chronic phase (>1 week) after the initial ischemic injury. The number of Treg cells in the ischemic brain increases for at least 1 month after stroke. These accumulated Treg cells are thought to promote functional recovery after stroke by inhibiting astrocyte proliferation (Ito et al., 2019). Additionally, Treg cell depletion inhibits the proliferation of neural stem cells 4 days after stroke, indicating the involvement of Treg cells in neurogenesis (Wang et al., 2015). These findings reveal that Treg cells are neural repair targets for AIS recovery. In the early stage of ischemia, endothelial progenitor cells can replace the damaged vascular endothelial cells and remodel the blood–brain barrier. The release of various nutritional factors can also protect other damaged cells. In the recovery period of cerebral infarction, vascular regeneration, neuroprotection, and nerve regeneration complement each other, and its potential mechanisms include neovascularization, which provides blood flow with nutrients. Endothelial progenitor cells can secrete chemical factors such as SDF-1 and VEGF to create a microenvironment suitable for nerve regeneration and survival (Chen B. et al., 2021). In addition, endogenous neural stem cells migrate to the periphery of the infarct along the newly formed blood vessels, promoting nerve regeneration (Figure 3).

6. Limitations

There are still many limitations in single-cell sequencing, which cause data bias and distortion: (1) Batch effect during technical operation (Li X. et al., 2020); (2) Cells get lost during preparation of single cell suspension (Xin et al., 2016); (3) Low cell activity leads to the failure of the reverse transcription (Li L.C. et al., 2018); (4) RNA with low abundance gets lost during reverse transcription (Wang et al., 2016); (5) Changes in gene transcriptome during the preparation of single cell suspension (Wang et al., 2016). Since the advent of single-cell sequencing, new dimension reduction methods have been emerging, such as single-cell harmful binomial matrix decomposition (Sun et al., 2019), single-cell bimodal clustering analysis (Kim et al., 2018), and new feature methods to speed up the analysis and processing speed and reduce the batch effect in experiments (Li X. et al., 2020). When using single-cell sequencing to analyze data, one should treat the analysis results dialectically and conduct experimental verification in various ways. Although single-cell sequencing can provide much information, the interaction between cells, the localization of stem cells in tissues, and the epigenetic modification of genes are still unclear. Therefore, follow-up research is needed by combining single-cell sequencing with metabolomics, spatial transcriptome, and epigenetic modification of genes.

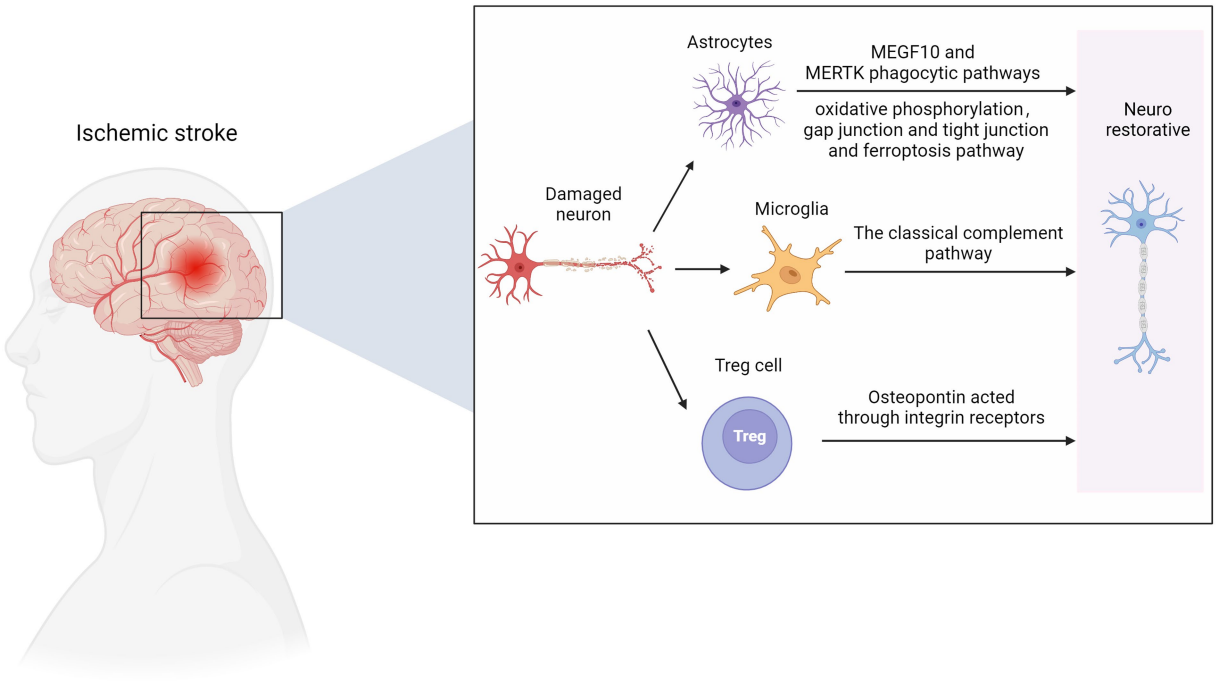

FIGURE 3
Nerve repair in ischemic stroke. MEGF10, multiple EGF like domains 10; MERTK, MER proto-oncogene, tyrosine kinase. Figure was created with Biorender.com.

7. Summary

In general, single-cell sequencing provides new information and direction for the molecular basis of AIS through dimensionality reduction and bioinformatics analysis and broadens our vision of AIS cell heterogeneity and cell expression-specific genes. Identifying specific genes expressed by cells can promote the application of molecular imaging research toward monitoring dynamic disease in AIS patients. It will open up a new field for exploring the pathogenesis of AIS and drug development based on cell subtype-specific molecules and lay a foundation for further research on the human brain after AIS.

Author contributions

XS: conceptualization and writing – original draft preparation. ML: conducting a research and investigation process and specifically performing the evidence collection. KS: presentation of the published work, specifically data presentation. YL: writing – reviewing and editing. ZG: writing – reviewing and editing and acquisition of the financial support for the project leading to this publication. All authors contributed to the article and approved the submitted version.

Funding

This study was supported by the special fund project for doctoral training program of Lanzhou University Second Hospital (no. YJS-BD-05); the clinical Research Center for neurological diseases of Gansu Province (no. 2020-0411-SFC-0025); and Cuiying Technology Innovation Project of Lanzhou University Second Hospital (no. CY2022-QN-A05).

Conflict of interest

The authors declare that the research was conducted in the absence of any commercial or financial relationships that could be construed as a potential conflict of interest.

Publisher's note

All claims expressed in this article are solely those of the authors and do not necessarily represent those of their affiliated organizations, or those of the publisher, the editors and the reviewers. Any product that may be evaluated in this article, or claim that may be made by its manufacturer, is not guaranteed or endorsed by the publisher.

References

Alessandrini, F., Ceresa, D., Appolloni, I., Pagani, F., Poliani, P. L., Marubbi, D., et al. (2020). Glioblastoma models driven by different mutations converge to the proneural subtype. *Cancer Lett.* 469, 447–455. doi: 10.1016/j.canlet.2019.11.010

Allen, N. J., and Lyons, D. A. (2018). Glia as architects of central nervous system formation and function. *Science* 362, 181–185. doi: 10.1126/science.aat0473

Amantea, D., Nappi, G., Bernardi, G., Bagetta, G., and Corasaniti, M. T. (2009). Post-ischemic brain damage: pathophysiology and role of inflammatory mediators. *FEBS J.* 276, 13–26. doi: 10.1111/j.1742-4658.2008.06766.x

Anderson, M. A., Burda, J. E., Ren, Y., Ao, Y., O'Shea, T. M., Kawaguchi, R., et al. (2016). Astrocyte scar formation aids central nervous system axon regeneration. *Nature* 532, 195–200. doi: 10.1038/nature17623

Aronowski, J., and Roy-O'reilly, M. A. (2019). Neutrophils, the felons of the brain. *Stroke* 50, e42–e43. doi: 10.1161/STROKEAHA.118.021563

Askew, K., Li, K., Olmos-Alonso, A., Garcia-Moreno, F., Liang, Y., Richardson, P., et al. (2017). Coupled proliferation and apoptosis maintain the rapid turnover of microglia in the adult brain. *Cell Rep.* 18, 391–405. doi: 10.1016/j.celrep.2016.12.041

Audet, G. N., Dineen, S. M., Quinn, C. M., and Leon, L. R. (2016). Altered hypothalamic inflammatory gene expression correlates with heat stroke severity in a conscious rodent model. *Brain Res.* 1637, 81–90. doi: 10.1016/j.brainres.2016.01.048

Bandler, R. C., Mayer, C., and Fishell, G. (2017). Cortical interneuron specification: the juncture of genes, time and geometry. *Curr. Opin. Neurobiol.* 42, 17–24. doi: 10.1016/j.conb.2016.10.003

Bernstein, D. L., and Rom, S. (2020). Let-7g* and mi R-98 reduce stroke-induced production of proinflammatory cytokines in mouse brain. *Front. Cell Dev. Biol.* 8:632. doi: 10.3389/fcell.2020.00632

Bonney, S. K., Sullivan, L. T., Cherry, T. J., Daneman, R., and Shih, A. Y. (2022). Distinct features of brain perivascular fibroblasts and mural cells revealed by in vivo two-photon imaging. *J. Cereb. Blood Flow Metab.* 42, 966–978. doi: 10.1177/0271678X211068528

Brioschi, S., Wang, W. L., Peng, V., Wang, M., Shchukina, I., Greenberg, Z. J., et al. (2021). Heterogeneity of meningeal B cells reveals a lymphopoietic niche at the CNS borders. *Science* 373:eabf9277. doi: 10.1126/science.abf9277

Bustamante, A., López-Cancio, E., Pich, S., Penalba, A., Giralt, D., García-Berrocoso, T., et al. (2017). Blood biomarkers for the early diagnosis of stroke: the stroke-Chip study. *Stroke* 48, 2419–2425. doi: 10.1161/STROKEAHA.117.017076

Calderon, T. M., Williams, D. W., Lopez, L., Eugenin, E. A., Cheney, L., Gaskill, P. J., et al. (2017). Dopamine increases CD14(+)CD16(+) monocyte transmigration across the blood brain barrier: implications for substance abuse and HIV Neuropathogenesis. *J. Neuroimmune Pharmacol.* 12, 353–370. doi: 10.1007/s11481-017-9726-9

Cegarra, C., Chaves, C., Déon, C., do, T. M., Dumas, B., Frenzel, A., et al. (2022). Exploring ITM2A as a new potential target for brain delivery. *Fluids Barriers CNS* 19:25. doi: 10.1186/s12987-022-00321-3

Chen, C., Ai, Q. D., Chu, S. F., Zhang, Z., and Chen, N. H. (2019). NK cells in cerebral ischemia. *Biomed. Pharmacother.* 109, 547–554. doi: 10.1016/j.biopha.2018.10.103

Chen, B., Banton, M. C., Singh, L., Parkinson, D. B., and Dun, X. P. (2021). Single cell transcriptome data analysis defines the heterogeneity of peripheral nerve cells in homeostasis and regeneration. *Front. Cell. Neurosci.* 15:624826. doi: 10.3389/fncel.2021.624826

Chen, M. L., Hong, C. G., Yue, T., Li, H. M., Duan, R., Hu, W. B., et al. (2021). Inhibition of mi R-331-3p and mi R-9-5p ameliorates Alzheimer's disease by enhancing autophagy. *Theranostics* 11, 2395–2409. doi: 10.7150/thno.47408

Chen, W., Qin, Y., and Liu, S. (2020). CCL20 signaling in the tumor microenvironment. *Adv. Exp. Med. Biol.* 1231, 53–65. doi: 10.1007/978-3-030-36667-4_6

Chen, R., Wu, X., Jiang, L., and Zhang, Y. (2017). Single-cell RNA-Seq reveals hypothalamic cell diversity. *Cell Rep.* 18, 3227–3241. doi: 10.1016/j.celrep.2017.03.004

Cho, Y. E., Lee, H., Bae, H. R., Kim, H., Yun, S., Vorn, R., et al. (2022). Circulating immune cell landscape in patients who had mild ischaemic stroke. *Stroke Vasc Neurol* 7, 319–327. doi: 10.1136/svn-2021-001224

Daneman, R., and Prat, A. (2015). The blood-brain barrier. *Cold Spring Harb. Perspect. Biol.* 7:a020412. doi: 10.1101/cshperspect.a020412

Dekker, R. J., Boon, R. A., Rondaij, M. G., Kragt, A., Volger, O. L., Elderkamp, Y. W., et al. (2006). KLF2 provokes a gene expression pattern that establishes functional quiescent differentiation of the endothelium. *Blood* 107, 4354–4363. doi: 10.1182/blood-2005-08-3465

Fawcett, J. W., and Asher, R. A. (1999). The glial scar and central nervous system repair. *Brain Res. Bull.* 49, 377–391. doi: 10.1016/S0361-9230(99)00072-6

Feigin, V., Brainin, M., Norrving, B., Martins, S., Sacco, R. L., Hacke, W., et al. (2022). World stroke organization (WSO): global stroke fact sheet 2022. *Int. J. Stroke* 17, 18–29. doi: 10.1177/17474930211065917

Feng, H., Moakley, D. F., Chen, S., McKenzie, M. G., Menon, V., and Zhang, C. (2021). Complexity and graded regulation of neuronal cell-type-specific alternative splicing revealed by single-cell RNA sequencing. *Proc. Natl. Acad. Sci. U. S. A.* 118:e2013056118. doi: 10.1073/pnas.2013056118

Gokce, O., Stanley, G. M., Treutlein, B., Neff, N. F., Camp, J. G., Malenka, R. C., et al. (2016). Cellular taxonomy of the mouse striatum as revealed by single-cell RNA-Seq. *Cell Rep.* 16, 1126–1137. doi: 10.1016/j.celrep.2016.06.059

Grønberg, N. V., Johansen, F. F., Kristiansen, U., and Hasseldam, H. (2013). Leukocyte infiltration in experimental stroke. *J. Neuroinflammation* 10:115. doi: 10.1186/1742-2094-10-115

Guo, K., Luo, J., Feng, D., Wu, L., Wang, X., Xia, L., et al. (2021). Single-cell RNA sequencing with combined use of bulk RNA sequencing to reveal cell heterogeneity and molecular changes at acute stage of ischemic stroke in mouse cortex penumbra area. *Front. Cell Dev. Biol.* 9:624711. doi: 10.3389/fcell.2021.624711

Guzik-Kornacka, A., Sliwa, A., Plucinska, G., and Lukasiuk, K. (2011). Status epilepticus evokes prolonged increase in the expression of CCL3 and CCL4 mRNA and protein in the rat brain. *Acta Neurobiol. Exp. (Wars)* 71, 193–207.

Heiss, W. D. (2000). Ischemic penumbra: evidence from functional imaging in man. *J. Cereb. Blood Flow Metab.* 20, 1276–1293. doi: 10.1097/00004647-200009000-00002

Hu, X., Leak, R. K., Shi, Y., Suenaga, J., Gao, Y., Zheng, P., et al. (2015). Microglial and macrophage polarization—new prospects for brain repair. *Nat. Rev. Neurol.* 11, 56–64. doi: 10.1038/nrneurol.2014.207

Huang, L., Nakamura, Y., Lo, E. H., and Hayakawa, K. (2019). Astrocyte signaling in the neurovascular unit after central nervous system injury. *Int. J. Mol. Sci.* 20:282. doi: 10.3390/ijms20020282

Iadecola, C., Buckwalter, M. S., and Anrather, J. (2020). Immune responses to stroke: mechanisms, modulation, and therapeutic potential. *J. Clin. Invest.* 130, 2777–2788. doi: 10.1172/JCI135530

Inoue, K., Sakuma, E., Morimoto, H., Asai, H., Koide, Y., Leng, T., et al. (2016). Serum- and glucocorticoid-inducible kinases in microglia. *Biochem. Biophys. Res. Commun.* 478, 53–59. doi: 10.1016/j.bbrc.2016.07.094

Ito, M., Komai, K., Mise-Omata, S., Iizuka-Koga, M., Noguchi, Y., Kondo, T., et al. (2019). Brain regulatory T cells suppress astrogliosis and potentiate neurological recovery. *Nature* 565, 246–250. doi: 10.1038/s41586-018-0824-5

Ji, B., Zhou, F., Han, L., Yang, J., Fan, H., Li, S., et al. (2017). Sodium Tanshinone IIA sulfonate enhances effectiveness Rt-PA treatment in acute ischemic stroke patients associated with ameliorating blood-brain barrier damage. *Transl. Stroke Res.* 8, 334–340. doi: 10.1007/s12975-017-0526-6

Jian, Z., Liu, R., Zhu, X., Smerin, D., Zhong, Y., Gu, L., et al. (2019). The involvement and therapy target of immune cells after ischemic stroke. *Front. Immunol.* 10:2167. doi: 10.3389/fimmu.2019.02167

Jiang, C., Kong, W., Wang, Y., Ziai, W., Yang, Q., Zuo, F., et al. (2017). Changes in the cellular immune system and circulating inflammatory markers of stroke patients. *Oncotarget* 8, 3553–3567. doi: 10.18632/oncotarget.12201

Kim, J., Song, T. J., Park, J. H., Lee, H. S., Nam, C. M., Nam, H. S., et al. (2012). Different prognostic value of white blood cell subtypes in patients with acute cerebral infarction. *Atherosclerosis* 222, 464–467. doi: 10.1016/j.atherosclerosis.2012.02.042

Kim, J., Stanescu, D. E., and Won, K. J. (2018). Cell BIC: bimodality-based top-down clustering of single-cell RNA sequencing data reveals hierarchical structure of the cell type. *Nucleic Acids Res.* 46:e124. doi: 10.1093/nar/gky698

Knotek, T., Janeckova, L., Kriska, J., Korinek, V., and Anderova, M. (2020). Glia and neural stem and progenitor cells of the healthy and ischemic brain: the workplace for the Wnt signaling pathway. *Genes (Basel)* 11:804. doi: 10.3390/genes11070804

Kriska, J., Janeckova, L., Kirdajova, D., Honsa, P., Knotek, T., Dzamba, D., et al. (2021). Wnt/β-catenin signaling promotes differentiation of ischemia-activated adult neural stem/progenitor cells to neuronal precursors. *Front. Neurosci.* 15:628983. doi: 10.3389/fnins.2021.628983

Kundishora, A. J., Peters, S. T., Pinard, A., Duran, D., Panchagnula, S., Barak, T., et al. (2021). DIAPH1 variants in non-east Asian patients with sporadic Moyamoya disease. *JAMA Neurol.* 78, 993–1003. doi: 10.1001/jamaneurol.2021.1681

Lee, Y. S., and Cho, Y. B. (2020). CCL7 signaling in the tumor microenvironment. *Adv. Exp. Med. Biol.* 1231, 33–43. doi: 10.1007/978-3-030-36667-4_4

Lee, J. H., Kim, J. Y., Noh, S., Lee, H., Lee, S. Y., Mun, J. Y., et al. (2021). Astrocytes phagocytose adult hippocampal synapses for circuit homeostasis. *Nature* 590, 612–617. doi: 10.1038/s41586-020-03060-3

Lehnardt, S. (2010). Innate immunity and neuroinflammation in the CNS: the role of microglia in toll-like receptor-mediated neuronal injury. *Glia* 58, 253–263. doi: 10.1002/glia.20928

Lerman, I., Bawany, F., Whitt, W., Esaa, F., Yon, J., Babkowski, N., et al. (2022). Prominent B-cell signature differentiates discoid from subacute cutaneous lupus erythematosus. *J. Invest. Dermatol.* 142, 2885–2895.e2. doi: 10.1016/j.jid.2022.03.033

Li, B. H., Garstka, M. A., and Li, Z. F. (2020). Chemokines and their receptors promoting the recruitment of myeloid-derived suppressor cells into the tumor. *Mol. Immunol.* 117, 201–215. doi: 10.1016/j.molimm.2019.11.014

Li, X., Lyu, J., Li, R., Jain, V., Shen, Y., del Águila, Á., et al. (2022). Single-cell transcriptomic analysis of the immune cell landscape in the aged mouse brain after ischemic stroke. *J. Neuroinflammation* 19:83. doi: 10.1186/s12974-022-02447-5

Li, P., Stetler, R. A., Leak, R. K., Shi, Y., Li, Y., Yu, W., et al. (2018). Oxidative stress and DNA damage after cerebral ischemia: potential therapeutic targets to repair the genome and improve stroke recovery. *Neuropharmacology* 134, 208–217. doi: 10.1016/j.neuropharm.2017.11.011

Li, X., Wang, K., Lyu, Y., Pan, H., Zhang, J., Stambolian, D., et al. (2020). Deep learning enables accurate clustering with batch effect removal in single-cell RNA-seq analysis. *Nat. Commun.* 11:2338. doi: 10.1038/s41467-020-15851-3

Li, L. C., Yu, X. X., Zhang, Y. W., Feng, Y., Qiu, W. L., and Xu, C. R. (2018). Single-cell transcriptomic analyses of mouse pancreatic endocrine cells. *J. Vis. Exp.* 139:58000. doi: 10.3791/58000-v

Li, Y., Zhu, Z. Y., Huang, T. T., Zhou, Y. X., Wang, X., Yang, L. Q., et al. (2018). The peripheral immune response after stroke-a double edge sword for blood-brain barrier integrity. *CNS Neurosci. Ther.* 24, 1115–1128. doi: 10.1111/cns.13081

Lin, W., Wang, Y., Chen, Y., Wang, Q., Gu, Z., and Zhu, Y. (2021). Role of calcium signaling pathway-related gene regulatory networks in ischemic stroke based on multiple WGCNA and single-cell analysis. *Oxidative Med. Cell. Longev.* 2021:8060477. doi: 10.1155/2021/8060477

Luo, R., Su, L. Y., Li, G., Yang, J., Liu, Q., Yang, L. X., et al. (2020). Activation of PPARA-mediated autophagy reduces Alzheimer disease-like pathology and cognitive decline in a murine model. *Autophagy* 16, 52–69. doi: 10.1080/15548627.2019.1596488

Ma, D., Feng, L., Cheng, Y., Xin, M., You, J., Yin, X., et al. (2018). Astrocytic gap junction inhibition by carbenoxolone enhances the protective effects of ischemic preconditioning following cerebral ischemia. *J. Neuroinflammation* 15:198. doi: 10.1186/s12974-018-1230-5

Ma, H., Zhou, Y., Li, Z., Zhu, L., Li, H., Zhang, G., et al. (2022). Single-cell RNA-sequencing analyses revealed heterogeneity and dynamic changes of metabolic pathways in astrocytes at the acute phase of ischemic stroke. *Oxidative Med. Cell. Longev.* 2022, 1–22. doi: 10.1155/2022/1817721

Madreiter-Sokolowski, C. T., Thomas, C., and Ristow, M. (2020). Interrelation between ROS and Ca2+ in aging and age-related diseases. *Redox Biol.* 36:101678. doi: 10.1016/j.redox.2020.101678

Marques, S., Zeisel, A., Codeluppi, S., van Bruggen, D., Mendanha Falcão, A., Xiao, L., et al. (2016). Oligodendrocyte heterogeneity in the mouse juvenile and adult central nervous system. *Science* 352, 1326–1329. doi: 10.1126/science.aaf6463

Martinez-Lage, M., Lynch, T. M., Bi, Y., Cocito, C., Way, G. P., Pal, S., et al. (2019). Immune landscapes associated with different glioblastoma molecular subtypes. *Acta Neuropathol. Commun.* 7:203. doi: 10.1186/s40478-019-0803-6

Mondal, S., Adhikari, N., Banerjee, S., Amin, S. A., and Jha, T. (2020). Matrix metalloproteinase-9 (MMP-9) and its inhibitors in cancer: A minireview. *Eur J Med Chem* 194:112260. doi: 10.1016/j.ejmech.2020.112260

Munji, R. N., Soung, A. L., Weiner, G. A., Sohet, F., Semple, B. D., Trivedi, A., et al. (2019). Profiling the mouse brain endothelial transcriptome in health and disease models reveals a core blood-brain barrier dysfunction module. *Nat. Neurosci.* 22, 1892–1902. doi: 10.1038/s41593-019-0497-x

Niu, B., Zhang, T., Hu, H., and Cao, B. (2017). Transcriptome sequencing reveals astrocytes as a therapeutic target in heat-stroke. *Neurosci. Bull.* 33, 627–640. doi: 10.1007/s12264-017-0156-8

Owolabi, M. O., Thrift, A. G., Mahal, A., Ishida, M., Martins, S., Johnson, W. D., et al. (2022). Primary stroke prevention worldwide: translating evidence into action. *Lancet Public Health* 7, e74–e85. doi: 10.1016/S2468-2667(21)00230-9

Peterfalvi, A., Molnar, T., Banati, M., Pusch, G., Miko, E., Bogar, L., et al. (2009). Impaired function of innate T lymphocytes and NK cells in the acute phase of ischemic stroke. *Cerebrovasc. Dis.* 28, 490–498. doi: 10.1159/000236527

Polosukhina, D., Singh, K., Asim, M., Barry, D. P., Allaman, M. M., Hardbower, D. M., et al. (2021). CCL11 exacerbates colitis and inflammation-associated colon tumorigenesis. *Oncogene* 40, 6540–6546. doi: 10.1038/s41388-021-02046-3

Profaci, C. P., Munji, R. N., Pulido, R. S., and Daneman, R. (2020). The blood-brain barrier in health and disease: important unanswered questions. *J. Exp. Med.* 217:e20190062. doi: 10.1084/jem.20190062

Réu, P., Khosravi, A., Bernard, S., Mold, J. E., Salehpour, M., Alkass, K., et al. (2017). The lifespan and turnover of microglia in the human brain. *Cell Rep.* 20, 779–784. doi: 10.1016/j.celrep.2017.07.004

Rolls, A., Shechter, R., and Schwartz, M. (2009). The bright side of the glial scar in CNS repair. *Nat. Rev. Neurosci.* 10, 235–241. doi: 10.1038/nrn2591

Rosenkranz, S. C., Shaposhnykov, A., Schnapauff, O., Epping, L., Vieira, V., Heidermann, K., et al. (2020). TRPV4-mediated regulation of the blood brain barrier is abolished during inflammation. *Front. Cell Dev. Biol.* 8:849. doi: 10.3389/fcell.2020.00849

Rusu, P., Shao, C., Neuerburg, A., Acikgöz, A. A., Wu, Y., Zou, P., et al. (2019). GPD1 specifically Marks dormant glioma stem cells with a distinct metabolic profile. *Cell Stem Cell* 25, 241–257.e8. doi: 10.1016/j.stem.2019.06.004

Saad, M. I., Alhayyani, S., Mcleod, L., Yu, L., Alanazi, M., Deswaerte, V., et al. (2019). ADAM17 selectively activates the IL-6 trans-signaling/ERK MAPK axis in KRAS-addicted lung cancer. *EMBO Mol. Med.* 11:e9976. doi: 10.15252/emmm.201809976

Shen, X. Y., Gao, Z. K., Han, Y., Yuan, M., Guo, Y. S., and Bi, X. (2021). Activation and role of astrocytes in ischemic stroke. *Front. Cell. Neurosci.* 17:755955. doi: 10.3389/fncel.2021.755955

Shi, X., Luo, L., Wang, J., Shen, H., Li, Y., Mamtilahun, M., et al. (2021). Stroke subtype-dependent synapse elimination by reactive gliosis in mice. *Nat. Commun.* 12:6943. doi: 10.1038/s41467-021-27248-x

Shi, L., Sun, Z., Su, W., Xu, F., Xie, D., Zhang, Q., et al. (2021). Treg cell-derived osteopontin promotes microglia-mediated white matter repair after ischemic stroke. *Immunity* 54, 1527–1542.e8. doi: 10.1016/j.immuni.2021.04.022

Shi, K., Tian, D. C., Li, Z. G., Ducruet, A. F., Lawton, M. T., and Shi, F. D. (2019). Global brain inflammation in stroke. *Lancet Neurol.* 18, 1058–1066. doi: 10.1016/S1474-4422(19)30078-X

Shi, Y., Wang, M., Mi, D., Lu, T., Wang, B., Dong, H., et al. (2021). Mouse and human share conserved transcriptional programs for interneuron development. *Science* 374:eabj6641. doi: 10.1126/science.abj6641

Skytthe, M. K., Graversen, J. H., and Moestrup, S. K. (2020). Targeting of CD163(+) macrophages in inflammatory and malignant diseases. *Int. J. Mol. Sci.* 21:5497. doi: 10.3390/ijms21155497

Smyth, L. C. D., Rustenhoven, J., Scotter, E. L., Schweder, P., Faull, R. L. M., Park, T. I. H., et al. (2018). Markers for human brain pericytes and smooth muscle cells. *J. Chem. Neuroanat.* 92, 48–60. doi: 10.1016/j.jchemneu.2018.06.001

Sousa, C., Golebiewska, A., Poovathingal, S. K., Kaoma, T., Pires-Afonso, Y., Martina, S., et al. (2018). Single-cell transcriptomics reveals distinct inflammation-induced microglia signatures. *EMBO Rep.* 19:e46171. doi: 10.15252/embr.201846171

Sun, S., Chen, Y., Liu, Y., and Shang, X. (2019). A fast and efficient count-based matrix factorization method for detecting cell types from single-cell RNAseq data. *BMC Syst. Biol.* 13:28. doi: 10.1186/s12918-019-0699-6

Sun, J., Zhang, W., Tan, Z., Zheng, C., Tang, Y., Ke, X., et al. (2020). Zika virus promotes CCN1 expression via the CaMKIIα-CREB pathway in astrocytes. *Virulence* 11, 113–131. doi: 10.1080/21505594.2020.1715189

Tang, H., Li, Y., Tang, W., Zhu, J., Parker, G. C., and Zhang, J. H. (2022). Endogenous neural stem cell-induced neurogenesis after ischemic stroke: processes for brain repair and perspectives. *Transl. Stroke Res.* doi: 10.1007/s12975-022-01078-5 Epub ahead of print. Erratum in: Transl Stroke Res.

Veys, K., Fan, Z., Ghobrial, M., Bouché, A., García-Caballero, M., Vriens, K., et al. (2020). Role of the GLUT1 glucose transporter in postnatal CNS angiogenesis and blood-brain barrier integrity. *Circ. Res.* 127, 466–482. doi: 10.1161/CIRCRESAHA.119.316463

Virani, S. S., Alonso, A., Benjamin, E. J., Bittencourt, M. S., Callaway, C. W., Carson, A. P., et al. (2020). American Heart Association Council on epidemiology and prevention statistics committee and stroke statistics subcommittee heart disease and stroke Statistics-2020 update: a report from the American Heart Association. *Circulation* 141, e139–e596. doi: 10.1161/CIR.0000000000000757

Wang, J., Sareddy, G. R., Lu, Y., Pratap, U. P., Tang, F., Greene, K. M., et al. (2020). Astrocyte-derived estrogen regulates reactive Astrogliosis and is neuroprotective following ischemic brain injury. *J. Neurosci.* 40, 9751–9771. doi: 10.1523/JNEUROSCI.0888-20.2020

Wang, Y. J., Schug, J., Won, K. J., Liu, C., Naji, A., Avrahami, D., et al. (2016). Single-cell transcriptomics of the human endocrine pancreas. *Diabetes* 65, 3028–3038. doi: 10.2337/db16-0405

Wang, J., Xie, L., Yang, C., Ren, C., Zhou, K., Wang, B., et al. (2015). Activated regulatory T cell regulates neural stem cell proliferation in the subventricular zone of normal and ischemic mouse brain through interleukin 10. *Front. Cell. Neurosci.* 9:361. doi: 10.3389/fncel.2015.00361

Wang, Y., Zhang, J. H., Sheng, J., and Shao, A. (2019). Immunoreactive cells after cerebral ischemia. *Front. Immunol.* 10:2781. doi: 10.3389/fimmu.2019.02781

Wanner, I. B., Anderson, M. A., Song, B., Levine, J., Fernandez, A., Gray-Thompson, Z., et al. (2013). Glial scar borders are formed by newly proliferated, elongated astrocytes that interact to corral inflammatory and fibrotic cells via STAT3-dependent mechanisms after spinal cord injury. *J. Neurosci.* 33, 12870–12886. doi: 10.1523/JNEUROSCI.2121-13.2013

Xie, Y., He, L., Lugano, R., Zhang, Y., Cao, H., He, Q., et al. (2021). Key molecular alterations in endothelial cells in human glioblastoma uncovered through single-cell RNA sequencing. *JCI Insight* 6:e150861. doi: 10.1172/jci.insight.150861

Xin, Y., Kim, J., Ni, M., Wei, Y., Okamoto, H., Lee, J., et al. (2016). Use of the Fluidigm C1 platform for RNA sequencing of single mouse pancreatic islet cells. *Proc. Natl. Acad. Sci. U. S. A.* 113, 3293–3298. doi: 10.1073/pnas.1602306113

Yan, J., Greer, J. M., Etherington, K., Cadigan, G. P., Cavanagh, H., Henderson, R. D., et al. (2009). Immune activation in the peripheral blood of patients with acute ischemic stroke. *J. Neuroimmunol.* 206, 112–117. doi: 10.1016/j.jneuroim.2008.11.001

Yong, Y. X., Yang, H., Lian, J., Xu, X. W., Han, K., Hu, M. Y., et al. (2019). Up-regulated micro RNA-199b-3p represses the apoptosis of cerebral microvascular endothelial cells in ischemic stroke through down-regulation of MAPK/ERK/EGR1 axis. *Cell Cycle* 18, 1868–1881. doi: 10.1080/15384101.2019.1632133

Yook, C., Kim, K., Kim, D., Kang, H., Kim, S. G., Kim, E., et al. (2019). A TBR1-K228E mutation induces Tbr1 upregulation, altered cortical distribution of interneurons, increased inhibitory synaptic transmission, and autistic-like behavioral deficits in mice. *Front. Mol. Neurosci.* 12:241. doi: 10.3389/fnmol.2019.00241

Zeisel, A., Muñoz-Manchado, A. B., Codeluppi, S., Lönnerberg, P., La Manno, G., Juréus, A., et al. (2015). Brain structure. Cell types in the mouse cortex and hippocampus revealed by single-cell RNA-seq. *Science* 347, 1138–1142. doi: 10.1126/science.aaa1934

Zheng, K., Lin, L., Jiang, W., Chen, L., Zhang, X., Zhang, Q., et al. (2021). Single-cell RNA-seq reveals the transcriptional landscape in ischemic stroke. *J. Cereb. Blood Flow Metab.* 42, 56–73. doi: 10.1177/0271678X211026770

Zhong, S., Zhang, S., Fan, X., Wu, Q., Yan, L., Dong, J., et al. (2018). A single-cell RNA-seq survey of the developmental landscape of the human prefrontal cortex. *Nature* 555, 524–528. doi: 10.1038/nature25980

Zubova, S. G., Suvorova, I. I., and Karpenko, M. N. (2022). Macrophage and microglia polarization: focus on autophagy-dependent reprogramming. *Front. Biosci. (Schol. Ed.)* 14:3. doi: 10.31083/j.fbs1401003

frontiers | Frontiers in Molecular Neuroscience

TYPE Review
PUBLISHED 11 May 2023
DOI 10.3389/fnmol.2023.1118078

OPEN ACCESS

EDITED BY
Maria Jose Sisalli,
University of Naples Federico II, Italy

REVIEWED BY
Zachary Freyberg,
University of Pittsburgh, United States
Stephanie Daumas,
Sorbonne Université, France

*CORRESPONDENCE
Weiqian Yan
✉ yanweiqian@csu.edu.cn

RECEIVED 07 December 2022
ACCEPTED 06 April 2023
PUBLISHED 11 May 2023

CITATION
Zhao C, Wang C, Zhang H and Yan W (2023) A mini-review of the role of vesicular glutamate transporters in Parkinson's disease. *Front. Mol. Neurosci.* 16:1118078. doi: 10.3389/fnmol.2023.1118078

A mini-review of the role of vesicular glutamate transporters in Parkinson's disease

Cheng Zhao[1,2,3], Chunyu Wang[1], Hainan Zhang[1] and Weiqian Yan[1]*

[1]Department of Neurology, The Second Xiangya Hospital, Central South University, Changsha, China, [2]National Clinical Research Center for Geriatric Disorders, Xiangya Hospital, Central South University, Changsha, China, [3]Department of Urology, Xiangya Hospital, Central South University, Changsha, China

Parkinson's disease (PD) is a common neurodegenerative disease implicated in multiple interacting neurotransmitter pathways. Glutamate is the central excitatory neurotransmitter in the brain and plays critical influence in the control of neuronal activity. Impaired Glutamate homeostasis has been shown to be closely associated with PD. Glutamate is synthesized in the cytoplasm and stored in synaptic vesicles by vesicular glutamate transporters (VGLUTs). Following its exocytotic release, Glutamate activates Glutamate receptors (GluRs) and mediates excitatory neurotransmission. While Glutamate is quickly removed by excitatory amino acid transporters (EAATs) to maintain its relatively low extracellular concentration and prevent excitotoxicity. The involvement of GluRs and EAATs in the pathophysiology of PD has been widely studied, but little is known about the role of VGLUTs in the PD. In this review, we highlight the role of VGLUTs in neurotransmitter and synaptic communication, as well as the massive alterations in Glutamate transmission and VGLUTs levels in PD. Among them, adaptive changes in the expression level and function of VGLUTs may exert a crucial role in excitatory damage in PD, and VGLUTs are considered as novel potential therapeutic targets for PD.

KEYWORDS

Parkinson's disease, glutamate, vesicular glutamate transporters, excitatory amino acid transporters, glutamate receptors

Introduction

Parkinson's disease (PD) is a progressive neurodegenerative disease, implicated in multiple neurotransmitter pathways and autonomic nervous system that is associated with a range of clinical features (Schapira et al., 2017). Two types of clinical features are relied upon in its diagnosis: motor symptoms, including bradykinesia, stiffness, resting tremor, and postural and balance difficulties and non-motor symptoms, including autonomic dysfunction, sleep disturbances, behavioral changes, sensory abnormalities, and other unclassifiable symptoms (Kalia and Lang, 2015). The motor features are predominantly attributed to the formation of intracytoplasmic inclusion called Lewy bodies and the loss of dopamine (DA) neurons in the substantia nigra pars compacta (SNpc). The broad spectrum of non-motor symptoms of PD usually precede motor dysfunction. With the increasing awareness of the importance and presence of non-motor symptoms, PD is considered as a multisystem disorder involving various neurotransmitters in the brain (Klingelhoefer and Reichmann, 2017). Considering that most symptoms precede the complete loss of DA neurons in SNpc, it is likely that neuronal

dysfunction precedes degeneration and other pathophysiological mechanisms drive the vulnerability of DA neurons.

The current standard drug therapy for PD is dopamimetic drugs, such as DA precursor levodopa (L-3,4-dihydroxyphenylalanine, L-DOPA), DA receptor agonists, and monoamine oxidase-B (MAO-B) inhibitors (Armstrong and Okun, 2020). In fact, the current DA replacement therapies neither improve most non-motor symptoms nor slow disease progression, highlighting the importance of studying the intervention of non-DA systems (Schapira et al., 2017). Indeed, various neurotransmitter systems are closely associated with the pathophysiology of PD (Sanjari et al., 2017). Among them, glutamate (Glu) is the most abundant transmitter in the central nervous system (CNS), and exerts vital effects on mediating the continuous feedback of basal ganglia circuits leading to DA dysregulation in the striatum (Wang et al., 2020). Emerging evidence suggests that glutamatergic transmission participates in the processes of PD, which is necessary for further study (Iovino et al., 2020; Pisanò et al., 2020; Lyu et al., 2021).

Glutamate-glutamine cycle

Glutamate is the primary excitatory neurotransmitter in the brain and plays critical role in the control of neuronal activity. Glutamate is released from presynaptic terminals, and then it interacts with glutamate receptors (GluRs) on the plasma membrane of postsynaptic neurons. When triggered by glutamate, several types of GluRs work together to regulate excitatory postsynaptic neurotransmission (Plaitakis and Shashidharan, 2000). The specific receptors activated by glutamate can be divided into two main families: ionotropic and metabotropic GluRs (iGluRs and mGluRs). The iGluRs, including kainate receptors, α-amino-3-hydroxy-5-methyl-4-isoxazolepropionic acid (AMPA) receptors, and N-methyl-d-aspartate (NMDA) receptors, are multimeric ion channels in charge of rapid excitatory transmission in the mammalian CNS (Bigge, 1999). mGluRs are members of the G-protein-coupled receptor superfamily that contain eight receptor subtypes, inducing slow excitatory responses, which contribute to long-lasting effects in synaptic strength called long-term potentiation (LTP) or long-term depression (LDP; Ferraguti and Shigemoto, 2006). In presynaptic neurons, glutamine is converted to glutamate by mitochondrial enzyme glutaminase, and then packaged by vesicular glutamate transporters (VGLUTs) into synaptic vesicles, followed by releasing into the synaptic cleft by stimulation (El et al., 2011). Glutamate in the synaptic cleft is removed by excitatory amino acid transporters (EAATs) situated on the neuronal plasma membrane, and is also able to transport glutamate to astrocyte or back to presynaptic terminals. Within the astrocyte, glutamate is transformed into glutamine by glutamine synthetase (GS), and then transported back to neurons sequentially through glutamine transporters on the membrane of astrocytes and neurons (Andersen and Schousboe, 2022; Figure 1). All these transporters facilitate the transport of glutamate, ensuring that glutamate is maintained with the appropriate concentration in the correct compartment.

Extracellular glutamate concentrations are mainly regulated via EAATs with high affinity. EAATs have five characterized mammalian subtypes, including glutamate/aspartate transporter (GLAST, also named EAAT1), glutamate transporter-1 (GLT-1, also named EAAT2), excitatory amino acid carrier-1 (EAAC1, also named EAAT3), EAAT4, and EAAT5. EAATs are proved to maintain the balance of extracellular glutamate concentrations and protect neurons from harmful overstimulation of GluRs (Magi et al., 2019). Noteworthy, Glutamate concentration is also regulated by modulating glutamate internalization into synaptic vesicles through VGLUTs (Shigeri et al., 2004). The expression and function of VGLUTs play an important role in glutamate release in presynaptic regions. The expression level of VGLUTs in each synaptic vesicle indicates the relative intensity of presynaptic glutamatergic innervation and control the quantal size of glutamatergic transmission (Daniels et al., 2006; Liguz-Lecznar and Skangiel-Kramska, 2007). The involvement of GluRs and EAATs in the pathophysiology of PD has been widely studied, but little is known about the role of VGLUTs in PD. Therefore, given that a comprehensive understanding of the pathophysiology and therapeutic targets of VGLUTs for PD can help in the development of new therapeutic approaches for PD. This article highlights the role of VGLUTs in neurotransmitter and synaptic communication, as well as the massive alterations in Glutamate transmission and VGLUTs levels in PD.

Distribution and molecular pharmacology of VGLUTs

Three subtypes of VGLUTs have been identified and characterized, named VGLUT1-3, which are encoded by solute vector gene *Slc17a6-8* (Bellocchio et al., 2000; Takamori et al., 2000). The distributions of the three VGLUTs barely overlap, delineating 3 complementary glutamate systems that VGLUT1 (*Slc17a7*) and VGLUT2 (*Slc17a6*) exert dominating neurophysiological impacts on almost all central neuronal circuits, whereas VGLUT3 (*Slc17a8*) participates in local transmission regulation (Fremeau et al., 2001; Schäfer et al., 2002). VGLUT1 and VGLUT2 are specific markers of glutamatergic neurons, which are co-expressed in most of the brain region, including the cerebral cortex, occipital lobe, frontal lobe, temporal lobe, cerebellum, amygdala, medulla, hippocampus, and putamen. Additionally, VGLUT2 is also expressed in many other parts of the brain, including substantia nigra, caudate nucleus, thalamus, subthalamic nucleus, and spinal cord (Fremeau et al., 2001; Kaneko and Fujiyama, 2002; Herzog et al., 2004; Hackett et al., 2011). Notably, VGLUT2 is the only vesicular glutamate transporter expressed in transgenic ventral tegmental area (VTA)/substantia nigra dopamine neurons (Kouwenhoven et al., 2020). VGLUT3 is only expressed in a few glutamate neurons in raphe nuclei, cerebral cortex, and cochlear inner hair cells (IHCs; Gras et al., 2002; Ruel et al., 2008; Hioki et al., 2010). VGLUT3 predominantly exists in scattered group of "non-glutamatergic" neurons, including cholinergic interneurons (ChIs) in the ventral and dorsal striatum, GABAergic neurons in the olfactory bulb, GABAergic cortical and hippocampal interneurons, and 5-hydroxytryptaminergic olecranon neurons (Somogyi et al., 2004; Gras et al., 2008; Tatti et al., 2014; Fasano et al., 2017). Moreover, VGLUT3 is widely expressed outside the brain, particularly in cochleae, retina, and spinal cord (Lee et al., 2014; Cheng et al., 2017).

These three transporters (VGLUT1-3) show strong sequence homology, particularly in the transmembrane structural domains that constitute the translocation pathway (Bellocchio et al., 2000; Takamori et al., 2000). In addition, Inherent transport activities are

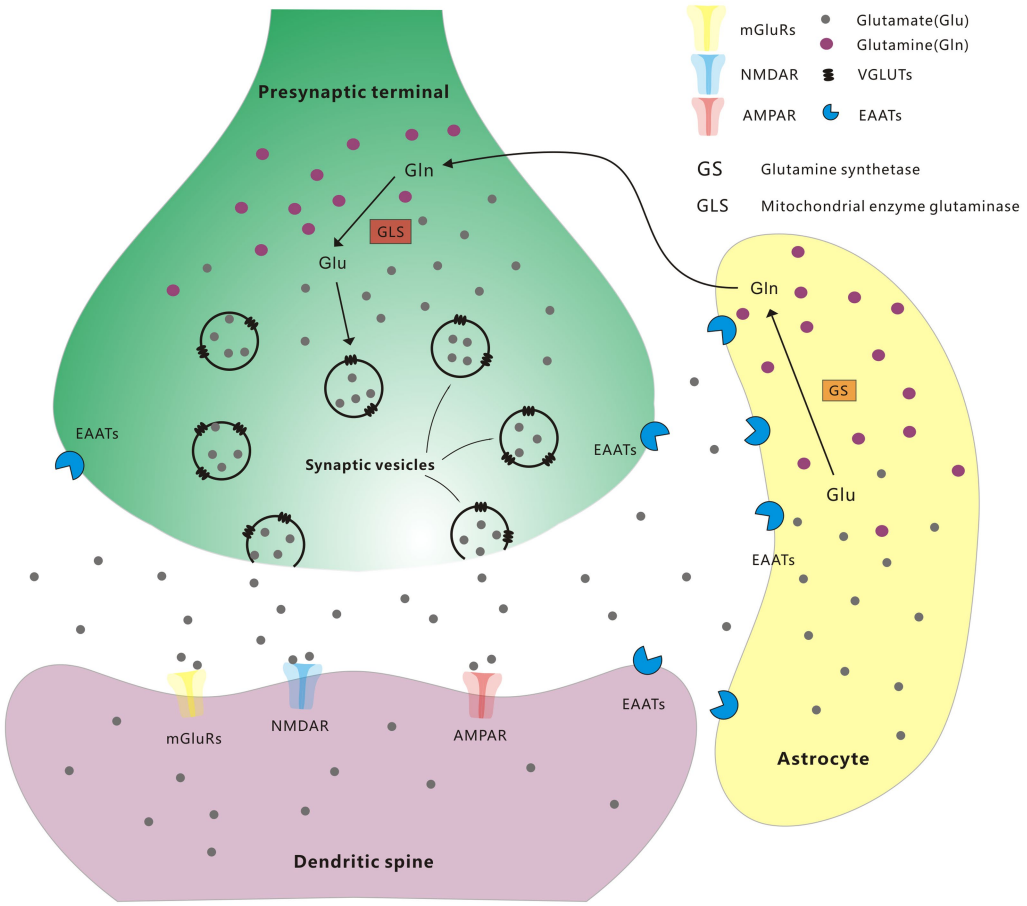

FIGURE 1
Glutamate-glutamine cycle.

found no difference among them. VGLUTs have relatively low affinity [K(m) = 1–2 mM] for glutamate, which make it difficult to identify VGLUTs inhibitors with high affinity (Thompson et al., 2005). VGLUTs are highly selective for glutamate which make them selectively targeted, thus the effect of pharmacological manipulations by small molecules do not disrupt other transport phenomena, like EAATs or GluRs (Thompson and Chao, 2020). In contrast to most plasma membrane transporters, the VGLUTs, like other endosomal neurotransmitter transporters, rely on the proton electrochemical gradient across the synaptic vesicle membrane generated by vacuolar-type H + -ATPase (V-ATPase; Blakely and Edwards, 2012). The difference is vesicular neurotransmitter transporters are driven by proton exchange and thus depend on the chemical component of $\Delta\mu H+$ (ΔpH), glutamate uptake by VGLUTs depends on the membrane potential ($\Delta\psi$), suggesting a mechanism of facilitated diffusion (Maycox et al., 1988). Subsequently, chloride (Cl^-) ions are reported to greatly stimulate glutamate uptake by synaptic vesicles *in vitro* (Wolosker et al., 1996). Increasing studies soon confirmed these initial results (Martineau et al., 2017; Eriksen et al., 2020; Chen et al., 2021). In conclusion, the vacuolar-type H + -ATPase generate transmembrane proton electrical gradient provide powers for VGLUTs, while VGLUTs binding with chloride, potassium, and protons regulate VGLUTs activity as well (Pietrancosta et al., 2020).

Molecular mechanism of VGLUTs in PD

In recent years, studies have indicated the subtle, but important, participation of VGLUTs-dependent glutamate/DA co-transmission and its roles in the regulation of different brain functions and dysfunctions (Buck et al., 2021c, 2022). In-depth study in the molecular mechanism of VGLUTs could result in decisive breakthroughs in the treatment of PD.

VGLUT1 and Parkinson's disease

Plenty of cortical excitatory neurons express VGLUT1, which represents a major isoform in the brain, accounting for about 80% of total glutamatergic vesicular transports (Fremeau et al., 2001). Glutamatergic neurotransmission in the striatum has been involved in the progression of PD. Biphasic and bilateral alterations in the levels of VGLUT1 and VGLUT2 protein expression of the striatum in hemiparkinsonian rats suggest significant time-dependent changes in glutamatergic neurotransmission from both types of striatal afferents (Massie et al., 2010). Study has revealed that glutamate is significantly reduced in synaptic vesicle-enriched membrane fractions of VGLUT1−/− mice, the absence of VGLUT1 may alter the ability of

releasing glutamate from nerve endings (Wojcik et al., 2004). The glutamatergic pathways exert significant functions in neuronal circuits related to PD.

The progressive degeneration of DA-capable cells in SNpc results in the imbalance within the cortico-basal ganglia loop, related to aberrant glutamatergic innervation in the brain (Orieux et al., 2000; Cilia et al., 2009). It has been reported that compared to controls, the protein level of VGLUT1 is decreased in the prefrontal cortex (PFC) of PD patients, revealing that VGLUT1 exerts the significant effects on glutamatergic damage in patients with PD (Kashani et al., 2007). Whereas, the study of Raju et al. has revealed the significantly increased total density of VGLUT1 in the striatum of PD monkeys after treatment with 1-methyl-4-phenyl-1,2,3,6-tetrahydropyridine (MPTP; Raju et al., 2008). In addition, El Arfani et al. have also noted alterations of different glutamate transporter expression levels in the bilaterally-lesioned 6-hydroxydopamine (6-OHDA) rat model, bilateral SNpc lesions inhibit the expression of VGLUT1 and showed a remarkable change after 2 weeks of injury in the striatum, but no significant changes were observed in the motor cortex (El et al., 2015). In a PD mouse model, the MPTP-induced expression of VGLUT1 protein is elevated in the medial PFC with loss of DA, while the expression of VGLUT1 in the dorsolateral striatum is significantly decreased (Pflibsen et al., 2015). These findings indicate that the remarkable variations in glutamate delivery transported by VGLUT1 may related to motor and cognitive deficits of PD.

Increasing evidence has demonstrated that as a treatment method for PD, electroacupuncture (EA) is able to facilitate the improvement of motor function in PD (Jia et al., 2010). In clinical practice, the subthalamic nucleus (STN) is considered as a pivotal target of deep brain stimulation for PD treatment, and VGLUT1 is closely involved in glutamate regulation of the cortical STN (Wang et al., 2018). Electroacupuncture can reverse 6-OHDA-induced VGLUT1 expression reduction in the STN (Zheng et al., 2019). Electroacupuncture promotes VGLUT1 expression in the ipsilateral STN and improves motor symptoms in PD rats, indicating that the overexpression of VGLUT1 in the STN may be associated with the role of EA in motor symptoms of PD via the cortical-STN pathway.

VGLUT2 and Parkinson's disease

VGLUT1 and VGLUT2 have complementary distributions throughout the adult brain. VGLUT2 predominantly exists in glutamate neurons of subcortical brain regions, such as SNpc, VTA, and thalamus (Kashani et al., 2007). Endogenous VGLUT2 has also been proved to express in a subpopulation of midbrain DA neurons (Kawano et al., 2006; Yamaguchi et al., 2011, 2015). A few (<20%) DA neurons in midbrain express detectable levels of VGLUT2 in the adulthood. However, the rate of co-localization of VGLUT2 and DA may increase during development (Mendez et al., 2008; Bérubé-Carrière et al., 2009). Consistently, it has been shown more than 90% of SNpc DA neurons presented a reporter indicative of past expression of VGLUT2 based on a fate mapping strategy (Steinkellner et al., 2018). VGLUT2 is expressed in SNpc DA neurons early in life, while most of these DA neurons present decreased expression of VGLUT2 at maturity. VGLUT2 facilitates the encapsulation of glutamate into synaptic vesicles *in vitro* (Kouwenhoven et al., 2020). Study have shown that VGLUT2 contributes to vesicular DA loading by increasing the pH gradient of vesicles (or vesicular hyper-acidification; Aguilar et al., 2017).

VGLUT2 functionally regulates the core co-release of glutamate and DA from VGLUT2+ DA neurons. VGLUT2 is the dominant subtype of VGLUTs existed in midbrain DA neurons (Bérubé-Carrière et al., 2009; Chuhma et al., 2009; Morales and Root, 2014; Morales and Margolis, 2017). Furthermore, VGLUT2 selectively deleted from DA neurons may influence the growth and survival of DA neurons in cell culture and development *in vivo* (Hnasko et al., 2010). Similarly, the loss of DA neurons in SNpc caused by overexpression of VGLUT2 is accompanied by changes in motor behavior of mice (Steinkellner et al., 2018). In general, these behavioral abnormalities are strongly linked to decreased striatal DA neurotransmission in involved hemispheres. Postmortem brain tissues from PD patients exhibit marked variations in expression of VGLUTs in the cerebral cortex and striatum, indicating the important role of VGLUTs in PD (Kashani et al., 2007). Previous research has shown the essential roles of VGLUT2 expression in DA neurons in normal emotional responses as well as behavioral activation mediated by psychostimulant (Birgner et al., 2010). Several studies have shown that downregulation of VGLUT2 expression exclusively in the STN of mice leads to reduced postsynaptic activity and behavioral hyperlocomotion, due to the strong modifications in both the STN and the striatum DA system (Schweizer et al., 2014, 2016). Moreover, MPTP-treated mouse model of PD has increased expression of VGLUT2 in the striatum in comparison to controls (Pflibsen et al., 2015).

VGLUT2 is deemed to promote the survival of DA neurons. Shen et al. have reported that VGLUT2 selectively deleted from DA neurons obviously increases the susceptibility of DA neurons to neurotoxin MPTP, and furthermore, upregulation of VGLUT2 in DA neurons prevented this vulnerability in VGLUT2 conditional Knock-out (KO) mice (Shen et al., 2018). This finding suggests that the absence or reduction of VGLUT2 expression in several DA neurons may be considered as a novel risk factor for the occurrence and progression of DA neurodegeneration in PD. Therefore, restoring the expression of VGLUT2 in DA neurons may be a potential and novel therapeutic method for PD or other neurodegenerative diseases. In contrast, Steinkellner et al. reported that the proportion of DA neurons expressing VGLUT2 approximately doubled after 6-OHDA injection in the striatum. Notably, although the neurotoxicity of 6-OHDA reduced the total DA neurons, the number of DA neurons containing elevated VGLUT2 transcripts was definitely increased, suggesting that 6-OHDA caused upregulation of VGLUT2 in transcriptional levels in adult SNpc DA neuron cells (Steinkellner et al., 2018). They further demonstrated that VGLUT2+ DA neurons enriched in surviving neurons in α-synuclein-induced dopaminergic neuronal injury, and VGLUT2 expression was found upregulated in brain tissue of PD patients (Steinkellner et al., 2022). This result is consistent with previous studies which revealed that neonatal striatal lesions or 6-OHDA treatment promote the expression of VGLUT2 (Dal Bo et al., 2008; Bérubé-Carrière et al., 2009). Buck et al. also found that the subpopulation of VGLUT2+ DA neurons are relatively protected from rotenone neurotoxicity (Buck et al., 2021a). In summary, the effects of different neurotoxicants produced an analogous change. The above findings implied that the neurotoxins-induced upregulation of the glutamatergic machinery in VTA and SNpc neurons and their projections may be part of a broader neuroprotective mechanism. Moreover, Buck et al. demonstrated that female drosophila has

elevated expression level of dVGLUT in DA neurons compared with male drosophila, and this finding is highly conserved across species, including flies, rodents, and humans. Moreover, they found that reducing the expression of dVGLUT in DA neurons eliminates females' better resilience to DA neuron loss throughout aging. dVGLUT is the core role in the selective DA neuron vulnerability to sex- and age-related DA neurodegeneration (Buck et al., 2021b).

Noteworthy, Heterologous expression of VGLUT2 with a sustained or high level is toxic to DA neurons, while endogenous expression of VGLUT2 with a low level might exert a protective effect (Buck et al., 2022). Glutamate co-entry through the vesicle of VGLUTs is able to drive VMAT2-mediated exchange, which can elevate the amount of DA and other cationic transmitters, as well as contribute to isolate toxic VMAT2 substrates, including 1-methyl-4-phenylpyridine (MPP^+) or 6-OHDA, away from sensitive cellular compartments (Dal Bo et al., 2008; Descarries et al., 2008). Therefore, the expressing of VGLUT2 is likely to explain the enhancive resistance of DA neurons to neurotoxins. DA-depletion has no influence in the expression of VGLUT1 and VGLUT3, but VGLUT2 expression is conspicuously reduced in almost all basal ganglia structures (Favier et al., 2013). High-frequency stimulation of the subthalamic nucleus (STN-HFS) can reverse the decrease in VGLUT2 expression, which provides evidence for the involvement of VGLUT2 in the regulation of basal ganglia circuitry, suggesting that VGLUT2 exert an important role in alleviating motor symptoms in PD (Favier et al., 2013). Since VGLUT2 is the only VGLUT produced by STN glutamatergic projections to SNpr, we speculate that during STN-HFS, information transmission through the trans-thalamic pathway has not been fully interrupted, despite its roles in the expression of VGLUT2 in SNpr are likely mediated by regulation of thalamic afferents.

VGLUT3 and Parkinson's disease

Both VGLUT1 and VGLUT2 are originally known as "typical" cortical and subcortical VGLUTs. However, VGLUT3 predominantly exists in scattered group of "non-glutamatergic" neurons, or only expresses in a few glutamate neurons (El et al., 2011). VGLUT3 represents a unique modulator of glutamate release from both non-glutamatergic and glutamatergic neurons in the brain (Favier et al., 2021). Although the distribution and quantity of VGLUT3 is limited, it plays a vital role in regulation glutamate signaling and thus modulates the activity of neural microcircuits (Favier et al., 2021). Currently, few studies have explored the role of VGLUT3 in PD, most studies focus on revealing the critical role of VGLUT3 in levodopa-induced dyskinesia (LID), which usually occurs in PD patients with long-term L-DOPA treatment (Divito et al., 2015; Gangarossa et al., 2016).

Reduction of DA transmission triggers profound adaptive changes in DA-sensitive brain structures, particularly the dorsal striatum. Striatal cholinergic interneurons (ChIs) are the main source of acetylcholine in the striatum. The increased striatal cholinergic tone is the main pathogenic mechanism among all the alterations associated with PD, as ChIs potently regulates local striatal microcirculation, which attracts intensive researchers to establish anticholinergic treatment for PD (McKinley et al., 2019). However, regulation of striatal ChIs directly leads to alterations in local striatal glutamate transmission (Tubert et al., 2016). VGLUT3 is highly expressed in striatum, and plays an important role in ChIs-mediated glutamate release (Gras et al., 2008). Meanwhile, the activity of GABAergic medium spiny neurons (MSNs) and fast-spiking GABAergic interneurons (FSIs) are related to the VGLUT3-dependent glutamate transmission (Favier et al., 2021). VGLUT3-KO mice show circadian-dependent hyperlocomotor activity, while conditional deletion of VGLUT3 from ChIs does not alter evoked DA release in the striatum or baseline locomotor activity (Divito et al., 2015). Loss of DA in 6-OHDA-lesioned mice is accompanied by increased expression of VGLUT3 and vesicular acetylcholine transporter (VAChT) in the striatum, and the VAChT levels remain high whereas the VGLUT3 expression decreases in LID mice (Gangarossa et al., 2016).

Conclusion

In this review, we summarized the distribution and functional characteristics of VGLUTs in the brain, and indicate the pivotal influence of glutamate transmission in the functional organization of neuronal circuits in PD, as well as the massive alterations in glutamate transmission and VGLUTs levels in PD. Among them, adaptive changes in the expression level and function of VGLUTs may exert a crucial role in excitatory damage in PD, and VGLUTs are considered as novel potential therapeutic targets for PD. Notably, recent years, there have been several authoritative studies on VGLUT2, and emerging evidence highlights that the balance of VGLUT2 expression in select DA neuronal populations may be a novel identified risk factor or therapeutic target in the progression of PD or other neurodegenerative diseases. Taken together, the structure, function, and regulatory mechanisms of VGLUTs will be a promising area of research in PD clinical practice.

Author contributions

WY contributed to the conception of the study. CZ contributed to search and organize literatures. WY and CZ wrote the manuscript. CW and HZ contributed equally to this work in administrative and material support. All authors contributed to the article and approved the submitted version.

Funding

This research was supported by the grant of National Natural Science Foundation of China (no. 81801123) to WY, Natural Science Foundation of Hunan Province (no. 2023JJ40865) to WY and Natural Science Foundation of Hunan Province (no. 2021JJ41055) to CZ.

Conflict of interest

The authors declare that the research was conducted in the absence of any commercial or financial relationships that could be construed as a potential conflict of interest.

Publisher's note

References

Aguilar, J. I., Dunn, M., Mingote, S., Karam, C. S., Farino, Z. J., Sonders, M. S., et al. (2017). Neuronal depolarization drives increased dopamine synaptic vesicle loading via VGLUT. *Neuron* 95, 1074–1088.e7. doi: 10.1016/j.neuron.2017.07.038

Andersen, J. V., and Schousboe, A. (2022). Glial glutamine homeostasis in health and disease. *Neurochem. Res.* 48, 1100–1128. doi: 10.1007/s11064-022-03771-1

Armstrong, M. J., and Okun, M. S. (2020). Diagnosis and treatment of parkinson disease: a review. *JAMA* 323, 548–560. doi: 10.1001/jama.2019.22360

Bellocchio, E. E., Reimer, R. J., Fremeau, R. J., and Edwards, R. H. (2000). Uptake of glutamate into synaptic vesicles by an inorganic phosphate transporter. *Science* 289, 957–960. doi: 10.1126/science.289.5481.957

Bérubé-Carrière, N., Riad, M., Dal Bo, G., Lévesque, D., Trudeau, L. E., and Descarries, L. (2009). The dual dopamine-glutamate phenotype of growing mesencephalic neurons regresses in mature rat brain. *J. Comp. Neurol.* 517, 873–891. doi: 10.1002/cne.22194

Bigge, C. F. (1999). Ionotropic glutamate receptors. *Curr. Opin. Chem. Biol.* 3, 441–447. doi: 10.1016/S1367-5931(99)80065-9

Birgner, C., Nordenankar, K., Lundblad, M., Mendez, J. A., Smith, C., le Grevès, M., et al. (2010). VGLUT2 in dopamine neurons is required for psychostimulant-induced behavioral activation. *Proc. Natl. Acad. Sci. U. S. A.* 107, 389–394. doi: 10.1073/pnas.0910986107

Blakely, R. D., and Edwards, R. H. (2012). Vesicular and plasma membrane transporters for neurotransmitters. *Cold Spring Harb. Perspect. Biol.* 4:a005595. doi: 10.1101/cshperspect.a005595

Buck, S. A., de Miranda, B. R., Logan, R. W., Fish, K. N., Greenamyre, J. T., and Freyberg, Z. (2021a). VGLUT2 is a determinant of dopamine neuron resilience in a rotenone model of dopamine neurodegeneration. *J. Neurosci.* 41, 4937–4947. doi: 10.1523/JNEUROSCI.2770-20.2021

Buck, S. A., Erickson-Oberg, M. Q., Bhatte, S. H., McKellar, C. D., Ramanathan, V. P., Rubin, S. A., et al. (2022). Roles of VGLUT2 and dopamine/glutamate co-transmission in selective vulnerability to dopamine neurodegeneration. *ACS Chem. Nerosci.* 13, 187–193. doi: 10.1021/acschemneuro.1c00741

Buck, S. A., Steinkellner, T., Aslanoglou, D., Villeneuve, M., Bhatte, S. H., Childers, V. C., et al. (2021b). Vesicular glutamate transporter modulates sex differences in dopamine neuron vulnerability to age-related neurodegeneration. *Aging Cell* 20:e13365. doi: 10.1111/acel.13365

Buck, S. A., Torregrossa, M. M., Logan, R. W., and Freyberg, Z. (2021c). Roles of dopamine and glutamate co-release in the nucleus accumbens in mediating the actions of drugs of abuse. *FEBS J.* 288, 1462–1474. doi: 10.1111/febs.15496

Chen, I., Pant, S., Wu, Q., Cater, R. J., Sobti, M., Vandenberg, R. J., et al. (2021). Glutamate transporters have a chloride channel with two hydrophobic gates. *Nature* 591, 327–331. doi: 10.1038/s41586-021-03240-9

Cheng, L., Duan, B., Huang, T., Zhang, Y., Chen, Y., Britz, O., et al. (2017). Identification of spinal circuits involved in touch-evoked dynamic mechanical pain. *Nat. Neurosci.* 20, 804–814. doi: 10.1038/nn.4549

Chuhma, N., Choi, W. Y., Mingote, S., and Rayport, S. (2009). Dopamine neuron glutamate cotransmission: frequency-dependent modulation in the mesoventromedial projection. *Neuroscience* 164, 1068–1083. doi: 10.1016/j.neuroscience.2009.08.057

Cilia, R., Marotta, G., Landi, A., Isaias, I. U., Mariani, C. B., Vergani, F., et al. (2009). Clinical and cerebral activity changes induced by subthalamic nucleus stimulation in advanced Parkinson's disease: a prospective case-control study. *Clin. Neurol. Neurosurg.* 111, 140–146. doi: 10.1016/j.clineuro.2008.09.018

Dal Bo, G., Bérubé-Carrière, N., Mendez, J. A., Leo, D., Riad, M., Descarries, L., et al. (2008). Enhanced glutamatergic phenotype of mesencephalic dopamine neurons after neonatal 6-hydroxydopamine lesion. *Neuroscience* 156, 59–70. doi: 10.1016/j.neuroscience.2008.07.032

Daniels, R. W., Collins, C. A., Chen, K., Gelfand, M. V., Featherstone, D. E., and DiAntonio, A. (2006). A single vesicular glutamate transporter is sufficient to fill a synaptic vesicle. *Neuron* 49, 11–16. doi: 10.1016/j.neuron.2005.11.032

Descarries, L., Bérubé-Carrière, N., Riad, M., Bo, G. D., Mendez, J. A., and Trudeau, L. E. (2008). Glutamate in dopamine neurons: Synaptic versus diffuse transmission. *Brain Res. Rev.* 58, 290–302. doi: 10.1016/j.brainresrev.2007.10.005

Divito, C. B., Steece-Collier, K., Case, D. T., Williams, S. P., Stancati, J. A., Zhi, L., et al. (2015). Loss of VGLUT3 produces circadian-dependent hyperdopaminergia and ameliorates motor dysfunction and l-Dopa-mediated dyskinesias in a model of parkinson's disease. *J. Neurosci.* 35, 14983–14999. doi: 10.1523/JNEUROSCI.2124-15.2015

El, A. A., Albertini, G., Bentea, E., Demuyser, T., Van Eeckhaut, A., Smolders, I., et al. (2015). Alterations in the motor cortical and striatal glutamatergic system and D-serine levels in the bilateral 6-hydroxydopamine rat model for Parkinson's disease. *Neurochem. Int.* 88, 88–96. doi: 10.1016/j.neuint.2015.07.005

El, M. S., Wallén-Mackenzie, A., Fortin, G. M., Descarries, L., and Trudeau, L. E. (2011). From glutamate co-release to vesicular synergy: vesicular glutamate transporters. *Nat. Rev. Neurosci.* 12, 204–216. doi: 10.1038/nrn2969

Eriksen, J., Li, F., and Edwards, R. H. (2020). The mechanism and regulation of vesicular glutamate transport: coordination with the synaptic vesicle cycle. *Biochim. Biophys. Acta Biomembr.* 1862:183259. doi: 10.1016/j.bbamem.2020.183259

Fasano, C., Rocchetti, J., Pietrajtis, K., Zander, J. F., Manseau, F., Sakae, D. Y., et al. (2017). Regulation of the hippocampal network by VGLUT3-positive CCK-GABAergic basket cells. *Front. Cell. Neurosci.* 11:140. doi: 10.3389/fncel.2017.00140

Favier, M., Carcenac, C., Drui, G., Boulet, S., El, M. S., and Savasta, M. (2013). High-frequency stimulation of the subthalamic nucleus modifies the expression of vesicular glutamate transporters in basal ganglia in a rat model of Parkinson's disease. *BMC Neurosci.* 14:152. doi: 10.1186/1471-2202-14-152

Favier, M., Pietrancosta, N., El, M. S., and Gangarossa, G. (2021). Leveraging VGLUT3 functions to untangle brain dysfunctions. *Trends Pharmacol. Sci.* 42, 475–490. doi: 10.1016/j.tips.2021.03.003

Ferraguti, F., and Shigemoto, R. (2006). Metabotropic glutamate receptors. *Cell Tissue Res.* 326, 483–504. doi: 10.1007/s00441-006-0266-5

Fremeau, R. J., Troyer, M. D., Pahner, I., Nygaard, G. O., Tran, C. H., Reimer, R. J., et al. (2001). The expression of vesicular glutamate transporters defines two classes of excitatory synapse. *Neuron* 31, 247–260. doi: 10.1016/s0896-6273(01)00344-0

Gangarossa, G., Guzman, M., Prado, V. F., Prado, M. A., Daumas, S., El, M. S., et al. (2016). Role of the atypical vesicular glutamate transporter VGLUT3 in l-DOPA-induced dyskinesia. *Neurobiol. Dis.* 87, 69–79. doi: 10.1016/j.nbd.2015.12.010

Gras, C., Amilhon, B., Lepicard, E. M., Poirel, O., Vinatier, J., Herb in, M., et al. (2008). The vesicular glutamate transporter VGLUT3 synergizes striatal acetylcholine tone. *Nat. Neurosci.* 11, 292–300. doi: 10.1038/nn2052

Gras, C., Herzog, E., Bellenchi, G. C., Bernard, V., Ravassard, P., Pohl, M., et al. (2002). A third vesicular glutamate transporter expressed by cholinergic and serotoninergic neurons. *J. Neurosci.* 22, 5442–5451. doi: 10.1523/JNEUROSCI.22-13-05442.2002

Hackett, T. A., Takahata, T., and Balaram, P. (2011). VGLUT1 and VGLUT2 mRNA expression in the primate auditory pathway. *Hear. Res.* 274, 129–141. doi: 10.1016/j.heares.2010.11.001

Herzog, E., Gilchrist, J., Gras, C., Muzerelle, A., Ravassard, P., Giros, B., et al. (2004). Localization of VGLUT3, the vesicular glutamate transporter type 3, in the rat brain. *Neuroscience* 123, 983–1002. doi: 10.1016/j.neuroscience.2003.10.039

Hioki, H., Nakamura, H., Ma, Y. F., Konno, M., Hayakawa, T., Nakamura, K. C., et al. (2010). Vesicular glutamate transporter 3-expressing nonserotonergic projection neurons constitute a subregion in the rat midbrain raphe nuclei. *J. Comp. Neurol.* 518, 668–686. doi: 10.1002/cne.22237

Hnasko, T. S., Chuhma, N., Zhang, H., Goh, G. Y., Sulzer, D., Palmiter, R. D., et al. (2010). Vesicular glutamate transport promotes dopamine storage and glutamate corelease in vivo. *Neuron* 65, 643–656. doi: 10.1016/j.neuron.2010.02.012

Iovino, L., Tremblay, M. E., and Civiero, L. (2020). Glutamate-induced excitotoxicity in Parkinson's disease: the role of glial cells. *J. Pharmacol. Sci.* 144, 151–164. doi: 10.1016/j.jphs.2020.07.011

Jia, J., Li, B., Sun, Z. L., Yu, F., Wang, X., and Wang, X. M. (2010). Electro-acupuncture stimulation acts on the basal ganglia output pathway to ameliorate motor impairment in parkinsonian model rats. *Behav. Neurosci.* 124, 305–310. doi: 10.1037/a0018931

Kalia, L. V., and Lang, A. E. (2015). Parkinson's disease. *Lancet* 386, 896–912. doi: 10.1016/S0140-6736(14)61393-3

Kaneko, T., and Fujiyama, F. (2002). Complementary distribution of vesicular glutamate transporters in the central nervous system. *Neurosci. Res.* 42, 243–250. doi: 10.1016/s0168-0102(02)00009-3

Kashani, A., Betancur, C., Giros, B., Hirsch, E., and El, M. S. (2007). Altered expression of vesicular glutamate transporters VGLUT1 and VGLUT2 in Parkinson disease. *Neurobiol. Aging* 28, 568–578. doi: 10.1016/j.neurobiolaging.2006.02.010

Kawano, M., Kawasaki, A., Sakata-Haga, H., Fukui, Y., Kawano, H., Nogami, H., et al. (2006). Particular subpopulations of midbrain and hypothalamic dopamine neurons express vesicular glutamate transporter 2 in the rat brain. *J. Comp. Neurol.* 498, 581–592. doi: 10.1002/cne.21054

Klingelhoefer, L., and Reichmann, H. (2017). Parkinson's disease as a multisystem disorder. *J. Neural Transm.* 124, 709–713. doi: 10.1007/s00702-017-1692-0

Kouwenhoven, W. M., Fortin, G., Penttinen, A. M., Florence, C., Delignat-Lavaud, B., Bourque, M. J., et al. (2020). VGluT2 expression in dopamine neurons contributes to postlesional striatal reinnervation. *J. Neurosci.* 40, 8262–8275. doi: 10.1523/JNEUROSCI.0823-20.2020

Lee, S., Chen, L., Chen, M., Ye, M., Seal, R. P., and Zhou, Z. J. (2014). An unconventional glutamatergic circuit in the retina formed by vGluT3 amacrine cells. *Neuron* 84, 708–715. doi: 10.1016/j.neuron.2014.10.021

Liguz-Lecznar, M., and Skangiel-Kramska, J. (2007). Vesicular glutamate transporters (VGLUTs): the three musketeers of glutamatergic system. *Acta Neurobiol. Exp.* 67, 207–218.

Lyu, S., Guo, Y., Zhang, L., Tang, G., Li, R., Yang, J., et al. (2021). Downregulation of astroglial glutamate transporter GLT-1 in the lateral habenula is associated with

depressive-like behaviors in a rat model of Parkinson's disease. *Neuropharmacology* 196:108691. doi: 10.1016/j.neuropharm.2021.108691

Magi, S., Piccirillo, S., Amoroso, S., and Lariccia, V. (2019). Excitatory amino acid transporters (EAATs): glutamate transport and beyond. *Int. J. Mol. Sci.* 20:5674. doi: 10.3390/ijms20225674

Martineau, M., Guzman, R. E., Fahlke, C., and Klingauf, J. (2017). VGLUT1 functions as a glutamate/proton exchanger with chloride channel activity in hippocampal glutamatergic synapses. *Nat. Commun.* 8:2279. doi: 10.1038/s41467-017-02367-6

Massie, A., Schallier, A., Vermoesen, K., Arckens, L., and Michotte, Y. (2010). Biphasic and bilateral changes in striatal VGLUT1 and 2 protein expression in hemi-Parkinson rats. *Neurochem. Int.* 57, 111–118. doi: 10.1016/j.neuint.2010.04.019

Maycox, P. R., Deckwerth, T., Hell, J. W., and Jahn, R. (1988). Glutamate uptake by brain synaptic vesicles. Energy dependence of transport and functional reconstitution in proteoliposomes. *J. Biol. Chem.* 263, 15423–15428. doi: 10.1016/S0021-9258(19)37605-7

McKinley, J. W., Shi, Z., Kawikova, I., Hur, M., Bamford, I. J., Sudarsana, D. S., et al. (2019). Dopamine deficiency reduces striatal cholinergic interneuron function in models of parkinson's disease. *Neuron* 103, 1056–1072.e6. doi: 10.1016/j.neuron.2019.06.013

Mendez, J. A., Bourque, M. J., Dal Bo, G., Bourdeau, M. L., Danik, M., Williams, S., et al. (2008). Developmental and target-dependent regulation of vesicular glutamate transporter expression by dopamine neurons. *J. Neurosci.* 28, 6309–6318. doi: 10.1523/JNEUROSCI.1331-08.2008

Morales, M., and Margolis, E. B. (2017). Ventral tegmental area: cellular heterogeneity, connectivity and behaviour. *Nat. Rev. Neurosci.* 18, 73–85. doi: 10.1038/nrn.2016.165

Morales, M., and Root, D. H. (2014). Glutamate neurons within the midbrain dopamine regions. *Neuroscience* 282, 60–68. doi: 10.1016/j.neuroscience.2014.05.032

Orieux, G., Francois, C., Féger, J., Yelnik, J., Vila, M., Ruberg, M., et al. (2000). Metabolic activity of excitatory parafascicular and pedunculopontine inputs to the subthalamic nucleus in a rat model of Parkinson's disease. *Neuroscience* 97, 79–88. doi: 10.1016/s0306-4522(00)00011-7

Pflibsen, L., Stang, K. A., Sconce, M. D., Wilson, V. B., Hood, R. L., Meshul, C. K., et al. (2015). Executive function deficits and glutamatergic protein alterations in a progressive 1-methyl-4-phenyl-1,2,3,6-tetrahydropyridine mouse model of Parkinson's disease. *J. Neurosci. Res.* 93, 1849–1864. doi: 10.1002/jnr.23638

Pietrancosta, N., Djibo, M., Daumas, S., El, M. S., and Erickson, J. D. (2020). Molecular, structural, functional, and pharmacological sites for vesicular glutamate transporter regulation. *Mol. Neurobiol.* 57, 3118–3142. doi: 10.1007/s12035-020-01912-7

Pisanò, C. A., Brugnoli, A., Novello, S., Caccia, C., Keywood, C., Melloni, E., et al. (2020). Safinamide inhibits in vivo glutamate release in a rat model of Parkinson's disease. *Neuropharmacology* 167:108006. doi: 10.1016/j.neuropharm.2020.108006

Plaitakis, A., and Shashidharan, P. (2000). Glutamate transport and metabolism in dopaminergic neurons of substantia nigra: implications for the pathogenesis of Parkinson's disease. *J. Neurol.* 247, II25–I35. doi: 10.1007/pl00007757

Raju, D. V., Ahern, T. H., Shah, D. J., Wright, T. M., Standaert, D. G., Hall, R. A., et al. (2008). Differential synaptic plasticity of the corticostriatal and thalamostriatal systems in an MPTP-treated monkey model of parkinsonism. *Eur. J. Neurosci.* 27, 1647–1658. doi: 10.1111/j.1460-9568.2008.06136.x

Ruel, J., Emery, S., Nouvian, R., Bersot, T., Amilhon, B., Van Rybroek, J. M., et al. (2008). Impairment of SLC17A8 encoding vesicular glutamate transporter-3, VGLUT3, underlies nonsyndromic deafness DFNA25 and inner hair cell dysfunction in null mice. *Am. J. Hum. Genet.* 83, 278–292. doi: 10.1016/j.ajhg.2008.07.008

Sanjari, M. H., Zare-Shahabadi, A., Rahmani, F., and Rezaei, N. (2017). Neurotransmission systems in Parkinson's disease. *Rev. Neurosci.* 28, 509–536. doi: 10.1515/revneuro-2016-0068

Schäfer, M. K., Varoqui, H., Defamie, N., Weihe, E., and Erickson, J. D. (2002). Molecular cloning and functional identification of mouse vesicular glutamate transporter 3 and its expression in subsets of novel excitatory neurons. *J. Biol. Chem.* 277, 50734–50748. doi: 10.1074/jbc.M206738200

Schapira, A., Chaudhuri, K. R., and Jenner, P. (2017). Non-motor features of Parkinson disease. *Nat. Rev. Neurosci.* 18, 435–450. doi: 10.1038/nrn.2017.62

Schweizer, N., Pupe, S., Arvidsson, E., Nordenankar, K., Smith-Anttila, C. J., Mahmoudi, S., et al. (2014). Limiting glutamate transmission in a Vglut2-expressing subpopulation of the subthalamic nucleus is sufficient to cause hyperlocomotion. *Proc. Natl. Acad. Sci. U. S. A.* 111, 7837–7842. doi: 10.1073/pnas.1323499111

Schweizer, N., Viereckel, T., Smith-Anttila, C. J., Nordenankar, K., Arvidsson, E., Mahmoudi, S., et al. (2016). Reduced Vglut2/Slc17a6 gene expression levels throughout the mouse subthalamic nucleus cause cell loss and structural disorganization followed by increased motor activity and decreased sugar consumption. *eNeuro.* 3, ENEURO.0264–ENEU16.2016. doi: 10.1523/ENEURO.0264-16.2016

Shen, H., Marino, R., McDevitt, R. A., Bi, G. H., Chen, K., Madeo, G., et al. (2018). Genetic deletion of vesicular glutamate transporter in dopamine neurons increases vulnerability to MPTP-induced neurotoxicity in mice. *Proc. Natl. Acad. Sci. U. S. A.* 115, E11532–E11541. doi: 10.1073/pnas.1800886115

Shigeri, Y., Seal, R. P., and Shimamoto, K. (2004). Molecular pharmacology of glutamate transporters, EAATs and VGLUTs. *Brain Res. Brain Res. Rev.* 45, 250–265. doi: 10.1016/j.brainresrev.2004.04.004

Somogyi, J., Baude, A., Omori, Y., Shimizu, H., El, M. S., Fukaya, M., et al. (2004). GABAergic basket cells expressing cholecystokinin contain vesicular glutamate transporter type 3 (VGLUT3) in their synaptic terminals in hippocampus and isocortex of the rat. *Eur. J. Neurosci.* 19, 552–569. doi: 10.1111/j.0953-816x.2003.03091.x

Steinkellner, T., Conrad, W. S., Kovacs, I., Rissman, R. A., Lee, E. B., Trojanowski, J. Q., et al. (2022). Dopamine neurons exhibit emergent glutamatergic identity in Parkinson's disease. *Brain* 145, 879–886. doi: 10.1093/brain/awab373

Steinkellner, T., Zell, V., Farino, Z. J., Sonders, M. S., Villeneuve, M., Freyberg, R. J., et al. (2018). Role for VGLUT2 in selective vulnerability of midbrain dopamine neurons. *J. Clin. Invest.* 128, 774–788. doi: 10.1172/JCI95795

Takamori, S., Rhee, J. S., Rosenmund, C., and Jahn, R. (2000). Identification of a vesicular glutamate transporter that defines a glutamatergic phenotype in neurons. *Nature* 407, 189–194. doi: 10.1038/35025070

Tatti, R., Bhaukaurally, K., Gschwend, O., Seal, R. P., Edwards, R. H., Rodriguez, I., et al. (2014). A population of glomerular glutamatergic neurons controls sensory information transfer in the mouse olfactory bulb. *Nat. Commun.* 5:3791. doi: 10.1038/ncomms4791

Thompson, C. M., and Chao, C. K. (2020). VGLUT substrates and inhibitors: a computational viewpoint. *Biochim. Biophys. Acta Biomembr.* 1862:183175. doi: 10.1016/j.bbamem.2020.183175

Thompson, C. M., Davis, E., Carrigan, C. N., Cox, H. D., Bridges, R. J., and Gerdes, J. M. (2005). Inhibitor of the glutamate vesicular transporter (VGLUT). *Curr. Med. Chem.* 12, 2041–2056. doi: 10.2174/0929867054637635

Tubert, C., Taravini, I., Flores-Barrera, E., Sánchez, G. M., Prost, M. A., Avale, M. E., et al. (2016). Decrease of a current mediated by kv1.3 channels causes striatal cholinergic interneuron hyperexcitability in experimental parkinsonism. *Cell Rep.* 16, 2749–2762. doi: 10.1016/j.celrep.2016.08.016

Wang, Y., Wang, Y., Liu, J., and Wang, X. (2018). Electroacupuncture alleviates motor symptoms and up-regulates vesicular glutamatergic transporter 1 expression in the subthalamic nucleus in a unilateral 6-Hydroxydopamine-lesioned hemi-parkinsonian rat model. *Neurosci. Bull.* 34, 476–484. doi: 10.1007/s12264-018-0213-y

Wang, J., Wang, F., Mai, D., and Qu, S. (2020). Molecular mechanisms of glutamate toxicity in parkinson's disease. *Front. Neurosci.* 14:585584. doi: 10.3389/fnins.2020.585584

Wojcik, S. M., Rhee, J. S., Herzog, E., Sigler, A., Jahn, R., Takamori, S., et al. (2004). An essential role for vesicular glutamate transporter 1 (VGLUT1) in postnatal development and control of quantal size. *Proc. Natl. Acad. Sci. U. S. A.* 101, 7158–7163. doi: 10.1073/pnas.0401764101

Wolosker, H., de Souza, D. O., and de Meis, L. (1996). Regulation of glutamate transport into synaptic vesicles by chloride and proton gradient. *J. Biol. Chem.* 271, 11726–11731. doi: 10.1074/jbc.271.20.11726

Yamaguchi, T., Qi, J., Wang, H. L., Zhang, S., and Morales, M. (2015). Glutamatergic and dopaminergic neurons in the mouse ventral tegmental area. *Eur. J. Neurosci.* 41, 760–772. doi: 10.1111/ejn.12818

Yamaguchi, T., Wang, H. L., Li, X., Ng, T. H., and Morales, M. (2011). Mesocorticolimbic glutamatergic pathway. *J. Neurosci.* 31, 8476–8490. doi: 10.1523/JNEUROSCI.1598-11.2011

Zheng, X., Huang, Z., Zhu, Y., Liu, B., Chen, Z., Chen, T., et al. (2019). Increase in glutamatergic terminals in the striatum following dopamine depletion in a rat model of parkinson's disease. *Neurochem. Res.* 44, 1079–1089. doi: 10.1007/s11064-019-02739-y

frontiers | Frontiers in Molecular Neuroscience

TYPE Review
PUBLISHED 25 May 2023
DOI 10.3389/fnmol.2023.1197853

OPEN ACCESS

EDITED BY
Laura Musazzi,
University of Milano Bicocca, Italy

REVIEWED BY
Ayse Ulusoy,
Helmholtz Association of German Research Centers (HZ), Germany
George K. Tofaris,
University of Oxford, United Kingdom

*CORRESPONDENCE
Arianna Bellucci
✉ arianna.bellucci@unibs.it

RECEIVED 31 March 2023
ACCEPTED 27 April 2023
PUBLISHED 25 May 2023

CITATION
Brembati V, Faustini G, Longhena F and Bellucci A (2023) Alpha synuclein post translational modifications: potential targets for Parkinson's disease therapy?
Front. Mol. Neurosci. 16:1197853.
doi: 10.3389/fnmol.2023.1197853

Alpha synuclein post translational modifications: potential targets for Parkinson's disease therapy?

Viviana Brembati, Gaia Faustini, Francesca Longhena and Arianna Bellucci*

Division of Pharmacology, Department of Molecular and Translational Medicine, University of Brescia, Brescia, Italy

Parkinson's disease (PD) is the most common neurodegenerative disorder with motor symptoms. The neuropathological alterations characterizing the brain of patients with PD include the loss of dopaminergic neurons of the nigrostriatal system and the presence of Lewy bodies (LB), intraneuronal inclusions that are mainly composed of alpha-synuclein (α-Syn) fibrils. The accumulation of α-Syn in insoluble aggregates is a main neuropathological feature in PD and in other neurodegenerative diseases, including LB dementia (LBD) and multiple system atrophy (MSA), which are therefore defined as synucleinopathies. Compelling evidence supports that α-Syn post translational modifications (PTMs) such as phosphorylation, nitration, acetylation, O-GlcNAcylation, glycation, SUMOylation, ubiquitination and C-terminal cleavage, play important roles in the modulation α-Syn aggregation, solubility, turnover and membrane binding. In particular, PTMs can impact on α-Syn conformational state, thus supporting that their modulation can in turn affect α-Syn aggregation and its ability to seed further soluble α-Syn fibrillation. This review focuses on the importance of α-Syn PTMs in PD pathophysiology but also aims at highlighting their general relevance as possible biomarkers and, more importantly, as innovative therapeutic targets for synucleinopathies. In addition, we call attention to the multiple challenges that we still need to face to enable the development of novel therapeutic approaches modulating α-Syn PTMs.

KEYWORDS

alpha synuclein, post translational modifications, Parkinson's disease, synucleinopathies, therapeutic targets, biomarkers

1. Introduction

Parkinson's disease (PD) is the second most common movement disorder, affecting 2% of the world population over 65 years of age (Baker and Graham, 2004).

Motor symptoms mainly arise from the loss of dopaminergic nigrostriatal neurons, that alters the homeostasis of basal ganglia networks (Hornykiewicz, 2001). Beyond motor manifestations, PD patients may also exhibit a wide range of non-motor and psychiatric symptoms, which are caused by functional changes in central nervous system (CNS) and peripheral network system (PNS) circuits (Pfeiffer, 2016; Engelender and Isacson, 2017; Takamatsu et al., 2018; Kulkarni et al., 2022).

Key neuropathological hallmark of PD is the deposition of insoluble proteinaceous inclusions in cell bodies and neurites (Gibb, 1986), which are called Lewy bodies (LB) and Lewy neurites (LN), respectively. In 1997, these were found to be mainly composed of alpha synuclein (α-Syn) insoluble fibrils (Spillantini et al., 1997). In the last decades, it has

been shown that α-Syn is particularly enriched at synaptic terminals, where it regulates synaptic function (Spillantini et al., 1997; Burre et al., 2010; Longhena et al., 2019). Since then, other disorders such as LB dementia (LBD), multiple system atrophy (MSA), Alzheimer's disease (AD) LB variant or neurodegeneration with brain iron accumulation (NBIA), have been found to be characterized by brain accumulation of insoluble α-Syn deposits, and have been defined as synucleinopathies (Spillantini et al., 1998; Spillantini, 1999; Spillantini and Goedert, 2016; Goedert et al., 2017).

Interestingly, α-Syn deposits have been observed also in the PNS innervating the gastrointestinal tract, blood, salivary glands, olfactory mucosa, skin, retina, adrenal gland, heart and muscles (Qualman et al., 1984; Fumimura et al., 2007; Beach et al., 2010; Gelpi et al., 2014; Zange et al., 2015; Stoessl, 2016; Rey et al., 2016a,b, 2018; Wakabayashi, 2020). This peripheral α-Syn pathology is thought to contribute to the onset of PD non-motor manifestations in the prodromal and symptomatic phase (Abbott et al., 2007).

Remarkably, numerous studies in experimental models of synucleinopathy, post-mortem PD brains and neuroimaging evidences support that α-Syn pathological aggregation can severely impair synaptic function, thus consequently perturbing neuronal network dynamics and inducing neurodegeneration (Bellucci et al., 2016, 2017; Longhena et al., 2017, 2019; Kulkarni et al., 2022). This notwithstanding, we still ignore the mechanisms that drive pathological α-Syn aggregation in neuronal cells, and this has hampered the development of innovative effective therapies that block α-Syn pathological deposition as disease modifying approaches for PD and other synucleinopathies (Fields et al., 2019; Lashuel, 2021; Oliveira et al., 2021; Engelender et al., 2022). Indeed, current α-Syn-targeting strategies mainly include immunotherapy-based removal of extracellular α-Syn fibrils, gene therapy-based reduction of α-Syn, general and non-selective small molecule inhibitors of protein aggregation and protein degradation enhancers, but we still miss a cutting edge approach interfering with the culprit of α-Syn aggregate formation.

Interestingly, several post translational modifications (PTMs) of α-Syn have been found to differently modulate α-Syn aggregation either by predisposing or interfering with it (Zhang et al., 2019; Table 1). Indeed, they can affect α-Syn aggregation propensity, solubility and turnover, membrane binding and interaction with other proteins and metals (Oueslati et al., 2010; Zhang et al., 2017, 2019; Bell and Vendruscolo, 2021; Bell et al., 2022a,b). Moreover, α-Syn PTMs can serve as markers for environmental changes, may play a role in gene expression by impinging on cellular responses to stimuli and are also under study as possible disease biomarkers for synucleinopathies (Vicente Miranda et al., 2017a; Fayyad et al., 2019; Vivacqua et al., 2019; Petricca et al., 2022; Sonustun et al., 2022).

In this review, we summarize and discuss the main findings on α-Syn PTMs, in order to define a route to decipher whether these modifications can be rationally considered as achievable druggable targets for synucleinopathies or effective biomarkers monitoring the progression or enabling patient stratification in these neurodegenerative disorders.

2. α-Syn and its post-translational modifications

α-Syn is a member of synuclein family, which also includes β-and γ-synuclein (Clayton and George, 1998). In humans, α-Syn is encoded by the SNCA gene located on chromosome 4q21 (Shibasaki et al., 1995; Lavedan, 1998).

Although the physiological role of α-Syn has not been fully elucidated yet, numerous studies demonstrated its involvement in the control of synaptic release. Indeed, it regulates synaptic vesicle clustering, the coupling and fusion of vesicles participating in SNARE complex assembly, the extent of phasic and tonic

TABLE 1 Functional consequences of the majorly studied α-Syn PTMs.

PTMs	Amino acid	Effects	References
Phoshorylation	ser87	Limits aggregation	Paleologou et al. (2010)
	ser129	Promotes aggregation	Fujiwara et al. (2002), Smith et al. (2005b), Karampetsou et al. (2017)
		Limits aggregation	Gorbatyuk et al. (2008), Oueslati et al. (2012), Tenreiro et al. (2014), Ghanem et al. (2022)
	tyr39	Promotes aggregation	Brahmachari et al. (2016), Mahul-Mellier et al. (2014), Dikiy et al. (2016)
	tyr125	Limits aggregation	Negro et al. (2002), Chen et al. (2009), Kosten et al. (2014)
Nitration	tyr39	Promotes oligomerization	Hodara et al. (2004)
	tyr125	Promotes dimerization	Takahashi et al. (2002), Hodara et al. (2004)
	tyr133	Promotes aggregation	Hodara et al. (2004)
	tyr136	Promotes aggregation	Hodara et al. (2004)
N-terminal acetylation		Inhibits aggregation	Bell et al. (2022a,b, 2023)
O-GlcNAcylation	thr72	Inhibits aggregation	Marotta et al. (2015), Levine et al. (2017, 2019)
	ser87	Inhibits aggregation	Lewis et al. (2017)
Glycation	lys	Promotes oligomerization	Vicente Miranda et al. (2017b)
SUMOylation	lys	Limits aggregation	Krumova et al. (2011)
	lys	Protects from degradation	Rott et al. (2017), Rousseaux et al. (2018)
Ubiquitination	lys	Promotes degradation	Tofaris et al. (2011), Engelender et al. (2022)

neurotransmitter release as well as neurotransmitter reuptake (Choi et al., 2013; Ghiglieri et al., 2018; Longhena et al., 2019). Moreover, α-Syn regulates mitochondrial function, fusion as well as mitochondria and endoplasmic reticulum interaction at mitochondria-associated membranes (MAM; Dauer et al., 2002; Ellis et al., 2005; Di Maio et al., 2016; Ludtmann et al., 2016; Menges et al., 2017; Faustini et al., 2019; Risiglione et al., 2021; Thorne and Tumbarello, 2022) and is involved in neuronal plasticity (Liu et al., 2004b, 2007; Watson et al., 2009; Ullman et al., 2011; Leite et al., 2022; Calabresi et al., 2023).

α-Syn is composed of 140 amino acids and its molecular weight is 14 kDa. α-Syn structure encompasses 3 domains: (1) the N-terminal region (residues 1–60), is positively charged and contains imperfect repeats with a highly conserved hexameric motif (KTKEGV), typically involved in the formation of amphipathic α-helices which mediate membrane binding (Clayton and George, 1998; George, 2002; Vamvaca et al., 2009); (2) the central hydrophobic region (residues 61–95), also known as non-amyloid component (NAC) portion, is prone to intermolecular interactions and is crucial for aggregation and fibril formation (Giasson et al., 2001; Ma et al., 2003); (3) the C-terminal region (residues 96–140) is highly enriched in acidic proline residues (Bellucci et al., 2012). This part of the protein reduces the NAC propensity for aggregation, mediates the majority of α-Syn interactions with proteins, metal ions and other ligands, including dopamine and polyamines, and harbors the majority of PTMs sites (Jensen et al., 1999; Paik et al., 1999; Giasson et al., 2003; Fernandez et al., 2004; Hoyer et al., 2004; Brown, 2007).

α-Syn does not present a defined structure in aqueous solutions and for this reason is defined "natively unfolded" (Stefanis, 2012), but it can shift to α-helix structure in association with membrane phospholipids, suggesting that it acquires different roles in different subcellular compartments based on its dynamic structure (Ahn et al., 2002). Indeed, in function of its capacity to acquire different conformations, α-Syn can interact with lipid membranes, enzymes, chaperones, synaptic and cytoskeletal proteins. Some studies also suggested a physiological α-helical structure forming dimers that counteract synaptic vesicle fission or tetramers that resist aggregation (Bartels et al., 2011; Wang et al., 2011; Medeiros et al., 2017).

Compelling evidence supports that PTMs play an important role in promoting conformational changes that make α-Syn more or less prone to aggregation (Table 1). Indeed, several PTMs such as phosphorylation, nitration, acetylation, glycation, truncation, ubiquitination, SUMOylation and O-GlcNAcylation can affect α-Syn structure. In particular, PTMs can either promote or inhibit α-Syn oligomerization, fibrillization and degradation (Feany and Bender, 2000; Fujiwara et al., 2002; Hodara et al., 2004; Smith et al., 2005a; Kasai et al., 2008; Lee et al., 2008; Rott et al., 2008, 2017; Tetzlaff et al., 2008; Danielson et al., 2009; Oueslati et al., 2010, 2013; Levine et al., 2017; Lewis et al., 2017; Zhang et al., 2019). Moreover, it has been described that LB contain phosphorylated, nitrated, ubiquitinated, SUMOylated and C-terminally truncated α-Syn, further supporting the role of PTMs in the modulation of α-Syn aggregation (Baba et al., 1998; Crowther et al., 1998; Giasson et al., 2000; Gomez-Tortosa et al., 2000; Campbell et al., 2001; Hasegawa et al., 2002; Anderson et al., 2006; Paleologou et al., 2010; Rott et al., 2017).

3. α-Syn post-translational modifications as possible biomarkers for PD and other synucleinopathies

Of note, α-Syn and post translational modified α-Syn in peripheral and accessible tissues have been investigated as possible biomarkers for the diagnosis of PD and other synucleinopathies. Nevertheless, since none of them has been validated across different cohorts so far, we still miss a clear cut evidence supporting their factual clinical significance (Witt et al., 2009; Pouclet et al., 2012; Shannon et al., 2012; Donadio et al., 2014, 2018; Sprenger et al., 2015; Zange et al., 2015; Stokholm et al., 2016; Vilas et al., 2016; Fereshtehnejad et al., 2017).

Biomarkers are defined as cellular, biochemical or molecular alterations that are measurable in biological samples such as human tissues, cells, or fluids (Hulka, 1990). The definition has been extended in order to define biomarkers as biological characteristics that can be objectively measured and evaluated as an indicator of normal biological processes, pathogenic processes, or pharmacological responses to a therapeutic intervention (Naylor, 2003). In particular, biomarkers include tools and technologies that can help disease prediction, cause, diagnosis, progression, regression, or the outcome of treatments (Mayeux, 2004). The importance of biomarkers is particularly relevant in the context of diseases affecting CNS, where it is impossible to have the direct access to the unhealthy tissue. CNS biomarkers detection can be pursued by positron emission tomography (PET) or magnetic resonance imaging (MRI) as well as by biological fluids [blood, cerebrospinal fluid (CSF), saliva], skin and gastrointestinal system biopsies or nasal mucosa analysis.

The fact that α-Syn can be found in different forms (monomeric, oligomeric, aggregated or post translational modified) in accessible and peripheral tissues such as CSF, blood, saliva, tears, colon, esophagus and skin (Tokuda et al., 2010; Devic et al., 2011; Foulds et al., 2011, 2012; Mollenhauer et al., 2013; Abd-Elhadi et al., 2015; Koehler et al., 2015; Chung et al., 2016; Cariulo et al., 2019; Fenyi et al., 2019; Hamm-Alvarez et al., 2019; Vivacqua et al., 2019; Maass et al., 2020; Wang et al., 2020b; Tanei et al., 2021; Bakhit et al., 2022), opened up the possibility to evaluate whether these different proteoforms may be useful for the diagnosis of PD and or other synucleinopathies (Witt et al., 2009; Pouclet et al., 2012; Shannon et al., 2012; Donadio et al., 2014, 2018; Sprenger et al., 2015; Zange et al., 2015; Stokholm et al., 2016; Vilas et al., 2016; Fereshtehnejad et al., 2017; Fayyad et al., 2019; Parnetti et al., 2019; Vivacqua et al., 2019, 2023; Wang et al., 2020b; Ganguly et al., 2021).

Several studies demonstrated that the levels of α-Syn phosphorylated at serine 129 (p-ser129), a PTM that is considered a marker of mature α-Syn aggregates (Ghanem et al., 2022), are elevated in the CSF and plasma of PD patients (Foulds et al., 2011, 2012; Wang et al., 2014; Landeck et al., 2016; Majbour et al., 2016a,b), while total α-Syn levels are decreased (Vivacqua et al., 2019, 2023). Remarkably, the levels of p-ser129 α-Syn were also found to significantly correlate with symptom severity in PD patients, suggesting that p-ser129 may serve as a biomarker for disease progression (Wang et al., 2014; Stewart et al., 2015).

In a recent study, increased levels of total and aggregated α-Syn in the membrane fraction of erythrocytes and high levels of p-ser129 α-Syn in cytosolic fractions were detected in PD cases versus healthy controls (Tian et al., 2019). Another report that analyzed oxidized and

p-ser129 α-Syn demonstrated that higher levels of total and proteinase K resistant α-Syn and p-ser129 α-Syn can be detected in PD patients with motor symptoms (without dementia) with a high degree of accuracy (Abd Elhadi et al., 2019). Interestingly, p-ser129 α-Syn can be detected in skin nerve fibers biopsies and saliva (Vivacqua et al., 2019, 2023; Bougea et al., 2019a; Infante et al., 2020; Wang et al., 2020a; De Bartolo et al., 2023). Interestingly, α-Syn isolated from the skin and saliva has aggregation seeding activity and could serve as a biomarker for PD and as a differential biomarker to distinguish synucleoinopathies from tauopathies (Wang et al., 2020b).

p-ser129 α-Syn has also been detected in the lysate of red blood cells in synucleinopathies (Tian et al., 2019; Li et al., 2020, 2021). Higher levels of both Tyrosine (tyr) 125-phosphorylated α-Syn (p-tyr125) and p-ser129 α-Syn can be also detected in the blood of PD patients (Foulds et al., 2011, 2013; Vicente Miranda et al., 2017a).

Two recent meta-analysis showed that patients with PD have higher blood oxidative stress (OS) markers such as malondialdehyde (MDA), 8-Oxo-2′-deoxyguanosine lipid hydro-peroxide, nitrate and ferritine and lower antioxidant activity of superoxide dismutase (SOD), glucose 6 phosphate dehydrogenase, catalase, and glutathione peroxidase (GPx) compared with healthy control (Khan and Ali, 2018). Nitration of tyr and tryptophan residues as a consequence of the formation of peroxynitrite byproducts easily occurs at OS sites, i.e., in inflamed tissue, and can alter the structure and function of proteins. Nitric oxide (NO) and superoxide react to form peroxynitrite which promotes the nitrification of tyr residues in proteins. Specifically, the nitro group ($-NO_2$) is added to replace a hydrogen atom in the 3′ position of the tyr phenolic ring to form 3-nitrotyrosine (Chavarria and Souza, 2013). Several studies reported the presence of nitrated α-Syn in *in vivo* and *in vitro* experimental models of PD and also in LB (Giasson et al., 2000; Yu et al., 2010; He et al., 2019; Manzanza et al., 2021; Simon et al., 2021; Magalhaes and Lashuel, 2022). Of note, Fernandez et al. (2013) reported the presence of tyr125/136 nitrated α-Syn in the CSF and serum of early PD patients, while a more recent study showed increased levels of nitrated α-Syn at tyr39 (n-tyr39) in the red blood cells of PD patients (Vicente Miranda et al., 2017a). In the same study, Vicente Miranda et al. (2017a) showed also reduced levels of SUMOylated α-Syn and increased levels of glycated α-Syn in PD patients erythrocytes with respect to controls. Since SUMOylation can increase α-Syn solubility and reduce aggregation (Krumova et al., 2011) and glycation can potentiate neuronal loss and motor impairment (Vicente Miranda et al., 2017b), the observed results may reflect brain α-Syn pathological alterations and toxicity (Vicente Miranda et al., 2017a,b).

These findings suggest that α-Syn PTMs, and in particular α-Syn nitration or phosphorylation, can be valuable biomarkers for synucleinopathies. This notwithstanding, we miss large cross-sectional and follow-up studies that will be pivotal for the implementation of post-translationally-modified α-Syn as a biomarker and we need to standardize the most reliable detection methods and several technical issues dealing with the detection or quantification of α-Syn have to be solved (Schmid et al., 2013; Mollenhauer et al., 2017; Magalhaes and Lashuel, 2022; Petricca et al., 2022). Indeed, the assay developed in the different studies exhibited different sensitivity and specificity and also led to conflicting results (Malek et al., 2014; Vivacqua et al., 2019, 2023; Bougea et al., 2019a,b; De Bartolo et al., 2023). For instance, Lin et al. (2019) recently reported a marked increase in total and phosphorylated α-Syn levels as well as in their ratio in the plasma of PD patients vs. healthy controls with assays exhibiting elevated specificity (AUC of ROC curves: 0.94, 0.91 and 0.74, respectively). This is in contrast to the findings of a previous study (Foulds et al., 2012) describing a reduction of total α-Syn and a parallel increase in phosphorylated α-Syn levels detected in the plasma of PD patients with a phosphorylated α-Syn assay exhibiting a ROC AUC = 0.68. Consistently, other reports showed that levels of phosphorylated α-Syn are increased in spite of the decrease of total α-Syn levels in plasma of PD patients (Hong et al., 2010; Gorostidi et al., 2012; Cariulo et al., 2019). When considering that because of sensitivity and specificity issues even CSF or plasma α-Syn cannot be considered as valuable markers of PD yet, it is clear that, as the reliable detection of post-translationally modified α-Syn is even more problematic, much work is warranted for achieving the exhaustive clinical translation of these kind of assay. This notwithstanding, the integrated measurement of α-Syn PTM may offer the possibility to single out patient-specific signatures that in the future could be of great help to settle precision-medicine-based approaches if disease-modifying therapies targeting α-Syn pathology will be developed.

4. Phosphorylation

Among α-Syn PTMs, phosphorylation is the most studied. The primary cause of this interest is mainly due to the fact that in normal brains only 4% of α-Syn is phosphorylated, whereas in LB extracted from PD brains 90% of α-Syn is phosphorylated at ser87 (p-ser87) and at ser129 (Anderson et al., 2006; Paleologou et al., 2010). Other sites of phosphorylation have been found on tyr residues at position 39, 125, 133, and 136.

Phosphorylation is the chemical addition of a phosphoryl group (PO^{3-}) to an organic molecule. Phosphorylation and dephosphorylation (the removal of a phosphoryl group) are carried out by enzymes (e.g., kinases, phosphatases) and the processes orchestrate a plethora of cellular functions in response to external stimuli. *In vitro* and cell culture-based studies have identified a number of kinases, which phosphorylate α-Syn at ser129 and/or ser87, including casein kinase I (CKI; ser87 and ser129), casein kinase II (CKII; ser129; Okochi et al., 2000), G protein-coupled receptor kinases (GRKs 1, 2, 5 and 6; ser129; Pronin et al., 2000), leucine-rich repeat kinase 2 (LRRK2; ser129; Qing et al., 2009b), polo-like kinase (PLK; ser129; Inglis et al., 2009, Mbefo et al., 2010) protein kinase C-related kinase (PKR; ser129; Reimer et al., 2018) and LK6/Mnk2a (ser129; Zhang et al., 2015).

α-Syn phosphorylation at tyr125 can be mediated by the proto-oncogene tyrosine-protein kinase Fyn (Nakamura et al., 2001) and SRC proto-oncogene non-receptor (Src) tyr kinases such as spleen associated tyrosine kinase (Syk), the non-receptor tyrosine-protein kinase Lyn, the protein tyrosine kinase expressed by the protooncogene c-fgr (Ellis et al., 2001; Negro et al., 2002). Syk also phosphorylates α-Syn at try133 and tyr136.

Although the contribution of α-Syn pathology to LRRK2-associated PD is debated (Schneider and Alcalay, 2017) and the relevance of LRRK2-mediated α-Syn phosphorylation in PD is still to be determined, several studies reported that LRRK2 co-localizes with α-Syn in the lower brainstem of PD and LBD patients at early stages (Alegre-Abarrategui et al., 2008; Qing et al., 2009b; Zimprich et al., 2011). Still, *in vitro* studies hint that G2019S-mutant LRRK2 exhibit

an improved ability to phosphorylate α-Syn on ser129 when compared to wt LRRK2 (Qing et al., 2009a).

On the other hand, the phosphatases involved in the dephosphorylation are phosphoprotein phosphatase 2A and 2C (PP2A and PP2C).

Increased ser129 α-Syn phosphorylation has been detected in PD, LBD and MSA (Kahle et al., 2000; Okochi et al., 2000; Fujiwara et al., 2002; Takahashi et al., 2003; Anderson et al., 2006). A recent study analyzing post-mortem tissue from PD and MSA patients at different disease stages reported that ser129 α-Syn phosphorylation is the dominant and earliest PTMs, while lower amounts of p-ser87 α-Syn appeared later along PD progression (Sonustun et al., 2022).

Almost all phosphorylation sites cluster at the C-terminal region of α-Syn (residues 120–140), which is involved in protein–protein, protein-ligand and protein-metal interactions, suggesting a possible role of the modification in the regulation of these functions. Only ser87 lies in the hydrophobic NAC region of α-Syn, which is essential for α-Syn aggregation and fibrillogenesis (El-Agnaf et al., 1998b).

Ser129 is the most studied phosphorylation site because it was linked with increased cytotoxicity and neuronal death (Zhang et al., 2015; Karampetsou et al., 2017; Zhong et al., 2017; Reimer et al., 2018). Furthermore, it has been described that p-ser129 enhances intracellular aggregate formation in SH-SY5Y cells (Smith et al., 2005b) and mediates cell death through activation of the unfolded protein response (UPR) pathway (Sugeno et al., 2008). Still, Karampetsou et al. (2017) observed that mice who received intrastriatal injection of p-ser129 α-Syn exhibited enhanced α-Syn pathology deposition and neurodegeneration in the substantia nigra (SN) compared to the mice injected with wild type (wt) α-Syn.

However, other studies in cellular and animal models claimed that phosphorylated α-Syn exherts a neuroprotective role (Gorbatyuk et al., 2008; Oueslati et al., 2012; Tenreiro et al., 2014; Ghanem et al., 2022). In particular, it has been demonstrated that p-ser129 phosphorylation occurs secondarily to α-Syn accumulation, reducing cytotoxicity and aggregation propensity of α-Syn (Ghanem et al., 2022). Interestingly, p-tyr125 α-Syn can also prevent α-Syn neurotoxicity and aggregation and is pivotal for ser129 phosphorylation (Kosten et al., 2014).

The role of p-ser87 is also controversial as this PTM falls in the NAC region of α-Syn, which is crucial for α-Syn aggregation and fibrillogenesis *in vitro* (Ueda et al., 1993; El-Agnaf et al., 1998a,b; Giasson et al., 2001). In addition, though p-ser87 phosphorylation is increased in the membrane fractions of *post mortem* brains of patients affected by LBD, MSA and AD and healthy controls and of rats overexpressing wt α-Syn, p-ser87 was found to reduce α-Syn membrane binding (Paleologou et al., 2010), supporting that this phosphorylation may be crucial for modulating the physiological effect of α-Syn on synaptic vesicle mobility. Moreover, the unilateral p-ser87 α-Syn overexpression in the nigrostriatal system of rats results in reduced formation of aggregates and does not exert toxicity for nigral dopaminergic neurons in contrast to what has been observed following wt α-Syn overexpression (Decressac et al., 2012; Lundblad et al., 2012; Oueslati et al., 2012; Faustini et al., 2018).

Differently, p-tyr125 was reported to decrease with aging and in PD brains, in *Drosophila melanogaster* and mice (Chen et al., 2009). As this phosphorylation has been found to reduce α-Syn oligomerization, it has been hypothesized that it may play a protective role against aggregate formation (Chen et al., 2009). On this line, Negro et al. (2002) showed that the kinase Syk phosphorylates the C-terminal tyr125 of α-Syn to block α-Syn fibrillation. Moreover, p-tyr125 facilitates the deposition of p-ser129 under physiological conditions (Kosten et al., 2014).

PLK2 has been found to phosphorylate α-Syn, but not β-or γ-syn, at ser129 in HEK293T cells and in primary neurons (Arawaka et al., 2006; Inglis et al., 2009; Mbefo et al., 2010). In particular, PLKs can phosphorylate both monomeric or fibrillary α-Syn (Waxman and Giasson, 2011) and overexpression of PLK2 enhances α-Syn turnover via the autophagic degradation pathway, thus suppressing its toxicity *in vivo* (Oueslati et al., 2013). Despite the role of PLK2 in centriole duplication and cell cycle regulation, PLK2 inhibitors do not appear to cause cytotoxicity nor genotoxicity *in vitro* or *in vivo* at doses and exposures that engage the target in rat (Fitzgerald et al., 2013), but clinical trials on PLK2 inhibitors have shown difficulties in targeting specifically PLK2 in order to avoid off-target-related side effects (Vancraenenbroeck et al., 2011).

c-Abelson tyrosine kinase (c-Abl) is a 120 kDa protein majorly known in relation to human leukemias. c-Abl is distributed in the nucleus and cytosol and is involved in a wide range of functions, including apoptosis and development of the CNS in which it affects neurogenesis, neurite outgrowth, and neuronal plasticity. Moreover, it is involved in several neurodegenerative diseases including PD (Tremblay et al., 2010; Imam et al., 2011). For instance, c-Abl is elevated in postmortem nigrostriatal region of PD patients (Ko et al., 2010; Imam et al., 2011) where it is majorly phosphorylated at tyr412 (Mehdi et al., 2016). c-Abl was found to phosphorylate parkin thus impairing its E3 ligase activity and leading to the loss of dopaminergic neurons in the SN (Ko et al., 2010). It has been described that c-Abl aberrant activation induced a progressive accumulation of α-Syn in the human A53T mutant α-Syn tg mouse model of genetic PD (Brahmachari et al., 2016) through the phosphorylation at tyr39 (Mahul-Mellier et al., 2014; Brahmachari et al., 2016; Dikiy et al., 2016), thus contributing to neurodegeneration. Furthermore, c-Abl is activated by OS (Brasher and Van Etten, 2000; Sun et al., 2000; Gonfloni et al., 2012), and in turn it disrupts antioxidant defense mechanisms driving oxidative injury (Li et al., 2004). It may thus be inferred that c-Abl inhibitors may impact on α-Syn pathology by affecting the phosphorylation and nitration state of the protein.

Consistently, Hebron et al. (2013) showed that c-Abl activation promotes α-Syn accumulation and that the treatment with nilotinib, a brain-permeable second-generation c-Abl inhibitor, developed from the first generation anticancer agent, named imatinib, favored the clearance of α-Syn, improved motor performances (Hebron et al., 2013), restored the levels of dopamine transporter (DAT) and dopamine production in the striatum as well as the expression of tyrosine hydroxylase (TH) in the SN (Hebron et al., 2013, Karuppagounder et al., 2014; Table 2).

Of note, results from nilotinib clinical trials showed that the drug could reduce oligomeric α-Syn (only at 150 mg dose) as well as phosphorylated tau. Nilotinib treatment also improved dopamine metabolism in patients with PD. In particular, it increased the levels of homovanillic acid (HVA) and 3,4-Dihydroxyphenylacetic acid (DOPAC) in the CSF (Pagan et al., 2016, 2020) but without improving motor and nonmotor outcomes.

Simuni et al. (2021) run a double-blind, placebo-controlled trial on 173 PD patients. The results about safety, tolerability, adverse effects and lack of the symptomatic effect of nilotinib were in line with

TABLE 2 Kinase-inhibitors tested in preclinical models of PD and in clinical trials.

Target	Mechanism of action	Molecule name	Results from studies in preclinical models	Results from clinical trials	Ongoing clinical trials	Direct or indirect effect on α-Syn Phosphorylation
c-Abl	Inhibition	Nilotininb	Hebron et al. (2013), Karuppagounder et al. (2014)	Pagan et al. (2016, 2019, 2020), Simuni et al. (2021)		Direct
	Inhibition	IkT-148,009	Karuppagounder et al. (2023)		NCT04350177; NCT05424276	Direct
	Inhibition	Vodobatinib (K0706 or SCC-138)	Mandhane et al. (2019)		NCT03316820; NCT03655236	Direct

the study by Pagan et al. (2020). However, they could not observe changes in biomarkers. Although these evidences support that nilotinib is not suitable for further testing the collected data did not exclude the importance of c-Abl modulation in PD therapeutic strategy (Simuni et al., 2021).

The fact that no clinically meaningful benefit in PD patients in two double-blind studies was reported, is discouraging, but this can find an explanation by the fact that nilotinib does not accumulate in the brain at concentrations sufficient to inhibit c-Abl. As a competitive inhibitor of c-Abl with an IC50 of ≈48 nM it would require a sustained concentration of 150 nM to exert the adequate functions (Pagan et al., 2019). Other c-Abl inhibitors such as IkT-148,009 and vodobatinib (Table 2), are currently under development. The chronic oral treatment with IkT-148,009 was found to significantly reduce p-tyr39 and p-ser129 α-Syn levels thus preventing neurodegeneration in the brain of human A53T mutated α-Syn transgenic (tg) mice and of mice who received striatal injections of mouse recombinant α-Syn pre-formed fibrils (PFF; Karuppagounder et al., 2023). IkT-148009 is a derivative of the commercial anticancer imatinib and it has an IC50 of 33 nM for c-Abl, an improvement in potency of more than 20-fold over imatinib (Werner and Olanow, 2022). The randomized phase I/Ib study in older adult or elderly healthy volunteer was then extended to PD patients to identify the safety, tolerability, maximum tolerated dose and the pharmacokinetic profile of the molecule in single doses up to 325 mg and multiple doses up to 100 mg (Clinical trial identifier: NCT04350177). A randomized, double-blind study in non-treated PD patients is also ongoing (Clinical trial identifier: NCT05424276).

Vodobatinib, also known as K0706 or as SCC-138 is a chemical mixture of other two commercial anticancer agents (Dasatinib and Ponatinib) and it has a reported IC50 for wt c-Abl of 0.9 nM (Antelope et al., 2019). In preclinical models of PD it has been shown that it inhibited preferentially, with a sub-nanomolar potency, the protein kinase activity of c-Abl. Moreover, it increased autophagic flux, it had appreciable BBB penetration *in vivo* and protected both 1-methyl-4-phenyl-1,2,3,6-tetrahydropyridine (MPTP) mice and rats overexpressing α-Syn from nigrostriatal neuron loss (Mandhane et al., 2019).

A phase I clinical trial showed that vodobatinib was well-tolerated and allowed the selection of two doses that are likely to produce therapeutic effects (Clinical trial identifier: NCT03316820). A new double-blind, placebo-controlled phase II study is now recruiting for evaluating the safety and effectiveness of the two selected K0706 doses in people with early PD who are not receiving dopaminergic therapy (Clinical trial identifier: NCT03655236). The primary endpoints focus on changes from baseline in the sum of Movement Disorder Society-Sponsored Revision of the Unified Parkinson's Disease Rating Scale (MDS-UPDRS) Parts 2 and 3, but among other outcome measures there will be the evaluation of CSF and blood K0706 levels and dopamine transporter single-photon emission computed tomography (DAT-SPECT).

Collectively, the above summarized studies on c-Abl inhibitors support that the use of protein kinase modulators in PD may be beneficial. Nevertheless, we need to achieve a deeper understanding of the role of the α-Syn phosphorylation and, more generally, on protein kinase and phosphatases activity in synucleinopathies, before to conclude that strategies modulating this PTM may constitute a possible therapeutic approach for this class of neurodegenerative disorders.

5. Nitration

Post-mortem PD brains are rich in lipid peroxidation products such as 4-hydroxyl-2-nonenal (HNE) as well as DNA and RNA oxidation products (Alam et al., 1997; Floor and Wetzel, 1998; Zhang et al., 1999). Moreover, several lines of evidence support that OS is involved in the degeneration of dopaminergic neurons in PD (Jenner and Olanow, 2006; Schapira and Tolosa, 2010).

OS is the result of a disequilibrium between the production of reactive oxygen species (ROS) or reactive nitrogen species (RNS) and the system for the detoxification leading to the production of free radicals byproducts that damage proteins, lipids, nucleic acids and organelles (Ryan et al., 2014). Although the brain represents only 2% of the body weight, it consumes 20% of the total body oxygen (Quastel and Wheatley, 1932; Magistretti and Pellerin, 1996), which is majorly converted in ROS. To defend against oxidative injuries, cells own a series of enzyme-based antioxidant mechanisms, such as glutathione (GSH), SOD and DJ-1. However, these systems are feeble in preventing the damage. In particular, nigral dopaminergic neurons are particularly sensitive to oxidative injuries as they own long, highly branched axons with a huge number of release sites that renders these cells bioenergentically demanding and at risk of developing mitochondrial OS (Pissadaki and Bolam, 2013). Nigral dopaminergic neurons also own a pacemaking activity characterized by broad and slow action potentials in the absence of synaptic input (Grace and Bunney, 1983). This activity engages continuously L-type Ca^{2+} channel, creating a basal mitochondrial OS in SN dopaminergic neurons (Guzman et al., 2010) and elevating intracellular Ca^{2+} levels (Wilson and Callaway, 2000; Chan et al., 2007). In light of the fact that cytoplasmic Ca^{2+} controls a huge number of pathways within a cell, its

presence inside a neuron must be strictly controlled, and it is rapidly sequestered or pumped back in an ATP-dependent manner, thus resulting highly energy demanding (Wilson and Callaway, 2000). Still, dopamine turnover by monoamine oxidases (MAO) is involved in the production of cytotoxic free radicals, causing the death of dopaminergic neurons (Greenamyre and Hastings, 2004). Among them, the MAO-derived dopamine catabolite 3,4-dihydroxyphenylacetaldehyde (DOPAL) exhibits an enhanced reactivity towards proteins especially at synaptic terminals (Rees et al., 2009) and has been recently found to contribute to the initiation of α-Syn-dependent impaired proteostasis and degeneration of neuronal projections in different experimental models of PD (Masato et al., 2023).

Consistently, it is well established that mitochondria dysfunction is crucially involved in the pathogenesis of PD. This is also supported by the fact that several gene mutations implicated in familial and idiopathic forms of PD are located on loci encoding for mitochondria-linked proteins (Moore et al., 2005; Abou-Sleiman et al., 2006; Schapira, 2008). Moreover, postmortem studies on the SN of sporadic PD patients reported a decreased activity of mitochondrial complex I and higher levels of iron in the SN (Mann et al., 1994; Keeney et al., 2006). Free iron is toxic since it can donate or accept an electron from neighboring molecules and cause damage to cellular components and it can create ROS through the Fenton and Haber-Weiss reaction, in which ferric iron (Fe^{3+}) and ferrous iron (Fe^{2+}) react with superoxide and hydrogen peroxide to form hydroxyl radical (Beard and Connor, 2003; Jomova and Valko, 2011; Eid et al., 2017). Neuromelanin, the dark colored granular pigment present in the dopaminergic neurons of the SN, has the ability to chelate metals, in particular the ferric Fe^{3+} form (Gerlach et al., 2003), thus blocking the Fenton reaction and protecting the cells from hydroxyl radical production. The huge increase of iron found in SN of PD brains might saturate the iron-chelating site of neuromelanin, increasing the production of free radical species. Finally, neuroinflammation can also contribute to OS in the PD brain (Mosley et al., 2006; Picca et al., 2020; Teleanu et al., 2022).

The interplay between α-Syn and OS is still not fully elucidated. *In vitro* and *in vivo* studies support that increased OS in the brain may promote α-Syn aggregation (Paxinou et al., 2001), but α-Syn itself can increase ROS production (Junn and Mouradian, 2002; Winklhofer and Haass, 2010) or it can bind to mitochondrial complex I causing mitochondrial dysfunction in turn favoring OS (Chinta et al., 2010; Winklhofer and Haass, 2010; Wilkaniec et al., 2013).

Nitrated α-Syn can be easily formed under OS conditions. α-Syn has four tyr residues, placed in positions 39 (at the N-terminal region), 125, 133, and 136 (at the C-terminal region). The positions of the nitration sites suggest a possible modulation of membrane binding ability (Hodara et al., 2004) and protein–protein and protein-metal interactions. α-Syn is sensitive to the presence of nitrating agents and the presence of peroxynitrite not only induces the deposition of 3-nitrotyrosines but also the formation of 3,3-dityrosine via the oxidation of tyr residues, which results in α-Syn dimers and oligomer formation (Souza et al., 2000). Danielson et al. (2009) demonstrated a selective 9-fold increase in nitration on tyr39 of α-Syn in oxidative cellular model of PD. In addition, nitration of tyr39 induces high rate of oligomerization (Hodara et al., 2004) similarly to n-tyr125 that contributes to α-Syn dimer formation upon the exposure of recombinant α-Syn to nitrating agents (Takahashi et al., 2002).

Interestingly, a recent study analyzing post-mortem tissue from PD and MSA patients at different disease stages reported that ser129 α-Syn phosphorylation is the dominant and earliest PTMs, followed by tyr39 nitration, while lower amounts of p-ser87 α-Syn appeared later along PD progression (Sonustun et al., 2022). However, in the MSA brain glial cytoplasmatic inclusions, neuronal inclusions and small threads are mainly positive for tyr39 nitrated while ser129 α-Syn can be mainly detected in Schwan cell and neuronal inclusions (Sonustun et al., 2022; Wakabayashi et al., 2022).

Nitrated α-Syn monomers and dimers have been shown to accelerate fibril formation while nitrated α-Syn oligomers inhibit this process (Hodara et al., 2004). This supports that improving the amount of nitrated α-Syn oligomers may delay the formation of mature fibrils. This notwithstanding, as we still ignore whether fibrils or oligomers are the major neurotoxic species in PD, it is hard to predict whether this may be beneficial or detrimental.

Nevertheless, it may be feasible that antioxidant supplementation may be used to reduce α-Syn nitration. In this framework, some antioxidant schemes have been attempted, such as the supplementation of vitamin C, E and β-carotene as well as an adequate diet (Percario et al., 2020). Vitamin A and its precursor β-carotene, have been involved in the destabilization of fibrillary α-Syn *in vitro* (Ono et al., 2004; Ono and Yamada, 2007). Vitamin E (i.e., α-tocopherol) and Vitamin C (i.e., ascorbic acid) are antioxidants that are thought to have a protective effect by either reducing or preventing oxidative damage, preventing or interacting directly with free radicals, respectively. A lot of studies tried to investigate the relation between the intake of vitamins and the protection from PD, but they generated only conflicting results (Kieburtz et al., 1994; Hellenbrand et al., 1996; Morens et al., 1996; de Rijk et al., 1997; Scheider et al., 1997; Etminan et al., 2005; Miyake et al., 2011; Hughes et al., 2016; Schirinzi et al., 2019; Zhao et al., 2019). It has been demonstrated that NXP031, a new compound composed of aptamin C and vitamin C, blocks α-Syn aggregation in the hippocampus of AAV-human α-Syn-injected mice (Song et al., 2022). Similarly, also vitamin B12 was found to inhibit α-Syn fibrillogenesis in *in vitro* models (Jia et al., 2019).

Recent studies on MPTP *in vivo* and *in vitro* models support that γ-and δ-tocotrienol reduces dopaminergic neuron toxicity and improves motor performances through estrogen receptor/PI3K/Akt signaling pathway activation, hence in an antioxidant-independent way (Matsura, 2019). The supplementation of α-and δ-tocotrienol significantly ameliorates motor behavior and prevents the loss of nigra dopaminergic neurons and striatal fibers and neuroinflammation in 6-Hydroxydopamine (6-OHDA)-injected rats (Kumari et al., 2021). The vitamin E family compound tocotrienol is currently under study as a potential agent to delay motor symptoms in PD patients at Hoehn & Yahr stage 2 in a phase II clinical trial (Clinical trial identifier: NCT04491383; Table 3).

This notwithstanding, a multicenter, phase II, randomized, double-blind trial in early drug-naïve PD patients evaluating the efficacy of the iron chelator deferiprone (Table 3) on disease progression indicate that 36 weeks of therapy with deferiprone could remove specifically, safely and gradually the iron content in the nigrostriatal system of PD patients but it worsened the progression of symptoms (Devos et al., 2022). Studies on the efficacy of deferiprone in experimental *in vivo* models of synucleinopathies led to conflicting results. Indeed, human A57T α-Syn tg mice showed improvement in behavioral performances upon deferiprone treatment but without

reduction of α-Syn aggregation (Carboni et al., 2017), while deferiprone treated mouse model of MSA exhibited rescued motor performance, higher neuronal survival and reduced density of α-Syn aggregates in SN (Shukla et al., 2021).

Another possible strategy to counteract OS is based on GSH rebalancing. In particular, since GSH is neither able to pass the blood brain barrier (BBB) nor the cellular membrane of neurons, the dietary supplementation of this enzyme is not possible. However, cysteine, which is rate-limiting in the GSH synthesis pathway, crosses both the BBB and most cell membranes. Therefore, cysteine and its derivative N-acetylcysteine have been investigated as a possible dietary supplementation to implement GSH amount, with several clinical trials ongoing (Table 3). Intravenous N-acetylcysteine injection increased blood GSH redox ratios in PD and healthy subjects and magnetic resonance spectroscopy (MRS) showed higher brain GSH concentrations in all subjects. This supports that it is possible to directly monitor GSH levels that could help during clinical trial to determine the activities and the doses of this antioxidant therapy (Holmay et al., 2013).

Another study aimed at assessing the effect of N-acetylcysteine on human embryonic stem cells-derived midbrain dopaminergic neurons treated with rotenone and on PD patients and showed that N-acetylcysteine exposure significantly improved the survival of midbrain dopaminergic neurons treated with rotenone (Monti et al., 2016). Furthermore, Dopamine Transporter scan (DaTscan) analysis on patients treated for 3 months with N-acetylcysteine resulted in increased DAT binding in the caudate and putamen (Monti et al., 2016). These results support a potential direct effect of N-acetylcysteine (Table 3) on the dopamine system in PD patients, but we still ignore whether this compound affects α-Syn nitration state though N-acetylcysteine has shown protective effects against the damage in dopaminergic terminals concomitant with a reduction in α-Syn levels in transgenic mice (Clark et al., 2010).

Coenzime Q10 (CoQ10) is a key component of the electron transport chain that leads to decreased free radical generation, and, in its reduced form, acts as a powerful antioxidant (Shults, 2005). CoQ10 levels were altered in PD cases (Matsubara, 1991; Shults et al., 1997; Molina et al., 2002) with a significant increase in the percentage of oxidized CoQ10 in affected patients (Sohmiya et al., 2004). Numerous studies in *in vitro* and *in vivo* models of PD demonstrated that CoQ10 protects neurons against MPTP and rotenone toxicity (Beal, 1998; Horvath et al., 2003; Menke et al., 2003; Sherer et al., 2003; Gille et al., 2004), and 1-Benzyl-1,2,3,4-tetrahydroisoquinol (Shavali et al., 2004; Table 3).

A randomized, double-blind, placebo-controlled, multicenter phase II study in early PD examined the effects of 300, 600, and 1,200 mg per day of CoQ10 vs. placebo. CoQ10 supplementation decreased functional decline in participants and increased platelet mitochondrial complex I and II/III activities. These results suggested a possible disease-modifying effect (Shults and Schapira, 2001). Based on these results, in a phase III study, the group tested whether high doses (1,200 and 2,400 mg/d) of CoQ10 could slow functional decline in early PD. The results showed that CoQ10 could be safely administered to patients with early PD, however no therapeutic efficacy was demonstrated (Parkinson Study Group et al., 2014).

The hydrophilic analogue of CoQ10, idebenone, is well-known antioxidant compound with better pharmacological properties. Clinical safety of idebenone was well described, and the molecule is

TABLE 3 List of OS modulators tested in preclinical models of PD and in clinical trials.

Target	Mechanism of action	Molecule name	Results from studies in preclinical models	Results from clinical trials	Ongoing clinical trials	Direct or indirect effect on α-Syn Nitration
Vitamin E	Supplementation	Tocotrienol	Kumari et al. (2021)		NCT04491383	N/A
Iron	Removing	Deferiprone		Devos et al. (2022)		Indirect (reduces a-Syn aggregates)
GSH	Supplementation	N-acetylcisteine	Monti et al. (2016)	Holmay et al. (2013), Monti et al. (2016)		Indirect (reduces a-Syn aggregates)
CoQ10	Supplementation	Coenzime Q10	Beal (1998), Horvath et al. (2003), Menke et al. (2003), Sherer et al. (2003), Gille et al. (2004), Shavali et al. (2004)	Shults and Schapira (2001), Parkinson Study Group et al. (2014)		Indirect
		Idebenone	Avci et al. (2021), He et al. (2021)		NCT03727295; NCT04152655	Indirect (induces a-Syn degradation)
Nrf2	Supplementation	Sulforaphane	Uddin et al. (2020)		NCT05084365	Indirect
Several pathways involved in oxidative stress	Inhibits pro-oxidative mechanism and enhances anti-oxidative systems	Melatonin	Li and Pelletier (1995), Gilad et al. (1998), Crespo et al. (1999), Reiter et al. (2002a,b, 2003, 2005), Dong et al. (2003), Lopez-Burillo et al. (2003), Rodriguez et al. (2004, 2007), Deng et al. (2006), Lopez et al. (2006), Winiarska et al. (2006), Sudnikovich et al. (2007)	Kunz and Bes (1999), Boeve et al. (2001), Kunz et al. (2004)	NCT02768077; NCT03258294; NCT02789592; NCT02359448; NCT04287543	Indirect

currently used to treat Freidrich's ataxia and AD (Orsucci et al., 2011; Montenegro et al., 2018). Two clinical trials assessing the efficacy and safety of idebenone in PD are currently ongoing (Clinical trial identifier: NCT03727295; NCT04152655) and results obtained on PD models are encouraging (Table 3). Indeed, idebenone improved motor coordination and locomotor activity while decreasing TH-positive neurons damage, lipid peroxidation, ferroptosis and other OS markers in rotenone-induced PD models (Avci et al., 2021). Moreover, idebenone activated autophagy and promoted α-Syn degradation by suppressing the AKT/mTOR pathway in SH-SY5Y overexpressing the A53T mutant form of α-Syn (He et al., 2021). This mechanism appears unusual for this compound, but recently idebenone has been demonstrated to act as cytoprotective molecule activating fundamental pathways rather than by functioning as a direct antioxidant agent (Gueven et al., 2021; He et al., 2021).

A new interesting agent for OS modulation is sulforaphane, a phytocompound belonging to the isothiocyanate family and owning lipophilic nature and a molecular size that makes it highly bioavailable (Schepici et al., 2020; Uddin et al., 2020). Its molecular target is nuclear factor erythroid 2 related factor 2 (Nrf2), which is a crucial controller of enzymes involved in antioxidation and detoxification of xenobiotics (Eggler et al., 2008; Zhang et al., 2013; Stefanson and Bakovic, 2014; Sajja et al., 2017). *In vitro* studies on cellular models of PD treated with sulforaphane showed reduced OS, cell damage and death (Uddin et al., 2020; Table 3). In line with the *in vitro* studies, *in vivo* experiments demonstrated that in C57BL/6 mice sulforaphane administration improved motor deficits and counteracted nigrostriatal dopaminergic neurons degeneration and apoptosis attenuating OS and neuroinflammation (Uddin et al., 2020). A phase II clinical trial is currently ongoing to evaluate the efficacy and safety of sulforaphane in PD patients (Clinical trial identifier: NCT05084365).

An interesting molecule to counteract OS is melatonin, a hormone produced endogenously by pineal gland and other tissues. It regulates circadian cycle and also plays a relevant role in neuroprotection, anti-inflammation and anti-oxidation. For all these reasons, it has been considered as a candidate for PD therapy (Table 3). Melatonin is an indoleamine and it can yield electron easily, hence it is a potent reducer agent. It acts as a scavenger for oxygen-and nitrogen-based reactive molecules (Reiter et al., 2002a,b, 2003; Lopez-Burillo et al., 2003; Sudnikovich et al., 2007) and it works as an inhibitor of inducible NO synthase (iNOS; Gilad et al., 1998; Crespo et al., 1999; Dong et al., 2003; Rodriguez et al., 2004, 2007; Lopez et al., 2006). The ability to interact with iNOS and peroxinitrite is the one that makes melatonin a special candidate for the treatment of OS as none of the previous mentioned antioxidant is able to exert this action. It has been demonstrated that melatonin also helps antioxidant enzymes, including SOD and GPx, stimulating the production of GSH (Rodriguez et al., 2004; Reiter et al., 2005; Winiarska et al., 2006). In addition, melatonin has been found to inhibit cyclooxygenase-2 reducing the severity of inflammation (Deng et al., 2006). In particular, it ameliorates inflammation blocking tumor necrosis factor-α (TNF-α; Li and Pelletier, 1995; Reiter et al., 2003) and it impacts on mitochondrial respiration, protecting both proteins of electron transport chain and mitochondrial DNA from oxidative damage (Reiter et al., 2008). Interestingly, melatonin has been found to reduce α-Syn secretion in rat adipose-derived mesenchymal stem cells (Ibrahim et al., 2022). Several phase II and III clinical trials are evaluating the effect of melatonin on sleep disturbances in PD patients (Clinical trial identifiers: NCT02768077; NCT03258294; NCT02789592; NCT02359448; NCT04287543; Table 3). Interestingly, trial NCT04287543 aimed at following the activity of mitochondrial complex I, the levels of MDA and 4-hydroxyalkene and the production of NO among the secondary outcome measures, but it was withdrawn because of COVID-19 pandemic. Other studies on exogenous melatonin investigated the effect of the molecule on rapid eye movement (REM) sleep behavior disorder (RBD), which is a prodromal sign for PD. Among them, the study by Kunz et al. (2004) demonstrated that medical melatonin increased REM sleep percentage to normal levels in patients with reduced REM sleep duration and re-organized REM sleep episode length during night-time sleep. The effect lasted for several weeks after the discontinuation of the therapy. Other studies reported a resolution of clinical RBD symptoms lasting for up to 3 years after discontinuation of melatonin treatment (Kunz and Bes, 1999; Boeve et al., 2001; Kunz et al., 2004).

It is worth considering that unfortunately the limitations offered by OS targeting therapeutic strategies are challenging. Moreover, despite OS is common to several diseases, it rarely constitutes the primary cause of a disease, supporting that the use of an antioxidant may have mild impact on pathology progression. Moreover, *in vitro* and *in vivo* evidences demonstrated that endogenous antioxidants support the progression of different types of tumors (Singh et al., 2008; DeNicola et al., 2011; Sayin et al., 2014; George and Abrahamse, 2020; Harris and DeNicola, 2020). This effect is even greater in older people, where the activation of Nrf2 pathway, which usually is chemopreventing, can be deleterious and it could predispose for tumor progression (Forman and Zhang, 2021). Still, all classical antioxidants, excluding melatonin, are potential electron donors and they exhibit both reduced and oxidized forms. In general, these oxidized molecules should be regenerated to the reduce form through a process of recycling that consumes GSH to be exploited or through a redox reaction that, eventually, oxidizes other molecules. This means that the classical antioxidant may act as prooxidant molecules, causing other damages. However, the toxic concentrations of most of these prooxidant regenerated compounds are extremely high and their toxic potential appears negligible.

Another issue is related to the discrepancy that exists in the ratio of *in vitro* vs. *in vivo* exogenous agents. In general, in *in vitro* studies free radicals are produced at much greater rates than what would be observed in real physiological or pathological conditions (Forman et al., 2014). In addition, antioxidant defenses may not be able to reach effective concentrations *in vivo*. Therefore, it is hard to think that antioxidant approaches may significantly impact on PD progression though we cannot exclude that they may contribute in reducing α-Syn nitration.

6. Acetylation

Protein acetylation is one of the major PTM found in eukaryotes, in which the acetyl group from acetyl coenzyme A is transferred to a specific site on a polypeptide chain. Acetylation is mostly known for the role on gene transcription regulation, indeed through the reversible accumulation of acetylation on the lysines (ac-lys) of the histones, the transcription is activated.

In humans, 80–90% of all proteins become co-translationally acetylated at their N-terminal (Nt) of the nascent polypeptide chains

(Arnesen, 2009; Aksnes et al., 2015) in an irreversible way. Nt-acetylation is a general mechanism for stabilizing α-helical structures in both proteins and peptides (Chakrabartty et al., 1993), and makes α-Syn resistant for amyloid aggregation enhancing both protein–protein and protein-membrane interaction (Bartels et al., 2014). Indeed, recent findings indicate that all the *in vivo* detectable α-Syn is post-translationally modified by an acetyl group attached to the amino group of the first N-terminal amino acid (Anderson et al., 2006; Bartels et al., 2011; Ohrfelt et al., 2011). This modification alters the charge and structure of α-Syn molecules affecting their interaction with lipid membranes, as well as their aggregation process (Bell et al., 2022a,b, 2023). It has been found that ac-lys impacts on α-Syn aggregation (Fauvet et al., 2012; Kang et al., 2012; Gruschus et al., 2013; Bu et al., 2017; de Oliveira et al., 2017) and that acetylated α-Syn and α-tubulin inhibit oligomers formation (Kazantsev and Kolchinsky, 2008). Interestingly, studies demonstrated that increases in histone acetylation are disease-dependently associated with PD progression (Park et al., 2016; Harrison et al., 2018; Toker et al., 2021) and histone-3 or-4 hyperacetylation is a key epigenetic change in dopaminergic neurons exposed to other PD-related neurotoxins. Conversely, the deacetylation of histones operated by histone deacetylase (HDAC) is implicated in the control of α-Syn toxicity. The activity of HDAC6 has been linked with PD pathogenesis (Lemos and Stefanova, 2020) and HDAC6 is highly expressed in LB in PD patients' brain sections, indicating that HDAC6 may play a key role in the clearance of those misfolded and aggregated protein (Kawaguchi et al., 2003; Du et al., 2010; Richter-Landsberg and Leyk, 2013). Indeed, HDAC6 decreased activity is an essential factor for impaired autophagic flux in PD pathophysiology (Wang et al., 2019). Several studies demonstrated that the inhibitors of HDAC worsen the motor abilities of mice and exacerbate cell death in primary neuron cells (Du et al., 2014), while other demonstrated that HDAC inhibitors restore axonal transport and motor behavior (Godena et al., 2014; Pinho et al., 2016), reduce ROS production, and alleviate dopaminergic neurotoxicity (Jian et al., 2017). Other studies demonstrated the protective effect of pan-HDAC inhibitors such as valproic acid, sodium butyrate, phenylbutyrate, suberoylanilide hydroxamic acid and trichostatin A in *in vitro* and *in vivo* models of PD acting through different mechanism listed in Table 4 (Gardian et al., 2004; Chen et al., 2007, 2012; Wu and Guo, 2008; Kidd and Schneider, 2010, 2011; Zhou et al., 2011, 2014; Rane et al., 2012; St Laurent et al., 2013; Harrison et al., 2015; Suo et al., 2015; Sharma et al., 2015a; Kim et al., 2019; Getachew et al., 2020; Hsu et al., 2020). The specific inhibitors of HDAC1, 2 and 3, RGFP109, K560, K-856, MS-275, MC-1568, and LMK235 also showed neuroprotection against α-Syn toxicity (Table 4; Johnston et al., 2013, Formisano et al., 2015, Choong et al., 2016, Hirata et al., 2018, Mazzocchi et al., 2021).

On this line, a recent phase I clinical trial investigated whether phenylbutyrate (Table 4) can increase the removal of α-Syn from the brain into the bloodstream (Clinical trial identifier: NCT02046434), but results are not available yet.

Sirtuins (SIRT) are nicotinamide adenine dinucleotide (NAD^+)-dependent HDAC, proteins implied in neurodegenerative disorders (Satoh and Imai, 2014). In mammals, there are seven members of the SIRT family: SIRT1-SIRT7. SIRT2 is the most abundant SIRT in the brain and its levels increase with aging (Maxwell et al., 2011). De Oliveira et al. (2017) recently described that SIRT2 interacts with and removes acetyl groups from α-Syn. They also demonstrated both *in vitro* and *in vivo* that the inhibition of SIRT2 decreased α-Syn toxicity (Outeiro et al., 2007; de Oliveira et al., 2017).

On the other hand, SIRT1 increases lifespan in mammals (Cohen et al., 2004), promotes mitochondrial biogenesis (Wenz, 2013), protects against neurodegeneration (Kim et al., 2007) and mitigates α-Syn pathology through the induction of the chaperone heat shock protein 70, which prevents the misfolding or clear the aggregates by degradation (Donmez et al., 2012). By reducing signs of aging, the SIRT1-activating drugs, such as resveratrol may have a role in the counteract of neurodegenerative diseases (Barger et al., 2008; Pearson et al., 2008). Indeed, resveratrol and its derivatives are able to alleviate motor and cognitive deficits and neuropathology in different mouse model of PD (Table 4; Guo et al., 2016, Zhang et al., 2018) and to reduce α-Syn toxicity and OS in *in vitro* models of the pathology (Albani et al., 2009; Arbo et al., 2020; Chau et al., 2021). Interestingly, though the bioavailability and brain penetration of resveratrol are problematic, some modified forms of this molecule have been developed to overcome these issues (Intagliata et al., 2019) and it has been demonstrated that one of the more bioavailable forms of resveratrol acts as a protein aggregation suppressor *in vitro* and *in vivo* (Mehringer et al., 2022).

The upstream regulation of SIRT through a replenishment of NAD within the brain has been attempted through the nicotinamide riboside supplementation. Brakedal et al. (2022) summarized the double-blinded, randomized, placebo-controlled phase I study of nicotinamide riboside in which they demonstrated a mild improvement in motor ability and a neuroprotective effect that was previously shown in murine, *Drosophila melanogaster* and induced pluripotent stem cells-based experimental models of noise induced hearing loss, amyotrophic lateral sclerosis, depression and PD (Table 4; Brown et al., 2014, Sorrentino et al., 2017, Schondorf et al., 2018, Han et al., 2020, Harlan et al., 2020, Xie et al., 2020). Nicotinamide riboside may target multiple processes implicated in the pathophysiology of the disease by upregulating the expression of genes involved in mitochondrial respiration, oxidative damage response, lysosomal and proteasomal function as well as by downregulating inflammatory cytokines in the central nervous system (Canto et al., 2012; Gong et al., 2013; Mehmel et al., 2020; Brakedal et al., 2022). In addition, it is possible that nicotinamide riboside may mitigate epigenomic dysregulation in PD by regulating histone acetylation. Increasing neuronal NAD levels would boost the activity of the NAD-dependent histone deacetylases of the SIRT family, potentially ameliorating histone hyperacetylation in PD.

7. O-GlcNAcylation

O-linked N-acetylglucosamine (O-GlcNAc) is a form of protein glycosylation in which N-acetylglucosamine (GlcNAc) residues are O-linked to ser and threonine (thr) hydroxyl groups of proteins (Butkinaree et al., 2010). The enzymes which control the levels of GlcNAc are O-GlcNAc transferase (OGT) which attaches O-GlcNAc and O-GlcNAcase (OGA), which instead removes the O-GlcNAc (Bond and Hanover, 2013).

O-GlcNAcylation reduces the aggregation propensity and the toxicity of amyloidogenic proteins including and α-Syn (Marotta et al., 2015; Levine et al., 2017; Lewis et al., 2017). α-Syn has several O-GlcNAcylation sites (Cole and Hart, 2001), especially located in the

TABLE 4 HDAC-modulators tested in preclinical models of PD and in clinical trials.

Target	Mechanism of action	Molecule name	Results from studies in preclinical models	Results from clinical trials	Ongoing clinical trials	Direct or indirect effect on α-Syn Acetylation
HDAC	Inhibition	Valproic acid	Chen et al. (2007), Wu and Guo (2008), Kidd and Schneider, (2011), Harrison et al. (2015); Kim et al. (2019), Hsu et al. (2020)			Indirect (JNK Pathway)
		Sodium butyrate	Rane et al. (2012), St Laurent et al. (2013), Sharma et al. (2015a), Getachew et al. (2020)			Indirect (activates autophagy)
		Phenylbutyrate	Gardian et al. (2004), Zhou et al. (2011)		NCT02046434	Indirect
		Suberoylanilide hydroxamic acid	Chen et al. (2012)			Indirect
		Trichostatin A	Zhou et al. (2014), Suo et al. (2015)			Indirect
HDAC1, 2 and 3	Inhibition	RGFP109	Johnston et al. (2013)			Indirect
		K560, K-856	Choong et al. (2016), Hirata et al. (2018)			Indirect
		MS-275, MC-1568	Formisano et al. (2015)			Indirect
		LMK235	Mazzocchi et al. (2021)			Indirect
SIRT1	Activation	Resveratrol	Albani et al. (2009), Guo et al. (2016), Zhang et al. (2018), Chau et al., 2021; Arbo et al. (2020), Mehringer et al. (2022)			Indirect
	Activation	Nicotinamide riboside	Schondorf et al. (2018)	Brakedal et al. (2022)		Indirect

NAC region of the protein (Marotta et al., 2015; Levine et al., 2017, 2019; Lewis et al., 2017). The O-GlcNAcylation at thr72 of α-Syn decreases aggregation propensity and toxicity in cultured cells (Marotta et al., 2015). Moreover, O-GlcNAcylation hampers the cleavage of α-Syn by calpain (Levine et al., 2017), a process involved in the formation of aggregates, and is implicated in the modulation of endocytic and autophagic pathways (Dufty et al., 2007). In addition, it has been demonstrated that pharmacological inhibition or the knockdown of OGA hampers α-Syn pre-formed fibrils internalization (Tavassoly et al., 2021).

Selective inhibitors of OGA are of interest for their potential to reduce the aggregation of the amyloidogenic proteins within brain (Selnick et al., 2019). In this context, thiamet G, a brain permeable molecule, has been shown to increase cerebral O-GlcNAc levels to hamper neurodegeneration and reduce phosphorylation and aggregation of tau (Liu et al., 2004a; Yuzwa et al., 2008; Gong et al., 2012). Moreover, thiamet G improves behavioral features in preclinical models of tauopathies (Yuzwa et al., 2008, 2012, 2014a,b; Yu et al., 2012; Borghgraef et al., 2013; Graham et al., 2014; Hastings et al., 2017). A novel, highly potent and selective OGA inhibitor, MK-8719, has been developed and showing promising results in *in vitro* and *in vivo* tauopathies model. The OGA inhibitor ASN120290, that has been recently assigned the Orphan Drug Designation for the treatment of progressive supranuclear palsy (PSP) by the Food and Drug Administration has granted to ASN120290 reduced neurofibrillary tangles in mouse model of tauopathy. Permanne et al. (2022) demonstrated that the administration of ASN120290 enhance α-Syn O-GlcNAcylation and slows the progression of motor impairment in a α-Syn tg mouse model of PD (Table 5). In June 2021, a phase I first-in-human trial assessing the diffusion of ASN121151 to the CNS and the safety and pharmacokinetic profile in elderly healthy and AD subjects has been started (Clinical trial identifier: NCT04759365). Furthermore, a multiple ascending doses PET study is currently ongoing to investigate the brain occupancy of OGA and the pharmacodynamic response in peripheral blood mononuclear cells after repeated doses of ASN121151 to healthy subjects (Clinical trial identifier: NCT05725005; Table 5).

8. Glycation

In the context of sugar-based modifications we can find glycation. Glycation is a non-enzymatic reaction that proceeds under hyperglycemia and during aging. Through the Maillard reaction the reduced carbohydrates and amino compounds form the intermediate Amadori products which in turn break down, thus creating a variety of different carbonyl and dicarbonyl intermediate products, including glyoxal and methylglyoxal (MGO) that are able to bound to the proteins (Hodge, 1955). Lastly, higher molecular weight species or advanced glycation end products (AGEs) can be formed from these lower molecular weight species (Henning and Glomb, 2016). These reactions are generally rather slow and their end products are very stable (Henning and Glomb, 2016). Therefore, short lived proteins are usually not involved in this process, however long-lived proteins, such as α-Syn can be modified in AGEs (Ahmed, 2005; Vicente Miranda and Outeiro, 2010). AGEs colocalize with α-Syn in LB in the SN (Munch et al., 2000) and glycated α-Syn has been identified in brain tissue from PD patients (Vicente Miranda et al., 2017b). MGO reacts

TABLE 5 Inhibitors of OGA tested in preclinical models of PD or in clinical trials.

Target	Mechanism of action	Molecule name	Results from studies in preclinical models	Results from clinical trials	Ongoing clinical trials	Direct or indirect effect on α-Syn O-GlcNAcylation
O-GlcNAcase	Inhibition	ASN120290	Permanne et al. (2022)			Direct
		ASN121151			NCT04759365; NCT05725005	Direct

with α-Syn to form oligomers, increasing the toxicity (Vicente Miranda et al., 2017b). In addition, diabetes is associated with the accumulation of AGEs (Kopytek et al., 2020) and patients with type 2 diabetes mellitus experience an increased risk to develop PD (Yang et al., 2017; Vaccari et al., 2021), indicating a possible insulin-modulating role in this latter condition. Both diabetes and PD are characterized by altered homeostasis of sugar metabolism (Dunn et al., 2014; Shamsaldeen et al., 2016; Trezzi et al., 2017). Interestingly, antidiabetic drugs have been suggested to exert a neuroprotective role both in PD models and in patients (Konig et al., 2018; Iravanpour et al., 2021). For instance, insulin modulates α-Syn expression and aggregation (Sharma et al., 2015b,c), regulates vesicular monoamine transporter 2 (VMAT2; Kong et al., 2020) and intranasal administration of insulin ameliorated mitochondrial function, motor impairment and dopaminergic neuron death in a rat model of PD (Iravanpour et al., 2021).

Glucagon-like peptide-1 (GLP1) is secreted in response to ingestion and absorption, preferably of carbohydrates and fats (Drucker and Nauck, 2006; Wu et al., 2015; Nauck and Meier, 2018). The binding of GLP1 to its receptor (GLP1R) induces the glucose-dependent pancreatic insulin secretion (Flock et al., 2007; Holst, 2007). It has been demonstrated that agonists (GLP1RA) such as exendin-4 (Ex-4) can regulate several functions related to neurodegeneration, OS and neurogenesis (Kim et al., 2017). Consistently, Ex-4 and derivatives showed beneficial effects in PD animal models (Bertilsson et al., 2008, Rampersaud et al., 2012, Liu et al., 2015, Palleria et al., 2017, Chen et al., 2018, Elbassuoni and Ahmed, 2019, Zhang et al., 2021; Table 6). Indeed, it has been demonstrated that GLP1RA ameliorates MPTP-induced neurotoxicity acting on mitophagy flux, OS and α-Syn aggregation in both the MPTP-mouse model of PD (Lin et al., 2021) and in α-Syn transgenic mice (Yun et al., 2018).

Phase II clinical trials assessing the effect of 12 or 24 months treatments with exenatide, a synthetic Ex-4 derivative, showed cognitive and motor benefits which persisted for 12 months after drug washout in moderate PD patients (Aviles-Olmos et al., 2013, 2014; Table 6). In a next randomized, placebo-controlled, double-blind trial the authors analyzed the improvements of exenatide treated PD patients regarding motor abilities (Athauda et al., 2017), mood and cognition (Athauda et al., 2018). A *post hoc* analysis showed that younger patients with lower MDS-UPDRS-2 scores and tremor-dominant phenotype had the best response to exenatide (Athauda et al., 2019b). Moreover, there was a positive trend in obese patients or those with insulin resistance (Athauda et al., 2019a). Several other trials are evaluating other GLP1RA such as liraglutide, semaglutide or lixisenatide (Clinical trial identifier: NCT02953665; NCT03659682; NCT03439943; Table 6).

Dipeptidyl peptidase 4 (DDP4) inhibitors such as Vildaglitpin, Saxagliptin, Linaglitptin and Sitaglitpin have also been tested in animals as blockers of peripheral GLP1 degradation (Abdelsalam and Safar, 2015; Nassar et al., 2015; Kabel et al., 2018). In humans DDP4 inhibitors administration showed decrease in PD incidence (Svenningsson et al., 2016; Brauer et al., 2020) and beneficial effect in diabetic PD patients (Jeong et al., 2021; Table 6).

The most common treatment for type 2 diabetes, metformin, showed promising results in MPTP animal models (Katila et al., 2017; Table 6). Moreover, it reduced mitochondrial respiration dysfunction, activating AMP-activated protein kinase (AMPK), which has pro-survival functions and increases α-Syn clearance in animal models of PD (Parekh et al., 2022). Recently, it has been demonstrated that metformin is able to control microglial and astrocyte activation, eventually leading to neuroprotection and controlling dyskinesia development (Ryu et al., 2020). So far, metformin treatments in humans gave rise to conflicting results (Wahlqvist et al., 2012; Ping et al., 2020).

Mitoglitazone, an antidiabetic molecule which was found to protect against MPTP toxicity in cells, rodents and nematodes, reduced the incidence of PD in diabetic patients (Brauer et al., 2015, 2020; Table 6) exerting a better effect when compared to metformin (Brakedal et al., 2017).

Furthermore, high doses of thiamine improved motor function in PD patients by acting on AGE levels (Karachalias et al., 2010; Costantini et al., 2013, 2015; Table 6).

Other molecules showed promising results in preclinical models such as, MGO-scavengers tenilsetam and aminoguanidine that reduced α-Syn aggregation while improving its clearance and motor behavior in a PD models (Vicente Miranda et al., 2017b; Table 6). Telmisartan an anti-hypertension molecule, which was shown to reduce AGEs levels in rodents, demonstrated a protective role in MPTP models (Sato et al., 2014; Table 6).

9. SUMOylation

The covalent addition of a small ubiquitin like modifiers (SUMO) is one of the PTM which characterizes α-Syn. SUMO is a 12 kDa protein attached covalently to the lys-residues of a protein and it is essential for normal cellular processes including cell cycle regulation, nuclear-cytosolic transport, gene transcription, protein stability, response to stress, apoptosis and many others functions (Matunis et al., 1996; Hershko and Ciechanover, 1998).

SUMOylation is mediated by a three-step reaction that involves SUMO activating enzyme (SAE1), Ubc9 conjugating enzyme and SUMO-E3 ligase (Muller et al., 2001; Wilkinson and Henley, 2010).

TABLE 6 Glycation-modifying agents tested in preclinical models of PD and in clinical trials.

Target	Mechanism of action	Molecule name	Results from studies in preclinical models	Results from clinical trials	Ongoing clinical trials	Direct or indirect effect on α-Syn Glycation
Glucagon-like peptide-1 receptor	Activation	Exendin-4	Bertilsson et al. (2008), Rampersaud et al. (2012), Liu et al. (2015), Palleria et al. (2017), Chen et al. (2018), Elbassuoni and Ahmed (2019), Zhang et al. (2021)			Indirect
	Activation	Exenatide		Aviles-Olmos et al. (2013, 2014), Athauda et al. (2017, 2018, 2019a,b)		Indirect
	Activation	Liraglutide			NCT02953665	Indirect
	Activation	Semaglutide			NCT03659682	Indirect
	Activation	Lixisenatide			NCT03439943	Indirect
DDP4	Inhibition	Vildaglitpin, Saxagliptin, Linaglitptin and Sitaglitpin	Abdelsalam and Safar (2015), Nassar et al. (2015), Kabel et al. (2018)	Svenningsson et al. (2016), Brauer et al. (2020), Jeong et al. (2021)		Indirect
Glucagon	Inhibition	Metformin	Katila et al. (2017), Parekh et al. (2022), Ryu et al. (2020)	Wahlqvist et al. (2012), Ping et al. (2020)		Indirect
		Mitoglitazone		Brauer et al. (2015, 2020), Brakedal et al. (2017)		Indirect
Advanced glycation end products levels	Reducing	Thiamine		Costantini et al. (2013, 2015), Karachalias et al. (2010)		Indirect
Methylglyoxal	Scavenging	Tenilsetam and aminoguanidine	Vicente Miranda et al. (2017a,b)			Indirect
Advanced glycation end products levels	Reducing	Telmisartan	Sato et al. (2014)			Indirect

10.3389/fnmol.2023.1197853

SUMO peptides can be recycled through a process of deSUMOylation by the SUMO proteases from the Ulp/SENP family.

SUMOylation machinery and protein SUMOylation dramatically increase in response to cellular stresses, and so in PD (Zhou et al., 2004; Enserink, 2015). Furthermore, rotenone-injected mice exhibit increased α-Syn and SUMO levels (Weetman et al., 2013). SUMOylation participates in several pathways connected to PD such as regulation of DJ-1 activity, modulation of transcription factors involved in mitochondrial and lysosomal biogenesis, and regulation of mitochondrial fission machinery (Harder et al., 2004; Ariga et al., 2013; Savyon and Engelender, 2020).

SUMO has been shown to enhance the solubility of aggregation-prone proteins like α-Syn, and impaired SUMOylation increased α-Syn aggregation and toxicity in HEK293 cells and a PD rat models (Krumova et al., 2011). On the other hand, SUMOylation competes with ubiquitination on the same lys residue, protecting the protein from degradation (Rott et al., 2017; Rousseaux et al., 2018). The discrepancies seen on α-Syn aggregation may be related to the different SUMO isoforms and SUMO-ligases that may be involved in the processes (Tatham et al., 2001; Bohren et al., 2004; Wilkinson and Henley, 2010).

The only tested molecule for the interference with E1-SUMO complex formation in PD like model, is ginkgolic acid (Fukuda et al., 2009; Table 7), which decreases the levels of SUMOylation stimulating the macroautophagic clearance of α-Syn aggregates (Vijayakumaran et al., 2019).

So far, SUMOylation targeting has been achieved especially in oncology, indeed spectomycin B1 had been proposed as therapeutic agent to cure breast cancer through the blocking of SUMOylation preventing the formation of the Ubc9-SUMO (Hirohama et al., 2013). In addition, the potent SAE inhibitor ML-792 impairs SUMO conjugation but also induces significant loss of viability in multiple cancer cell lines (He et al., 2017). On the other hand, global cellular SUMOylation is enhanced in response to interferons (Maroui et al., 2018).

10. Ubiquitination

The ubiquitin–proteasome system (UPS) mediates the degradation of proteins in mammalian cells (Ross and Pickart, 2004). The addition of multiple molecules of ubiquitin, a conserved 8.5-kDa polypeptide, constitute the signal for proteasome-mediated degradation. Ubiquitin–substrate ligation is mediated by different enzymatic steps which are mainly mediated by E3 ligases. These latter recognize specific substrate-based signals in a manner that is frequently regulated by covalent modification (Weissman, 2001), in which the first ubiquitin is covalently joined to proteins through an isopeptide bond between the C-terminus of ubiquitin and a lys residue, and must be proteolytically processed by ubiquitin C-terminal hydrolases (UCHs) before it can acquire activity (Weissman, 2001). Additional ubiquitins are then linked to the first one to form a polyubiquitin chain that is a potent attractive signal for the regulatory complex of the proteasome. The UPS is vitally important for protecting cells against the toxic effects of misfolded proteins (Engelender et al., 2022). The 26S proteasome consists of more than 60 subunits. It is composed by: (1) a central, barrel-shaped catalytic (20S) complex carrying multiple active sites, which are sequestered in an interior chamber that is only accessible through a narrow axial pore; (2) two distally positioned regulatory (19S) complexes which unfold the substrate polypeptide chain and translocate it through this pore and into the active-site chamber, using integral chaperone subunits placed immediately adjacent to the axial pore of the 20S complex (Ross and Pickart, 2004). Of note, studies in the post-mortem brains of sporadic PD patients showed that LB contain ubiquitinated α-Syn that is not associated with UPS impairment (Tofaris et al., 2003). However, even non-ubiquitinated α-Syn appears to be degraded by the 20S proteasome (Tofaris et al., 2001), supporting the occurrence of ubiquitin-independent mechanism of UPS-mediated α-Syn degradation in synucleinopathies.

Studies in cell models or purified systems led to conflicting results either supporting that both 20S and 26S proteasomes degrade α-Syn or failing to detect α-Syn accumulation upon UPS inhibition (Bennett et al., 1999; Tofaris et al., 2001, 2011; Webb et al., 2003; Emmanouilidou et al., 2010; Shabek et al., 2012) hinting that the UPS may play a relevant role in degrading a fraction of α-Syn, whose relative abundance may vary between cell types and experimental conditions (Stefanis et al., 2019).

Promoting the activity of the UPS can thus be considered as a possible therapeutic strategy for combating α-Syn accumulation (Engelender et al., 2022; Table 8). For instance, following evidence that p38 mitogen-activated protein kinase (MAPK) negatively regulates proteasome activity, the p38 MAPK inhibitor PD169316 has been identified as a proteasome activator that decreases α-Syn toxicity in cells (Braun et al., 2021; Engelender et al., 2022). Several p38 MAPK inhibitors tested in clinical trials for chronic inflammatory diseases and cancer may also be considered as possible UPS stimulators, though their neuroprotective effects may not be solely ascribed to UPS induction. Indeed, studies in experimental models of synucleinopathies and of other neurodegenerative diseases such as AD have shown that p38 MAPK plays a relevant role in mediating other key processes involved in neurodegeneration, neuroinflammation and disease protein-mediated brain damage (Giovannini et al., 2002, 2008; Cuenda and Rousseau, 2007).

Alternatively, compounds that work as gate-openers of the 20S proteasome by preventing the barrel closing may also promote α-Syn clearing (Forster and Hill, 2003; Jones et al., 2017). For instance, chlorpromazine and some derivatives devoid of dopamine receptors D2 binding were shown to promote the degradation of α-Syn by interacting with the 20S subunits and preventing its closure (Jones et al., 2017).

Another strategy to increase proteasomal activity is to modulate the phosphorylation status of its subunits that are influenced by several protein kinases (Kors et al., 2019). In particular, cAMP-dependent protein kinase A (PKA) phosphorylates the 19S subunits Rpt6 and Rpn6, leading to activation of 20S proteolytic activities in a

TABLE 7 SUMOylation inhibitors tested in preclinical models of PD.

Target	Mechanism of action	Molecule name	Results from studies in preclinical models	Direct or indirect effect on α-Syn SUMOylation
E1-SUMO complex	Inhibition	Ginkgolik acid	Fukuda et al. (2009)	Direct

TABLE 8 UPS modulators tested in preclinical models of PD.

Target	Mechanism of action	Molecule name	Results from studies in preclinical models	Direct or indirect on ubiquitinated or non-ubiquitinated α-Syn
p38 MAPK	Inhibition	PD169316	Braun et al. (2021)	Indirect
PKA	Activation	forskolin and analogues	Sanders and Rajagopal (2020)	Indirect
Phosphodiesterases	Inhibition	rolipram, cilostazol, vinpocetine and others	Prickaerts et al. (2017)	Indirect
20S proteasome subunit	Gate opening	chlorpromazine and some derivatives	Forster and Hill (2003), Jones et al. (2017)	Indirect
α-Syn + proteasome	α-Syn targeting to proteasome	β-synuclein-based TAT + proteasome degron petptide	Jin et al. (2021)	Direct
α-Syn	α-Syn ubiquitination and targeting to proteasome	PROTAC	Kargbo (2020)	Direct

process that may involve changes in proteasomal conformation (Zhang et al., 2007; Lokireddy et al., 2015). Despite the benefits of PKA activators, no positive outcome on improving cognition has been observed in clinical trials with forskolin analogs (Sanders and Rajagopal, 2020). On the other hand, several clinical trials assessing the efficacy of phosphodiesterase inhibitors are currently under way, including rolipram, cilostazol and vinpocetine (Prickaerts et al., 2017) and may hold promise for treating synucleinopathies.

A more recent approach to promote the proteasomal degradation of disease proteins is cell-penetrating peptides that specifically interact with the target protein and the proteasome. One promising peptide consists of a portion of β-synuclein peptide that interacts with α-Syn, which was fused to the cell-penetrating peptide TAT and a proteasomal degron and significantly decreased the neuronal levels of α-Syn via proteasome as well as neurotoxicity in mice (Jin et al., 2021).

Finally, the proteasomal degradation of disease proteins can also be improved Proteolysis Targeting Chimeric (PROTAC) compounds (Sakamoto et al., 2001). The technology relies on the fusion of a ligand for the target protein to a ligand for an E3 ubiquitin-ligase, such as cereblon and Van Hippel-Landau (VHL; Au et al., 2020). α-Syn-targeting PROTAC are currently in preclinical development (Kargbo, 2020).

11. Discussion

The evidence summarized in this review highlights the relevance of α-Syn PTMs in PD pathophysiology. In the last few years, α-Syn PTMs have been investigated as biomarker for the diagnosis and progression of PD and other synucleinopathies. Moreover, studies supporting that PTMs control structural changes in α-Syn thus influencing its aggregation propensity, have blossomed great interest for the development of innovative therapeutic strategies, that by modulating α-Syn PTM, could reduce its pathological aggregation or spreading. Interestingly, some novel therapeutic strategies modulating α-Syn PTMs are already under investigation in clinical trials. This notwithstanding, further studies are warranted to better clarify the role of PTMs on α-Syn pathophysiology, to confirm the translational potential of PTMs-modifying drugs in synucleinopathies as well as to disclose whether the evaluation of α-Syn PTMs in peripheral tissues can be a valuable readout to monitor the effect of such approaches.

Author contributions

FL, GF, VB, and AB conceived the manuscript. VB and AB collected references, wrote the main text, and prepared illustrations and tables. AB revised manuscript text and tables. All authors contributed to the article and approved the submitted version.

Funding

We are grateful to the Michael J. Fox Foundation for Parkinson's Research, NY, USA (grant ID: MJFF-021179), the Multiple system atrophy coalition, USA, and the MIUR PRIN 2017-1065.

Conflict of interest

The authors declare that the research was conducted in the absence of any commercial or financial relationships that could be construed as a potential conflict of interest.

Publisher's note

References

Abbott, R. D., Ross, G. W., Petrovitch, H., Tanner, C. M., Davis, D. G., Masaki, K. H., et al. (2007). Bowel movement frequency in late-life and incidental Lewy bodies. *Mov. Disord.* 22, 1581–1586. doi: 10.1002/mds.21560

Abd-Elhadi, S., Honig, A., Simhi-Haham, D., Schechter, M., Linetsky, E., Ben-Hur, T., et al. (2015). Total and proteinase K-resistant alpha-synuclein levels in erythrocytes, determined by their ability to bind phospholipids, associate with Parkinson's disease. *Sci. Rep.* 5:11120. doi: 10.1038/srep11120

Abd Elhadi, S., Grigoletto, J., Poli, M., Arosio, P., Arkadir, D., and Sharon, R. (2019). Alpha-synuclein in blood cells differentiates Parkinson's disease from healthy controls. *Ann. Clin. Transl. Neurol.* 6, 2426–2436. doi: 10.1002/acn3.50944

Abdelsalam, R. M., and Safar, M. M. (2015). Neuroprotective effects of vildagliptin in rat rotenone Parkinson's disease model: role of RAGE-NFkappaB and Nrf2-antioxidant signaling pathways. *J. Neurochem.* 133, 700–707. doi: 10.1111/jnc.13087

Abou-Sleiman, P. M., Muqit, M. M., and Wood, N. W. (2006). Expanding insights of mitochondrial dysfunction in Parkinson's disease. *Nat. Rev. Neurosci.* 7, 207–219. doi: 10.1038/nrn1868

Ahmed, N. (2005). Advanced glycation endproducts--role in pathology of diabetic complications. *Diabetes Res. Clin. Pract.* 67, 3–21. doi: 10.1016/j.diabres.2004.09.004

Ahn, B. H., Rhim, H., Kim, S. Y., Sung, Y. M., Lee, M. Y., Choi, J. Y., et al. (2002). Alpha-synuclein interacts with phospholipase D isozymes and inhibits pervanadate-induced phospholipase D activation in human embryonic kidney-293 cells. *J. Biol. Chem.* 277, 12334–12342. doi: 10.1074/jbc.M110414200

Aksnes, H., Hole, K., and Arnesen, T. (2015). Molecular, cellular, and physiological significance of N-terminal acetylation. *Int. Rev. Cell Mol. Biol.* 316, 267–305. doi: 10.1016/bs.ircmb.2015.01.001

Alam, Z. I., Jenner, A., Daniel, S. E., Lees, A. J., Cairns, N., Marsden, C. D., et al. (1997). Oxidative DNA damage in the parkinsonian brain: an apparent selective increase in 8-hydroxyguanine levels in substantia nigra. *J. Neurochem.* 69, 1196–1203. doi: 10.1046/j.1471-4159.1997.69031196.x

Albani, D., Polito, L., Batelli, S., De Mauro, S., Fracasso, C., Martelli, G., et al. (2009). The SIRT1 activator resveratrol protects SK-N-BE cells from oxidative stress and against toxicity caused by alpha-synuclein or amyloid-beta (1-42) peptide. *J. Neurochem.* 110, 1445–1456. doi: 10.1111/j.1471-4159.2009.06228.x

Alegre-Abarrategui, J., Ansorge, O., Esiri, M., and Wade-Martins, R. (2008). LRRK2 is a component of granular alpha-synuclein pathology in the brainstem of Parkinson's disease. *Neuropathol. Appl. Neurobiol.* 34, 272–283. doi: 10.1111/j.1365-2990.2007.00888.x

Anderson, J. P., Walker, D. E., Goldstein, J. M., De Laat, R., Banducci, K., Caccavello, R. J., et al. (2006). Phosphorylation of Ser-129 is the dominant pathological modification of alpha-synuclein in familial and sporadic Lewy body disease. *J. Biol. Chem.* 281, 29739–29752. doi: 10.1074/jbc.M600933200

Antelope, O., Vellore, N. A., Pomicter, A. D., Patel, A. B., Van Scoyk, A., Clair, P. M., et al. (2019). BCR-ABL1 tyrosine kinase inhibitor K0706 exhibits preclinical activity in Philadelphia chromosome-positive leukemia. *Exp. Hematol.* 77, 36–40.e2. doi: 10.1016/j.exphem.2019.08.007

Arawaka, S., Wada, M., Goto, S., Karube, H., Sakamoto, M., Ren, C. H., et al. (2006). The role of G-protein-coupled receptor kinase 5 in pathogenesis of sporadic Parkinson's disease. *J. Neurosci.* 26, 9227–9238. doi: 10.1523/JNEUROSCI.0341-06.2006

Arbo, B. D., Andre-Miral, C., Nasre-Nasser, R. G., Schimith, L. E., Santos, M. G., Costa-Silva, D., et al. (2020). Resveratrol derivatives as potential treatments for Alzheimer's and Parkinson's disease. *Front. Aging Neurosci.* 12:103. doi: 10.3389/fnagi.2020.00103

Ariga, H., Takahashi-Niki, K., Kato, I., Maita, H., Niki, T., and Iguchi-Ariga, S. M. (2013). Neuroprotective function of DJ-1 in Parkinson's disease. *Oxidative Med. Cell. Longev.* 2013:683920. doi: 10.1155/2013/683920

Arnesen, T. (2009). Protein N-terminal acetylation: NAT 2007-2008 Symposia. *BMC Proc.* 3:S1. doi: 10.1186/1753-6561-3-S6-S1

Athauda, D., Gulyani, S., Karnati, H. K., Li, Y., Tweedie, D., Mustapic, M., et al. (2019a). Utility of neuronal-derived exosomes to examine molecular mechanisms that affect motor function in patients with Parkinson disease: a secondary analysis of the exenatide-PD trial. *JAMA Neurol.* 76, 420–429. doi: 10.1001/jamaneurol.2018.4304

Athauda, D., Maclagan, K., Budnik, N., Zampedri, L., Hibbert, S., Aviles-Olmos, I., et al. (2019b). Post hoc analysis of the exenatide-PD trial-factors that predict response. *Eur. J. Neurosci.* 49, 410–421. doi: 10.1111/ejn.14096

Athauda, D., Maclagan, K., Budnik, N., Zampedri, L., Hibbert, S., Skene, S. S., et al. (2018). What effects might exenatide have on non-motor symptoms in Parkinson's disease: a post hoc analysis. *J. Parkinsons Dis.* 8, 247–258. doi: 10.3233/JPD-181329

Athauda, D., Maclagan, K., Skene, S. S., Bajwa-Joseph, M., Letchford, D., Chowdhury, K., et al. (2017). Exenatide once weekly versus placebo in Parkinson's disease: a randomised, double-blind, placebo-controlled trial. *Lancet* 390, 1664–1675. doi: 10.1016/S0140-6736(17)31585-4

Au, Y. Z., Wang, T., Sigua, L. H., and Qi, J. (2020). Peptide-based PROTAC: the predator of pathological proteins. *Cell Chem. Biol.* 27, 637–639. doi: 10.1016/j.chembiol.2020.06.002

Avci, B., Gunaydin, C., Guvenc, T., Yavuz, C. K., Kuruca, N., and Bilge, S. S. (2021). Idebenone ameliorates rotenone-induced Parkinson's disease in rats through decreasing lipid peroxidation. *Neurochem. Res.* 46, 513–522. doi: 10.1007/s11064-020-03186-w

Aviles-Olmos, I., Dickson, J., Kefalopoulou, Z., Djamshidian, A., Ell, P., Soderlund, T., et al. (2013). Exenatide and the treatment of patients with Parkinson's disease. *J. Clin. Invest.* 123, 2730–2736. doi: 10.1172/JCI68295

Aviles-Olmos, I., Dickson, J., Kefalopoulou, Z., Djamshidian, A., Kahan, J., Ell, P., et al. (2014). Motor and cognitive advantages persist 12 months after exenatide exposure in Parkinson's disease. *J. Parkinsons Dis.* 4, 337–344. doi: 10.3233/JPD-140364

Baba, M., Nakajo, S., Tu, P. H., Tomita, T., Nakaya, K., Lee, V. M., et al. (1998). Aggregation of alpha-synuclein in Lewy bodies of sporadic Parkinson's disease and dementia with Lewy bodies. *Am. J. Pathol.* 152, 879–884.

Baker, M. G., and Graham, L. (2004). The journey: Parkinson's disease. *BMJ* 329, 611–614. doi: 10.1136/bmj.329.7466.611

Bakhit, Y., Schmitt, I., Hamed, A., Ibrahim, E. A. A., Mohamed, I. N., El-Sadig, S. M., et al. (2022). Methylation of alpha-synuclein in a Sudanese cohort. *Parkinsonism Relat. Disord.* 101, 6–8. doi: 10.1016/j.parkreldis.2022.05.009

Barger, J. L., Kayo, T., Vann, J. M., Arias, E. B., Wang, J., Hacker, T. A., et al. (2008). A low dose of dietary resveratrol partially mimics caloric restriction and retards aging parameters in mice. *PLoS One* 3:e2264. doi: 10.1371/annotation/c54ef754-1962-4125-bf19-76d3ec6f19e5

Bartels, T., Choi, J. G., and Selkoe, D. J. (2011). Alpha-synuclein occurs physiologically as a helically folded tetramer that resists aggregation. *Nature* 477, 107–110. doi: 10.1038/nature10324

Bartels, T., Kim, N. C., Luth, E. S., and Selkoe, D. J. (2014). N-alpha-acetylation of alpha-synuclein increases its helical folding propensity, GM1 binding specificity and resistance to aggregation. *PLoS One* 9:e103727. doi: 10.1371/journal.pone.0103727

Beach, T. G., Adler, C. H., Sue, L. I., Vedders, L., Lue, L., White Iii, C. L., et al. (2010). Multi-organ distribution of phosphorylated alpha-synuclein histopathology in subjects with Lewy body disorders. *Acta Neuropathol.* 119, 689–702. doi: 10.1007/s00401-010-0664-3

Beal, M. F. (1998). Excitotoxicity and nitric oxide in Parkinson's disease pathogenesis. *Ann. Neurol.* 44, S110–S114. doi: 10.1002/ana.410440716

Beard, J. L., and Connor, J. R. (2003). Iron status and neural functioning. *Annu. Rev. Nutr.* 23, 41–58. doi: 10.1146/annurev.nutr.23.020102.075739

Bell, R., Castellana-Cruz, M., Nene, A., Thrush, R. J., Xu, C. K., Kumita, J. R., et al. (2022a). Effects of N-terminal acetylation on the aggregation of disease-related alpha-synuclein variants. *J. Mol. Biol.* 167825

Bell, R., Castellana-Cruz, M., Nene, A., Thrush, R. J., Xu, C. K., Kumita, J. R., et al. (2023). Effects of N-terminal acetylation on the aggregation of disease-related alpha-synuclein variants. *J. Mol. Biol.* 435:167825. doi: 10.1016/j.jmb.2022.167825

Bell, R., Thrush, R. J., Castellana-Cruz, M., Oeller, M., Staats, R., Nene, A., et al. (2022b). N-terminal acetylation of alpha-synuclein slows down its aggregation process and alters the morphology of the resulting aggregates. *Biochemistry* 61, 1743–1756. doi: 10.1021/acs.biochem.2c00104

Bell, R., and Vendruscolo, M. (2021). Modulation of the interactions between alpha-synuclein and lipid membranes by Post-translational modifications. *Front. Neurol.* 12:661117. doi: 10.3389/fneur.2021.661117

Bellucci, A., Antonini, A., Pizzi, M., and Spano, P. (2017). The end is the beginning: Parkinson's disease in the light of brain imaging. *Front. Aging Neurosci.* 9:330. doi: 10.3389/fnagi.2017.00330

Bellucci, A., Mercuri, N. B., Venneri, A., Faustini, G., Longhena, F., Pizzi, M., et al. (2016). Review: Parkinson's disease: from synaptic loss to connectome dysfunction. *Neuropathol. Appl. Neurobiol.* 42, 77–94. doi: 10.1111/nan.12297

Bellucci, A., Navarria, L., Zaltieri, M., Missale, C., and Spano, P. (2012). Alpha-synuclein synaptic pathology and its implications in the development of novel therapeutic approaches to cure Parkinson's disease. *Brain Res.* 1432, 95–113. doi: 10.1016/j.brainres.2011.11.031

Bennett, M. C., Bishop, J. F., Leng, Y., Chock, P. B., Chase, T. N., and Mouradian, M. M. (1999). Degradation of alpha-synuclein by proteasome. *J. Biol. Chem.* 274, 33855–33858. doi: 10.1074/jbc.274.48.33855

Bertilsson, G., Patrone, C., Zachrisson, O., Andersson, A., Dannaeus, K., Heidrich, J., et al. (2008). Peptide hormone exendin-4 stimulates subventricular zone neurogenesis in the adult rodent brain and induces recovery in an animal model of Parkinson's disease. *J. Neurosci. Res.* 86, 326–338. doi: 10.1002/jnr.21483

Boeve, B. F., Silber, M. H., Ferman, T. J., Lucas, J. A., and Parisi, J. E. (2001). Association of REM sleep behavior disorder and neurodegenerative disease may reflect an underlying synucleinopathy. *Mov. Disord.* 16, 622–630. doi: 10.1002/mds.1120

Bohren, K. M., Nadkarni, V., Song, J. H., Gabbay, K. H., and Owerbach, D. (2004). A M55V polymorphism in a novel SUMO gene (SUMO-4) differentially activates heat shock transcription factors and is associated with susceptibility to type I diabetes mellitus. *J. Biol. Chem.* 279, 27233–27238. doi: 10.1074/jbc.M402273200

Bond, M. R., and Hanover, J. A. (2013). O-GlcNAc cycling: a link between metabolism and chronic disease. *Annu. Rev. Nutr.* 33, 205–229. doi: 10.1146/annurev-nutr-071812-161240

Borghgraef, P., Menuet, C., Theunis, C., Louis, J. V., Devijver, H., Maurin, H., et al. (2013). Increasing brain protein O-GlcNAc-ylation mitigates breathing defects and mortality of Tau.P301L mice. *PLoS One* 8:e84442. doi: 10.1371/journal.pone.0084442

Bougea, A., Koros, C., and Stefanis, L. (2019a). Salivary alpha-synuclein as a biomarker for Parkinson's disease: a systematic review. *J. Neural Transm. (Vienna)* 126, 1373–1382. doi: 10.1007/s00702-019-02062-4

Bougea, A., Stefanis, L., Paraskevas, G. P., Emmanouilidou, E., Vekrelis, K., and Kapaki, E. (2019b). Plasma alpha-synuclein levels in patients with Parkinson's disease: a systematic review and meta-analysis. *Neurol. Sci.* 40, 929–938. doi: 10.1007/s10072-019-03738-1

Brahmachari, S., Ge, P., Lee, S. H., Kim, D., Karuppagounder, S. S., Kumar, M., et al. (2016). Activation of tyrosine kinase c-Abl contributes to alpha-synuclein-induced neurodegeneration. *J. Clin. Invest.* 126, 2970–2988. doi: 10.1172/JCI85456

Brakedal, B., Dolle, C., Riemer, F., Ma, Y., Nido, G. S., Skeie, G. O., et al. (2022). The NADPARK study: a randomized phase I trial of nicotinamide riboside supplementation in Parkinson's disease. *Cell Metab.* 34:e6. doi: 10.1016/j.cmet.2022.02.001

Brakedal, B., Flones, I., Reiter, S. F., Torkildsen, O., Dolle, C., Assmus, J., et al. (2017). Glitazone use associated with reduced risk of Parkinson's disease. *Mov. Disord.* 32, 1594–1599. doi: 10.1002/mds.27128

Brasher, B. B., and Van Etten, R. A. (2000). c-Abl has high intrinsic tyrosine kinase activity that is stimulated by mutation of the Src homology 3 domain and by autophosphorylation at two distinct regulatory tyrosines. *J. Biol. Chem.* 275, 35631–35637. doi: 10.1074/jbc.M005401200

Brauer, R., Bhaskaran, K., Chaturvedi, N., Dexter, D. T., Smeeth, L., and Douglas, I. (2015). Glitazone treatment and incidence of Parkinson's disease among people with diabetes: a retrospective cohort study. *PLoS Med.* 12:e1001854. doi: 10.1371/journal.pmed.1001854

Brauer, R., Wei, L., Ma, T., Athauda, D., Girges, C., Vijiaratnam, N., et al. (2020). Diabetes medications and risk of Parkinson's disease: a cohort study of patients with diabetes. *Brain* 143, 3067–3076. doi: 10.1093/brain/awaa262

Braun, A. R., Liao, E. E., Horvath, M., Kalra, P., Acosta, K., Young, M. C., et al. (2021). Potent inhibitors of toxic alpha-synuclein identified via cellular time-resolved FRET biosensors. *NPJ Parkinsons Dis.* 7:52. doi: 10.1038/s41531-021-00195-6

Brown, D. R. (2007). Interactions between metals and alpha-synuclein--function or artefact? *FEBS J.* 274, 3766–3774. doi: 10.1111/j.1742-4658.2007.05917.x

Brown, K. D., Maqsood, S., Huang, J. Y., Pan, Y., Harkcom, W., Li, W., et al. (2014). Activation of SIRT3 by the NAD(+) precursor nicotinamide riboside protects from noise-induced hearing loss. *Cell Metab.* 20, 1059–1068. doi: 10.1016/j.cmet.2014.11.003

Bu, B., Tong, X., Li, D., Hu, Y., He, W., Zhao, C., et al. (2017). N-terminal acetylation preserves alpha-Synuclein from Oligomerization by blocking intermolecular hydrogen bonds. *ACS Chem. Neurosci.* 8, 2145–2151. doi: 10.1021/acschemneuro.7b00250

Burre, J., Sharma, M., Tsetsenis, T., Buchman, V., Etherton, M. R., and Sudhof, T. C. (2010). Alpha-synuclein promotes SNARE-complex assembly in vivo and in vitro. *Science* 329, 1663–1667. doi: 10.1126/science.1195227

Butkinaree, C., Park, K., and Hart, G. W. (2010). O-linked beta-N-acetylglucosamine (O-GlcNAc): extensive crosstalk with phosphorylation to regulate signaling and transcription in response to nutrients and stress. *Biochim. Biophys. Acta* 1800, 96–106. doi: 10.1016/j.bbagen.2009.07.018

Calabresi, P., Mechelli, A., Natale, G., Volpicelli-Daley, L., Di Lazzaro, G., and Ghiglieri, V. (2023). Alpha-synuclein in Parkinson's disease and other synucleinopathies: from overt neurodegeneration back to early synaptic dysfunction. *Cell Death Dis.* 14:176. doi: 10.1038/s41419-023-05672-9

Campbell, B. C., Mclean, C. A., Culvenor, J. G., Gai, W. P., Blumbergs, P. C., Jakala, P., et al. (2001). The solubility of alpha-synuclein in multiple system atrophy differs from that of dementia with Lewy bodies and Parkinson's disease. *J. Neurochem.* 76, 87–96. doi: 10.1046/j.1471-4159.2001.00021.x

Canto, C., Houtkooper, R. H., Pirinen, E., Youn, D. Y., Oosterveer, M. H., Cen, Y., et al. (2012). The NAD(+) precursor nicotinamide riboside enhances oxidative metabolism and protects against high-fat diet-induced obesity. *Cell Metab.* 15, 838–847. doi: 10.1016/j.cmet.2012.04.022

Carboni, E., Tatenhorst, L., Tonges, L., Barski, E., Dambeck, V., Bahr, M., et al. (2017). Deferiprone rescues behavioral deficits induced by mild Iron exposure in a mouse model of alpha-synuclein aggregation. *NeuroMolecular Med.* 19, 309–321. doi: 10.1007/s12017-017-8447-9

Cariulo, C., Martufi, P., Verani, M., Azzollini, L., Bruni, G., Weiss, A., et al. (2019). Phospho-S129 alpha-synuclein is present in human plasma but not in cerebrospinal fluid as determined by an ultrasensitive immunoassay. *Front. Neurosci.* 13:889. doi: 10.3389/fnins.2019.00889

Chakrabartty, A., Doig, A. J., and Baldwin, R. L. (1993). Helix capping propensities in peptides parallel those in proteins. *Proc. Natl. Acad. Sci. U. S. A.* 90, 11332–11336. doi: 10.1073/pnas.90.23.11332

Chan, C. S., Guzman, J. N., Ilijic, E., Mercer, J. N., Rick, C., Tkatch, T., et al. (2007). Rejuvenation' protects neurons in mouse models of Parkinson's disease. *Nature* 447, 1081–1086. doi: 10.1038/nature05865

Chau, E., Kim, H., Shin, J., Martinez, A., and Kim, J. R. (2021). Inhibition of alpha-synuclein aggregation by AM17, a synthetic resveratrol derivative. *Biochem. Biophys. Res. Commun.* 574, 85–90. doi: 10.1016/j.bbrc.2021.08.049

Chavarria, C., and Souza, J. M. (2013). Oxidation and nitration of alpha-synuclein and their implications in neurodegenerative diseases. *Arch. Biochem. Biophys.* 533, 25–32. doi: 10.1016/j.abb.2013.02.009

Chen, L., Periquet, M., Wang, X., Negro, A., Mclean, P. J., Hyman, B. T., et al. (2009). Tyrosine and serine phosphorylation of alpha-synuclein have opposing effects on neurotoxicity and soluble oligomer formation. *J. Clin. Investig.* 119, 3257–3265. doi: 10.1172/JCI39088

Chen, P. S., Wang, C. C., Bortner, C. D., Peng, G. S., Wu, X., Pang, H., et al. (2007). Valproic acid and other histone deacetylase inhibitors induce microglial apoptosis and attenuate lipopolysaccharide-induced dopaminergic neurotoxicity. *Neuroscience* 149, 203–212. doi: 10.1016/j.neuroscience.2007.06.053

Chen, S., Yu, S. J., Li, Y., Lecca, D., Glotfelty, E., Kim, H. K., et al. (2018). Author correction: post-treatment with PT302, a long-acting Exendin-4 sustained release formulation, reduces dopaminergic neurodegeneration in a 6-Hydroxydopamine rat model of Parkinson's disease. *Sci. Rep.* 8:13953. doi: 10.1038/s41598-018-31455-w

Chen, S. H., Wu, H. M., Ossola, B., Schendzielorz, N., Wilson, B. C., Chu, C. H., et al. (2012). Suberoylanilide hydroxamic acid, a histone deacetylase inhibitor, protects dopaminergic neurons from neurotoxin-induced damage. *Br. J. Pharmacol.* 165, 494–505. doi: 10.1111/j.1476-5381.2011.01575.x

Chinta, S. J., Mallajosyula, J. K., Rane, A., and Andersen, J. K. (2010). Mitochondrial alpha-synuclein accumulation impairs complex I function in dopaminergic neurons and results in increased mitophagy in vivo. *Neurosci. Lett.* 486, 235–239. doi: 10.1016/j.neulet.2010.09.061

Choi, B. K., Choi, M. G., Kim, J. Y., Yang, Y., Lai, Y., Kweon, D. H., et al. (2013). Large alpha-synuclein oligomers inhibit neuronal SNARE-mediated vesicle docking. *Proc. Natl. Acad. Sci. U. S. A.* 110, 4087–4092. doi: 10.1073/pnas.1218424110

Choong, C. J., Sasaki, T., Hayakawa, H., Yasuda, T., Baba, K., Hirata, Y., et al. (2016). A novel histone deacetylase 1 and 2 isoform-specific inhibitor alleviates experimental Parkinson's disease. *Neurobiol. Aging* 37, 103–116. doi: 10.1016/j.neurobiolaging.2015.10.001

Chung, S. J., Kim, J., Lee, H. J., Ryu, H. S., Kim, K., Lee, J. H., et al. (2016). Alpha-synuclein in gastric and colonic mucosa in Parkinson's disease: limited role as a biomarker. *Mov. Disord.* 31, 241–249. doi: 10.1002/mds.26473

Clark, J., Clore, E. L., Zheng, K., Adame, A., Masliah, E., and Simon, D. K. (2010). Oral N-acetyl-cysteine attenuates loss of dopaminergic terminals in alpha-synuclein overexpressing mice. *PLoS One* 5:e12333. doi: 10.1371/journal.pone.0012333

Clayton, D. F., and George, J. M. (1998). The synucleins: a family of proteins involved in synaptic function, plasticity, neurodegeneration and disease. *Trends Neurosci.* 21, 249–254. doi: 10.1016/S0166-2236(97)01213-7

Cohen, H. Y., Miller, C., Bitterman, K. J., Wall, N. R., Hekking, B., Kessler, B., et al. (2004). Calorie restriction promotes mammalian cell survival by inducing the SIRT1 deacetylase. *Science* 305, 390–392. doi: 10.1021/acschembio.8b00466

Cole, R. N., and Hart, G. W. (2001). Cytosolic O-glycosylation is abundant in nerve terminals. *J. Neurochem.* 79, 1080–1089. doi: 10.1046/j.1471-4159.2001.00655.x

Costantini, A., Pala, M. I., Compagnoni, L., and Colangeli, M. (2013). High-dose thiamine as initial treatment for Parkinson's disease. *BMJ Case Rep.* 2013:bcr2013009289. doi: 10.1136/bcr-2013-009289

Costantini, A., Pala, M. I., Grossi, E., Mondonico, S., Cardelli, L. E., Jenner, C., et al. (2015). Long-term treatment with high-dose thiamine in Parkinson disease: an open-label pilot study. *J. Altern. Complement. Med.* 21, 740–747. doi: 10.1089/acm.2014.0353

Crespo, E., Macias, M., Pozo, D., Escames, G., Martin, M., Vives, F., et al. (1999). Melatonin inhibits expression of the inducible NO synthase II in liver and lung and prevents endotoxemia in lipopolysaccharide-induced multiple organ dysfunction syndrome in rats. *FASEB J.* 13, 1537–1546. doi: 10.1096/fasebj.13.12.1537

Crowther, R. A., Jakes, R., Spillantini, M. G., and Goedert, M. (1998). Synthetic filaments assembled from C-terminally truncated alpha-synuclein. *FEBS Lett.* 436, 309–312. doi: 10.1016/S0014-5793(98)01146-6

Cuenda, A., and Rousseau, S. (2007). p38 MAP-kinases pathway regulation, function and role in human diseases. *Biochim. Biophys. Acta* 1773, 1358–1375. doi: 10.1016/j.bbamcr.2007.03.010

Danielson, S. R., Held, J. M., Schilling, B., Oo, M., Gibson, B. W., and Andersen, J. K. (2009). Preferentially increased nitration of alpha-synuclein at tyrosine-39 in a cellular oxidative model of Parkinson's disease. *Anal. Chem.* 81, 7823–7828. doi: 10.1021/ac901176t

Dauer, W., Kholodilov, N., Vila, M., Trillat, A. C., Goodchild, R., Larsen, K. E., et al. (2002). Resistance of alpha-synuclein null mice to the parkinsonian neurotoxin MPTP. *Proc. Natl. Acad. Sci. U. S. A.* 99, 14524–14529. doi: 10.1073/pnas.172514599

De Bartolo, M. I., Vivacqua, G., Belvisi, D., Mancinelli, R., Fabbrini, A., Manzo, N., et al. (2023). A combined panel of salivary biomarkers in de novo Parkinson's disease. *Ann. Neurol.* 93, 446–459. doi: 10.1002/ana.26550

De Oliveira, R. M., Vicente Miranda, H., Francelle, L., Pinho, R., Szego, E. M., Martinho, R., et al. (2017). Correction: the mechanism of sirtuin 2-mediated exacerbation of alpha-synuclein toxicity in models of Parkinson disease. *PLoS Biol.* 15:e1002601. doi: 10.1371/journal.pbio.1002601

De Rijk, M. C., Breteler, M. M., Den Breeijen, J. H., Launer, L. J., Grobbee, D. E., Van Der Meche, F. G., et al. (1997). Dietary antioxidants and Parkinson disease. The rotterdam study. *Arch. Neurol.* 54, 762–765. doi: 10.1001/archneur.1997.00550180070015

Decressac, M., Mattsson, B., Lundblad, M., Weikop, P., and Bjorklund, A. (2012). Progressive neurodegenerative and behavioural changes induced by AAV-mediated overexpression of alpha-synuclein in midbrain dopamine neurons. *Neurobiol. Dis.* 45, 939–953. doi: 10.1016/j.nbd.2011.12.013

Deng, W. G., Tang, S. T., Tseng, H. P., and Wu, K. K. (2006). Melatonin suppresses macrophage cyclooxygenase-2 and inducible nitric oxide synthase expression by inhibiting p52 acetylation and binding. *Blood* 108, 518–524. doi: 10.1182/blood-2005-09-3691

Denicola, G. M., Karreth, F. A., Humpton, T. J., Gopinathan, A., Wei, C., Frese, K., et al. (2011). Oncogene-induced Nrf2 transcription promotes ROS detoxification and tumorigenesis. *Nature* 475, 106–109. doi: 10.1038/nature10189

Devic, I., Hwang, H., Edgar, J. S., Izutsu, K., Presland, R., Pan, C., et al. (2011). Salivary alpha-synuclein and DJ-1: potential biomarkers for Parkinson's disease. *Brain* 134:e178. doi: 10.1093/brain/awr015

Devos, D., Labreuche, J., Rascol, O., Corvol, J. C., Duhamel, A., Guyon Delannoy, P., et al. (2022). Trial of Deferiprone in Parkinson's Disease. *N. Engl. J. Med.* 387, 2045–2055. doi: 10.1056/NEJMoa2209254

Di Maio, R., Barrett, P. J., Hoffman, E. K., Barrett, C. W., Zharikov, A., Borah, A., et al. (2016). Alpha-synuclein binds to TOM20 and inhibits mitochondrial protein import in Parkinson's disease. *Sci. Transl. Med.* 8:342ra78. doi: 10.1126/scitranslmed.aaf3634

Dikiy, I., Fauvet, B., Jovicic, A., Mahul-Mellier, A. L., Desobry, C., El-Turk, F., et al. (2016). Semisynthetic and in vitro phosphorylation of alpha-synuclein at Y39 promotes functional partly helical membrane-bound states resembling those induced by PD mutations. *ACS Chem. Biol.* 11, 2428–2437. doi: 10.1021/acschembio.6b00539

Donadio, V., Incensi, A., El-Agnaf, O., Rizzo, G., Vaikath, N., Del Sorbo, F., et al. (2018). Skin alpha-synuclein deposits differ in clinical variants of synucleinopathy: an in vivo study. *Sci. Rep.* 8:14246. doi: 10.1038/s41598-018-32588-8

Donadio, V., Incensi, A., Leta, V., Giannoccaro, M. P., Scaglione, C., Martinelli, P., et al. (2014). Skin nerve alpha-synuclein deposits: a biomarker for idiopathic Parkinson disease. *Neurology* 82, 1362–1369. doi: 10.1212/WNL.0000000000000316

Dong, W. G., Mei, Q., Yu, J. P., Xu, J. M., Xiang, L., and Xu, Y. (2003). Effects of melatonin on the expression of iNOS and COX-2 in rat models of colitis. *World J. Gastroenterol.* 9, 1307–1311. doi: 10.3748/wjg.v9.i6.1307

Donmez, G., Arun, A., Chung, C. Y., Mclean, P. J., Lindquist, S., and Guarente, L. (2012). SIRT1 protects against alpha-synuclein aggregation by activating molecular chaperones. *J. Neurosci.* 32, 124–132. doi: 10.1523/JNEUROSCI.3442-11.2012

Drucker, D. J., and Nauck, M. A. (2006). The incretin system: glucagon-like peptide-1 receptor agonists and dipeptidyl peptidase-4 inhibitors in type 2 diabetes. *Lancet* 368, 1696–1705. doi: 10.1016/S0140-6736(06)69705-5

Du, G., Liu, X., Chen, X., Song, M., Yan, Y., Jiao, R., et al. (2010). Drosophila histone deacetylase 6 protects dopaminergic neurons against alpha-synuclein toxicity by promoting inclusion formation. *Mol. Biol. Cell* 21, 2128–2137. doi: 10.1091/mbc.e10-03-0200

Du, Y., Wang, F., Zou, J., Le, W., Dong, Q., Wang, Z., et al. (2014). Histone deacetylase 6 regulates cytotoxic alpha-synuclein accumulation through induction of the heat shock response. *Neurobiol. Aging* 35, 2316–2328. doi: 10.1016/j.neurobiolaging.2014.04.029

Dufty, B. M., Warner, L. R., Hou, S. T., Jiang, S. X., Gomez-Isla, T., Leenhouts, K. M., et al. (2007). Calpain-cleavage of alpha-synuclein: connecting proteolytic processing to disease-linked aggregation. *Am. J. Pathol.* 170, 1725–1738. doi: 10.2353/ajpath.2007.061232

Dunn, L., Allen, G. F., Mamais, A., Ling, H., Li, A., Duberley, K. E., et al. (2014). Dysregulation of glucose metabolism is an early event in sporadic Parkinson's disease. *Neurobiol. Aging* 35, 1111–1115. doi: 10.1016/j.neurobiolaging.2013.11.001

Eggler, A. L., Gay, K. A., and Mesecar, A. D. (2008). Molecular mechanisms of natural products in chemoprevention: induction of cytoprotective enzymes by Nrf2. *Mol. Nutr. Food Res.* 52, S84–S94. doi: 10.1002/mnfr.200700249

Eid, R., Arab, N. T., and Greenwood, M. T. (2017). Iron mediated toxicity and programmed cell death: a review and a re-examination of existing paradigms. *Biochim. Biophys. Acta, Mol. Cell Res.* 1864, 399–430. doi: 10.1016/j.bbamcr.2016.12.002

El-Agnaf, O. M., Bodles, A. M., Guthrie, D. J., Harriott, P., and Irvine, G. B. (1998a). The N-terminal region of non-a beta component of Alzheimer's disease amyloid is responsible for its tendency to assume beta-sheet and aggregate to form fibrils. *Eur. J. Biochem.* 258, 157–163.

El-Agnaf, O. M., Jakes, R., Curran, M. D., Middleton, D., Ingenito, R., Bianchi, E., et al. (1998b). Aggregates from mutant and wild-type alpha-synuclein proteins and NAC peptide induce apoptotic cell death in human neuroblastoma cells by formation of beta-sheet and amyloid-like filaments. *FEBS Lett.* 440, 71–75.

Elbassuoni, E. A., and Ahmed, R. F. (2019). Mechanism of the neuroprotective effect of GLP-1 in a rat model of Parkinson's with pre-existing diabetes. *Neurochem. Int.* 131:104583. doi: 10.1016/j.neuint.2019.104583

Ellis, C. E., Murphy, E. J., Mitchell, D. C., Golovko, M. Y., Scaglia, F., Barcelo-Coblijn, G. C., et al. (2005). Mitochondrial lipid abnormality and electron transport chain impairment in mice lacking alpha-synuclein. *Mol. Cell. Biol.* 25, 10190–10201. doi: 10.1128/MCB.25.22.10190-10201.2005

Ellis, C. E., Schwartzberg, P. L., Grider, T. L., Fink, D. W., and Nussbaum, R. L. (2001). Alpha-synuclein is phosphorylated by members of the Src family of protein-tyrosine kinases. *J. Biol. Chem.* 276, 3879–3884. doi: 10.1074/jbc.M010316200

Emmanouilidou, E., Stefanis, L., and Vekrellis, K. (2010). Cell-produced alpha-synuclein oligomers are targeted to, and impair, the 26S proteasome. *Neurobiol. Aging* 31, 953–968. doi: 10.1016/j.neurobiolaging.2008.07.008

Engelender, S., and Isacson, O. (2017). The threshold theory for Parkinson's Disease. *Trends Neurosci.* 40, 4–14. doi: 10.1016/j.tins.2016.10.008

Engelender, S., Stefanis, L., Oddo, S., and Bellucci, A. (2022). Can we treat neurodegenerative Proteinopathies by enhancing protein degradation? *Mov. Disord.* 37, 1346–1359. doi: 10.1002/mds.29058

Enserink, J. M. (2015). Sumo and the cellular stress response. *Cell Div* 10:4. doi: 10.1186/s13008-015-0010-1

Etminan, M., Gill, S. S., and Samii, A. (2005). Intake of vitamin E, vitamin C, and carotenoids and the risk of Parkinson's disease: a meta-analysis. *Lancet Neurol.* 4, 362–365. doi: 10.1016/S1474-4422(05)70097-1

Faustini, G., Longhena, F., Varanita, T., Bubacco, L., Pizzi, M., Missale, C., et al. (2018). Synapsin III deficiency hampers alpha-synuclein aggregation, striatal synaptic damage and nigral cell loss in an AAV-based mouse model of Parkinson's disease. *Acta Neuropathol.* 136, 621–639. doi: 10.1007/s00401-018-1892-1

Faustini, G., Marchesan, E., Zonta, L., Bono, F., Bottani, E., Longhena, F., et al. (2019). Alpha-Synuclein preserves mitochondrial fusion and function in neuronal cells. *Oxidative Med. Cell. Longev.* 2019:4246350. doi: 10.1155/2019/4246350

Fauvet, B., Fares, M. B., Samuel, F., Dikiy, I., Tandon, A., Eliezer, D., et al. (2012). Characterization of semisynthetic and naturally Nalpha-acetylated alpha-synuclein in vitro and in intact cells: implications for aggregation and cellular properties of alpha-synuclein. *J. Biol. Chem.* 287, 28243–28262. doi: 10.1074/jbc.M112.383711

Fayyad, M., Salim, S., Majbour, N., Erskine, D., Stoops, E., Mollenhauer, B., et al. (2019). Parkinson's disease biomarkers based on alpha-synuclein. *J. Neurochem.* 150, 626–636. doi: 10.1111/jnc.14809

Feany, M. B., and Bender, W. W. (2000). A Drosophila model of Parkinson's disease. *Nature* 404, 394–398. doi: 10.1038/35006074

Fenyi, A., Leclair-Visonneau, L., Clairembault, T., Coron, E., Neunlist, M., Melki, R., et al. (2019). Detection of alpha-synuclein aggregates in gastrointestinal biopsies by protein misfolding cyclic amplification. *Neurobiol. Dis.* 129, 38–43. doi: 10.1016/j.nbd.2019.05.002

Fereshtehnejad, S. M., Zeighami, Y., Dagher, A., and Postuma, R. B. (2017). Clinical criteria for subtyping Parkinson's disease: biomarkers and longitudinal progression. *Brain* 140, 1959–1976. doi: 10.1093/brain/awx118

Fernandez, C. O., Hoyer, W., Zweckstetter, M., Jares-Erijman, E. A., Subramaniam, V., Griesinger, C., et al. (2004). NMR of alpha-synuclein-polyamine complexes elucidates the mechanism and kinetics of induced aggregation. *EMBO J.* 23, 2039–2046. doi: 10.1038/sj.emboj.7600211

Fernandez, E., Garcia-Moreno, J. M., Martin De Pablos, A., and Chacon, J. (2013). May the evaluation of nitrosative stress through selective increase of 3-nitrotyrosine proteins other than nitroalbumin and dominant tyrosine-125/136 nitrosylation of serum alpha-synuclein serve for diagnosis of sporadic Parkinson's disease? *Antioxid. Redox Signal.* 19, 912–918. doi: 10.1089/ars.2013.5250

Fields, C. R., Bengoa-Vergniory, N., and Wade-Martins, R. (2019). Targeting alpha-Synuclein as a therapy for Parkinson's Disease. *Front. Mol. Neurosci.* 12:299. doi: 10.3389/fnmol.2019.00299

Fitzgerald, K., Bergeron, M., Willits, C., Bowers, S., Aubele, D. L., Goldbach, E., et al. (2013). Pharmacological inhibition of polo like kinase 2 (PLK2) does not cause chromosomal damage or result in the formation of micronuclei. *Toxicol. Appl. Pharmacol.* 269, 1–7. doi: 10.1016/j.taap.2013.02.012

Flock, G., Baggio, L. L., Longuet, C., and Drucker, D. J. (2007). Incretin receptors for glucagon-like peptide 1 and glucose-dependent insulinotropic polypeptide are essential for the sustained metabolic actions of vildagliptin in mice. *Diabetes* 56, 3006–3013. doi: 10.2337/db07-0697

Floor, E., and Wetzel, M. G. (1998). Increased protein oxidation in human substantia nigra pars compacta in comparison with basal ganglia and prefrontal cortex measured with an improved dinitrophenylhydrazine assay. *J. Neurochem.* 70, 268–275. doi: 10.1046/j.1471-4159.1998.70010268.x

Forman, H. J., Davies, K. J., and Ursini, F. (2014). How do nutritional antioxidants really work: nucleophilic tone and Para-hormesis versus free radical scavenging in vivo. *Free Radic. Biol. Med.* 66, 24–35. doi: 10.1016/j.freeradbiomed.2013.05.045

Forman, H. J., and Zhang, H. (2021). Author correction: targeting oxidative stress in disease: promise and limitations of antioxidant therapy. *Nat. Rev. Drug Discov.* 20:652. doi: 10.1038/s41573-021-00267-5

Formisano, L., Guida, N., Laudati, G., Mascolo, L., Di Renzo, G., and Canzoniero, L. M. (2015). MS-275 inhibits aroclor 1254-induced SH-SY5Y neuronal cell toxicity by preventing the formation of the HDAC3/REST complex on the synapsin-1 promoter. *J. Pharmacol. Exp. Ther.* 352, 236–243. doi: 10.1124/jpet.114.219345

Forster, A., and Hill, C. P. (2003). Proteasome degradation: enter the substrate. *Trends Cell Biol.* 13, 550–553. doi: 10.1016/j.tcb.2003.09.001

Foulds, P., Mann, D. M., and Allsop, D. (2012). Phosphorylated alpha-synuclein as a potential biomarker for Parkinson's disease and related disorders. *Expert. Rev. Mol. Diagn.* 12, 115–117. doi: 10.1586/erm.12.5

Foulds, P. G., Diggle, P., Mitchell, J. D., Parker, A., Hasegawa, M., Masuda-Suzukake, M., et al. (2013). A longitudinal study on alpha-synuclein in blood plasma as a biomarker for Parkinson's disease. *Sci. Rep.* 3:2540. doi: 10.1038/srep02540

Foulds, P. G., Mitchell, J. D., Parker, A., Turner, R., Green, G., Diggle, P., et al. (2011). Phosphorylated alpha-synuclein can be detected in blood plasma and is potentially a useful biomarker for Parkinson's disease. *FASEB J.* 25, 4127–4137. doi: 10.1096/fj.10-179192

Fujiwara, H., Hasegawa, M., Dohmae, N., Kawashima, A., Masliah, E., Goldberg, M. S., et al. (2002). Alpha-Synuclein is phosphorylated in synucleinopathy lesions. *Nat. Cell Biol.* 4, 160–164. doi: 10.1038/ncb748

Fukuda, I., Ito, A., Hirai, G., Nishimura, S., Kawasaki, H., Saitoh, H., et al. (2009). Ginkgolic acid inhibits protein SUMOylation by blocking formation of the E1-SUMO intermediate. *Chem. Biol.* 16, 133–140. doi: 10.1016/j.chembiol.2009.01.009

Fumimura, Y., Ikemura, M., Saito, Y., Sengoku, R., Kanemaru, K., Sawabe, M., et al. (2007). Analysis of the adrenal gland is useful for evaluating pathology of the peripheral autonomic nervous system in lewy body disease. *J. Neuropathol. Exp. Neurol.* 66, 354–362. doi: 10.1097/nen.0b013e3180517454

Ganguly, U., Singh, S., Pal, S., Prasad, S., Agrawal, B. K., Saini, R. V., et al. (2021). Alpha-synuclein as a biomarker of Parkinson's disease: good, but not good enough. *Front. Aging Neurosci.* 13:702639. doi: 10.3389/fnagi.2021.702639

Gardian, G., Yang, L., Cleren, C., Calingasan, N. Y., Klivenyi, P., and Beal, M. F. (2004). Neuroprotective effects of phenylbutyrate against MPTP neurotoxicity. *NeuroMolecular Med.* 5, 235–241. doi: 10.1385/NMM:5:3:235

Gelpi, E., Navarro-Otano, J., Tolosa, E., Gaig, C., Compta, Y., Rey, M. J., et al. (2014). Multiple organ involvement by alpha-synuclein pathology in Lewy body disorders. *Mov. Disord.* 29, 1010–1018. doi: 10.1002/mds.25776

George, J. M. (2002). The Synucleins. *Genome Biol.* 3:Reviews3002. doi: 10.1186/gb-2001-3-1-reviews3002

George, S., and Abrahamse, H. (2020). Redox potential of antioxidants in cancer progression and prevention. *Antioxidants* 9:1156. doi: 10.3390/antiox9111156

Gerlach, M., Double, K. L., Ben-Shachar, D., Zecca, L., Youdim, M. B., and Riederer, P. (2003). Neuromelanin and its interaction with iron as a potential risk factor for dopaminergic neurodegeneration underlying Parkinson's disease. *Neurotox. Res.* 5, 35–44. doi: 10.1007/BF03033371

Getachew, B., Csoka, A. B., Bhatti, A., Copeland, R. L., and Tizabi, Y. (2020). Butyrate protects against salsolinol-induced toxicity in SH-SY5Y cells: implication for Parkinson's disease. *Neurotox. Res.* 38, 596–602. doi: 10.1007/s12640-020-00238-5

Ghanem, S. S., Majbour, N. K., Vaikath, N. N., Ardah, M. T., Erskine, D., Jensen, N. M., et al. (2022). Alpha-synuclein phosphorylation at serine 129 occurs after initial protein deposition and inhibits seeded fibril formation and toxicity. *Proc. Natl. Acad. Sci. U. S. A.* 119:e2109617119. doi: 10.1073/pnas.2109617119

Ghiglieri, V., Calabrese, V., and Calabresi, P. (2018). Alpha-Synuclein: from early synaptic dysfunction to Neurodegeneration. *Front. Neurol.* 9:295. doi: 10.3389/fneur.2018.00295

Giasson, B. I., Duda, J. E., Forman, M. S., Lee, V. M., and Trojanowski, J. Q. (2001). Prominent perikaryal expression of alpha-and beta-synuclein in neurons of dorsal root ganglion and in medullary neurons. *Exp. Neurol.* 172, 354–362. doi: 10.1006/exnr.2001.7805

Giasson, B. I., Duda, J. E., Murray, I. V., Chen, Q., Souza, J. M., Hurtig, H. I., et al. (2000). Oxidative damage linked to neurodegeneration by selective alpha-synuclein nitration in synucleinopathy lesions. *Science* 290, 985–989. doi: 10.1126/science.290.5493.985

Giasson, B. I., Forman, M. S., Higuchi, M., Golbe, L. I., Graves, C. L., Kotzbauer, P. T., et al. (2003). Initiation and synergistic fibrillization of tau and alpha-synuclein. *Science* 300, 636–640. doi: 10.1126/science.1082324

Gibb, W. R. (1986). Idiopathic Parkinson's disease and the Lewy body disorders. *Neuropathol. Appl. Neurobiol.* 12, 223–234. doi: 10.1111/j.1365-2990.1986.tb00136.x

Gilad, E., Wong, H. R., Zingarelli, B., Virag, L., O'connor, M., Salzman, A. L., et al. (1998). Melatonin inhibits expression of the inducible isoform of nitric oxide synthase in murine macrophages: role of inhibition of NFkappaB activation. *FASEB J.* 12, 685–693. doi: 10.1096/fasebj.12.9.685

Gille, G., Hung, S. T., Reichmann, H., and Rausch, W. D. (2004). Oxidative stress to dopaminergic neurons as models of Parkinson's disease. *Ann. N. Y. Acad. Sci.* 1018, 533–540. doi: 10.1196/annals.1296.066

GioVannini, M. G., Cerbai, F., Bellucci, A., Melani, C., Grossi, C., Bartolozzi, C., et al. (2008). Differential activation of mitogen-activated protein kinase signalling pathways in the hippocampus of CRND8 transgenic mouse, a model of Alzheimer's disease. *Neuroscience* 153, 618–633. doi: 10.1016/j.neuroscience.2008.02.061

Giovannini, M. G., Scali, C., Prosperi, C., Bellucci, A., Vannucchi, M. G., Rosi, S., et al. (2002). Beta-amyloid-induced inflammation and cholinergic hypofunction in the rat brain in vivo: involvement of the p38MAPK pathway. *Neurobiol. Dis.* 11, 257–274. doi: 10.1006/nbdi.2002.0538

Godena, V. K., Brookes-Hocking, N., Moller, A., Shaw, G., Oswald, M., Sancho, R. M., et al. (2014). Increasing microtubule acetylation rescues axonal transport and locomotor deficits caused by LRRK2 Roc-COR domain mutations. *Nat. Commun.* 5:5245. doi: 10.1038/ncomms6245

Goedert, M., Jakes, R., and Spillantini, M. G. (2017). The synucleinopathies: twenty years on. *J. Parkinsons Dis.* 7, S51–S69. doi: 10.3233/JPD-179005

Gomez-Tortosa, E., Newell, K., Irizarry, M. C., Sanders, J. L., and Hyman, B. T. (2000). Alpha-synuclein immunoreactivity in dementia with Lewy bodies: morphological staging and comparison with ubiquitin immunostaining. *Acta Neuropathol.* 99, 352–357. doi: 10.1007/s004010051135

Gonfloni, S., Maiani, E., Di Bartolomeo, C., Diederich, M., and Cesareni, G. (2012). Oxidative stress, DNA damage, and c-Abl signaling: at the crossroad in neurodegenerative diseases? *Int. J. Cell. Biol.* 2012:683097. doi: 10.1155/2012/683097

Gong, B., Pan, Y., Vempati, P., Zhao, W., Knable, L., Ho, L., et al. (2013). Nicotinamide riboside restores cognition through an upregulation of proliferator-activated receptor-gamma coactivator 1alpha regulated beta-secretase 1 degradation and mitochondrial gene expression in Alzheimer's mouse models. *Neurobiol. Aging* 34, 1581–1588. doi: 10.1016/j.neurobiolaging.2012.12.005

Gong, C. X., Liu, F., and Iqbal, K. (2012). O-GlcNAc cycling modulates neurodegeneration. *Proc. Natl. Acad. Sci. U. S. A.* 109, 17319–17320. doi: 10.1073/pnas.1215395109

Gorbatyuk, O. S., Li, S., Sullivan, L. F., Chen, W., Kondrikova, G., Manfredsson, F. P., et al. (2008). The phosphorylation state of Ser-129 in human alpha-synuclein determines neurodegeneration in a rat model of Parkinson disease. *Proc. Natl. Acad. Sci. U. S. A.* 105, 763–768. doi: 10.1073/pnas.0711053105

Gorostidi, A., Bergareche, A., Ruiz-Martinez, J., Marti-Masso, J. F., Cruz, M., Varghese, S., et al. (2012). Alphalpha-synuclein levels in blood plasma from LRRK2 mutation carriers. *PLoS One* 7:e52312. doi: 10.1371/journal.pone.0052312

Grace, A. A., and Bunney, B. S. (1983). Intracellular and extracellular electrophysiology of nigral dopaminergic neurons—3. Evidence for electrotonic coupling. *Neuroscience* 10, 333–348. doi: 10.1016/0306-4522(83)90137-9

Graham, D. L., Gray, A. J., Joyce, J. A., Yu, D., Omoore, J., Carlson, G. A., et al. (2014). Increased O-GlcNAcylation reduces pathological tau without affecting its normal phosphorylation in a mouse model of tauopathy. *Neuropharmacology* 79, 307–313. doi: 10.1016/j.neuropharm.2013.11.025

Greenamyre, J. T., and Hastings, T. G. (2004). Biomedicine. Parkinson's--divergent causes, convergent mechanisms. *Science* 304, 1120–1122. doi: 10.1126/science.1098966

Gruschus, J. M., Yap, T. L., Pistolesi, S., Maltsev, A. S., and Lee, J. C. (2013). NMR structure of calmodulin complexed to an N-terminally acetylated alpha-synuclein peptide. *Biochemistry* 52, 3436–3445. doi: 10.1021/bi400199p

Gueven, N., Ravishankar, P., Eri, R., and Rybalka, E. (2021). Idebenone: when an antioxidant is not an antioxidant. *Redox Biol.* 38:101812. doi: 10.1016/j.redox.2020.101812

Guo, Y. J., Dong, S. Y., Cui, X. X., Feng, Y., Liu, T., Yin, M., et al. (2016). Resveratrol alleviates MPTP-induced motor impairments and pathological changes by autophagic degradation of alpha-synuclein via SIRT1-deacetylated LC3. *Mol. Nutr. Food Res.* 60, 2161–2175. doi: 10.1002/mnfr.201600111

Guzman, E., Taylor, G., Charleston, B., and Ellis, S. A. (2010). Induction of a cross-reactive CD8(+) T cell response following foot-and-mouth disease virus vaccination. *J. Virol.* 84, 12375–12384. doi: 10.1128/JVI.01545-10

Hamm-Alvarez, S. F., Okamoto, C. T., Janga, S. R., Feigenbaum, D., Edman, M. C., Freire, D., et al. (2019). Oligomeric alpha-synuclein is increased in basal tears of Parkinson's patients. *Biomark. Med* 13, 941–952. doi: 10.2217/bmm-2019-0167

Han, S., Du, Z., Liu, K., and Gong, S. (2020). Nicotinamide riboside protects noise-induced hearing loss by recovering the hair cell ribbon synapses. *Neurosci. Lett.* 725:134910. doi: 10.1016/j.neulet.2020.134910

Harder, Z., Zunino, R., and Mcbride, H. (2004). Sumo1 conjugates mitochondrial substrates and participates in mitochondrial fission. *Curr. Biol.* 14, 340–345. doi: 10.1016/j.cub.2004.02.004

Harlan, B. A., Killoy, K. M., Pehar, M., Liu, L., Auwerx, J., and Vargas, M. R. (2020). Evaluation of the NAD(+) biosynthetic pathway in ALS patients and effect of modulating NAD(+) levels in hSOD1-linked ALS mouse models. *Exp. Neurol.* 327:113219. doi: 10.1016/j.expneurol.2020.113219

Harris, I. S., and Denicola, G. M. (2020). The complex interplay between antioxidants and ROS in Cancer. *Trends Cell Biol.* 30, 440–451. doi: 10.1016/j.tcb.2020.03.002

Harrison, I. F., Crum, W. R., Vernon, A. C., and Dexter, D. T. (2015). Neurorestoration induced by the HDAC inhibitor sodium valproate in the lactacystin model of Parkinson's is associated with histone acetylation and up-regulation of neurotrophic factors. *Br. J. Pharmacol.* 172, 4200–4215. doi: 10.1111/bph.13208

Harrison, I. F., Smith, A. D., and Dexter, D. T. (2018). Pathological histone acetylation in Parkinson's disease: Neuroprotection and inhibition of microglial activation through SIRT 2 inhibition. *Neurosci. Lett.* 666, 48–57. doi: 10.1016/j.neulet.2017.12.037

Hasegawa, M., Fujiwara, H., Nonaka, T., Wakabayashi, K., Takahashi, H., Lee, V. M., et al. (2002). Phosphorylated alpha-synuclein is ubiquitinated in alpha-synucleinopathy lesions. *J. Biol. Chem.* 277, 49071–49076. doi: 10.1074/jbc.M208046200

Hastings, N. B., Wang, X., Song, L., Butts, B. D., Grotz, D., Hargreaves, R., et al. (2017). Inhibition of O-GlcNAcase leads to elevation of O-GlcNAc tau and reduction of tauopathy and cerebrospinal fluid tau in rTg4510 mice. *Mol. Neurodegener.* 12:39. doi: 10.1186/s13024-017-0181-0

He, P. K., Gao, Y. Y., Lyu, F. J., Chen, J. N., Zhang, Y. H., Nie, K., et al. (2021). Idebenone-activating Autophagic degradation of alpha-synuclein via inhibition of AKT-mTOR pathway in a SH-SY5Y-A53T model of Parkinson's disease: a network pharmacological approach. *Evid. Based Complement. Alternat. Med.* 2021:8548380. doi: 10.1155/2021/8548380

He, X., Riceberg, J., Soucy, T., Koenig, E., Minissale, J., Gallery, M., et al. (2017). Probing the roles of SUMOylation in cancer cell biology by using a selective SAE inhibitor. *Nat. Chem. Biol.* 13, 1164–1171. doi: 10.1038/nchembio.2463

He, Y., Yu, Z., and Chen, S. (2019). Alpha-synuclein nitration and its implications in Parkinson's disease. *ACS Chem. Neurosci.* 10, 777–782. doi: 10.1021/acschemneuro.8b00288

Hebron, M. L., Lonskaya, I., and Moussa, C. E. (2013). Nilotinib reverses loss of dopamine neurons and improves motor behavior via autophagic degradation of alpha-

synuclein in Parkinson's disease models. *Hum. Mol. Genet.* 22, 3315–3328. doi: 10.1093/hmg/ddt192

Hellenbrand, W., Boeing, H., Robra, B. P., Seidler, A., Vieregge, P., Nischan, P., et al. (1996). Diet and Parkinson's disease. II: a possible role for the past intake of specific nutrients. Results from a self-administered food-frequency questionnaire in a case-control study. *Neurology* 47, 644–650. doi: 10.1212/WNL.47.3.644

Henning, C., and Glomb, M. A. (2016). Pathways of the Maillard reaction under physiological conditions. *Glycoconj. J.* 33, 499–512. doi: 10.1007/s10719-016-9694-y

Hershko, A., and Ciechanover, A. (1998). The ubiquitin system. *Annu. Rev. Biochem.* 67, 425–479. doi: 10.1146/annurev.biochem.67.1.425

Hirata, Y., Sasaki, T., Kanki, H., Choong, C. J., Nishiyama, K., Kubo, G., et al. (2018). New 5-aryl-substituted 2-aminobenzamide-type HDAC inhibitors with a diketopiperazine group and their ameliorating effects on ischemia-induced neuronal cell death. *Sci. Rep.* 8:1400. doi: 10.1038/s41598-018-19664-9

HIrohama, M., Kumar, A., Fukuda, I., Matsuoka, S., Igarashi, Y., Saitoh, H., et al. (2013). Spectomycin B1 as a novel SUMOylation inhibitor that directly binds to SUMO E2. *ACS Chem. Biol.* 8, 2635–2642. doi: 10.1021/cb400630z

Hodara, R., Norris, E. H., Giasson, B. I., Mishizen-Eberz, A. J., Lynch, D. R., Lee, V. M., et al. (2004). Functional consequences of alpha-synuclein tyrosine nitration: diminished binding to lipid vesicles and increased fibril formation. *J. Biol. Chem.* 279, 47746–47753. doi: 10.1074/jbc.M408906200

Hodge, J. E. (1955). The Amadori rearrangement. *Adv. Carbohydr. Chem.* 10, 169–205. doi: 10.1016/s0096-5332(08)60392-6

Holmay, M. J., Terpstra, M., Coles, L. D., Mishra, U., Ahlskog, M., Oz, G., et al. (2013). N-Acetylcysteine boosts brain and blood glutathione in Gaucher and Parkinson diseases. *Clin. Neuropharmacol.* 36, 103–106. doi: 10.1097/WNF.0b013e31829ae713

Holst, J. J. (2007). The physiology of glucagon-like peptide 1. *Physiol. Rev.* 87, 1409–1439. doi: 10.1152/physrev.00034.2006

Hong, Z., Shi, M., Chung, K. A., Quinn, J. F., Peskind, E. R., Galasko, D., et al. (2010). DJ-1 and alpha-synuclein in human cerebrospinal fluid as biomarkers of Parkinson's disease. *Brain* 133, 713–726. doi: 10.1093/brain/awq008

Hornykiewicz, O. (2001). Chemical neuroanatomy of the basal ganglia--normal and in Parkinson's disease. *J. Chem. Neuroanat.* 22, 3–12. doi: 10.1016/S0891-0618(01)00100-4

Horvath, T. L., Diano, S., Leranth, C., Garcia-Segura, L. M., Cowley, M. A., Shanabrough, M., et al. (2003). Coenzyme Q induces nigral mitochondrial uncoupling and prevents dopamine cell loss in a primate model of Parkinson's disease. *Endocrinology* 144, 2757–2760. doi: 10.1210/en.2003-0163

Hoyer, W., Cherny, D., Subramaniam, V., and Jovin, T. M. (2004). Impact of the acidic C-terminal region comprising amino acids 109-140 on alpha-synuclein aggregation in vitro. *Biochemistry* 43, 16233–16242. doi: 10.1021/bi048453u

Hsu, S. W., Hsu, P. C., Chang, W. S., Yu, C. C., Wang, Y. C., Yang, J. S., et al. (2020). Protective effects of valproic acid on 6-hydroxydopamine-induced neuroinjury. *Environ. Toxicol.* 35, 840–848. doi: 10.1002/tox.22920

Hughes, K. C., Gao, X., Kim, I. Y., Rimm, E. B., Wang, M., Weisskopf, M. G., et al. (2016). Intake of antioxidant vitamins and risk of Parkinson's disease. *Mov. Disord.* 31, 1909–1914. doi: 10.1002/mds.26819

Hulka, B. S. (1990). Principles of bladder cancer screening in an intervention trial. *J. Occup. Med.* 32, 812–816. doi: 10.1097/00043764-199009000-00011

Ibrahim, H. A. M., Hussein, A. M., Gabr, M., El-Saeed, R. A., Ammar, O. A., Mosa, A. A. H., et al. (2022). Effect of melatonin on alpha synuclein and autophagy in dopaminergic neuronal differentiation of adipose mesenchymal stem cells. *Res. Sq.* doi: 10.21203/rs.3.rs-1746786/v

Imam, S. Z., Zhou, Q., Yamamoto, A., Valente, A. J., Ali, S. F., Bains, M., et al. (2011). Novel regulation of parkin function through c-Abl-mediated tyrosine phosphorylation: implications for Parkinson's disease. *J. Neurosci.* 31, 157–163. doi: 10.1523/JNEUROSCI.1833-10.2011

Infante, R., Scaglione, C., Incensi, A., Rizzo, G., Liguori, R., and Donadio, V. (2020). A longitudinal skin biopsy study of phosphorylated alpha-synuclein in a patient with Parkinson disease and orthostatic hypotension. *J. Neuropathol. Exp. Neurol.* 79, 813–816. doi: 10.1093/jnen/nlaa048

Inglis, K. J., Chereau, D., Brigham, E. F., Chiou, S. S., Schobel, S., Frigon, N. L., et al. (2009). Polo-like kinase 2 (PLK2) phosphorylates alpha-synuclein at serine 129 in central nervous system. *J. Biol. Chem.* 284, 2598–2602. doi: 10.1074/jbc.C800206200

Intagliata, S., Modica, M. N., Santagati, L. M., and Montenegro, L. (2019). Strategies to improve resveratrol systemic and topical bioavailability: an update. *Antioxidants* 8:244. doi: 10.3390/antiox8080244

Iravanpour, F., Dargahi, L., Rezaei, M., Haghani, M., Heidari, R., Valian, N., et al. (2021). Intranasal insulin improves mitochondrial function and attenuates motor deficits in a rat 6-OHDA model of Parkinson's disease. *CNS Neurosci. Ther.* 27, 308–319. doi: 10.1111/cns.13609

Jenner, P., and Olanow, C. W. (2006). The pathogenesis of cell death in Parkinson's disease. *Neurology* 66, S24–S36. doi: 10.1212/WNL.66.10_suppl_4.S24

Jensen, P. H., Hager, H., Nielsen, M. S., Hojrup, P., Gliemann, J., and Jakes, R. (1999). Alpha-synuclein binds to Tau and stimulates the protein kinase A-catalyzed tau phosphorylation of serine residues 262 and 356. *J. Biol. Chem.* 274, 25481–25489. doi: 10.1074/jbc.274.36.25481

Jeong, S. H., Chung, S. J., Yoo, H. S., Hong, N., Jung, J. H., Baik, K., et al. (2021). Beneficial effects of dipeptidyl peptidase-4 inhibitors in diabetic Parkinson's disease. *Brain* 144, 1127–1137. doi: 10.1093/brain/awab015

Jia, L., Wang, Y., Wei, W., Zhao, W., Lu, F., and Liu, F. (2019). Vitamin B12 inhibits alpha-synuclein fibrillogenesis and protects against amyloid-induced cytotoxicity. *Food Funct.* 10, 2861–2870. doi: 10.1039/C8FO02471E

Jian, W., Wei, X., Chen, L., Wang, Z., Sun, Y., Zhu, S., et al. (2017). Inhibition of HDAC6 increases acetylation of peroxiredoxin1/2 and ameliorates 6-OHDA induced dopaminergic injury. *Neurosci. Lett.* 658, 114–120. doi: 10.1016/j.neulet.2017.08.029

Jin, J. W., Fan, X., Del Cid-Pellitero, E., Liu, X. X., Zhou, L., Dai, C., et al. (2021). Development of an alpha-synuclein knockdown peptide and evaluation of its efficacy in Parkinson's disease models. *Commun. Biol.* 4:232. doi: 10.1038/s42003-021-01746-6

Johnston, T. H., Huot, P., Damude, S., Fox, S. H., Jones, S. W., Rusche, J. R., et al. (2013). RGFP109, a histone deacetylase inhibitor attenuates L-DOPA-induced dyskinesia in the MPTP-lesioned marmoset: a proof-of-concept study. *Parkinsonism Relat. Disord.* 19, 260–264. doi: 10.1016/j.parkreldis.2012.07.001

Jomova, K., and Valko, M. (2011). Importance of iron chelation in free radical-induced oxidative stress and human disease. *Curr. Pharm. Des.* 17, 3460–3473. doi: 10.2174/138161211798072463

Jones, C. L., Njomen, E., Sjogren, B., Dexheimer, T. S., and Tepe, J. J. (2017). Small molecule enhancement of 20S proteasome activity targets intrinsically disordered proteins. *ACS Chem. Biol.* 12, 2240–2247. doi: 10.1021/acschembio.7b00489

Junn, E., and Mouradian, M. M. (2002). Human alpha-synuclein over-expression increases intracellular reactive oxygen species levels and susceptibility to dopamine. *Neurosci. Lett.* 320, 146–150. doi: 10.1016/S0304-3940(02)00016-2

Kabel, A. M., Omar, M. S., Alhadhrami, A., Alharthi, S. S., and Alrobaian, M. M. (2018). Linagliptin potentiates the effect of l-dopa on the behavioural, biochemical and immunohistochemical changes in experimentally-induced Parkinsonism: role of toll-like receptor 4, TGF-beta1, NF-kappaB and glucagon-like peptide 1. *Physiol. Behav.* 188, 108–118. doi: 10.1016/j.physbeh.2018.01.028

Kahle, P. J., Neumann, M., Ozmen, L., and Haass, C. (2000). Physiology and pathophysiology of alpha-synuclein. Cell culture and transgenic animal models based on a Parkinson's disease-associated protein. *Ann. N. Y. Acad. Sci.* 920, 33–41. doi: 10.1111/j.1749-6632.2000.tb06902.x

Kang, L., Moriarty, G. M., Woods, L. A., Ashcroft, A. E., Radford, S. E., and Baum, J. (2012). N-terminal acetylation of alpha-synuclein induces increased transient helical propensity and decreased aggregation rates in the intrinsically disordered monomer. *Protein Sci.* 21, 911–917. doi: 10.1002/pro.2088

Karachalias, N., Babaei-Jadidi, R., Rabbani, N., and Thornalley, P. J. (2010). Increased protein damage in renal glomeruli, retina, nerve, plasma and urine and its prevention by thiamine and benfotiamine therapy in a rat model of diabetes. *Diabetologia* 53, 1506–1516. doi: 10.1007/s00125-010-1722-z

Karampetsou, M., Ardah, M. T., Semitekolou, M., Polissidis, A., Samiotaki, M., Kalomoiri, M., et al. (2017). Phosphorylated exogenous alpha-synuclein fibrils exacerbate pathology and induce neuronal dysfunction in mice. *Sci. Rep.* 7:16533. doi: 10.1038/s41598-017-15813-8

Kargbo, R. B. (2020). PROTAC compounds targeting alpha-synuclein protein for treating neurogenerative disorders: Alzheimer's and Parkinson's diseases. *ACS Med. Chem. Lett.* 11, 1086–1087. doi: 10.1021/acsmedchemlett.0c00192

Karuppagounder, S. S., Brahmachari, S., Lee, Y., Dawson, V. L., Dawson, T. M., and Ko, H. S. (2014). The c-Abl inhibitor, nilotinib, protects dopaminergic neurons in a preclinical animal model of Parkinson's disease. *Sci. Rep.* 4:4874. doi: 10.1038/srep04874

Karuppagounder, S. S., Wang, H., Kelly, T., Rush, R., Nguyen, R., Bisen, S., et al. (2023). The c-Abl inhibitor IkT-148009 suppresses neurodegeneration in mouse models of heritable and sporadic Parkinson's disease. *Sci. Transl. Med.* 15:eabp9352.

Kasai, T., Tokuda, T., Yamaguchi, N., Watanabe, Y., Kametani, F., Nakagawa, M., et al. (2008). Cleavage of normal and pathological forms of alpha-synuclein by neurosin in vitro. *Neurosci. Lett.* 436, 52–56. doi: 10.1016/j.neulet.2008.02.057

Katila, N., Bhurtel, S., Shadfar, S., Srivastav, S., Neupane, S., Ojha, U., et al. (2017). Metformin lowers alpha-synuclein phosphorylation and upregulates neurotrophic factor in the MPTP mouse model of Parkinson's disease. *Neuropharmacology* 125, 396–407. doi: 10.1016/j.neuropharm.2017.08.015

Kawaguchi, Y., Kovacs, J. J., Mclaurin, A., Vance, J. M., Ito, A., and Yao, T. P. (2003). The deacetylase HDAC6 regulates aggresome formation and cell viability in response to misfolded protein stress. *Cells* 115, 727–738. doi: 10.1016/S0092-8674(03)00939-5

Kazantsev, A. G., and Kolchinsky, A. M. (2008). Central role of alpha-synuclein oligomers in neurodegeneration in Parkinson disease. *Arch. Neurol.* 65, 1577–1581. doi: 10.1001/archneur.65.12.1577

Keeney, P. M., Xie, J., Capaldi, R. A., and Bennett, J. P. Jr. (2006). Parkinson's disease brain mitochondrial complex I has oxidatively damaged subunits and is functionally impaired and misassembled. *J. Neurosci.* 26, 5256–5264. doi: 10.1523/JNEUROSCI.0984-06.2006

Khan, Z., and Ali, S. A. (2018). Oxidative stress-related biomarkers in Parkinson's disease: a systematic review and meta-analysis. *Iran. J. Neurol.* 17, 137–144.

Kidd, S. K., and Schneider, J. S. (2010). Protection of dopaminergic cells from MPP+-mediated toxicity by histone deacetylase inhibition. *Brain Res.* 1354, 172–178. doi: 10.1016/j.brainres.2010.07.041

Kidd, S. K., and Schneider, J. S. (2011). Protective effects of valproic acid on the nigrostriatal dopamine system in a 1-methyl-4-phenyl-1,2,3,6-tetrahydropyridine mouse model of Parkinson's disease. *Neuroscience* 194, 189–194. doi: 10.1016/j.neuroscience.2011.08.010

Kieburtz, K., Mcdermott, M., Como, P., Growdon, J., Brady, J., Carter, J., et al. (1994). The effect of deprenyl and tocopherol on cognitive performance in early untreated Parkinson's disease. Parkinson study group. *Neurology* 44, 1756–1759. doi: 10.1212/WNL.44.9.1756

Kim, D., Nguyen, M. D., Dobbin, M. M., Fischer, A., Sananbenesi, F., Rodgers, J. T., et al. (2007). SIRT1 deacetylase protects against neurodegeneration in models for Alzheimer's disease and amyotrophic lateral sclerosis. *EMBO J.* 26, 3169–3179. doi: 10.1038/sj.emboj.7601758

Kim, D. S., Choi, H. I., Wang, Y., Luo, Y., Hoffer, B. J., and Greig, N. H. (2017). A new treatment strategy for Parkinson's disease through the gut-brain axis: the glucagon-like peptide-1 receptor pathway. *Cell Transplant.* 26, 1560–1571. doi: 10.1177/0963689717721234

Kim, T., Song, S., Park, Y., Kang, S., and Seo, H. (2019). HDAC inhibition by valproic acid induces neuroprotection and improvement of PD-like behaviors in LRRK2 R1441G transgenic mice. *Exp. Neurobiol.* 28, 504–515. doi: 10.5607/en.2019.28.4.504

Ko, H. S., Lee, Y., Shin, J. H., Karuppagounder, S. S., Gadad, B. S., Koleske, A. J., et al. (2010). Phosphorylation by the c-Abl protein tyrosine kinase inhibits parkin's ubiquitination and protective function. *Proc. Natl. Acad. Sci. U. S. A.* 107, 16691–16696. doi: 10.1073/pnas.1006083107

Koehler, N. K., Stransky, E., Meyer, M., Gaertner, S., Shing, M., Schnaidt, M., et al. (2015). Alpha-synuclein levels in blood plasma decline with healthy aging. *PLoS One* 10:e0123444. doi: 10.1371/journal.pone.0123444

Kong, Y., Zhou, H., Feng, H., Zhuang, J., Wen, T., Zhang, C., et al. (2020). Elucidating the relationship between diabetes mellitus and Parkinson's disease using (18) F-FP-(+)-DTBZ, a positron-emission tomography probe for vesicular monoamine transporter 2. *Front. Neurosci.* 14:682.

Konig, A., Vicente Miranda, H., and Outeiro, T. F. (2018). Alpha-synuclein glycation and the action of anti-diabetic agents in Parkinson's disease. *J. Parkinsons Dis.* 8, 33–43. doi: 10.3233/JPD-171285

Kopytek, M., Zabczyk, M., Mazur, P., Undas, A., and Natorska, J. (2020). Accumulation of advanced glycation end products (AGEs) is associated with the severity of aortic stenosis in patients with concomitant type 2 diabetes. *Cardiovasc. Diabetol.* 19:92. doi: 10.3389/fnins.2020.00682

Kors, S., Geijtenbeek, K., Reits, E., and Schipper-Krom, S. (2019). Regulation of proteasome activity by (Post-)transcriptional mechanisms. *Front. Mol. Biosci.* 6:48. doi: 10.3389/fmolb.2019.00048

Kosten, J., Binolfi, A., Stuiver, M., Verzini, S., Theillet, F. X., Bekei, B., et al. (2014). Efficient modification of alpha-synuclein serine 129 by protein kinase CK1 requires phosphorylation of tyrosine 125 as a priming event. *ACS Chem. Neurosci.* 5, 1203–1208. doi: 10.1021/cn5002254

Krumova, P., Meulmeester, E., Garrido, M., Tirard, M., Hsiao, H. H., Bossis, G., et al. (2011). Sumoylation inhibits alpha-synuclein aggregation and toxicity. *J. Cell Biol.* 194, 49–60. doi: 10.1083/jcb.201010117

Kulkarni, A. S., Burns, M. R., Brundin, P., and Wesson, D. W. (2022). Linking alpha-synuclein-induced synaptopathy and neural network dysfunction in early Parkinson's disease. *Brain Commun.* 4:fcac165. doi: 10.1093/braincomms/fcac165

Kumari, P., Ghosh, D., Vanas, A., Fleischmann, Y., Wiegand, T., Jeschke, G., et al. (2021). Structural insights into alpha-synuclein monomer-fibril interactions. *Proc. Natl. Acad. Sci. U. S. A.* 118:e2012171118. doi: 10.1073/pnas.2012171118

Kunz, D., and Bes, F. (1999). Melatonin as a therapy in REM sleep behavior disorder patients: an open-labeled pilot study on the possible influence of melatonin on REM-sleep regulation. *Mov. Disord.* 14, 507–511. doi: 10.1002/1531-8257(199905)14:3<507::AID-MDS1021>3.0.CO;2-8

Kunz, D., Mahlberg, R., Muller, C., Tilmann, A., and Bes, F. (2004). Melatonin in patients with reduced REM sleep duration: two randomized controlled trials. *J. Clin. Endocrinol. Metab.* 89, 128–134. doi: 10.1210/jc.2002-021057

Landeck, N., Hall, H., Ardah, M. T., Majbour, N. K., El-Agnaf, O. M., Halliday, G., et al. (2016). A novel multiplex assay for simultaneous quantification of total and S129 phosphorylated human alpha-synuclein. *Mol. Neurodegener.* 11:61. doi: 10.1186/s13024-016-0125-0

Lashuel, H. A. (2021). Rethinking protein aggregation and drug discovery in neurodegenerative diseases: why we need to embrace complexity? *Curr. Opin. Chem. Biol.* 64, 67–75. doi: 10.1016/j.cbpa.2021.05.006

Lavedan, C. (1998). The synuclein family. *Genome Res.* 8, 871–880. doi: 10.1101/gr.8.9.871

Lee, J. T., Wheeler, T. C., Li, L., and Chin, L. S. (2008). Ubiquitination of alpha-synuclein by Siah-1 promotes alpha-synuclein aggregation and apoptotic cell death. *Hum. Mol. Genet.* 17, 906–917. doi: 10.1093/hmg/ddm363

Leite, K., Garg, P., Spitzner, F. P., Guerin Darvas, S., Bahr, M., Priesemann, V., et al. (2022). Alpha-synuclein impacts on intrinsic neuronal network activity through reduced levels of cyclic AMP and diminished numbers of active presynaptic terminals. *Front. Mol. Neurosci.* 15:868790. doi: 10.3389/fnmol.2022.868790

Lemos, M., and Stefanova, N. (2020). Histone deacetylase 6 and the disease mechanisms of alpha-synucleinopathies. *Front. Synaptic. Neurosci.* 12:586453. doi: 10.3389/fnsyn.2020.586453

Levine, P. M., De Leon, C. A., Galesic, A., Balana, A., Marotta, N. P., Lewis, Y. E., et al. (2017). O-GlcNAc modification inhibits the calpain-mediated cleavage of alpha-synuclein. *Bioorg. Med. Chem.* 25, 4977–4982. doi: 10.1016/j.bmc.2017.04.038

Levine, P. M., Galesic, A., Balana, A. T., Mahul-Mellier, A. L., Navarro, M. X., De Leon, C. A., et al. (2019). Alpha-synuclein O-GlcNAcylation alters aggregation and toxicity, revealing certain residues as potential inhibitors of Parkinson's disease. *Proc. Natl. Acad. Sci. U. S. A.* 116, 1511–1519. doi: 10.1073/pnas.1808845116

Lewis, Y. E., Galesic, A., Levine, P. M., De Leon, C. A., Lamiri, N., Brennan, C. K., et al. (2017). O-GlcNAcylation of alpha-synuclein at serine 87 reduces aggregation without affecting membrane binding. *ACS Chem. Biol.* 12, 1020–1027. doi: 10.1021/acschembio.7b00113

Li, B., Wang, X., Rasheed, N., Hu, Y., Boast, S., Ishii, T., et al. (2004). Distinct roles of c-Abl and Atm in oxidative stress response are mediated by protein kinase C delta. *Genes Dev.* 18, 1824–1837. doi: 10.1101/gad.1223504

Li, S., and Pelletier, G. (1995). Effects of pinealectomy and melatonin on gonadotropin-releasing hormone (GnRH) gene expression in the male rat brain. *Endocrine* 3, 533–536. doi: 10.1007/BF02738829

Li, X. Y., Li, W., Li, X., Li, X. R., Sun, L., Yang, W., et al. (2021). Alterations of erythrocytic phosphorylated alpha-synuclein in different subtypes and stages of Parkinson's disease. *Front. Aging Neurosci.* 13:623977. doi: 10.3389/fnagi.2021.623977

Li, X. Y., Yang, W., Li, X., Li, X. R., Li, W., Song, Q., et al. (2020). Phosphorylated alpha-synuclein in red blood cells as a potential diagnostic biomarker for multiple system atrophy: a pilot study. *Parkinsons Dis.* 2020:8740419. doi: 10.1155/2020/8740419

Lin, T. K., Lin, K. J., Lin, H. Y., Lin, K. L., Lan, M. Y., Wang, P. W., et al. (2021). Glucagon-Like Peptide-1 Receptor Agonist Ameliorates 1-Methyl-4-Phenyl-1,2,3,6-Tetrahydropyridine (MPTP) Neurotoxicity Through Enhancing Mitophagy Flux and Reducing alpha-Synuclein and Oxidative Stress. *Front. Mol. Neurosci.* 14:697440. doi: 10.3389/fnmol.2021.697440

Lin, C. H., Liu, H. C., Yang, S. Y., Yang, K. C., Wu, C. C., and Chiu, M. J. (2019). Plasma pS129-alpha-synuclein is a surrogate biofluid marker of motor severity and progression in Parkinson's disease. *J. Clin. Med.* 8:1601. doi: 10.3390/jcm8101601

Liu, F., Iqbal, K., Grundke-Iqbal, I., Hart, G. W., and Gong, C. X. (2004a). O-GlcNAcylation regulates phosphorylation of tau: a mechanism involved in Alzheimer's disease. *Proc. Natl. Acad. Sci. U. S. A.* 101, 10804–10809. doi: 10.1073/pnas.0400348101

Liu, S., Fa, M., Ninan, I., Trinchese, F., Dauer, W., and Arancio, O. (2007). Alpha-synuclein involvement in hippocampal synaptic plasticity: role of NO, cGMP, cGK and CaMKII. *Eur. J. Neurosci.* 25, 3583–3596. doi: 10.1111/j.1460-9568.2007.05569.x

Liu, S., Ninan, I., Antonova, I., Battaglia, F., Trinchese, F., Narasanna, A., et al. (2004b). Alpha-synuclein produces a long-lasting increase in neurotransmitter release. *EMBO J.* 23, 4506–4516. doi: 10.1038/sj.emboj.7600451

Liu, W., Jalewa, J., Sharma, M., Li, G., Li, L., and Holscher, C. (2015). Neuroprotective effects of lixisenatide and liraglutide in the 1-methyl-4-phenyl-1,2,3,6-tetrahydropyridine mouse model of Parkinson's disease. *Neuroscience* 303, 42–50. doi: 10.1016/j.neuroscience.2015.06.054

Lokireddy, S., Kukushkin, N. V., and Goldberg, A. L. (2015). cAMP-induced phosphorylation of 26S proteasomes on Rpn6/PSMD11 enhances their activity and the degradation of misfolded proteins. *Proc. Natl. Acad. Sci. U. S. A.* 112, E7176–E7185. doi: 10.1073/pnas.1522332112

Longhena, F., Faustini, G., Missale, C., Pizzi, M., Spano, P., and Bellucci, A. (2017). The contribution of alpha-Synuclein spreading to Parkinson's Disease Synaptopathy. *Neural Plast.* 2017:5012129. doi: 10.1155/2017/5012129

Longhena, F., Faustini, G., Spillantini, M. G., and Bellucci, A. (2019). Living in promiscuity: the multiple Partners of alpha-synuclein at the synapse in physiology and pathology. *Int. J. Mol. Sci.* 20:141. doi: 10.3390/ijms20010141

Lopez-Burillo, S., Tan, D. X., Mayo, J. C., Sainz, R. M., Manchester, L. C., and Reiter, R. J. (2003). Melatonin, xanthurenic acid, resveratrol, EGCG, vitamin C and alpha-lipoic acid differentially reduce oxidative DNA damage induced by Fenton reagents: a study of their individual and synergistic actions. *J. Pineal Res.* 34, 269–277. doi: 10.1034/j.1600-079X.2003.00041.x

Lopez, L. C., Escames, G., Tapias, V., Utrilla, P., Leon, J., and Acuna-Castroviejo, D. (2006). Identification of an inducible nitric oxide synthase in diaphragm mitochondria from septic mice: its relation with mitochondrial dysfunction and prevention by melatonin. *Int. J. Biochem. Cell Biol.* 38, 267–278. doi: 10.1016/j.biocel.2005.09.008

Ludtmann, M. H., Angelova, P. R., Ninkina, N. N., Gandhi, S., Buchman, V. L., and Abramov, A. Y. (2016). Monomeric alpha-synuclein exerts a physiological role on brain ATP synthase. *J. Neurosci.* 36, 10510–10521. doi: 10.1523/JNEUROSCI.1659-16.2016

Lundblad, M., Decressac, M., Mattsson, B., and Bjorklund, A. (2012). Impaired neurotransmission caused by overexpression of alpha-synuclein in nigral dopamine neurons. *Proc. Natl. Acad. Sci. U. S. A.* 109, 3213–3219. doi: 10.1073/pnas.1200575109

Ma, Q. L., Chan, P., Yoshii, M., and Ueda, K. (2003). Alpha-synuclein aggregation and neurodegenerative diseases. *J. Alzheimers Dis.* 5, 139–148. doi: 10.3233/JAD-2003-5208

Maass, F., Rikker, S., Dambeck, V., Warth, C., Tatenhorst, L., Csoti, I., et al. (2020). Increased alpha-synuclein tear fluid levels in patients with Parkinson's disease. *Sci. Rep.* 10:8507. doi: 10.1038/s41598-020-65503-1

Magalhaes, P., and Lashuel, H. A. (2022). Opportunities and challenges of alpha-synuclein as a potential biomarker for Parkinson's disease and other synucleinopathies. *NPJ Parkinsons Dis.* 8:93. doi: 10.1038/s41531-022-00357-0

Magistretti, P. J., and Pellerin, L. (1996). Cellular mechanisms of brain energy metabolism. Relevance to functional brain imaging and to neurodegenerative disorders. *Ann. N. Y. Acad. Sci.* 777, 380–387.

Mahul-Mellier, A. L., Fauvet, B., Gysbers, A., Dikiy, I., Oueslati, A., Georgeon, S., et al. (2014). C-Abl phosphorylates alpha-synuclein and regulates its degradation: implication for alpha-synuclein clearance and contribution to the pathogenesis of Parkinson's disease. *Hum. Mol. Genet.* 23, 2858–2879. doi: 10.1093/hmg/ddt674

Majbour, N. K., Vaikath, N. N., Eusebi, P., Chiasserini, D., Ardah, M., Varghese, S., et al. (2016a). Longitudinal changes in CSF alpha-synuclein species reflect Parkinson's disease progression. *Mov. Disord.* 31, 1535–1542. doi: 10.1002/mds.26754

Majbour, N. K., Vaikath, N. N., Van Dijk, K. D., Ardah, M. T., Varghese, S., Vesterager, L. B., et al. (2016b). Oligomeric and phosphorylated alpha-synuclein as potential CSF biomarkers for Parkinson's disease. *Mol. Neurodegener.* 11:7. doi: 10.1186/s13024-016-0072-9

Malek, N., Swallow, D., Grosset, K. A., Anichtchik, O., Spillantini, M., and Grosset, D. G. (2014). Alpha-synuclein in peripheral tissues and body fluids as a biomarker for Parkinson's disease - a systematic review. *Acta Neurol. Scand.* 130, 59–72. doi: 10.1111/ane.12247

Mandhane, S., Soni, D., Jani, K., Sengupta, P., Patel, A., Bambal, R., et al. (2019). K0706, a potent orally bioavailable brain-penetrating selective inhibitor of cABL protein tyrosine kinase, exhibits neuroprotective activity in preclinical models of Parkinson's disease [online] Available at: https://www.mdsabstracts.org/abstract/k0706-a-potent-orally-bioavailable-brain-penetrating-selective-inhibitor-of-cabl-protein-tyrosine-kinase-exhibits-neuroprotective-activity-in-preclinical-models-of-parkinsons-disease/ [Accessed May 3, 2023].

Mann, V. M., Cooper, J. M., Daniel, S. E., Srai, K., Jenner, P., Marsden, C. D., et al. (1994). Complex I, iron, and ferritin in Parkinson's disease substantia nigra. *Ann. Neurol.* 36, 876–881. doi: 10.1002/ana.410360612

Manzanza, N. O., Sedlackova, L., and Kalaria, R. N. (2021). Alpha-synuclein post-translational modifications: implications for pathogenesis of Lewy body disorders. *Front. Aging Neurosci.* 13:690293. doi: 10.3389/fnagi.2021.690293

Marotta, N. P., Lin, Y. H., Lewis, Y. E., Ambroso, M. R., Zaro, B. W., Roth, M. T., et al. (2015). O-GlcNAc modification blocks the aggregation and toxicity of the protein alpha-synuclein associated with Parkinson's disease. *Nat. Chem.* 7, 913–920. doi: 10.1038/nchem.2361

Maroui, M. A., Maarifi, G., Mcmanus, F. P., Lamoliatte, F., Thibault, P., and Chelbi-Alix, M. K. (2018). Promyelocytic leukemia protein (PML) requirement for interferon-induced global cellular SUMOylation. *Mol. Cell. Proteomics* 17, 1196–1208. doi: 10.1074/mcp.RA117.000447

Masato, A., Plotegher, N., Terrin, F., Sandre, M., Faustini, G., Thor, A., et al. (2023). DOPAL initiates alphaSynuclein-dependent impaired proteostasis and degeneration of neuronal projections in Parkinson's disease. *NPJ Parkinsons Dis.* 9:42. doi: 10.1038/s41531-023-00485-1

Matsubara, T. (1991). Interleukin 6 activities and tumor necrosis factor-alpha levels in serum of patients with Kawasaki disease. *Arerugi* 40, 147–154.

Matsura, T. (2019). Protective effect of tocotrienol on in vitro and in vivo models of Parkinson's disease. *J. Nutr. Sci. Vitaminol. (Tokyo)* 65, S51–S53. doi: 10.3177/jnsv.65.S51

Matunis, M. J., Coutavas, E., and Blobel, G. (1996). A novel ubiquitin-like modification modulates the partitioning of the ran-GTPase-activating protein RanGAP1 between the cytosol and the nuclear pore complex. *J. Cell Biol.* 135, 1457–1470. doi: 10.1083/jcb.135.6.1457

Maxwell, M. M., Tomkinson, E. M., Nobles, J., Wizeman, J. W., Amore, A. M., Quinti, L., et al. (2011). The Sirtuin 2 microtubule deacetylase is an abundant neuronal protein that accumulates in the aging CNS. *Hum. Mol. Genet.* 20, 3986–3996. doi: 10.1093/hmg/ddr326

Mayeux, R. (2004). Biomarkers: potential uses and limitations. *NeuroRx* 1, 182–188. doi: 10.1602/neurorx.1.2.182

Mazzocchi, M., Goulding, S. R., Wyatt, S. L., Collins, L. M., Sullivan, A. M., and O'keeffe, G. W. (2021). LMK235, a small molecule inhibitor of HDAC4/5, protects dopaminergic neurons against neurotoxin-and alpha-synuclein-induced degeneration in cellular models of Parkinson's disease. *Mol. Cell. Neurosci.* 115:103642. doi: 10.1016/j.mcn.2021.103642

Mbefo, M. K., Paleologou, K. E., Boucharaba, A., Oueslati, A., Schell, H., Fournier, M., et al. (2010). Phosphorylation of synucleins by members of the polo-like kinase family. *J. Biol. Chem.* 285, 2807–2822. doi: 10.1074/jbc.M109.081950

Medeiros, A. T., Soll, L. G., Tessari, I., Bubacco, L., and Morgan, J. R. (2017). Alpha-synuclein dimers impair vesicle fission during clathrin-mediated synaptic vesicle recycling. *Front. Cell. Neurosci.* 11:388. doi: 10.3389/fncel.2017.00388

Mehdi, S. J., Rosas-Hernandez, H., Cuevas, E., Lantz, S. M., Barger, S. W., Sarkar, S., et al. (2016). Protein kinases and Parkinson's disease. *Int. J. Mol. Sci.* 17:1585. doi: 10.3390/ijms17091585

Mehmel, M., Jovanovic, N., and Spitz, U. (2020). Nicotinamide Riboside-the current state of research and therapeutic uses. *Nutrients* 12:1616. doi: 10.3390/nu12061616

Mehringer, J., Navarro, J. A., Touraud, D., Schneuwly, S., and Kunz, W. (2022). Phosphorylated resveratrol as a protein aggregation suppressor in vitro and in vivo. *RSC Chem. Biol.* 3, 250–260. doi: 10.1039/D1CB00220A

Menges, S., Minakaki, G., Schaefer, P. M., Meixner, H., Prots, I., Schlotzer-Schrehardt, U., et al. (2017). Alpha-synuclein prevents the formation of spherical mitochondria and apoptosis under oxidative stress. *Sci. Rep.* 7:42942. doi: 10.1038/srep42942

Menke, T., Gille, G., Reber, F., Janetzky, B., Andler, W., Funk, R. H., et al. (2003). Coenzyme Q10 reduces the toxicity of rotenone in neuronal cultures by preserving the mitochondrial membrane potential. *Biofactors* 18, 65–72. doi: 10.1002/biof.5520180208

Miyake, Y., Fukushima, W., Tanaka, K., Sasaki, S., Kiyohara, C., Tsuboi, Y., et al. (2011). Dietary intake of antioxidant vitamins and risk of Parkinson's disease: a case-control study in Japan. *Eur. J. Neurol.* 18, 106–113. doi: 10.1111/j.1468-1331.2010.03088.x

Molina, J. A., De Bustos, F., Ortiz, S., Del Ser, T., Seijo, M., Benito-Leon, J., et al. (2002). Serum levels of coenzyme Q in patients with Lewy body disease. *J. Neural Transm. (Vienna)* 109, 1195–1201. doi: 10.1007/s00702-001-0761-5

Mollenhauer, B., Batrla, R., El-Agnaf, O., Galasko, D. R., Lashuel, H. A., Merchant, K. M., et al. (2017). A user's guide for alpha-synuclein biomarker studies in biological fluids: Perianalytical considerations. *Mov. Disord.* 32, 1117–1130. doi: 10.1002/mds.27090

Mollenhauer, B., Trautmann, E., Taylor, P., Manninger, P., Sixel-Doring, F., Ebentheuer, J., et al. (2013). Total CSF alpha-synuclein is lower in de novo Parkinson patients than in healthy subjects. *Neurosci. Lett.* 532, 44–48. doi: 10.1016/j.neulet.2012.11.004

Montenegro, L., Turnaturi, R., Parenti, C., and Pasquinucci, L. (2018). Idebenone: novel strategies to improve its systemic and local efficacy. *Nanomaterials* 8:87. doi: 10.3390/nano8020087

Monti, D. A., Zabrecky, G., Kremens, D., Liang, T. W., Wintering, N. A., Cai, J., et al. (2016). N-acetyl cysteine may support dopamine neurons in Parkinson's disease: preliminary clinical and cell line data. *PLoS One* 11:e0157602. doi: 10.1371/journal.pone.0157602

Moore, D. J., West, A. B., Dawson, V. L., and Dawson, T. M. (2005). Molecular pathophysiology of Parkinson's disease. *Annu. Rev. Neurosci.* 28, 57–87. doi: 10.1146/annurev.neuro.28.061604.135718

Morens, D. M., Grandinetti, A., Waslien, C. I., Park, C. B., Ross, G. W., and White, L. R. (1996). Case-control study of idiopathic Parkinson's disease and dietary vitamin E intake. *Neurology* 46, 1270–1274. doi: 10.1212/WNL.46.5.1270

Mosley, R. L., Benner, E. J., Kadiu, I., Thomas, M., Boska, M. D., Hasan, K., et al. (2006). Neuroinflammation, oxidative stress and the pathogenesis of Parkinson's Disease. *Clin. Neurosci. Res.* 6, 261–281. doi: 10.1016/j.cnr.2006.09.006

Muller, S., Hoege, C., Pyrowolakis, G., and Jentsch, S. (2001). SUMO, ubiquitin's mysterious cousin. *Nat. Rev. Mol. Cell Biol.* 2, 202–210. doi: 10.1038/35056591

Munch, G., Luth, H. J., Wong, A., Arendt, T., Hirsch, E., Ravid, R., et al. (2000). Crosslinking of alpha-synuclein by advanced glycation endproducts--an early pathophysiological step in Lewy body formation? *J. Chem. Neuroanat.* 20, 253–257. doi: 10.1016/S0891-0618(00)00096-X

Nakamura, T., Yamashita, H., Takahashi, T., and Nakamura, S. (2001). Activated Fyn phosphorylates alpha-synuclein at tyrosine residue 125. *Biochem. Biophys. Res. Commun.* 280, 1085–1092. doi: 10.1006/bbrc.2000.4253

Nassar, N. N., Al-Shorbagy, M. Y., Arab, H. H., and Abdallah, D. M. (2015). Saxagliptin: a novel antiparkinsonian approach. *Neuropharmacology* 89, 308–317. doi: 10.1016/j.neuropharm.2014.10.007

Nauck, M. A., and Meier, J. J. (2018). Incretin hormones: their role in health and disease. *Diabetes Obes. Metab.* 20, 5–21. doi: 10.1111/dom.13129

Naylor, S. (2003). Biomarkers: current perspectives and future prospects. *Expert. Rev. Mol. Diagn.* 3, 525–529. doi: 10.1586/14737159.3.5.525

Negro, A., Brunati, A. M., Donella-Deana, A., Massimino, M. L., and Pinna, L. A. (2002). Multiple phosphorylation of alpha-synuclein by protein tyrosine kinase Syk prevents eosin-induced aggregation. *FASEB J.* 16, 210–212. doi: 10.1096/fj.01-0517fje

Ohrfelt, A., Zetterberg, H., Andersson, K., Persson, R., Secic, D., Brinkmalm, G., et al. (2011). Identification of novel alpha-synuclein isoforms in human brain tissue by using an online nanoLC-ESI-FTICR-MS method. *Neurochem. Res.* 36, 2029–2042. doi: 10.1007/s11064-011-0527-x

Okochi, M., Walter, J., Koyama, A., Nakajo, S., Baba, M., Iwatsubo, T., et al. (2000). Constitutive phosphorylation of the Parkinson's disease associated alpha-synuclein. *J. Biol. Chem.* 275, 390–397. doi: 10.1074/jbc.275.1.390

Oliveira, L. M. A., Gasser, T., Edwards, R., Zweckstetter, M., Melki, R., Stefanis, L., et al. (2021). Alpha-synuclein research: defining strategic moves in the battle against Parkinson's disease. *NPJ Parkinsons Dis.* 7:65. doi: 10.1038/s41531-021-00203-9

Ono, K., and Yamada, M. (2007). Vitamin a potently destabilizes preformed alpha-synuclein fibrils in vitro: implications for Lewy body diseases. *Neurobiol. Dis.* 25, 446–454. doi: 10.1016/j.nbd.2006.10.010

Ono, K., Yoshiike, Y., Takashima, A., Hasegawa, K., Naiki, H., and Yamada, M. (2004). Vitamin a exhibits potent antiamyloidogenic and fibril-destabilizing effects in vitro. *Exp. Neurol.* 189, 380–392. doi: 10.1016/j.expneurol.2004.05.035

Orsucci, D., Mancuso, M., Ienco, E. C., Logerfo, A., and Siciliano, G. (2011). Targeting mitochondrial dysfunction and neurodegeneration by means of coenzyme Q10 and its analogues. *Curr. Med. Chem.* 18, 4053–4064. doi: 10.2174/092986711796957257

Oueslati, A., Fournier, M., and Lashuel, H. A. (2010). Role of post-translational modifications in modulating the structure, function and toxicity of alpha-synuclein: implications for Parkinson's disease pathogenesis and therapies. *Prog. Brain Res.* 183, 115–145. doi: 10.1016/S0079-6123(10)83007-9

Oueslati, A., Paleologou, K. E., Schneider, B. L., Aebischer, P., and Lashuel, H. A. (2012). Mimicking phosphorylation at serine 87 inhibits the aggregation of human alpha-synuclein and protects against its toxicity in a rat model of Parkinson's disease. *J. Neurosci.* 32, 1536–1544. doi: 10.1523/JNEUROSCI.3784-11.2012

Oueslati, A., Schneider, B. L., Aebischer, P., and Lashuel, H. A. (2013). Polo-like kinase 2 regulates selective autophagic alpha-synuclein clearance and suppresses its toxicity in vivo. *Proc. Natl. Acad. Sci. U. S. A.* 110, E3945–E3954. doi: 10.1073/pnas.1309991110

Outeiro, T. F., Kontopoulos, E., Altmann, S. M., Kufareva, I., Strathearn, K. E., Amore, A. M., et al. (2007). Sirtuin 2 inhibitors rescue alpha-synuclein-mediated toxicity in models of Parkinson's disease. *Science* 317, 516–519. doi: 10.1126/science.1143780

Pagan, F., Hebron, M., Valadez, E. H., Torres-Yaghi, Y., Huang, X., Mills, R. R., et al. (2016). Nilotinib effects in Parkinson's disease and dementia with Lewy bodies. *J. Parkinsons Dis.* 6, 503–517. doi: 10.3233/JPD-160867

Pagan, F. L., Hebron, M. L., Wilmarth, B., Torres-Yaghi, Y., Lawler, A., Mundel, E. E., et al. (2020). Nilotinib effects on safety, tolerability, and potential biomarkers in Parkinson Disease: a phase 2 randomized clinical trial. *JAMA Neurol.* 77, 309–317. doi: 10.1001/jamaneurol.2019.4200

Pagan, F. L., Hebron, M. L., Wilmarth, B., Torres-Yaghi, Y., Lawler, A., Mundel, E. E., et al. (2019). Pharmacokinetics and pharmacodynamics of a single dose Nilotinib in individuals with Parkinson's disease. *Pharmacol. Res. Perspect.* 7:e00470. doi: 10.1002/prp2.470

Paik, S. R., Shin, H. J., Lee, J. H., Chang, C. S., and Kim, J. (1999). Copper(II)-induced self-oligomerization of alpha-synuclein. *Biochem. J.* 340, 821–828.

Paleologou, K. E., Oueslati, A., Shakked, G., Rospigliosi, C. C., Kim, H. Y., Lamberto, G. R., et al. (2010). Phosphorylation at S87 is enhanced in synucleinopathies, inhibits alpha-synuclein oligomerization, and influences synuclein-membrane interactions. *J. Neurosci.* 30, 3184–3198. doi: 10.1523/JNEUROSCI.5922-09.2010

Palleria, C., Leo, A., Andreozzi, F., Citraro, R., Iannone, M., Spiga, R., et al. (2017). Liraglutide prevents cognitive decline in a rat model of streptozotocin-induced diabetes independently from its peripheral metabolic effects. *Behav. Brain Res.* 321, 157–169. doi: 10.1016/j.bbr.2017.01.004

Parekh, P., Sharma, N., Sharma, M., Gadepalli, A., Sayyed, A. A., Chatterjee, S., et al. (2022). AMPK-dependent autophagy activation and alpha-synuclein clearance: a putative mechanism behind alpha-mangostin's neuroprotection in a rotenone-induced mouse model of Parkinson's disease. *Metab. Brain Dis.* 37, 2853–2870. doi: 10.1007/s11011-022-01087-1

Park, G., Tan, J., Garcia, G., Kang, Y., Salvesen, G., and Zhang, Z. (2016). Regulation of histone acetylation by autophagy in Parkinson disease. *J. Biol. Chem.* 291, 3531–3540. doi: 10.1074/jbc.M115.675488

Parkinson Study GroupBeal, M. F., Oakes, D., Shoulson, I., Henchcliffe, C., Galpern, W. R., et al. (2014). A randomized clinical trial of high-dosage coenzyme Q10 in early Parkinson disease: no evidence of benefit. *JAMA Neurol.* 71, 543–552. doi: 10.1001/jamaneurol.2014.131

Parnetti, L., Gaetani, L., Eusebi, P., Paciotti, S., Hansson, O., El-Agnaf, O., et al. (2019). CSF and blood biomarkers for Parkinson's disease. *Lancet Neurol.* 18, 573–586. doi: 10.1016/S1474-4422(19)30024-9

Paxinou, E., Chen, Q., Weisse, M., Giasson, B. I., Norris, E. H., Rueter, S. M., et al. (2001). Induction of alpha-synuclein aggregation by intracellular nitrative insult. *J. Neurosci.* 21, 8053–8061. doi: 10.1523/JNEUROSCI.21-20-08053.2001

Pearson, K. J., Baur, J. A., Lewis, K. N., Peshkin, L., Price, N. L., Labinskyy, N., et al. (2008). Resveratrol delays age-related deterioration and mimics transcriptional aspects of dietary restriction without extending life span. *Cell Metab.* 8, 157–168. doi: 10.1016/j.cmet.2008.06.011

Percario, S., Da Silva Barbosa, A., Varela, E. L. P., Gomes, A. R. Q., Ferreira, M. E. S., Moreira, D. N. A., et al. (2020). Oxidative stress in Parkinson's Disease: potential benefits of antioxidant supplementation. *Oxidative Med. Cell. Longev.* 2020:2360872. doi: 10.1155/2020/2360872

Permanne, B., Sand, A., Ousson, S., Neny, M., Hantson, J., Schubert, R., et al. (2022). O-GlcNAcase inhibitor ASN90 is a multimodal drug candidate for Tau and alpha-synuclein proteinopathies. *ACS Chem. Neurosci.* 13, 1296–1314. doi: 10.1021/acschemneuro.2c00057

Petricca, L., Chiki, N., Hanna-El-Daher, L., Aeschbach, L., Burai, R., Stoops, E., et al. (2022). Comparative analysis of Total alpha-synuclein (alphaSYN) immunoassays reveals that they do not capture the diversity of modified alphaSYN proteoforms. *J. Parkinsons Dis.* 12, 1449–1462. doi: 10.3233/JPD-223285

Pfeiffer, R. F. (2016). Non-motor symptoms in Parkinson's disease. *Parkinsonism Relat. Disord.* 22, S119–S122. doi: 10.1016/j.parkreldis.2015.09.004

Picca, A., Guerra, F., Calvani, R., Marini, F., Biancolillo, A., Landi, G., et al. (2020). Mitochondrial signatures in circulating extracellular vesicles of older adults with Parkinson's disease: results from the EXosomes in PArkiNson's disease (EXPAND) study. *J. Clin. Med.* 9:504. doi: 10.3390/jcm9020504

Ping, F., Jiang, N., and Li, Y. (2020). Association between metformin and neurodegenerative diseases of observational studies: systematic review and meta-analysis. *BMJ Open Diabetes Res. Care* 8:e001370. doi: 10.1136/bmjdrc-2020-001370

Pinho, B. R., Reis, S. D., Guedes-Dias, P., Leitao-Rocha, A., Quintas, C., Valentao, P., et al. (2016). Pharmacological modulation of HDAC1 and HDAC6 in vivo in a zebrafish model: therapeutic implications for Parkinson's disease. *Pharmacol. Res.* 103, 328–339. doi: 10.1016/j.phrs.2015.11.024

Pissadaki, E. K., and Bolam, J. P. (2013). The energy cost of action potential propagation in dopamine neurons: clues to susceptibility in Parkinson's disease. *Front. Comput. Neurosci.* 7:13. doi: 10.3389/fncom.2013.00013

Pouclet, H., Lebouvier, T., Coron, E., Rouaud, T., Flamant, M., Toulgoat, F., et al. (2012). Analysis of colonic alpha-synuclein pathology in multiple system atrophy. *Parkinsonism Relat. Disord.* 18, 893–895. doi: 10.1016/j.parkreldis.2012.04.020

Prickaerts, J., Heckman, P. R. A., and Blokland, A. (2017). Investigational phosphodiesterase inhibitors in phase I and phase II clinical trials for Alzheimer's disease. *Expert Opin. Investig. Drugs* 26, 1033–1048. doi: 10.1080/13543784.2017.1364360

Pronin, A. N., Morris, A. J., Surguchov, A., and Benovic, J. L. (2000). Synucleins are a novel class of substrates for G protein-coupled receptor kinases. *J. Biol. Chem.* 275, 26515–26522. doi: 10.1074/jbc.M003542200

Qing, H., Wong, W., Mcgeer, E. G., and Mcgeer, P. L. (2009a). Lrrk2 phosphorylates alpha synuclein at serine 129: Parkinson disease implications. *Biochem. Biophys. Res. Commun.* 387, 149–152. doi: 10.1016/j.bbrc.2009.06.142

Qing, H., Zhang, Y., Deng, Y., Mcgeer, E. G., and Mcgeer, P. L. (2009b). Lrrk2 interaction with alpha-synuclein in diffuse Lewy body disease. *Biochem. Biophys. Res. Commun.* 390, 1229–1234. doi: 10.1016/j.bbrc.2009.10.126

Qualman, S. J., Haupt, H. M., Yang, P., and Hamilton, S. R. (1984). Esophageal Lewy bodies associated with ganglion cell loss in achalasia. Similarity to Parkinson's disease. *Gastroenterology* 87, 848–856. doi: 10.1016/0016-5085(84)90079-9

Quastel, J. H., and Wheatley, A. H. (1932). Oxidations by the brain. *Biochem. J.* 26, 725–744. doi: 10.1042/bj0260725

Rampersaud, N., Harkavyi, A., Giordano, G., Lever, R., WhittON, J., and WHitton, P. (2012). Exendin-4 reverts behavioural and neurochemical dysfunction in a pre-motor rodent model of Parkinson's disease with noradrenergic deficit. *Br. J. Pharmacol.* 167, 1467–1479. doi: 10.1111/j.1476-5381.2012.02100.x

Rane, P., Shields, J., Heffernan, M., Guo, Y., Akbarian, S., and King, J. A. (2012). The histone deacetylase inhibitor, sodium butyrate, alleviates cognitive deficits in pre-motor stage PD. *Neuropharmacology* 62, 2409–2412. doi: 10.1016/j.neuropharm.2012.01.026

Rees, J. N., Florang, V. R., Eckert, L. L., and Doorn, J. A. (2009). Protein reactivity of 3,4-dihydroxyphenylacetaldehyde, a toxic dopamine metabolite, is dependent on both the aldehyde and the catechol. *Chem. Res. Toxicol.* 22, 1256–1263. doi: 10.1021/tx9000557

Reimer, L., Vesterager, L. B., Betzer, C., Zheng, J., Nielsen, L. D., Kofoed, R. H., et al. (2018). Inflammation kinase PKR phosphorylates alpha-synuclein and causes alpha-synuclein-dependent cell death. *Neurobiol. Dis.* 115, 17–28. doi: 10.1016/j.nbd.2018.03.001

Reiter, R. J., Paredes, S. D., Korkmaz, A., Jou, M. J., and Tan, D. X. (2008). Melatonin combats molecular terrorism at the mitochondrial level. *Interdiscip. Toxicol.* 1, 137–149. doi: 10.2478/v10102-010-0030-2

Reiter, R. J., Sainz, R. M., Lopez-Burillo, S., Mayo, J. C., Manchester, L. C., and Tan, D. X. (2003). Melatonin ameliorates neurologic damage and neurophysiologic deficits in experimental models of stroke. *Ann. N. Y. Acad. Sci.* 993, 35–47. discussion 48-53. doi: 10.1111/j.1749-6632.2003.tb07509.x

Reiter, R. J., Tan, D. X., and Allegra, M. (2002a). Melatonin: reducing molecular pathology and dysfunction due to free radicals and associated reactants. *Neuro Endocrinol. Lett.* 23, 3–8.

Reiter, R. J., Tan, D. X., and Burkhardt, S. (2002b). Reactive oxygen and nitrogen species and cellular and organismal decline: amelioration with melatonin. *Mech. Ageing Dev.* 123, 1007–1019. doi: 10.1016/s0047-6374(01)00384-0

Reiter, R. J., Tan, D. X., Leon, J., Kilic, U., and Kilic, E. (2005). When melatonin gets on your nerves: its beneficial actions in experimental models of stroke. *Exp. Biol. Med.* 230, 104–117. doi: 10.1177/153537020523000205

Rey, N. L., George, S., and Brundin, P. (2016a). Review: spreading the word: precise animal models and validated methods are vital when evaluating prion-like behaviour of alpha-synuclein. *Neuropathol. Appl. Neurobiol.* 42, 51–76. doi: 10.1111/nan.12299

Rey, N. L., George, S., Steiner, J. A., Madaj, Z., Luk, K. C., Trojanowski, J. Q., et al. (2018). Spread of aggregates after olfactory bulb injection of alpha-synuclein fibrils is

associated with early neuronal loss and is reduced long term. *Acta Neuropathol.* 135, 65–83. doi: 10.1007/s00401-017-1792-9

Rey, N. L., Steiner, J. A., Maroof, N., Luk, K. C., Madaj, Z., Trojanowski, J. Q., et al. (2016b). Widespread transneuronal propagation of alpha-synucleinopathy triggered in olfactory bulb mimics prodromal Parkinson's disease. *J. Exp. Med.* 213, 1759–1778. doi: 10.1084/jem.20160368

Richter-Landsberg, C., and Leyk, J. (2013). Inclusion body formation, macroautophagy, and the role of HDAC6 in neurodegeneration. *Acta Neuropathol.* 126, 793–807. doi: 10.1007/s00401-013-1158-x

Risiglione, P., Zinghirino, F., Di Rosa, M. C., Magri, A., and Messina, A. (2021). Alpha-Synuclein and mitochondrial dysfunction in Parkinson's disease: the emerging role of VDAC. *Biomol. Ther.* 11:718. doi: 10.3390/biom11050718

Rodriguez, C., Mayo, J. C., Sainz, R. M., Antolin, I., Herrera, F., Martin, V., et al. (2004). Regulation of antioxidant enzymes: a significant role for melatonin. *J. Pineal Res.* 36, 1–9. doi: 10.1046/j.1600-079X.2003.00092.x

Rodriguez, M. I., Escames, G., Lopez, L. C., Lopez, A., Garcia, J. A., Ortiz, F., et al. (2007). Chronic melatonin treatment reduces the age-dependent inflammatory process in senescence-accelerated mice. *J. Pineal Res.* 42, 272–279. doi: 10.1111/j.1600-079X.2006.00416.x

Ross, C. A., and Pickart, C. M. (2004). The ubiquitin-proteasome pathway in Parkinson's disease and other neurodegenerative diseases. *Trends Cell Biol.* 14, 703–711. doi: 10.1016/j.tcb.2004.10.006

Rott, R., Szargel, R., Haskin, J., Shani, V., Shainskaya, A., Manov, I., et al. (2008). Monoubiquitylation of alpha-synuclein by seven in absentia homolog (SIAH) promotes its aggregation in dopaminergic cells. *J. Biol. Chem.* 283, 3316–3328. doi: 10.1074/jbc.M704809200

Rott, R., Szargel, R., Shani, V., Hamza, H., Savyon, M., Abd Elghani, F., et al. (2017). SUMOylation and ubiquitination reciprocally regulate alpha-synuclein degradation and pathological aggregation. *Proc. Natl. Acad. Sci. U. S. A.* 114, 13176–13181. doi: 10.1073/pnas.1704351114

Rousseaux, M. W., Revelli, J. P., Vazquez-Velez, G. E., Kim, J. Y., Craigen, E., Gonzales, K., et al. (2018). Depleting Trim28 in adult mice is well tolerated and reduces levels of alpha-synuclein and tau. *elife* 7:e36768. doi: 10.7554/eLife.36768

Ryan, B. J., Lourenco-Venda, L. L., Crabtree, M. J., Hale, A. B., Channon, K. M., and Wade-Martins, R. (2014). Alpha-synuclein and mitochondrial bioenergetics regulate tetrahydrobiopterin levels in a human dopaminergic model of Parkinson disease. *Free Radic. Biol. Med.* 67, 58–68. doi: 10.1016/j.freeradbiomed.2013.10.008

Ryu, Y. K., Go, J., Park, H. Y., Choi, Y. K., Seo, Y. J., Choi, J. H., et al. (2020). Metformin regulates astrocyte reactivity in Parkinson's disease and normal aging. *Neuropharmacology* 175:108173. doi: 10.1016/j.neuropharm.2020.108173

Sajja, R. K., Prasad, S., Tang, S., Kaisar, M. A., and Cucullo, L. (2017). Blood-brain barrier disruption in diabetic mice is linked to Nrf2 signaling deficits: role of ABCB10? *Neurosci. Lett.* 653, 152–158. doi: 10.1016/j.neulet.2017.05.059

Sakamoto, K. M., Kim, K. B., Kumagai, A., Mercurio, F., Crews, C. M., and Deshaies, R. J. (2001). Protacs: chimeric molecules that target proteins to the Skp1-Cullin-F box complex for ubiquitination and degradation. *Proc. Natl. Acad. Sci. U. S. A.* 98, 8554–8559. doi: 10.1073/pnas.141230798

Sanders, O., and Rajagopal, L. (2020). Phosphodiesterase inhibitors for Alzheimer's disease: a systematic review of clinical trials and epidemiology with a mechanistic rationale. *J. Alzheimers Dis. Rep.* 4, 185–215. doi: 10.3233/ADR-200191

Sato, K., Yamashita, T., Kurata, T., Lukic, V., Fukui, Y., Hishikawa, N., et al. (2014). Telmisartan reduces progressive oxidative stress and phosphorylated alpha-synuclein accumulation in stroke-resistant spontaneously hypertensive rats after transient middle cerebral artery occlusion. *J. Stroke Cerebrovasc. Dis.* 23, 1554–1563. doi: 10.1016/j.jstrokecerebrovasdis.2013.12.051

Satoh, A., and Imai, S. (2014). Systemic regulation of mammalian ageing and longevity by brain sirtuins. *Nat. Commun.* 5:4211. doi: 10.1038/ncomms5211

Savyon, M., and Engelender, S. (2020). SUMOylation in alpha-Synuclein homeostasis and pathology. *Front. Aging Neurosci.* 12:167. doi: 10.3389/fnagi.2020.00167

Sayin, V. I., Ibrahim, M. X., Larsson, E., Nilsson, J. A., Lindahl, P., and Bergo, M. O. (2014). Antioxidants accelerate lung cancer progression in mice. *Sci. Transl. Med.* 6:221ra15. doi: 10.1126/scitranslmed.3007653

Schapira, A. H. (2008). Mitochondrial dysfunction in neurodegenerative diseases. *Neurochem. Res.* 33, 2502–2509. doi: 10.1007/s11064-008-9855-x

Schapira, A. H., and Tolosa, E. (2010). Molecular and clinical prodrome of Parkinson disease: implications for treatment. *Nat. Rev. Neurol.* 6, 309–317. doi: 10.1038/nrneurol.2010.52

Scheider, W. L., Hershey, L. A., Vena, J. E., Holmlund, T., and Marshall, J. R.Freudenheim (1997). Dietary antioxidants and other dietary factors in the etiology of Parkinson's disease. *Mov. Disord.* 12, 190–196. doi: 10.1002/mds.870120209

Schepici, G., Bramanti, P., and Mazzon, E. (2020). Efficacy of sulforaphane in neurodegenerative diseases. *Int. J. Mol. Sci.* 21:8637. doi: 10.3390/ijms21228637

Schirinzi, T., Martella, G., Imbriani, P., Di Lazzaro, G., Franco, D., Colona, V. L., et al. (2019). Dietary vitamin E as a protective factor for Parkinson's disease: clinical and experimental evidence. *Front. Neurol.* 10:148. doi: 10.3389/fneur.2019.00148

Schmid, A. W., Fauvet, B., Moniatte, M., and Lashuel, H. A. (2013). Alpha-synuclein post-translational modifications as potential biomarkers for Parkinson disease and other synucleinopathies. *Mol. Cell. Proteomics* 12, 3543–3558. doi: 10.1074/mcp.R113.032730

Schneider, S. A., and Alcalay, R. N. (2017). Neuropathology of genetic synucleinopathies with parkinsonism: review of the literature. *Mov. Disord.* 32, 1504–1523. doi: 10.1002/mds.27193

Schondorf, D. C., Ivanyuk, D., Baden, P., Sanchez-Martinez, A., De Cicco, S., Yu, C., et al. (2018). The NAD+ precursor nicotinamide riboside rescues mitochondrial defects and neuronal loss in iPSC and Fly models of Parkinson's disease. *Cell Rep.* 23, 2976–2988. doi: 10.1016/j.celrep.2018.05.009

Selnick, H. G., Hess, J. F., Tang, C., Liu, K., Schachter, J. B., Ballard, J. E., et al. (2019). Discovery of MK-8719, a potent O-GlcNAcase inhibitor as a potential treatment for Tauopathies. *J. Med. Chem.* 62, 10062–10097. doi: 10.1021/acs.jmedchem.9b01090

Shabek, N., Herman-Bachinsky, Y., Buchsbaum, S., Lewinson, O., Haj-Yahya, M., Hejjaoui, M., et al. (2012). The size of the proteasomal substrate determines whether its degradation will be mediated by mono-or polyubiquitylation. *Mol. Cell* 48, 87–97. doi: 10.1016/j.molcel.2012.07.011

Shamsaldeen, Y. A., Mackenzie, L. S., Lione, L. A., and Benham, C. D. (2016). Methylglyoxal, a metabolite increased in diabetes is associated with insulin resistance, vascular dysfunction and neuropathies. *Curr. Drug Metab.* 17, 359–367. doi: 10.2174/1389200217666151222155216

Shannon, K. M., Keshavarzian, A., Mutlu, E., Dodiya, H. B., Daian, D., Jaglin, J. A., et al. (2012). Alpha-synuclein in colonic submucosa in early untreated Parkinson's disease. *Mov. Disord.* 27, 709–715. doi: 10.1002/mds.23838

Sharma, S., Taliyan, R., and Ramagiri, S. (2015a). Histone deacetylase inhibitor, trichostatin A, improves learning and memory in high-fat diet-induced cognitive deficits in mice. *J. Mol. Neurosci.* 56, 1–11. doi: 10.1007/s12031-014-0461-x

Sharma, S. K., Chorell, E., Steneberg, P., Vernersson-Lindahl, E., Edlund, H., and Wittung-Stafshede, P. (2015b). Insulin-degrading enzyme prevents alpha-synuclein fibril formation in a nonproteolytical manner. *Sci. Rep.* 5:12531. doi: 10.1038/srep12531

Sharma, S. K., Chorell, E., and Wittung-Stafshede, P. (2015c). Insulin-degrading enzyme is activated by the C-terminus of alpha-synuclein. *Biochem. Biophys. Res. Commun.* 466, 192–195. doi: 10.1016/j.bbrc.2015.09.002

Shavali, S., Carlson, E. C., Swinscoe, J. C., and Ebadi, M. (2004). 1-Benzyl-1,2,3,4-tetrahydroisoquinoline, a Parkinsonism-inducing endogenous toxin, increases alpha-synuclein expression and causes nuclear damage in human dopaminergic cells. *J. Neurosci. Res.* 76, 563–571. doi: 10.1002/jnr.20082

Sherer, T. B., Betarbet, R., Testa, C. M., Seo, B. B., Richardson, J. R., Kim, J. H., et al. (2003). Mechanism of toxicity in rotenone models of Parkinson's disease. *J. Neurosci.* 23, 10756–10764. doi: 10.1523/JNEUROSCI.23-34-10756.2003

Shibasaki, Y., Baillie, D. A., St Clair, D., and Brookes, A. J. (1995). High-resolution mapping of SNCA encoding alpha-synuclein, the non-A beta component of Alzheimer's disease amyloid precursor, to human chromosome 4q21.3-->q22 by fluorescence in situ hybridization. *Cytogenet. Cell Genet.* 71, 54–55.

Shukla, J. J., Stefanova, N., Bush, A. I., Mccoll, G., Finkelstein, D. I., and Mcallum, E. J. (2021). Therapeutic potential of iron modulating drugs in a mouse model of multiple system atrophy. *Neurobiol. Dis.* 159:105509. doi: 10.1016/j.nbd.2021.105509

Shults, C. W. (2005). Therapeutic role of coenzyme Q(10) in Parkinson's disease. *Pharmacol. Ther.* 107, 120–130. doi: 10.1016/j.pharmthera.2005.02.002

Shults, C. W., Haas, R. H., Passov, D., and Beal, M. F. (1997). Coenzyme Q10 levels correlate with the activities of complexes I and II/III in mitochondria from parkinsonian and nonparkinsonian subjects. *Ann. Neurol.* 42, 261–264. doi: 10.1002/ana.410420221

Shults, C. W., and Schapira, A. H. (2001). A cue to queue for CoQ? *Neurology* 57, 375–376. doi: 10.1212/WNL.57.3.375

Simon, C., Soga, T., Okano, H. J., and Parhar, I. (2021). Alpha-synuclein-mediated neurodegeneration in dementia with Lewy bodies: the pathobiology of a paradox. *Cell Biosci.* 11:196. doi: 10.1186/s13578-021-00709-y

Simuni, T., Fiske, B., Merchant, K., Coffey, C. S., Klingner, E., Caspell-Garcia, C., et al. (2021). Efficacy of Nilotinib in patients with moderately advanced Parkinson disease: a randomized clinical trial. *JAMA Neurol.* 78, 312–320. doi: 10.1001/jamaneurol.2020.4725

Singh, A., Boldin-Adamsky, S., Thimmulappa, R. K., Rath, S. K., Ashush, H., Coulter, J., et al. (2008). RNAi-mediated silencing of nuclear factor erythroid-2-related factor 2 gene expression in non-small cell lung cancer inhibits tumor growth and increases efficacy of chemotherapy. *Cancer Res.* 68, 7975–7984. doi: 10.1158/0008-5472.CAN-08-1401

Smith, W. W., Jiang, H., Pei, Z., Tanaka, Y., Morita, H., Sawa, A., et al. (2005a). Endoplasmic reticulum stress and mitochondrial cell death pathways mediate A53T mutant alpha-synuclein-induced toxicity. *Hum. Mol. Genet.* 14, 3801–3811. doi: 10.1093/hmg/ddi396

Smith, W. W., Margolis, R. L., Li, X., Troncoso, J. C., Lee, M. K., Dawson, V. L., et al. (2005b). Alpha-synuclein phosphorylation enhances eosinophilic cytoplasmic inclusion formation in SH-SY5Y cells. *J. Neurosci.* 25, 5544–5552. doi: 10.1523/JNEUROSCI.0482-05.2005

Sohmiya, M., Tanaka, M., Tak, N. W., Yanagisawa, M., Tanino, Y., Suzuki, Y., et al. (2004). Redox status of plasma coenzyme Q10 indicates elevated systemic oxidative stress in Parkinson's disease. *J. Neurol. Sci.* 223, 161–166. doi: 10.1016/j.jns.2004.05.007

Song, M. K., Adams, L., Lee, J. H., and Kim, Y. S. (2022). NXP031 prevents dopaminergic neuronal loss and oxidative damage in the AAV-WT-alpha-synuclein mouse model of Parkinson's disease. *PLoS One* 17:e0272085. doi: 10.1371/journal.pone.0272085

Sonustun, B., Altay, M. F., Strand, C., Ebanks, K., Hondhamuni, G., Warner, T. T., et al. (2022). Pathological relevance of Post-Translationally modified alpha-synuclein (pSer87, pSer129, nTyr39) in idiopathic Parkinson's Disease and multiple system atrophy. *Cells* 11:906. doi: 10.3390/cells11050906

Sorrentino, L., Cossu, F., Milani, M., Aliverti, A., and Mastrangelo, E. (2017). Structural bases of the altered catalytic properties of a pathogenic variant of apoptosis inducing factor. *Biochem. Biophys. Res. Commun.* 490, 1011–1017. doi: 10.1016/j.bbrc.2017.06.156

Souza, J. M., Giasson, B. I., Chen, Q., Lee, V. M., and Ischiropoulos, H. (2000). Dityrosine cross-linking promotes formation of stable alpha-synuclein polymers. Implication of nitrative and oxidative stress in the pathogenesis of neurodegenerative synucleinopathies. *J. Biol. Chem.* 275, 18344–18349. doi: 10.1074/jbc.M000206200

Spillantini, M. G. (1999). Parkinson's disease, dementia with Lewy bodies and multiple system atrophy are alpha-synucleinopathies. *Parkinsonism Relat. Disord.* 5, 157–162. doi: 10.1016/S1353-8020(99)00031-0

Spillantini, M. G., Crowther, R. A., Jakes, R., Hasegawa, M., and Goedert, M. (1998). Alpha-Synuclein in filamentous inclusions of Lewy bodies from Parkinson's disease and dementia with lewy bodies. *Proc. Natl. Acad. Sci. U. S. A.* 95, 6469–6473. doi: 10.1073/pnas.95.11.6469

Spillantini, M. G., and Goedert, M. (2016). Synucleinopathies: past, present and future. *Neuropathol. Appl. Neurobiol.* 42, 3–5. doi: 10.1111/nan.12311

Spillantini, M. G., Schmidt, M. L., Lee, V. M., Trojanowski, J. Q., Jakes, R., and Goedert, M. (1997). Alpha-synuclein in Lewy bodies. *Nature* 388, 839–840. doi: 10.1038/42166

Sprenger, F. S., Stefanova, N., Gelpi, E., Seppi, K., Navarro-Otano, J., Offner, F., et al. (2015). Enteric nervous system alpha-synuclein immunoreactivity in idiopathic REM sleep behavior disorder. *Neurology* 85, 1761–1768. doi: 10.1212/WNL.0000000000002126

St Laurent, R., Obrien, L. M., and Ahmad, S. T. (2013). Sodium butyrate improves locomotor impairment and early mortality in a rotenone-induced Drosophila model of Parkinson's disease. *Neuroscience* 246, 382–390. doi: 10.1016/j.neuroscience.2013.04.037

Stefanis, L. (2012). Alpha-synuclein in Parkinson's disease. *Cold Spring Harb. Perspect. Med.* 2:a009399. doi: 10.1101/cshperspect.a009399

Stefanis, L., Emmanouilidou, E., Pantazopoulou, M., Kirik, D., Vekrellis, K., and Tofaris, G. K. (2019). How is alpha-synuclein cleared from the cell? *J. Neurochem.* 150, 577–590. doi: 10.1111/jnc.14704

Stefanson, A. L., and Bakovic, M. (2014). Dietary regulation of Keap1/Nrf2/ARE pathway: focus on plant-derived compounds and trace minerals. *Nutrients* 6, 3777–3801. doi: 10.3390/nu6093777

Stewart, T., Sossi, V., Aasly, J. O., Wszolek, Z. K., Uitti, R. J., Hasegawa, K., et al. (2015). Phosphorylated alpha-synuclein in Parkinson's disease: correlation depends on disease severity. *Acta Neuropathol. Commun.* 3:7. doi: 10.1186/s40478-015-0185-3

Stoessl, A. J. (2016). Salivary gland biopsy for diagnosis of Parkinson's disease? *Lancet Neurol.* 15, 654–656. doi: 10.1016/S1474-4422(16)30031-X

Stokholm, M. G., Danielsen, E. H., Hamilton-Dutoit, S. J., and Borghammer, P. (2016). Pathological alpha-synuclein in gastrointestinal tissues from prodromal Parkinson disease patients. *Ann. Neurol.* 79, 940–949. doi: 10.1002/ana.24648

Sudnikovich, E. J., Maksimchik, Y. Z., Zabrodskaya, S. V., Kubyshin, V. L., Lapshina, E. A., Bryszewska, M., et al. (2007). Melatonin attenuates metabolic disorders due to streptozotocin-induced diabetes in rats. *Eur. J. Pharmacol.* 569, 180–187. doi: 10.1016/j.ejphar.2007.05.018

Sugeno, N., Takeda, A., Hasegawa, T., Kobayashi, M., Kikuchi, A., Mori, F., et al. (2008). Serine 129 phosphorylation of alpha-synuclein induces unfolded protein response-mediated cell death. *J. Biol. Chem.* 283, 23179–23188. doi: 10.1074/jbc.M802223200

Sun, X., Majumder, P., Shioya, H., Wu, F., Kumar, S., Weichselbaum, R., et al. (2000). Activation of the cytoplasmic c-Abl tyrosine kinase by reactive oxygen species. *J. Biol. Chem.* 275, 17237–17240. doi: 10.1074/jbc.C000099200

Suo, H., Wang, P., Tong, J., Cai, L., Liu, J., Huang, D., et al. (2015). NRSF is an essential mediator for the neuroprotection of trichostatin a in the MPTP mouse model of Parkinson's disease. *Neuropharmacology* 99, 67–78. doi: 10.1016/j.neuropharm.2015.07.015

Svenningsson, P., Wirdefeldt, K., Yin, L., Fang, F., Markaki, I., Efendic, S., et al. (2016). Reduced incidence of Parkinson's disease after dipeptidyl peptidase-4 inhibitors-a nationwide case-control study. *Mov. Disord.* 31, 1422–1423. doi: 10.1002/mds.26734

Takahashi, M., Kanuka, H., Fujiwara, H., Koyama, A., Hasegawa, M., Miura, M., et al. (2003). Phosphorylation of alpha-synuclein characteristic of synucleinopathy lesions is recapitulated in alpha-synuclein transgenic Drosophila. *Neurosci. Lett.* 336, 155–158. doi: 10.1016/S0304-3940(02)01258-2

Takahashi, T., Yamashita, H., Nakamura, T., Nagano, Y., and Nakamura, S. (2002). Tyrosine 125 of alpha-synuclein plays a critical role for dimerization following nitrative stress. *Brain Res.* 938, 73–80. doi: 10.1016/S0006-8993(02)02498-8

Takamatsu, Y., Fujita, M., Ho, G. J., Wada, R., Sugama, S., Takenouchi, T., et al. (2018). Motor and nonmotor symptoms of Parkinson's disease: antagonistic pleiotropy phenomena derived from alpha-synuclein evolvability? *Parkinsons Dis.* 2018:5789424. doi: 10.1155/2018/5789424

Tanei, Z. I., Saito, Y., Ito, S., Matsubara, T., Motoda, A., Yamazaki, M., et al. (2021). Lewy pathology of the esophagus correlates with the progression of Lewy body disease: a Japanese cohort study of autopsy cases. *Acta Neuropathol.* 141, 25–37. doi: 10.1007/s00401-020-02233-8

Tatham, M. H., Jaffray, E., Vaughan, O. A., Desterro, J. M., Botting, C. H., Naismith, J. H., et al. (2001). Polymeric chains of SUMO-2 and SUMO-3 are conjugated to protein substrates by SAE1/SAE2 and Ubc9. *J. Biol. Chem.* 276, 35368–35374. doi: 10.1074/jbc.M104214200

Tavassoly, O., Yue, J., and Vocadlo, D. J. (2021). Pharmacological inhibition and knockdown of O-GlcNAcase reduces cellular internalization of alpha-synuclein preformed fibrils. *FEBS J.* 288, 452–470. doi: 10.1111/febs.15349

Teleanu, D. M., Niculescu, A. G., Lungu, I., Radu, C. I., Vladacenco, O., Roza, E., et al. (2022). An overview of oxidative stress, neuroinflammation, and neurodegenerative diseases. *Int. J. Mol. Sci.* 23:5938. doi: 10.3390/ijms23115938

Tenreiro, S., Reimao-Pinto, M. M., Antas, P., Rino, J., Wawrzycka, D., Macedo, D., et al. (2014). Phosphorylation modulates clearance of alpha-synuclein inclusions in a yeast model of Parkinson's disease. *PLoS Genet.* 10:e1004302. doi: 10.1371/journal.pgen.1004302

Tetzlaff, J. E., Putcha, P., Outeiro, T. F., Ivanov, A., Berezovska, O., Hyman, B. T., et al. (2008). CHIP targets toxic alpha-Synuclein oligomers for degradation. *J. Biol. Chem.* 283, 17962–17968. doi: 10.1074/jbc.M802283200

Thorne, N. J., and Tumbarello, D. A. (2022). The relationship of alpha-synuclein to mitochondrial dynamics and quality control. *Front. Mol. Neurosci.* 15:947191. doi: 10.3389/fnmol.2022.947191

Tian, C., Liu, G., Gao, L., Soltys, D., Pan, C., Stewart, T., et al. (2019). Erythrocytic alpha-Synuclein as a potential biomarker for Parkinson's disease. *Transl. Neurodegener.* 8:15. doi: 10.1186/s40035-019-0155-y

Tofaris, G. K., Kim, H. T., Hourez, R., Jung, J. W., Kim, K. P., and Goldberg, A. L. (2011). Ubiquitin ligase Nedd4 promotes alpha-synuclein degradation by the endosomal-lysosomal pathway. *Proc. Natl. Acad. Sci. U. S. A.* 108, 17004–17009. doi: 10.1073/pnas.1109356108

Tofaris, G. K., Layfield, R., and Spillantini, M. G. (2001). Alpha-synuclein metabolism and aggregation is linked to ubiquitin-independent degradation by the proteasome. *FEBS Lett.* 509, 22–26. doi: 10.1016/S0014-5793(01)03115-5

Tofaris, G. K., Razzaq, A., Ghetti, B., Lilley, K. S., and Spillantini, M. G. (2003). Ubiquitination of alpha-synuclein in Lewy bodies is a pathological event not associated with impairment of proteasome function. *J. Biol. Chem.* 278, 44405–44411. doi: 10.1074/jbc.M308041200

Toker, L., Tran, G. T., Sundaresan, J., Tysnes, O. B., Alves, G., Haugarvoll, K., et al. (2021). Genome-wide histone acetylation analysis reveals altered transcriptional regulation in the Parkinson's disease brain. *Mol. Neurodegener.* 16:31. doi: 10.1186/s13024-021-00450-7

Tokuda, T., Qureshi, M. M., Ardah, M. T., Varghese, S., Shehab, S. A., Kasai, T., et al. (2010). Detection of elevated levels of alpha-synuclein oligomers in CSF from patients with Parkinson disease. *Neurology* 75, 1766–1772. doi: 10.1212/WNL.0b013e3181fd613b

Tremblay, M. A., Acker, C. M., and Davies, P. (2010). Tau phosphorylated at tyrosine 394 is found in Alzheimer's disease tangles and can be a product of the Abl-related kinase, Arg. *J. Alzheimers Dis.* 19, 721–733. doi: 10.3233/JAD-2010-1271

Trezzi, J. P., Galozzi, S., Jaeger, C., Barkovits, K., Brockmann, K., Maetzler, W., et al. (2017). Distinct metabolomic signature in cerebrospinal fluid in early parkinson's disease. *Mov. Disord.* 32, 1401–1408. doi: 10.1002/mds.27132

Uddin, M. S., Mamun, A. A., Jakaria, M., Thangapandiyan, S., Ahmad, J., Rahman, M. A., et al. (2020). Emerging promise of sulforaphane-mediated Nrf2 signaling cascade against neurological disorders. *Sci. Total Environ.* 707:135624. doi: 10.1016/j.scitotenv.2019.135624

Ueda, K., Fukushima, H., Masliah, E., Xia, Y., Iwai, A., Yoshimoto, M., et al. (1993). Molecular cloning of cDNA encoding an unrecognized component of amyloid in Alzheimer disease. *Proc. Natl. Acad. Sci. U. S. A.* 90, 11282–11286. doi: 10.1073/pnas.90.23.11282

Ullman, O., Fisher, C. K., and Stultz, C. M. (2011). Explaining the structural plasticity of alpha-synuclein. *J. Am. Chem. Soc.* 133, 19536–19546. doi: 10.1021/ja208657z

Vaccari, C., Grotto, D., Pereira, T. D. V., De Camargo, J. L. V., and Lopes, L. C. (2021). GLP-1 and GIP receptor agonists in the treatment of Parkinson's disease: translational systematic review and meta-analysis protocol of clinical and preclinical studies. *PLoS One* 16:e0255726. doi: 10.1371/journal.pone.0255726

Vamvaca, K., Volles, M. J., and Lansbury, P. T. Jr. (2009). The first N-terminal amino acids of alpha-synuclein are essential for alpha-helical structure formation in vitro and membrane binding in yeast. *J. Mol. Biol.* 389, 413–424. doi: 10.1016/j.jmb.2009.03.021

Vancraenenbroeck, R., Lobbestael, E., Maeyer, M. D., Baekelandt, V., and Taymans, J. M. (2011). Kinases as targets for Parkinson's disease: from genetics to therapy. *CNS Neurol. Disord. Drug Targets* 10, 724–740. doi: 10.2174/187152711797247858

Vicente Miranda, H., Cassio, R., Correia-Guedes, L., Gomes, M. A., Chegao, A., Miranda, E., et al. (2017a). Posttranslational modifications of blood-derived alpha-synuclein as biochemical markers for Parkinson's disease. *Sci. Rep.* 7:13713. doi: 10.1038/s41598-017-14175-5

Vicente Miranda, H., and Outeiro, T. F. (2010). The sour side of neurodegenerative disorders: the effects of protein glycation. *J. Pathol.* 221, 13–25. doi: 10.1002/path.2682

Vicente Miranda, H., Szego, E. M., Oliveira, L. M. A., Breda, C., Darendelioglu, E., De Oliveira, R. M., et al. (2017b). Glycation potentiates alpha-synuclein-associated neurodegeneration in synucleinopathies. *Brain* 140, 1399–1419. doi: 10.1093/brain/awx056

Vijayakumaran, S., Nakamura, Y., Henley, J. M., and Pountney, D. L. (2019). Ginkgolic acid promotes autophagy-dependent clearance of intracellular alpha-synuclein aggregates. *Mol. Cell. Neurosci.* 101:103416. doi: 10.1016/j.mcn.2019.103416

Vilas, D., Iranzo, A., Tolosa, E., Aldecoa, I., Berenguer, J., Vilaseca, I., et al. (2016). Assessment of alpha-synuclein in submandibular glands of patients with idiopathic rapid-eye-movement sleep behaviour disorder: a case-control study. *Lancet Neurol.* 15, 708–718. doi: 10.1016/S1474-4422(16)00080-6

Vivacqua, G., Mason, M., De Bartolo, M. I., Wegrzynowicz, M., Calo, L., Belvisi, D., et al. (2023). Salivary alpha-synuclein RT-QuIC correlates with disease severity in de novo Parkinson's disease. *Mov. Disord.* 38, 153–155. doi: 10.1002/mds.29246

Vivacqua, G., Suppa, A., Mancinelli, R., Belvisi, D., Fabbrini, A., Costanzo, M., et al. (2019). Salivary alpha-synuclein in the diagnosis of Parkinson's disease and progressive supranuclear palsy. *Parkinsonism Relat. Disord.* 63, 143–148. doi: 10.1016/j.parkreldis.2019.02.014

Wahlqvist, M. L., Lee, M. S., Hsu, C. C., Chuang, S. Y., Lee, J. T., and Tsai, H. N. (2012). Metformin-inclusive sulfonylurea therapy reduces the risk of Parkinson's disease occurring with type 2 diabetes in a Taiwanese population cohort. *Parkinsonism Relat. Disord.* 18, 753–758. doi: 10.1016/j.parkreldis.2012.03.010

Wakabayashi, K. (2020). Where and how alpha-synuclein pathology spreads in Parkinson's disease. *Neuropathology* 40, 415–425. doi: 10.1111/neup.12691

Wakabayashi, K., Miki, Y., Tanji, K., and Mori, F. (2022). Neuropathology of multiple system atrophy, a glioneuronal degenerative disease. *Cerebellum*, doi: 10.1007/s12311-022-01407-2 [Epub ahead of print].

Wang, D. B., Kinoshita, C., Kinoshita, Y., Sopher, B. L., Uo, T., Lee, R. J., et al. (2019). Neuronal susceptibility to beta-amyloid toxicity and ischemic injury involves histone deacetylase-2 regulation of endophilin-B1. *Brain Pathol.* 29, 164–175. doi: 10.1111/bpa.12647

Wang, N., Garcia, J., Freeman, R., and Gibbons, C. H. (2020a). Phosphorylated alpha-synuclein within cutaneous autonomic nerves of patients with Parkinson's disease: the implications of sample thickness on results. *J. Histochem. Cytochem.* 68, 669–678. doi: 10.1369/0022155420960250

Wang, W., Perovic, I., Chittuluru, J., Kaganovich, A., Nguyen, L. T., Liao, J., et al. (2011). A soluble alpha-synuclein construct forms a dynamic tetramer. *Proc. Natl. Acad. Sci. U. S. A.* 108, 17797–17802. doi: 10.1073/pnas.1113260108

Wang, X. Y., Kang, W. Y., Yang, Q., Zhang, L. Y., Chen, S. D., and Liu, J. (2014). Using gastrocnemius sEMG and plasma alpha-synuclein for the prediction of freezing of gait in Parkinson's disease patients. *PLoS One* 9:e89353. doi: 10.1371/journal.pone.0116382

Wang, Z., Becker, K., Donadio, V., Siedlak, S., Yuan, J., Rezaee, M., et al. (2020b). Skin alpha-synuclein aggregation seeding activity as a novel biomarker for Parkinson disease. *JAMA Neurol.* 78, 1–11. doi: 10.1001/jamaneurol.2020.3311

Watson, J. B., Hatami, A., David, H., Masliah, E., Roberts, K., Evans, C. E., et al. (2009). Alterations in corticostriatal synaptic plasticity in mice overexpressing human alpha-synuclein. *Neuroscience* 159, 501–513. doi: 10.1016/j.neuroscience.2009.01.021

Waxman, E. A., and Giasson, B. I. (2011). Characterization of kinases involved in the phosphorylation of aggregated alpha-synuclein. *J. Neurosci. Res.* 89, 231–247. doi: 10.1002/jnr.22537

Webb, J. L., Ravikumar, B., Atkins, J., Skepper, J. N., and Rubinsztein, D. C. (2003). Alpha-Synuclein is degraded by both autophagy and the proteasome. *J. Biol. Chem.* 278, 25009–25013. doi: 10.1074/jbc.M300227200

Weetman, J., Wong, M. B., Sharry, S., Rcom-H'cheo-Gauthier, A., Gai, W. P., Meedeniya, A., et al. (2013). Increased SUMO-1 expression in the unilateral rotenone-lesioned mouse model of Parkinson's disease. *Neurosci. Lett.* 544, 119–124. doi: 10.1016/j.neulet.2013.03.057

Weissman, A. M. (2001). Themes and variations on ubiquitylation. *Nat. Rev. Mol. Cell Biol.* 2, 169–178. doi: 10.1038/35056563

Wenz, T. (2013). Regulation of mitochondrial biogenesis and PGC-1alpha under cellular stress. *Mitochondrion* 13, 134–142. doi: 10.1016/j.mito.2013.01.006

Werner, M. H., and Olanow, C. W. (2022). Parkinson's disease modification through Abl kinase inhibition: an opportunity. *Mov. Disord.* 37, 6–15. doi: 10.1002/mds.28858

Wilkaniec, A., Strosznajder, J. B., and Adamczyk, A. (2013). Toxicity of extracellular secreted alpha-synuclein: its role in nitrosative stress and neurodegeneration. *Neurochem. Int.* 62, 776–783. doi: 10.1016/j.neuint.2013.02.004

Wilkinson, K. A., and Henley, J. M. (2010). Mechanisms, regulation and consequences of protein SUMOylation. *Biochem. J.* 428, 133–145. doi: 10.1042/BJ20100158

Wilson, C. J., and Callaway, J. C. (2000). Coupled oscillator model of the dopaminergic neuron of the substantia nigra. *J. Neurophysiol.* 83, 3084–3100. doi: 10.1152/jn.2000.83.5.3084

Winiarska, K., Fraczyk, T., Malinska, D., Drozak, J., and Bryla, J. (2006). Melatonin attenuates diabetes-induced oxidative stress in rabbits. *J. Pineal Res.* 40, 168–176. doi: 10.1111/j.1600-079X.2005.00295.x

Winklhofer, K. F., and Haass, C. (2010). Mitochondrial dysfunction in Parkinson's disease. *Biochim. Biophys. Acta* 1802, 29–44. doi: 10.1016/j.bbadis.2009.08.013

Witt, M., Bormann, K., Gudziol, V., Pehlke, K., Barth, K., Minovi, A., et al. (2009). Biopsies of olfactory epithelium in patients with Parkinson's disease. *Mov. Disord.* 24, 906–914. doi: 10.1002/mds.22464

Wu, T., Thazhath, S. S., Marathe, C. S., Bound, M. J., Jones, K. L., Horowitz, M., et al. (2015). Comparative effect of intraduodenal and intrajejunal glucose infusion on the gut-incretin axis response in healthy males. *Nutr. Diabetes* 5:e156. doi: 10.1038/nutd.2015.6

Wu, Y., and Guo, S. W. (2008). Histone deacetylase inhibitors trichostatin A and valproic acid induce cell cycle arrest and p21 expression in immortalized human endometrial stromal cells. *Eur. J. Obstet. Gynecol. Reprod. Biol.* 137, 198–203. doi: 10.1016/j.ejogrb.2007.02.014

Xie, X., Yu, C., Zhou, J., Xiao, Q., Shen, Q., Xiong, Z., et al. (2020). Nicotinamide mononucleotide ameliorates the depression-like behaviors and is associated with attenuating the disruption of mitochondrial bioenergetics in depressed mice. *J. Affect. Disord.* 263, 166–174. doi: 10.1016/j.jad.2019.11.147

Yang, Y. W., Hsieh, T. F., Li, C. I., Liu, C. S., Lin, W. Y., Chiang, J. H., et al. (2017). Increased risk of Parkinson disease with diabetes mellitus in a population-based study. *Medicine (Baltimore)* 96:e5921. doi: 10.1097/MD.0000000000009419

Yu, Y., Zhang, L., Li, X., Run, X., Liang, Z., Li, Y., et al. (2012). Differential effects of an O-GlcNAcase inhibitor on tau phosphorylation. *PLoS One* 7:e35277. doi: 10.1371/journal.pone.0051967

Yu, Z., Xu, X., Xiang, Z., Zhou, J., Zhang, Z., Hu, C., et al. (2010). Nitrated alpha-synuclein induces the loss of dopaminergic neurons in the substantia nigra of rats. *PLoS One* 5:e9956. doi: 10.1371/journal.pone.0015623

Yun, S. P.., Kim, D., Kim, S., Kim, S., Karuppagounder, S. S., Kwon, S. H., et al. (2018). Biopsiesalpha-Synuclein accumulation and GBA deficiency due to L444P GBA mutation contributes to MPTP-induced parkinsonism. *Mol Neurodegener.* 13:1. doi: 10.1186/s13024-017-0233-5

Yuzwa, S. A., Cheung, A. H., Okon, M., Mcintosh, L. P., and Vocadlo, D. J. (2014a). O-GlcNAc modification of tau directly inhibits its aggregation without perturbing the conformational properties of tau monomers. *J. Mol. Biol.* 426, 1736–1752. doi: 10.1016/j.jmb.2014.01.004

Yuzwa, S. A., Macauley, M. S., Heinonen, J. E., Shan, X., Dennis, R. J., He, Y., et al. (2008). A potent mechanism-inspired O-GlcNAcase inhibitor that blocks phosphorylation of tau in vivo. *Nat. Chem. Biol.* 4, 483–490. doi: 10.1038/nchembio.96

Yuzwa, S. A., Shan, X., Jones, B. A., Zhao, G., Woodward, M. L., Li, X., et al. (2014b). Pharmacological inhibition of O-GlcNAcase (OGA) prevents cognitive decline and amyloid plaque formation in bigenic tau/APP mutant mice. *Mol. Neurodegener.* 9:42. doi: 10.1186/1750-1326-9-42

Yuzwa, S. A., Shan, X., Macauley, M. S., Clark, T., Skorobogatko, Y., Vosseller, K., et al. (2012). Increasing O-GlcNAc slows neurodegeneration and stabilizes tau against aggregation. *Nat. Chem. Biol.* 8, 393–399. doi: 10.1038/nchembio.797

Zange, L., Noack, C., Hahn, K., Stenzel, W., and Lipp, A. (2015). Phosphorylated alpha-synuclein in skin nerve fibres differentiates Parkinson's disease from multiple system atrophy. *Brain* 138, 2310–2321. doi: 10.1093/brain/awv138

Zhang, F., Hu, Y., Huang, P., Toleman, C. A., Paterson, A. J., and Kudlow, J. E. (2007). Proteasome function is regulated by cyclic AMP-dependent protein kinase through phosphorylation of Rpt6. *J. Biol. Chem.* 282, 22460–22471. doi: 10.1074/jbc.M702439200

Zhang, J., Lei, H., Chen, Y., Ma, Y. T., Jiang, F., Tan, J., et al. (2017). Enzymatic O-GlcNAcylation of alpha-synuclein reduces aggregation and increases SDS-resistant soluble oligomers. *Neurosci. Lett.* 655, 90–94. doi: 10.1016/j.neulet.2017.06.034

Zhang, J., Li, X., and Li, J. D. (2019). The roles of post-translational modifications on alpha-synuclein in the pathogenesis of Parkinson's diseases. *Front. Neurosci.* 13:381. doi: 10.3389/fnins.2019.00381

Zhang, J., Perry, G., Smith, M. A., Robertson, D., Olson, S. J., Graham, D. G., et al. (1999). Parkinson's disease is associated with oxidative damage to cytoplasmic DNA and RNA in substantia nigra neurons. *Am. J. Pathol.* 154, 1423–1429. doi: 10.1016/S0002-9440(10)65396-5

Zhang, L. F., Yu, X. L., Ji, M., Liu, S. Y., Wu, X. L., Wang, Y. J., et al. (2018). Resveratrol alleviates motor and cognitive deficits and neuropathology in the A53T alpha-synuclein mouse model of Parkinson's disease. *Food Funct.* 9, 6414–6426. doi: 10.1039/C8FO00964C

Zhang, L. Y., Jin, Q. Q., Holscher, C., and Li, L. (2021). Glucagon-like peptide-1/glucose-dependent insulinotropic polypeptide dual receptor agonist DA-CH5 is superior to exendin-4 in protecting neurons in the 6-hydroxydopamine rat Parkinson model. *Neural Regen. Res.* 16, 1660–1670. doi: 10.4103/1673-5374.303045

Zhang, S., Xie, J., Xia, Y., Yu, S., Gu, Z., Feng, R., et al. (2015). LK6/Mnk2a is a new kinase of alpha synuclein phosphorylation mediating neurodegeneration. *Sci. Rep.* 5:12564. doi: 10.1038/srep12564

Zhang, Y. C., Gan, F. F., Shelar, S. B., Ng, K. Y., and Chew, E. H. (2013). Antioxidant and Nrf2 inducing activities of luteolin, a flavonoid constituent in Ixeris sonchifolia Hance, provide neuroprotective effects against ischemia-induced cellular injury. *Food Chem. Toxicol.* 59, 272–280. doi: 10.1016/j.fct.2013.05.058

Zhao, X., Zhang, M., Li, C., Jiang, X., Su, Y., and Zhang, Y. (2019). Benefits of vitamins in the treatment of Parkinson's Disease. *Oxidative Med. Cell. Longev.* 2019:9426867. doi: 10.1155/2019/9426867

Zhong, C. B., Chen, Q. Q., Haikal, C., Li, W., Svanbergsson, A., Diepenbroek, M., et al. (2017). Age-dependent alpha-synuclein accumulation and phosphorylation in the enteric nervous system in a transgenic mouse model of Parkinson's disease. *Neurosci. Bull.* 33, 483–492. doi: 10.1007/s12264-017-0179-1

Zhou, C., Ji, J., Shi, M., Yang, L., Yu, Y., Liu, B., et al. (2014). Suberoylanilide hydroxamic acid enhances the antitumor activity of oxaliplatin by reversing the oxaliplatin-induced Src activation in gastric cancer cells. *Mol. Med. Rep.* 10, 2729–2735. doi: 10.3892/mmr.2014.2548

Zhou, W., Bercury, K., Cummiskey, J., Luong, N., Lebin, J., and Freed, C. R. (2011). Phenylbutyrate up-regulates the DJ-1 protein and protects neurons in cell culture and in animal models of Parkinson disease. *J. Biol. Chem.* 286, 14941–14951. doi: 10.1074/jbc.M110.211029

Zhou, W., Ryan, J. J., and Zhou, H. (2004). Global analyses of sumoylated proteins in *Saccharomyces cerevisiae*. Induction of protein sumoylation by cellular stresses. *J. Biol. Chem.* 279, 32262–32268. doi: 10.1074/jbc.M404173200

Zimprich, A., Benet-Pages, A., Struhal, W., Graf, E., Eck, S. H., Offman, M. N., et al. (2011). A mutation in VPS35, encoding a subunit of the retromer complex, causes late-onset Parkinson disease. *Am. J. Hum. Genet.* 89, 168–175. doi: 10.1016/j.ajhg.2011.06.008

frontiers | Frontiers in Molecular Neuroscience

TYPE Original Research
PUBLISHED 20 June 2023
DOI 10.3389/fnmol.2023.1191324

OPEN ACCESS

EDITED BY
Maria Jose Sisalli,
University of Naples Federico II, Italy

REVIEWED BY
Tuan Leng Tay,
Boston University, United States
Jae-Ick Kim,
Ulsan National Institute of Science and Technology, Republic of Korea

*CORRESPONDENCE
Julien Gasser
✉ Julien.Gasser@ucb.com
Irena Kadiu
✉ Irena.Kadiu@ucb.com

RECEIVED 21 March 2023
ACCEPTED 24 May 2023
PUBLISHED 20 June 2023

CITATION
Gasser J, Gillet G, Valadas JS, Rouvière L, Kotian A, Fan W, Keaney J and Kadiu I (2023) Innate immune activation and aberrant function in the R6/2 mouse model and Huntington's disease iPSC-derived microglia. *Front. Mol. Neurosci.* 16:1191324. doi: 10.3389/fnmol.2023.1191324

Innate immune activation and aberrant function in the R6/2 mouse model and Huntington's disease iPSC-derived microglia

Julien Gasser[1]*, Gaelle Gillet[1], Jorge S. Valadas[1], Laura Rouvière[1], Apoorva Kotian[2], Wenqiang Fan[1], James Keaney[1] and Irena Kadiu[1]*

[1]Neuroinflammation Focus Area, Neuroscience Research, UCB Biopharma SRL, Braine-l'Alleud, Belgium, [2]Development Science, UCB Biopharma SRL, Slough, United Kingdom

Huntington's disease (HD) is an inherited autosomal dominant neurodegenerative disease caused by CAG repeats in exon 1 of the *HTT* gene. A hallmark of HD along with other psychiatric and neurodegenerative diseases is alteration in the neuronal circuitry and synaptic loss. Microglia and peripheral innate immune activation have been reported in pre-symptomatic HD patients; however, what "activation" signifies for microglial and immune function in HD and how it impacts synaptic health remains unclear. In this study we sought to fill these gaps by capturing immune phenotypes and functional activation states of microglia and peripheral immunity in the R6/2 model of HD at pre-symptomatic, symptomatic and end stages of disease. These included characterizations of microglial phenotypes at single cell resolution, morphology, aberrant functions such as surveillance and phagocytosis and their impact on synaptic loss *in vitro* and *ex vivo* in R6/2 mouse brain tissue slices. To further understand how relevant the observed aberrant microglial behaviors are to human disease, transcriptomic analysis was performed using HD patient nuclear sequencing data and functional assessments were conducted using induced pluripotent stem cell (iPSC)-derived microglia. Our results show temporal changes in brain infiltration of peripheral lymphoid and myeloid cells, increases in microglial activation markers and phagocytic functions at the pre-symptomatic stages of disease. Increases in microglial surveillance and synaptic uptake parallel significant reduction of spine density in R6/2 mice. These findings were mirrored by an upregulation of gene signatures in the endocytic and migratory pathways in disease-associated microglial subsets in human HD brains, as well as increased phagocytic and migratory functions of iPSC-derived HD microglia. These results collectively suggest that targeting key and specific microglial functions related to synaptic surveillance and pruning may be therapeutically beneficial in attenuating cognitive decline and psychiatric aspects of HD.

KEYWORDS

microglia, phagocytosis, migration, neuroinflammation, Huntington's disease, dendritic spines, R6/2 model, cyTOF

Introduction

Huntington's disease (HD) is a fatal neurodegenerative disorder caused by a polyglutamine (polyQ) repeat expansion in the *HTT* gene. It encodes for mutant Huntingtin (mHTT), a ubiquitous protein with an abnormally long PolyQ stretch, contributing to systemic and central nervous system (CNS) toxicities through gain-of-toxic function interference with normal protein folding, induced oxidative stress, and programmed cell death.

Peripheral widespread systemic toxicity and mHTT pathology has been reported in blood leukocytes, liver, pancreas, kidney and cardiac cells among others (Sassone et al., 2009; van der Burg et al., 2009). Human leukocytes express high levels of mHTT (Moscovitch-Lopatin et al., 2010; Weiss et al., 2012). These cells display activated phenotypes characterized by increased pro-inflammatory cytokines (TNF, IL1β, IL6, IL8, etc.) and lowered tissue-trophic factors such as transforming growth factor-β1 (TGF-β1) in the serum or exaggerated pro-inflammatory response to lipopolysaccharide (LPS) in cell culture (Schure et al., 2010; Di Pardo et al., 2013). Increased leukocyte activation and increased brain infiltration of NFκB-active monocytes has been reported as early as pre-symptomatic stages of disease and correlates with rates of disease progression (Di Pardo et al., 2013). In animal models of HD including R6/2 mice, peripheral innate immunity has been shown to be dysregulated; however, it remains unclear due to contradicting reports what functions are impacted and their involvement in murine mHTT pathobiology (Kwan et al., 2012; Träger et al., 2015; Lee et al., 2018).

In the CNS, mHTT toxicity is displayed in the form of selective vulnerability of medium spiny neurons (MSNs) and corticostriatal projection neurons (CPNs) modulating movement and cognition, respectively. Selective loss of MSNs and CPNs leads to progressive degeneration of basal ganglia and cortex manifesting as cognitive, behavioral, and motor disturbances including memory loss, depression and choreic (involuntary) movement. Although mHTT is the primary disease trigger in HD, the progressive loss of neuronal subtypes is thought to be non-cell autonomous. Neighboring cells such as microglia, essential for optimal neuronal/circuitry function and survival, are thought to contribute to the non-cell autonomous degeneration mechanisms in HD through increased release of pro-inflammatory and oxidative stress factors and maladaptive synaptic pruning. Imaging studies have established a link between synaptic density and cognitive performance across a range of neurodegenerative disease characterized by cognitive decline (Delva et al., 2022; Mecca et al., 2022). In HD in particular, imaging studies utilizing ^{11}C-UCB-J, a radioligand targeting synaptic vesicle protein 2A (SV2A), have shown the degree of synaptic loss (starting in the striatum) associates with earlier onset of cognitive and motor symptoms (Delva et al., 2022). Additionally, increased signal of ^{11}C-(R)-PK11195, a positron emission tomography (PET) radioligand of microglial/glial translocator protein (TSPO) in striatum and cortex correlated with dopamine receptor loss and could predict disease onset and clinical severity (Tai et al., 2007; Politis et al., 2011). Autonomous microglial activation has been reported in various rodent models of HD including R6/2 characterized by increased Iba1 staining in regions of brain pathology (Crotti et al., 2014); However, what Iba1+ increases and microglial activation signifies in terms of functional impact on disease pathobiology in HD remains unclear.

Currently, only symptomatic treatments are available. These temporarily address some of the HD disease symptoms without impacting the underlying disease pathobiology or progressive degeneration. Therefore, a thorough understanding of the non-cell autonomous mechanistic drivers of disease progression in human disease and interrogating their presence in rodent models among other tools for testing of therapeutic hypotheses is critical. More specifically, understanding what microglial functions are dysregulated in disease and their impact on neuronal health is the first step in identification of therapeutic targets that will potentially correct the underlying problem.

Our study addresses some of these knowledge gaps in HD human microglial functional pathobiology through comprehensive imaging, transcriptomic, phenotypic, and functional interrogation of human HD tissues/cells, and the R6/2 mouse model. It provides novel insights into disrupted innate immune biologies in HD as potential hypothesis entry points for testing of neuroimmune modulators as future therapies for HD.

Materials and methods

Animals

R6/2 transgenic mice (B6CBA-Tg (HDexon1)62Gpb/3 J, Jackson Labs # 006494) and non-transgenic litter mates (ntg) were in-licensed from King's College London. Mice were housed in ventilated cages with nesting cups (Kraft paper, CARFIL QUALITY, Beyntellus 3) on a 12/12 h light/dark cycle with lights on at 06:00 h and had al libitum access to rodent chow (Safe, Plant diets & Custom diet, Route de Saint Bris – 89,290 Augy – France) and tap water. The temperature in the husbandry was maintained at 20–22°C and humidity at about 40%. Following a habituation period of a minimum 1 week, mice were euthanized, and tissues collected at 7, 9, 10, 13, and 15 weeks of age for *ex vivo*, *in vitro* functional and biochemical assays. All experimental procedures and humane endpoints were carefully reviewed and approved by a local Animal Experimentation and Well-Being Ethical Committee compliant with national legislation guidelines (Belgian Royal Decree regarding the protection of laboratory animals of May 29th, 2013) and the European directive (2010/63/EU). Additionally, all animal experiments were carried out in an AAALAC accredited facility.

Human iPSC cell lines and tissues

Post-mortem frozen human brain tissues from the pre-central gyrus and the middle frontal gyrus of HD cases and non-demented controls were obtained from the Netherlands Brain Bank, Netherlands Institute for Neuroscience, Amsterdam (open access[1]). All Material has been collected from donors from whom written informed consent for brain autopsy and the use of the material and clinical information for research purposes had been obtained by the NBB. An HD patient iPSCs line heterozygous for pathologic CAG

1 www.brainbank.nl

repeats in the HTT gene (one allele within the normal range, ~18 repeats, and the other allele ~40 repeats) were obtained under informed consent from European Bank for induced pluripotent Stem Cells (EBiSC, RCi004-A). These lines showed the presence of Pluripotency markers (e.g., SSEA4, TRA-1-81, OCT4, and SOX2) and ability to differentiate to endo-, meso-and ectodermal cell types. The isogenic control line with 21 CAG repeats on both alleles of the HTT gene was generated at Bioneer. Human brain samples negative for prion disease and iPSC lines that tested negative for infectious pathogens were cleared for use by the Ethics Committee of UCB Biopharma and registered by the UCB Biobank in compliance with applicable local legislature (Belgian Royal Decree on Biobanks of January 9th, 2018).

Mouse bone marrow derived macrophage (BMDM) cell culture

WT and R6/2 litter mates were euthanized using a lethal dose of isoflurane followed by cervical dislocation. BMDM were isolated from femurs, tibias, humerus, and radius of 6 R6/2 and 6 WT mice flushing with 1x HBSS using a syringe with a 30-gauge needle. Flushed bone morrow was strained through a 40 µm filter (Falcon, 352340) followed by centrifugation at 300 xg for 10 min. The pellet was resuspended in 1 mL of DMEM-Glutamax supplemented with 20 ng/mL macrophage colony-stimulating factor (M-CSF), 1% penicillin–streptomycin 10,000 U/mL and 10% endotoxin-low heat-inactivated FBS. Cell numbers and viability were assessed using the Countess II automated cell counter (ThermoFisher Scientific). Monocytes in the bone marrow mix were allowed to adhere and differentiate in culture at 37°C, 5% CO_2, for 7 days prior to use in functional assays. Floating non-monocytic cells were removed from the cultures through complete media exchanges every 2 days.

Generation of pluripotent stem cell-derived microglia (iMGL)

iPSC HD and isogenic control lines were maintained in 6-well plates in feeder free conditions in complete mTESR plus medium (Stem Cell Technologies) for at least 2 passages. Two days before the start of the differentiation, iPSCs were cultured in complete Essential 8 Flex medium (ThermoFisher Scientific). Cells were fed fresh media daily, passaged every 4–5 days and maintained in a humidified incubator (20% O_2, 5% CO2, 37°C).

The differentiation of iPSC to iMGL was performed as described previously in Abud et al. (2017) with some modifications. Briefly, on day-1, iPSCs were dissociated to single cells and plated in complete Essential 8 Flex medium (with 10 µM Y-27632 dihydrochloride, Abcam) at 0.75 × 10^6 iPSCs per well in AggreWell™ 400 in 6-well plates pre-treated with Anti-Adherence Solution (Stem Cell Technologies). On day 0, the embryoid bodies were ready for iHPC generation and were cultured in T225 culture flasks (pre-treated with Anti-Adherence Solution from Stem Cell Technologies). iPSCs were first differentiated in induced Hematopoietic progenitor cells (iHPC) for 15 days. iHPC were collected by filtration through a 37 µm reversible cell strainer, centrifuged and resuspended in CryoStor® CS10 (Stemcell Technologies) and stored in liquid nitrogen. Frozen iHPC were thawed in iHPC medium and then differentiated to iMGL for 14 days with iMGL Differentiation base medium, as described in Abud et al. (2017).

BMDM and iMGL migration assay

BMDMs were seeded at a density of 50,000 cells/insert in 2-well culture insert 24-well plates (Ibidi). Cells were incubated at 37°C in 5% CO_2 for 24 h. Culture inserts were then carefully removed followed leaving an unpopulated "scratched" area and the cell monolayer with fresh complete medium and imaging of the scratch area using an EVOS digital inverted light microscope. Extent of microglia cell migration into the scratch area was quantified using a customized ImageJ script.

iMGL cultured for 30 days were replated in a clear bottom 96-well plate (ImageLock) coated with poly-D-lysine (1 mg/mL) at 40,000 cells per well and were allowed to rest at 37°C in 5% CO_2 for 1 h. Cells were then mechanically removed from the center of the well with a Incucyte® 96-Well Woundmaker Tool. Migration of iMGL to the generated wound was measured in images acquired in Incucyte S3 (Sartorius) using the Relative Wound Density metric (percentage of cells that migrated to the wound compared to the cells that remained in the unscratched area).

Assessment of phagocytic activity in murine BMDM and human iMGL cell cultures

To assess phagocytic function in BMDM from transgenic and litter mate control mice, cells were plated at a density of 30,000 cells/well in 96-well poly-D-lysine-coated plates, and allowed to rest at 37°C, and 5% CO_2 overnight. Cells were then exposed to pHrodo Red Zymosan Bioparticles™ (12.5 µg/mL per well; ThermoFisher Scientific) for 1 h at 37°C in 5% CO_2. Cells were washed once with 1X PBS for 5 min and fixed in 4% PFA for 10 min at RT. PFA was removed and fixed cells were washed twice with 1X PBS. Fixed cells were stained with either HCS CellMask Blue or Alexa Fluor 488 Phalloidin containing DAPI (ThermoFisher Scientific) to enable accurate cell segmentation and zymosan particle counting. Images were acquired using the Leica TCS SP5 II confocal microscope and IN-Cell Analyzer 6,000 system with cell segmentation and particle counting performed using the IN-Cell Developer Toolbox v1.9. Phagocytic index was measured as follows:

Phagocytic Index = (No. of particles/cell) × (% of phagocytic cells).

For synaptosome uptake measurements, co-localization of pHrodo-red signal and CellMask Blue was performed using a custom MATLAB application and results expressed using the Pearson coefficient.

For measurements of phagocytic uptake in iMGL derived from HD and isogenic control lines, cells cultured for 30 days in 6-well plates were replated in 384-well poly-D-lysine and laminin-coated plates (Corning) at 5,000 cells per well and were allowed to rest at 37°C in 5% CO_2 for 1 h. Separate wells were treated with 5 µM Cytochalasin D (an inhibitor of actin polymerization) or vehicle (complete medium). After 1 h, cells exposed to pHrodo™ Red

Zymosan Bioparticles™ (0.5 µg/mL per well, ThermoFisher Scientific). Uptake of zymosan bioparticles was measured by the pHrodo™ fluorescent intensity per cell confluence in images acquired in Incucyte S3 (Sartorius).

Tissue processing for CyTOF mass cytometry

Mice were anesthetized using isoflurane/O_2 mix in an induction chamber (Dräger Fabius, 8604200-14). Absence of reactivity to pain was tested by tail and paw pinch followed by transcardial perfusion with 1X HBSS (10 U/mL heparin) using a peristaltic pump at a rate of 6 mL/min for 5 min. Forebrains and spleens were collected in 5 mL of ice-cold 1X HBSS and stored on ice until tissue collection was completed. Brains were dissociated using the Papain Dissociation System (Worthington) by two sequential triturations and incubation for 15 min at 37°C. Single cell suspensions were filtered through a 40 µm cell strainer in 50 mL Falcon tubes and resuspended in 30% Percoll in AutoMACS running buffer (Miltenyi Biotec) at room temperature (RT) and centrifuged for 15 min at 500 xg with no brake to generate a floating top layer of myelin. Following myelin removal, 1X AutoMACS running buffer was added to the remaining volume, any pelleted cells were resuspended. Cells were filtered again through 40 µm cell strainers and centrifuged at 300 xg for 10 min at RT to obtain an immune cell-enriched pellet. The experimental workflow is summarized in Supplementary Figure S2.

Spleens were homogenized by mechanical dissociation followed by red blood cell lysis using 1X RBC lysis buffer (ThermoFisher Scientific) for 10 min at RT per manufacturer's recommendation. Following RBC lysis, samples were supplemented with 1X PBS, filtered through a 40 µm cell strainer and centrifuged at 300 xg for 10 min. Following a centrifugation at 300 xg for 5 min, a cocktail of 32 metal tag-conjugated antibodies (1:100) in Maxpar staining buffer was added to the cells and incubated for 1 h at 4° C. Information on antibody panel used for cytometry including clone and source is included in Supplementary Table S1. Several monoclonal antibodies were conjugated to metal tags in-house using the Maxpar 8X antibody labeling kit (Fluidigm) according to manufacturer's protocol. All labelled antibodies were quality-controlled in-house for correct labeling prior to use.

Following immunostaining, cells were washed by three sequential centrifugations at 300 xg for 5 min at 4°C in Maxpar staining buffer followed by fixation with 4% PFA in 1X PBS overnight at 4°C.

iPSC microglia surface staining for CyTOF mass cytometry

Cells were gently detached through medium exchange and washed once in Maxpar cell staining buffer. Following a centrifugation at 300 xg for 5 min a cocktail of 34 metal tag-conjugated antibodies (1:100; Supplementary Table S3) in Maxpar staining buffer was added to the cells and incubated for 1 h at 4°C. Following immunostaining, cells were washed by three sequential centrifugations at 300 xg for 5 min at 4°C in Maxpar staining buffer followed by fixation with 4% PFA in PBS overnight at 4°C.

Mass cytometry data acquisition and analysis

Prior to data acquisition, fixed cells were incubated with Maxpar 191/193Ir DNA Intercalator (50 nM final concentration, Fluidigm) diluted in 4% PFA in PBS at 4°C overnight. Cells were washed twice in Maxpar H_2O (Fluidigm) and centrifuged at 800 xg for 15 min at RT. Cells were resuspended in EQ Four Element Calibration beads (Fluidigm) diluted in Maxpar H_2O (1:4), filtered through a 40 µm cell strainer to remove cellular aggregates and debris followed by data acquisition on a Helios mass cytometer (Fluidigm). The full sample volume was acquired at an event rate of maximum 500 events/s.

Mass cytometry data were analyzed using different computational tools available in Cytobank.[2] Normalization beads were gated out and single live cells were then gated based on DNA content and cell length to exclude debris and doublets. Identification of immune cell subsets was then performed using traditional bivariate gating (Supplementary Figure S2). In brain, cell populations were defined based the following gating strategy: microglia/resident myeloid, $CD45^{low}CD11b^{+}CX3CR1^{+}$; neutrophils, $CD45^{high}CD11b^{+}Ly\text{-}6G^{+}$; monocytes/macrophages, $CD45^{high}CD11b^{+}Ly\text{-}6G^{-}$; dendritic cells, $CD45^{high}CD11b^{+}CD11c^{+}$; T cells, $CD45^{high}CD11b^{low}CD3^{+}$. In spleen immune subsets were defined as follows: CD4 T helper cells: $CD45^{+}CD3^{+}CD4^{+}CD8^{-}$; CD8 cytotoxic T cells: $CD45^{+}CD3^{+}CD4^{-}CD8^{-}$; B cells, $CD45^{+}CD19^{+}CD3^{-}$; NK cells: $CD45^{+}CD335^{+}$; Neutrophils: $CD45^{+}CD3^{-}CD19^{-}CD11b^{+}Ly\text{-}6G^{+}$; Monocytes/macrophages: $CD45^{+}CD3^{-}CD19^{-}CD11b^{+}Ly\text{-}6G^{-}$; Dendritic cells: $CD45^{+}CD3^{-}CD19^{-}CD11b^{+}CD11c^{+}Ly\text{-}6G^{-}$; Mast cells: $CD45^{+}FceRIa^{+}$. Differentiated iMGL were identified as $CD45^{+}$ cells. The percentage of each cell population was calculated out of the total of $CD45^{+}$ cells. To visualize all live immune cells or all iMGL in a single two-dimensional map, we applied an unsupervised high-dimensional data analysis on concatenated fcs files pooling cells equally and randomly sampled from all mice or samples in each group, using the t-distributed stochastic linear embedding (t-SNE) algorithm available on Cytobank (viSNE algorithm).

Synaptosome purification

Six-month-old Sprague Dawley rats were anesthetized with isoflurane and brains were dissected, placed in 10 volumes of ice cold HEPES-buffered sucrose (0.32 M sucrose, 4 mM HEPES pH 7.4) and homogenized using a Dounce homogenizer. Homogenate was spun at 1,000 xg at 4°C for 10 min to remove the pelleted nuclear fraction (P1). Supernatant was spun at 15,000 xg for 20 min to yield a crude synaptosomal pellet (P2), which was resuspended in 10 volumes of HEPES-buffered sucrose. After centrifugation at 10,000 xg for an additional 15 min at 4°C, the washed crude synaptosomal fraction (P2') was layered in ultra-clear centrifuge tubes (Beckman) onto 4 mL of 1.2 M sucrose and centrifuged at 230,000 xg for 15 min (Beckman SW40Ti). The interphase was collected, layered onto 4 mL of 0.8 M sucrose and centrifuged at 230,000 xg for 15 min to yield the

2 https://cytobank.org

synaptosome pellet. Purified synaptosomes were conjugated with pHrodo™ Red succinimidyl ester (ThermoFisher Scientific, P36600) in 0.1 M sodium carbonate (pH 9.0) by incubation for 2 h at RT with gentle agitation. Unbound pHrodo™ dye was removed by multiple rounds of washing and centrifugation with 1X HBSS and pHrodo™-conjugated synaptosomes were then resuspended in 5% DMSO in 1X HBSS and stored at −80°C until further use.

Immunoblotting

Using a cordless pestle motor for 1 min homogenization per sample (VWR), human and mouse brain tissues were homogenized on ice in 1X RIPA buffer (Sigma-Aldrich) containing protease and phosphatase inhibitors (Roche). BMDM and tissue lysates were centrifuged at 15,000 xg for 20 min at 4°C and protein concentration was assessed in the supernatant (BCA protein assay kit, ThermoFisher Scientific, 23,225, United States). Equal amounts of protein in Laemmli sample buffer (Biorad) were separated by gel electrophoresis using 4–12% Bis-Tris polyacrylamide gels (Invitrogen) and transferred to PVDF membranes (Merck Millipore). Nonspecific binding was blocked by incubating membranes for 1 h in TBS blocking buffer (Odyssey, Licor) followed by overnight incubation at 4°C with the following primary antibodies: anti-C1q (Abcam, ab11861, 1:500), anti-C3 (Abcam, ab97462, 1:250), anti-TSPO (Abcam, ab109497, 1:5,000), and anti-β-actin (Cell Signaling technology, 3700S/4970S, 1:5,000). Blots were washed three times in 1X TBS with 0.1% Tween-20 (TBS-T) followed by incubation for 1 h with fluorophore-conjugated secondary antibodies (Licor, IRDye 680LT Goat anti Mouse/Rabbit, 1:1,000) at RT. After three additional washes in TBS-T, blots were imaged using the Odyssey CLx Imaging system (Licor). ImageJ was used to quantify protein levels normalizing to actin levels as a loading control.

Microglial phagocytosis in acute mouse brain sections

Microglial phagocytic activity in R6/2 mice and WT littermate control acute brain sections was assessed as previously described in Keaney et al. (2019). Briefly, 300 µm brain slices were generated from transgenic and litter mate controls following euthanasia and kept in pH and temperature-controlled conditions. Slices were then incubated with pHRodo-conjugated zymosan beads or synaptosomes for 1 h at 37°C and 4% CO2, non-phagocytosed beads & synaptosomes were removed by gentle washing of the tissue sections followed by fixation with 4% PFA for 1 h at RT. Fixed slices were incubated for 3 h with blocking solution (5% normal goat serum, 0.05% Triton-X in PBS) followed by incubation with anti-Iba1 (polyclonal Guinea Pig, dilution 1:500, Synaptic Systems, 234004) for 48 h. Slices were washed three times for 15 min in 1X PBS and incubated with secondary antibody (anti-guinea pig IgG, Alexa488; Thermo Fisher Scientific, 1:1,000) for 3 h at RT. After washing three times for 5 min in 1X PBS, slices were counterstained with DAPI (ThermoFisher Scientific, D1306) and mounted onto glass slides. Images were acquired using the Zeiss LSM880 confocal microscope. The number of particles engulfed by Iba1-positive microglia and microglia morphological features were quantified. Experimental workflow is summarized in Supplementary Figure S3.

Microglia morphology analysis

Multiple z-stack images (20–30 stacked images, 8–10 µm thickness) of Iba1-positive microglia were captured from random areas of *ex vivo* acute brain slices using the Zeiss Axioscan and flattened using Zeiss ZEN 2.3 software. Microglial morphology analysis was performed using a customized morphology Fiji-script developed in collaboration with Prof. Winnok de Vos (University of Antwerp).

Quantification of synaptic markers by mass spectrometry (LC–MS/MS)

Mouse and human brain tissues (Supplementary Table S2) or sections were homogenized (1-part tissue and 4-parts RIPA buffer) using an ultrasonicator (Covaris). Samples were sonicated three times and after each cycle of sonication, the sample were centrifuged at 1,000 xg for 5 min. The supernatant was collected, and remaining pellet was further homogenized, repeating the procedure twice. The supernatants collected from the two consecutive runs were centrifuged at 1,000 xg for 10 min to remove any cell debris. Twenty microliters of homogenate (~400 µg total protein) were reduced and alkylated using tris (2-carboxyethyl) phosphine (TCEP) and iodoacetamide. The protein was then precipitated by adding 6 volumes of cold acetone stepwise with vigorous mixing and incubated at −20°C for 2 h. After incubation samples were centrifuged at 20,000 xg for 15 min. The supernatant was discarded and the resulting pellet was washed with acetone:water (6:1 v/v). After the washing step, the pellet was air dried and suspended in 200 mM ammonium bicarbonate buffer containing trypsin at an enzyme substrate ratio of 1:10. Stable labelled peptide cocktail was added at this stage and the mixture was incubated overnight at 37°C in an Eppendorf thermomixer. After digestion the samples were diluted 1:1 with 95:5 water:acetonitrile containing 0.1% formic acid.

Data was acquired using AB Sciex QTRAP 6500 triple quadruple mass spectrometer coupled to a Schimadzu LC system. Chromatographic separation was achieved on an Aeris C18 peptide column (100 × 2.1 mm, 2.6 µm) running at 0.5 mL/min. Aqueous mobile phase consisted of water with 0.1% formic acid and organic mobile phase consisted of acetonitrile with 0.1% formic acid. The digested samples containing both endogenous and labelled peptides were analyzed by scheduled Multiple Reaction Monitoring (MRM) method monitoring 101 transitions over 30 min run time.

Golgi-Cox staining, imaging, and quantitation of dendritic spines

Frozen mouse and human tissues were immersed in a 5 mL/1 cm^3 tissue Golgi-Cox impregnation solution (FD Rapid GolgiStain™ Kit, FDNeuroTechnologies, INC). The solution was changed 24 h after the first immersion. After 2 weeks impregnation, samples were transferred into a washing solution (solution C) and stored at RT in the dark for at least 72 h. Sagittal sections (100 µm) were mounted on microscope slides, dried, and stained for 10 min before being dehydrated and cleared in xylene (QPS Neuropharmacology, Austria). Slides were imaged on a confocal microscope (63x/1.40 Oil DIC, Zeiss LSM 880) using the reflection mode, z-stacking (100 µm range, 0.5 µm interval) and tiling options. Neurons

from the region of interest fulfilling the following criteria were imaged: (1) the presence of untruncated dendrites, (2) a consistent/dark impregnation along the entire extent of arborization, and (3) a relative isolation from neighboring stained neurons to avoid interference and ensure accuracy of dendritic spine counting. Striatal and middle frontal gyrus neurons were imaged in mice and human brains, respectively. Eight neurons per donor/animal were imaged. Once acquired, the 3D stacks were flattened into a 2D image. The 2D images were opened in ImageJ, each neurite length measured via the freehand line tool, and each spine counted manually. All tissue sample IDs were blinded for experimenters at all steps of the analysis and until completion of the study.

Single nuclei transcriptome analysis

Single nuclei RNA sequencing dataset from post-mortem caudate and putamen tissue of HD and control donors deposited in NBCI GEO: GSE152058 (Lee et al., 2020) was analyzed with a main focus in microglia. Count matrices were loaded into the R (v4.1.0) package Seurat (v4.3.0) (Butler et al., 2018). SCTransform (v0.3.5) was used for count normalization with regressing out the percentage of mitochondria genes. The top principal components (PCs), determined by the ElbowPlot function, were selected for dimensionality reduction, clustering and visualization with UMAP. Marker genes for each cluster were identified with FindAllMarkers function in Seurat (v4.3.0) with the following criteria: adjusted p-value <0.05, log fold change ≥0.25, and genes detected in >25% of the cells within its corresponding cluster. Top markers of microglial subclusters were showed by a heatmap plot using DoHeatmap function in Seurat (v4.3.0). Pseudobulk differential expressed genes were shown in a volcano plot using EnhancedVolcano package (v1.12.0). Gene oncology (GO) analysis was performed in DAVID using differential expressed genes (Huang et al., 2009; Sherman et al., 2022). Significantly upregulated GO terms were shown by bar plots via GraphPad Prism 9 or GOPlot package (v1.0.2).

Statistical analysis

All data are presented as means/individual values ± standard error of the mean (SEM). Data and statistical analysis were performed in GraphPad Prism. Mass cytometry data were analyzed using the unpaired Student's t-test with discovery determined using the two-stage linear step-up procedure of Benjamini, Krieger and Yekutieli, and a False Discovery Rate (FDR; Q) of 10%. Unpaired two-tailed Student's t-test was also used to analyze Western blot data. A Two-way ANOVA followed by Sidak's multiple comparison was used for spine density and *ex vivo* phagocytosis assays. Linear/non-linear regressions were performed for body weight evolution and human microglial function over time.

Results

HD R6/2 mice display a progressive disease phenotype

The R6/2 mouse model has been extensively used as a preclinical model of HD and as such a wealth of information on its disease phenotypes and progression has been reported. This model displays progressive motor dysfunction, weight loss and brain atrophy in the cerebral cortex and the striatum (Stack et al., 2005). To ensure the disease progression of mice housed in our facilities closely resembles the reported phenotypes and progression we assessed body, brain and spleen weight longitudinally at 7, 10, or 15 weeks of age (Supplementary Figure S1). We confirmed a progressive drop in body weight starting at 7 weeks of age, with significant decreases compared to WT litter mates starting at 10 weeks of age (Supplementary Figure S1A). Reduction in the body weight was paralleled by visible and significant decreases in spleen and brain weight in R6/2 mice at pre-and post-symptomatic stages of disease (7–15 weeks of age; Supplementary Figures S1B–D). These findings confirmed R6/2 mice display gross alterations in immune and neurodegenerative phenotypes in line with previous reports (Lee et al., 2018).

Ex vivo mass cytometry reveals phenotypic and functional hyperactivity in peripheral innate immunity of R6/2 mice

Mutant huntingtin can induce both autonomous and non-cell autonomous innate immune activation starting at pre-symptomatic stages of human disease. It is unclear whether heightened inflammatory responses are also present in the R6/2 model. A study from Pido-Lopez et al. described a hyperactive innate immune response in R6/2 mice and when blunted by chlodronate-induced depletion attenuated systemic inflammation (Pido-Lopez et al., 2018). Conversely, Lee et al. report that innate and adaptive immune responses in R6/2 mice are impaired and that stimulation with LPS/TLR4 pathway activation reverses these deficiencies resulting in beneficial behavior and survival outcomes (Lee et al., 2018). Beyond these contradictory findings, to date no phenotypic or functional characterization of peripheral innate and CNS immunity has been performed in the course of disease progression. As such, to get a holistic view on peripheral and CNS immune status in R6/2 mice we performed *ex vivo* mass cytometry studies of spleen and brain at 9 weeks (early symptomatic) and 13 weeks (late symptomatic disease) of age. A CyTOF mass cytometry panel of antibodies was assembled to define distinct immune cell populations and gain insights into their phenotypes.

Mass cytometry analysis of spleens revealed no changes in cell numbers across innate and adaptive cell populations in the spleen at 9 weeks of age (Figures 1A,C) and a decrease in the $CD4^+$ T helper cells as well as the innate immune subsets including NK, monocyte, dendritic and mast cells in the R6/2 mice at 13 weeks of age (Figures 1B,D). Phenotypic characterization revealed significant increases in regulators of phagocytic activity (CD68, CD206), cytoskeletal rearrangement (migratory and homing signals, CD11b, CD11c, CD44, CD49d), and antigen presentation (CD8+ T cell cross-priming: CD40, CD80, F4/80, CD127, CD169) at pre-symptomatic and to a lesser degree at the symptomatic stages of disease. These data collectively suggest a heightened inflammatory response prior to symptom onset and likely cell exhaustion and death at the late stages of disease (Figures 1E,F).

To further corroborate the functional implications of these phenotypic observations we generated bone morrow-derived macrophage (BMDM) cultures for WT and R6/2 mice at timepoints

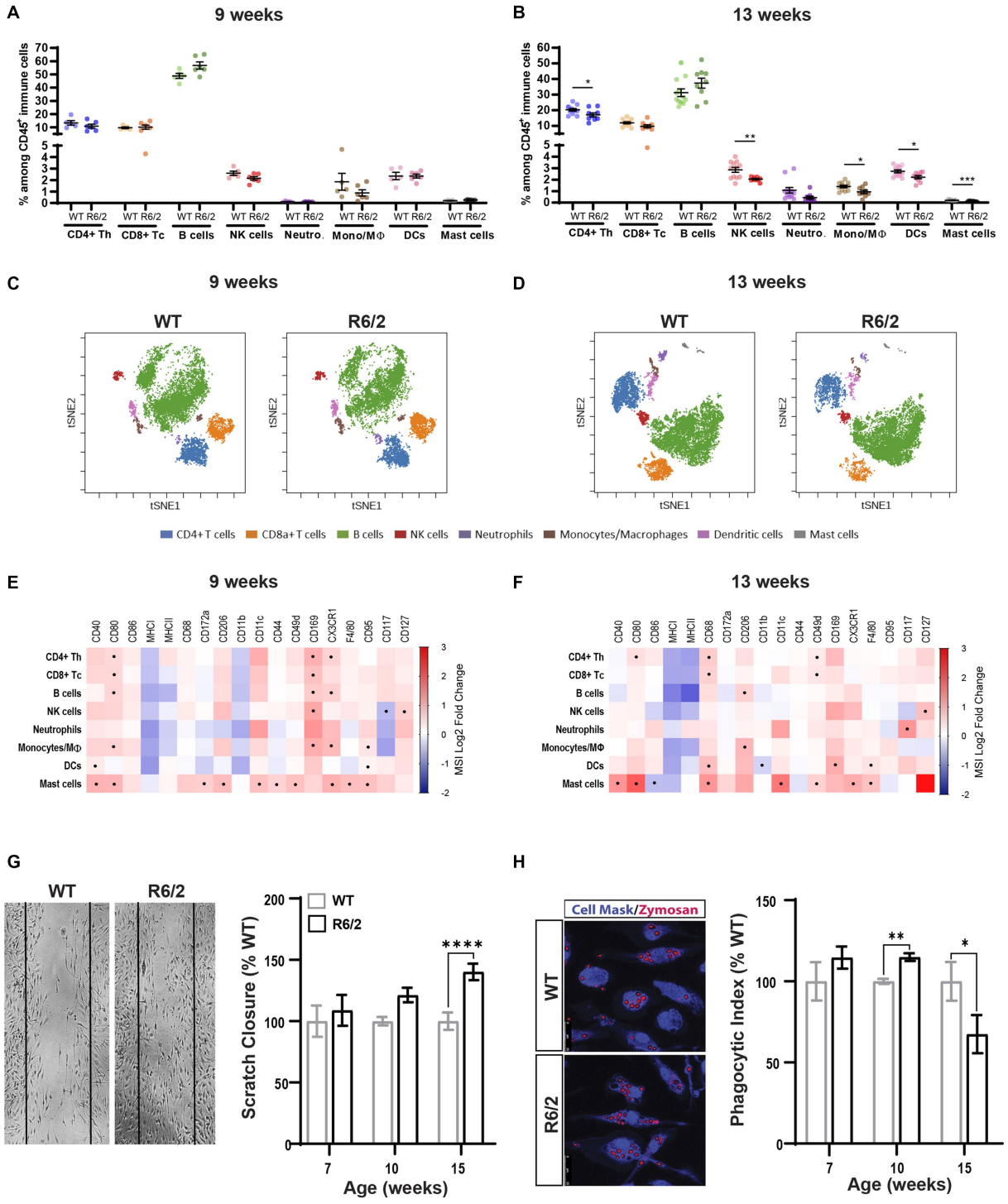

FIGURE 1
Immune phenotyping and functional characterization of peripheral immunity in R6/2 mice. **(A,B)** Relative abundance of the immune subsets among all CD45+ immune cells in the spleen compartment in 9-and 13-week-old mice. CD4+ Th: CD4 positive T helper lymphocyte; CD8+ Tc: CD8 positive T cytotoxic lymphocyte: B cells: B lymphocytes; NK cells: Natural killer cells; Neutro: Neutrophils; Mono/MΘ: monocytes/macrophages; DCs: dendritic cells. **(C,D)** Representative two-dimensional projections of single-cell data generated by t-SNE of immune cell populations in WT vs. R6/2 mice at **(C)** 9 and **(D)** 13 weeks. **(E,F)** Heatmap representation summarizing levels of expression markers in immune cells populations at 9 and 13weeks. Boxes marked with the symbol (•) show statistically significant genotype effect on marker expression (*p*-value equal to or less than 0.05). CRs: cytokine-related receptors. Data are presented as mean±SEM. FDR with two-stage step-up method of Benjamini, Krieger and Yekutieli (Q=10%); *p<0.05, **p<0.01, ****p<0.0001. **(G)** Longitudinal assessment of migratory function in WT and R6/2 BMDM measured as scratch surface area closure due to cell invasion including representative image at 15 weeks of age. **(H)** Uptake of pHrodamine-conjugated zymosan particles in BMDMD isolated from femurs of aging WT and R6/2 mice including representative image at 10weeks of age. Data represents mean values ± SEM. Statistical significance was evaluated using Two Way ANOVA, Sidák multiple comparison test, *p<0.05, **p<0.01, ****p<0.0001; ns, not significant. N=4–5 animals.

pre-and post-phenotypic characterization. Cells were first tested for any alterations in their ability to invade the surface area of the mechanical scratch in the cell culture wells over a 24 h period. Small and non-significant increases of migratory activity of R6/2 BMDM were measured at ages of 7 and 10 weeks reaching statistical significance at 15 weeks of age (Figure 1G). Next, we assessed phagocytic functions by exposing WT and R6/2 BMDM to pHRodo Zymosan™ bioparticles (which fluoresce when internalized into acidified endocytic compartments) for 24 h. A significant increase of phagocytic activity in the R6/2 mouse BMDMs at 10 weeks of age was measured aligning with earlier phenotypic observations (Figure 1H). A significant decrease in phagocytosis was observed at 15 weeks of age, likely due to overall decrease in cellular fitness at end stages of disease.

Immune phenotyping of R6/2 brain tissue reveals altered microglia activation states and peripheral immune cell influx to the CNS compartment

To determine whether the aberrant peripheral inflammatory tone was paralleled in microglia we performed mass cytometry of the brain homogenates collected from the same cohort of WT and R6/2 mice. Microglial activation states and peripheral immune cell presence/infiltration were assessed in parallel. At 9 weeks of age there were no significant changes in microglia cell numbers and a slight increase in mononuclear phagocyte numbers (perivascular, choroid plexus or infiltrating macrophages). At 13 weeks microglial numbers decreased accompanied by increasing cellular heterogeneity due to infiltration of peripheral myeloid and lymphoid immune subsets in the brain of R6/2 mice (Figures 2A,B). Assessment of cell surface marker levels in t-SNE revealed a phenotypic shift in microglia in both early and late stages of disease for the R6/2 mice (Figures 2C,D). At pre-symptomatic stages microglia (and infiltrating neutrophilic populations) increased inflammatory markers such as CD68 and F4/80. With disease progression additional markers including MHCI, CD11c and CD44 were increased in both monocytes and microglia further supporting a phenotypic shift toward a pro-inflammatory state (Figures 2E,F).

Microglial heterogeneity increases with disease progression in R6/2 mice

Next, we performed in depth profiling of microglial populations ($CX3CR1^{+}/CD45^{low/med}$) to further investigate whether a shift to enhanced inflammatory responses was characteristic of all brain microglia. Mass cytometry data from WT and R6/2 mice were mapped in viSNE revealed four clusters of microglia in R6/2 and WT mice at 9 weeks of age (Figure 3A). R6/2 microglia in clusters 1 and 4 displayed increased antigen presentation, phagocytic and migration markers. Interestingly, the increase in these subsets countered a decrease in microglia cluster 2 lacking all activation markers (potentially homeostatic; Figures 3A,C,E). An increase of microglial phenotypic heterogeneity was observed with age and disease progression to advanced stages. At 13 weeks of age six microglial clusters distinct from those in week 9 were identified. Cluster 5 and 7 microglia, characterized by elevated levels of co-stimulatory molecules, phagocytic and migratory markers were significantly increased in R6/2 mice, while cluster 10 microglia lacking any of the above-mentioned markers (homeostatic) were significantly decreased (Figures 3B,D,F).

R6/2 Microglia are morphologically distinct and display heightened phagocytic synaptic uptake

Following characterization of microglial populations, we examined the impact of the observed phenotypic alterations on microglial function. Since migration/surveillance and phagocytic regulators were increased in R6/2 microglia we assessed microglial morphology and phagocytic uptake in a complex 3-dimensional environment consisting of acute 300 µm brain slices pre-and post-phenotypic characterization time points. Brain sections generated from 7-, 10-, and 15-week-old mice were exposed to synaptosomes conjugated to pHRodamine. Synaptosomes were utilized to compare propensities for synapse recognition and uptake between WT and R6/2 microglia during disease progression. One-hour post-zymosan or synaptosome exposure brain sections were washed, fixed in PFA and stained for Iba1. Images of acute sections were analyzed for microglial morphology (surrogate for migratory activity) and phagocytic uptake of $pHrodo^{+}$ particles by Iba1-positive cells, excluding pHRodamine signal from phagocytic non-microglial cells (i.e., astrocytes). Although this particular assay does not capture synaptic pruning by microglia in real time, it provides insights on the functional states of the microglia and alternations in propensity of synapse recognition and uptake in a 3 dimensional native and complex environment.

Images and morphological analysis of microglia revealed a significant decrease in microglial ramifications measured by number of processes and process length in 10-week-old and 7-and 10-week-old R6/2 mice, respectively. At these ages R6/2 microglia displayed enlarged soma and shorter less abundant filopodial processes indicative of increased phagocytic function and motility (Figures 4A,B). Functional assessment of zymosan engulfment (macro-phagocytosis) showed non-significant differences in phagocytosed particle numbers and in numbers of phagocytic microglia at 7 and 10 and 15 weeks of age (Figures 4C,D). Next, we questioned whether R6/2 microglia showed an increased propensity for synaptic uptake. Acute exposure of R6/2 and WT brain slices to pHrodamine-conjugated synaptosomes showed significant uptake by R6/2 microglia at 7 and 10 weeks of age (Figures 4E,F). A significant decrease in synaptosome uptake was observed at the end stages of the disease (week 15; Figure 4F), potentially reflecting a microglial state characterized by an overwhelming cellular debris burden due to progressive neurodegeneration at the end stages of disease and a "shift in priorities" from synaptic pruning to overall phagocytic debris clearance.

R6/2 mice display complement dysregulation, microglial activation, and reduced synaptic density

Next, we questioned whether the observed enhanced microglial synaptic uptake would be reflected in reduced spine density in the aging R6/2 mice. To this end we assessed expression levels of complement factor C3 implicated in synaptic uptake and pre-(VGLUT1/2, synapsin, synaptophysin, SV2A/C) and post-synaptic markers (PSD95). Dendritic spine imaging of Golgi stained forebrains

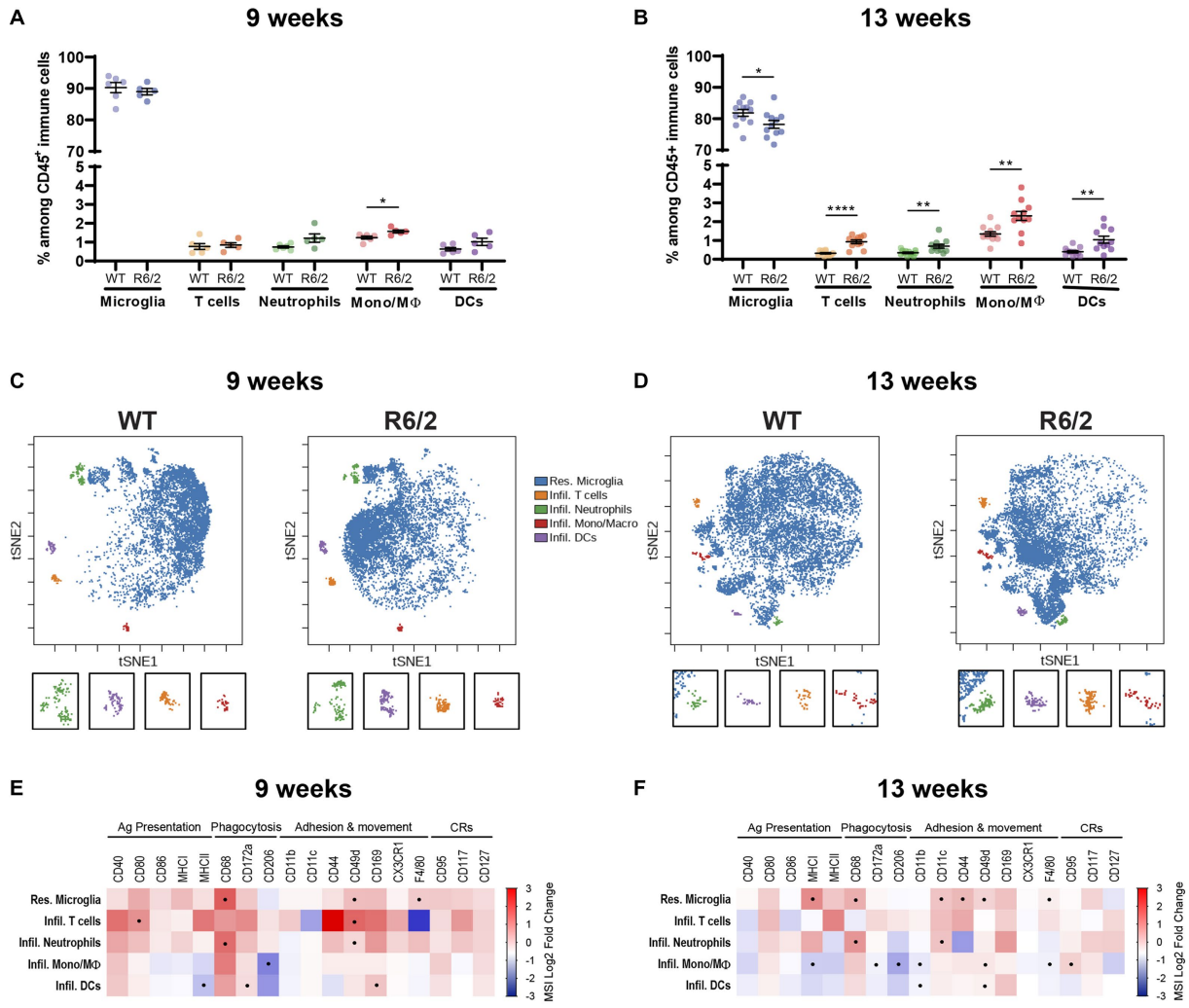

FIGURE 2
Characterization of the brain's resident and infiltrating immune cells populations by mass cytometry. **(A,B)** Relative abundance of the immune subsets among all CD45+ immune cells in the brain compartment in 9-and 13-week-old mice. Mono/MΘ: monocytes/macrophages; DCs: dendritic cells. **(C,D)** Representative two-dimensional projections of single-cell data generated by t-SNE of immune cell populations in WT vs. R6/2 mice at 9 and 13 weeks. **(E,F)** Heatmap representation summarizing levels of expression markers in immune cells populations at **(E)** 9 and **(F)** 13weeks. Boxes marked with the symbol (•) show statistically significant alterations in marker expression. CRs: cytokine-related receptors. *N*=6 (9 weeks) – 11 (13 weeks) animals/condition. Data are presented as mean±SEM; FDR with two-stage step-up method of Benjamini, Krieger and Yekutieli (*Q*=10%); **p*<0.05, ***p*<0.01, *****p*<0.0001.

was also performed to assess spine density and overall arborization in R6/2 mice. C3 levels were significantly increased at 10 weeks of age but not at pre-symptomatic or late stages of disease (Figure 5A). No changes were observed in levels of pre-synaptic markers except for VGLUT1 at the terminal stages of disease (Figures 5B–E). In contrast a significant reduction of post-synaptic marker PSD95 was noted as early as pre-symptomatic stages of disease (7 weeks of age) and throughout disease (Figure 5F). Decreased levels of PSD95 were paralleled by significant loss of spines in primary through quaternary branching of striatal neurons in R6/2 mice (Figures 5G–I).

Next, we questioned whether the state of synaptic architecture observed in R6/2 was reflected in human disease. Densitometry analysis of complement factors C1Q and C3 normalized to actin showed no significant changes in complement levels (Figures 6A,B); However, significant increase of translocator protein TSPO (Figure 6C) as a measure of inflammatory microglia was observed. Mass spectrometry analysis for the same pre-and post-synaptic markers showed no differences between non-demented controls (NDC) and HD brains (Supplementary Table S2; Figures 6C–H). Golgi-Cox staining of middle-frontal gyrus neurons showed a non-significant decrease in synaptic density in secondary branching of HD striatal neurons (Figures 6I,J).

Microglia activation is characterized by upregulation of regulators of phagocytic and migratory functions in HD brain single cell sequencing data sets

To get a broader view of microglial population heterogeneity and key pathways dysregulated in disease-associated microglia we re-analyzed single nuclei RNA sequencing public datasets

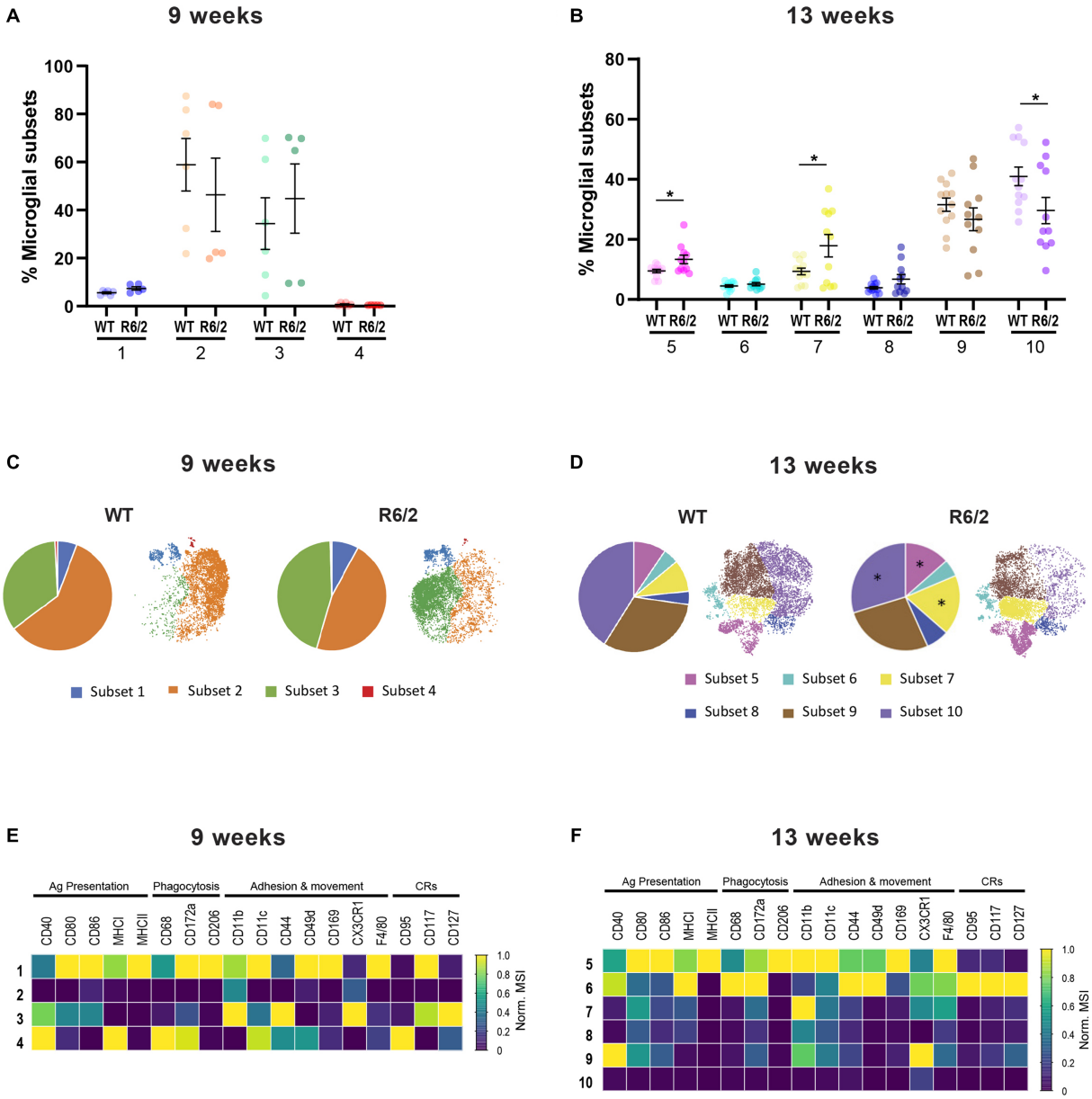

FIGURE 3
Characterization by mass cytometry of microglia heterogeneity in R6/2 mice. **(A,B)** Relative abundance of the microglia subsets among total population in the brain compartment in 9-and 13-week-old mice. **(C,D)** Pie charts and viSNE clustering showing the representation of microglial subsets in WT and R6/2 mice at 9 and 13weeks. **(E,F)** Heatmap capturing levels of expression markers in microglia subsets at 9 and 13weeks. CRs: cytokine-related receptors. *N*=6 (9weeks) – 11 (13weeks) animals/condition; data are presented as mean±SEM; FDR with two-stage step-up method of Benjamini, Krieger and Yekutieli (*Q*=10%); *p<0.05.

generated and reported by Lee et al. (2020). Analysis of datasets from 14 HD and 14 age-matched non-demented controls identified distinct cell populations including microglia, astrocytes, oligodendrocytes, OPCs, endothelial cells, ependymal cells, medium spiny neurons (MSN) and other neuron subtypes (Figure 7A). Further clustering of microglia resulted in 19 subclusters of microglia (Figure 7B) which suggests high level of heterogeneity of microglial populations. Five microglia clusters (1, 5, 9, 10, 11) unique to NDCs and 7 disease-specific microglia clusters (4, 6, 12, 13, 15, 16, 17) were identified (Figure 7B). Furthermore, when disease staging was considered as an analysis criterium, data showed certain microglia subsets cluster in a grade stage dependent manner, with clusters 4, 12, 13, 15 originating from brains at stage 3 of the disease and cluster 6 mainly from stage 4 (Figure 7B).

To further reveal the identity of these microglia subclusters, we performed differential gene expression analysis and found the majority of the microglia are in homeostatic stage which expressed high levels of CX3CR1 and P2RY12 (Figures 7C,D). A population of cycling microglia as defined by the expression of proliferation markers MKI67 and TOP2A and a cluster of macrophages defined by the expression of F13A1 and LYVE1 were identified (Figure 7C) (Hammond et al., 2019). Gene ontology analysis of disease-associated

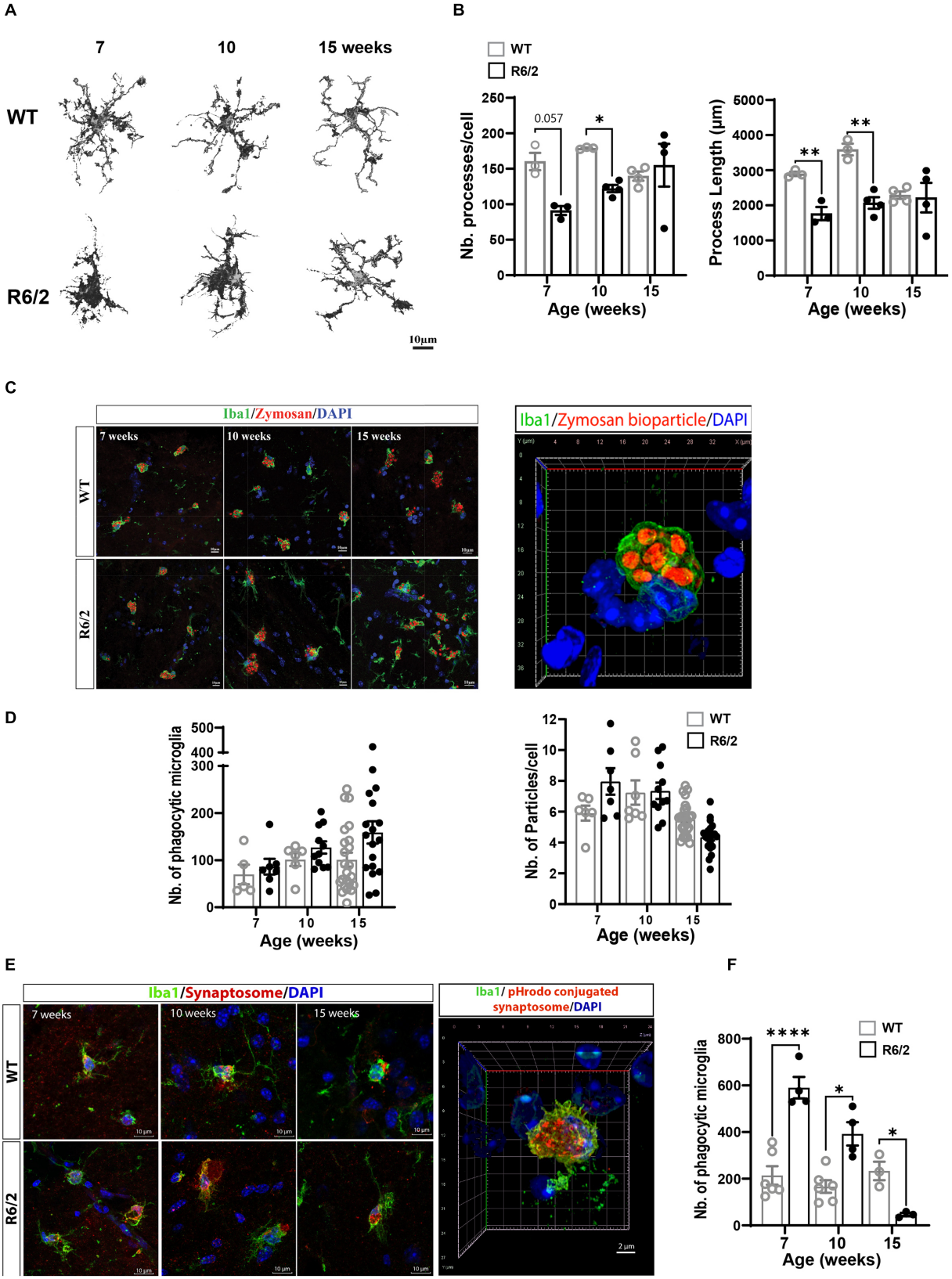

FIGURE 4
Ex vivo microglial morphology and phagocytic function in aging R6/2 mice. **(A)** Microglia morphological changes with age in WT and R6/2 mice. **(B)** Comparative quantitation of microglia filopodial branching during disease progression in R62 vs. age-and litter-matched WT mice. **(C)** Representative 3D-reconstructed image of a phagocytic microglia labeled with Iba1 (green; nuclei DAPI blue) displaying internalized pHrodo™ conjugated zymosan bioparticles™ (red). **(D)** Longitudinal assessment of microglial phagocytosis of zymosan bioparticles in aging WT and R6/2 mice (n=5–23 brain slices/condition, N=3–4 animals/condition). **(E)** Representative images of *ex vivo* microglial stained with Iba1 (green; nuclei DAPI blue)

(Continued)

FIGURE 4 (CONTINUED)
phagocytosis of pHrodamine-conjugated synaptosomes (red). **(F)** Comparative quantitation of the number of synaptosomes-phagocytosing microglia in aging WT and R6/2 mice (n=3–6 brain slices/condition, N=2–4 animals/condition. Statistical significance was evaluated using Two-Way ANOVA, Sidák multiple comparison test, *p<0.05, **p<0.01, ****p<0.0001; ns, not significant).

microglia in clusters 4 and 6 (representative of stage 3 and 4, respectively) was performed with the upregulated genes from each cluster. Distinct pathway enrichments in microglia from stage 3 and stage 4 brains were observed. Interestingly, cell migration, endocytosis, cell adhesion, signal transduction and inflammatory response were significantly upregulated in HD brains and were highly prioritized by the gene ontology analysis (Figures 7D–G).

Human HD iMGL are characterized by highly phagocytic and migratory phenotypes and functions

Next, we questioned whether increases in gene signatures regulating phagocytic and migratory pathways in human HD microglia signified overactive phagocytic and migratory phenotypes and functions. An HD patient iPSC line heterozygous for pathologic CAG repeats in the HTT gene (~18 repeats in one allele, and ~40 repeats in the other) and its isogenic control were induced to differentiate into iMGL. Following 25 days in culture, iMGL were detached and immunostained with a panel of metal-conjugated antibodies against cell surface regulators of essential microglial functions such as adhesion/migration, antigen presentation, and phagocytosis (Supplementary Table S3). High dimensional analysis at single cell resolution revealed 8 microglial sub-clusters, suggesting cells at day 25 in culture represent various states of maturity and activation (Figure 8A). A decrease in representation of cluster 1 characterized by high expression of tolerogenic receptors including CD83, CD163, CD169, and CSFR2 was observed in the HD line. This was paralleled by increased representation of clusters 4 and 5, characterized by high expression of adhesion, migration, and phagocytosis/lysosomal clearance receptors. Interestingly, representation of cluster 8 displaying high levels of peripheral innate immune markers such as CD45, CCR2, and complement receptor 3 (CR3) typically identifying cells of hematopoietic/monocytic lineage was increased in the HD line. This suggests a potential delayed maturity or propensity of HD stem cell subset to differentiate into monocytic lineage (Figures 8A,B).

Next, we assessed whether these phenotypic shifts observed by mass cytometry matched phagocytic and functional outcomes. Longitudinal functional assessment of phagocytic function by time lapse imaging showed both isogenic and HD lines were able to phagocytose and completely suppress phagocytic uptake in the presence of cytochalasin D (actin cytoskeleton polymerization inhibitor). A linear (Figure 8C) and nonlinear/exponential (Figure 8D) regression were performed to evaluate longitudinal variations in phagocytosis/migration and compare slopes differences, and a t-test at 24 h to compare two means. HD iMGL showed significantly enhanced particle uptake of pHRhodamine zymosan bioparticles with significant differences in slopes ($p < 0.0001$) and at the 24 h timepoint ($p = 0.01$; Figure 8C). Increased phagocytic activity was paralleled by a significantly increased migratory activity measured as scratch area invasion/closure by mHTT iMGL (k coefficient difference $p = 0.0106$; mean difference at 24 h $p = 0.0028$; Figure 8D). Interestingly, culture fluids collected form the same zymosan-stimulated microglia showed significantly higher levels of pro-inflammatory cytokine release (IL-6) by the HD cells compared to their isogenic controls, supporting their increased propensity for enhanced inflammatory response compared to isogenic controls (data not shown).

Discussion

It is widely recognized that microglia may contribute to non-cell autonomous neurotoxicity and exacerbation of disease progression in various neurodegenerative diseases. Transcriptomics studies in animal models and more recently human brain tissues, have reported mHTT-and neuronal death-dependent microglial activation; however, what "activation" signifies and what cellular functions are ultimately impacted by deregulated gene transcripts have not been fully explored (Crotti et al., 2014). This study aimed at filling some of these gaps by establishing connections between microglial phenotypic alterations, functional behaviors, and impact on neuronal pathology in the R6/2 mouse model, human diseased tissues, and cellular systems. One outstanding question that remained given the decreases in spleen size with disease progression was: What phenotypic and functional changes occurred in the periphery pre-and post-symptomatic stages? The data regarding innate immune compartment to date is unclear with reports suggesting either deficiency or hyperactivation of immune response in HD rodent models (Lee et al., 2018; Pido-Lopez et al., 2018). Mass cytometry of the spleens and functional assessment of BMDMs showed an increase in regulators of phagocytosis and chemotaxis at pre-symptomatic stages followed by altered functional outcomes at symptomatic and end stages of disease. It is worth noting that *ex vivo* mass cytometry revealed presence of classical peripheral immune cell markers in the brains of R6/2 mice. We annotated these subsets as monocytes, neutrophils or DCs cells based on a combination of 3–4 markers present in the CyTOF panel and taking into consideration levels of CD45 expression in each subset. Due to the pathological inflammatory context and similar genetic makeup, we cannot exclude the possibility that these cells can also represent a subset of activated microglia, perivascular macrophages, or meningeal and choroid plexus innate immune cells. Peripheral immune cells have also been reported in HD human brain tissue; however, their implication in HD pathobiology requires additional investigation (Di Pardo et al., 2013).

The primary focus of our study was the microglia. More specifically we investigated how specific functions related to synaptic pruning such as phagocytosis and neuronal surveillance (morphology/

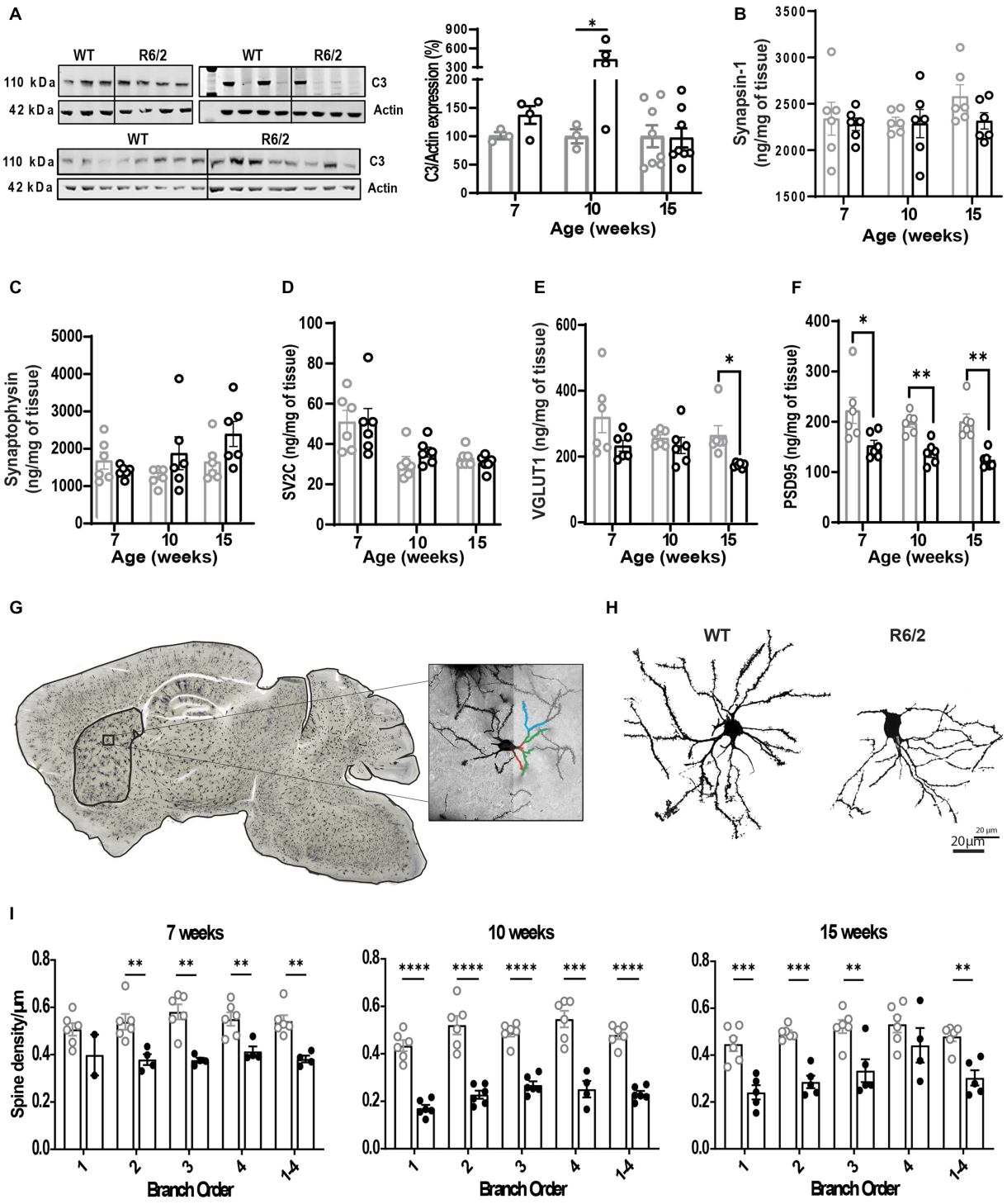

FIGURE 5
Altered synaptic architecture in aging R6/2 mice. **(A)** Representative image and densitometry analysis of complement factor C3 in WT and R6/2 brain homogenates at 7, 10, and 15weeks of age normalized to actin. Quantitative measurements by mass spectrometry of pre-synaptic proteins synapsin-1 **(B)**, synaptophysin **(C)**, SV2C **(D)**, VGLUT1 **(E)** and post-synaptic protein PSD95 **(F)** in brain homogenates of WT and R6/2 mice at 7,10, and 15weeks of age. **(G)** Bright field confocal image of a Golgi-Cox stained R6/2 brains, with a visual illustration of the manual neurite and dendritic spine tracing in striatal neurons. **(H)** High resolution bright field image of WT and R6/2 striatal neurons at 10weeks of age. **(I)** Manual quantification of neurite branching and dendritic spine density in the striatal neurons of WT and R6/2 mice at 7, 10, and 15 weeks of age. *N*=6 mice/condition; *n*=8 neurons/mouse. Data shown as mean/individual values ± SEM. Analysis utilizing Two Way ANOVA, Sidák multiple comparison test, **p*<0.05, ***p*<0.01, ****p*<0.001, *****p*<0.0001. ns, not significant.

chemotaxis) were impacted, considering the phenotypic alterations in these pathways. Immune phenotyping at single cell resolution demonstrated the presence of various microglial subsets in the R6/2 mice. This heterogeneity can be likely attributed to regionally-and

10.3389/fnmol.2023.1191324

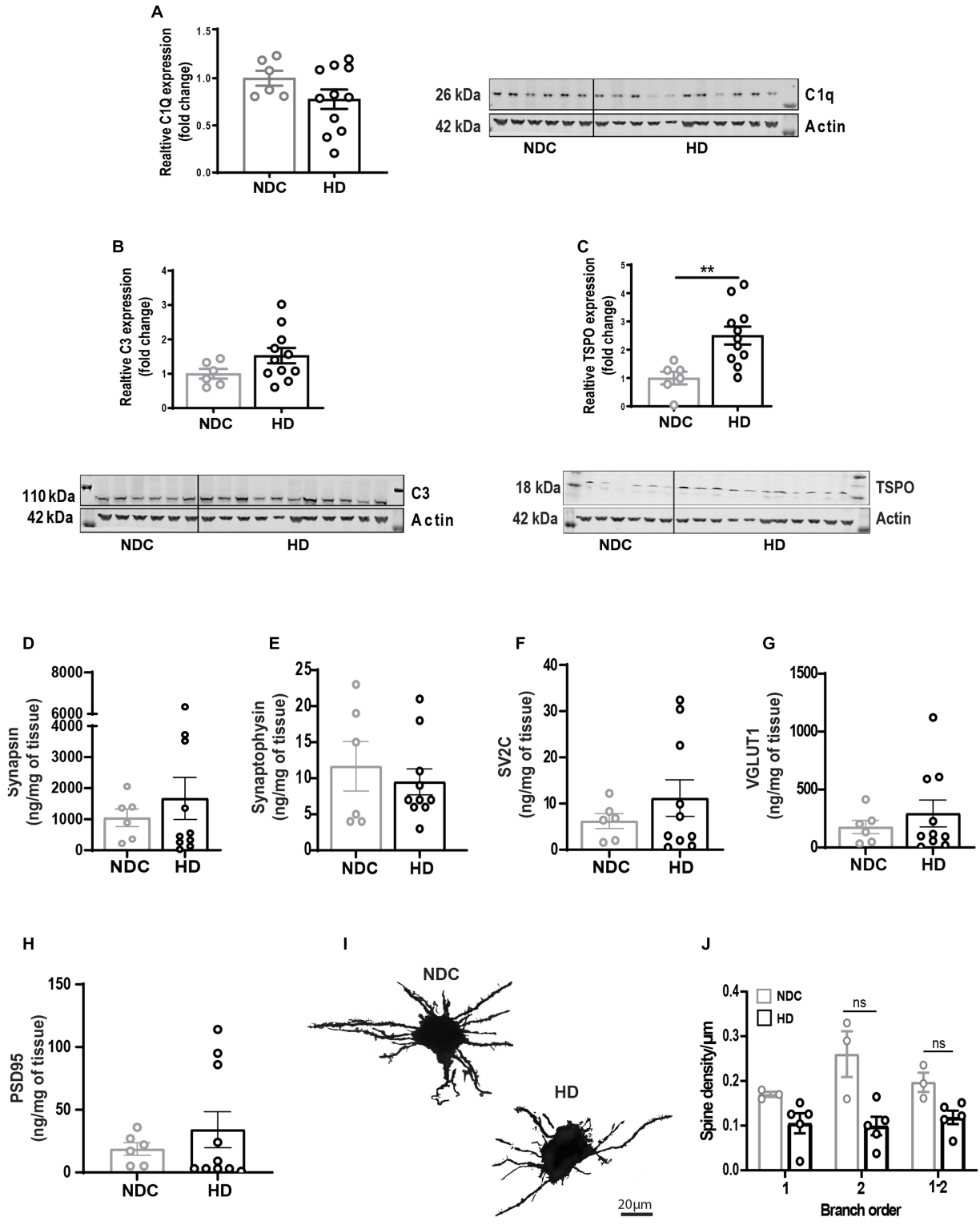

FIGURE 6
State of synaptic architecture in human HD brains. **(A–C)** Densitometry analysis of complement factors C1Q, C3, and glial activation marker TSPO western blots of human non demented controls (NDC) and HD brain homogenates (normalized to actin). Longitudinal evaluation by mass cytometry of pre-synaptic markers synapsin **(D)**, synaptophysin **(E)**, SV2c **(F)**, VGLUT1 **(G)** and post-synaptic marker PSD-95 **(H)** in human NDC and HD brain homogenates. **(I,J)** High magnification bright field confocal image of Golgi-Cox-stained middle frontal gyrus neurons and manual quantification of neurite branching and dendritic spine density in human NDC and HD. Data represented as mean/individual values ±SEM. *N*=3–5 donors/condition; *n*=8 neurons/donor. Statistical analysis was performed using Unpaired *t*-test (western blots) and Two Way ANOVA, Sidák multiple comparison test, $^{**}p<0.01$. ns, not significant.

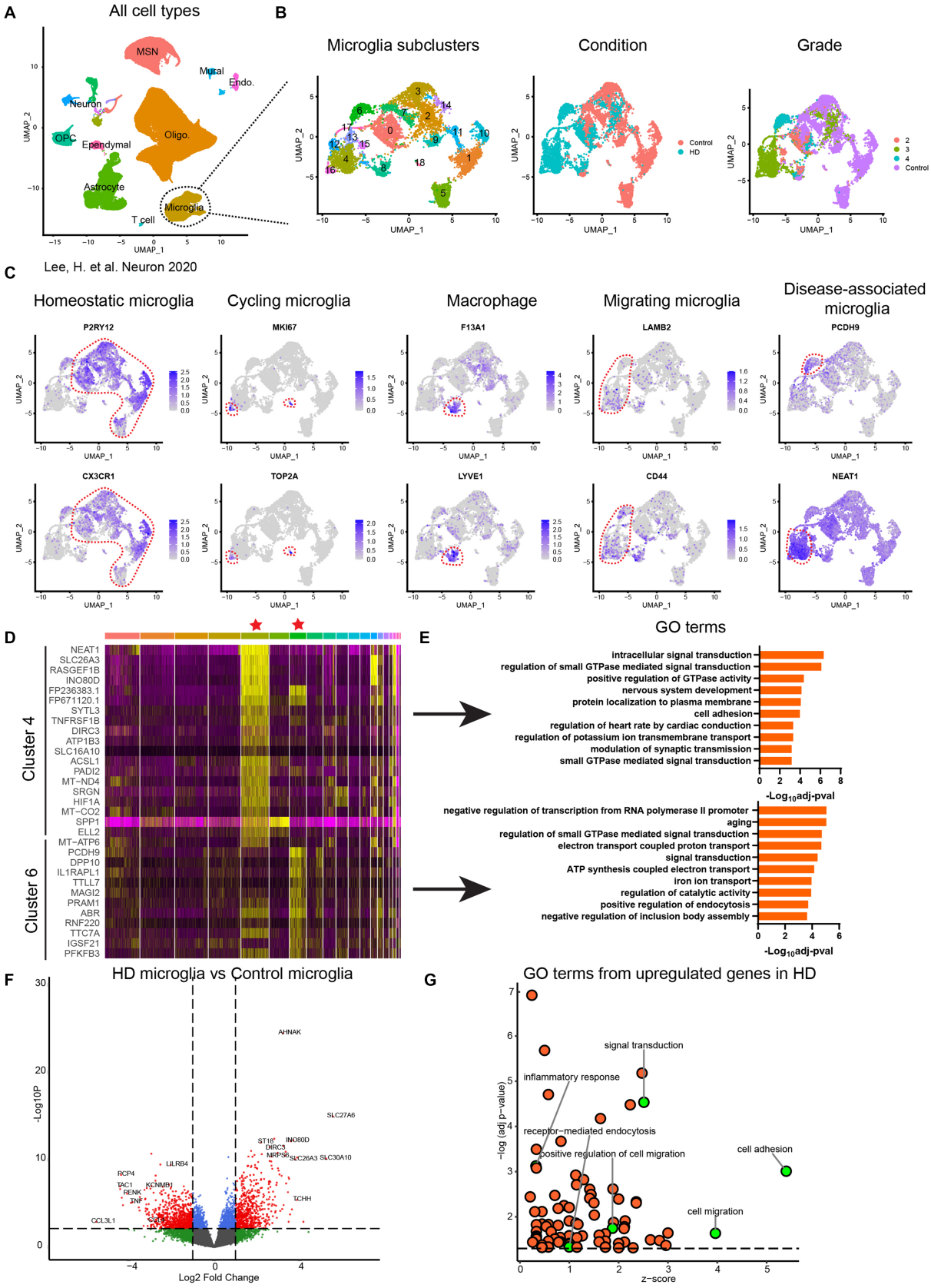

FIGURE 7
Transcriptomic characterization of human HD primary microglia. **(A)** Uniform Manifold Approximation and Projection (UMAP) of single nuclei transcriptome from published data set (Lee et al., 2020) comprising 125,467 nuclei from 14 unaffected control and 14 HD caudate and putamen samples. MSN: medium spiny neuron; Oligo.: oligodendrocyte; OPC: oligodendrocyte progenitor cell; Endo.: endothelial cell. **(B)** Subcluster

(Continued)

FIGURE 7 (CONTINUED)
identification corresponding to disease associated microglia. **(C)** Identification of microglia subpopulations based on the top markers of each cluster. **(D)** Heatmap of differential expressed genes in cluster 4 and cluster 6 compared to other clusters. **(E)** Enriched gene oncology (GO) terms of cluster 4 and cluster 6 based on upregulated genes in each cluster. **(F)** Differential gene expression analysis of whole microglia population without considering subclusters. Dash line indicates p=0.05. **(G)** GO analysis based on the differential expressed genes in **(F)**. Dash line indicates p=0.05.

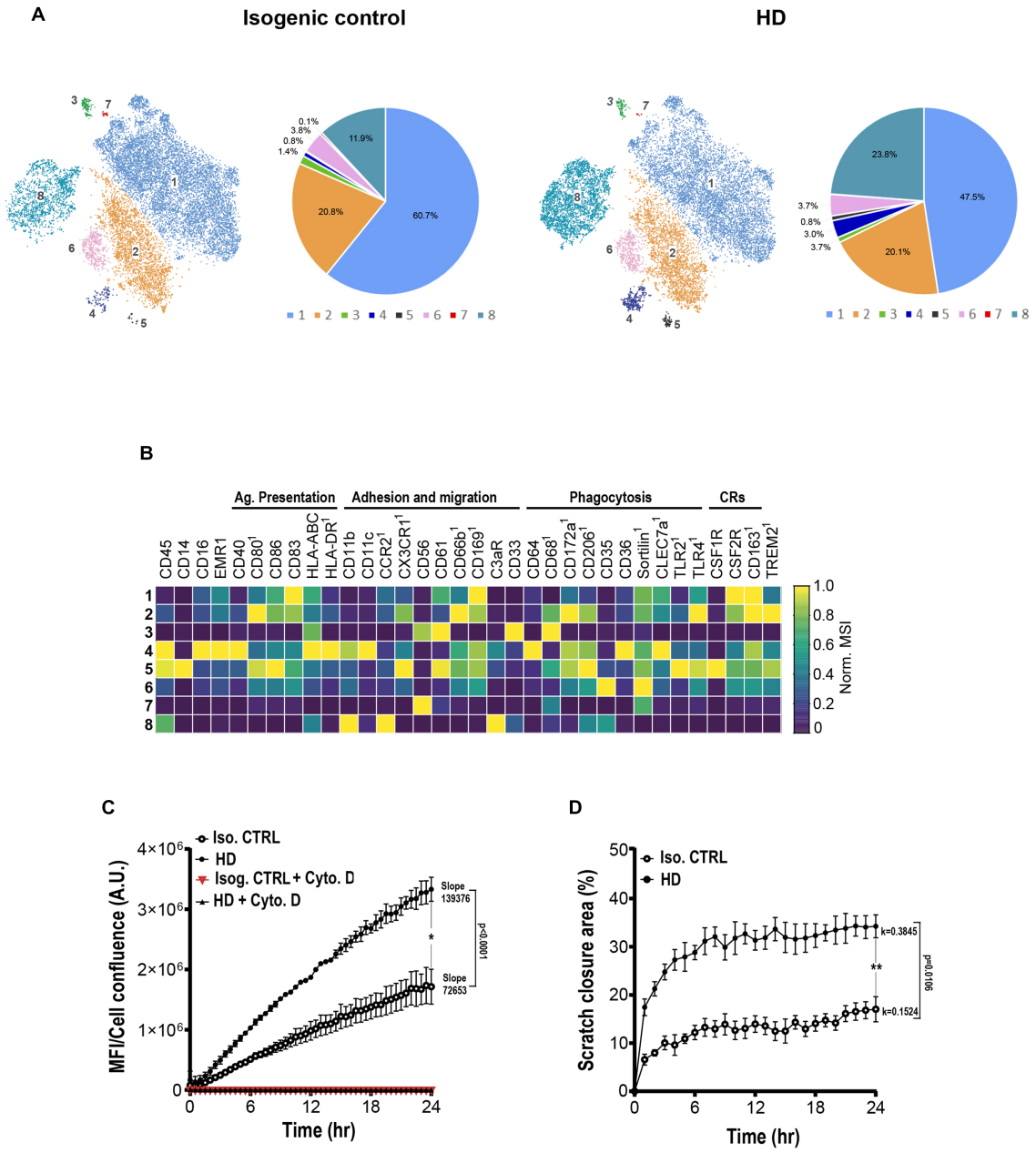

FIGURE 8
HD iPSC-derived microglia show enhanced phagocytosis and migration. **(A)** Representative mass cytometry t-SNE clustering and subset representation of human isogenic and HD iMGL. 15,000 cells per condition were randomly sampled. **(B)** Heatmap capturing levels of lineage, phagocytosis, migration and cytokine receptor cell markers in each microglial cluster. [1]Marker showing low mean signal intensity (MSI<5). **(C)** Graphic capturing longitudinal time lapse imaging over 24h of pHrodo™ labelled zymosan uptake by isogenic and HD patient iMGL. Data includes blockade of phagocytosis with actin cytoskeleton inhibitor cytochalasin D. Fluorescence intensity was normalized to cell confluence. **(D)** Graphic representation of time lapse imaging of isogenic and HD iMGL migration to the scratch area over 24h. Relative wound cellular density represents the proportion of migrating cells over time. Data from N=3 independent iMGL differentiation experiments and n=3 technical replicates. A linear **(C)** and nonlinear/exponential **(D)** regression were performed to evaluate longitudinal variations in phagocytosis/migration and compare slopes differences, and an unpaired t-test at 24h to compare two means, *p<0.05, **p<0.01. Data captured as mean±S.D.

metabolically-distinct microglial phenotypes and in the context of disease proximity to neuronal degeneration. Furthermore, basal ganglia are densely populated by microglia potentially contributing to heightened selective loss of striatal neurons in HD (Mittelbronn et al., 2001; Tan et al., 2020).

We assessed phagocytic activity in the entire surface areas of the brain slices and observed increased phagocytic activity of synaptosomes in the R6/2 microglia as early as pre-symptomatic stages of disease. The acute slice model was chosen to keep microglia in their complex environment omitting the caveats of cellular sorting and plastic-induced activation in functional assessment of brain isolated microglia (Cadiz et al., 2022). It is worth noting the differences in assay sensitivity of zymosan uptake vs. synaptosomes, with the synaptosome uptake being a more relevant and sensitive measure of alterations in phagocytosis. Assessment of R6/2 microglial functions required both assays given their more subtle phenotypes compared to HD iPSC microglia which displayed ameboid rather than ramified morphology *in vitro*. Synaptosome uptake by iMGLs was unquantifiable due to overly saturated signal *in vitro*. As such we resorted to a less sensitive approach such as zymosan uptake which showed significantly increased uptake in HD iMGL compared to isogenic control. Cytokine measurements in the culture fluids of iMGL exposed to zymosan showed an increased propensity for IL-6 and IL-8 release (data not shown). We recognize that one should not draw generalized conclusions for microglia function in HD based on hyperactivity observed in one donor line. Several donor lines with higher numbers of poly-Q repeats were also tested; however, no functional data were generated due to very poor overall health and viability of these cells when differentiated to iMGLs. Our observations with the high polyQ repeat lines align with others reporting significantly higher apoptotic activity in iMGL lines carrying over 80 polyQ repeats compared to those in the 30–40 range (O'Regan et al., 2021). Our iMGL *in vitro* data suggests mHTT can trigger an inflammatory phenotype in these cells independent of any non-cell autonomous activation cues from dying neurons in the complex brain environment.

In conclusion, our data from R6/2 mice, human cell and tissue-based systems collectively point to an autonomous and non-cell autonomous induction of innate immune inflammation, aberrant microglial migratory/surveillance and phagocytic functions associated with profound synaptic loss. It is broadly recognized that mHTT can cause multi-system toxicity that contributes to poor prognosis; however, in the context of neurological symptoms a microglial/innate immune modulator selectively targeting microglial aberrant functions such as synaptic overpruning may hold potential in attenuating progression of cognitive and motor decline in HD.

Data availability statement

The datasets presented in this study can be found in online repositories. The names of the repository/repositories and accession number(s) can be found in the article/Supplementary material.

Ethics statement

The studies involving human participants were reviewed and approved by UCB Biobank and Ethics Committee of UCB Biopharma. The patients/participants provided their written informed consent to participate in this study.

Author contributions

JG and IK designed the studies. GG, JV, JK, AK, WF, and JG performed experiments and analyzed the data. JG and IK wrote the manuscript. All authors contributed to the article and approved the submitted version.

Acknowledgments

The authors would like to thank Gregory Szczesny and Sasker Grootjans (UCB) for development of the co-localization script. The authors thank Martine Geraerts (UCB) for providing iPSC mHTT mutant lines and their isogenic controls. The authors would like to thank Winnok de Vos (University of Antwerp) for his contribution in the development of a custom-made script for assessing cell morphology. The authors would like to thank UCB statisticians Phil Stanley and Etienne Hannon for their support with the statistical analysis.

Conflict of interest

The authors declare that this study was funded in its entirety by UCB Biopharma SRL. The funder had the following involvement in the study: all authors were employees of UCB at the time of execution of the study. The funder was involved in the funding of the study in its entirety, as well as study design, collection, analysis, interpretation of data, the writing of this article, and the decision to submit it for publication.

Publisher's note

Supplementary material

The Supplementary material for this article can be found online at: https://www.frontiersin.org/articles/10.3389/fnmol.2023.1191324/full#supplementary-material

References

Abud, E. M., Ramirez, R. N., Martinez, E. S., Healy, L. M., Nguyen, C. H. H., Newman, S. A., et al. (2017). iPSC-derived human microglia-like cells to study neurological diseases. *Neuron* 94, 278–293.e9. doi: 10.1016/j.neuron.2017.03.042

Butler, A., Hoffman, P., Smibert, P., Papalexi, E., and Satija, R. (2018). Integrating single-cell transcriptomic data across different conditions, technologies, and species. *Nat. Biotechnol.* 36, 411–420. doi: 10.1038/nbt.4096

Cadiz, M. P., Jensen, T. D., Sens, J. P., Zhu, K., Song, W.-M., Zhang, B., et al. (2022). Culture shock: microglial heterogeneity, activation, and disrupted single-cell microglial networks *in vitro*. *Mol. Neurodegener.* 17:26. doi: 10.1186/s13024-022-00531-1

Crotti, A., Benner, C., Kerman, B. E., Gosselin, D., Lagier-Tourenne, C., Zuccato, C., et al. (2014). Mutant huntingtin promotes autonomous microglia activation via myeloid lineage-determining factors. *Nat. Neurosci.* 17, 513–521. doi: 10.1038/nn.3668

Delva, A., Michiels, L., Koole, M., Van Laere, K., and Vandenberghe, W. (2022). Synaptic damage and its clinical correlates in people with early Huntington disease: a PET study. *Neurology* 98, e83–e94. doi: 10.1212/WNL.0000000000012969

Di Pardo, A., Alberti, S., Maglione, V., Amico, E., Cortes, E. P., Elifani, F., et al. (2013). Changes of peripheral TGF-β1 depend on monocytes-derived macrophages in Huntington disease. *Mol. Brain* 6:55. doi: 10.1186/1756-6606-6-55

Hammond, T. R., Dufort, C., Dissing-Olesen, L., Giera, S., Young, A., Wysoker, A., et al. (2019). Single-cell RNA sequencing of microglia throughout the mouse lifespan and in the injured brain reveals complex cell-state changes. *Immunity* 50, 253–271.e6. doi: 10.1016/j.immuni.2018.11.004

Huang, D. W., Sherman, B. T., and Lempicki, R. A. (2009). Systematic and integrative analysis of large gene lists using DAVID bioinformatics resources. *Nat. Protoc.* 4, 44–57. doi: 10.1038/nprot.2008.211

Keaney, J., Gasser, J., Gillet, G., Scholz, D., and Kadiu, I. (2019). Inhibition of Bruton's tyrosine kinase modulates microglial phagocytosis: therapeutic implications for Alzheimer's disease. *J. Neuroimmune Pharmacol.* 14, 448–461. doi: 10.1007/s11481-019-09839-0

Kwan, W., Träger, U., Davalos, D., Chou, A., Bouchard, J., Andre, R., et al. (2012). Mutant huntingtin impairs immune cell migration in Huntington disease. *J. Clin. Invest.* 122, 4737–4747. doi: 10.1172/JCI64484

Lee, H., Fenster, R. J., Pineda, S. S., Gibbs, W. S., Mohammadi, S., Davila-Velderrain, J., et al. (2020). Cell type-specific transcriptomics reveals that mutant huntingtin leads to mitochondrial RNA release and neuronal innate immune activation. *Neuron* 107, 891–908.e8. doi: 10.1016/j.neuron.2020.06.021

Lee, S. W., Park, H. J., Im, W., Kim, M., and Hong, S. (2018). Repeated immune activation with low-dose lipopolysaccharide attenuates the severity of Huntington's disease in R6/2 transgenic mice. *Anim. Cells Syst.* 22, 219–226. doi: 10.1080/19768354.2018.1473291

Mecca, A. P., O'Dell, R. S., Sharp, E. S., Banks, E. R., Bartlett, H. H., Zhao, W., et al. (2022). Synaptic density and cognitive performance in Alzheimer's disease: a PET imaging study with [^{11} C]UCB-J. *Alzheimers Dement.* 18, 2527–2536. doi: 10.1002/alz.12582

Mittelbronn, M., Dietz, K., Schluesener, H. J., and Meyermann, R. (2001). Local distribution of microglia in the normal adult human central nervous system differs by up to one order of magnitude. *Acta Neuropathol.* 101, 249–255. doi: 10.1007/s004010000284

Moscovitch-Lopatin, M., Weiss, A., Rosas, H.D., and Ritch, J. (2010). Optimization of an HTRF assay for the detection of soluble mutant huntingtin in human Buffy coats: A potential biomarker in blood for Huntington disease. Available at: https://www.ncbi.nlm.nih.gov/pmc/articles/PMC3015780/.

O'Regan, G. C., Farag, S. H., Casey, C. S., Wood-Kaczmar, A., Pocock, J. M., Tabrizi, S. J., et al. (2021). Human Huntington's disease pluripotent stem cell-derived microglia develop normally but are abnormally hyper-reactive and release elevated levels of reactive oxygen species. *J. Neuroinflammation* 18:94. doi: 10.1186/s12974-021-02147-6

Pido-Lopez, J., Andre, R., Benjamin, A. C., Ali, N., Farag, S., Tabrizi, S. J., et al. (2018). *In vivo* neutralization of the protagonist role of macrophages during the chronic inflammatory stage of Huntington's disease. *Sci. Rep.* 8:11447. doi: 10.1038/s41598-018-29792-x

Politis, M., Pavese, N., Tai, Y. F., Kiferle, L., Mason, S. L., Brooks, D. J., et al. (2011). Microglial activation in regions related to cognitive function predicts disease onset in Huntington's disease: a multimodal imaging study. *Hum. Brain Mapp.* 32, 258–270. doi: 10.1002/hbm.21008

Sassone, J., Colciago, C., Cislaghi, G., Silani, V., and Ciammola, A. (2009). Huntington's disease: the current state of research with peripheral tissues. *Exp. Neurol.* 219, 385–397. doi: 10.1016/j.expneurol.2009.05.012

Schure, U., Magnusson, A., André, R., Rabbanian, S., Lowdell, M. W., Bjorkqvist, M., et al. (2010). A18 cellular signalling of human monocytes in Huntington's disease. *J. Neurol. Neurosurg. Neuropsychiatry* 81:A6-A6. doi: 10.1136/jnnp.2010.222570.18

Sherman, B. T., Hao, M., Qiu, J., Jiao, X., Baseler, M. W., Lane, H. C., et al. (2022). DAVID: a web server for functional enrichment analysis and functional annotation of gene lists (2021 update). *Nucleic Acids Res.* 50, W216–W221. doi: 10.1093/nar/gkac194

Stack, E. C., Kubilus, J. K., Smith, K., Cormier, K., Del Signore, S. J., Guelin, E., et al. (2005). Chronology of behavioral symptoms and neuropathological sequela in R6/2 Huntington's disease transgenic mice. *J. Comp. Neurol.* 490, 354–370. doi: 10.1002/cne.20680

Tai, Y. F., Pavese, N., Gerhard, A., Tabrizi, S. J., Barker, R. A., Brooks, D. J., et al. (2007). Imaging microglial activation in Huntington's disease. *Brain Res. Bull.* 72, 148–151. doi: 10.1016/j.brainresbull.2006.10.029

Tan, Y.-L., Yuan, Y., and Tian, L. (2020). Microglial regional heterogeneity and its role in the brain. *Mol. Psychiatry* 25, 351–367. doi: 10.1038/s41380-019-0609-8

Träger, U., Andre, R., Magnusson-Lind, A., Miller, J. R. C., Connolly, C., Weiss, A., et al. (2015). Characterisation of immune cell function in fragment and full-length Huntington's disease mouse models. *Neurobiol. Dis.* 73, 388–398. doi: 10.1016/j.nbd.2014.10.012

van der Burg, J. M., Björkqvist, M., and Brundin, P. (2009). Beyond the brain: widespread pathology in Huntington's disease. *Lancet Neurol.* 8, 765–774. doi: 10.1016/S1474-4422(09)70178-4

Weiss, A., Träger, U., Wild, E. J., Grueninger, S., Farmer, R., Landles, C., et al. (2012). Mutant huntingtin fragmentation in immune cells tracks Huntington's disease progression. *J. Clin. Invest.* 122, 3731–3736. doi: 10.1172/JCI64565

Glossary

BBB	Blood brain barrier
BMDM	Bone marrow derived macrophages
DAM	Disease-associated microglia
CNS	Central nervous system
CSF1R	Colony stimulating factor 1 receptor
CyTOF	Mass cytometry by time of flight
FDR	False discovery rate
HD	Huntington's disease
HTT	Huntingtin protein
iHPC	Induced hematopoietic progenitor cells
iMGL	hiPSC-induced microglia
iPSC	Induced pluripotent stem cells
PFA	Paraformaldehyde
PLX3397	Pexidartinib
PolyQ	Polyglutamine
snRNAseq	Single nucleus RNA sequencing
TCEP	Tris (2-carboxyethyl)phosphine
Tg	Transgenic
t-SNE	t-distributed stochastic neighbor embedding
VEGF	Vascular endothelial growth factor
WT	Wild type

Frontiers in
Molecular Neuroscience

Leading research into the brain's molecular structure, design and function

Part of the most cited neuroscience series, this journal explores and identifies key molecules underlying the structure, design and function of the brain across all levels.

Discover the latest Research Topics

See more →

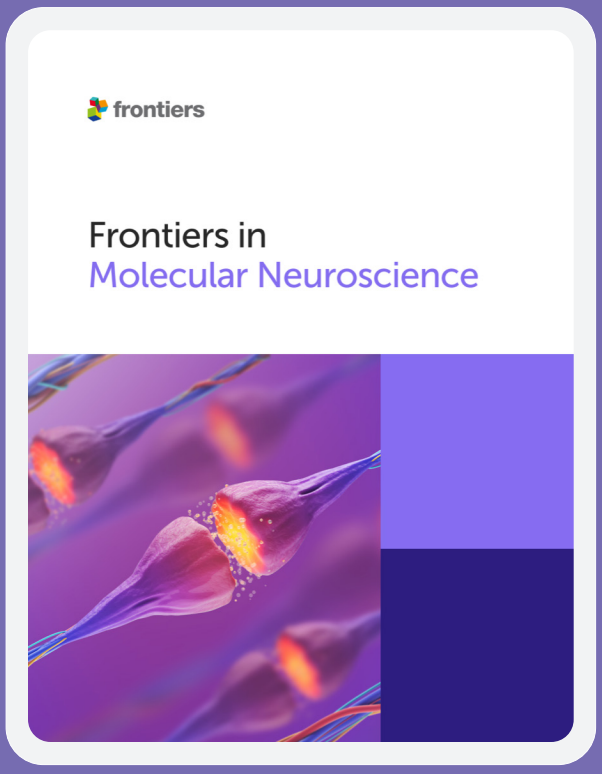

Frontiers

Avenue du Tribunal-Fédéral 34
1005 Lausanne, Switzerland
frontiersin.org

Contact us

+41 (0)21 510 17 00
frontiersin.org/about/contact